Virchows Arch (2012) 460:1–2
DOI 10.1007/s00428-011-1176-9

INVITED EDITORIAL

Virchows Archiv: Quo vadis?

Fred T. Bosman

Received: 16 November 2011 / Accepted: 16 November 2011 / Published online: 10 January 2012
© Springer-Verlag 2012

Each time I receive an issue of Virchows Archiv (The European Journal of Pathology), I realise with a feeling of pride that I am part of an incredible tradition in medical publication: 165 years of continuous pathology publishing! The journal was founded by our intellectual forebear Rudolf Virchow as 'Archiv für Pathologische Anatomie und Physiologie und für Klinische Medicin' in 1847. The first change in name occurred in 1903 when, for the 171st volume, the name of the founder was added to the name of the journal. Thus it became 'Virchows Archiv fuer Pathologische Anatomie und Physiologie und für Klinische Medizin'. With foresight the editors of the journal in 1968 decided to create two different sections of the journal: volume 344 had part A dedicated to 'Pathologische Anatomie und Histologie' and part B dedicated to 'Zellpathologie', later changed into 'Pathological Anatomy and Histology' and 'Cell Pathology'. These changes anticipated the important impact that the development of molecular biology would have on our understanding of the mechanisms involved in disease and the implications of this knowledge for the practice of diagnostic histo- and cytopathology. The journal also started to accept papers written in English, which in the second half of the twentieth century had become the new 'lingua franca' of science. Just a decade later, English became the sole language for the journal, with another name change: the German name versions disappeared. Again with foresight, the designation 'Molecular Pathology' was added to part B. In 1994, another decade later—we were now at volume 424—the two sections were fused, underlining the notion that cellular and molecular mechanisms of disease are an intricate part of pathology, be it in research or in diagnostic practice. The global orientation of the journal was reflected in the subtitle 'An International Journal of Pathology'. In 1999 the journal became officially associated with the European Society of Pathology and, with volume 454 in 2009, the journal metamorphosed in appearance (some like the flashy almost psychedelic colours, others do not) and again in name: the subtitle became 'The European Journal of Pathology'.

I have accepted the invitation to take over as editor in chief from January 2012. I stand in awe of those who have brought the journal to where it is today. Great names from the past such as Lubarsch, Hamperl, Uehlinger, Doerr, Seifert and, in recent decades, Victor Gould, Sir Colin Berry, Philipp Heitz, Manfred Dietel, Vincenso Eusebi, Günter Klöppel, who ran the journal from 1994 to 2003, Pierre Bedossa; the three latter names still being on the list of managing editors. Last but not least, Heinz Höfler, the outgoing editor in chief. We owe an immense, respectful debt of gratitude to Heinz for the energy with which he has handled the journal and his vision, whereby he has brought the journal to its present position: at the forefront of pathology publishing in an era of rapid change, in terms of both the transformation in publishing and the molecular revolution in biomedicine.

The fun part of taking on this responsibility is the opportunity to reflect on the future and to endeavour to maintain the journal in the mainstream of pathology publishing in these very dynamic times. A group of dedicated pathologists came together in the summer of 2011 to anticipate the future of pathology and the directions the journal would need to take to remain in that

F. T. Bosman (✉)
University Institute of Pathology, Lausanne University Hospital,
Rue du Bugnon 25,
1011 Lausanne, Switzerland
e-mail: fred.bosman@chuv.ch

mainstream. So what came out of this? What should the identity of the journal be? Where do we want to go?

Quite a bit of time was spent on a discussion regarding the mission statement: 'To advance the scientific basis of human pathology by the publication of high quality research (including molecular and translational studies) and thereby contribute to patient care.' Publication should be regarded in this context not as passive waiting for submitted papers but actively encouraging new generations of pathologists to engage in scientific observation and to publish their data, as well as the active dissemination of new findings in the electronic age. We also set out to define the type of manuscript that would be characteristic of the journal's content. Evidence-based pathology was chosen as the essential prerequisite: 'Manuscripts of original studies reinforcing the evidence base of modern diagnostic pathology, using immunocytochemical, molecular and ultrastructural techniques, will be welcomed. In addition, papers on the critical evaluation of diagnostic criteria but also broadsheets and guidelines with a solid evidence base will be considered. Consideration will also be given to reports of work in other fields relevant to the understanding of human pathology as well as manuscripts on the application of new methods and techniques in pathology.' Purely experimental pathology, as important as it remains for understanding mechanisms of disease, will not be one of the core interests of the journal. 'Submission of purely experimental articles is discouraged but manuscripts on experimental work applicable to diagnostic pathology are welcomed.' In this era of personalised medicine, biomarker studies will be of increasing importance and therefore 'Biomarker studies are welcomed' when they follow stringent methodological principles 'but need to abide by strict rules (e.g. REMARK—the NCI/EORTC reporting recommendations for tumour marker prognostic studies) of adequate sample size and relevant marker choice. Single marker studies on limited patient series without validated application will as a rule, not be considered.' This will include retrospective histopathological analysis of tissue from prospective studies, notably from tissue samples collected in the context of clinical trials. Unique case studies can be exciting and enlightening but 'Case reports will only be considered when they provide substantial new information with an impact on understanding disease or diagnostic practice.' So these will be the guiding principles for the future development of the journal.

Obviously, what authors and editors want is only one side of the coin. Readers should have an important voice in determining the content of the journal and a readership survey will be circulated shortly. When the message arrives in your mailbox, please do not delete it right away but take a few minutes to complete it; we need your input. To make you aware of what the journal publishes an email alert with a table of contents will be sent out to all subscribers and all others who enlist for this service. To increase interest in original papers published in the journal an annual Virchows Archiv, prize will be awarded: a short list of outstanding papers will be voted on by the editorial board and the prize will be awarded at the annual European Congress of Pathology. To attract more attention to good papers we publish, there will be an effort to improve their titles and to make the abstracts more informative. So do not be surprised if the editorial office suggests a more declarative title for your accepted paper. To lure potential authors to Virchows Archiv, members of the editorial team will actively solicit papers at European Congresses and European Society of Pathology courses. As others have done (we do not pretend to be totally original), we will publish an annual review issue as of 2013. The topics of the annual review issues will have a strong evidence-based pathology/guideline orientation. There will be a few new 'fun' items; for example, we will publish facsimiles of papers published by our intellectual ancestors over the last 50–100 years. We are seriously considering a 'News and views' section at the beginning of the journal. The journal would like to be informative to a broad readership and to keep that readership abreast of what is new out there; this will be the primary goal of this new section. Other ideas are to increase the visibility of the journal through a Facebook page and an item in Wikipedia. My grandchildren use these social media and even I have realised their potential and would like them to be able to appreciate what our discipline is all about.

You might think 'ambitions, ambitions, let us wait and see what happens.' You are right. Making plans is easy. Getting to where we want to be will take a lot of energy. I am fortunate not to have to do this all by myself. A skilled and dedicated editorial team is there to actively contribute. A partially renewed crew of editorial board members will be challenged to participate in this adventure. An office and a dedicated and experienced secretary (Dagmar Schmöe, what would we be without her?) provide essential infrastructural support. The Springer office is on board. But we need you out there: the author to share new knowledge through publishing in Virchows Archiv; the reader to digest its content, apply it in practice and comment or initiate new studies. For all of us this is going to be a fascinating adventure.

Virchows Arch (2012) 460:3–8
DOI 10.1007/s00428-011-1179-6

REVIEW AND PERSPECTIVES

Personalized cancer medicine and the future of pathology

H. Moch · P. R. Blank · M. Dietel · G. Elmberger · K. M. Kerr · J. Palacios · F. Penault-Llorca · G. Rossi · T. D. Szucs

Received: 1 September 2011 / Revised: 8 November 2011 / Accepted: 24 November 2011 / Published online: 6 December 2011
© Springer-Verlag 2011

Abstract In February 2011, a group of pathologists from different departments in Europe met in Zurich, Switzerland, to discuss opportunities and challenges for pathology in the era of personalized medicine. The major topics of the meeting were assessment of the role of pathology in personalized medicine, its future profile among other biomedical disciplines with an interest in personalized medicine as well as the evolution of companion diagnostics. The relevance of novel technologies for genome analysis in clinical practice was discussed. The participants recognize that there should be more initiatives taken by the pathology community in companion diagnostics and in the emerging field of next-generation sequencing and whole genome analysis. The common view of the participants was that the pathology community has to be mobilized for stronger engagement in the future of personalized medicine. Pathologists should be aware of the challenges and the analytical opportunities of the new technologies. Challenges of clinical trial design as well as insurance and reimbursement questions were addressed. The pathology community has the responsibility to lead medical colleagues into embracing this new area of genomic medicine. Without this effort, the discipline of pathology risks losing its key position in molecular tissue diagnostics.

Keywords Translational research · Next-generation sequencing · Whole genome analysis · Molecular pathology

H. Moch (✉)
Institute of Surgical Pathology, University Hospital Zurich,
Schmelzbergstrasse 12,
CH-8091, Zurich, Switzerland
e-mail: holger.moch@usz.ch

P. R. Blank
Institute of Social and Preventive Medicine, University of Zurich,
Zurich, Switzerland

M. Dietel
Institute of Pathology, University Hospital Charité,
Berlin, Germany

G. Elmberger
Department of Pathology, Karolinska University Hospital,
Stockholm, Sweden

K. M. Kerr
Department of Pathology, Aberdeen Royal Infirmary & Aberdeen
University Medical School,
Fosterhill,
Aberdeen, Scotland, UK

J. Palacios
Department of Pathology, Hospital Universitario Virgen
del Rocío/Instituto de Investigacions Biomédicas (IBIS) Sevilla,
Sevilla, Spain

F. Penault-Llorca
Department of Pathology, Centre Jean Perrin
et Université d'Auvergne,
Clermont-Ferrand Cedex, France

G. Rossi
Section of Pathologic Anatomy, Azienda Policlinico di Modena,
Modena, Italy

T. D. Szucs
European Center of Pharmaceutical Medicine, University of Basel,
Basel, Switzerland

Background

In the past, pathologists have defined cancer subtypes based on anatomic origin, clinical behavior, and microscopic morphology. Therapy was based on morphological classification and extent of spread as translated in stage, as well as protein-based tests such as immunohistochemistry. Although immunohistochemistry is still the most frequently used approach for cancer subtyping beyond morphology, the past 10 years have brought a revolution in the understanding of the molecular pathology of cancer [1]. We are increasingly aware of its enormous complexity, mainly due to the emerging technologies to characterize cancer and to derive its molecular characteristics, which are increasingly relevant in the practice of oncology. Molecular technologies, such as the identification of characteristic translocations in leukemias and lymphomas and categorization of tumor types based on expression profiling, had changed our understanding of certain cancers [2, 3]. In solid tumors, the identification of erbB2/*HER2* amplification in breast and gastroesophageal cancer led to the development of anti-HER2 therapeutics (trastuzumab, a monoclonal antibody; lapatinib, a small molecule tyrosine kinase inhibitor) that inhibit this protein specifically [4, 5]. Additional examples include *c-kit* and *PDGFRalpha* mutations in gastrointestinal stromal tumors [6], tyrosine kinase mutations of the *EGFR* gene in lung cancer [7, 8], mutations in the *BRAF* gene in melanoma [9], or the *EML-ALK* gene rearrangement in lung cancer [10]; all of which have the potential to render tumors extraordinarily sensitive to specific inhibitors. Certain biomarkers can also indicate when patients will not respond to a specific therapy, e.g., *K-RAS* mutations which render colorectal cancers unresponsive to anti-epidermal growth factor receptor (anti-EGFR) therapy with cetuximab or panitumumab [11, 12]. In recent years, pathologists have contributed profound knowledge to the understanding of these molecular alterations in specific tumor types [13]. In many of these examples, routine clinical practice has changed dramatically. However, the majority of patients have tumors that do not carry these particular genetic changes which therefore do not respond to such treatment. The percentage of patients responding to these new drugs is often below 30%. Therefore, future tasks include profiling these cancers further and to identify additional molecular aberrations that will lead to better therapies. This should be the focus of intensive research projects in pathology.

The goal of personalized cancer medicine is to understand the specific characteristics underlying a particular individual's disease and then match therapy to the molecular characteristics of this case. "The right drug, the right dose, for the right patient, at the right time" is the goal of personalized medicine [1]. The personalized approach has two major problems: complex biology and complex economics [14, 15]. The European Medicines Agency has already approved around 15 drugs for cancer therapy that have been designed to hit a particular molecular target. The pathways involved are often multiple with complex interactions between them which are mostly not well understood [16, 17]. Alterations in various genes, other than the predicted therapeutic target, can also significantly affect the response of a patient to a targeted therapy. As an example, inhibition of the mTOR pathway increases mitogen-activated protein kinase activity [18]. Therefore, the complex network of molecular alterations, signaling pathways, the cellular context, and the response to a particular therapeutic regimen represents a challenge for future approaches in personalized medicine.

The economic dimension is due to the fact that most targeted drugs are extremely expensive. As a result, healthcare systems and insurance companies are confronted with huge problems caused by rising health care expenditures. Targeted drugs need to be accompanied by predictive molecular diagnostic tests to identify suitable patients, yet many healthcare systems have no mechanism to pay for these tests. These companion "one-gene tests" are the domain of molecular pathology. Molecular pathologists have the expertise and the knowledge about many gene mutations identified by molecular tests; they have developed quality standards for testing, and they have developed fellowship training programs in Europe.

The movement towards personalized genomic medicine is currently associated with the development of novel high throughput genomic technologies. These tests reach beyond traditional personalized medicine, enabling the adoption of personalized genomic medicine. Pathologists should be at the forefront of embracing such new technologies [19]. An understanding of modern technologies that profile DNA, RNA, proteins, and metabolites will be essential for pathologists to make personalized medicine a reality [19].

Next-generation genomic sequencing—threat or opportunity?

The human genome sequence was completed more than 10 years ago. Improvements in sequencing technologies led to the "less than 1,000-dollar genome", which is now a reality. At the moment, these new technologies are widely used in research, but they have the potential to revolutionize medical practice. Next-generation sequencing technology may lead to fundamental changes in medical care, where pathologists could provide the necessary knowledge of interpreting genomic information in the context of the disease. However, pathologists have no "birthright" to this technology [19]. Therefore, next-generation sequencing (NGS) may challenge their traditional role. Other medical disciplines and private companies have now their own

interest in these technologies, even as clinical diagnostic tests [20]. Such drivers are further pushing pathologists to demonstrate their expertise in this rapidly evolving area of personalized medicine. One area where a desperate need exists is in the organization and coordination of programs for training in genomic medicine during the pathology residency period. Pathologists should seize the opportunity to take the lead in the translation of these new technologies and to demonstrate their value as routine diagnostic tests.

Pathologists also have to prove that genome-based testing is cost-effective, sufficiently rapid, and can optimize evidence-based precision diagnostics [21, 22]. The pathology community cannot claim ownership of these most recent technological innovations in genome sequencing, but should demonstrate competence in this field. Clinical genetic testing is also performed by various other specialties, e.g., clinical pathology, clinical genetics, oncology, clinical chemistry, microbiology, and pharmacology. With NGS, private, non-hospital-based companies have begun to offer genetic testing that might bypass pathology. Examples include OncotypeDX with their breast cancer assay determining the expression of the 21-gene panel [23] or new start-up companies like Foundation Medicine, offering NGS approaches to cancer genome analyses for personalized medicine. When NGS and whole genome analysis (WGA) can be performed at costs that significantly undercut current charges for single-gene testings, many other institutions outside pathology will offer such clinical tests. It may be that current "one-gene tests" are replaced by NGS testing that will be more powerful and more cost-effective. It is imperative that pathologists take the lead, demonstrating which tests are most powerful and most cost-effective [21, 22, 24]. Only when well-designed clinical studies convincingly demonstrate the predictive value of NGS- or WGA-based tests, will the implementation of such molecular tumor profiling become accepted and integrated in diagnosis and treatment of cancer. Personalized diagnostic technologies will aid in the stratification of patients with specific molecular alterations for a clinical trial. It has been shown in the past that pathologists can significantly contribute to clinical trials, e.g., EORTC trials with colorectal carcinoma patients [25]. These well-designed trials allowed identifying the relevance of k-RAS mutations in colorectal cancer. In the future, clinical trial design will be based on a genotype that can be targeted, rather than the morphological classification. Selection of patients on the basis of the mutations their cancer carries will be challenging, but might be the way to go for types of cancer with specific mutations at lower frequencies. NSCLC patients, for instance, can harbor activating mutations in EGFR, but also k-RAS, BRAF, or translocations involving ALK. Such alterations may be present in less than 2% of patients with prostate, gastric cancer, and melanoma, but these may be sensitive to RAF or MEK inhibitors [26]. The understanding of specific molecular pathways can also help to interpret clinical trial data and enhance our understanding of the biology of response or resistance. Well-designed clinical trials, in combination with novel genomic technologies, will require the involvement of pathologists' expertise, which as a consequence must be involved very early in the design of clinical trials [27].

Above all, when genomic tests of tumors are considered, it is essential that the test be performed on nucleic acid extracts *from tumor cells.* Certainly for solid tumors, only pathologists can make this determination; *genomic analysis in the absence of pathologic assessment risks the generation of meaningless results.*

Pathology today—strengths and weaknesses

Personalized genomic medicine is an issue for the entire field of medicine. The medical community now has the task of integrating this new domain into medical practice [19]. Pathology should take leadership in personalized genomic medicine by partnering with other medical disciplines. Diverse disciplines such as genetics, clinical chemistry, microbiology, immunology, and bioinformatics are engaged in molecular diagnostics. These specialists should work closely together with pathologists. At the moment, pathologists are important members of all tumor boards, where individualized treatment decisions are made. We rely on our clinical colleagues to send us specimens from patients who have sought medical attention for a specific problem; the case is assessed, diagnosed, and interpreted and a report is issued. Pathologists are able to develop a "diagnostic algorithm" with conventional histopathology in combination with immunohistochemistry [28]. This basic evaluation can be supplemented by disease-specific analyses such as other "one-gene tests", and potentially WGA or NGS. Therefore, pathologists are in a pivotal position to include and integrate genomic results with tissue-based morphological assessments to generate a complete report for the treating oncologist and the patient (Fig. 1).

In Europe, pathologists have different strategies to demonstrate competence and expertise in molecular testing. In Germany, a quality assurance initiative has been organized. Interlaboratory tests as part of a quality assurance initiative in pathology (QuIP) are run under the auspices of the German Society of Pathology. Similarly, in Italy and Spain, two quality assurance systems for molecular testing of EGFR and KRAS mutations under the supervision of the National Associations of Oncology (AIOM) and Pathology (SIAPEC) and the Spanish Society of Pathology, respectively, have been validated. The QuIP system sets quality standards for all molecular pathology testings. Similar systems exist in the UK for a number of tissue-based molecular tests, organized by UK-NEQAS, while EMQN and the European Society of Pathology also organize molecular testing

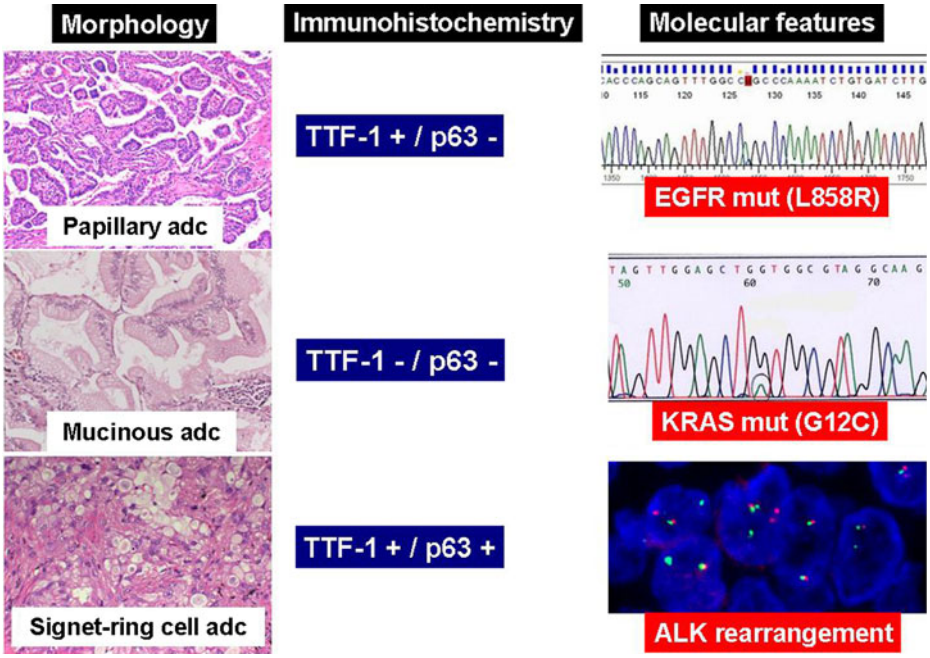

Fig. 1 Integration of conventional histopathology, immunohistochemistry, and disease-specific genetic results in lung cancer

quality assurance programs in various European countries. These systems demonstrate the expertise of pathology to perform such tests and to provide the respective quality assurance programs. National and international recommendations for mutational analysis of EGFR in lung cancer have been also published [29–32].

Given the high cost of targeted therapies and the requirement that these expensive drugs cannot be prescribed without testing, France has found its own solution: In 2005, the country confirmed payment for treatment of every citizen shown to be likely to benefit from targeted drugs. Its National Cancer Institute set up 28 platforms for molecular genetics at those university hospitals and cancer centers with expertise in both molecular and pathological analyses. Biopsy samples of cancer tissues are sent from all over France, to these platforms for a battery of around 20 genetic tests. If in the tissues a molecular signature is identified in any signaling pathway targeted by one of the drugs, the patient gets treated with it. The Czech Republic has a similar system. The French platforms have tested samples from around 50,000 people with lung cancer for alterations in the EGF pathway [14]. Advantages of the centralized system include reduced cost due to large volumes of tests, easier quality control, and free of charge testing for patients. On the other hand, tests are frequently performed outside the primary hospital and tissues have to be sent to an external platform. This can result in a delay of receiving the test results. Given these differences, a European commission's health directorate should help by encouraging European countries to harmonize their health technology assessment by giving recommendations.

Personalized medicine has ethical, legal, and social implications. Privacy issues are a concern for many patients, which must give their consent for treatment. The public has to be educated with regard to the impact of genomic testing. This is a relevant issue for the EU health directory. Furthermore, the requirements for informed consent documents should be harmonized in the European Union. There is a need to protect patients' data, e.g., against discrimination (issues related to health insurance and employment). Patients should not have to fear discrimination. Testing for BRCA1 and BRCA2 genes (implicated in familial breast and ovarian cancer syndromes) were early examples for the contribution of germline features to disease prognosis. Public education on the potential benefits of personalized cancer medicine and individualized treatments are important for its widespread acceptance. When novel next-generation sequencing technologies enter into clinical medicine and become standard of care, public education programs on the ethical, legal, and social implications are needed for patient protection [33].

Conclusions

The meeting participants agreed that there is a need to develop a European strategy to ensure that pathologists are involved in the performance, interpretation, and regulation of omics-based clinical testing, while recognizing the importance of clinical trial-based evidence for performing any particular test. Testing for testing's sake serves no useful purpose. Pathologists have

to develop programs of training and education in genomic medicine, especially in the evolving technologies of NGS and WGA. The European Society of Pathology should assess the current landscape of molecular testing and the reimbursement situation. It should identify barriers and recommend specific actions required to develop a European plan for integration of genomic testing and its interpretation into pathology. It should be shown that if pathologists take the lead in this arena, substantial benefits will be realized, not only for the patient, but also for society at large. The new technologies are very complex. Therefore, the European Society of Pathology should assume leadership when it comes to regulatory challenges for such technologies when performed in pathology laboratories. This includes evaluation of the performance claims of the tests based upon scientific evidence. Tests to be performed in a diagnostic and therapeutic context should be certified after technical validation, notably but not only when it comes to many "in-house-developed tests". The European Society of Pathology should publish standards on assay validation and performance. Consensus recommendations to clinicians and oncologists would also be helpful for personalized medicine, especially in a time with competing test on a commercial market. The European Society of Pathology, through its working group in molecular pathology, should distribute information on clinical trials and issue guidelines on clinical policy in oncology based on the "levels of evidence" approach. Guidelines of the European Society of Pathology would be helpful for different countries to select specific technologies into routine tissue testing.

The future of pathology lies in personalized medicine [19, 34, 35]. Pathologists have the obligation to take a lead in changing both their role, and prevailing attitudes towards that role, away from "just looking into the microscope", towards "integrating the results of both histology and molecular diagnostics" for the benefit of patients. Pathologists must learn to manage the clinical decision-making process by coordinating histological diagnosis and molecular measurements. Pathologists must get prepared to understand their new role, expand their profile, and take new responsibilities.

Acknowledgments We thank Mrs. B. Terrier for support in writing this article. The panel meeting of European pathologists held at the Institute of Surgical Pathology Zurich, Switzerland, was supported by Pfizer Inc.

References

1. Stricker T, Catenacci DV, Seiwert TY (2011) Molecular profiling of cancer—the future of personalized cancer medicine: a primer on cancer biology and the tools necessary to bring molecular testing to the clinic. Semin Oncol 38:173–185
2. Perou CM, Sorlie T, Eisen MB et al (2000) Molecular portraits of human breast tumours. Nature 406:747–752
3. Alizadeh AA, Eisen MB, Davis RE et al (2000) Distinct types of diffuse large B-cell lymphoma identified by gene expression profiling. Nature 403:503–511
4. Geyer CE, Forster J, Lindquist D et al (2006) Lapatinib plus capecitabine for HER2-positive advanced breast cancer. N Engl J Med 355:2733–2743
5. Hortobagyi GN (2005) Trastuzumab in the treatment of breast cancer. N Engl J Med 353:1734–1736
6. Rubin BP, Heinrich MC, Corless CL (2007) Gastrointestinal stromal tumour. Lancet 369:1731–1741
7. Lynch TJ, Bell DW, Sordella R et al (2004) Activating mutations in the epidermal growth factor receptor underlying responsiveness of non-small-cell lung cancer to gefitinib. N Engl J Med 350:2129–2139
8. Maemondo M, Inoue A, Kobayashi K et al (2010) Gefitinib or chemotherapy for non-small-cell lung cancer with mutated EGFR. N Engl J Med 362:2380–2388
9. Flaherty KT, Puzanov I, Kim KB et al (2010) Inhibition of mutated, activated BRAF in metastatic melanoma. N Engl J Med 363:809–819
10. Soda M, Choi YL, Enomoto M et al (2007) Identification of the transforming EML4-ALK fusion gene in non-small-cell lung cancer. Nature 448:561–566
11. Amado RG, Wolf M, Peeters M et al (2008) Wild-type KRAS is required for panitumumab efficacy in patients with metastatic colorectal cancer. J Clin Oncol 26:1626–1634
12. Jimeno A, Messersmith WA, Hirsch FR, Franklin WA, Eckhardt SG (2009) KRAS mutations and sensitivity to epidermal growth factor receptor inhibitors in colorectal cancer: practical application of patient selection. J Clin Oncol 27:1130–1136
13. Gabrielson E, Berg K, Anbazhagan R (2001) Functional genomics, gene arrays, and the future of pathology. Mod Pathol 14:1294–1299
14. Anonymous (2011) Getting personal. Nature 473:253–254
15. Luciano JS, Andersson B, Batchelor C et al (2011) The translational medicine ontology and knowledge base: driving personalized medicine by bridging the gap between bench and bedside. J Biomed Semantics 2(Suppl 2):S1
16. Dahinden C, Ingold B, Wild P et al (2010) Mining tissue microarray data to uncover combinations of biomarker expression patterns that improve intermediate staging and grading of clear cell renal cell cancer. Clin Cancer Res 16:88–98
17. Jones S, Zhang X, Parsons DW et al (2008) Core signaling pathways in human pancreatic cancers revealed by global genomic analyses. Science 321:1801–1806
18. Carracedo A, Ma L, Teruya-Feldstein J et al (2008) Inhibition of mTORC1 leads to MAPK pathway activation through a PI3K-dependent feedback loop in human cancer. J Clin Invest 118:3065–3074
19. Tonellato PJ, Crawford JM, Boguski MS, Saffitz JE (2011) A national agenda for the future of pathology in personalized medicine: report of the proceedings of a meeting at the Banbury Conference Center on genome-era pathology, precision diagnostics, and preemptive care: a stakeholder summit. Am J Clin Pathol 135:668–672
20. Salzberg SL, Pertea M (2010) Do-it-yourself genetic testing. Genome Biol 11:404
21. Blank PR, Moch H, Szucs TD, Schwenkglenks M (2011) KRAS and BRAF mutation analysis in metastatic colorectal cancer: a cost-effectiveness analysis from a Swiss perspective. Clin Cancer Res 17:6338–6346
22. Blank PR, Schwenkglenks M, Moch H, Szucs TD (2010) Human epidermal growth factor receptor 2 expression in early breast cancer patients: a Swiss cost-effectiveness analysis of different predictive assay strategies. Breast Cancer Res Treat 124:497–507
23. Paik S, Shak S, Tang G et al (2004) A multigene assay to predict recurrence of tamoxifen-treated, node-negative breast cancer. N Engl J Med 351:2817–2826

24. Blank PR, Dedes KJ, Szucs TD (2010) Cost effectiveness of cytotoxic and targeted therapy for metastatic breast cancer: a critical and systematic review. PharmacoEconomics 28:629–647
25. Roth AD, Tejpar S, Delorenzi M et al (2010) Prognostic role of KRAS and BRAF in stage II and III resected colon cancer: results of the translational study on the PETACC-3, EORTC 40993, SAKK 60–00 trial. J Clin Oncol 28:466–474
26. Palanisamy N, Ateeq B, Kalyana-Sundaram S et al (2010) Rearrangements of the RAF kinase pathway in prostate cancer, gastric cancer and melanoma. Nat Med 16:793–798
27. AMP Whole Genome Analysis Working Group (2011) The Association for Molecular Pathology's approach to supporting a global agenda to embrace personalized genomic medicine. J Mol Diagn 13:249–251
28. Dietel M, Sers C (2006) Personalized medicine and development of targeted therapies: the upcoming challenge for diagnostic molecular pathology. A review. Virchows Arch 448:744–755
29. Pirker R, Herth FJ, Kerr KM et al (2010) Consensus for EGFR mutation testing in non-small cell lung cancer: results from a European workshop. J Thorac Oncol 5:1706–1713
30. Marchetti A, Normanno N, Pinto C et al (2010) Recommendations for mutational analysis of EGFR in lung carcinoma. Pathologica 102:119–126
31. Kulesza P, Ramchandran K, Patel JD (2011) Emerging concepts in the pathology and molecular biology of advanced non-small cell lung cancer. Am J Clin Pathol 136:228–238
32. van Krieken JH, Jung A, Kirchner T et al (2008) KRAS mutation testing for predicting response to anti-EGFR therapy for colorectal carcinoma: proposal for an European quality assurance program. Virchows Arch 453:417–431
33. Macconaill LE, Van Hummelen P, Meyerson M, Hahn WC (2011) Clinical implementation of comprehensive strategies to characterize cancer genomes: opportunities and challenges. Cancer Discov 1:297
34. Cagle PT, Allen TC, Dacic S et al (2011) Revolution in lung cancer: new challenges for the surgical pathologist. Arch Pathol Lab Med 135:110–116
35. Kerr K (2011) Personalized medicine for lung cancer: new challenges for pathology. Histopathology. doi:10.1111/j.1365-2559.2011.03854.x

Virchows Arch (2012) 460:9–18
DOI 10.1007/s00428-011-1166-y

REVIEW AND PERSPECTIVE

Adrenocortical neoplasia: evolving concepts in tumorigenesis with an emphasis on adrenal cortical carcinoma variants

Ronald R. de Krijger · Thomas G. Papathomas

Received: 6 September 2011 / Revised: 28 September 2011 / Accepted: 31 October 2011 / Published online: 16 November 2011
© The Author(s) 2011. This article is published with open access at Springerlink.com

Abstract Adrenocortical carcinoma (ACC) is a rare, heterogeneous malignancy with a poor prognosis. According to WHO classification 2004, ACC variants include oncocytic ACCs, myxoid ACCs and ACCs with sarcomatous areas. Herein, we provide a comprehensive review of these rare subtypes of adrenocortical malignancy and emphasize their clinicopathological features with the aim of elucidating aspects of diagnostic categorization, differential diagnostics and biological behavior. The issue of current terminology, applied to biphasic tumors with pleomorphic, sarcomatous or sarcomatoid elements arising in adrenal cortex, is also discussed. We additionally present emerging evidence concerning the adrenal cortical tumorigenesis and the putative adenoma–carcinoma sequence as well.

Keywords Adrenal cortical neoplasia · Adenoma · Carcinoma · ACC variants · Oncocytic · Myxoid · Sarcomatoid · Carcinosarcoma

Introduction

Adrenocortical carcinoma (ACC) is a rare heterogeneous malignancy with an incidence of 0.7–2.0 cases per million population per year [1]. Although the diagnosis of malignancy is easy in most cases, mainly due to advanced stage at presentation, strictly intra-adrenal tumors must be evaluated for malignant potential [2]. In this regard, several multiparametric scoring systems, including the Hough scoring system, the Weiss scoring system, the Van Slooten scoring system and the Weiss revisited index [3, 4], and, also recently, diagnostic algorithms, such as the stepwise discriminate diagnostic system and the simplified diagnostic algorithm [5, 6], have been generated. The latter takes into account the presence of a disrupted reticulin framework, which constitutes the first step of this diagnostic approach, as being the single most sensitive feature of malignancy. Other parameters include mitotic count >5⁄50 HPF, presence of necrosis and venous invasion [6].

Currently, the Weiss scoring system is the most popular among multiparametric scoring systems, owing to its reliability and relative simplicity (Table 1) [1, 7]. Nevertheless, the Weiss system suffers particular limitations including (1) lack of reproducibility of several criteria, (2) "borderline" tumors with a Weiss score of 2 or 3, (3–4) oncocytic and myxoid variants of adrenocortical tumors and (5) pediatric adrenocortical neoplasms [2, 7]. The latter are frequently characterized by a limited malignant potential especially in children<5 years of age, despite the presence of impressively atypical histologic features (Fig. 1), which could be attributed either to a low stage upon presentation or to a putative origin from a cell of the fetal adrenal cortex [8].

The objectives of this review are (1) to present emerging evidence concerning the adrenocortical tumorigenesis in order to address the issue of an adenoma–carcinoma sequential progression as well as to further elucidate the incompletely understood pathophysiology of this aggressive neoplasia and (2) to describe in detail the rare variants of ACC to increase awareness of their clinicopathological features and the potential diagnostic challenges.

R. R. de Krijger (✉) · T. G. Papathomas
Department of Pathology, Josephine Nefkens Institute,
Erasmus MC—University Medical Center Rotterdam,
P.O. Box 2040, 3000 CA Rotterdam, The Netherlands
e-mail: r.dekrijger@erasmusmc.nl

T. G. Papathomas
e-mail: t.papathomas@erasmusmc.nl

Table 1 Weiss system for assessing malignant potential of adrenocortical neoplasms [2, 3]

Histological features to be evaluated
Diffuse architecture (greater than one third of the tumor)
Clear cells comprising 25% or less of the tumor
High nuclear grade (grade 3 or 4 according to Fuhrman criteria)
Mitotic rate ≥ 6 per 50 high-power fields
Atypical mitotic figures
Necrosis
Venous invasion
Sinusoidal invasion
Capsular invasion

The presence of three or more criteria highly correlates with malignant behavior

Part I. Histogenesis of conventional adrenocortical carcinomas

A hotly debated issue is whether or not adenomas progress stepwise to carcinoma. Given (1) the differences between benign and malignant tumors in terms of transcriptome and genetic alterations, (2) the epidemiology of adrenal incidentaloma and ACC and (3) the low incidence of progression (5–25%) of clinically inapparent adrenal masses to hyperfunction or an increase in size by at least 1 cm coupled with (4) the lack of clear evolution from benign, non-secreting adenoma to ACC in untreated cases [9, 10], it seems that multistep progression from benign to malignant is unlikely for adrenal cortical neoplasms.

However, not all evidence points in that direction. Fewer genetic aberrations were found in adenomas than in carcinomas. Most (72–86%) distinct alterations seen in the adenomas were also present in carcinomas [11, 12]. Furthermore, the positive correlation between the number of alterations detected by comparative genomic hybridization (CGH) and tumor size [11, 13] supports the notion of an adenoma–carcinoma sequence. Additional evidence in favor of such a sequence derives from X-chromosome inactivation pattern analysis which shows monoclonal ACCs along with ACAs of polyclonal or monoclonal origin. Allelotyping with microsatellites and a few reported cases provide support for an adrenal adenoma–carcinoma sequence [14–20].

With regard to the latter, Bernard et al. [17] reported on an intriguing case of a localized adrenal neoplasm composed of two different components exhibiting different pathological features: a central zone of a Weiss score (5) and a peripheral zone of a Weiss score (0). The former zone displayed complete LOH at the *TP53* (17p13.3) gene locus, uniparental disomy at the 11p15 locus, overexpression of the *IGF-II* gene and numerous CGH changes, with gains at chromosomes 4, 5p, 10, 12p, 16p, 19 and 20 and losses at chromosomes 2 and 11. The outer zone did not show any of these genetic abnormalities. A similar case was presented by Trezzi et al. [18] as a dedifferentiated adrenal cortical neoplasm comprising a sharply outlined, hemorrhagic, central nodule (ACC) and an outer ring zone (ACA), while Gaujoux et al. [19] included one heterogeneous ACT in a small series consisting of an ACC component (Weiss score 6) developed within an ACA component (Weiss score 1). The malignant component exhibited diffuse cytoplasmic and focal nuclear β-catenin accumulation and harbored a β-catenin gene (CTNNB1) mutation, whereas the benign component showed only focal cytoplasmic staining and no such mutation. No *TP53* somatic mutation was found in the ACC and ACA components. Similarly, Schmitt et al. [20] presented an ACA case showing frank heterogeneity both by means of H&E staining (atypia, hyperchromasia, nucleoli and atypical mitoses) and immunohistochemistry, including perinuclear dot-like immunoreactivity for IGF-II, nuclear staining for CDK4 and Ki67 labeling index > 5%. These particular areas within the adenoma were interpreted as small

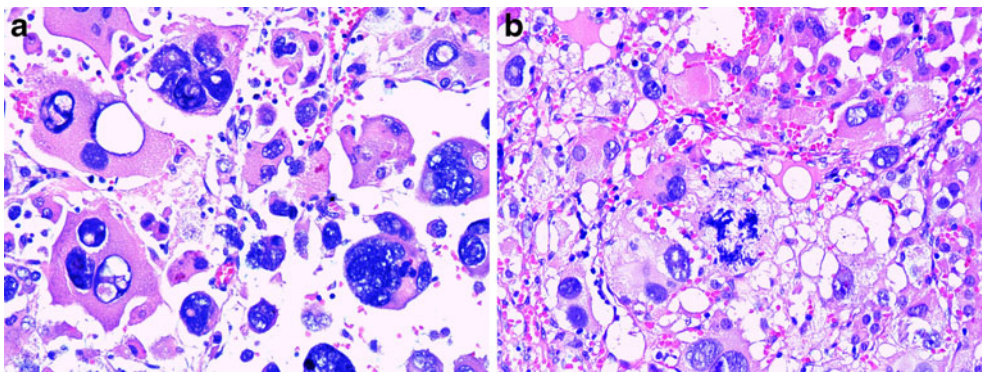

Fig. 1 Two areas from a pediatric adrenal cortical neoplasm, weighing 88 g. Large, multinucleated tumor giant cells, with hyperchromatic nuclei and nuclear pseudoinclusions in a few, among smaller tumor cells displaying high nuclear/cytoplasmic ratio and hyperchromatic nuclei (**a**). Tumor cells with moderately atypical nuclei and an atypical mitotic figure near the center of the field (**b**). Despite these worrisome histological features, this neoplasm had a benign biological behavior

foci of malignant transformation, in accordance with a van Slooten index > 8.

Whether the fact that different scoring systems yield different diagnoses in individual ACTs [20, 21] points to a multistep process remains to be clarified. It is tempting to speculate that in a process of clonal evolution, one dominant clone may overtake neighboring subclones to an extent that the ACA component is no longer visible.

Recent evidence has suggested multistep tumorigenesis within the group of ACCs [9]. In particular, transcriptome analysis has established an ACC subclassification into two distinct subgroups with different outcomes [22–24], consistent with the notion that ACC survival and outcome vary greatly mainly due to different molecular defects modulating the tumor phenotype and, to a lesser extent, to tumor stage at diagnosis [25]. However, ACCs in the poor prognosis group displayed more advanced disease, subsequently confounding the issue of whether these subgroups correspond to distinct stages of the same disease or to distinct ACC types. Statistical independence of transcriptome-based prognostic information from stage seems to argue in favor of the latter [26].

In an effort to further elucidate the molecular genetics of the poor-outcome ACC group, Ragazzon et al. [25] identified three subgroups by using unsupervised clustering analysis: (1) p53 group, encompassing all tumors with a *TP53* mutation, (2) β-catenin group, containing all tumors with beta-catenin nuclear staining, and (3) x group, with neither p53 nor β-catenin altered pathways, but enriched in cell cycle and metabolism genes. Moreover, IGF-II overexpression has been shown in approximately 90% of ACCs, with *paternal unidisomy* and *loss of imprinting* being the underlying mechanisms accounting for this markedly elevated expression in familial ACC cases associated with Beckwith–Wiedemann Syndrome, while additional mechanisms of transcriptional regulation are likely to be involved in sporadic ACCs [9, 23]. In this context, Ragazzon et al. [25] did refer to widespread IGF-II overexpression among both subgroups, highlighting its importance in adrenocortical tumorigenesis, but concomitantly suggesting a role for additional genomic alterations promoting the development of the most aggressive tumors [25, 27]. Prior to IGF-II overexpression, it appears that ACC loses nephroblastoma overexpressed (nov) expression [28], in line with the finding of a significantly reduced novH expresssion correlated with the acquisition of a malignant tumoral phenotype [29].

Several lines of evidence suggest that the activation of the Wnt/β-catenin signaling pathway is important in adrenocortical oncogenesis [19, 25, 30–37]. In fact, it has been demonstrated that this activation, as assessed by abnormal nuclear and/or cytoplasmic β-catenin accumulation with or without somatic activating CTNNB1 mutations, is involved both in benign and malignant adrenocortical tumors [19, 31–33]. It is of particular interest to note that CTNNB1 mutations (1) were detected only in macronodules of primary pigmented nodular adrenocortical disease cases, suggesting that these are secondary genetic events contributing to the nodular development of the disease and potentially implying a more aggressive phenotype [19, 34], (2) were related to a specific phenotype of larger and non-secreting ACAs, indicating a less differentiated state [33], and (3) were associated with decreased overall and disease-free survival in ACCs, suggesting a specific effect on tumor biology in terms of progression towards a more aggressive phenotype within the group of ACCs [25, 35]. Altogether, these observations, along with data stemming from an experimental mouse model [30], do not completely clarify whether the activation of Wnt/beta-catenin signaling pathway is an early or a late event in the development of adrenal neoplasms.

Part II. Adrenocortical carcinoma variants

Oncocytic adrenocortical neoplasms

Oncocytic adrenocortical neoplasms (OAN) represent a rare group of neoplasms with approximately 115 cases reported in the literature [38–44]. Kakimoto et al. [38] first described this particular histological variant in 1986, which was followed by numerous reports either in the form of single cases or of small series, with the largest one comprising 13 cases [39].

Accurate classification of OAN is important. Given that OANs display (1) cells with eosinophilic cytoplasm, clear cell population as a rule consisting of less than 25% of the tumor volume, (2) high-grade nuclear atypia in at least a subgroup of neoplastic cells and (3) almost always diffuse architecture and since these inherent histological parameters do not confer a poor prognosis [45], applying the Weiss system to this subset of adenocortical neoplasms will lead to a diagnosis of ACC, which is not appropriate given the benign behavior of most of these lesions.

Bisceglia and colleagues [46] developed criteria for the classification of oncocytic adrenocortical tumors (Table 2). These were based on parameters of the Weiss system and constituted the Lin–Weiss–Bisceglia (LWB) system: (1) *major criteria* (a mitotic rate of more than 5 mitoses per 50 high-power fields, any atypical mitoses or venous invasion), (2) *minor criteria* [large size (>10 cm and/or > 200 gr), necrosis, capsular invasion or sinusoidal invasion] and (3) *definitional criteria* (predominantly cells with eosinophilic-granular cytoplasm, high nuclear grade and diffuse architectural pattern). The latter are not used as they

Table 2 Lin–Weiss–Bisceglia (LWB) system for diagnostic categorization of oncocytic adrenocortical neoplasms [42]

Major criteria
Mitotic count >5 per 50 high-power fields
Atypical mitoses
Venous invasion
Minor criteria
Size >10 cm and/or weight >200 g
Necrosis
Sinusoidal invasion
Capsular invasion

The presence of one major criterion indicates malignancy, one to four minor criteria present indicates uncertain malignant potential, and the absence of all major and minor criteria is indicative of benign biological behavior

are present in all subgroups of pure oncocytic neoplasms and are not determinants of biological behavior. According to the proposed working rules, the presence of any one of the major criteria indicates malignancy (*oncocytic adrenocortical carcinoma*), and the presence of one to four minor criteria is indicative of uncertain potential (*borderline oncocytic neoplasm of uncertain malignant potential*) (Fig. 2), while the absence of all major and minor criteria indicates benign behavior (*adrenocortical oncocytoma*) [46]. In addition, Bisceglia et al. [45] proposed categories for oncocytic adrenocortical tumors as follows: (1) *pure oncocytic tumor*, if a tumor is exclusively or almost entirely composed (greater than 90%) of oncocytic cells, (2) *mixed oncocytic tumor*, when a clear cell component is also present (ranging from 10% to 50%), and (3) *ordinary adrenocortical tumor with focal oncocytic changes*, if the oncocytic component is not a predominant one (less than 50% of the tumor mass).

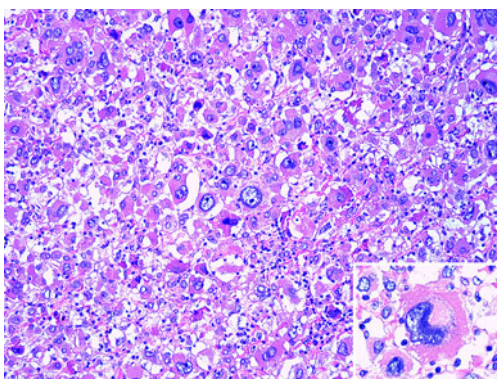

Fig. 2 Section of an oncocytic adrenocortical neoplasm, weighing >200 g; in the presence of only one minor criterion (according to the Lin–Weiss–Bisceglia classification), a diagnosis of borderline oncocytic neoplasm of uncertain malignant potential was finally rendered. Diffuse growth pattern of tumor cells, characteristically displaying abundant eosinophilic, granular cytoplasm and at least focal high nuclear atypia. Marked degree of nuclear pleomorphism (*inset*). These would lead to a Weiss score 3, probably overestimating the biological behavior of this lesion

It is critical to extensively sample an oncocytic adrenocortical neoplasm for several reasons. First, one should discriminate a pure oncocytic tumor either from an ordinary adrenocortical tumor with focal oncocytic changes or its conventional counterpart of the compact cell type in order not to incorrectly apply the Weiss system and accordingly inadequately estimate its biological behavior [45]. Second, an oncocytic tumor can only be labeled as pure after quantifying each individual component (oncocytic and clear) since pure and mixed oncocytic tumors do not seem to share similar clinical outcome [45]. In this regard, immunohistochemistry using antimitochondrial antibodies can support the recognition of oncocytic differentiation and help to accurately quantify the oncocytic component. Of note, adrenocortical cells are, by nature, rich in mitochondria and therefore positive, so only strong, diffuse and finely granular staining should be taken as indicative of oncocytic differentiation, as suggested by Wong et al. [39] with respect to mES-13 staining. Moreover, the differential diagnostic spectrum of OANs also includes the oncocytic variant of pheochromocytoma, the granular cell variant of clear cell renal cell carcinoma, the eosinophilic variant of chromophobe renal cell carcinoma and the hepatocellular carcinoma [45, 46].

In an effort to further delineate and elucidate this subtype of adrenocortical neoplasia, Wong et al. [39] provided a comprehensive review and retrospectively applied the LWB criteria to all reported cases with sufficient information, along with 13 previously unpublished cases. Of note, they validated the effectiveness of the LWB criteria in predicting malignant potential and provided preliminary evidence supporting the concept of a more favorable prognosis for oncocytic adrenocortical carcinomas in comparison with their conventional counterparts. Moreover, they found approximately 30% of OANs to be functional while emphasizing the frequency of small oncocytes in several cases of their series [39], accordingly including in their view of the oncocyte not only cells with *abundant* granular eosinophilic cytoplasm.

Myxoid adrenocortical neoplasms

In keeping with the current notion that myxoid extracellular matrix is a histological feature that can be found in both physiological and pathological conditions, *non-neoplastic* (e.g. myxedema) as well as *neoplastic* (benign/malignant epithelial or mesenchymal tumors) [47], myxoid change has been recognized rarely also in neoplasms of adrenal cortical origin. The myxoid substance has been shown to be *Alcian-blue* positive and negative or focally weak positive for *PAS*

stain and *mucicarmine*. In particular, there have been thus far 46 reports of myxoid adrenocortical neoplasms (MANs) [48–65]: 17 myxoid adrenocortical adenomas [49–58], 2 borderline MANs [48, 50] and 27 myxoid adrenocortical carcinomas [48, 49, 59–65]. These cases were either published as isolated case reports or were presented in small series, with the largest ones each consisting of 14 cases [48, 49].

The reported age range of MANs (46 cases) is 16 to 82 years, with a mean and a median age of 51 and 51.5 years, respectively. In general, cases in females slightly outnumber those in males (26:20). Hormone hypersecretion occurs frequently in these tumors; only 13 out of 42 cases were non-functioning (eight adenomas, one borderline and four carcinomas), whereas five patients had biochemical evidence of hormone production (two adenomas, one borderline and two carcinomas). The remaining 24 cases with an available endocrine evaluation presented with clinical evidence of hormone overproduction: 16 with Cushing-related symptoms, 4 with Conn syndrome, 2 with symptoms due to cortisol and androgens, 1 with gynecomastia and breast pain and 1 with virilization (4 adenomas and 20 carcinomas). Although it had been suggested that the functional status could be associated with the presence of myxoid material, non-functioning tumors displaying a higher percentage of myxoid areas and being lipid depleted [61], no definite conclusions can be reached on morphological grounds. In fact, eight cases showing a myxoid area > 70 % were hormonally active [48–50, 62, 63], whereas another eight cases with a similar myxoid content were non-functional [48, 51, 53–55, 57, 59, 60]. The proportion of myxoid change varied in all reported cases from 5% to approximately 100% of the total area. Interestingly, neurofilament (NF) expression has been recently found to be related more to the extent of myxoid changes and, therefore, suggested as a potential characteristic of *myxoid ACC*s with a predominant (> 70 %) myxoid component [48]. This, along with the fact that the expression of neuroendocrine/neuronal markers such as NF and CD56 was mostly restricted to the myxoid areas of *conventional ACCs with focal myxoid change*, seems to imply a peculiar association between NF expression and myxoid change [48].

An important point is the distinction of myxoid borderline/malignant ACTs into two subgroups as proposed by Papotti et al. [48]: *myxoid ACCs* and *conventional ACCs with focal myxoid changes*. This is based on a different type of myxoid change, growth pattern, cell size, nuclear atypia and cell cytoplasm. Myxoid ACCs are usually characterized by (1) extensive myxoid areas separated from conventional ACC areas, if present, (2) trabecular/microacinar growth pattern, (3) small, uniform cell size, (4) mild nuclear atypia and (5) scant, eosinophilic cell cytoplasm, whereas *conventional ACCs with focal myxoid changes* are characterized by (1) focal myxoid areas (< 20% of the total area) always merging with conventional ACC areas, (2) solid/diffuse growth pattern, (3) large, heterogenous cell size, (4) moderate to high nuclear atypia and (5) abundant, granular eosinophilic cell cytoplasm. Nevertheless, two cases of the former subset showed overlapping features such as solid growth pattern and pleomorphism as well. In addition, the same investigators [48] suggested that only the former subgroup actually belongs to the distinctive myxoid variant of ACTs, with the latter potentially representing the result of myxoid degenerative changes (Fig. 3). Whether or not these subgroups have a distinct biologic behavior needs to be further elucidated.

In the histopathological assessment of these lesions, it is critical first to exclude potential morphological mimics, including *metastatic tumors* affecting the adrenal gland (breast carcinomas, salivary or skin adnexal carcinomas of adenoid cystic type and neuroendocrine tumors) [48] as well as primary *retroperitoneal neoplasms* with myxoid areas (chordomas, myxomas, lipomas or liposarcomas, leiomyomas or leiomyosarcomas, benign or malignant nerve sheath tumors, extraskeletal myxoid chondrosarcomas, gastrointestinal stromal tumors and myxoid malignant fibrous histiocytomas) [49, 50, 63]. The presence of typical foci of adrenocortical differentiation, along with an immunohistochemical profile similar to that of the conventional ACT, provides valuable aid in excluding these mimics [48, 50, 51]. In addition, accurate assessment of malignant potential in any given tumor of the myxoid variant is important. In this regard, the issue of whether the Weiss scoring system is adequate to reliably predict malignancy in MANs is currently being questioned because:

(1) A MAN case lacking morphological signs of malignancy (Weiss score 1/clear cell cytoplasm present in less than 25% of the tumor cells) and diagnosed as myxoid borderline ACT [59] subsequently did demonstrate an aggressive clinical behavior (peritoneal spread), with a dismal outcome 68 months following the initial diagnosis [48]. Another such tumor of uncertain malignant potential (Weiss score 1/clear cell cytoplasm present in less than 25% of the tumor cells) has been recently described by the same group, with no evidence of recurrence or metastasis 9 months following surgical resection. Both cases were characterized by the same extent of myxoid area (90%), growth pattern, Weiss score and low Ki67 labeling index (3% and 4%, respectively). Interestingly, the latter case had an intact reticulin network as opposed to the former, which displayed stromal framework disruption as confirmed by the reticulin stain [48].

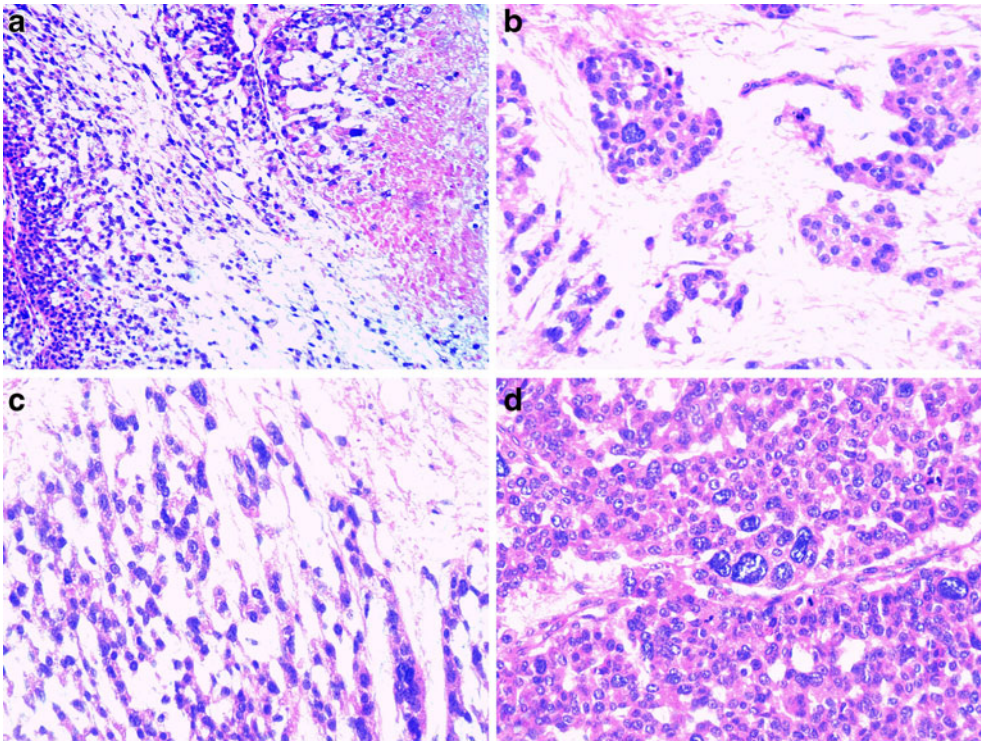

Fig. 3 Section of a myxoid adrenocortical carcinoma showing a necrotic area at the right of the field (**a**). Tumor cells are arranged in a small nested (**b**) or trabecular/cord-like (**c**) growth pattern focally displaying marked nuclear atypia (**b**–**c**). Area of conventional adrenocortical carcinoma (60–70% of total area in histologic sections); neoplastic cells are arranged in an interanastomosing trabecular pattern showing severe nuclear atypia near the center of the field (**d**)

(2) Another MAN of borderline malignancy (average mitoses 3/10 HPFs, mild to moderate nuclear pleomorphism, cells with ample predominantly eosinophilic cytoplasm, occasional clear cells and a tumor weight of 94 g) did not recur or metastasize after a follow-up period of 18 months [50]. In addition, four out of six myxoid ACAs reported in a series by Brown et al. [49] were large (≥ 6 cm), showed focal capsular invasion and a mitotic activity of ≥ 1/10 HPFs in the absence of recurrence or metastatic disease after a mean follow-up period of 12 years. It should be stressed that 9 out of 17 myxoid ACAs were relatively large (≥ 6 cm), a feature further challenging the prediction of a benign clinical course [49, 50, 54–57].

(3) Some of the Weiss score parameters were hard to assess in the myxoid areas, while others could be identified in a variable percentage according to observations made by Papotti et al. [48] in the subset of myxoid ACCs. In particular, diffuse growth pattern was never a feature, atypia was minimal or absent, and small vessel invasion was less apparent due to myxoid areas in contrast to necrosis, "dark" cell cytoplasm and mitotic figures which were the only readily apparent criteria. In keeping with this, Hsieh et al. [62] reported on a myxoid ACC showing an extensive myxoid area (80% of the tumor area) of Weiss score (3) and a non-myxoid component of Weiss score (6); the latter consisted of three growth patterns (trabecular, solid and clear cell), each exhibiting different Weiss score parameters. Moreover, Brown et al. [49] noted that mitoses, when present, were generally less frequent in myxoid areas, while extensive extracapsular involvement was a feature only of carcinomas.

Adrenocortical carcinomas with a sarcomatous or sarcoma-like component

According to WHO classification 2004, *oncocytic* ACCs, *myxoid* ACCs and ACCs *with sarcomatous areas* are regarded as rare variants of ACC [66]. Whether the latter variant should be designated *carcinosarcoma* or *sarcomatoid carcinoma*, as previously suggested by Sturm and colleagues [67] in agreement with the WHO terminology applied to biphasic tumors with pleomorphic, sarcomatous or sarcomatoid elements arising in other organs [68], is still unsettled. Nevertheless, nine cases of this unusual variant have been previously reported [67, 69–76], with only four corresponding to true carcinosarcomas [69, 72–74], consistent with the concept that carcinosarcomas are tumors composed of morphologically malignant epithelial and *specialized* mesenchymal elements, easily recognizable histologically as forms of mesenchymal malignancy resembling osteosarcoma, chondrosarcoma, rhabdomyosarcoma, angiosarcoma or liposarcoma (Fig. 4) [77]. Adrenal carcinosarcomas, like their counterparts in other organ systems, were mainly characterized by a rhabdomyosarcomatous component (three out of four) [69, 73, 74], while only one case was characterized by a mixture of osteosar-

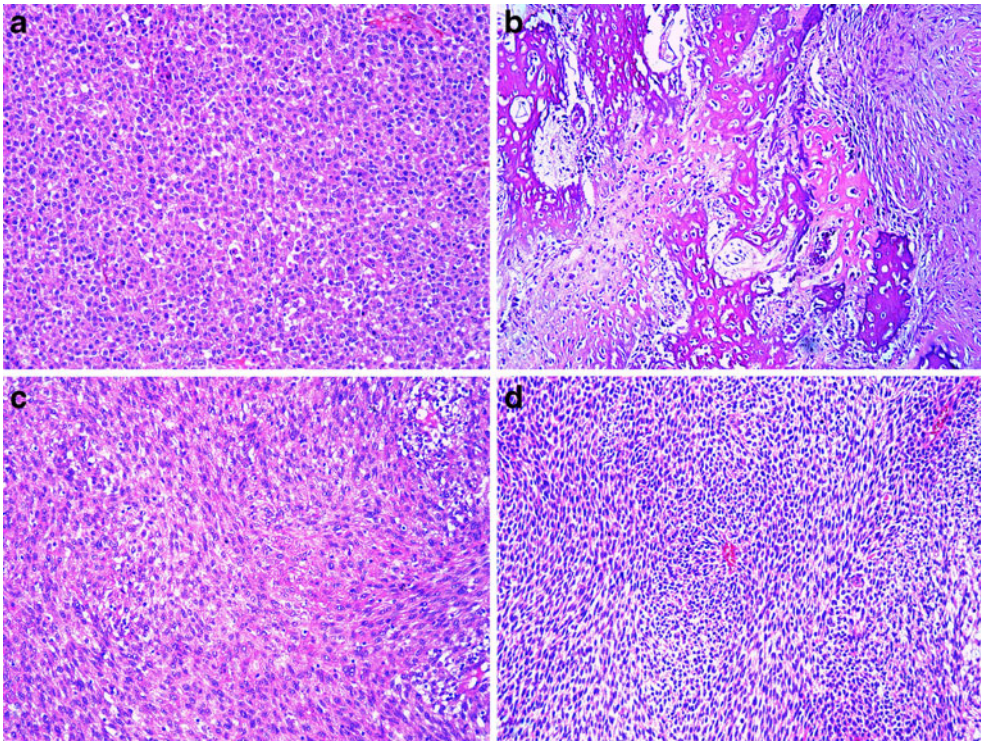

Fig. 4 Sections of an adrenocortical carcinosarcoma comprising a well-differentiated carcinomatous component (**a**) and a sarcomatous component demonstrating osteosarcomatous differentiation (**b**) along with areas of uniform spindle cells arranged in a fascicular (**c**) or herringbone (**d**) growth pattern

coma and chondrosarcoma [72]. The remaining five biphasic cases without heterologous elements did have a spindle cell component [67, 70, 71, 75, 76], with three out of five also showing variably giant cells in the sarcomatous component [67, 70, 75].

Another unique malignant biphasic neoplasm arising as a primary tumor of the adrenal gland is the *adrenocortical blastoma*. This functional (virilizing) malignant tumor has been reported in an infant, and it consisted of a mixture of immature epithelial and mesenchymal elements, along with slit-like spaces partially lined by primitive epithelial cells, focally recapitulating the morphology of the normal embryologic development of the adrenal cortex [78]. There have been no additional cases reported, and therefore, the question whether this neoplasm is indeed restricted to the pediatric age group [79] similar to pleuropulmonary blastoma (virtually restricted) but in contrast to pulmonary blastoma [77] remains unresolved.

Of interest, only two out of four carcinosarcomas were functional, presenting with clinical signs either of hyperaldosteronism or of virilization [72, 73], whereas all adrenocortical sarcomatoid carcinomas were non-functioning [67, 70, 71, 75, 76].

Although the limited number of reported cases does not allow any definite conclusion, adrenocortical carcinosarcomas and sarcomatoid carcinomas have similar clinical outcome (postoperative survival ranging from 2 days to 12 months; median 6 months) [69] and therefore have a worse prognosis than their conventional counterparts [67]. This dramatically aggressive behavior may be attributed not only to advanced stage at presentation but also in part to inherent biological properties potentially deriving by progression (dedifferentiation) from a pre-existing *better differentiated* ACC, in analogy to the undifferentiated (anaplastic) carcinoma of the thyroid gland [66, 80]. This endows cells with migratory and invasive properties, epithelial-mesenchymal transition, stemness, prevention of apoptosis and senescence, and it contributes to immunosuppression and notably confers resistance to chemotherapy and immunotherapy [81].

Although various theories have been proposed with regard to the histogenesis of carcinosarcomas, namely (1) the *composition* tumor theory (paradoxically requiring a non-malignant non-epithelial component as a reactive proliferative response induced by the epithelial component via paracrine secretion), (2) the *collision* or *biclonal* tumor theory (a collision between two synchronous, histogenetically independent, biclonal tumors), (3) the *conversion* tumor theory (neoplastic transformation within a monoclonal tumor recapitulating the naturally occurring event of conversion of epithelial to mesenchymal cells during embryogenesis) [81] and (4) the *combination* or *divergent* tumor theory (deriving from a common monoclonal stem cell precursor) [82–85], molecular genetic evidence of monoclonality supports the single pluripotential stem-cell-divergence hypothesis and the epithelial-to-mesenchymal transition as well [83–85]. With regard to ACCs *with sarcomatous areas*, evidence emerging from the immunophenotypical profile of the sarcomatous component (focal retaining of Melan-A, synaptophysin and

calretinin positivity) [69] and the presence of transitional (intermingled) zones between carcinomatous and sarcomatous components [67, 70, 73] seem to imply such a putative transition. Differences of the mitotic count in the distinct elements [7/10 HPF (epithelioid component) versus 30/10 HPF (pleomorphic/spindle cell component)] [69] and the presence only of the sarcomatous component either in large veins into the periadrenal fat [67] or in well-established metastases [71, 74] are consistent with a dedifferentiation process.

Aberrant phenotypical differentiation observed in this particular variant includes both neural and melanocytic differentiation (NSE, S100 and HMB-45 immunoreactivity) [70, 71]. Although melanocytic differentiation, suggestive of a *divergent* evolutionary pathway, has been reported in carcinosarcomas of other anatomic locations [86–89], pathologists should always keep in mind to first exclude the possibilities of a metastatic melanoma, a collision tumor consisting of an ACC and *a primary or metastatic* melanoma (not yet reported) and a primary perivascular epithelioid cell tumor [90]. Other differential diagnostic considerations include composite pheochromocytoma with a malignant peripheral nerve sheath tumor component (the latter with or without divergent differentiation into mesenchymal elements such as rhabdomyo-, osteo-, chondro-, angio- and/or fibro-sarcomatous components) [91, 92], metastatic carcinoma with sarcomatous or sarcoma-like areas and metastatic neoplasm with sarcomatoid elements other than carcinomas (melanoma or germ cell tumor), as well as primary retroperitoneal sarcomas [69]. Given that adrenal biphasic tumors, in contrast to those arising in epithelial organs, are unlikely to express cytokeratins while focal smooth muscle differentiation is a common finding, thorough sampling of the resected tumor is of critical importance in order to reveal the co-existent carcinomatous component and subsequently prove the adrenal origin on immunohistochemical grounds [67, 69].

Since ACCs *with sarcomatous areas* are highly aggressive tumors and a sarcomatous or sarcomatoid component seems to be a predictor of shorter survival in ACC, the question arises whether the Weiss scoring system should be applied to this extremely rare ACC variant. In fact, ACCs *with sarcomatous areas* regroup the majority of Weiss histological criteria [67]. In this setting, Sturm and colleagues [67] have proposed that a sarcomatous or sarcomatoid component should be well circumscribed and represent at least 10% of the tumor bulk to establish this unusual diagnosis. Nevertheless, the sarcomatous or sarcomatoid component is not included in the Weiss system, further confounding this issue when dealing with a biphasic tumor demonstrating a predominant non-carcinomatous component [67, 69]; in such cases, the criterion of diffuse architecture (greater than 1/3) is being obviously challenged.

Conclusion

In summary, we discussed the issue of multistep tumorigenesis in adrenocortical neoplasia and provided an overview of the ACN variants in order to make histopathologists aware of the clinicopathological spectrum. It is important to correctly characterize their biological potential, which is occasionally not an easy task for myxoid and oncocytic adrenocortical tumors. In this context, applying the Weiss scoring system on the latter would definitely tilt the diagnostic balance towards malignancy in a similar way as pediatric ACNs (pathologically malignant but benign-behaving tumors) [8], whereas underdiagnosis could potentially be the case with regard to the myxoid ones. In this setting, even the multistep tumorigenic processes are hard to take apart and analyze, while evidence for a distinct biological behavior is either preliminary [39] or unestablished [48] due to the small number of reported cases, limited follow-up period, insufficient data and heterogeneity. Whenever pathologists report on these variants singly or as part of larger series, it is recommended to note the diagnostic subcategory, as has been previously suggested (pure oncocytic tumor/mixed oncocytic tumor/ordinary adrenocortical tumor with focal oncocytic changes, myxoid ACCs/conventional ACCs with focal myxoid changes and carcinosarcoma/sarcomatoid carcinoma) [39, 48].

Conflict of interest statement We declare that we have no conflict of interest.

Open Access This article is distributed under the terms of the Creative Commons Attribution Noncommercial License which permits any noncommercial use, distribution, and reproduction in any medium, provided the original author(s) and source are credited.

References

1. Fassnacht M, Libe R, Kroiss M, Allolio B (2011) Adrenocortical carcinoma: a clinician's update. Nat Rev Endocrinol 7:323–335
2. McNicol AM (2011) Update on tumours of the adrenal cortex, phaeochromocytoma and extra-adrenal paraganglioma. Histopathology 58:155–168
3. Lau SK, Weiss LM (2009) The Weiss system for evaluating adrenocortical neoplasms: 25 years later. Hum Pathol 40:757–768
4. Aubert S, Wacrenier A, Leroy X et al (2002) Weiss system revisited: a clinicopathologic and immunohistochemical study of 49 adrenocortical tumors. Am J Surg Pathol 26:1612–1619
5. Blanes A, Diaz-Cano SJ (2007) Histologic criteria for adrenocortical proliferative lesions: value of mitotic figure variability. Am J Clin Pathol 127:398–408
6. Volante M, Bollito E, Sperone P et al (2009) Clinicopathological study of a series of 92 adrenocortical carcinomas: from a proposal of simplified diagnostic algorithm to prognostic stratification. Histopathology 55:535–543
7. Tissier F (2010) Classification of adrenal cortical tumors: what limits for the pathological approach? Best Pract Res Clin Endocrinol Metab 24:877–885

8. Dehner LP, Hill DA (2009) Adrenal cortical neoplasms in children: why so many carcinomas and yet so many survivors? Pediatr Dev Pathol 12:284–291
9. Bertherat J, Bertagna X (2009) Pathogenesis of adrenocortical cancer. Best Pract Res Clin Endocrinol Metab 23:261–271
10. Grumbach MM, Biller BM, Braunstein GD et al (2003) Management of the clinically inapparent adrenal mass ("incidentaloma"). Ann Intern Med 138:424–429
11. Sidhu S, Marsh DJ, Theodosopoulos G et al (2002) Comparative genomic hybridization analysis of adrenocortical tumors. J Clin Endocrinol Metab 87:3467–3474
12. Gruschwitz T, Breza J, Wunderlich H, Junker K (2010) Improvement of histopathological classification of adrenal gland tumors by genetic differentiation. World J Urol 28:329–334
13. Kjellman M, Larsson C, Bäckdahl M (2001) Genetic background of adrenocortical tumor development. World J Surg 25:948–956
14. Gicquel C, Leblond-Francillard M, Bertagna X et al (1994) Clonal analysis of human adrenocortical carcinomas and secreting adenomas. Clin Endocrinol (Oxf) 40:465–477
15. Beuschlein F, Reincke M, Karl M et al (1994) Clonal composition of human adrenocortical neoplasms. Cancer Res 54:4927–4932
16. Kjellman M, Roshani L, Teh BT et al (1999) Genotyping of adrenocortical tumors: very frequent deletions of the MEN1 locus in 11q13 and of a 1-centimorgan region in 2p16. J Clin Endocrinol Metab 84:730–735
17. Bernard MH, Sidhu S, Berger N et al (2003) A case report in favor of a multistep adrenocortical tumorigenesis. J Clin Endocrinol Metab 88:998–1001
18. Trezzi R, Poli F, Fellegara G (2009) "Dedifferentiated" adrenal cortical neoplasm. Int J Surg Pathol 17:343–344
19. Gaujoux S, Tissier F, Groussin L et al (2008) Wnt/beta-catenin and 3',5'-cyclic adenosine 5'-monophosphate/protein kinase A signaling pathways alterations and somatic beta-catenin gene mutations in the progression of adrenocortical tumors. J Clin Endocrinol Metab 93:4135–4140
20. Schmitt A, Saremaslani P, Schmid S et al (2006) IGFII and MIB1 immunohistochemistry is helpful for the differentiation of benign from malignant adrenocortical tumours. Histopathology 49:298–307
21. van't Sant HP, Bouvy ND, Kazemier G et al (2007) The prognostic value of two different histopathological scoring systems for adrenocortical carcinomas. Histopathology 51:239–245
22. de Reyniès A, Assié G, Rickman DS et al (2009) Gene expression profiling reveals a new classification of adrenocortical tumors and identifies molecular predictors of malignancy and survival. J Clin Oncol 27:1108–1115
23. Giordano TJ, Kuick R, Else T et al (2009) Molecular classification and prognostication of adrenocortical tumors by transcriptome profiling. Clin Cancer Res 15:668–676
24. Laurell C, Velázquez-Fernández D, Lindsten K et al (2009) Transcriptional profiling enables molecular classification of adrenocortical tumours. Eur J Endocrinol 161:141–152
25. Ragazzon B, Libé R, Gaujoux S et al (2010) Transcriptome analysis reveals that p53 and {beta}-catenin alterations occur in a group of aggressive adrenocortical cancers. Cancer Res 70:8276–8281
26. Ragazzon B, Assié G, Bertherat J (2011) Transcriptome analysis of adrenocortical cancers: from molecular classification to the identification of new treatments. Endocr Relat Cancer 18:R15–R27
27. Bussey KJ, Demeure MJ (2009) Genomic and expression profiling of adrenocortical carcinoma: application to diagnosis, prognosis and treatment. Future Oncol 5:641–655
28. Bussey KJ, Demeure MJ (2011) Toward a pathway-centered approach for the treatment of adrenocortical carcinoma. Curr Opin Oncol 23:34–44
29. Martinerie C, Gicquel C, Louvel A et al (2001) Altered expression of novH is associated with human adrenocortical tumorigenesis. J Clin Endocrinol Metab 86:3929–3940
30. Berthon A, Sahut-Barnola I, Lambert-Langlais S et al (2010) Constitutive beta-catenin activation induces adrenal hyperplasia and promotes adrenal cancer development. Hum Mol Genet 19:1561–1576
31. Tissier F, Cavard C, Groussin L et al (2005) Mutations of beta-catenin in adrenocortical tumors: activation of the Wnt signaling pathway is a frequent event in both benign and malignant adrenocortical tumors. Cancer Res 65:7622–7627
32. Tadjine M, Lampron A, Ouadi L, Bourdeau I (2008) Frequent mutations of beta-catenin gene in sporadic secreting adrenocortical adenomas. Clin Endocrinol (Oxf) 68:264–270
33. Bonnet S, Gaujoux S, Launay P et al (2011) Wnt/{beta}-catenin pathway activation in adrenocortical adenomas is frequently due to somatic CTNNB1-activating mutations, which are associated with larger and nonsecreting tumors: a study in cortisol-secreting and -nonsecreting tumors. J Clin Endocrinol Metab 96:E419–E426
34. Tadjine M, Lampron A, Ouadi L et al (2008) Detection of somatic beta-catenin mutations in primary pigmented nodular adrenocortical disease (PPNAD). Clin Endocrinol (Oxf) 69:367–373
35. Gaujoux S, Grabar S, Fassnacht M et al (2011) β-catenin activation is associated with specific clinical and pathologic characteristics and a poor outcome in adrenocortical carcinoma. Clin Cancer Res 17:328–336
36. Durand J, Lampron A, Mazzuco TL, Chapman A, Bourdeau I (2011) Characterization of differential gene expression in adrenocortical tumors harboring {beta}-catenin (CTNNB1) mutations. J Clin Endocrinol Metab 96:E1206–E1211
37. Chapman A, Durand J, Ouadi L, Bourdeau I (2011) Identification of genetic alterations of AXIN2 gene in adrenocortical tumors. J Clin Endocrinol Metab (Epub ahead of print)
38. Kakimoto S, Yushita Y, Sanefuji T et al (1986) Non-hormonal adrenocortical adenoma with oncocytoma-like appearances. Hinyokika Kiyo 32:757–763
39. Wong DD, Spagnolo DV, Bisceglia M et al (2011) Oncocytic adrenocortical neoplasms—a clinicopathologic study of 13 new cases emphasizing the importance of their recognition. Hum Pathol 42:489–499
40. Saad R, Marsault S, Coloby P (2011) Adrenocortical oncocytic cells tumor: case report and review of literature. Prog Urol 21:288–290
41. Mwandila M, Waller H, Stott V, Mercer P (2010) A case of a testosterone-secreting oncocytic adrenocortical carcinoma. N Z Med J 123:80–82
42. Rosenkrantz AB, Do RK, Hajdu CH (2010) Imaging appearance of bulk fat within an oncocytic adrenocortical neoplasm, a rare and potentially malignant tumour. Br J Radiol 83:e204–e207
43. Cham E, Watkin W, Goldschmidt R, Liu L (2010) Fine needle aspiration cytology of adrenocortical oncocytic neoplasm: a case report. Acta Cytol 54:627–634
44. Ohtake H, Kawamura H, Matsuzaki M et al (2010) Oncocytic adrenocortical carcinoma. Ann Diagn Pathol 14:204–208
45. Bisceglia M, Ben-Dor D, Pasquinelli G (2005) Oncocytic adrenocortical tumors. Pathol Case Rev 10:228–242
46. Bisceglia M, Ludovico O, Di Mattia A et al (2004) Adrenocortical oncocytic tumors: report of 10 cases and review of the literature. Int J Surg Pathol 12:231–243
47. Willems SM, Wiweger M, van Roggen JF, Hogendoorn PC (2010) Running GAGs: myxoid matrix in tumor pathology revisited: what's in it for the pathologist? Virchows Arch 456:181–192
48. Papotti M, Volante M, Duregon E et al (2010) Adrenocortical tumors with myxoid features: a distinct morphologic and phenotypical variant exhibiting malignant behavior. Am J Surg Pathol 34:973–983
49. Brown FM, Gaffey TA, Wold LE, Lloyd RV (2000) Myxoid neoplasms of the adrenal cortex: a rare histologic variant. Am J Surg Pathol 24:396–401
50. Raparia K, Ayala AG, Sienko A, Zhai QJ, Ro JY (2008) Myxoid adrenal cortical neoplasms. Ann Diagn Pathol 12:344–348

51. Dundr P, Novák K (2003) Pseudoglandular myxoid adenoma of the adrenal gland. Pathol Res Pract 199:493–496
52. Honda K, Kashima K, Daa T et al (2001) Myxoid adrenal cortical adenoma. Pathol Int 51:887–891
53. Jang KY, Chung MJ, Moon WS et al (2009) Adrenocortical adenoma with unusual myxoid histological pattern: a case report. Pathology 41:188–191
54. Ishida M, Yoshida K, Miyamoto K et al (2008) Cytological features of myxoid adrenocortical adenoma with a pseudoglandular component: a case report with differential diagnostic considerations. Diagn Cytopathol 36:576–580
55. Fine SW, Pindzola JA, Uhlman EJ, Epstein JI (2005) Pathologic quiz case: a 64-year-old man with an adrenal mass. Myxoid adrenal cortical neoplasm. Arch Pathol Lab Med 129:541–542
56. De Padua M, Rajagopal V (2008) Myxoid adrenal adenoma with focal pseudoglandular pattern. Indian J Med Sci 62:199–203
57. Zhu Y, Wu YX, Zhang CY et al (2008) Myxoid adrenocortical adenoma: a case report. Chin Med J (Engl) 121:1598–1600
58. Lu HS, Gan MF, Chen HS, Huang SQ (2008) Adrenal myelolipoma within myxoid cortical adenoma associated with Conn's syndrome. J Zhejiang Univ Sci B 9:500–505
59. Bollito ER, Papotti M, Porpiglia F et al (2004) Myxoid adrenocortical adenoma with a pseudoglandular pattern. Virchows Arch 445:414–418
60. Tang CK, Harriman BB, Toker C (1979) Myxoid adrenal cortical carcinoma: a light and electron microscopic study. Arch Pathol Lab Med 103:635–638
61. Forsthoefel KF (1994) Myxoid adrenal cortical carcinoma. A case report with differential diagnostic considerations. Arch Pathol Lab Med 118:1151–1153
62. Hsieh MS, Chen JH, Lin LW (2010) Myxoid adrenal cortical carcinoma presenting as primary hyperaldosteronism: case report and review of the literature. Int J Surg Pathol (Epub ahead of print)
63. Karim RZ, Wills EJ, McCarthy SW, Scolyer RA (2006) Myxoid variant of adrenocortical carcinoma: report of a unique case. Pathol Int 56:89–94
64. Suresh B, Kishore TA, Albert AS, Joy A (2005) Myxoid adrenal cortical carcinoma—a rare variant of adrenocortical carcinoma. Indian J Med Sci 59:505–507
65. Izumi M, Serizawa H, Iwaya K et al (2003) A case of myxoid adrenocortical carcinoma with extensive lipomatous metaplasia. Arch Pathol Lab Med 127:227–230
66. DeLellis RA, Lloyd RV, Heitz PU, Eng C (2004) World Health Organization classification of tumours. Pathology and genetics of tumours of endocrine organs. IARC, Lyon
67. Sturm N, Moulai N, Laverrière MH et al (2008) Primary adrenocortical sarcomatoid carcinoma: case report and review of literature. Virchows Arch 452:215–219
68. Travis WD, Brambilla E, Muller-Hermelink HK, Harris CC (2004) World Health Organization classification of tumours. Pathology and genetics of tumours of the lung, pleura, thymus and heart. IARC, Lyon
69. Sasaki K, Desimone M, Rao HR, Huang GJ, Seethala RR (2010) Adrenocortical carcinosarcoma: a case report and review of the literature. Diagn Pathol 5:51
70. Coli A, Di Giorgio A, Castri F (2010) Sarcomatoid carcinoma of the adrenal gland: a case report and review of literature. Pathol Res Pract 206:59–65
71. Lee MS, Park IA, Chi JG et al (1997) Adrenal carcinosarcoma—a case report. J Korean Med Sci 12:374–377
72. Barksdale SK, Marincola FM, Jaffe G (1993) Carcinosarcoma of the adrenal cortex presenting with mineralocorticoid excess. Am J Surg Pathol 17:941–945
73. Fischler DF, Nunez C, Levin HS et al (1992) Adrenal carcinosarcoma presenting in a woman with clinical signs of virilization. A case report with immunohistochemical and ultrastructural findings. Am J Surg Pathol 16:626–631
74. Decorato JW, Gruber H, Petti M, Levowitz BS (1990) Adrenal carcinosarcoma. J Surg Oncol 45:134–136
75. Collina G, Maldarizzi F, Betts CM, Eusebi V (1989) Primary sarcomatoid carcinoma of the adrenal gland. First case report. Virchows Arch A Pathol Anat Histopathol 415:161–167
76. Okazumi S, Asano T, Ryu M et al (1987) Surgical resection of adrenal carcinoma extending into the vena cava, right atrium and ventricle: case report and review of the literature. Nippon Geka Gakkai Zasshi 88:231–238
77. Weissferdt A, Moran CA (2011) Malignant biphasic tumors of the lungs. Adv Anat Pathol 18:179–189
78. Molberg K, Vuitch F, Stewart D, Albores-Saavedra J (1992) Adrenocortical blastoma. Hum Pathol 23:1187–1190
79. Lack EE (2007) Tumors of the adrenal glands and extraadrenal paraganglia—volume 8 (Afip Atlas of Tumor Pathology Series 4). American Registry of Pathology, Washington
80. Liu J, Brown RE (2010) Immunohistochemical detection of epithelialmesenchymal transition associated with stemness phenotype in anaplastic thyroid carcinoma. Int J Clin Exp Pathol 3:755–762
81. Thiery JP, Acloque H, Huang RY, Nieto MA (2009) Epithelial-mesenchymal transitions in development and disease. Cell 139:871–890
82. Guarino M, Tricomi P, Giordano F, Cristofori E (1996) Sarcomatoid carcinomas: pathological and histopathogenetic considerations. Pathology 28:298–305
83. Jin Z, Ogata S, Tamura G et al (2003) Carcinosarcomas (malignant mullerian mixed tumors) of the uterus and ovary: a genetic study with special reference to histogenesis. Int J Gynecol Pathol 22:368–373
84. Dacic S, Finkelstein SD, Sasatomi E, Swalsky PA, Yousem SA (2002) Molecular pathogenesis of pulmonary carcinosarcoma as determined by microdissection-based allelotyping. Am J Surg Pathol 26:510–516
85. Thompson L, Chang B, Barsky SH (1996) Monoclonal origins of malignant mixed tumors (carcinosarcomas). Evidence for a divergent histogenesis. Am J Surg Pathol 20:277–285
86. Roma AA, Malpica A, Deavers MT (2011) Malignant melanoma arising in an ovarian carcinosarcoma: case report and review of the literature. Int J Gynecol Pathol 30:158–162
87. Liu J, Wu H (2011) Carcinosarcoma of female urethra with melanocytic differentiation. Int J Clin Exp Pathol 4:206–209
88. Amant F, Moerman P, Davel GH et al (2001) Uterine carcinosarcoma with melanocytic differentiation. Int J Gynecol Pathol 20:186–190
89. Kajo K, Zubor P, Spacek J, Ryska A (2007) Carcinosarcoma of the uterus with melanocytic differentiation. Pathol Res Pract 203:753–758
90. Zarineh A, Silverman JF (2011) Adrenal perivascular epithelioid cell tumor: a case report with discussion of differential diagnoses. Arch Pathol Lab Med 135:499–502
91. Sakaguchi N, Sano K, Ito M et al (1996) A case of von Recklinghausen's disease with bilateral pheochromocytoma-malignant peripheral nerve sheath tumors of the adrenal and gastrointestinal autonomic nerve tumors. Am J Surg Pathol 20:889–897
92. Gupta R, Sharma A, Arora R, Vijayaraghavan M (2009) Composite phaeochromocytoma with malignant peripheral nerve sheath tumour and rhabdomyosarcomatous differentiation in a patient without von Recklinghausen disease. J Clin Pathol 62:659–661

Virchows Arch (2012) 460:19–46
DOI 10.1007/s00428-011-1177-8

ORIGINAL ARTICLE

Management of precancerous conditions and lesions in the stomach (MAPS): guideline from the European Society of Gastrointestinal Endoscopy (ESGE), European Helicobacter Study Group (EHSG), European Society of Pathology (ESP), and the Sociedade Portuguesa de Endoscopia Digestiva (SPED)

M. Dinis-Ribeiro · M. Areia · A. C. de Vries · R. Marcos-Pinto · M. Monteiro-Soares · A. O'Connor · C. Pereira · P. Pimentel-Nunes · R. Correia · A. Ensari · J. M. Dumonceau · J. C. Machado · G. Macedo · P. Malfertheiner · T. Matysiak-Budnik · F. Megraud · K. Miki · C. O'Morain · R. M. Peek · T. Ponchon · A. Ristimaki · B. Rembacken · F. Carneiro · E. J. Kuipers · on behalf of MAPS Participants

Received: 5 August 2011 / Revised: 13 October 2011 / Accepted: 19 October 2011 / Published online: 22 December 2011
© Springer-Verlag 2011

Abstract Atrophic gastritis, intestinal metaplasia, and epithelial dysplasia of the stomach are common and are associated with an increased risk for gastric cancer. In the absence of guidelines, there is wide disparity in the management of patients with these premalignant conditions. The European Society of Gastrointestinal Endoscopy, the European Helicobacter Study Group, the European Society of Pathology, and the Sociedade Portuguesa de Endoscopia Digestiva have therefore combined efforts to develop evidence-based guidelines on the management of patients with precancerous conditions and lesions of the stomach. A multidisciplinary group of 63 experts from 24 countries developed these recommendations by means of repeat online voting and a meeting in June 2011 in Porto, Portugal. The recommendations emphasize the increased

MAPS Participants include: Cathomas G (Switzerland), Fedorov ED (Russia), Figueiredo P (Portugal), Goldis A (Romania), Leja M (Latvia), Moehler M (Germany), Plesea E (Romania), Bergman J (the Netherlands), Hamoudi W (Jordan), Almeida R, Annibale B, Lobo LA, Balaban YH, Boeriu A, Burette A, Mallet AC, David L, Delchier J-C, Dobru ED, Fernandes C, Kahaleh M, Kashin S, Lomba-Viana R, Lunet N, Marakhouski K, Moreira-Dias L, Ferreira CF, Pais TP, Rollán A, Sadio A, Santos C, Chu K-M, D'Ambra G, Ellul P, van Grieken N, Lamarque D, Najeeb AA

M. Dinis-Ribeiro (✉) · P. Pimentel-Nunes
Department of Gastroenterology,
Portuguese Oncology Institute of Porto,
Rua Dr. Bernardino de Almeida,
4200-072 Porto, Portugal
e-mail: mdinisribeiro@gmail.com

M. Areia
Department of Gastroenterology,
Portuguese Oncology Institute of Coimbra,
Coimbra, Portugal

A. C. de Vries · E. J. Kuipers
Department of Gastroenterology and Hepatology, Erasmus MC,
Rotterdam, the Netherlands

R. Marcos-Pinto
Department of Gastroenterology, Centro Hospitalar do Porto,
Porto, Portugal

M. Dinis-Ribeiro · M. Areia · M. Monteiro-Soares · R. Correia
Centre for Research in Health Technologies and Information
Systems (CINTESIS), Medical Faculty, University of Porto,
Porto, Portugal

cancer risk in patients with gastric atrophy and metaplasia and the need for adequate staging in the case of high-grade dysplasia, and they focus on treatment and surveillance indications and methods.

Keywords Atrophic gastritis · Intestinal metaplasia · Dysplasia · Precancerous conditions · Precancerous lesions · Gastric cancer · Endoscopy · Pepsinogen · Diagnosis · Management · Follow-up · Therapy · Diagnosis · *Helicobacter pylori* · Guideline

Introduction

Gastric cancer remains a major problem worldwide. The intestinal type of gastric cancer develops through a cascade of well-defined and recognizable precursors (inflammation–metaplasia–dysplasia–carcinoma sequence) [1]. It has been argued that the identification and surveillance of patients with such precursor conditions and lesions may lead to early diagnosis of gastric cancer. Indeed, this may be an important measure for prevention of death due to gastric cancer both in Western and Asian countries. However, even though such lesions are commonly found in everyday practice, there are no international recommendations to guide clinicians in their care of individuals with these changes. This leads to wide heterogeneity of practice and to failure to diagnose patients with curable forms of cancer. Standardization of management is likely to benefit patients and may also be cost-effective by focusing resources on patients with the greatest risk.

This consensus project aimed to summarize current evidence on the management of patients with precancerous conditions and lesions and to propose guidelines for the diagnosis and management of individuals with chronic gastritis, atrophy, intestinal metaplasia, or dysplasia. This guideline does not address methodologies for screening these lesions in general populations or the assessment and

R. Marcos-Pinto
Institute of Biomedical Sciences, University of Porto (ICBAS/UP),
Porto, Portugal

A. O'Connor · C. O'Morain
Gastroenterology Department, AMNCH/TCD,
Adelaide and Meath Hospital/Trinity College,
Dublin, Ireland

C. Pereira
Molecular Oncology Research Group,
Portuguese Oncology Institute of Porto,
Porto, Portugal

A. Ensari
Department of Pathology, Ankara University Medical School,
Ankara, Turkey

J. M. Dumonceau
Département de Gastroénterologie et d'Hépatopancréatologie,
H.U.G. Hôpital Cantonal,
Geneva, Switzerland

J. C. Machado · F. Carneiro
Institute of Molecular Pathology and Immunology
of the University of Porto (IPATIMUP),
Porto, Portugal

G. Macedo
Department of Gastroenterology, Centro Hospitalar S. João/
Medical Faculty,
Porto, Portugal

P. Malfertheiner
Klinik der Gasroenterologie, Hepatologie und Infektologie,
Otto von Guericke Universität Magdeburg,
Magdeburg, Germany

T. Matysiak-Budnik
Service d'Hépato-Gastroentérologie, Hôtel Dieu, CHU de Nantes,
Nantes, France

F. Megraud
Laboratoire de Bacteriologie, Inserm U853, Université Bordeaux,
Bordeaux, France

K. Miki
Japan Research Foundation of Prediction,
Diagnosis and Therapy for Gastric Cancer (JRF PDT GC),
Tokyo, Japan

R. M. Peek
Division of Gastroenterology,
Vanderbilt University School of Medicine,
Nashville, TN, USA

T. Ponchon
Department of Digestive Diseases, Hôpital Edouard Herriot,
Lyon, France

A. Ristimaki
Department of Pathology, HUSLAB and Haartman Institute,
Helsinki University Central Hospital,
University of Helsinki,
Helsinki, Finland

A. Ristimaki
Genome-Scale Biology, Research Program Unit,
University of Helsinki,
Helsinki, Finland

B. Rembacken
Centre for Digestive Diseases, The General Infirmary at Leeds,
Leeds, UK

F. Carneiro
Department of Pathology,
Medical Faculty/Centro Hospitalar S. João,
Porto, Portugal

management of patients with other precancerous conditions, such as pernicious anemia, Ménétrier disease, or gastric stump, or treatment for gastric adenocarcinoma.

Scope and key questions

We addressed the management, that is, the diagnostic assessment, treatment, and follow-up, of individuals with atrophic gastritis, or intestinal metaplasia or dysplasia of the gastric mucosa. Specific issues were included: What is the optimal diagnostic approach for patients with gastric precancerous conditions/lesions? Which patients are at higher risk and would benefit from surveillance to detect early-stage cancer? Should they receive pharmacological interventions to reduce the risk of developing cancer? If so, are such measures cost-effective?

Methods

These recommendations were developed according to the process described by the Appraisal of Guidelines for Research and Evaluation Collaboration [2].

Selection of working panel

In May 2010, three authors (M.D.R., E.J.K., and F.C.), on behalf of the European Society of Gastrointestinal Endoscopy (ESGE), the Sociedade Portuguesa de Endoscopia Digestiva, the European Helicobacter Study Group, and the European Society of Pathology, assembled a panel of European gastroenterologists and pathologists, including clinical experts and young researchers trained in literature search and evidence-based medicine (see "Appendix").

This panel met in October 2010 in Barcelona and agreed on the methodology to be applied and on a set of key questions and preliminary statements to guide a literature search. The panel further worked in subgroups (Table 1) to perform a systematic search for evidence, to review statements on the basis of quality-rated evidence, and to report graded statements and recommendations accordingly. Subsequently, representatives from European national societies of digestive endoscopy and pathology and individual members (see "Appendix") considered the applicability of the evidence and draft statements. This was done by means of two online sessions for voting and comments, followed by a second meeting held in June 2011 in Porto, Portugal.

A total of 63 participants contributed (all online and 45 in Porto), including participants from Belarus, Belgium, Brazil, China, Chile, Finland, France, Germany, Iraq, Ireland, Italy, Jordan, Latvia, Malta, Portugal, Romania, Russia, Slovakia, Sudan, Switzerland, the Netherlands, Turkey, UK, and USA. In addition, nine national societies were represented (Germany, Jordan, Latvia, Portugal, Romania, Russia, Slovakia, Switzerland, and the Netherlands).

Table 1 Panel subgroups according to key questions

Key questions	Working group
Which are the precancerous lesions in the stomach? Which outcomes to prevent/avoid?	Fátima Carneiro, Ernst Kuipers, Mário Dinis-Ribeiro
Is there evidence to use endoscopic methods to improve diagnosis?	Miguel Areia, Pedro Pimentel-Nunes, AnneMarie de Vries, Bjorn Rembacken, Ernst Kuipers, Mário Dinis-Ribeiro
Which care should be taken on biopsies (number and sites) for a correct diagnosis and staging?	Ricardo Marcos-Pinto, Bjorn Rembacken, Kazumasa Miki, José Carlos Machado, Fátima Carneiro, Ernst Kuipers, Mário Dinis-Ribeiro
Should other sources of data be added for staging?	Ricardo Marcos-Pinto, Carina Pereira, José Carlos Machado, Miguel Areia, AnneMarie de Vries, Fátima Carneiro, Ernst Kuipers, Mário Dinis-Ribeiro, Thierry Ponchon, Bjorn Rembacken, Kazumasa Miki
Is there evidence to use non-invasive methods to improve diagnosis?	Miguel Areia, Ernst Kuipers, Mário Dinis-Ribeiro, Kazumasa Miki
Should these patients be followed up?	AnneMarie de Vries, Ernst Kuipers, Mário Dinis-Ribeiro, Ricardo Marcos-Pinto, Carina Pereira
Does the type, the severity, and the extension of the lesion influence the prognosis of these patients?	AnneMarie de Vries, Ernst Kuipers, Mário Dinis-Ribeiro, Thierry Ponchon, Bjorn Rembacken, Kazumasa Miki, José Carlos Machado, Ricardo Marcos-Pinto, Carina Pereira, Fátima Carneiro
Is there a role for *Helicobacter pylori* eradication?	Anthony O'Connor, Pedro Pimentel-Nunes, Ernst Kuipers, Mário Dinis-Ribeiro, Peter Malfertheiner, Tamara Matysiak-Budnik, Francis Megraud, Carina Pereira, Ari Ristimaki
Is there a role for other therapies?	Anthony O'Connor, Carina Pereira, Ernst Kuipers, Mário Dinis-Ribeiro, Peter Malfertheiner, Tamara Matysiak-Budnik, Francis Megraud, Pedro Pimentel-Nunes
May it/these strategies be cost-effective?	Miguel Areia, Richard Peek, Jean-Marc Dumonceau, Ernst Kuipers, Mário Dinis-Ribeiro

Literature search

A literature search using PubMed up to November 2010 was carried out. A small working group from the panel dealt with each question and each string/query and identified key references which were supplied to the entire panel and participants.

Grading of evidence

Each working group rated the quality level of the available evidence and the strength of recommendations by using both the Grading of Recommendations, Assessment, Development, and Evaluation process [3, 4] and the system of the Scottish Intercollegiate Guidelines Network [5]. Researchers prioritized data from randomized clinical trials (RCTs) when available and performed meta-analyses when applicable. Each paper was individually assessed by two investigators using a methodological tool that was identical for all topics reviewed in the guidelines. Discrepant assessment results were discussed by the full working group. Tables with the assessment of individual manuscripts are available upon request.

For each question, the working group summarized the quantity, quality, and consistency of evidence, and they discussed the external validity of studies and whether the study conclusions were applicable to the target population for the guidelines. The group recorded the overall level of evidence addressing the key question and made a graded recommendation pertaining to the key question (for evidence levels and recommendation grades, see Table 2). It is important to emphasize that the grading does not relate to the importance of the recommendation but to the strength of the supporting evidence.

Other factors that influenced the grading of a recommendation were taken into account by the participants, including (a) any evidence of potential harms associated with implementation of a recommendation, (b) clinical impact on the target population and impact on resource consumption, (c) whether and to what extent any patient populations might be particularly advantaged or disadvantaged by the recommendations, and (d) opportunities and obstacles regarding implementation in daily clinical practice.

Consensus process and applicability

A hybrid approach was used to obtain the final version of statements, starting with an online consultation followed by a final meeting in Porto, in June 2011. Online questionnaires

Table 2 Scottish Intercollegiate Guidelines Network system: definitions of levels of evidence and recommendation grades

Levels	
1++	High-quality meta-analyses, systematic reviews of RCTs, or RCTs with a very low risk of bias
1+	Well conducted meta-analyses, systematic reviews of RCTs, or RCTs with a low risk of bias
1–	Meta-analyses, systematic reviews or RCTs, or RCTs with a high risk of bias
2++	High-quality systematic reviews of case–control or cohort studies
	OR High-quality case–control or cohort studies with a very low risk of confounding, bias, or chance and a high probability that the relationship is causal
2+	Well conducted case–control or cohort studies with a low risk of confounding, bias, or chance and a moderate probability that the relationship is causal
2–	Case–control or cohort studies with a high risk of confounding, bias, or chance and a significant risk that the relationship is not causal
3	Non-analytic studies, e.g., case reports, case series
4	Expert opinion
Grades	
A	At least one meta-analysis, systematic review, or RCT rated as 1++, and directly applicable to the target population
	OR a systematic review of RCTs
	OR A body of evidence consisting principally of studies rated as 1+, directly applicable to the target population, and demonstrating overall consistency of results
B	A body of evidence including studies rated as 2++, directly applicable to the target population, and demonstrating overall consistency of results
	OR Extrapolated evidence from studies rated as 1++ or 1+
C	A body of evidence including studies rated as 2+, directly applicable to the target population and demonstrating overall consistency of results
	OR Extrapolated evidence from studies rated as 2++
D	Evidence level 3 or 4
	OR Extrapolated evidence from studies rated as 2+

RCT randomized controlled trial

(MedQuest) were devised to allow participants to vote anonymously on statements. During the first round, the panel members were asked to vote on their agreement with evidence-based statements, and in a second round, all participants, that is, panelists, society representatives, and individual members, were asked to vote on their agreement with statements but also on the level of applicability. At this stage, a collection of summarized references were available to all participants. The final discussion took place in June 2011 in Porto, during a 1-day consensus conference, where data were presented and discussed; this was followed by re-voting and attribution of grades to the final statements.

Voting was on a six-point scale: a, agree strongly; b, agree moderately; c, just agree; d, just disagree; e, disagree moderately; and f, disagree strongly. Prior to the voting process, it was defined that a statement would be accepted if more than 75% of the participants voted a, b, or c. In addition, in the second round, all participants were also specifically queried regarding the level of applicability to their own practice and in their country, when this was relevant.

Reporting

The present manuscript summarizes the results of this entire process and was reviewed by all participants. Moreover, all ESGE individual members and national societies were asked to send their contributions.

Agreement results are presented as proportions of voters agreeing with the statements. The online voting results are presented for the statements that remained unchanged during the Porto meeting. For those for which a new voting process was conducted during the meeting in Porto, the final results for that meeting are presented. We also present a flow chart of the final results.

Results

Summary of recommendations

Conventional white light endoscopy cannot accurately differentiate between and diagnose preneoplastic gastric conditions/lesions (evidence level 2++, recommendation grade B). Thus, magnification chromoendoscopy or narrow-band imaging (NBI) endoscopy with or without magnification may be offered in these cases as it improves diagnosis of such lesions (evidence level 2++, recommendation grade B). In addition, at least four biopsies of the proximal and distal stomach, on the lesser and greater curvature, are needed for adequate assessment of premalignant gastric conditions (evidence level 2+, recommendation grade C). Systems for histopathological staging [e.g., operative link for gastritis assessment (OLGA) and operative link for gastric intestinal metaplasia (OLGIM) assessment] may be useful for identifying subgroups of patients with different risks of progression to gastric cancer (evidence level 2++, recommendation grade C), namely those with extensive lesions (i.e., atrophy and/or intestinal metaplasia in both antrum and corpus). Although only low potential applicability was reported by participants for this indicator, low serum pepsinogen (PG) levels can also predict this phenotype (evidence level 2++, recommendation grade C) and, in such patients, *Helicobacter pylori* serology may also be useful for further detection of high-risk individuals (evidence level 2++, recommendation grade C). Beyond a family history of gastric cancer (evidence level 2++, recommendation grade B), neither age, gender, *H. pylori* virulence factors nor host genetic variations change these clinical recommendations (evidence level 4, recommendation grade D). Patients with extensive atrophy and/or extensive intestinal metaplasia should be offered endoscopic surveillance (evidence level 2++, recommendation grade B) every 3 years (evidence level 4, recommendation grade D). Further studies are needed, however, to accurately estimate the cost–effectiveness of such an approach (evidence level 1, recommendation grade B). Patients with mild-to-moderate atrophy/intestinal metaplasia only in antrum do not need follow-up (evidence level 4, recommendation grade D). If *H. pylori* infection is present, eradication should be offered to prevent high-grade dysplasia or carcinoma (evidence level 1+, recommendation grade B). Currently, the use of cyclooxygenase-2 (COX-2) inhibitors or the use of dietary supplementation with antioxidants (ascorbic acid and beta-carotene) is not endorsed as approaches to decrease the risk of progression of gastric precancerous lesions (evidence level 1+, recommendation grade B). Patients with dysplasia without a visible endoscopic lesion should be closely followed up, either immediately and 6 to 12 months thereafter, or within 12 months (evidence level 2+, recommendation grade C), respectively, for those with high-grade or low-grade dysplasia. Those with dysplasia or cancer within an endoscopically visible lesion should undergo staging and resection. A flow chart for the proposed management of patients with atrophic gastritis, gastric intestinal metaplasia, or gastric epithelial dysplasia is shown in Fig. 1.

Definitions and outcomes to prevent

Gastric carcinogenesis

1. Patients with chronic atrophic gastritis or intestinal metaplasia should be considered to be at higher risk for gastric adenocarcinoma [agree 96% (vote: a, 68%; b, 18%; c, 10%; d, 2%; e, 2%)].

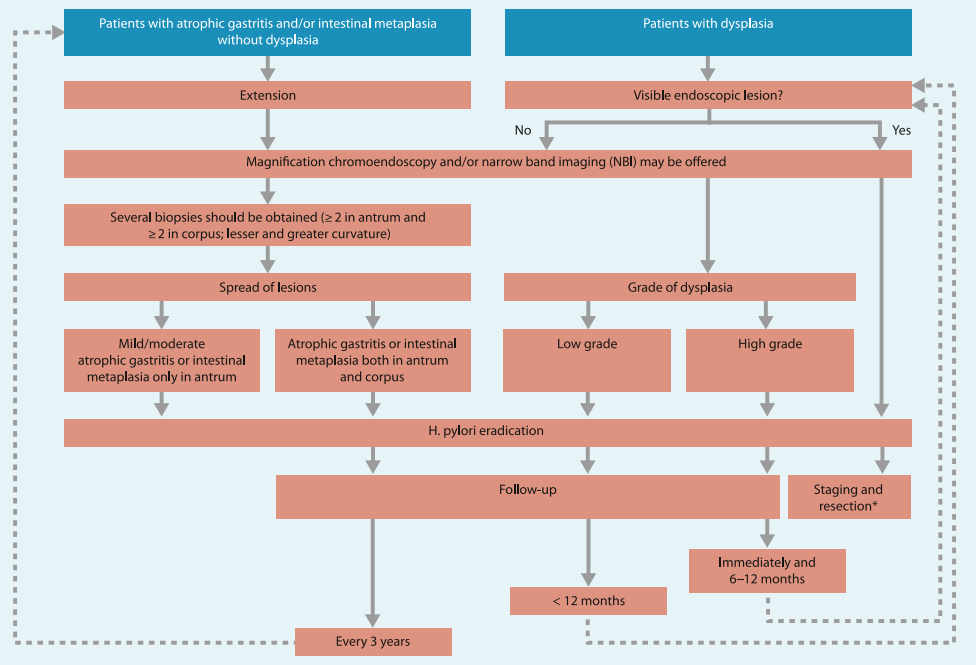

Fig. 1 Summary of proposed management for patients with atrophic gastritis, gastric intestinal metaplasia and gastric epithelial dysplasia. *The further management is not covered by this guideline

2. High-grade dysplasia and invasive carcinoma should be regarded as the outcomes to be prevented when patients with chronic atrophic gastritis or intestinal metaplasia are managed [agree 96% (vote: a, 72%; b, 14%; c, 10%; d, 4%)].
3. Patients with endoscopically visible high-grade dysplasia or carcinoma should undergo staging and adequate management [agree 100% (vote: a, 94%; b, 2%; c, 4%)].

In most instances, the development of so-called intestinal gastric adenocarcinoma represents the culmination of an inflammation–metaplasia–dysplasia–carcinoma sequence, known as the Correa cascade of multistep gastric carcinogenesis, where a progression may occur from normal mucosa through chronic non-atrophic gastritis (Fig. 2a, b), atrophic gastritis (Fig. 2c, d), and intestinal metaplasia (Fig. 2e, f), to dysplasia (Fig. 2g) and carcinoma [6–8]. This model has been consistently confirmed in different studies [9, 10].

Precancerous conditions

Mucosal gastric atrophy and intestinal metaplasia confer a high risk for the development of gastric cancer as they constitute the background in which dysplasia and intestinal-type gastric adenocarcinoma develop [7, 11–13]. Thus, chronic atrophic gastritis and intestinal metaplasia are considered to be *precancerous conditions*.

Chronic atrophic gastritis should be diagnosed and graded on the basis of the presence of chronic inflammatory cells, including lymphocytes and plasma cells that expand the lamina propria, and the disappearance of the normal glands [14–16]. In the gastric body/fundus, this is associated with a loss of specialized cells and thus a reduction of gastric secretory functions. The severity of gland loss (atrophy) should be graded although inter- and intra-observer agreements are both poor.

Individuals may develop different phenotypes of chronic gastritis due to different genetic profiles and environmental exposure:

- Cases of inflammatory changes *limited to the antrum* and without gland atrophy and/or intestinal metaplasia are defined as *diffuse antral gastritis*.
- Cases of gland atrophy and/or intestinal metaplasia distributed *multifocally* including the lesser curvature of the corpus and fundus are defined as *multifocal atrophic gastritis*. This phenotype may be described as "extensive," whereas the term "marked" is used to define a severity grade at a particular site.

The overall background changes in the stomach should therefore be described in terms of the severity and distribution of any premalignant conditions/lesions. Several classification schemes have been developed for chronic gastritis and preneoplastic changes.

At present, the updated Sydney System is generally used both in clinical practice and in research, combining topographic, morphological, and etiological information in reporting systems designed to include both grading and staging of gastritis. In addition, the systems known as

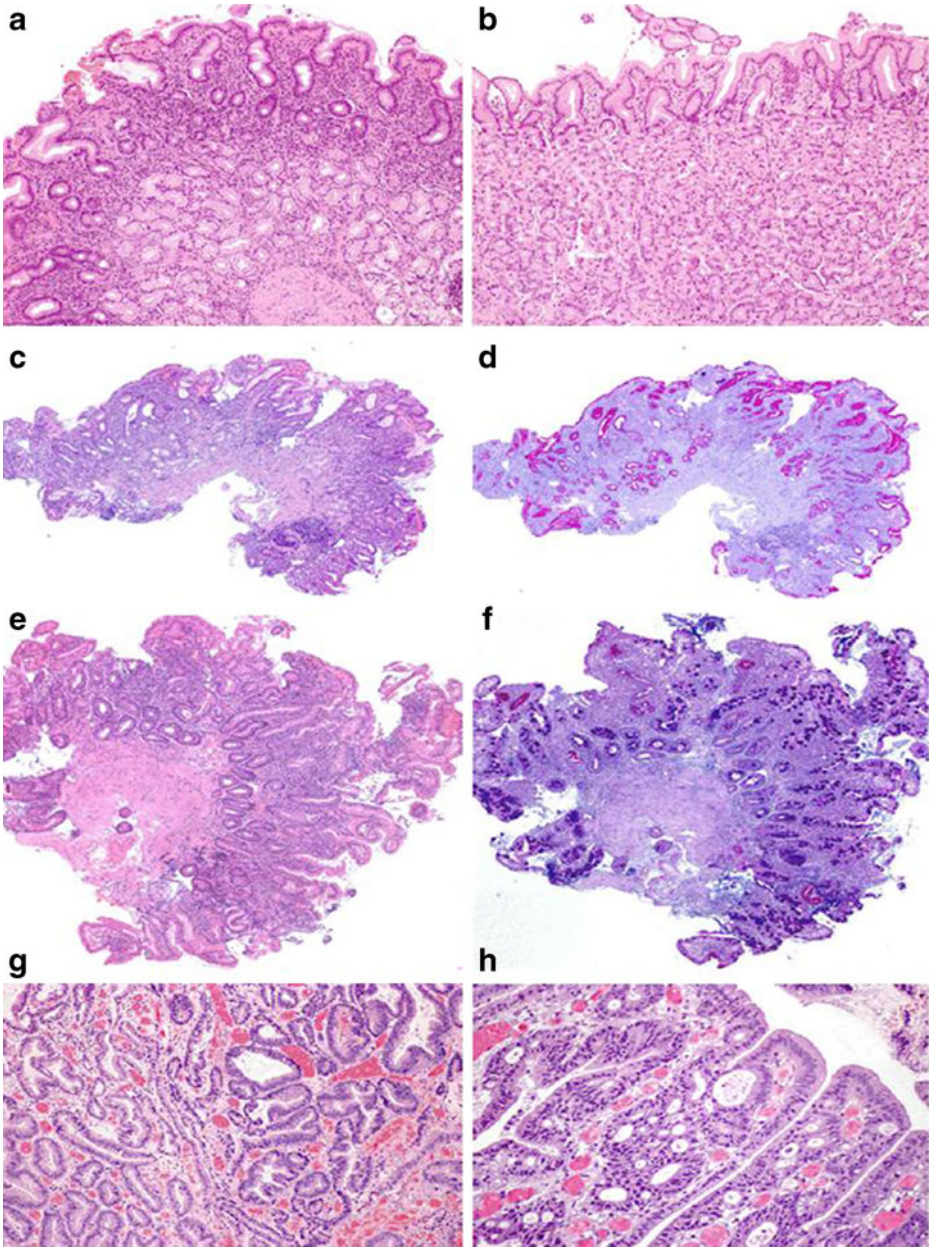

Fig. 2 Morphologic changes in gastric mucosa during gastric carcinogenesis. **a**, **b** Non-atrophic gastritis, without gland atrophy and/or intestinal metaplasia: **a** antrum [hematoxylin and eosin (H&E), ×40]; **b** corpus (H&E, ×100). **c**, **d** Moderate atrophy of deep antral glands (gland loss between 30% and 60%), without intestinal metaplasia: **c** H&E staining, ×40; **d** Periodic acid–Schiff (PAS)–Alcian blue staining, ×40, highlighting gland loss and a single focus of intestinal metaplasia in the superficial part of the gastric mucosa. **e**, **f** Severe atrophy of antral mucosa, with loss of more than 60% of original mucous-secreting glands, replaced by intestinal metaplasia: **e** H&E, ×40; **f** PAS–Alcian blue, ×40. **g**, **h** Dysplasia and intramucosal carcinoma: **g** low-grade (*left*) and high-grade (*right*) dysplasia (H&E, ×100); **h** intramucosal carcinoma (H&E, ×200)

OLGA and OLGIM assessment have been proposed for staging of gastritis (see below). However, most classifications are still difficult to use in clinical practice, and when applied, they have the disadvantage of considerable inter- and intra-observer variation.

Nevertheless, these systems seem to be more relevant and easy to apply than subtyping of intestinal metaplasia. *Intestinal metaplasia* may be classified as "complete" or "incomplete." Complete intestinal metaplasia ("small-intestinal" or type I) displays goblet and absorptive cells, decreased expression of gastric mucins (MUC1, MUC5AC, and MUC6), and expression of MUC2, an intestinal mucin. Incomplete intestinal metaplasia ("enterocolic" or type IIA/II and "colonic" or type IIB/III) displays goblet and columnar non-absorptive cells [17–20], in which gastric mucins (MUC1, MUC5AC, and MUC6) are coexpressed with MUC2 [17–20]. In Filipe's classification, the typing of intestinal metaplasia (types I, II, and III) was based on the detection of sialomucin and sulphomucin by high iron diamine–Alcian blue staining (this approach was discontinued due to toxicity of the reagents). Currently used classifications also take into consideration the presence of Paneth cells (complete metaplasia) or crescent architecture changes, dedifferentiation, and degree of absence of Paneth cells (incomplete metaplasia), as well as the pattern and type of mucin expression [20]. Moreover, some studies indicate a

positive correlation between the degree of incomplete intestinal metaplasia and the extent of intestinal metaplasia. However, the use of immunohistochemistry or other special techniques in order to subtype intestinal metaplasia is not widespread in routine diagnostics.

Recently, another pattern of metaplasia, termed spasmolytic polypeptide-expressing metaplasia (SPEM), has been described. This is characterized by the expression of the TFF2 spasmolytic polypeptide that is associated with oxyntic atrophy. SPEM, which characteristically develops in the gastric body and fundus, appears to share some characteristics with pseudopyloric metaplasia, has a strong association with chronic infection with *H. pylori* and with gastric adenocarcinoma, and may represent another pathway to gastric neoplasia [21]. At present, identification of SPEM is considered an investigational parameter.

Precancerous lesions

Gastric dysplasia represents the penultimate stage of the gastric carcinogenesis sequence, is defined as histologically unequivocal neoplastic epithelium without evidence of tissue invasion, and is thus a direct neoplastic precancerous lesion [22]. It is characterized by cellular atypia reflective of abnormal differentiation and disorganized glandular architecture [23–26]. Correct diagnosis and grading of dysplasia are critical because they predict both the risk of malignant transformation and the risk of metachronous gastric cancer. In fact, the reported progression rates of dysplasia to gastric cancer vary greatly, from 0% to 73% per year [27–48]. These variations can probably be explained by diverse factors such as differences in study design and populations under study and also differences in definitions and assessment of gastric dysplasia.

There are well-known differences between Japanese and European/North American pathologists in categorizing gastric dysplasia that in some classifications is designated as intraepithelial neoplasia. For instance, in Japan, non-invasive intramucosal neoplastic lesions with high-grade cellular and architectural atypia are termed "non-invasive intramucosal carcinoma," whereas the same lesions are diagnosed as high-grade dysplasia by most pathologists in the West [49, 50].

In an attempt to resolve this issue, several proposals have been made regarding the terminology for the morphological spectrum of lesions, including the Padova and Vienna classifications and, more recently, the World Health Organization (WHO) classification.

The WHO recently reiterated the classification of dysplasia/intraepithelial neoplasia. Acknowledging the widespread use of both "dysplasia" and "intraepithelial neoplasia", it uses these terms as synonymous (in this paper, dysplasia is the term that will be used from now on). According to the current WHO classification [51], the following diagnostic categories should thus be considered:

1. Negative for intraepithelial neoplasia/dysplasia
2. Indefinite for intraepithelial neoplasia/dysplasia
3. Low-grade intraepithelial neoplasia/dysplasia
4. High-grade intraepithelial neoplasia/dysplasia
5. Intramucosal invasive neoplasia/intramucosal carcinoma.

In the stomach and as far as the present guidelines are concerned, category 1, *negative for intraepithelial neoplasia/dysplasia*, includes chronic atrophic gastritis and intestinal metaplasia. Where there is doubt as to whether a lesion is neoplastic or non-neoplastic (i.e., reactive or regenerative), particularly in small biopsies exhibiting inflammation, the diagnosis should be *indefinite for intraepithelial neoplasia/dysplasia*. In such cases, the dilemma is usually solved by cutting deeper levels, by obtaining additional biopsies, or after correcting for possible etiologies.

Intraepithelial neoplasia/dysplasia comprises unequivocally epithelial neoplastic proliferations characterized by variable cellular and architectural atypia, but without convincing evidence of invasion. *Low-grade intraepithelial neoplasia/dysplasia* shows minimal architectural disarray and only mild-to-moderate cytological atypia. The nuclei are elongated, polarized, and basally located, and mitotic activity is mild-to-moderate (Fig. 2g, left). *High-grade intraepithelial neoplasia/dysplasia* comprises neoplastic cells that are usually cuboidal, rather than columnar, with a high nucleus-to-cytoplasm ratio, prominent amphophilic nucleoli, more pronounced architectural disarray, and numerous mitoses, which can be atypical. Importantly, the nuclei frequently extend into the luminal aspect of the cell, and nuclear polarity is usually lost (Fig. 2g, right). Most patients harboring lesions classified as *high-grade dysplasia* are at high risk for either synchronous invasive carcinoma or its rapid development [34] (see below).

Intramucosal invasive neoplasia/intramucosal carcinoma defines carcinomas that invade the lamina propria and are distinguished from intraepithelial neoplasia/dysplasia not only by desmoplastic changes that can be minimal or absent but also by distinct structural anomalies, such as marked glandular crowding, excessive branching, budding, and fused or cribriforming glands (Fig. 2h). The diagnosis of intramucosal carcinoma indicates that there is an increased risk of lymphatic invasion and lymph node metastasis. However, endoscopic techniques allow treatment without open surgery, particularly for lesions ≤2 cm in size and for those that are well differentiated with no lymphatic invasion. Guidelines for endoscopic treatment of gastric adenocarcinoma are beyond the scope of this manuscript.

Diagnosis and staging

Endoscopy

4. Conventional white light endoscopy cannot accurately differentiate and diagnose preneoplastic gastric conditions (evidence level2++, recommendation grade B) [agree 94% (vote: a, 46%; b, 24%; c, 24%; d, 4%; e, 2%)].
5. Magnification chromoendoscopy and NBI, with or without magnification, improve the diagnosis of gastric preneoplastic conditions/lesions (evidence level 2++, recommendation grade B) [agree 98% (vote: a, 47%; b, 27%; c, 24%; d, 2%); 83% of voters stated that they would apply this statement; 67% of those representing national societies mentioned that it would also be applicable (63%) or widely applicable (4%) in their countries].
6. Within this context, diagnostic upper gastrointestinal endoscopy should include gastric biopsies sampling (evidence level 4, recommendation grade D) [agree 93% (vote: a, 66%; b, 18%; c, 9%; d, 7%)].

Some studies have evaluated whether conventional white light endoscopy can reliably distinguish *H. pylori* gastritis and gastric preneoplastic lesions from normal mucosa. In a pioneer study, Atkins and Benedict concluded that correlation between endoscopy and histology was poor [52]. This was confirmed in a subsequent prospective study, where Bah et al. concluded that it is not possible to reliably diagnose *H. pylori* gastritis with endoscopy alone [53]. Antral nodularity appears to be the only endoscopic sign with a high positive predictive value (>90%) for *H. pylori* infection; however, it is, except in children, only present in a minority of patients with *H. pylori* gastritis [53–56]. Absence of rugae and presence of visible vessels in the gastric mucosa predict severe atrophy but with a relatively low sensitivity [57]. Intestinal metaplasia may appear as thin, white mucosal deposits [58]; however, the value of this or other endoscopic signs for the diagnosis of intestinal metaplasia remains unestablished. Taken together, these studies show that conventional endoscopy cannot reliably diagnose *H. pylori* gastritis, atrophy, or intestinal metaplasia [52, 54–58].

There is inconsistent evidence that new high-resolution endoscopes are more reliable. Some studies show low accuracy for the diagnosis of gastric mucosal inflammation, atrophy, and metaplasia, particularly with patients aged below 50 years and in particular when they have mild atrophy or metaplasia [59], but others suggest a good accuracy [60]. In addition to low accuracy, endoscopy findings were associated with low reproducibility [61], and therefore, current evidence suggests that conventional endoscopy cannot be relied upon to correctly identify patients with atrophy or intestinal metaplasia.

Studies have suggested that chromoendoscopy, particularly with magnification, helps to identify lesions of intestinal metaplasia and dysplasia. Dinis-Ribeiro et al. proposed a classification for the diagnosis of these lesions that was reproducible and highly accurate [62]. The accuracy and reproducibility of this chromoendoscopy classification with methylene blue was maintained when it was submitted to external validation [63]. Chromoendoscopy using other solutions, such as indigo carmine, acetic acid, or hematoxylin, was also associated with high accuracy for the diagnosis of these lesions, particularly for dysplasia [64, 65]. Tanaka et al. reported that the use of acetic acid was superior to that of indigo carmine [65].

However, high-resolution magnifying endoscopy without chromoendoscopy also appears superior to standard endoscopy, allowing great accuracy for the diagnosis of *H. pylori* gastritis, intestinal metaplasia, and dysplasia [66, 67]. No comparative study of magnification with or without chromoendoscopy has been made for the diagnosis of these lesions, despite the suggestion of Tanaka et al. that enhanced magnification chromoendoscopy with acetic acid is superior to conventional magnification endoscopy and indigo carmine chromoendoscopy [65].

So, current evidence suggests that magnification chromoendoscopy (MCE) improves accuracy for the detection of preneoplastic gastric lesions. However, this technique lengthens the time of the endoscopic procedure and adds to the workload of gastroenterology departments. Besides, patient tolerance, even with sedation, may be compromised. Taking all these considerations together, routine performance of MCE cannot be recommended, and its use should be restricted to centers experienced in this technique.

The recent technology of NBI has been found to have good sensitivity and specificity for the diagnosis of gastric lesions [68–77]. However, there is no agreement on which NBI patterns are associated with gastric precancerous lesions. The NBI classification systems varied between studies, there was no external validation, and reproducibility was seldom evaluated. Only two studies used NBI without magnification [76, 77]. The latter method, which could be applied in routine clinical practice in contrast to magnification NBI which is not practicable in an everyday clinical setting, requires some level of expertise and a type of scope that is available in only a few centers. Nevertheless, this indicates that NBI may be useful for the identification of different gastric lesions. However, before this technology can be endorsed, a simple classification system will have to be agreed upon and independently validated in a large prospective multicenter study.

It follows that the best available endoscopic method should be offered to individual patients, but within the

context of optimal identification of patients with precancerous conditions, diagnostic upper gastrointestinal endoscopy should include sampling with gastric biopsies.

Biopsy sampling

7. Atrophic gastritis and intestinal metaplasia are often unevenly distributed throughout the stomach. For adequate staging and grading of gastric precancerous conditions, at least four non-targeted biopsies of two topographic sites (at the lesser and greater curvature, from both the antrum and the corpus) should be taken and clearly labeled in separate vials; additional target biopsies of lesions should be taken (evidence level 2+, recommendation grade C) [agree 100% (vote: a, 61%; b, 25%; c, 14%); 90% of voters stated that they would apply this statement; 80% of those representing national societies mentioned that it would also be applicable (60%) or widely applicable (20%) in their countries].
8. Systems for histopathological staging (e.g., OLGA and OLGIM assessment) may be useful for categorization of risk of progression to gastric cancer (evidence level 2++, recommendation grade C) [agree 98% (vote: a, 39%; b, 41%; c, 18%; e, 2%); 90% of voters stated that they would apply this statement; 70% of those representing national societies mentioned that it would also be applicable in their countries].

Biopsy specimens of the stomach are essential to the establishment and grading of preneoplastic gastric lesions. The updated Sydney System is the most widely accepted for classification and grading of gastritis [14]. The system was primarily designed to provide standardization for reporting of gastric biopsies. The updated version recommended five biopsies, two from the antrum (3 cm from the pylorus, greater and lesser curvatures), one from the incisura, and two from the corpus (one from the lesser curvature, 4 cm proximal to the incisura, and one from the middle of the greater curvature); these sites were arbitrarily chosen. Although this biopsy protocol generally correctly establishes *H. pylori* status and chronic gastritis, the number of biopsies is controversial with regard to adequate staging of premalignant gastric lesions, mainly because of the multifocal nature of these lesions [78–82]. This multifocal nature affects their detectability, in turn affecting decisions regarding the patient's therapy or future surveillance [1, 6].

Five good-quality studies [78–80, 83, 84], in different population settings, addressed the number of biopsies needed for a precise grading of gastritis and intestinal metaplasia. el-Zimaity and Graham [80] concluded that the biopsy protocol recommended by the Sydney System underestimated the presence of intestinal metaplasia and could identify corpus atrophy only when it was extensive; these authors recommended a minimum of eight biopsies. On the other hand, Guarner et al. [79] concluded that the Sydney recommendations for biopsy sites and number were sensitive for identification of *H. pylori* infection and preneoplastic lesions (in geographic areas with a high prevalence of gastric cancer). The additional value of biopsies from the incisura angularis is unclear and remains insufficiently established. Although this location is considered to be an area of early onset of atrophic–metaplastic transformation [85, 86], other studies reported that additional incisura biopsies added little information to those obtained from antrum and corpus [78, 83]. On the other hand, de Vries et al. [84] in a multicenter study, in a low gastric cancer risk population, evaluated the yield from endoscopic surveillance of premalignant gastric lesions, by standardized biopsy protocols with 12 non-targeted and additional targeted biopsies, in 112 patients with a previous histologically confirmed diagnosis of intestinal metaplasia or dysplasia. The highest prevalence of premalignant lesions was found in the incisura (40%), followed by the antrum (35%) and lesser curvature of the corpus (33%). The non-targeted lesser curvature biopsies had a higher yield compared with those from the greater curvature of the corpus. A biopsy protocol consisting of seven non-targeted biopsies (three antrum, one incisura, three from corpus, with one from the greater and two from the lesser curvature) was able to diagnose intestinal metaplasia in 97% of cases and all cases of dysplasia or cancer. Moreover, despite the low number of cases of gastric dysplasia in this study, it was shown that non-targeted biopsies were important for diagnosing dysplasia or even cancer.

The variability of sampling methods and results obtained is related to the prevalence of premalignant lesions in the studied population. Fewer biopsies are needed for accurate diagnosis and staging in high-risk populations where the extent of the lesions is higher [83, 87, 88]. Even when extensive biopsy protocols are used, the inevitable sampling errors may affect the identification of the premalignant lesions which are frequently patchy [14, 80, 89, 90] and can be missed on follow-up [91]. However, the greater the extent of the lesion, the more likely it is to be found with regular biopsy sampling.

Although the Sydney system and its updated version [14] have contributed to uniformity of reporting of gastric preneoplastic lesions, they are not intended to be gastric cancer risk prediction tools. The aim of the recently established OLGA staging system is to translate the histopathological data into a standardized report, with information on the gastric condition (topography and extent of the atrophic changes) and subgrouping of patients by cancer risk [92, 93]. Initially, two cross-sectional validation studies concluded that OLGA provides relevant clinical information, with identification of a subpopulation of patients (OLGA stage

III/IV) with gastric premalignant lesions with high risk for gastric cancer and thus potentially eligible for surveillance of these lesions [94, 95]. Recently, Rugge et al. [96] described a cohort of patients with premalignant gastric conditions/lesions followed for 12 years. Only two patients with OLGA grade III/IV developed invasive neoplasias [P= 0.001; relative risk (RR)=18.56]. Because the OLGA system is based on the severity and extent of atrophy, a condition with low interobserver agreement [14, 97], Capelle et al. [98] introduced a modified system based on intestinal metaplasia, OLGIM, with which there is a high level of interobserver concordance [99]. The agreement between pathologists was moderate for atrophy (k=0.6) and higher for intestinal metaplasia (k=0.9). Application of the OLGIM assessment was associated with categorization of fewer patients into the high-risk stages III and IV. This has at least in theory the additional advantage that use of the OLGIM system would select a smaller population for whom surveillance would need to be considered. More studies on feasibility and reproducibility in different epidemiological contexts are needed to validate these classification systems [94].

Among these data, we have two good-quality studies [96, 98] suggesting that for the identification of patients with severe atrophic changes, namely extensive atrophy and/or intestinal metaplasia, which identify patients at risk for dysplasia and/or cancer, biopsies should be taken in the corpus. In addition, other good-quality case–control studies provided different conclusions, suggesting a minimum of four and a maximum of eight biopsies for adequate staging and/or surveillance [78–80, 83, 84].

On this basis, the panel concluded that one should sample *at least* two biopsies from the antrum (greater and lesser curvature) and two biopsies from the corpus (greater and lesser curvature) to identify patients with atrophy and/or intestinal metaplasia. Biopsy samples should be submitted for pathological examination in different vials labeled according to the site of the sampling [14, 94].

Non-invasive assessment

9. Serum pepsinogen levels can predict extensive atrophic gastritis (evidence level 2++, recommendation grade C) [agree 92% (vote: a, 30%; b, 28%; c, 34%; d, 4%; e, 4%); 68% of voters stated that they would apply this statement; only 50% of those representing national societies mentioned that it would be applicable in their countries].
10. In patients with low pepsinogen test levels, *H. pylori* serology may be useful for further detection of high-risk individuals (evidence level 2++, recommendation grade C) [agree 76% (vote: a, 26%; b, 10%; c, 40%; d, 18%; e, 4%; f, 2%); 77% of voters stated that they would apply this statement; 80% of those representing national societies mentioned that it would also be applicable (70%) or widely applicable (10%) in their countries].

Serum PGs are related to atrophic changes in gastric mucosa and consist of two types: PGI, which is mainly secreted by the fundic mucosa, and PGII secreted by chief cells but also by the pyloric glands and the proximal duodenal mucosa. Inflammation of the gastric mucosa leads to an increase in both PGI and PGII serum levels, usually with a more marked increase of PGII and thus a decrease in the PGI/II ratio. With the development of atrophy and loss of specialized cells, both PGI and PGII may decrease, but PGI usually shows a more marked decrease than PGII; thus, there is a further decline in the PGI/II ratio (see review by Kuipers [100]). Thus, a low PGI level, a low PGI/II ratio, or both are good indicators of atrophic changes in the gastric mucosa.

Many studies have been conducted that compare the levels of the serum pepsinogens with the features of the gastric mucosa as characterized by endoscopy with biopsies, in different countries and populations and using several different cutoff values. The reporting of results in terms of sensitivities and specificities but also as differences in serum pepsinogen mean levels, as correlations, or as odds ratios makes it difficult to compare or generalize studies.

In a meta-analysis published in 2004, Dinis-Ribeiro et al. [101] combined 42 studies that included 27 population studies (296,553 patients) and 15 selected-population studies (4,385 patients) and looked for the best cutoff for dysplasia diagnosis. A combination of PGI <50 ng/mL and a PGI/PGII ratio 3.0 provided the best results, with a sensitivity of 65%, a specificity of 74–85%, and a negative predictive value >95%. Most of the studies comparing serum pepsinogen levels with the histological assessment of the gastric mucosa were cross-sectional studies, from screening populations to selected high-risk patients. Usually in these studies the gastroenterologist and the pathologist were blinded to each other's findings, and both tests were done simultaneously.

When the study outcome was the extent of atrophy of the gastric corpus, values ranged between sensitivities of 9.4% to 92.3% and specificities of 9.9% to 100% [102–120], but other methods of reporting results found statistically significantly lower mean values of serum pepsinogen in extensive atrophic gastritis [106, 111, 121–124], significant correlations between atrophy extent and serum pepsinogen values [102, 125, 126], or significant odds/likelihood ratios for progression of atrophy to the corpus [113, 127, 128].

When the study outcome was the presence or extent of intestinal metaplasia, results presented sensitivity values of 15–75% and specificity values of 92.2–97.8% [103, 116,

129], or significant odds ratios [127, 128, 130]. When the study outcome was dysplasia/gastric cancer, some well-designed cohort studies were found reporting large numbers of patients followed up for many years, together with several other case series reports or case–control studies.

The best evidence on the risk associated with premalignant gastric lesions comes from well-designed cohort studies, preferably with long follow-up times, including a large number of patients and with small numbers lost to follow-up. At least six cohort studies fulfilling these criteria have been published to date. Watabe et al. [131] conducted a cohort study of 6,983 patients for 4.7 years and found that *H. pylori*-positive patients with a PGI <70 ng/mL and a PGI/II ratio <3.0 had a hazard ratio (HR) for gastric cancer of 6.0 [95% confidence intervals (CI) 2.4–14.5]; in *H. pylori*-negative patients with the same pepsinogen profile, the HR increased to 8.2 (3.2–21.5). Yamaji et al. [132], in a study with 6,158 patients followed for 4.7 years, found an HR of 6.2 (2.9–13.0), while Yanaoka et al. [133, 134], in 5,209 patients followed for 10 years, obtained a HR of 2.77 (1.46–5.26). Ohata et al. [135] studied a cohort of 4,655 patients for 7.7 years after collecting serum for pepsinogen and *H. pylori* antibodies; they concluded that in patients who were *H. pylori*-positive, with chronic atrophic gastritis by pepsinogen definition, the HR was 14.85 (1.96–107.7), while for patients who were *H. pylori*-negative with severe chronic atrophic gastritis, the HR increased to 61.85 (5.6–682.64). Oishi et al. [136] followed 2,466 patients for 12 years and found that a PGI level <70 ng/mL with a PGI/II ratio <3.0 was linked with an HR for gastric cancer of 3.42 (1.92–6.11) and a PGI <30 ng/mL with a PGI/II ratio <2.0 related to an HR of 4.43 (2.18–7.82). Finally, Dinis-Ribeiro et al., in a cohort of 100 patients followed for 3 years, found that the combination of incomplete intestinal metaplasia and a PGI/PGII ratio <3 was significantly associated with progression to dysplasia, with an HR of 13.9 (1.6–122.1) when compared with patients with only chronic atrophic gastritis or complete intestinal metaplasia [137].

Some of these studies also evaluated the presence of *H. pylori* and found that the most advanced and severe cases of gastric atrophy judged by the pepsinogen assessment, when combined with a negative *H. pylori* serology, probably due to a spontaneous disappearance of *H. pylori* antibody, were associated with an even greater progression to dysplasia and cancer. The values of hazard ratios of severely atrophic *H. pylori*-negative cases versus less atrophic *H. pylori*-positive cases were 8.2 (3.2–21.5) versus 6.0 in the study of Watabe et al. [131], 131.98 (11.95–1,457.36) versus 2.77 in that of Yanaoka et al. [133, 134], and 61.85 (5.6–682.64) versus 14.85 in that of Ohata et al. [135]. Yamaji et al. also found an increased incidence of gastric cancer, from 0.37% cases per year for the less atrophic *H. pylori-positive* cases to 0.53% cases per year in the severely atrophic *H. pylori*-negative cases [132].

On the issue of acceptability of examinations to patients, Miki et al. conducted a screening by serum pepsinogen in 101,892 patients. This indicated 21,178 endoscopies, of which 13,789 were effectively done (65%): 125 cancers were diagnosed, 80% of them at an early stage [138]. Several case–control studies comparing gastric cancer patients with healthy controls, including a range of 84 to 511 cases per study, found statistically significant odds ratios (ORs) for cancer, ranging from 2.24–12.0 for a PGI level <50 ng/mL to an OR of 2.78–10.92 for a PGI/PGII ratio <3 [139–155].

In diagnostic studies, detection of cancer by serum pepsinogen presented sensitivities of 66.7–84.6% and specificities of 73.5–81.5% [156–158], lower mean pepsinogen values compared with non-cancer patients [121, 122, 159], and a positive correlation with lower PGI/PGII ratio values [160]. Comparative studies of serum pepsinogen and gastric X-ray concluded that the positive predictive value was superior for serum pepsinogen (1.4% versus 0.8%) especially before the age of 50 years [161, 162].

Nevertheless, it was noted that most studies came from Japan and that different laboratory methodologies and different population settings may require cutoff adjustment. Therefore, the term “low level of pepsinogens” was preferred over a defined cutoff value.

Additional diagnostic factors

11. Family history of gastric cancer should be taken into account in the follow-up of precancerous conditions (evidence level 2++, recommendation grade B) [agree 96% (vote: a, 58%; b, 22%; c, 16%; d, 4%); 98% voters stated that they would apply this statement; 100% of those representing national societies mentioned that it would also be applicable (90%) or widely applicable (10%) in their countries].
12. Even though diverse studies assessed age, gender, and *H. pylori* virulence factors as well as host genetic variations, no clinical recommendations can be made for targeted management based on these factors with regard to diagnosis and surveillance (evidence level 4, recommendation grade D) [agree 82% (vote: a, 42%; b, 4%; c, 36%; d, 14%; e,2%; f, 2%)].

It has long been recognized that 10% of cases of gastric cancer exhibit some kind of familial aggregation. Of these, only 1–3% are clearly vertically inherited familial syndromes, such as hereditary diffuse gastric cancer [163, 164], Lynch syndrome [165, 166], Peutz–Jeghers syndrome [167, 168], and familial adenomatous polyposis [169], in which the risk of gastric cancer and carcinogenesis is well

established. For the remainder, the significance of family history and familial clustering of gastric cancer is not clearly determined. Having a first-degree relative with gastric cancer is a risk factor for gastric cancer with an OR varying from 2 to 10 in relation to geographic region and ethnicity [170]. A large study from Turkey reported an OR of 10.1 for siblings of gastric cancer patients, although these results were not adjusted for environmental factors [171]. Other European (OR 1.8–3.5), American (OR 2.2), and Asian (OR 1.5–9.9) case–control studies consistently provided corroboration that having a family history of gastric cancer is a risk factor [172–179]. Adjustment for environmental factors did not alter the risk. Interestingly, the Lauren intestinal type of gastric cancer was more strongly associated with family history of gastric cancer than the diffuse type [177, 180]. It is believed that this familial clustering of gastric cancer is due to an inherited genetic susceptibility, shared environmental or lifestyle factors, or a combination of these in different populations. A recent meta-analysis [181] of 11 studies addressed *H. pylori* infection and prevalence of premalignant conditions/lesions in first-degree relatives of gastric cancer patients. For the total of 1,500 cases and 2,638 controls, the pooled OR for cases to have *H. pylori* gastritis was 1.93 (95% CI 1.41–2.61), and it was 2.20 (1.27–3.82) for atrophy and 1.98 (1.36–2.88) for intestinal metaplasia. Altogether, these data show that first-degree relatives of gastric cancer patients have an increased prevalence of *H. pylori* infection and premalignant conditions/lesions, as well as an increased risk for gastric cancer. To the best of our knowledge, there are no studies aiming to assess whether the premalignant conditions/lesions in relatives of a gastric cancer patient progress more rapidly through the carcinogenic cascade to gastric cancer than similar lesions in matched controls in a general population.

Assuming the gene–environment interaction for gastric cancer, multiple risk factors have been linked to the multistep progression from chronic non-atrophic gastritis to atrophic gastritis, intestinal metaplasia, dysplasia, and finally cancer [6]. *H. pylori* plays a pivotal role in this progression and has been classified as a type 1 carcinogen in 1994 by the WHO [182]. It is believed that the combination of a virulent organism in a genetically susceptible host is associated with more severe chronic inflammation and more rapid progression to gastric cancer, at least for Lauren's intestinal type [183–185]. Different strains of *H. pylori* vary in their carcinogenic potential, with those containing virulence factor CagA inducing a high degree of inflammation. A meta-analysis of 16 case–control studies showed that among *H. pylori*-infected individuals, infection with CagA-positive strains further increases the risk for gastric cancer by 1.64-fold [186]. Other bacterial virulence factors, such as the CagA forms encoding multiple EPIYA-C type segments and strains that harbor VacA signal region type s1 and mid-region m1 [187], have also been related to an increased risk for gastric cancer. Nevertheless, there are no studies addressing the clinical usefulness of genotyping *H. pylori* strains with regard to the management and surveillance of gastric premalignant conditions/lesions.

An immense number of studies have addressed the issue of genes and genetic variations and their implications for gastric carcinogenesis, although their relevance has not always been clear. In the last few years, the role of host genetic interleukin polymorphisms has been widely studied in relation to gastric carcinogenesis. The best characterized are those that play a role in the inflammatory response to *H. pylori* infection and inflammation of the gastric mucosa, leading to mucosal atrophy and progression to gastric cancer. These in particular include IL-1B, IL1-receptor antagonist (IL-1RN), IL8, IL10, and TNF-α. Early studies by El-Omar et al. [188] showed an association of gastric cancer risk with the interleukin 1 genotypes IL-1B-511T, IL-1B-31T, and the IL1-receptor antagonist type *2/*2, with ORs of 2.5, 2.6, and 3.7 for development of gastric cancer among homozygotic carriers of these alleles compared with non-carriers. Results from other studies were inconsistent because of variations in allele frequencies in different ethnic groups, tumor type and location, *H. pylori* infection, methodologies, and quality of studies [189, 190]. Three powered meta-analyses found an association of IL-1B and IL-1RN*2 risk in Caucasians but not in Asians [191–193], and another study found a null association in both populations [194]. Another recent meta-analysis [190] found an increased cancer risk for IL-RN*2 carriers, a risk that was specific to non-Asian populations and for distal cancers; the analysis restricted for high-quality studies or *H. pylori*-positive cases and controls disclosed an association with the carrier and the homozygosity status. Regarding Asian populations, reduced risk was observed with IL-1B-31C carrier status (in high-quality studies). Caucasian carriers of TNF-α-308A were found to be at an increased risk for gastric cancer in a recent meta-analysis [195]. At present, the heterogeneity of results makes it difficult to translate them into recommendations for daily clinical practice.

Surveillance

Dysplasia

13. Patients with low-grade dysplasia in the absence of an endoscopically defined lesion should receive follow-up within 1 year after diagnosis. In the presence of an endoscopically defined lesion, endoscopic resection should be considered, to obtain a more accurate histological diagnosis (evidence level 2+, recommendation grade C) [agree 98% (vote: a, 60%; b, 26%; c, 13%; d, 2%); 96% of voters stated that they would apply this

statement; 90% of those representing national societies mentioned that it would be applicable (80%) or widely applicable (10%) in their countries].

14. For patients with high-grade dysplasia in the absence of endoscopically defined lesions, immediate endoscopic reassessment with extensive biopsy sampling and surveillance at 6-month to 1-year intervals is indicated (evidence level 2+, recommendation grade C) [agree 98% (vote: a, 69%; b, 17%; c, 12%; d, 2%); 100% of voters stated that they would apply this statement; 100% of those representing national societies mentioned that it would be applicable (70%) or widely applicable (30%) in their countries].

As mentioned above, differences exist between studies from the West and from Asia in reported progression rate of severe dysplasia. A large prospective study in China included 546 patients with dysplasia: Within 5 years of follow-up, progression rates to gastric cancer were 0.6% per year for mild dysplasia (now generally called low-grade dysplasia) and 1.4% for severe dysplasia (now generally called high-grade dysplasia) [32]. The largest Western study included 7,616 patients with mild-to-moderate dysplasia and 562 with severe dysplasia: Within 5 years' follow-up, the annual incidence of gastric cancer was 0.6% for mild-to-moderate dysplasia and 6% for severe dysplasia [28].

High-grade dysplasia-associated risk Most patients harboring lesions classified as high-grade dysplasia are at high risk for either synchronous invasive carcinoma or its rapid development [34]. In a cohort of patients with premalignant gastric lesions, approximately 25% of patients with high-grade dysplasia received a diagnosis of gastric cancer within 1 year of follow-up [28]. This finding implies that thorough endoscopic and histological re-evaluation shortly after initial diagnosis is indicated, and resection needs to be considered in the case of endoscopically defined lesions, either through endoscopy (endoscopic mucosal resection) or surgery [45, 196–198].

Low-grade dysplasia-associated risk Gastric cancer risk in patients with low-grade dysplasia is similar to or even considerably higher than the risk of cancer after removal of colonic adenomas, or in patients with Barrett's esophagus, or in those with long-standing inflammatory bowel disease [199–201]. In comparison with patients harboring high-grade dysplasia, patients with low-grade dysplasia seem to show a smaller risk to progress to invasive carcinoma of 7% (95% CI 6–8%) [28, 29, 33–37, 42, 43, 45, 202–204].

Thus, at least endoscopic surveillance at regular intervals seems to be indicated, although cost–effectiveness requires further evaluation. When repeated endoscopy with surveillance biopsy sampling confirms the presence of low-grade dysplasia, continued surveillance is warranted. When low-grade dysplasia cannot be confirmed during re-evaluation endoscopy, it is unclear for how long surveillance should be continued.

Of major importance is the fact that low-grade and high-grade dysplasia may present as endoscopically visible, depressed, or elevated lesions [34, 201] but may also present as minute or flat lesions that may be isolated or multifocal [7]. Thus, the disappearance of dysplasia or its assumed disappearance, as evaluated by successive current videoendoscopy biopsies during follow-up procedures, does not rule out the possible progression to invasive cancer [37, 44, 197, 205].

It seems therefore reasonable to propose high-quality endoscopic follow-up for patients with low-grade dysplasia [33, 37, 202, 206], expanding this to endoscopic resection of the most severe lesions in some patients [197, 203, 207]. In fact, a histological diagnosis of low-grade dysplasia in forceps biopsies, obtained from an endoscopically defined lesion, may be upgraded to a diagnosis of high-grade dysplasia or even adenocarcinoma after endoscopic mucosal resection (EMR) [208, 209]. In a Korean patient series, such an upgraded diagnosis after EMR occurred in up to 19% of low-grade dysplasia diagnoses on biopsy forceps specimens [209]. However, previously mentioned progression rates of low-grade dysplasia in large series seem discrepant with these findings. Moreover, in 3% to 5% of gastric neoplasia diagnoses on forceps biopsy tissue, EMR does not confirm this diagnosis [209, 210]. Nevertheless, EMR may be considered in patients with low-grade dysplasia with an endoscopically defined lesion, in order to obtain a more accurate histological diagnosis.

Atrophy or intestinal metaplasia

15. Endoscopic surveillance should be offered to patients with extensive atrophy and/or intestinal metaplasia (i.e., atrophy and/or intestinal metaplasia in the antrum and corpus) (evidence level 2++, recommendation grade B) [agree 94% (vote: a, 60%; b, 15%; c, 19%; d, 4%; f, 2%); 91% of voters stated that they would apply this statement; 80% of those representing national societies mentioned that it would be applicable in their countries].
16. Patients with extensive atrophy and/or intestinal metaplasia should receive follow-up every 3 years after diagnosis (evidence level 4, recommendation grade D) [agree 86% (vote: a, 43%; b, 20%; c, 23%; d, 12%; f, 2%); 90% of voters stated that they would apply this statement; 80% of those representing national societies mentioned that it would be applicable (70%) or widely applicable (10%) in their countries].

17. For those patients with mild-to-moderate atrophy/intestinal metaplasia restricted to the antrum, there is no evidence to recommend surveillance (evidence level 4, recommendation grade D) [Agree 99% (vote: a, 87%; b, 13%; c, 9%; d, 1%)].

As early detection of gastric cancer leads to improved survival, surveillance of premalignant gastric conditions/lesions may be important, as shown in several studies. Rates of progression in patients with atrophic gastritis, and intestinal metaplasia vary between, respectively, 0% to 1.8% and 0% to 10% per year. Overall, gastric cancer risk is too low to justify endoscopic surveillance in all patients with atrophic gastritis and intestinal metaplasia. Therefore, additional risk factors for progression toward gastric cancer need to be identified in these categories of patients.

First, the intragastric distribution and extent of intestinal metaplasia has been identified as a risk factor for gastric cancer. Atrophic gastritis tends to show a diffuse intragastric pattern, whereas intestinal metaplasia tends to be multifocal [44]. Several studies have shown that gastric cancer risk increases in patients with extensive intragastric lesions [211–214]. Two forms of extensive intestinal metaplasia have been identified. In the so-called magenstrasse or transitional zones distribution, intestinal metaplasia is found over the lesser curvature from cardia to pylorus and is especially common in the transitional zones (from cardia to corpus, from corpus to antrum), and in the "diffuse distribution," the gastric mucosa is diffusely replaced by intestinal-type mucosa, except for in the fundic region [215]. These topographical patterns of intestinalization show an increased risk for cancer [OR=5.7 (95% CI 1.3–26) and OR=12.2 (2.0–72.9), respectively]. To establish the extent of atrophic gastritis and intestinal metaplasia, three methods can be used: endoscopic assessment, histological assessment of biopsy specimens, and serology. In Asian countries, the presence and extent of premalignant gastric conditions/lesions are frequently established at endoscopy. For the presence of atrophic gastritis, the Kimura classification is used [216]. However, this method requires considerable experience on the part of endoscopists. In addition, biopsy sampling can be used to estimate the intragastric extent of lesions and the severity of atrophic gastritis, and intestinal metaplasia can be assessed according to the Sydney System. As has been suggested by the OLGA and OLGIM classifications, both the intragastric extent and severity of atrophic gastritis and intestinal metaplasia within biopsy samples determines gastric cancer risk. Finally, serologic testing for pepsinogens, gastrin, and *H. pylori* antibodies has great potential for establishing the intragastric extent of atrophic gastritis. Serology identifies individuals at increased risk of progression toward dysplasia and gastric cancer and is currently used in certain Japanese gastric cancer screening programs to identify patients to whom follow-up should be offered [101].

Secondly, individuals with a positive family history of gastric cancer carry an increased risk of premalignant gastric conditions/lesions and gastric cancer. The risk of atrophic gastritis in these individuals is approximately seven times higher compared with that of controls [188].

Thirdly, the type of intestinal metaplasia has been suggested as a risk factor for gastric cancer development. In a few studies, type III or incomplete intestinal metaplasia was associated with an increased risk for development of gastric cancer [19, 217, 218]. However, these observations have not been confirmed in other studies [219, 220]. Therefore, subtyping of intestinal metaplasia is not recommended for clinical practice.

Therapy

Eradication of H. pylori

18. *H. pylori* eradication heals non-atrophic chronic gastritis and it may lead to partial regression of atrophic gastritis (evidence level 1+, recommendation grade B) [agree 96% (vote: a, 70%; b, 16%; c, 10%; d, 4%); 98% of voters stated they would apply this statement; 90% of those representing national societies mentioned that it would be applicable (40%) or widely applicable (50%) in their countries].
19. In patients with intestinal metaplasia, *H. pylori* eradication does not appear to reverse intestinal metaplasia but it may slow progression to neoplasia, and therefore, it is recommended (evidence level 1+, recommendation grade B) [agree 96% (vote: a, 50%; b, 24%; c, 22%; d, 4%); 100% of voters stated they would apply this statement; 90% of those representing national societies mentioned that it would be applicable (or widely applicable (30%)) in their countries].
20. *H. pylori* eradication is recommended for patients with previous neoplasia after endoscopic or surgical therapy (evidence level 1++, recommendation grade A) [agree 96% (vote: a, 80%; b, 8%; c, 8%; d, 4%); 96% of voters stated they would apply this statement; 100% of those representing national societies mentioned that it would be applicable or widely applicable (50%) in their countries].

In rodent models, *H. pylori* eradication has been shown to have a prophylactic effect on gastric cancer [221–223]. However, studies on *H. pylori* eradication in humans have shown less consistent results. There is no dispute that *H. pylori* eradication leads to healing of non-atrophic gastritis,

but the evidence is not so clear for gastric atrophy and intestinal metaplasia.

A recent randomized study and a meta-analysis showed that in early stages of disease such as chronic gastritis and gastric atrophy without metaplasia, *H. pylori* eradication markedly improves gastric histology toward normal [224, 225]. Another systematic review also concluded that atrophic gastritis can regress within 1–2 years after *H. pylori* eradication [226].

A more recent meta-analysis on this subject suggests that gastric atrophy, however, may be reversible only in the corpus and not in the antrum [227]. The probability of reversal of gastric atrophy appears to be dependent on the extent and topographic location of atrophy [227]; however, it is unclear whether the effects of *H. pylori* eradication vary with the location and extent of atrophy.

In contrast to gastritis and atrophy, the effect of *H. pylori* eradication on gastric intestinal metaplasia is controversial. Some authors completely refute the idea of reversibility of intestinal metaplasia after *H. pylori* eradication [228, 229]. A lower *H. pylori* colonization of metaplastic areas may indicate a limited benefit for eradication. Two meta-analyses on this subject also concluded that there is no significant improvement in intestinal metaplasia after *H. pylori* eradication [225, 227]. Nevertheless, in a randomized trial, after 6 years of follow-up, Correa et al. showed that in patients with preneoplastic lesions, effective anti-*H. pylori* treatment and dietary supplementation with antioxidant micronutrients may interfere with the precancerous process, mostly by increasing the rate of regression of cancer precursor conditions/lesions including intestinal metaplasia [230]. This regression of atrophy and intestinal metaplasia was further confirmed after 12 years of follow-up [231]. Nevertheless, it remains to be proven whether eradication at these stages reduces the risk of cancer.

A large-scale randomized trial in China failed to demonstrate that *H. pylori* eradication led to a significant decrease in the rate of gastric cancer [232]. However, in the same study, considering only the group of patients without preneoplastic conditions/lesions at baseline, the risk of cancer in a period of 7.5 years was reduced after *H. pylori* eradication (zero versus six cases, $P=0.02$). A subsequent meta-analysis, including four randomized intervention studies with a follow-up ranging from 5 to 12 years comparing *H. pylori* eradication versus placebo for prevention of gastric cancer, showed a non-statistically significant trend in favor of eradication therapy. Further analysis with inclusion of non-randomized studies with follow-up of 3–8.5 years showed a significant reduction in cancer incidence after eradication [233]. The same authors recently updated their meta-analysis, and in a pooled analysis of six studies with a total of 6,695 participants followed from 4 to 10 years, they found that the relative risk for gastric cancer following *H. pylori* eradication was 0.65 (95% CI 0.43–0.98) [234]. These authors concluded that while *H. pylori* eradication seems to reduce gastric cancer, however, that might be relevant in only a subset of participants, probably in the early stages of gastritis (non-atrophic) [233, 234]. Another systematic review also concluded that there is sufficient clinical evidence that *H. pylori* eradication has a role in the prevention of gastric cancer in patients with chronic non-atrophic gastritis and with atrophic gastritis [226]. Indeed, a large prospective study (mean follow-up of 9.4 years) also suggested that *H. pylori* eradication before the development of intestinal metaplasia is probably more effective in reducing gastric cancer incidence [235].

Moreover, four prospective trials (follow-up range 3–8.5 years) that evaluated the effect of *H. pylori* eradication in patients with premalignant conditions/lesions to the end point of gastric cancer failed to show a significant reduction in cancer risk [231, 232, 236, 237]. And one non-randomized prospective study (mean follow-up 8.6 years) demonstrated a significant reduction of gastric cancer development after successful *H. pylori* eradication in comparison with those with persistent *H. pylori* infection [238]. However, in the same cohort, cancer still developed after 14 years of follow-up in some *H. pylori*-negative patients, suggesting that even after cure of infection, cancer can still develop [239]. Nevertheless, in studies involving patients who had previously undergone endoscopic resection of cancer, the majority of whom had extensive intestinal metaplasia, the risk of cancer was significantly reduced after successful *H. pylori* eradication and in a short period of time (3 years) [240, 241].

Indeed, at least, *H. pylori* eradication seems to decrease the progression of gastric intestinal metaplasia [236, 242, 243]. However, even after successful *H. pylori* eradication, gastric cancer still develops in the context of intestinal metaplasia [235, 239]. Therefore, the evidence is not clear regarding whether *H. pylori* eradication will reduce the risk of cancer in patients with extensive intestinal metaplasia, although there is some evidence that it slows progression. Based on these literature data, the consensus panel came to the view that *H. pylori* eradication should be considered in a case-by-case approach in patients with intestinal metaplasia, taking into account the extent of metaplasia and the degree of *H. pylori* colonization.

H. pylori eradication is recommended by several societies and guidelines for gastric cancer patients who undergo subtotal gastrectomy [244–247]. Indeed, eradication of *H. pylori* in patients with previous endoscopic resection of tumors decreases the rate of occurrence of new tumors and the severity of intestinal metaplasia [241]. These results were

confirmed in a multicenter randomized control trial [240]. In this open-label study, 272 patients were allocated for eradication or no eradication, with similar baseline characteristics in both groups; after 3 years of follow-up, 24 metachronous lesions had developed in the non-eradication group compared with nine new lesions in the eradication group ($P<0.01$). Another study showed that *H. pylori* eradication in this high-risk population was a cost-effective strategy [248]. All these studies showed this protective effect after a short period of time (3 years).

Concerning the effect of *H. pylori* eradication on the progression of gastric dysplasia, the data are scarce and contradictory [230, 231, 237]. So far, most of the evidence suggests that dysplastic lesions are not affected by eradication. However, patients with dysplasia may benefit from eradication because of a decreased incidence of metachronous lesions. Taking these considerations together, in patients with a previous history of gastric cancer, including dysplasia, *H. pylori* eradication is strongly recommended.

Additional measures

21. Currently, the use of COX-2 inhibitors cannot be supported as an approach to decrease the risk of progression of gastric precancerous lesions (evidence level 1+, recommendation grade B) [agree 96% (vote: a, 50%; b, 20%; c, 26%; d, 2%; e, 2%)].
22. The use of dietary supplementation with antioxidants (ascorbic acid and beta-carotene) cannot be supported as a therapy to reduce the prevalence of atrophy or intestinal metaplasia (evidence level 1+, recommendation grade B) [agree 96% (vote: a, 63%; b, 14%; c, 19%; d, 4%)].

Meta-analyses of observational studies demonstrated that long-term non-selective inhibition of COX, through the use of non-steroidal anti-inflammatory drugs (NSAIDs), is an effective chemopreventive strategy for gastric cancer development [249, 250]. The available literature on the efficacy of the use of COX-2 inhibitors to prevent the progression of gastric precancerous lesions is restricted to five clinical studies conducted exclusively in Asian populations. The overall evidence regardless of type of drug used is inconsistent. Apart from one well-designed placebo-controlled RCT [251], the evidence suggesting a preventive effect of these chemopreventive agents on precancerous lesions outcome is drawn from low-quality studies, comprising one small RCT [252], one pilot study [253], and two prospective cohorts [254, 255]. These were conducted in very heterogeneous populations (first-degree relatives of gastric cancer patients, dyspeptic patients with rheumatologic diseases, early gastric cancer patients, etc.) that compromise the generalizability and interpretation of data.

Three selective COX-2 inhibitors were considered: rofecoxib, etodolac, and celecoxib. Rofecoxib for 2 years in an RCT did not have a significant benefit in terms of intestinal metaplasia regression after *H. pylori* eradication [251]. Yanaoka et al. reported a higher metachronous cancer incidence in patients treated with 300 mg/day of etodolac, after a mean follow-up period of 4.2 years. Interestingly, no significant change in the extent of precancerous conditions/lesions was observed despite etodolac treatment [254].

Most studies focused on whether celecoxib, a selective COX-2, could decrease the severity of gastric precancerous conditions/lesions following *H. pylori* eradication. In patients receiving celecoxib in a small randomized trial, a 67% improvement in gastric precancerous lesion histology was observed ($P<0.001$, versus 16.1% in the placebo group) after 12 weeks [252]. In a pilot study, following 8 weeks of intervention, in 29% of patients, a complete regression of persistent intestinal metaplasia was noticed in those with confirmed *H. pylori* eradication [253]. Furthermore, in those patients without complete regression, an improvement in intestinal metaplasia severity was noticed ($P<0.007$) [253]. Additionally, Yang et al. [255] observed that dyspeptic chronic users of celecoxib for rheumatologic diseases presented a higher regression rate of intestinal metaplasia than non-NSAID users (42% versus 20%; RR=2.9, 95% CI 1.88–6.91) but only after *H. pylori* eradication.

Therefore, there is some evidence supporting the involvement of celecoxib in the regression of gastric precancerous conditions/lesions, namely intestinal metaplasia, that could motivate the design of larger RCTs with longer follow-up. Furthermore, regular use of non-selective NSAIDs, including aspirin, has been associated with a decreased risk for gastric cancer development, as observed in a recent large retrospective cohort [256] and meta-analyses [250]. Further prospective clinical trials are needed to address the effects of these non-specific COX inhibitors on the progression of gastric lesions.

Three chemoprevention trials specifically designed to evaluate the effects of antioxidant vitamin supplementation on gastric precancerous lesions have been reported [230, 237, 257]. These randomized double-blind placebo-controlled trials, conducted in populations at high risk for gastric cancer, presented conflicting results, and their quality is compromised by significant loss to follow-up/withdrawal observed in two of the studies [230, 257].

Correa et al. [230] reported that patients randomized to single active intervention with ascorbic acid (1 g twice daily), beta-carotene (30 mg/day), or anti-*H. pylori* therapy were three times more likely to show an improvement in the histology of their lesions after a 6-year follow-up period. However, this antioxidant benefit disappeared after a further 6 years with no vitamin supplementation, as shown in a re-evaluation at 12 years after the inception of the study [231].

In contrast, a long-term trial in Linqu County, Shandong, China reported no favorable effect on the prevalence of gastric precancerous conditions/lesions after 7.2 years of intervention with vitamin supplements (capsule with 250 mg ascorbic acid, 100 IU vitamin E, and 37.5 μL selenium, twice daily) [237]. Similarly, Plummer et al. [257], in a study involving patients randomized to receive either vitamins (capsule with 250 mg ascorbic acid, 200 mg vitamin E, and 6 mg beta-carotene/thrice daily) or placebo for 3 years, did not observe any significant association between vitamin supplementation and the progression/regression of gastric precancerous conditions/lesions.

These studies were carried out in populations with a high incidence of gastric cancer in Columbia, Venezuela, and China [230, 237, 257]. It is as yet unclear to what extent these results can be generalized to populations with a low incidence of gastric cancer.

Cost–effectiveness

23. After endoscopic resection of early gastric cancer, *H. pylori* eradication is cost-effective (evidence level 1+, recommendation grade B) [agree 100% (vote: a, 79%; b, 14%; c, 7%)].
24. Currently available evidence does not allow an accurate estimation of the cost–effectiveness of surveillance for premalignant gastric conditions worldwide (evidence level 2+, recommendation grade C) [agree 98% (vote: a, 41%; b, 16%; c, 41%; d, 2%)].

Most of the studies on cost–effectiveness of *H. pylori* eradication for gastric cancer prevention report on models with a population screening scenario, which is outside the scope of this manuscript. Only a few studies dealt with the issue of surveillance after an incidental diagnosis of a gastric premalignant condition/lesion. Most of these studies compared strategies of screening for and treating *H. pylori* versus no screening from the public healthcare provider's perspective, used estimates from systematic reviews of the literature, and conducted sensitivity analyses with results that were consistent in most strategies. Despite involving populations with very different gastric cancer risks and also the use of diverse models, all studies concluded that the screening option is cost-effective compared with no screening [258–270].

Concerning the possibility of *H. pylori* eradication after EMR of a gastric precancerous lesion, Shin et al. [248] developed a Markov model based on a randomized clinical trial conducted by Fukase et al. [240] precisely on this topic. They used a very wide set of clinical health estimates derived from an extensive search of the literature, and costs were based on the perspective of the Korean public healthcare provider. The results showed that in the base-case assumptions, *H. pylori* eradication was less costly than no eradication (US $29,780 versus 30,594) and also provided more benefits (mean life expectancy of 13.60 versus 13.55). Thus, treatment of 10,000 persons would lead to a net saving of US $814,200 and around 50 life-years saved (LYS) would be gained. This strategy was dominant (less costly and more effective), but the usual calculation of the incremental cost–effectiveness ratio (ICER) value was not performed. By conducting one-way and three-way sensitivity analyses, the authors confirmed the robustness of the model, with a dominant ICER conclusion for the strategy of eradication in almost every scenario or providing very cost-effective values (always below US $3,852 per LYS).

Concerning the cost–effectiveness of secondary surveillance of incidentally detected precancerous conditions/lesions, studies in the published literature provide conflicting results, mainly due to different estimates for lesion progression to dysplasia or cancer. Yeh et al. [271] compared several strategies, from neither surveillance nor treatment to surveillance of various precancerous gastric conditions/lesions at several frequencies followed by treatment with EMR or surgery. The model was cost-effective for men over 50 years with dysplasia treated by EMR with annual surveillance [cost per quality-adjusted life-year (QALY) US $39,800], but not for patients with intestinal metaplasia (cost per QALY US $544,500 for surveillance every 10 years). Hassan et al. [272], using a model for the American population, revealed an incremental cost–effectiveness ratio above $70,000 per life-year saved for an yearly endoscopy versus no surveillance in patients with intestinal metaplasia, while in a model derived from a Portuguese cohort, Dinis-Ribeiro et al. [137] obtained a cost of only 1,868€ per QALY in a protocol of yearly magnification chromoendoscopy and pepsinogen measurement.

These conflicting results might arise from very different estimates of the yearly rates for progression of conditions (0.00–0.012% per year for dysplasia to invasive cancer in the study of Yeh et al. [271], 0.18% for intestinal metaplasia to cancer in Hassan et al. [272], and 12.8–56.0% for intestinal metaplasia to dysplasia in the study by Dinis-Ribeiro et al. [137]) and might also arise from the differing cost estimates included in the models (cost per endoscopy of US $871 versus US $358 in the studies by Yeh at al. and Hassan et al., respectively [271, 272]). Moreover, no study except that of Dinis-Ribeiro et al. [137] considered different stages of premalignant gastric conditions/lesions.

Research agenda

The extensive examination of the literature and the discussion within the consensus panel led to the research agenda described below, with the possibility of a review in 3 to 5 years:

- Reliability studies for histopathological staging systems for precancerous conditions and for endoscopic features
- Large multicenter cohort studies to derive and validate clinical decision rules addressing the value of variables other than the phenotype of lesion extent, such as age, gender, *H. pylori* virulence factors, and genetic profiles
- Large multicenter cohort studies to further clarify stages involved in gastric carcinogenesis, such as the elucidation of the role of SPEM
- Standardization and validation of endoscopic features with new endoscopic technologies and randomized trials to address the benefit per-patient in this setting (diagnosis of intestinal metaplasia and atrophy in corpus and diagnosis of superficial lesions)
- Further clarification of the role of *H. pylori* eradication and other therapies in prevention of gastric cancer
- Observational and/or decision analysis studies addressing follow-up intervals and cost–benefit of these strategies
- Studies to address methodologies and target populations for the screening of these lesions in Western countries

Acknowledgments These guidelines were made possible through the financial support of the European Society of Gastrointestinal Endoscopy (ESGE) and the Sociedade Portuguesa de Endoscopia Digestiva (SPED). Olympus (Europe), Casen-Fleet (Portugal), and Angelini (Portugal) gave educational grants to ESGE and SPED. We would also like to acknowledge Eng. Jorge Jacome for his support through MedQuest development and the Secretariats of ESGE (Hilary Hamilton and Nicola Oremus) and SPED (Maria José Ilharco).w

Conflict of interest statement We declare that we have no conflict of interest.

Appendix

All contributors are listed below in alphabetic order, according to their role (Working Group, as national representative, or as an individual) and their participation in the Porto meeting (* indicates those who voted online only and not at the Porto meeting).

Panel of Experts or Young Investigators (Working Group)

Miguel Areia, Gastroenterology Department, Portuguese Oncology Institute; Fátima Carneiro, European Society of Pathology, Porto Faculty of Medicine, Serviço de Anatomia Patológica, Porto, Portugal; Annemarie de Vries, Erasmus MC University Medical Center Rotterdam, Gastroenterology and Hepatology, Rotterdam, the Netherlands; Mário Dinis-Ribeiro, Servico de Gastrenterologia, Instituto Portugues de Oncologia Francisco Gentil, Porto, Portugal; Jean-Marc Dumonceau, Département de Gastroénterologie et d'Hépato-pancréatologie, H.U.G. Hôpital Cantonal, Geneva, Switzerland; *Arzu Ensari, Department of Pathology, Ankara University Medical School, Turkey; Ernst J. Kuipers, Department of Gastroenterology and Hepatology, Erasmus MC, Rotterdam, the Netherlands; Guilherme Macedo, IPATIMUP, Porto, Portugal; Jose Carlos Machado, Department of Gastroenterology, Hospital de S. João/Porto Faculty of Medicine, Portugal; Peter Malfertheiner, Klinik der Gasroenterologie, Hepatologie und Infektologie, Otto von Guericke Universität Magdeburg, Germany; Ricardo Marcos-Pinto, Gastroenterology Department, Centro Hospitalar do Porto, Portugal; Tamara Matysiak-Budnik, Service d'Hépato-Gastroentérologie, Hôtel Dieu, CHU de Nantes, France; Francis Megraud, Inserm U853 and Université Bordeaux, Laboratoire de Bacteriologie, Bordeaux, France; Kazumasa Miki, Japan Research Foundation of Prediction, Diagnosis and Therapy for Gastric Cancer (JRF PDT GC), Tokyo, Japan; Matilde Monteiro-Soares CINTESIS, Porto Faculty of Medicine, Portugal; Anthony O'Connor, AMNCH/TCD, Adelaide and Meath Hospital/Trinity College, Dublin Tallagh, Ireland; Colm O'Morain, Department of Gastroenterology, Adelaide and Meath Hospital, Dublin, Ireland; Richard Peek, Division of Gastroenterology, Vanderbilt University School of Medicine, Nashville, USA; Carina Pereira, Grupo de Oncologia Molecular, Instituto Português de Oncologia do Porto FG, EPE, Porto, Portugal; Pedro Pimentel-Nunes, Servico de Gastrenterologia, IPO-Porto, Portugal, and Department of Physiology, Cardiovascular Research and Development Unit, Medical Faculty, Porto, Portugal; Thierry Ponchon, Hopital Edouard Herriot, Department of Digestive Diseases, Lyon, France; Björn Rembacken, Centre for Digestive Diseases, The General Infirmary at Leeds, UK; Ari Ristimaki, Department of Pathology, HUSLAB and Haartman Institute, Helsinki University Central Hospital and University of Helsinki, Helsinki, Finland.

National representatives

Gieri Cathomas (Switzerland, pathology), Head of the Cantonal Institute for Pathology, President Swiss Society of Gastrointestinal Pathology, Cantonal Institute for Pathology, Liestal, Switzerland; Evgeny D. Fedorov (Russia), Russia State Medical University, Moscow University Hospital; Pedro Manuel Narra de Figueiredo (Portugal), Hospitais da Universidade de Coimbra, Serviço de Gastrenterologia,

Coimbra, Portugal; Adrian Goldis (Romania), Clinic of Gastroenterology Algomed, Timisoara, Romania; Marcis Leja (Latvia), University of Latvia, Latvian Society of Gastroenterology, Hospital Linezers, Riga, Latvia; Markus Moehler (Germany), 1. Medizinische Klinik und Poliklinik der Johannes-Gutenberg Universität Mainz, Germany; Emil Plesea (Romania, pathology), Department of Pathology, University of Medicine and Pharmacy, Craiova, Romania; *Jacques Bergman (the Netherlands), Department of Gastroenterology and Hepatology, Academic Medical Center Amsterdam, the Netherlands; *Waseem Hamoudi (Jordan), Jordanian Society of Gastroenterology, Amman, Jordan.

As individuals

Raquel Almeida, IPATIMUP, Porto, Portugal; Bruno Annibale, Dipartimento Medico-chirurgico di scienze cliniche, Tecnobiomediche e medicina traslazionale, Section of Gastroenterology, Rome, Italy; Luís Azevedo Lobo, Gastroenterology Department, Pedro Hispano Hospital, ULS Matosinhos, Senhora da Hora, Portugal; Yasemin Hatice Balaban, Hacettepe University, Gastroenterology Unit, Ankara, Turkey; Alina Boeriu, Gastroenterology Department, University of Medicine, Targu Mures, Romania; Alain Burette, Gastroenterology Department, CHIREC, Brussels, Belgium; Anne Courillon Mallet, Service Hépato-gastroentérologie, Centre Hospitalier de Villeneuve St Georges, Villeneuve St Georges, France; Leonor David, IPATIMUP, Porto, Portugal; Jean-Charles Delchier, Service d'hépatogastroentérologie, Hôpital Henri Mondor, Créteil, France; Ecaterina Daniela Dobru, Gastroenterology Department, University of Medicine and Pharmacy, TG. Mures, Romania; Carlos Fernandes, C. H. Vila Nova de Gaia/Espinho, Portugal; Michel Kahaleh, Division of Gastroenterology/Hepatology, University of Virginia Health System, Charlottesville, USA; Sergey Kashin, Yaroslavl Regional Cancer Hospital, Yaroslavl, Russia; Rafael Lomba-Viana, Porto, Portugal; Nuno Lunet, University of Porto Medical School, Department of Clinical Epidemiology, Predictive Medicine and Public Health, Porto, Portugal; Kirill Marakhouski, Minsk, Belarus; Luis Moreira-Dias, Instituto Português De Oncologia Do Porto, Serviço De Gastrenterologia, Porto, Portugal; Carlos Noronha Ferreira, Serviço de Gastrenterologia e Hepatologia, Hospital de Santa Maria-Centro Hospitalar Lisboa Norte, Lisbon, Portugal; Teresa Pinto Pais, Portugal; Antonio Rollán, Gastroenterology Department, Clinica Alemana, Santiago, Chile; Ana Sadio, IPATIMUP, Porto, Portugal; Carlos Figueiredo Costa Santos, Casa Saude Boavista, Porto, Portugal; *Joao Santos Barbosa, Lisbon, Portugal; *Kent-Man Chu, Department of Surgery, The University of Hong Kong, Queen Mary Hospital, Pokfulam, Hong Kong; *Giancarlo D'Ambra, Rome, Italy; *Pierre Ellul, Mater Dei Hospital, Sliema, Malta; *Nicole van Grieken, Department of Pathology, VU University Medical Center, Amsterdam, the Netherlands; *Dominique Lamarque, Service Hépato-Gastroentérologie, Oncologie digestive, Hôpital Ambroise Paré, Boulogne-Billancourt, France; *Akram Ajeel Najeeb, Medical City, Bab Al-Mudhaam, Baghdad, Iraq.

References

1. Correa P (1988) A human model of gastric carcinogenesis. Cancer Res 48:3554–3560
2. Collaboration AGREE (2003) Development and validation of an international appraisal instrument for assessing the quality of clinical practice guidelines: the AGREE project. Qual Saf Health Care 12:18–23
3. Atkins D, Best D, Briss PA, Working Group GRADE et al (2004) Grading quality of evidence and strength of recommendations. BMJ 328:1490
4. Guyatt GH, Oxman AD, Vist GE, Kunz R, Falck-Ytter Y, Alonso-Coello P, Schünemann HJ, GRADE working group (2008) GRADE: an emerging consensus on rating quality of evidence and strength of recommendations. BMJ 336:924–926
5. Harbour R, Miller J (2001) A new system for grading recommendations in evidence-based guidelines. BMJ 323:334–336
6. Correa P (1992) Human gastric carcinogenesis: a multistep and multifactorial process—First American Cancer Society Award Lecture on Cancer Epidemiology and Prevention. Cancer Res 52:6735–6740
7. Kapadia CR (2003) Gastric atrophy, metaplasia and dysplasia. A clinical perspective. J Clin Gastroenterol 36:S29–S36
8. Carneiro F, Machado JC, David L, Reis C, Nogueira AM, Sobrinho-Simões M (2001) Current thoughts on the histopathogenesis of gastric cancer. Eur J Cancer Prev 10:101–102
9. Ihamäki T, Saukkonen M, Siurala M (1978) Long term observation of subjects with normal mucosa and with superficial gastritis: results of 23–27 years follow-up examination. Scand J Gastroenterol 13:771–775
10. Ormiston MC, Gear MW, Codling BW (1982) Five year follow-up study of gastritis. J Clin Pathol 35:757–760
11. Laurén P (1965) The two histological main types of gastric carcinoma: diffuse and so-called intestinal-type carcinoma. Acta Pathol Microbiol Scand 64:31–49
12. Fukao A, Hisamichi S, Ohsato M, Fujino N, Endo N, Iha M (1993) Correlation between the prevalence of gastritis and gastric cancer in Japan. Cancer Causes Control 4:17–20
13. Genta RM (1998) Review article: gastric atrophy and atrophic gastritis—nebulous concepts in search of a definition. Aliment Pharmacol Ther 12:17–23
14. Dixon MF, Genta RM, Yardley JH, Correa P (1994) Classification and grading of gastritis. The updated Sydney System. International Workshop on the Histopathology of Gastritis, Houston 1994. Am J Surg Pathol 20:1161–1181
15. Misiewicz JJ (1991) The Sydney System: a new classification of gastritis. Introduction. J Gastroenterol Hepatol 6:207–208
16. Plummer M, Buiatti E, Lopez G, Peraza S, Vivas J, Oliver W, Muñoz N (1997) Histological diagnosis of precancerous lesions of the stomach: a reliability study. Int J Epidemiol 26:716–720
17. Filipe MI, Potet F, Bogomoletz WV, Dawson PA, Fabiani B, Chauveinc P, Fenzy A, Gazzard B, Golfain D, Zeegen R (1985) Incomplete sulphomucin-secreting intestinal metaplasia for gastric cancer. Preliminary data from a prospective study from three centres. Gut 26:1319–1326

18. Filipe MI, Barbatis C, Sandey A, Ma J (1988) Expression of intestinal mucin antigens in the gastric epithelium and its relationship with malignancy. Hum Pathol 19:19–26
19. Silva S, Filipe MI, Pinho A (1990) Variants of intestinal metaplasia in the evolution of chronic atrophic gastritis and gastric alcer. A follow up study. Gut 31:1097–1104
20. Reis CA, David L, Correa P, Carneiro F, de Bolós C, Garcia E, Mandel U, Clausen H, Sobrinho-Simões M (1999) Intestinal metaplasia of human stomach displays distinct patterns of mucin (MUC1, MUC2, MUC5AC and MUC6) expression. Cancer Res 59:1003–1007
21. Gutiérrez-González L, Wright NA (2008) Biology of intestinal metaplasia in 2008: more than a simple phenotypic alteration. Dig Liver Dis 40:510–522
22. Correa P (1985) Clinical implications of recent developments in gastric cancer pathology and epidemiology. Semin Oncol 12:2–10
23. Genta RM, Rugge M (1999) Gastric precancerous lesions: heading for an international consensus. Gut 45:I5–I8
24. Guindi M, Riddell RH (2001) The pathology of epithelial premalignancy of the gastrointestinal tract. Best Pract Res Clin Gastroenterol 15:191–210
25. Riddell RH (1996) Premalignant and early malignant lesions in the gastrointestinal tract: definitions, terminology and problems. Am J Gastroenterol 91:864–872
26. Odze RD, Riddell RH, Bosman FT, Carneiro F, Fléjou J-F, Geboes K, Genta RM, Hattori T, Hruban RH, van Krieken JHJM, Lauwers GY, Offerhaus GJA, Rugge M, Shimizu M, Shimoda T, Theise ND, Vieth M (2010) Premalignant lesions of the digestive system. In: Bosman FT, Carneiro F, Hruban RH, Theise ND (eds) WHO classification of tumours of the digestive system, 4th edn. IARC, Lyon
27. Park SY, Jeon SW, Jung MK, Cho CM, Tak WY, Kweon YO, Kim SK, Choi YH (2008) Long-term follow-up study of gastric intraepithelial neoplasias: progression from low-grade dysplasia to invasive carcinoma. Eur J Gastroenterol Hepatol 20:966–970
28. de Vries AC, van Grieken NC, Looman CW, Casparie MK, de Vries E, Meijer GA, Kuipers EJ (2008) Gastric cancer risk in patients with premalignant gastric lesions: a nationwide cohort study in the Netherlands. Gastroenterology 134:945–952
29. Yamada H, Ikegami M, Shimoda T, Takagi N, Maruyama M (2004) Long-term follow-up study of gastric adenoma/dysplasia. Endoscopy 36:390–396
30. Dinis-Ribeiro M, Lopes C, da Costa-Pereira A, Guilherme M, Barbosa J, Lomba-Viana H, Silva R, Moreira-Dias L (2004) A follow up model for patients with atrophic chronic gastritis and intestinal metaplasia. J Clin Pathol 57:177–182
31. Whiting JL, Sigurdsson A, Rowlands DC, Hallissey MT, Fielding JW (2002) The long term results of endoscopic surveillance of premalignant gastric lesions. Gut 50:378–381
32. You WC, Li JY, Blot WJ et al (1999) Evolution of precancerous lesions in a rural Chinese population at high risk of gastric cancer. Int J Cancer 83:615–619
33. Kokkola A, Haapiainen R, Laxén F, Puolakkainen P, Kivilaakso E, Virtamo J, Sipponen P (1996) Risk of gastric carcinoma in patients with mucosal dysplasia associated with atrophic gastritis: a follow-up study. J Clin Pathol 49:979–984
34. Rugge M, Farinati F, Baffa R, Sonego F, Di Mario F, Leandro G, Valiante F (1994) Gastric epithelial dysplasia in the natural history of gastric cancer: a multicenter prospective follow-up study. Interdisciplinary Group on Gastric Epithelial Dysplasia. Gastroenterology 107:1288–1296
35. Bearzi I, Brancorsini D, Santinelli A, Rezai B, Mannello B, Ranaldi R (1994) Gastric dysplasia: a ten-year follow-up study. Pathol Res Pract 190:61–68
36. Di Gregorio C, Morandi P, Fante R, De Gaetani C (1993) Gastric dysplasia. A follow-up study. Am J Gastroenterol 88:1715–1719
37. Fertitta AM, Comin U, Terruzzi V et al (1993) Clinical significance of gastric dysplasia: a multicenter follow-up study. Gastrointestinal Endoscopic Pathology Study Group. Endoscopy 25:265–268
38. Farinati F, Rugge M, Di Mario F, Valiante F, Baffa R (1993) Early and advanced gastric cancer in the follow-up of moderate and severe gastric dysplasia patients. A prospective study. I.G.G.E.D.—Interdisciplinary Group on Gastric Epithelial Dysplasia. Endoscopy 25:261–264
39. Rugge M, Farinati F, Di Mario F, Baffa R, Valiante F, Cardin F (1991) Gastric epithelial dysplasia: a prospective multicenter follow-up study from the Interdisciplinary Group on Gastric Epithelial Dysplasia. Hum Pathol 22:1002–1008
40. Rugge M, Baffa R, Farinati F, Di Mario F, Guido M, Valiante F, Ninfo V (1991) Epithelial dysplasia in atrophic gastritis. Bioptical follow-up study. Ital J Gastroenterol 23:70–73
41. Koch HK, Oehlert M, Oehlert W (1990) An evaluation of gastric dysplasia in the years 1986 and 1987. Pathol Res Pract 186:80–84
42. Lansdown M, Quirke P, Dixon MF, Axon AT, Johnston D (1990) High grade dysplasia of the gastric mucosa: a marker for gastric adenocarcinoma. Gut 31:977–983
43. Coma del Corral MJ, Pardo-Mindan FJ, Razquin S, Ojeda C (1990) Risk of cancer in patients with gastric dysplasia. Follow-up study of 67 patients. Cancer 65:2078–2085
44. Correa P, Haenszel W, Cuello C, Zavala D, Fontham E, Zarama G, Tannenbaum S, Collazos T, Ruiz B (1990) Gastric precancerous process in a high risk population: cohort follow-up. Cancer Res 50:4737–4740
45. Saraga EP, Gardiol D, Costa J (1987) Gastric dysplasia. A histological follow-up study. Am J Surg Pathol 11:788–796
46. Andersson AP, Lauritsen KB, West F, Johansen A (1987) Dysplasia in gastric mucosa: prognostic significance. Acta Chir Scand 153:29–31
47. Aste H, Sciallero S, Pugliese V, Gennaro M (1986) The clinical significance of gastric epithelial dysplasia. Endoscopy 18:174–176
48. Farini R, Pagnini CA, Farinati F, Di Mario F, Cardin F, Vianello F, Rugge M, Naccarato R (1983) Is mild gastric epithelial dysplasia an indication for follow-up? J Clin Gastroenterol 5:307–310
49. Riddell RH, Goldman H, Ransohoff DF et al (1983) Dysplasia in inflammatory bowel disease: standardized classification with provisional clinical applications. Hum Pathol 14:931–968
50. Lauwers GY, Shimizu M, Correa P et al (1999) Evaluation of gastric biopsies for neoplasia: differences between Japanese and Western pathologists. Am J Surg Pathol 23:511–518
51. Lauwers GY, Carneiro F, Graham DY, Curado M-P, Franceschi S, Montgomery E, Tatematsu M, Hattori T (2010) Gastric carcinoma. In: Bosman FT, Carneiro F, Hruban RH, Theise ND (eds) WHO Classification of tumours of the digestive system, 4th edn. IARC, Lyon, pp 48–58
52. Atkins L, Benedict EB (1956) Correlation of gross gastroscopic findings with gastroscopic biopsy in gastritis. N Engl J Med 254:641–644
53. Bah A, Saraga E, Armstrong D, Vouillamoz D, Dorta G, Duroux P, Weber B, Froehlich F, Blum AL, Schnegg JF (1995) Endoscopic features of *Helicobacter pylori*-related gastritis. Endoscopy 27:593–596
54. Calabrese C, Di Febo G, Brandi G, Morselli-Labate AM, Areni A, Scialpi C, Biasco G, Miglioli M (1999) Correlation between endoscopic features of gastric antrum, histology and *Helicobacter pylori* infection in adults. Ital J Gastroenterol Hepatol 31:359–365

55. Carpenter HA, Talley NJ (1995) Gastroscopy is incomplete without biopsy: clinical relevance of distinguishing gastropathy from gastritis. Gastroenterology 108:917–924
56. Loffeld RJ (1999) Diagnostic value of endoscopic signs of gastritis: with special emphasis to nodular antritis. Neth J Med 54:96–100
57. Redéen S, Petersson F, Jönsson KA, Borch K (2003) Relationship of gastroscopic features to histological findings in gastritis and *Helicobacter pylori* infection in a general population sample. Endoscopy 35:946–950
58. Stathopoulos G, Goldberg RD, Blackstone MO (1990) Endoscopic diagnosis of intestinal metaplasia. Gastrointest Endosc 36:544–545
59. Eshmuratov A, Nah JC, Kim N et al (2010) The correlation of endoscopic and histological diagnosis of gastric atrophy. Dig Dis Sci 55:1364–1375
60. Yan SL, Wu ST, Chen CH, Hung YH, Yang TH, Pang VS, Yeh YH (2010) Mucosal patterns of *Helicobacter pylori*-related gastritis without atrophy in the gastric corpus using standard endoscopy. World J Gastroenterol 16:496–500
61. Laine L, Cohen H, Sloane R, Marin-Sorensen M, Weinstein WM (1995) Interobserver agreement and predictive value of endoscopic findings for *H. pylori* and gastritis in normal volunteers. Gastrointest Endosc 42:420–423
62. Dinis-Ribeiro M, da Costa-Pereira A, Lopes C et al (2003) Magnification chromoendoscopy for the diagnosis of gastric intestinal metaplasia and dysplasia. Gastrointest Endosc 57:498–504
63. Areia M, Amaro P, Dinis-Ribeiro M et al (2008) External validation of a classification for methylene blue magnification chromoendoscopy in premalignant gastric lesions. Gastrointest Endosc 67:1011–1018
64. Mouzyka S, Fedoseeva A (2008) Chromoendoscopy with hematoxylin in the classification of gastric lesions. Gastric Cancer 11:15–21, discussion 21–22
65. Tanaka K, Toyoda H, Kadowaki S, Hamada Y, Kosaka R, Matsuzaki S, Shiraishi T, Imoto I, Takei Y (2008) Surface pattern classification by enhanced magnification endoscopy for identifying early gastric cancers. Gastrointest Endosc 67:430–437
66. Anagnostopoulos GK, Yao K, Kaye P et al (2007) High-resolution magnification endoscopy can reliably identify normal gastric mucosa, *Helicobacter pylori*-associated gastritis, and gastric atrophy. Endoscopy 39:202–207
67. Gonen C, Simsek I, Sarioglu S, Akpinar H (2009) Comparison of high resolution magnifying endoscopy and standard videoendoscopy for the diagnosis of *Helicobacter pylori* gastritis in routine clinical practice: a prospective study. Helicobacter 14:12–21
68. Tahara T, Shibata T, Nakamura M, Yoshioka D, Okubo M, Arisawa T, Hirata I (2009) Gastric mucosal pattern by using magnifying narrow-band imaging endoscopy clearly distinguishes histological and serological severity of chronic gastritis. Gastrointest Endosc 70:246–253
69. Bansal A, Ulusarac O, Mathur S, Sharma P (2008) Correlation between narrow band imaging and nonneoplastic gastric pathology: a pilot feasibility trial. Gastrointest Endosc 67:210–216
70. Kato M, Kaise M, Yonezawa J, Toyoizumi H, Yoshimura M, Yoshida Y, Kawamura M, Tajiri H (2010) Magnifying endoscopy with narrow-band imaging achieves superior accuracy in the differential diagnosis of superficial gastric lesions identified with white-light endoscopy: a prospective study. Gastrointest Endosc 72:523–529
71. Ezoe Y, Muto M, Horimatsu T, Minashi K, Yano T, Sano Y, Chiba T, Ohtsu A (2010) Magnifying narrow-band imaging versus magnifying white-light imaging for the differential diagnosis of gastric small depressive lesions: a prospective study. Gastrointest Endosc 71:477–484
72. Kadowaki S, Tanaka K, Toyoda H et al (2009) Ease of early gastric cancer demarcation recognition: a comparison of four magnifying endoscopy methods. J Gastroenterol Hepatol 24:1625–1630
73. Uedo N, Ishihara R, Iishi H et al (2006) A new method of diagnosing gastric intestinal metaplasia: narrow-band imaging with magnifying endoscopy. Endoscopy 38:819–824
74. Okubo M, Tahara T, Shibata T, Nakamura M, Yoshioka D, Maeda Y, Yonemura J, Ishizuka T, Arisawa T, Hirata I (2011) Changes in gastric mucosal patterns seen by magnifying NBI during *H. pylori* eradication. J Gastroenterol 46:175–182
75. Kaise M, Kato M, Urashima M et al (2009) Magnifying endoscopy combined with narrow-band imaging for differential diagnosis of superficial depressed gastric lesions. Endoscopy 41:310–315
76. Capelle LG, Haringsma J, da Vries AC, Steyerberg EW, Biermann K, van Dekken H, Kuipers EJ (2010) Narrow band imaging for the detection of gastric intestinal metaplasia and dysplasia during surveillance endoscopy. Dig Dis Sci 55:3442–3448
77. Alaboudy AA, Elbahrawy A, Matsumoto S, Yoshizawa A (2011) Conventional narrow-band imaging has good correlation with histopathological severity of *Helicobacter pylori* gastritis. Dig Dis Sci 56:1127–1130
78. Eriksson NK, Färkkilä MA, Voutilainen ME, Arkkila PE (2005) The clinical value of taking routine biopsies from the incisura angularis during gastroscopy. Endoscopy 37:532–536
79. Guarner J, Herrera-Goepfert R, Mohar A, Smith C, Schofield A, Halperin D, Sanchez L, Parsonnet J (2003) Diagnostic yield of gastric biopsy specimens when screening for preneoplastic lesions. Hum Pathol 34:28–31
80. el-Zimaity HM, Graham DY (1999) Evaluation of gastric mucosal biopsy site and number for identification of *Helicobacter pylori* or intestinal metaplasia: role of the Sydney System. Hum Pathol 30:72–77
81. Rugge M, Genta RM (2005) Staging and grading of chronic gastritis. Hum Pathol 36:228–233
82. Kashin S, Pavlov A, Gono K, Nadezhin A (2010) Endoscopic diagnosis of early gastric cancer and gastric precancerous lesions. In: Pasechnikov VD (ed) Gastric cancer: diagnosis, early prevention, and treatment, 1st edn. Nova Science, Hauppauge, pp 197–233
83. Satoh K, Kimura K, Taniguchi Y et al (1998) Biopsy sites suitable for the diagnosis of *Helicobacter pylori* infection and the assessment of the extent of atrophic gastritis. Am J Gastroenterol 93:569–573
84. de Vries AC, Haringsma J, de Vries RA, Ter Borg F, van Grieken NC, Meijer GA, van Dekken H, Kuipers EJ (2010) Biopsy strategies for endoscopic surveillance of pre-malignant gastric lesions. Helicobacter 15:259–264
85. Rugge M, Cassaro M, Pennelli G, Leandro G, Di Mario F, Farinati F (2003) Atrophic gastritis: pathology and endoscopy in the reversibility assessment. Gut 52:1387–1388
86. Ricuarte O, Gutierrez O, Cardona H, Kim JG, Dy G, el-Zimaity HM (2005) Atrophic gastritis in young children and adolescents. J Clin Pathol 58:1189–1193
87. You WC, Blot WJ, Li JY et al (1993) Precancerous gastric lesions in a population at high risk of stomach cancer. Cancer Res 53:1317–1321
88. Dursun M, Yilmaz S, Yükselen V, Kilinç N, Canoruç F, Tuzcu A (2004) Evaluation of optimal gastric mucosal biopsy site and number for identification of *Helicobacter pylori*, gastric atrophy and intestinal metaplasia. Hepatogastroenterology 51:1732–1735
89. el-Zimaity HM, al-Assi MT, Genta RM, Graham DY (1995) Confirmation of successful therapy of *Helicobacter pylori*

infection: number and site of biopsies or a rapid urease test. Am J Gastroenterol 90:1962–1964
90. el-Zimaity HM, Ota H, Graham DY, Akamatsu T, Katsuyama T (2002) Patterns of gastric atrophy in intestinal type gastric carcinoma. Cancer 94:1428–1436
91. el-Zimaity HM, Ramchatesingh J, Saeed MA, Graham DY (2001) Gastric intestinal metaplasia: subtypes and natural history. J Clin Pathol 54:679–683
92. Rugge M, Correa P, Di Mario F et al (2008) OLGA staging for gastritis: a tutorial. Dig Liver Dis 40:650–658
93. Rugge M, Genta RM, OLGA group (2005) Staging gastritis: an international proposal. Gastroenterology 129:1807–1808
94. Rugge M, Meggio A, Pennelli G, Piscioli F, Giacomelli L, De Pretis G, Graham DY (2007) Gastritis staging in clinical practice: the OLGA staging system. Gut 56:631–636
95. Satoh K, Osawa H, Yoshizawa M, Nakano H, Hirasawa T, Kihira K, Sugano K (2008) Assessment of atrophic gastritis using the OLGA system. Helicobacter 13:225–229
96. Rugge M, de Boni M, Pennelli G, de Bona M, Giacomelli L, Fassan M, Basso D, Plebani M, Graham DY (2010) Gastritis OLGA-staging and gastric cancer risk: a twelve year clinico-pathological follow-up study. Aliment Pharmacol Ther 31:1104–1111
97. el-Zimaity HM, Graham DY, al-Assi MT, Malaty H, Karttunen TJ, Graham DP, Huberman RM, Genta RM (1996) Interobserver variation in the histopathological assessment of *Helicobacter pylori* gastritis. Hum Pathol 27:35–41
98. Capelle LG, de Vries AC, Haringsma J, Ter Borg F, de Vries RA, Bruno MJ, van Dekken H, Meijer J, van Grieken NC, Kuipers EJ (2010) The staging of gastritis with the OLGA system by using intestinal metaplasia as an accurate alternative for atrophic gastritis. Gastrointest Endosc 71:1150–1158
99. Guarner J, Herrera-Goepfert R, Mohar A, Sanchez L, Halperin D, Ley C, Parsonnet J (1999) Interobserver variability in application of the revised Sydney classification for gastritis. Hum Pathol 30:1431–1434
100. Kuipers EJ (2003) In through the out door: serology for atrophic gastritis. Eur J Gastroenterol Hepatol 15:877–879
101. Dinis-Ribeiro M, Yamaki G, Miki K, Costa-Pereira A, Matsukawa M, Kurihara M (2004) Meta-analysis on the validity of pepsinogen test for gastric carcinoma, dysplasia or chronic atrophic gastritis screening. J Med Screen 11:141–147
102. Graham DY, Nurgalieva ZZ, El-Zimaity HM, Opekun AR, Campos A, Guerrero L, Chavez A, Cardenas V (2006) Noninvasive versus histologic detection of gastric atrophy in a Hispanic population in North America. Clin Gastroenterol Hepatol 4:306–314
103. Haj-Sheykholeslami A, Rakhshani N, Amirzargar A, Rafiee R, Shahidi SM, Nikbin B, Khoshavi F, Massarrat S (2008) Serum pepsinogen I, pepsinogen II, and gastrin 17 in relatives of gastric cancer patients: comparative study with type and severity of gastritis. Clin Gastroenterol Hepatol 6:174–179
104. Hartleb M, Wandzel P, Waluga M, Matyszczyk B, Boldys H, Romañczyk T (2004) Non-endoscopic diagnosis of multifocal atrophic gastritis; efficacy of serum gastrin-17, pepsinogens and *Helicobacter pylori* antibodies. Acta Gastroenterol Belg 67:320–326
105. Iijima K, Abe Y, Kikuchi R, Koike T, Ohara S, Sipponen P, Shimosegawa T (2009) Serum biomarker tests are useful in delineating between patients with gastric atrophy and normal, healthy stomach. World J Gastroenterol 15:853–859
106. Inoue M, Kobayashi S, Matsuura A, Hamajima N, Tajima K, Tominaga S (1998) Agreement of endoscopic findings and serum pepsinogen levels as an indicator of atrophic gastritis. Cancer Epidemiol Biomarkers Prev 7:261–263
107. Kim HY, Kim N, Kang JN, Park YS, Lee DH, Kim YR, Kim JS, Jung HC, Song IS (2009) Clinical meaning of pepsinogen test and *Helicobacter pylori* serology in the health check-up population in Korea. Eur J Gastroenterol Hepatol 21:606–612
108. Knight T, Wyatt J, Wilson A, Greaves S, Newell D, Hengels K, Corlett M, Webb P, Forman D, Elder J (1996) *Helicobacter pylori* gastritis and serum pepsinogen levels in a healthy population: development of a biomarker strategy for gastric atrophy in high risk groups. Br J Cancer 73:819–824
109. Leja M, Kupcinkas L, Funka K, Sudraba A, Jonaitis L, Ivanauskas A, Janciauskas D, Kiudelis G, Chiu HM, Lin JT (2009) The validity of a biomarker method for indirect detection of gastric mucosal atrophy versus standard histopathology. Dig Dis Sci 54:2377–2384
110. Ley C, Mohar A, Guarner J, Herrera-Goepfert R, Figueroa LS, Halperin D, Parsonnet J (2001) Screening markers for chronic atrophic gastritis in Chiapas, Mexico. Cancer Epidemiol Biomarkers Prev 10:107–112
111. Nardone G, Rocco A, Staibano S, Mezza E, Autiero G, Compare D, De Rosa G, Budillon G (2005) Diagnostic accuracy of the serum profile of gastric mucosa in relation to histological and morphometric diagnosis of atrophy. Aliment Pharmacol Ther 22:1139–1146
112. Pasechnikov VD, Chukov SZ, Kotelevets SM, Mostovov AN, Mernova VP, Polyakova MB (2005) Invasive and non-invasive diagnosis of *Helicobacter pylori*-associated atrophic gastritis: a comparative study. Scand J Gastroenterol 40:297–301
113. Ricci C, Vakil N, Rugge M et al (2004) Serological markers for gastric atrophy in asymptomatic patients infected with *Helicobacter pylori*. Am J Gastroenterol 99:1910–1915
114. Rollan A, Ferreccio C, Gederlini A, Serrano C, Torres J, Harris P (2006) Noninvasive diagnosis of gastric mucosal atrophy in an asymptomatic population with high prevalence of gastric cancer. World J Gastroenterol 12:7172–7178
115. Sierra R, Une C, Ramírez V et al (2006) Association of serum pepsinogen with atrophic body gastritis in Costa Rica. Clin Exp Med 6:72–78
116. Sitas F, Smallwood R, Jewell D, Millard PR, Newell DG, Meuwissen SG, Moses S, Zwiers A, Forman D (1993) Serum anti-*Helicobacter pylori* IgG antibodies and pepsinogens A and C as serological markers of chronic atrophic gastritis. Cancer Epidemiol Biomarkers Prev 2:119–123
117. Storskrubb T, Aro P, Ronkainen J et al (2008) Serum biomarkers provide an accurate method for diagnosis of atrophic gastritis in a general population: the Kalixanda study. Scand J Gastroenterol 43:1448–1455
118. Sun LP, Gong YH, Wang L, Yuan Y (2007) Serum pepsinogen levels and their influencing factors: a population-based study in 6990 Chinese from North China. World J Gastroenterol 13:6562–6567
119. Wu KC, Li HT, Qiao TD et al (2004) Diagnosis of atrophic body gastritis in Chinese patients by measuring serum pepsinogen. Chin J Dig Dis 5:22–27
120. Väänänen H, Vauhkonen M, Helske T et al (2003) Non-endoscopic diagnosis of atrophic gastritis with a blood test. Correlation between gastric histology and serum levels of gastrin-17 and pepsinogen I: a multicentre study. Eur J Gastroenterol Hepatol 15:885–891
121. Cao Q, Ran ZH, Xiao SD (2007) Screening of atrophic gastritis and gastric cancer by serum pepsinogen, gastrin-17 and *Helicobacter pylori* immunoglobulin G antibodies. J Dig Dis 8:15–22
122. Chung HW, Kim JW, Lee JH, Song SY, Chung JB, Kwon OH, Lim JB (2009) Comparison of the validity of three biomarkers for gastric cancer screening: carcinoembryonic antigen, pepsinogens, and high sensitive C-reactive protein. J Clin Gastroenterol 43:19–26
123. Kiyohira K, Yoshihara M, Ito M, Haruma K, Tanaka S, Chayama K (2003) Serum pepsinogen concentration as a marker of *Helicobacter pylori* infection and the histologic grade of gastritis:

evaluation of gastric mucosa by serum pepsinogen levels. J Gastroenterol 38:332–338
124. Oksanen A, Sipponen P, Miettinen A, Sarna S, Rautelin H (2000) Evaluation of blood tests to predict normal gastric mucosa. Scand J Gastroenterol 35:791–795
125. Di Mario F, Cavallar LG, Moussa AM et al (2006) Usefulness of serum pepsinogens in *Helicobacter pylori* chronic gastritis: relationship with inflammation, activity, and density of the bacterium. Dig Dis Sci 51:1791–1795
126. Kreuning J, Lindeman J, Biemond I, Lamers CB (1995) Serological parameters in assessment of degree of gastritis in healthy volunteers. Dig Dis Sci 40:609–614
127. Con SA, Con-Wong R, Con-Chin GR et al (2007) Serum pepsinogen levels, *Helicobacter pylori* CagA status, and cytokine gene polymorphisms associated with gastric premalignant lesions in Costa Rica. Cancer Epidemiol Biomarkers Prev 16:2631–2636
128. Dinis-Ribeiro M, da Costa-Pereira A, Lopes C, Barbosa J, Guilherme M, Moreira-Dias L, Lomba-Viana H, Silva R, Abreu N, Lomba-Viana R (2004) Validity of serum pepsinogen I/II ratio for the diagnosis of gastric epithelial dysplasia and intestinal metaplasia during the follow-up of patients at risk for intestinal-type gastric adenocarcinoma. Neoplasia 6:449–456
129. Urita Y, Hike K, Torii N, Kikuchi Y, Kanda E, Sasajima M, Miki K (2004) Serum pepsinogens as a predicator of the topography of intestinal metaplasia in patients with atrophic gastritis. Dig Dis Sci 49:795–801
130. de Vries AC, Haringsma J, de Vries RA, ter Borg F, Nagtzaam NM, Steyerberg EW, van Dekken H, Kuipers EJ (2009) The use of clinical, histologic, and serologic parameters to predict the intragastric extent of intestinal metaplasia: a recommendation for routine practice. Gastrointest Endosc 70:18–25
131. Watabe H, Mitsushima T, Yamaji Y, Okamoto M, Wada R, Kokubo T, Doi H, Yoshida H, Kawabe T, Omata M (2005) Predicting the development of gastric cancer from combining *Helicobacter pylori* antibodies and serum pepsinogen status: a prospective endoscopic cohort study. Gut 54:764–768
132. Yamaji Y, Watabe H, Yoshida H, Kawabe T, Wada R, Mitsushima T, Omata M (2009) High-risk population for gastric cancer development based on serum pepsinogen status and lifestyle factors. Helicobacter 14:81–86
133. Yanaoka K, Oka M, Mukoubayashi C et al (2008) Cancer high-risk subjects identified by serum pepsinogen tests: outcomes after 10-year follow-up in asymptomatic middle-aged males. Cancer Epidemiol Biomarkers Prev 17:838–845
134. Yanaoka K, Oka M, Yoshimura N et al (2008) Risk of gastric cancer in asymptomatic, middle-aged Japanese subjects based on serum pepsinogen and *Helicobacter pylori* antibody levels. Int J Cancer 123:917–926
135. Ohata H, Kitauchi S, Yoshimura N et al (2004) Progression of chronic atrophic gastritis associated with *Helicobacter pylori* infection increases risk of gastric cancer. Int J Cancer 109:138–143
136. Oishi Y, Kiyohara Y, Kubo M et al (2006) The serum pepsinogen test as a predictor of gastric cancer: the Hisayama study. Am J Epidemiol 163:629–637
137. Dinis-Ribeiro M, da Costa-Pereira A, Lopes C, Moreira-Dias L (2007) Feasibility and cost-effectiveness of using magnification chromoendoscopy and pepsinogen serum levels for the follow-up of patients with atrophic chronic gastritis and intestinal metaplasia. J Gastroenterol Hepatol 22:1594–1604
138. Miki K, Fujishiro M, Kodashima S, Yahagi N (2009) Long-term results of gastric cancer screening using the serum pepsinogen test method among an asymptomatic middle-aged Japanese population. Dig Endosc 21:78–81
139. Aromaa A, Kosunen TU, Knekt P, Maatela J, Teppo L, Heinonen OP, Härkönen M, Hakama MK (1996) Circulating anti-*Helicobacter pylori* immunoglobulin A antibodies and low serum pepsinogen I level are associated with increased risk of gastric cancer. Am J Epidemiol 144:142–149
140. Fukuda H, Saito D, Hayashi S et al (1995) *Helicobacter pylori* infection, serum pepsinogen level and gastric cancer: a case–control study in Japan. Jpn J Cancer Res 86:64–71
141. Kikuchi S, Wada O, Miki K, Nakajima T, Nishi T, Kobayashi O, Inaba Y (1994) Serum pepsinogen as a new marker for gastric carcinoma among young adults. Research Group on Prevention of Gastric Carcinoma among Young Adults. Cancer 73:2695–2702
142. Knekt P, Teppo L, Aromaa A, Rissanen H, Kosunen TU (2006) *Helicobacter pylori* IgA and IgG antibodies, serum pepsinogen I and the risk of gastric cancer: changes in the risk with extended follow-up period. Int J Cancer 119:702–705
143. Kodoi A, Yoshihara M, Sumii K, Haruma K, Kajiyama G (1995) Serum pepsinogen in screening for gastric cancer. J Gastroenterol 30:452–460
144. Kokkola A, Louhimo J, Puolakkainen P, Alfthan H, Haglund C, Rautelin H (2005) *Helicobacter pylori* infection and low serum pepsinogen I level as risk factors for gastric carcinoma. World J Gastroenterol 11:1032–1036
145. Kwak MS, Kim N, Lee HS, Lee HE, Jung HC, Song IS (2010) Predictive power of serum pepsinogen tests for the development of gastric cancer in comparison to the histologic risk index. Dig Dis Sci 55:2275–2282
146. Miki K, Ichinose M, Kawamura N et al (1989) The significance of low serum pepsinogen levels to detect stomach cancer associated with extensive chronic gastritis in Japanese subjects. Jpn J Cancer Res 80:111–114
147. Nomura AM, Stemmermann GN, Samloff IM (1980) Serum pepsinogen I as a predictor of stomach cancer. Ann Intern Med 93:537–540
148. Parsonnet J, Samloff IM, Nelson LM, Orentreich N, Vogelman JH, Friedman GD (1993) *Helicobacter pylori*, pepsinogen, and risk for gastric adenocarcinoma. Cancer Epidemiol Biomarkers Prev 2:461–466
149. Parthasarathy G, Maroju NK, Kate V, Ananthakrishnan N, Sridhar mg (2007) Serum pepsinogen I and II levels in various gastric disorders with special reference to their use as a screening test for carcinoma stomach. Trop Gastroenterol 28:166–170
150. Ren JS, Kamangar F, Qiao YL, Taylor PR, Liang H, Dawsey SM, Liu B, Fan JH, Abnet CC (2009) Serum pepsinogens and risk of gastric and oesophageal cancers in the General Population Nutrition Intervention Trial cohort. Gut 58:636–642
151. Sasazuki S, Inoue M, Iwasaki M, Otani T, Yamamoto S, Ikeda S, Hanaoka T, Tsugane S, Japan Public Health Center Study Group (2006) Effect of *Helicobacter pylori* infection combined with CagA and pepsinogen status on gastric cancer development among Japanese men and women: a nested case–control study. Cancer Epidemiol Biomarkers Prev 15:1341–1347
152. Shiotani A, Iishi H, Uedo N, Kumamoto M, Nakae Y, Ishiguro S, Tatsuta M, Graham DY (2005) Histologic and serum risk markers for noncardia early gastric cancer. Int J Cancer 115:463–469
153. So JB, Yeoh KG, Moochala S, Chachlani N, Ho J, Wong WK, Mack P, Goh PM (2002) Serum pepsinogen levels in gastric cancer patients and their relationship with *Helicobacter pylori* infection: a prospective study. Gastric Cancer 5:228–232
154. Sugiu K, Kamada T, Ito M, Kaya S, Tanaka A, Kusunoki H, Hata J, Haruma K (2006) Anti-parietal cell antibody and serum pepsinogen assessment in screening for gastric carcinoma. Dig Liver Dis 38:303–307
155. Yoshihara M, Hiyama T, Yoshida S, Ito M, Tanaka S, Watanabe Y, Haruma K (2007) Reduction in gastric cancer mortality by screening based on serum pepsinogen concentration: a case–control study. Scand J Gastroenterol 42:760–764

156. Hattori Y, Tashiro H, Kawamoto T, Kodama Y (1995) Sensitivity and specificity of mass screening for gastric cancer using the measurement of serum pepsinogens. Jpn J Cancer Res 86:1210–1215
157. Kitahara F, Kobayashi K, Sato T, Kojima Y, Araki T, Fujino MA (1999) Accuracy of screening for gastric cancer using serum pepsinogen concentrations. Gut 44:693–697
158. Westerveld BD, Pals G, Lamers CB et al (1987) Clinical significance of pepsinogen A isozymogens, serum pepsinogen A and C levels, and serum gastrin levels. Cancer 59:952–958
159. You WC, Blot WJ, Zhang L et al (1993) Serum pepsinogens in relation to precancerous gastric lesions in a population at high risk for gastric cancer. Cancer Epidemiol Biomarkers Prev 2:113–117
160. Yoshihara M, Sumii K, Haruma K, Kiyohira K, Hattori N, Kitadai Y, Komoto K, Tanaka S, Kajiyama G (1998) Correlation of ratio of serum pepsinogen I and II with prevalence of gastric cancer and adenoma in Japanese subjects. Am J Gastroenterol 93:1090–1096
161. Miki K, Ichinose M, Ishikawa KB et al (1993) Clinical application of serum pepsinogen I and II levels for mass screening to detect gastric cancer. Jpn J Cancer Res 84:1086–1090
162. Miki K, Morita M, Sasajima M, Hoshina R, Kanda E, Urita Y (2003) Usefulness of gastric cancer screening using the serum pepsinogen test method. Am J Gastroenterol 98:735–739
163. Pharoah PD, Guilford P, Caldas C, International Gastric Cancer Linkage Consortium (2001) Incidence of gastric cancer and breast cancer in CDH1 (E-cadherin) mutation carriers from hereditary diffuse gastric cancer families. Gastroenterology 121:1348–1353
164. Fitzgerald RC, Hardwick R, Huntsman D et al (2010) Hereditary diffuse gastric cancer: updated consensus guidelines for clinical management and directions for future research. J Med Genet 47:436–444
165. Watson P, Vasen HF, Mecklin JP, Bernstein I, Aarnio M, Järvinen HJ, Myrhøj T, Sunde L, Wijnen JT, Lynch HT (2008) The risk of extra-colonic, extra-endometrial cancer in the Lynch syndrome. Int J Cancer 123:444–449
166. Capelle LG, Van Grieken NC, Lingsma HF, Steyerberg EW, Klokman WJ, Bruno MJ, Vasen HF, Kuipers EJ (2010) Risk and epidemiological time trends of gastric cancer in Lynch syndrome carriers in the Netherlands. Gastroenterology 138:487–492
167. Giardiello FM, Brensinger JD, Tersmette AC, Goodman SN, Petersen GM, Booker SV, Cruz-Correa M, Offerhaus JA (2000) Very high risk of cancer in familial Peutz–Jeghers syndrome. Gastroenterology 119:1447–1453
168. van Lier mg, Westerman AM, Wagner A, Looman CW, Wilson JH, de Rooij FW, Lemmens VE, Kuipers EJ, Mathus-Vliegen EM, van Leerdam ME (2011) High cancer risk and increased mortality in patients with Peutz–Jeghers syndrome. Gut 60:141–147
169. Offerhaus GJ, Giardiello FM, Krush AJ, Booker SV, Tersmette AC, Kelley NC, Hamilton SR (1992) The risk of upper gastrointestinal cancer in familial adenomatous polyposis. Gastroenterology 102:1980–1982
170. Yaghoobi M, Bijarchi R, Narod SA (2009) Family history and the risk of gastric cancer. Br J Cancer 102:237–242
171. Bakir T, Can G, Erkul S, Siviloglu C (2000) Stomach cancer history in the siblings of patients with gastric carcinoma. Eur J Cancer Prev 9:401–408
172. La Vecchia C, Negri E, Franceschi S, Gentile A (1992) Family history and the risk of stomach and colorectal cancer. Cancer 70:50–55
173. Palli D, Galli M, Caporaso NE, Cipriani F, Decarli A, Saieva C, Fraumeni JF Jr, Buiatti E (1994) Family history and risk of stomach cancer in Italy. Cancer Epidemiol Biomarkers Prev 3:15–18
174. García-González MA, Lanas A, Quintero E et al (2007) Gastric cancer susceptibility is not linked to pro- and anti-inflammatory cytokine gene polymorphisms in whites: a nationwide multicenter study in Spain. Am J Gastroenterol 102:1878–1892
175. Dhillon PK, Farrow DC, Vaughan TL et al (2001) Family history of cancer and risk of esophageal and gastric cancers in the United States. Int J Cancer 93:148–152
176. Minami Y, Tateno H (2003) Associations between cigarette smoking and the risk of four leading cancers in Miyagi Prefecture, Japan: a multi-site case–control study. Cancer Sci 94:540–547
177. Eto K, Ohyama S, Yamaguchi T, Wada T, Suzuki Y, Mitsumori N, Kashiwagi H, Anazawa S, Yanaga K, Urashima M (2006) Familial clustering in subgroups of gastric cancer stratified by histology, age group and location. Eur J Sur Oncol 32:743–748
178. Hong SH, Kim JW, Kim HG, Park IK, Ryoo JW, Lee CH, Sohn YK, Lee JY (2006) Glutathione S-transferases (GSTM1, GSTT1 and GSTP1) and N-acetyltransferase 2 polymorphisms and the risk of gastric cancer. J Prev Med Public Health 39:135–140
179. Foschi R, Lucenteforte E, Bosetti C, Bertuccio P, Tavani A, La Vecchia C, Negri E (2008) Family history of cancer and stomach cancer risk. Int J Cancer 123:1429–1432
180. Bernini M, Barbi S, Roviello F, Scarpa A, Moore P, Pedrazzani C, Beghelli S, Marrelli D, de Manzoni G (2006) Family history of gastric cancer: a correlation between epidemiologic findings and clinical data. Gastric Cancer 9:9–13
181. Rokkas T, Sechopoulos P, Pistiolas D, Margantinis G, Koukoulis G (2010) *Helicobacter pylori* infection and gastric histology in first-degree relatives of gastric cancer patients: a meta-analysis. Eur J Gastroenterol Hepatol 22:1128–1133
182. IARC Working Group on the Evaluation of Carcinogenic Risks to Humans (1994) Schistosomes, liver flukes and *Helicobacter pylori*. IARC Working Group on the Evaluation of Carcinogenic Risks to Humans Lyon, 7–14 June 1994. IARC Monogr Eval Carcinog Risks Hum 61:1–241
183. Figueiredo C, Machado JC, Pharoah P et al (2002) *Helicobacter pylori* and interleukin 1 genotyping: an opportunity to identify high-risk individuals for gastric carcinoma. J Natl Cancer Inst 94:1680–1687
184. Amieva MR, El-Omar EM (2008) Host–bacterial interactions in *Helicobacter pylori* infection. Gastroenterology 134:306–323
185. Machado JC, Figueiredo C, Canedo P et al (2003) A proinflammatory genetic profile increases the risk for chronic atrophic gastritis and gastric carcinoma. Gastroenterology 125:364–371
186. Huang JQ, Zheng GF, Sumanac K, Irvine EJ, Hunt RH (2003) Meta-analysis of the relationship between cagA seropositivity and gastric cancer. Gastroenterology 125:1636–1644
187. Basso D, Zambon CF, Letley DP et al (2008) Clinical relevance of *Helicobacter pylori* cagA and vacA gene polymorphisms. Gastroenterology 135:91–99
188. El-Omar EM, Carrington M, Chow WH (2000) Interleukin-1 polymorphisms associated with increased risk of gastric cancer. Nature 404:398–402
189. Yin M, Hu Z, Tan D, Ajani JA, Wei Q (2009) Molecular epidemiology of genetic susceptibility to gastric cancer: focus on single nucleotide polymorphisms in gastric carcinogenesis. Am J Transl Res 1:44–54
190. Persson C, Canedo P, Machado JC, El-Omar EM, Forman D (2011) Polymorphisms in inflammatory response genes and their association with gastric cancer: a HuGE systematic review and meta-analyses. Am J Epidemiol 173:259–270
191. Wang P, Xia HH, Zhang JY, Dai LP, Xu XQ, Wang KJ (2007) Association of interleukin-1 gene polymorphisms with gastric cancer: a meta-analysis. Int J Cancer 120:552–562
192. Camargo MC, Mera R, Correa P, Peek RM Jr, Fontham ET, Goodman KJ, Piazuelo MB, Sicinschi L, Zabaleta J, Schneider

BG (2006) Interleukin-1beta and interleukin-1 receptor antagonist gene polymorphisms and gastric cancer: a meta-analysis. Cancer Epidemiol Biomarkers Prev 15:1674–1687
193. Xue H, Lin B, Ni P, Xu H, Huang G (2010) Interleukin-1B and interleukin-1 RN polymorphisms and gastric carcinoma risk: a meta-analysis. J Gastroenterol Hepatol 25:1604–1617
194. Kamangar F, Cheng C, Abnet CC, Rabkin CS (2006) Interleukin-1B polymorphisms and gastric cancer risk—a meta-analysis. Cancer Epidemiol Biomarkers Prev 15:1920–1928
195. Loh M, Koh KX, Yeo BH, Song CM, Chia KS, Zhu F, Yeoh KG, Hill J, Iacopetta B, Soong R (2009) Meta-analysis of genetic polymorphisms and gastric cancer risk: variability in associations according to race. Eur J Cancer 45:2562–2568
196. Schlemper RJ, Riddell RH, Kato Y et al (2000) The Vienna classification of gastrointestinal epithelial neoplasia. Gut 47:251–255
197. Rugge M, Leandro G, Farinati F, Di Mario F, Sonego F, Cassaro M, Guido M, Ninfo V (1995) Gastric epithelial dysplasia. How clinicopathologic background relates to management. Cancer 76:376–382
198. Rugge M, Cassaro M, Di Mario F, Leo G, Leandro G, Russo VM, Pennelli G, Farinati F, Interdisciplinary Group on Gastric Epithelial Dysplasia (IGGED) (2003) The long term outcome of gastric non-invasive neoplasia. Gut 52:1111–1116
199. de Jonge PJ, van Blankenstein M, Looman CW, Casparie MK, Meijer GA, Kuipers EJ (2010) Risk of malignant progression in patients with Barrett's oesophagus: a Dutch nationwide cohort study. Gut 59:1030–1036
200. Stryker SJ, Wolff BG, Culp CE, Libbe SD, Ilstrup DM, MacCarty RL (1987) Natural history of untreated colonic polyps. Gastroenterology 93:1009–1013
201. Munkholm P (2003) Review article: the incidence and prevalence of colorectal cancer in inflammatory bowel disease. Aliment Pharmacol Ther 18(Suppl 2):1–5
202. Weinstein WM, Goldstein N (1994) Gastric dysplasia and its management. Gastroenterology 107:1543–1559
203. Ching CK (1995) Can we justify resecting all gastric epithelial dysplastic lesions? Gastroenterology 108:1955–1956
204. Abraham SC, Montgomery EA, Singh VK, Yardley JH, Wu TT (2000) Gastric adenomas: intestinal type and gastric type adenomas differ in the risk of adenocarcinoma and presence of background mucosal pathology. Am J Surg Pathol 26:1276–1285
205. Hosokawa O, Watanabe K, Hatorri M, Douden K, Hayashi H, Kaizaki Y (2001) Detection of gastric cancer by repeat endoscopy within a short time after negative examination. Endoscopy 33:301–305
206. de Dombal FT, Price AB, Thompson H, Williams GT, Morgan AG, Softley A, Clamp SE, Unwin BJ (1990) The British Society of Gastroenterology early gastric cancer/dysplasia survey: an interim report. Gut 31:115–120
207. Sipponen P, Kekki M, Siurali M (1983) Atrophic chronic gastritis and intestinal metaplasia in gastric cancer: comparison with a representative population sample. Cancer 52:1062–1068
208. Hull MJ, Mino-Kenudson M, Nishioka NS et al (2006) Endoscopic mucosal resection: an improved diagnostic procedure for early gastroesophageal epithelial neoplasms. Am J Surg Pathol 30:114–118
209. Kim YJ, Park JC, Kim JH, Shin SK, Lee SK, Lee YC, Chung JB (2010) Histologic diagnosis based on forceps biopsy is not adequate for determining endoscopic treatment of gastric adenomatous lesions. Endoscopy 42:620–626
210. Kim ES, Jeon SW, Park SY et al (2009) Where has the tumor gone? The characteristics of cases of negative pathologic diagnosis after endoscopic mucosal resection. Endoscopy 41:739–745
211. Cassaro M, Rugge M, Gutierrez O, Leandro G, Graham DY, Genta RM (2000) Topographic patterns of intestinal metaplasia and gastric cancer. Am J Gastroenterol 95:1431–1438
212. Morson BC (1955) Carcinoma arising from areas of intestinal metaplasia in the gastric mucosa. Br J Cancer 9:377–385
213. Vannella L, Lahner E, Osborn J, Bordi C, Miglione M, Delle Fave G, Annibale B (2010) Risk factors for progression to gastric neoplastic lesions in patients with atrophic gastritis. Aliment Pharmacol Ther 31:1042–1050
214. Lahner E, Bordi C, Cattaruzza MS, Iannoni C, Milione M, Delle Fave G, Annibale B (2005) Long-term follow-up in atrophic body gastritis patients: atrophy and intestinal metaplasia are persistent lesions irrespective of *Helicobacter pylori* infection. Aliment Pharmacol Ther 22:471–481
215. Van Zanten SJ, Dixon MF, Lee A (1999) The gastric transitional zones: neglected links between gastroduodenal pathology and helicobacter ecology. Gastroenterology 116:1217–1229
216. Kimura A, Takemoto T (1969) An endoscopic recognition of the atrophic border and its significance in chronic gastritis. Endoscopy 1:87–97
217. Rokkas T, Filipe MI, Sladen GE (1991) Detection of an increased incidence of early gastric cancer in patients with intestinal metaplasia type III who are closely followed up. Gut 32:1110–1113
218. Tosi P, Filipe MI, Luzi P, Miracco C, Santopietro R, Lio R, Sforza V, Barbini P (1993) Gastric intestinal metaplasia type III cases are classified as low-grade dysplasia on the basis of morphometry. J Pathol 169:73–78
219. Ramesar KC, Sanders DS, Hopwood D (1987) Limited value of type III intestinal metaplasia in predicting risk of gastric carcinoma. J Clin Pathol 40:1287–1290
220. Conchillo JM, Houben G, de Bruïne A, Stockbrügger R (2001) Is type III intestinal metaplasia an obligatory precancerous lesion in intestinal-type gastric carcinoma? Eur J Cancer Prev 10:307–312
221. Nozaki K, Shimizu N, Ikehara Y, Inoue M, Tsukamoto T, Inada K, Tanaka H, Kumagai T, Kaminishi M, Tatematsu M (2003) Effect of early eradication on *Helicobacter pylori*-related gastric carcinogenesis in Mongolian gerbils. Cancer Sci 94:235–239
222. Shimizu N, Ikehara Y, Inada K et al (2000) Eradication diminishes enhancing effects of *Helicobacter pylori* infection on glandular stomach carcinogenesis in Mongolian gerbils. Cancer Res 60:1512–1514
223. Maruta F, Sugiyama A, Ishizone S, Miyagawa S, Ota H, Katsuyama T (2005) Eradication of *Helicobacter pylori* decreases mucosal alterations linked to gastric carcinogenesis in Mongolian gerbils. J Gastroenterol 40:104–105
224. Pimanov SI, Makarenko EV, Voropaeva AV, Matveenko ME, Voropaev EV (2008) *Helicobacter pylori* eradication improves gastric histology and decreases serum gastrin, pepsinogen I and pepsinogen II levels in patients with duodenal ulcer. J Gastroenterol Hepatol 23:1666–1671
225. Rokkas T, Pistiolas D, Sechopoulos P, Robotis I, Margantinis G (2007) The long-term impact of *Helicobacter pylori* eradication on gastric histology: a systematic review and meta-analysis. Helicobacter 12(Suppl 2):32–38
226. de Vries AC, Kuipers EJ (2007) Review article: *Helicobacter pylori* eradication for the prevention of gastric cancer. Aliment Pharmacol Ther 26(Suppl 2):25–35
227. Wang J, Xu L, Shi R, Huang X, Li SW, Huang Z, Zhang G (2011) Gastric atrophy and intestinal metaplasia before and after *Helicobacter pylori* eradication: a meta-analysis. Digestion 83:253–260
228. Annibale B, Aprile MR, D'ambra G, Caruana P, Bordi C, Delle Fave G (2000) Cure of *Helicobacter pylori* infection in atrophic body gastritis patients does not improve mucosal atrophy but reduces hypergastrinemia and its related effects on body ECL-cell hyperplasia. Aliment Pharmacol Ther 14:625–634
229. Satoh K, Kimura K, Takimoto T, Kihira K (1998) A follow-up study of atrophic gastritis and intestinal metaplasia after eradication of *Helicobacter pylori*. Helicobacter 3:236–240

230. Correa P, Fontham ET, Bravo JC et al (2000) Chemoprevention of gastric dysplasia: randomized trial of antioxidant supplements and anti-*Helicobacter pylori* therapy. J Natl Cancer Inst 92:1881–1888
231. Mera R, Fontham ET, Bravo LE, Bravo JC, Piazuelo MB, Camargo MC, Correa P (2005) Long term follow up of patients treated for *Helicobacter pylori* infection. Gut 54:1536–1540
232. Wong BC, Lam SK, Wong WM (2004) *Helicobacter pylori* eradication to prevent gastric cancer in a high-risk region of China: a randomized controlled trial. JAMA 291:187–194
233. Fuccio L, Zagari RM, Minardi ME, Bazzoli F (2007) Systematic review: *Helicobacter pylori* eradication for the prevention of gastric cancer. Aliment Pharmacol Ther 25:133–141
234. Fuccio L, Zagari RM, Eusebi LH, Laterza L, Cennamo V, Ceroni L, Grilli D, Bazzoli F (2009) Meta-analysis: can *Helicobacter pylori* eradication treatment reduce the risk for gastric cancer? Ann Intern Med 151:121–128
235. Kim N, Park RY, Cho SI, Lim SH, Lee KH, Lee W, Kang HM, Lee HS, Jung HC, Song IS (2008) *Helicobacter pylori* infection and development of gastric cancer in Korea: long-term follow-up. J Clin Gastroenterol 42:448–454
236. Leung WK, Lin SR, Ching JY, To KF, Ng EK, Chan FK, Lau JY, Sung JJ (2004) Factors predicting progression of gastric intestinal metaplasia: results of a randomised trial on *Helicobacter pylori* eradication. Gut 53:1244–1249
237. You WC, Brown LM, Zhang L et al (2006) Randomized double-blind factorial trial of three treatments to reduce the prevalence of precancerous gastric lesions. J Natl Cancer Inst 98:974–983
238. Take S, Mizuno M, Ishiki K, Nagahara Y, Yoshida T, Yokota K, Oguma K, Okada H, Shiratori Y (2005) The effect of eradicating *Helicobacter pylori* on the development of gastric cancer in patients with peptic ulcer disease. Am J Gastroenterol 100:1037–1042
239. Take S, Mizuno M, Ishiki K, Yoshida T, Ohara N, Yokota K, Oguma K, Okada H, Yamamoto K (2011) The long-term risk of gastric cancer after the successful eradication of *Helicobacter pylori*. J Gastroenterol 46:318–324
240. Fukase K, Kato M, Kikuchi S et al (2008) Effect of eradication of *Helicobacter pylori* on incidence of metachronous gastric carcinoma after endoscopic resection of early gastric cancer: an open-label, randomised controlled trial. Lancet 372:392–397
241. Uemura N, Mukai T, Okamoto S, Yamaguchi S, Mashiba H, Taniyama K, Sasaki N, Haruma K, Sumii K, Kajiyama G (1997) Effect of *Helicobacter pylori* eradication on subsequent development of cancer after endoscopic resection of early gastric cancer. Cancer Epidemiol Biomarkers Prev 6:639–642
242. Toyokawa T, Suwaki K, Miyake Y, Nakatsu M, Ando M (2010) Eradication of *Helicobacter pylori* infection improved gastric mucosal atrophy and prevented progression of intestinal metaplasia, especially in the elderly population: a long-term prospective cohort study. J Gastroenterol Hepatol 25:544–547
243. Yang HB, Sheu BS, Wang ST, Cheng HC, Chang WL, Chen WY (2009) H. pylori eradication prevents the progression of gastric intestinal metaplasia in reflux esophagitis patients using long-term esomeprazole. Am J Gastroenterol 104:1642–1649
244. Malfertheiner P, Megraud F, O'Morain C, Bazzoli F, El-Omar E, Graham D, Hunt R, Rokkas T, Vakil N, Kuipers EJ (2007) Current concepts in the management of *Helicobacter pylori* infection: the Maastricht III Consensus Report. Gut 56:772–781
245. Lam SK, Talley NJ (1998) Report of the 1997 Asia Pacific Consensus Conference on the management of *Helicobacter pylori* infection. J Gastroenterol Hepatol 13:1–12
246. Malfertheiner P, Mégraud F, O'Morain C, Hungin AP, Jones R, Axon A, Graham DY, Tytgat G, European Helicobacter Pylori Study Group (EHPSG) (2002) Current concepts in the management of *Helicobacter pylori* infection—the Maastricht 2-2000 Consensus Report. Aliment Pharmacol Ther 16:167–180
247. Fock KM, Katelaris P, Sugano K (2009) Second Asia-Pacific Consensus Guidelines for *Helicobacter pylori* infection. J Gastroenterol Hepatol 24:1587–1600
248. Shin DW, Yun YH, Choi IJ, Koh E, Park SM (2009) Cost–effectiveness of eradication of *Helicobacter pylori* in gastric cancer survivors after endoscopic resection of early gastric cancer. Helicobacter 14:536–544
249. Wang WH, Huang JQ, Zheng GF, Lam SK, Karlberg J, Wong BC (2003) Nonsteroidal anti-inflammatory drug use and the risk of gastric cancer: a systematic review and meta-analysis. J Natl Cancer Inst 95:1784–1791
250. Tian W, Zhao Y, Liu S, Li X (2010) Meta-analysis on the relationship between nonsteroidal anti-inflammatory drug use and gastric cancer. Eur J Cancer Prev 19:288–298
251. Leung WK, Ng EK, Chan FK, Chan WY, Chan KF, Auyeung AC, Lam CC, Lau JY, Sung JJ (2006) Effects of long-term rofecoxib on gastric intestinal metaplasia: results of a randomized controlled trial. Clin Cancer Res 12:4766–4772
252. Zhang LJ, Wang SY, Huo XH et al (2009) Anti-*Helicobacter pylori* therapy followed by celecoxib on progression of gastric precancerous lesions. World J Gastroenterol 15:2731–2738
253. Hung KH, Yang HB, Cheng HC, Wu JJ, Sheu BS (2010) Short-term celecoxib to regress long-term persistent gastric intestinal metaplasia after *Helicobacter pylori* eradication. J Gastroenterol Hepatol 25:48–53
254. Yanaoka K, Oka M, Yoshimura N et al (2010) Preventive effects of etodolac, a selective cyclooxygenase-2 inhibitor, on cancer development in extensive metaplastic gastritis, a *Helicobacter pylori*-negative precancerous lesion. Int J Cancer 126:1467–1473
255. Yang HB, Cheng HC, Sheu BS, Hung KH, Liou MF, Wu JJ (2007) Chronic celecoxib users more often show regression of gastric intestinal metaplasia after *Helicobacter pylori* eradication. Aliment Pharmacol Ther 25:455–461
256. Wu CY, Wu MS, Kuo KN, Wang CB, Chen YJ, Lin JT (2010) Effective reduction of gastric cancer risk with regular use of nonsteroidal anti-inflammatory drugs in *Helicobacter pylori*-infected patients. J Clin Oncol 28:2952–2957
257. Plummer M, Vivas J, Lopez G et al (2007) Chemoprevention of precancerous gastric lesions with antioxidant vitamin supplementation: a randomized trial in a high-risk population. J Natl Cancer Inst 99:137–146
258. Mason J, Axon AT, Forman D et al (2002) The cost–effectiveness of population *Helicobacter pylori* screening and treatment: a Markov model using economic data from a randomized controlled trial. Aliment Pharmacol Ther 16:559–568
259. Parsonnet J, Harris RA, Hack HM, Owens DK (1996) Modelling cost–effectiveness of *Helicobacter pylori* screening to prevent gastric cancer: a mandate for clinical trials. Lancet 348:150–154
260. Davies R, Crabbe D, Roderick P, Goddard JR, Raftery J, Patel P (2002) A simulation to evaluate screening for *Helicobacter pylori* infection in the prevention of peptic ulcers and gastric cancers. Health Care Manag Sci 5:249–258
261. Roderick P, Davies R, Raftery J, Crabbe D, Pearce R, Bhandari P, Patel P (2003) The cost–effectiveness of screening for *Helicobacter pylori* to reduce mortality and morbidity from gastric cancer and peptic ulcer disease: a discrete-event simulation model. Health Technol Assess 7:1–86
262. Roderick P, Davies R, Raftery J, Crabbe D, Pearce R, Patel P, Bhandari P (2003) Cost-effectiveness of population screening for *Helicobacter pylori* in preventing gastric cancer and peptic ulcer disease, using simulation. J Med Screen 10:148–156

263. Leivo T, Salomaa A, Kosunen TU, Tuominen R, Färkkilä M, Linna M, Sintonen H (2004) Cost–benefit analysis of *Helicobacter pylori* screening. Health Policy 70:85–96
264. Dan YY, So JB, Yeoh KG (2006) Endoscopic screening for gastric cancer. Clin Gastroenterol Hepatol 4:709–716
265. Yeh JM, Kuntz KM, Ezzati M, Goldie SJ (2009) Exploring the cost–effectiveness of *Helicobacter pylori* screening to prevent gastric cancer in China in anticipation of clinical trial results. Int J Cancer 124:157–166
266. Lee YC, Lin JT, Wu HM, Liu TY, Yen MF, Chiu HM, Wang HP, Wu MS, Hsiu-Hsi Chen T (2007) Cost–effectiveness analysis between primary and secondary preventive strategies for gastric cancer. Cancer Epidemiol Biomarkers Prev 16:875–885
267. Lee HY, Park EC, Jun JK, Choi KS, Hahm MI (2010) Comparing upper gastrointestinal X-ray and endoscopy for gastric cancer diagnosis in Korea. World J Gastroenterol 16:245–250
268. Xie F, Luo N, Blackhouse G, Goeree R, Lee HP (2008) Cost–effectiveness analysis of *Helicobacter pylori* screening in prevention of gastric cancer in Chinese. Int J Technol Assess Health Care 24:87–95
269. Xie F, Luo N, Lee HP (2008) Cost effectiveness analysis of population-based serology screening and 13C-urea breath test for *Helicobacter pylori* to prevent gastric cancer: a Markov model. World J Gastroenterol 14:3021–3027
270. Fendrick AM, Chernew ME, Hirth RA, Bloom BS, Bandekar RR, Scheiman JM (1999) Clinical and economic effects of population-based *Helicobacter pylori* screening to prevent gastric cancer. Arch Intern Med 159:142–148
271. Yeh JM, Hur C, Kuntz KM, Ezzati M, Goldie SJ (2010) Cost–effectiveness of treatment and endoscopic surveillance of precancerous lesions to prevent gastric cancer. Cancer 116:2941–2953
272. Hassan C, Zullo A, Di Giulio E, Annibale B, Lahner E, De Francesco V, Ierardi E (2010) Cost–effectiveness of endoscopic surveillance for gastric intestinal metaplasia. Helicobacter 15:221–226

These guidelines represent a consensus of best practice based on the available evidence at the time of preparation. They may not apply in all situations and should be interpreted in the light of specific clinical situations and resource availability. Further controlled clinical studies may be needed to clarify aspects of these statements, and revision may be necessary as new data appear. Clinical consideration may justify a course of action at variance to these recommendations. These guidelines are intended to be an educational device to provide information that may assist endoscopists in providing care to patients. They are not rules and should not be construed as establishing a legal standard of care or as encouraging, advocating, requiring, or discouraging any particular treatment.

Virchows Arch (2012) 460:47–60
DOI 10.1007/s00428-011-1175-x

ORIGINAL ARTICLE

MHC class II expression in pancreatic tumors: a link to intratumoral inflammation

Matthias M. Gaida · Thilo Welsch · Esther Herpel · Darjus F. Tschaharganeh · Lars Fischer · Peter Schirmacher · G. Maria Hänsch · Frank Bergmann

Received: 2 July 2011 / Revised: 28 October 2011 / Accepted: 9 November 2011 / Published online: 27 November 2011
© Springer-Verlag 2011

Abstract Major histocompatibility complex class II antigens (MHC class II) are constitutively expressed by professional antigen presenting cells and present antigenic peptides to specific CD4+ T lymphocytes. MHC class II expression, however, can also be induced on epithelial cells and in a variety of solid tumors. We tested MHC class II expression on tissue samples derived from patients with pancreatic ductal adenocarcinoma (PDAC) and pancreatic endocrine tumors (PET). Immunohistochemistry revealed MHC class II expression in 86 of 112 (76.8%) PDAC samples and in 30 of 43 (70.0%) PET samples. In PDAC and PET, MHC class II expression correlated significantly with severity and activity of intratumoral inflammation, as well as with the infiltration of CD4+ T lymphocytes. High MHC class II expression significantly correlated with a better histological grade of differentiation in PDAC. In vitro MHC class II expression could be induced on PDAC tumor cell lines by interferon-γ. These cells were then able to present the staphylococci enterotoxin B superantigen to T lymphocytes, which resulted in T cell proliferation. Our findings suggest that MHC class II expression on pancreatic tumor cells is induced by the intratumoral inflammatory reaction in pancreatic tumors.

Keywords Pancreatic cancer · Pancreatic endocrine tumor · MHC class II · Intratumoral inflammation · T cell proliferation

M. M. Gaida · E. Herpel · D. F. Tschaharganeh · P. Schirmacher · F. Bergmann (✉)
Institute of Pathology, University of Heidelberg,
Im Neuenheimer Feld 220,
69120 Heidelberg, Germany
e-mail: frank.bergmann@med.uni-heidelberg.de

T. Welsch · L. Fischer
Department of General Surgery, University of Heidelberg,
Im Neuenheimer Feld 110,
69120 Heidelberg, Germany

G. M. Hänsch
Institute of Immunology, University of Heidelberg,
Im Neuenheimer Feld 305,
69120 Heidelberg, Germany

Introduction

Pancreatic ductal adenocarcinoma (PDAC) is a highly aggressive neoplasm, ranking fourth in cancer-related deaths in western countries [1]. Tumors are significantly influenced by the cross-talk among the tumor cells and by their microenvironment, particularly the tissue-resident cells such as fibroblasts, or the tumor-infiltrating lymphocytes and the inflammatory cells [2]. The intratumoral inflammation in the PDAC microenvironment is often distinct, and multiple interactions between tumor cells and cells of the immune system have been previously described, but the impact on tumor progression is not yet understood [3–5]. Systemically increased C-reactive protein concentrations, a marker for an active inflammatory constitution, correlates with shorter survival of PDAC patients [6]. Moreover, an intensive interplay between pancreatic tumor cells and inflammatory cells has been reported [3]. Cytokines released by tumor infiltrating lymphocytes were shown to enhance the invasion of pancreatic cancer cells [4, 7], while neutrophil-derived lipocalin provided an anti-tumoral and anti-metastatic effect in PDAC [8].

Key findings include the fact that PDAC cells are specifically recognized by autologous T lymphocytes [9] and that chemokines or their receptors, such as CXCL14 or CXCL16 and its corresponding receptor CXCR6, are found in PDAC that could mediate interactions with inflammatory

cells in particular [10–13]. Moreover, major histocompatibility antigen (MHC) class I and class II are found on a variety of tumor cells, including pancreatic adenocarcinoma cells [14], and it has been assumed that they provide the immunologic recognition structure of the tumor by presenting either an "altered self" or a "non-self antigen" to T lymphocytes [15, 16].

The constitutive MHC class II expression is restricted to professional antigen presenting cells, such as dendritic cells, monocytes, and B lymphocytes. MHC class II expression, however, can be induced in non-neoplastic tissue under inflammatory conditions, particularly on epithelial cells like keratinocytes or intestinal mucosa [17, 18]. MHC class II antigens are also expressed by human malignancies, e.g. in Ewing sarcoma [15], malignant melanoma [19], renal cell carcinoma [20], colon carcinoma [21], breast cancer [22], and squamous cell carcinoma of the larynx [22, 23]. MHC class II expression has been associated with better tumor differentiation and a better prognosis, e.g. in colon, breast and larynx carcinoma [21–24].

Expression of MHC class II in PDAC tissue was indicated by two preliminary studies, comprising only a small number of patients [14, 25], on isolated cells of primary PDAC [9], and on pancreatic adenocarcinoma cell lines [14]. These first studies reported that approximately 30% of PDAC tissues revealed MHC class II positivity [14, 25]. In the present study, we examined MHC class II expression in a large series of 112 PDAC patients and for comparison additionally of 43 patients with PET and assessed the correlation with clinical and pathological parameters focussing the intratumoral inflammation. To gain insight into the functional role of MHC class II expression in tumors, we tested whether pancreatic cancer cells that were induced to express MHC class II molecules were able to activate T lymphocytes using staphylococcus enterotoxin B as a model superantigen [26]. We found a strong correlation between MHC class II expression by pancreatic tumor cells and the intratumoral inflammatory reaction, particularly with respect to the infiltration of CD4+ T lymphocytes. Moreover, the in vitro data provided evidence for the propensity of MHC class II positive tumor cells to induce the proliferation of T lymphocytes. Taken together, our data suggest that the proinflammatory microenvironment induces the MHC class II expression on the tumor, and the tumor cell, in turn, might participate in a localized immune reaction.

Material and methods

Patients

PDAC tumor tissue samples were obtained from 112 patients (46 female, 66 male; age range, 39–85 years; mean, 64.9 years; median, 66.0 years). In 84 patients the tumors were located in the pancreatic head, 7 in the body, 13 in the body and tail, and 8 were in the tail. The tissue specimens were formalin-fixed and paraffin-embedded.

Based on haematoxylin and eosin (H&E) staining, the diagnosis of PDAC and the tumor stage were established according the criteria recommended by the World Health Organization (WHO) (2010) [27] and the UICC criteria (2009) [28]. Pathological examination revealed a pT3 stage in 110 patients and pT1 and pT2 stages in one case each. Regional lymph node metastases (pN1) occurred in 98 patients and metastases to other organs (liver and/or non-regional lymph nodes) were seen in 13 cases (pM1). Four PDAC were well-differentiated (G1), 75 moderately (G2) and 33 poorly differentiated (G3). Follow-up information was available for 104 patients: 61 patients died from the cancer within 25–1,187 days after the operation (mean, 427 days; median, 347 days), 37 patients were alive after a follow-up of 15–1,044 days (mean, 551 days; median, 663 days), and six patients died of non-cancer-related disease and were thus excluded from further analysis (Table 1).

The study furthermore comprised 43 samples of primary PET (21 females, 22 males; age range, 13–85 years; mean, 56.0 years; median, 60 years). In 23 cases, the tumors were located in the pancreatic head, four were in the body, five

Table 1 Clinical and pathological parameters of PDAC patients

Patients (n=112)	PDAC
Gender (F/M) (n=112)	46, 66
Age [years]	39–85 (mean, 64.9; median, 66.0)
Location of tumor	Head, 84
	Body, 7
	Body and tail, 13
	Tail, 8
pT	pT1, 1
	pT2, 1
	pT3, 110
	pT4, 0
pN	pN0, 14
	pN1, 98
pM	pM0, 99
	pM1, 13
G	G1, 4
	G2, 75
	G3, 33
Survival (n=104 patients)	Death of disease, 61 patients; 25–1,187 days (mean, 427; median, 347)
	Alive, 37 patients; 15–1,044 days (mean, 551; median, 663)
	Non-cancer-related death, 6 patients

were in the body and tail, and 11 cases were found in the tail. Using the criteria established by the World Health Organization of 2004 [29] and of 2010 [30] and the criteria of the European Neuroendocrine Tumor Society (ENETS) [31], diagnosis and tumor stage were established. The PET were classified as benign well-differentiated endocrine tumors (n=6), well-differentiated endocrine tumors of uncertain behavior (n=8), well-differentiated endocrine carcinoma (n=25) and poorly differentiated endocrine carcinoma (n=4). According to the WHO classification of 2010, 35 cases were classified as neuroendocrine tumor and eight as neuroendocrine carcinoma. No case revealed a pT4, 28 cases a pT3, six cases a pT2 and nine cases a pT1 stage. Regional lymph node metastases (pN1) were detected in 20 cases. Distant organ metastases (liver and/or non-regional lymph nodes) were observed in nine cases (pM1). According to their mitotic activity and proliferative activity, 21 cases were graded as G1, 14 cases as G2, and 8 as G3. Immunohistochemistry revealed positivity for the neuroendocrine markers synaptophysin and chromogranin A in all 43 cases. All 43 cases were immunohistochemically evaluated for hormone expression. Immunohistochemical stains showed expression of insulin in 12 cases, gastrin in ten cases, glucagon, pancreatic polypeptide and somatostatin in three cases, each, and serotonin in one case. Of these tumors, functional activity was clinically determined in 16 patients (37% of patients, 11 insulinomas, 4 gastrinomas, one glucagonoma). Twenty-seven cases clinically revealed no functional activity (63% of patients). Four patients had a hereditary syndrome (MEN 1 syndrome). Follow-up information was available for 37 patients: eight patients died of their tumors within 1–1,258 days postoperatively (mean, 477 days; median, 260 days) and 29 patients were alive after a follow-up of 47 to 4,980 days (mean, 1,480 days; median, 1,466 days) (Table 2).

The study was approved by the Ethics Committee of the University of Heidelberg and written informed consent was obtained from the patients.

Immunohistochemistry

Paraffin-embedded tissue sections (4 μm) were used for the immunohistochemical analyses. Immunostaining was performed as previously described [32], using the avidin–biotin complex method. Prior to antibody incubation, heat pre-treatment in an antigen retrieval solution (DAKO; pH 9.0) was performed. Primary antibodies included a mouse monoclonal antibody to MHC class II (Abcam, Cambridge, UK; diluted 1:250) and a mouse monoclonal antibody to CD4 (Novocastra, Newcastle, UK; diluted 1:10). MHC class II staining was performed on tissue microarrays from 112 PDAC samples, 43 PET samples and ten normal pancreas samples. To validate these immunohistochemical results obtained from the microarrays, 16 and 26 of the cases were additionally stained for MHC class II and CD4, respectively, using whole tissue tumor sections, revealing comparable results.

Scoring of inflammation, CD4+ T lymphocyte infiltration and MHC class II expression

The severity of the inflammation was evaluated microscopically on whole tumor sections, using a previously reported scoring system [33]. Briefly, the severity was determined as absent (score, 0), mild (score, 1), moderate (score, 2) or severe (score, 3), depending on the accumulation of inflammatory cells (lymphocytes, plasma cells, macrophages) and the formation of lymph follicles. The activity of inflammation was semiquantitatively scored as absent (score, 0), mild (score, 1) or moderate to severe (score, 2), depending on the density of neutrophil granulocytes.

The immunohistochemical MHC class II expression (distribution) of the tumor cells was determined semiquantitatively as score, 0 for 0%; score, 1 for 1–5%; score, 2 for 5–25%; score, 3 for 25–50%; score, 4 for 50–75% and score, 5 for 75–100% positive tumor cells according to a previously reported scale for the immunohistochemical evaluation of the expression of MHC molecules [15, 34, 35]. This scoring system includes also a semiquantification of the staining intensity, as grouped in no staining (score, 0), weak staining intensity (score, 1), moderate staining intensity (score, 2) or strong staining intensity (score, 3). According to Berghuis et al. we used an immunoreactivity score (in accordance to the Allred-Score), in which the summation of both scores was composed [15].

CD4+ T lymphocytes have been described to interact with MHC class II molecules [36]. To test the correlation between the MHC class II expression on PDAC and PET and the infiltration of CD4+ lymphocytes, the CD4+ T lymphocytes were counted in ten representative high power fields (HPF) of each case in 112 PDAC and in 21 PET cases.

TMA specimen and the corresponding whole tissue sections were compared, and the ratio between the mean number of CD4+ infiltrating cells in sections with high MHC class II expression and those without any expression was calculated. The ratio (CD4+ lymphocytes in high MHC class II expressing tumors/CD4+ lymphocytes in non-MHC class II expressing tumors) was 4.0 in whole tissue sections and 3.8 in TMA; thus a valid tool for the quantification of CD4+ lymphocytes was generated. Next, we compared the expression pattern and intensity of MHC class II with the number of infiltrating CD4+ T lymphocytes. Furthermore, we correlated the infiltrate of CD4+ lymphocytes in tumors with MHC class II expression (irrespective of the quantity of positively staining cells) versus tumors without any expression. Moreover, we selected 13 cases without MHC class II expression and 13 cases with notably high MHC

Table 2 Clinical and pathological parameters of PET patients

Patients (n=43)	PET
Gender (F/M) (n=43)	21, 22
Age [years]	13–85 (mean, 56.0; median, 60.0)
Location of tumor	Head, 23
	Body, 4
	Body and tail, 5
	Tail, 11
Diagnosis (WHO 2004)	Well-differentiated endocrine tumor, 6
	Well-differentiated endocrine tumor of uncertain behaviour, 8
	Well-differentiated endocrine carcinoma, 25
	Poorly differentiated endocrine carcinoma, 4
Diagnosis (WHO 2010)	Neuroendocrine tumor, 35
	Neuroendocrine carcinoma, 8
pT	pT1, 9
	pT2, 6
	pT3, 28
	pT4, 0
pN	pN0, 10
	pN1, 20
	pNx, 13
pM	pM0, 34
	pM1, 9
G	G1, 21
	G2, 14
	G3, 8
Endocrine markers	Chromogranin A, 43
	Synaptophysin, 43
Immunohistochemical hormone expression	Insulin, 12 (27.9% of 43 cases)
	Gastrin, 10 (23.2% of 43 cases)
	Glucagon, 3 (7.0% of 43 cases)
	Pancreatic polypeptide, 3 (7.0% of 43 cases)
	Somatostatin, 3 (7.0% of 43 cases)
	Serotonin, 1 (2.3% of 43 cases)
Clinically determined functional activity	Insulinoma, 11 (25.6% of 43 cases)
	Gastrinoma, 4 (9.3% of 43 cases)
	Glucagonoma, 1 (2.3% of 43 cases)
Hereditary syndrome	4
Survival (n=37 patients)	Death of disease, 8 patients; 1–1,258 days (mean, 477; median, 260)
	Alive, 29 patients; 47–4,980 days (mean, 1,480; median, 1,466)

class II expression (more than 75% positive cells, moderate to strong staining intensity) to compare the infiltration of CD4+ T lymphocytes.

Cytofluorometry and induction of MHC class II expression on pancreatic cancer cell lines

The pancreatic tumor cell lines Capan-1, MiaPaca-2, BxPC-3, Panc-1, SU8686, AspC1, (ATCC, Rockville, MD, USA), T3M4 and Colo-357 (R.S. Metzgar Duke University, Durham, NC, USA) were cultivated in RPMI 1640, supplemented with 10 % fetal calf serum, 1% L-glutamine and 1% penicillin/streptomycin (all obtained from Invitrogen, Karlsruhe, Germany). For induction of MHC class II expression, the cells were seeded into 6-well plates (NUNC, Roskilde, Denmark; 1×10^5/ml), and cultivated with interferon-γ (Serotec, Düsseldorf, Germany; 100 U/ml) for 24 and 48 h, respectively. Next, the cells were washed,

removed from the plates by treatment with EDTA/Trypsin (Invitrogen) and suspended in phosphate-buffered saline (PBS) containing 1% bovine serum albumin and 0.1% sodium azide. To detect MHC class II surface expression, 5 μl PE-labelled antibody (anti-HLA-DR-DQ-DP; Biozol, Eching, Germany) was added. Mouse IgG-PE (BD Pharmingen, Heidelberg, Germany) was used as an isotype control. After 30 min, the cells were washed, resuspended in 1% paraformaldehyde in PBS and antibody binding was measured by FACScalibur® (Becton and Dickinson, Heidelberg, Germany).

MHC class II-mediated superantigen presentation of pancreatic tumor cells to CD4+ T lymphocytes

The pancreatic cell lines Colo-357 and SU8686 were cultivated in the presence of interferon-γ to induce MHC class II expression as described above and then irradiated for 14 min (60 Gy) to prevent their proliferation. T lymphocytes were isolated from the peripheral blood of a healthy donor according to established methods. In brief, heparinized blood was layered onto PolymorphPrep® (Axis-Shield, Oslo, Norway), and the mononuclear cell fraction was recovered according to the protocol of the supplier. T lymphocytes were separated from the mononuclear cell fraction by magnetic beads separation using anti-CD3 beads (MACS Miltenyi Biotec, Bergisch Gladbach, Germany). The T lymphocytes were adjusted to 1×10^6/ml in RPMI supplemented with 10% fetal calf serum, 1% HEPES, 1% L-glutamine, and 1% penicillin/streptomycin (all obtained from Invitrogen) and 100 μl were placed into a round-bottom 96-well culture plate. The irradiated pancreatic cells (100 μl in the concentrations indicated in the respective experiment) were added with or without staphylococci enterotoxin B (SEB; 2 ng/well; Sigma-Aldrich, Munich, Germany). After 48 h, ^{3}H-thymindine was added (1 μCi/well) for another 24 h and incorporation into the cells of radioactivity was measured. For comparison, pancreatic cancer cells without previous interferon-γ stimulation were used, as were T lymphocytes alone and pancreatic cancer cells alone with or without SEB. The T lymphocyte proliferation was determined as mean value of five replicas, and the differences between groups were determined using ANOVA.

Statistical analysis

For statistical analysis of survival, the non-parametric logrank test was performed. Correlation of MHC class II expression with clinical and pathological parameters was performed using Spearman's rho analysis. Correlation of MHC class II staining with the density of CD4+ T lymphocytes was calculated with the Spearman's rho analysis and the Mann–Whitney *U* test, respectively. For the array analysis, the staining results were grouped as described above. Significance levels were defined as $p<0.05$. The statistical analyses were carried out with the SPSS software version 18.0 for Windows (SPSS Inc., Chicago, USA). Graphs were made using OriginPro7.5 software (Additive Software, Friedrichsdorf, Germany).

Results

Correlation of MHC class II expression with the severity and activity of intratumoral inflammatory reaction in PDAC and PET

Intratumoral inflammation was assessed by analysing and quantifying the infiltrating leucocytes, and the activity of inflammatory reaction was judged by the presence of neutrophils as indicators of an acute reaction. Inflammatory activity was seen in 108 of the 112 PDAC cases, while in PET—though inflammation was seen in 32 of 43 cases—only 22 cases revealed an inflammatory activity (data summarized in Fig. 1 and Table 3).

As shown in Fig. 2 and Table 4, MHC class II antigen expression on tumor cells was seen in 86 of the 112 PDAC cases (76.8%); of these six cases revealed 1–5% positive tumor cells (score, 1), five cases 5–25% positive tumor cells (score, 2), 44 cases 25–50% positive tumor cells (score, 3), 12 cases 50–75% positive tumor cells (score, 4) and 19 cases more than 75% positive tumor cells (score, 5). The staining intensity was predominately weak to moderate and significantly correlated with the distribution of MHC class II expression ($p<0.0001$). In PET, 30 of the 43 cases (70.0%) revealed MHC class II expression; of these two cases revealed 1–5% positive tumor cells (score, 1), one case 5–25% positive tumor cells (score, 2), 16 cases 25–50% positive tumor cells (score, 3), five cases 50–75% positive tumor cells (score, 4) and six cases more than 75% positive tumor cells (score, 5). In both types of tumor cells, an immunohistochemical staining of MHC class II on the cellular membrane, as well as a cytoplasmatic immunopositivity was detected [37]. Antigen-presenting inflammatory cells served as internal positive control. Additionally, stained normal pancreas tissue revealed no MHC class II expression in acini, ducts and islets of normal pancreas tissue.

MHC class II antigen expression on PDAC cancer cells showed a significant positive correlation with the severity of the inflammation ($p=0.001$) as well as with the activity of the inflammation ($p=0.007$). Furthermore, the MHC class II staining intensity correlated positively

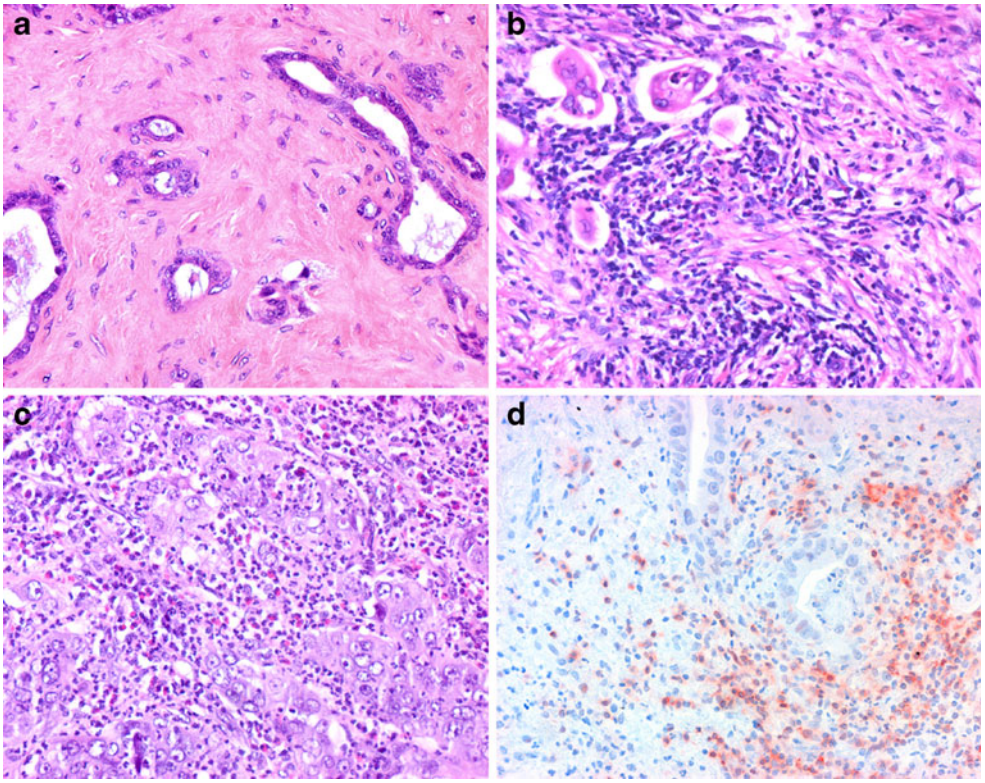

Fig. 1 **a** PDAC tumor tissue revealing no significant (score, 0) inflammation. **b** PDAC tissue revealing a severe (score, 3) intratumoral inflammatory reaction. **c** PDAC specimen with densely, mixed inflammatory infiltration dominated by neutrophil granulocytes, as indicator for a severe inflammatory activity (score, 2). **d** High infiltrate of CD4+ T lymphocytes

with the severity ($p<0.001$) and the activity of the inflammation ($p=0.002$).

Using the immunoreactivity score, a positive correlation between severity ($p<0.001$) and activity ($p=0.001$) and the MHC class II expression was seen. Again, PET yielded essentially similar results, a positive correlation of MHC class II antigen expression with the severity of the intratumoral inflammation ($p<0.001$) and with the activity of the intratumoral inflammation ($p<0.001$) was seen; MHC class II staining intensity correlated with the severity ($p=0.003$) and the activity of the intratumoral inflammation ($p<0.001$). The immunoreactivity score revealed a significant positive correlation between the MHC class II expression and the severity ($p<0.001$) and the activity ($p<0.001$).

Among the infiltrating leucocytes, CD4+ lymphocytes were detected. In PDAC, the expression pattern of MHC class II as well as the staining intensity correlated significantly with the number of infiltrating CD4+ T lymphocytes ($p<0.001$ for each parameter). Similar results were detected for PET tissues, in which MHC class II dispersion ($p=0.003$) and staining intensity ($p<0.001$) correlated significantly with the number of infiltrating CD4+ T lymphocytes. Scored by the immunoreactivity score, the MHC class II expression correlated significantly with the number CD4+ T lymphocytes in PDAC ($p<0.001$) and PET ($p=0.007$). In addition, we analysed the density of CD4+ T lymphocytes in MHC class II negative tumors versus tumors expressing MHC class II, irrespective of the staining pattern and the intensity. Here, the density of CD4+ T lymphocytes was higher in tissues containing MHC class II-positive tumor cells (irrespective of focal or diffuse staining pattern) compared to tissues with tumor cells negative for MHC class II ($p<0.001$ for PDAC; $p<0.01$ for PET). In PDAC tissue without MHC class II expression, the number of CD4+ cells ranged from zero to six cells per 10 HPF (mean, 1.5; median, 1), in samples revealing MHC class II expression, the number of CD4+ lymphocytes ranged from 0 to 97 cells per 10 HPF (mean, 11.4; median, 5). In

Table 3 Severity and activity of intratumoral inflammation in PDAC and PET

Number of cases	Severity of inflammation	Activity of inflammation
PDAC ($n=112$)	Total: 112/112 (100.0%)	Total: 108/112 (96.4%)
	Score 3: 20/112 (17.8%)	Score 2: 51/112 (45.5%)
	Score 2: 80/112 (71.4%)	Score 1: 57/112 (50.9%)
	Score 1: 12/112 (10.7%)	
	Score 0: 0/112	Score 0: 4 /112 (3.6%)
PET ($n=43$)	Total: 32/43 (74.4%)	Total: 22/32 (68.8%)
	Score 3: 0/43	Score 2: 2/32 (6.3%)
	Score 2: 5/43 (11.6%)	Score 1: 20/32 (62.5%)
	Score 1: 27/43 (62.8%)	
	Score 0: 11/43 (25.6%)	Score 0: 10/32 (31.2%)

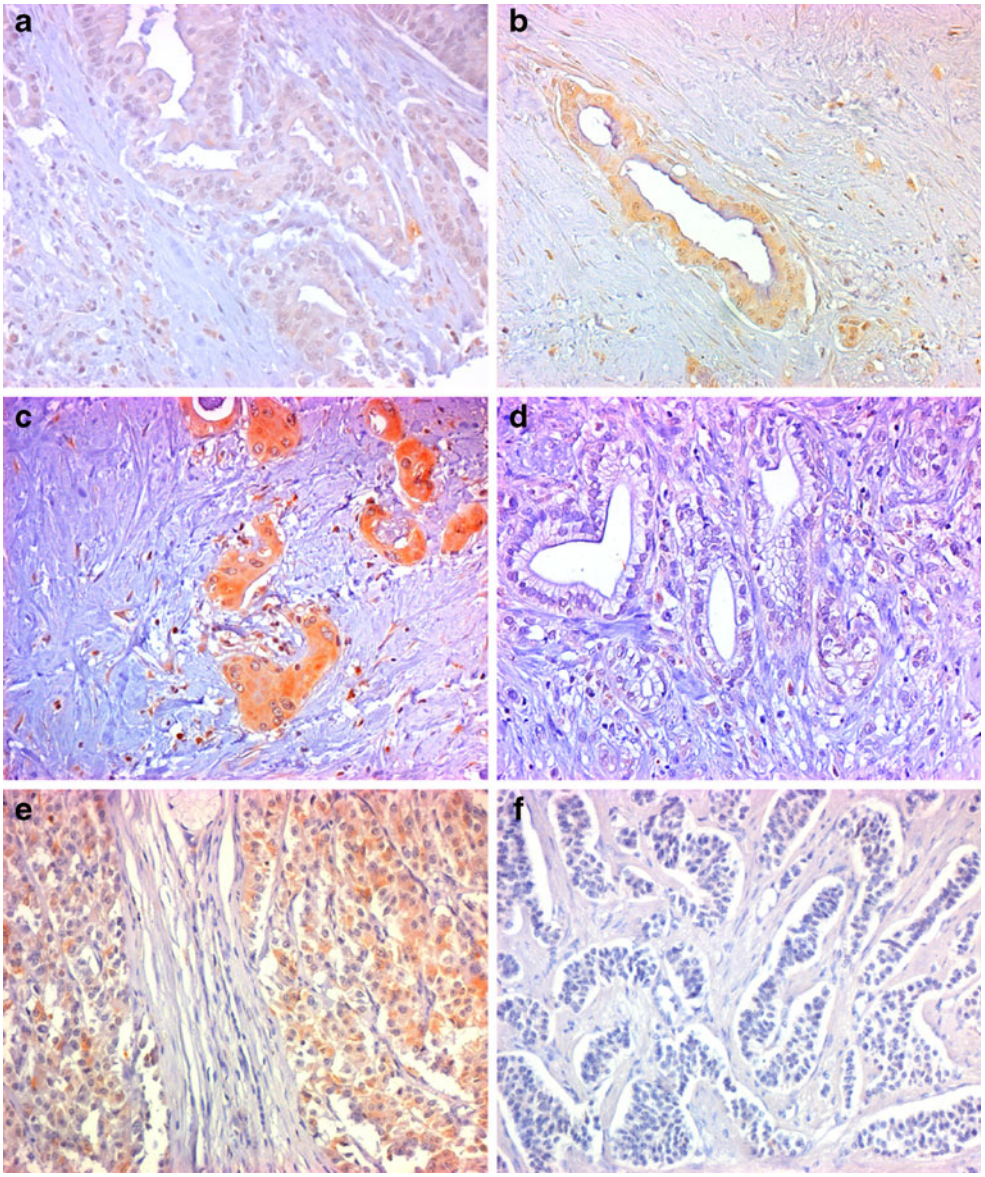

Fig. 2 Immunohistochemical analyses of MHC class II expression on PDAC cells and endocrine tumor cells revealed different staining intensities, classified as, weak staining intensity (score, 1), moderate staining intensity (score, 2) or strong staining intensity (score, 3) or no staining (score, 0). **a** Exemplarily PDAC specimen with weak (score, 1), **b** moderate (score, 2), **c** strong staining intensity (score, 3). **d** No staining (score, 0). **e** Endocrine tumor cells with moderate staining (score, 2), **f** without staining (score, 0). Immune cells served in each case as an internal positive control

PET without MHC class II expression, the number of CD4+ lymphocytes ranged between zero and one cell per 10 HPF (mean, 0.6; median, 1), in samples revealing MHC class II expression, the number of CD4+ lymphocytes ranged from zero to eight cells per 10 HPF (mean, 2.5; median, 2). In whole tissue sections of PDAC, CD4+ T lymphocytes could be detected in all 26 investigated cases. In cancer tissue without MHC class II expression, the density of CD4+ T lymphocytes ranged from five to 90 CD4+ T lymphocytes per 10 HPF (mean, 24.6; median, 14). Cases revealing a high MHC class II expression (more than 75% positive cells, moderate to strong staining intensity) showed a significantly higher density of CD4+ T lymphocytes ($p<0.0002$), ranging from six to 201 CD4+ T lymphocytes per 10 HPF (mean, 102.7; median, 104) (data summarized in Figs. 3, 4 and 5).

Correlation of MHC class II expression in PDAC and PET with clinical and pathological parameters

The expression of MHC class II in PDAC (distribution, intensity and the immunoreactivity score) showed a significantly negative correlation with the tumor grade ($p=0.001$), but not with the local tumor stage (pT), the presence of regional lymph node metastases (pN), distant metastases (pM) or patient gender. No correlation between the survival of the patients and MHC class II expression ($p=0.70$) or intensity ($p=0.88$) was found. In PET, the distribution of the MHC class II ($p=0.042$) and the calculated immunoreactivity score ($p=0.027$) significantly correlated with the local tumor stage (pT).

MHC class II expression parameters (distribution, intensity and the immunoreactivity score) revealed no

Table 4 MHC class II expression in PDAC and PET with percentage of immunoreactive tumor cells

Number of cases	MHC class II expression	MHC class II intensity	Immunoreactivity score
PDAC (n=112)	Total, 86/112 (76.8%)	Strong, 9/86 (10.5%)	0, 26/112 (23.2%)
	>75%, 19/86 (22.1%)	Moderate, 32/86 (37.2%)	2, 5/112 (4.5%)
	50–75%, 12/86 (13.9%)	Weak, 45/86 (52.3%)	3, 5/112 (4.5%)
	25–50%, 44/86 (51.2%)		4, 29/112 (25.9%)
	5–25%, 5/86 (5.8%)		5, 22/112 (19.7%)
	1–5%, 6/86 (7.0%)		6, 8/112 (7.1%)
			7, 8/112 (7.1%)
			8, 9/112 (8.0%)
PET (n=43)	Total, 30/43 (70.0%)	Strong, 0/30 (0.0%)	0, 13/43 (30.0%)
	>75%, 6/30 (20.0%)	Moderate, 13/30 (43.3%)	2, 8/43 (18.7%)
	50–75%, 5/30 (16.7%)	Weak, 17/30 (56.7%)	3, 4/43 (9.3%)
	25–50%, 16/30 (53.3%)		4, 1/43 (2.3%)
	5–25%, 1/30 (3.3%)		5, 4/43 (9.3%)
	1–5%, 2/30 (6.7%)		6, 8/43 (18.7%)
			7, 5/43 (11.6%)
			8, 0/43 (0%)

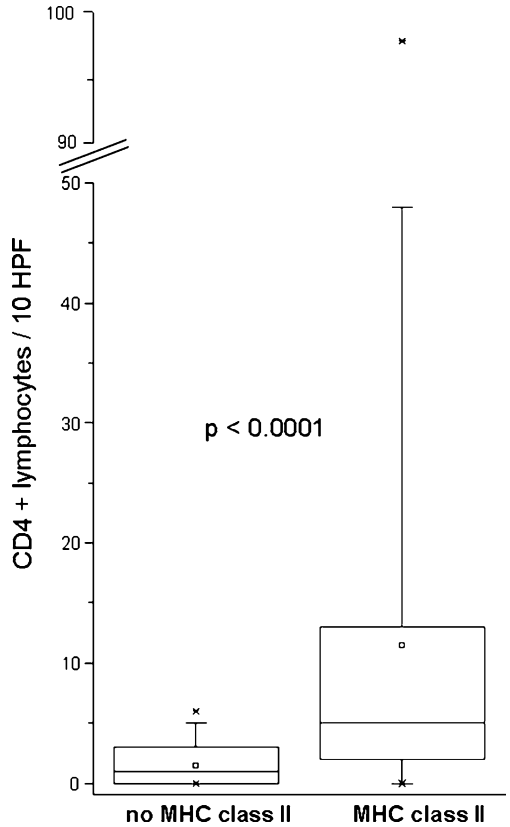

Fig. 3 In PDAC a significantly higher density of CD4+ T lymphocytes was found in tissues revealing MHC class II expression versus no expression (PDAC: p<0.0001). In PDAC tissue without MHC class II expression, the number of CD4+ cells ranged from 0 to 6 cells per 10 HPF (mean, 1.5; median, 1); in samples revealing MHC class II expression, the number of CD4+ lymphocytes ranged from 0 to 97 cells per 10 HPF (mean, 11.4; median, 5)

significant correlation between the diagnostic tumor classification (WHO 2004 and 2010 and ENETS), histopathological grading, hormone expression of insulin or glucagon, functional activity, presence of a hereditary syndrome (MEN 1 syndrome), or gender of the patients. The endocrine

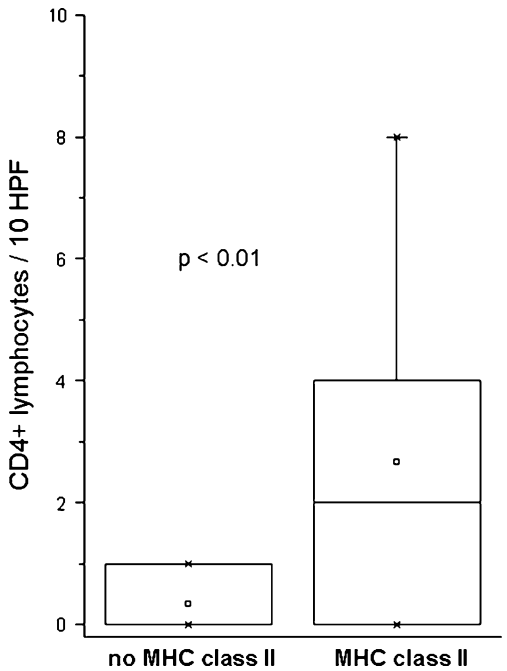

Fig. 4 In PET, a significantly higher density of CD4+ T lymphocytes in tissues revealing MHC class II expression versus no expression could be shown (p<0.01). In PET without MHC class II expression, the number of CD4+ lymphocytes ranged between 0 and 1 cell per 10 HPF (mean, 0.6; median, 1); in PET revealing MHC class II expression, the number of CD4+ lymphocytes ranged from 0 to 8 cells per 10 HPF (mean, 2.5; median, 2)

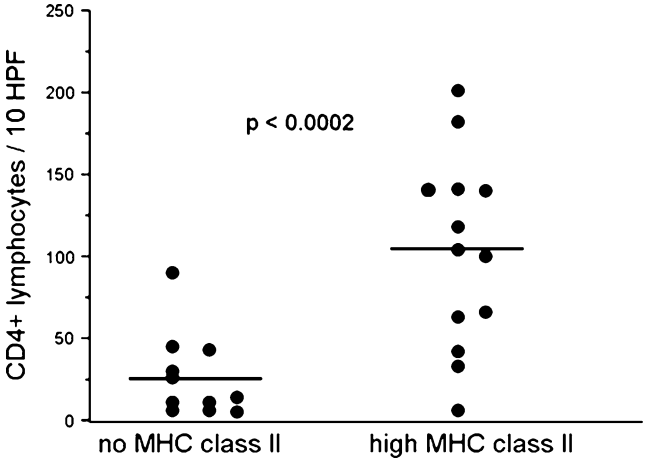

Fig. 5 All 26 investigated PDAC specimen contained CD4+ T lymphocytes. In cancer specimen without MHC class II expression (*left bar*), CD4+ T lymphocytes ranged from 5 to 90 cells per 10 HPF (mean, 24.6; median, 14). Cases revealing high MHC class II expression showed a significantly higher density of CD4+ T lymphocytes ($p<0.0002$), ranging from 6 to 201 cells per 10 HPF (mean, 102.7; median, 104)

carcinomas among the collective showed no correlation between the MHC class II expression and the presence or absence of regional lymph node (pN) or distant organ metastases (pM). No correlation with patient survival could be demonstrated with respect to distribution ($p=0.91$) or intensity ($p=0.40$).

MHC class II-positive PDAC tumor cells present superantigen to T lymphocytes and mediate T cell activation

MHC class II surface expression was evaluated on pancreatic cancer cells lines Capan-1, MiaPaca-2, BxPC-3, Panc-1, SU8686, AspC1, T3M4 and Colo-357. As determined by cytofluorometry, cultured cells were negative for MHC class II. Following cultivation with interferon-γ, MHC class II surface expression could be induced to high levels (21.4% to 44.4%), measured as the percent of cells expressing MHC class II on the following cell lines: SU8686 (44.4%), AspC-1 (43.7%), T3M4 (29.9%), Capan-1 (24.5%), BxPC3 (21.4%) and not at all or to a lesser extent on Panc-1 (4.8%) Colo-357 (4.0%) and MiaPaca-2 (1.4%) (data for SU8686 are shown in Fig. 6; data for all cells summarised in Table 5).

To assess the functionality of the MHC class II antigens, two of the tumor cell lines, one expressing high levels of MHC class II antigens (SU8686; 44.4% MHC class II expressing cells after incubation with interferon-γ), and one expressing little to no MHC class II antigens (Colo-357; 4.0% MHC class II expressing cells after incubation with interferon-γ), as determined by FACS analysis, were chosen and cultivated with interferon-γ for 48 h. The tumor cells were irradiated to prevent their proliferation and then co-cultivated with isolated T cells and staphylococci enterotoxin B (SEB), a well-established "super" antigen. Proliferation of T lymphocytes was then measured after 36 h. Co-cultivation of T lymphocytes with SEB and SU8686, pre-incubated with interferon-γ, resulted in profound T lymphocyte proliferation, compared to T cells co-cultivated with SU8686 without prior interferon-γ exposure, or to T cells cultivated in the absence of SU8686 or SEB (Figs. 7 and 8). Colo-357 that only acquired little MHC class II induced little to no proliferation of the T lymphocytes.

Discussion

In the present study, we focussed on rather specialized interaction molecules, the MHC class II complex (HLA-DR, DP, DQ) because as specialized recognition molecules they could provide a link between the local inflammation and the specific immune response. Under physiological conditions, constitutive expression of MHC class II molecules is restricted to professional antigen presenting

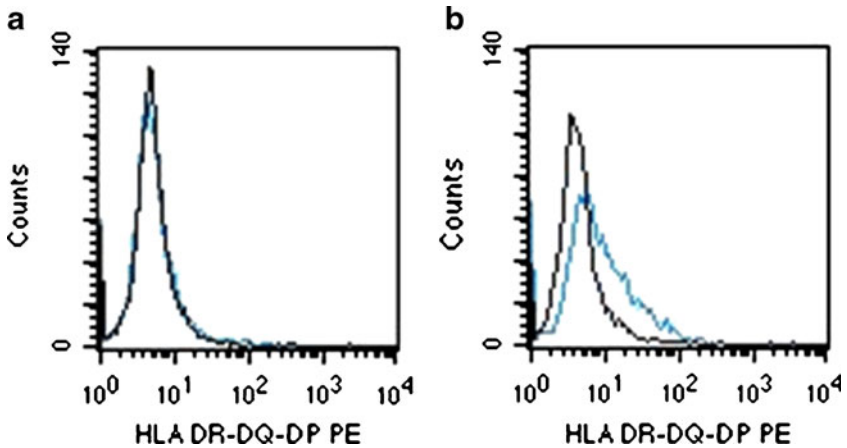

Fig. 6 MHC class II expression on the pancreatic tumor cell line SU8686 as determined by cytofluorometry. **a** Untreated cells do not express MHC class II (*left panel*); **b** following culture with interferon-γ for 48 h, MHC class II expression was seen (*right panel*). The *dotted line* indicates the antibody to HLA-DR-DQ-DP and the *thick line* indicates the isotype control

Table 5 Induction of MHC class II expression on ductal pancreatic tumor cell lines (48 h), measured as the percent of cells expressing MHC class II

Cell line	MHC class II expression		Isotype (IgG) control	
	Culture without interferon-γ	Following culture with interferon-γ	Culture without interferon-γ	Following culture with interferon-γ
AspC-1	4.1%	43.7%	3.9%	4.4%
BxPC3	4.0%	21.4%	4.2%	6.2%
Capan1	0.3%	24.5%	0.4%	0.9%
Colo-357	0.4%	4.0%	0.5%	1.0%
MiaPaca	0.5%	1.4%	0.7%	1.3%
SU8686	2.8%	44.4%	2.2%	6.9%
T3M4	0.2%	29.9%	1.0%	0.4%
Panc-1	2.0%	4.8%	3.1%	3.7%

cells, including dendritic cells, monocytes and B lymphocytes. MHC class II molecules bind processed antigenic peptides and present them to the antigen-specific T cell receptors on CD4+ T lymphocytes. The ensuing antigen-specific T cell activation is dependent on appropriate co-stimulatory signals and can be modified by the cytokines within the microenvironment [38, 39]. MHC class II expression, however, is not limited to antigen presenting cells. Under inflammatory conditions, polymorphonuclear neutrophils [26] and epithelial cells [40] acquire MHC class II molecules. Moreover, a variety of tumor cells express MHC class II [21–24]. The data for pancreatic ductal adenocarcinoma are rather limited. In two studies MHC class II expression in three out of eight patients [14] and in 11 out of 37 patients [25] was described. According to another study, expression of MHC class II could not be demonstrated by cytofluorometry in untreated, primary PDAC cells of 19 patients [9], while others found MHC class II on cultured PDAC lines [14] that could be induced by interferon-γ [14, 25]. In our series, MHC class II expression was detected in the majority of PDAC (76.8%) and of PET (70.0%). MHC class II expression correlated positively with the severity and the activity of the inflammatory reaction, and notably, with the infiltration of CD4+ T lymphocytes. Since the latter produce interferon-γ, the major effector cytokine for induction of MHC class II antigens in professional and non-professional antigen presenting cells [41], these data suggest that the infiltrating CD4+ T lymphocytes induce the MHC class II expression on the tumor cells. The fact that infiltrating T lymphocytes or PDAC tissue-derived tumor-reactive T lymphocytes release interferon-γ has been shown before [3, 42, 43]; moreover, we found that interferon-γ induced surface expression of MHC class II antigen on pancreatic tumor cell lines. Additionally, stained normal pancreas tissue revealed no MHC class II expression, reflecting the MHC class II expression as an effect induced by the inflammatory microenvironment in the tumor.

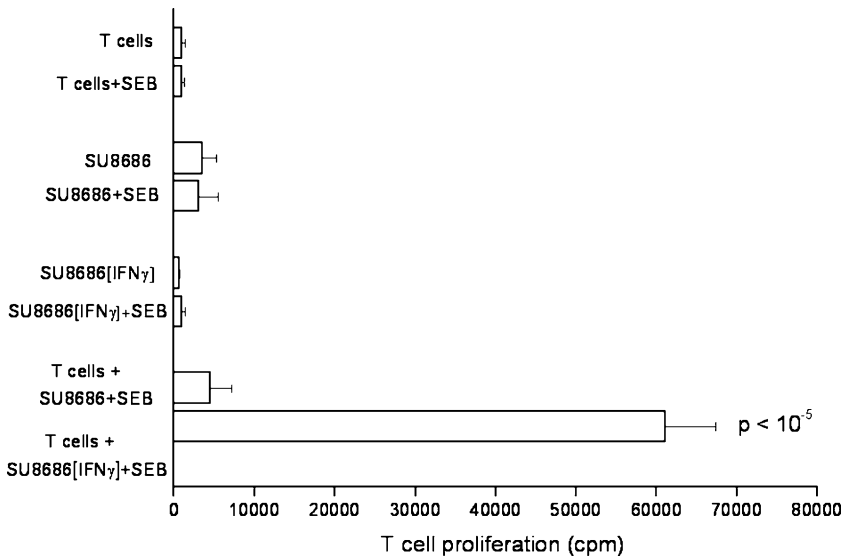

Fig. 7 Induction of T lymphocyte proliferation by the interferon-γ-treated pancreas tumor cell line SU8686 and staphylococci enterotoxin B (SEB). SU8686—either pre-treated with interferon-γ or not—were cultivated with T cells of a healthy donor in absence or presence of SEB. After 3 days, proliferation was measured as incorporation of ^{3}H-thymidine

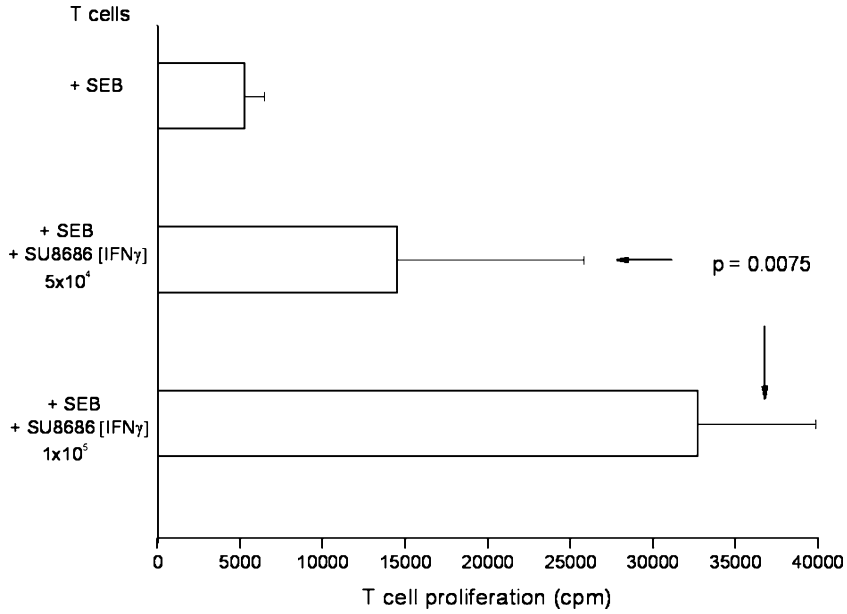

Fig. 8 Two concentrations of interferon-γ-treated SU8686 were used, SEB and T cells of a healthy donor. Values are given as counts per minute (*cpm*); shown is the mean ± SD of 5 replica)

The fact that the cell lines varied with regard to MHC class II expression could reflect their differentiation status: well or moderately differentiated cell lines such as Capan-1, Su8686 T3M4 or AsPC1 acquired more MHC class II after interferon-γ stimulation compared to the poorly differentiated cell lines Panc-1 or Colo-357. These data are in accordance to our histological findings, in which high levels of MHC class II expression coincided with a better histological differentiation grade. De-differentiation of the tumors may probably cause a loss of MHC class II antigen expression of tumor cells. In our study, the presence or absence of lymph node or distant metastases did not correlate with MHC class II expression in the PDAC collective, nor did the pT stage, the latter obviously due to the fact that 110 patients revealed a pT3 status. In PET, pT stage correlated significantly with the expression of MHC class II expression by endocrine tumor cells.

MHC class II expression did not correlate with lymph node or organ metastases, corresponding to the findings of Monti et al., who tested pancreatic cancer cell lines either cultivated from the primary tumors or from metastases revealing no differences of MHC class II expression [44].

So far, the functional role of MHC class II molecules on tissue cells is poorly understood. Except for the special situation in the thymus, in which thymus epithelial cells present self-antigens and thereby contribute to the shaping of the T cell repertoire, only in vitro data are available showing that MHC class II on tissue cells such as keratinocytes [45], tubular epithelial cells [46] or synovial fibroblasts [47] can present superantigen to T cells, thereby inducing their proliferation. The special situation of superantigens, such as, the staphylococcus enterotoxin (SE) B used as reliable model superantigen in our study, is that they bind to the non-variable region of the MHC class II molecule without prior processing and are recognised by a large number of CD4+ T lymphocytes in a MHC class II-dependent but unrestricted and antigen-unspecific manner. Binding results in the activation of T cells, apparent as proliferation [48]. Under our experimental conditions, we found that pancreatic tumor cell lines induced to express MHC class II antigens were able to trigger T cell proliferation when SEB was present.

The role of activated T cells, particularly that of CD4+ T lymphocytes, is currently under intense investigation and pro- or antitumorigenic functions have been described, depending on the cytokine environment [49–51]. Pancreatic tumor cells are specifically recognized by autologous T lymphocytes [9]. Based on these observations and our results, MHC class II antigens on pancreatic tumor cells might serve as a means to present tumor-associated antigens. According to the classical dogma, MHC class II molecules present processed exogenous antigens as opposed to self-antigens that are presented by MHC class I. This strict segregation, however, no longer holds true, and multiple alternative antigen-presenting pathways involving MHC class II antigens have been described [52]. In that, MHC class II expression on pancreatic tumor cells could participate in the CD4+ T lymphocyte-mediated arrest of carcinogenesis. However, no correlation between MHC class II expression and patient survival was seen in our study, which is quite in contrast to data on patients with colorectal cancer, in which MHC class II expression correlated with a better survival [21]. The generally dismal prognosis of PDAC patients with a 5-year survival rate of less than 5% assembling all components like aggressive and invasive tumor growth, early metastasis and resistance to radiation

and chemotherapy [53], overbalances probably the effects of the MHC class II-mediated immune reaction and of the surrounding inflammatory infiltrate in PDAC. For PET, correlations with MHC class II molecules and survival should be performed in a larger series including longer follow-up periods to obtain reliable results. Nevertheless, the inflammatory infiltrate, influencing the tumor cell growth, tumor cell migration or tumor neoangiogenesis [10, 12, 54], might also be an important factor in PET biology. As previously shown for malignant melanoma, even scarce inflammatory infiltrates may significantly affect the tumor biology and the resulting prognosis of the patients [55].

The question arises whether the expression of MHC class II antigens on tumor cells might have some benefit for patients with PDAC or PET. A major problem in the host defence and by analogy of immunologic-based therapies is the "tumor-immune-escape" [56], which—at least in part—is due to the downregulation of recognition structures on the tumor cells, including MHC molecules [14]. In this context, pancreatic ductal adenocarcinomas [25] as well as pancreatic endocrine tumor cells [57], are characterized to reveal a loss of MHC class I molecules, probably to escape a CD8+ T cell-mediated cytotoxic reaction. A direct relationship between the expression profiles of MHC class I and class II molecules could not be demonstrated in a study for PDAC, though both molecules are inducible by interferon-γ [25]. Consequently, in various clinical trials, e.g. on malignant melanoma, interferon was applied to induce MHC class I and MHC class II molecules and as consequence levels of melanoma-specific CD4+ T lymphocytes increased [58, 59]. Since MHC class II can be induced also on pancreatic cancer cells, an interferon-γ-based therapy is worth considering, especially in better differentiated cancers. On the other hand, a note of caution is imperative: MHC class molecules can also induce antigen-specific anergy of T lymphocytes, e.g. when co-stimulatory signals on the target cells are missing [60]. In conclusion, our findings suggest that MHC class II expression on pancreatic tumor cells is induced by the intratumoral inflammatory reaction in pancreatic tumors and might play an important role in the interaction of the inflammatory cells with pancreatic tumors.

Acknowledgements We thank Prof. Dr. Ulrich Abel, Department of Medical Biometry, University of Heidelberg for the professional evaluation of the biostatistics. We thank Mrs. Birgit Prior, Institute for Immunology, University of Heidelberg and Mrs. Sarah Messnard, Institute of Pathology, University of Heidelberg for their excellent technical support.

Conflict of interest statement None of the authors declare a conflict of interest.

References

1. Jemal A, Siegel R, Ward E, Hao Y, Xu J, Thun MJ (2009) Cancer statistics, 2009. CA Cancer J Clin 59(4):225–249
2. Hanahan D, Weinberg RA (2000) The hallmarks of cancer. Cell 100(1):57–70
3. Kleeff J, Beckhove P, Esposito I, Herzig S, Huber PE, Lohr JM, Friess H (2007) Pancreatic cancer microenvironment. Int J Cancer 121(4):699–705
4. Welsch T, Kleeff J, Friess H (2007) Molecular pathogenesis of pancreatic cancer: advances and challenges. Curr Mol Med 7 (5):504–521
5. Greer JB, Whitcomb DC (2009) Inflammation and pancreatic cancer: an evidence-based review. Curr Opin Pharmacol 9 (4):411–418
6. Tingstedt B, Johansson P, Andersson B, Andersson R (2007) Predictive factors in pancreatic ductal adenocarcinoma: role of the inflammatory response. Scand J Gastroenterol 42(6):754–759
7. Esposito I, Menicagli M, Funel N, Bergmann F, Boggi U, Mosca F, Bevilacqua G, Campani D (2004) Inflammatory cells contribute to the generation of an angiogenic phenotype in pancreatic ductal adenocarcinoma. J Clin Pathol 57(6):630–636
8. Bolignano D, Donato V, Lacquaniti A, Fazio MR, Bono C, Coppolino G, Buemi M (2010) Neutrophil gelatinase-associated lipocalin (NGAL) in human neoplasias: a new protein enters the scene. Cancer Lett 288(1):10–16
9. Schmitz-Winnenthal FH, Escobedo LV, Beckhove P, Schirrmacher V, Bucur M, Ziouta Y, Volk C, Schmied B, Koch M, Antolovic D, Weitz J, Buchler MW, Z'Graggen K (2006) Specific immune recognition of pancreatic carcinoma by patient-derived CD4 and CD8 T cells and its improvement by interferon-gamma. Int J Oncol 28(6):1419–1428
10. Wente MN, Gaida MM, Mayer C, Michalski CW, Haag N, Giese T, Felix K, Bergmann F, Giese NA, Friess H (2008) Expression and potential function of the CXC chemokine CXCL16 in pancreatic ductal adenocarcinoma. Int J Oncol 33(2):297–308
11. Gaida MM, Gunther F, Wagner C, Friess H, Giese NA, Schmidt J, Hansch GM, Wente MN (2008) Expression of the CXCR6 on polymorphonuclear neutrophils in pancreatic carcinoma and in acute, localized bacterial infections. Clin Exp Immunol 154 (2):216–223
12. Wente MN, Mayer C, Gaida MM, Michalski CW, Giese T, Bergmann F, Giese NA, Buchler MW, Friess H (2008) CXCL14 expression and potential function in pancreatic cancer. Cancer Lett 259(2):209–217
13. Koshiba T, Hosotani R, Miyamoto Y, Ida J, Tsuji S, Nakajima S, Kawaguchi M, Kobayashi H, Doi R, Hori T, Fujii N, Imamura M (2000) Expression of stromal cell-derived factor 1 and CXCR4 ligand receptor system in pancreatic cancer: a possible role for tumor progression. Clin Cancer Res 6(9):3530–3535
14. Scupoli MT, Sartoris S, Tosi G, Ennas MG, Nicolis M, Cestari T, Zamboni G, Martignoni G, Lemoine NR, Scarpa A, Accolla RS (1996) Expression of MHC class I and class II antigens in pancreatic adenocarcinomas. Tissue Antigens 48(4 Pt 1):301–311
15. Berghuis D, de Hooge AS, Santos SJ, Horst D, Wiertz EJ, van Eggermond MC, van den Elsen PJ, Taminiau AH, Ottaviano L, Schaefer KL, Dirksen U, Hooijberg E, Mulder A, Melief CJ, Egeler RM, Schilham MW, Jordanova ES, Hogendoorn PC, Lankester AC (2009) Reduced human leukocyte antigen expression in advanced-stage Ewing sarcoma: implications for immune recognition. J Pathol 218(2):222–231
16. Townsend A, Bodmer H (1989) Antigen recognition by class I-restricted T lymphocytes. Annu Rev Immunol 7:601–624
17. Albanesi C, Cavani A, Girolomoni G (1998) Interferon-gamma-stimulated human keratinocytes express the genes necessary for

the production of peptide-loaded MHC class II molecules. J Invest Dermatol 110(2):138–142
18. Fais S, Capobianchi MR, Marcheggiano A, Iannoni C, Pallone F (1992) MHC class II antigens on the epithelial cells of the human gastrointestinal tract. Gastroenterology 102(1):377–378
19. Ruiter DJ, Bergman W, Welvaart K, Scheffer E, van Vloten WA, Russo C, Ferrone S (1984) Immunohistochemical analysis of malignant melanomas and nevocellular nevi with monoclonal antibodies to distinct monomorphic determinants of HLA antigens. Cancer Res 44(9):3930–3935
20. Dengjel J, Nastke MD, Gouttefangeas C, Gitsioudis G, Schoor O, Altenberend F, Muller M, Kramer B, Missiou A, Sauter M, Hennenlotter J, Wernet D, Stenzl A, Rammensee HG, Klingel K, Stevanovic S (2006) Unexpected abundance of HLA class II presented peptides in primary renal cell carcinomas. Clin Cancer Res 12(14 Pt 1):4163–4170
21. Walsh MD, Dent OF, Young JP, Wright CM, Barker MA, Leggett BA, Bokey L, Chapuis PH, Jass JR, Macdonald GA (2009) HLA-DR expression is associated with better prognosis in sporadic Australian clinicopathological Stage C colorectal cancers. Int J Cancer 125 (5):1231–1237
22. Concha A, Esteban F, Cabrera T, Ruiz-Cabello F, Garrido F (1991) Tumor aggressiveness and MHC class I and II antigens in laryngeal and breast cancer. Semin Cancer Biol 2(1):47–54
23. Esteban F, Concha A, Huelin C, Perez-Ayala M, Pedrinaci S, Ruiz-Cabello F, Garrido F (1989) Histocompatibility antigens in primary and metastatic squamous cell carcinoma of the larynx. Int J Cancer 43(3):436–442
24. Andersen SN, Rognum TO, Lund E, Meling GI, Hauge S (1993) Strong HLA-DR expression in large bowel carcinomas is associated with good prognosis. Br J Cancer 68(1):80–85
25. Pandha H, Rigg A, John J, Lemoine N (2007) Loss of expression of antigen-presenting molecules in human pancreatic cancer and pancreatic cancer cell lines. Clin Exp Immunol 148(1):127–135
26. Radsak M, Iking-Konert C, Stegmaier S, Andrassy K, Hansch GM (2000) Polymorphonuclear neutrophils as accessory cells for T-cell activation: major histocompatibility complex class II restricted antigen-dependent induction of T-cell proliferation. Immunology 101(4):521–530
27. Bosman FT, Carneiro F, Hruban RH, Theise ND (eds) (2010) World Health Organisation classification of tumours. Pathology and genetics of tumours of the digestive system. Ductal adenocarcinoma of the pancreas. IARC Press, Lyon
28. Sobin LH, Gospodarowicz MK, Wittekind C (2009) TNM classification of malignant tumours, 7th edition. Wiley, Oxford
29. Heitz PU, Komminoth P, Perren A (2004) Tumours of endocrine organs: pathology and genetics World Health Organisation classification of tumors. IARC press, Lyon
30. Bosman FT, Carneiro F, Hruban RH, Theise ND (2010) World Health Organisation classification of tumours. Pathology and genetics of tumours of the digestive system. Neuroendocrine neoplasms of the pancreas. IARC press, Lyon
31. Rindi G, Kloppel G, Alhman H, Caplin M, Couvelard A, de Herder WW, Erikssson B, Falchetti A, Falconi M, Komminoth P, Korner M, Lopes JM, McNicol AM, Nilsson O, Perren A, Scarpa A, Scoazec JY, Wiedenmann B (2006) TNM staging of foregut (neuro)endocrine tumors: a consensus proposal including a grading system. Virchows Arch 449(4):395–401
32. Bergmann F, Breinig M, Hopfner M, Rieker RJ, Fischer L, Kohler C, Esposito I, Kleeff J, Herpel E, Ehemann V, Friess H, Schirmacher P, Kern MA (2009) Expression pattern and functional relevance of epidermal growth factor receptor and cyclooxygenase-2: novel chemotherapeutic targets in pancreatic endocrine tumors? Am J Gastroenterol 104(1):171–181
33. Ceyhan GO, Bergmann F, Kadihasanoglu M, Erkan M, Park W, Hinz U, Giese T, Muller MW, Buchler MW, Giese NA, Friess H (2007) The neurotrophic factor artemin influences the extent of neural damage and growth in chronic pancreatitis. Gut 56(4):534–544
34. Bijen CB, Bantema-Joppe EJ, de Jong RA, Leffers N, Mourits MJ, Eggink HF, van der Zee AG, Hollema H, de Bock GH, Nijman HW (2010) The prognostic role of classical and nonclassical MHC class I expression in endometrial cancer. Int J Cancer 126(6):1417–1427
35. Rolland P, Deen S, Scott I, Durrant L, Spendlove I (2007) Human leukocyte antigen class I antigen expression is an independent prognostic factor in ovarian cancer. Clin Cancer Res 13 (12):3591–3596
36. Itano AA, Jenkins MK (2003) Antigen presentation to naive CD4 T cells in the lymph node. Nat Immunol 4(8):733–739
37. Rocha N, Neefjes J (2008) MHC class II molecules on the move for successful antigen presentation. EMBO J 27(1):1–5
38. Radfar S, Wang Y, Khong HT (2009) Activated CD4+ T cells dramatically enhance chemotherapeutic tumor responses in vitro and in vivo. J Immunol 183(10):6800–6807
39. DeNardo DG, Barreto JB, Andreu P, Vasquez L, Tawfik D, Kolhatkar N, Coussens LM (2009) CD4(+) T cells regulate pulmonary metastasis of mammary carcinomas by enhancing protumor properties of macrophages. Cancer Cell 16(2):91–102
40. Han DC, Huang GT, Lin LM, Warner NA, Gim JS, Jewett A (2003) Expression of MHC Class II, CD70, CD80, CD86 and pro-inflammatory cytokines is differentially regulated in oral epithelial cells following bacterial challenge. Oral Microbiol Immunol 18(6):350–358
41. Giacomini P, Tecce R, Gambari R, Sacchi A, Fisher PB, Natali PG (1988) Recombinant human IFN-gamma, but not IFN-alpha or IFN-beta, enhances MHC- and non-MHC-encoded glycoproteins by a protein synthesis-dependent mechanism. J Immunol 140 (9):3073–3081
42. Tang KF, Chan SH, Loh KS, Chong SM, Wang D, Yeoh KH, Hu H (1999) Increased production of interferon-gamma by tumour infiltrating T lymphocytes in nasopharyngeal carcinoma: indicative of an activated status. Cancer Lett 140(1–2):93–98
43. Schmitz-Winnenthal FH, Volk C, Z'Graggen K, Galindo L, Nummer D, Ziouta Y, Bucur M, Weitz J, Schirrmacher V, Buchler MW, Beckhove P (2005) High frequencies of functional tumor-reactive T cells in bone marrow and blood of pancreatic cancer patients. Cancer Res 65(21):10079–10087
44. Monti P, Marchesi F, Reni M, Mercalli A, Sordi V, Zerbi A, Balzano G, Di Carlo V, Allavena P, Piemonti L (2004) A comprehensive in vitro characterization of pancreatic ductal carcinoma cell line biological behavior and its correlation with the structural and genetic profile. Virchows Arch 445(3):236–247
45. Nickoloff BJ, Mitra RS, Green J, Shimizu Y, Thompson C, Turka LA (1993) Activated keratinocytes present bacterial-derived superantigens to T lymphocytes: relevance to psoriasis. J Dermatol Sci 6(2):127–133
46. Schulz H, Karau A, Filsinger S, Schoels M, Kabelitz D, Richter R, Hansch GM (1998) Tubular epithelial cells as accessory cells for superantigen-induced T cell activation. Exp Nephrol 6(1):67–73
47. Kraft M, Filsinger S, Kramer KL, Kabelitz D, Hansch GM, Schoels M (1995) Synovial fibroblasts as accessory cells for staphylococcal enterotoxin-mediated T-cell activation. Immunology 85(3):461–466
48. Fanger NA, Liu C, Guyre PM, Wardwell K, O'Neil J, Guo TL, Christian TP, Mudzinski SP, Gosselin EJ (1997) Activation of human T cells by major histocompatability complex class II expressing neutrophils: proliferation in the presence of super-antigen, but not tetanus toxoid. Blood 89(11):4128–4135
49. Muller-Hermelink N, Braumuller H, Pichler B, Wieder T, Mailhammer R, Schaak K, Ghoreschi K, Yazdi A, Haubner R, Sander CA, Mocikat R, Schwaiger M, Forster I, Huss R,

Weber WA, Kneilling M, Rocken M (2008) TNFR1 signaling and IFN-gamma signaling determine whether T cells induce tumor dormancy or promote multistage carcinogenesis. Cancer Cell 13 (6):507–518
50. Marzo AL, Kinnear BF, Lake RA, Frelinger JJ, Collins EJ, Robinson BW, Scott B (2000) Tumor-specific CD4+ T cells have a major "post-licensing" role in CTL mediated anti-tumor immunity. J Immunol 165(11):6047–6055
51. Fukunaga A, Miyamoto M, Cho Y, Murakami S, Kawarada Y, Oshikiri T, Kato K, Kurokawa T, Suzuoki M, Nakakubo Y, Hiraoka K, Itoh T, Morikawa T, Okushiba S, Kondo S, Katoh H (2004) CD8+ tumor-infiltrating lymphocytes together with CD4+ tumor-infiltrating lymphocytes and dendritic cells improve the prognosis of patients with pancreatic adenocarcinoma. Pancreas 28(1):e26–e31
52. Lindner R, Unanue ER (1996) Distinct antigen MHC class II complexes generated by separate processing pathways. EMBO J 15(24):6910–6920
53. Li D, Xie K, Wolff R, Abbruzzese JL (2004) Pancreatic cancer. Lancet 363(9414):1049–1057
54. Strieter RM, Burdick MD, Mestas J, Gomperts B, Keane MP, Belperio JA (2006) Cancer CXC chemokine networks and tumour angiogenesis. Eur J Cancer 42(6):768–778
55. Clemente CG, Mihm MC Jr, Bufalino R, Zurrida S, Collini P, Cascinelli N (1996) Prognostic value of tumor infiltrating lymphocytes in the vertical growth phase of primary cutaneous melanoma. Cancer 77(7):1303–1310
56. von Bernstorff W, Voss M, Freichel S, Schmid A, Vogel I, Johnk C, Henne-Bruns D, Kremer B, Kalthoff H (2001) Systemic and local immunosuppression in pancreatic cancer patients. Clin Cancer Res 7(3 Suppl):925s–932s
57. Ye X, Kralli A, Ge R, Ricciardi RP, Knowles BB (1994) Down-regulation of MHC class I antigen in insulinoma cells controlled by the R1 element of the H-2 enhancer. Oncogene 9(4):1195–1204
58. Lotem M, Machlenkin A, Hamburger T, Nissan A, Kadouri L, Frankenburg S, Gimmon Z, Elias O, David IB, Kuznetz A, Shiloni E, Peretz T (2009) Autologous melanoma vaccine induces antitumor and self-reactive immune responses that affect patient survival and depend on MHC class II expression on vaccine cells. Clin Cancer Res 15(15): 4968–4977
59. Propper DJ, Chao D, Braybrooke JP, Bahl P, Thavasu P, Balkwill F, Turley H, Dobbs N, Gatter K, Talbot DC, Harris AL, Ganesan TS (2003) Low-dose IFN-gamma induces tumor MHC expression in metastatic malignant melanoma. Clin Cancer Res 9(1):84–92
60. Schwartz RH (1996) Models of T cell anergy: is there a common molecular mechanism? J Exp Med 184(1):1–8

Virchows Arch (2012) 460:61–68
DOI 10.1007/s00428-011-1174-y

ORIGINAL ARTICLE

Expression of Raf-1 kinase inhibitory protein in carcinoma of the ampulla of Vater

Hyun-Soo Kim · Sun Ho Lee · Kyu Yeoun Won · Gou Young Kim · Yong-Koo Park · Youn Wha Kim

Received: 29 September 2011 / Revised: 2 November 2011 / Accepted: 8 November 2011 / Published online: 20 November 2011
© Springer-Verlag 2011

Abstract Raf-1 kinase inhibitor protein (RKIP) has emerged as a significant metastatic suppressor in a variety of human malignancies. We have recently demonstrated that reduced expression of RKIP is significantly associated with invasion and metastasis in periampullary carcinomas, including pancreatic carcinoma, gallbladder carcinoma, and extrahepatic bile duct carcinoma. In this study, we evaluated RKIP expression in ampulla of Vater (AoV) carcinoma and investigated its prognostic significance. Immunostaining for RKIP was performed for 80 and 21 cases with primary and nodal metastatic AoV carcinoma, respectively. RKIP expression was reduced in 32.5% (26/80) and 66.7% (14/21) of primary and nodal metastatic AoV carcinoma cases, respectively. This distribution of RKIP expression was statistically significant ($P<0.001$). The reduction in RKIP expression was significantly associated with the presence of nodal ($P=0.008$) and distant ($P=0.002$) metastases, a higher TNM stage group ($P=0.010$), lymphatic invasion ($P<0.001$), vascular invasion ($P<0.001$), and a shorter disease-free survival (DFS; $P=0.028$) and distant metastasis-free survival (DMFS; $P=0.005$). In addition, reduced RKIP expression was an independent prognostic predictor for worse DFS and DMFS ($P=0.032$ and $P=0.036$, respectively). Our data suggest that a reduction in RKIP expression contributes to invasion and metastasis in AoV carcinoma and is a significant prognostic marker in patients with AoV carcinoma.

Keywords Raf kinase inhibitory protein · Metastasis · Ampulla of Vater · Carcinoma · Immunohistochemistry

H.-S. Kim
Aerospace Medical Research Center, Aerospace Medical Center, Republic of Korea Air Force,
Cheongwon-gun, Chungcheongbuk-do, Republic of Korea

S. H. Lee · K. Y. Won · G. Y. Kim · Y.-K. Park · Y. W. Kim (✉)
Department of Pathology, School of Medicine,
Kyung Hee University,
1 Hoegi-dong, Dongdaemun-gu,
130-702, Seoul, Republic of Korea
e-mail: kimyw@khu.ac.kr

Introduction

Raf-1 kinase inhibitory protein (RKIP), also known as phosphatidylethanolamine-binding protein 1, has been implicated as a modulator of several fundamental signal transduction pathways that control cellular growth, differentiation, apoptosis, and migration, including the mitogen-activated protein kinase (MAPK) pathway, nuclear factor–kappa B (NF–κB) pathway, and G protein-coupled receptor (GPCR) pathway [1–5]. RKIP blocks Raf-1-induced phosphorylation of MAPK/extracellular signal-regulated kinase (ERK) kinase (MEK), via direct binding to Raf-1 or MEK, and consequently inhibits the activation of ERK. In addition to its modulation of the MAPK pathway, RKIP inhibits NF–κB activity by interacting with upstream NF–κB activators such as the NF–κB-inducing kinase and TGF-β-activated kinase 1 [5]. RKIP also inhibits GPCR kinase 2 (GRK2), a negative feedback inhibitor of GPCR [4, 6]. RKIP that has been phosphorylated by protein kinase C is released from Raf-1 and binds to GRK2, blocking its activity and enhancing GPCR signaling.

Recently, RKIP was identified as a suppressor of metastasis. RKIP expression has been shown to be significantly reduced in a variety of human carcinomas,

and a significant association of reduced RKIP expression with invasion and metastasis has been reported in carcinomas of the colorectum [7, 8], stomach [9], breast [10], nasopharynx [11], and ovary [12] and in malignant melanoma [13]. Furthermore, in a study using an orthotopic murine model, restoration of RKIP in metastatic prostate carcinoma cells inhibited cell invasion in vitro and lung metastasis in vivo, suggesting that RKIP suppresses the metastatic potential of prostate carcinoma cells [14].

Carcinoma of the ampulla of Vater (AoV) is a relatively uncommon tumor that accounts for approximately 6% of all periampullary carcinomas [15]. In most series, the resectability rate is higher and the prognosis is better when AoV carcinoma is compared with other periampullary carcinomas [16]. However, reported series of AoV carcinoma usually contain small numbers of patients, making definitive conclusions difficult. Furthermore, given the rarity of this malignancy, prognostic indicators of survival remain poorly defined.

We have recently demonstrated that reduced RKIP expression is significantly associated with lymphovascular invasion and metastasis in periampullary carcinomas, including pancreatic carcinoma [17], gallbladder carcinoma [18], and extrahepatic bile duct carcinoma [19]. We have also provided evidence suggesting that reduced RKIP expression is a significant prognostic marker for worse postoperative survival in patients with periampullary carcinomas [17–19]. The evidence for an important role of RKIP in tumor progression prompted us to evaluate the expression of RKIP in AoV carcinoma and to investigate its association with clinicopathological characteristics and patient outcomes.

Materials and methods

Tumor samples

This study included 80 patients with AoV carcinoma who underwent pylorus-preserving pancreaticoduodenectomy with lymphadenectomy at Kyung Hee University Hospital between January 1994 and December 2008 and did not have a microscopically residual tumor. Of the 80 cases with primary AoV carcinoma, 25 had nodal metastasis; in 21 of the 25 cases, sufficient amounts of metastatic tumor tissue (nodal metastatic AoV carcinoma) were available. No preoperative chemotherapy or radiotherapy had been performed. Two independent pathologists (H.-S.K. and Y.W.K.) reviewed all hematoxylin-and-eosin-stained slides and performed immunohistochemical staining on the most representative slide from each case. Clinicopathological characteristics, including sex, age, tumor size, histological grade, histological subtype (pancreaticobiliary or intestinal), pathological tumor stage, nodal metastasis, distant metastasis, local recurrence, TNM stage group, lymphatic invasion, vascular invasion, and perineural invasion were assessed. The tumors were postoperatively staged according to the seventh edition of the American Joint Committee on Cancer Staging System [20]. No distant metastasis was identified at the time of surgery. Research protocols for the use of human tissue were approved by and conducted in accordance with the policies of the Institutional Review Board at Kyung Hee University Hospital. Informed consent was obtained from all subjects.

Immunohistochemistry

RKIP expression was assessed by immunohistochemistry using the Bond Polymer Intense Detection System (Vision BioSystems, Mount Waverley, VIC, Australia) according to the manufacturer's instructions, with minor modifications. In brief, 4-μm sections of formalin-fixed, paraffin-embedded tissue were deparaffinized using the Bond Dewax Solution (Vision BioSystems), and antigen retrieval was performed using the Bond ER Solution (Vision BioSystems) for 30 min at 100°C. Endogenous peroxidase activity was quenched by incubation with hydrogen peroxide for 5 min. The sections were incubated for 15 min at ambient temperature with a polyclonal rabbit antibody against RKIP (1:200, Santa Cruz Biotechnology, Santa Cruz, CA, USA) using a biotin-free polymeric horseradish peroxidase linker antibody conjugate system in the Bond-maX™ autostainer (Vision BioSystems). Nuclei were counterstained with hematoxylin. The positive control sample was normal human AoV mucosa. The negative control sample was the same normal tissue without antibody.

Evaluation of immunohistochemical staining

Immunohistochemical RKIP expression was analyzed using a semi-quantitative scoring method, as described previously [7, 17–19, 21, 22]. Briefly, the score is the sum of the percentage of positive tumor cells (0, none; 1, <25%; 2, 25–49%; and 3, ≥50%) and the staining intensity (0, negative; 1, weak; 2, moderate; and 3, strong). Specimens with sums between 0 and 2 were scored as negative; sums of 3 and 4 were scored as weakly positive, and sums of 5 and 6 were scored as positive. All slides were examined and scored by two independent pathologists (H.-S.K. and Y.W.K.), who were blinded to the clinicopathological data and patient identity. Disagreements between the two pathologists were resolved by consensus.

Statistical analysis

The chi-square test or Fisher's exact test was performed to compare RKIP expression between primary and nodal metastatic AoV carcinoma and to examine the relationship between RKIP expression and clinicopathological characteristics. Univariate and multivariate survival analyses were used to determine the prognostic significance of RKIP expression in patients with AoV carcinoma. Disease-free survival (DFS) was defined as the interval from surgery to the first appearance of local recurrence or distant metastasis. Distant metastasis-free survival (DMFS) was defined as the interval from surgery to the first appearance of distant metastasis. Loss to follow-up, death from a cause other than carcinoma, and survival until the end of the follow-up period were regarded as censoring events. Curves for DFS and DMFS were drawn according to the Kaplan–Meier method, and differences were analyzed by applying the log-rank test for univariate survival analysis. Multivariate survival analysis was performed using the Cox proportional hazard models (95% confidence interval) with a backward stepwise method to remove the least significant variables from the model. Statistical analyses were performed using SPSS ver. 15.0 (SPSS Inc., Chicago, IL, USA). Statistical significance was defined as a P value of less than 0.05.

Results

The patients' ages ranged from 26 to 75 (median, 58 years). Of the 80 patients, 38 (47.5%) had ≥ pT3 tumors. The TNM stage group was I in 32 (40.0%) patients, II in 47 (58.8%), and III in one (1.2%). Fifty-one (63.8%) cases had lymphatic vessel invasion, and 12 (15.0%) cases had histological blood vessel invasion.

Normal AoV mucosa demonstrated uniform, strong cytoplasmic RKIP immunoreactivity (Fig. 1a). Of 80 cases with primary AoV carcinoma, RKIP expression was positive in 54 (67.5%; Fig. 1b), weakly positive in eight (10.0%), and negative in 18 (22.5%; Fig. 1c). Of 21 cases with nodal metastatic AoV carcinoma, RKIP expression was positive in six (28.6%), weakly positive in one (4.8%), and negative in 14 (66.7%; Fig. 1d). The difference in RKIP expression between primary and nodal metastatic AoV carcinoma was statistically significant (P<0.001).

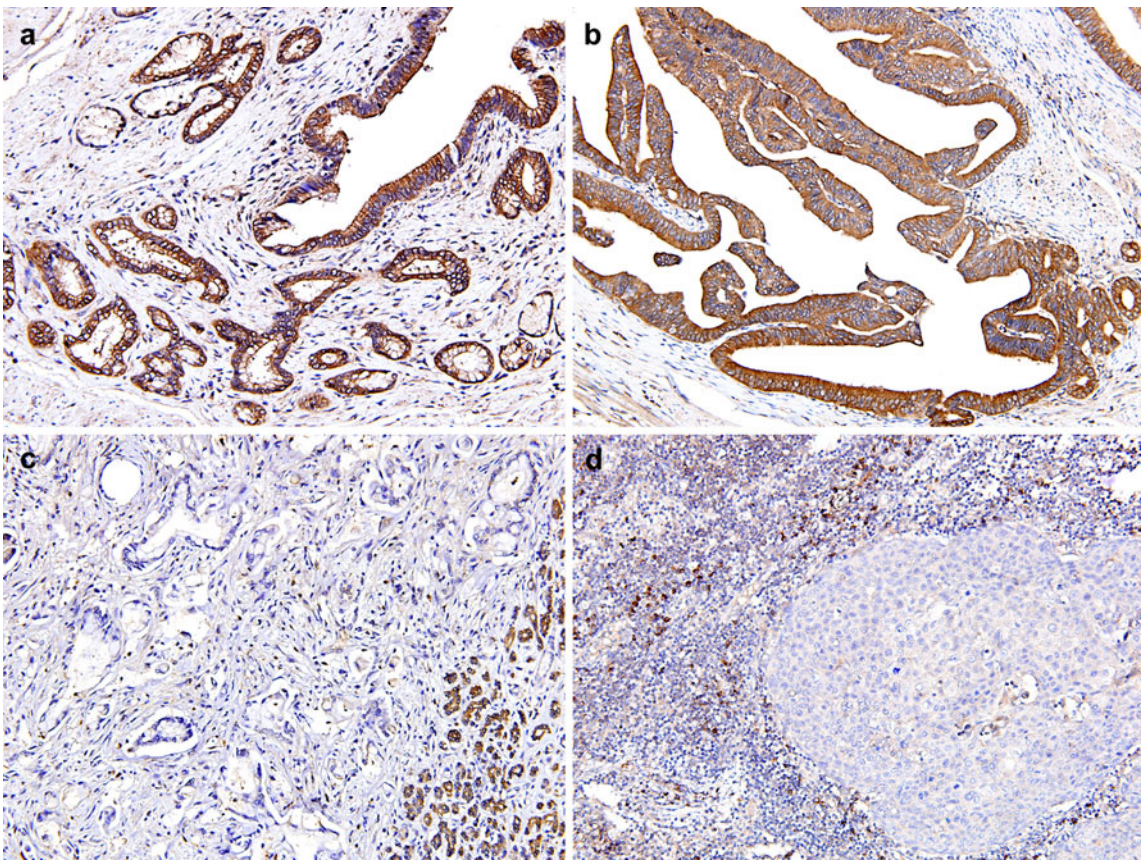

Fig. 1 RKIP immunoreactivity in normal AoV mucosa, primary AoV carcinoma, and nodal metastatic AoV carcinoma. **a** Localization of RKIP in the cytoplasm of normal AoV epithelia. **b** Positive RKIP immunoreactivity in primary AoV carcinoma. Reduced RKIP expression in **c** primary and **d** nodal metastatic AoV carcinoma (polymer method; original magnification, ×200)

Table 1 Association of RKIP expression with clinicopathological characteristics

Characteristics	Total (n=80)	Number of cases (%)			P value
		Negative	Weakly positive	Positive	
Sex					
Man	40 (50.0)	8 (20.0)	3 (7.5)	29 (72.5)	0.425
Woman	40 (50.0)	10 (25.0)	5 (2.5)	25 (62.5)	
Age (year-old)					
≥58	45 (56.3)	9 (20.0)	4 (8.9)	32 (71.1)	0.461
<58	35 (43.7)	9 (25.7)	4 (1.4)	22 (62.9)	
Tumor size (cm)					
≥2	50 (62.5)	9 (18.0)	6 (12.0)	35 (70.0)	0.336
<2	30 (37.5)	9 (30.0)	2 (6.7)	19 (63.3)	
Histological grade					
Well	15 (18.7)	2 (13.3)	2 (3.3)	11 (73.3)	0.141
Moderate	57 (71.3)	12 (21.1)	6 (0.5)	39 (68.4)	
Poor	8 (10.0)	4 (50.0)	0 (0.0)	4 (50.0)	
Histological subtype					
Pancreatobiliary	19 (31.1)	5 (26.3)	3 (15.8)	11 (57.9)	0.425
Intestinal	61 (68.9)	13 (21.3)	5 (8.2)	43 (70.5)	
Pathological tumor stage					
pT1	7 (8.7)	0 (0.0)	0 (0.0)	7 (100.0)	0.059
pT2	35 (43.8)	8 (22.9)	3 (8.6)	24 (68.6)	
pT3	37 (46.3)	9 (24.3)	5 (3.5)	23 (62.2)	
pT4	1 (1.2)	1 (100.0)	0 (0.0)	0 (0.0)	
Nodal metastasis					
Present	25 (31.2)	10 (40.0)	3 (2.0)	12 (48.0)	0.008*
Absent	55 (68.8)	8 (14.5)	5 (9.1)	42 (76.4)	
Distant metastasis					
Present	20 (25.0)	9 (45.0)	3 (5.0)	8 (40.0)	0.002*
Absent	60 (75.0)	9 (15.0)	5 (8.3)	46 (76.7)	
Local recurrence					
Present	7 (8.7)	3 (42.9)	0 (0.0)	4 (57.1)	0.311
Absent	73 (91.3)	15 (20.5)	8 (1.0)	50 (68.5)	
Stage group					
Ia	7 (8.7)	0 (0.0)	0 (0.0)	7 (100.0)	0.010*
Ib	25 (31.3)	5 (20.0)	3 (2.0)	17 (68.0)	
IIa	23 (28.8)	3 (13.0)	2 (8.7)	18 (78.3)	
IIb	24 (30.0)	9 (37.5)	3 (2.5)	12 (50.0)	
III	1 (1.2)	1 (100.0)	0 (0.0)	0 (0.0)	
Lymphatic invasion					
Present	51 (63.8)	18 (35.3)	5 (9.8)	28 (54.9)	<0.001*
Absent	29 (36.2)	0 (0.0)	3 (10.3)	26 (89.7)	
Vascular invasion					
Present	12 (15.0)	12 (100.0)	0 (0.0)	0 (0.0)	<0.001*
Absent	68 (85.0)	6 (8.8)	8 (1.8)	54 (79.4)	
Perineural invasion					
Present	7 (8.7)	1 (14.3)	2 (8.6)	4 (57.1)	0.944
Absent	73 (91.3)	17 (23.3)	6 (8.2)	50 (68.5)	

*P value is statistically significant

RKIP was expressed homogeneously throughout the whole tumor. In correlating RKIP expression with clinicopathological characteristics (Table 1), the reduction in RKIP expression was significantly associated with the presence of nodal (P=0.008) and distant (P=0.002) metastases, a higher TNM stage group (P=0.010), lymphatic invasion (P<0.001), and vascular invasion (P<0.001).

Adequate clinical follow-up information was available for all 80 patients with AoV carcinoma; the median follow-up was 45.5 months. Of the 80 patients, 35 (43.8%) patients died during the follow-up period, and the remaining 45 (56.3%) were alive at the end of the study. In 23 (28.8%) patients, distant metastasis or local recurrence was found during the follow-up period. Univariate analysis for DFS showed that reduced RKIP expression (P=0.028; Fig. 2a), a higher TNM stage group (P=0.021), lymphatic invasion (P=0.001), and vascular invasion (P=0.012) were significant predictors for a worse DFS (Table 2). Multivariate analysis showed reduced RKIP expression (P=0.032) and lymphatic invasion (P=0.006) to be independent prognostic factors predicting a worse DFS (Table 2).

Distant metastasis was detected during the follow-up period in 20 (25.0%) patients. Univariate analysis revealed that reduced RKIP expression (P=0.005; Fig. 2b), local recurrence (P=0.001), lymphatic invasion (P=0.003), and vascular invasion (P=0.003) were significantly associated with a worse DMFS (Table 2). At the multivariate level, reduced RKIP expression (P=0.036), local recurrence (P=0.020), and lymphatic invasion (P=0.018) proved to be independent prognostic factors for a worse DMFS (Table 2).

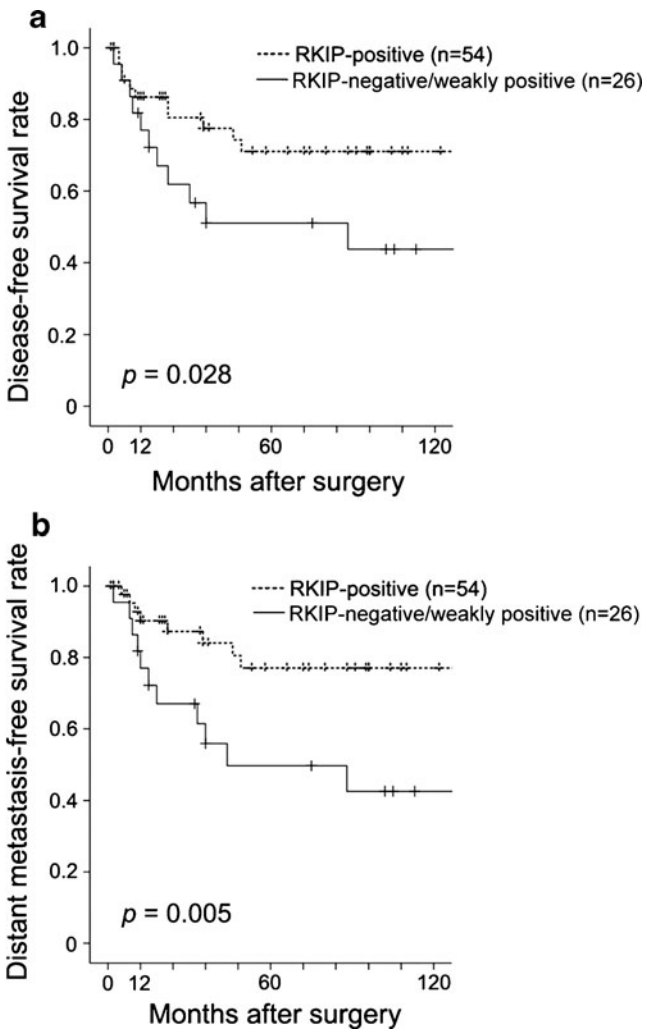

Fig. 2 Kaplan–Meier curves for **a** DFS and **b** DMFS are indicated by the *solid line* in patients with RKIP-negative or weakly positive AoV carcinoma and by the *dotted line* in patients with RKIP-positive AoV carcinoma

Discussion

This is the first study to date reporting the expression of RKIP in AoV carcinoma, using immunohistochemical staining. We observed that nodal metastatic AoV carcinoma (66.7%) had significantly reduced RKIP expression, compared with primary AoV carcinoma (32.5%). Consistent with this finding, we have recently demonstrated a significant difference in RKIP expression between primary gallbladder carcinoma (42.3%) and nodal metastatic gallbladder carcinoma (68.8%) [18]. Al-Mulla et al. [7] also showed that RKIP expression was significantly reduced in 38.6% and 72.0% of cases with primary and metastatic colorectal carcinoma, respectively. In addition, 48% and 89% of cases with primary and metastatic prostate carcinomas had reduced RKIP expression, respectively [23]. These data support the notion that RKIP functions as a suppressor of metastasis. In addition, we demonstrated that a reduction in RKIP expression is significantly associated with a higher TNM stage group, lymphovascular invasion, and the presence of nodal and distant metastases, representing a 7.1- and 9.7-fold greater risk for nodal and distant metastases in patients with RKIP-negative or weakly positive AoV carcinoma compared with patients with RKIP-positive AoV carcinoma, respectively. This agrees with results from our recent studies showing a significant association between a reduction in RKIP expression and the presence of nodal and distant metastases in pancreatic carcinoma [17] and lymphatic invasion and the presence of nodal metastasis in extrahepatic bile duct carcinoma [19]. It has also been observed that a reduction in RKIP expression is significantly associated with tumor progression and metastasis in breast carcinoma [10, 24], colorectal carcinoma [8], ovarian carcinoma [12], and malignant melanoma [13]. Taken together, our data suggest that a reduction in RKIP expression is involved in invasion and metastasis in AoV carcinoma.

Table 2 Factors predicting worse outcome of patients with AoV carcinoma (univariate and multivariate survival analyses)

Characteristics	Disease-free survival			Distant metastasis-free survival		
	Univariate	Multivariate		Univariate	Multivariate	
	P value	HR (95% CI)	*P* value	*P* value	HR (95% CI)	*P* value
Sex, man vs. woman	0.726	NA		0.905	NA	
Age (year-old), ≥ 58 vs. < 58	0.908	NA		0.894	NA	
Tumor size (cm), ≥ 2 vs. < 2	0.245	NA		0.452	NA	
Histological grade, moderate/poor vs. well	0.155	NA		0.086	NA	
Histological subtype, pancreatobiliary vs. intestinal	0.873	NA		0.927	NA	
Pathological tumor stage, pT3-4 vs. pT1-2	0.081	NA		0.230	NA	
Nodal metastasis, present vs. absent	0.544	NA		0.270	NA	
Distant metastasis, present vs. absent	NA			NA		
Local recurrence, present vs. absent	NA			0.001*	4.140 (1.251–3.697)	0.020*
Stage group, III vs. I–II	0.021*	2.154 (0.715–6.490)	0.173	0.054	NA	
Lymphatic invasion, present vs. absent	0.001*	7.656 (1.771–33.098)	0.006*	0.003*	6.059 (1.356–7.069)	0.018*
Vascular invasion, present vs. absent	0.012*	1.843 (0.737–4.609)	0.191	0.003*	1.932 (0.534–6.995)	0.316
Perineural invasion, present vs. absent	0.052	NA		0.513	NA	
RKIP expression, negative/weakly positive vs. positive	0.028*	5.262 (1.150–7.083)	0.032*	0.005*	3.649 (1.087–5.253)	0.036*

HR hazard ratio, *CI* confidence interval, *NA* not available

**P* value is statistically significant

We further demonstrated that a reduction in RKIP expression is significantly associated with a shorter DFS and DMFS in patients with AoV carcinoma. This relationship was maintained after adjusting for other conventional characteristics in the multivariate analysis, indicating that reduced RKIP expression is an independent predictor for worse DFS and DMFS in patients with AoV carcinoma. This result is consistent with our recent data demonstrating that reduced RKIP expression is an independent prognostic factor predicting worse DMFS in patients with pancreatic carcinoma [17] and previous data showing that a reduction in RKIP expression predicted a shorter survival time for patients with colorectal carcinoma [7, 8], prostate carcinoma [23], or gastric carcinoma [9]. RKIP expression therefore may be used as a significant prognostic marker in patients with AoV carcinoma.

The frequency of reduced RKIP expression in human carcinomas has been reported to vary between 1.9% and 88.2% [9–12, 17, 18, 22–27]. The following reasons may underlie such a discrepancy: differences in tumor location and histology, sample size, and intrinsic tumor heterogeneity; differences in the antibodies used; use of antigen retrieval and staining procedures with varying degrees of sensitivity; and lack of a standard evaluation method for immunohistochemical staining. In this study, RKIP expression was reduced in 32.5% of AoV carcinomas. We have observed a reduction in RKIP expression in 57.1% of pancreatic carcinomas [17], 42.3% of gallbladder carcinomas [18], and 55.0% of extrahepatic bile duct carcinomas [19]. In general, AoV carcinoma is considered to have a better prognosis than other periampullary carcinomas. We speculate that the lower frequency of reduced RKIP expression in AoV carcinoma may be partly attributable to the more favorable prognosis of AoV carcinoma compared with that of pancreatic carcinoma, gallbladder carcinoma, or extrahepatic bile duct carcinoma. Additionally, the higher frequency of reduced RKIP expression in periampullary carcinomas compared with colorectal carcinomas (33.8%) [7], breast carcinomas (1.9% and 10.5%) [10, 24], or nasopharyngeal carcinomas (23.3%) [11] may reflect a common characteristic feature of periampullary carcinomas: strong invasion and early metastasis.

Activation of the Ras/Raf/MEK/ERK pathway has been observed in a variety of human carcinomas and has been suggested to play a major role in tumor progression and metastasis [28]. Activated ERK can lead to cancer cell migration via enhanced myosin light-chain kinase [29] and cancer cell invasion via enhanced induction of matrix metalloproteinase [30, 31]. RKIP binds to Raf-1 or MEK and interferes with MEK phosphorylation and activation by Raf-1, interrupting ERK activation and thereby suppressing invasion and metastasis. However, it was interesting to observe that 15.0% (12/80) and 10.0% (8/80) of patients who suffered nodal and distant metastases, respectively, had positive RKIP expression. This result may be attributed to several factors that can affect RKIP activity or activate ERK, regardless of the status of RKIP. First, activated B-

Raf can activate MEK/ERK independently of RKIP [32]. Trakul et al. [33] demonstrated that RKIP regulates Raf-1 but not B-Raf, suggesting that B-Raf can activate ERK independent of RKIP. Second, protein kinase C has been shown to phosphorylate RKIP, which results in the dissociation of Raf-1 and RKIP [6]. Third, activation of vascular endothelial growth factor (VEGF) receptor-3 by VEGF-C or VEGF-D induces the activation of ERK, thereby promoting lymphangiogenesis and nodal metastasis [34]. Thus, activated ERK, regardless of the presence of RKIP, may induce the expression of genes involved in cancer cell invasion, migration, and metastasis.

In conclusion, we have demonstrated that a reduction in RKIP expression is significantly associated with lympho-vascular invasion and the presence of nodal and distant metastases in AoV carcinoma and can independently predict worse DFS and DMFS of patients with AoV carcinoma. These results suggest that RKIP plays a role in suppressing invasion and metastasis in AoV carcinoma.

Conflict of interest statement We declare that we have no conflict of interest.

References

1. Yeung K, Seitz T, Li S, Janosch P, McFerran B, Kaiser C, Fee F, Katsanakis KD, Rose DW, Mischak H, Sedivy JM, Kolch W (1999) Suppression of Raf-1 kinase activity and MAP kinase signalling by RKIP. Nature 401:173–177
2. Park S, Yeung ML, Beach S, Shields JM, Yeung KC (2005) RKIP downregulates B-Raf kinase activity in melanoma cancer cells. Oncogene 24:3535–3540
3. Odabaei G, Chatterjee D, Jazirehi AR, Goodglick L, Yeung K, Bonavida B (2004) Raf-1 kinase inhibitor protein: structure, function, regulation of cell signaling, and pivotal role in apoptosis. Adv Cancer Res 91:169–200
4. Kroslak T, Koch T, Kahl E, Hollt V (2001) Human phosphatidylethanolamine-binding protein facilitates heterotrimeric G protein-dependent signaling. J Biol Chem 276:39772–39778
5. Yeung KC, Rose DW, Dhillon AS, Yaros D, Gustafsson M, Chatterjee D, McFerran B, Wyche J, Kolch W, Sedivy JM (2001) Raf kinase inhibitor protein interacts with NF–kappaB-inducing kinase and TAK1 and inhibits NF–kappaB activation. Mol Cell Biol 21:7207–7217
6. Lorenz K, Lohse MJ, Quitterer U (2003) Protein kinase C switches the Raf kinase inhibitor from Raf-1 to GRK-2. Nature 426:574–579
7. Al-Mulla F, Hagan S, Behbehani AI, Bitar MS, George SS, Going JJ, Garcia JJ, Scott L, Fyfe N, Murray GI, Kolch W (2006) Raf kinase inhibitor protein expression in a survival analysis of colorectal cancer patients. J Clin Oncol 24:5672–5679
8. Minoo P, Zlobec I, Baker K, Tornillo L, Terracciano L, Jass JR, Lugli A (2007) Loss of raf-1 kinase inhibitor protein expression is associated with tumor progression and metastasis in colorectal cancer. Am J Clin Pathol 127:820–827
9. Chatterjee D, Sabo E, Tavares R, Resnick MB (2008) Inverse association between Raf kinase inhibitory protein and signal transducers and activators of transcription 3 expression in gastric adenocarcinoma patients: implications for clinical outcome. Clin Cancer Res 14:2994–3001
10. Hagan S, Al-Mulla F, Mallon E, Oien K, Ferrier R, Gusterson B, Garcia JJ, Kolch W (2005) Reduction of Raf-1 kinase inhibitor protein expression correlates with breast cancer metastasis. Clin Cancer Res 11:7392–7397
11. Chen Y, Ouyang GL, Yi H, Li MY, Zhang PF, Li C, Li JL, Liu YF, Chen ZC, Xiao ZQ (2008) Identification of RKIP as an invasion suppressor protein in nasopharyngeal carcinoma by proteomic analysis. J Proteome Res 7:5254–5262
12. Li HZ, Wang Y, Gao Y, Shao J, Zhao XL, Deng WM, Liu YX, Yang J, Yao Z (2008) Effects of Raf kinase inhibitor protein expression on metastasis and progression of human epithelial ovarian cancer. Mol Cancer Res 6:917–928
13. Schuierer MM, Bataille F, Hagan S, Kolch W, Bosserhoff AK (2004) Reduction in Raf kinase inhibitor protein expression is associated with increased Ras-extracellular signal-regulated kinase signaling in melanoma cell lines. Cancer Res 64:5186–5192
14. Fu Z, Smith PC, Zhang L, Rubin MA, Dunn RL, Yao Z, Keller ET (2003) Effects of raf kinase inhibitor protein expression on suppression of prostate cancer metastasis. J Natl Cancer Inst 95:878–889
15. Brennan M (1995) Surgical management of peripancreatic cancer. In: Bland KI, Karakousis CP, Copeland EM (eds) Atlas of surgical oncology. W. B. Saunders Company, Philadelphia, pp 473–485
16. Sarmiento JM, Nagomey DM, Sarr MG, Farnell MB (2001) Periampullary cancers: are there differences? Surg Clin North Am 81:543–555
17. Kim HS, Kim GY, Lim SJ, Kim YW (2010) Loss of Raf-1 kinase inhibitory protein in pancreatic ductal adenocarcinoma. Pathology 42:655–660
18. Kim HS, Kim GY, Lim SJ, Park YK, Kim YW (2010) Reduced expression of Raf-1 kinase inhibitory protein is a significant prognostic marker in patients with gallbladder carcinoma. Hum Pathol 41:1609–1616
19. Kim HS, Kim GY, Lim SJ, Kim YW (2010) Expression of Raf-1 kinase inhibitory protein in extrahepatic bile duct carcinoma. Korean J Pathol 44:234–242
20. Edge SB, Byrd DR, Compton CC, Fritz AG, Greene FL, Trotti A (2010) AJCC Cancer staging manual, 7th edn. Springer, New York
21. Kim HS, Kim GY, Lim SJ, Kim YW (2010) Raf-1 kinase inhibitory protein expression in thyroid carcinomas. Endocr Pathol 21:253–257
22. Al-Mulla F, Hagan S, Al-Ali W, Jacob SP, Behbehani AI, Bitar MS, Dallol A, Kolch W (2008) Raf kinase inhibitor protein: mechanism of loss of expression and association with genomic instability. J Clin Pathol 61:524–529
23. Fu Z, Kitagawa Y, Shen R, Shah R, Mehra R, Rhodes D, Keller PJ, Mizokami A, Dunn R, Chinnaiyan AM, Yao Z, Keller ET (2006) Metastasis suppressor gene Raf kinase inhibitor protein (RKIP) is a novel prognostic marker in prostate cancer. Prostate 66:248–256
24. Li HZ, Gao Y, Zhao XL, Liu YX, Sun BC, Yang J, Yao Z (2009) Effects of Raf kinase inhibitor protein expression on metastasis and progression of human breast cancer. Mol Cancer Res 7:832–840
25. Kim SH, Kim HJ, Park YN, Cho SH (2001) The expression of extracellular signal regulated kinase (ERK) in non-small cell lung carcinoma. Korean J Pathol 35:361–367
26. Lee HC, Tian B, Sedivy JM, Wands JR, Kim M (2006) Loss of Raf kinase inhibitor protein promotes cell proliferation and migration of human hepatoma cells. Gastroenterology 131:1208–1217
27. Wang J, Yang YH, Wang AQ, Yao B, Xie G, Feng G, Zhang Y, Cheng ZS, Hui L, Dai TZ, Du XB, Wang D (2010) Immunohistochemical detection of the Raf kinase inhibitor protein in

nonneoplastic gastric tissue and gastric cancer tissue. Med Oncol 27:219–223
28. Hoshino R, Chatani Y, Yamori T, Tsuruo T, Oka H, Yoshida O, Shimada Y, Ari-i S, Wada H, Fujimoto J, Kohno M (1999) Constitutive activation of the 41-/43-kDa mitogen-activated protein kinase signaling pathway in human tumors. Oncogene 18:813–822
29. Klemke RL, Cai S, Giannini AL, Gallagher PJ, de Lanerolle P, Cheresh DA (1997) Regulation of cell motility by mitogen-activated protein kinase. J Cell Biol 137:481–492
30. Kajanne R, Miettinen P, Mehlem A, Leivonen SK, Birrer M, Foschi M, Kahari VM, Leppa S (2007) EGF-R regulates MMP function in fibroblasts through MAPK and AP-1 pathways. J Cell Physiol 212:489–497
31. McCawley LJ, Li S, Wattenberg EV, Hudson LG (1999) Sustained activation of the mitogen-activated protein kinase pathway. A mechanism underlying receptor tyrosine kinase specificity for matrix metalloproteinase-9 induction and cell migration. J Biol Chem 274:4347–4353
32. Peraldi P, Frodin M, Barnier JV, Calleja V, Scimeca JC, Filloux C, Calothy G, Van Obberghen E (1995) Regulation of the MAP kinase cascade in PC12 cells: B-Raf activates MEK-1 (MAP kinase or ERK kinase) and is inhibited by cAMP. FEBS Lett 357:290–296
33. Trakul N, Menard RE, Schade GR, Qian Z, Rosner MR (2005) Raf kinase inhibitory protein regulates Raf-1 but not B-Raf kinase activation. J Biol Chem 280:24931–24940
34. Salameh A, Galvagni F, Bardelli M, Bussolino F, Oliviero S (2005) Direct recruitment of CRK and GRB2 to VEGFR-3 induces proliferation, migration, and survival of endothelial cells through the activation of ERK, AKT, and JNK pathways. Blood 106:3423–3431

Virchows Arch (2012) 460:69–76
DOI 10.1007/s00428-011-1171-1

ORIGINAL ARTICLE

Frozen section analysis of sentinel lymph nodes in patients with breast cancer does not impair the probability to detect lymph node metastases

Eva V. E. Madsen · Jan van Dalen · Joost van Gorp · Poultje M. P. van Oort · Thijs van Dalen

Received: 23 July 2011 / Revised: 28 September 2011 / Accepted: 4 November 2011 / Published online: 25 November 2011
© The Author(s) 2011. This article is published with open access at Springerlink.com

Abstract Intra-operative frozen section analysis (FS analysis) of sentinel lymph nodes (SLNs) in patients with breast cancer can prevent a second operation for axillary lymph node dissection. In contrast, loss of tissue during FS analysis may impair the probability to detect lymph node metastases. To determine the effect of tissue loss on the probability of detection of metastases, dimensions and tissue loss resulting from intra-operative frozen section analysis were measured for 21 SLNs. In a mathematical model, the influence of tissue loss on the probability to detect metastases was calculated in relation to SLN size for various pathology protocols: an American, a widely used European, the extensive 'Milan' and the Dutch protocol. For median-sized SLN 11×8×5 mm (length×width×height), FS analysis led to a median loss of 680 μm (13.6%) of the height of the SLN. Irrespective of SLN size or used pathology protocol, the probability of detecting 2 mm metastases remained unchanged or even increased (0–12.8%). Moreover, the probability to detect 0.2 mm metastases increased for the majority of tested combinations of SLN size, tissue loss and used protocol. Only when combining maximum tissue loss and smallest SLN size in the Dutch protocol, or when applying the extensive Milan protocol on a median-sized SLN, the probability to detect 0.2 mm metastases decreased by 2.7% and 14.3%, respectively. Contrary to 'common knowledge', doing FS analysis of SLNs does not impair the probability to detect lymph node metastases.

Keywords Frozen section · Sentinel lymph node · Lymphatic metastasis · Breast cancer · Mathematical model

E. V. E. Madsen (✉) · P. M. P. van Oort · T. van Dalen
Department of Surgery, Diakonessenhuis,
Bosboomstraat 1,
3582 KE, Utrecht, The Netherlands
e-mail: eve_madsen@hotmail.com

J. van Dalen
Department of Mathematical Science,
RSM Erasmus University Rotterdam,
Rotterdam, The Netherlands

J. van Gorp
Department of Pathology, Diakonessenhuis,
Utrecht, The Netherlands

Introduction

Sentinel lymph node (SLN) biopsy has proven to be an accurate staging procedure in breast cancer patients and has replaced axillary lymph node dissection (ALND) in clinically 'node negative' axillas [1]. Though the SLN procedure has led to a more thorough inspection of these lymph nodes in general, their specific examination varies substantially throughout Europe [2] and the USA [3].

Intra-operative frozen section (FS) analysis of an SLN enables ALND to be performed during the same operation if tumour metastases are detected. When an SLN is prepared for FS analysis, part of the lymph node is sacrificed to obtain a reliable cut from the SLN for pathological examination. This loss of tissue may influence the probability to detect small lymph node metastases. As such, it may be a reason to discourage the use of FS analysis [4–6].

In the present study, the loss of SLN tissue during FS analysis is measured and the effect of the tissue loss on the probability to detect metastases within an SLN for four different, commonly used protocols is calculated.

Materials and methods

Intra-operative FS analysis and definitive pathology examination of SLNs (applying the Dutch guideline for evaluating SLNs)

In our hospital since 2000, intra-operative FS analysis of SLNs is routinely performed in breast cancer patients. Following retrieval of axillary SLNs, lymph nodes are transported to the pathology department and processed by the pathologist. After clearing the node from surrounding fat, SLNs are bisected along their longest axis. The two emerging halves are then frozen in Tissue-tek (Klinipath, Duiven, The Netherlands) after which preparatory cuts are taken from the centre of the nodes at variable intervals until appropriately examinable cuts are obtained from both halves. Appropriate cuts are slices that comprise an (almost) complete cross section from the lymph node. These intra-operative cuts are stained with haematoxylin–eosin (HE) and are examined by the pathologist for the presence of metastases. The remaining tissue is subsequently formalin-fixed and examined according to the Dutch guideline for evaluating SLNs, i.e. taking three cuts from either half starting from the centre with 250 μm distance between two cuts. SLNs thicker than 10 mm are sectioned into 2-mm slices. According to the protocols, samples are stained both with HE and immunohistochemically with antibodies to cytokeratin [7].

The study was approved by the institutional ethics committee. The size of SLNs was measured and tissue loss during the FS procedure was assessed. For a range of SLN sizes, the influence of the varying amount of tissue loss on the probability to detect metastases was calculated in a mathematical model, representing the processing of SLNs according to the Dutch pathology protocol. Subsequently, the influence of applying existing, alternative examination protocols was determined.

Establishing the size of an SLN

The dimensions of 21 SLNs obtained during breast surgery of ten consecutive female patients with cT1-2N0 breast cancer were measured by a pathologist after clearance of surrounding fat and before fixation. Length, height and width of the SLN were measured in millimetres (mm). In order to estimate the volume of an SLN, a triaxial, ellipsoid shape is assumed with parameters (half-lengths) a_x (width), a_y (depth) and b (height) (Appendix A; Fig. 4)

Tissue loss associated with frozen section analysis

For intra-operative FS analysis, an SLN is first bisected along its longest axis. FS are prepared from the cut surface (centre part) and preparatory FS are cut until a first section can be obtained that contains a complete cross section from the SLN (Fig. 1). Tissue loss was estimated by counting the number of preparatory sections cut on a cryostat (Leica CM1850) multiplied by the section thickness.

Calculating the influence of tissue loss on the probability of detecting metastases in the SLN

The Dutch guideline for evaluating SLNs advocates to bisect SLNs and to take three cuts from both halves starting from the centre with 250 μm distance between two cuts (or cuts at 2-mm intervals when an SLN is thicker than 10 mm). In a previous study [8], a model was presented to calculate the probability of detecting metastases in an SLN. This probability can be interpreted as the complementary risk of missing metastases that remain unnoticed due to their location in the outer areas of the SLNs or in the tissue between the cuts.

In the present study, we adopt and adapt this model to assess the probability of detecting the smallest (0.2 mm) and the largest (2 mm) single micrometastasis (TNM-N-class pN1mi) when performing FS analysis. The metastasis is represented as a ball shape with diameter m. A circular shape of a micrometastasis and a random location of the micrometastasis within the SLN are assumed (Appendix A; Fig. 4). The probability of detecting a metastasis in a particular tissue is roughly determined as the ratio of the volume covered by the histological examination and the total volume of the tissue (V). The pathology protocols, described below, all divide the unfixed tissue into two halves, after which a number of cuts n with height c and a distance d are taken from either half. The number of cuts depends on the protocol and the size of the SLN. If a metastasis with size m is present in the tissue and intersects with the examined section, it is assumed to be discovered with certainty. For preparing intra-operative FS, the two halves are levelled, cut

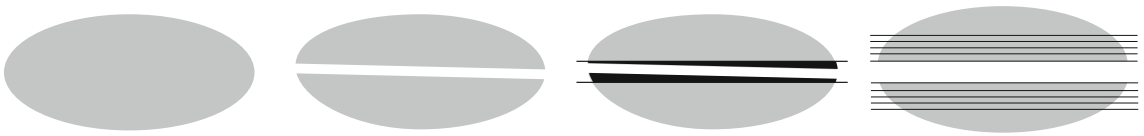

Fig. 1 Graphical presentation of bisecting an SLN, wasting tissue (*black*) by cutting preparative sections for FS analysis and further examination of the SLN. *SLN* sentinel lymph node

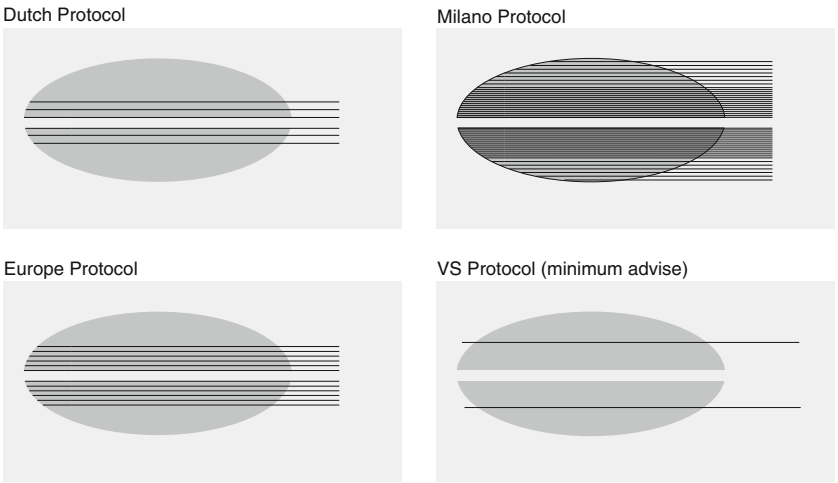

Fig. 2 Graphical presentation of the various pathology protocols

surface up, to ensure that the FS covers the full surface of both halves (Fig. 1). Thus, the potential waste is taken from the middle segment of the lymph node. The wasted tissue is assumed to have a total height w, of which w_L concerns the lower half, and w_U the upper half of the tissue. The choice of which half of the tissue is the lower or upper part is immaterial; the distinction between different amounts of waste from both halves merely adds flexibility to the model. Conceptually, wasting tissue has two opposite effects on the probability of detecting metastases during FS examination. On the one hand, the wasting tissue might cause the pathologist to miss metastases which reduces the probability of detection (the pure waste effect). On the other hand, levelling of the tissue halves has the effect of covering more of the periphery of the lymph node, which may actually increase the probability of detection (the advancement effect). The precise consequences of wasted tissue for the detection probability will depend on the pathology protocol, the size of the metastasis, the wasted volume and the size of the SLN. The specifics of the mathematical model are summarised in Appendix A.

The effect of FS analysis when alternative pathology protocols for the examination of SLNs followed

The effect of FS analysis has been studied for three commonly used protocols in addition to the Dutch protocol: the American pathology guideline [4], the 'Milan' protocol as described by Veronesi [1] and the protocol described by Cserni [2] as the most commonly used practice in Europe. While the Dutch protocol takes three cuts from either half of the tissue at a distance of d=250 μm, American guidelines suggest sectioning SLNs at 2-mm intervals after bisecting the SLN. The protocol described by Cserni as the most commonly used in Europe takes six cuts from both halves at a distance of d=150 μm. The most extensive Milan protocol takes 15 cuts from both halves at a distance of d=50 μm, after which the remaining tissue is cut at 100 μm. The vertical size of the cuts is c=5 μm for all protocols except the Milan protocol in which c=4 μm. The specifics of these protocols are graphically represented in Fig. 2. The effect of FS analysis on the probability of detection has been assessed for various combinations of the

Table 1 Probability to detect 0.2-mm metastases in SLNs without and with frozen section analysis

	Small SLN		Median SLN		Large SLN	
	7×6×4 mm		11×8×5 mm		20×10×10 mm	
	Without FS	With FS	Without FS	With FS	Without FS	With FS
Minimum amount of lost tissue during FS (72 μm)	44.0%	46.7%	35.8%	38.1%	18.3%	19.5%
Median amount of lost tissue during FS (680 μm)	44.0%	47.4%	35.8%	39.8%	18.3%	21.2%
Maximum amount of lost tissue during FS (1,250 μm)	44.0%	41.3%	35.8%	36.7%	18.3%	20.8%

Probability values were calculated for the various combinations of minimum, median and maximum tissue loss and minimum, median and maximum SLN size

SLN sentinel lymph node, *FS* frozen section

Table 2 Probability to detect 2-mm metastases in SLNs without and with frozen section analysis

	Small SLN		Median SLN		Large SLN	
	7×6×4 mm		11×8×5 mm		20×10×10 mm	
	Without FS	With FS	Without FS	With FS	Without FS	With FS
Minimum amount of lost tissue during FS (72 μm)	100%	100%	100%	100%	69.1%	70.0%
Median amount of lost tissue during FS (680 μm)	100%	100%	100%	100%	69.1%	76.4%
Maximum amount of lost tissue during FS (1,250 μm)	100%	100%	100%	100%	69.1%	81.9%

Probability values were calculated for the various combinations of minimum, median and maximum tissue loss and minimum, median and maximum SLN size

SLN sentinel lymph node, *FS* frozen section

different sized SLNs and the different amounts of wasted tissue corresponding with the different pathology protocols.

Results

The median size of the 21 examined SLNs was 11×8×5 mm (range 7×6×4–20×10×10 mm; length×width×height). After bisecting the SLN, cutting preparatory sections from the centre of the SLN led to a median loss in the height of tissue of 680 μm (range 72–1,250 μm). This tissue loss comprised 13.6% (range 1.4–25%) of the height of a median SLN.

In Table 1, the probability to detect metastatic involvement in SLNs of different sizes as well as the influence of FS related tissue loss is shown for 0.2-mm metastases when SLNs are processed according to the Dutch pathology protocol. The probability to detect 0.2-mm metastases only decreased when the maximum amount of tissue was wasted when examining the smallest SLN. In that case, the probability to detect a 0.2-mm metastasis decreased from 44.0% to 41.3%. For all other combinations, the probability of detection increased when doing FS analysis, the increase of this chance to detect a 0.2-mm metastasis ranging between 0.9% and 4.0%.

The probabilities of detecting 2.0-mm metastases are shown in Table 2. For small- and median-sized SLNs, the probability of detection remained 100%, irrespective of doing FS analysis. For large SLNs, in which the probability of detection of 2.0-mm metastasis without FS analysis is 69.1%, the use of FS analysis increased the probability of detection, and the increase of the detection probability varied between 0.9% and 12.8%.

The effect of FS analysis is graphically represented in Fig. 3. When applying the Dutch guideline for the pathology examination of SLNs, the loss of tissue from the centre of the SLN resulted in an advancement of the examined area towards the outer areas of the SLN, on average leading to a higher probability to detect metastases.

In Table 3, the effect of tissue loss resulting from FS analysis is summarised for the alternative pathology protocols, i.e. the Milan, the European and the American protocol. For 0.2-mm metastases, the probability of detection increased for the European and American protocol, from 55.8% to 57.7% and from 12.3 to 18.1% respectively. Only in the extensive Milan protocol, a 14.3% decrease to detect 0.2-mm metastases was observed when doing FS analysis. The probability of detecting 2.0-mm metastases remained the same for the European and the Milan protocol, i.e. 100%, and it increased when applying the American protocol from 94.5% to 99.5%.

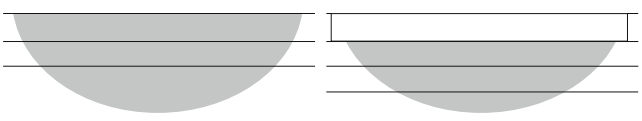

Fig. 3 Graphical presentation of the effect of tissue loss from the centre of the SLN: advancement of examined tissue towards the outer area. *SLN* sentinel lymph node

Table 3 Effect of frozen section on detection probabilities when applying alternative pathology protocols for SLN examination

	Metastasis size	Without FS	With FS
European protocol	0.2 mm	55.8%	57.7%
	2 mm	100%	100%
Milan protocol	0.2 mm	100%	85.7%
	2 mm	100%	100%
Dutch protocol	0.2 mm	35.8%	39.8%
	2 mm	100%	100%
American protocol	0.2 mm	12.3%	18.1%
	2 mm	94.5%	99.5%

SLN sentinel lymph node, *FS* frozen section

Discussion

In the present study, a beneficial effect of FS analysis on the probability to detect micrometastases in SLNs is observed. Despite losing approximately 14% of tissue from the centre of the SLN, the probability to detect the smallest micrometastasis in an SLN of median size with median tissue loss increased by 4%, while the probability to detect the smallest macrometastasis remained unchanged (100%) for the Dutch pathology protocol. Variations in the probability of detection depend on the size of the SLN and the amount of wasted tissue. These paradoxical findings were confirmed for most of the other pathology protocols.

According to our knowledge, no studies have been performed that actually measure the potentially adverse effect of tissue loss resulting from FS analysis. However, various authors have hypothesised a substantial effect of lost tissue due to FS analysis [5, 6]. Based on this assumption, 'conventional wisdom' has been ground for dissuasion of this intra-operative technique. In addition, this presumed effect is the main reason to advocate other intra-operative techniques such as touch imprint cytology or intra-operatively assessing greater volumes of SLNs or even whole lymph nodes without losing tissue by one-step nucleic acid amplification [9, 10].

The observed paradoxically increased probability to detect small lymph node metastases when doing FS analysis can be explained in a number of ways. Firstly, the median loss of tissue due to FS analysis was 680 μm. Serial sectioning is in itself accompanied by a risk of 'missing' metastases that are smaller than the interval between the cuts (250 μm according to the Dutch guidelines). Conceptually, the observed loss of 680 μm may be viewed as an extension of the cut interval by 430 μm (680 instead of 250 μm). Furthermore, if a metastasis is larger than the height of wasted tissue, the probability to detect such a metastasis remains unaffected. Finally, losing tissue from the centre of the node leads to an advancement of the sections to be analysed microscopically towards the outer areas of the SLN. So, the loss of 430 μm from the centre of the node is accompanied by examining 680 μm deeper into the periphery of an SLN. This 'advancement' effect increases the probability to detect metastases in case of pathology protocols that advocate examining the central part of the lymph node. This effect is absent in case of protocols advocating extensive serial sectioning of the entire SLN, e.g. the Milan protocol.

Thus, preparing SLNs during FS analysis and thereby sacrificing tissue will initially have a favourable effect on the probability to detect metastases but, with on-going loss, will eventually result in a decreased probability. Differences in applied protocols and the absence of consensus regarding a minimum metastasis size that should be detected under all circumstances preclude formulating a rule of thumb that can be used to suggest what proportion of an SLN can be sacrificed during FS analysis without compromising the detection probability. Then again, the results of the present study demonstrate that the wasted tissue never compromised the chance to detect lymph node metastases when commonly used protocols are applied.

Only when using the protocol as described by Veronese et al. [1], which implies cutting the entire SLN at 50-μm intervals, the probability to detect 0.2 mm was decreased by 14.3% (from 100% to 85.7%) while the chance to detect the smallest macrometastasis was unimpaired. Then again, few other institutions advocate such an extensive examination of SLNs. In this respect, it is noteworthy that the probability to detect a 0.2-mm metastasis was very limited in all protocols except for the Milan protocol, as demonstrated in a previous study [8]. Given the ongoing discussion regarding the prognostic effect of micrometastases and isolated tumour cells [11, 12], this may be a reason to consider a more extensive protocol.

The present study has a number of limitations. In designing the model, a number of assumptions were adopted such as the ellipsoid shape of an SLN, the circular-shaped metastasis, as well as the random position of the metastasis within an SLN. Furthermore, we assumed that subsequent definitive pathology examination was not associated with tissue loss irrespective of the use of FS analysis, whereas in reality, tissue loss accompanies the final pathological examination too. Furthermore, in this model, a lymph node metastasis is assumed to be single, whereas the probability of detecting metastases increases with the number of metastases in the SLN. As a rule of thumb, the probability to detect at least one of multiple metastases will increase for all examination protocols, and the effect of FS analysis will never lead to an increased risk of missing metastases.

In summary, contrary to our expectation as well as 'common knowledge', FS analysis of sentinel lymph nodes by bisecting lymph nodes, wasting of preparative sections from the centre does not impair the probability to detect lymph node metastases.

Acknowledgements The meticulous work in the pathology laboratory from L. Smeets is greatly appreciated. The authors thank T. van Velsen, communication designer, for designing the figures used in this manuscript.

Conflict of interest The authors declare that they have no conflict of interest

Open Access This article is distributed under the terms of the Creative Commons Attribution Noncommercial License which permits any noncommercial use, distribution, and reproduction in any medium, provided the original author(s) and source are credited.

Appendix A

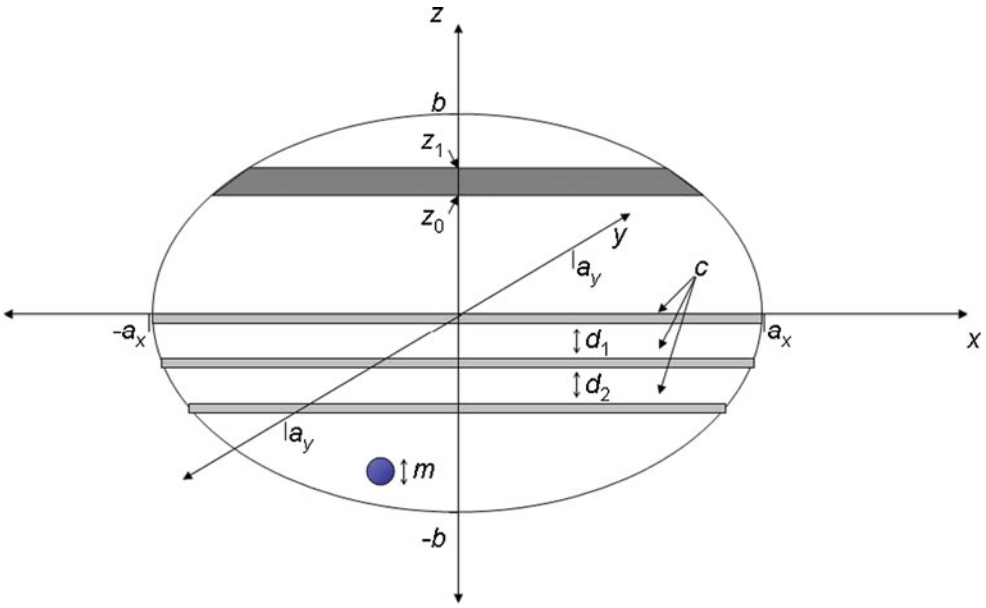

Fig. 4 The model to determine the probability of detecting micrometastases in SLN with and without frozen section analysis

This appendix presents the mathematical model to determine the probability of detecting micrometastases in an SLN with and without frozen section analysis. The pathological protocols considered in the present paper all divide the raw tissue into two halves. From each half, one frozen section with height *fc* and *n* cuts with height *c* are taken at inter-cut distance *d*; if no frozen section analysis is applied, then the height of the frozen section is simply equal to zero, *fc*=0. The number of cuts depends on the protocol and the size of the tissue. If a metastasis with size *m* is present in the tissue and intersects with the inspected cuts, it is assumed to be detected with certainty. During the preparation of the cutting process, the two halves are levelled to ensure that the first cut covers the full surface of the remaining half. The implied waste is taken from the midst of the original tissue. It is assumed to have a total height *w*, of which w_L concerns the lower half, and w_U the upper half of the tissue. The choice of which half of the tissue is the lower or upper part is immaterial; the distinction between different amounts of waste from both halves merely adds flexibility to the model. The occurrence of pathological waste has two opposite effects on the probability of detecting metastases. On the one hand, waste may lead the pathologists to definitively miss a metastasis, which reduces the probability of detection (the pure waste effect). On the other hand, levelling of the tissue halves causes the volume covered by the pathological inspection to include more of the outer parts of the tissue, which may actually increase the probability of detection (the advancement effect). The precise consequences on the detection probability of wasted tissue will depend on the size of the metastasis, the wasted volume and the total volume of the tissue.

General assumptions

We model a given tissue by means of a triaxial ellipsoid with parameters (half-lengths): a_x (width), a_y (depth) and b (height); $a_x \geq a_y \geq b > 0$. The volume of the entire ellipsoid is obtained as $V = 4\pi\ a_x\ a_y\ b/3$, while the volume of an arbitrary (horizontal) slice from this ellipsoid between points z_0 and z_1, $-b \leq z_0 \leq z_1 \leq b$, can be derived as:

$$I(z_0, z_1) = \pi a_x a_y \left((z_1 - z_0) - \frac{1}{3b^2} \left(z_1^3 - z_0^3 \right) \right) \tag{1}$$

Obviously, $V = I(-b, b)$. The probability p of detecting a metastasis, if it is present, is defined as the total tissue volume covered by the pathological inspection (V_{PI}) corrected for waste (U_W) and unobserved volume due to metastases smaller than the inter-cut distance ($U_{m<d}$) divided by the tissue volume (V):

$$p = \frac{V_{\mathrm{PI}} - U_W - U_{m<d}}{V} \tag{2}$$

Further formalisation will distinguish between situations without and with pathological waste.

The case of no waste

In the absence of waste, assuming frozen section and symmetric halves, the total tissue volume covered by the pathological inspection is equal to:

$$V_{\mathrm{PI}} = I[-(fc + c + (n-1)(c+d) + m); \quad fc + c + (n-1)(c+d) + m] \tag{3}$$

with n the number of cuts. The volume unseen due to waste is obviously void, U_W=0. Metastases with size equal or larger than the inter-cut space ($m \geq d$) will always be detected, if they are within this inspected volume ($U_{m<d}$=0). Smaller metastases ($m<d$) within the inspected volume may be missed when they lie between two cuts without intersecting them. Considering cuts j and j+1, j=1, …, n-1, the inter-cut volume unobserved by the pathologist can be approximated as the average of $I[fc + c + (j-1)(c+d); fc + j(c+d) - m]$ and $I[fc + c + (j-1)(c+d) + m; fc + j(c+d)]$. Alternatively, one could approximate this unseen volume by $I[fc + c + (j-1)(c+d) + m/2; fc + j(c+d) - m/2)$, but the difference between the two approaches is marginal. Assuming symmetry, the total volume unseen by the pathological inspection in the case of small metastases ($m<d$) is equal to:

$$U_{m<d} = \sum_{j=1}^{n-1} [I[fc + c + (j-1)(c+d); \quad fc + j(c+d) - m] + I[fc + c + (j-1)(c+d) + m; \quad fc + j(c+d)]] \tag{4}$$

The probability of detection can now be calculated using Eq. 2.

The case of waste

In the case that the pathological process involves waste, the probability of detection is affected through a larger total volume covered by the inspection (the advancement effect) and a possibly unseen part of wasted tissue (the pure waste effect). Relaxing the assumption of symmetric tissue halves and recalling that w_L and w_U refer to the wasted heights from the lower and upper tissue halves, respectively, the total inspected volume before correction becomes:

$$V_{\mathrm{PI}} = I[-(w_L + fc + c + (n_L - 1)(c+d) + m); \; 0] + I[0; \quad w_U + fc + c + (n_U - 1)(c+d) + m] \tag{5}$$

with n_L and n_U the possibly different numbers of cuts from the lower and upper tissue halves, respectively. The total tissue volume covered by the inspection is larger than that in the case of no waste, which positively affects the probability of detection. However, the occurrence of pathological waste implies that metastases in the wasted tissue might go undetected. Again, two situations may be discerned: large metastases with a size greater than the total height of the wasted material ($m \geq w = w_L + w_U$) and small metastases ($m<w$). In the former case, $m \geq w$, the metastasis will always intersect with the first cut on either half. Consequently, the wasting has no adverse effects on the detection of the metastases, and no waste correction is needed (U_W=0). In the latter case, $m<w$, some metastases may be missed when they fall in between the first cuts on both tissue halves without intersecting them. In line with the unobserved parts of the inter-cut spaces, we approximate the unobserved part of the wasted tissue by:

$$U_W = (I[-w_L + m; w_U] + I[-w_L; w_U - m])/2 \tag{6}$$

Again, this could be approximated by $I(-w_L + m/2; w_U - m/2)$, leading to a marginally different outcome. Furthermore, the unobserved parts of the inter-cut spaces due to small metastases ($m<d$) simply generalise from Eq. 4. Taking into account the waste (w_L and w_U), possibly different numbers of cuts on the upper and lower halves (n_L and n_U), and not imposing symmetry, the unseen volume of tissue during pathological inspection ($U_{m<d}$) is obtained as:

$$\begin{aligned} U_{m<d,L} &= \sum_{j=1}^{n_L-1} [I[-(w_L + fc + c + (j-1)(c+d); \; -(w_L + fc + j(c+d) - m)] + \\ &\quad + I[-(w_L + fc + c + (j-1)(c+d) + m); \; -(w_L + fc + c + j(c+d))]]/2 \\ U_{m<d,U} &= \sum_{j=1}^{n_U-1} [I[w_U + fc + c + (j-1)(c+d); \; w_U + fc + j(c+d) - m] + \\ &\quad + I[w_U + fc + c + (j-1)(c+d) + m; \; w_U + fc + c + j(c+d)]]/2 \\ U_{m<d} &= U_{m<d,L} + U_{m<d,U} \end{aligned} \tag{7}$$

Having the corrections for waste and unseen inter-cut spaces, the probability of detection is determined using Eq. 2.

References

1. Veronesi U, Paganelli G, Viale G et al (2006) Sentinel-lymph-node biopsy as a staging procedure in breast cancer: update of a randomised controlled study. Lancet Oncol 7(12):983–990
2. Cserni G, Amendoeira I, Apostolikas N et al (2004) Discrepancies in current practice of pathological evaluation of sentinel lymph nodes in breast cancer. Results of a questionnaire based survey by the European Working Group for Breast Screening Pathology. J Clin Pathol 57(7):695–701
3. Weaver DL (2010) Pathology evaluation of sentinel lymph nodes in breast cancer: protocol recommendations and rationale. Mod Pathol 23(Suppl 2):S26–S32
4. Lyman GH, Giuliano AE, Somerfield MR et al (2005) American Society of Clinical Oncology guideline recommendations for sentinel lymph node biopsy in early-stage breast cancer. J Clin Oncol 23(30):7703–7720
5. Van Diest PJ, Torrenga H, Borgstein PJ, Pijpers R, Bleichrodt RP, Rahusen FD, Meijer S (1999) Reliability of intraoperative frozen section and imprint cytological investigation of sentinel lymph nodes in breast cancer. Histopathology 35(1):14–18
6. Varga Z, Rageth C, Saurenmann E, Honegger C, von Orelli S, Fehr M, Fink D, Seifert B, Moch H, Caduff R (2008) Use of intraoperative stereomicroscopy for preventing loss of metastases during frozen sectioning of sentinel lymph nodes in breast cancer. Histopathology 52(5):597–604
7. Vereniging van Integrale Kankercentra (VIKC): Oncoline, Richtlijnen oncologische zorg. http://www.oncoline.nl. Mamma; Mammacarcinoom (1.1); Pathologie na chirurgie; Okselstadiëring. Accessed 23 July 2011
8. Madsen EV, van Dalen J, van Gorp J, Borel RInkes IH, van Dalen T (2008) Strategies for optimizing pathologic staging of sentinel lymph nodes in breast cancer patients. Virchows Arch 453(1):17–24
9. Snook KL, Layer GT, Jackson PA et al (2011) Multicentre evaluation of intraoperative molecular analysis of sentinel lymph nodes in breast carcinoma. Br J Surg 98(4):527–535
10. Visser M, Jiwa M, Brink AA, Pol RP, van Diest P, Snijders PJ, Meijer CJ (2008) Intra-operative rapid diagnostic method based on CK19 mRNA expression for the detection of lymph node metastases in breast cancer. Int J Cancer 122(11):2562–2567
11. Tjan-Heijnen VC, de Boer M (2009) Minimal lymph node involvement and outcome of breast cancer. The results of the Dutch MIRROR study. Discov Med 8(42):137–139
12. Gobardhan PD, Elias SG, Madsen EV et al (2011) Prognostic value of lymph node micrometastases in breast cancer: a multicenter cohort study. Ann Surg Oncol 18(6):1657–1664

Virchows Arch (2012) 460:77–87
DOI 10.1007/s00428-011-1169-8

ORIGINAL ARTICLE

PIK3CA mutations and loss of ARID1A protein expression are early events in the development of cystic ovarian clear cell adenocarcinoma

Sohei Yamamoto · Hitoshi Tsuda · Masashi Takano · Seiichi Tamai · Osamu Matsubara

Received: 7 August 2011 / Revised: 26 October 2011 / Accepted: 2 November 2011 / Published online: 26 November 2011
© Springer-Verlag 2011

Abstract Somatic mutations of PIK3CA and ARID1A are the most common genetic alterations observed in ovarian clear cell adenocarcinomas (CCA). In a previous report, we showed that PIK3CA gene mutations and loss of ARID1A expression occur early during the development of CCA. In the present study, using direct genomic DNA sequencing for exons 9 and 20 of PIK3CA and immunohistochemistry for ARID1A protein expression, we analyzed the association of these molecular alterations with various clinicopathological parameters in a total of 90 cases of primary ovarian CCA, including 42 previously examined cases. The presence of PIK3CA mutations, identified in 34 (39%) of the 88 informative cases, was significantly associated with a grossly cystic tumor, the presence of adjacent endometriosis, prominent papillary architecture of tumor growth, the presence of hyalinized and mucoid stroma, and the absence of clear cell adenofibroma components ($P<0.05$, each). There was no significant association of PIK3CA mutations with other clinical variables, such as age, clinical stage, or clinical outcome of the patients. The intensity of immunoreactivity for ARID1A was assigned as negative, weakly positive, and strongly positive in 44%, 22%, and 33% of tumors, respectively. Compared to tumors immunoreactive for ARID1A, ARID1A-negative tumors were significantly associated with the presence of adjacent endometriosis ($P=0.025$), but there was no statistically supported association with other examined clinicopathological parameters. Compared with CCAs strongly positive for ARID1A, CCAs negative for ARID1A more frequently harbor PIK3CA mutations ($P=0.013$). PIK3CA gene mutations and ARID1A immunohistochemistry lacked prognostic significance. These data further support the idea that these molecular alterations occur as very early events during tumor development of ovarian CCA.

Keywords PIK3CA · ARID1A · Clear cell carcinoma · Histopathology · Endometriosis · Clear cell adenofibroma

S. Yamamoto (✉) · O. Matsubara
Department of Basic Pathology,
National Defense Medical College,
3-2 Namiki, Tokorozawa, Saitama 359-8513, Japan
e-mail: dr21001@ndmc.ac.jp

M. Takano
Department of Obstetrics and Gynecology,
National Defense Medical College,
3-2 Namiki, Tokorozawa, Saitama 359-8513, Japan

S. Tamai
Department of Laboratory Medicine,
National Defense Medical College Hospital,
3-2 Namiki, Tokorozawa, Saitama 359-8513, Japan

H. Tsuda
Department of Pathology and Clinical Laboratories,
National Cancer Center Hospital,
5-1-1 Tsukiji, Chuo-ku, Tokyo 104-0045, Japan

Introduction

Among ovarian carcinomas, clear cell adenocarcinoma (CCA) has been recognized as a distinct clinicopathological entity in view of its characteristic histology, frequent concurrence of endometriotic lesions, and highly chemotherapy-resistant nature, resulting in an extremely poor prognosis when surgical cytoreduction is insufficient [1–4]. Although little is known about CCA pathogenesis, somatic mutations of the *PIK3CA* and *ARID1A* (the AT-rich interactive domain 1A) genes are the most common molecular genetic alterations identified in ovarian CCAs [5–8].

The phosphatidylinositol 3-kinases (PI3K) are widely expressed lipid kinases that catalyze the production of the second messenger phosphatidylinositol 3,4,5-triphosphate (PIP3), which in turn contributes to the recruitment and activation of a wide range of downstream targets, including Akt [9]. Increased PI3K activity via gain of function has been shown in a number of human cancers: *PIK3CA*, which encodes the catalytic subunit p110a of PI3K, is located on chromosome 3q26.3, and it has been suggested that amplification of this locus increases PI3K activity [10]. Moreover, Samuels et al. identified somatic mutations of *PIK3CA* in several types of human cancer [11]. Functional analysis revealed that several "hotspot" mutants, such as E542K, E545K, and H1047R, increase lipid kinase activity and induce cellular transformation [12]. Somatic activating mutations of *PIK3CA* have been reported in CCAs with very high frequency (32–46%) [5, 6], and these mutations are evident at the endometriotic epithelium adjacent to CCA [6], suggesting that *PIK3CA* mutations are very early events during the development of endometriosis-associated ovarian CCAs.

Somatic mutations in the *PIK3CA* gene have been identified in various human cancers, including cancer of the colon, stomach, breast, brain, lung, uterus (endometrium), and ovary [11, 13–16]. Recent reports have highlighted the prognostic role of *PIK3CA* mutations as a marker for poor outcome in patients with colorectal carcinomas [17, 18]. Sartore-Bianchi et al. [18] showed that PIK3CA mutations are significantly associated with clinical resistance to panitumumab or cetuximab in a cohort of 110 patients with metastatic colon cancer. In their study, tumors harboring *PIK3CA* mutations had worse clinical outcome in terms of progression-free survival [18]. *PIK3CA* mutations have also been associated with paclitaxel resistance in transformed breast epithelial cells [19], and PI3K signaling in general has been linked with resistance to a number of other cancer therapies.

ARID1A is located in the chromosome 1p36 region and encodes a large nuclear protein involved in chromatin remodeling. ARID1A (also known as BAF250a), the protein encoded by the *ARID1A* gene, is a key component of the multi-protein SWI/SNF chromatin remodeling complex present in all eukaryotes, and it is believed to confer specificity in the regulation of gene expression [20]. The SWI/SNF complex uses ATP to mobilize nucleosomes, modulating the accessibility of promoters to transcriptional activation or repression, and is involved in the regulation of many cellular processes, including development, differentiation, proliferation, and DNA repair [21, 22]. Previous functional assays suggest that *ARID1A* is a tumor-suppressor gene [23]. Recently, with the use of whole exome and transcriptome sequencing, two independent studies have reported novel somatic mutations of the *ARID1A* gene in 43% and 56% of ovarian CCAs, suggesting a major role of *ARID1A* in the pathogenesis of this carcinoma [7, 8]. Moreover, our recent immunohistochemical analysis suggested that loss of ARID1A protein expression appears to be a very early molecular event in ovarian clear cell carcinogenesis, regardless of the putative carcinogenic pathway involved (i.e., endometriosis-associated pathway and clear cell adenofibroma-associated pathway) [24].

To date, it has been unclear whether the presence of molecular alterations of *PIK3CA* and ARID1A is of some clinicopathological value in ovarian CCAs. Therefore, in this study, we investigated these molecular alterations in a number of surgically resected ovarian CCA cases as a means to study their clinicopathological significance and thus clarify their role in the pathogenesis of this disease. Moreover, given the frequent concurrence of *PIK3CA* mutations and loss of ARID1A protein expression in ovarian CCAs as shown in our recent study [24], we have assessed possible relationships between *PIK3CA* mutations and ARID1A alterations in a larger number of CCA cases. Because immunohistochemical analysis of clear cell and endometrioid carcinomas of the ovary showed that loss of ARID1A protein expression was highly correlated with the presence of *ARID1A* mutations [7, 25] and because *ARID1A* mutations are randomly distributed in 20 exons and most of these are the insertion/deletion type of mutations, making it very challenging to detect in formalin-fixed paraffin-embedded specimens [7, 8], we used protein expression by immunohistochemistry as a readout of ARID1A alterations.

Materials and methods

Cases enrolled and clinicopathological parameters analyzed

Ninety cases of primary ovarian CCA, as a consecutive series, were identified from the files of the Department of Laboratory Medicine, National Defense Medical College Hospital, Japan. These 90 patients underwent surgical resection between 1986 and 2007, and none had undergone chemotherapy or radiation therapy before surgery. All specimens were formalin-fixed and paraffin-embedded, and tumors were classified according to the criteria of the World Health Organization [1]. Histopathological slides of the surgical specimens were available for all 90 cases. The number of 4-μm-thick hematoxylin and eosin-stained histopathological slides examined per case was 7.1 on average, ranging from 3 to 20. The research protocol was approved by the Ethics Committee of the National Defense Medical College, Tokorozawa, Japan.

The tumors were macroscopically classified as either cystic or non-cystic; cystic tumors were defined as those with main carcinoma components presenting as a grossly identifiable cyst; otherwise, they were classified as non-cystic tumors. The presence of endometriosis, which included both endometriotic implants and endometriotic cysts, and its location (anywhere and/or adjacent) were histologically examined and recorded. The designation "endometriosis anywhere" included endometriosis within the ovarian tumor, residual ipsilateral ovarian tissue, the contralateral normal ovary, or extra-ovarian sites. Endometriosis adjacent to the carcinoma was defined as (1) existing in histological continuity with, or adjacent to, the CCA, or (2) endometriotic cyst in which CCA was observed regardless of the presence of histological continuity between the carcinoma and endometriotic epithelium [26, 27]. The presence of clear cell adenofibroma components was also assessed according to previously described histopathological criteria [26, 28]. Cytological atypia within the endometriotic epithelium or clear cell adenofibroma components was not considered in this study.

The distinction between different architectural patterns of tumor growth (tubulocystic, papillary, and solid or diffuse) was based on the predominant component in a given specimen. Nuclear grade of carcinoma cells was considered to be high when the tumor contained highly pleomorphic nuclei (variation in nuclear size of >4:1) with vesicular chromatin and large eosinophilic nucleoli visible under low (×10) magnification; otherwise, they were classified as low nuclear grade. The nuclear grade was determined based on the highest grade evaluation, providing it comprised at least 10% of the tumor. The presence or absence of hyalinized or mucoid stroma, which are considered to be characteristic histological features of CCA [1, 29], was evaluated, according to the histological features of these stromal changes in CCA described in a previous report by Kato et al. [29]. To qualify as hyalinized or mucoid changes in the cancer stroma, these changes had to comprise at least 10% of the sections examined.

Other clinicopathological details such as patient age, clinical stage of the disease, size and laterality of tumor, residual tumor after initial cytoreductive surgery, clinical response to chemotherapy, regional lymph node status, and overall survival were assessed. The age of the patients ranged from 35 to 75 years (mean 53 years). Clinical staging of disease was done according to the International Federation of Gynecology and Obstetrics system. Of the 90 cases enrolled, 49 (54%) were stage I; 9 (10%), stage II; 27 (30%), stage III; and 5 (6%), stage IV. Of the 90 patients, 88 (98%) received postoperative platinum-based chemotherapy after the initial surgery. A second-look operation or second reductive surgery was performed, depending on the surgeon's preference. Clinical response to chemotherapy was assessed for the 27 patients with measurable residual tumor (regardless of size) after initial surgery, evaluated by ultrasonography or computed tomography, and classified into complete response, partial response, stable disease, or progressive disease, according to the new Response Evaluation Criteria for Solid Tumours (RECIST) guidelines [30]. Follow-up was calculated from the date of initial definitive surgery to the date of either the last follow-up or death. The average follow-up period after initial surgery was 52.0 months and ranged between 2 and 182 months. Thirty (33%) of 90 patients died because of their tumor burden, and one patient died because of another cause.

Mutation assay of the *PIK3CA* gene

In ovarian CCAs, more than 85% of mutations in *PIK3CA* have been found in the helical (exon 9) and kinase domains (exon 20) [5, 6]; therefore, we restricted our analyses to these two regions of the gene. Carcinoma components from the 90 enrolled cases were analyzed for somatic mutations of the *PIK3CA* gene using direct genomic DNA sequencing. Details of these methods have been described in our previous study [6]. Briefly, exons 9 and 20 of the *PIK3CA* gene were amplified using PCR for genomic DNA. PCR was performed using AmpliTaq Gold (Applied Biosystems, Foster City, CA, USA), and the primers for PCR and sequencing conditions were as previously described [6]. The PCR products were subsequently subjected to direct sequencing PCR with BigDye terminator V 3.1/1.1 cycle sequencing reagents (Applied Biosystems). The samples were finally analyzed on an ABI PRISM 3130 Genetic Analyzer (Applied Biosystems) with DNA Sequencing Analysis Software v5.2 (Applied Biosystems). If the carcinoma components were judged to be harboring a *PIK3CA* mutation, genomic DNA from the corresponding normal tissue was isolated and subjected to genetic analysis to confirm the somatic nature of the tumor mutations. As a part of these analyses, we used data previously described [6, 24].

Immunohistochemistry for ARID1A protein detection

Carcinoma components from the 90 enrolled cases were analyzed for *ARID1A* protein expression. All of the selected formalin-fixed and paraffin-embedded specimens were cut into 4-μm-thick serial sections and analyzed by immunohistochemistry. A commercially available polyclonal rabbit anti-ARID1A antibody (Sigma-Aldrich, HPA005456, diluted 1:50) was used as a primary antibody for ARID1A protein detection [31]. Sections were deparaffinized and boiled in an autoclave at 121°C for 15 min in a 0.01-mol/L citrate buffer (pH 6.0) and then allowed to cool at room temperature. Endogenous peroxidase was blocked using 5% hydrogen

peroxide. The slides were incubated at 4°C overnight with primary antibodies and then reacted with a dextran polymer reagent combined with secondary antibodies and peroxidase for 1 h at room temperature. Specific antigen–antibody reactions were visualized with 0.2% diaminobenzidine tetrahydrochloride and hydrogen peroxide, and counterstaining was performed using Mayer's hematoxylin. Non-neoplastic cells, including endothelial cells, fibroblasts, and lymphocytes, typically show ARID1A nuclear immunoreactivity and serve as positive internal controls. As negative controls, sections without the primary antibody were used.

By referring to the immunoreactive intensity in background stromal cells as a standard, the intensity of staining in the carcinoma cells was scored using a three-tier system as follows: negative (undetectable; no discernible staining in tumor cells with positive immunoreaction in background stromal cells), weakly positive (definite nuclear immunoreactions but less intense than that of background stromal cells), and strongly positive (immunoreaction intensity equal to or greater than that of background cells). Because majority of the given cases showed diffusely (>80% of the cells of interest) positive or homogeneously negative results for the ARID1A immunoreaction, we did not consider the distribution (or percentage of stained cells) of the immunoreaction.

Statistical analysis

Statistical analyses were performed using the StatMate III software (ATMS, Tokyo, Japan). Comparisons between parameters were made using the chi-squared test. For survival analysis, Kaplan–Meier curves were drawn, and differences between the curves were calculated by the log-rank test. Differences of $P<0.05$ were considered to be statistically significant.

Results

Pathological findings of tumors

Tumor size varied from 5.0 to 30.0 cm (mean 13.2 cm). Of the 90 cases, primary tumors were located at the left and right ovaries in 33 (37%) and 53 (59%) cases, respectively, and tumors involving both ovaries accounted for the remaining four (4%) cases.

From the gross appearance, 60 (67%) and 30 (33%) of the 90 tumors were defined as cystic and non-cystic tumors, respectively. Histologically, endometriotic lesions were present in 59 (66%) of the 90 cases, and 28 (47%) of these 59 lesions presented with endometriosis adjacent to CCA. Clear cell adenofibroma components were present in 14 (16%) cases, and 2 (14%) of these 14 cases had endometriosis away from the carcinoma components. Prominent architectural pattern of tumor cell growth was assigned as tubulocystic, papillary, or solid/diffuse in 32 (36%), 49 (54%), and 9 (10%) cases, respectively. Hyalinized stroma and mucoid stroma in the carcinoma components were present in 72 (80%) and 48 (53%) cases, respectively.

PIK3CA mutations and ARID1A immunoreaction in ovarian CCA

Sequencing chromatograms for *PIK3CA* exons 9 and 20 were obtained from 88 (98%) of the 90 cases examined, and *PIK3CA* somatic mutations were identified in 34 (39%) cases. Of these, 28 (82%) tumors carried mutations in the kinase domain (exon 20) and six (18%) in the helical domain (exon 9) (Fig. 1). No carcinomas carried more than one mutation in exons 9 and 20. All observed mutations were missense somatic mutations and are listed in Table 1. Three mutation hotspots were found; 23 (82%) of the 28 mutations in exon 20 were H1047R substitutions. Of the six mutations in exon 9, two (33%) were of the E542K type and two (33%) were of the E545K type. Immunoreactivity for ARID1A was assigned as negative, weakly positive, and strongly positive in 40 (44%), 20 (22%), and 30 (33%) tumors, respectively (Fig. 2).

Correlation of *PIK3CA* mutations with pathological parameters

Compared with *PIK3CA* mutation-negative tumors, tumors harboring *PIK3CA* mutations were frequently composed of

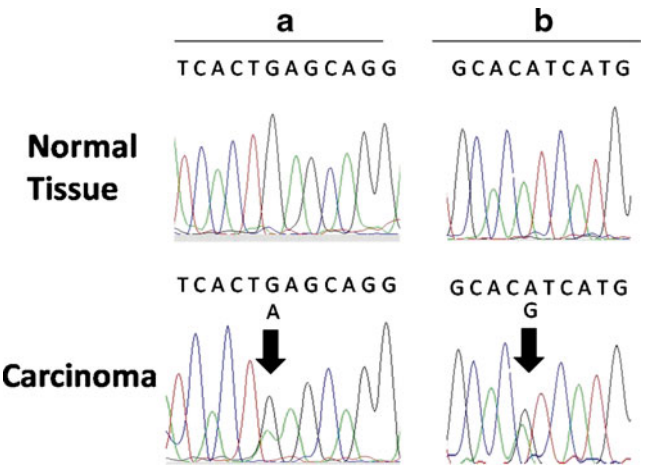

Fig. 1 Sequencing chromatograms for *PIK3CA* exon 9 (**a**) and 20 (**b**) in two representative cases. **a** *Arrow*, peak of the G→A substitution at nucleotide 1,633 resulting in the E545K mutation. **b** *Arrow*, peak of the A→G substitution at nucleotide 3,140 resulting in the H1047R mutation. Normal tissues of both panels show wild-type sequence for each exon, confirming that these mutations are somatic

Table 1 Summary of *PIK3CA* mutations in ovarian clear cell adenocarcinomas

Exon	Nucleotide	Codon	No. of patients (%)
9	G1624A	E542K	2 (6)
9	G1633A	E545K	2 (6)
9	A1634C	E545A	1 (3)
9	A1634T	E545V	1 (3)
Subtotal			6 (18)
20	C3139A	H1047N	1 (3)
20	A3140G	H1047R	23 (68)
20	A3140T	G1047L	1 (3)
20	G3146A	G1049D	2 (6)
20	G3148A	G1050S	1 (3)
Subtotal			28 (82)
Total			34 (100)

a grossly cystic tumor, and this difference was statistically significant (88% vs. 54%, P=0.0018). Positivity for *PIK3CA* mutations was significantly associated with the presence of endometriosis adjacent to the carcinoma (P=0.049) and the absence of clear cell adenofibroma components (P=0.036). Endometriotic lesions in any location were more frequently detected in the *PIK3CA* mutation-positive tumors than in the mutation-negative tumors, but this difference was not statistically significant (71% vs. 63%, P=0.462) (Table 2).

Twenty-four (70.5%) and 6 (18%) of the 34 *PIK3CA* mutation-positive tumors were prominently composed of papillary architectures and tubulo-cystic architectures, respectively, of tumor cells growth. On the other hand, in the 54 *PIK3CA* mutation-negative tumors, 23 (43%) and 26 (48%) were predominantly composed of papillary and tubulo-cystic architectural patterns, respectively. Consequently, there was a significant association between the mutational status of *PIK3CA* and the prominent architectural patterns of CCA tumor cell growth (P=0.014). When the PIK3CA mutation-positive tumors were compared with the mutation-negative tumors, hyalinized and mucoid stroma were more frequently detected in the former with statistically significant differences (hyalinized, 94% vs. 70%, P=0.0056; mucoid, 74% vs. 41%, P=0.0027). In terms of the nuclear grade of carcinoma cells, frequencies of high grade features were not statistically different between the mutation-positive and mutation-negative tumors (35% vs. 44%, P=0.395).

Of the 88 cases informative for *PIK3CA* mutation status, 39 (44%), 20 (23%), and 29 (33%) were assigned as negative, weakly positive, and strongly positive for ARID1A immunoreactivity, respectively. The rates of

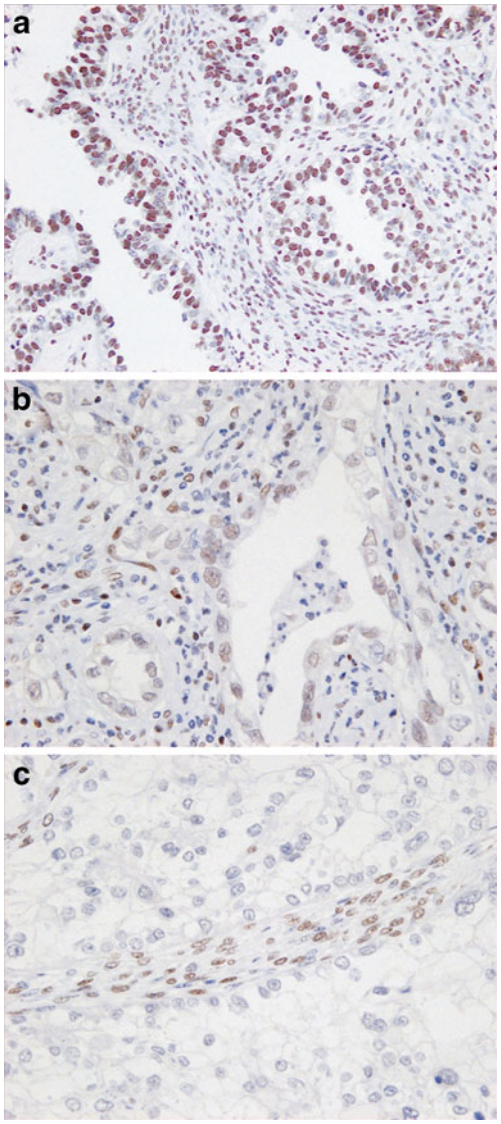

Fig. 2 ARID1A immunoreactivity in three representative ovarian clear cell adenocarcinoma (CCA) cases. **a** A CCA case showing diffuse and strong nuclear immunoreactivity for ARID1A. **b** A CCA case showing weak immunoreactivity for ARID1A. Immunoreactivity in the carcinoma cells was less intense than that in background stromal cells. **c** A CCA case exhibiting no ARID1A protein expression. The stromal cells in the three cases, showing moderate to strong immunoreactivity, serve as an internal positive control. The cases shown in **a**, **b**, and **c** were assigned as strongly positive, weakly positive, and negative for ARID1A protein expression, respectively, and the former two (**a** and **b**) were defined as ARID1A-positive and **c** was defined as ARID1A-negative carcinomas, respectively. Immunoperoxidase stain, original magnification×200 for **a** and×400 for **b** and **c**

ARID1A-negative (undetectable) tumors were higher in the *PIK3CA* mutation-positive tumors than in the *PIK3CA* mutation-negative tumors (53% vs. 39%), but this was not statistically different (P=0.196). However, *PIK3CA* mutations were more frequently detected in the

Table 2 The relation of *PIK3CA* mutation and ARID1A expression with various pathological parameters

	Number of cases (%)				
	Status of *PIK3CA*		ARID1A immunoreaction		
	Mutant	WT	Negative	Positive	
Variables			Undetectable	Weak	Strong
Grossly cystic tumor					
No	4 (12)	25 (46)	11 (28)	4 (20)	15 (50)
Yes	30 (88)	29 (54)	29 (72)	16 (80)	15 (50)
		***P*=0.0018**		*P*=0.293[a];	*P*=0.054[b]
Endometriosis (anywhere)					
Absent	10 (29)	20 (37)	12 (30)	3 (15)	16 (53)
Present	24 (71)	34 (63)	28 (70)	17 (85)	14 (47)
		P=0.462		*P*=0.427[a];	***P*=0.049**[b]
Endometriosis (adjacent)					
Absent	19 (56)	41 (76)	23 (57)	16 (80)	23 (77)
Present	15 (44)	13 (24)	17 (43)	4 (20)	7 (23)
		***P*=0.049**		***P*=0.025**[a];	*P*=0.066[b]
Clear cell adenofibroma					
Absent	32 (94)	42 (78)	34 (85)	18 (90)	24 (80)
Present	2 (6)	12 (22)	6 (15)	2 (10)	6 (20)
		***P*=0.036**		*P*=0.897[a];	*P*=0.583[b]
Prominent growth architecture					
Tubulo/cystic	6 (18)	26 (48)	12 (30)	7 (35)	13 (43)
Papillary	24 (70)	23 (43)	25 (62)	11 (55)	13 (43)
Solid/diffuse	4 (12)	5 (9)	3 (8)	2 (10)	4 (14)
		***P*=0.014**		*P*=0.380[a];	*P*=0.273[b]
Nuclear grade					
Lower	22 (65)	30 (56)	26 (65)	13 (65)	15 (50)
Higher	12 (35)	24 (44)	14 (35)	7 (35)	15 (50)
		P=0.395		*P*=0.386[a];	*P*=0.207[b]
Hyalinized stroma					
Absent	2 (6)	16 (30)	6 (15)	2 (10)	10 (33)
Present	32 (94)	38 (70)	34 (85)	18 (90)	20 (67)
		***P*=0.0056**		*P*=0.289[a];	*P*=0.071[b]
Mucoid stroma					
Absent	9(26)	32 (59)	16 (40)	8 (40)	18 (60)
Present	25 (74)	22 (41)	24 (60)	12 (60)	12 (40)
		***P*=0.0027**		*P*=0.257[a];	*P*=0.098[b]
ARID1A expression					
Negative	18 (53)	21 (39)			
Weakly positive	11 (32)	9 (17)			
Strongly positive	5 (15)	24 (44)			
	P=0.196[a];	***P*=0.013**[b]			
Total	34 (100)	54 (100)	40 (100)	20 (100)	30 (100)

Bold type indicates statistically significant difference

[a]Comparison between ARID1A-negative and ARID1A-positive tumors

[b]Comparison between ARID1A-negative and ARID1A-strong tumors

tumors negative for ARID1A expression than in the tumors strongly positive for ARID1A, and this difference was statistically significant (46% vs. 17%, *P*=0.013).

Correlation of ARID1A immunoreactivity with pathological parameters

Comparing ARID1A-negative tumors with ARID1A-positive (either weak or strong immunoreaction) tumors reveals that endometriotic lesions adjacent to carcinoma were more frequently detected in the former, and this difference was statistically significant (43% vs. 22%, P= 0.025). There was no significant association of ARID1A expression status (negative vs. positive) with other pathological parameters examined. However, when ARID1A-negative tumors were compared with the tumors that were strongly positive for ARID1A immunoreaction, the endometriotic lesions (anywhere) were more frequently documented in the former (70% vs. 47%, P=0.049) (Table 2).

Correlation of *PIK3CA* mutations and ARID1A immunoreactivity with other clinicopathological parameters

There was no significant association between the presence of *PIK3CA* mutations or immunoreactive patterns for ARID1A protein expression and age at disease presentation, clinical stage of disease, tumor size and laterality, presence of residual tumor after initial surgery, response to chemotherapies of tumors, lymph node metastases, or overall patient survival (P>0.05) (Table 3; Fig. 3).

Discussion

In the present study, we sought to determine whether *PIK3CA* mutations and loss of ARID1A protein expression were correlated with histopathological features of ovarian CCAs and whether these alterations had prognostic or clinicopathological significance. The main findings of our investigation can be summarized as follows: (a) the presence of *PIK3CA* mutations in CCA was highly correlated with various histopathological tumor features; (b) *PIK3CA* mutations were not correlated with clinical stage of tumors or the clinical outcome of patients with ovarian CCA; (c) immunoreactivity for ARID1A in CCAs did not correlate with histopathological or clinicopathological parameters examined, although a close association between the negativity for ARID1A immunoreaction and the presence of endometriotic lesions was statistically supported; and (d) the presence of *PIK3CA* mutations was significantly associated with a loss of ARID1A protein expression in CCA. In this study, we used a three-tier scoring system for ARID1A immunoreactions (negative, weakly positive, and strongly positive), and significant associations of ARID1A expression with some parameters examined were only found when strong expression was compared to negative expression. Although complete absence of immunoreactivity for ARID1A protein in tumor cells may be a surrogate marker for *ARID1A* mutations, the meaning of weakened immunoreaction is so far not clear. Therefore, it would be of interest to know whether this weak expression of ARID1A expression also indicates impairment of protein function due to ARID1A gene mutations.

This study has identified *PIK3CA* mutations in 39% of ovarian CCAs, and this frequency is similar to that seen in a previous report by Kuo et al. [5], where the prevalence was estimated to be 33–46%. However, in the present study, most of these *PIK3CA* mutations were localized in exon 20 and were mainly of the H1047R type, while the mutations in the helical domain (exon 9) accounted for only 18% of all mutational events. In two previous studies, mutations in exon 9 and the H1047R mutation substitution in exon 20 comprised 38–41% and 30–35% of all *PIK3CA* mutation types, respectively [5, 8]. Although several factors, such as sample size and methods used for the mutation assay, might lead to these conflicting results, it can be speculated that the contribution of *PIK3CA* mutations to the pathogenesis of ovarian CCAs may vary with ethnicity, for example, in Asian and Caucasian populations. This suggests that the different amino acid changes could exert distinct functional effects on the oncogenic properties of the PI3K enzyme. However, in our series, the difference of domain involved by *PIK3CA* mutations (i.e., exon 9 vs. exon 20) did not correlate with any histopathological or clinicopathological parameters examined (data not shown).

The current study characterizes pathological features of ovarian CCAs harboring *PIK3CA* mutations as follows: the tumors usually manifest a grossly cystic appearance, and the cancer cells prominently grow with a papillary architecture and with hyalinized and/or mucoid stroma. Moreover, *PIK3CA*-mutated tumors were significantly associated with the presence of adjacent endometriotic lesions and the absence of clear cell adenofibroma components. Recently, ovarian CCAs have been believed to be composed of a heterogeneous group of tumors, some arising from an endometriosis and others from a clear cell adenofibroma [1, 6, 26, 28, 32, 33]. Veras et al. [32] reported that CCA manifesting as a macroscopically cystic tumor could be a distinct clinicopathological entity of ovarian CCA, that is, tumor cell growth was very frequently (over 90%) associated with coexisting endometriotic lesions and commonly composed of predominant papillary architectures. In contrast, CCAs with clear cell adenofibroma components usually show non-cystic gross appearance and prominent tubulocystic architectural patterns [32, 33]. Moreover, in a previous study by Kato et al. [29], mucoid stromal changes in CCAs were highly associated with papillary architectural growth and frequently coexisted with hyalinized stromal changes. Considering the

Table 3 The relation of *PIK3CA* mutation and ARID1A expression with other clinico-pathological variables

	Number of cases (%)				
	Status of *PIK3CA*		ARID1A immunoreaction		
	Mutant	WT	Negative	Positive	
Variables			Undetectable	Weak	Strong
Patients age					
≤53[a]	22 (65)	26 (48)	21 (53)	13 (65)	15 (50)
≥53[a]	12 (35)	28 (52)	19 (47)	7 (35)	15 (50)
		P=0.129		*P*=0.740[a];	*P*=0.836[b]
Clinical stage of disease					
I	19 (56)	28 (52)	23 (58)	11 (55)	15 (50)
II/III/IV	15 (44)	26 (48)	17 (42)	9 (45)	15 (50)
		P=0.712		*P*=0.603[a];	*P*=0.533[b]
Tumor size					
≤13 cm[a]	18 (53)	35 (65)	22 (55)	13 (65)	19 (63)
>13 cm[a]	16 (47)	19 (35)	18 (45)	7 (35)	11 (37)
		P=0.268		*P*=0.386[a];	*P*=0.484[b]
Tumor laterality					
Left	15 (44)	18 (33)	15 (38)	6 (30)	12 (40)
Right	17 (50)	34 (63)	22 (55)	14 (70)	17 (57)
Bilateral	2 (6)	2 (4)	3 (7)	0	1 (3)
		P=0.480		*P*=0.609[a];	*P*=0.840[b]
Residual tumor after initial surgery					
Absent	25 (74)	36 (67)	27 (68)	15 (75)	21 (70)
Present	9 (26)	18 (33)	13 (32)	5 (25)	9 (30)
		P=0.497		*P*=0.643[a];	*P*=0.824[b]
Chemo-effect					
CR/PR	3 (33)	7 (39)	6 (46)	2 (40)	2 (22)
SD/PD	6 (67)	11 (61)	7 (54)	3 (60)	7 (78)
		P=0.778		*P*=0.293[a];	*P*=0.246[b]
Lymph node metastasis					
Absent	22 (79)	24 (80)	23 (77)	10 (83)	13 (81)
Present	6 (21)	6 (20)	7 (23)	2 (17)	3 (19)
Unknown	6	24	10	8	14
		P=0.893		*P*=0.607[a];	*P*=0.516[b]
5-year survival	63.8%	64.9%	77.1%	67.5%	50.5%
		P=0.915		*P*=0.235[a];	*P*=0.119[b]
Total	34(100)	54(100)	40(100)	20(100)	30(100)

CR complete response, *PR* partial response, *SD* stable disease, *PD* progressive disease

[a]Mean value

[b]Comparison between ARID1A-negative and ARID1A-positive tumors

[c]Comparison between ARID1A-negative and ARID1A-strong tumors

data available, we speculate that *PIK3CA* mutations contribute to the pathogenesis of a subset of ovarian CCA, namely, those derived from endometriotic cysts, rather than from clear cell adenofibroma, in which carcinoma cells commonly grow as prominent papillary architectures with hyalinized and/or mucoid stroma.

From another viewpoint, the findings of this study help not only in understanding the pathogenesis of ovarian CCAs but also in clustering CCAs more likely to harbor *PIK3CA* mutations. Indeed, the grossly cystic feature in conjunction with the prominent papillary growth pattern and with hyalinized and mucoid stromal changes indicates the presence of *PIK3CA* mutations with a positive predictive value of 78% and a negative predictive value of 75% with likelihood ratio of 5.72 (data not shown in the results). A case of a *PIK3CA* mutation-positive CCA representing all of these features is shown in Fig. 4, and these pathological features seemed to be almost concordant with the "cystic clear cell carcinoma" designated by Veras et al. [32] (see Fig. 2 in their report).

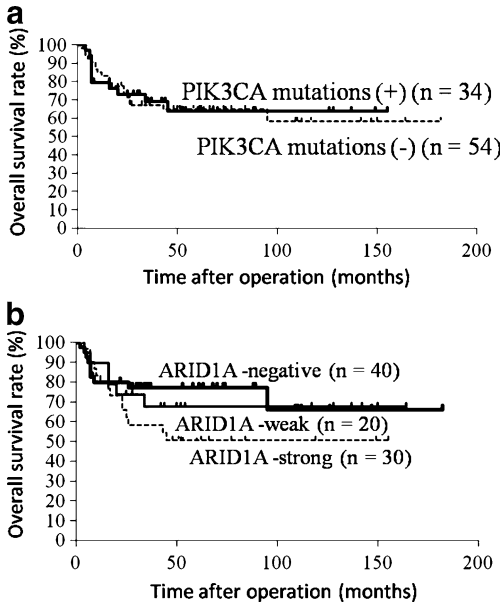

Fig. 3 Overall survival curves for patients with clear cell adenocarcinoma (CCA), stratified by **a** *PIK3CA* mutations detected by direct genomic DNA sequence and **b** immunoreactive intensities for ARID1A protein expression. **a** Kaplan–Meier curves demonstrate the lack of significant prognostic impact of the *PIK3CA* mutations for patients with ovarian CCA. **b** Although the ARID1A-strong group shows a trend of shorter overall survival than the other two groups (ARID1A-negative and ARID1A-weak groups), these differences are not statistically significant. *ARID1A-negative* the tumor group negative for ARID1A immunoreaction, *ARID1A-weak* the tumor group weakly positive for ARID1A, *ARID1A-strong* the tumor group strongly positive for ARID1A

One of the explanations for the lack of correlation between *PIK3CA* mutations or ARID1A immunoreactivity and clinical stage or clinical outcome of patients is that these molecular alterations occur as very early events during tumor development of ovarian CCA [6, 24]. As one of our previous studies demonstrated, *PIK3CA* mutations could be detected in the endometriotic epithelium adjacent to the *PIK3CA* mutation-positive CCAs, even in those that displayed no evidence of cytological atypia, strongly suggesting that mutations of the *PIK3CA* gene occur before the development of the atypical precancerous lesions (e.g., atypical endometriosis) [6]. In addition, loss of ARID1A expression and somatic mutations of *ARID1A* gene were reported in the atypical endometriosis adjacent to CCA [7]. Moreover, our recent immunohistochemical analysis showed that loss of ARID1A protein expression in the putative precursor lesions of ovarian CCA occurred specifically in cases in which the corresponding carcinoma was negative for ARID1A expression. In the majority of the ARID1A-negative carcinoma cases, the deficiency of ARID1A immunoreaction was already evident at the stage of precursor lesions lacking cytological atypia (i.e., non-atypical endometriosis adjacent to carcinoma or benign clear cell adenofibroma), suggesting that loss of ARID1A protein also occurs as a very early event in CCA tumorigenesis [24]. Therefore, *PIK3CA* mutations and loss of ARID1A protein expression may initiate tumor development of CCA, but may not be critical for tumor progression in this carcinoma.

Our recent report showed frequent concurrence of *PIK3CA* mutations and deficient immunoreactivity for ARID1A in ovarian CCAs [24], and the present statistical

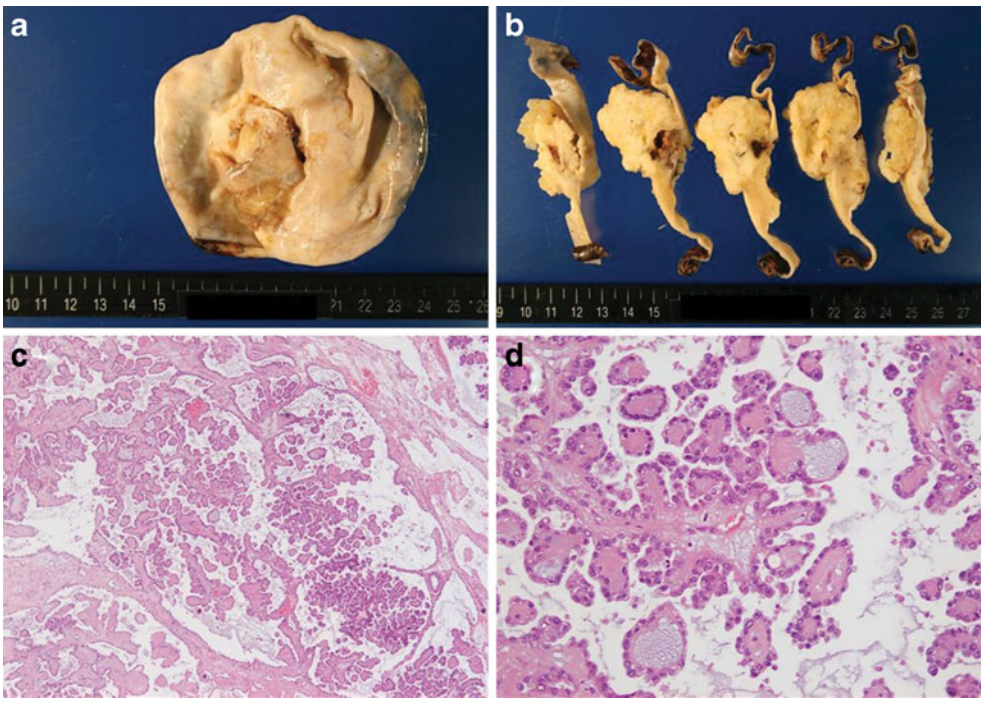

Fig. 4 Representative macroscopic (**a**, **b**) and microscopic (**c**, **d**) findings of the ovarian clear cell adenocarcinoma (CCA) harboring *PIK3CA* mutations. **a** Macroscopic appearance of an ovarian cystic tumor. **b** In cut sections, a cancerous solid component protrudes into the cystic lumen. **c** Microscopic findings of the cancerous components in **a.** Tumor cells grow in a prominent papillary architectural pattern. **c**, **d** High power view of **c**. Stroma components in the papillary core show both hyalinized and mucoid changes. These findings are similar to those of the "cystic clear cell carcinoma" designated by Veras et al. [29]. **c**, **d** HE stain, original magnification×40 for **c** and×200 for **d**

analysis using a large number of CCA cases confirmed these findings. Consequently, it is interesting to consider whether the ARID1A pathway can crosstalk with the PI3K signaling pathway and how inactivation of ARID1A may contribute to the development of ovarian CCA. It might be speculated that somatic mutations of tumor suppressor genes such as *ARID1A* can directly lead to epigenetic changes in tumor cells through specific modifications of chromatin proteins. By altering the accessibility of transcription factors to chromatin, additional mutations in the PI3 kinase pathways (e.g., *PIK3CA* mutation) could take advantage of its oncogenic properties. Identification of the possible interactions between these molecular alterations during tumor development of CCA is important for the understanding of its pathogenesis, guidance of proper management, and development of new therapeutic strategies of this highly lethal type of ovarian cancer.

In conclusion, mutations in the *PIK3CA* gene seem to be associated with the pathogenesis of a subgroup of ovarian CCAs, namely, cystic CCA showing prominent papillary tumor cell growth with hyalinized and/or mucoid stromal changes, which could be derived from adjacent endometriosis. Weak prognostic impacts of *PIK3CA* mutations or ARID1A alterations in patients with CCA may support the idea that both *PIK3CA* mutations and ARID1A alterations occur as very early events in the CCA tumorigenesis, initiating tumor development. The meaning of low immunoreactivity for ARID1A and possible interactions or potential crosstalk between the PI3K signaling pathway and the ARID1A pathway should be analyzed in the future.

Acknowledgments This work was supported in part by a grant-in-aid for promotion of defense medicine from the Ministry of Defense, Japan (S.Y., O.M.), by a grant-in-aid for cancer research from the Ministry of Health, Labor, and Welfare, Japan (H.T.), and by a grant from the Foundation for Promotion of Cancer Research (S.Y. and H. T.). We are grateful to Ms. Kozue Suzuki, Department of Basic Pathology, National Defense Medical College, Saitama, Japan, for her technical assistance.

Conflicts of interest The authors declare no actual or potential conflicts of interest associated with this study.

References

1. Lee KR, Tavassoli FA, Part J et al (2003) Surface epithelial-stromal tumours. In: Tavassoli FA, Devilee P (eds) World Health Organization classification of tumours. Pathology and genetics of tumours of the breast and female genital organs. IARC, Lyon, pp 117–145
2. Chan JK, Teoh D, Hu JM et al (2008) Do clear cell ovarian carcinomas have poorer prognosis compared to other epithelial cell types? A study of 1411 clear cell ovarian cancers. Gynecol Oncol 109:370–376
3. Mizuno M, Kikkawa F, Shibata K et al (2006) Long-term follow-up and prognostic factor analysis in clear cell adenocarcinoma of the ovary. J Surg Oncol 94:138–143
4. Takano M, Kikuchi Y, Yaegashi N et al (2006) Clear cell carcinoma of the ovary: a retrospective multicentre experience of 254 patients with complete surgical staging. Br J Cancer 94:1369–1374
5. Kuo KT, Mao TL, Jones S et al (2009) Frequent activating mutations of PIK3CA in ovarian clear cell carcinoma. Am J Pathol 174:1597–1601
6. Yamamoto S, Tsuda H, Takano M et al (2011) PIK3CA mutation is an early event in the development of endometriosis-associated ovarian clear cell adenocarcinoma. J Pathol 225:189–194
7. Wiegand KC, Shah SP, Al-Agha OM et al (2010) ARID1A mutations in endometriosis-associated ovarian carcinomas. N Engl J Med 363:1532–1543
8. Jones S, Wang TL, Shih I et al (2010) Frequent mutations of chromatin remodeling gene *ARID1A* in ovarian clear cell carcinoma. Science 330:228–231
9. Stokoe D, Stephens LR, Copeland T et al (1997) Dual role of phosphatidylinositol-3,4,5-trisphosphate in the activation of protein kinase B. Science 277:567–570
10. Shayesteh L, Lu Y, Kuo WL et al (1999) PIK3CA is implicated as an oncogene in ovarian cancer. Nat Genet 21:99–102
11. Samuels Y, Wang Z, Bardelli A et al (2004) High frequency of mutations of the PIK3CA gene in human cancers. Science 304:554
12. Kang S, Bader AG, Vogt PK (2005) Phosphatidylinositol 3-kinase mutations identified in human cancer are oncogenic. Proc Natl Acad Sci USA 102:802–807
13. Broderick DK, Di C, Parrett TJ et al (2004) Mutations of PIK3CA in anaplastic oligodendrogliomas, high-grade astrocytomas, and medulloblastomas. Cancer Res 64:5048–5050
14. Lee JW, Soung YH, Kim SY et al (2005) PIK3CA gene is frequently mutated in breast carcinomas and hepatocellular carcinomas. Oncogene 24:1477–1480
15. Velho S, Oliveira C, Ferreira A et al (2005) The prevalence of PIK3CA mutations in gastric and colon cancer. Eur J Cancer 41:1649–1654
16. Hayes MP, Wang H, Espinal-Witter R et al (2006) PIK3CA and PTEN mutations in uterine endometrioid carcinoma and complex atypical hyperplasia. Clin Cancer Res 12:5932–5935
17. Ogino S, Nosho K, Kirkner GJ et al (2009) PIK3CA mutation is associated with poor prognosis among patients with curatively resected colon cancer. J Clin Oncol 27:1477–1484
18. Sartore-Bianchi A, Martini M, Molinari F et al (2009) PIK3CA mutations in colorectal cancer are associated with clinical resistance to EGFR-targeted monoclonal antibodies. Cancer Res 69:1851–1857
19. Isakoff SJ, Engelman JA, Irie HY et al (2005) Breast cancer-associated PIK3CA mutations are oncogenic in mammary epithelial cells. Cancer Res 65:10992–11000
20. Reisman D, Glaros S, Thompson EA (2009) The SWI/SNF complex and cancer. Oncogene 28:1653–1668
21. Sif S, Saurin AJ, Imbalzano AN et al (2001) Purification and characterization of mSin3A-containing Brg1 and hBrm chromatin remodeling complexes. Genes Dev 15:603–618
22. Wang W, Xue Y, Zhou S et al (1996) Diversity and specialization of mammalian SWI/SNF complexes. Genes Dev 10:2117–2130
23. Ho L, Crabtree GR (2010) Chromatin remodelling during development. Nature 463:474–484
24. Yamamoto S, Tsuda H, Takano M, et al (2011) Loss of ARID1A protein expression occurs as an early event in ovarian clear-cell carcinoma development and frequently coexists with *PIK3CA* mutations. Mod Pathol (in press)

25. Maeda D, Mao TL, Fukayama M et al (2010) Clinicopathological significance of loss of ARID1A immunoreactivity in ovarian clear cell carcinoma. Int J Mol Sci 11:5120–5128
26. Yamamoto S, Tsuda H, Takano M et al (2008) Expression of platelet-derived growth factors and their receptors in ovarian clear-cell carcinoma and its putative precursors. Mod Pathol 21:115–124
27. Yamamoto S, Tsuda H, Miyai K et al (2010) Cumulative alterations of p27-related cell-cycle regulators in the development of endometriosis-associated ovarian clear cell adenocarcinoma. Histopathology 56:740–749
28. Yamamoto S, Tsuda H, Takano M et al (2008) Clear-cell adenofibroma can be a clonal precursor for clear-cell adenocarcinoma of the ovary: a possible alternative ovarian clear-cell carcinogenic pathway. J Pathol 216:103–110
29. Kato N, Takeda J, Fukase M et al (2010) Alternate mucoid and hyalinized stroma in clear cell carcinoma of the ovary: manifestation of serial stromal remodeling. Mod Pathol 23:881–888
30. Therasse P, Arbuck SG, Eisenhauer EA et al (2000) New guidelines to evaluate the response to treatment in solid tumors. European Organization for Research and Treatment of Cancer, National Cancer Institute of the United States, National Cancer Institute of Canada. J Natl Cancer Inst 92:205–216
31. Guan B, Mao TL, Panuganti PK et al (2011) Mutation and loss of expression of ARID1A in uterine low-grade endometrioid carcinoma. Am J Surg Pathol 35:625–632
32. Veras E, Mao TL, Ayhan A et al (2009) Cystic and adenofibromatous clear cell carcinomas of the ovary: distinctive tumors that differ in their pathogenesis and behavior: a clinicopathologic analysis of 122 cases. Am J Surg Pathol 33:844–853
33. Yamamoto S, Tsuda H, Yoshikawa T et al (2007) Clear cell adenocarcinoma associated with clear cell adenofibromatous components: a subgroup of ovarian clear cell adenocarcinoma with distinct clinicopathologic characteristics. Am J Surg Pathol 31:999–1006

Virchows Arch (2012) 460:89–93
DOI 10.1007/s00428-011-1178-7

ORIGINAL ARTICLE

Carbonic anhydrase IX is expressed in mesothelioma and metastatic clear cell renal cell carcinoma of the lung

Mitchell L. Ramsey · Benjamin J. Yuh · Matthew T. Johnson · Anjana V. Yeldandi · Debra L. Zynger

Received: 12 October 2011 / Revised: 10 November 2011 / Accepted: 22 November 2011 / Published online: 6 December 2011
© Springer-Verlag 2011

Abstract High immunohistochemical expression of carbonic anhydrase IX (CAIX) is found in clear cell renal cell carcinoma (ccRCC), but no studies have assessed CAIX in metastatic ccRCC (mccRCC) of the lung. As 75% of patients with mccRCC show lung involvement, characterization of protein expression in these lesions is warranted. This investigation analyzed CAIX immunohistochemical expression in pulmonary/pleural tumors including mccRCC (n=22), mesothelioma (n=19), squamous cell carcinoma (n=27), small cell carcinoma (n=9), and adenocarcinoma (n=49), as well as other mesothelial lesions (n=4). Membranous immunoreactivity was semiquantitatively evaluated for percent of cells stained and intensity. All cases of mccRCC (1+, 4.5%; 3+, 95.5%) and mesothelioma (2+, 10.5%; 3+, 89.5%) expressed CAIX. Most cases of lung squamous cell carcinoma (0, 11.1%; 1+, 25.9%; 2+, 22.2%; 3+, 40.7%) and small cell carcinoma were reactive (0, 11.1%; 1+, 22.2%; 2+, 33.3%; 3+, 33.3%), while CAIX was detected less frequently in pulmonary adenocarcinoma (0, 61.2%; 1+, 16.3%; 2+, 12.2%; 3+, 10.2%). In addition, CAIX was positive in adenomatoid tumor (3+, 100%) and mesothelial hyperplasia (3+, 100%). We demonstrate that CAIX is sensitive for mccRCC within the lung and a novel immunohistochemical marker for mesothelial proliferations, notably mesothelioma. Variable immunoreactivity is present among primary pulmonary epithelial tumors. Knowledge of expression overlap between these entities may prevent an incorrect interpretation of immunohistochemical results, particularly when limited tissue is available. As new carbonic anhydrase inhibitors are being evaluated, testing additional tumors for CAIX may lead to novel treatment options.

Keywords Carbonic anhydrase IX · CAIX · Mesothelioma · Metastatic · Clear cell renal cell carcinoma · Lung

M. L. Ramsey · B. J. Yuh · D. L. Zynger (✉)
Department of Pathology,
The Ohio State University Medical Center,
410 W 10th Ave., E401 Doan Hall,
Columbus, OH 43210, USA
e-mail: debra.zynger@osumc.edu

M. T. Johnson
Department of Urology,
The Ohio State University Medical Center,
Columbus, OH 43210, USA

A. V. Yeldandi
Department of Pathology,
Northwestern University Feinberg School of Medicine,
Chicago, IL 60611, USA

Introduction

Carbonic anhydrase IX (CAIX) is a transmembrane, zinc-containing metalloenzyme that catalyzes reversible reactions of the bicarbonate buffer system to regulate pH in hypoxic conditions [1–3]. CAIX is overexpressed in aggressive tumors where rapid growth limits available oxygen [3–5]. However, CAIX is not limited to cancerous cells but is present in gastric mucosa, larger bile ducts, and several other locations [3, 6, 7]. In addition, Northern blot analysis and immunohistochemistry techniques were used to demonstrate expression of CAIX in nonneoplastic mesothelial cells [1, 3, 6].

CAIX has been well described as a diagnostic marker for clear cell renal cell carcinoma (ccRCC) [3, 7–11], with a few studies noting generally high expression in metastatic ccRCC (mccRCC) [3, 7, 8]. Although 85% of ccRCC recurrences present within 3 years, ccRCC is known for late metastases to the lung, liver, bone, and brain [9, 12, 13]. When metastatic, approximately 75% of tumors have lung involvement [14]. However, CAIX expression of mccRCC

Table 1 CAIX immunohistochemical expression in pulmonary lesions

	Percentage of cells stained				Intensity (mean)
	0 (<5%)	1+ (5%–10%)	2+ (11%–50%)	3+ (>50%)	
Metastatic ccRCC to the lung (n=22)	0	1 (4.5%)	0	21 (95.5%)	2.9
Mesothelioma of the pleura (n=19)	0	0	2 (10.5%)	17 (89.5%)	2.8
Mesothelial hyperplasia of the pleura (n=1)	0	0	0	1 (100%)	3.0
Adenomatoid tumor (n=3)	0	0	0	3 (100%)	2.7
Squamous cell carcinoma of the lung (n=27)	3 (11.1%)	7 (25.9%)	6 (22.2%)	11 (40.7%)	2.3
Small cell carcinoma of the lung (n=9)	1 (11.1%)	2 (22.2%)	3 (33.3%)	3 (33.3%)	2.3
Adenocarcinoma of the lung (n=49)	30 (61.2%)	8 (16.3%)	6 (12.2%)	5 (10.2%)	0.8
Nonneoplastic lung (bronchial epithelium/pneumocytes) (n=24)	24 (100%)	0	0	0	0

mccRCC within the lung and pleural mesothelioma have consistent CAIX expression. Squamous cell carcinoma and small cell carcinoma have variable expression, while adenocarcinoma has infrequent diffuse expression.

has not yet been evaluated in these metastases. Understanding the expression overlap between primary lung tumors and mccRCC to the lung is relevant for diagnosis and potential treatment. Some patients with mccRCC have shown favorable outcomes with treatment by interferon-α monotherapy, interleukin (IL)-2, or combination therapy [14, 15]. Recent advances in the sulfamide, sulfamate, and sulfonamide series may provide alternative treatments through CAIX inhibition [16]. Regarding primary lung tumors, previous articles report variable expression of CAIX in non-small cell lung carcinoma [17, 18]. Expression of CAIX in mesothelioma effusions was identified via reverse transcriptase polymerase chain reaction, but mesothelioma has yet to be tested by immunohistochemical analysis [17].

This study aims to assess CAIX protein expression of mccRCC in the lung, epithelial lung tumors, and pleural mesothelioma via immunohistochemistry. Better understanding of the expression profile will aid in diagnostics and may lead to novel treatment opportunities.

Materials and methods

Archived formalin-fixed, paraffin-embedded tissue blocks were obtained from The Ohio State University Medical Center and Northwestern Memorial Hospital. Tissues from 130 tumors were sampled, which contained eight types of neoplasms and nonneoplastic conditions. All diagnoses were based on World Health Organization histologic criteria [19].

Four-micrometer-sections were dried at 55°C for 3 h then subjected to heat-induced epitope retrieval for 25 min at pH 6.0 on a Leica-Bond Autostainer. The slides were incubated with diluted CAIX monoclonal antibody (Leica, NCL-L-CAIX, 1:100) for 30 min. Bond Polymer Refine Detection kit was applied, and the sections were counterstained with hematoxylin.

Immunohistochemical scoring was based on membranous reactivity and was recorded semiquantitatively as follows: negative (0, <5% of cells stained), focally positive (1+, 5%–10% of cells stained), positive (2+, 11%–50% of cells stained), or diffusely positive (3+, >50% of cells stained). Staining intensity was averaged across the lesion and graded from 0 to 3, with 3 being the most intense. Non-mccRCC was used as a positive control, and ccRCC lacking the CAIX primary antibody was used as a negative control. When possible, cases were also evaluated for CAIX staining in bronchial epithelium and alveolar pneumocytes.

Results

Table 1 depicts the immunohistochemical results for CAIX expression in lung lesions.

All mccRCC cases (n=22; 12 biopsies, 10 resections) demonstrated positivity, with only 1 case that did not exhibit diffuse expression (1+, 4.5%; 3+, 95.5%) (Fig. 1a and b). Three cases with sarcomatoid differentiation were included, one of which had focal staining (Fig. 1c and d). The mean intensity for mccRCC was high (2.9).

Fig. 1 CAIX expression in lung lesions. (**a**, **b**) Hematoxylin and eosin and CAIX immunohistochemical stains of mccRCC with diffuse, membranous reactivity. Alveolar pneumocytes are negative (*upper left*) (×20). (**c**, **d**) mccRCC with sarcomatoid differentiation demonstrating diffuse, moderate expression (×20). (**e**, **f**) Epithelioid mesothelioma exhibiting strong and diffuse membranous and cytoplasmic reactivity (×20). (**g**, **h**) The sarcomatoid focus in a biphasic mesothelioma expresses CAIX strongly in a membranocytoplasmic pattern (×20). (**i**, **j**) Adenomatoid tumor displays strong, diffuse membranous and cytoplasmic reactivity (×20). (**k**, **l**) Squamous cell carcinoma of the lung highly expresses CAIX, notably at the periphery of tumor nests (×20). (**m**, **n**) Small cell carcinoma with strong, diffuse membranous staining (×20). (**o**, **p**) Primary lung adenocarcinoma is negative for membranous CAIX reactivity with weak focal cytoplasmic expression (×20)

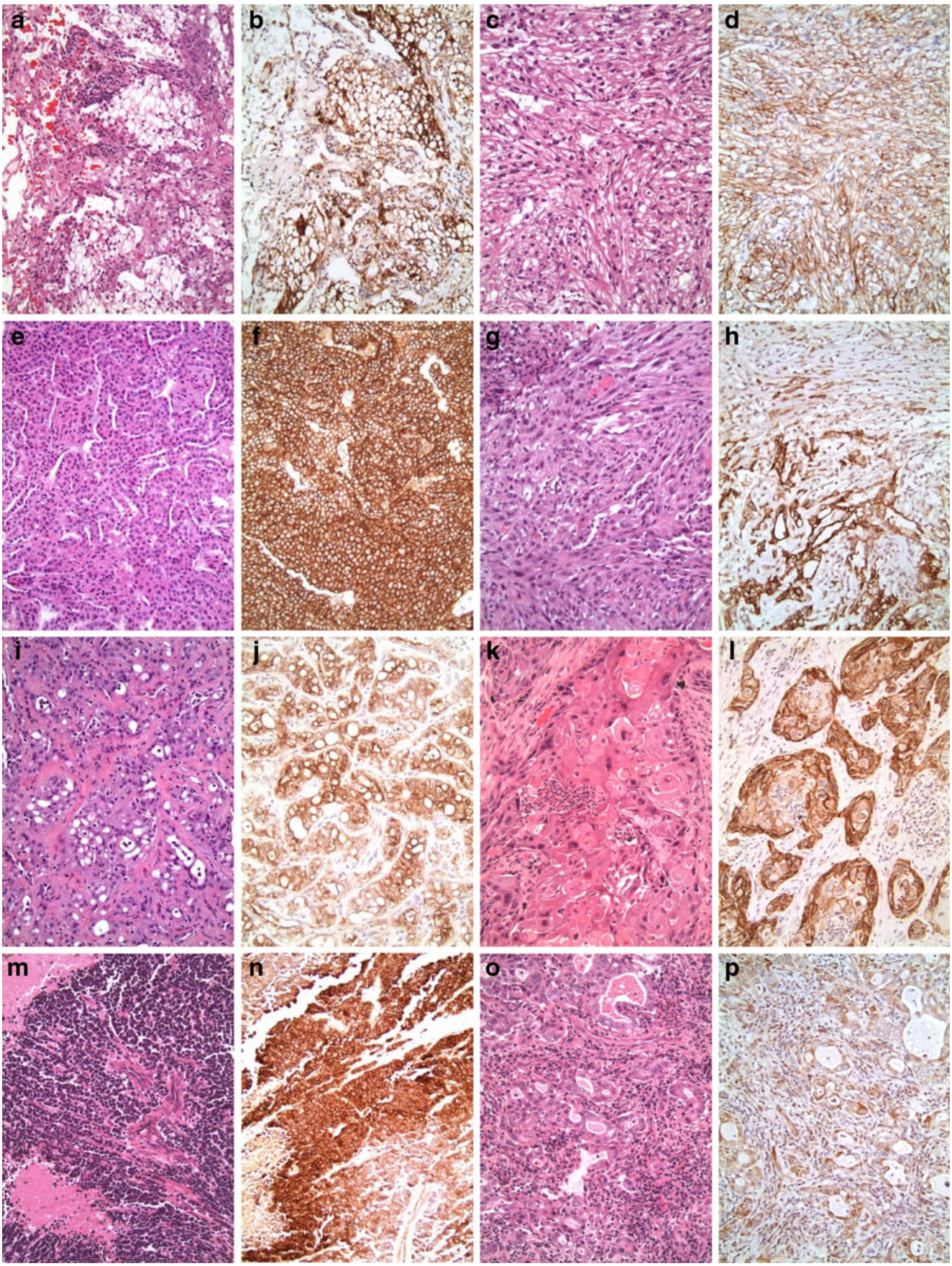
a
b
c
d
e
f
g
h
i
j
k
l
m
n
o
p

All cases of pleural mesothelioma (n=19; 13 biopsies, 6 resections) expressed CAIX strongly and diffusely (2+, 10.5%; 3+, 89.5%; mean intensity=2.8) (Fig. 1e and f). Mesothelioma included epithelioid (n=14) and biphasic subtypes (spindle cell and epithelioid) (n=5), with no appreciable difference in reactivity (Fig. 1g and h). Other mesothelial lesions with strong and diffuse reactivity include mesothelial hyperplasia (n=1 biopsy) of the pleura (3+, 100%; intensity=3.0) and adenomatoid tumor of the testicle (n=2 resections) and fallopian tube (n=1 resection) (3+, 100%; mean intensity=2.7) (Fig. 1i and j).

Regarding epithelial lung primary tumors, squamous cell carcinoma (n=27 resections) had the highest percentage of diffusely positive cases (0, 11.1%; 1+, 25.9%; 2+, 22.2%; 3+, 40.7%; mean intensity=2.3) (Fig. 1k and l). In squamous cell carcinoma, expression was most intense at the periphery of squamous nests. Small cell carcinoma of the lung (n=9 resections) had variable reactivity (0, 11.1%; 1+, 22.2%; 2+, 33.3%; 3+, 33.3%; mean intensity=2.3) (Fig. 1m and n). Lung adenocarcinoma (n=49 resections) was predominately negative with occasional diffuse expression (0, 61.2%, 1+, 16.3%; 2+, 12.2%; 3+, 10.2%; mean intensity=0.8) (Fig. 1o and p).

Associated nonneoplastic lung tissues were evaluated for CAIX expression (n=24). Among these, bronchial epithelium (n=15) was consistently negative for membranous expression (0, 100%; mean intensity=0), although 53.3% revealed strong and diffuse cytoplasmic staining. Alveolar pneumocytes were negative for CAIX (0, 100%; mean intensity=0) (Fig. 1a and b, upper left). Pleural nonneoplastic mesothelium (n=3) had strong and diffuse expression (3+, 100%; mean intensity=3.0). A single case contained bronchial submucosal glandular tissue, which was negative (0, 100%; mean intensity=0).

Discussion

CAIX has been identified as a reliable marker for ccRCC, with promising results for mccRCC [3, 7–11]. While it is known that mccRCC commonly involves the lung, there are no reports specifically detailing the expression of CAIX in mccRCC of the lung [14]. This study aims to test lung tumors for CAIX expression to determine the diagnostic utility of this marker as well as potential candidacy for CAIX-related treatments.

Nonneoplastic mesothelium has been reported to diffusely express CAIX via immunohistochemistry [6]. Using reverse transcriptase polymerase chain reaction to assay malignant pleural effusions in patients with a history of mesothelioma, researchers detected CAIX gene expression in seven of eight cases [17]. We describe for the first time the immunohistochemical expression of CAIX in pleural mesothelioma. Concordant with prior preliminary data, CAIX was detected in all cases of mesothelioma, including biopsies and resections. Membranous expression was strong and diffuse in 89.5% of tumors, with similar expression seen in epithelioid and biphasic subtypes. Other mesothelial proliferations, including mesothelial hyperplasia of the pleura and adenomatoid tumor, were diffusely positive. CAIX appears to be an additional novel mesothelial marker.

We demonstrated CAIX immunohistochemical expression in all cases of mccRCC in the lung, including resections and biopsies. Published data reveal high CAIX expression in 69% to 75% of mccRCC, with metastases generally expressing CAIX less than the primary tumor [3, 7, 8, 20, 21]. While lung metastases were likely included in earlier studies, specific data for metastatic sites were not provided [3, 7, 8, 20, 21]. The few cases with sarcomatoid differentiation that we examined had less consistent expression. Similarly, Tickoo et al. [22] found 82% of organ confined sarcomatoid ccRCC to express CAIX compared with 95% of ccRCC without sarcomatoid differentiation. As anticipated, CAIX has a high sensitivity for mccRCC of the lung.

Among primary lung tumors, we report CAIX expression in 89% of squamous cell carcinoma, 89% of small cell carcinoma, and 39% of adenocarcinoma. Squamous cell carcinoma and small cell carcinoma varied in percentage of reactive cells. Both tumors did have a substantial subset that was diffusely positive and could mimic the expression seen in mccRCC and mesothelioma. Prior authors observed CAIX expression in 58% to 96% of pulmonary squamous cell carcinoma [23–25]. We found adenocarcinoma to be predominately negative with only 10% of cases diffusely positive, unlike the other neoplasms. A range of CAIX expression of 30%–81% in lung adenocarcinoma has been noted in the literature [23–25]. Kim et al. [23, 24] concluded that CAIX expression is significantly higher in squamous cell carcinoma than in adenocarcinoma, compatible with our data. No former studies have assessed CAIX expression in small cell carcinoma of the lung for comparison. In light of the variable reactivity in primary lung epithelial tumors, CAIX does not seem to be a useful diagnostic marker for these lesions, although diffuse expression of CAIX does not favor a diagnosis of pulmonary adenocarcinoma.

The potential roles for CAIX include serum and radiologic diagnostics as well as guiding or predicting therapeutic response [7, 10, 16, 21, 26, 27]. While the usual treatment for primary ccRCC is surgical, targeted therapy has resulted in improved long-term disease-free survival in those with metastatic disease. Higher CAIX expression tends to increase the efficacy of IL-2, and CAIX screening may improve patient selection for higher-dose IL-2 regimens [10, 26, 27]. Numerous publications describe the usage of IL-2 for treatment of mccRCC, and by extension, other CAIX-expressing tumors may be implicated [7, 21, 26]. In addition to IL-2 (and

interferon-α combination treatments), recent advances in carbonic anhydrase inhibiting drugs may result in treatment options for a variety of CAIX-dependent tumors arising from the sulfamide, sulfonamide, and sulfamate series [16].

In conclusion, CAIX immunohistochemical expression has a high sensitivity for mccRCC and pleural mesothelioma. However, it is important to note the overlap of primary lung tumor reactivity. In the wake of numerous reports of CAIX-based treatment for ccRCC, there may be future applications in diagnostic assessment, treatment, and radiologic imaging of CAIX-expressing lung tumors.

Conflict of interest statement We declare that we have no conflict of interest.

References

1. Stillebroer AB, Mulders PFA, Boerman OC et al (2010) Carbonic anhydrase IX in renal cell carcinoma: implications for prognosis, diagnosis, and therapy. Eur Urol 58:75–83
2. Kon-no H, Ishii G, Nagai K et al (2006) Carbonic anhydrase IX expression is associated with tumor progression and a poor prognosis of lung adenocarcinoma. Lung Cancer 54(3):409–418
3. Leibovich BC, Sheinin Y, Lohse CM et al (2007) Carbonic anhydrase IX is not an independent predictor of outcome for patients with clear cell renal cell carcinoma. J Clin Oncol 25:4757–4764
4. Malentacchi F, Simi L, Nannelli C et al (2009) Alternative splicing variants of carbonic anhydrase IX in human non-small cell lung cancer. Lung Cancer 64:271–276
5. Patard J, Fergelot P, Karakiewicz PI et al (2009) Low CAIX expression and absence of VHL gene mutation are associated with tumor aggressiveness and poor survival of clear cell renal cell carcinoma. Int J Cancer 123(2):395–400
6. Ivanov S, Liao SY, Ivanova A et al (2001) Expression of hypoxia-inducible cell-surface transmembrane carbonic anhydrases in human cancer. Am J Pathol 158(3):905–919
7. Tostain J, Li G, Gentil-Perret A et al (2010) Carbonic anhydrase 9 in clear cell renal cell carcinoma: a marker for diagnosis, prognosis and treatment. Eur J Cancer 46:3141–3148
8. Liao SY, Aurelio ON, Jan K et al (1997) Identification of the MN/CA9 protein as a reliable diagnostic biomarker of clear cell carcinoma of the kidney. Cancer Res 57:2827–2831
9. Genega EM, Ghebremichael M, Najarian R et al (2010) Carbonic anhydrase IX expression in renal neoplasms: correlation with tumor type and grade. Am J Clin Pathol 134:873–879
10. Leppert JT, Lam JS, Pantuck AJ et al (2005) Carbonic anhydrase IX and the future of molecular markers in renal cell carcinoma. BJU Int 96:281–285
11. Al-Hamadie HA, Alden D, Qin LX et al (2008) Carbonic anhydrase IX expression in clear cell renal cell carcinoma: an immunohistochemical study comparing 2 antibodies. Am J Surg Pathol 32 (3):377–382
12. McNichols DW, Segura JW, DeWeerd JH (1981) Renal cell carcinoma: long-term survival and late recurrence. J Urol 126:17–23
13. Janzen NK, Kim HL, Figlin RA et al (2003) Surveillance after radical or partial nephrectomy for localized renal cell carcinoma and management of recurrent disease. Urol Clin North Am 30:843–852
14. Bukowski RM (1997) Natural history and therapy of metastatic renal cell carcinoma: the role of interleukin-2. Cancer 80:1198–1220
15. Motzer RJ, Bacik J, Mariani T et al (2002) Treatment outcome and survival associated with metastatic renal cell carcinoma of non-clear-cell histology. J Clin Oncol 20:2376–2381
16. Winum JY, Scozzafava A, Montera JL et al (2009) Inhibition of carbonic anhydrase IX: a new strategy against cancer. Anticancer Agents Med Chem 9:693–702
17. Li G, Passebosc-Faure K, Feng G et al (2007) MN/CA9: a potential gene marker for detection of malignant cells in effusions. Biomarkers 12(2):214–220
18. Ilie M, Mazure NM, Hofman V et al (2010) High levels of carbonic anhydrase IX in tumour tissue and plasma are biomarkers of poor prognostic in patients with non-small cell lung cancer. Br J Cancer 102:1627–1635
19. Travis WD, Brambilla E, Muller-Hermelink HK et al (2004) World Health Organization classification of tumors: pathology and genetics of tumours of the lung, pleura, thymus and heart. IARC, Lyon
20. Choueiri TK, Regan MM, Rosenberg JE et al (2010) Carbonic anhydrase IX and pathological features as predictors of outcome in patients with metastatic clear-cell renal cell carcinoma receiving vascular endothelial growth factor-targeted therapy. BJU Int 106:772–778
21. Bui MH, Seligson D, Han K et al (2003) Carbonic anhydrase IX is an independent predictor of survival in advanced renal clear cell carcinoma: implications for prognosis and therapy. Clin Cancer Res 9:802–811
22. Tickoo SK, Alden D, Olgac S (2007) Immunohistochemical expression of hypoxia inducible factor-1α and its downstream molecules in sarcomatoid renal cell carcinoma. J Urol 177:1258–1263
23. Kim SJ, Rabbani ZN, Vollmer RT (2004) Carbonic anhydrase IX in early-stage non-small cell lung cancer. Clin Cancer Res 10:7925–7933
24. Kim SJ, Rabbani ZN, Dewhirst MW (2005) Expression of HIF-1alpha, CA IX, VEGF, and MMP-9 in surgically resected non-small cell lung cancer. Lung Cancer 49:325–335
25. Vermylen P, Roufosse C, Burny A (1999) Carbonic anhydrase IX antigen differentiates between preneoplastic malignant lesions in non-small cell lung carcinoma. Eur Respir J 14:806–811
26. Atkins M, Regan M, McDermott D (2005) Carbonic anhydrase IX expression predicts outcome of interleukin 2 therapy for renal cancer. Clin Cancer Res 11(10):3714–3721
27. Atkins MB, Choueiri TK, Cho D (2009) Treatment selection for patients with metastatic renal cell carcinoma. Cancer 115(10):2327–2333

Virchows Arch (2012) 460:95–102
DOI 10.1007/s00428-011-1168-9

ORIGINAL ARTICLE

Peripheral chondrosarcoma progression is associated with increased type X collagen and vascularisation

Carlos E. de Andrea · Malgorzata I. Wiweger · Judith V. M. G. Bovée · Salvatore Romeo · Pancras C. W. Hogendoorn

Received: 10 August 2011 / Revised: 31 October 2011 / Accepted: 2 November 2011 / Published online: 25 November 2011
© The Author(s) 2011. This article is published with open access at Springerlink.com

Abstract Endochondral bone formation requires a cartilage template, known as the growth plate, and vascular invasion, bringing osteoblasts and osteoclasts. Endochondral chondrocytes undergo sequences of cell division, matrix secretion, cell hypertrophy, apoptosis, and matrix calcification/mineralisation. In this study, two critical steps of endochondral bone formation, the deposition of collagen X-rich matrix and blood vessel attraction/invasion, were investigated by immunohistochemistry. Fourteen multiple osteochondromas and six secondary peripheral chondrosarcomas occurring in patients with multiple osteochondromas were studied and compared to epiphyseal growth plate samples. Mutation analysis showed all studied patients (expect one) to harbour a germ-line mutations in either *EXT1* or *EXT2*. Here, we described that homozygous mutations in *EXT1/EXT2*, which are causative for osteochondroma formation, are likely to affect terminal chondrocyte differentiation and vascularisation in the osteocartilaginous interface. Contrastingly, terminal chondrocyte differentiation and vascularisation seem to be unaffected in secondary peripheral chondrosarcoma. In addition, osteochondromas with high vascular density displayed a higher proliferation rate. A similar apoptotic rate was observed in osteochondromas and secondary peripheral chondrosarcomas. Recently, it has been shown that cells with functional *EXT1* and *EXT2* are outnumbering *EXT1/EXT2* mutated cells in secondary peripheral chondrosarcomas. This might explain the increased type X collagen production and blood vessel attraction in these malignant tumours.

Keywords Growth plate · Osteochondroma · Peripheral chondrosarcoma · Type X collagen · Angiogenesis · Bone tumour

C. E. de Andrea · M. I. Wiweger · J. V. M. G. Bovée · P. C. W. Hogendoorn (✉)
Department of Pathology, Leiden University Medical Center, PO Box 9600, L1-Q, 2300 RC Leiden, The Netherlands
e-mail: P.C.W.Hogendoorn@lumc.nl

S. Romeo
Department of Pathology, Treviso Regional Hospital, Piazza dell' Ospedale 1, 31100 Treviso, Italy

Introduction

Elongation of long bones is a complex process that requires a cartilage template, known as the epiphyseal growth plate, and a strict coordination and synchronisation of cell–cell and cell–matrix signalling events [1]. The key events in this process can be divided into two major sequential morphogenesis phases. The first phase is characterised by the proliferation of the growth plate chondrocytes, which maintains the pool of cells needed for bone lengthening. The second phase is a multistep process characterised by the hypertrophy of proliferating chondrocytes and bone formation. Hypertrophic chondrocytes increase their volume and secrete a specialised extracellular matrix rich in type X collagen [2]. The ossifying collagen X-rich matrix attracts blood vessels and bone precursor cells, allowing bone development [3].

The process of endochondral ossification is also observed in cartilaginous tumours [4]. An active endochondral ossification takes place deep to the cartilage cap of osteochondroma and secondary peripheral chondrosarcoma [5].

Osteochondromas are the most common benign bone tumours at childhood and adolescence [6]. They can occur either as a sporadic lesion or multiple tumours in hereditary multiple osteochondromas syndrome (previously known as hereditary multiple exostoses) [7]. Osteochondromas are caused by mutations in either *EXT1* or *EXT2* genes [7].

They are pedunculated or sessile cartilage-capped bony projections from the metaphyses of endochondral bones adjacent to the growth plate [5]. In less than 1% of patients with sporadic osteochondromas and 1–3% of patients with multiple osteochondromas at the age of 30–60 years, an osteochondroma may eventually transform into a secondary peripheral chondrosarcoma [8].

Whereas osteochondromas have been linked to homozygous mutations in *EXT1* or *EXT2* genes, cells with functional *EXT1* and *EXT2* have been shown to be the predominant subclone in secondary peripheral chondrosarcomas [9].

Mutations in *EXT1* have been demonstrated to impair angiogenesis in mice [10] and to affect endochondral bone formation by reducing type X collagen deposition [11]. Endochondral bone formation has been shown to be affected in the homozygous *dak/ext2* zebrafish mutant [12].

EXT1 and *EXT2* genes encode enzymes that catalyse the biosynthesis of heparan sulphate. Heparan sulphate is a key component of the extracellular matrix acting as co-receptors for signalling molecules, including vascular endothelial growth factors (VEGF), fibroblast growth factors (FGF), and others [13, 14]. The impact of mutations in *EXT1* or *EXT2* genes with regards to production of a collagen X-rich matrix and attraction of blood vessels in osteochondromas and secondary peripheral chondrosarcomas has not been investigated so far.

Here, we describe that terminal chondrocyte differentiation and vascularisation are affected in osteochondromas. Contrastingly, these two critical steps of endochondral bone formation seem to be unaffected in secondary peripheral chondrosarcomas.

Materials and methods

Patient material

Paraffin-embedded tissues from 14 osteochondromas and 6 low-grade secondary peripheral chondrosarcomas from patients with multiple osteochondromas, collected between 1991 and 2008, were retrieved from the files of the Leiden University Medical Centre (Table 1). One patient had two tumours from distinct location included in this study. For comparison, paraffin-embedded epiphyseal growth plates ($n=3$) were obtained from orthopaedic resections for pathological conditions not related to osteochondroma or chondrosarcoma. Clinical information and the thickness of the cartilage cap were obtained from pathology/radiology reports. All samples were handled in a coded fashion, and all procedures were performed according to the ethical guidelines in "Code for Proper Secondary Use of Human Tissue in the Netherlands" (Dutch Federation of Medical Scientific Societies).

Immunohistochemistry

Deparaffinised sections were treated with testicular hyaluronidase (2 mg/ml in 0.1-M Tris saline, pH 5.0; Sigma-Aldrich, St Louis, MO, USA, 60 min at 37°C) and proteinase K (5 μl/ml in 0.1-M Tris-buffered saline, pH 5.0; DakoCytomation, Carpinteria, CA, USA) followed by overnight incubation at 4°C with monoclonal antibody to collagen X (clone X53, 1:100, Quartett, Berlin, Germany), as previously described [4, 15]. Monoclonal antibody to CD31 (clone JC70A, 1:10,000, DakoCytomation, Glostrup, Denmark), cleaved caspase-3 (clone 5A1E, 1:100, Cell Signaling Technology, Danvas, MA, USA), and Ki-67 (clone MIB-1, 1:100, Dako, Glostrup, Germany) were used as earlier described [16–18]. The thickness of collagen X-rich matrix was evaluated jointly by two observers (C.E.A. and S.R.). The thickest collagen X stained area was identified in each section and measured by an eye-piece graticule, as described in Fig. 1a. The apoptotic rate was defined as the number of apoptotic cells (positive for caspase-3) out of the total number of nucleated cells. The proliferation rate was determined by counting the numbers of Ki-67-positive cells.

Estimating vascular density by Chalkley counting

The Chalkley counting method has been previously described in detail [19]. Briefly, the three most vascular areas (hot spots) of each section stained with CD31 were selected and analysed (Fig. 1b). Each vascular hotspot was viewed at×200 magnification, and a 25-point Chalkley graticule was applied and oriented to permit the maximum number of points to hit in or within the CD31 stained blood vessels [19, 20]. The Chalkley count for each section was taken as the mean value of the three counts and performed by two observers independently (C.E.A. and J.V.M.G.B.).

Mutation analysis

Eleven patients were screened by direct sequencing for DNA mutations in the coding sequence of *EXT1* or *EXT2* genes [21]. After informed consent, DNA was isolated from resected tumours. If no alterations were found, a multiplex ligation-dependent probe amplification assay designed for *EXT1* and *EXT2* genes was performed to identify possible large deletions, as previously described [22]. Mutation analysis from six patients has been previously reported [15, 23, 24] (Table 1).

Statistical analysis

Results are expressed as the means with a measure of variability (standard deviation, S.D.). Statistical significance was calculated by one-way analysis of variance with

Table 1 Clinical information of patients with osteochondroma and secondary peripheral chondrosarcoma

Case #	Sample	Age (years)	Gender	Location	*EXT* mutation analysis[a] (type of mutation)	Cartilage cap thickness (mm)
L-741	GP	2	M	Femur	–	–
L-996	GP	8	M	Femur	–	–
L-1142	GP	12	F	Tibia	–	–
L-1234	GP	8	F	Femur	–	–
L-298	OC	24	M	Femur	*EXT1* exon 3: c.1121 G > A, p.W374X (ns)[b]	6
L-317	OC	31	M	Tibia	None in *EXT1* or *EXT2*[b]	4
L-332	OC	25	M	Femur	None in *EXT1* or *EXT2*[b]	5.5
L-523	OC	20	M	Tibia	*EXT1* del codon 235–239 (del Pro-Leu-Phe-Ser-Lys)[b]	5
L-524	OC	26	M	Tibia	*EXT1* codon 164 GAC > CAC (Asp > His), exon 1: c.1212 G > C, p. D164H[b]	4.5
L-722	OC	15	F	Radius	*EXT2* IVS7+1 G > A[b]	1.5
L-726	OC	6	M	Rib	*EXT2* IVS7+1 G > A	6
L-841	OC	14	F	Femur	*EXT2* deletion exon 6+7 (del)[b]	8
L-1094	OC	6	M	Femur	*EXT2* del exon 6+7	3
L-1143	OC	39	M	Femur	NA	2
L-2029	OC	23	F	Femur	*EXT2* exon 7: IVS7+1 G > A	3.5
L-2069	OC	11	M	Tibia	*EXT1* exon 1 c.538_539delAG, p.Ser180fsX7[b]	5.5
L-2160	OC	48	F	Scapula	*EXT1* exon1 c.538_539delAG, p.Ser180fsX17	6
L-2350	OC	53	F	Femur	*EXT2* exon 7: IVS7+1 G>A	1
L-951	PCH	24	M	Fibula	NA	8
L-2117	PCH	37	M	Humerus	*EXT1* exon 2: c.1056+1 G>A	12
L-114	PCH	39	M	Femur	*EXT2* exon 5: 764 T>C, L255P (uv)[b]	12
L-578	PCH	22	F	Femur	*EXT2* deletion exon 6+7 (del)	11
L-2254	PCH	33	F	Pelvis	*EXT2* exon 6 c.980delG, p.Gly327AlafsX5	8
L-2372	PCH	54	M	Rib	NA	13

GP epiphyseal growth plate, *OC* osteochondroma, *PCH* low grade secondary peripheral chondrosarcoma, *NA* not analysed

[a] Mutation nomenclature was according to the Nomenclature Working Group [30]; *ns* non-sense, *del* deletion, *uv* unclassified variant, *fs* frame shift, *pm* polymorphism

[b] Results of mutation previously reported [15, 23, 24]

Bonferroni's multiple comparison tests. Spearman's rank correlation coefficient was calculated to verify statistical dependence between two variables. Both tests were performed using the SPSS 16.0 software package (IBM, Somers, NY, USA). P values <0.05 were considered significant.

Results

Collagen X-rich matrix in peripheral cartilaginous tumours

The epiphyseal growth plate is organised in columns of stacked chondrocytes (Fig. 2a). The interface between cartilaginous and osseous parts in the growth plate (osteocartilaginous interface) was well defined and formed by hypertrophic chondrocytes immersed in a strong stained collagen X-rich matrix (Fig. 2d). In the growth plate, the collagen X-rich matrix was restricted to the hypertrophic zone and had, on average, 0.8 (± 0.47) mm thickness.

Osteochondromas showed less structured tissue organisation. The osteocartilaginous interface was also less well defined (Fig. 2b). The collagen X-rich matrix was restricted to the hypertrophic zone and had, on average, 1.5 (± 1.48) mm thickness. Additionally, in osteochondroma, not all chondrocytes with a hypertrophic morphology expressed type X collagen (Fig. 2e), and when type X collagen was present, the staining was mainly seen around the chondrocytes and not across the matrix (Fig. 2e). In osteochondromas, no correlation was found between the age of the patient and the thickness of the collagen X-rich matrix (Spearman's coefficient =0.25).

Secondary peripheral chondrosarcomas showed no structured tissue organisation (Fig. 2c) and had an average cap thickness of 10 mm. Secondary peripheral

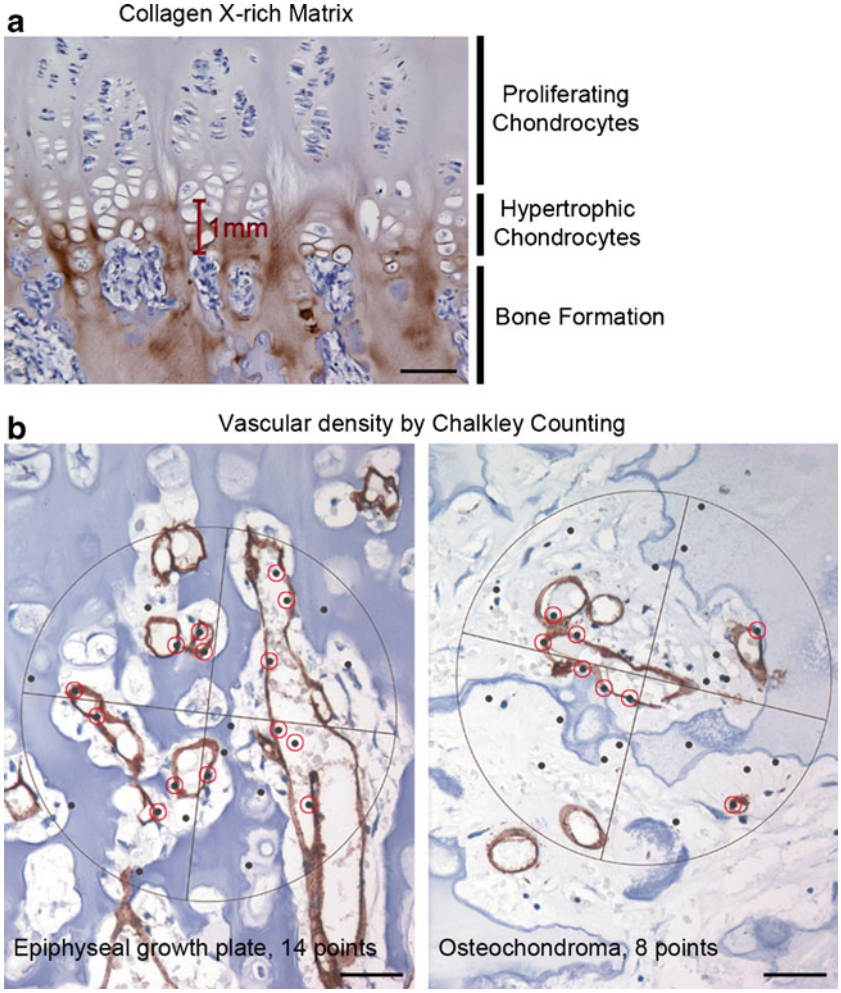

Fig. 1 Collagen X-rich matrix and vascular density by Chalkley counting. Collagen X-rich matrix produced by hypertrophic chondrocytes was measured from the beginning to the end of the hypertrophic zone (**a**). Chalkley count reflects the number of grid points that hit CD31 stained vessels (*red circles*) (**b**). It is more of an estimate of the relative area than a true vessel count (**a** *scale bar* 10 μm; **b** *scale bars* 5 μm)

chondrosarcomas showed a thick, uniformly and strongly stained collagen X-rich matrix (Fig. 2f) with an average 6.5 (± 3.66) mm thickness. Type X collagen expression in secondary peripheral chondrosarcomas was not restricted to the osteocartilaginous interface but was also detected throughout the extracellular tumour matrix and close to the perichondrium (data not shown). In secondary peripheral chondrosarcomas, no correlation was found between the age of the patient and the thickness of the collagen X-rich matrix (Spearman's coefficient =0.01).

In osteochondromas and secondary peripheral chondrosarcomas, the thickness of the collagen X-rich matrix correlated with the thickness of the cartilage cap (Spearman's coefficient =0.63) (Fig. 2g).

Similar apoptotic rates were observed in osteochondromas and secondary peripheral chondrosarcomas and had values of 35 (± 0.16) % vs. 36 (± 0.15) %, respectively (P= 0.847).

Vascular density in the ossification area

Invasion of blood vessels is a critical step towards ossification of the collagen X-rich matrix. Strong CD31 staining was observed along the cell membrane of endothelial cells in the epiphyseal growth plate, osteochondroma, and secondary peripheral chondrosarcoma. The median CD31 vascular density in the growth plate osteocartilaginous interface was significantly higher than in osteochondroma, with a value of 10.8 (± 0.83) vs. 6.1 (± 1.79), respectively (P= 0.007) (Fig. 3a, b, d). Interestingly, no differences in vascularisation of the osteocartilaginous interface were observed between the growth plate and secondary peripheral chondrosarcoma; a value of 10.8 (± 0.83) vs. 10 (± 0.70) was, respectively, found (P= 0.464) (Fig. 3a, c, d). Moreover, an irregular distribution of blood vessels was identified in the osteocartilaginous interface of osteochondromas and peripheral chondrosarcomas, but not in the epiphyseal growth plates.

In osteochondromas and secondary peripheral chondrosarcomas, no association between the age of the patient and vascular density was found (Spearman's rho correlation coefficient =0.39 and 0.27, respectively).

In osteochondromas, the proliferation rate ranged from 0–24% in 9 cases to 25–49% in 5 cases. The cases with a higher proliferation rate (25–49%) showed a higher

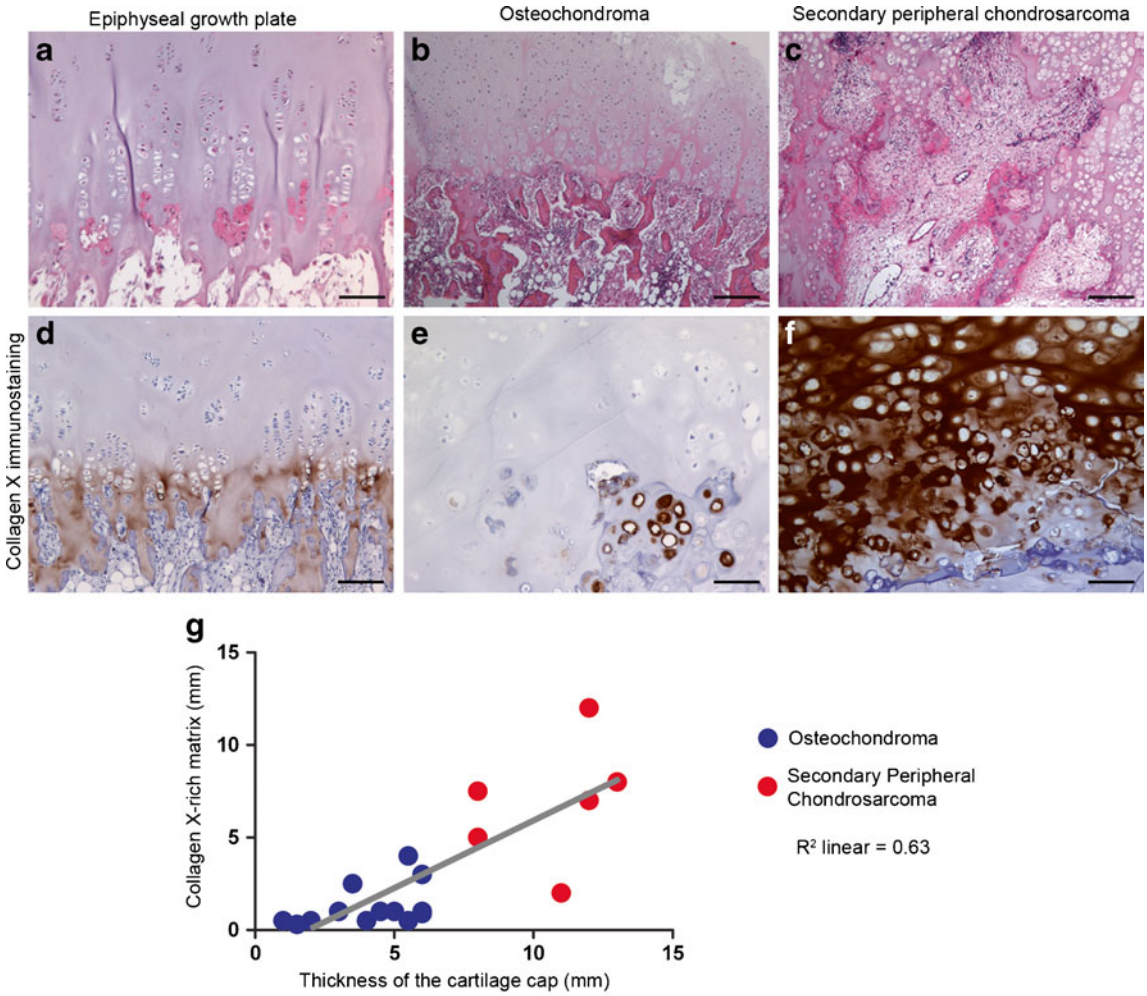

Fig. 2 Collagen X-rich matrix. The epiphyseal growth plate is organised in columns of stacked chondrocytes (**a**). Osteochondromas show less structured organisation (**b**), and secondary peripheral chondrosarcomas (**c**) display no clear organisation. Hypertrophic chondrocytes secrete a collagen X-rich matrix, which, ultimately, is replaced by bone (**d**). In osteochondromas, chondrocytes with a hypertrophic morphology are not always secreting collagen X (**e**). In secondary peripheral chondrosarcoma, a thick layer of collagen X-rich matrix is observed (**f**). In osteochondromas and secondary peripheral chondrosarcomas, the thickness of the cartilage cap correlates with the thickness of collagen X-rich matrix (**g**) (*scale bars* 10 μm)

vascular density when compared to the cases with a lower proliferation rate (0–24%); a value of 8 (± 0.83) vs. 5.2 (± 1.58) was, respectively, found ($P = 0.008$).

Mutation analysis

Fifteen of 16 patients with multiple osteochondromas demonstrated a mutation in *EXT1* or *EXT2* (Table 1). One patient, from whom two distinct tumours were studied (L-317 and L-332), displayed no mutations in *EXT1* or *EXT2*. Additionally, no correlation was found between mutation type and (a) either tumour type ($P=0.564$) (b) or the thickness of the collagen X-rich matrix ($P=0.564$) (c) or vascular density ($P=0.556$).

Discussion

In this study, two crucial steps of endochondral ossification, formation of a collagen X-rich matrix and invasion/attraction of blood vessels, were assessed and compared in the epiphyseal growth plate and peripheral cartilaginous tumours (osteochondroma and secondary peripheral chondrosarcoma). The protein expression level of type X collagen in human osteochondroma was shown to be similar to the one found in human epiphyseal growth plate [4]. Interestingly, in the *EXT1* heterozygous mutant mice, in situ hybridisation studies have demonstrated that the mRNA expression of type X collagen is reduced in the growth plate as compared to wild-type mice [11, 25]. In

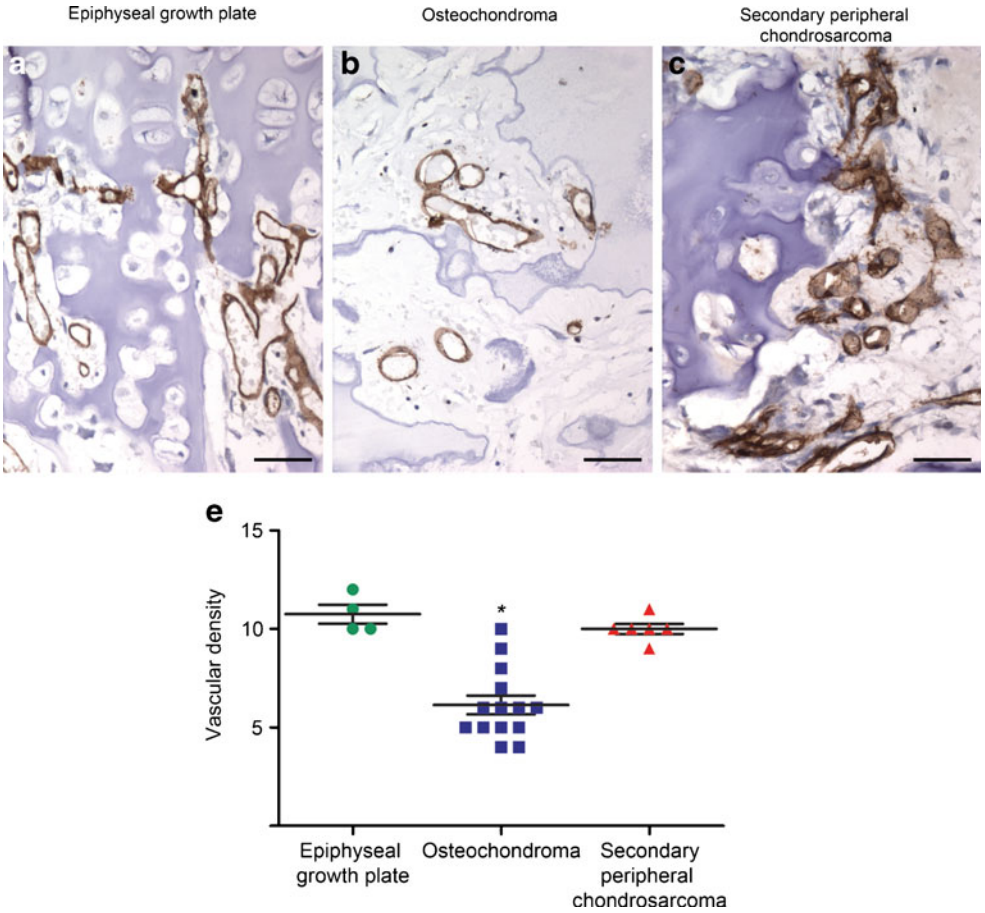

Fig. 3 Vascular density in the ossification zone. The epiphyseal growth plate (**a**, **d**) and secondary peripheral chondrosarcoma (**c**, **d**) show similar vascular density. Osteochondroma displays low vascular density (**b**, **d**) (*asterisk* indicates $P<0.05$; *scale bars* 5 μm)

addition, endochondral bone formation has been shown to be affected in the homozygous *dak/ext2* zebrafish mutant [12]. The reduced type X collagen expression in the *EXT1* mutant mice and the delay in endochondral ossification in the homozygous *dak/ext2* zebrafish mutant suggest that *EXT1* and *EXT2* genes play a role in terminal chondrocyte differentiation and the replacement of hypertrophic chondrocytes by bone.

Here, we describe that not all of the osteochondroma cells undergo terminal differentiation. These cells, although displaying a hypertrophic phenotype, do not express type X collagen (Fig. 2e). This may suggest that mutations in *EXT1* or *EXT2* genes may affect terminal chondrocyte differentiation in humans. Interestingly, progression of osteochondroma towards secondary peripheral chondrosarcoma showed an increased production of type X collagen. Therefore, the secondary peripheral chondrosarcoma cells expressing abundant type X collagen indicated that they have undergone terminal chondrocyte differentiation.

Osteochondromas and secondary peripheral chondrosarcoma had a similar apoptotic rate. This indicates that, although secondary peripheral chondrosarcoma cells undergo terminal differentiation, the differentiation process does not induce apoptosis. Hence, low cell death seems to contribute to the relatively rapid growth of peripheral chondrosarcoma.

Several pro-angiogenic growth factors, such as FGF-2 and VEGFs, bind to heparan sulphate proteoglycans [26]. Heparan sulphate proteoglycans have been shown to regulate the distribution of these signalling molecules throughout the extracellular matrix and their receptor binding affinity [27]. Syndecan-2 is a cell surface heparan sulphate proteoglycan [26]. Syndecan-2 has been demonstrated to bind to VEGF, thereby regulating the distribution of VEGF nearby its receptor [28]. Interestingly, in osteochondromas, syndecan-2 is no longer located in the plasma membrane, but is shown to be accumulated in the Golgi apparatus [24]. The abnormal intracellular location of syndecan-2 may affect the distribution of VEGF, explaining the low efficiency of the osteochondroma cells in attracting blood vessels. Osteochondromas with high vascular density in the osteocartilaginous interface displayed a higher proliferation rate. This might suggest that proliferation of tumour cells is associated with increased vascularisation in the osteocartilaginous interface. Interestingly, secondary peripheral chondrosarcomas showed

similar efficiency in attracting blood vessels as the epiphyseal growth plate.

We have recently shown that cells with functional *EXT1* and *EXT2* genes are the predominant subclone in secondary peripheral chondrosarcomas [9]. Therefore, the increased type X collagen deposition and blood vessel attraction in the osteocartilaginous interface of secondary peripheral chondrosarcoma are possibly associated with cells with functional *EXT1* and *EXT2* genes. In addition, collagen X-rich matrix formation and vascularisation might be useful prognostic markers of neoplastic transformation of an osteochondroma, but further validation is required before they can be proposed as a routine and as a reliable diagnostic tool.

In conclusion, we show that terminal chondrocyte differentiation and vascularisation are affected in osteochondromas, suggesting that *EXT1* and *EXT2* genes are critical for endochondral bone formation. Terminal chondrocyte differentiation and vascularisation seem to be unaffected in secondary peripheral chondrosarcomas, which might be associated with the presence of cells with functional *EXT1* and *EXT2* genes.

Acknowledgments This work was supported by the European network of excellence EuroBoNeT (http://www.eurobonet.eu) grant number 018814 (LSHC-CT-2006-018814).

Conflict of interest The authors declare that they have no conflict of interest.

Open Access This article is distributed under the terms of the Creative Commons Attribution Noncommercial License which permits any noncommercial use, distribution, and reproduction in any medium, provided the original author(s) and source are credited.

References

1. Kronenberg HM (2003) Developmental regulation of the growth plate. Nature 423:332–336
2. Kuhn JL, DeLacey JH, Leenellett EE (1996) Relationship between bone growth rate and hypertrophic chondrocyte volume in New Zealand white rabbits of varying ages. J Orthop Res 14:706–711
3. Ballock RT, O'Keefe RJ (2003) The biology of the growth plate. J Bone Joint Surg Am 85-A:715–726
4. Aigner T, Frischolz S, Dertinger S, Beier F, Girkontaité I, Von der Mark K (1997) Type X collagen expression and hypertrophic differentiation in chondrogenic neoplasias. Histochem Cell Biol 107:435–440
5. Khurana J, Abdul-Karim F (2002) Bovée JVMG Osteochondroma. In: Fletcher CDM, Unni KK, Mertens F (eds) World Health Organization classification of tumours. Pathology and genetics of tumours of soft tissue and bone. IARC Press, Lyon (France), pp 234–236
6. van den Berg H, Kroon HM, Slaar A, Hogendoorn P (2008) Incidence of biopsy-proven bone tumors in children: a report based on the Dutch pathology registration "PALGA". J Pediatr Orthop 28(1):29–35
7. Bovee JVMG, Hogendoorn PCW, Wunder JS, Alman BA (2010) Cartilage tumours and bone development: molecular pathology and possible therapeutic targets. Nat Rev Cancer 10:481–488
8. Dorfman HD, Czerniak B, Kotz R, Vanel D, Park YK, Unni KK (2002) WHO classification of tumours of bone: introduction. In: Fletcher CDM, Unni KK, Mertens F (eds) World Health Organization classification of tumours. Pathology and genetics of tumours of soft tissue and bone. IARC Press, Lyon, pp 226–232
9. de Andrea CE, Reijnders CM, Kroon HM, de Jong D, Hogendoorn PC, Szuhai K et al (2011) Secondary peripheral chondrosarcoma evolving from osteochondroma as a result of outgrowth of cells with functional EXT. Oncogene. doi:10.1038/onc.2011.311
10. Kucharzewska P, Welch JE, Birgersson J, Belting M (2010) Establishment of heparan sulphate deficient primary endothelial cells from EXT-1(flox/flox) mouse lungs and sprouting aortas. In Vitro Cell Dev Biol Anim 46:577–584
11. Hilton MJ, Gutierrez L, Martinez DA, Wells DE (2005) *EXT1* regulates chondrocyte proliferation and differentiation during endochondral bone development. Bone 36:379–386
12. Wiweger MI, Avramut CM, de Andrea CE, Prins FA, Koster AJ, Ravelli RB et al (2011) Cartilage ultrastructure in proteoglycan-deficient zebrafish mutants brings to light new candidate genes for human skeletal disorders. J Pathol 223:531–542
13. Hufnagel L, Kreuger J, Cohen SM, Shraiman BI (2006) On the role of glypicans in the process of morphogen gradient formation. Dev Biol 300:512–522
14. Hacker U, Nybakken K, Perrimon N (2005) Heparan sulphate proteoglycans: the sweet side of development. Nat Rev Mol Cell Biol 6:530–541
15. Reijnders CM, Waaijer CJ, Hamilton A, Buddingh' EP, Dijkstra SP, Ham J et al (2010) No haploinsufficiency but loss of heterozygosity for EXT in multiple osteochondromas. Am J Pathol 177:1946–1957
16. Verbeke SL, Fletcher CD, Alberghini M, Daugaard S, Flanagan AM, Parratt T et al (2010) A reappraisal of hemangiopericytoma of bone; analysis of cases reclassified as synovial sarcoma and solitary fibrous tumor of bone. Am J Surg Pathol 34:777–783
17. Schrage YM, Machado I, Meijer D, Briaire-de Bruijn I, van den Akker B, Taminiau AHM et al (2010) COX-2 expression in chondrosarcoma: a role for celecoxib treatment? Eur J Cancer 46:616–624
18. de Andrea CE, Wiweger M, Prins F, Bovee JVMG, Romeo S, Hogendoorn PCW (2010) Primary cilia organization reflects polarity in the growth plate and implies loss of polarity and mosaicism in osteochondroma. Lab Invest 90:1091–1101
19. Vermeulen PB, Gasparini G, Fox SB, Toi M, Martin L, McCulloch P et al (1996) Quantification of angiogenesis in solid human tumours: an international consensus on the methodology and criteria of evaluation. Eur J Cancer 32A:2474–2484
20. Hansen S, Grabau DA, Sorensen FB, Bak M, Vach W, Rose C (2000) The prognostic value of angiogenesis by Chalkley counting in a confirmatory study design on 836 breast cancer patients. Clin Cancer Res 6:139–146
21. Vink GR, White SJ, Gabelic S, Hogendoorn PCW, Breuning MH, Bakker E (2004) Mutation screening of *EXT1* and *EXT2* by direct sequence analysis and MLPA in patients with multiple osteochondromas: splice site mutations and exonic deletions account for more than half of the mutations. Eur J Hum Genet 13:470–474

22. White SJ, Vink GR, Kriek M, Wuyts W, Schouten J, Bakker B et al (2004) Two-color multiplex ligation-dependent probe amplification: detecting genomic rearrangements in hereditary multiple exostoses. Hum Mutat 24:86–92
23. Bovee JVMG, Cleton-Jansen AM, Wuyts W, Caethoven G, Taminiau AHM, Bakker E et al (1999) EXT-mutation analysis and loss of heterozygosity in sporadic and hereditary osteochondromas and secondary chondrosarcomas. Am J Hum Genet 65:689–698
24. Hameetman L, David G, Yavas A, White SJ, Taminiau AHM, Cleton-Jansen AM et al (2007) Decreased EXT expression and intracellular accumulation of HSPG in osteochondromas and peripheral chondrosarcomas. J Pathol 211:399–409
25. Koziel L, Kunath M, Kelly OG, Vortkamp A (2004) *EXT1*-dependent heparan sulfate regulates the range of Ihh signaling during endochondral ossification. Dev Cell 6:801–813
26. Iozzo RV (2001) Heparan sulfate proteoglycans: intricate molecules with intriguing functions. J Clin Invest 108:165–167
27. Bernfield M, Gotte M, Park PW, Reizes O, Fitzgerald ML, Lincecum J et al (1999) Functions of cell surface heparan sulfate proteoglycans. Annu Rev Biochem 68:729–777
28. Chen E, Hermanson S, Ekker SC (2004) Syndecan-2 is essential for angiogenic sprouting during zebrafish development. Blood 103:1710–1719

Virchows Arch (2012) 460:103–108
DOI 10.1007/s00428-011-1172-0

ORIGINAL ARTICLE

Fatty lesions in intra-articular loose bodies: a histopathological study of non-primary synovial chondromatosis cases

Susumu Matsukuma · Hiroaki Takeo · Kenji Okada · Kimiya Sato

Received: 17 September 2011 / Accepted: 4 November 2011 / Published online: 18 November 2011
© Springer-Verlag 2011

Abstract Intra-articular loose bodies (ILBs) are not uncommon conditions in patients with various joint diseases. Their morphological alterations have been investigated in detail, but little attention has been paid to their fatty lesions. In this study, we examined fatty bone marrow, fat cells without bone marrow structures (extramedullary fat cells), and their necrotic changes in 55 ILBs surgically removed from 42 patients, excluding primary synovial chondromatosis cases. The presence of viable re-vascularized vessels with or without enchondral ossification could discriminate 19 re-attached ILBs from 36 true free ILBs. Fatty bone marrow was found in 25 ILBs, and its necrosis was recognized in 11 (44.0%) of them. Extramedullary fat cells, characterized by single or clustered fat cells focally or multifocally distributed in fibrous or cartilaginous stroma, were identified in seven true free ILBs (7of 55, 12.7%), and all of them were focally necrotic. Unique lipomembranous changes were detected in 7 (12.7%) of 55 ILBs; they were found in 4 (36.4%) of 11 ILBs of necrotic bone marrow and were associated with 3 (42.9%) of 7 necrotic extramedullary fatty lesions. These changes were highlighted by periodic-acid Schiff and Masson's trichrome stain more clearly. We concluded that extramedullary fat cells represent lipometaplasia in ILBs with no blood supply. We considered that lipomembranous changes in ILBs can be a useful hallmark for necrotic bone marrow or necrosis of extramedullary lipometaplastic lesions.

S. Matsukuma (✉) · H. Takeo · K. Okada · K. Sato
Department of Pathology,
Japan Self-Defense Forces Central Hospital,
Ikejiri 1-2-24, Setagaya-ku,
Tokyo 154-0001, Japan
e-mail: skuma@cocoa.plala.or.jp

Keywords Intra-articular loose body · Lipometaplasia · Lipomembranous change · Fat cell · Lipodystrophy · Bone marrow

Introduction

Intra-articular loose bodies (ILBs) are not uncommon findings in patients with various types of underlying arthritis or joint diseases, including osteochondritis dissecans, traumatic osteochondral fracture, primary synovial chondromatosis, osteoarthrosis, and primary epiphyseal osteonecrosis [1–7]. Many researchers have described metaplastic, proliferative, and degenerative changes in ILBs, such as the formation of cartilaginous and/or osseous lamellae, resorptive changes of mineralized tissues, and enchondral ossification [2–13]. Our recent examination of ILBs incidentally found focal fat cells with lipomembranous changes, which are known to be a unique form of fat necrosis [14, 15]. We speculated that these fatty lesions may represent remnants of necrotic bone marrow, but they were not accompanied by bone marrow structures. To date, such fatty lesions have been poorly investigated in ILBs [16]. There have been no articles clearly describing lipometaplasia in ILBs, although secondary enchondral ossification induces fatty bone marrow [4, 13]. In this study, we examined fat cells with bone marrow structures (fatty bone marrow), fat cells without bone marrow structures (extramedullary fat cells), and their necrotic changes in ILBs, and attempted to delineate their histopathological characteristics. Primary synovial chondromatosis is a distinct cause of ILBs [3, 4, 7, 12]. However, this disease is characterized by lobular or clustered growth of metaplastic cartilage in the synovium [3, 5–7, 12, 17], and the possible contamination of synovium-derived fat cells in

ILBs cannot be ruled out. Therefore, this study avoided cases of primary synovial chondromatosis.

Materials and methods

The surgical pathology files of the Department of Pathology, Japan Self-Defense Forces Central Hospital (from September 1978 to May 2011), were searched for cases of surgically removed ILBs excluding cases of primary synovial chondromatosis. A total of 55 ILBs from 42 patients (41 males and 1 female), with a mean age of 31.3 years (range, 16–54 years), were examined. Thirty-seven ILBs were removed from 29 knee joints, 15 ILBs were removed from 10 elbow joints, 2 ILBs were removed from 2 ankle joints, and 1 ILB was removed from a shoulder joint. Clinical information was obtained from the request forms of pathologic examination and/or the patients' medical records. All specimens were fixed in 10% buffered formalin, and 44 calcified and/or ossified specimens were decalcified using formic acid. They were additionally cut and stained with hematoxylin and eosin (H&E). Selected sections were stained with periodic acid–Schiff (PAS) and Masson's trichrome and were immunostained using antibodies against alpha-smooth muscle actin (ASMA; 1A4, Nichirei Corp., Tokyo, Japan), CD34 (QBEnd10, Dako, Glostrup, Denmark), and S-100 protein (Nichirei). Re-attachment of ILBs is known to occur and induce re-vascularization and enchondral ossification [4, 13]. Therefore, on the basis of the presence of these features, ILBs were divided into true free ILBs and re-attached ILBs. “Fat cell necrosis” or “necrotic changes of fat cells,” rather than lipomembranous changes, were assessed by disappearing nuclei of fat cells.

Results

The histopathological findings of ILBs are summarized in Table 1. Fifty-five ILBs were classified into 14 cartilaginous bodies composed of articular cartilage, 38 osteocartilaginous bodies containing both osseous and articular or metaplastic cartilaginous components, and 3 osseous bodies containing mature bones. They were divided into 19 re-attached ILBs and 36 true free ILBs. Re-vascularized vessels in 19 re-attached ILBs showed focal co-immunoreactivity of ASMA and CD34. One true free ILB, which was composed of mature bone and fatty bone marrow, focally contained re-vascularized vessels. However, these vessels were completely occlusive and were immunohistochemically positive for ASMA but negative for CD34. We interpreted this body as re-detached free ILB that had been previously attached to the synovium and enchondrally ossified.

Fatty bone marrow and extramedullary fat cells were found in 25 ILBs and 7 ILBs, respectively. Eleven (44.0%) of 25 ILBs of fatty bone marrow were totally or partially necrotic (Fig. 1). One re-detached free ILB also demonstrated focal necrotic changes of bone marrow. All extramedullary fatty lesions were focally necrotic. Lipomembranous changes were identified in 7 (12.7%) of 55 ILBs; 4 were found in necrotic bone marrow lesions (Fig. 1b), and 3 were associated with extramedullary fat cells (Figs. 2b and 3c). Focal lipomembranous changes were difficult to recognize on H&E-stained sections alone, but they were highlighted by Masson's trichrome stain (Fig. 1c) and PAS (Fig. 2c) more clearly. Extramedullary fat cells and lipomembranous changes were found only in true free bodies. In addition, we focally identified necrotic trabecular-like bones that were embedded in or surrounded by metaplastic cartilaginous tissues (Fig. 3b).

Table 1 Histopathological features of 55 intra-articular loose bodies

	Total (n=55)	True free bodies (n=36)	Re-attached bodies (n=19)
Cartilaginous/osteocartilaginous/osseous bodies	14/38/3	14/22/0	0/16/3
The formation of cartilaginous lamellae	30 (54.5%)	20 (55.6%)	10 (52.6%)
The formation of osseous lamellae	26 (47.3%)	19 (52.8%)	7 (36.8%)
Resorptive changes of mineralized tissues	15 (27.3%)	13 (36.1%)	2 (10.5%)
Active enchondral ossification	11 (20.0%)	0 (0%)	11 (57.9%)
Fatty bone marrow	25 (45.5%)	7 (19.4%)	18 (94.7%)
Bone marrow necrosis	11 (20.0%)	7 (19.4%)	4 (21.1%)
Lipomembranous changes of bone marrow	4 (7.2%)	4 (11.1%)	0 (0%)
Extramedullary fat cells	7 (12.7%)	7 (19.4%)	0 (0%)
Fat cell necrosis of extramedullary fat cells	7 (12.7%)	7 (19.4%)	0 (0%)
Lipomembranous changes of extramedullary fat cells	3 (5.5%)	3 (8.3%)	0 (0%)
Marrow-like necrotic bones	3 (5.5%)	2 (5.6%)	1 (5.3%)
Lipomembranous changes (total)	7 (12.7%)	7 (19.4%)	0 (0%)

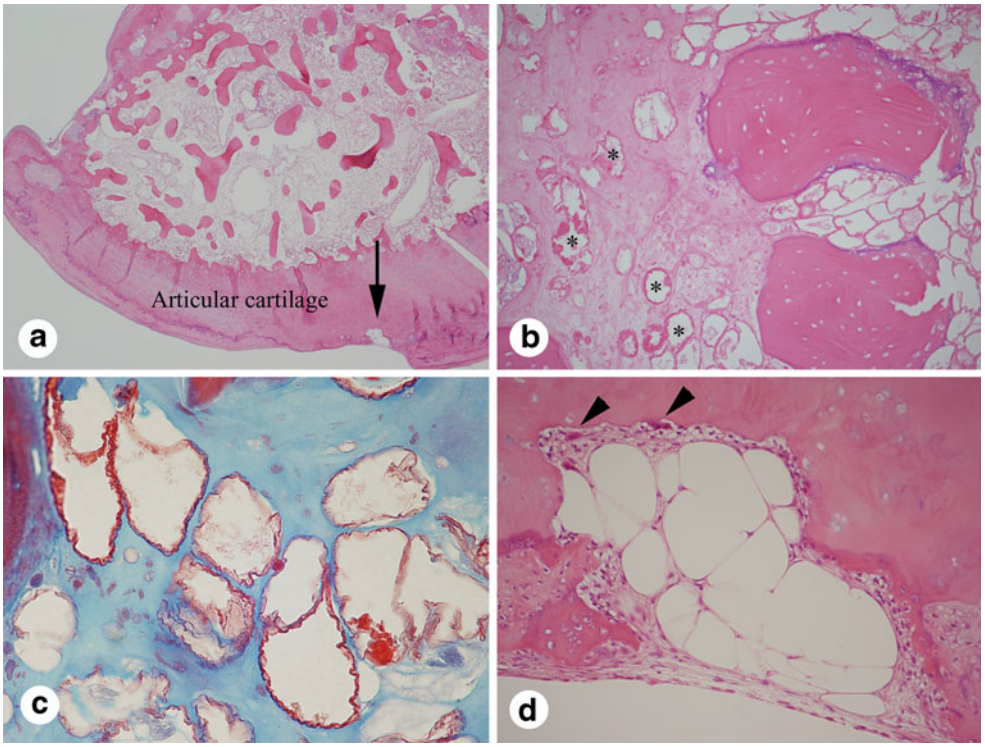

Fig. 1 Intra-articular loose body containing necrotic bone marrow (body no. 2). **a** Low-power view showing totally necrotic bone marrow attached to articular cartilage in the *central portion* and extramedullary fat cells in the *peripheral portion* (*arrow*), which is distinctly distant from bone marrow (H&E, ×20). **b** Necrotic bones and bone marrow showing fat cell necrosis and lipomembranous changes (*asterisks*) (H&E, ×200). **c** Masson's trichrome stain highlighting lipomembranous changes in necrotic bone marrow (×600). **d** Extramedullary fat cells in peripheral resorptive stroma with osteoclasts (*arrowheads*) (H&E, ×300)

These lesions were termed "marrow-like necrotic bones" and were found in three ILBs (3 of 55, 5.5%). Articular cartilage was unclear in one of them, and tidemarks between the necrotic bones and the attached articular cartilage were inconspicuous in the other two. Hence, the assessment of these lesions could not rule out possible non-specific necrosis of metaplastic osseous fragments.

Clinicopathological features of seven ILBs containing extramedullary fat cells are summarized in Table 2. All of these ILBs had articular cartilaginous components. Extramedullary fat cells, singly or in clusters, were focally or multifocally distributed in fibrous or cartilaginous tissues involving the peripheral/surface portions of six ILBs and the central to peripheral portion of one ILB. They were frequently associated with resorptive changes with or without osteoclasts (Figs. 1d and 2b). In one ILB (body no. 6), fat cells and immature lipocyte-like microvacuolated cells were observed (Fig. 3d, e). Necrotic bone marrow or marrow-like necrotic bones were also present in two ILBs, but extramedullary fat cells were detected distinctly distant from these lesions (Figs. 1a and 3a). Weak positive immunostaining for S-100 protein was recognized in extramedullary viable fat cells of three ILBs (bodies no.1, 6, and 7).

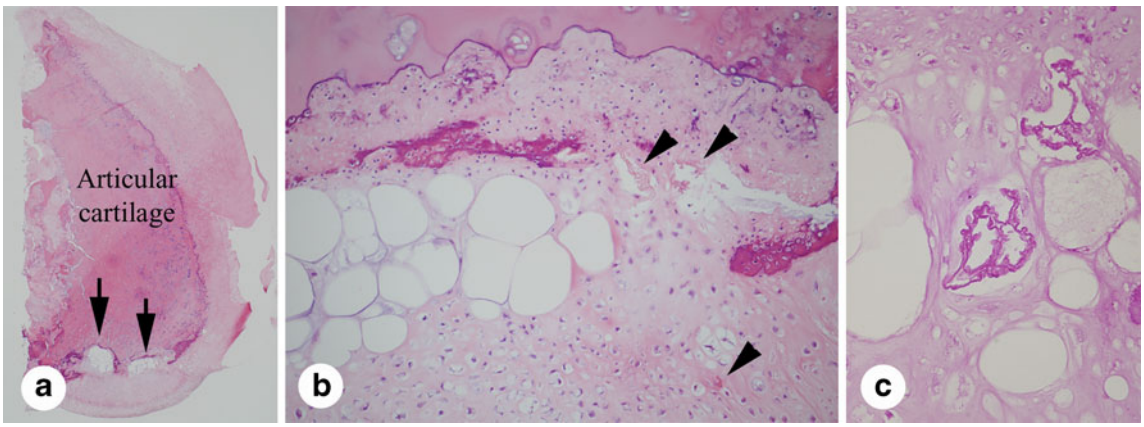

Fig. 2 Intra-articular loose body with extramedullary fat cells (body no. 4). **a** Low-power view showing articular cartilage, scattered osseous lamination, and fat cells with no structure of bone marrow (*arrows*) (H&E, ×20). **b** Extramedullary fat cells and lipomembranous changes (*arrowheads*) in resorptive stroma (H&E, ×200). **c** PAS stain highlighting scattered lipomembranous changes near extramedullary fat cells (×400)

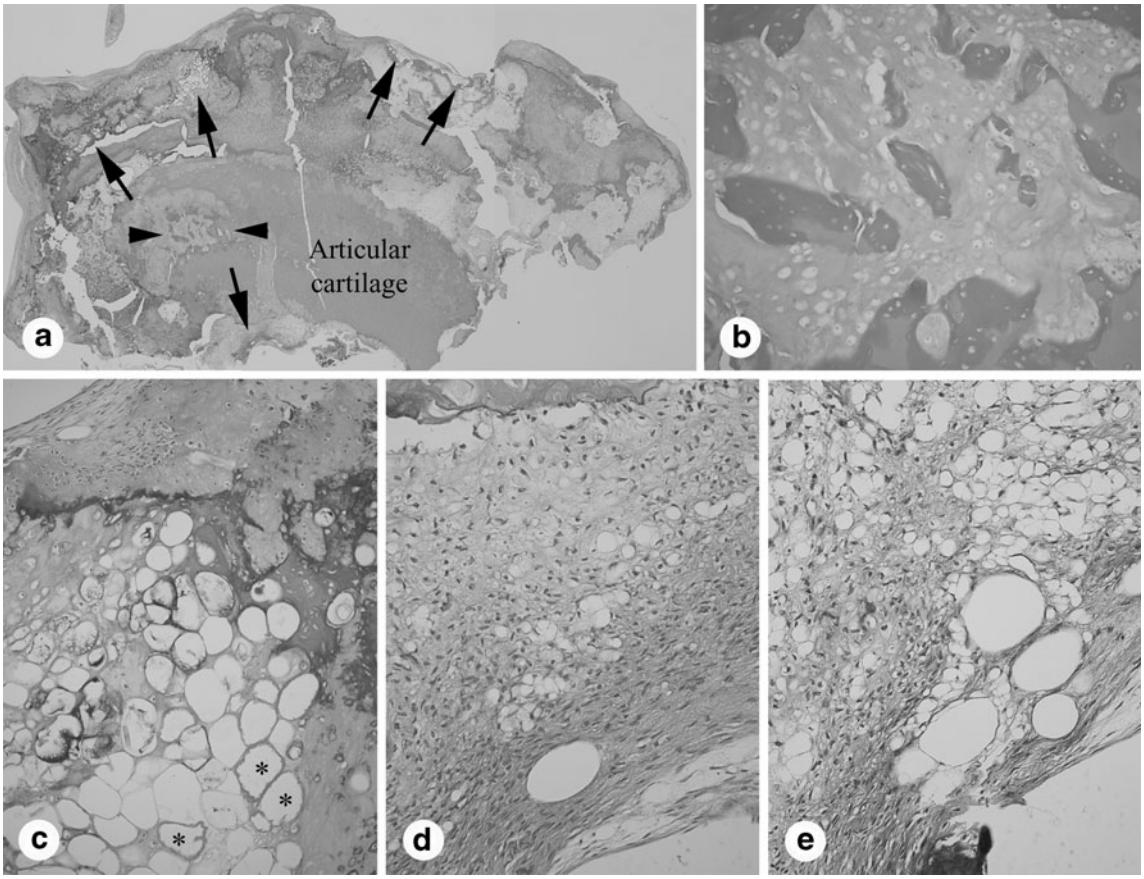

Fig. 3 Intra-articular loose body with marrow-like necrotic bones and extramedullary fat cells (body no. 6). **a** Low-power view showing articular cartilage, marrow-like necrotic bones (*arrowheads*), and multifocal fat cells with no bone marrow structures (*arrows*) (H&E, ×20). **b** Marrow-like necrotic bones embedded in metaplastic cartilaginous tissues with no convincing features of fat cell necrosis, lipomembranous changes, or tidemark (H&E, ×200). **c** Extramedullary fat cell necrosis and lipomembranous changes (*asterisks*) in the *upper peripheral portion* of the low-power view (H&E, ×100). **d** Extramedullary mature fat cells and microvacuolated cells in the *lower peripheral portion* of the low-power view (H&E, ×400). **e** The serial section showing immature lipocyte-like microvacuolated cells in fibrous stroma more clearly (Masson's trichrome stain, ×400)

Table 2 Clinicopathological features of seven intra-articular loose bodies with extramedullary fat cells

Body no.	Age (years)	Sex	Site of joint	Size (cm)	Necrotic bone marrow	Marrow-like necrotic bones	Histopathological findings of extramedullary fat cells				
							Distribution	Location	Associated resorptive changes	Necrotic changes[b]	Lipomembranous changes
1	23	M	Elbow	1.2	None	None	Multifocal	Peripheral	Present	Present	None
2	46	M	Elbow	1.6	Present[a]	None	Focal	Peripheral	Present	Present	None
3	28	M	Knee	1.3	None	None	Focal	Peripheral	Present	Present	None
4	36	M	Knee	0.8	None	None	Multifocal	Peripheral	Present	Present	Present
5	54	F	Knee	0.9	None	None	Multifocal	Central to peripheral	Present	Present	Present
6	49	M	Elbow	1.3	Unclear	Present[a]	Multifocal	Peripheral	Present	Present	Present
7	50	M	Elbow	2.0	None	None	Focal	Peripheral	Present	Present	None

F female, *M* male

[a] Lipomembranous changes were not found

[b] Assessed by fat cells with disappearing nuclei rather than lipomembranous changes

Discussion

This study revealed extramedullary fat cells in 7 (12.7%) of 55 ILBs, characterized by single or clustered fat cells in fibrous or cartilaginous tissues with no distinct features of bone marrow. Total absorption of necrotic bones could develop in re-vascularized condition [3, 6, 10, 13], and we initially speculated that this could involve remnants of fatty bone marrow. However, all seven ILBs with extramedullary fat cells were true free bodies without blood supply, and total absorption of marrow bones seems less likely. In two ILBs, necrotic bone marrow or marrow-like necrotic bones were present, but fat cells were distinctly distant from these structures. In addition, the multifocal distribution of fat cells could not be explained by the remnants of bone marrow alone. These findings suggested that extramedullary fat cells represent lipometaplasia in ILBs without blood supply. To our knowledge, such fatty lesions have not been described in previous articles clearly. Only Strangeways [16] mentioned the presence of fat cell-like structures in resorptive stroma, and the illustrated features in this article somewhat resemble immature lipocyte-like microvacuolated features in our study. Moreover, our study revealed extramedullary lipometaplasia in 7 (19.4%) of 36 true free ILBs. Except for one re-detached enchondrally ossified ILB, lipometaplasia was identified in 7 (20.0%) of 35 true free bodies with no re-vascularized vessels. These fat cells were focally or totally necrotic, which may indicate the vulnerability of fat cells. However, diversely, viable and S-100 protein-positive metaplastic fat cells were identified in three true free ILBs. These findings suggest that metaplastic fat cells can survive directly or indirectly by nourishment from synovial fluid.

Lipometaplasia, adipocytic metaplasia, or fatty infiltration is not uncommon in other tissues and could arise from pluripotent mesenchymal cells or ASMA-positive pericytes adjacent to blood vessels [18, 19]. In this study, however, no ILBs with extramedullary lipometaplasia had ASMA-positive vessels, and the vessel-dependent lipocytic origin is difficult to be considered. These findings resembled the uncertain source of osteoblasts and osteoclasts in ossified ILBs without blood supply [4]. Migram [4] described that these osteoblasts and osteoclasts are probably derived from the synovial membrane as free cells in synovial spaces, and there may be a similar origin of metaplastic fat cells. On the other hand, some experimental studies [20, 21] have shown the lipogenetic differentiation in cell cultures of human articular cartilage and have indicated the presence of mesenchymal progenitor cells in articular cartilage [20] or a multipotent population of dedifferentiated articular chondrocytes themselves [21]. In our study, all ILBs with extramedullary lipometaplasia possessed detached articular cartilage. Metaplastic fat cells were always identified in fibrous or cartilaginous stroma. These findings suggest that progenitor cells derived from articular cartilage, dedifferentiated chondrocytes, or other stromal cells transform into fat cells. Unfortunately, this study revealed no convincing features of such transformation, and further studies are necessary to elucidate these pathogeneses.

Lipomembranous changes, also called membranocystic changes [22], lipodystrophy-like changes [22, 23], or membranous fat necrosis [15], are characterized by convoluted microcystic changes lined by PAS-positive membranous structures having fine, feathery projections [14, 15, 22–24]. They are stained red with Masson's trichrome or Azan-Mallory stain and blue with Luxol fast blue [15, 23, 24]. They were first mentioned in a rare lipid metabolic disease [24], but are currently considered a form of fat necrosis frequently found in ischemic conditions [14, 23]. Lipomembranous changes have been noted in bone marrow affected by membranous dystrophy [24] and in avascular bone necrosis [2], but such changes have not been described in ILBs. The current study identified lipomembranous changes in 36.4% (4 of 11) of ILBs of necrotic bone marrow and 42.9% (3 of 7) of necrotic extramedullary lipometaplasia. These incidences appear to be similar to that (38%) of lipomembranous changes in subcutaneous fat affected by thromboangiitis obliterans [23]. In the current study, lipomembranous changes were singly recognizable in fibrous or cartilaginous tissues on decalcified sections and were highlighted by PAS and Masson's trichrome stain more clearly. These findings suggest that lipomembranous changes in ILBs can be a useful hallmark for bone marrow necrosis or necrosis of lipometaplastic fat cells.

Various non-specific morphological alterations can occur in ILBs and progressively modify the initial features, leading to difficulty in assessing the source of ILBs [2–4, 6–13]. Previous articles have emphasized the usefulness of histopathological examination of ILBs and have proposed some histological markers for evaluating their sources or origins [3, 4, 7, 13]. Bone marrow necrosis is considered a useful marker for primary necrosis of subchondral bone or de-vascularized necrosis of detached bone; the former represents primary osteonecrosis or osteochondritis dissecans [1, 2, 4, 6], and the latter is possibly associated with traumatic fracture or osteoarthrosis [2, 6]. Re-detached enchondrally ossified bodies would demonstrate similar non-specific necrosis of bone marrow, and such features were confirmed in this study. Lipomembranous changes are a useful hallmark for necrotic bone marrow, but the possibility of necrotic extramedullary lipometaplasia should be ruled out.

Thus, this study revealed that extramedullary lipometaplasia occurs occasionally in true free ILBs. Metaplastic fat cells can survive in synovial fluid. Moreover, this study detected unique lipomembranous changes in 7 (12.7%) of 55 ILBs examined. Lipomembranous changes are considered

a distinctive hallmark for bone marrow necrosis or necrotic lipometaplastic lesions.

Conflict of interest We declare that we have no conflict of interest.

References

1. Aurich M, Anders J, Trommer T et al (2006) Histological and cell biological characterization of dissected cartilage fragments in human osteochondritis dissecans of the femoral condyle. Arch Orthop Trauma Surg 126:606–614
2. Ishida T, Imamura T (2003) Surgical pathology of non-neoplastic bone and joint diseases. Bunkoudo, Tokyo, In Japanese
3. Milgram JW (1977) The classification of loose bodies in human joints. Clin Orthop Relat Res 124:282–291
4. Milgram JW (1990) Radiologic and histologic pathology of nontumorous diseases of bones and joints. Northbook Publishing Company, Northbook
5. O'Connell JX (2000) Pathology of the synovium. Am J Clin Pathol 114:773–784
6. Phemister DB (1924) The causes of and changes in loose bodies arising from the articular surface of the joint. J Bone Joint Surg 6:278–315
7. Villacin AB, Brigham LN, Bullough PG (1979) Primary and secondary synovial chondrometaplasia: histopathologic and clinicoradiologic differences. Hum Pathol 10:439–451
8. Barrie HJ (1978) Intra-articular loose bodies regarded as organ cultures in vivo. J Pathol 125:163–169
9. Barrie HJ (1980) Hypertrophy and laminar calcification of cartilage in loose bodies as probable evidence of an ossification abnormality. J Pathol 132:161–168
10. Milgram JW (1977) The development of loose bodies in human joints. Clin Orthop Relat Res 124:292–303
11. Milgram JW, Gilden JJ, Gilula LA (1996) Multiple loose bodies: formation, revascularization, and resorption. A 29-year followup study. Clin Orthop Relat Res 322:152–157
12. Saotome K, Tamai K, Koguchi Y, Sakai H, Yamaguchi T (1999) Growth potential of loose bodies: an immunohistochemical examination of primary and secondary synovial osteochondromatosis. J Orthop Res 17:73–79
13. Saotome K, Tamai K, Osada D, Oshima F, Koguchi Y, Hoshikawa A (2006) Histologic classification of loose bodies in osteoarthrosis. J Orthop Sci 11:607–613
14. McNutt NS, Moreno A, Contreras F (2005) Inflammatory diseases of the subcutaneous fat. In: Elder DE, Elenitsas R, Johnson BL Jr, Murphy GF (eds) Lever's histopathology of the skin, 9th edn. Lippincott Williams & Wilkins, Philadelphia, pp 519–549
15. Poppiti RJ Jr, Margulies M, Cabello B, Rywlin AM (1986) Membranous fat necrosis. Am J Surg Pathol 10:62–69
16. Strangeways TSP (1920) Observations on the nutrition of articular cartilage. Brit Med J 1:661–663
17. Davis RI, Hamilton A, Biggart JD (1998) Primary synovial chondromatosis: a clinicopathologic review and assessment of malignant potential. Hum Pathol 29:683–688
18. Brooks JSJ, Perosio PM (1997) Adipose tissue. In: Sternberg SS (ed) Histology for pathologist, 2nd edn. Lippincott-Raven, Philadelphia, pp 167–196
19. Farrington-Rock C, Crofts NJ, Doherty MJ, Ashton BA, Griffin-Jones C, Canfield AE (2003) Chondrogenic and adipogenic potential of microvascular pericytes. Circulation 110:2226–2232
20. Alsalameh S, Amin R, Gemba T, Lotz M (2004) Identification of mesenchymal progenitor cells in normal and osteoarthritic human articular cartilage. Arthritis Rheum 50:1522–1532
21. de la Fuente R, Abad JL, García-Castro J et al (2004) Dedifferentiated adult articular chondrocytes: a population of human multipotent primitive cells. Exp Cell Res 297:313–328
22. Machinami R (1983) Membranous lipodystrophy-like changes in ischemic necrosis of the legs. Virchows Arch [Pathol Anat] 399:191–205
23. Machinami R (1984) Incidence of membranous lipodystrophylike change among patients with limb necrosis caused by chronic arterial obstruction. Arch Pathol Lab Med 108:823–826
24. Nasu T, Tsukahara Y, Terayama K (1973) A lipid metabolic disease–"membranous lipodystrophy"–an autopsy case demonstrating numerous peculiar membrane-structures composed of compound lipid in bone and bone marrow and various adipose tissues. Acta Pathol Jpn 23:539–558

Virchows Arch (2012) 460:109–117
DOI 10.1007/s00428-011-1162-2

INVITED COMMENTARY

The birth of the clinicopathological method in France: the rise of morbid anatomy in France during the first half of the nineteenth century

Paul P. de Saint-Maur

Received: 14 October 2011 / Accepted: 19 October 2011 / Published online: 25 November 2011
© Springer-Verlag 2011

Abstract Morbid anatomy underwent extraordinary development in Paris during the last years of the eighteenth and the first half of the nineteenth century, for both philosophical and political reasons. The protagonists of this progress were primarily clinicians whose purpose was to link symptoms with pathological lesions and to elaborate a pertinent nosology. Pierre-Joseph Desault and Jean-Nicolas Corvisart were the forerunners, along with Xavier Bichat, a genius who died before he was able to realize his full potential. Guillaume Dupuytren, a renowned surgeon, founded an Anatomical Society with enthusiastic students; while Gaspard-Laurent Bayle and René-Theophile Laennec studied tuberculosis and developed the principles of clinicopathological correlations. Laennec's invention of the stethoscope in 1816 constituted a dramatic improvement of the possibilities of clinical examination and effectively established the clinicopathological method. A chair of morbid anatomy was created in 1835 for J. Cruveilhier, while a museum of morbid anatomy was established thanks to a 200,000 francs donation on behalf of G. Dupuytren. The French practitioners, however, did not believe that the microscope would play a major part in further medical progress, and after the revolution of 1848, the so-called School of Paris declined.

Keywords Morbid anatomy · Pathological museum · Clinicopathological method · Anatomical society · Tuberculosis · Auscultation

P. P. de Saint-Maur (✉)
Saint-Maur des fossés, France
e-mail: gpsaintmaur@free.fr

During the second half of the eighteenth century in all countries of Europe, the opening of the corpses of deceased patients had become a common procedure, and numerous cases of 'morbid anatomy' dissections had been gathered [17, 29].

This performance and collection of morbid anatomy cases was especially prominent in Italy with Giovanni Baptista Morgagni (1682–1771), England with John Hunter (1728–1793), Germany with Johan Gottlieb Walter (1734–1818) and Johan Frederich Meckel (1781–1823) and Holland with Eduard Sandifort (1742–1814) and Sebald Justinus Brugmans (1763–1819).

Subsequent advances resulted from the work of French practitioners especially in Paris and were stimulated, in large part, by the philosophical concepts of the age of enlightenment and the upheavals of the French Revolution (1789–1799) [1, 19]. One of the acts of the Revolution, among many others, was the suppression of medical schools and the opening of medical practice to everyone. Such a situation of anarchy could not last, and in 1793, three medical schools were created in Montpellier, Strasbourg and Paris on the initiative of Antoine François de Fourcroy (1755–1809), chemist, physician and politician. These medical schools were founded on principles quite differently from previous 'old regime' medical schools. Henceforth, the course of learning became the same for surgeons and medical practitioners, whereas before the revolution, surgeons had a non-academic course and were to a degree vassals of medical doctors.

Pierre-Jean-Georges Cabanis (1757–1808) provided much of the theoretical basis of the new teaching method of medicine, and his thoughts may be summarized in his own words: "the real apprenticeship of the physician must take place at the patient's bed side, not in books". Cabanis actually was the friend and follower of the philosopher De

Condillac (1715–1780), who in his turn continued the philosophy of the British philosopher, John Locke (1632–1704), and also was the inventor of 'sensationism'; as a consequence, Cabanis intended to develop a sensation-based medicine.

However, at the same time, there were many medical practitioners in Paris hospitals, whose appointments dated from before the revolution. They employed the opening of corpses in their medical practice. Three of these practitioners deserve particular mention because of their own contributions to medicine, and because some of their trainees were pioneers in the development of morbid anatomy.

Antoine Portal (1742–1832) held the chair of anatomy at "Collège de France" in 1769; his lessons, published in 1804, contributed to the rise of morbid anatomy [29]. He was, in 1789, probably the first to describe amyloid in the liver, when he noted a lard-like substance in an elderly woman's liver, and he was also the first to describe bleeding due to esophageal varices. Strangely enough, he did not appreciate Morgagni's work "De Sedibus et Causis Morborum", considering that the work was "incomplete in many aspects and unsuitable for practitioners" [29].

At about the same time, Pierre-Joseph Desault (1744–1796) was surgeon at Hôtel-Dieu Hospital. He made many dissections and had some specimens moulded in wax. Some of these specimens are still to be found in Dupuytren Museum (Fig. 1). His two most famous pupils were Xavier Bichat and Jean-Nicolas Corvisart who both contributed to the concept of clinicopathology.

The first one, Xavier Bichat (Fig. 2), born in 1771, the year of Morgagni's death, died in 1802 at the age of 31, probably of tubercular meningitis. However, the amount of work he accomplished in such a short life is quite amazing.

Born in a small town near Lyon, he began his medical training with his father, who was a medical doctor, and Marc-Antoine Petit, a surgeon in the Hôtel-Dieu of Lyon, no medical school existing at that time. He was a military surgeon for a while and, in 1793, prompted by the political troubles in Lyon, came to Paris and soon was the devoted pupil of Desault in Hôtel-Dieu hospital of Paris.

Bichat invented the concept of tissues without in fact using the microscope. By simple methods (e.g. cooking, freezing, treatment with chemicals), he was able to identify and characterize 21 different tissues [7], providing an initial foundation for the concept of tissue-based disease. Henceforth, the idea spread that a given lesion might be characteristic of a specific tissue, rather than a particular organ, and could therefore be encountered in various organs. Following the general precepts developed by John Hunter, Bichat raised the question of agonic lesions and their interpretation. He was a thorough supporter of morbid anatomy, although in his work he was more of a physiologist than a clinician.

In 1801, referring to the principles of observation-based medicine and the idea that medicine had to be learned at the patient bedside, he wrote—"Had You written notes all day long during 20 years at patient's bedside, on diseases (…) everything will still be for you confusion in symptoms which, without any relation to anything, shall only offer a sequence of inconsistent phenomena. Just open a few corpses: you immediately will notice the vanishing of the darkness that observation alone was unable to dispel" [6]. Michel Foucault [19] considers this statement to be the 'very birth certificate' of clinicopathological method and offers this comment: "…the great gap in the history of occidental medicine dates definitely back to the moment

Fig. 1 Two wax mouldings of a syphilitic aneurysm of the aorta: external view and dissection. Specimen of JJ Desault, 1792 (Courtesy Dupuytren Museum)

Fig. 2 Xavier Bichat: statue by David d'Angers erected in 1857 in the courtyard of the old medical school of Paris

when clinical experience became the clinicopathological look"

Bichat gave private lectures on morbid anatomy but never wrote a treatise of the matter which, in his opinion, should have been the task of maturity, a maturity that he never reached because of his early demise. The notes of his lectures, collected by PA Béclard, were published after his death [8].

The second important student of Desault was Jean-Nicolas Corvisart (1755–1821) cured by Desault of an ominous dissection wound. He later became physician of the Charité Hospital and first physician of Emperor Napoleon. Corvisart's accuracy in predicting which lesions would be found at the autopsy of his patients was famous.

In 1806, he wrote his most renowned work "Essai sur les maladies organiques du coeur et des gros vaisseaux" [12]. In his foreword, he reveals his concern for clinicopathologic correlation, saying that he had dreamt of completing Morgagni's classical work by writing a "De Sedibus et Causis Morborum per Signa Diagnostica Investigatis et per Anatomen Confirmatis". He had many students, among them his most renowned pupils Guillaume Dupuytren (1777–1835), Gaspard-Laurent Bayle (1774–1816) and René-Théophile Laennec (1781–1826).

Guillaume Dupuytren as a trainee of Corvisart at the Charité Hospital was in 1796 in charge of autopsies. Two years later, he was appointed Chief of Anatomical Tutorials in the medical school, where he performed many autopsies and gathered a great amount of anatomical documents. In 1802, he became the second surgeon of Hotel-Dieu Hospital. In 1803, he defended his doctorate thesis "Propositions sur quelques points d'anatomie, de physiologie et d'anatomie pathologique" [18]. Beginning his proposals concerning morbid anatomy, he wrote: "A general impulse drives nowadays every good nature mind to the study of morbid anatomy and this branch of medicine seems to be rich enough in facts so as to form from now on a separate science able to make its way by following its own principles". As a matter of fact, as he wrote in the prelude of this thesis, he was obliged by the law to defend his thesis after only a short laps of time and therefore offered these proposals, instead of more general and presumably more detailed considerations that he intended to formulate, as an introduction to a major treatise on morbid anatomy that he was preparing but never completed.

In 1802, Gaspard Laurent Bayle (1774–1816) joined the team of Corvisart and was Dupuytren's demonstrator in anatomical tutorials. The same year, 1802, he defended his doctoral thesis entitled "Considérations sur la nosologie, la médecine d'observation et la médecine pratique" [3].The great nosologist Philippe Pinel was on the examining board. Bayle cautiously expressed the opinion that the search for lesions might be the best way to elaborate a relevant nosology. This was in keeping with Bichat's ideas [7].

René–Théophile Laennec was Corvisart's trainee during the same period, and he established a close friendship with Bayle, which lasted until Bayle's death in 1816. In 1802, Laennec issued a paper on a case of mitral stenosis and gave in 1803, like Dupuytren, private lectures on morbid anatomy. However, his thesis in 1804 was rather old fashioned and written in Latin, consisting of "Propositions sur la doctrine d'Hippocrate".

These three men would lay the foundation for anatomic pathology in France for the decennia to come.

The anatomical society

On the 4th of December 1803, Dupuytren, together with Bayle and Laennec, assembled the best and most practical students belonging to the medical school to found an "Anatomical Society" [27, 28, 32], part of the "Society of the Medical School". The express purpose was to gather and discuss anatomical and pathological findings made during autopsies and dissections performed in the medical school. The regulations of the new society specified that it ".... was born from the general feeling that the everyday discoveries made by people admitted in the dissecting

rooms of the medical school should be put in common and used for the purpose of general education … The goal of the society would be the study of anatomy and physiology of in the state of health and illness" [27]. Seventy members put their names down at the foundation. There were 180 members just 11 months later, and the regulations had to be changed: the students who wished to join the society had to be sponsored by a member and would not be admitted before they had submitted some reports or cases. For 5 years, the society met every week, first on Sundays and then on Wednesdays. The average number of members attending the meetings was about 30 [28]. The members reported 'viva voce' and had to write down the case when asked. In 1804, the members were invited to gather cases from the hospitals in which they practiced. The story and the proceedings of the society have been thoroughly investigated [28]. The proceedings of the 37 first meetings were published in 1983 [32].

As an example, discussion about the following selection of subjects took place at the 12th meeting in 1804:

Report about an aneurysma of aorta (Boucher)
Tubercular liver: chemical study has shown a great amount of fat unrelated to the tubercular lesion which never contains fat (Delaroche).
Fatty pancreas (Dupuytren)
Lack of septum lucidum (Delaroche)
Organic brain lesions in children (Baron)
Organic heart lesions: case of mitral stenosis (Flaubert)
Lung of tubercular phtisis(Galaizeau)
Organic disease of uterus (Lenoble) (probably carcinoma of cervix)
Tumours of both ovaries (Pitet)
Honey like stuff found in a large cyst of the neck (Dupuytren)
Proposal of a choice for diplomas and stamp of the society (Fig. 3).

356 lectures were registered during the first 3.5 years of the society, a great part of them being issued in the "Bulletin de la Faculté". Despite this energetic beginning, the society did not last more than 6 years and was dissolved in 1809.

A major reason for this dissolution appeared to be the deep dissension between the President, Dupuytren, and Laennec, the Vice President, which began a year after the foundation of the society. In 1804, Laennec had issued a "Note sur l'anatomie pathologique", and Dupuytren accused him of plagiary [27].

Both men were the followers of Corvisart and Bichat, and their ideas were consequently very similar. However, this violent attack was a demonstration of the well-known rude and impolite nature of Dupuytren. He was fiercely ambitious, could not bear not to be first everywhere and used all possible means, honest or dishonest, to thrust aside his challengers. PF Percy (1754–1825), military surgeon of Napoleon's great army and Dupuytren's fellow professor, admired his surgical skills but said that Dupuytren was "the first as a surgeon and the last as a man". J. Lisfranc (1790–1847), who was 'surgeon in second' at Hôtel-Dieu, under Dupuytren's authority, but subsequently resigned, called Dupuytren "the brigand of Hôtel-Dieu".

The birth of the clinicopathological method

Thus, the clinicopathological method resulted from a body of convergent ideas and arose as the result of a scientific revolution that had originated during the eighteenth century [21].

In 1810, Georges Cuvier (1777–1832), founder of palaeontology and one of the greatest French scientists of that time, was asked by the imperial government to write a report on the state of science in France [17]. As for Medicine, he wrote that the opening of corpses, so-called morbid anatomy, had become very productive, due to the work of Portal, Dupuytren, Bayle, Laennec and others, who, following the example of Bichat, were especially concerned with the correlation between demonstrable organic lesions and clinical symptoms. Dupuytren was then professor for "medecine opératoire" and surgeon of Hôtel-Dieu Hospital.

In 1810, Bayle, then a consultant at la Charité Hospital, issued his most renowned work, "Recherches sur la phtisie pulmonaire"[4]. At that time, phthisis had a clinical definition: every consumption with pulmonary symptoms was termed phthisis. In his book, Bayle broke with the ideas of Corvisart and Pinel, who considered that the diseases should be defined by the clinical symptoms. Pinel, for instance, defined phthisis as a disease with "…cough, difficulty to breath, hectic fever and sometimes purulent expectoration". Conversely, Bayle stated definitively that the disease should be defined by the lesion found at the opening of the corpses at autopsy. Through studying a large number of cases in the most precise way, he intended to describe and define the correlations between the different organic lesions of the lungs and the different sorts of phthisis which resulted from them. His definition of phthisis was "every lesion of the lung which spontaneous evolution is a progressive disorganization of this viscera with ensuing ulceration and ultimately death". His book not only described in a quite new and accurate manner the pulmonary lesions of tuberculosis but also included lesions of some non-tubercular diseases.

This morphological approach was further developed in 1812 in Panckoucke's 'Dictionnaire des sciences médicales'.

Fig. 3 Guillaume Dupuytren's diploma as member of the Anatomical Society. (Courtesy Dupuytren Museum)

Laennec and Bayle each wrote à paper for the article "Morbid anatomy". Laennec's paper [22] is entitled "Anatomie Pathologique" and begins with Laennec's definition of morbid anatomy:

> Morbid anatomy is a science which purpose is the knowledge of the perceptible changes in the organs of human body arising during the state of illness. Opening corpses is the mean to acquire this knowledge; however, in order to become directly useful and immediately applicable to practical medicine, it must be brought together with the observation of the symptoms and changes in functions which coincide with the different kinds of changes of the organs.

Bayle's paper [5], more practical, is entitled: "Morbid anatomy (general considerations about the help which morbid anatomy can supply in the medicine)".

As an introductory matter, Bayle points out that the advantages of morbid anatomy, in some way a new science, are under discussion. Some enthusiasts want to generalize them, while other practitioners, very learned but virtually ignorant of this branch of medicine, underestimate them. As a matter of fact, they are some diseases in which the study of morbid anatomy can bring no help, some diseases in which it is of very little utility and others of which the knowledge can be completed or improved by the careful search of lesions, which may be found after the death in the organs involved by the disease.

Bayle sums up his paper by a few statements: morbid anatomy is useful for the classification of many diseases. It only shows us organic lesions and brings absolutely no enlightening about the immediate causes of the diseases. It can almost never let us know about the immediate cause of death. In every disease in which organic lesions can induce serious symptoms and result in death, morbid anatomy provides major enlightening, and it is not possible to do without it, namely to settle a clear classification and manage cautiously the patients suffering from these fearsome diseases.

A further breakthrough came in 1816 when Laennec invented the stethoscope and developed methods of auscultation at Hospital Necker, where he had been appointed (Fig. 4). 'Immediate auscultation', listening directly with the ear to the chest, was considered as of little importance because of its poor results [20]. However,

Fig. 4 Portrait of Laennec. Bas relief on the wall of Necker Hospital, Rue de Sévres in Paris. "In this hospital, Laennec discovered auscultation"

'Mediate auscultation', through the medium of the stethoscope resulted in dramatic change because it became possible to link, more clearly defined sounds with specific pathological lesions of the chest revealed by autopsy. Continuing with the studies of Bayle, Laennec, after 3 years of obstinate work, issued one of the masterworks of the whole history of medicine the "Traité de l'auscultation mediate" which remains the monument of the clinicopathological method [23]. The book was translated into English as soon as 1821 by John Forbes. A second enlarged edition was issued the year of Laennec's death in 1826. The book was devoted to the study of the diseases of the heart and lungs by means of the stethoscope and was divided into three parts, namely heart diseases, lung tuberculosis and non-tubercular diseases of the lung (such as lobar pneumonia, abcesses, bronchectasia, emphysema and so on). Pulmonary apoplexia (later to be called Laennec's infarct) is described, but Laennec did not establish the link with pulmonary embolism, due perhaps to uncertainty about the ante-mortem nature of clots found in the pulmonary arteries [26]. Incidentally, Laennec coined the name cirrhosis for a lesion of the liver with a tawny discoloration that he had seen in one of his patients.

According to a French professor of pneumology writing in 1981 [11], the three parts of the treatise are of unequal value. The section concerning heart disease was judged to be rather poor and only recapitulates and develops Corvisart's teaching, probably because Laennec was more an anatomist than a physiologist. The section on tuberculosis was, however, thought to be excellent. Laennec assembled and described the variable tubercular lesions and their evolution with outstanding accuracy, demonstrating for the first time that they all were consequences of the same disease. Regrettably, however, the contagious nature of tuberculosis was denied. The third section was a delight; no errors are to be found, and the descriptions are still valid today.

That tuberculosis was not contagious was a general acknowledged opinion of the time and remained so until 1865. The fact that many people could cohabit with tubercular patients without contracting the disease was considered as a proof of the fact. If someone was contaminated, it was admitted that he was naturally prone to have tuberculosis. Ironically, both Bayle and Laennec died of tuberculosis, which they certainly contracted from their patients.

In 1825, Pierre-Charles-Alexandre Louis (1787–1872) published his "Recherches anatomicopathologiques sur la phtisie" [25]. From 1821 to 1825, Louis had followed 1,960 patients, 358 of which died, 127 having phthisis. He performed many autopsies and agreed with Laennec about the definition of phthisis. His purpose, however, was not only clinicopathological correlation but also what he termed a "numerical method", essentially medical statistics. He was one of the founders of epidemiology.

The chair of morbid anatomy in Paris

In 1813, after Dupuytren had visited the museum of morbid anatomy of Strasbourg as general inspector of medical schools, a chair of morbid anatomy was founded in Strasbourg for Johann Friederich Lobstein (1777–1835). Lobstein subsequently published, in 1829, a treatise of morbid anatomy, which had a large distribution [24].

In Paris, however, there was no chair of morbid anatomy until 1835, when Jean Cruveilhier (1791–1874) was appointed to the position. Jean Cruveilhier was born in Limousin, a province in the south-eastern part of France, which also was Dupuytren's birth place 14 years earlier. He was the son and grandson of surgeons. After hesitating between priesthood and medical studies, he came to Paris and was admitted in 1812, as head of the list at the competitive examination that selected the "Internes des hôpitaux". As an 'interne', he was a resident for 4 years in Dupuytren's department at Hôtel-Dieu Hospital. For the rest of his long life, he remained a great admirer and supporter of Dupuytren. In 1816, he defended his thesis "Essai sur l'anatomie pathologique en general" [13], putting into words many of the ideas of Dupuytren, who had inspired this work. The thesis contains a short chapter on the history of pathology with the following assertion about his mentor "… at the same time (1803) M Dupuytren gave in Paris his first course of morbid anatomy; being chief of anatomical tutorials he had a large field in which he could exercise his outstanding skill for observation. He has been the first (and no one will dispute him the glory of this achievement) to reassemble the scattered pieces of morbid anatomy".

A few lines later, he stated that the fundamental ideas of Dupuytren have been followed by many practitioners, the most distinguished of them being Bayle and Laennec. Two years later, Pierre Rayer (1797–1876) in his thesis "Sommaire d'une histoire abrégée de l'anatomie pathologique" [30] wrote almost exactly the same thing, wisely perhaps, because Dupuytren was on the board of examiners!

After his thesis, Cruveilhier returned home, intending to spend his life as the successor of his father, a surgeon in a small town. However, in 1823, his father asked him to go back to Paris in order to undertake the competitive examination for an appointment as a lecturer. Again he succeeded, again as head of the list. Owing to the influence of Dupuytren, he then was appointed as professor for "médecine opératoire" in the medical school of Montpellier. In 1825, he decided to return home once again. But again, this was not to happen because he was asked by the

chancellor of the university to come back to Paris as professor for 'normal anatomy'. The chancellor, Monseigneur Fraysinnous, was a bishop; he had selected Cruveilhier not only because of his proficiency but also because he was a devote Roman Catholic. Cruveilhier accepted, and this was the beginning of a brilliant academic career.

In 1826, Cruveilhier reconstituted the anatomical society; Dupuytren and Laennec, still alive, were offered the titles of honorary president. Laennec died shortly thereafter, whereas Dupuytren did attend a few meetings [28]. Cruveilhier was elected permanent president, an appointment that he held for 44 years. The anatomical society is still well, alive and active today, although its name has been changed to "Société Française de Pathologie".

In 1828, Cruveilhier began the publication of an atlas [14, 15] that still is one of the most gorgeous medical books ever issued. The work was composed of a series of sections appearing at intervals with text and many lithographic illustrations of outstanding quality. The last section was issued in 1842. The book contains the first precise description of peptic ulcer ("ulcére rond") (Fig. 5), and most lesions may perfectly be identified today. It is fascinating that some of the lithographs show diseases that were only described many decades later, such as spindle cell haemangioma (Fig. 5) or Peutz–Jeghers polyps.

It was not a surprise that Dupuytren, when he initiated the foundation of the first pathology chair in Paris, indicated that this should be given to Jean Cruveilhier. By 1835, Dupuytren had been first surgeon of two kings, had an enormous practice and consequently had become very wealthy. Nonetheless, he was reported to be greatly disappointed on learning, when he went to London, that Sir Astley Cooper, Sergeant-Surgeon to King George IV, was three times as rich as he! [27]. However that may be, Dupuytren left a legacy of 200,000 francs to establish the Paris chair. At that time, the founding of a chair meant giving sufficient capital such that the interest would be enough to settle the salary of the professor. The amount of 200,000 francs was not quite sufficient for this purpose. The Dean, Matthieu Orfila (1787–1853), professor for forensic medicine, solved the difficulty. He persuaded the government to provide all of the money for the foundation of the chair and then convinced Dupuytren to use his legacy for the foundation of a museum of morbid anatomy. Shortly after, Dupuytren's death in 1835, the chair was established, and no objection could be raised to the appointment of Cruveilhier.

As for the museum, it was given Dupuytren's name and was settled in a large gothic building that for several centuries had been a convent refectory and was a renowned political meeting point during the French revolution. At its opening, the museum contained about a thousand specimens: wax mouldings (Fig. 1), glass jars, dried bones and dissected specimens, both desiccated and glycerinated, prepared by the faculty, and including some that were the heritage of societies suppressed by the revolution, such as the Royal Academy of Surgery. The museum stayed in the same building for a century, was closed in 1939, reopened in the 1960s and transferred in another part of the faculty of medicine where it still stands today. The refectory, after being restored, is nowadays an exhibition hall.

Other influential French pathologists

Cruveilhier was by no means the only one to practice gross morbid anatomy and to employ it for clinicopathological correlation. In fact, most hospital practitioners performed some morbid anatomical dissections, and the discoveries of the time were plentiful. Among them, we recall Gabriel Andral (1797–1876) who was appointed as a lecturer the same year as Cruveilhier. In 1829, he issued a "Précis d'Anatomie-Pathologique" [2] which, in the opinion of Ackerknecht [1], was markedly superior to Lobstein's treatise issued the same year and may really be considered

Fig. 5 Two plates of Cruveilhier's atlas [14, 15]. *Left* perforated ulcer of duodenum (Courtesy Dupuytren Museum). *Right* "Erectile tumors" of the hand and forearm, probably spindle cell haemangioma. The clinical history of the patient was not known

as the height of the classical morbid anatomy of the school of Paris. In the foreword, Andral said he intended to make morbid anatomy the principal basis for the art of diagnosis and treatment. He admitted, however, that morbid anatomy was only one of the many standpoints from which the science of a diseased man could be considered. Fourteen years later, he wrote "Essai d'hématologie pathologique" with chemical and microscopic observations, one of the first books on this topic.

Pierre Rayer (1793–1867) was Cruveilhier's contemporary. He was one of the pioneers of dermatopathology and was also the first in France to take special interest in kidney disease. In his treatise and atlas [31], he described hydronephrosis and coined the name for it. The treatise included a chapter on adrenals (capsules surrénales), which were not mentioned in the Cruveilhier Atlas (Fig. 6). The chapter is barely seven lines long: "They are in the human body two small organs which, because of their little importance and the unintelligibility of their functions, seem not to be a possible location for any lesion. These organs with indistinct and poor functions, and without any known disease are adrenals (suprarenal capsules). However several cases of my own prove that these small organs may show various changes (abscesses, tubercular and cancerous lesions). Moreover, they exhibit fairly often internal hemorrhages which, in some cases, rare indeed, change them into small or large tumors; I have seen death resulting from these". Is it possible to be at the same time, both more precise and more concise?

Jean Baptiste Bouillaud (1796–1881) was professor at La Charité Hospital in 1831. He wrote many books. His major contribution has been the study of rheumatic heart disease. He definitely demonstrated the connection between rheumatic fever and valvular heart diseases and specified the usual conditions of the occurrence of the latter [9, 10].

Fig. 7 Monument in memory of Victor Cornil. Cloister of institute des Cordeliers. The corpse and the microscope

In 1848, another revolution occurred in France and spread to other countries of Europe and especially to Berlin where R. Virchow was involved. J. Cruveilhier was 57 years old and had already been a professor of morbid anatomy in Paris for 13 years. After issuing his atlas, he published between 1849 and 1865 his "Traité d'Anatomie Pathologique générale» in five tomes [16]. In the foreword, issued in 1849, he gave the following definition: "morbid anatomy is the clinic of unfortunate cases". In practice, with very few exceptions, every practitioner in Paris agreed with him, considering morbid anatomy as the basis of nosology and semeiology and nothing else.

In 1829, Andral had already written that morbid anatomy should be the basis of the art of curing but no one thought that morbid anatomy could provide much value in finding the causes of the disease [1, 19], in keeping with Bayle's statement of 1812 [5].

These ingrained convictions most likely were the main reason for the lack of interest of the school of Paris for the

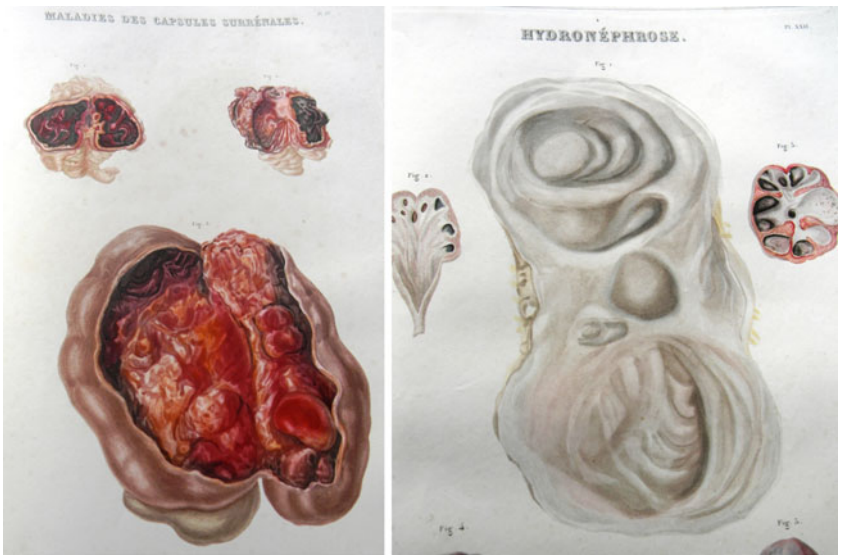

Fig. 6 Two plates of Reyers "Traité des maladies des reins" [31]. *Right* Hydronephrosis. *Left* Haematoma of adrenals, the grey organ at the *bottom* of the picture is the kidney. (Courtesy Dupuytren Museum)

use of the microscope. Cruveilhier and the faculty of Paris failed to recognize the promise of microscope, unlike Hughes Bennett in Edinburgh and Virchow in Berlin [33]. Thus, Paris remained isolated for several decades from the remarkable advances that the microscope was to bring to pathology elsewhere.

Cruveilhier remained professor until 1866, and there was no public teaching of histopathology in Paris. His successor, Alfred Vulpian (1826–1887), initiated some teaching but was more interested in physiopathology than in histopathology. Vulpian's successor was J.M. Charcot (1825–1893) who was not a histopathologist and left the chair in 1882 for a chair of neurology. The first histopathologist as professor in Paris was Victor Cornil (1837–1908), third successor of Cruveilhier, who had been for a while Virchow's student; he occupied the chair from 1882 to 1907 and made sure that France became connected once more with the developments of pathology elsewhere in Europe (Fig. 7).

References

1. Acherknecht EH (1967) Medicine at the Paris hospital 1794–1848. Baltimore. Translated in French: La médecine hospitalière à Paris (1794–1848) Payot Paris (1986)
2. Andral G (1829) Précis d'Anatomie Pathologique. Gabon, Paris
3. Bayle GL (1802) Considérations sur la nosologie, la médecine d'observation et la médecine pratique…Thèse Paris 1802; Available at http://www.bium.univparis5.fr
4. Bayle GL (1810) Recherches sur la phtisie pulmonaire. Gabon, Paris
5. Bayle GL (1812) Anatomie Pathologique (Considérations générales sur les secours que l'Anatomie Pathologique peut fournir à la médecine) in «Dictionnaire des sciences médicales de Panckoucke» Tome II, Paris, pages 61–78. Available at http://www.bium.univparis5.fr/
6. Bichat X (1801) Anatomie générale appliquée à la physiologie et à la médecine Paris. Foreword p.XCIX
7. Bichat X. (1801) Anatomie générale appliquée à la physiologie et à la medicine Paris.
8. Bichat X (1825) Anatomie pathologique: dernier cours de Xavier Bichat d'après un manuscrit autographe de P-A Béclard avec une notice sur la vie et les travaux de Bichat par FG Boisseau. JB Baillière, Paris
9. Bouillaud J-B (1836) Nouvelles recherches sur le rhumatisme articulaire aigu. J.B Baillière, Paris
10. Bouillaud J-B (1845) Traité clinique du rhumatisme articulaire aigu et de la loi de coïncidence des inflammations du coeur avec cette maladie. J.B Baillière, Paris
11. Bourgeois P (1981) Laennec et son temps. Sem Hop Paris 57(47–48):2047–2056
12. Corvisart JN (1806) Essai sur les maladies et les lésions organiques du coeur et des gros vaisseaux. Migneret, Paris
13. Cruveilhier J (1816) Essai sur l'Anatomie-Pathologique en général. Thèse Paris 1816. Available at http://www.bium.univparis5.fr
14. Cruveilhier J (1829–1842) Anatomie pathologique du corps humain ou description avec figures lithographiées des différentes altérations morbides dont le corps humain est susceptible. Paris Baillière Tome IXéme livraison (ulcère gastrique) Available at http://www.bium.univparis5.fr
15. idem Tome II XXIIIème livraison Available at http://www.bium.univparis5.fr
16. Cruveilhier J (1849) Traité d'Anatomie pathologique générale Tome 1. JB Baillière, Paris, p.37
17. Cuvier GC (1810) Rapport historique sur les progrès des sciences naturelles depuis 1789 et sur leur état actuel. Paris Imprimerie Impériale
18. Dupuytren G (1803) Propositions sur quelques points d'anatomie, de physiologie et d'anatomie pathologique. Thèse Paris 1803. Available at http://www.bium.univparis5.fr
19. Foucault M (1963) Naissance de la Clinique.- Quadrige/PUF 8 ème édition 2009
20. Grmek MD (1981) L'invention de l'auscultation médiate, retouches à un cliché historique.-Revue du palais de la découverte. Numéro spécial 22, p.107–116
21. Imbault-Huart MJ (1981) Bayle, Laennec et la méthode anatomo-clinique.-Revue du palais de la découverte. Numéro spécial 22, p.79–90
22. Laennec RTH (1812) Anatomie Pathologique in «Dictionnaire des sciences médicales de Panckoucke» Tome II, pages 46–61 Paris. Available at http://www.bium.univparis5.fr
23. Laennec RTH (1819) De l'auscultation médiate ou traité du diagnostic des maladies du poumon et du coeur fondé principalement sur ce nouveau moyen d'investigation. Brosson et Chaudé, Paris
24. Lobstein JF (1829) Traité et atlas d'anatomie pathologique. Levrault, Paris
25. Louis PCA (1825) Recherches anatomico-pathologiques sur la phtisie. Précédées du rapport fait à l'Académie royale de médecine par MM Bourdois, Royer-Collard et Chomel. Gabon & Cie, Paris
26. Mann RJ, Mann FD (1981) Laennec as a critical pathologist. J Hist Med All.sc. XXXVI 446–454
27. Orcel L, Vetter Th (1976) Dupuytren, Cruveilhier et la Société Anatomique. Arch Anat Cyt Path 24(2):167–179
28. Palluault F (2003) Étudiants et praticiens au service de la médecine: la Société anatomique de Paris de 1803 à 1873: étude institutionnelle et prosopographique. Edition numérisée BIUM 2003. http://www.bium.univparis5.fr/histmed
29. Portal A (1803) Cours d'anatomie médicale. 4 volumes Paris Baudouin an XII
30. Rayer P (1816) Sommaire d'une histoire abrégée de l'Anatomie Pathologique. Thèse Paris. Available at http://www.bium.univparis5.fr
31. Rayer P (1837) Traité des maladies des reins. JB Baillères, Paris
32. Société Anatomique(1996) Société Anatomique de Paris: procès-verbaux du 12 Frimaire An 12 jusques au 1er Fructidor An 12: Texte intégral du manuscrit original établi et présenté par Marie-Françoise Garreau. Paris SFANP
33. Virchow R (1847) Ueber die Reform des pathologischen und therapeutischen Anschauungen durch die mikroscopische Untersuchungen. Arch Path Anat I:207–255

Virchows Arch (2012) 460:119–122
DOI 10.1007/s00428-011-1170-2

CASE REPORT

CD99 is expressed in chordoid glioma and suggests ependymal origin

Alfredo E. Romero-Rojas · Julio A. Díaz-Pérez · Lina M. Ariza-Serrano

Received: 2 August 2011 / Revised: 24 October 2011 / Accepted: 3 November 2011 / Published online: 20 November 2011
© Springer-Verlag 2011

Introduction

Chordoid glioma (CG) is a neoplasm of the central nervous system (CNS), first described in 1995 by Wanschitz et al. [1], which is located exclusively in the third ventricle and hypothalamic region [2]. The origin of the CG is unclear, as it has characteristics similar to meningioma or chordoid chordoma, which is why some authors consider it a variant of these neoplasms [3]. It expresses glial fibrillary acidic protein (GFAP), which has led authors [4] to consider it to have a glial nature. In 1998 the CG was first described as a particular clinicopathologic entity, and since then few cases have published. Ependymal differentiation has been proposed as possible lineage of origin of this neoplasm [3, 5]. Recently, the use of CD99 has been proposed to support ependymal differentiation [6, 7]. We evaluate immunochemical expression of CD99 in the differential diagnosis of a case of CG.

A. E. Romero-Rojas
National Institute of Cancer,
Bogota, Colombia

J. A. Díaz-Pérez
University of Santander,
Bucaramanga, Colombia

J. A. Díaz-Pérez (✉) · L. M. Ariza-Serrano
UCSD Moores Cancer Center,
3855 Health Science Dr. MC0820,
La Jolla, CA 92037, USA
e-mail: jdiazperez@ucsd.edu

J. A. Díaz-Pérez
e-mail: patologia@udes.edu.co

Case report

Our patient is a 39-year-old male who developed headache, nausea, and progressive ataxia 20 days before he came to our institution. The computed axial tomography scan of the head showed a biventricular obstructive hydrocephalus due to the presence of a 4-cm mass in the anterior surface of the third ventricle, occluding the foramina of Monro. The lesion was hyperdense on CT and isointense in cranial magnetic resonance imaging (MRI) sequences in both T1 and T2 (Fig. 1). An emergency ventriculoperitoneal shunt was put in place. Upon surgical intervention a yellowish mass, firm with mucoid content was found.

A histopathological study revealed a neoplasm composed of epithelioid cells with uniform round nuclei, surrounded by moderate cytoplasm, distributed in nests and cords and surrounded by mucoid stroma with occasional lymphocytes (Fig. 2). The neoplastic cells were positive for CD99 (MIC-2, dilution 1:100 ThermoScientific) and PAGF (GF-2, dilution 1:50 Dako Cytomation) but negative for E-cadherin, CEA, CK7, CK19, CK20, EMA, and progesterone receptors (Fig. 3). The Ki67 proliferation index was 1%. A diagnosis of third ventricle CG grade II (WHO) was made. After a follow of 36 months, patient is in complete remission with CT documentation.

Discussion

GC has recently been included (2000) in the CNS tumor Classification by WHO as a neuroepithelial tumor of uncertain histogenesis and is considered as a grade II lesion in terms of its biological behavior [8]. CG are solitary neoplasms, with particular morphological, clinical, histopathological,

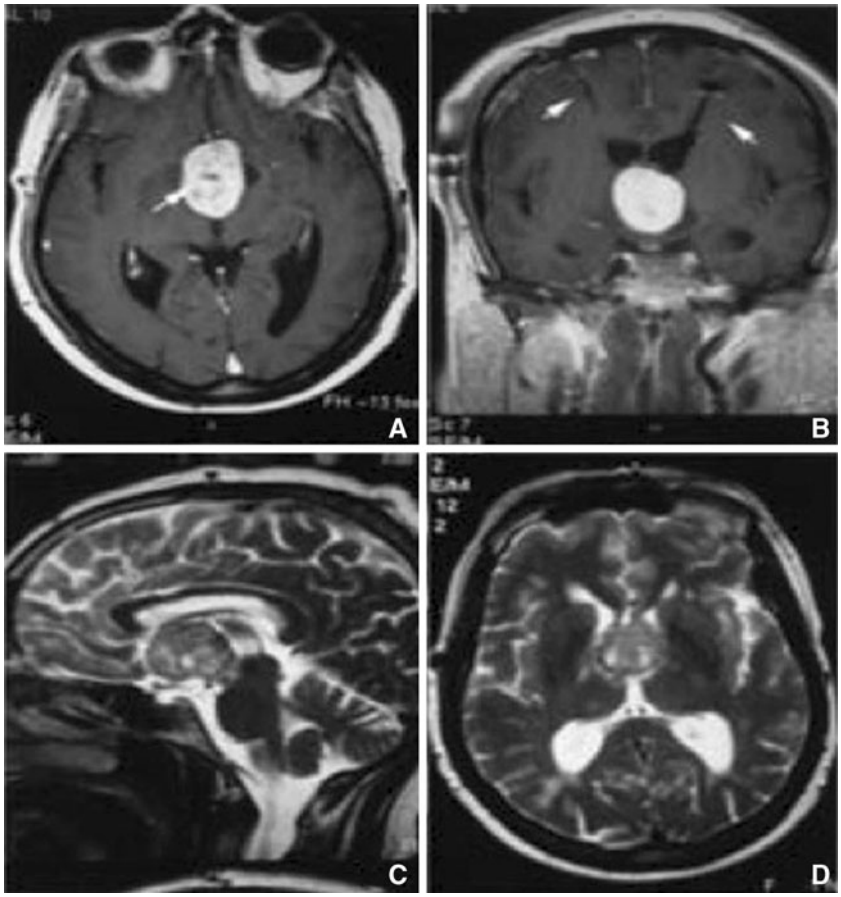

Fig. 1 The superior T1 sequences identifies areas of low intratumoral uptake (**a**, *arrow*). The coronal image (**b**) shows the artifact produced by ventricular drainage (*arrows*). The lower courts are sagittal images and axial T2 MRI, which shows isointense tumor and the absence of vasogenic edema (**c**, **d**)

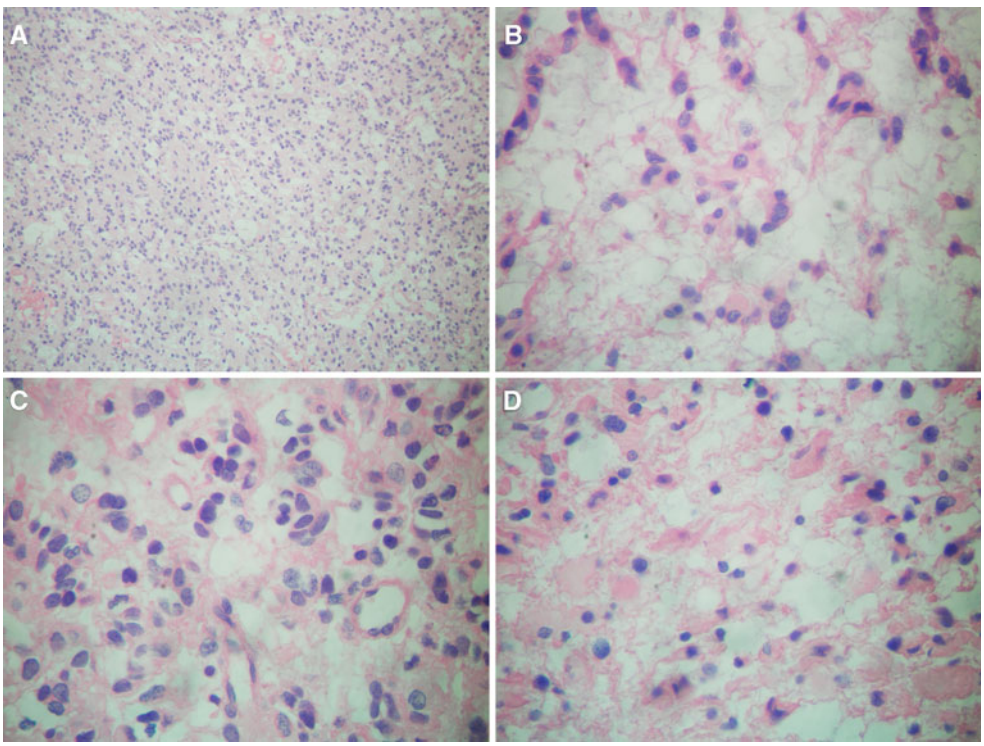

Fig. 2 The histopathological study has recognized a tumor (**a**, ×4) composed of many polygonal and oval cells with scant cytoplasm and uniform nuclei, forming cords and aggregates on a myxoid stroma (**b**, ×10); these cells had no atypia or mitosis (**c** and **d**, ×40). (Hematoxylin and eosin)

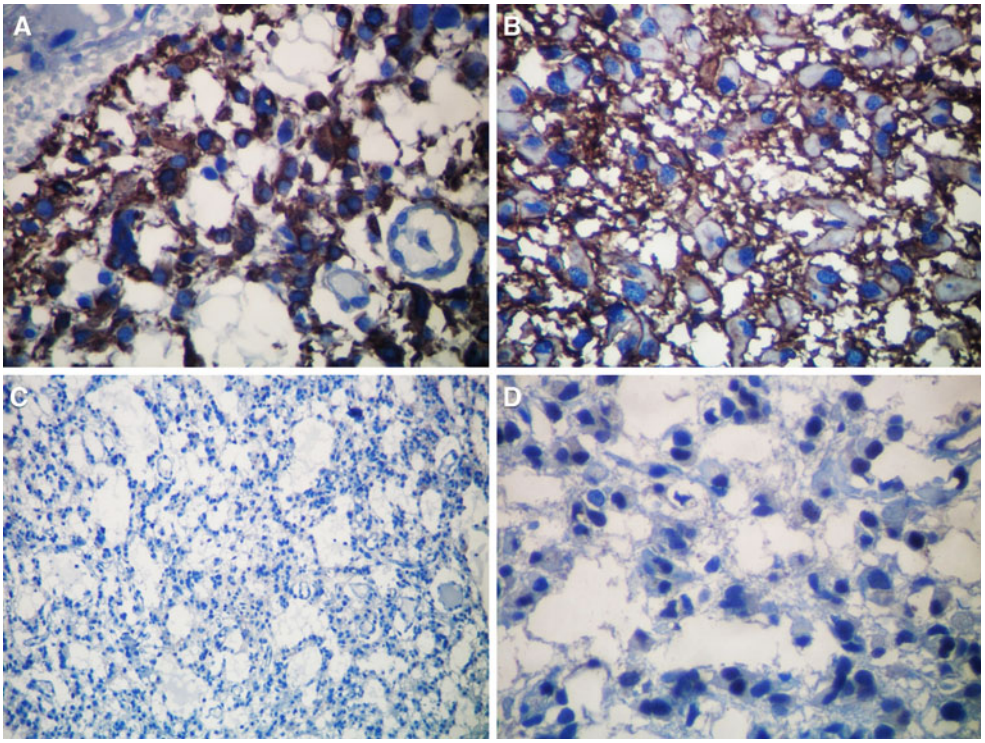

Fig. 3 The GC neoplastic cells were positive for GFAP (**a**) and CD99 (**b**), and negative for EMA (**c**) and CK19 (**d**) (×40)

immunophenotypical, and ultrastructural characteristics [9]. Only 45 cases have been reported. It is usually seen in female adult (mean age of 45 years) [2, 9], although cases have been reported in infants [9]. The clinical features are related to obstructive hydrocephalus due to a space-occupying lesion, producing symptoms such as lethargy, ataxia, urinary incontinence, vomiting, diabetes insipidus, and headache [2, 9]. CG as an incidental finding has been reported as well [10].

Because of its anatomical location and pathological features, it has been suggested that CG might be derived from specialized ependymal cover [5]. Evidence of ependymal histogenesis was provided by the ultrastructural demonstration of microvilli-like structures and hemidesmosomes in these tumors [11]. These findings were confirmed in other studies [12]. A possible origin of the CG in tanycytic cells, specialized ependymal cells, with abundant cytoplasmic intermediate filaments, a basal lamina, and secretory granules has been proposed [3] but the absence of intercellular junctions argues against this hypothesis [13].

Other authors have considered a possible origin in the subcommissural organ, located in the third ventricle at the entrance of the aqueduct of Sylvius, which disappears in the first years of life [13, 14]. Chromosomal abnormalities and amplification of oncogenes, which also occur in astrocytomas, meningiomas, and chordomas, have been described in CG [15].

Amplification in EGFR, CDK4 or MDM2 proto-oncogenes, or TP53 or CDKN2A mutations, as commonly seen in astrocytomas, has been reported [15, 16]. No NG2 gene inactivation has been found, as often found in meningiomas. Furthermore, a possible origin in the *lamina terminalis* has been proposed [13]. The histogenesis of CG is therefore unclear.

Grossly, these neoplasms measuring 2.5 to 3.5 cm are well circumscribed and occasionally cystic (19% of reported cases) [8, 9]. Histopathologically, this neoplasm is composed of cords and groups of epithelioid cells with eosinophilic cytoplasm and a monomorphous nucleus without (atypical) mitoses. These are embedded in lakes of mucin, which gives a chordoid appearance [9], with prominent lymphocytic infiltration. Other features such as chondroid metaplasia and papillary formations have also been described [12]. The adjacent brain parenchyma shows reactive astrocytes with Rosenthal fibers and moderate lymphocytic infiltrate [14]. Occasionally, high-grade features such as high number of mitosis, necrosis, and microvascular proliferation have been reported [2].

In the present case, immunochemical expression of CD99 was found. Other neoplasms which express CD99 such as PNET, rhabdomyosarcoma, neuronal/ganglionar tumor, and extrerenal rhabdoid tumor were ruled out by immunohistochemistry. GFAP expression confirmed the glial nature of the neoplasm. The CG cells can express vimentin, CD34, and E-cadherin and focally EMA, cytokeratin, and S100, but not synaptophysin, NF, neuron-specific enolase, desmin, or factor VIII [2, 9]. The rich intercellular matrix is positive for laminin and collagen type IV [3].

All reported cases had a low Ki67 proliferation index [2]. Growth of these tumors is slow [8], and the mortality and morbidity is related to surgery, rather than to the behavior of this tumor [2, 9].

In conclusion, the expression of CD99, which was never described before in CG, supports the hypothesis of an ependymal diferentiation and we propose to add this marker to the diagnostic panel for GC diagnosis.

Conflict of interest None.

References

1. Wanschitz J, Schmidbauer M, Maier H, Rossler K, Vorkapic P, Budka H (1995) Suprasellar meningioma with expression of glial fibrillary acidic protein: a peculiar variant. Acta Neuropathol 90:539–544
2. Kurian KM, Summers DM, Statham PF, Smith C, Bell JE, Ironside JW (2005) Third ventricular chordoid glioma: clinicopathological study of two cases with evidence for a poor clinical outcome despite low grade histological features. Neuropathol Appl Neurobiol 31(4):354–361
3. Sato K, Kubota T, Ishida M, Yoshida K, Takeuchi H, Handa Y (2003) Immunohistochemical and ultrastructural study of chordoid glioma of the third ventricle: its tanycytic differentiation. Acta Neuropathol 106 (2):176–180
4. Brat DJ (2006) The elusive origin of chordoid glioma. Arch Pathol Lab Med 130(4):437–438
5. Pasquier B, Peoc'h M, Morrison AL, Gay E, Pasquier D, Grand S, Sindou M, Kopp N (2002) Chordoid glioma of the third ventricle: a report of two new cases, with further evidence supporting an ependymal differentiation, and review of the literature. Am J Surg Pathol 26:1330–1342
6. Mahfouz S, Aziz AA, Gabal SM, el-Sheikh S (2008) Immunohistochemical study of CD99 and EMA expression in ependymomas. Medscape J Med 10(2):41
7. Choi YL, Chi JG, Suh YL (2001) CD99 immunoreactivity in ependymoma. Appl Immunohistochem Mol Morphol 9(2):125–129
8. Brat DJ, Scheithauer BW (2007) Chordoid glioma of the third ventricle. In: Louis DN, Ohgaki H, Weistler OD, Cavenee WK (eds) WHO classification of tumours of the central nervous system, 4th edn. Intl. Agency for Research, Lyon
9. Buccoliero AM, Caldarella A, Gallina P, Di Lorenzo N, Taddei A, Taddei GL (2004) Chordoid glioma: clinicopathologic profile and differential diagnosis of an uncommon tumor. Arch Pathol Lab Med 128(11):e141–e145
10. Gallina P, Pansini G, Mouchaty H, Mura R, Buccoliero AM, Di L (2007) An incidentally detected third ventricle chordoid glioma. Neurol India 55(4):406–407
11. Cenacchi G, Roncaroli F, Cerasoli S, Ficarra G, Merli GA, Giangaspero F (2001) Chordoid glioma of the third ventricle: an ultrastructural study of three cases with a histogenetic hypothesis. Am J Surg Pathol 25:401–405
12. Jain D, Sharma MC, Sarkar C, Suri V, Rishi A, Garg A, Vaishya S (2008) Chordoid glioma: report of two rare examples with unusual features. Acta Neurochir (Wien) 150(3):295–300
13. Leeds NE, Lang FF, Ribalta T, Sawaya R, Fuller GN (2006) Origin of chordoid glioma of the third ventricle. Arch Pathol Lab Med 130(4):460–464
14. Galloway M, Afshar F, Geddes JF (2001) Chordoid glioma: an uncommon tumour of the third ventricle. Br J Neurosurg 15 (2):147–150
15. Reifenberger G, Weber T, Weber RG et al (1999) Chordoid glioma of the third ventricle: immunohistochemical and molecular genetic characterization of a novel tumor entity. Brain Pathol 9:617–626
16. Held-Feindt J, Forstreuter F, Pufe T, Mentlein R (2001) Influence of the somatostatin receptor sst2 on growth factor signal cascades in human glioma cells. Brain Res Mol Brain Res 87(1):12–21

Virchows Arch (2012) 460:123–127
DOI 10.1007/s00428-011-1183-x

CASE REPORT

Eosinophilic myenteric ganglionitis as a cause of chronic intestinal pseudo-obstruction

Ariadne H. A. G. Ooms · Joanne Verheij · Jessie M. Hulst · John Vlot · Cynthia van der Starre · Lissy de Ridder · Ronald R. de Krijger

Received: 13 August 2011 / Revised: 30 November 2011 / Accepted: 5 December 2011 / Published online: 16 December 2011
© The Author(s) 2011. This article is published with open access at Springerlink.com

Abbreviations

Anti-SMA	Anti-smooth muscle actin
CIPO	Chronic intestinal pseudo-obstruction
ENS	Enteric nervous system
GINMD	Gastrointestinal neuromuscular disorders
HPF	High power field
ICC	Interstitial cells of Cajal
IL-5	Interleukin-5

Introduction

Chronic intestinal pseudo-obstruction (CIPO) represents a rare and severe condition characterized by failure of the intestinal tract to propel its contents normally [1, 2]. The condition presents with clinical features such as abdominal pain, vomiting, distended abdomen, constipation, and diarrhea [1, 2]. These symptoms resemble an intestinal mechanical obstruction in the absence of a demonstrable lesion occluding the gut. It is thought that this can result from disturbance of the intestinal motor function, supplied by the enteric nervous system (ENS). The neurons of the ENS are contained in two groups of ganglia: the myenteric (Auerbach's) and the submucosal (Meissner's) plexuses.

The ENS has the unique ability to control most gut functions, such as regulating vascular tone, secretion/absorption, and gut motility [3, 4]. Given these important functions of the ENS, it is not surprising that damage to the ENS results in digestive disorders and reduced quality of life. Human and experimental evidence indicates that inflammation can occur in the ENS, resulting in severe intestinal motor impairment. Inflammation of the ENS has indeed been observed in some cases of CIPO [3, 5, 6].

Many efforts have been made to classify CIPO. Based on histological examination, CIPO may be categorized as primary, secondary, or idiopathic in nature [1]. Primary CIPO can be classified into three major categories of gastrointestinal neuromuscular disorders (GINMD): mesenchymopathies, myopathies, and neuropathies, depending on the predominant involvement of interstitial cells, smooth muscle cells, or enteric neurons, respectively [1, 7]. The enteric neuropathies underlying CIPO can be subdivided into two major entities: (a) degenerative neuropathies, without any evident inflammatory response and (b) inflammatory neuropathies, referred to as myenteric ganglionitis [3, 8]. Inflammation within the myenteric ganglia is a recognized primary cause of CIPO, but the mechanisms through which the dysfunction occurs and the mechanisms leading to enteric neuropathies remain poorly understood [3, 4]. In this case report, we present the first male neonate with eosinophilic myenteric ganglionitis

A. H. A. G. Ooms (✉) · R. R. de Krijger
Department of Pathology, Josephine Nefkens Institute,
Erasmus MC—University Medical Centre,
P.O. 2040, 3000 CA, Rotterdam, The Netherlands
e-mail: a.ooms@erasmusmc.nl

J. Verheij
Department of Pathology, AMC,
Amsterdam, The Netherlands

J. M. Hulst · L. de Ridder
Department of Pediatric Gastroenterology, Erasmus MC—Sophia,
Rotterdam, The Netherlands

J. Vlot
Department of Pediatric Surgery, Erasmus MC—Sophia,
Rotterdam, The Netherlands

C. van der Starre
Neonatal and Pediatric ICU, Erasmus MC—Sophia,
Rotterdam, The Netherlands

underlying CIPO and report his successful recovery following steroid treatment.

Clinical history

A boy was born prematurely at 25 weeks through a primary Caesarean section, weighing 940 grams (>−2.5 SD). Two weeks later he suffered from necrotizing enterocolitis for which he underwent a right hemicolectomy as well as resection of 10 cm of jejunum. However, in the months following surgery, the infant continued to have poor feeding tolerance with a distended abdomen and severe constipation. At 6 months of age, the boy weighed 4.1 kg (−2.5 SD), despite total parental feeding. At 4 months of age, he developed signs of obstruction (distended abdomen, vomiting, and gastric retentions) and a laparotomy was performed. During surgery, there was no stricture at the ileocolonic anastomosis. Although there was no stricture, a milk curd was found proximal to the anastomosis and the anastomosis was resected. Rectal full thickness biopsies were taken to rule out Hirschsprung's disease. The laboratory results showed a variable number of eosinophils (0.1×10^9/l to 1.0×10^9/l) and during a short period of time peripheral eosinophilia was present until treatment started. Laboratory results further showed a normal amount of serum IgE and tests for antinuclear and smooth muscle autoantibodies were negative. Because of the feeding difficulties, the patient was treated with an amino acid-based infant formula for 4 months. Major improvement of the infant's condition only occurred after starting anti-inflammatory treatment, using intravenous prednisone and subsequently oral beclomethasone 200 mg three times daily. Within 1–2 weeks after starting the beclomethasone, enteral nutrition could be increased to complete enteral feeding. After 6 months of hospitalization, the patient was discharged in good condition. Follow-up for 7 months after discharge showed that the patient still needs corticosteroids and steroid-containing enemas have been added to the therapy during flares of the gastrointestinal problems, which has a positive effect on his feeding tolerance. After 18 months of follow-up after hospitalization, the child eats normally and does not need any medication.

Materials and methods

Patient

Informed consent for publication was obtained from the parents.

Histological methods

A hemicolectomy specimen as well as 10 cm of jejunum was received. Later, full thickness rectal biopsies were taken during surgery for a pseudo-obstruction as well as the anastomosis created during the previous surgery. Histological sections were prepared and examined by routine methods. Enzyme histochemistry with acetylcholinesterase was performed on frozen sections of the biopsies to exclude Hirschsprung's disease. Immunohistochemistry using CD117 was applied on formalin-fixed paraffin-embedded sections form the resection specimen to demonstrate the presence of interstitial cells of Cajal (ICCs). The number of eosinophils per high power field (HPF, i.e., 400×) was counted in the resection specimens.

On the same slides, we performed immunohistochemical analysis with PGP9.5 to demonstrate the presence of enteric neurons. In addition, we applied anti-smooth muscle actin (anti-SMA) to demonstrate the presence of a normal layer of smooth muscle.

Results

Histological findings

In the biopsies, there was no evidence of hypo- or aganglionosis. Histological examination of the resected bowel segment showed a striking presence of eosinophils, especially in the myenteric plexus with affinity for the neurons and ganglion cells (range 8–43/HPF; mean 16/HPF) (Fig. 1). This was located in the ileum as well as in the colon. There was no significant increase of lymphocytes surrounding the ganglion cells as in lymphocytic ganglionitis. Retrospectively, histological examination of slides of the previously removed necrotic bowel also showed the presence of eosinophils with affinity for the ganglion cells.

Immunohistochemical findings

Immunohistochemistry with CD117 showed an apparently normal c-Kit labeling pattern, since we found CD117 positive cells in the colon as well as in the ileum. These were located in the myenteric plexus, in the submucosa, and interspersed in the muscle layer. This indicated a normal number of interstitial cells of Cajal (Fig. 2a, b). Immunohistochemistry with acetylcholinesterase showed a normal amount of acetylcholinesterase-positive neuronal fibers in the muscularis mucosae and

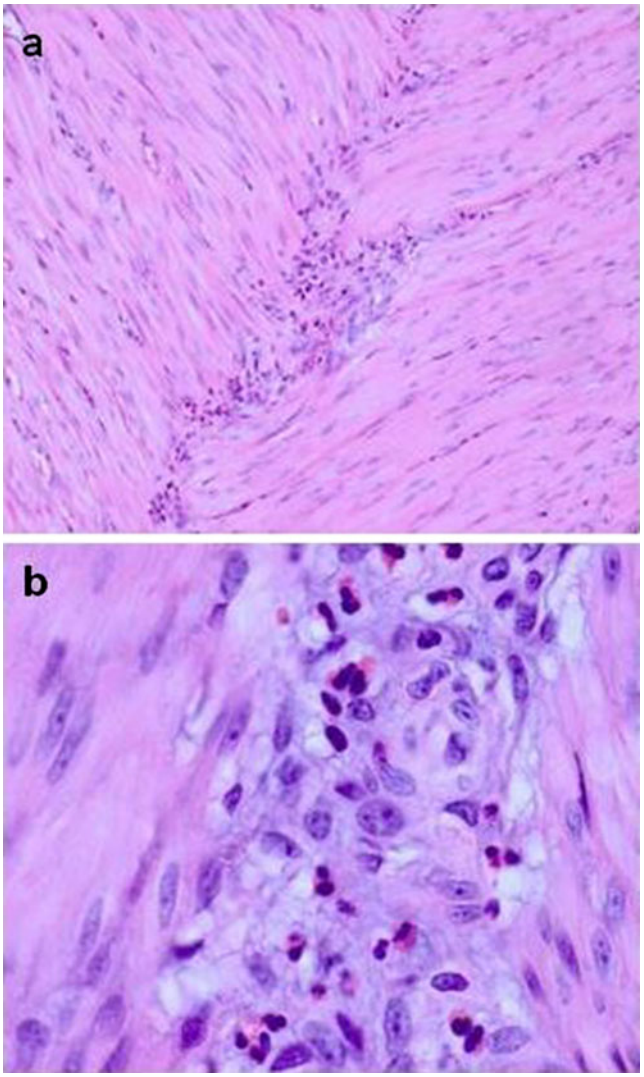

Fig. 1 Hematoxylin/eosin (H/E)-stained sections of full thickness biopsies from our patient demonstrating the presence of eosinophils in the myenteric plexus. **a** Overview of muscular layer with myenteric plexus. **b** Detail of myenteric plexus with infiltrating eosinophilic granulocytes between the ganglion cells and neurons without obvious cellular destruction

lamina propria, as well as in the submucosal neurons (data not shown).

Immunohistochemical analysis with PGP9.5 showed the presence of an apparently normal number of enteric neurons, even with the presence of eosinophils in the immediate vicinity (Fig. 2c). This indicates that the eosinophilic infiltrate did not lead to degeneration of the neurons. In addition we used immunohistochemical analysis with antibodies against smooth muscle actin (anti-SMA) to show there was a normal amount of smooth muscle cells (Fig. 2d).

Discussion

We describe the second neonatal case of eosinophilic myenteric ganglionitis, causing a rare and highly morbid functional intestinal obstruction syndrome, referred to as CIPO [2]. This represents a rare syndrome characterized by impaired gastrointestinal propulsion, which causes symptoms of gastrointestinal obstruction, in the absence of any lesion occluding the intestinal lumen [2]. The intestine depends on the ENS for its functionally important patterns of movement [9]. Current evidence indicates that alterations in the ENS, including functional impairment of neurons, are associated with uncoordinated motor activities, resulting in altered transit of intestinal contents potentially leading to CIPO [8].

Schappi et al. [2] described three cases, all female in contrast to our patient. The three cases described were aged 1 month, 11 and 15 years. The clinical presentation of the first two patients is similar to our case: vomiting, constipation, and marked abdominal distension for several days. The third case had a more acute event. The neonate also experienced a peripheral blood eosinophilia (1.15×10^9/l) as did our case before he was treated. However, in our case there was no elevation in serum IgE, as was described in the first two cases. Smooth muscle and antinuclear autoantibodies were weakly positive in the neonatal case, not described in the second, and negative in the third case as in our patient. In our patient no anorectal inflammatory manometry was performed.

In our patient the clinical picture was obscured at first by necrotizing enterocolitis in this premature infant. However, after surgery the patient continued to have feeding difficulties. The patient developed signs of a gastrointestinal obstruction, but during surgery this turned out to be a pseudo-obstruction. When examining the bowel specimen, it was noticed that there was an eosinophilic myenteric ganglionitis. The eosinophils were specifically located around the ganglion cells, with some scattered eosinophils in the submucosa and tunica muscularis. In the second and third cases described by Schappi et al. there seems to be a more extensive involvement of all layers of the bowel, but with a larger collection of eosinophils around the myenteric plexus. Unfortunately, they do not provide a count of the eosinophils. IL-5, a potent eosinophil chemoattractant, has been suggested as a humoral factor playing a role in gut dysmotility. IL-5 expression by the myenteric ganglions was demonstrated by Schappi et al. in his patients with eosinophilic myenteric ganglionitis. Unfortunately we did not have the means to demonstrate IL-5 expression in our patient.

In the neonatal case and the second case of Schappi et al. Hirschsprung's disease was considered, as was done in our case. Full thickness rectal biopsies in those children and in

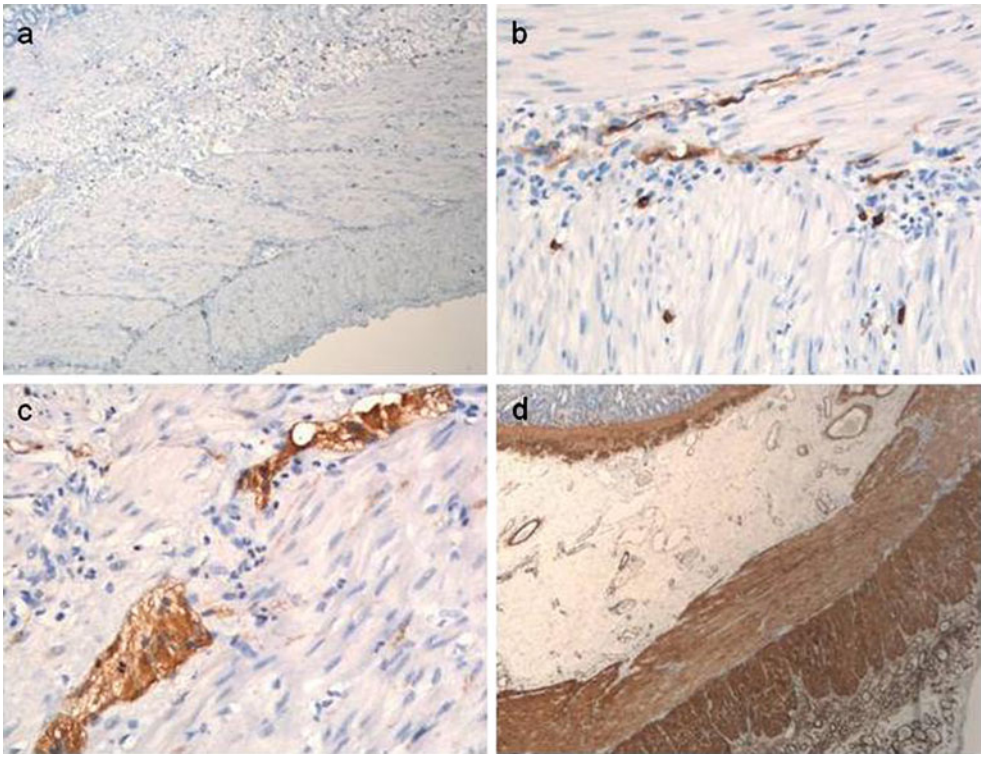

Fig. 2 Immunohistochemistry on sections of the resection specimen from our patient. **a**, **b** Overview (**a**; 40×) and detail (**b**; 200×) of a slide form the bowel resection stained for CD117, highlighting the ICCs, with an apparently normal distribution and number. **c** Detail (200×) of the myenteric plexus stained for PGP9.5, highlighting the neurons. An apparently normal number can be appreciated. **d** Overview (40×) of a slide stained for anti-SMA, in which a normal pattern of smooth muscle cells can be seen

our case also showed the presence of normal ganglia and neurons within the submucosal and myenteric plexus, as well as a normal acetylcholinesterase staining pattern. In all cases described as well as in our case, there was no significant lymphocytic infiltrate.

We applied immunohistochemistry with CD117 antibodies to analyze the number of interstitial cells of Cajal, which are thought to be required for normal gut motility and are also implicated in some forms of GINMD. ICCs are found widespread throughout the gastrointestinal tract, distributed along a variety of locations. In the colon, distinct networks can be found in the myenteric plexus and more loosely in the submucosa. In the small bowel, the same networks can be found in the myenteric plexus and in addition more loosely in the deep muscular plexus. Single ICCs can also be found interspersed between muscle cells in the muscle layer [10, 11]. CD117 also stains mast cells, which were excluded by comparing with the H&E and by looking at the contour of the cell, since mast cells do not have processes whereas ICCs do [10, 11]. Until now, there are no normal reference values for the range of ICC numbers when applying immunohistochemistry. Most reports use immunofluorescence on frozen tissue samples instead of immunohistochemistry on paraffin-embedded material [10, 11]. It is believed that immunohistochemistry does not detect all ICCs [10]. Therefore, we examined our slides for the presence of the ICCs in the previously named locations, especially in those with the presence of eosinophils. In addition we used PGP-9.5 and anti-SMA to demonstrate the presence of a normal amount of enteric neurons and smooth muscle cells, respectively. These immunohistochemical stainings also showed a normal amount of neurons and smooth muscle cells.

By excluding the above-mentioned cells as a cause of the pseudo-obstruction, it appears more likely that there is a functional rather than anatomically detectable cause for the pseudo-obstruction in this patient. However, we cannot entirely exclude this, as we have not performed quantitative analysis of the enteric neurons. Similar to the patients demonstrated by Schappi et al. there was no clinical improvement in the gastrointestinal dysmotility syndrome with an amino acid-based formula as the sole source of nutrition for at least 3 months in our patient as compared to 2 months in the neonatal case described by Schappi et al. However, all patients, including our patient, did respond rapidly to steroids [2]. We used the same steroid (beclomethason) in the same dosage as in the previously published neonatal case. The other cases were treated with (methyl)prednisolone and azathioprine. Our patient could tolerate complete enteral feeding within 1–2 weeks. In contrast to the previously published patients, our patient is completely without medication after 18 months of follow-up, not requiring a maintenance dose of steroids.

In conclusion, this case illustrates that a GINMD, such as myenteric ganglionitis, should be considered in patients with CIPO, since it may be treated with an elemental diet and steroids.

Conflict of interest statement We declare that we have no conflict of interest.

Open Access This article is distributed under the terms of the Creative Commons Attribution Noncommercial License which permits any noncommercial use, distribution, and reproduction in any medium, provided the original author(s) and source are credited.

References

1. Antonucci A, Fronzoni L, Cogliandro L, Cogliandro RF, Caputo C, De Giorgio R, Pallotti F, Barbara G, Corinaldesi R, Stanghellini V (2008) Chronic intestinal pseudo-obstruction. World J Gastroenterol 14(19):2953–2961
2. Schappi MG, Smith VV, Milla PJ, Lindley KJ (2003) Eosinophilic myenteric ganglionitis is associated with functional intestinal obstruction. Gut 52(5):752–755
3. De Giorgio R, Camilleri M (2004) Human enteric neuropathies: morphology and molecular pathology. Neurogastroenterol Motil 16(5):515–531. doi:10.1111/j.1365-2982.2004.00538.x
4. Lacy BE, Weiser K (2006) Gastrointestinal motility disorders: an update. Dig Dis 24(3–4):228–242. doi:10.1159/000092876
5. De Giorgio R, Barbara G, Stanghellini V, De Ponti F, Salvioli B, Tonini M, Velio P, Bassotti G, Corinaldesi R (2002) Clinical and morphofunctional features of idiopathic myenteric ganglionitis underlying severe intestinal motor dysfunction: a study of three cases. Am J Gastroenterol 97(9):2454–2459. doi:10.1111/j.1572-0241.2002.06002.x
6. Khan WI, Collins SM (2006) Gut motor function: immunological control in enteric infection and inflammation. Clin Exp Immunol 143(3):389–397. doi:10.1111/j.1365-2249.2005.02979.x
7. Knowles CH, De Giorgio R, Kapur RP, Bruder E, Farrugia G, Geboes K, Lindberg G, Martin JE, Meier-Ruge WA, Milla PJ, Smith VV, Vandervinden JM, Veress B, Wedel T (2010) The London Classification of gastrointestinal neuromuscular pathology: report on behalf of the Gastro 2009 International Working Group. Gut 59(7):882–887
8. Di Nardo G, Blandizzi C, Volta U, Colucci R, Stanghellini V, Barbara G, Del Tacca M, Tonini M, Corinaldesi R, De Giorgio R (2008) Review article: molecular, pathological and therapeutic features of human enteric neuropathies. Aliment Pharmacol Ther 28(1):25–42. doi:10.1111/j.1365-2036.2008.03707.x
9. Furness JB (2008) The enteric nervous system: normal functions and enteric neuropathies. Neurogastroenterol Motil 20(Suppl 1):32–38. doi:10.1111/j.1365-2982.2008.01094.x
10. Farrugia G (2008) Interstitial cells of Cajal in health and disease. Neurogastroenterol Motil 20(Suppl 1):54–63
11. Gomez-Pinilla PJ, Gibbons SJ, Sarr MG, Kendrick ML, Shen KR, Cima RR, Dozois EJ, Larson DW, Ordog T, Pozo MJ, Farrugia G (2011) Changes in interstitial cells of cajal with age in the human stomach and colon. Neurogastroenterol Motil 23(1):36–44. doi:10.1111/j.1365-2982.2010.01590.x, Epub 02010 Aug 01519

Virchows Arch (2012) 460:129–130
DOI 10.1007/s00428-012-1197-z

INVITED COMMENTARY

The times have changed: molecular pathology is here to stay

A commentary on: Analytical performance of a PCR assay for the detection of KRAS mutations (codons 12/13 and 61) in formalin-fixed paraffin-embedded tissue samples of colorectal carcinoma, by Lee et al. In this issue

J. Han van Krieken · Gerald Hoefler

Received: 2 January 2012 / Accepted: 15 January 2012 / Published online: 23 February 2012
© The Author(s) 2012. This article is published with open access at Springerlink.com

Molecular pathology is now an integral part of diagnostic pathology. This has brought excitement and responsibilities to us as pathologists and molecular biologists in pathology—excitement, due to the many new possibilities we have for diagnosis, prediction of outcome, and response to therapy of disease, and responsibilities, since we need to perform the tests with high accuracy, which requires expertise. But is this different from conventional histology and immunohistochemistry? At the time of Virchow, histopathology brought about enormous excitement, and as we are all aware, the responsibilities became rapidly clear. The first attempt to diagnose a tumor in 1882, on a biopsy of a Crown Prince, resulted in a failure, which led to many publications on this topic. Many of us remember the early days of immunohistochemistry, again enormous excitement, many publications (still ongoing) on its use, and obviously, great responsibilities since without immunohistochemistry, many diagnoses are impossible or, at the least, unreliable. But the pathologists looking down the microscope remained the final decision makers. And we all know that a good pathologist can make a correct diagnosis on a poor slide and/or a poor immunostained slide, but without knowledge and experience, even the best slide does not suffice. For molecular pathology, it is different.

J. H. van Krieken (✉)
Department of Pathology,
Radboud University Nijmegen Medical Centre,
PO Box 9101, 6500HB Nijmegen, The Netherlands
e-mail: j.vankrieken@pathol.umcn.nl

G. Hoefler
Institute of Pathology, Medizinische Universitat Graz,
Graz, Austria
e-mail: Gerald.hoefler@medunigraz.at

For molecular tests (excluding fluorescent in situ hybridization, which is often regarded by pathologists as a bit fancier immunostain), the tissue is ground, DNA or RNA is extracted and processed, and bands, or colors or letters, appear on a screen, blot, or paper. These need to be interpreted in the context of the histological and immunohistochemical findings in order for a final conclusion to be drawn. This needs teamwork between a molecular biologist and pathologist, and both need to understand each other's trade. For pathologists, it is important to realize that there are factors that may influence the molecular results, factors such as fixation, tissue processing, and DNA extraction to name just a few. For molecular biologists, these issues are well known, but they also need to be informed about the exact diagnosis and the absolute and relative quantity of tumor cells and other potential test confounders. Not only that, both need to be aware of the test characteristics specific to the questions asked. That this is crucial can be learned from the KRAS story in colorectal cancer.

EGFR targeting agents have a modest effect on metastasized colorectal cancer. As it turned out, they are only effective on tumors with a wild-type KRAS gene, but in patients with a KRAS mutated tumor, the drug even has a negative effect. It is therefore mandatory that the test is performed with high accuracy. Therefore, the European Society of Pathology has initiated a European external quality assurance system, which is now in its fourth year [1–3]. Through this program, it has become clear not only that many different test systems can provide reliable results, but also that about 10–15% of the laboratories committed unacceptable mistakes (the good news, however, is that after feedback, these laboratories performed significantly better). It has also become clear that there are major differences in the pre-analytical phase between laboratories, that there are problems when, in a sample, the

percentage of tumor cells to be tested is low, and that DNA extraction methods matter.

In this issue, Lee et al. describe a novel PCR-based method for KRAS testing and compare the results with the most commonly used test, Sanger sequencing [4]. This latter method is quite robust, but may show failures in case the sample contains a low percentage of tumor cells. The TaqMelt PCR assay—the cobas® KRAS Mutation Test—designed to detect 19 mutations in codons 12, 13, and 61 was shown to be superior in samples with a low percentage of tumor cells. The paper also discusses some of the issues which are relevant in molecular pathology of today and is therefore a valuable contribution to the literature, both for pathologists and for molecular biologists. It is, however, not the only commercial test system that provides highly accurate results in such samples. It is important that experiences like those from Lee et al. are published. The results of the ESP KRAS EQA system will be published as well. In this way, a large database with knowledge on methods of DNA extraction and test platforms will be built up. Such data will enable pathologists and molecular biologists to make an argued choice for test systems for any particular question. These choices are important, since each new method that is going to be used for molecular pathology needs in-house validation, prior to its application. This implies that one cannot change too often from one test to another, even though developments in methods of molecular testing evolve extremely fast.

Open Access This article is distributed under the terms of the Creative Commons Attribution License which permits any use, distribution, and reproduction in any medium, provided the original author(s) and the source are credited.

References

1. van Krieken JH, Jung A, Kirchner T, Carneiro F, Seruca R, Bosman FT, Quirke P, Fléjou JF, Plato Hansen T, de Hertogh G, Jares P, Langner C, Hoefler G, Ligtenberg M, Tiniakos D, Tejpar S, Bevilacqua G, Ensari A (2008) KRAS mutation testing for predicting response to anti-EGFR therapy for colorectal carcinoma: proposal for an European quality assurance program. Virchows Arch 453(5):417–431, Epub 2008 Sep 18. Review. Erratum in: Virchows Arch. 2009 Feb; 454(2):233–5
2. Bellon E, Ligtenberg MJ, Tejpar S, Cox K, de Hertogh G, de Stricker K, Edsjö A, Gorgoulis V, Höfler G, Jung A, Kotsinas A, Laurent-Puig P, López-Ríos F, Hansen TP, Rouleau E, Vandenberghe P, van Krieken JJ, Dequeker E (2011) External quality assessment for KRAS testing is needed: setup of a European program and report of the first joined regional quality assessment rounds. Oncologist 16(4):467–478, Epub 2011 Mar 26. PubMed PMID: 21441573
3. Dequeker E, Ligtenberg MJ, Vander Borght S, van Krieken JH (2011) Mutation analysis of KRAS prior to targeted therapy in colorectal cancer: development and evaluation of quality by a European external quality assessment scheme. Virchows Arch 459 (2):155–160, Epub 2011 Jun 24. PubMed PMID: 21701884
4. Sung Lee, Victoria H. Brophy, Jianli Cao, Margot Velez, Corey Hoeppner, Stephen Soviero, H. Jeffrey Lawrence (2012) Analytical performance of a PCR assay for the detection of KRAS mutations (codons 12/13 and 61) in formalin-fixed paraffin-embedded tissue samples of colorectal carcinoma. Virchows Arch. doi:10.1007/s00428-011-1180-0

Virchows Arch (2012) 460:131–140
DOI 10.1007/s00428-011-1184-9

ORIGINAL ARTICLE

Nucleic acids from long-term preserved FFPE tissues are suitable for downstream analyses

Natalie Ludyga · Barbara Grünwald · Omid Azimzadeh · Sonja Englert · Heinz Höfler · Soile Tapio · Michaela Aubele

Received: 8 September 2011 / Revised: 27 November 2011 / Accepted: 13 December 2011 / Published online: 22 January 2012
© Springer-Verlag 2012

Abstract Tissues used for clinical diagnostics are mostly formalin-fixed and paraffin-embedded (FFPE) which provides many advantages. However, the quality of the obtained nucleic acids (NA) is reduced and this turns out to be a challenge for further molecular analyses. Although the spectrum of analyses of NA extracted from FFPE tissue has increased, the standard operating procedures for NA isolation from old tissue blocks still need to be improved. Here, we compared the efficiency of different NA extraction methods, using FFPE tissues of variable age and origin, with respect to downstream analyses. Our study showed that the phenol–chloroform isoamyl alcohol (PCI) and the commercial Qiagen protocol yielded samples with highest purity. The PCI protocol delivered the longest amplicons even from samples from the 1970s. We developed a short (1 h) tissue lysis procedure that turned out to be highly time- and cost-effective when DNA quality was tested using single and multiplex PCR. Compared to a 1-day lysis-protocol, the amplicons were only 100 bp shorter. In addition, single-copy genes used in daily routine were successfully amplified from long-term stored FFPE samples following 1-h tissue-lysis. The RNA integrity numbers (RIN) determined on RNA isolated from FFPE tissues indicated degraded RNA; however, all RINs were above the generally agreed threshold of 1.4. We showed that, depending on the purpose of the analysis, NA retrieved from FFPE tissues older than 40 years may be successfully used for molecular analysis.

Keywords Long-term preserved FFPE tissue · DNA · RNA · Rapid tissue lysis · PCR

Natalie Ludyga and Barbara Grünwald contributed equally to this work.

N. Ludyga · B. Grünwald · S. Englert · H. Höfler · M. Aubele (✉)
Institute of Pathology, Helmholtz Zentrum München,
German Research Center for Environmental Health,
Ingolstaedter Landstrasse 1,
85764 Neuherberg, Germany
e-mail: aubele@helmholtz-muenchen.de

O. Azimzadeh · S. Tapio
Institute of Radiation Biology, Helmholtz Zentrum München,
German Research Center for Environmental Health,
Ingolstaedter Landstrasse 1,
85764 Neuherberg, Germany

H. Höfler
Institute of Pathology, Technische Universität München,
Trogerstrasse 18,
81675 Munich, Germany

Introduction

In pathology archives, tissue samples are stored as formalin-fixed paraffin-embedded (FFPE) blocks, a common way to preserve specimens for a longer time period. FFPE tissue is relatively stable for several decades allowing applications for retrospective NA analyses, such as for prediction of therapy response and clinical outcome [1]. The advantages of FFPE tissue include easy handling, long-term cheap storage, suitability for immunohistochemical analyses, and low cost of large-scale application [2, 3]. However, formalin decreases the efficiency of PCR due to protein cross-linking. In addition, the degradation of nucleic acids increases during storage depending on the pH value of the fixative [4]. Nevertheless, due to the worldwide abundance and the associated great potential of diagnostic pathology tissue archives, many groups have used FFPE tissues for nucleic acid extraction and further analysis [5–9]. In recent years, using FFPE specimens of different origin and storage times, a variety of methods for DNA/RNA isolation and subsequent assay have

been developed. It was shown that PCR products between 100 and 300 bp could be generated from FFPE material [8]. Additionally, Gilbert and colleagues [10] reported a multiplex PCR procedure combined with minisequencing for high-throughput SNP typing applicable to 25-year-old FFPE tissue. Epigenetic studies performed with DNA isolated from 30-year-old FFPE tissue have been reported [11].

The scope of the present study was to establish standard operation procedures for DNA and RNA isolation from up to 40-year-old FFPE material in order to determine the quality and quantity of the NA samples obtained. We compared the properties of NA after extraction using commercially available kits from Qiagen (QG) and Norgen (NG) as well as the phenol–chloroform isoamyl alcohol (PCI) protocol. In addition, we developed a rapid lysis method to validate the quality of the FFPE tissue. The extraction protocols were ranked according to the suitability of the extracts for performing PCR and the obtained RIN value (RNA integrity number). For the amplification reaction, primers targeting three house-keeping genes (β-actin, GAPDH, and TBP) and targeting single-copy genes EGFR exon 19 and 21 were applied. The short (1 h) tissue lysis method turned out to be an efficient tool for testing the length of amplifiable fragments. Extractions using the PCI protocol and Qiagen kit resulted in the highest purity of NA. Furthermore, the longest PCR fragments and the highest RIN values from about 40-year-old FFPE materials were achieved by PCI extraction.

Materials and methods

Cellular material

NA were extracted from the following materials: (1) FFPE breast cancer specimens stored between 10 and 40 years (originating from three different pathology institutes); FFPE and frozen human colon tissue from the same patient from 2002; immortalized T47D breast cancer cells isolated from fresh cell culture; (2) T47D FFPE blocks fixed in formalin at pH 7 and pH 4.

For NA extraction, we used three 8-μm-thick sections of archival FFPE blocks, six 8-μm-thick sections of T47D cell blocks, 40 8-μm-thick sections of frozen colon tissue, or 5×10^6 freshly prepared T47D cells.

Preparation of FFPE blocks from T47D breast cancer cell line

T47D breast cancer cells were cultured in RPMI-1640 medium (Sigma-Aldrich, Steinheim, Germany) supplemented with 10% fetal bovine serum "Gold" (PAA Laboratories, Cölbe, Germany), 10 μg/ml bovine pancreas insulin (Sigma-Aldrich), and 1% penicillin–streptomycin (10,000 U/ml from Invitrogen, Darmstadt, Germany) at 37°C and 5% CO_2 in a humidified incubator. The FFPE T47D cell blocks were prepared as described previously with some modifications [12]. Briefly, 2×10^6 T47D cells were harvested and washed twice with D-PBS (Dulbecco's PBS, Gibco®, Invitrogen, Darmstadt, Germany). The pellet was resuspended in human plasma, before adding bovine thrombin (both from Sigma-Aldrich, Schnelldorf, Germany), and mixed immediately. The pellets were left for several minutes to agglomerate, brought into biopsy capsules (Leica, Nussloch, Germany), and subsequently fixed in 4% phosphate-buffered formaldehyde at pH 7 or at pH 4 for 16 h. Pellets were dehydrated and embedded in paraffin using a tissue processor (Sakura Tissue-Tek VIP from GMI Inc., Ramsey, USA).

Isolation of NA

The tissue section, which was used for extraction, was hematoxylin and eosin stained, scanned, and the area measured with the polygon tool (dotSlide 2.0, slide scanner; Olympus Deutschland GmbH, Hamburg, Germany). The area varied in size about 30-fold (between 0.26 cm^2 and 7.53 cm^2) due to different tissue or cell amounts, origins (breast or colon), and tumor size within the blocks. Deparaffinization of the FFPE sections was performed in Eppendorf tubes using xylene, followed by descending ethanol series. After final centrifugation and removing the supernatant, tubes were left open (10 min) for evaporation of residual ethanol. For NA extraction, two commercially available kits (Qiagen and Norgen) or the phenol–chloroform isoamyl alcohol extraction protocol were used. NA were isolated three times for DNA and two times for RNA using the different protocols. For comparison of the NA yields from three different extraction methods, a three-times-standard deviation was calculated [13]. All NA yields outside this range were considered significantly different and marked in Fig. 1 with an asterisk.

NA isolation from FFPE material using qiagen kit (QG)

DNA was extracted using the QIAamp DNA FFPE tissue kit (#56404; Qiagen, Hilden, Germany) according to manufacturer's instructions, with the following modifications: after 3 h of lysis with 40 μl proteinase K (20 mg/ml, Roche, Mannheim, Germany), 2 μl 100 mg/ml DNase-free RNase A (Qiagen) was added and the mixture was incubated for 2 min at room temperature before adding buffer AL. DNA was eluted with 30 μl TE buffer (10 mM Tris, 1 mM EDTA). RNA was extracted using the RNeasy FFPE kit (#74404; Qiagen) according to the manufacturer's instructions. RNA was eluted with 25 μl ultra-pure water and immediately supplemented with RNase Inhibitor (RiboLock™, Fermentas, St. Leon-Rot, Germany). For 1-h lysis–PCR,

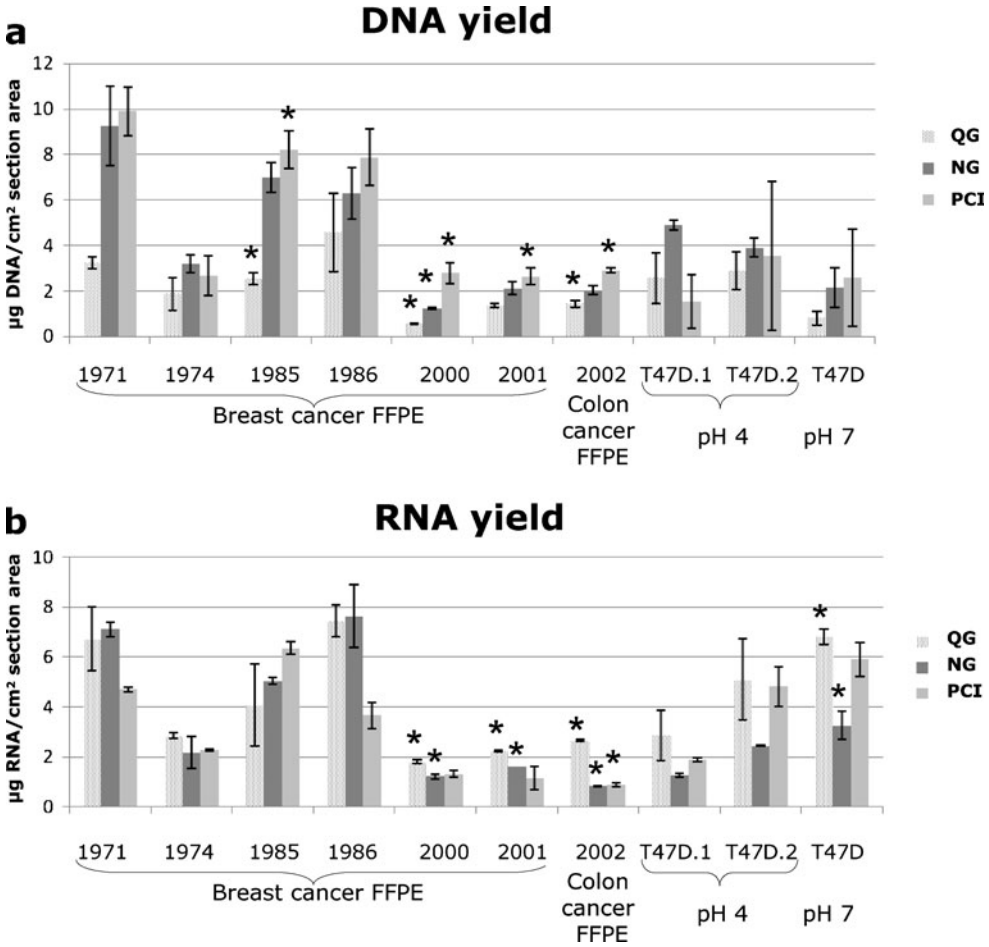

Fig. 1 Histograms showing total DNA (**a**) and RNA (**b**) amounts, respectively. Yield for each extraction method from all 10 FFPE blocks normalized by the actual tissue area measured in a subsequent section. Nucleic acids have been extracted with the Qiagen kit (*QG*), the Norgen Kit (*NG*), and a phenol–chloroform isoamyl alcohol protocol (*PCI*), and NA yields were determined spectrophotometrically. NA amounts, which are significantly different from the other extraction methods in terms of ±3-times-SD, are marked by *asterisks*

PCR-ready lysis solution (see PCI protocol) was used instead of the ATL buffer, followed by DNA purification via Qiagen silica columns.

NA isolation from FFPE material using norgen (NG)

The FFPE RNA/DNA purification kit (#25000; Norgen Biotek, Ontario, Canada) was used according to the manufacturer's instructions. After 1 h of lysis, 31 µl (10%) of the lysate was taken, heat-inactivated (10 min, 95°C), and used as PCR template. With the remaining lysate, incubation was continued as indicated in the manufacturer's protocol (1-day lysis). An additional RNA digestion step was introduced before adding binding solution (as described above). Lysis was carried out for 24 h for DNA and 3 h for RNA. DNA was eluted with 40 µl TE buffer and RNA with 25 µl ultra-pure water, and immediately supplemented with RNase Inhibitor (RiboLock™, Fermentas).

NA isolation from FFPE material using phenol–chloroform isoamyl alcohol (PCI)

The following PCR-ready lysis buffer was used for DNA and RNA extraction: 40 mM Tris, 1 mM EDTA (Sigma-Aldrich) and 0.5% Tween-20 (Carl Roth, Kalsruhe, Germany) in ultra-pure water. Deparaffinized and dried cell pellets were resuspended in 200 µl PCR-ready lysis solution, and 50 µl proteinase K was added. For extraction of DNA, samples were incubated under constant agitation (60°C, 1 h), vortexed, and 25 µl (10%) lysate was retained, heat-inactivated, and used as PCR template (1-h lysis). Lysis of the remaining sample was continued (1-day lysis). After heat inactivation of proteinase K (10 min, 90°C), 2 µl RNase A was added to each sample as described above. An equal volume of phenol–chloroform isoamyl alcohol solution (25:24:1) was added to the sample, vortexed, and centrifuged. Upper phases were transferred into new tubes and an equal volume of chloroform (EMSURE® by Merck, Darmstadt, Germany) was added, vortexed, and centrifuged. Upper phases were transferred into new tubes, 0.1 vol of 3 M sodium acetate pH 5.5 (Ambion, Austin, USA) was added, and tubes were vortexed before addition of 1 vol of isopropanol followed by precipitation of DNA (−20°C, overnight). The precipitated DNA was centrifuged, supernatants were removed, and pellets were washed twice with 70% ethanol. Then, pellets were dried at 35°C, 40 µl TE buffer was added, and tubes were heated (1 h, 45°C) for complete solubilization. For extraction of RNA, samples were incubated under constant agitation (55°C, 2 h), 0.1 vol of

3 M sodium acetate pH 4.0 was added, vortexed, and after addition of an equal volume of phenol–chloroform isoamyl alcohol solution, samples were incubated (4°C, 15 min). The following centrifugation led to separation of two phases, of which the upper was transferred into a new tube, mixed with an equal volume of chloroform, and again centrifuged. Then, the upper phase was transferred into a new tube, and 1 μl glycogen and 1 vol of isopropanol were added. RNA was precipitated (−20°C, overnight), then centrifuged and washed twice with 70% ethanol. Pellets were dried at 35°C, 25 μl ultra-pure water was added, and all tubes were heated (15 min, 55°C) for complete solubilization.

NA extraction from frozen tissue and T47D cells

Extraction of DNA and RNA from frozen colon tissue (25 mg of 8-μm tissue section) and from 5×10^6 fresh T47D cells was performed using the QIAamp DNA Mini Kit and the RNeasy Mini Kit (#51304 and #74104; Qiagen), respectively, according to the manufacturer's instructions. Purified DNA was eluted twice with 200 μl TE buffer and stored at −20°C. Purified RNA was eluted with 50 μl ultra-pure water and supplemented with RNase inhibitor.

Spectrophotometrical measurements

The total amounts of NA obtained with the three 1-day lysis extraction methods were measured using a spectrophotometer (NanoDrop ND-100; PEQLAB Biotechnologie, Erlangen, Germany). The amount of DNA obtained after 1-h lysis could not be spectrophotometrically determined due to sample consistency. For each sample, DNA and RNA concentrations, OD ratio 260/280 nm indicating protein contamination, and OD ratio 260/230 nm, indicating contamination with solvents, salts, and organic compounds, were determined in triplicate.

Microcapillary electrophoretic RNA separation

RNA degradation and RNA integrity numbers (RINs) for double RNA extractions with each method from each block were determined (Agilent 2100 Bioanalyzer; Agilent, Santa Clara, USA) according to the manufacturer's instructions after additional denaturation of the ladder (2 min, 70°C) before use. RNA (500 ng/μl) was diluted in RNase-free ultra-pure water. The software automatically generates the ratio of the 18S and 28S rRNA and a RNA integrity number (RIN) from 1 to 10, based on the entire electrophoretic trace of a sample. An RNA sample with RIN 1 is considered to be completely degraded, whereas RIN 10 indicates intact RNA [14]. A RIN above the minimum acceptable value of 1.4 is considered as still useful for analysis [15]. The average RNA quality is expressed as the average RIN ± standard deviation.

PCR-based assays

To assess the length of the maximum amplifiable PCR fragment, 10 primer pairs targeting three different human house-keeping genes [β-actin, GAPDH, and the TATA box binding protein (TBP), see Table 1] were designed for the amplification of fragments with an increasing length between 100 bp and 1,338 bp. The four primer pairs for the shortest fragments were used in a multiplex PCR, generating simultaneously 100, 150, 200, and 300 bp long fragments. For the amplification of EGFR exon 19 and exon 21, four primers (Table 1) and PCR conditions as published [16] were used. The PCR master mix contained 1.16× reaction buffer for BioThermAB™ Hot Start Taq DNA Polymerase (Ares Bioscience, Köln, Germany) and 232 μM of each dNTP (dNTP set, 4×100 μmol; Fermentas). For every PCR reaction after 1-day lysis, 1 μl of extract (100 ng/μl) and after 1-h lysis also 1 μl of lysate (concentration could not be determined) were used as templates. All other PCR reactions were performed under identical conditions: initial denaturation (4 min, 94°C), followed by 35 cycles of denaturation (1 min, 94°C), annealing (1 min, 64°C), elongation (1 min, 72°C), and a final elongation (7 min, 72°C). The PCR products were visualized by 1% agarose gel electrophoresis and stained with ethidium bromide.

Results and discussion

The NA amount depended on the isolation method and on FFPE material age

In spite of the many advantages formalin fixation of tissue samples for diagnostic purposes has to offer [2, 3], the use of FFPE material for molecular analysis remains problematic. While the tissue morphology is well preserved, the degradation of nucleic acids continues, in particular due to a time-dependent decrease of pH [4].

The correlation between the pH and NA quality was also observed in our study. The amount of DNA, after isolation with the PCI protocol, was higher than with the (commercially available) kits. However, the PCI extraction resulted in a higher variation in DNA yield between the three replicates (Fig. 1a). This outcome is associated with a DNA loss in silica columns and several processing steps, typical for conventional isolation methods, which is furthermore influenced by particularities of the used laboratory protocol. In Fig. 1a and b, the NA amounts, which are significantly different from the other extraction methods in terms of ±3-times-SD, are marked by asterisks.

We observed that the age and origin of the FFPE sample influenced the isolation efficiency. However, the DNA yield from 40-year-old FFPE material was relatively high in comparison to FFPE material, a 10-year-old block. Interestingly,

Table 1 Sequences and names of primers used for single and multiplex PCR, amplicon length (bp), and corresponding number. Sequences for the last four primers for the amplification of exon 19 and exon 21 of EGFR were used as published before [16] *F* forward, *R* reverse

Primer name	Primer sequence in 5′–3′ orientation	Amplicon length (bp)	Number/name
TBP-100 F TBP-100R	AACTTCGCTTCCGCTGGCCC AGTGCAGTGGTGGCCTTCGC	100	1
ACTB-142 F ACTB-142R	CCTGTGTTATCTTGGAGGTCCCCTGAAG ACCGTAGAGTGGTCACTCAATGAAG	142	2
GAPDH-200 F GAPDH-200R	GGGAAGTCAGGTGGAGCGAGGC TTGCGGTGGAAATGTCCTTTTCCAACTACC	200	3
ACTB-307/968 F ACTB-307R	CTTGAGGAGGTGGGAAGGGACTATTTGG CCCCTACCCCAACTTGACTTTGATTCCA	307	4
ACTB-411 F ACTB-411R	AAGTTCCCAAGCACAGAAGAGAACCTGT CTTCCTAGTGCTCTCCTATGCACCCTTC	411	5
GAPDH-500 F GAPDH-500R	GAAAAGGACATTTCCACCGCAAAATGGC GGTCAGAAATTAACTGGACAGGGCAAGC	500	6
GAPDH-687 F GAPDH-687R	ATTAGCCCAGTTTCATGCAGCAGAGAGA GGTGACTCAGCAGAGAAGACTTGAGGAG	687	7
GAPDH-781 F GAPDH-781R	AAAATCGGTAAAAATGCCCACCTCGCAT ATCAGCTAAAGATGTGCTTCCTCCGTGT	781	8
ACTB-968R	CTTCAGGGGACCTCCAAGATAACACAGG	968	9
ACTB-1338 F ACTB-1338R	CTGTGGCATCCACGAAACTACCTTCAAC CCAAATAGTCCCTTCCCACCTCCTCAAG	1338	10
EGFR-E19F EGFR-E19R	CGTCTTCCTTCTCTCTCTGT CCACACAGCAAAGCAGAAAC	148	Exon 19
EGFR-E21F EGFR-E21R	CCAGGAACGTACTGGTGAAA TGACCTAAAGCCACCTCCTT	129	Exon 21

the DNA amount derived from freshly prepared FFPE block fixed at pH 4, a pH value typical for long-term stored FFPE material, was reasonably good and higher than from samples from recent years (Fig. 1a). Furthermore, the composition of tissue samples differs in relation to tissue composition, such as inflammatory cells and parenchymal cells, resulting in differences in cell density and therefore different NA amounts in a given tissue surface area.

The RNA yield between the three isolation methods showed more consistency than for that for DNA; consequently, the determined standard deviation for respective replicates was lower than for DNA (Fig. 1b). The RNA amount isolated from older FFPE samples was slightly higher than that from tissues from recent years. The RNA yield from freshly prepared T47D cell blocks, fixed at pH 7, was much higher than the DNA amount obtained from the same sample, probably due to the isolation of RNA from exponentially growing cells cultivated at optimal conditions. In general, the NA yield depended on the origin of individual tissue blocks: breast cancer tissue fixed in 1971 or 1985 yielded higher NA amounts than breast cancer fixed in 2001 or fresh T47D cell blocks (fixed at pH 4) (Fig. 1a, b). As the exact fixation and storage conditions for archival samples are normally not known, we suppose that the variation of the NA content is due to variations in tissue condition and preservation between individual samples. This hypothesis is in accordance with the study by Bonin et al. [5] comparing different isolation protocols using colon, ovarian, and lung cancer tissues that showed variable NA yields.

The highest NA purity was obtained with PCI protocol and qiagen kit

The highest purity for DNA was obtained using PCI and Qiagen protocols (Fig. 2a). Only five out of all 30 DNA isolates using Norgen or Qiagen protocols did not reach the threshold of 1.8 (OD 260/280), indicating high protein contamination. Generally, using the Norgen protocol resulted in lysates highly contaminated with organic compounds and solvents (Fig. 2b, OD 260/230), and this method therefore should not be used for isolation of high purity NA using FFPE tissue.

Concerning the purity of RNA, all OD 260/280 values exceeded the threshold of 1.8, the lowest value being 1.83 and the highest 2.03, indicating low protein contamination (Fig. 2c). The OD 260/230 values of the Qiagen and PCI RNA lysates were above the threshold of 1.8, indicating that the RNA lysates were relatively pure (Fig. 2d). RNA isolated using the Norgen protocol showed low purity and was highly contaminated with salts, solvents, or organic compounds.

In summary, for both DNA and RNA, lysates obtained using PCI and Qiagen methods showed the highest purity. Our results confirmed previously published data showing satisfactory results for the Qiagen kits for extraction of DNA or RNA from FFPE tissue [11].

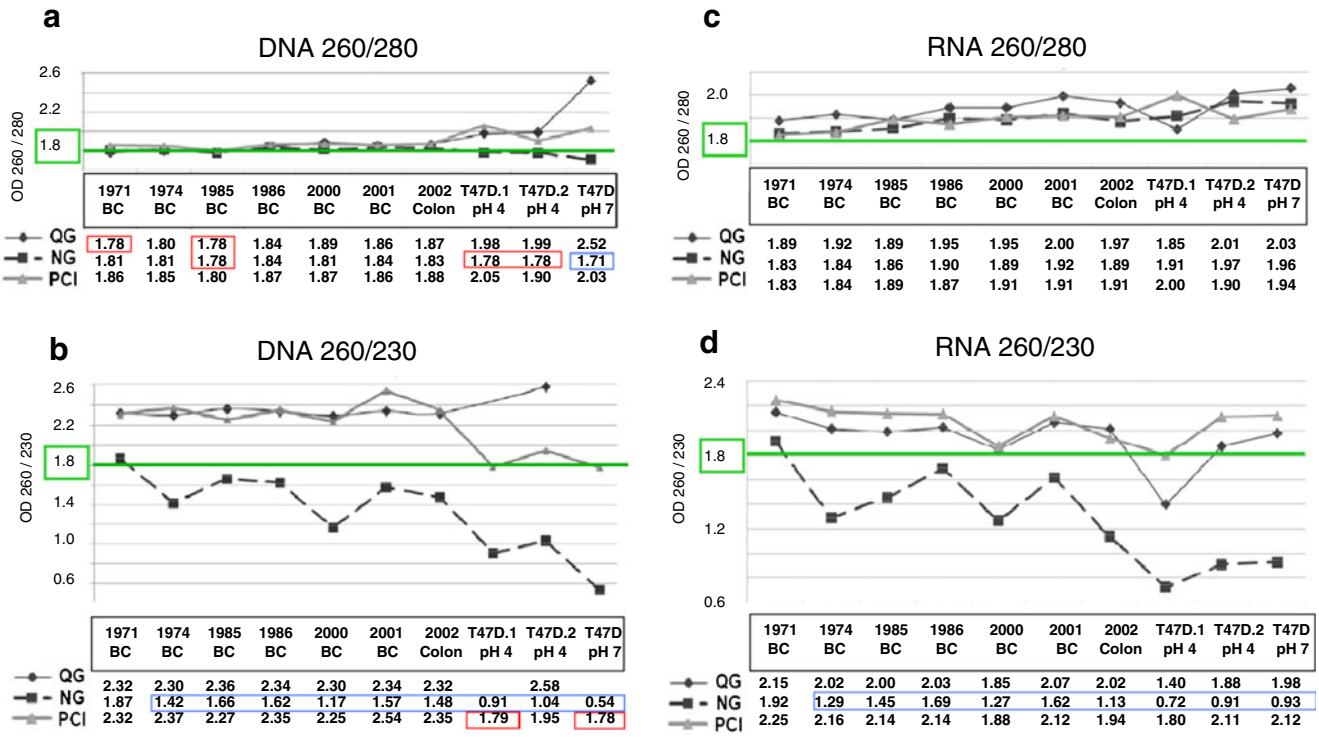

Fig. 2 Plots and tables of the OD 260/280 and OD 260/230 values for DNA (**a**, **b**) and RNA (**c**, **d**) for each extraction method from all 10 FFPE tissue blocks. Nucleic acids have been extracted with the Qiagen kit (*QG*), the Norgen kit (*NG*), or the phenol–chloroform isoamyl alcohol protocol (*PCI*), and OD values were determined spectrophotometrically. The threshold of 1.8 is marked; isolates which undermatch the threshold are framed in *red* (strongly—*blue frame*)

RNA isolated from FFPE tissue is highly degraded but still useful

For the assessment of RNA length, RIN (RNA integrity number) values for all isolates were established. RIN value of 1 indicates completely degraded RNA, whereas RIN value of 10 indicates intact RNA. A RIN value of 1.4 was considered as a minimum for successful execution of further analyses, such as RNA expression arrays [14, 15]. In all our samples, regardless of extraction methods and age of the sample, RIN values higher than 1.4 were achieved. No big differences were detected between the used extraction methods using the same breast cancer tissue (Fig. 3a). The Qiagen protocol was used for frozen colon tissue, the corresponding FFPE tissue as well as for fresh T47D cells (Fig. 3b). Here, the determined RIN for freshly prepared T47D cells was 10. RNA isolated from frozen colon tissue had a RIN value of 8.7, whereas the corresponding FFPE colon tissue had a value of 2.20. In Fig. 3c, an overview of all average RIN values per sample according to extraction method is shown. The average RIN values of FFPE tissue from 1971 to 2002 varied between 1.80 and 3.65, obtained after Qiagen extraction, between 2.3 and 2.5 after Norgen extraction and between 2.3 and 2.7 after PCI extraction. For frozen colon tissue from 2002 and fresh T47D cells, higher RIN values of 8.03 and 10, respectively, were obtained.

In general, independent from the extraction protocol, all FFPE samples showed a high level of degradation, confirming earlier studies [15, 17]. The high fragmentation of RNA from FFPE material is highly associated with the addition of methylol groups by formalin during fixation [9, 18, 19]. In comparison to DNA, RNA is more susceptible to degradation as it is a single strand. However, all samples showed RIN values higher than 1.4 and could be thus used for further analysis.

Fragmentation of genomic DNA increases with the age of FFPE material

As shown in Fig. 4a, DNA smear caused by fragmentation was detected in all three individually extracted samples using the same block. Similarly different FFPE samples, including the recently prepared blocks from the T47D cells fixed at pH 4, showed a different degree of DNA fragmentation. In contrast, isolates from the T47D cell block, fixed in formalin at pH 7, showed high molecular weight DNA (Fig. 4a). Therefore, the size of DNA fragments seemed not only to be influenced by the age or the pH value decrease during the storage but also by variations in the sample preparation methods. The latter is demonstrated in Fig. 4a in which samples from breast cancer (from year 2000) and colon cancer (from year 2002) showed a DNA smear and a

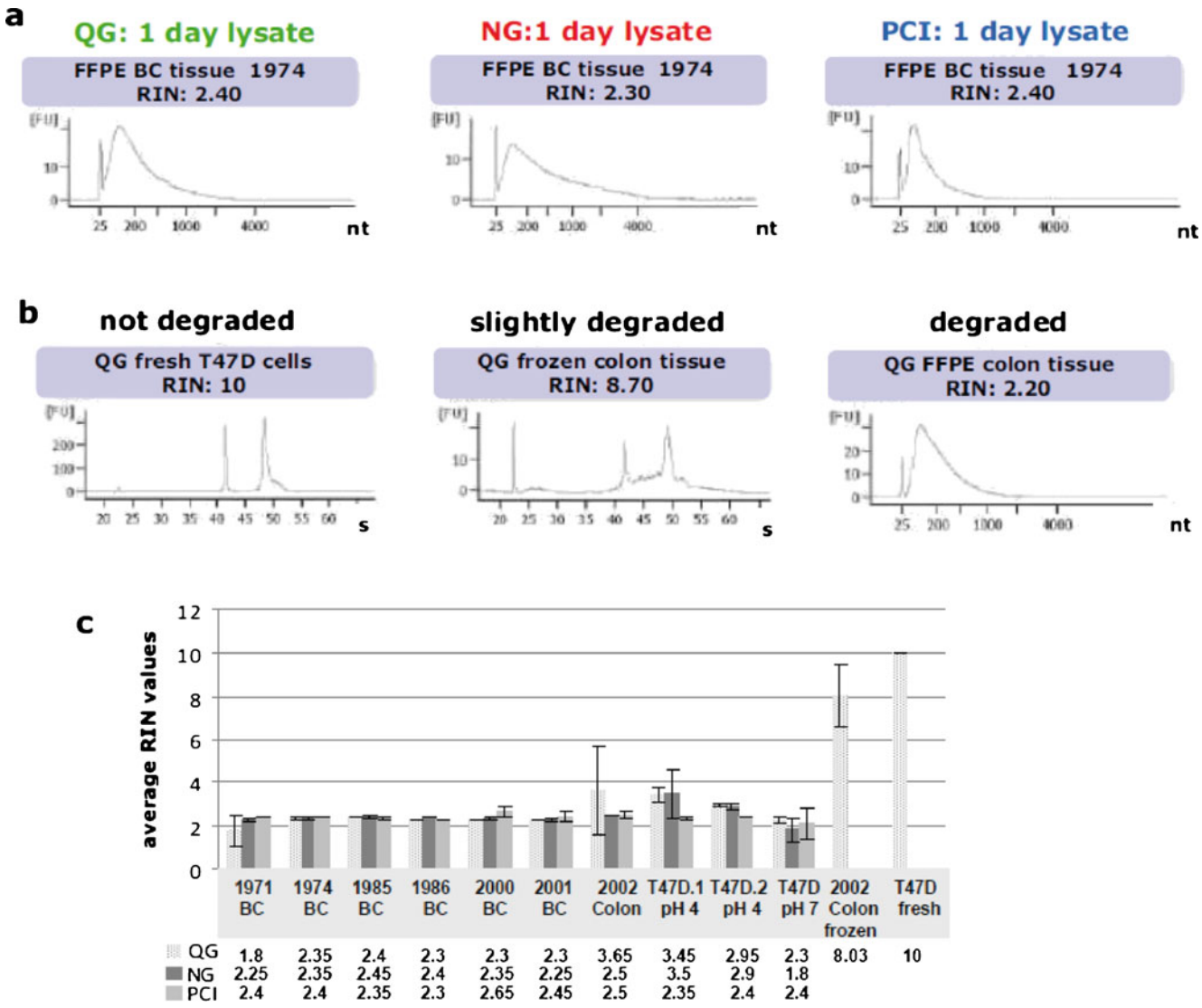

Fig. 3 Representative electropherogram curves from selected samples. **a** No difference between the different extraction methods, applied on a breast cancer (*BC*) FFPE tissue block from 1974. **b** RNA degradation shown by the electropherogram curve: *not degraded*: two distinct and sharp peaks at around 41 seconds (*s*) and 47 seconds correspond to the 18S and 28S rRNA, *slightly degraded*: a raised baseline along with less distinct 18S and 28S rRNA peaks and broad peaks between 25 and 200 nucleotides (*nt*) indicate small, degraded RNA products and tRNA in the frozen colon tissue, and *degraded*: the absence of 18S and 28S rRNA peaks shows a complete degradation of the RNA in the corresponding FFPE colon tissue sample, dependent on the degree of fragmentation the software shifts to a different scaling, e.g., from (s) to (nt). **c** Plot and table with the average RIN values per block or material for all 10 FFPE tissue blocks, frozen colon tissue, and fresh T47D cells. All extractions were carried out in duplicate, except from frozen colon tissue (*Colon frozen*) and fresh T47D cells, where extractions were carried out in triplicate. In the block "*1986 BC*", only one RIN value could be determined

band of high molecular DNA, whereas breast cancer sample of similar age (2001) only showed a degraded DNA smear.

In general, DNA fragmentation was strongly associated with the storage time: the older the FFPE sample the shorter the fragments, as shown in Fig. 4a. DNA fragmentation was compared between DNA isolated from freshly prepared T47D cells, recently prepared T47D FFPE blocks, and over 5-year-old T47D FFPE blocks. High molecular weight DNA was detected in fresh T47D cells and in recently prepared T47D FFPE cell blocks, while over 5-year-old T47D FFPE blocks yielded only a degraded DNA smear (Fig. 4b).

No significant differences were observed between the three different protocols for DNA isolation. Huang et al. [20] detected fragment sizes between 15 and 30 kb of extracted DNA from FFPE tissue. These results are comparable with freshly prepared FFPE material also tested by us as shown in Fig. 4b.

1-h lysis–PCR of FFPE material is a rapid novel method to validate DNA quality

To obtain information about the quality of DNA from long-term preserved FFPE tissue blocks using a rapid and low-

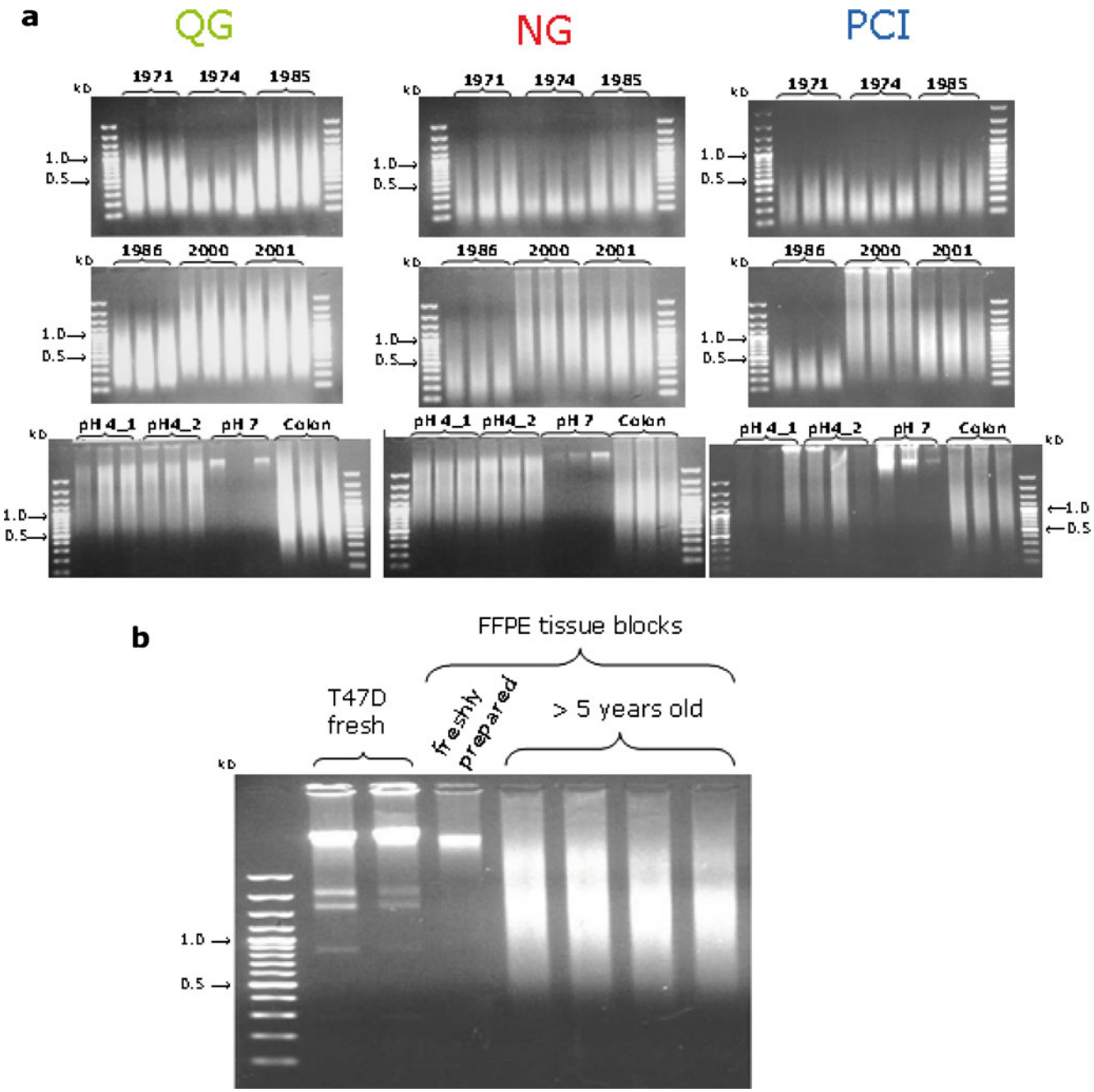

Fig. 4 Fragmentation of DNA extracted from different samples. **a** 1 μg genomic DNA from three individual extraction approaches per block were loaded on an agarose gel. From T47D cell line, two blocks were fixed in formalin pH 4; one was fixed in formalin pH 7. The used extraction protocols were Qiagen kit (*QG*), Norgen kit (*NG*), and phenol–chloroform isoamyl alcohol extraction (*PCI*). **b** 1 μg genomic DNA from fresh T47D cells, from recently prepared FFPE fixed, and from over 5-year-old FFPE T47D cell blocks (FFPE, >5 years old) were loaded

cost protocol, we tested a short (1 h) tissue lysis method using PCR as an endpoint (1-h lysis–PCR). Ten different primer pairs targeting three house-keeping genes (β-actin, GAPDH, and TBP) were used, resulting in amplified sequences varying in length between 100 bp and 1,338 bp. Amplification results were compared to PCR amplification data obtained after continued overnight lysis and subsequent purification steps (1-day lysis–PCR).

In Fig. 5a, representative examples are shown for PCR products obtained using the PCI method combined with 1-h lysis–PCR or 1-day lysis–PCR from breast cancer FFPE tissue from 1986 and from a FFPE T47D cell block, fixed at pH 7. The amplifications were performed in triplicate and the results indicate that the maximum amplifiable PCR fragment from the 1986 sample after 1-h lysis was 300 bp (lane 4). From the respective 1-day lysis–PCR, an additional

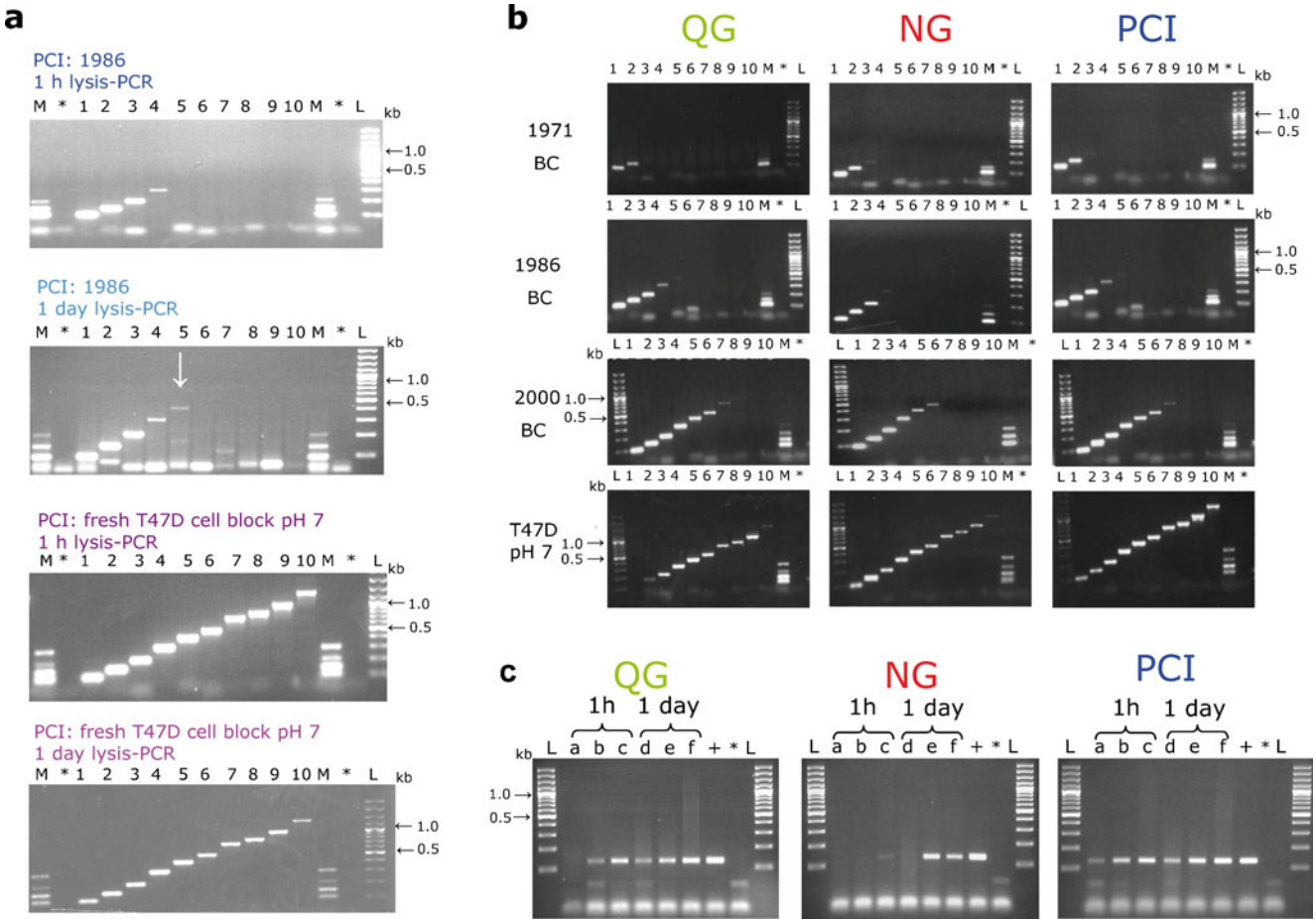

Fig. 5 Maximum amplifiable PCR products from DNA extracted from different FFPE samples. **a** Representative examples of PCR fragments obtained after 1-h lysis–PCR and after 1-day lysis–PCR with DNA isolated with PCI protocol. *M* multiplex PCR, *L* ladder, * negative control. Numbers *1–10* indicate fragment lengths shown in Table 1; *white arrow* indicates the 411 bp fragment. **b** Comparison of maximum amplifiable PCR products obtained after DNA extractions from different breast cancer (*BC*) FFPE tissues and T47D cells using the three different protocols and followed PCR (1-day lysis–PCR). **c** Examples of amplifications of 129 bp long EGFR exon 21 using three different protocols for 1-h and 1-day lysis, *a* lysate from 1971, *b* from 1986, *c* from 2000, *d* extract from 1971, *e* from 1986, *f* from 2000. +: positive control

weak 411 bp long PCR fragment was obtained (indicated by an arrow in Fig. 5a, lane 5). The 1-h lysis–PCR using PCI protocol generally yielded longer PCR fragments than the 1-h lysates from the Norgen or Qiagen kit, in particular with DNA derived from older FFPE samples (data not shown). The 1-day lysis–PCR results were highly comparable between the methods, although the maximum amplifiable DNA fragments were generated using the PCI protocol.

In Fig. 5b, examples of 1-day lysis–PCR assays using the three protocols are shown. The results confirm that the older the FFPE samples the shorter the DNA fragment size. DNA templates isolated with the PCI protocol resulted in longer PCR fragments than the silica column-based Norgen and Qiagen kits, probably due to the higher sensitivity and better DNA yield of the former method. Using the PCI protocol, weak bands of high molecular DNA were sometimes detected (Fig. 4a).

Importantly, our novel 1-h lysis–PCR method gave similar maximum fragment lengths amplified from long-term stored FFPE tissue as reported previously [6, 8]. Furthermore, in addition to the single PCR assays, multiplex PCR using four primer pairs for amplification of fragments between 100 bp and 300 bp was successfully performed using 1-h lysis–PCR method, although the 1-day lysis–multiplex PCR led to somewhat longer fragments (100 bp) with respective lysates (Fig. 5a, b). This is an efficient test to determine maximum amplifiable DNA after 1-h tissue lysis.

Furthermore, amplification of EGFR exon 19 and exon 21 from FFPE samples was performed using PCR published previously [16]. To demonstrate that 1-h lysates can be used for the amplification of single copy genes, these target regions were selected as representative targets in daily routine analysis. Representative examples of amplification of EGFR exon 21 from DNA obtained after 1-h and 1-day lysis using three protocols are illustrated in Fig. 5c. Here, 129 bp

long PCR fragments were generated even from 1-h lysates after DNA isolation from FFPE tissue from 1971 following PCI and QG protocol. The NG protocol was less effective in comparison to PCI and QG protocol. These PCR results are in agreement with our PCR results obtained by amplification of house-keeping genes, indicating that the PCI and QG protocols are most effective for DNA isolation and subsequent PCR. Furthermore, 1-h tissue lysis is as efficient as 1-day lysis for successful amplification of single copy genes even from over 40-year-old FFPE tissue samples.

In conclusion, fixation and storage conditions may make FFPE material unsuitable for further analysis. The development of tests for the prediction of therapy response makes it crucial to exploit available FFPE tissue banks using standard techniques. We established standard operation procedures for DNA/RNA isolation from long-term preserved FFPE tissue which can be routinely used in molecular diagnostic laboratories. We identify advantages and disadvantages of different methods. The Qiagen method and the PCI protocol resulted in highly pure nucleic acid samples. The maximum PCR amplicons were achieved after DNA extraction using the PCI protocol. However, this method, due to more preparatory steps, showed higher variation between the replicates. Importantly, an efficient novel method for tissue lysis and NA amplification (1-h lysis–PCR) and a multiplex PCR were established as a tool for rapid validation of the quality of DNA derived from long-term preserved FFPE tissue. As this approach delivered most relevant information on DNA quality, it might replace other more time-consuming and expensive isolation protocols.

Acknowledgments The authors thank Nina Weber and Katrin Lindner for great technical assistance. This work was supported by a grant from the European Community's Seventh Framework Programme (FP7, EURATOM) contract no. 232628 (STORE—Sustaining access to Tissues and data frOm Radiobiological Experiments).

Conflict of interest The authors declare that they have no conflict of interest.

References

1. Abrahamsen HN, Steiniche T, Nexo E, Hamilton-Dutoit SJ, Sorensen BS (2003) Towards quantitative mRNA analysis in paraffin-embedded tissues using real-time reverse transcriptase–polymerase chain reaction: a methodological study on lymph nodes from melanoma patients. J Mol Diagn 5:34–41
2. Kayser K, Stute H, Lübcke J, Wazinski U (1988) Rapid microwave fixation—a comparative morphometric study. Histochem J 20:347–352
3. Perlmutter MA, Best CJ, Gillespie JW, Gathright Y, González S, Velasco A, Linehan WM, Emmert-Buck MR, Chuaqui RF (2004) Comparison of snap freezing versus ethanol fixation for gene expression profiling of tissue specimens. J Mol Diagn 6:371–377
4. Gilbert MT, Haselkorn T, Bunce M, Sanchez JJ, Lucas SB, Jewell LD, Van Marck E, Worobey M (2007) The isolation of nucleic acids from fixed, paraffin-embedded tissues—which methods are useful when? PLoS One 2:e537
5. Bonin S, Hlubek F, Benhattar J, Denkert C, Dietel M, Fernandez PL, Höfler G, Kothmaier H, Kruslin B, Mazzanti CM et al (2010) Multicentre validation study of nucleic acids extraction from FFPE tissues. Virchows Arch 457:309–317
6. Huijsmans CJ, Damen J, van der Linden JC, Savelkoul PH, Hermans MH (2010) Comparative analysis of four methods to extract DNA from paraffin-embedded tissues: effect on downstream molecular applications. BMC Res Notes 3:239
7. Torrente MC, Ríos C, Misad C, Ramírez R, Acuña M, Cifuentes L (2010) DNA extraction from formalin-fixed laryngeal biopsies: comparison of techniques. Acta Otolaryngol 131:330–333
8. Bonin S, Petrera F, Niccolini B, Stanta G (2003) PCR analysis in archival postmortem tissues. Mol Pathol 56:184–186
9. Jacobson TA, Lundahl J, Mellstedt H, Moshfegh A (2011) Gene expression analysis using long-term preserved formalin-fixed and paraffin-embedded tissue of non-small cell lung cancer. Int J Oncol 38:1075–1081
10. Gilbert MT, Sanchez JJ, Haselkorn T, Jewell LD, Lucas SB, Van Marck E, Børsting C, Morling N, Worobey M (2007) Multiplex PCR with minisequencing as an effective high-throughput SNP typing method for formalin-fixed tissue. Electrophoresis 28:2361–2367
11. Kristensen LS, Wojdacz TK, Thestrup BB, Wiuf C, Hager H, Hansen LL (2009) Quality assessment of DNA derived from up to 30 years old formalin fixed paraffin embedded (FFPE) tissue for PCR-based methylation analysis using SMART-MSP and MS-HRM. BMC Cancer 9:453
12. Koch I, Slotta-Huspenina J, Hollweck R, Anastasov N, Höfler H, Quintanilla-Martinez L, Fend F (2006) Real-time quantitative RT–PCR shows variable, assay-dependent sensitivity to formalin fixation: implications for direct comparison of transcript levels in paraffin-embedded tissues. Diagn Mol Pathol 15:149–156
13. Pukelsheim F (1994) The three-sigma-rule. Am Stat 48:88–91
14. Schroeder A, Mueller O, Stocker S, Salowsky R, Leiber M, Gassmann M, Lightfoot S, Menzel W, Granzow M, Ragg T (2006) The RIN: an RNA integrity number for assigning integrity values to RNA measurements. BMC Mol Biol 7:3
15. Ribeiro-Silva A, Zhang H, Jeffrey SS (2007) RNA extraction from ten year old formalin-fixed paraffin-embedded breast cancer samples: a comparison of column purification and magnetic bead-based technologies. BMC Mol Biol 8:118
16. Tomizawa Y, Iijima H, Sunaga N, Sato K, Takise A, Otani Y, Tanaka S, Suga T, Saito R, Ishizuka T, Dobashi K, Minna JD, Nakajima T, Mori M (2005) Clinicopathologic significance of the mutations of the epidermal growth factor receptor gene in patients with non-small cell lung cancer. Clin Cancer Res 11:6816–6822
17. Jarzab M, Rózanowski P, Kowalska M, Zebracka J, Rudnicka L, Stobiecka E, Jarzab B, Stachura J, Pawlega J (2008) Optimization of the method of RNA isolation from paraffin blocks to assess gene expression in breast cancer. Pol J Pathol 59:85–91
18. Masuda N, Ohnishi T, Kawamoto S, Monden M, Okubo K (1999) Analysis of chemical modification of RNA from formalin-fixed samples and optimization of molecular biology applications for such samples. Nucleic Acids Res 27:4436–4443
19. von Smolinski D, Leverkoehne I, von Samson-Himmelstjerna G, Gruber AD (2005) Impact of formalin-fixation and paraffin-embedding on the ratio between mRNA copy numbers of differently expressed genes. Histochem Cell Biol 124:177–188
20. Huang WY, Sheehy TM, Moore LE, Hsing AW, Purdue MP (2010) Simultaneous recovery of DNA and RNA from formalin-fixed paraffin-embedded tissue and application in epidemiologic studies. Cancer Epidemiol Biomarkers Prev 19:973–977

Virchows Arch (2012) 460:141–149
DOI 10.1007/s00428-011-1180-0

ORIGINAL ARTICLE

Analytical performance of a PCR assay for the detection of KRAS mutations (codons 12/13 and 61) in formalin-fixed paraffin-embedded tissue samples of colorectal carcinoma

Sung Lee · Victoria H. Brophy · Jianli Cao · Margot Velez · Corey Hoeppner · Stephen Soviero · H. Jeffrey Lawrence

Received: 3 October 2011 / Revised: 22 November 2011 / Accepted: 28 November 2011 / Published online: 16 December 2011
© The Author(s) 2011. This article is published with open access at Springerlink.com

Abstract KRAS mutation testing is mandatory before prescribing anti-epidermal growth factor monoclonal antibodies in the treatment of advanced colorectal cancer. We describe the performance of a TaqMelt polymerase chain reaction (PCR) assay—the cobas® KRAS Mutation Test—designed to detect 19 mutations in codons 12, 13, and 61. The limit of detection was determined using DNA blends from cell lines, plasmids, and formalin-fixed paraffin-embedded tissue specimens. Assay performance was compared to Sanger sequencing using a panel of 188 specimens. Discordant specimens were subjected to next generation pyrosequencing (454). Assay repeatability was assessed using a panel of six specimens. A >95% correct mutation call rate was obtained in all specimen types with ~5% mutant alleles at DNA inputs of 0.8–6.3 ng per PCR reaction; 100% detection rate was observed at the recommended DNA input of 50 ng. The positive percent agreement with Sanger was 97.5% (79/81) for codons 12/13 and 85.7% (6/7) for codon 61. Negative percent agreement was 94.4% (101/107) for codon 12/13 and 99.4% (180/181) for codon 61. Nine of 10 discordant specimens yielded 454 results consistent with the cobas® results. With repeated testing, the assay showed a correct call rate of 100% (192/192) for all operators, instruments, reagent lots, and days tested. The cobas® test detects KRAS mutations in codons 12, 13, and 61 at a limit of detection of <5%. The PCR assay was more sensitive and specific than Sanger sequencing, and performance was highly reproducible. Test performance was not influenced by various endogenous interfering substances or common gut microbes.

S. Lee · V. H. Brophy · J. Cao · M. Velez · C. Hoeppner · S. Soviero · H. J. Lawrence (✉)
Roche Molecular Systems, Inc,
4300 Hacienda Drive,
Pleasanton, CA 94588, USA
e-mail: jeffrey.lawrence@roche.com

Keywords KRAS mutations · Molecular diagnostics · Colorectal cancer · Polymerase chain reaction (PCR)

Background

Mutations in the KRAS gene that lead to its constitutive activation have been identified in 24–43% of colorectal cancer (CRC) tumors and are common in other tumor types such as pancreatic, lung, thyroid, and myeloid leukemia [1–3]. These gain of function mutations lead to epidermal growth factor receptor (EGFR)-independent activation of intracellular signaling pathways, resulting in tumor cell proliferation, protection against apoptosis, increased invasion and metastasis, and activation of tumor-induced angiogenesis [4]. The presence of activating mutations has been shown in randomized clinical trials to play a crucial role in predicting non-responsiveness in patients with advanced CRC who receive the anti-EGFR monoclonal antibodies cetuximab and panitumumab [5–9]. The majority of activating mutations in CRC tumors occur in codons 12 (~82%) and 13 (~17%) of exon 2 of the KRAS gene; however, mutations in codon 61 (exon 3) have also been described [10]. Codon 61 mutations have been shown to result in constitutive activation of KRAS just as codon 12 and 13 mutations do [11, 12], and limited clinical data indicate that codon 61 mutations may predict non-response to anti-EGFR monoclonal antibody therapy [13–15].

The high level evidence supporting the clinical utility of KRAS mutation status in predicting response to anti-EGFR monoclonal antibodies has led to specific requirements for KRAS mutation testing by European and US regulatory authorities [16, 17]. Major oncology guidelines, including those of the European Society for Medical Oncology [18] and the American Society of Clinical Oncology [19], have

all embraced the recommendation that these antibodies be restricted to patients with KRAS wild-type colorectal cancers.

Bi-directional Sanger sequencing, which theoretically can identify all possible mutations in an exon, has been a common reference method for detecting somatic mutations in tumor specimens. However, Sanger sequencing suffers from limited sensitivity for low-level mutant alleles, particularly in formalin-fixed paraffin-embedded tissue (FFPET) specimens, and has a slow turnaround time [20]. A number of other KRAS mutation detection methods, including allele-specific PCR assays, high-resolution melting analysis, and pyrosequencing, have been developed [21, 22]. These other methods have been reported to have varying levels of sensitivity and specificity for detecting KRAS mutations and there is currently no uniform standard for KRAS mutation testing.

There is a clear need for a well-validated, robust, and reproducible method. The European Union in vitro Diagnostic (IVD) Medical Device Directive 98/79/EC requires that IVDs "achieve the performance…stated by the manufacturer" for a variety of test attributes such as limits of detection, analytical sensitivity and specificity, reproducibility/repeatability, and potential interfering and cross-reacting substances. Aligning with the European Union IVD directives and optimizing the analytical performance of a mutation assay requires thorough validation testing on different specimen types (including the intended use of FFPET specimens) as well as a comprehensive understanding of the impact of specimen attributes, such as the tumor content, the levels of amplifiable DNA, necrosis, and the influence of endogenous and exogenous interfering substances.

We set out to design a robust, accurate molecular diagnostic test to identify patients who have CRC tumors with somatic mutations in codons 12 and 13 of exon 2 or 61 of exon 3 of the KRAS gene and who are therefore unlikely to benefit from therapy with anti-EGFR monoclonal antibodies. The cobas® KRAS Mutation Test (Roche Molecular Systems, Branchburg, NJ, USA), for use with the cobas® 4800 System v2.0 is a TaqMelt™ real-time PCR test intended to detect 19 mutations in codons 12 and 13 of exon 2 and 61 of exon 3 of the KRAS gene using DNA derived from FFPET from human CRC tumors. In this report, we present data on the analytic performance of the cobas® test.

Material and methods

Materials

FFPET specimens from CRC tumors were purchased from US commercial vendors: Discovery Life Sciences, Inc. (Los Osos, CA, USA); BioServe (Beltsville, MD, USA); ProteoGenex (Culver City, CA, USA); CureLine, Inc. (San Francisco, CA, USA); and Indivumed, Inc. (Kensington, MD, USA). The FFPET specimens from vendors were from CRC stages I to IV with a majority from stages II and III. Estimated tumor content ranged from 25% to 80%.

Cobas® KRAS mutation test

The cobas® KRAS Mutation Test kit (cobas® test) is a TaqMelt™-based PCR assay (Fig. 1). The testing process consists of two main steps: manual specimen preparation to obtain genomic DNA from FFPET and PCR amplification and detection of target DNA using complementary primer pairs and two oligonucleotide probes labeled with different fluorescent dyes. The PCR primers are designed to amplify defined sections of exons 2 and 3 of the KRAS gene, and fluorescently labeled oligonucleotide probes detect mutations in codons 12, 13, and 61, which fall within these exons.

DNA extraction: DNA is extracted from a single, deparaffinized 5 μm section of FFPET following the standard procedure described in the cobas® DNA Sample Preparation Kit package insert. A deparaffinized specimen is lysed by incubation at an elevated temperature with a protease and chaotropic lysis/binding buffer that releases nucleic acid and protects the released genomic DNA from DNases. Subsequently, isopropanol is added to the lysis mixture that is then centrifuged through a column with a glass fiber filter. Unbound substances, such as salts, proteins, and other cellular impurities, are removed by centrifugation. The adsorbed nucleic acids are washed and then eluted with an aqueous solution. The amount of genomic DNA is spectrometrically determined and adjusted to a fixed concentration of 2 ng/μL.

PCR amplification and detection: The target DNA is amplified and detected on the cobas® 4800 system, which measures the fluorescence generated by specific PCR products, using the amplification and detection reagents provided in the cobas® KRAS Mutation Test kit (Fig. 1). Mutation detection is achieved by melting curve analysis, using an automated result interpretation software package (KRAS Assay Specific Analysis Package v1.0). Based on melting temperatures and peak heights for mutants and wild types, mutation status of each specimen was determined. A mutant control, a negative control, and a calibrator are included in each run to confirm the validity of the run. Amplification, detection, quality control analysis, and result interpretation are automated on the system; raw data and melting curves are not reported. The DNA isolation, amplification/detection, and result reporting can be performed in less than 8 h. The test kit is configured such that users running a minimum of three specimens can achieve the full number of 24 reportable results per kit; as many as 45 specimens can be processed in a single test run.

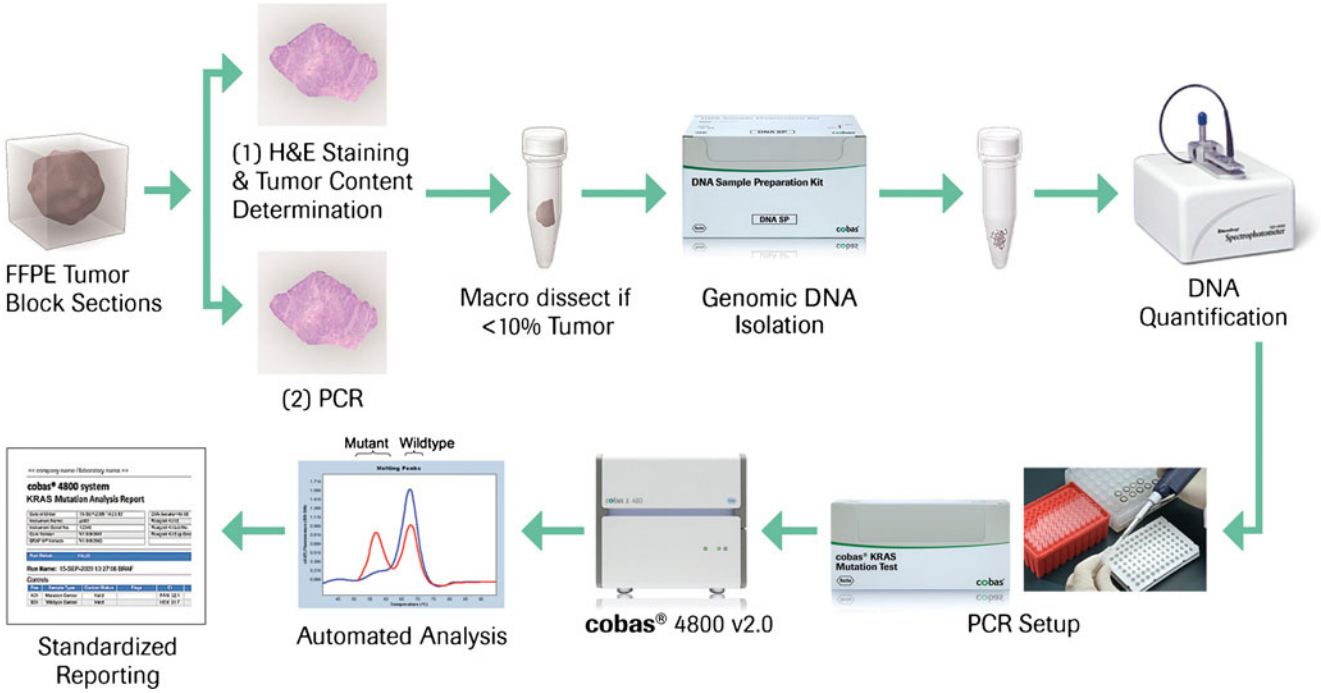

Fig. 1 Assay workflow. Two 5-μm sections are prepared from each FFPET specimen—one section is used for H&E staining to assess tumor content and the other section is used for DNA isolation. If the tumor content is greater than 10%, which all of the specimens for the studies in this report were, then no macro-dissection is required. Genomic DNA is isolated using the cobas® DNA Sample Preparation Kit and two 25-μL aliquots (one aliquot for codon 12/13 of exon 2 and the other aliquot for codon 61 of exon 3) of the resulting extract that is adjusted to 2 ng/μL of DNA are amplified using cobas z 480 analyzer. Change in fluorescence during melting steps is automatically analyzed for melting temperatures and peak heights for mutants and wild types to determine mutation status of each specimen

Sanger sequencing

DNA prepared from FFPET specimens using the same extraction method as described for the cobas® test were sequenced by 2X bi-directional Sanger sequencing by a Clinical Laboratory Improvement Amendments (CLIA)-certified laboratory (SeqWright, Houston, TX) using a validated protocol.

454 quantitative massively parallel pyrosequencing

Specimens which gave discordant cobas® test and Sanger test results were retested using a quantitative massively parallel pyrosequencing method (454 GS Titanium, 454 Life Sciences, Branford, CT) by a CLIA-certified laboratory (SeqWright, Houston, TX) using a validated protocol. Additionally, a randomly selected subset of specimens with concordant cobas® test and Sanger results were tested by 454 sequencing to confirm the accuracy of mutation status. The validated limit of detection for the 454 KRAS protocol was 1%.

Limit of detection

The limit of detection (LOD) of the cobas® test was evaluated for one predominant mutation in codon 12 (GAT), codon 13 (GAC), and codon 61 (CAC) of the KRAS gene with ~5% mutation. Testing on 24–72 replicates per panel member at different levels of DNA input was conducted using the following specimen types:

- FFPET specimens,
- DNA extracted from CRC FFPET mutant and wild-type specimens,
- DNA extracted and blended from two CRC mutant and wild-type cell lines for codons 12 and 13, and
- DNA from one mutant plasmid for codon 61 blended with wild-type KRAS cell line DNA.

Testing was performed using three lots of the cobas® test kit and one lot of the cobas® DNA Sample Preparation Kit. DNA extracted from each specimen type was then serially diluted to DNA input levels ranging from 50.0 to 0.4 ng per reaction well, in order to simulate varying degrees of DNA degradation that may occur with formalin fixation. 454 sequencing was used to assess percent mutant alleles for DNA extracted from each specimen type. Sensitivity was determined based on a correct mutation call rate of ≥95% and by Probit analysis.

In a separate analysis, the LOD was evaluated for 16 additional KRAS mutation genotypes. Due to the lack of naturally occurring specimens with ~5% mutant alleles,

FFPET DNA and plasmid blends at ~5% mutation (as assessed by 454 sequencing) were prepared including:

- Five FFPET blends representing five KRAS codon 12 mutations,
- Five blends (four plasmid and one FFPET) representing five KRAS codon 13 mutations, and
- Six blends (two plasmid and four FFPET) representing six KRAS codon 61 mutations.

Before cobas® testing, the mutation status and mutation percentage of the specimens were verified by 2X bi-directional Sanger sequencing and 454 sequencing, respectively.

Analytic sensitivity and specificity—methods correlation with Sanger sequencing

The analytic performance of the cobas® test was evaluated by comparing two lots of the cobas® KRAS test to 2X bi-directional Sanger Sequencing using 188 vendor-purchased CRC FFPET specimens. Each cobas® test reagent lot was paired with a separate lot of the cobas® DNA Sample Preparation Kit. Specimens were tested in a blinded fashion for the presence of codon 12, 13, and 61 mutations. Positive and negative percent agreements between the cobas® test and Sanger test results were determined. Discrepant analysis was performed by testing specimens with discordant cobas® test and Sanger results with 454 sequencing for resolution. In addition, 50 randomly selected specimens with concordant Sanger and cobas® test results were tested by 454 sequencing in order to provide further verification of the correct call rate.

Repeatability

The repeatability of the cobas® test was evaluated across different reagent lots, days, operators, and instruments with six FFPET CRC specimens, two KRAS wild-type, and four KRAS mutation positive. The materials used in the repeatability testing are:

- One cobas® DNA Sample Preparation Kit lot,
- Two cobas® KRAS Mutation Test Kit lots,
- Two operators, and
- Four cobas® 4800 System v.2.0.

Each operator performed one run per reagent lot per day for 4 days for a total of 16 runs with two replicates of each of the six specimens.

Interfering endogenous substances

The effects of endogenous substances, hemoglobin and triglycerides, on the performance of the cobas® test were investigated in 10 CRC FFPET specimens. The specimens were selected for mutation status based on Sanger and/or 454 sequencing. Five specimens were KRAS mutation positive and five were wild type. Four 5-μm sections were extracted for each specimen, one each in the following:

- Tissue Lysis Buffer + Proteinase K (TLB/PK) (control),
- TLB/PK + saline (solvent control),
- TLB/PK + 2 g/L hemoglobin (CLSI-recommended test concentrations), and
- TLB/PK + 37 mM triglycerides.

Hemoglobin and triglycerides were added during the lysis step of DNA extraction and were not subjected to deparaffinization. All DNA extracts were tested for interference of mutation detection using the cobas® test.

Interference by common colon-related microorganisms

The effects of colon-related microorganisms on the performance of the cobas® test were investigated in 10 FFPET CRC specimens. The specimens were selected for mutation status based on Sanger and/or 454 sequencing. Five specimens were KRAS mutation positive and five were wild type. Approximately one million colony-forming units of *Bacteroides caccae*, *Prevotella intermedia*, and *Escherichia coli* was added during the lysis step of DNA extraction. Phosphate-buffered saline and blank controls were also tested. One 5-μm section of each specimen was extracted and all DNA extracts were tested for interference of mutation detection using the cobas® test.

Cross-reactivity

The cross-reactivity of the cobas® test with a panel of KRAS silent mutations and KRAS homolog plasmids was assessed. Plasmids containing one each of three silent codon 12 mutations and three silent codon 13 mutations were prepared in a background of wild-type cell line DNA and tested in the presence and absence of 5% KRAS mutant DNA. Additionally, cross-reactivity and interference of the cobas® test were assessed with highly homologous RAS gene sequences present in the human genome (HRAS, NRAS, and pseudogene KRAS1P). Six plasmids (KRAS codon 12/13 pseudogene, codon 61 pseudogene, NRAS exon 2, NRAS exon 3, HRAS exon 2, and HRAS exon 3) were blended with KRAS wild-type DNA (K562 cell line DNA) and tested in the presence and absence of 5% KRAS mutant DNA. Each blend was tested in triplicate.

Necrosis

The impact of tissue necrosis on the performance of the cobas® test was evaluated in duplicate in 20 FFPET CRC specimens with varying percentages of necrotic tissue (5–70%) as

Table 1 Summary of limit of detection (LOD) results for the three most predominant KRAS mutations

KRAS mutation	Specimen type and ID	Mutation (%)	Lowest DNA input (ng/PCR) for a mutation rate ≥95%
Codon 12 (exon 2) GGT>G**A**T	FFPET specimen	4.3	3.1
	FFPET blend #1	4.2	3.1
	FFPET blend #2	4.7	3.1
	Cell line blend	5.3	0.8
Codon 13 (exon 2) GGC>G**A**C	FFPET blend #1	5.0	3.1
	FFPET blend #2	4.6	1.6
	FFPET blend #3	7.2	1.6
	Cell line blend	4.9	1.6
Codon 61 (exon 3) CAA>CA**C**	FFPET blend #1	4.4	3.1
	FFPET blend #2	5.5	3.1
	FFPET blend #3	3.8	6.3
	Plasmid blend	5.8	6.3

FFPET formalin-fixed paraffin-embedded tissue

assessed by an external pathologist. Mutation status was verified by Sanger sequencing. The FFPET specimens used were:

- Ten wild-type specimens with 30–70% necrotic tissue,
- Five KRAS codon 12 mutants with 30–45% necrotic tissue,
- Four KRAS codon 13 mutants with 15–50% necrotic tissue, and
- One KRAS codon 61 mutant with 5% necrotic tissue.

Results

Limit of detection

For the LOD analysis for the three predominant mutations in codons 12, 13, and 61, ≥95% correct mutation call rates were obtained across all specimen types with approximately 5% mutant alleles (as assessed by 454) at a DNA input of 0.8–6.3 ng per reaction well (Table 1). A 100% correct mutation call rate for the remaining 16 mutations in codons 12, 13, and 61 for all specimens was obtained at the recommended DNA input of 50 ng per reaction well (Table 2).

Methods correlation

The analytic performance of the cobas® test and 2X bi-directional Sanger sequencing was compared with a total of 188 FFPET vendor-purchased specimens using two different cobas® test reagent lots. Concordance between the cobas® test and Sanger sequencing for each lot was 97.5% positive percent agreement (PPA) and 94.4% negative percent agreement (NPA) for codon 12/13 and 85.7% PPA and 99.4% NPA for codon 61 (Table 3, columns A and B). Eight discordant results for codon 12/13 and two for codon 61 were subjected to 454 sequencing. Six specimens were reported mutation-detected codon 12/13 by the cobas® test and mutation not detected by Sanger. 454 results agreed with the cobas® test in five of the six cases. The other two specimens were reported mutation not detected codon 12/13 by the cobas® test and mutation detected by Sanger. 454 agreed with the cobas®

Table 2 Limit of detection (LOD) results for the remaining 16 KRAS mutations at ~5% at recommended DNA input of 50 ng per reaction well

					Correct call rate	
Sample	Codon	Mutation	Valid replicates	KRAS mutation test results (codon)	Correct mutation calls	Accuracy (%)
1	12	GGT>**A**GT	24	12/13	24	100
2	12	GGT>**C**GT	24	12/13	24	100
3	12	GGT>**T**GT	24	12/13	24	100
4	12	GGT>G**C**T	24	12/13	24	100
5	12	GGT>G**T**T	24	12/13	24	100
6	13	GGC>**A**GC	24	12/13	24	100
7	13	GGC>**C**GC	24	12/13	24	100
8	13	GGC>**T**GC	24	12/13	24	100
9	13	GGC>G**C**C	24	12/13	24	100
10	13	GGC>G**T**C	24	12/13	24	100
11	61	CAA>**A**AA	24	61	24	100
12	61	CAA>**G**AA	24	61	24	100
13	61	CAA>C**T**A	24	61	24	100
14	61	CAA>C**G**A	26	61	26	100
15	61	CAA>C**C**A	24	61	24	100
16	61	CAA>CA**T**	24	61	24	100

test in both cases. Therefore, 454 sequencing results agreed with the cobas® test for seven of the eight discrepant specimens. One unique specimen per lot remained discordant for codon 12/13 mutation status after 454 sequencing. Both discordant specimens displayed low peak heights in the cobas assay, suggesting the presence of very low levels of mutant alleles. After discordant resolution with 454 sequencing, the PPA for codon 12/13 was 100% and the NPA was 99% (Table 3, column C). 454 sequencing results of the two discordant specimens for codon 61 agreed with the cobas® test. After discordant resolution with 454 sequencing, the PPA and the NPA for codon 61 were 100% (Table 3, column D). In addition to the 10 discrepant specimens, 50 specimens with concordant cobas® test and Sanger sequencing results (26 codon 12/13 mutations, 6 codon 61 mutations, and 18 mutation not detected specimens) were subjected to 454 sequencing. The 454 sequencing results for all 50 concordant specimens were concordant with the Sanger sequencing and cobas® KRAS test results.

Repeatability

All 16 repeatability runs were valid. The cobas® test had a mutation result accuracy of 100% (192/192 replicates) across all specimens, reagent lots, operators, and instruments combined (Table 4).

Interfering substances

No interference was observed for any of the 10 specimens tested for potential endogenous interfering substances (hemoglobin and triglycerides) at Clinical and Laboratory Standards Institute recommended test concentrations of 2 g/L and 37 mM, respectively. None of the exogenous colon-related microorganisms tested interfered with the cobas® test. All five of the KRAS wild-type specimens spiked with an exogenous substance gave valid results of "mutation not detected", while all five KRAS-mutant specimens spiked with an exogenous substance gave valid results of "mutation detected" for the correct codon. Both study controls gave valid and accurate mutation results (data not shown).

Cross-reactivity

The cobas® test did not cross-react with either KRAS silent mutations in codons 12/13 or highly homologous RAS gene sequences. When tested in a wild-type background, all plasmid blends tested with either KRAS silent mutations or KRAS homologs resulted in "mutation not detected". When tested in a background of 5% KRAS-mutant DNA, all plasmid blends

Table 3 Methods correlation between mutation findings with the cobas® mutation test and Sanger sequencing (columns A and B) and combined Sanger and 454/GS20 sequencing resolution (columns C and D)

A					B					C					D				
Codon 12/13		2X bi-directional Sanger sequencing			Codon 61		2X bi-directional Sanger sequencing			Codon 12/13		Sanger sequencing, resolved with 454 sequencing			Codon 61		Sanger sequencing, resolved with 454 sequencing		
		MD	MND	Totals			MD	MND	Totals			MD	MND	Totals			MD	MND	Totals
cobas® KRAS	MD	79	6	85	cobas® KRAS	MD	6	1	7	cobas® KRAS	MD	84	1	85	cobas® KRAS	MD	7	0	7
	MND	2	101	103		MND	1	180	181		MND	0	103	103		MND	0	181	181
	Totals	81	107	188		Totals	7	181	188		Totals	84	104	188		Totals	7	181	188
Positive agreement, 97.5% (95% CI, 91.4–99.3)					Positive agreement, 85.7% (95% CI, 48.7–97.4)					Positive agreement, 100% (95% CI, 95.6–100)					Positive agreement, 100% (95% CI, 64.6–100)				
Negative agreement, 94.4% (95% CI, 88.3–97.4)					Negative agreement, 99.4% (95% CI, 96.9–99.9)					Negative agreement, 99.0% (95% CI, 94.8–99.8)					Negative agreement, 100% (95% CI, 97.9–100)				
Overall agreement, 95.7% (95% CI, 91.8–97.8)					Overall agreement, 98.9% (95% CI, 96.2–99.7)					Overall agreement, 99.5% (95% CI, 97.0–99.9)					Overall agreement, 100% (95% CI, 98.0–100)				

MD mutation detected, *MND* wild type for codons 12/13 or 61

Table 4 Repeatability—cobas® KRAS mutation test accuracy by test day, reagent lot, operator, and instrument

Test day	Reagent lot	Run	Operator	Instrument ID	Incorrect results	Valid results	Accuracy (%)
1	1	1	A	1	0	12	100
		2	B	2	0	12	100
	2	3	A	3	0	12	100
		4	B	4	0	12	100
2	1	5	A	3	0	12	100
		6	B	2	0	12	100
	2	7	A	1	0	12	100
		8	B	4	0	12	100
3	1	9	A	1	0	12	100
		10	B	2	0	12	100
	2	11	A	3	0	12	100
		12	B	4	0	12	100
4	1	13	A	3	0	12	100
		14	B	2	0	12	100
	2	15	A	1	0	12	100
		16	B	4	0	12	100
				Total	0	192	100

resulted in "mutation detected" for the correct codon (data not shown).

Necrosis

No interference from necrotic tissue was observed when evaluating the performance of the cobas® test. Results for all specimens were concordant with Sanger and 454 sequencing results. Necrosis up to 70% did not affect cobas® test performance (data not shown).

Discussion

KRAS testing is now mandatory for patients with CRC being considered for treatment with anti-EGFR monoclonal antibodies such as cetuximab (Erbitux®, Bristol Myers Squibb and Merck-Serono) and panitumumab (Vectibix®, Amgen). Several methods for KRAS testing currently exist, from commercially available CE-marked test kits to laboratory-developed tests, but there are limited data to support the performance of individual methods over others [21–23]. With the lack of standardization for KRAS testing, there is a widely recognized need for external quality assessment programs and standards [24, 25]. Indeed, a number of recent studies have highlighted the variability of mutation test results from different clinical laboratories [26, 27]. As results directly affect patient therapy, KRAS tests should be thoroughly validated on clinically relevant specimen types (including FFPET) with optimal analytical performance that encompasses a comprehensive understanding of the impact of specimen attributes, such as the levels of amplifiable DNA; the tumor content of FFPET specimens used for analysis; tissue necrosis; and the influence of endogenous and exogenous interfering substances.

The cobas® test was thoroughly evaluated with 23 unique performance verification studies and in 188 CRC clinical specimens. Here, we have reported results on six of these studies, including methods correlation with Sanger sequencing, limit of detection, repeatability, interfering substances, cross-reactivity, and necrosis. These verification tests were performed in FFPET specimens as well as DNA derived from cell lines and plasmids. Specimen attributes that were evaluated were: tumor cell content, potential effects of endogenous and exogenous interfering substances, cross-reactivity with KRAS silent mutations and KRAS homologs, and proportion of necrotic tissue in the FFPET specimen. These analytic performance attributes have not been published for other KRAS testing methods.

Concordance between the cobas® test and sequencing (Sanger plus 454) was 99.5% for codon 12/13 and 100% for codon 61. The cobas® test had a ≥95% correct mutation call rate across all specimen types with ~5% mutant alleles at a DNA input of 0.8–6.3 ng/PCR, and a 100% correct mutation call rate across all specimen types for the recommended DNA input of 50 ng per reaction well. The ability of this assay to detect KRAS mutations at lower DNA inputs reduces the likelihood that mutations will be missed in poor-quality FFPET samples with limited amounts of amplifiable DNA. Because we did not perform a systematic assessment of samples with <5% mutant alleles, the detectability of lower levels of mutation with this assay is uncertain.

The cobas® test had a mutation result accuracy of 100% for all specimens and operators combined in the repeatability study. Neither endogenous interfering factors (hemoglobin or triglycerides) nor the presence of exogenous colon-related microorganisms interfered with the test results. The cobas® test does not cross-react with KRAS silent mutations or KRAS homologs from the RAS gene family. The cobas® test gave 100% correct mutation call in FFPET specimens with up to 70% necrosis and ≥95% correct mutation call rate in specimens with low tumor content at ≤50 ng per reaction well.

In contrast to other KRAS testing kits, such as the *therascreen*® KRAS test (Qiagen, Manchester, UK), which identifies seven somatic mutations in codons 12 (six mutations) and 13 (one mutation), the cobas® test identifies 19 mutations in codons 12, 13, and 61. Based on data from the Catalogue of Somatic Mutations in Cancer (COSMIC) database [10], the additional 12 mutations detected by the cobas test represent approximately 2% of all KRAS mutations or approximately 1% of all CRC cases. However, recent studies suggest that codon 61 mutations are more prevalent than reflected in the COSMIC data [28, 29]. Thus, more comprehensive KRAS mutation coverage may help to improve the selection of patients for this treatment [15]. The analytical studies presented in this paper demonstrate that the cobas® KRAS Mutation Test is a thoroughly validated, robust, and reproducible companion diagnostic test for the detection of the KRAS mutation in CRC tumors from patients under consideration for treatment with anti-EGFR monoclonal antibodies.

Acknowledgments We acknowledge Felice Shieh for her contributions to manuscript preparation.

Conflict of interest All authors are full-time employees of Roche Molecular Systems, Inc., Pleasanton, CA.

Open Access This article is distributed under the terms of the Creative Commons Attribution Noncommercial License which permits any noncommercial use, distribution, and reproduction in any medium, provided the original author(s) and source are credited.

References

1. Bos JL (1989) ras oncogenes in human cancer: a review. Cancer Res 49(17):4682–4689
2. Andreyev HJ, Norman AR, Cunningham D, Oates J, Dix BR, Iacopetta BJ, Young J, Walsh T, Ward R, Hawkins N, Beranek M, Jandik P, Benamouzig R, Jullian E, Laurent-Puig P, Olschwang S, Muller O, Hoffmann I, Rabes HM, Zietz C, Troungos C, Valavanis C, Yuen ST, Ho JW, Croke CT, O'Donoghue DP, Giaretti W, Rapallo A, Russo A, Bazan V, Tanaka M, Omura K, Azuma T, Ohkusa T, Fujimori T, Ono Y, Pauly M, Faber C, Glaesener R, de Goeij AF, Arends JW, Andersen SN, Lovig T, Breivik J, Gaudernack G, Clausen OP, De Angelis PD, Meling GI, Rognum TO, Smith R, Goh HS, Font A, Rosell R, Sun XF, Zhang H, Benhattar J, Losi L, Lee JQ, Wang ST, Clarke PA, Bell S, Quirke P, Bubb VJ, Piris J, Cruickshank NR, Morton D, Fox JC, Al-Mulla F, Lees N, Hall CN, Snary D, Wilkinson K, Dillon D, Costa J, Pricolo VE, Finkelstein SD, Thebo JS, Senagore AJ, Halter SA, Wadler S, Malik S, Krtolica K, Urosevic N (2001) Kirsten ras mutations in patients with colorectal cancer: the 'RASCAL II' study. Br J Cancer 85(5):692–696. doi:10.1054/bjoc.2001.1964
3. Samowitz WS, Curtin K, Schaffer D, Robertson M, Leppert M, Slattery ML (2000) Relationship of Ki-ras mutations in colon cancers to tumor location, stage, and survival: a population-based study. Cancer Epidemiol Biomarkers Prev 9(11):1193–1197
4. Ciardiello F, Tortora G (2008) EGFR antagonists in cancer treatment. N Engl J Med 358(11):1160–1174. doi:10.1056/NEJMra0707704
5. Van Cutsem E, Kohne CH, Lang I, Folprecht G, Nowacki MP, Cascinu S, Shchepotin I, Maurel J, Cunningham D, Tejpar S, Schlichting M, Zubel A, Celik I, Rougier P, Ciardiello F (2011) Cetuximab plus irinotecan, fluorouracil, and leucovorin as first-line treatment for metastatic colorectal cancer: updated analysis of overall survival according to tumor KRAS and BRAF mutation status. J Clin Oncol 29(15):2011–2019. doi:10.1200/JCO.2010.33.5091
6. Bokemeyer C, Bondarenko I, Makhson A, Hartmann JT, Aparicio J, de Braud F, Donea S, Ludwig H, Schuch G, Stroh C, Loos AH, Zubel A, Koralewski P (2009) Fluorouracil, leucovorin, and oxaliplatin with and without cetuximab in the first-line treatment of metastatic colorectal cancer. J Clin Oncol 27(5):663–671
7. Amado RG, Wolf M, Peeters M, Van Cutsem E, Siena S, Freeman DJ, Juan T, Sikorski R, Suggs S, Radinsky R, Patterson SD, Chang DD (2008) Wild-type KRAS is required for panitumumab efficacy in patients with metastatic colorectal cancer. J Clin Oncol 26 (10):1626–1634
8. Karapetis CS, Khambata-Ford S, Jonker DJ, O'Callaghan CJ, Tu D, Tebbutt NC, Simes RJ, Chalchal H, Shapiro JD, Robitaille S, Price TJ, Shepherd L, Au HJ, Langer C, Moore MJ, Zalcberg JR (2008) K-ras mutations and benefit from cetuximab in advanced colorectal cancer. N Engl J Med 359(17):1757–1765. doi:10.1056/NEJMoa0804385
9. Tol J, Koopman M, Cats A, Rodenburg CJ, Creemers GJ, Schrama JG, Erdkamp FL, Vos AH, van Groeningen CJ, Sinnige HA, Richel DJ, Voest EE, Dijkstra JR, Vink-Borger ME, Antonini NF, Mol L, van Krieken JH, Dalesio O, Punt CJ (2009) Chemotherapy, bevacizumab, and cetuximab in metastatic colorectal cancer. N Engl J Med 360(6):563–572
10. Catalog Of Somatic Mutations In Cancer (COSMIC) database, v. 54 (2011) (http://www.sanger.ac.uk/perl/genetics/CGP/cosmic)
11. Der CJ, Finkel T, Cooper GM (1986) Biological and biochemical properties of human rasH genes mutated at codon 61. Cell 44 (1):167–176
12. Scheffzek K, Ahmadian MR, Kabsch W, Wiesmuller L, Lautwein A, Schmitz F, Wittinghofer A (1997) The Ras-RasGAP complex: structural basis for GTPase activation and its loss in oncogenic Ras mutants. Science 277(5324):333–338
13. Loupakis F, Ruzzo A, Cremolini C, Vincenzi B, Salvatore L, Santini D, Masi G, Stasi I, Canestrari E, Rulli E, Floriani I, Bencardino K, Galluccio N, Catalano V, Tonini G, Magnani M, Fontanini G, Basolo F, Falcone A, Graziano F (2009) KRAS codon 61, 146 and BRAF mutations predict resistance to cetuximab plus irinotecan in KRAS codon 12 and 13 wild-type metastatic colorectal cancer. Br J Cancer 101(4):715–721
14. De Roock W, Claes B, Bernasconi D, De Schutter J, Biesmans B, Fountzilas G, Kalogeras KT, Kotoula V, Papamichael D, Laurent-Puig P, Penault-Llorca F, Rougier P, Vincenzi B, Santini D, Tonini G, Cappuzzo F, Frattini M, Molinari F, Saletti P, De Dosso S, Martini M, Bardelli A, Siena S, Sartore-Bianchi A, Tabernero J, Macarulla T, Di Fiore F, Gangloff AO, Ciardiello F, Pfeiffer P, Qvortrup C, Hansen TP, Van Cutsem E, Piessevaux H, Lambrechts D, Delorenzi M, Tejpar S (2010) Effects of KRAS, BRAF, NRAS, and PIK3CA mutations on the efficacy of cetuximab plus

chemotherapy in chemotherapy-refractory metastatic colorectal cancer: a retrospective consortium analysis. Lancet Oncol 11 (8):753–762
15. Molinari F, Felicioni L, Buscarino M, De Dosso S, Buttitta F, Malatesta S, Movilia A, Luoni M, Boldorini R, Alabiso O, Girlando S, Soini B, Spitale A, Di Nicolantonio F, Saletti P, Crippa S, Mazzucchelli L, Marchetti A, Bardelli A, Frattini M (2011) Increased detection sensitivity for KRAS mutations enhances the prediction of anti-EGFR monoclonal antibody resistance in metastatic colorectal cancer. Clin Cancer Res 17(14):4901–4914. doi:10.1158/1078-0432.CCR-10-3137
16. Agency EM (2008) Committee for Medicinal Products for Human Use post-authorisation summary of positive opinion for Erbitux., vol doc. Ref
17. Administration USFaD (2009) cetuximab (Erbitux) and panitumumab (Vectibix)
18. Van Cutsem E, Oliveira J (2009) Advanced colorectal cancer: ESMO clinical recommendations for diagnosis, treatment and follow-up. Ann Oncol 20(Suppl 4):61–63. doi:10.1093/annonc/mdp130
19. Allegra CJ, Jessup JM, Somerfield MR, Hamilton SR, Hammond EH, Hayes DF, McAllister PK, Morton RF, Schilsky RL (2009) American Society of Clinical Oncology provisional clinical opinion: testing for KRAS gene mutations in patients with metastatic colorectal carcinoma to predict response to anti-epidermal growth factor receptor monoclonal antibody therapy. J Clin Oncol 27(12):2091–2096
20. Querings S, Altmuller J, Ansen S, Zander T, Seidel D, Gabler F, Peifer M, Markert E, Stemshorn K, Timmermann B, Saal B, Klose S, Ernestus K, Scheffler M, Engel-Riedel W, Stoelben E, Brambilla E, Wolf J, Nurnberg P, Thomas RK (2011) Benchmarking of mutation diagnostics in clinical lung cancer specimens. PLoS One 6(5): e19601. doi:10.1371/journal.pone.0019601
21. Gao J, Li YY, Sun PN, Shen L (2010) Comparative analysis of dideoxy sequencing, the KRAS StripAssay and pyrosequencing for detection of KRAS mutation. World J Gastroenterol 16(38):4858–4864
22. Angulo B, Garcia-Garcia E, Martinez R, Suarez-Gauthier A, Conde E, Hidalgo M, Lopez-Rios F (2010) A commercial real-time PCR kit provides greater sensitivity than direct sequencing to detect KRAS mutations: a morphology-based approach in colorectal carcinoma. J Mol Diagn 12(3):292–299
23. Whitehall V, Tran K, Umapathy A, Grieu F, Hewitt C, Evans TJ, Ismail T, Li WQ, Collins P, Ravetto P, Leggett B, Salto-Tellez M, Soong R, Fox S, Scott RJ, Dobrovic A, Iacopetta B (2009) A multicenter blinded study to evaluate KRAS mutation testing methodologies in the clinical setting. J Mol Diagn 11(6):543–552
24. van Krieken H, Tol J (2009) Setting future standards for KRAS testing in colorectal cancer. Pharmacogenomics 10(1):1–3
25. Dequeker E, Ligtenberg MJ, Vander Borght S, van Krieken JH (2011) Mutation analysis of KRAS prior to targeted therapy in colorectal cancer: development and evaluation of quality by a European external quality assessment scheme. Virchows Arch 459(2):155–160. doi:10.1007/s00428-011-1094-x
26. Bellon E, Ligtenberg MJ, Tejpar S, Cox K, de Hertogh G, de Stricker K, Edsjo A, Gorgoulis V, Hofler G, Jung A, Kotsinas A, Laurent-Puig P, Lopez-Rios F, Hansen TP, Rouleau E, Vandenberghe P, van Krieken JJ, Dequeker E (2011) External quality assessment for KRAS testing is needed: setup of a European program and report of the first joined regional quality assessment rounds. Oncologist 16 (4):467–478
27. Beau-Faller M, Degeorges A, Rolland E, Mounawar M, Antoine M, Poulot V, Mauguen A, Barbu V, Coulet F, Pretet JL, Bieche I, Blons H, Boyer JC, Buisine MP, de Fraipont F, Lizard S, Olschwang S, Saulnier P, Prunier-Mirebeau D, Richard N, Danel C, Brambilla E, Chouaid C, Zalcman G, Hainaut P, Michiels S, Cadranel J (2011) Cross-validation study for epidermal growth factor receptor and KRAS mutation detection in 74 blinded non-small cell lung carcinoma samples: a total of 5550 exons sequenced by 15 molecular French laboratories (evaluation of the EGFR mutation status for the administration of EGFR-TKIs in non-small cell lung carcinoma [ERMETIC] project—part 1). J Thorac Oncol 6(6):1006–1015. doi:10.1097/JTO.0b013e318211dcee
28. Richman SD, Seymour MT, Chambers P, Elliott F, Daly CL, Meade AM, Taylor G, Barrett JH, Quirke P (2009) KRAS and BRAF mutations in advanced colorectal cancer are associated with poor prognosis but do not preclude benefit from oxaliplatin or irinotecan: results from the MRC FOCUS trial. J Clin Oncol 27 (35):5931–5937
29. Gaedcke J, Grade M, Jung K, Schirmer M, Jo P, Obermeyer C, Wolff HA, Herrmann MK, Beissbarth T, Becker H, Ried T, Ghadimi M (2010) KRAS and BRAF mutations in patients with rectal cancer treated with preoperative chemoradiotherapy. Radiother Oncol 94 (1):76–81

Virchows Arch (2012) 460:151–155
DOI 10.1007/s00428-012-1193-3

ORIGINAL ARTICLE

A multi-centre pathologist survey on pathological processing and regression grading of colorectal cancer resection specimens treated by neoadjuvant chemoradiation

Runjan Chetty · Pelvender Gill · Dhirendra Govender · Adrian Bateman · Hee Jin Chang · David Driman · Fraser Duthie · Marisa Gomez · Eleanor Jaynes · Cheok Soon Lee · Michael Locketz · Claudia Mescoli · Corwyn Rowsell · Anne Rullier · Stefano Serra · Neil Shepherd · Eva Szentgyorgyi · Rajkumar Vajpeyi · Lai Mun Wang

Received: 21 October 2011 / Revised: 12 December 2011 / Accepted: 3 January 2012 / Published online: 13 January 2012
© Springer-Verlag 2012

Abstract To ascertain the approach and degree of consensus of pathologists in the handling and regression grading of colorectal cancer resection specimens treated with neoadjuvant chemoradiation, a ten-part questionnaire was circulated to 18 gastrointestinal pathologists in eight countries. The questions were specific and addressed pertinent issues related to colorectal cancer with neoadjuvant chemoradiation. There is a lack of consensus on how to handle the specimen, number of sections taken, correlation with pre- and post-operative radiological imaging, and especially, regression grading schema employed. Consensus in the form of guidelines is required so that the pathological assessment

R. Chetty · P. Gill · L. M. Wang
Department of Cellular Pathology/Biomedical Research Centre/
Nuffield Department of Clinical Laboratory Sciences,
John Radcliffe Hospital and University of Oxford,
Oxford, UK

D. Govender · M. Locketz
Division of Anatomical Pathology, University of Cape Town/
Groote Schuur Hospital,
Cape Town, South Africa

A. Bateman · E. Jaynes
Department of Cellular Pathology,
Southampton University Hospitals NHS Trust,
Southampton, UK

H. J. Chang
Center for Colorectal Cancer, Research Institute & Hospital,
National Cancer Center,
Goyang, South Korea

D. Driman
Department of Pathology, London Health Sciences Centre/
University of Western Ontario,
London, Canada

F. Duthie
Department of Pathology, Western Infirmary,
Glasgow, Scotland, UK

M. Gomez
Department of Pathology, Hospital de Navarra,
Pamplona, Spain

C. S. Lee
Department of Pathology,
Liverpool & Royal Prince Alfred Hospital,
University of Western Sydney,
Sydney, Australia

C. Mescoli
Department of Diagnostic Sciences & Special Therapies,
Pathology Unit, University of Padova,
Padova, Italy

C. Rowsell
Department of Pathology,
Sunnybrook Health Science Center/University of Toronto,
Toronto, Canada

A. Rullier
Department of Pathology,
CHU Bordeaux, France

S. Serra · E. Szentgyorgyi · R. Vajpeyi
Department of Pathology,
University Health Network/University of Toronto,
Toronto, Canada

of these specimens will provide clinically relevant information for patient management, irrespective of location.

Keywords Colorectal cancer · Regression grading · Neoadjuvant chemoradiation · Pathology reporting

Preoperative (neoadjuvant) chemoradiation for colorectal cancer is an important treatment modality of colorectal carcinoma and is used worldwide to improve local control and downstage the cancer [1–3]. Histological tumour response (measured by complete or partial tumour regression) to this form of therapy has been associated with increased patient survival [4–6].

With neoadjuvant therapy becoming more commonly used, the handling and reporting of such specimens have changed routine diagnostic practice for pathologists. The histological tumour response to the preoperative treatment is evaluated as the grade of regression. Oesophageal cancers were the first cancers to be treated with neoadjuvant therapy and the Mandard grading of regression was formulated for these cases [7]. Subsequently, Dworak et al. proposed a similar system for rectal cancer [8]. However, as Bateman and colleagues [9] pointed out, studies attempting to relate the degree of tumour response to clinical outcome have produced conflicting results, with some finding no evidence of improved survival [10] and others identifying a correlation between a good tumour response and better long-term outcome [11–13].

It is also clear that within the pathology fraternity there is also great variation in whether such cancers are accorded a regression grading score, what grading scheme is employed and indeed, how these schemas are applied. In order to ascertain the level of concordance, 18 gastrointestinal (GI) pathologists with an interest in colorectal cancer were asked to participate in a survey.

Materials and methods

A questionnaire was compiled consisting of ten questions that would assist in ascertaining the incidence, approach and style of practice of GI pathologists in eight countries around the world. The questions were collated into a simple word document (Table 1) and circulated electronically to 18 GI pathologists. One respondent did not use regression grading for these cancers and the practice in this centre was to use the ypTNM system without specific attention paid to regression grading per se. Thus, there were 17 participants from 13 centres. Having more than one participant from the same centre would allow for the assessment of variation in practice within the same department. Responses were collated, anonymised and then synthesised into a range of responses per question.

Results

Results from the questionnaire are summarised as follows:

1. The average number of cases seen annually is 53 (range, 10 to 300) within the respective departments.
2. Grossing protocol for specimens

   Eight participants did not have a standardised grossing method on how to submit sections from cases following neoadjuvant therapy, while nine participants claimed to have a grossing protocol that was based on published methods and internal institutional standards.
3. Are the gross specimens previewed and/or grossed by the reporting pathologist?

   Twelve participants grossed/dissected the cases personally, while five participants did not.
4. Is post-surgery radiological imaging performed?

   Ten participants did not perform post-surgery radiological imaging of the resected specimen (usually

Table 1 Questionnaire for pathology assessment of rectal cancer post-chemoradiation

1. How many resection/total mesorectal excision (TME) cases with preoperative chemoradiation are encountered in your department annually?
2. Is there a specific grossing protocol for such specimens?
3. Are the gross specimens previewed and/or grossed by the reporting pathologist?
4. Is post-surgery imaging of the specimen performed?
5. Is the gross specimen correlated with imaging?
6. (a) Average number of sections/blocks taken:
(b) Is the specimen submitted in toto?
(c) If not in toto is further tissue resubmitted?
(d) Is sampling restricted to fibrous and/or suspicious for tumour areas only?
7. What grading system do you use? Why?
8. How do you reach a final grading score?
9. Do the oncologists ask for a regression grade/score?
10. Do you think there is a need for uniformity in grading regression?

N. Shepherd
Gloucestershire Cellular Pathology Laboratory,
Cheltenham General Hospital,
Cheltenham, UK

R. Chetty (✉)
Department of Cellular Pathology & Nuffield Department of Clinical Laboratory Sciences, Level 1, Academic Centre,
John Radcliffe Hospital,
Headley Way,
Oxford OX3 9DU, UK
e-mail: runjan.chetty@gmail.com

MRI), and seven performed radiological assessment of the resected specimen.

5. Is the gross specimen correlated with imaging?

   Only two participants (who did not perform post-surgery imaging of the resected specimen) correlated the preoperative imaging to the gross specimen, whereas, the majority of the group did not perform radiological imaging correlation. Five participants indicated that correlation was frequently obtained at a multidisciplinary team meeting.

6. (a) Average number of sections/blocks taken per case

   The average number of blocks taken was 16, with a range from 4 to 35.

   (b) Is the entire area of macroscopic abnormality submitted in toto?

   Eight participants submitted in toto routinely and the other nine did not.

   (c) If not in toto, is further tissue resubmitted?

   Of the nine participants who did not submit in toto, two participants did not resubmit tissue, whereas the other seven participants did resubmit if no abnormality was evident on histological examination and/or surgeon/radiologist queries histological findings.

   (d) Is sampling restricted to fibrous and/or suspicious for tumour areas only?

   Six participants restricted sampling to fibrous tissue, two did not respond to this question and nine participants sample more widely than only the fibrous tissue, including randomly around proximal and distal margins and normal-looking rectum around the lesion. In discussion of the post-survey results, all participants also stated they sampled incidental pathology such as polyps, diverticula and any other mucosal lesions.

7. What grading system do you use? Why?

   Four participants used the RCPath system, four used the AJCC guidelines, four used the Mandard system, three used the Dworak grading system, one used a local hospital system and one used an unspecified grading system.

8. How do you reach a final grading score?

   Participants reached final grading by a variety of means. Five participants made an overall assessment of all slides and produced a composite regression score. Seven scored on the worst area, in terms of residual tumour, seen microscopically irrespective of what other sections showed. Two adhered strictly to the criteria set up by whichever system they employed, such as the Royal College of Pathologists system. One participant took the macroscopic appearances into account before appending a regression grade to the tumour. Two participants did not respond to this question.

9. Do the oncologists ask for a regression grade/score?

   Three participants did not respond this question; of the 14 participants who did answer, six participants claimed that the oncologist did ask for a regression grading, which often is incorporated into the report, while the remaining eight said the oncologists in their institutions did not ask for it.

10. Do you think there is a need for uniformity in grading regression?

    Three abstained, 11 agreed and 3 disagreed stating that the uniformity depends on the needs of the oncologist and the needs of the local institution.

Discussion

Adjuvant chemoradiotherapy following surgery was the standard of care in the management of rectal cancer until the German clinical trial comparing pre- and post-operative chemoradiation clearly established a role for preoperative chemoradiation [14]. Neoadjuvant chemoradiation is now indicated for all or almost all patients with cT3/T4 N0 rectal cancer determined either by transrectal ultrasound (TRUS) or MRI. Relative indications for neoadjuvant chemoradiotherapy include the presence of clinically node-positive rectal cancer in a patient with an MRI or TRUS-staged T1/2 rectal cancer, a distal rectal tumour for which an abdomino-perineal resection is thought to be necessary and a tumour which appears to invade the mesorectal fascia on preoperative imaging, due to decreased likelihood of achieving a tumour-free circumferential resection margin with surgery as the first line of treatment. For all of these clinical situations, absolute conclusive evidence to support benefit for preoperative chemoradiotherapy is lacking except for T3/T4 rectal cancers. However, rectal surgery has morbidity and complications, and if surgery can be avoided in many cases, then alternate modes of treatment need to be explored.

It has been stated that with preoperative chemoradiation, 25% of cases achieve a ‘pathological complete response’ [15]. The role of the pathologist in assessing whether a tumour has been successfully down-staged is axiomatic because of the prognostic value of regression grading.

Neoadjuvant chemoradiation for oesophageal carcinomas resulted in Mandard and colleagues establishing histological parameters by which regression could be gauged [7]. They recognised that regression impacted both on the cancer cells, which showed degenerative features and necrosis, and the stromal as well [7]. Stromal changes included fibrosis, inflammation, giant cells and a granulomatous response to ghost tumour cells and keratin [7]. Based on these histological features, Mandard et al. suggested five grades of regression ranging from complete regression (grade 1) to no

regression (grade 5) [7]. Several have adapted the Mandard grading system to grade regression in other sites such as the rectum.

To address regression in the rectum, Dworak and colleagues suggested a tumour regression grading system (TRG) based on the histological degree of tumour regression and fibrosis present in a rectal cancer specimen after preoperative treatment [8]. This system is based on the grading scheme suggested by Mandard et al. [7]; however, Dworak et al. reversed their grading with grade 0 reflecting no regression and grade 4 being complete regression [8]. The histological parameters they used to assess regression grading included: tumour mass, fibrosis, radiation-induced vascular change and peritumoural inflammation [8]. Thus, these two grading systems formed the basis of modifications that have been suggested more recently and provided pathologists with criteria on which they could approach regression grading.

Rodel and colleagues showed that TRG was of prognostic significance when assessed in 385 patients receiving preoperative chemoradiation [16]. Five-year disease-free survival was 86% for TRG 4 (no viable tumour cells or a pathological complete response), 75% for TRG 2 and TRG 3 grouped together and 63% for TRG 0 and TRG 1 grouped together [15]. So, pathology is pivotal in determining prognosis in this group of patients treated by neoadjuvant chemoradiation. The need for standardisation of reporting and the difficulties associated with histopathological variations following different regimens of neoadjuvant chemoradiation have been discussed by Nagtegaal and colleagues [17, 18].

As has already been pointed out and concluded from this survey, the pathologist's success in finding residual apparently viable cells depends on how assiduously they search, how many sections and blocks are processed, and importantly, on how to apply the various grading systems that are available [19]. However, this paper also contends that 'there is no standardised practice' to both sampling and grading [19]. To address this problem, the following was suggested by the second European Rectal Cancer Consensus Conference on multidisciplinary rectal cancer management [20]: 'To declare a complete pathological response, initially at least 5 tissue blocks should be taken from the tumour site. If there is no tumour present in these, the whole tumour area should be blocked. If still no tumour is present, three levels should be cut from each tumour block. If still no tumour is present, there is a pathological complete response' [20]. This appears to be the only published guideline on the pathological handling or processing of colorectal specimens (the vast majority of cases being rectal resections) treated with neoadjuvant chemoradiation. As can be seen from the responses to question 6, there does not appear to be a uniform approach to sampling these specimens. There is tremendous inter-pathologist and institutional variation. However, it is clear that there should be uniformity of handling of these specimens and we would recommend that optimally the entire grossly/macroscopically abnormal area be sampled in toto. If this is not feasible, we would endorse the suggestion of the second European Rectal Cancer Consensus Conference as a minimum guideline. On grading, the conference submitted that the most practical subdivision for the grading of tumour regression is: no response, signs of response, near complete response and complete response, which is the basis of the Royal College of Pathologists (implemented in 2007) [21] and Dworak guidelines on grading of regression.

Several grading systems for regression exist: Mandard, Dworak, rectal cancer regression grade (RCRG) its modification and finally the one suggested by the Royal College of Pathologists, UK [7–9, 12, 21]. While there are variations in the way these grading schemes are applied, they are all underpinned by the amount of residual tumour and evidence of response to treatment (fibrosis, mucin pools). Regression is graded depending on the relative proportion/extent of these elements. The participants used grading systems that they were familiar with, colleagues had recommended, their centres have used historically by consensus or recommended by practice guidelines established by responsible authorities such the Royal College of Pathologists, UK.

Imaging pre- and post-treatment is routinely performed to assess radiological regression and/or response to neoadjuvant chemoradiation. The two questions in the study regarding imaging related to the post-surgical specimen. In some centres, the post-operative specimen is also imaged (question 4) to assist the pathologist with identification of the tumour site and extent. It is also possible to map out and take sections from radiologically suspicious areas. Question 5 related to comparing the resection specimen with the post-chemoradiation and pre-surgical imaging. This also allows the pathologist to identify residual tumour and aid with sampling of the most appropriate areas.

It is evident from the survey that there is considerable variation in the approach, handling, assessment and final grading of regression of specimens treated with neoadjuvant chemoradiation, despite various organisations identifying and providing guidelines. It is interesting to note that 11 of the participants expressed a desire for consensus in the grading system used. Clearly, this should be guided by best practice principles, ease of application and reproducibility. As Bateman and colleagues pointed out, there is some inter-observer variability in applying some of the different grading schema, even between two pathologists [9]. This would be magnified if more pathologists participated and is implicit in some of the answers returned in the questionnaire, especially surrounding the application of the criteria in a given system. It seems reasonable to assume that the system with the least amount of stratification and subjectivity would

present the best way forward. Ultimately, the clinician needs to know whether or not pathological complete response is present. It behoves the pathologist to provide the most accurate interpretation of regression as it has prognostic and possible further therapeutic ramifications.

Conflict of interest There is no conflict of interest.

References

1. Gerard A, Buyse M, Nordlinger B et al (1998) Preoperative radiotherapy as adjuvant treatment in rectal cancer: final results of a randomized study of the European Organization for Research and Treatment of Cancer (EORTC). Ann Surg 208:606–614
2. Janjan NA, Khoo VS, Abbruzzese J et al (1999) Tumor downstaging and sphincter preservation with preoperative chemoradiation in locally advanced rectal cancer: the M.D. Anderson Center experience. Int J Radiat Oncol Biol Phys 44:1027–1038
3. Camma C, Giunta M, Fiorica F et al (2000) Preoperative radiotherapy for resectable rectal cancer: a meta-analysis. JAMA 284:1008–1015
4. Kaminsky-Forrett MC, Conroy T, Luporsi E et al (1998) Prognostic implications of downstaging following preoperative radiation therapy for operable T3–T4 rectal cancer. Int J Radiat Oncol Biol Phys 42:935–941
5. Mohiuddin M, Hayne M, Regine WF et al (2000) Prognostic significance of postchemoradiation stage following preoperative chemotherapy and radiation for advanced/recurrent rectal cancers. Int J Radiat Oncol Biol Phys 48:1075–1080
6. Medich D, McGinty J, Parda D et al (2001) Preoperative chemoradiotherapy and radical surgery for locally advanced distal rectal adenocarcinoma. Dis Colon Rectum 44:1123–1128
7. Mandard AM, Dalibard F, Mandard JC et al (1994) Pathologic assessment of tumor regression after preoperative chemoradiotherapy of esophageal carcinoma: clinicopathologic correlations. Cancer 73:2680–2686
8. Dworak O, Keilholz L, Hoffmann A (1997) Pathological features of rectal cancer after preoperative radiochemotherapy. Int J Colorectal Dis 12:19–23
9. Bateman AC, Jaynes E, Bateman AR (2009) Rectal cancer staging post neoadjuvant therapy—how should the changes be assessed? Histopathology 54:713–721
10. Pucciarelli S, Toppan P, Friso ML et al (2004) Complete pathologic response following preoperative chemoradiation therapy for middle to lower rectal cancer is not a prognostic factor for a better outcome. Dis Colon Rectum 47:1798–1807
11. Bouzourene H, Bosman FT, Seelentag W, Matter M, Coucke P (2002) Importance of tumour regression assessment in predicting the outcome in patients with locally advanced rectal carcinoma who are treated with preoperative radiotherapy. Cancer 94:1121–1130
12. Wheeler JMD, Dodds E, Warren BF et al (2004) Preoperative chemoradiotherapy and total mesorectal excision surgery for locally advanced rectal cancer: correlation with rectal cancer regression grade. Dis Colon Rectum 47:2025–2031
13. Vecchio FM, Valentini V, Minsky BD et al (2005) The relationship of pathologic tumour regression grade (TRG) and outcomes after preoperative therapy in rectal cancer. Int J Radiat Oncol Biol Phys 62:752–760
14. Sauer R, Becker H, Hohenberger W et al (2004) Preoperative versus postoperative chemoradiotherapy for rectal cancer. N Engl J Med 351:1731–1740
15. O'Neill BDP, Brown G, Heald RJ et al (2007) Non-operative treatment after neoadjuvant chemoradiotherapy for rectal cancer. Lancet Oncol 8:625–633
16. Rodel C, Martus P, Papadoupolos T et al (2005) Prognostic significance of tumor regression after preoperative chemoradiotherapy for rectal cancer. J Clin Oncol 23:8688–8696
17. Nagtegaal ID, Klein E, Kranenbarg J et al (2000) Pathology data in the central databases of multicenter randomized trials need to be based on pathology reports and controlled by trained quality managers. J Clin Oncol 18:1771–1779
18. Nagtegaal ID, Marijnen CAM, Kranenbarg EK et al (2002) Short-term preoperative radiotherapy interferes with the determination of pathological parameters in rectal cancer. J Pathol 197:20–27
19. Glynne-Jones R, Anyamene N (2006) Just how useful an endpoint is complete pathological response after neoadjuvant chemoradiation in rectal cancer? Int J Radiat Oncol Biol Phys 66:319–320
20. Valentini V, Aristei C, Glimelius B et al (2009) Multidisciplinary rectal cancer management: 2nd European Rectal Cancer Consensus Conference (EURECA-CC2). Radiother Oncol 92:148–163
21. Williams GT, Quirke P, Shepherd NA (2007) Royal College of Pathologists' Dataset for Colorectal Cancer, 2nd revision. http://www.rcpath.org/resources/pdf/G049-ColorectalDataset-Sep07.pdf

Virchows Arch (2012) 460:157–161
DOI 10.1007/s00428-011-1188-5

ORIGINAL ARTICLE

Decreased mucosal expression of intestinal alkaline phosphatase in children with coeliac disease

Kriszta Molnár · Ádám Vannay · Erna Sziksz · Nóra Fanni Bánki · Hajnalka Győrffy · András Arató · Antal Dezsőfi · Gabor Veres

Received: 3 November 2011 / Revised: 12 December 2011 / Accepted: 26 December 2011 / Published online: 20 January 2012
© Springer-Verlag 2012

Abstract A major function of the enzyme intestinal alkaline phosphatase (iAP) is the detoxification of lipopolysaccharide (LPS), the ligand of Toll-like receptor 4 (TLR4). Hence, iAP has a role in the defence of maintaining intestinal barrier integrity. As intestinal barrier integrity is impaired in coeliac disease (CD), we tested the expression and localization of iAP in duodenal mucosa specimens from children with newly diagnosed CD (n=10), with CD on gluten-free diet (GFD) (n=5) and compared to those from ten healthy children. The mRNA and protein expression was determined by RT-PCR and Western blot analysis, respectively. Tissue localization of iAP and TLR4 was determined by immunofluorescence staining. iAP protein expression level was significantly lower than normal in newly diagnosed CD, while it was normalised in children on GFD. iAP and TLR4 colocalized at the epithelial surface of duodenal mucosa in each group of subjects enrolled. The finding of decreased iAP protein levels in newly diagnosed CD is consistent with its role in decreased intestinal barrier integrity. The latter may be the result of decreased LPS-detoxifying ability.

Keywords Intestinal alkaline phosphatase · Toll-like receptor · Duodenal biopsy · Children · Coeliac disease

K. Molnár · A. Arató · A. Dezsőfi · G. Veres (✉)
1st Department of Paediatrics, Semmelweis University,
Bókay u. 53,
H-1083, Budapest, Hungary
e-mail: veres.gabor@med.semmelweis-univ.hu

Á. Vannay · E. Sziksz
Research Group for Paediatrics and Nephrology,
Semmelweis University and Hungarian Academy of Sciences,
Budapest, Hungary

N. F. Bánki
SE-MTA "Lendulet" Diabetes Research Group,
Budapest, Hungary

H. Győrffy
2nd Department of Pathology, Semmelweis University,
Budapest, Hungary

Introduction

Coeliac disease (CD) is a chronic enteropathy that is triggered by chronic exposure to gluten protein of wheat, barley and rye. Both the innate and the adaptive parts of the immune system are involved in its pathogenesis in genetically predisposed individuals [1, 2]. The diagnosis of CD is based on serologic tests, mucosal biopsy and the effects of gluten-free diet (GFD) on the symptoms [3]. The innate immune system in the pathogenesis of CD includes Toll-like receptors (TLR), a family of bacterial and viral pattern recognition receptors [4]. Under physiological circumstances TLRs play a crucial role in preserving a regulated homeostasis within the gut by the elimination of pathogens and toleration against commensal microbes [5]. TLR4, a member of the transmembrane receptor TLR family, is activated by lipopolysaccharide (LPS) present in the outer membrane of Gram-negative bacteria [6]. The uncontrolled activation of TLR4 may induce mucosal loss and induction of a proinflammatory cascade [7]. Recently, our group has shown increased mRNA and protein levels of TLR4 in the duodenal mucosa of children with newly diagnosed CD, and these levels further increased in CD patients on GFD [8]. In addition, we found a higher prevalence of TLR4-positive dendritic cells and monocytes in the peripheral blood of patients newly diagnosed with CD compared to controls [9].

The enzyme intestinal alkaline phosphatase (iAP) is expressed in large quantity on the apical surface of the

enterocytes [10]. iAP may play a pivotal role in the maintenance of intestinal barrier integrity by detoxification of LPS, the ligand of TLR4 [11, 12]. iAP is able to dephosphorylate the disphosphoryl lipid A part of LPS. This avoids pathological activation of TLR4 and the MyD88-dependent signalling events [13]. The precise role of iAP in CD is not defined, but according to previous studies in an animal model of inflammatory bowel disease, exogenously administered iAP improved the histological signs of inflammation [14]. A recent clinical study also reinforced the beneficial effects of exogenous iAP products in inflammatory bowel disease patients [15]. For CD, the data available for iAP suggest that iAP enzyme activity decreases in the duodenal biopsy specimens and strongly correlates with histological signs [16], but the iAP protein levels were not investigated.

The aim of our study was to collect additional data on iAP protein and mRNA expression in CD. We also tested whether or not iAP and TLR4 are colocalized in duodenal mucosa.

Materials and methods

Patients and duodenal biopsies

We enrolled ten children (two boys, eight girls; median age, 4 years; range, 2–12 years) with newly diagnosed CD and five children (two boys, three girls; median age, 12 years; range, 6–13 years) with GFD-treated CD and ten controls (five boys, five girls; median age, 9.5 years; range, 2–16 years) in the study. CD was diagnosed by the criteria of the European Society for Paediatric Gastroenterology, Hepatology and Nutrition [17, 18]. Screening for CD was performed using IgA anti-tissue transglutaminase [19]. High level of anti-tissue transglutaminase and villous atrophy was demonstrated in all patients with newly diagnosed CD. Children on GFD had full clinical and histological remission supported by normal blood levels of anti-tissue transglutaminases. The time frame between the first and the second biopsies of patients on GFD (GFD-treated CD) was 1.5 years (range, 0.5–2.5 years). The control group included children with chronic abdominal pain or chronic diarrhoea referred to the outpatient clinic. Normal blood levels of anti-tissue transglutaminases were demonstrated, and no histological alterations were present in their duodenal biopsy specimens. The subjects' anthropometric parameters in each group were comparable (Table 1). Written informed consent was obtained from parents prior to the procedure. The study was approved by the Semmelweis University Regional and Institutional Committee and Research Ethics.

RNA isolation and real-time PCR

Total RNA was isolated from the duodenal biopsy samples. Total RNA was reverse-transcribed to generate first-strand cDNA. iAP mRNA expression was determined by real-time PCR on a Light Cycler480 (Roche Diagnostics, Mannheim, Germany). PCRs were performed containing RealTime ready Catalog Assay primer (Roche Diagnostics), Brilliant II QPCR Master Mix (Stratagene, Cedar Creek, TX, USA) and cDNA. Conditions for iAP include one cycle, 95°C, 10 min (denaturation), followed by several cycles at 95°C, 20 s and 60°C, 1 min (annealing and extension). The internal control was glyceraldehyde-3-phosphate dehydrogenase (GAPDH). The mRNA expression of GAPDH was determined using Brilliant II Fast SYBR Green QPCR Master Mix (Stratagene), PCR primers (forward: 5-CAC CAC CAT GGA GAA GGC TG-3′; reverse: 5-GTG ATG GCA TGG

Table 1 Clinical characteristics of newly diagnosed patients with CD and patients treated on GFD

Patient		Gender	Age (years)	Main symptom	IEL/100	Marsh modification
1	CD	F	3	Weight loss	80	3b
2	CD	F	3	Weight loss	72–85	3b–3c
3	CD	F	2	Weight loss, diarrhoea	80–90	3c
4	CD	F	7	Iron deficiency	50–60	3b–3c
5	CD	M	12	Coeliac disease screening	55–70	2
6	CD	F	5	Coeliac disease screening	40–50	2
7	CD	F	3	Iron deficiency	85	3b
8	CD	F	10	Growth failure	65	3b
9	CD	M	2	Iron deficiency	50	3c
10	CD	F	5	Coeliac disease screening	72–80	3b
11	GFD	F	12	Chronic abdominal pain	20–25	0
12	GFD	M	6	–	10–15	0
13	GFD	M	7	–	3–4	0
14	GFD	F	13	–	10	0
15	GFD	F	16	–	6	0

Threshold of duodenal intraepithelial lymphocytes at villus tip and per 100 enterocytes (IEL/100)

M male, *F* female

ACT GTG-3′, Invitrogen, CA, USA) and cDNA. Conditions for GAPDH include one cycle, 95°C, 2 min followed by 50 cycles at 95°C, 20 s, and 60°C, 40 s. Results were analysed by Light-Cycler software 480 (Roche Diagnostics).

Protein isolation and Western blotting

Duodenal biopsy samples were homogenized in lysing solution, and the total protein concentrations were analysed by DC Protein Assay (Bio-Rad Laboratories, Hercules, CA, USA). An equal amount of protein samples, 0.5 μg from each sample, was separated by 10% sodium dodecyl sulphate–polyacrylamide gel electrophoresis (120 V, 40 mA, 120 min) (Penguin™ Dual-Gel Water Cooler Systems, Owl, NH, USA) and transferred to nitrocellulose membrane (GE Healthcare, Little Chalfont, UK) (70 V, 220 mA, 120 min) (MiniTank™ electroblotter, Owl). Membranes were blocked in 1% fat-free dry milk solution (1 h) and incubated with iAP-specific rabbit polyclonal antibody (1:1,000, 1 h) (AbCam, Cambridge, UK). Equal protein loading was confirmed by ß-actin-specific (C-11) goat polyclonal IgG antibody (1:100) (Santa Cruz Biotechnology Inc., Santa Cruz, CA, USA). The membrane was incubated with peroxidase-conjugated secondary anti-rabbit IgG or donkey anti-goat IgG antibodies (1:2,000, 30 min) (Santa Cruz Biotechnology Inc.). Immunoreactive bands were visualized using the enhanced chemiluminescence Western blotting detection reagents (GE Healthcare). Bands were analysed with software Image J. 1.42q (National Institutes of Health, USA). The values were expressed as relative optical density.

Immunofluorescence staining

The snap-frozen duodenal biopsy samples were imbedded in Shandon cryomatrix (ThermoElectron Co., Waltham, MA, USA) and cut to 3–4-μm slides. For iAP and TLR4 double immunofluorescence, iAP-specific rabbit polyclonal antibody and TLR4-specific goat polyclonal antibody were applied (1:100, 1 h) (Abcam Plc). Alexa Fluor 488 donkey anti-goat and Alexa Fluor 568 goat anti-rabbit antibodies were used as secondary antibodies (Invitrogen). Zeiss LSM 510 Meta confocal laser scanning microscope (Carl Zeiss, Jena, Germany) was used with ×20 Plan Apochromat (NA= 0.8) and ×63 Plan Apochromat oil immersion differential interference contrast objectives (NA=1.4).

Statistical analysis

Data were analysed using Statistica 7.0 software (StatSoft Inc., Tulsa, OK, USA). After testing the normality with Shapiro–Wilk's test, nonparametric Mann–Whitney *U* test was used. Values of $p \leq 0.05$ were considered to be significant and expressed as mean±SD.

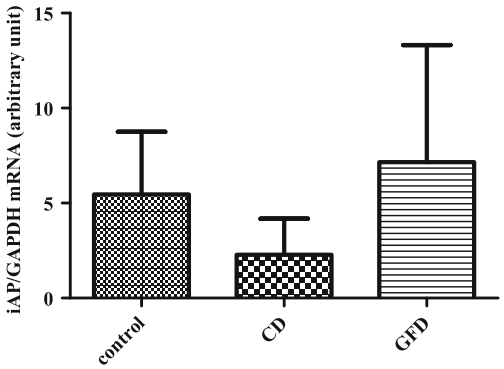

Fig. 1 iAP mRNA expression in the duodenal mucosa of children with coeliac disease (*CD*), children on *GFD* and healthy controls. mRNA expression of iAP was determined by computerized analysis of RT-PCR. Optical density of the investigated RT-PCR products was corrected for that of GAPDH. Data are expressed as mean±SD. The mRNA expression of iAP in duodenal mucosa of newly diagnosed patients with CD was not significantly decreased in comparison to patients with GFD and healthy controls

Results

iAP mRNA expression

Real-time PCR was performed to determine the mRNA expression of iAP in children with newly diagnosed CD,

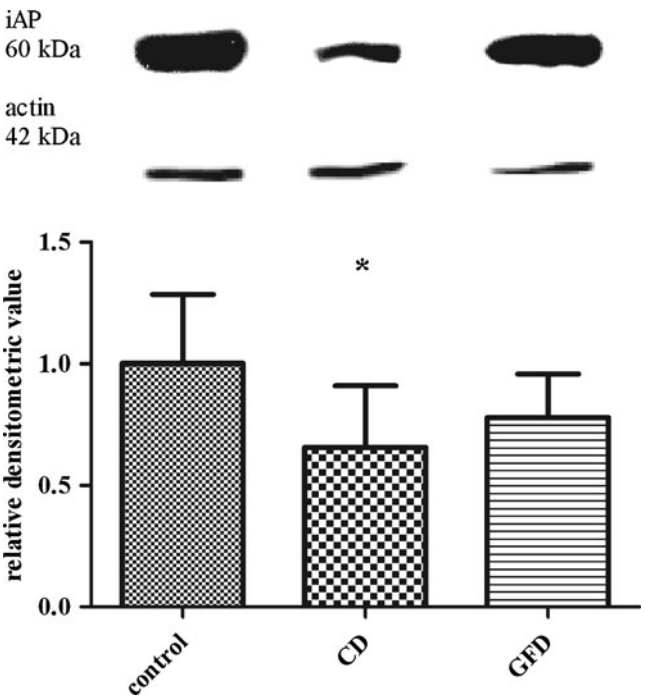

Fig. 2 Protein levels of iAP in the duodenal mucosa of children with newly diagnosed CD, children on GFD, and healthy controls. Western blot analysis reveals one distinct band at a molecular weight of 60 kDa with rabbit polyclonal antibody specific to human iAP in the duodenal biopsy specimens of children with CD and with GFD, and healthy controls (**a**). Data for protein levels of iAP were obtained by computerized analysis of the Western blots (**b**). Data are expressed as mean±SD. Analysis of significance was performed by Mann–Whitney *U* test. *$p<0.05$ vs. control

children with GFD, and healthy controls. As shown in Fig. 1, iAP mRNA expression was decreased in the duodenal mucosa of children with newly diagnosed CD compared to healthy controls; however, the difference failed to reach significance. There was no significant difference in children maintained on GFD and newly diagnosed CD groups, but the iAP mRNA expression of the GFD group has started to normalise.

iAP protein levels

We performed Western blot analysis in the duodenal biopsy specimens from newly diagnosed CD patients, children with GFD, and healthy controls, which revealed one distinct band at 60 kDa. The amount of iAP protein in newly diagnosed children with CD was significantly decreased when compared to controls (33%, $p<0.05$) (Fig. 2). iAP protein levels of patients on GFD were higher than those of CD patients but lower than those of controls (Fig. 2).

Localization of iAP and TLR4 in the duodenum

Immunofluorescence staining was performed to investigate the possible colocalization of iAP and TLR4 in patients with CD, children with GFD, and healthy controls (Fig. 3). iAP and TLR molecules clearly colocalized in a dot-like pattern in all groups studied. iAP was restricted to the epithelial surface of the duodenal mucosa, but no immunofluorescent signal was detected in goblet cells, in immune cells of the lamina propria or in the Lieberkühn cells.

Discussion

To the best of our knowledge, we are the first to demonstrate the alteration of protein expression of iAP and the localization of iAP and TLR4 in the duodenal mucosa of children with newly diagnosed CD, children maintained on GFD, and healthy controls. We found significantly reduced iAP protein levels in the duodenal mucosa of newly diagnosed CD patients, compared to healthy controls. The iAP protein levels of children maintained on GFD were lower than those of controls, but higher than those of patients with CD.

iAP is a recently identified enzyme with a major role in intestinal barrier integrity. Its possible contribution to CD is highlighted by Prasad et al. who reported that the activity of iAP and other brush-border enzymes correlates with histologically moderate and severe lesions in CD duodenal specimens [16] and that these abnormalities vanish on GFD [20, 21]. In line with these results, we found decreased iAP protein levels in newly diagnosed patients with CD that tended to normalise on GFD. We have also shown in a previous study that the increased expression of tight-junction molecules such as claudin 2 and 3 might contribute

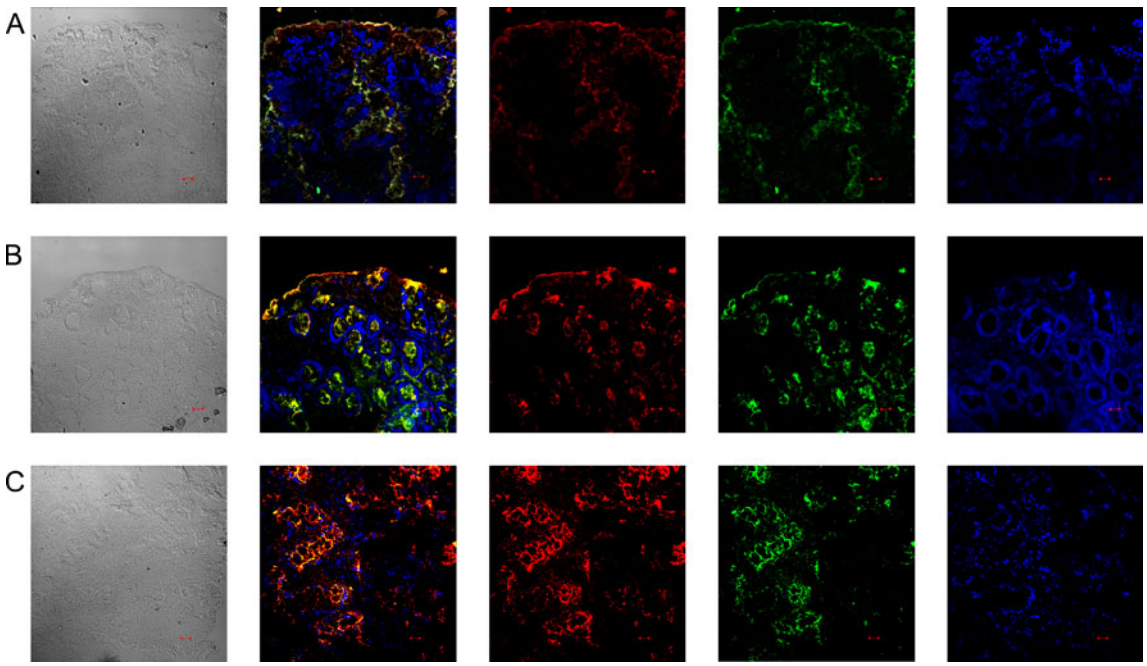

Fig. 3 Localization of iAP and TLR4 in duodenal mucosa of healthy controls, children with newly diagnosed CD and children on GFD. Immunofluorescent staining using anti-iAP and anti-TLR4 antibodies staining were performed. Representative example sections of duodenum are shown: healthy controls (**a**), children with CD (**b**) and patients treated with GFD (**c**). Differential interference contrast was used for the observation of non-labelled tissues. Double-positive cells for iAP and TLR4 are seen as *yellow* clusters. iAP (*red*) and TLR4 (*green*) were equally intense only at the epithelial surface in all groups studied. Nuclei are stained with *blue*. *Bar*=20 μm

to the change of barrier function of the duodenal mucosa [22] and to increased permeability and consequential malabsorption. The decreased level of iAP may be a further element contributing to the degradation of intestinal barrier integrity [11]. Nevertheless, the decreased iAP level in untreated patients with CD is probably an inflammation-related, nonspecific finding for CD; however, our results (colocalization with TLR, TLR–LPS-detoxifying ability) may add new pieces to the puzzle of the pathomechanism of CD.

The possible contribution of iAP to intestinal barrier integrity is thought to be mediated by its action on TLR ligands. Indeed, we observed that iAP and TLR4 occur in a colocalized manner. Previously, we have shown increased TLR4 expression in newly diagnosed patients with CD [8]. Theoretically, the lower-than-normal iAP together with a higher-than-normal TLR4 expression results in an imbalance in iAP/TLR4 ratio and, hence, an increased inflammatory response to LPS present in the gut. These data support that innate immunity and, particularly, TLRs are major players in disturbed intestinal barrier integrity in CD.

In summary, we found decreased iAP duodenal mucosal protein expression in children with newly diagnosed CD. In addition, a strong colocalization of iAP and TLR4 at the epithelial surface of duodenal mucosa was found. These findings suggest that iAP plays an important role in the restitution of mucosal barrier integrity and in innate immunity.

Acknowledgements We thank Mária Bernáth for her excellent technical assistance. This work was supported by grants OTKA-76316, OTKA-K81117, TÁMOP 4.2.2. B-10/1-2010-2013, and ETT-028-02. Gábor Veres and Ádam Vannay are holders of the János Bolyai Research grant; this article was supported by the János Bolyai Research Scholarship of the Hungarian Academy of Sciences.

Conflict of interest We declare that we have no conflict of interest.

References

1. Maynard CL, Weaver CT (2011) Immunology: context is key in the gut. Nature 471:169–170
2. Dickson BC, Streutker CJ, Chetty R (2006) Coeliac disease: an update for pathologists. J Clin Pathol 59:1008–1016
3. Ensari A (2010) Gluten-sensitive enteropathy (celiac disease): controversies in diagnosis and classification. Arch Pathol Lab Med 134:826–836
4. Cario E (2008) Barrier-protective function of intestinal epithelial Toll-like receptor 2. Mucosal Immunol 1(Suppl 1):S62–S66
5. Abreu M, Fukata M, Arditi M (2005) TLR signaling in the gut in health and disease. J Immunol 174:4453–4460
6. Triantafilou M, Triantafilou K (2002) Lipopolysaccharide recognition: CD14, TLRs and the LPS-activation cluster. Trends Immunol 23:301–304
7. Baumgart D, Thomas S, Przesdzing I, Metzke D, Bielecki C, Lehmann S, Lehnardt S, Dörffel Y, Sturm A, Scheffold A, Schmitz J, Radbruch A (2009) Exaggerated inflammatory response of primary human myeloid dendritic cells to lipopolysaccharide in patients with inflammatory bowel disease. Clin Exp Immunol 157:423–436
8. Szebeni B, Veres G, Dezsofi A, Rusai K, Vannay A, Bokodi G, Vásárhelyi B, Korponay-Szabó I, Tulassay T, Arató A (2007) Increased mucosal expression of Toll-like receptor (TLR)2 and TLR4 in coeliac disease. J Pediatr Gastroenterol Nutr 45:187–193
9. Cseh Á, Vásárhelyi B, Szalay B, Molnár K, Nagy-Szakál D, Treszl A, Vannay Á, Arató A, Tulassay T, Veres G (2011) Immune phenotype of children with newly diagnosed and gluten-free diet-treated celiac disease. Dig Dis Sci 56:792–798
10. Lallès JP (2010) Intestinal alkaline phosphatase: multiple biological roles in maintenance of intestinal homeostasis and modulation by diet. Nutr Rev 68:323–332
11. Bates J, Akerlund J, Mittge E, Guillemin K (2007) Intestinal alkaline phosphatase detoxifies lipopolysaccharide and prevents inflammation in zebrafish in response to the gut microbiota. Cell Host Microbe 2:371–382
12. Goldberg RF, Austen WG, Zhang X, Munene G, Mostafa G, Biswas S, McCormack M, Eberlin KR, Nguyen JT, Tatlidede HS, Warren HS, Narisawa S, Millán JL, Hodin RA (2008) Intestinal alkaline phosphatase is a gut mucosal defense factor maintained by enteral nutrition. Proc Natl Acad Sci U S A 105:3551–3556
13. Geddes K, Philpott D (2008) A new role for intestinal alkaline phosphatase in gut barrier maintenance. Gastroenterology 135:8–12
14. Tuin A, Poelstra K, de Jager-Krikken A, Bok L, Raaben W, Velders M, Dijkstra G (2009) Role of alkaline phosphatase in colitis in man and rats. Gut 58:379–387
15. Lukas M, Drastich P, Konecny M, Gionchetti P, Urban O, Cantoni F, Bortlik M, Duricova D, Bulitta M (2010) Exogenous alkaline phosphatase for the treatment of patients with moderate to severe ulcerative colitis. Inflamm Bowel Dis 16:1180–1186
16. Prasad K, Thapa B, Nain C, Sharma A, Singh K (2008) Brush border enzyme activities in relation to histological lesion in pediatric celiac disease. J Gastroenterol Hepatol 23:e348–e352
17. Ribes-Koninckx C, Mearin M, Korponay-Szabó I, Shamir R, Husby S, Ventura A, Branski D, Catassi C, Koletzko S, Mäki M, Troncone R, Zimmer K, The ESPGHAN Working Group on Coeliac Disease Diagnosis (2012) Coeliac disease diagnosis: espghan 1990 Criteria or need for a change? Results of a questionnaire. J Pediatr Gastroenterol Nutr 54(1):15–19
18. Meijer JW, Wahab PJ, Mulder CJ (2003) Small intestinal biopsies in celiac disease: duodenal or jejunal? Virchows Arch 442:124–128
19. Dalgic B, Sari S, Basturk B, Ensari A, Egritas O, Bukulmez A, Baris Z, TurkishCeliac Study Group (2011) Prevalence of celiac disease in healthy Turkish school children. Am J Gastroenterol 106:1512–1517
20. Gorgun J, Portyanko A, Marakhouski Y, Cherstvoy E (2009) Tissue transglutaminase expression in celiac mucosa: an immunohistochemical study. Virchows Arch 455:363–373
21. Wahab PJ, Meijer JW, Mulder CJ (2002) Histologic follow-up of people with celiac disease on a gluten-free diet: slow and incomplete recovery. Am J Clin Pathol 118:459–463
22. Szakál DN, Gyorffy H, Arató A, Cseh A, Molnár K, Papp M, Dezsofi A, Veres G (2010) Mucosal expression of claudins 2, 3 and 4 in proximal and distal part of duodenum in children with coeliac disease. Virchows Arch 456:245–250

Virchows Arch (2012) 460:163–169
DOI 10.1007/s00428-011-1181-z

ORIGINAL ARTICLE

Expression level of the mitotic checkpoint protein and G2–M cell cycle regulators and prognosis in gastrointestinal stromal tumors in the stomach

Aya Fujita · Hidetaka Yamamoto · Masakazu Imamura · Norimoto Nakamura · Yoshihiko Maehara · Masazumi Tsuneyoshi · Yoshinao Oda

Received: 21 July 2011 / Revised: 26 October 2011 / Accepted: 29 November 2011 / Published online: 22 December 2011
© Springer-Verlag 2011

Abstract The biological behavior of gastrointestinal stromal tumors (GISTs) ranges from benign to malignant, and the risk of an adverse outcome is correlated with the location of the primary tumor, tumor size, and mitotic counts. Cell cycle regulators are potentially associated with the tumorigenesis and progression of GISTs. Checkpoint with forkhead and ring finger (CHFR) functions as an important checkpoint protein in the early to mid-prophase to regulate mitosis. In this study, we evaluated the expression of CHFR and several cell cycle regulators, including cyclin A, cyclin B1, cdc2, and cdk2, by immunohistochemical staining in 53 cases of primary gastric GISTs, and compared the immunohistochemical results with the clinicopathological factors or the GIST risk grades as modified by Miettinen et al. Of the 53 cases, 18 (34%) showed decreased nuclear CHFR expression. Decreased CHFR expression was correlated with higher mitotic counts [>5/50 high-power fields (HPFs)] (p=0.039) and a high-risk grade (p=0.0475), but not with expression of other cell cycle regulators. Higher cyclin A labeling index (LI, >1.5%), cyclin B1 LI (>0.25%), cdc2 LI (>1.16%), Ki-67 LI (>4.9%), mitotic counts (>5/50 HPF) and high-risk grade were each associated with shorter disease-free survival (p=0.0017, p=0.003, p=0.0471, p=0.002, p<0.001, and p=0.0017, respectively). Our results suggest that modified risk grade and increased expression of G2–M regulators such as cyclin A, cyclin B1, and cdc2 are useful for predicting the biological behavior of gastric GISTs. In addition, decreased CHFR expression may play a role in increased proliferative activity of higher grade GISTs.

Keywords Gastrointestinal stromal tumor · Stomach · Cell cycle · CHFR · Cyclin A · Cyclin B1 · cdc2

A. Fujita · H. Yamamoto · M. Imamura · N. Nakamura · M. Tsuneyoshi · Y. Oda (✉)
Department of Anatomic Pathology,
Graduate School of Medical Sciences, Kyushu University,
3-1-1 Maidashi, Higashi-ku,
Fukuoka 812-8582, Japan
e-mail: oda@surgpath.med.kyushu-u.ac.jp

M. Imamura · Y. Maehara
Department of Surgery and Science,
Graduate School of Medical Sciences, Kyushu University,
Fukuoka, Japan

Introduction

Gastrointestinal stromal tumor (GIST) is the most common mesenchymal tumor arising from the digestive tracts, including the stomach and small intestine, and is characterized by immunohistochemical expression of KIT protein [1, 2]. GISTs have a gain-of-function mutation of the *KIT* gene or platelet-derived growth factor receptor alpha (*PDGFRA*) gene [3–7]. The biological behavior of GISTs ranges from benign to malignant, and it is difficult to draw a sharp line between benign and malignant lesions based on histomorphological features only. Several studies have demonstrated that a higher mitotic count and larger tumor size were both related to poorer prognosis of the GISTs. After the consensus meeting in 2001 at the National Institutes of Health (NIH), the risk grading advocated by Fletcher et al. [1] became widely used. This grading system classifies GISTs into four degrees (very low, low, intermediate, and high grade) based on a combination of tumor size and mitotic counts per 50 high-power fields (HPFs). These grading systems have been applied to both gastric and intestinal GISTs (Table 1).

Table 1 Risk grading system for gastric GISTs

Mitosis (HPF)	Size (cm)	Group	Modified risk grade by Miettien et al.[a]	Conventional risk grade by Fletcher et al.[b]
≤5/50	≤2	1	No risk (0%)[c]	Very low
	>2≤5	2	Very low (1.9%)[c]	Low
	>5≤10	3a	Low (3.6%)[c]	Intermediate
	>10	3b	Moderate (12%)[c]	High
>5/50	≤2	4	Possibly no risk[d]	Intermediate
	>2≤5	5	Moderate (16%)[c]	Intermediate
	>5≤10	6a	High (55%)[c]	High
	>10	6b	High (86%)[c]	High

[a]Ref. [2, 8]
[b]Ref. [1]
[c]Ratio of metastases
[d]Tentative grade because of small number cases

Recently, based on a very large numbers of GISTs, Miettinen et al. [2] reported that gastric GISTs have a better outcome than intestinal GISTs of similar size and mitotic rate. Large (>10 cm) gastric GISTs with low mitotic rates (<5/50 HPF) carried a risk of metastasis of only 10%, whereas tumors of similar size and mitotic rate arising in the small intestine had a high risk (>30%) of aggressive behavior. Apparently, gastric GISTs with low mitotic activity are less aggressive than previously assumed. Therefore, in the modified risk grading system proposed by Miettinen et al. [2], gastric GISTs with <5/50 HPFs were downgraded, irrespective of tumor size (Table 1) [8]. However, even this modified GIST risk grade does not perfectly predict the outcome of an individual patient with GIST. Thus, additional prognostic markers are needed.

Several studies have reported the possible prognostic value of the expression of cell cycle regulatory proteins, in particular G1–S regulators. Decreased expression of p16INK4a was associated with a poorer prognosis in GIST [9–11]. At the molecular level, decreased expression of p16INK4a protein is closely linked with loss of chromosome 9p and additional genetic or epigenetic alteration of the *p16* gene.

Checkpoint with forkhead and ring finger (CHFR) functions as an important G2–M checkpoint protein by keeping Aurora-A, Aurora-B, Plk1, and cyclin B1/cdc2 inactive [12–14]. CHFR was found downregulated in several established tumor cell lines and human carcinoma tissue samples, such as oral squamous cell carcinoma, gastric cancer, lung cancer, and breast cancer [15–18]. In a previous study, we evaluated the prognostic value of the level of expression of cell cycle regulators, including p53, p16, p21, p27, cyclin D1, cyclin E, cyclin A, cyclin B1, cdk2, and cdc2 in GISTs [19]. Overexpression of G2–M regulators, cyclin A, cyclin B1, and cdc2, was associated with the Ki-67 LI. In addition, conventional risk grade (high risk), tumor size (≧5 cm), mitotic counts (≧5/50 HPF), Ki-67 LI (≧4.92%), cyclin A LI (≧1.61%), and cdc2 LI (≧1.25%) were significantly associated with worse prognosis of patients with GIST. The cohort in that study, however, included both gastric and small intestinal GISTs, although recent studies revealed that biological behavior of gastric GISTs was different from that of small intestinal GISTs. Therefore, we decided to reappraise the prognostic value of the above factors according to the primary site of GISTs.

As mentioned above, mitotic counts seem to more strongly influence prognosis, particularly in gastric GIST, compared with tumor size. However, which underlying molecular mechanisms are involved in the increased mitotic index is poorly understood. The aim of this study was therefore to elucidate

Table 2 Summary of clinicopathological findings and risk grade in 53 cases of gastric GISTs

		Risk grade			
		Very low and no (*n*=16)	Low (*n*=12)	Moderate (*n*=8)	High (*n*=17)
Gender	Male	9	4	4	9
	Female	7	8	4	8
Age (mean, years)		62.4	68.8	68.8	61.1
Histologic type	Spindle	10	8	6	13
	Epithelioid	1	1	0	3
	Mixed	5	3	2	1
Necrosis and/or Hemorrhage	Absent	8	12	6	14
	Present	8	0	2	3

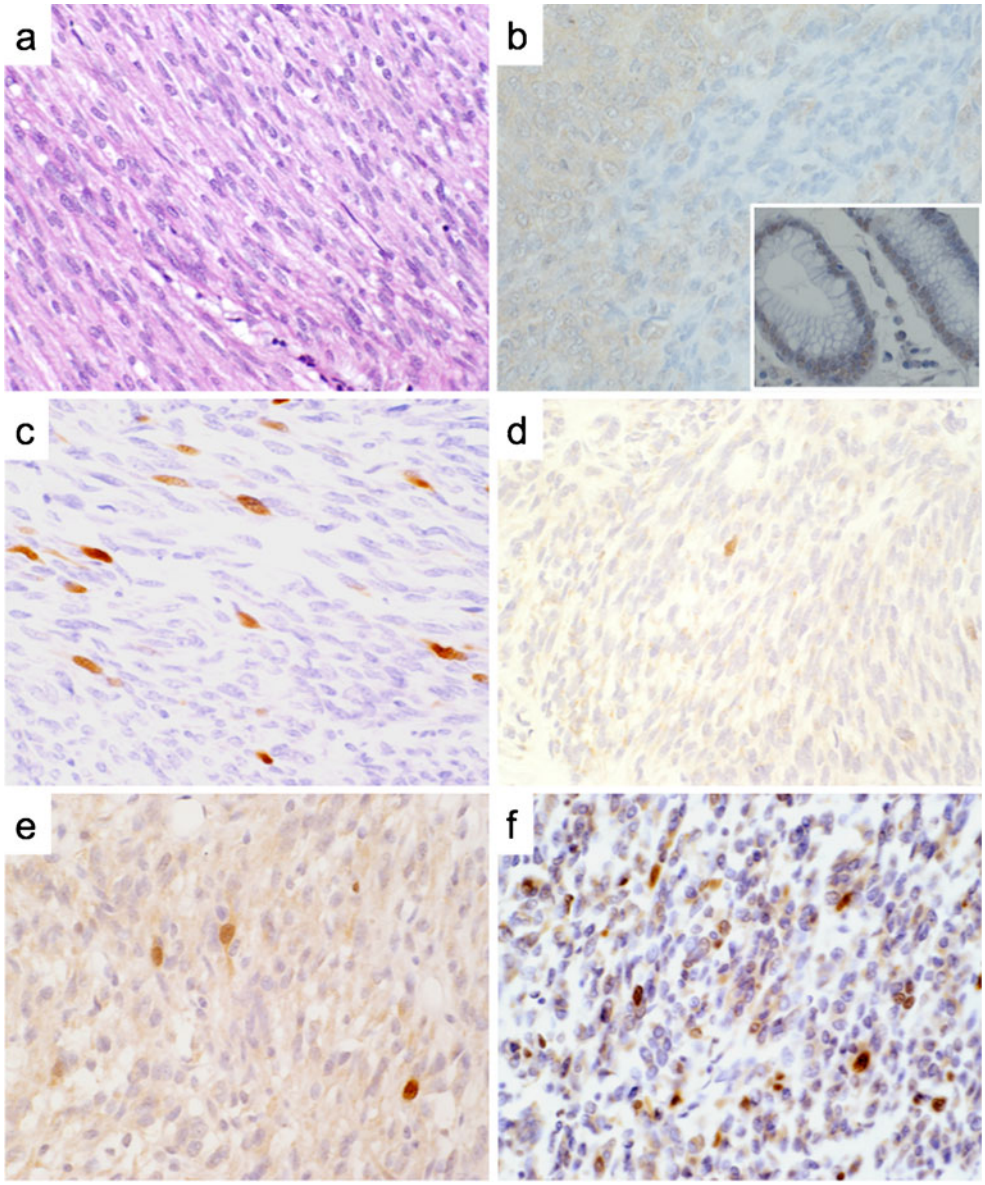

Fig. 1 Immunohistochemical staining of gastric GISTs. **a** A representative case of GIST, spindle cell type. **b** Moderate-risk grade GIST showing loss of nuclear CHFR expression (*inset* positive nuclear CHFR expression in the normal mucosa adjacent to GIST). **c** High-risk grade GIST showing positive expression of cyclin A, LI 6.8%. **d** High-risk grade GIST showing positive expression of cyclin B1, LI 0.3%. **e** Low-risk grade GIST showing positive expression of cdc2, LI 3.5%. **f** High-risk grade GIST showing high Ki-67 LI, 21.2%

the potential role of the level of expression of CHFR and related cell cycle regulators in the mitotic activity and biological behavior of gastric GISTs.

Materials and methods

Case materials

Specimens from 53 primary gastric GISTs were obtained from the Department of Anatomic Pathology of Kyushu University between 1986 and 2002. All 53 cases has been included in a previous study [19] and concerned surgical resection specimens. The diagnosis was made based on histopathologic features on H&E-stained sections and on the consistent immunohistochemical expression of KIT. The modified (Miettinen) risk grade of each tumor was determined based on tumor size and mitotic counts per 50 HPFs in the most mitotically active areas [8]. This study was approved by the surveillance committee of Kyushu University (number 22-114).

Immunohistochemical study

Histologic sections (3 μm thick) of 10% formalin-fixed, paraffin-embedded tissue samples were used for immunohistochemistry.

Table 3 The correlations between cell cycle markers and tumor size, mitotic figures, or risk grade in gastric GISTs

		Tumor size (cm)		*p* value	Mitotic figures			Risk grade		*p* value
		≤5	>5		≤5/50 HPF	>5/50 HPF		Very low, low, or moderate	High	
Cyclin A	Low (≤1.5%)	16	22	0.556	27	11	0.0114[a]	29	9	0.041[a]
	High (>1.5%)	5	10		5	10		7	8	
Cyclin B	Low (≤0.25%)	19	23	0.089	27	15	0.256	30	12	0.286
	High (>0.25%)	2	9		5	6		6	5	
cdc2	Low (≤1.16%)	13	24	0.301	23	14	0.686	25	12	0.933
	High (>1.16%)	8	8		9	7		11	5	
cdk2	Low (≤25.38%)	13	22	0.607	22	13	0.607	26	9	0.171
	High (>25.38%)	8	10		10	8		10	8	
Ki-67	Low (≤4.9%)	16	17	0.09	24	9	0.0218[a]	26	7	0.03[a]
	High (>4.9%)	5	15		8	12		10	10	
CHFR	Negative	6	12	0.502	6	12	0.039[a]	9	9	0.0475[a]
	Positive	15	20		26	9		27	8	

[a] Statistically significant

Expression of c-KIT, CD34, Ki-67, cyclin A, cyclin B1, cdc2, and cdk2 was reported in a previous study [19]. For CHFR we used H0055743-M01, dilution 1/600 (Abnova, Taipei, Taiwan) with incubation at 4°C overnight, followed by staining with the dextran polymer method (Envision+, DAKO). 3,3′-Diaminobenzidine tetrahydrochloride was used as a chromogen to visualize the immunoreaction, and the sections were counterstained with hematoxylin. For CHFR, we defined any nuclear immunostaining as positive, and no nuclear staining as negative, as CHFR was reported to function in the nucleus [20, 21]. The labeling indices (in percent) for Ki-67, cyclin A, cyclin B1, cdc2, and cdk2 were as previously reported (Table 3, [19]).

Statistical analysis

The correlation between the expression of cell cycle regulators and clinicopathological factors (size, mitosis, or risk grade) was analyzed by the chi-square test or the Wilcoxon's test. For univariate and multivariate analyses of disease-free survival (DFS), we used the Kaplan–Meier method with the log-rank test and the Cox proportional hazard model, respectively.

Results

Clinicopathological findings

Clinicopathological data for patients with gastric GISTs are summarized in Table 2. The 53 patients comprised 26 males and 27 females, ranging in age from 34 to 93 years (mean, 63.4 years old). The diameter of tumors ranged from 0.9 to 22 cm (mean, 7.63 cm). Histologically, 37 tumors were spindle cell type, 5 were epithelioid type, and 11 were mixed type. According to the Miettinen risk grade, 1 tumor was classified as no risk (group 1), 15 were classified as very low risk (group 2), 12 as low risk (group 3a), 8 as moderate risk (groups 3b and 5), and the remaining 17 as high risk (groups 6a and 6b). There were no cases classified as group 4 (possibly no risk). In this study, we considered the no risk case together with very low-risk cases. Six cases were found to have distant and/or peritoneal metastases at the initial operation: of these four cases were high grade (liver metastasis in two cases; peritoneal metastasis in one; both peritoneal and lymph node metastases in one), and two cases were low grade (liver metastasis in one, and both peritoneal and lymph node metastases in another one).

Immunohistochemical findings with clinicopathological correlations

Of the 53 gastric GISTs, 18 cases (34%) showed decreased nuclear CHFR expression (Fig. 1) while the labeling index for cyclin A, cyclin B1, cdc2, and cdk2 varied (Fig. 1) as listed

Fig. 2 Disease-free survival analysis for 47 patients with gastric GISTs that had neither metastases nor peritoneal dissemination at initial operation. **a** GIST patients with higher cyclin A expression have significantly shorter DFS (p=0.0017). **b** GIST patients with higher cyclin B1 expression have significantly shorter DFS (p=0.003). **c** GIST patients with higher cdc2 expression have significantly shorter DFS (p=0.0471). **d** GIST patients with higher Ki-67 LI have significantly shorter DFS (p=0.002). **e** GIST patients with more frequent mitoses (>5 out of 50 HPFs) have significantly shorter DFS than those with fewer mitoses (p<0.001). **f** GIST patients in the high-risk grade had significantly shorter DFS than those in the very low-, low-, or moderate-risk grade (p=0.0017). **g** GIST patients with larger tumors (>5 cm) tended to have shorter DFS than those with smaller tumors, but this relationship was not statistically significant. **h** CHFR expression level is not correlated with DFS (p=0.545)

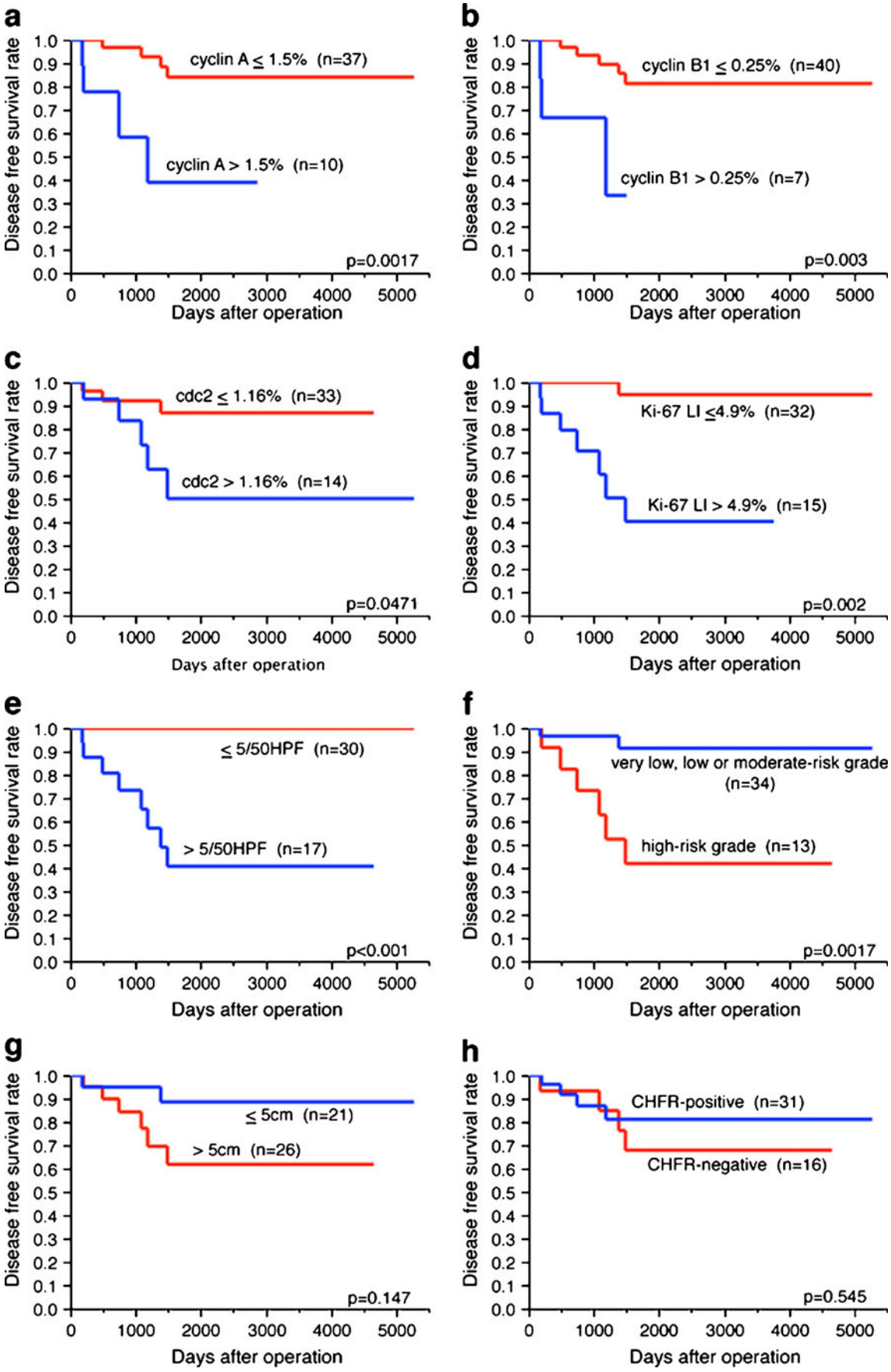
a
Disease free survival rate
cyclin A ≤ 1.5% (n=37)
cyclin A > 1.5% (n=10)
p=0.0017
Days after operation
b
Disease free survival rate
cyclin B1 ≤ 0.25% (n=40)
cyclin B1 > 0.25% (n=7)
p=0.003
Days after operation
c
Disease free survival rate
cdc2 ≤ 1.16% (n=33)
cdc2 > 1.16% (n=14)
p=0.0471
Days after operation
d
Disease free survival rate
Ki-67 LI ≤4.9% (n=32)
Ki-67 LI > 4.9% (n=15)
p=0.002
Days after operation
e
Disease free survival rate
≤ 5/50HPF (n=30)
> 5/50HPF (n=17)
p<0.001
Days after operation
f
Disease free survival rate
very low, low or moderate-risk grade (n=34)
high-risk grade (n=13)
p=0.0017
Days after operation
g
Disease free survival rate
≤ 5cm (n=21)
> 5cm (n=26)
p=0.147
Days after operation
h
Disease free survival rate
CHFR-positive (n=31)
CHFR-negative (n=16)
p=0.545
Days after operation

in Table 3. The correlations between the clinicopathological parameters and the expression level of each cell cycle marker are summarized in Table 3. Reduced expression of CHFR correlated with higher mitotic counts (>5/50 HPFs, $p=0.039$) and high-risk grade ($p=0.0475$), but not with tumor size ($p=0.502$) or other cell cycle regulators (data not shown). The increased expression of cyclin A was significantly correlated with higher mitotic count ($p=0.0114$) and higher risk ($p=0.041$), but was not with tumor size ($p=0.556$). Ki-67 LI was correlated with higher mitotic count ($p=0.0218$) and higher risk grade ($p=0.03$). The expression level of cell cycle regulators other than CHFR, cyclin A, and Ki-67 was not significantly correlated with clinicopathological factors, including mitosis, tumor size, and risk grade.

Prognostic significance of both classic pathologic features and cell cycle immunomarkers

Follow-up information was available for 53 patients, and the follow-up period ranged from 1 to 175.3 months (median, 48.5 months; mean, 58.6 months). The prognostic value of several factors (e.g., tumor size, mitosis, risk grade, histologic type, and cell cycle-related proteins) for DFS was analyzed in 47 cases, excluding 6 cases with peritoneal and/or distant metastases at the initial operation. Of the 47 cases, 8 (17%) cases had relapsed; 4 cases had metastases in the liver, 1 case in the liver and peritoneum, 2 cases in the peritoneum, and 1 case in the remnant portion of stomach. The eight cases with relapse comprised seven high-grade GISTs and one moderate-grade GIST.

Higher cyclin A LI (>1.5%), cyclin B1 LI (>0.25%), cdc2 LI (>1.16%), Ki-67 LI (>4.9%), mitotic counts (>5/50 HPF), and high-risk grade were all associated with shorter DFS by univariate analysis ($p=0.0017$, $p=0.003$, $p=0.0471$, $p=0.002$, $p<0.001$, and $p=0.0017$, respectively; Fig. 2a–f and Table 4). Tumor diameter and the expression levels of CHFR did not correlate with DFS (Fig. 2g–h). On multivariate analysis, higher mitotic counts as well as higher Ki-67 LI and cdk2 were also significantly associated with shorter DFS ($p<0.0001$, $p=0.0007$, and $p=0.021$, respectively; Table 4).

Discussion

In the current study, we reevaluated the prognostic value of the expression of cell cycle-related markers in gastric GISTs based on the modified risk grading system. We found that increased expression of cyclin B1, in addition to cyclin A and cdc2, correlates with a worse prognosis in gastric GISTs. Decreased expression of CHFR protein did not correlate with GIST prognosis.

The risk grading system, which does not draw a sharp line between "benign" and "malignant" lesions, has been in use since the consensus workshop at NIH in 2001. Recently, based on a more detailed subclassification of large numbers of GISTs, Miettinen et al. proposed a modified grading system [8]. Although group 3b (>10 cm, ≦5 mitoses/50 HPF) and group 6 (>5 or >10 cm, >5mitoses/50 HPF) had been classified as high-risk grade in Fletcher's/NIH system, Miettinen et al. found that group 3b GISTs had a better outcome than group 6, suggesting that large gastric GISTs with low mitotic activity are less aggressive than previously assumed. We found higher mitotic counts (>5/50 HPFs) and modified grade (high grade) significantly correlated with worse prognosis, but not tumor size (>5 cm). Our data support the modified grading system for predicting the biological behavior of gastric GISTs.

In a previous study, including both gastric and intestinal GISTs, we showed that higher expression of cyclin A, cdc2, and Ki-67; higher mitotic counts; and high-risk grade correlated with worse prognosis. As the biological behavior of GIST is different depending on the primary site, we reappraised the clinicopathological significance of levels of expression of cell cycle regulators in gastric GIST. We previously reported that higher LI for cyclin A, cdc2, and Ki-67 and mitotic counts as

Table 4 Univariate and multivariate analyses for prognostic factors in gastric GIST

Variables	*p* value	
	Univariate	Multivariate
Tumor size (≤5 vs >5 cm)	0.147	0.14
Mitosis (≤5/50 vs >5/50 HPF)	<0.001[a]	<0.0001[a]
Risk grade (very low, low, moderate vs high)	0.0017[a]	Not included
Ki-67 (≤4.9% vs >4.9%)	0.002[a]	0.0007[a]
Histological type (epithelioid vs mixed and spindle)	0.179	0.442
Hemorrhage or necrosis (absent or present)	0.102	0.201
CHFR (negative vs positive)	0.545	0.152
Cyclin A (≤1.5% vs >1.5%)	0.0017[a]	0.413
Cyclin B1 (≤0.25% vs >0.25%)	0.003[a]	0.797
cdc2 (≤1.16% vs >1.16%)	0.0471	0.993
cdk2 (≤25.38% vs >25.38%)	0.69	0.021[a]

[a]Statistically significant

well as high-risk grade associate with a shorter DFS. We found that higher cyclin B1 LI correlates with shorter DFS, but cyclin B1 expression had no prognostic significance.

Although increased mitotic activity is a strong prognostic indicator in gastric GIST, the fundamental mechanisms underlying increased mitoses are poorly understood in GISTs. CHFR is one of the checkpoint proteins regulating early the G2–M transition and is downregulated in various cancers; furthermore, it delays the transition from early to mid-prophase by keeping the Aurora-A, -B, cyclin B1/cdc2 complex, and PLK inactive [12–14]. In several studies on carcinomas, the decrease or loss of CHFR expression was associated with higher mitotic indices, suggesting that CHFR functions as a tumor suppressor gene [15–18]. We earlier reported that decreased CHFR expression is correlated with a high mitotic rate and poor prognosis in malignant peripheral nerve sheath tumors [20]. The molecular mechanism leading to the downregulation of CHFR has been reported to be the methylation of the promoter region of the *CHFR* gene [17, 21, 22]. In contrast, hypermethylation of the promoter region of *CHFR* gene was less frequent (9.8%) in GIST [23]. Recently, loss of *CHFR* DNA copy number has been suggested as an alternative mechanism of inactivation of CHFR in esophageal adenocarcinoma [24]. In the current study, we found that decreased expression of CHFR protein was present in 34% (18 out of 53 cases) of gastric GIST but we failed to find a close relationship between the expression levels of CHFR and its possible targets, such as cyclin A and cyclin B1. This result suggests that in GIST, cyclin A and cyclin B1 might be controlled mainly by other cell cycle regulators, such as Aurora kinase [25, 26].

In conclusion, our results support Miettinen's modified risk grade system for predicting the biological behavior of gastric GISTs. In addition, increased expression of G2–M regulators, such as cyclin A, cyclin B1 and cdc2, may be useful for predicting the biological behavior of gastric GISTs. Although reduced CHFR expression correlated with higher mitotic counts, it did not have independent prognostic value.

Acknowledgment This study was supported in part by the Grants-in-Aid for Scientific Research from the Japan Society for the Promotion of Science, Tokyo, Japan (Grant Number 22790346; H. Yamamoto).

Conflict of interest statement We declare that we have no conflict of interest.

References

1. Fletcher CD, Bermann JJ, Corless C et al (2002) Diagnosis of gastrointestinal stromal tumors: a consensus approach. Hum Pathol 33:459–465
2. Miettinen M, Lasota J (2006) Gastrointestinal stromal tumors: pathology and prognosis at different sites. Semin Diagn Pathol 23:70–83
3. Lasota J, Miettinen M (2006) KIT and PDGFRA mutations in gastrointestinal stromal tumors (GISTs). Semin Diagn Pathol 23:91–102
4. Hirota S, Isozaki K, Moriyama Y et al (1998) Gain-of function mutations of c-kit in human gastrointestinal stromal tumors. Science 279:577–580
5. Heinrich MC, Corless CL, Duensing A et al (2003) PDGFRA activating mutations in gastrointestinal stromal tumors. Science 299:708–710
6. Hirota S, Ohashi A, Nishida T et al (2003) Gain-of function mutations of platelet-derived growth factor receptor alpha gene in gastrointestinal stromal tumors. Gastroenterology 125:660–667
7. Yamamoto H, Oda Y, Kawaguchi K et al (2004) c-kit and PDGFRA mutations in extragastrointestinal stromal tumor (gastrointestinal stromal tumor of the soft tissue). Am J Surg Pathol 28:479–488
8. Miettinen M, Sobin LH, Lasota J (2005) Gastrointestinal stromal tumors of the stomach. A clinicopathologic, immunohistochemical, and molecular genetic study of 1765 cases with long-term follow up. Am J Surg Pathol 29:52–68
9. Schimieder M, Wolf S, Danner B et al (2008) p16 expression differentiates high-risk gastrointestinal stromal tumor and predicts poor outcome. Neoplasia 10(10):1154–1625
10. Schneider-Stock R, Boltze C, Lasota J et al (2003) High prognostic value of p16INK4 alterations in gastrointestinal stromal tumors. J Clin Oncol 21(9):1688–1697
11. Haller F, Lobke C, Ruschhaoupt M et al (2008) Loss of 9p leads to p16INK4A down-regulation and enables RB/E2F1-dependent cell cycle promotion in gastrointestinal stromal tumors (GISTs). J Pathol 215:253–262
12. Scolnick DM, Halazonetis TD (2000) *Chfr* defines a mitotic stress check-point that delays entry into metaphase. Nature 406:430–435
13. Summes MK, Bothos J, Halazonetis TD (2005) The CHFR mitotic checkpoint protein delays cell cycle progression by excluding cyclin B1 from the nucleus. Oncogene 24:2589–2598
14. Kang D, Chen J, Wong J et al (2002) The checkpoint protein Chfr is a ligase that ubiquitinates Plk1 and inhibits Cdc2 at the G2 to M transition. J Cell Biol 56:249–259
15. Ogi K, Toyota M, Mita H et al (2005) Small interfering RNA-induced CHFR silencing sensitizes oral squamous cell cancer cells to microtubule inhibitors. Cancer Biol Ther 4:773–780
16. Satoh A, Toyota M, Itoh F et al (2003) Epigenetic inactivation of CHFR and sensitivity to microtubule inhibitors in gastric cancer. Cancer Res 63:8606–8613
17. Mizuno K, Osada H, Konishi H et al (2002) Aberrant hypermethylation of the *CHFR* prophase checkpoint gene in human lung cancers. Oncogene 21:2328–2333
18. Erson AE, Petty EM (2004) *CHFR*-associated early G2/M checkpoint defects in breast cancer cells. Mol Carcinog 39:26–33
19. Nakamura N, Yamamoto H, Yao T et al (2005) Prognostic significance of abnormalities of cell-cycle regulatory proteins in gastrointestinal stromal tumor and relevance of the risk-grading system. Hum Pathol 36:828–837
20. Kobayashi C, Oda Y, Takahira T et al (2006) Aberrant expression of CHFR in malignant peripheral nerve sheath tumors. Mod Pathol 19:524–532
21. Daniels MJ, Marson A, Venkitaraman AR (2004) PML bodies control the nuclear dynamics and function of the CHFR mitotic checkpoint protein. Nat Struct Mol Biol 11:1114–1121
22. Toyota M, Sasaki Y, Satoh A et al (2003) Epigenetic inactivation of CHFR in human tumors. Proc Nati Acad Sci U S A 100:7818–7823
23. Igarashi S, Suzuki H, Niinuma T et al (2010) A novel correlation between *LINE-1* hypomethylation and the malignancy of gastrointestinal stromal tumors. Clin Cancer Res 16:5114–4123
24. Soutto M, Peng D, Razvi M et al (2010) Epigenetic and genetic silencing of CHFR in esophageal adenocarcinomas. Cancer 116:4033–4042
25. Marumoto T, Hirota T, Morisaki T et al (2002) Roles of aurora-A kinase in mitotic entry and G2 checkpoint in mammalian cells. Genes Cells 7:1173–1182
26. Hirota T, Kunitoku N, Sasayama T et al (2003) Aurora-A and an interacting activator, the LIM protein Ajuba, are required for mitotic commitment in human cells. Cell 114:585–598

Virchows Arch (2012) 460:171–181
DOI 10.1007/s00428-011-1185-8

ORIGINAL ARTICLE

KIT protein expression and mutational status of KIT gene in pituitary adenomas

Olivera Casar-Borota · Stine Lyngvi Fougner · Jens Bollerslev · Jahn Marthin Nesland

Received: 19 June 2011 / Revised: 11 December 2011 / Accepted: 12 December 2011 / Published online: 3 January 2012
© Springer-Verlag 2011

Abstract KIT protein expression and mutational status of KIT gene in different types of tumours have been intensively studied since Imatinib Mesylate, KIT/PDGFRA tyrosine kinase inhibitor became available. However, only one immunohistochemical study on KIT expression in pituitary adenomas has been published. There are currently no reports on mutational status of KIT gene in pituitary adenomas. We have immunohistochemically investigated KIT expression in 252 pituitary adenomas and found cytoplasmic reactivity in 52.4% and membranous reactivity in 8.3% of all adenomas. There was statistically significant difference in KIT expression between clinically non-functioning, growth hormone- and adrenocorticotroph hormone-producing adenomas. The group with membranous expression was dominated by somatotropinomas and clinically non-functioning adenomas. KIT expression in a subset of adenomas was also confirmed by western blot analysis of 48 adenomas. Immunohistochemical KIT expression was correlated with basic clinical data and in a cohort of acromegalic patients with additional data (somatostatin receptor type 2A expression, response to somatostatin analogue treatment and mutational status of gsp oncogene). Exons 9, 11, 13 and 17 of KIT gene were searched for mutations in the tumours with membranous KIT expression and in a minority of tumours with cytoplasmic KIT expression using denaturing high-performance liquid chromatography and in suspected cases sequencing of one or more exons. No mutations in the examined exons were found. Our results may suggest a role of KIT in the pathogenesis of a subset of pituitary adenomas and point out the need for further research to find out if KIT-reactive adenomas could be sensitive to Imatinib Mesylate.

Keywords Pituitary adenomas · KIT (CD 117) · Imatinib Mesylate · DHPLC

O. Casar-Borota · J. M. Nesland
Faculty of Medicine, University of Oslo,
0027 Oslo, Norway

O. Casar-Borota · J. M. Nesland
Division of Pathology, Oslo University Hospital, Rikshospitalet,
0027 Oslo, Norway

O. Casar-Borota
Department of Laboratory Medicine/Pathology,
Umeå University Hospital,
901 85 Umeå, Sweden

O. Casar-Borota
Department of Medical Biosciences, Umeå University,
901 85 Umeå, Sweden

O. Casar-Borota (✉)
Department of Clinical Pathology and Cytology,
Uppsala University Hospital,
751 85 Uppsala, Sweden
e-mail: olivera.casar.borota@medbio.umu.se

O. Casar-Borota
Department of Immunology, Genetics and Pathology,
Uppsala University,
751 85 Uppsala, Sweden

S. L. Fougner · J. Bollerslev
Section of Specialized Endocrinology,
Oslo University Hospital,
0407 Oslo, Norway

S. L. Fougner
Research Institute for Internal Medicine,
University of Oslo,
0027 Oslo, Norway

S. L. Fougner
Department of Endocrinology,
St. Olavs Hospital,
Trondheim University Hospital,
7006 Trondheim, Norway

Introduction

KIT is a 145-kDa transmembrane protein which belongs to the receptor tyrosine kinases class III, which also includes platelet-derived growth factor receptor alpha and beta (PDGFRA/B), macrophage colony-stimulating factor receptor and FMS-like tyrosine kinase-3. Activation of KIT by binding to its ligand SCF induces downstream signalling leading to activation of various transcription factors ultimately regulating cell survival, proliferation, differentiation, migration, cell adhesion and chemotaxis [1–3]. The KIT gene has been mapped to the pericentromeric location of the long arm of chromosome 4 (4q12), in the proximity of the highly homologous gene encoding for the PDGFRA [1].

Expression of KIT protein is found in mast cells and a subset of hematopoietic stem cells [4, 5] but also in a wide range of non-hematopoietic cell types, including melanocytes and basal cells of the skin, breast epithelium, germ cells, Cajal cells of gastrointestinal tract, sweat gland epithelia and some neuronal cells in the cerebellum [4, 6, 7].

A number of studies has focused on the role of KIT in human malignancies since the introduction of Imatinib Mesylate (Gleevec), a selective tyrosine kinase inhibitor of KIT and PDGFR. Thus, KIT was found to be expressed in the majority of gastrointestinal stromal tumours (GISTs) [8], acute myeloid leukaemia [5], mastocytosis [9] and adenoid cystic carcinomas of salivary gland [10]. A significant number of KIT-positive tumours was identified among neuroendocrine tumours with different locations [11–14] and among germinal cell tumours [15]. Soft tissue tumours other than GIST and germinal cell tumours are rarely KIT-positive [16]. KIT expression has also been reported in melanocytic tumours [17] and carcinomas of the lung [18], ovarium [19], breast [20], colon [21], prostate [22] and kidney [23].

Gain-of-function mutations in the KIT gene leading to anti-apoptotic signals and tissue growth have been well documented in several malignancies, notably acute myeloid leukaemia [24], systemic mastocytosis [25], germinal cell tumours of the seminoma type [15], GISTs [26, 27] and adenoid cystic carcinoma of the salivary gland [10] but are rare in other human tumours despite the widespread expression of KIT. The great majority of KIT mutations reported in human tumours involved exons 11 and 17. Rarely, mutations in exons 9 and 13 were observed and very rarely in other loci [28].

KIT expression in pituitary adenomas and in normal pituitary gland was first reported in 2008 [29]. However, it is currently unknown whether any of the mutations in the KIT gene are associated with pituitary adenomas.

The aims of our study were to (1) investigate if KIT may have a pathogenetic role in the development of pituitary adenomas by examining the expression of KIT in a series of 252 pituitary adenomas of different types using immunohistochemistry and in a limited number of adenomas by using western blot as well; (2) correlate data on KIT expression with clinical data as age, gender and recurrence rate; (3) correlate data on KIT expression with somatostatin receptor type 2A expression, response to somatostatin analogue (SMS) treatment and mutational status of the alpha subunit of the stimulating G-protein (gsp oncogene) which links the growth hormone (GH)-releasing hormone to the adenyl cyclase in a previously described cohort of acromegalic patients [30] and (4) investigate mutational status of KIT exons 9, 11, 13 and 17 in adenomas which were selected on the basis of KIT expression at the plasma membrane or intracellularly.

Materials and methods

Materials

The examined material includes pituitary adenoma tissue from 252 adult patients of both genders operated at Rikshospitalet, Oslo, Norway in a period from 2000 to 2007, as well as patients with acromegaly and corticotroph adenomas operated since 1998. Sixty-four patients were operated two or more times, and for these patients, biopsy material before 2000, but not older than 1998, was included. The tumours were classified based on the immunohistochemical expression of anterior pituitary hormones and clinical symptoms following WHO Classification of Pituitary tumours from 2004 [31]. Among 252 patients, 152 had non-functioning pituitary adenoma (NFPA), 64 patients had acromegaly due to pure GH- or mixed growth hormone–prolactin (GH-PRL)-producing adenomas, 23 patients had adrenocorticotroph hormone (ACTH)-producing adenomas, 10 patients had prolactinomas, 2 patients had thyroid-stimulating hormone (TSH)-producing adenoma and 1 patient had GH-PRL-TSH-producing adenoma with clinical signs of hyperproduction of all three hormones (Table 1). The regional ethical committee approved the study. Written informed consent was obtained from all living patients.

Methods

Light microscopy

Five-micron sections from buffered formalin-fixed, paraffin-embedded tumour tissue routinely hematoxylin–eosin stained were re-examined. Areas of representative tumour tissue were selected for micro-tissue arrays. Thirteen micro-tissue arrays were constructed containing replicate 1-mm cores from formalin-fixed, paraffin-embedded tissue samples [32].

Table 1 Clinical features, immunohistochemical hormone expression and KIT expression in the examined pituitary adenomas

Clinic	Number	Hormone expression	Number	KIT expression		
				0	1	2
NFPA	152	Null cell	70	27	41	2
		FSH/LH	63	27	32	4
		ACTH	15	10	2	3
		alpha-Subunit	4	0	3	1
Acromegaly	64	GH	33	12	12	9
		GH/PRL	31	14	15	2
Cushing/Nelson	19/4	ACTH	23	7	16	0
Prolactinomas	10	PRL	10	2	8	0
TSHoma	2	TSH	2	0	2	0
GH-PRL-TSHoma	1	GH-PRL-TSH	1	0	1	0
Total (% of total number)	252 (100%)		252 (100%)	99 (39.3%)	132 (52.4%)	21 (8.3%)

KIT expression was detected in different immunohistochemical and clinical types of pituitary adenomas with totally 52.4% of tumours showing cytoplasmic expression (class 1) and 8.3% of tumours showing membranous expression (class 2)

Immunohistochemistry

The following antibodies were used for immunohistochemical classification of the adenomas: anti-GH (DAKO, polyclonal, code no. A0570, 1:1,600), anti-ACTH (DAKO, monoclonal, Clone 02A3, code no. M3501, 1:1,200), anti-prolactin (DAKO, polyclonal, code no. A0569, 1:400), anti-TSH (DAKO, monoclonal, Clone 0042, code no. M3503, 1:160), anti-follicle-stimulating hormone (FSH; Thermo Scientific, monoclonal, Clone FSH03, Ab-3, 1:3,000), anti-luteinizing hormone (LH; Thermo Scientific, monoclonal, Clone LH01, Ab-1, 1:3,000) and anti-human chorionic gonadotroph hormone alpha subunit (hCG alpha; Affinity Bioreagents, monoclonal, Clone INN-hFSH-132, cat no. MA1-25038, 1:400). Staining was performed on the tissue arrays, applying a Ventana automatic immunostainer.

Immunohistochemical analysis with anti-KIT antibody was performed on the sections from all 13 micro-tissue arrays using the Dako EnVision™+System, Peroxidase (3′ 3-diaminobenzidine tetrahydrochloride, DAB) (K4011, Dako Corporation, CA, USA) and Dakoautostainer. Deparaffinized sections were microwaved in 10 mM Tris–1 mM EDTA, pH 9.0 to unmask the epitopes. Sections were treated with 0.03% hydrogen peroxide (H_2O_2) for 5 min to block endogenous peroxidase. The sections were incubated with polyclonal rabbit anti-KIT antibody (Dako, code A4502, dilution 1:100) for 30 min at room temperature. The sections were then incubated with peroxidase-labelled polymer conjugated to goat anti-rabbit antibody for 30 min, stained for 10 min with DAB and then counterstained with haematoxylin, dehydrated and mounted in Diatex. A section from seminoma was used as a positive control. Negative control was performed omitting the primary antibody. Both positive and negative controls gave satisfactory results (Fig. 1a, b).

Three semiquantitative classes were used to describe the immunohistochemical expression of KIT protein: (0) no expression or expression of any intensity in less than 10% of the tumour cells, (1) cytoplasmic expression in more than 10% of the cells and (2) membranous expression with or without cytoplasmic expression in more than 10% of the cells. Tumours with membranous expression (class 2) were further examined by immunohistochemical analyses of whole sections from the paraffin blocks to confirm the results from the tissue arrays.

Western blot

A small piece was cut from frozen tissue from total of 48 pituitary adenomas and transferred to an Eppendorf tube. Ice-cold NP-40 lysis buffer (1% NP-40; 10% glycerol; 20 mM Tris–HCl pH 7.5; 137 mM sodium chloride; 100 mM sodium fluoride; 1 mM sodium vanadate; 1 mM phenylmethylsulphonyl fluoride; 0.025 mg/mL each of aprotinin, leupeptin and pepstatin and 10 μL/mL phosphatase inhibitor cocktail I and II) was added and tissue was cut with a small scissor before carefully pipetting the lysate up and down. Amount of buffer was adjusted to sample size (approximately 500 μL for a piece with diameter 0.5 cm). Cells were lysed for 2 h in ice-cold lysis buffer. All inhibitors were from Sigma-Aldrich (St. Louis, MO, USA). Samples were vortexed every 15 min. Protein concentration was determined by Bradford analysis (Bio-Rad Laboratories, Hercules, CA, USA).

Protein lysates (25 μg per lane) were separated by sodium dodecyl sulphate–polyacrylamide gel electrophoresis and blotted onto Immobilon-P membranes (Millipore, Billerica, MA, USA). Membranes were blocked for 1 h in 5% nonfat dry milk (Bio-Rad Laboratories) in Tris-buffered

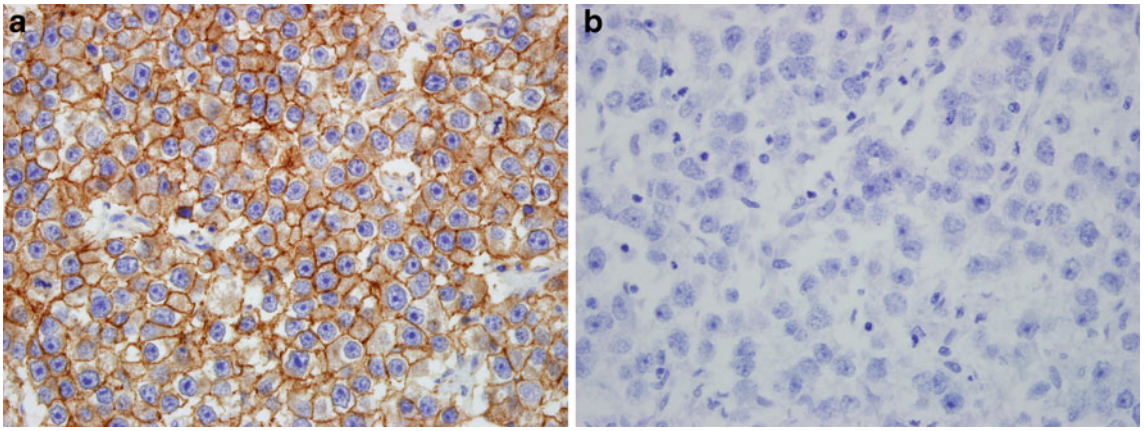

Fig. 1 Positive (**a**) and negative (**b**) control for KIT. Strong membranous expression of KIT in seminoma tumour cells (**a**) and no reactivity when omitting the primary antibody (**b**) (×400)

saline-containing 0.1% Tween (TBST). Blots were incubated with anti-human KIT rabbit polyclonal antibody (Dako-Cytomation, Glostrup, Denmark) in 5% milk in TBST for 2 h at the room temperature. Anti-α-tubulin mouse monoclonal antibody (Calbiochem, San Diego, CA, USA) was used as loading control. HRP-conjugated anti-rabbit IgG and HRP-conjugated anti-mouse secondary antibodies were from Promega (Madison, WI, USA). The ECL plus western blotting detection system (GE Healthcare, Buckinghamshire, England) was used for visualization.

Clinical information

Relevant clinical information was obtained from the medical records. Age, sex and rate of recurrence were all included in the clinicopathological correlations and statistical analyses. For the somatotroph patients' cohort, additional clinical data were correlated with KIT expression.

Analyses of the somatotroph patients' cohort

Among 64 patients with somatotroph adenomas included in the study, a cohort of 57 patients has previously been described [30, 33]. Tumour DNA for gsp mutational analysis was available in 56 of the patients, and immunohistochemical expression of somatostatin receptor subtype 2a (SSTR2a) had previously been performed in 54 patients [30]. Tumour size was measured on preoperative MRI scans, using the formula width × height × length × 0.5. An acute octreotide test to assess acute octreotide response was done in 50 patients as described previously. Twenty-two of these patients had received preoperative treatment with octreotide, a SMS, and the long-term effect of octreotide defined by the reduction of insulin growth factor 1 after 6 months preoperative SMS treatment was assessed in 20 of these patients, in addition to nine patients treated with SMS postoperatively. None of the patients had received radiation therapy prior to surgery

Mutational analysis of KIT gene

Genomic DNA was isolated either from fresh frozen tumour tissue or from formalin-fixed, paraffin-embedded tumour tissue using EZ1 DNA kit (Qiagen) according to the manufacturer's instructions. KIT exons 9, 11, 13 and 17 were screened for mutations using denaturing high-performance liquid chromatography (DHPLC). Prior to screening for heterozygous fragments by DHPLC analysis, PCR products were heated to 95°C and cooled 1.5°C/min down to 25°C to optimise heteroduplex formation. Aliquots of 5 μL of reannealed PCR products were injected on a semi-automated 3500 High Throughput Wave System (Transgenomics WAVE™, UK) using an elution gradient and an oven temperature as predicted by WAVEMAKER Software version 4.1 (Transgenomic). The products were eluted with a 0.1-M triethylammonium acetate gradient at a flow rate of 1.5 mL/min. The start and end points of the gradient were adjusted according to the size of the PCR products using algorithms provided by WAVEMAKER. Heterozygous profiles were identified by visual inspection of the chromatograms on the basis of the appearance of additional and earlier eluting peaks. Homozygous profiles showed only one peak.

DNA from the tumours with suspected mutation in DHPLC was sequenced for mutations in KIT exons 9, 11, 13 and 17. PCR products depicting heteroduplexes were purified (Exo-Sap IT, GE Healthcare Europe GMBH (Amersham Biosciences Europe GMBH)) and sequenced in both directions according to manufacturers instruction (ABI BigDye® Terminator Cycle Sequencing Kit v 3.1 on the ABI3130x; Applied Biosystems). Sequencing primers were the same as for the amplification reactions prior to DHPLC (Table 2).

Table 2 Primers used in DHPLC and sequencing of KIT exons 9, 11, 13 and 17

	Primers	Primers sequence	PCR product (bp)
1	1712 KIT exon 9 F 1749 KIT exon 9 R	CTAGAGTAAGCCAGGGCTTTTGT CAGAGCCTAAACATCCCCTTAAATTG	275
2	1704 KIT exon 11 F 1751 KIT exon 11 R	GACTGAGACAATAATTATTAAAAGGTGATC GTACCCAAAAAGGTGACATGG	223
3	1716 KIT exon 13 F 1717 KIT exon 13 R	CATCAGTTTGCCAGTTGTGCT TAACCTGACAGACAATAAAAGGCAG	204
4	1757 KIT exon 17 F 1758 KIT exon 17 R	GTTTTCACTCTTTACAAGTTAAAATGAATTTAAATGG TGCAGGACTGTCAAGCAGAGAATG	219

Statistical analyses

The statistical analyses were performed using SPSS software (SPSS, Chicago, IL, USA). Differences in proportions were analysed using Pearson chi-square test. Comparisons of continuous variables between the three KIT groups were done using Kruskal–Wallis test. P value <0.05 was considered significant.

Results

KIT protein expression

Within the group of 252 patients, immunohistochemical expression of KIT protein was detected in tumours from 153 patients (60.7%). In 132 tumours (52.4%), a cytoplasmic expression corresponding to class 1 (Fig. 2) was detected, while 21 tumours (8.3%) showed moderate to strong membranous KIT expression (Fig. 3) with or without cytoplasmic reactivity in more than 10% of the tumour cells corresponding to class 2. Among 132 class 1 KIT-positive adenomas, 78 were NFPAs (41 null cell, 32 gonadotroph adenomas, 3 alpha subunit and 2 silent ACTH adenomas), 27 GH/GH-PRL-, 16 ACTH-producing adenomas and 8 prolactinomas. Among 21 class 2 KIT-positive adenomas, 10 were of NFPA type (two null cell, three silent corticotroph adenomas, one alpha subunit and four gonadotroph adenomas) and 11 of somatotroph type (nine GH/two GH-PRL producing) (Table 1). All tumours showing membranous expression of KIT in tissue arrays were further assessed in the sections from the paraffin blocks. The analyses showed full concordance with the results obtained in the tissue arrays. KIT expression was heterogeneous in the tumour tissue cores in the microarrays. Some tumours showed more focal expression while others were almost diffusely positive. In the whole sections stained from paraffin blocks of the tumours with membranous KIT expression in tissue microarrays, the proportion of the tumour cells with membranous expression varied from 20% to 80% and was often combined with weaker or stronger cytoplasmic expression in some tumour areas. There was no KIT expression in 99 (39.3%) pituitary adenomas of different types (Fig. 4).

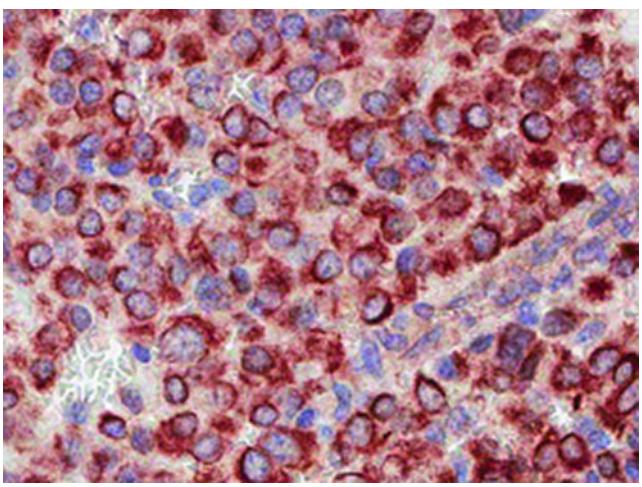

Fig. 2 Cytoplasmic expression of KIT. Strong cytoplasmic KIT expression corresponding to class 1 in a plurihormonal GH/prolactin/TSH-producing adenoma (anti-KIT immunohistochemistry, ×400)

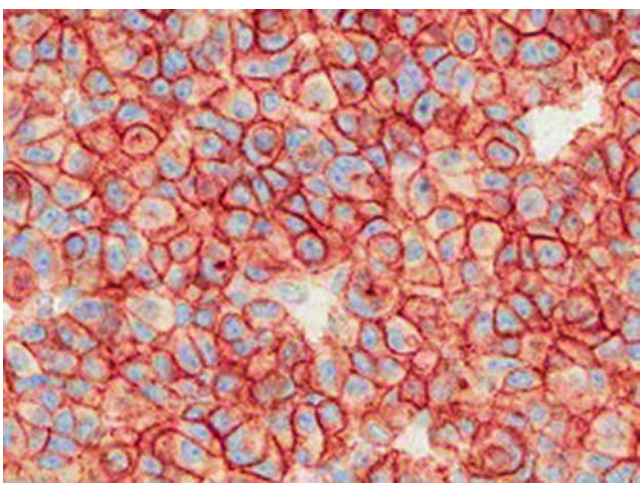

Fig. 3 Membranous expression of KIT. Strong membranous KIT expression corresponding to class 2 in a GH-producing adenoma (anti-KIT immunohistochemistry, ×400)

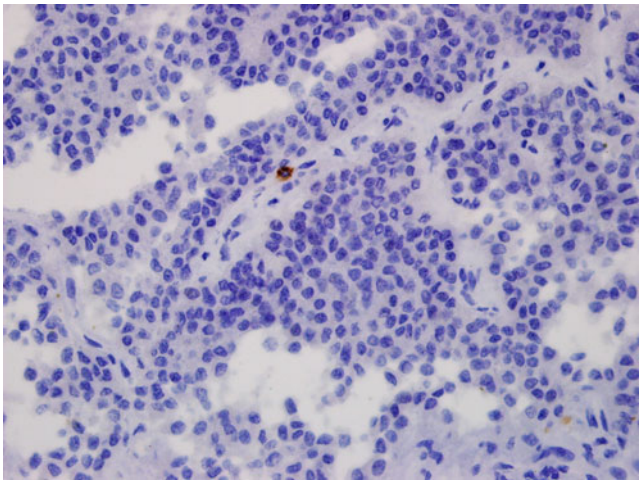

Fig. 4 No detectable KIT expression in tumour cells of clinically non-functioning pituitary adenoma. A single KIT-reactive cell probably represents a mast cell

There was statistically significant difference (P=0.024) in the KIT expression between three largest groups of pituitary adenomas, NFPAs, somatotroph and corticotroph adenomas. The class 2 group with membranous KIT expression was dominated by somatotropinomas and NFPAs in almost the same proportion. If classified according to the tumour type, the highest proportion of adenomas with membranous expression was found in the somatotroph group (17.2% of all somatotropinomas), followed by NFPAs (6.6% of all NFPAs). No corticotroph adenomas showed membranous KIT expression, but as many as 69.6% showed cytoplasmic expression. The proportion of KIT-negative adenomas was similar in all three groups (Table 3).

There was no statistically significant difference in the KIT expression related to the gender and age of the patients.

Table 3 Distribution of adenomas according to KIT expression in the three largest groups of adenomas

		KIT expression			Total
		0	1	2	
NFPA	Count	64	78	10	152
	% within clinic	42.1	51.3	6.6	100.0
Acromegaly	Count	26	27	11	64
	% within clinic	40.6	42.2	17.2	100.0
Cushing syndrome	Count	7	16	0	23
	% within clinic	30.4	69.6	0	100.0
Total	Count	97	121	21	239
	% within clinic	40.6	50.6	8.8	100.0

There was statistically significant difference in KIT expression between NFPAs, somatotroph and corticotroph adenomas. Pearson chi-square test, P=0.024

There was no statistically significant difference in KIT expression in non-recurrent and recurrent tumours of any adenoma type (data not shown).

KIT protein expression examined by immunoblotting

Forty-eight adenomas of different hormonal type representing all three immunohistochemical KIT classes were analysed by immunoblotting. Four different patterns of KIT positive signals were observed (Fig. 5): (1) a strong double signal with a prominent band at about 150 kDa and a weaker band at about 130 kDa, (2) a strong single-band signal at about 150 kDa, (3) a weak single-band signal at about 150 kDa and (4) no detectable signal.

Six adenomas showed the double-band signal, out of them five GH-producing adenomas with membranous KIT expression characterized by immunohistochemistry and one silent ACTH-adenoma which did not show immunohistochemically detectable KIT in the TMA cores. Sixteen adenomas were characterized by a strong single-band signal, out of which 12 belonging to the class 1 of KIT positive tumours with cytoplasmic expression, 3 belonging to the class 2 of KIT positive tumours with membranous expression and 1 tumour nonreactive for KIT in tissue microarray. NFPA-, ACTH-, GH- and prolactin-producing adenomas were represented in this group. Weak, one-band signal was observed in nine adenomas (four without detectable KIT on immunohistochemistry, two with cytoplasmic and three with membranous KIT expression). No detectable KIT expression was found in 17 adenomas, 11 out of them showing cytoplasmic KIT expression, 5 being KIT-negative and 1 showing membranous KIT expression in immunohistochemical analysis. These results were correlated with the immunohistochemical analysis in Table 4 and further compared with the clinical type of adenoma in Table 5.

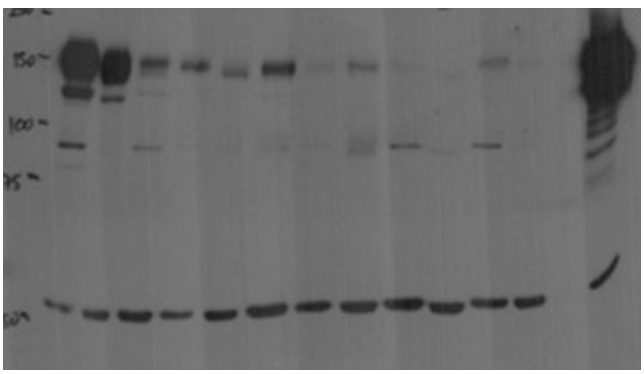

Fig. 5 KIT protein detected by western blot. Four different patterns are observed: (1) a double-band signal at around 150 and 130 kDa (likely representing differently glycosylated protein isoforms), (2) a strong single-band signal at around 150 kDa, (3) a weak single-band signal at around 150 kDa and (4) no detectable signal. The *last lane to the right* is a positive control from KIT-reactive GIST

Table 4 Distribution of adenomas examined by immunoblotting according to the pattern of signals and KIT expression analysed by immunohistochemistry

Detectable amount of KIT was found in 31 (64.6%) of total of 48 adenomas analysed by immunoblotting

Immunohistochemistry	Western blot				Total
	No signal	Weak signal	Strong single	Strong double	
No expression	5	4	1	1	11
Cytoplasmic	11	2	12	0	25
Membranous	1	3	3	5	12
Total	17	9	16	6	48

KIT protein expression in the previously described acromegaly cohort

In the cohort of 57 previously described acromegalic patients, 24 (42.1%) patients had KIT class 0 tumours, 22 (38.6%) KIT class 1 tumours and 11 (19.3%) KIT class 2 tumours. No differences were found in KIT expression between the groups of preoperatively octreotide treated and non-treated patients. There was no difference in baseline characteristics including patient age, preoperative hormone levels or tumour size and invasiveness in the three tumour groups regarding KIT expression. There was also no difference in SMS efficacy between the groups, neither in acute nor in long-term response. KIT expression was not significantly correlated to gsp mutation (Table 6) or to SSTR2a expression (Table 7). However, among the adenomas with membranous expression of KIT, 10 out of 11 adenomas were gsp mutation negative (Table 6) and nine out of 10 adenomas had high SSTR2a expression (Table 7). Examples of GH-adenomas with focal and diffuse sstr2A expression are shown in Fig. 6. Example of the most frequently detected gsp mutation is shown in Fig. 7.

Mutational status of KIT exons 9, 11, 13 and 17

DNA was extracted from tumour tissue from 40 patients, including 20 of 21 patients with KIT class 2 expression, 16 of 132 patients with KIT class 1 expression and 4 patients without KIT expression. From 22 tumours, DNA was extracted from frozen tumour tissue and from 18 biopsies from paraffin-embedded tumour tissue. DNA extracted from paraffin embedded tissue from five tumours was not of satisfactory quality for further analyses. DNA extracted from other 35 adenomas was screened for mutation in exons 9, 11, 13 and 17 of KIT gene by DHPLC. In 21 adenomas (8 classified as class 2, 11 classified as class 1 and 2 classified as class 0 regarding KIT immunohistochemical expression), no abnormality was revealed in any of the exons screened by DHPLC analysis. In four adenomas (two corresponding to class 2, one corresponding to class 1 and one corresponding to class 0), inconclusive results were obtained in one or two of four exons and no abnormalities found in the other exons. In 10 adenomas (seven classified as class 2 and three classified as class 1 regarding KIT expression) sequencing of one or more exons of the KIT gene was performed because of the suspected mutation in DHPLC analysis (Fig. 8). No mutations were detected by sequencing.

Discussion

In the present study, we have shown that KIT protein is expressed at cytoplasmic and/or membranous level in a considerable proportion of pituitary adenomas. The expression of KIT varied significantly between different clinical and immunohistochemical types of the pituitary adenomas, but there was no apparent correlation between KIT expression and the clinical data including patients' age, sex or tumour recurrence rate. In the cohort of the acromegalic patients, there was a tendency of high sstr2a expression and negative gsp mutational status in KIT reactive tumours, but we demonstrated no correlation with other clinical parameters. In a subset of adenomas, we have confirmed

Table 5 Distribution of different clinical types of adenomas in relation to the immunoblotting results

GH-adenomas dominated in the group of adenomas with strong double-band signal for KIT in immunoblotting

Clinics	WB pattern				Total
	No signal	Weak signal	Strong single	Strong double	
NFPA	12	7	11	1	31
GH	1	0	1	5	7
ACTH	2	2	1	0	5
Prolactin	0	0	3	0	3
TSH	2	0	0	0	2
Total	17	9	16	6	48

Table 6 Correlation between KIT expression and Gsp mutational status in the cohort of acromegalic patients

Gsp mutation	KIT			Total
	0	1	2	
Positive	12	13	10	35
Negative	12	8	1	21
Total	24	21	11	56

Despite the lack of clinical correlation, there was a clear predominance of gsp positive adenomas in the class 2 adenomas with membranous KIT expression. Pearson chi-square test, $P=0.068$

KIT expression by immunoblotting. Finally, we did not detect any mutations in KIT exons 9, 11, 13 and 17 in the tumours with membranous KIT expression and in a minority of the tumours which expressed KIT in the cytoplasm.

Cytoplasmic immunohistochemical KIT expression, sometimes with a membranous reinforcement, was previously reported in a subset of pituitary adenomas of ACTH, FSH/LH, αSU and null cell type [29]. In our material, in addition to cytoplasmic KIT expression in different types of pituitary adenomas, we could also detect membranous expression in a subset of somatotroph and clinically non-functioning adenomas. The membranous KIT expression is considered to be especially important for a functional KIT receptor and in some studies only membranous expression in tumour cells has been considered positive [34]. The cytoplasmic staining may reflect internalization of KIT receptor following its activation [35]. These data suggest a pathogenetic role of KIT in a subset of pituitary adenomas.

We found significantly different KIT expression between the three largest adenoma groups in our material, NFPAs, somatotroph and corticotroph adenomas, with somatotroph and non-functioning adenomas dominating the class 2 with membranous expression and ACTH adenomas dominating the class 1 tumours with cytoplasmic KIT expression. In the somatotroph adenomas, we detected KIT expression both at the cytoplasmic and at the membranous level. Conversely, La Rosa et al. found no KIT reactivity in any of the examined GH adenomas [29]. This discrepancy could be explained at least in part by a relatively small number of cases examined by La Rosa et al (seven GH-producing adenomas in La Rosas studies vs. 64 adenomas in our study). Interestingly, the coexpression of GH and KIT in normal pituitary cells was also absent in La Rosas study [29]. Our findings therefore suggest that pathological activation of KIT may be a possible pathogenetic factor in GH-producing adenomas. However, despite the high proportion of KIT reactive adenomas in the somatotroph group, the lack of KIT mutations, poor correlation with clinical parameters and the availability of other therapeutic alternatives for acromegalic patients such as dopamine agonists, somatostatin analogues, GH antagonists or combinations [36] make the search for possible candidates for Imatinib Mesylate therapy among acromegalic patients less attractive. This is further supported by the fact that all KIT-positive somatotroph adenomas in our material showed also high proportion of sstr2A-positive tumour cells, making them sensitive for somatostatin analogue treatment.

Table 7 Correlation between KIT expression and sstr2A expression in the tumour tissue in the cohort of acromegalic patients

Sstr 2A expression	KIT			Total
	0	1	2	
<75% positive cells	8	11	1	20
>75% positive cells	15	10	9	34
Total	23	21	10	54

The somatotroph adenomas with high sstr2A expression predominated among adenomas with the membranous KIT expression. Pearson chi-square, $P=0.07$

However, patients with clinically NFPAs do not have any established medical therapy other than surgery or irradiation. It would therefore be important to further define a possible pathogenetic role of KIT in NFPAs.

Cytoplasmic KIT expression has previously been described in normal ACTH-producing pituitary cells [29] suggesting the role for KIT in differentiation and metabolic regulation of ACTH cells. A previous experimental study showed developing of intermediate lobe pituitary adenomas similar to human ACTH adenomas in the transgenic mice carrying c-kit/SV40 T antigen fusion gene [37]. Both our study and La Rosa et al. report that the considerable proportion of ACTH adenomas is KIT reactive (69.6% in our study). These data indicate a regulatory role of KIT in the development of ACTH-producing adenomas. Additionally, we have found KIT expression in other tumour types, but the number of the examined cases was too low for any conclusion.

We did not find any correlation between KIT expression and patient age, gender and the tumour recurrence rate. The lack of correlation between KIT expression and tumour recurrence rate in our material suggests that KIT, even if involved in pathogenesis of a subset of pituitary adenomas, does not contribute to the more aggressive clinical outcome, at least measured by the recurrence frequency.

In order to confirm that KIT protein is present in pituitary adenoma tissue, we carried out immunoblot analysis of 48 adenomas of different types and belonging to the different groups according to the immunohistochemical expression of KIT. Although the number of samples analysed was too low for statistical analysis and correlation with clinical data, there were several interesting observations obtained from this analysis. Firstly, high expression level of KIT in the form of a strong, single-band or double-band signal was detected in 22 of 48 adenomas. The majority of these

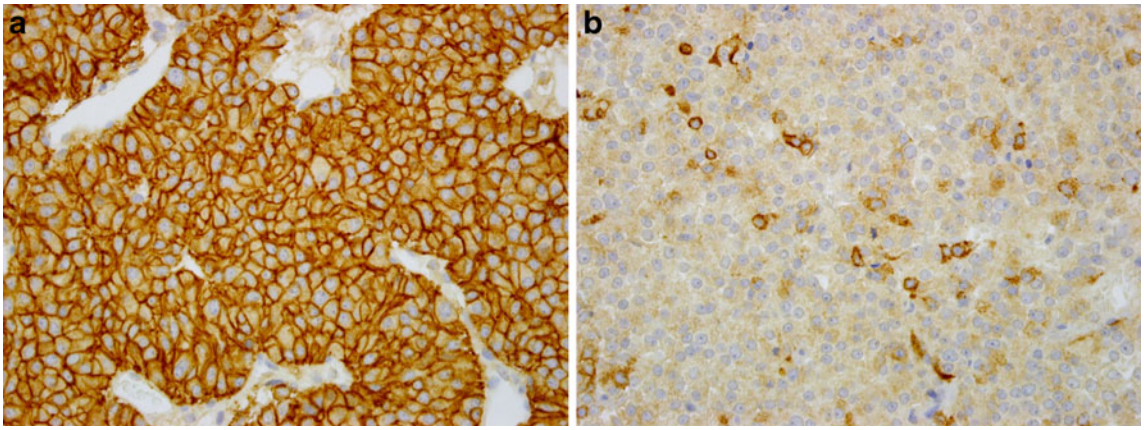

Fig. 6 Somatostatin receptor type 2A expression in GH-producing adenomas. **a** Strong, diffuse expression of SSTR2A in all tumour cells. **b** Focal expression of SSTR2A in some tumour cells

adenomas (20 out of 22) showed cytoplasmic or membranous expression of KIT by immunohistochemistry. Secondly, a weak signal was detected in nine adenomas. Detectable amount of KIT was found in 31 (64.6%) of 48 analysed adenomas which corresponds well to the total proportion of 60.7% of all adenomas with immunohistochemically detected KIT expression. Some discrepancies between the immunohistochemical and immunoblotting results, such as in the case of some adenomas with a cytoplasmic expression of KIT but without detectable KIT expression in immunoblotting analysis, or the presence of immunohistochemically negative adenomas in the group of adenomas showing a weak signal for KIT in immunoblotting, could be explained by the heterogeneity in the expression of KIT, presence of non-adenomatous tissue such as inflammatory cells, normal pituitary tissue, fibrous tissue or blood in the frozen specimens or differences in the sensitivity between immunohistochemistry and immunoblotting which could exist and give slightly different results especially for those adenomas showing weaker immunoreactivity in either of the analyses. Another interesting observation from immunoblotting analysis was the presence of a strong, double-band signal for six adenomas, among which five were GH-producing adenomas with membranous KIT expression. The most probable explanation for such strong signal in the tumours with membranous KIT expression is that KIT is likely to be metabolically stable once it is incorporated into the plasma membrane. The presence of bands of approximately 150 and 130 kDa can be explained by different levels of glycosylation of KIT [38]. We have also speculated that a weaker band of 130 kDa could represent a truncated form of KIT. Thus, immunoblotting has confirmed the presence of KIT in a subset of pituitary adenomas, although extensive analysis including a larger number of cases should be

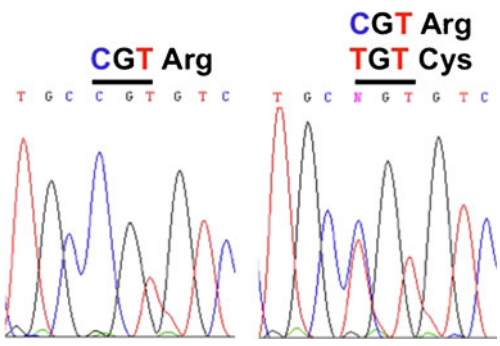

Fig. 7 Gsp mutation in a GH-producing adenoma. Gsp point mutation in codon 201 resulting in replacement of arginine by cysteine was the most frequent mutation detected in the cohort of GH-producing adenomas

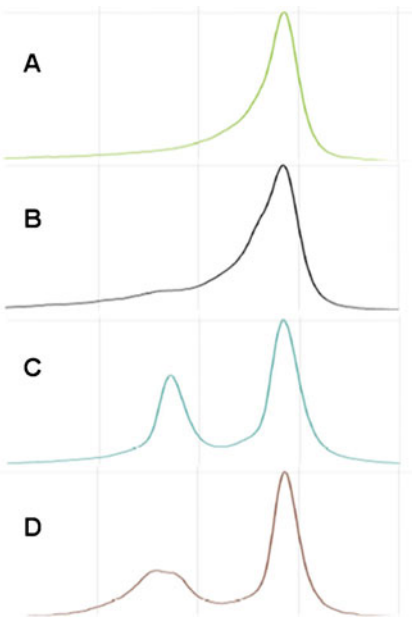

Fig. 8 DHPLC chromatograms of KIT exon 11 PCR products: **a** negative control (human male genomic DNA). **b** GH-producing pituitary adenomas. **c** c.1667-1681del in a GIST. **d** c.1676 T>A in a GIST. KIT exon 11 PCR product of the pituitary adenoma sample in **b** was sequenced due to the small deviation of the elution profile from that of the negative control and found to be negative

carried out in order to establish the statistical correlation with the clinical data.

The great majority of KIT mutations reported in human tumours involved exons 11 and 17. Rarely, mutations in exons 9 and 13 were observed and very rarely in other loci, such as exon 8 in some cases of acute myeloid leukemias and intron 17 in renal papillary carcinomas [28]. We used DHPLC to screen KIT exons 9, 11, 13 and 17 in all but one adenoma with membranous KIT expression, a minority of adenomas with diffuse cytoplasmic expression and a few adenomas without KIT expression (35 adenomas in total). DHPLC is regarded as one of the most sensitive techniques available for mutation screening [39] and is well established in the screening of KIT gene. In the cases with suspected mutations, sequencing of one or more exons was performed. Even though we were unable to identify any specific mutations in the examined exons of the KIT gene, the possibility still remains that some of these tumours may be responsive to Imatinib Mesylate.

In GISTs, the presence of KIT mutation is predictive for responsiveness to Imatinib Mesylate. The response is best in tumours with exon 11 mutation and moderate in tumours with exon 9 mutation. The tumours with exon 17 mutation are resistant to Imatinib Mesylate treatment. The response is poor in tumours with wild-type KIT, although Imatinib Mesylate inhibits effectively wild-type KIT and PDGFRs in vitro [40].

Although the most common site of mutations in GISTs, exons 9, 11, 13 and 17 may not be the representative site for mutations in pituitary adenomas. Additionally, mutations in receptor tyrosine kinases other then KIT should be considered, as it was found that some immunohistochemically KIT-negative GISTs do have PDGFR mutations [41]. Response to Imatinib Mesylate was observed in some, but not all, patients with PDGFR-mutant tumours. The signal transduction mechanisms for PDGFRA-mutant tumours were indistinguishable from the KIT-mutant tumours, suggesting that PDGFRA can substitute for KIT in GIST oncogenesis and that PDGFR-mutated tumours can respond to Imatinib Mesylate therapy [40, 42]. Additionally, Imatinib Mesylate may contribute to tumour growth reduction due to its anti-angiogenic properties via PDGFRs inhibition [43]. This indicates a need for further characterization of mutations in receptor tyrosine kinases other than KIT, particularly mutations in PDGFR in pituitary adenomas.

Additionally, KIT, PDGFRA or other proteins inhibited by Imatinib Mesylate may be activated by other mechanisms than gene mutation, such as gene fusion and amplification, autocrine and paracrine stimulation of the receptor by its ligand, loss of phosphatase activity, cross-activation by another kinases and promoter activation/inactivation via methylation/demethylation [44]. Therefore, the absence of KIT mutation in a tumour does not exclude the possibility that Imatinib or other tyrosine kinase inhibitors may be effective as drug therapies.

Conclusions

(1) The expression of KIT in a subset of pituitary adenomas suggests a possible role of this protein in the pathogenesis of pituitary adenomas. The KIT inhibitor Imatinib Mesylate may prove to be an adjuvant therapy for patients with NFPAs and Cushing's disease, as there are no approved medical therapeutic options in these patients. (2) KIT, even if involved in pathogenesis of a subset of pituitary adenomas, does not seem to contribute to the more aggressive clinical outcome. (3) Despite the high proportion of somatotroph adenomas in the group of tumours with membranous expression of KIT in our study, absence of mutation in the examined exons of KIT, no correlation with clinical data and high proportion of KIT-reactive tumours with high sstr2A expression make them less attractive candidates for Imatinib Mesylate therapy. (4) Absence of mutation in exons 9, 11, 13 and 17 of KIT gene does not necessary exclude the possible responsiveness of pituitary adenomas to Imatinib Mesylate. Search for mutations in other exons of the KIT gene as well as in kinases other than KIT, such as PDGFRs, would be of interest to clarify this issue, especially in the group of clinically non-functioning and ACTH-producing pituitary adenomas.

Acknowledgements The authors thank Ellen Hellesylt for assistance with the immunohistochemical analyses, Sarah L. Ariansen and Lilach Kleinberg for assistance with the DHPLC analysis, Anne Katrine Rosnes for assistance with the western blot analysis and Dr Jasmina N. Jovanovic for critical reading of the manuscript.

Disclosure/conflict of interest The authors declare that they have no conflict of interest.

References

1. Yarden Y, Kuang W-J, Yang-Feng T, Coussens L, Munemitsu S, Dull T et al (1987) Human proto-oncogene c-kit: a new cell surface receptor tyrosine kinase for an unidentified ligand. EMBOJ 6:3341–3351
2. Ashman LK (1999) The biology of stem cell factor and its receptor c-kit. Int J Biochem Cell Biol 31:1037–1051
3. Pawson T (2002) Regulation and targets of receptor tyrosine kinases. Eur J Cancer 38(Suppl 5):S3–S10
4. Tsuura Y, Hiraki H, Watanabe K, Igarashi S, Shimamura K, Fukuda T et al (1994) Preferential localization of c-kit product in tissue mast cells, basal cells of skin, epithelial cells of breast, small cell lung carcinoma and seminoma/dysgerminoma in human: immunohistochemical study on formalin-fixed, paraffin-embedded tissues. Virchows Arch 424:135–141
5. Escribano L, Ocqueteau M, Almeida J, Orfao A, San Miguel JF (1998) Expression of the c-kit (CD117) molecule in normal and malignant hematopoiesis. Leuk Lymphoma 30:459–466
6. Natali PG, Nicotra MR, Sures I, Santoro E, Bigotti A, Ullrich A (1992) Expression of c-kit receptor in normal and transformed human nonlymphoid tissues. Cancer Res 52:6139–6143
7. Huizinga JD, Thuneberg L, Klüppel M, Malysz J, Mikkelsen HB, Bernstein A (1995) W/kit gene required for intestinal cells of Cajal and for intestinal pacemaker activity. Nature 373:347–349

8. Sarlomo-Rikala M, Kovatich A, Barusevicius A, Miettinen M (1998) CD117: a sensitive marker for gastrointestinal stromal tumours that is more specific than CD34. Mod Pathol 11:728–734
9. Lim KH, Pardanani A, Tefferi A (2008) KIT and mastocytosis. Acta Haematol 119:194–198
10. Vila L, Liu H, Al-Quran SZ, Coco DP, Dong HJ, Liu C (2009) Identification of c-kit gene mutations in primary adenoid cystic carcinoma of the salivary gland. Mod Pathol 22:1296–1302
11. Akintola-Ogunremi O, Pfeifer JD, Tan BR, Yan Y, Zhu X, Hart J et al (2003) Analysis of protein expression and gene mutation of c-kit in colorectal neuroendocrine carcinomas. Am J Surg Pathol 27:1551–1558
12. Pelosi G, Masullo M, Leon ME, Veronesi G, Spaggiari L, Pasini F et al (2004) CD117 immunoreactivity in high-grade neuroendocrine tumors of the lung: a comparative study of 39 large-cell neuroendocrine carcinomas and 27 surgically resected small-cell carcinomas. Virchows Arch 445:449–455
13. Swick BL, Ravdel L, Fitzpatrick JE, Robinson WA (2007) Merkel cell carcinoma: evaluation of KIT (CD117) expression and failure to demonstrate activating mutations in the C-KIT proto-oncogene —implications for treatment with imatinib mesylate. J Cutan Pathol 34:324–329
14. Veras E, Deavers MT, Silva EG, Malpica A (2007) Ovarian nonsmall cell neuroendocrine carcinoma. A clinicopathologic and immunohistochemical study of 11 cases. Am J Surg Pathol 31:774–782
15. Kemmer K, Corless CL, Fletcher JA, McGreevey L, Haley A, Griffith D et al (2004) KIT mutations are common in testicular seminomas. Am J Pathol 164:305–313
16. Hornick JL, Fletcher CDM (2002) Immunohistochemical staining for KIT (CD117) in soft tissue sarcomas is very limited in distribution. Am J Clin Pathol 117:188–193
17. Takahashi H, Saitoh K, Kishi H, Parsons PG (1995) Immunohistochemical localization of stem cell factor (SCF) with comparison of its receptor c-Kit protooncogene product (c-KIT) in melanocytic tumors. Virchows Arch 427:283–288
18. Pelosi G, Barisella M, Pasini F, Leon ME, Veronesi G, Spaggiari L et al (2004) CD117 immunoreactivity in stage I adenocarcinoma and squamous cell carcinoma of the lung: relevance to prognosis in a subset of adenocarcinoma patients. Mod Pathol 17:711–721
19. Lassus H, Sihto H, Leminen A, Nordling S, Joensuu H, Nupponen NN et al (2004) Genetic alterations and protein expression of KIT and PDGFRA in serous ovarian carcinoma. Br J Cancer 91:2048–2055
20. Simon R, Panussis S, Maurer R, Spichtin H, Glatz K, Tapia C et al (2004) KIT (CD117)-positive breast cancers are infrequent and lack KIT gene mutations. Clin Cancer Res 10:178–183
21. Preto A, Moutinho C, Velho S, Oliveira C, Rebocho AP, Figueiredo J et al (2007) A subset of colorectal carcinomas express c-KIT protein independently of BRAF and/or KRAS activation. Virchows Arch 450:619–626
22. Simak R, Capodieci P, Cohen DW, Fair WR, Scher H, Melamed J et al (2000) Expression of c-kit and kit ligand in benign and malignant prostatic tissues. Histol Histopathol 15:365–374
23. Miliaras D, Karasavvidou F, Papanikolaou A, Sioutopoulou D (2004) KIT expression in fetal, normal adult, and neoplastic renal tissues. J Clin Pathol 57:463–466
24. Beghini A, Rapamonti CB, Cairoli R (2004) KIT activating mutations: incidence in adult and pediatric acute myeloid leukemia, and identification of internal tandem duplication. Haematologica 89:920–925
25. Orfao A, Garcia-Montero AC, Sanchez L, Escribano L (2007) Recent advances in the understanding of mastocytosis: the role of KIT mutations. Br J Haematol 138:12–30
26. Hirota S, Isozaki K, MoriyamaY HK, Nishida T, Ishiguro S et al (1998) Gain-of-function mutations of c-kit in human gastrointestinal stromal tumours. Science 279:577–580
27. Miettinen M, Lasota J (2006) Gastrointestinal stromal tumors. Review on morphology, molecular pathology, prognosis, and differential diagnosis. Arch Pathol Lab Med 130:1466–1478
28. Miettinen M, Lasota J (2005) KIT (CD117): a review on expression in normal and neoplastic tissues, and mutations and their clinicopathologic correlation. Appl Immunohistochem Mol Morphol 13:205–220
29. La Rosa S, Uccella S, Dainese L, Marchet S, Placidi C, Vigetti D et al (2008) Characterization of C-Kit (CD117) expression in human normal pituitary cells and pituitary adenomas. Endocr Pathol 19:104–111
30. Fougner SL, Casar Borota O, Berg JP, Hald JK, Ramm-Pettersen J, Bollerslev J (2008) The clinical response to somatostatin analogues in acromegaly is related to the somatostatin receptor subtype 2a protein expression of the adenoma. Clin Endocrinol (Oxf) 68:458–465
31. Lloyd RV, Kovacs K, Young WF Jr, Farrell WE, Asa SL, Trouillas J et al (2004) Pituitary tumours: introduction. In: DeLellis RA, Lloyd RV, Heitz PU, Eng C (eds) World Health Organization classification of tumours. Pathology and genetics of tumours of endocrine organs. IARC, Lyon, pp 10–13
32. Kononen J, Bubendorf L, Kallioniemi A, Barlund M, Schraml P, Leighton S et al (1998) Tissue microarrays for high-throughput molecular profiling of tumor specimens. Nat Med 4:844–847
33. Fougner SL, Lekva T, Casar Borota O, Hald JK, Bollerslev J, Berg JP (2010) The expression of E-cadherin in somatotroph pituitary adenomas is related to tumor size, invasiveness, and somatostatin analog response. J Clin Endocrinol Metab 95:2334–2342
34. Jones C, Rodriguez-Pinilla M, Lambros M, Bax D, Messahel B, Vujanic GM et al (2007) C-kit overexpression, without gene amplification and mutation, in paediatric renal tumors. J Clin Pathol 60:1226–1231
35. Lennartsson J, Jelacic T, Linnekin D, Shivakrupa R (2005) Normal and oncogenic forms of the receptor tyrosine kinase Kit. Stem Cells 23:16–43
36. Bollerslev J, Fougner SL, Berg JP (2009) New directions in pharmacological treatment of acromegaly. Expert Opin Investig Drugs 18(1):13–22
37. Bossé P, Bernex F, De Sepulveda P, Salaün P, Panthier J-J (1997) Multiple neuroendocrine tumours in transgenic mice induced by c-kit-SV40 T antigen fusion genes. Oncogene 14:2661–2670
38. Merkwitz C, Lochhead P, Tsikolia N, Koch D, Sygnecka K, Sakurai M et al (2011) Expression of KIT in the ovary, and the role of somatic precursor cells. Progr Histochem Cytochem 46:131–184
39. Xiao W, Oefner PJ (2001) Denaturing high-performance liquid chromatography: a review. Hum Mutat 17:439–474
40. Heinrich MC, Corless CL, Demetri GD, Blanke CD, von Mehren M, Joensuu H et al (2003) Kinase mutations and imatinib response in patients with metastatic gastrointestinal stromal tumors. J Clin Oncol 21:4342–4349
41. Medeiros F, Corless CL, Duensing A, Hornick JL, Oliveira AM, Heinrich MC et al (2004) KIT-negative gastrointestinal stromal tumors. Proof of concept and therapeutic implications. Am J Surg Pathol 28:889–894
42. Corless CL, Fletcher JA, Heinrich MC (2004) Biology of gastrointestinal stromal tumors. J Clin Oncol 22:3813–3825
43. Pietras K, Sjöblom T, Rubin K, Heldin C-H, Östman A (2003) PDGF receptors as cancer drug targets. Cancer Cell 3:439–443
44. Sihto H, Sarlomo-Rikala M, Tynninen O, Tanner M, Andersson LC, Franssila K et al (2005) KIT and platelet-derived growth factor receptor alpha tyrosine kinase gene mutations and KIT amplifications in human solid tumors. J Clin Oncol 23:49–57

Virchows Arch (2012) 460:183–191
DOI 10.1007/s00428-011-1190-y

ORIGINAL ARTICLE

LYVE-1 upregulation and lymphatic invasion correlate with adverse prognostic factors and lymph node metastasis in neuroblastoma

Pramila Ramani · Josiah V Dungwa · Margaret T. May

Received: 26 August 2011 / Revised: 12 December 2011 / Accepted: 26 December 2011 / Published online: 13 January 2012
© Springer-Verlag 2012

Abstract Neuroblastoma (NB) accounts for 15% of all childhood cancer deaths. The majority of patients have widespread lymphatic and/or haematogenous metastases at diagnosis, but lymphangiogenesis has not been well documented. Sixty-seven NBs were immunostained for the lymphatic endothelial marker, LYVE-1, and the lymphatic density (LD) and lymphatic invasion (LI), were counted in LYVE-1-expressing lymphatics. LYVE-1-stained lymphatic vessels and LI were present in 26/67 (39%) and 14/67 (21%) of the NBs, respectively. Central LD (CLD) and LI were higher in NBs from stage 4 (p=0.012, p=0.004, respectively), high-risk group (p=0.030, p=0.002), NBs with high mitosis karyorrhexis index (MKI) (p=0.011, p=0.005), unfavourable histology group (p=0.040, p=0.017) and distant lymph node metastasis (LNM) (p<0.001 for each). Marginal LD (MLD) was higher in patients with LNM (p<0.001). CLD and MLD correlated with LI (p<0.001 each). Total LYVE-1 protein levels, quantified by a sensitive enzyme-linked immunosorbent assay (n=55), were also higher in NBs from patients with stage 4 disease (p=0.046), high-risk group (p=0.028), *MYCN*-amplified NBs (p=0.034) and LNM (p=0.038). Kaplan–Meier analysis showed that the presence of CLD was associated with both worse OS at 5 years (77% [95% CI: 62–87%] versus 60% [95% CI: 32–80%], p=0.062) and EFS (74% [95% CI: 58–85%] versus 43% [95% CI: 15–69%], p=0.070) and LI with OS (71% [95% CI: 57–81%] versus 56% [95% CI: 26–78%], p=0.055). Significant upregulation of LYVE-1 and the presence of LI in patients with stage 4 and high-risk disease, *MYCN*-amplification and LNM suggests that LYVE-1 may have value as predictors of outcome.

Keywords Neuroblastoma · LYVE-1 · Lymphatic density · Lymph node metastasis · Lymphatic invasion

Abbreviations

NB	Neuroblastoma
LYVE-1	Lymphatic vessel endothelial hyaluronan receptor-1
LD	Lymphatic density
CLD	Central lymphatic density
MLD	Marginal lymphatic density
LNM	Lymph node metastasis
LI	Lymphatic invasion

Introduction

Neuroblastoma (NB) is the most common extra-cranial solid paediatric cancer and is responsible for approximately 15% of all childhood cancer deaths, as reviewed by Maris [1].

Electronic supplementary material The online version of this article (doi:10.1007/s00428-011-1190-y) contains supplementary material, which is available to authorized users.

P. Ramani · J. V. Dungwa
Department of Histopathology, Bristol Royal Infirmary, Bristol BS2 8HW, UK

J. V. Dungwa
e-mail: pajvd@bristol.ac.uk

P. Ramani (✉) · J. V. Dungwa
School of Cellular and Molecular Medicine, School of Medical Sciences, University of Bristol, University Walk, Bristol BS8 1TD, UK
e-mail: pramila.ramani@bristol.ac.uk

M. T. May
School of Social and Community Medicine, University of Bristol, Canynge Hall, 39 Whatley Road, Bristol BS8 2PS, UK
e-mail: m.t.may@bristol.ac.uk

NBs arise from tissue of the sympathetic nervous system and frequently originate in the adrenal medulla or the sympathetic abdominal ganglia. However, NBs can also arise in the neck, chest and pelvis. The International Neuroblastoma Staging System defines five stages of NBs: stages 1 through 4 and 4-special (4 s) [1]. Stage 4 s tumours occur in children <18 months old and are widely disseminated but have a good prognosis and are capable of spontaneous regression. Adverse prognostic factors include an age ≥18 months at diagnosis, an abdominal location of the primary tumour [2] and specific genetic abnormalities, such as *MYCN* oncogene amplification, the loss of chromosome 1p or the gain of chromosome 17q [1]. Pathology is also an important prognostic indicator [2, 3]. Differentiated ganglioneuromas (GNs) lie at the benign end of the spectrum, and undifferentiated or poorly differentiated NBs with a high mitosis karyorrhexis index (MKI) lie at the most malignant end of the spectrum [3]. The majority of patients with NBs have widespread lymphatic and/or haematogenous metastases at diagnosis. Whereas angiogenesis has been studied extensively (reviewed by Rossler) [4], few reports have examined lymphangiogenesis in NBs [5–11].

Increased lymphatic density (LD) and lymphatic invasion (LI) are correlated with the incidence of lymph node metastasis (LNM) and poor prognosis in some human cancers (comprehensively reviewed by Sleeman) [12]. Specific staining for lymphatic vessels has been facilitated by the discovery of several proteins that recognise lymphatic endothelial cells (LECs), such as podoplanin and the transcription factor prospero-related homeobox gene-1 (PROX1) [13, 14]. The hyaluronan receptor LYVE-1 has been widely used for the detection of tumour-associated lymphatic vessels in different types of tumours [12, 15, 16]. However, the only published investigation of LYVE-1 in NB reports on only a small number of samples [6]. Moreover, the presence or absence of LI was not commented on, and no correlative data on LI, clinicopathological or biological variables are available. We performed a comprehensive expression analysis of LYVE-1 in a series of malignant neuroblastic tumours to determine the following: (1) the sensitivity of LYVE-1 in detecting LD and LI by immunohistochemistry, (2) the potential role of LD and LI based on their associations with clinicopathological and biological features and (3) the value of LD and LI as predictors of outcome.

Patients and methods

Patients

The study cohort consisted of 85 consecutive patients with NBs (including ganglioneuroblastomas, GNBs) treated at Bristol Children's Hospital between January 1994 and June 2009. The study was approved by the South Bristol and North Somerset Research Ethics Committee (09/H0106/06). Written informed consent was obtained from parents, legal guardians or subjects for clinical information and use of tumour samples surplus to diagnostic requirements. Staging was based on the International Neuroblastoma Staging System [17]. Subjects were treated according to the appropriate clinical protocols based on clinicopathological and biological characteristics. Clinical information was extracted from the medical records, and all patient data were de-identified. The tumours were classified into prognostic groups according to the International Neuroblastoma Pathology Classification (INPC) system [3]: 79 NBs and 6 GNBs (4 intermixed and 2 nodular subtypes).

Tissue samples

Samples were obtained from the Paediatric Pathology files of the Bristol Royal Infirmary. All of the samples were obtained at primary resection (stages 1 and 2) or before chemotherapy was administered (stages 3 and 4). For immunohistochemistry, paraffin-embedded tissues were available for 67 NBs (including all GNBs). Paraffin-embedded sections were not available from 18 NBs because of insufficient viable tumour material remaining in the tissue blocks. For LYVE-1 protein assays, snap-frozen tissue samples, comprising at least 70% viable tumoural tissue, were available for 55 NBs (including the 18 NBs that did not have paraffin-embedded tissue sections).

Enzyme-linked immunosorbent assay (ELISA)

Snap-frozen tissue samples were homogenised in an ice-cold lysis buffer composed of 1% Triton X-100 buffer containing 1:100 dilutions of protease and phosphatase inhibitor cocktails (Sigma-Aldrich, Dorset, UK). After homogenisation, the samples were centrifuged at 12,000×*g* for 15 min at 4°C. Total protein was quantified using the Bradford assay following the manufacturer's instructions (Sigma-Aldrich, Dorset, UK).

The concentration of LYVE-1 total protein was measured using the human LYVE-1 Duoset ELISA kit (DY2089, R&D Systems, Abingdon, UK) according to the manufacturer's instructions. Standard curves were constructed using two-fold serial dilutions of recombinant LYVE-1 protein (range 0–2,000 pg/ml). Optical densities were determined using a spectrophotometer at λ=450 nm with a corrective reading at λ=570 nm. Each test was performed in triplicate, and the mean values were used. The intraassay and interassay variation were both <10%.

Immunohistochemistry

Four-micrometer-thick consecutive sections from paraffin-embedded blocks were stained using a BOND-III automated immunostainer (Leica Biosystems, Milton Keynes, UK). Rabbit anti-human LYVE-1 polyclonal antibody (5 μg/ml, Abcam, Cambridge, UK) was applied to the sections for 1.5 h and detected using the Bond™ Polymer Refine Detection system (DS9800, Leica Novocastra, Milton Keynes, UK). Omission of the primary antibody was used as a negative control.

Assessment of lymphatic vessel density (LD)

LYVE-1-stained sections were scanned at low magnification (×10 eyepiece, ×10 objective) to identify the 'hot spots' showing the maximum number of lymphatics. Three 'hot spots' within each tumour section were counted at ×200 magnification (×10 eyepiece, ×20 objective) with a surface area of 1.23 mm^2. The sum of lymphatic vessels was divided by the sum of the surface area of all counted fields to obtain the mean lymphatic density (LD)/mm^2. Vessels with a clearly defined lumen or well-defined linear vessel shape, but not single endothelial cells, were taken into account for LD determination. Intratumoural lymphatic hotspots from the central (CLD) and marginal (MLD) (<2 mm from the margin of tumour) regions of the tumour were counted as previously described [18] by two independent observers blinded to the clinical data. LYVE-1-stained lymphatic vessels were assessed for the presence or absence of lymphatic invasion (LI).

Statistical analysis

Patients were divided into high-risk and non-high-risk groups. Patients with non-amplified *MYCN* stage 1, 2 and 3 tumours and children <18 months at presentation with stage 4 and 4 s NBs that lacked *MYCN* amplification were classified as non-high-risk. Patients with stage 3 *MYCN*-amplified tumours and children ≥18 months of age with stage 4 disease were classified as high risk. Only two tumour-related deaths occurred among stages 1, 2 and 3, so we combined these stages.

Associations between the LYVE-1-LDs and LYVE-1 total protein levels and the clinicopathological and biological variables were compared using the Mann–Whitney or Cuzick test for trend (MKI and stage) tests. χ^2 tests were used to test whether the presence or absence of LI was independent of other variables. Spearman's rank correlation was used to test for correlations between CLD, MLD and LYVE protein.

Overall survival (OS) was determined from the time of diagnosis to the last follow-up or tumour-specific-related death. Event-free survival (EFS) was calculated from the time of diagnosis until the time of first occurrence of relapse, progression, secondary malignancy or death or until the time of last contact if none of these occurred. Patients with poor or no response to therapy were excluded from the EFS analysis (n=7, all stage 4). A patient with co-incidental stage 2 NB and stage 4 alveolar rhabdomyosarcoma died.

For comparison of groups in survival analyses, LYVE-1-LDs were categorised as absent versus present because the medians were zero. LYVE-1 total protein level was dichotomised at 2 pg/μg protein, which was close to the median value. OS and EFS were estimated using the Kaplan–Meier (KM) method, and the differences in survival of the LYVE-1 subgroups were compared using the log-rank test. We used

Table 1 Clinicopathological and biological characteristics of the NB cohort (n=85)

Variable	Frequency (%)
Stage	
1	6 (7)
2	15 (18)
3	16 (19)
4	45 (53)
4 s	3 (4)
Age (months)	
<18	36 (42)
≥18	49 (58)
Risk group	
Non-high-risk	42 (49)
High-risk	43 (51)
Primary tumour site	
Extra-abdominal	17 (20)
Abdominal	68 (80)
MKI	
High	38 (45)
Intermediate	18 (21)
Low	29 (34)
INPC	
Favourable	35 (41)
Unfavourable	50 (59)
MYCN status	
Non-amplified	59 (69)
Amplified	21 (25)
Unknown	5 (6)
Deletion 1p	
Present	22 (26)
Absent	46 (54)
Unknown	17 (20)
17q gain	
Present	35 (41)
Absent	23 (27)
Unknown	27 (32)

NB neuroblastoma including ganglioneuroblastomas, *INPC* International Neuroblastoma Pathology Classification, *MKI* mitosis-karyorrhexis index

Schoenfeld residuals to test the proportional hazards assumption for all Cox models fitted to the data and found no evidence that this assumption was not valid. Univariable Cox regression models were used to estimate the unadjusted hazard ratio for tumour-related death and relapse for each of the prognostic factors.

The statistical analyses were performed using the Stata 11.0 software package (Stata for Windows, StataCorp, Texas, US).

Results

Clinicopathological characteristics of the cohort

The clinicopathological characteristics of the 85 NB patients (including GNBs) are summarised in Table 1. The median age at presentation was 20.14 months (range 0.03–188.3 months), and the median follow-up time of all the survivors was 75 months (range 14.0–195.0 months).

LYVE-1 expression in neuroblastic tumours

Lymphatic density

LYVE-1 expression was present mainly in the LECs but was also seen in scattered macrophages in the tumoural and stromal compartments. Lymphatics in the central part of the tumour were generally collapsed (Fig. 1a), and the marginal lymphatics were larger with wider lumens (Fig. 1b). However, lymphatics in the central part of the tumour were easily visualised when they contained tumour emboli (Fig. 1c).

The lymphatic count was 0 for 41/67 (61%) of patients. However, a significantly higher proportion of NBs exhibited MLD compared to NBs with CLD (39% vs. 26%, respectively, $p<0.001$) (Table 2). The CLD could not be assessed in two NBs because the biopsies contained peripheral tumoural tissue only and the biopsies were 2 mm in depth.

LYVE-1 total protein expression

As a result of the relatively low LD counts, the number of NBs stained by immunohistochemistry and the commercial availability of a sensitive ELISA, LYVE-1 protein were quantified in tumour lysates. LYVE-1 protein was detected in all 55 NBs analysed (median 1.62 pg/μg, range 0.0005–61.59 pg/μg total protein).

Lymphatic invasion (LI)

Immunostaining with LYVE-1 highlighted the presence of lymphatic invasion (LI) by tumour emboli in 14/67 (21%) NBs and nodular GNBs (Table 2), but none of the intermixed GNBs were positive for LI. The lymphatics in the marginal as well as central regions showed tumour emboli (Fig. 1b, c).

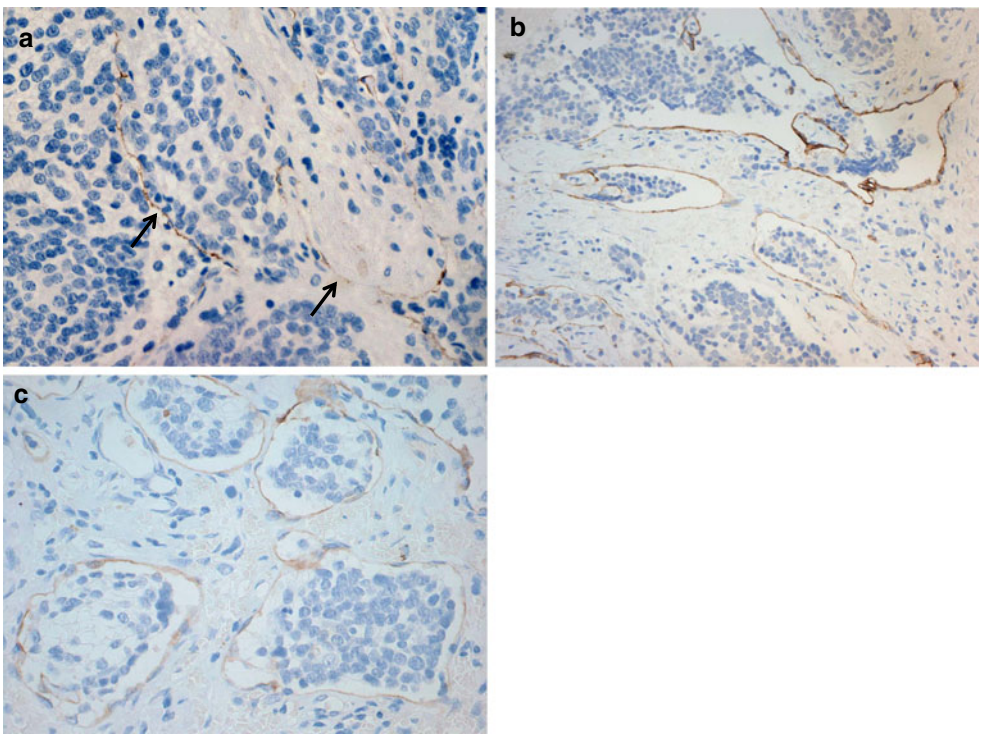

Fig. 1 Immunohistochemical expression of LYVE-1 in NBs. **a** Collapsed lymphatics (*black arrow*) in the central regions of the NB. **b** Large, dilated lymphatics in the marginal areas of NB containing tumour emboli. **c** LYVE-1-expressing lymphatics in the central region of NB show luminal occlusion by NB tumour emboli

Table 2 Relationship between LD and LI with clinicopathological and biological variables

	CLD			MLD			LI present	
All NBs								
Frequency	26% (17/65)			39% (26/67)			(14/67) 21%	
Mean (SE)	0.518 (0.195)			0.987 (0.276)				
Score range	0–9.00			0–11.6				
Variables	Number	Mean/mm^2 (SE)	*p*-value	Number	Mean/mm^2 (SE)	*p*-value	Percent	*p*-value[a]
Age (months)								
<18	28	0.098(0.043)		31	0.392(0.110)		6/31 (19)	
≥18	37	0.903(0.378)	0.320	36	1.428(0.475)	0.790	8/36 (22)	>0.999
Stage								
1, 2, 4 s	23	0.022(0.015)		24	0.469(0.187)		1/24 (4)	
3	12	0.208(0.126)		12	0.583(0.272)		1/12 (2)	
4	30	1.094(0.454)	**0.012**[b]	31	1.528(0.551)	0.558[b]	12/31(39)	**0.004**
Risk group								
Non-high-risk	37	0.095(0.045)		39	0.513(0.143)		3/39 (8)	
High-risk	28	1.150(0.483)	**0.030**	28	1.625(0.604)	0.920	11/28(39)	**0.002**
Site								
Extra-abdominal	14	0.087(0.090)		14	0.261(0.154)		1/14 (7)	
Abdominal	51	0.560(0.282)	0.260	53	0.943(0.342)	0.810	13/53(25)	0.269
MKI								
Low	24	0.093(0.067)		25	0.382(0.195)		0/25	
Intermediate	14	0.087(0.073)		15	1.301(0.796)		5/15 (33)	
High	27	0.946(0.499)	**0.011**[b]	27	0.911(0.486)	0.940[b]	9/27 (33)	**0.005**
INPC								
Favourable	33	0.080(0.050)		34	0.541(0.238)		3/34 (9)	
Unfavourable	32	0.831(0.430)	**0.040**	33	1.064(0.497)	0.990	11/33(33)	**0.017**
MYCN status								
Non-amplified	47	0.207(0.085)		49	0.824(0.301)		9/49 (18)	
Amplified	13	1.595(1.060)	0.440	13	1.033(0.905)	0.540	4/13 (31)	0.444
1p deletion								
Absent	37	0.143(0.070)		39	0.677(0.262)		8/39 (21)	
Present	14	1.800(0.965)	**0.020**	13	1.759(1.151)	0.650	6/13 (46)	0.086
17q gain								
Absent	19	0.118(0.075)		21	0.721(0.518)		5/21 (24)	
Present	21	1.229(0.676)	0.220	20	1.113(0.675)	0.510	7/20(35)	0.506
LNM								
Absent	51	0.063(0.034)		53	0.324(0.110)		4/53 (8)	
Present	14	1.843(0.878)	**<0.001**	14	2.672(1.100)	**<0.001**	10/14(71)	**<0.001**

All *p*-values were calculated using Mann–Whitney test unless otherwise stated

[a] χ^2 test

[b] Cuzick test for trend

SE standard error, *CLD* central lymphatic density, *MLD* marginal lymphatic density, *INPC* International Neuroblastoma Pathology Classification, *MKI* mitosis karyorrhexis index, *LNM* lymph node metastasis, *LI* lymphatic invasion

The association of the LDs, LI and total protein with clinicopathological and biological variables

The relationships between LD and LI with clinicopathological and biological variables are shown in Table 2.

LYVE-1-LD

CLD was higher in NBs from patients with stage 4 disease (p=0.012), high-risk group NBs (p=0.030), NBs with high MKI (p=0.011), unfavourable histology (p=0.040) and 1p

deletion (p=0.020) (Table 2). The data also show that CLD is increased in children ≥18 months at age of diagnosis, NBs from the primary abdominal site, *MYCN* amplification and chromosome 17q gain (Table 2). Similarly, MLD was higher in NBs with each of the adverse clinicopathological and biological variables, although p values indicated that there was insufficient power to exclude the possibility that differences may have been due to chance (Table 2).

LI

LI was higher in patients with stage 4 disease (p=0.004), high-risk group (p=0.002) and in NBs with high MKI (p=0.005) and unfavourable histology (p=0.017) (Table 2). LI also appeared to be increased in children ≥18 months at age of diagnosis, NBs from primary abdominal site, *MYCN* amplification and chromosome 17q gain (Table 2).

LYVE-1 total protein

The relationship between LYVE-1 protein expression in 55 NBs and the clinical, pathological and biological variables is shown in Fig. 2 and Supplementary File 1. There was an increase in LYVE-1 total protein levels in NB biopsies from stage 4 patients (Fig. 2a, p=0.046), high-risk group (Fig. 2b, p=0.028), LNM (Fig. 2c, p=0.035) and those with *MYCN* amplification (Fig. 2d, p=0.034). LYVE-1 total protein was higher in tumours with a high compared with intermediate or low MKI (median, 2.95 vs. 1.10 and 0.59 pg/μg total protein, respectively, p=0.157), tumours with unfavourable compared with favourable histology NBs (median, 2.30 vs. 0.51 pg/μg total protein, respectively, p=0.357), tumours with 1p deletion versus NBs without (median, 1.59 vs. 0.88 pg/μg total protein, respectively, p=0.626) and tumours with a gain of the 17q chromosome versus NBs without (median, 3.56 vs. 0.44 pg/μg total protein, respectively, p=0.126). There was no evidence of association between LYVE-1 protein levels and age at diagnosis, primary tumour location, INPC pathology prognostic group, MKI, deletion 1p or 17q gain (Supplementary File 1).

Correlation between LD, LI and LNM

CLD and MLD were strongly correlated (n=65, rho=0.605, p<0.001). CLD correlated with LI (rho=0.611, p<0.001) as did MLD (rho=0.638, p<0.001). Both CLD and MLD were higher in patients with LNM (p<0.001 for each, Table 2). A higher proportion of patients with LI showed LNM (p<0.001, Table 2).

Survival analysis

At the last follow-up, 26 of 85 patients (31%) had died, and 9 patients (10%) were alive with recurrent disease. All eight of the patients with poor or no response to therapy died.

In the univariable Cox proportional hazard regression analyses, age ≥18 months at diagnosis (p=0.038), clinical stage 4 (p<0.001), high-risk group (p<0.001), high MKI value (p=0.001), *MYCN*-amplification (p=0.001), 1p deletion (p<0.001) and 17q gain (p=0.032) were associated with lower OS (Table 3).

Similarly, age ≥18 months at diagnosis (p=0.015), clinical stage 4 (p<0.001), high-risk group (p<0.001), high MKI value (p=0.004), INPC pathology unfavourable prognostic group (p<0.001), 1p deletion (p<0.001) and 17q gain (p=0.022) were associated with worse EFS. There was a

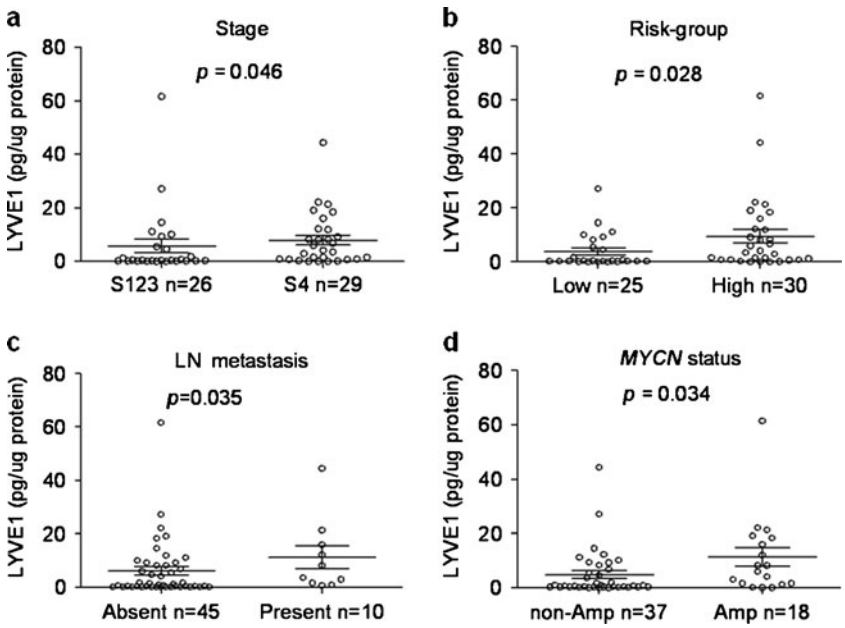

Fig. 2 Increased LYVE-1 total protein levels in NBs from **a** stage 4 patients, **b** high-risk group, **c** LN metastasis and **d** those with *MYCN* amplification. Each data point (*open circle*) represents protein concentration for each sample, and the *horizontal line* represents the median values. All p-values calculated using Mann–Whitney U-test

Table 3 Univariate Cox proportional hazards regression for NBs and GNBs

Variable		Deaths/*n*	Overall survival		Events/*n*	Event-free survival	
			HR (CI)	*p*-value		HR (CI)	*p*-value
Age (months)	<18	6/36	1		6/34	1	
	≥18	20/49	2.64 (1.06–6.59)	**0.038**	22/44	3.04 (1.24–7.59)	**0.015**
Stage	1–3,4 s	2/40	1		7/40	1	
	4	24/45	19.15 (4.46–82.17)	**<0.001**	21/38	5.22 (2.17–12.56)	**<0.001**
Risk group	Non-high-R	2/42	1		7/42	1	
	High-R	24/43	19.68 (4.59–84.29)	**<0.001**	21/36	5.41 (2.26–12.98)	**<0.001**
Site	Extra A	3/17	1		6/17	1	
	Abdo	23/68	2.76 (0.82–9.29)	0.101	22/61	1.26 (0.51–3.13)	0.613
MKI	Low/Interm	8/47	1		11/45	1	
	High	18/38	4.31(1.84–10.12)	**0.001**	17/33	3.10 (1.42–6.76)	**0.004**
INPC	FH	0/33			4/35	1	
	UH	26/32		0.072[a]	24/43	8.79 (2.97–25.99)	**<0.001**
MYCN status	Non-A	12/59	1		17/56	1	
	Amplified	11/21	3.88 (1.69–8.92)	**0.001**	9/18	2.15 (0.95–4.85)	0.066
1p deletion	Absent	5/46	1		7/45	1	
	Present	14/22	9.75 (3.47–27.41)	**<0.001**	13/18	7.91 (3.11–20.07)	**<0.001**
17q gain	Absent	2/23	1		2/22	1	
	Present	13/35	5.13 (1.15–22.81)	**0.032**	14/32	5.69 (1.29–25.12)	**0.022**
MLD	0	10/41	1		13/39	1	
	>0	7/26	1.12 (0.42–2.93)	0.824	6/23	0.83 (0.31–2.18)	0.700
CLD	0	10/49	1		12/46	1	
	>0	7/16	2.43 (0.93–6.40)	0.071	7/14	2.32 (0.91–5.92)	0.078
LYVE-1 protein	<2	9/30	1		8/29	1	
	≥2	7/25	1.12 (0.42–3.02)	0.818	5/23	0.92 (0.38–2.26)	0.863
LI	Absent	19/69	1		22/65	1	
	Present	7/16	2.29 (0.96–5.46)	0.062	6/13	1.87 (0.76–4.64)	0.175
LNM	Absent	19/70	1		20/65	1	
	Present	7/15	2.15 (0.90–5.13)	0.086	8/13	2.62 (1.14–6.01)	**0.023**

[a] Pearson χ^2 test. Presence or absence of LD was used as the cut-off for LD. Total LYVE-1 protein threshold of 2 pg/μg protein was used as the cut-off for protein

GNB ganglioneuroblastoma, *R* risk, *Extra-A* extra-abdominal, *Abdo* abdominal, *INPC* International Neuroblastoma Pathology Classification, *FH* favourable histology prognostic group, *UH* unfavourable pathology prognostic group, *Non-A MYCN* non-amplified, *MKI* mitosis karyorrhexis index, *Interm* intermediate, *CLD* central lymphatic density, *MLD* marginal lymphatic density, *LI* lymphatic invasion, *LNM* lymph node metastasis, *HR* hazard rate, *CI* confidence interval

strong association between distant LNM and shorter EFS and a weaker association with worse OS (Table 3).

The estimated overall survival (OS) at 5 years was 68% (95% CI: 56–77%) (Fig. 3a), and the estimated 5-year event-free survival (EFS) was 62% (95% CI: 50–72%) (Fig. 3b). Kaplan–Meier analysis showed that the presence of CLD was associated with both worse OS at 5 years (77% [95% CI: 62–87%] versus 60% [95% CI: 32–80%], $p=0.062$) (Fig. 3c) and EFS (74% [95% CI: 58–85%] versus 43% [95% CI: 15–69%], $p=0.070$) (Fig. 3d) and LI with OS (71% [95% CI: 57–81%] versus 56% [95% CI: 26–78%], $p=0.055$). However, as the sample size is small and there are few events, confidence intervals for survival estimates are wide, and therefore, observed differences in survival may be due to chance. There was no evidence of an association between MLD or total protein and OS or EFS (Table 3).

Discussion

This study represents the first detailed expression analysis of the lymphatic endothelial marker LYVE-1 in biopsies of NB patients and is the first examination of the relationship

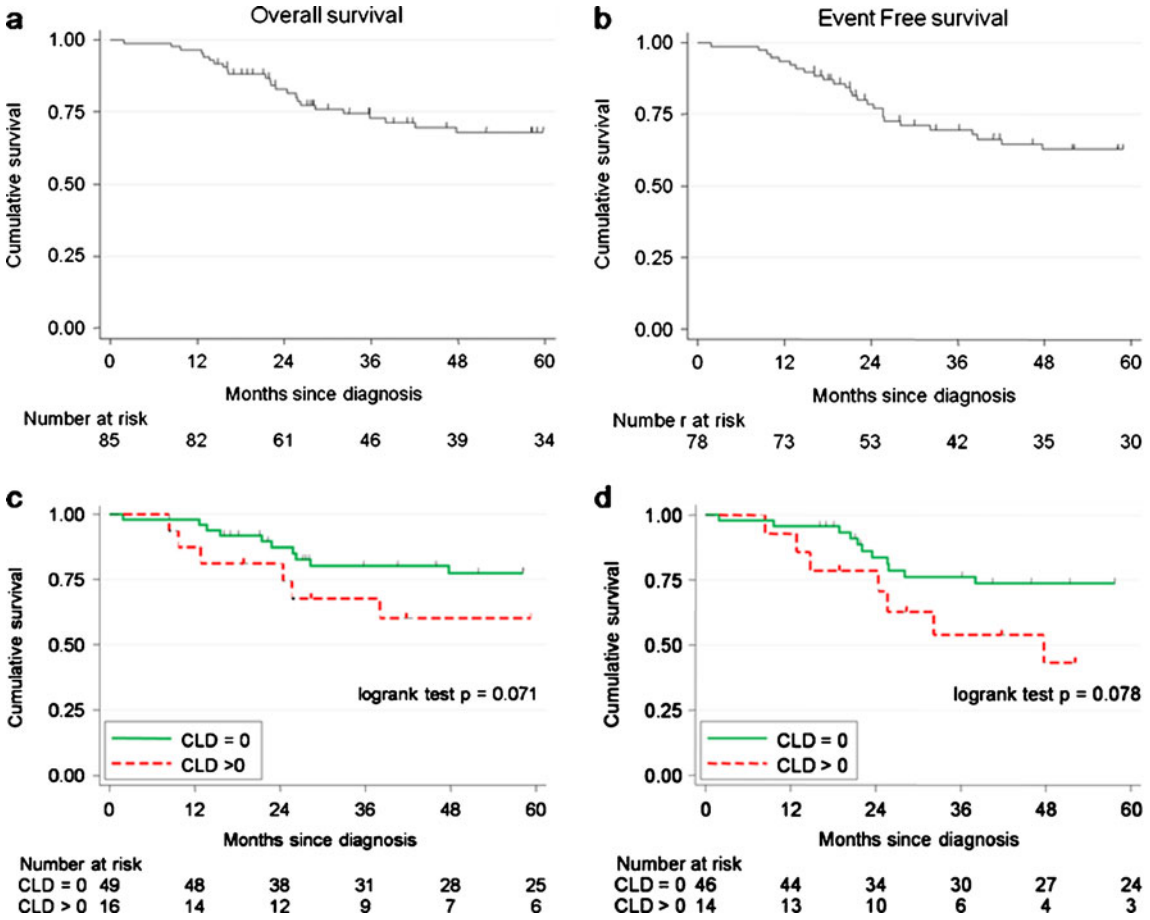

Fig. 3 Kaplan–Meier curves showing **a** overall survival (OS) and **b** event-free survival (EFS) of all patients in the study (85 NBs); worse **c** OS and **d** EFS rates in patients with LYVE-1 central lymphatic density (CLD >0) than those without

between the expression levels of this marker, clinicopathological and biological features and the prognosis of the patients.

LYVE-1 detected intratumoural lymphatics in up to 39% of 67 NBs, in contrast to 72% reported in the only previous study of 25 NBs [6]. Variations in the sensitivity of antibodies from different sources may provide a possible explanation for this difference. However, similar to the previous study in NBs [6], we noted LYVE-1 positive intratumoural lymphatics in the central and peripheral regions of the NBs. Most of the LYVE-1-expressing lymphatics in the central, deeper parts of the tumour were small and collapsed, although they were easily visualised when tumour emboli were present. In contrast, the marginal lymphatics in the peripheral parts of the NBs were larger with widely patent lumina. There was also a significant difference in the lymphatic count between the central and marginal areas of the NBs, which is in line with previous studies of other cancers [15, 16, 18, 19].

In our cohort, CLD and MLD were highly correlated with each other, and all of the associations for MLD were similar to those with CLD, but a little less strong. Increased CLD was associated with key adverse prognostic factors, such as inclusion in the high-risk group. We also observed a significant increase in NBs from patients with stage 4 tumours, in line with those of the previous study of 25 NBs [6].

The primary significance of the increased number and size of lymphatic vessels is that they provide a possible conduit for the spread of NB cells. Intravasation into tumoural vessels is an essential step in the metastatic cascade, and the presence of LI is an important pathological feature for assessing the risk of recurrence and metastasis. Immunostaining by LYVE-1 confirmed the presence of LI by NB tumour emboli and also showed a strong relationship between LI and various adverse prognostic features. Moreover, increased CLD and MLD strongly correlated with LI and LNM. As expected, the presence of LI correlated with distant LNM. Furthermore, both LD and LI showed a trend towards a poorer OS, whereas LNM showed a trend towards poorer OS and EFS. Our results are in line with recent findings on melanomas [20], tumours that share an embryonic origin with NBs, and various epithelial cancers, as

reviewed by Sleeman [12]. It is likely that a study including a larger cohort would show a significant relationship between LI and survival.

Quantification of total LYVE-1 protein using a sensitive ELISA assay also showed that LYVE-1 levels were significantly higher in the NBs of patients in an advanced stage, in the high-risk group or those with *MYCN*-amplified NBs. To our knowledge, LYVE-1 total protein, which measures expression in LEC and a subset of macrophages, has not been utilised in any other published clinical studies. The results obtained by immunohistochemistry were concordant with the data obtained by ELISA; increased LYVE-1 protein levels were also seen in NBs with similarly adverse prognostic features and distant LNM. However, LYVE-1 total protein levels did not show a significant association with OS or EFS in patients. Based on these findings, prospective studies including a larger number of samples from patients with NB may be useful to determine whether ELISA assays for LYVE-1 protein levels have clinical utility in providing prognostic data on the biological behaviour of NBs.

In summary, our results show for the first time that increased LYVE-1 (both LD and total protein levels) and LI are closely associated with key adverse risk factors and LNM. Distant LN involvement by NB is significantly correlated with EFS. These findings suggest that LYVE1 LD and LI may predict the outcome.

Acknowledgments The authors would like to thank Above and Beyond Charities of the University Hospitals Bristol Foundation Trust for their financial support and Ince & Co for their private donation. The authors are grateful to Mr. P.B. Savage for providing laboratory facilities.

Conflict of interest The authors declare that there is no conflict of interest. No part of the article has been published or submitted elsewhere, and there are no financial relationships that may lead to conflict of interest. The manuscript has been read and approved by all authors.

References

1. Maris JM, Hogarty MD, Bagatell R et al (2007) Neuroblastoma. Lancet 369:2106–2120
2. Cohn SL, Pearson AD, London WB et al (2009) The International Neuroblastoma Risk Group (INRG) classification system: an INRG Task Force report. J Clin Oncol 27:289–297
3. Shimada H, Ambros IM, Dehner LP et al (1999) The International Neuroblastoma Pathology Classification (the Shimada system). Cancer 86:364–372
4. Rossler J, Taylor M, Geoerger B et al (2008) Angiogenesis as a target in neuroblastoma. Eur J Cancer 44:1645–1656
5. Lagodny J, Juttner E, Kayser G et al (2007) Lymphangiogenesis and its regulation in human neuroblastoma. Biochem Biophys Res Commun 352:571–577
6. Ribatti D, Nico B, Cimpean AM et al (2010) Podoplanin and LYVE-1 expression in lymphatic vessels of human neuroblastoma. J Neurooncol 100:151–152
7. Becker J, Wang B, Pavlakovic H et al (2010) Homeobox transcription factor Prox1 in sympathetic ganglia of vertebrate embryos: correlation with human stage 4 s neuroblastoma. Pediatr Res 68:112–117
8. Becker J, Pavlakovic H, Ludewig F et al (2010) Neuroblastoma progression correlates with downregulation of the lymphangiogenesis inhibitor sVEGFR-2. Clin Cancer Res 16:1431–1441
9. Eggert A, Ikegaki N, Kwiatkowski J et al (2000) High-level expression of angiogenic factors is associated with advanced tumor stage in human neuroblastomas. Clin Cancer Res 6:1900–1908
10. Komuro H, Kaneko S, Kaneko M et al (2001) Expression of angiogenic factors and tumor progression in human neuroblastoma. J Cancer Res Clin Oncol 127:739–743
11. Nowicki M, Konwerska A, Ostalska-Nowicka D et al (2008) Vascular endothelial growth factor (VEGF)-C—a potent risk factor in children diagnosed with stadium 4 neuroblastoma. Folia Histochem Cytobiol 46:493–499
12. Sleeman JP, Thiele W (2009) Tumor metastasis and the lymphatic vasculature. Int J Cancer 125:2747–2756
13. Baluk P, McDonald DM (2008) Markers for microscopic imaging of lymphangiogenesis and angiogenesis. Ann N Y Acad Sci 1131:1–12
14. Van der Auwera I, Cao Y, Tille JC et al (2006) First international consensus on the methodology of lymphangiogenesis quantification in solid human tumours. Br J Cancer 95:1611–1625
15. Beasley NJ, Prevo R, Banerji S et al (2002) Intratumoral lymphangiogenesis and lymph node metastasis in head and neck cancer. Cancer Res 62:1315–1320
16. Van der Auwera I, Van den Eynden GG, Colpaert CG et al (2005) Tumor lymphangiogenesis in inflammatory breast carcinoma: a histomorphometric study. Clin Cancer Res 11:7637–7642
17. Maris JM (2010) Recent advances in neuroblastoma. N Engl J Med 362:2202–2211
18. Gombos Z, Xu X, Chu CS et al (2005) Peritumoral lymphatic vessel density and vascular endothelial growth factor C expression in early-stage squamous cell carcinoma of the uterine cervix. Clin Cancer Res 11:8364–8371
19. Straume O, Jackson DG, Akslen LA (2003) Independent prognostic impact of lymphatic vessel density and presence of low-grade lymphangiogenesis in cutaneous melanoma. Clin Cancer Res 9:250–256
20. Dadras SS, Paul T, Bertoncini J et al (2003) Tumor lymphangiogenesis: a novel prognostic indicator for cutaneous melanoma metastasis and survival. Am J Pathol 162:1951–1960

Virchows Arch (2012) 460:193–202
DOI 10.1007/s00428-011-1191-x

ORIGINAL ARTICLE

Rab25 is overexpressed in Müllerian serous carcinoma compared to malignant mesothelioma

Kjersti Brusegard · Helene Tuft Stavnes · Dag André Nymoen · Kjersti Flatmark · Claes G. Trope · Ben Davidson

Received: 2 November 2011 / Revised: 15 December 2011 / Accepted: 26 December 2011 / Published online: 17 January 2012
© Springer-Verlag 2012

Abstract Rab25, an epithelial-specific member of the Rab family of small GTPases, was previously shown to be overexpressed in ovarian/primary peritoneal serous carcinoma compared to malignant mesothelioma using gene expression arrays. The objective of this study was to validate this finding at the mRNA and protein level. Quantitative PCR analysis of 112 Müllerian serous carcinomas (84 effusions, 28 primary ovarian carcinomas) and 22 malignant mesotheliomas (19 effusions, 3 solid specimens) showed significantly higher *RAB25* mRNA expression in the former tumor ($p<0.001$). Immunohistochemical analysis of Rab25 protein expression in 245 effusions showed significantly higher expression of this protein in Müllerian serous carcinoma compared to malignant mesothelioma (189/209 vs. 12/36 positive tumors, respectively; $p<0.001$). Immunostaining of 101 patient-matched solid Müllerian carcinoma specimens (34 primary carcinomas, 67 metastases) showed expression levels comparable to effusions (94/101 positive specimens; $p>0.05$). Rab25 mRNA and protein expression levels in Müllerian carcinoma effusions did not correlate with overall or progression-free survival. Our data confirm that Rab25 effectively differentiates Müllerian carcinomas from malignant mesothelioma at the mRNA and protein level, suggesting a role in the diagnostic work-up of serosal cancers.

Keywords Rab25 · Müllerian carcinoma · Malignant mesothelioma · Serous effusions · Diagnosis · Quantitative real-time PCR · Immunohistochemistry

K. Brusegard · H. T. Stavnes · D. A. Nymoen · B. Davidson (✉)
Department of Pathology, Norwegian Radium Hospital,
Oslo University Hospital,
0424 Oslo, Norway
e-mail: bend@medisin.uio.no

K. Flatmark
Department of Tumor Biology, Institute for Cancer Research,
Norwegian Radium Hospital, Oslo University Hospital,
0424 Oslo, Norway

C. G. Trope
Department of Gynecologic Oncology,
Norwegian Radium Hospital, Oslo University Hospital,
0424 Oslo, Norway

C. G. Trope · B. Davidson
Institute of Clinical Medicine, Faculty of Medicine,
University of Oslo,
0424 Oslo, Norway

K. Flatmark
Department of Gastroenterological Surgery,
Norwegian Radium Hospital, Oslo University Hospital,
0424 Oslo, Norway

Introduction

The Rab GTPases are small GTP-binding proteins that form the largest family within the Ras superfamily of small GTPases, and over 70 human Rab genes have been identified [1–5]. The various Rab GTPases are localized to the cytosolic face of specific intracellular membranes, where they serve as coordinators of vesicle traffic. The Rab proteins take part in control of membrane identity and regulate the functions of vesicle budding, uncoating, motility, and fusion [2, 6]. As regulatory proteins, their mode of action is to alternate between two conformational states: the active GTP-bound form and the inactive GDP-bound form [1, 7].

In contrast to most of the Rab proteins that have a ubiquitous distribution, Rab25 was found to have an epithelial distribution. Prominent expression of Rab25 has been observed throughout the gastrointestinal mucosa, with the highest expression seen in the ileum and colon. High levels of expression are also present in the lungs and kidneys, with

a very minor and variable level of expression seen in splenic tissue. No expression of Rab25 has been seen in the brain, heart, liver, skeletal muscle, or the gastric wall [8]. Together with its paralogues, Rab11a and Rab11b, Rab25 is located in polarized epithelial cells where it exerts its function of regulating polarized endocytic recycling [9, 10].

Several Rab GTPases, including Rab25, have been examined for being potential drivers in carcinogenesis [11]. Studies have shown that Rab25, located at chromosome 1q22, is amplified at the DNA level and overexpressed at the RNA level in ovarian cancer and that these changes are associated with poor patient outcome. The underlying mechanisms effecting poor prognosis were hypothesized to be related to the intrinsic ability of Rab25 to promote anchorage-independent growth, decreased apoptosis and increased proliferation, and aggressiveness in vivo [12]. Increased Rab25 levels were also observed in other forms of cancer such as prostate cancer and transitional cell carcinoma of the bladder, providing further indication as to its involvement in carcinogenesis [13].

The dysregulation of Rab25 has been shown in transcription profiling analysis of various cancer tissues [14]. However, in contrast to its overexpression in the cancer types mentioned above, Rab25 was reported to be a tumor suppressor in colon carcinogenesis, and its expression in clinical cancer specimens was found to be decreased compared to normal mucosa independent of stage [15, 16]. Data are less conclusive in breast cancer. It was previously reported that Rab25 was overexpressed in this tumor [12]. However, recent studies have shown that Rab25 expression is actually significantly decreased compared to normal breast tissue, at least in hormone receptor-negative cancers [17].

Ovarian carcinoma (OC) is the second most common gynecological cancer, and it has the highest death toll among the gynecologic cancers, with more than 50% of the diagnosed women dying from this disease [18]. The poor outcome of OC is due to the fact that the majority of patients are presenting with advanced stage III/IV disease. Despite efforts to improve treatment of the disease by focus on early stage detection and the combination of aggressive surgery with improved chemotherapy protocols, the mortality rate of OC has largely remained unchanged.

The serosal cavities, including the peritoneal, pleural, and pericardial spaces, are frequently affected by cancer. The presence of cancer cells in effusions at these anatomic sites is evidence of advanced stage disease with metastatic spread, and regardless of the tumor site of origin, marks disease progression and is associated with poor survival [19, 20]. One of the most challenging differential diagnoses in serosal cancer is between Müllerian serous carcinoma and malignant mesothelioma (MM); tumors that are closely related in terms of clinical presentation, morphology, and immunohistochemical phenotype.

We recently reported on the differential expression of 189 genes in ovarian/primary peritoneal serous carcinoma (OC/PPC) compared with diffuse malignant peritoneal mesothelioma (DMPM) using cDNA microarray technology [21]. Among the differentially expressed genes, *RAB25* was identified as a gene that is significantly overexpressed in OC/PPC effusions compared to DMPM effusions. The present study evaluated the diagnostic value of Rab25 mRNA and protein expression levels in differentiating Müllerian carcinoma from malignant mesothelioma and analyzed the prognostic role of this molecule in Müllerian carcinoma effusions.

Material and methods

Patients and material

Effusions The material analyzed in the present study using quantitative real-time PCR (qPCR) consisted of 103 fresh-frozen effusions and 31 surgical specimens (total=134). Effusions consisted of 84 Müllerian serous carcinomas and 19 MM, submitted for routine diagnostic purposes to the Department of Pathology, Norwegian Radium Hospital, during the period 1998–2011. Müllerian serous carcinoma effusions (64 peritoneal, 20 pleural) were obtained from 84 patients diagnosed with the International Federation of Gynecology and Obstetrics (FIGO) stage II–IV OC (n=70), PPC (n=10), or carcinoma of the fallopian tube (n=4). Clinicopathologic data for patients with Müllerian serous carcinoma effusions were obtained from the Department of Gynecologic Oncology at the Norwegian Radium Hospital and are summarized in Table 1. The majority of the patients (75/84; 89%) received platinum-based chemotherapy at diagnosis.

The 19 MM effusions consisted of 14 pleural and 5 peritoneal specimens. All were from patients diagnosed with MM of the epithelioid or biphasic type in biopsy specimens.

Effusion specimens were centrifuged immediately after tapping, and cell pellets were frozen at −70°C in equal amounts of RPMI 1640 medium containing 50% fetal calf serum and 20% dimethyl sulfoxide. Smears and hematoxylin and eosin (H&E)-stained cell block sections were reviewed by a surgical pathologist experienced in cytopathology (BD). Diagnoses were based on morphology and immunohistochemistry. The antibody panel used for differentiating Müllerian serous carcinoma from MM and for establishing the malignant character of the mesothelial cell proliferations included Ber-EP4, B72.3, and in some cases BG8, as epithelial markers, and calretinin and desmin as mesothelial markers, the latter differentiating reactive from malignant mesothelial cells. The EMA staining pattern (thick brush-like membrane expression vs. combined membrane and cytoplasmic) was additionally used to differentiate malignant mesothelioma from adenocarcinoma, whereas WT-1 was added to the panel

Table 1 Clinicopathologic data of the Müllerian serous carcinoma effusion cohort analyzed using quantitative PCR (n=84 patients)

Parameter		Number of patients
Age		34–87 years (mean=61)
Histological grade[a]	1	4
	2	20
	3	50
	NA[b]	10
FIGO stage	II	1
	III	46
	IV	37
Effusion site	Peritoneum	64
	Pleura	20
Residual disease	≤1 cm	28
	>1 cm	43
	NA[c]	13
Chemoresponse at diagnosis	Complete	45
	Incomplete[d]	35
	ND[e]	4

[a] FIGO system

[b] NA = not available, including effusions from inoperable patients where biopsy was too small for grading and patients operated in other hospitals, for which the primary tumor could not be accessed for assessment of grade

[c] Nine patients who were inoperable and four patients with no record

[d] Partial response/stable disease/progression

[e] ND = not determined, including patients who received no chemotherapy and patients who died before chemoresponse could be assessed

as marker of serous differentiation in Müllerian carcinoma specimens. The tumor cell population was >50% in all specimens analyzed in this study.

Surgical specimens In addition to the above-mentioned effusions, 28 primary serous OC and 3 DMPM specimens were examined. Histological grade (FIGO system) of the 28 OC was as follows: grade 1, 5 tumors; grade 2, 5 tumors; and grade 3, 18 tumors. FIGO stage was as follows: I, 1 patient; II, 1 patient; III, 20 patients; and IV, 6 patients. Residual disease volume was available for 24 patients, of whom 16 were debulked to ≤1 cm and 8 to >1 cm.

Surgical specimens were snap frozen and kept at −70°C with no medium. Frozen sections from all tumors were evaluated to ensure the presence of a >50% tumor component and absence of necrosis. H&E-stained sections from these tumors were reviewed in order to establish tumor type and histological grade.

Quantitative real-time PCR

Total RNA was extracted using the automated sample preparation instrument QiaCube® and the RNeasy Mini Kit® (Qiagen, Hilden, Germany). mRNA was reverse-transcribed into cDNA using Superscript III Reverse Transcriptase (Invitrogen, Carlsbad, CA, USA). The *RAB25* (NM_020387.2) assay covered exon junction 1-2. Primer specificity was validated by gel electrophoresis. The assay was controlled for primer dimers using the NetPrimer software by PREMIER Biosoft, as well as for single nucleotide polymorphisms through the NCBI database. Primer efficiency was tested using Power SYBR Green (Applied Biosystems, Foster City, CA, USA) with a dilution series of synthetic oligonucleotides as template. The qPCR reaction was run using the Platinum qPCR SuperMix-UDG with ROX solution (Invitrogen) and quantified on the Applied Biosystems 7900HT Sequence Detection System.

Primer and probe sequences are as follows:

forward primer 5′-GGGGAATGGAACTGAGGAA GATTATAACT-3′;
reverse primer 5′-CGTGAATCGGGAGAGTA GATTGGTC-3′; and Probe Fam 5′-CAAGGTGGTGCT GATCGGCGAATCA -3′ non-fluorescent quencher.

An array of 12 reference genes (TaqMan low-density array human endogenous control panel; Applied Biosystems) was tested to identify the most uniformly expressed transcript in effusions specimens. Based on these results, the expression levels of *RAB25* were normalized against the housekeeping gene beta-glucuronidase (*GUS*). The *GUS* primer and probe sequences have been published elsewhere [22]. Standard curves for the *GUS* assay were commercially produced and purchased from Ipsogen (Marseille, France). Synthetic oligonucleotides were used as standard curve for *RAB25*. Standard curves were used to obtain copy numbers of *RAB25* and *GUS*. The copy number for *RAB25* was divided by the copy number of *GUS* to obtain normalized values for *RAB25* mRNA levels. These normalized values were used for the statistics.

Immunohistochemistry

A total of 245 effusions (209 Müllerian serous carcinomas and 36 MM) were analyzed. As with the qPCR series, clinicopathologic data for this cohort of patients with Müllerian serous carcinoma effusions were obtained from the Department of Gynecologic Oncology at the Norwegian Radium Hospital. They are summarized in Table 2. MM effusions were, as in the qPCR series, from patients diagnosed with MM of the epithelioid or biphasic type in biopsy specimens.

A series of 101 serous OC (34 primary carcinomas, 67 solid metastases) on tissue microarray slides (2-mm cores) was additionally immunostained. The majority of metastases (n=39) were omental, the remaining ones obtained from various other intraperitoneal sites, with the exception of one

Table 2 Clinicopathologic data of the Müllerian serous carcinoma effusion cohort analyzed using immunohistochemistry (n=208 patients)[a]

Parameter		Number of patients
Age		34–88 years (mean=61)
Histological grade[b]	1	14
	2	51
	3	123
	NA[c]	20
FIGO stage	I	1
	II	2
	III	126
	IV	79
Effusion site	Peritoneum	170
	Pleura	38
Residual disease	≤1 cm	81
	>1 cm	96
	NA[d]	31
Chemoresponse at diagnosis	Complete	117
	Incomplete[e]	80
	ND[f]	11

[a] One of 209 patients with incomplete clinical data

[b] FIGO system

[c] NA = not available, including effusions from inoperable patients where biopsy was too small for grading and patients operated in other hospitals, for which the primary tumor could not be accessed for assessment of grade

[d] Twelve patients who were inoperable and 19 patients with no record

[e] Partial response/stable disease/progression

[f] ND = not determined, including patients who received no chemotherapy and patients who died before chemoresponse could be assessed

lymph node metastasis. Specimens were patient-matched tumors from 46 of the patients with Müllerian carcinoma effusions studied using immunohistochemistry (IHC).

Paraffin-embedded sections were subjected to deparaffinization and epitope retrieval by the use of the Dako PT-Link (Dako, Glostrup, Denmark) with a high-pH (50× Tris–EDTA buffer pH 9) target retrieval solution (Dako). Sections were then incubated with 0.03% hydrogen peroxide to inhibit endogenous peroxidase. Sections were subsequently incubated for 30 min with a mouse monoclonal anti-Rab25 antibody purchased from Novus Biologicals (Littleton, CO, USA), diluted 1:500. Visualization was achieved using the EnVisionTM FLEX+peroxidase system (Dako). Positive control for Rab25 protein expression consisted of OC sections previously shown to express this protein. Negative controls consisted of sections that underwent similar staining procedure with normal IgG of the corresponding isotype as the primary antibody (IgG2A). Staining extent was scored by a surgical pathologist experienced in cytopathology (BD) using a scale of 0 to 4, corresponding to percentage of immunoreactive tumor cells of 0%, 1–5%, 6–25%, 26–75%, and 76–100%, respectively. A subset (n=100) of the 346 samples was scored together with the author of this study, and interobserver concordance was excellent, with 90% total agreement on score. In cases with discordant scores, the difference was of one scoring level and consensus was easily reached upon discussion.

Statistical analysis

Statistical analysis was performed using the SPSS-PC package (Version 18; Chicago, IL, USA). Probability of <0.05 was considered significant. The Mann–Whitney U test was used to analyze the differences in Rab25 mRNA and protein expression between Müllerian carcinoma and MM. The same test was applied to the comparative analysis of *RAB25* mRNA expression in Müllerian carcinoma effusions vs. primary OC. The Wilcoxon signed ranks test was applied to the patient-matched analyses of Rab25 protein expression in primary OC vs. effusions, primary OC vs. solid metastases, and effusions vs. solid metastases. Comparative analysis of all effusions, primary OC, and solid metastases was performed using the Kruskal–Wallis H test. Comparative analysis of Rab25 expression in omental vs. non-omental metastases were executed using the Mann–Whitney U test.

The Mann–Whitney U test was additionally applied to analyses investigating the association between gene expression and clinicopathologic parameters (effusion site, age, histological grade, FIGO stage, residual disease volume, previous chemotherapy, and response to chemotherapy at diagnosis) for patients with Müllerian carcinoma effusions. For these analyses, clinicopathologic parameters were grouped as follows: age, ≤60 vs. >60 years; histological grade, 1–2 vs. 3; FIGO stage, III vs. IV; residual disease volume, ≤1 vs. >1 cm; previous chemotherapy, yes vs. no; response to chemotherapy at diagnosis, complete vs. partial response/stable disease/progression.

Survival data were available for all Müllerian carcinoma patients. Univariate survival analyses of progression-free survival (PFS) and overall survival (OS) were executed using the Kaplan–Meier method and groups compared with the log rank test. For this analysis, expression levels were grouped as low or high based on median values.

Results

Rab25 is overexpressed in Müllerian carcinoma compared to MM at the mRNA and protein level

Comparative analysis of *RAB25* mRNA expression in Müllerian carcinoma and MM effusions using qPCR showed marked differences between these two tumor entities.

Müllerian carcinoma effusions had a *RAB25* copy number range of 1 to 3,204 (median, 416), whereas MM effusions had no copies (16 specimens) or one copy (3 specimens) of this transcript ($p<0.001$; Fig. 1). The three solid MM specimens had 0–2 copies.

Primary OC had *RAB25* expression range of 22 to 3,386 (median, 763). In statistical analysis, the difference between Müllerian carcinoma effusions and primary OC was not significant, although one observed a trend for a higher *RAB25* expression in the latter group ($p=0.062$). Values of the reference gene GUS showed little variation across different samples, irrespective of tumor type or anatomic site (Fig. 1).

Rab25 protein expression was analyzed in 346 tumors, consisting of 209 Müllerian carcinoma effusions, 36 MM effusions, and 101 solid OC. Rab25 was expressed in the cytoplasm of tumor cells in 189/209 (90%) OC/PPC effusions, with the following staining score: 0, 20; 1, 14; 2, 26; 3,46, and 4, 103 (Fig. 2a–c). In MM effusions, Rab25 was expressed in the cytoplasm of 12/36 (33%) specimens, with the following staining score: 0, 24; 1, 3; 2, 2; 3, 6, and 4, 1 (Fig. 2d). Nuclear expression was observed in 33/209 Müllerian carcinoma effusions, but none of the MM cases (Fig. 2e, f). Mann–Whitney *U* test was performed separately for cytoplasmic and nuclear staining. This test showed a

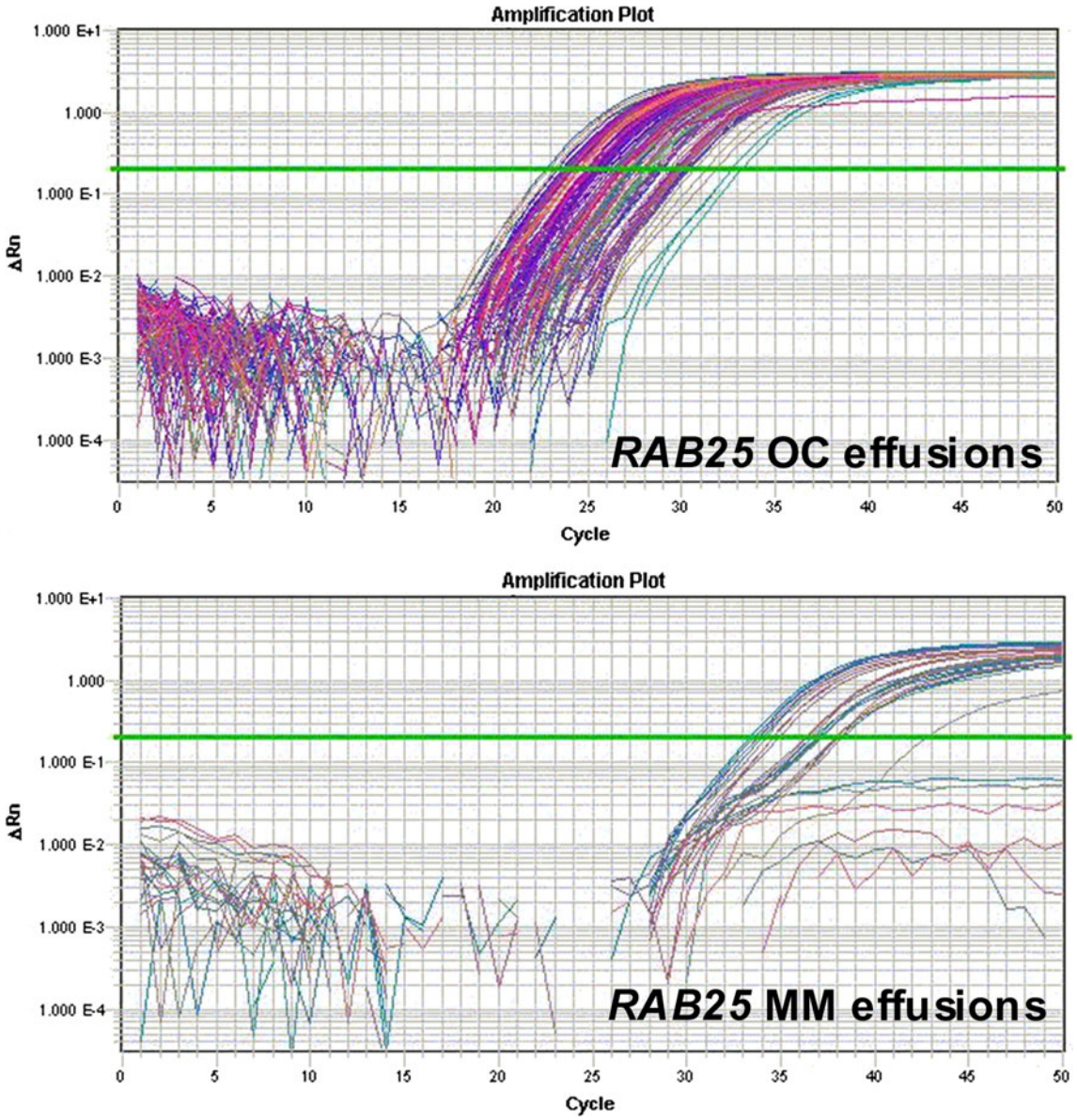

Fig. 1 *RAB25* and *GUS* mRNA expressions in Müllerian serous carcinoma and malignant mesothelioma (*MM*) effusions. qPCR amplification plots for *RAB25* and *GUS* mRNA in Müllerian serous carcinoma and MM effusions. Cases were run in triplicate. *RAB25* mRNA expression is much higher in Müllerian carcinoma compared to MM effusions, whereas the reference gene *GUS* is uniformly expressed

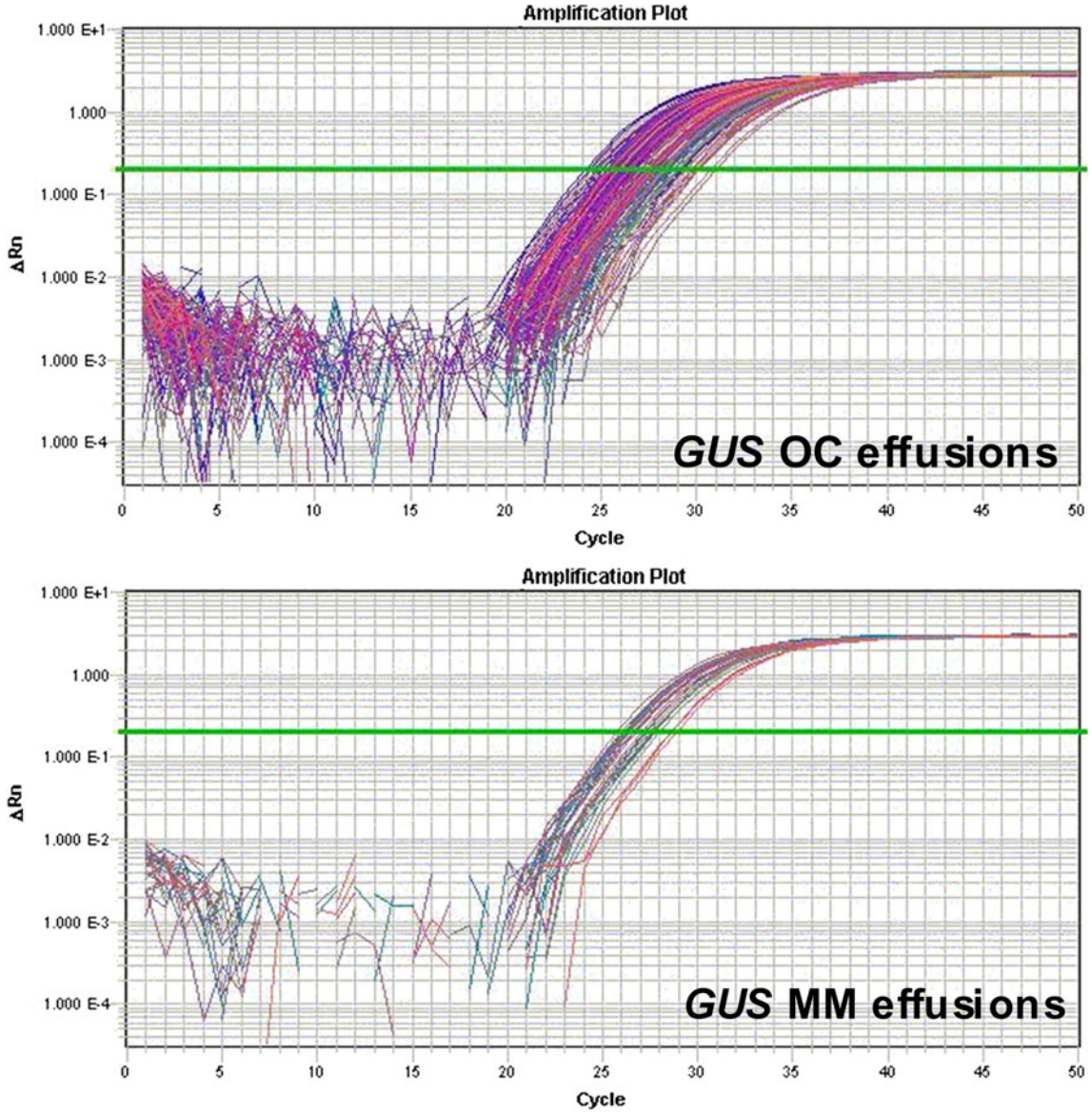

Fig. 1 (continued)

significantly higher Rab25 protein in the Müllerian carcinoma effusions compared to MM effusions for both subcellular locations (cytoplasmic staining: mean rank=135.88 and 48.24 for Müllerian carcinoma and MM respectively, $p<0.001$; nuclear staining: mean rank=125.84 and 106.50 for Müllerian carcinoma and MM respectively, $p=0.011$).

Rab25 was expressed in the cytoplasm of tumor cells in 31/34 (91%) primary OC, with the following staining score: 0, 3; 1, 4; 2, 1; 3, 6, and 4, 20. In solid metastases, Rab25 was expressed in the cytoplasm of 63/67 (94%) specimens, with the following staining score: 0, 4; 1, 14; 2, 7; 3, 13, and 4, 29 (Fig. 2g–i). Nuclear Rab25 was found in 13 specimens, including 5 primary OC and 8 metastases. Wilcoxon signed ranks analysis of the association between IHC results and anatomic site showed no significant differences in Rab25 cytoplasmic or nuclear staining between patient-matched primary OC and solid metastases or between effusions and solid primary or metastatic lesions ($p>0.05$; data not shown). Comparison of Rab25 protein expression in all effusions, primary OC, and solid metastases, rather than in patient-matched cases, similarly demonstrated no significant differences, as did comparison of omental vs. non-omental metastases ($p>0.05$ for both; data not shown). Positive and negative controls were satisfactory in all experiments.

Rab25 expression in Müllerian carcinoma is not significantly related to disease outcome

RAB25 mRNA expression in Müllerian carcinoma effusions was significantly associated with younger patient

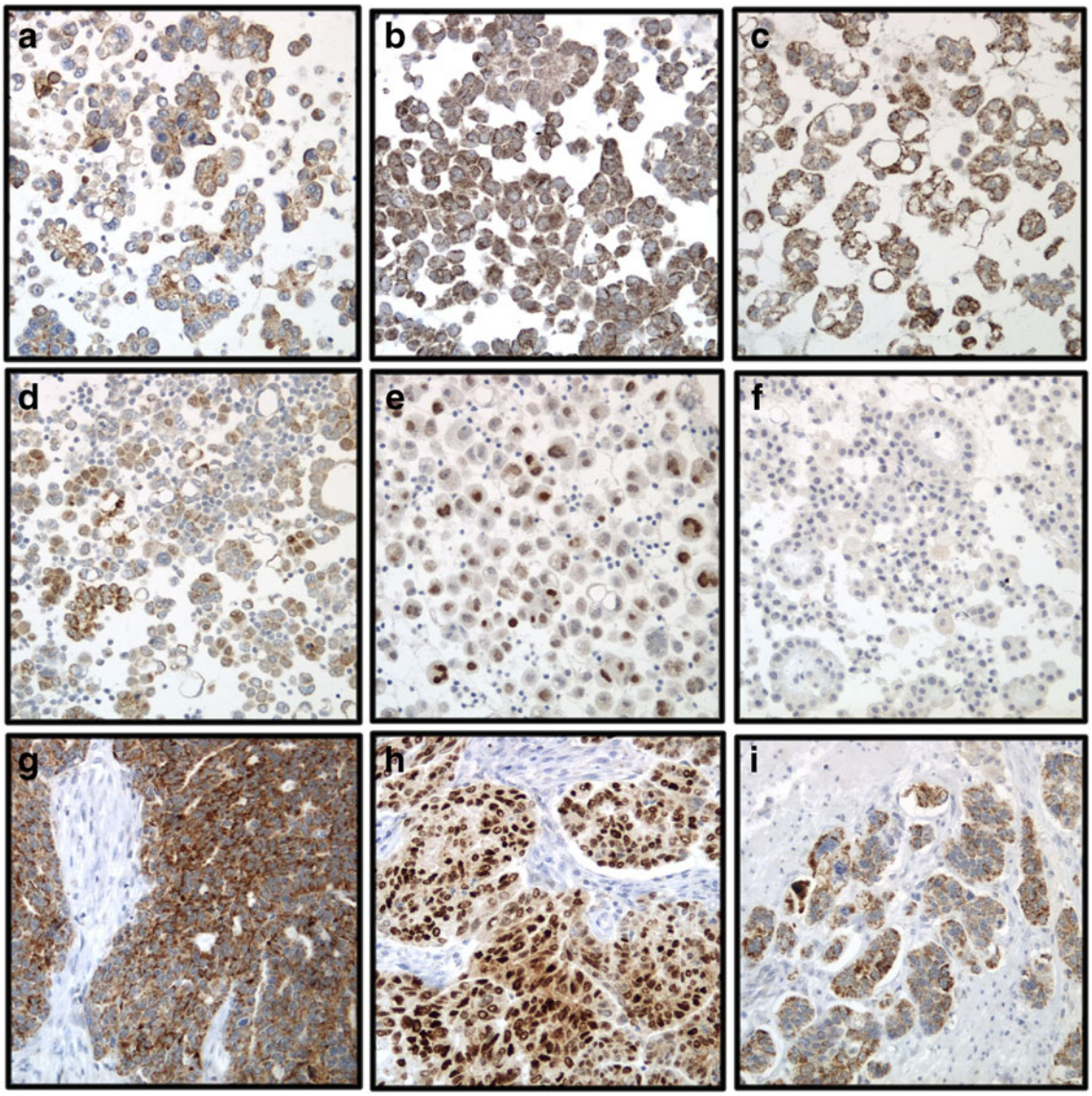

Fig. 2 Rab25 protein expression in Müllerian carcinoma. Examples of Rab25 immunostaining in Müllerian serous carcinoma and MM. **a–e** Müllerian serous carcinoma effusions: examples of cytoplasmic staining (**a–c**), cytoplasmic and focal nuclear staining (**d**), and nuclear staining (**e**); **f** negative staining in a malignant mesothelioma effusion; **g–i** primary and metastatic serous ovarian carcinoma: cytoplasmic (**g**) and nuclear staining in a primary ovarian carcinoma (**h**) and cytoplasmic staining in a colon metastasis (**i**)

age (mean rank=48.23 and 35.57 for patients aged ≤60 vs. >60 years, respectively; $p=0.018$) but was unrelated to effusion site (pleura vs. peritoneum), histological grade, FIGO stage, residual disease volume, and response to chemotherapy at diagnosis. Expression was similarly unrelated to previous exposure to chemotherapy ($p>0.05$; data not shown).

Rab25 nuclear expression by IHC was directly related to higher histological grade (mean rank=98.87 and 86.23 for grade 3 vs. grade 1–2 tumors, respectively; $p=0.018$) and was unrelated to the other clinicopathologic parameters ($p>0.05$; data not shown). Cytoplasmic expression was unrelated to any of these parameters.

The follow-up period for the 84 Müllerian carcinoma patients with effusions analyzed using qPCR ranged from 1 to 87 months (median, 24 months). PFS ranged from 0 to 66 months (median, 4 months), with 34 patients never achieving a progression-free period. At the last follow-up, 1 patient was alive with no evidence of disease, 3 patients were alive without disease, and 80 patients were dead of disease.

The follow-up period for 208 Müllerian carcinoma patients with effusions analyzed using IHC (one patient without full clinical data) ranged from 1 to 110 months (median, 26 months). PFS ranged from 0 to 66 months (median, 6 months), with 78 patients never achieving a

progression-free period. At the last follow-up, 3 patients were alive with no evidence of disease, 16 patients were alive without disease, and 188 patients were dead of disease. One patient died of unrelated cause.

No significant association was found between Rab25 mRNA or protein expression and OS or PFS. However, higher *RAB25* mRNA expression levels in Müllerian carcinoma effusions were associated with a trend for shorter PFS (6 vs. 9 months; $p=0.071$), which was additionally observed in analysis limited to the 42 patients with primary diagnosis prechemotherapy specimens (4 vs. 11 months; $p=0.104$), whereas Rab25 protein cytoplasmic expression in primary diagnosis specimens was associated with a trend for longer OS (38 vs. 27 months; $p=0.079$).

Discussion

The differentiation of Müllerian serous carcinoma from MM may pose difficulties, as these tumors morphologically resemble each other and co-express many of the diagnostic markers used in effusion diagnosis. It is therefore vital to identify and validate new high-throughput markers that can aid in differentiating these two cancer types. Previous studies have shown elevated or decreased expression levels of Rab25 in multiple cancer types compared to normal tissue [12–17]. Nevertheless, with the exception of our previous Affymetrix gene expression microarray analysis [21], the role of Rab25 in differentiating between various cancer types has not been explored to date.

The present study validates the findings of our microarray analysis, where *RAB25* was identified as a potential marker for differentiating Müllerian serous carcinoma from MM [21]. We measured Rab25 mRNA levels and protein expression in Müllerian serous carcinoma compared to MM and observed significantly higher expression levels of both Rab25 mRNA and protein in the former tumor. Previous work by our group has shown that the mRNA of the folate receptor genes *FOLR1* and *FOLR3*, *SCARA3* (Scavenger receptor class A, member 3), *EHF* (Ets homologous factor) and *PRAME* (preferentially expressed antigen of melanoma) are overexpressed in Müllerian serous carcinoma compared to MM and/or breast carcinoma, while *TNXB* (Tenascin-X) and *PINCH-2* (Particularly interesting new cysteine-histidine-rich) mRNA levels have the opposite transcription pattern [23–28]. Based on these studies and additional ones that are in preparation, we are in the process of developing a diagnostic qPCR panel for effusion diagnosis. Furthermore, despite the small number of MM biopsies analyzed in the present study, our findings suggest that the diagnostic role of *RAB25* may apply to surgical specimens as well, as mRNA levels of this gene were high in primary OC and very low in MM specimens.

RAB25 transcript levels in Müllerian serous carcinoma effusions were comparable in peritoneal and pleural specimens. This concurs with previous comparative studies of cancer-associated molecules by our group, which have revealed striking similarities between tumor cells in these two serosal cavities [20, 29]. Our finding adds to a series of previous observations supporting the hypothesis that cancer cells in peritoneal effusions, similarly to those in pleural effusions, are of a fully metastatic nature.

When comparing gene expression levels of *RAB25* between primary OC and Müllerian carcinoma effusions, we found a trend for higher *RAB25* expression at the former anatomic site. From these results, one can infer that there is decreased expression of *RAB25* as the tumor progresses and metastasizes from its solid form to effusions. The altered expression profile of tumor cells in effusions can result from a change in the microenvironment. When the tumor cells are part of solid organs they are complemented by various cell populations such as stromal myofibroblasts, endothelial cells, and leukocytes. Within solid organs, tumor cells are able to induce leaky vessels and obtain nutrients and oxygen, in addition to gaining access to the circulation. When present in effusions, however, tumor cells are in a unique microenvironment with reduced direct access to oxygen and nutrients and no longer in interaction with stromal myofibroblasts and endothelial cells [29]. The decreased expression levels of *RAB25* in Müllerian carcinoma effusions compared to primary OC may be the result of such a change in the microenvironment.

Alterations of genetic and epigenetic factors lead to deregulation of gene expression in cancer cells in comparison to normal cells. Our findings suggest that these alterations are not random. Metastatic cells within the same microenvironment display a conserved expression pattern that correlates to their tissue of origin. The molecular basis for the difference in Rab25 expression between Müllerian serous carcinoma and MM, as well as its reduced expression in effusions compared to solid lesions, is nevertheless not understood at present. Rab family members, including Rab25, are part of the Ras superfamily of small GTPases. Mutations in Ras genes in general [2, 30], and in Rab genes in particular [31, 32], are involved in a range of neurodegenerative, metabolic, and autoimmune diseases, as well as in cancer, and may well be the molecular basis for the reduced or absent expression of Rab25 in MM. An alternative, which may also be relevant for Müllerian serous carcinoma effusions, would be gene hypermethylation, which has been reported for Rab32 in several carcinoma types [33, 34] or deletion, as reported for Rab36 in malignant Rhabdoid tumors [35].

The clinical role of Rab25 in ovarian carcinoma has been studied previously but is undecided at present. Cheng et al. found that increased *RAB25* expression levels were

associated with markedly decreased disease-free survival and OS [12]. In contrast, Sheach et al. found that Rab25 protein expression levels in ovarian cancers did not correlate with survival. The latter group did observe that among patients with tumors expressing high Rab25 protein levels, those with mucinous or endometrioid carcinoma had better survival than those with serous, clear cell, or undifferentiated carcinoma, which was not found in low Rab25 expressors [36]. In our cohort, which consisted uniformly of serous carcinomas, we observed significantly higher mRNA expression in Müllerian carcinoma effusions from younger patients, as well as significant association between the presence of nuclear Rab25 protein expression and high histological grade (grade 3). However, no significant relationship was observed between Rab25 mRNA or protein expression and chemoresponse or survival. We did, however, find a trend for higher *RAB25* mRNA expression levels in effusion specimens from patients who had shorter PFS, which was additionally observed in analysis limited to patients with pre-chemotherapy effusions. In contrast, we found a trend for longer OS for patients with pre-chemotherapy primary diagnosis effusions displaying high Rab25 protein cytoplasmic expression. While these results appear contradictory, mRNA levels often correlate poorly with protein expression, especially when one is measured quantitatively (qPCR) and the other semiquantitatively at best (IHC). In the present study, the cohorts analyzed using these two methods were additionally different. At any rate, the prognostic role of Rab25 in metastatic Müllerian carcinoma remains at present undecided.

Our finding of Rab25 nuclear staining was surprising, as Rab proteins are known to be mostly cytosolic proteins. However there are studies that show Rab25-related proteins to be localized to the nucleus. One of these proteins, Rab-like protein 1B, was shown to play an important part in breast tumorigenesis [37]. Another nucleus-associated protein is Ran. The Ran protein resides on a branch of the Rab subfamily, and it is involved in nuclear import and export [5]. If confirmed in additional studies, nuclear Rab25 may have a yet uncharacterized biological role in Müllerian carcinoma.

In conclusion, qPCR analysis and IHC confirmed that Rab25 effectively differentiates Müllerian carcinomas from MM at the mRNA and protein levels, suggesting that Rab25 may be a novel marker in the diagnostic panel of serosal tumors. Although our data do not support a role for Rab25 as a prognostic marker in Müllerian carcinoma, its frequent expression in this tumor may suggest a role as a therapeutic target. K-Ras, member of the Ras family, regulates epidermal growth factor receptor and has in recent years proven to be a successful target for drug therapy. Rab family members are currently investigated for their potential relevance in the context of targeted therapy using small molecules [32], and may, in view of their wide range of regulatory functions, prove to be novel drug targets.

Acknowledgments This study was supported by grants from the Norwegian Cancer Society and the Research Foundation at the Norwegian Radium Hospital and by the Inger and John Fredriksen Foundation for Ovarian Cancer Research.

Conflict of interest statement We declare that we have no conflict of interest.

References

1. Stenmark H, Olkkonen VM. The Rab GTPase family (2001) Genome Biol 2:REVIEWS3007
2. Stenmark H (2009) Rab GTPases as coordinators of vesicle traffic. Nat Rev Mol Cell Biol 10:513–523
3. Seabra MC, Mules EH, Hume AN (2002) Rab GTPases, intracellular traffic and disease. Trends Mol Med 8:23–30
4. Schwartz SL, Cao C, Pylypenko O, Rak A, Wandinger-Ness A (2007) Rab GTPases at a glance. J Cell Sci 120:3905–3910
5. Colicelli J (2004) Human RAS superfamily proteins and related GTPases. Sci STKE 2004(250):RE13
6. Stein MP, Dong J, Wandinger-Ness A (2003) Rab proteins and endocytic trafficking: potential targets for therapeutic intervention. Adv Drug Deliv Rev 55:1421–1437
7. Zerial M, McBride H (2001) RAB proteins as membrane organizers. Nat Rev Mol Cell Biol 2:107–117
8. Goldenring JR, Shen KR, Vaughan HD, Modlin IM (1993) Identification of a small GTP-binding protein, Rab25, expressed in the gastrointestinal mucosa, kidney, and lung. J Biol Chem 268:18419–18422
9. Wang X, Kumar R, Navarre J, Casanova JE, Goldenring JR (2000) Regulation of vesicle trafficking in Madin-Darby canine kidney cells by Rab11a and Rab25. J Biol Biochem 275:29138–29146
10. Casanova JE, Wang X, Kumar R, Bhartur SG, Navarre J, Woodrum JE, Altschuler Y, Ray GS, Goldenring JR (1999) Association of Rab25 and Rab11a with the apical recycling system of polarized Madin-Derby canine kidney cells. Mol Biol Cell 10:47–61
11. Tang BL (2010) Is Rab25 a tumor promoter or suppressor-context dependency on RCP status? Tumor Biol 31:359–361
12. Cheng KW, Lahad JP, Kuo WL, Lapuk A, Yamada K, Auersperg N, Liu J, Smith-McCune K, Lu KH, Fishman D, Gray JW, Mills GB (2004) The RAB25 small GTPase determines aggressiveness of ovarian and breast cancers. Nat Med 10:1251–1256
13. Cheng KW, Lahad JP, Gray JW, Mills GB (2005) Emerging role of RAB GTPases in cancer and human disease. Cancer Res 65:2516–2519
14. Agarwal R, Jurisica I, Mills GB, Cheng KW (2009) The emerging role of the RAB25 small GTPase in cancer. Traffic 10:1561–1568
15. Nam KT, Lee HJ, Smith JJ, Lapierre LA, Kamath VP, Chen X, Aronow BJ, Yeatman TJ, Bhartur SG, Calhoun BC, Condie B, Manley NR, Beauchamp RD, Coffey RJ, Goldenring JR (2010) Loss of Rab25 promotes the development of intestinal neoplasia in mice and is associated with human colorectal adenocarcinomas. J Clin Invest 120:840–849
16. Goldenring JR, Nam KT (2011) Rab25 as a tumour suppressor in colon carcinogenesis. Br J Cancer 104:33–36
17. Cheng JM, Volk L, Janaki DK, Vyakaranam S, Ran S, Rao KA (2010) Tumor suppressor function of Rab25 in triple-negative breast cancer. Int J Cancer 126:2799–2812
18. American Cancer Society. Cancer facts and figures 2010. Estimated new cancers cases and deaths by sex for all sites. Available at:

http://www.cancer.org/Research/CancerFactsFigures/CancerFactsFigures/cancer-facts-and-figures-2010. Accessed 31 July 2010
19. Davidson B (2004) Malignant effusions: from diagnosis to biology. Diagn Cytopathol 31:246–254
20. Davidson B (2007) Biological characteristics of cancers involving the serosal cavities. Crit Rev Oncog 13:189–227
21. Davidson B, Zhang Z, Kleinberg L, Li M, Flørenes V, Wang TL, Shih leM (2006) Gene expression signatures differentiate ovarian/peritoneal serous carcinoma from diffuse malignant peritoneal mesothelioma. Clin Cancer Res 12:5944–5950
22. Beillard E, Pallisgaard N, van der Velden VH, Bi W, Dee R, van der Schoot E, Delabesse E, Macintyre E, Gottardi E, Saglio G, Watzinger F, Lion T, van Dongen JJ, Hokland P, Gabert J (2003) Evaluation of candidate control genes for diagnosis and residual disease detection in leukemic patients using "real-time" quantitative reverse-transcriptase polymerase reaction (RQ-PCR)—a Europe against cancer program. Leukemia 17:2474–2486
23. Bock AJ, Nymoen DA, Brenne K, Kærn J, Davidson B (2011) *SCARA3* mRNA is overexpressed in ovarian carcinoma compared with breast carcinoma effusions. Hum Pathol. doi:10.1016/j.humpath.2011.06.003
24. Yuan Y, Nymoen DA, Dong HP, Bjørang O, Shih leM, Low PS, Trope CG, Davidson B (2009) Expression of the folate receptor genes *FOLR1* and *FOLR3* differentiates ovarian carcinoma from breast carcinoma and malignant mesothelioma in serous effusions. Hum Pathol 40:1453–1460
25. Brenne K, Nymoen DA, Hetland TE, Trope CG, Davidson B (2011) Expression of the Ets transcription factor EHF in serous ovarian carcinoma effusions is a marker of poor survival. Hum Pathol. doi:10.1016/j.humpath.2011.05.023
26. Yuan Y, Nymoen DA, Stavnes HT, Rosnes AK, Bjørang O, Wu C, Nesland JM, Davidson B (2009) Tenascin-X is a novel diagnostic marker of malignant mesothelioma. Am J Surg Pathol 33:1673–1682
27. Yuan Y, Dong HP, Nymoen DA, Nesland JM, Wu C, Davidson B (2011) PINCH-2 expression in cancers involving serosal effusions using quantitative PCR. Cytopathology 22:22–29
28. Brenne K, Nymoen DA, Reuven R, Davidson B (2012) PRAME (Preferentially expressed antigen of melanoma) is a novel marker for differentiating serous carcinoma from malignant mesothelioma. Am J Clin Pathol (in press)
29. Davidson B (2007) Anatomic site-related expression of cancer associated molecules in ovarian carcinoma. Curr Cancer Drug Targets 7:109–120
30. Oxford G, Theodorescu D (2003) Ras superfamily monomeric G proteins in carcinoma cell motility. Cancer Lett 189:117–128
31. Mitra S, Cheng KW, Mills GB (2011) Rab GTPases implicated in inherited and acquired disorders. Semin Cell Dev Biol 22:57–68
32. Agola J, Jim P, Ward H, Basuray S, Wandinger-Ness A (2011) Rab GTPases as regulators of endocytosis, targets of disease and therapeutic opportunities. Clin Genet 80:305–318
33. Schulmann K, Mori Y, Croog V, Yin J, Olaru A, Sterian A, Sato F, Wang S, Xu Y, Deacu E, Berki AT, Hamilton JP, Kan T, Abraham JM, Schmiegel W, Harpaz N, Meltzer SJ (2005) Molecular phenotype of inflammatory bowel disease-associated neoplasms with microsatellite instability. Gastroenterology 129:74–85
34. Shibata D, Mori Y, Cai K, Zhang L, Yin J, Elahi A, Hamelin R, Wong YF, Lo WK, Chung TK, Sato F, Karpeh MS Jr, Meltzer SJ (2006) RAB32 hypermethylation and microsatellite instability in gastric and endometrial adenocarcinomas. Int J Cancer 119:801–806
35. Mori T, Fukuda Y, Kuroda H, Matsumura T, Ota S, Sugimoto T, Nakamura Y, Inazawa J (1999) Cloning and characterization of a novel Rab-family gene, Rab36, within the region at 22q11.2 that is homozygously deleted in malignant rhabdoid tumors. Biochem Biophys Res Commun 254:594–600
36. Sheach LA, Adeney EM, Kucukmetin A, Wilkinson SJ, Fisher AD, Elattar A, Robson CN, Edmondson RJ (2009) Androgen-related expression of G-proteins in ovarian cancer. Br J Cancer 101:498–503
37. Montalbano J, Jin W, Sheikh MS, Huang Y (2007) RBEL1 is a novel gene that encodes a nucleocytoplasmic Ras superfamily GTP-binding protein and is overexpressed in breast cancer. J Biol Chem 282:37640–37649

Virchows Arch (2012) 460:203–209
DOI 10.1007/s00428-011-1192-9

ORIGINAL ARTICLE

Angiomatoid change in polyps of the nasal and paranasal regions: an underrecognized and commonly misdiagnosed lesion—report of 45 cases

Ladislav Hadravsky · Alena Skalova · Denisa Kacerovska · Dmitry V. Kazakov · Zdenek Chudacek · Michal Michal

Received: 29 September 2011 / Revised: 12 December 2011 / Accepted: 27 December 2011 / Published online: 12 January 2012
© Springer-Verlag 2012

Abstract We present 45 patients with angiomatoid polyps of the nasal and paranasal regions (APNPRs), which are underrecognized lesions which may cause considerable diagnostic difficulties. There were 32 men and 13 women in our series. The average age at diagnosis was 49 years in men and 54.3 years in women. Locations were known in 41 cases and included the nasal septum (14), maxillary sinus (12), ethmoid sinuses (5), lateral wall of the nasal cavity (5), sphenoid sinus (1), and nasal cavity, not otherwise specified (4). X-ray or computed tomography was performed in 19 cases and revealed bone erosions/deviations in four cases. Initial misdiagnoses submitted by referring pathologists were reported in 20/32 of the consultation cases. Our study confirms that APNPRs are benign lesions which often recur and sometimes multiple recurrences are seen. APNPRs sometimes cause severe changes of the skeletal bones especially in recurrent lesions. Awareness of the above described features and familiarity with the clinical presentation of APNPRs is the best way to avoid a misdiagnosis.

L. Hadravsky · A. Skalova · D. Kacerovska · D. V. Kazakov · M. Michal
Department of Pathology, Medical Faculty,
Charles University in Prague,
Plzeň, Czech Republic

Z. Chudacek
Department of Radiology, Medical Faculty,
Charles University in Prague,
Plzeň, Czech Republic

M. Michal (✉)
Sikl's Department of Pathology, Medical Faculty Hospital,
Alej Svobody 80,
304 60, Plzeň, Czech Republic
e-mail: michal@medima.cz

Keywords Nose · Paranasal region · Inflammatory polyp · Choanal polyp · Angiomatoid nasal polyp · Nasopharyngeal angiofibroma · Angiosarcoma

Introduction

Angiomatoid polyps of the nasal and paranasal regions (APNPRs) are little known lesions among pathologists. As recently pointed out by Heffner [1], secondary changes resulting from infarction may impart unusual histopathological appearances causing considerable diagnostic difficulties, and these features have not been adequately described in the literature so far. Despite a handful of reports describing these secondary changes in the nasal and paranasal inflammatory polyps [2–5], no systematic study focusing on this phenomenon exists, as far as we are aware. The significance of these features lies in the fact that their misinterpretation as malignant may result in unnecessary aggressive treatment of the patients. This study was undertaken to better define this diagnostically important lesion.

Material and methods

All cases from the Pilsen Faculty Hospital routine files and the consultation files of two authors (MM and AS) stored under designations "angiomatoid nasal polyp", "vascular changes in nasal polyps", "angiosarcoma-like changes in nasal polyps", and "sarcomatoid changes in nasal polyps" were retrieved. Histological slides were reviewed and clinical information was obtained from the referring pathologists and patients' clinicians. For all 45 included cases, tissue samples were fixed in 4% formaldehyde and paraffin-embedded.

Sections (5 μm thick) were stained with routine methods. Of the 45 cases included, 13 cases were found in the routine files, whereas 9 and 23 cases were derived from the consultation files of two of the authors AS and MM, respectively.

Results

Clinical data

There were 32 men and 13 women. The detailed clinical information and follow-up was available in 27 cases. The average age at diagnosis was 49 years in men (range, 13–84 years) and 54.3 years in women (range, 18–83 years). The most commonly reported symptoms were recurrent epistaxis (21/27), nasal obstruction (16/27), mucus or pus discharge (5/27), and pain in the paranasal sinuses (3/27). The average size of APNPR was 25.7 mm (range, 5–80 mm). Locations were known in 41 cases and included the nasal septum (14), maxillary sinus (12), ethmoid sinuses (5), lateral wall of the nasal cavity (5), sphenoid sinus (1), and nasal cavity, not otherwise specified (4). X-ray or computed tomography was performed in 19 cases and revealed bone erosions/deviations in four cases. A history of allergy was obtained in 44% (11/25) of patients and was mostly related to dust, mites, pollen, hey, honey, antibiotics, nuts, chlorine, and cold. Six patients had a history of a malignant neoplasm elsewhere (endometrial adenocarcinoma, rectal carcinoma, colonic carcinoma, renal carcinoma, lymphoma, plasmacytoma and cutaneous basal cell carcinoma). Initial misdiagnoses submitted by referring pathologists were reported in 20/32 of the consultation cases, and in 3/20 cases, more than one diagnosis was suggested (angiofibroma 8/20, hemangioma 6/20, hemangiopericytoma 4/20, angiosarcoma 3/20, pyogenic granuloma and hemangioendothelioma, each 2/20). For the rest of the 12 cases of the consultations, either no diagnosis or a descriptive diagnosis pointing to a necrosis in a polyp was given by the referring pathologists.

Of the 27 patients with available follow-up, no case showed metastasis or an infiltrative behavior and none of the patients died of the disease. However, a local recurrence was recorded in nine of the patients (30%). The recurrence was histologically confirmed in these patients.

Histopathological features

Histologically, APNPRs were formed by a conspicuous proliferation of small vessels, mostly capillaries within a myxoid background (Fig. 1). In nearly half of the cases, a vessel thrombosis (Fig. 2) or vessels with histological signs of an organizing thrombus or postthrombotic vessel changes were noted. Various heavy deposition of fibrin in the organizing thrombi and in their vicinity was a rule. At least a small focus of tissue necrosis was found in all cases, and often, vascular proliferation, stromal atypia in fibroblastic cells, endothelial cells, or myoid cells forming the vessel wall were present in the proximity of the necrotic areas. In six cases, the stromal atypia was conspicuous to resemble a sarcoma (Fig. 3). Cellular foci of a capillary proliferation with various degrees of atypia simulating angiosarcoma were also frequently found (Fig. 4). In many cases, there were areas with capillary proliferation arranged in a lobular fashion indistinguishable from pyogenic granuloma [6]. In most cases, the superficial epithelium adjacent to necrotic areas underwent various degrees of pseudoepitheliomatous hyperplasia (Fig. 5). In five cases, metaplastic and reactive changes on the scull bones were found (Fig. 6a, b), and these corresponded to marked skeletal bone changes observed on radiological investigations (Fig. 7a–d). Variously expressed mucinous stromal leakage, due to obstruction of the small salivary glands, was observed in 12 cases (Fig. 8a, b). Focally, areas of keloid scarring tissue representing probably a reparative process were found (Fig. 9a, b). In no case did we find a necrotizing sialometaplasia in the glandular epithelium [7]. Mitoses were rare to absent and atypical mitoses were not present.

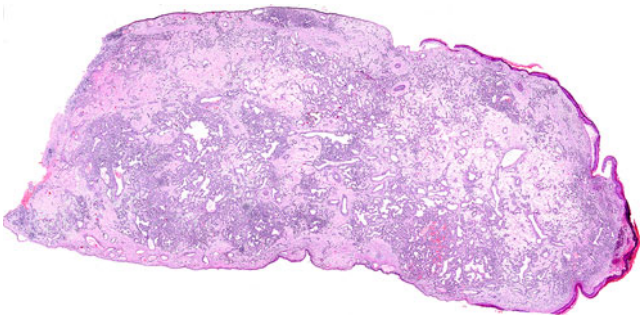

Fig. 1 Scanning magnification of polyp with angiomatoid change

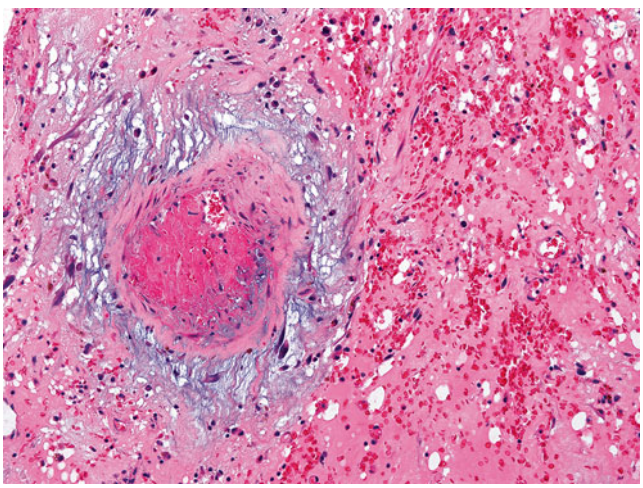

Fig. 2 Vessel thrombosis

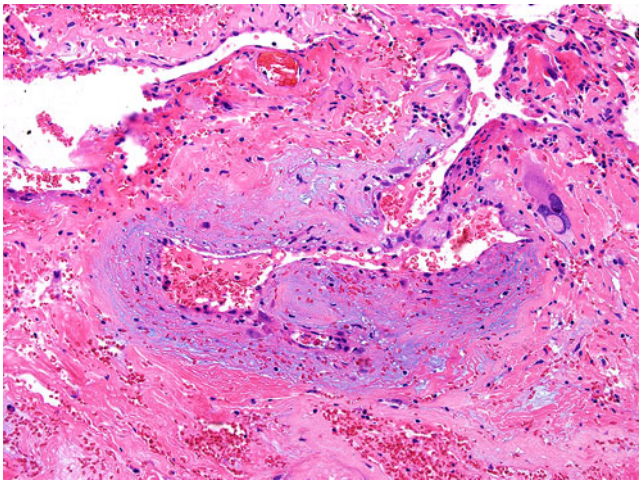

Fig. 3 Postthrombotic changes with stromal atypias

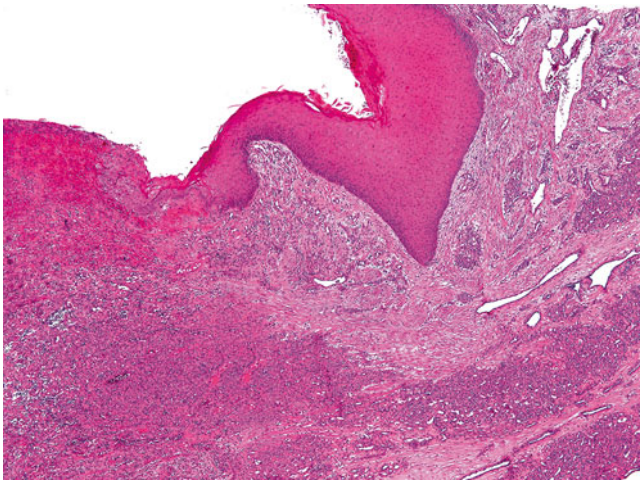

Fig. 5 Pseudoepitheliomatous hyperplasia adjacent to necrosis

Discussion

Nasal and paranasal inflammatory polyps can undergo secondary changes, which may be a source of diagnostic difficulties. In spite of the fact that these lesions are not extremely rare [1] and, in our view, all pathologists practicing head and neck pathology must have encountered them in their routine work, we are not aware of any major clinicopathologic study fully describing them. The best known pseudomalignant feature appears to be atypical pseudosarcomatous changes involving stromal cells imparting sarcomatous appearance described by various groups of authors [5, 8–14]. Nasal and paranasal inflammatory polyps with secondary vascular changes may account for further difficulties in the interpretation of these lesions. There are several isolated case reports documenting these vascular changes, but very diverse and unrelated names were given by the authors while describing this phenomenon, including "maxillary sinus hematoma" [4], "organized hematoma of the maxillary sinus" [2], "hemorrhagic pseudotumor of the maxillary sinus" [3], "infarcted angiomatous polyps" [15], and "angiectatic nasal polyp" [5],

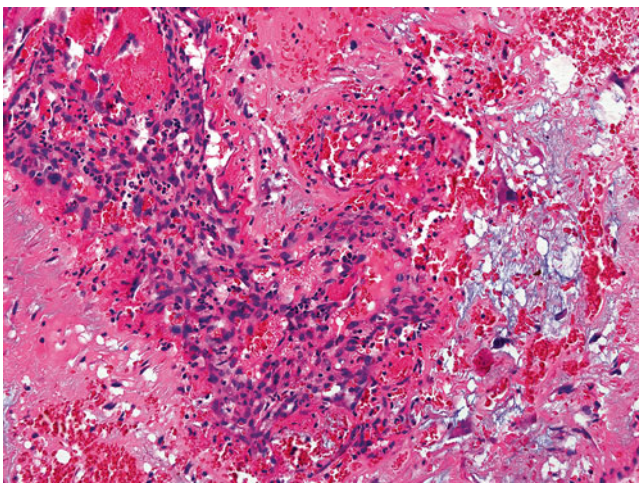

Fig. 4 Proliferation of capillaries with atypias simulating angiosarcoma and mucous spillage into the stroma

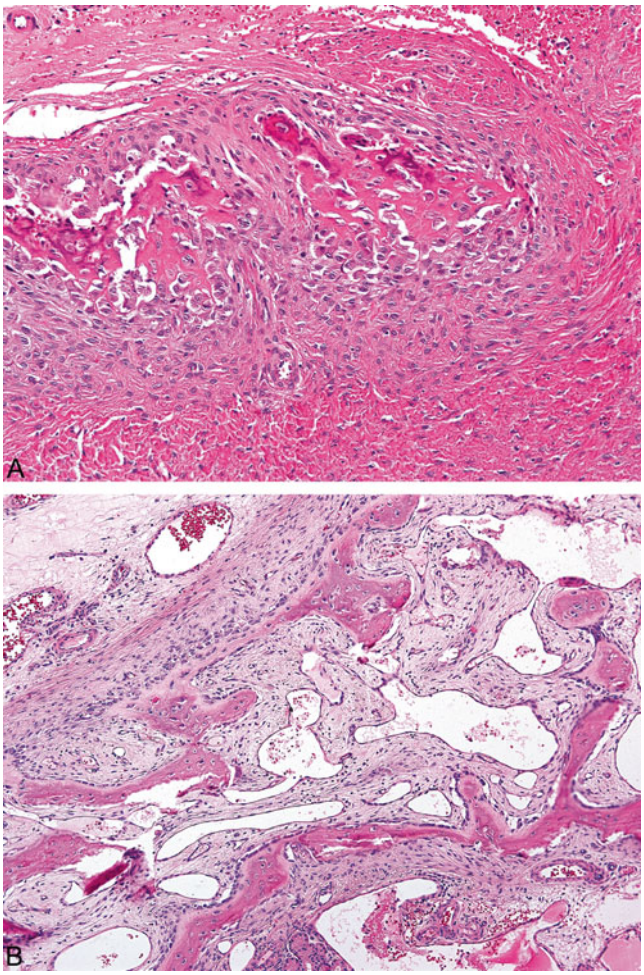

Fig. 6 **a**, **b** Reactive changes of skeletal bone. **b** Lesion in a patient with recurrent polyp. The skeletal changes in this patient might be a consequence of a previous process

Fig. 7 **a** Case no. 6: non-enhanced CT of the paranasal sinuses—right maxillary sinus and nasal cavity entirely filled with a solid mass. The medial wall of the right maxillary sinus destroyed in its dorsal half. **b** Case no. 7: non-enhanced CT of the paranasal sinuses—a solid mass in the frontal part of the left nasal cavity. The nasal septum is severely deviated to the left. **c** Case no. 18: non-enhanced CT of the paranasal sinuses—right maxillary sinus and nasal cavity entirely filled with a solid mass. The medial wall of the right maxillary sinus destroyed in its dorsal half. Severe mass effect with deviation of the nasal septum to the left. **d** Case no. 43: non-enhanced CT of the paranasal sinuses—a solid mass filling the right nasal cavity. Focal defects in the bone lamina of the nasal septum and the medial wall of the right maxillary sinus

reflecting the great diagnostic confusion caused by these polyps.

The most likely explanation of vascular changes in the paranasal inflammatory polyps can be inferred from the anatomical position of the majority of these polyps. They originate mostly in the maxillary sinus. Antrochoanal polyps are polyps that arise in the maxillary sinus and extend into the middle meatus projecting posteriorly through the ipsilateral choana. Those polyps that arise in the maxillary sinus and extend into the middle meatus projecting anteriorly are known as antronasal polyps. Less frequently, the origin of sinonasal polyps is in the sphenoid and ethmoid sinuses. They pass through the sinus ostia via a small stalk into the nasal cavity, so that the main bulk of the lesion occurs usually in the nasal cavity [16]. The growth rate may be prominent, and the polyps sometimes extend as far as into the nasopharynx or even oropharynx. Because the polyps may form a large mass with a small stalk and because the stalk extends through a relatively small channel causing a compression and stasis of the feeder vessel, these polyps are particularly subject to secondary changes resulting from chronic or subacute vascular compromise. Rarely, even strangulation with necrosis resulting in "autopolypectomy" has been reported [17–19].

Because a minority of APNPRs occurring in the nasal septum and lateral walls of the nasal cavity manifest angiomatoid changes identical to those seen in lesions involving the maxillary sinus and ethmoid and sphenoid sinuses, it is apparent that necrosis may be induced by other means than the strangulation of the stalks of antrochoanal polyps. The most possible explanation appears to be the local pressure caused by the bulky size of the nasal polyp which often entirely obtrudes the whole nasal cavity.

The histology of the secondary changes may range from a simple increase in stromal fibrosis to more striking alterations resulting from hemorrhagic infarction, including vascular proliferations simulating angiosarcoma. Reparative changes, especially those occurring in patients with recurrent disease, may result in a large keloid scar, a lesion potentially confused with desmoid fibromatosis [20] (Fig. 9a, b).

The above mechanisms and the extension of the polyp through the paranasal sinus ostium in the lateral nasal cavity wall partly explain bone erosions [1]. Because in our series we have found bone reactive changes in the vicinity of the necrotic polyp masses, it can be suggested that the bone necrosis and subsequent reparative skeletal bone process are related to the necrosis of the polyps. In some patients, this bone loss may be impressive. Several cases in our series

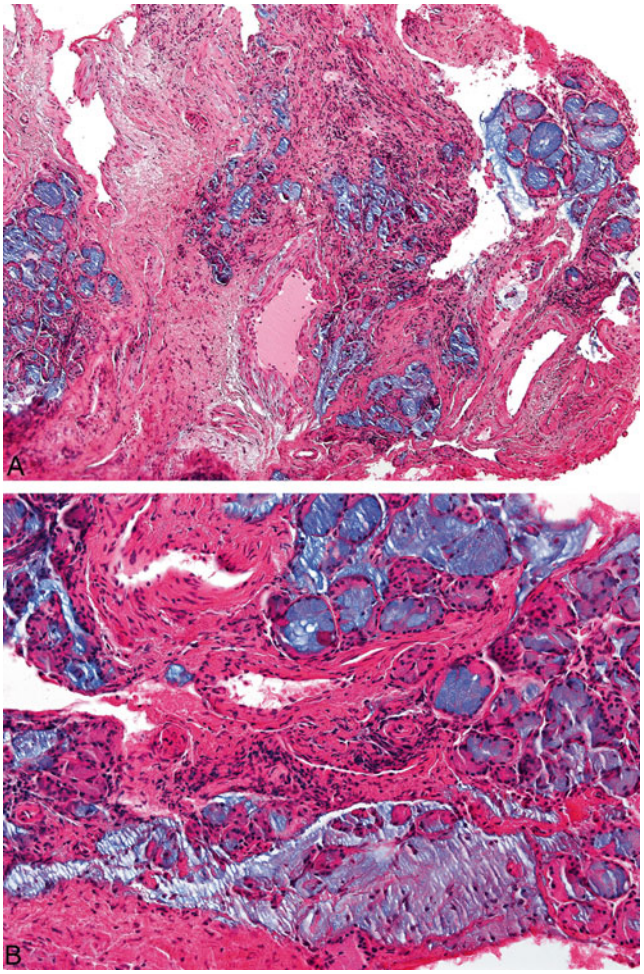

Fig. 8 **a**, **b** Mucinous spillage into the stroma

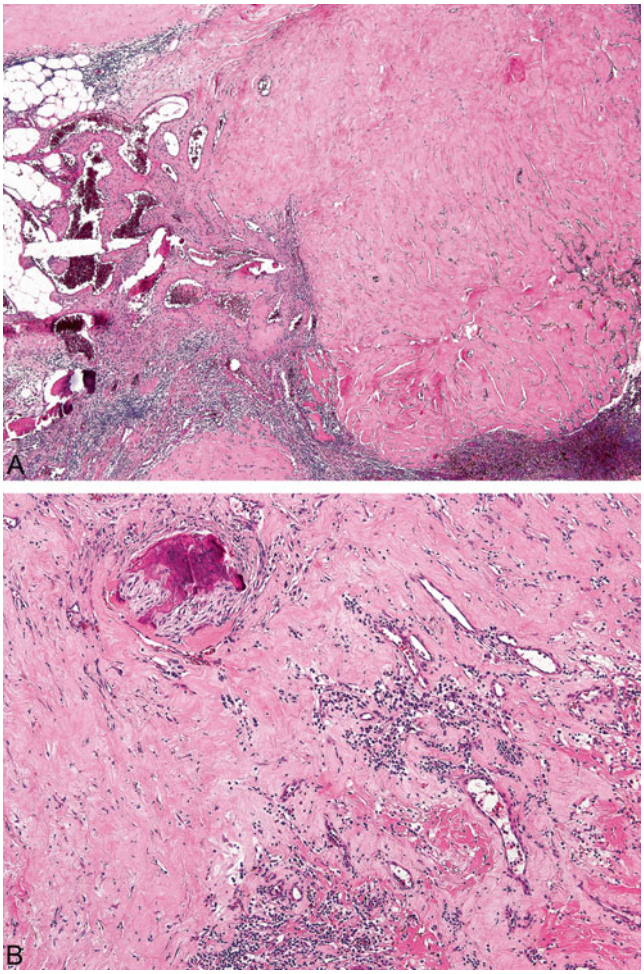

Fig. 9 **a**, **b** Keloid scarring

revealed variously severe deviations of the nasal septum (Fig. 7a–d). The bone loss is usually located in the region of the lateral nasal cavity–medial maxillary sinus wall, but sometimes it can be more lateral and includes the ethmo-orbital lamina papyracea [1]. There are on record cases of nasal polyps with severe destruction of the skull bones [21, 22], and in one case, it caused even blindness of the patient [23]. This skeletal bone defect may further contribute to the clinical–radiologic impression of an infiltrative growth and possible malignancy.

Another interesting histological feature observed in 12 cases was the spillage of mucus into the stroma caused by the obstruction of mucous secreting glands within the sinuses (Fig. 8a, b). In several cases, this feature was so prominent that it simulates a primary mucinous neoplasm originating from minor salivary glands.

The above described secondary changes in the nasal and paranasal inflammatory polyps were encountered over a wide age range, including children, and there was a considerable (32:13) male predominance in our series. Many types of allergies due to penicillin, tetracycline, deoxymykoin, ampicillin, hey, honey, dust, pollen, mites, cold, and chlorine in nearly half of the patients in whom the history of the disease was available were recorded. It therefore appears that the angiomatous changes may occur in polyps of various etiologies.

APNPRs are benign lesions, but they can present with pseudomalignant clinical and morphological features, and as reflected by the diagnoses rendered by the referring pathologists, they are often misinterpreted as more aggressive or even malignant lesions [1]. Reactive changes in APNPRs may impart a histological resemblance to various benign and malignant tumors of the nasal and paranasal regions, the most important of which are nasopharyngeal angiofibroma, sinonasal hemangiopericytoma (glomangiopericytoma), or angiosarcoma. Although various degrees of stromal atypia were a rather common finding, in six cases, the atypia amounted to such a degree when a sarcoma was considered as a diagnosis. The most severe atypias were usually seen around the thrombotic vessels often accompanied by foci of necrosis, so that the sarcoma type in differential diagnosis was practically always angiosarcoma. These misdiagnoses may lead to unnecessary aggressive treatment. A

diagnostically misinterpreted case appeared in court as a malpractice claim [1].

An important lesion to differentiate from APNPR is nasopharyngeal angiofibroma. Nasopharyngeal angiofibroma is a lesion with aggressive growth, which in large tumors may even have intracranial extension and which often requires extensive surgical approach [24]. It occurs nearly exclusively in young boys. These clinical features (age and gender) can help in differentiating between nasopharyngeal angiofibroma and APNPRs in most cases, because only a minority of APNPRs occurs in this age/gender group. In our consultations, some referring pathologists have encountered several recurrences of APNPRs which lead them to suggest a diagnosis of nasopharyngeal angiofibroma. Besides these two cases, a diagnosis of nasopharyngeal angiofibroma was suggested in nearly one third of the referral cases in our series. Clinically, APNPR can also be differentiated from nasopharyngeal angiofibroma by the location of the lesion. Appearance of an expansile nasal tumor without a nasopharyngeal mass excludes the diagnosis of nasopharyngeal angiofibroma. In addition, anterior and posterior ethmoidal arteries are not often involved as the main feeding vessels, and if they are found, the possibility of a primary nasal mass should be considered instead of a nasopharyngeal mass [25]. Furthermore, nasopharyngeal angiofibromas are broad-based lesions that are difficult to be surgically removed. If a lesion is easily extirpated as is the case with most APNPRs, the diagnosis of angiofibroma should be questioned. Histologically, nasopharyngeal angiofibroma differs from APNPR by its long and very thin slit-like vascular channels, which are relatively uniformly distributed in a given area of the tumor. These vascular structures typically have very thin walls with irregularly thickened muscular layer [26]. Sometimes, the vessels in nasopharyngeal angiofibroma look like having a deficiently and irregularly formed muscular vessel wall. The stromal collagen has a wavy pattern resembling a fascia and the stromal cells have a stellate shape.

Mills et al. described an entity of "lobular capillary hemangioma" of the nasal cavity [6]. These lesions may primarily arise in the mucosa of the nasal cavity without antecedent polyps, and as such, they should be differentiated from secondary vascular changes in inflammatory nasal polyps. In some cases, there might be, however, an overlap between these two entities or when primary lobular capillary hemangioma has a polypoid configuration, and these two entities might be, especially in partial excision, indistinguishable.

Sinonasal hemangiopericytoma (glomangiopericytoma) presents usually as a solid proliferation of cells which often manifest as a myoid differentiation and lack vascular thrombotic changes and necroses, and the latter features invariably present in APNPR [27, 28]. The most helpful feature in the diagnosis of APNPR is the finding of the rest of the well-preserved inflammatory polyps devoid of necrosis and secondary changes, which in our experience, may be found in most cases. Even in cases showing no recognizable residua of an inflammatory polyp, there may be large areas of hypocellular fibrinoid tissue that is not very vascular. These features characteristic of inflammatory polyps can be helpful in avoiding misdiagnosis [1].

The last and most important differential diagnostic consideration is angiosarcoma. It should be kept in mind that angiosarcomas in this anatomic area are vanishingly rare and most pathologists will probably never encounter one in the paranasal region in their whole professional life. It is likely that most of the few reports of sinonasal angiosarcomas in fact are mistaken diagnoses [1]. While we have found in our consultation and routine files 45 cases of APNPRs, we have encountered only a single case of paranasal angiosarcoma among nearly 100,000 consultation cases and more than 2,000,000 routine cases.

In summary, this study confirms that angiomatoid APNPRs are benign lesions which often recur and sometimes multiple recurrences are seen. It is important to note that all the above described histological reactive pseudomalignant changes are much more common in APNPRs than it is apparent from tissue material in our series because, especially in the referral cases, the material submitted for consultation was quite limited, and in these cases, usually a single block was available for the study. APNPRs sometimes cause severe changes of the skeletal bones especially in recurrent lesions. The authors do not consider APNPRs to represent a new entity, but a change that may simulate various entities in the nasal and paranasal regions.

Conflicts of interest We declare that we have no conflict of interest.

References

1. Heffner DK (2010) Sinonasal angiosarcoma? Not likely (a brief description of infarcted nasal polyps). Ann Diagn Pathol 14:233–234
2. Lee B-J, Heo S-C (2003) Organized hematoma of the maxillary sinus. Acta Otolaryngol 123:869–872
3. Lee PK, Wu JK, Ludemann JP (2004) Hemorrhagic pseudotumor of the maxillary sinus. J Otolaryngol 3:206–208
4. Lim M, Lew-Gor S, Ramsay A (2008) Maxillary sinus hematoma. J Laryngol Otol 122:210–212
5. Yfantis HG, Drachenberg CB, Gray W, Papadimitriou JC (2000) Angiectatic nasal polyps that clinically simulate a malignant process. Report of 2 cases and a review of the literature. Arch Pathol Lab Med 124:406–410
6. Mills SE, Cooper PH, Fechner RE (1980) Lobular capillary hemangioma: the underlying lesion of pyogenic granuloma. A study of 73 cases from the oral and nasal mucous membranes. Am J Surg Pathol 4:471–479
7. Bell GW, Loukota RA (1996) Necrotizing sialometaplasia coincident with ipsilateral infarcted antral polyps. Br J Oral Maxillofac Surg 34:129–131

8. Batsakis JG, Sneige N (1992) Choanal and angiomatous polyps of the sinonasal tract. Ann Otol Rhinol Laryngol 101:623–625
9. Compagno J, Hyams VJ, Lepore ML (1976) Nasal polyposis with stromal atypia. Review of follow-up study of 14 cases. Arch Pathol Lab Med 100:224–226
10. Kindbloom LG, Angerval L (1984) Nasal polyps with atypical stromal cells: a pseudosarcomatous lesion: a light and electron-microscopic and immunohistochemical investigation with implications on the type and nature of the mesenchymal cells. Acta Pathol Microbiol Immunol Scand 92:65–72
11. Lewis JS (2008) Spindle cell lesions—neoplastic or non-neoplastic? Spindle cell carcinoma and other spindle cell lesions of the head and neck. Head and Neck Pathol 2:103–108
12. Mills SE, Gaffey MJ, Frierson HF (2000) Antrochoanal polyps. In: Atlas of tumor pathology. Tumors of the upper aerodigestive tract and ear. NCBI, Bethesda
13. Nakayama M, Wenig BM, Heffner DK (1995) Atypical stromal cells in inflammatory nasal polyps: immunohistochemical and ultrastructural analysis in defining histogenesis. Laryngoscope 105:127–134
14. Tuziak T, Kran A, Woyke S (1995) Edematous nasal polyp with atypical stromal cells misdiagnosed cytologically as rhabdomyosarcoma. Acta Cytol 39:521–524
15. Sheahan P, Crotty PL, Hamilton S, Colreavy M, McShane D (2004) Infarcted angiomatous polyps. Rhinology 262:225–230
16. De Vuysere S, Hermans R, Marchal G (2001) Sinochoanal polyp and its variant, the angiomatous polyp. Head Neck Radiol 11:55–58
17. Ole-Lengine L, Manni JJ (1993) A strangulated antrochoanal polyp. J Laryngol Otol 107:342–343
18. Pruna X, Ibanez JM, Santamaria G, Serres X, Inaraja L, Vilar F (1997) Antrochoanal autopolypectomy: CT findings. Eur Radiol 7:571–572
19. Rashid A-MH, Soosay G, Morgan D (1994) Unusual presentation of a nasal (antrochoanal) polyp. Br J Clin Pract 48:108–109
20. Gnepp DR, Henley J, Weiss S, Heffner D (1996) Desmoid fibromatosis of the sinonasal tract and nasopharynx. A clinicopathologic study of 25 cases. Cancer 78:2572–2579
21. Sheanan P, Crotty PL, Hamilton S, Colreavy M, McShane D (2005) Infarcted angiomatous nasal polyps. Eur Arch Otorhinolaryngol 262:225–230
22. Winestock DP, Bartlett PC, Sondheimer FK (1978) Benign nasal polyps causing bone destruction in the nasal cavity and paranasal sinuses. Laryngoscope 88:675–679
23. Rejowski JE, Caldarelli DD, Campanella RS, Penn RD (1982) Nasal polyps causing bone destruction and blindness. Otolaryngol Head neck Surg 90:505–506
24. Radkovski D, McGill T, Healy GB, Ohlms L, Jones DT (1997) Angiofibroma. Changes in staging and treatment. Arch Ololaryngol Head Neck Surg 123:115–116
25. Som PM, Cohen A, Sacher M, Coi I-S, Bryan NR (1982) The angiomatous polyp and the angiofibroma: two different lesions. Radiology 144:329–334
26. Heffner DK (1983) Problems in pediatric otorhinolaryngic pathology. II. Vascular tumors and lesions of the sinonasal tract and nasopharynx. Int J Pediatr Otolaryngol 5:125–138
27. Eichhorn JH, Dickersin GR, Bhan AK, Goodman ML (1990) Sinonasal hemangiopericytoma. A reassessment with electron microscopy, immunohistochemistry, and long-term follow-up. Am J Surg Pathol 14:856–866
28. Thompson LD, Miettinen M, Wenig BM (2003) Sinonasal type hemangiopericytoma: a clinicopathologic and immunephenotypic analysis of 104 cases showing perivascular myoid differentiation. Am J Surg Pathol 27:737–749

Virchows Arch (2012) 460:211–221
DOI 10.1007/s00428-011-1182-y

ORIGINAL ARTICLE

Immunohistochemical diagnosis of Fabry nephropathy and localisation of globotriaosylceramide deposits in paraffin-embedded kidney tissue sections

Carmen Valbuena · Dina Leitão · Fátima Carneiro · João Paulo Oliveira

Received: 22 July 2011 / Revised: 22 November 2011 / Accepted: 24 November 2011 / Published online: 29 December 2011
© Springer-Verlag 2011

Abstract Fabry disease (FD) is a rare X-linked lysosomal storage disorder of glycosphingolipids, mostly globotriaosylceramide (Gb3). Proteinuric chronic kidney disease develops frequently, and recognition of Fabry nephropathy on a kidney biopsy may be the first clue to the underlying diagnosis. Since the accumulated glycosphingolipids are largely extracted by the paraffin-embedding procedure, the most characteristic feature of Fabry nephropathy on routine light microscopy (LM) is nonspecific cell vacuolization. To test whether residual Gb3 in kidney tissue might be exploited for the specific diagnosis of Fabry nephropathy, paraffin-embedded kidney biopsies of nine FD patients (one boy, four men, four women) and of a female carrier of a mild genetic mutation, with no evidence of Fabry nephropathy, were immunostained with an anti-Gb3 antibody. The adult biopsies were additionally co-stained with a lysosomal marker (anti-lysosomal-associated membrane protein 2 (anti-LAMP2) antibody). The distribution of Gb3 deposits was scored per cell type and compared to the histological scorings of glycosphingolipid inclusions on semi-thin sections. FD patients had residual Gb3 in all types of glomerular, tubular, interstitial and vascular kidney cells. The highest expression of LAMP2 was seen in tubular cells, but there were no meaningful associations between LAMP2 expression and prevalence of Gb3 deposits on different kidney cell types. The histological scorings of glycosphingolipid inclusions were relatively higher than the corresponding immunohistochemical scorings of Gb3 deposits. In the mildly affected female, Gb3 expression was limited to tubular cells, a pattern similar to controls. Gb3 immunostaining allows the specific diagnosis of Fabry nephropathy even in kidney biopsies routinely processed for LM.

Keywords Fabry disease · Kidney biopsy · Immunohistochemistry · Globotriaosylceramide (Gb3) · Lysosomal-associated membrane protein 2 (LAMP2)

C. Valbuena (✉) · F. Carneiro
Department of Pathology,
Hospital São João,
Alameda Prof. Hernâni Monteiro,
4200-319 Porto, Portugal
e-mail: valbuena@med.up.pt

C. Valbuena · F. Carneiro · J. P. Oliveira
Faculty of Medicine,
University of Porto (FMUP),
Porto, Portugal

D. Leitão · F. Carneiro
Department of Pathology,
Institute of Molecular Pathology
and Immunology of the University of Porto (IPATIMUP),
Porto, Portugal

C. Valbuena · J. P. Oliveira
Department of Nephrology and Unit of Research & Development
in Nephrology (FCT-725),
Hospital São João,
Porto, Portugal

J. P. Oliveira
Department of Human Genetics, Faculty of Medicine,
University of Porto,
Porto, Portugal

Introduction

Fabry disease (FD) is an X-linked storage disorder of neutral glycosphingolipids (GSL) caused by deficient activity of the lysosomal enzyme α-galactosidase [1, 2]. The pathogenic basis of FD is continuous accumulation of, in particular, globotriaosylceramide (Gb3), but the mechanisms underlying tissue injury and disease progression are still incompletely

understood. Chronic kidney disease (CKD), cardiomyopathy and stroke are major causes of morbidity and early mortality in affected adults [1, 2]. Although the phenotypic expression in females is often less severe and more variable, up to two thirds of the heterozygotes ultimately become symptomatic and have major organ involvement [2, 3]. The diagnosis is often missed or delayed, particularly if early-onset neuropathic and/or cutaneous manifestations, or a positive family history, are lacking [2].

Identification of GSL deposits in affected organs by light microscopy (LM) [4] or electron microscopy (EM) [5, 6] has been regarded as an ancillary diagnostic method of FD, particularly useful in patients with renal involvement [6]. However, as GSL are almost entirely extracted by non-polar solvents (e.g., ethanol, xylene) used in the standard paraffin-embedding procedure [7], cellular vacuolization remains as the most distinctive LM feature of FD. Vacuolization of kidney cells is also a non-specific feature of several other disorders affecting the kidneys (Table 1), some of them more prevalent than FD [8–10]. Staining of formalin-fixed paraffin-embedded (FFPE) LM specimens with lipid-soluble dyes or periodic acid-Schiff (PAS) is also negative [6, 7]. Frozen sections allow the widest range of histochemical methods available for GSL identification to be carried out [7] but freezing leads to loss of fine cellular details and staining reactions are not specific for Gb3. Thus, even though the lamellate, myelin-like ultrastructure of Gb3 inclusions is not pathognomonic, EM is the most reliable approach to identify GSL deposits in Fabry patients' tissues including the kidneys [1, 11]. On semi-thin (ST) toluidine blue- or methylene blue-stained EM scout sections evaluated by LM, GSL deposits are easily identified as dark blue inclusions [12]. However, freezing of tissue samples and/or processing for EM are often not routinely performed, and the diagnosis of FD can easily be missed on standard LM assessment of kidney biopsies.

Highly specific anti-Gb3 monoclonal antibodies [13] have been employed to confirm Gb3 accumulation in the kidney biopsy of a female with FD, using an indirect immunofluorescence technique in frozen sections [14], and to detect Gb3 in FFPE sections of the kidney and other organ samples collected at autopsy of a classically affected Fabry male [15]. The latter study provided robust evidence that a

Table 1 Medical diseases affecting the kidney parenchyma, with histological vacuolization of cells [8–10]

Disease	Podocytes	Mesangial cells	Glomerular capillary endothelium	Proximal tubular cells	Distal tubular cells	Interstitial cells	Vascular smooth muscle cells	Vascular endothelium
Aspartylglycosaminuria	±							
Fabry disease	±	±	±		±	±	±	±
Fucosidosis	±							
Gaucher disease						±		
Glycogen storage disease type I				±	±			
GM1 gangliosidosis	±	±						
Hurler's disease	±			±				
I-cell disease	±			±				
LCAT deficiency		±	±			±	±	±
Lipoprotein glomerulopathy						±		
Mannosidosis	±							
Metachromatic leukodystrophy				±	±			
Nephrosialidosis	±			±	±	±		±
Neuronal ceroid lipofuscinosis	±		±	±	±			
Niemann–Pick disease	±		±	±	±	±		
Sandhoff disease	±			±				
Type III hyperlipoproteinemia		±						
Alport disease						±		
Nephrotic range proteinuria	±					±		
Minimal change disease				±	±	±		

GM1 monosialotetrahexosylganglioside, *LCAT* lecithin/cholesterol acyltransferase, + vacuolization present

significant amount of Gb3, or parts thereof containing the antigen specificity recognized by the monoclonal antibodies, remained within cells even after standard tissue processing for LM.

We aimed to assess whether these monoclonal antibodies could be effectively used for the immunohistochemical identification of Gb3 in archive FFPE kidney biopsies of Fabry patients, as a routine diagnostic tool for Fabry nephropathy. Further goals were to estimate the relative abundance of lysosomes in different kidney cell types of adult Fabry patients, using an anti-lysosomal-associated membrane protein 2 (anti-LAMP2) antibody as lysosomal marker and to analyse whether Gb3 deposits always colocalised with LAMP2.

Subjects, materials and methods

The protocol of this study was approved by the institutional Health Ethics Board.

Patients and biopsies

All kidney biopsies of patients diagnosed with FD processed at the Pathology Department of a large university hospital between January 1, 1977 and December 31, 2007 were identified using a computerised database search. Cases for whom paraffin blocks were still available in archive were selected for this study. The original haematoxylin–eosin stained microscope slides, EM photomicrographs and ST (1 μm) scout sections were reviewed by the same pathologist (CV) highly experienced in the kidney pathology of FD.

Relevant clinical details and laboratory data were retrieved from the patient's hospital records. In all cases, the diagnosis of FD had been established by the demonstration of deficient leukocyte or plasma α-galactosidase activity and/or identification of a mutation of the α-galactosidase gene (*GLA*).

Immunohistochemical protocols

Double immunohistochemical staining was performed on 10% buffered FFPE 2-μm-thick sections, newly prepared from the archive paraffin blocks. An endomyocardial biopsy from an affected male with cardiac involvement was used as positive control. Kidney tissue samples of two adult males without evidence of kidney disease were used as tissue negative controls. Negative control sections were additionally prepared by replacing the primary antibodies in the immunohistochemical protocol with normal rabbit immunoglobulin (negative control rabbit immunoglobulin fraction, 20 mg/ml; Dako, Denmark). All immunohistochemical procedures were carried out at room temperature. Commercial reagents and reaction kits were used according to the manufacturer's instructions.

The microscope slides were initially deparaffinized in xylene, rehydrated through an ethanol gradient and washed for 20 min in phosphate-buffered saline (PBS). Endogenous peroxidase activity was quenched by 3% hydrogen peroxide in methanol for 30 min. Inhibition of tissue non-specific epitopes was achieved by incubating the slides for 5 min with a blocking solution (UltraVision Block; Lab Vision Corp., Fremont, CA, USA).

Double immunohistochemical detection of Gb3 and LAMP2 in kidney biopsies of adults

The murine anti-Gb3 primary antibody (anti-Gb3(CD77), IgG, 1 mg/ml, clone BGR23; Seikagaku, Tokyo, Japan) was diluted to 1:100 with an antibody diluent (Lab Vision Antibody Diluent; Lab Vision Corp.), applied to the slides and let to incubate overnight in a humidity control chamber. Detection of bound primary antibody was achieved with a commercial kit (UltraVision Detection System Anti-Polyvalent, Alk-Phos/Fast Red; Lab Vision Corp.). In short, the slides were washed three times for 5 min in PBS, incubated with the biotinylated goat anti-polyvalent secondary antibody for 15 min and rinsed twice for 5 min in PBS. The streptavidin–alkaline phosphatase complex was then applied and incubated for 15 min. After rinsing twice for 5 min in PBS, the slides were incubated for 90 min with the chromogen/substrate solution (Fast Red/Naphthol Phosphate Substrate).

LAMP2 immunoreactivity was identified with a commercial kit (DAB + Chromogen//REAL™ EnVision™ Detection System, Peroxidase/DAB+, Rabbit/Mouse; Dako). The slides were initially washed in PBS for 10 min and then let to incubate for 120 min with a mouse monoclonal anti-LAMP2 antibody (Anti-LAMP2(H4B4), IgG, 200 μg/ml; Santa Cruz Biotechnology, Santa Cruz, CA, USA), diluted to 1:100 with an antibody diluent (Lab Vision Antibody Diluent). Following 30 min incubation with the detection reagent (REAL™ EnVision™/HRP, Rabbit/Mouse; Dako), the slides were washed in PBS for 10 min and incubated for 1.5 min with a diaminobenzidine chromogen (REAL™ DAB + Chromogen; Dako) in a buffered hydrogen peroxide solution (REAL™ Substrate Buffer; Dako). After fast washing in distilled water and PBS, the slides were lightly counterstained with Mayer's haematoxylin and mounted with 10% buffered glycerine in PBS. Gb3 immunoreactivity was identified by a bright red precipitate, and LAMP2 immunoreactivity was identified by a crisp brown precipitate.

Immunohistochemical detection of Gb3 in the kidney biopsy of a child

Immunohistochemical detection of Gb3 was also performed in the kidney biopsy of a young boy but using a higher dilution

Table 2 Demographic, clinical and laboratory data of patients with Fabry disease at the time of kidney biopsy

Case ID	Gender	Age	*GLA* mutation	αGal(L)	CKD stage	uProt	Biopsy indication
H07-13445	M	7	p.C94S	0.54	1	–	Baseline assessment pre-ERT
H04-4366	M	19	c.305_749[2]dupEx2_Ex4	0.07	1	+++	Proteinuria
H05-9169	M	20	c.305_749[2]dupEx2_Ex4	0.59	1	+++	Baseline assessment pre-ERT
H05-6791	M	21	p.239ΔI	0.38	1	+	Baseline assessment pre-ERT
H05-7176	M	40	p.153ΔD	0.25	2	+++	Baseline assessment pre-ERT
H99-4183	F	32	p.R220X	20	3	++++	Proteinuria (nephrotic)
H05-9180	F	42	c.305_749[2]dupEx2_Ex4	18	1	+	Baseline assessment
H03-3708	F	45	p.R220X	18	2	++	Baseline assessment pre-ERT
H05-6994	F	50	p.239ΔI	20	2	+	Baseline assessment pre-ERT
H05-9092[a]	F	29	p.R118C[a]	44	1	+++	Proteinuria

Age in full years.

M male, *F* female, *GLA* α-galactosidase gene, α *Gal (L)*α-galactosidase residual activity in leukocytes (Normal laboratory range 36-80 nMol/h/mg), *CKD* chronic kidney disease (Stages according to estimated glomerular filtration rate (eGFR), based on serum creatinine levels, race, gender and age: "1" = eGFR ≥ 90 ml/min/1.73 m^2 , "2"=eGFR 89–60 ml/min/1.73 m^2 and "3"=eGFR 59–30 ml/min/1.73 m^2), *uProt* proteinuria (Highest level recorded before the kidney biopsy, expressed in milligrams per day: "–" <150 mg/day, "+" 150–300 mg/day, "++" 300–1,000 mg/day, "+++" 1,000–3,500 mg/day, "++++" >3,500 mg/day), *ERT* enzyme replacement therapy

[a] Urine Gb3 levels were found to be consistently within the normal range in this female; hemizygous males for the *GLA* p.R118C mutation excrete normal levels of lysoGb3 in the urine

of the primary antibody (1:300) and the DAB + Chromogen// REAL™ EnVision™ Detection System, Peroxidase/DAB+, Rabbit/Mouse commercial kit to detect bound antibody. After washing three times for 2 min in PBS, the slides were incubated with the primary antibody overnight, in a humidity control chamber. Following washing three times for 5 min in PBS, the slides were incubated with the Dako REAL™ EnVision™/HRP, Rabbit/Mouse detection reagent for 30 min and then washed again twice in PBS for 5 min. Finally, the slides were incubated with the buffered hydrogen peroxide diaminobenzidine chromogen solution for 5 min (REAL™ DAB + Chromogen/REAL™ Substrate Buffer). After washing 10 min in PBS, the slides were counterstained with Mayer's haematoxylin and then mounted with a permanent mounting medium (SUB-XTM Mounting Medium; Surgipath Europe, Peterborough, UK). Gb3 immunoreactivity was identified by a crisp brown precipitate.

Gb3 and LAMP2 immunostaining assessment

The quality of the double immunostaining technique was first checked on the positive and the negative controls. Gb3 immunoreactivity was semi-quantitatively graded according to the tertiles of the proportion of cells of each type that showed positive reactions. LAMP2 immunoreactivity was semi-quantitatively graded according to the relative average intensity staining of each cell type.

Toluidine blue- or methylene blue-stained, plastic-embedded EM scout sections were used to semi-quantify the GSL inclusions in the different kidney cell types, as published elsewhere [16]. The semi-quantification of GSL inclusions in the EM scout sections was correlated to the Gb3 immunostaining data.

Statistics

Ages at the time of kidney biopsy are presented as mean± standard deviation and were compared between genders with the unpaired Student's *t* test. Spearman correlation was used to measure the association between the Gb3 and LAMP2 immunoreactivity scores and selected demographic, clinical and histological parameters. Statistical significance was assumed for test p values <0.05.

Results

Patients and kidney biopsy material

A total of ten paraffin blocks of kidney biopsies from ten patients (five males, mean age 21.4±11.8 years; five females, mean age 39.6±8.8 years; $p=0.02$) were available for the immunohistochemical studies. The biopsies had been performed as baseline assessment for enzyme replacement therapy (ERT; $n=7$, including a 7-year-old boy) or as diagnostic workup for proteinuria ($n=3$). Two further cases were excluded because the archive paraffin block could not be located or did not contain enough tissue. Demographic and

Table 3 Semi-quantification of immunohistochemical Gb3 and LAMP2 staining and comparison of the semi-quantification of Gb3 immunostaining with the semi-quantification of Gb3 inclusions in semi-thin sections, according to their prevalence per kidney cell type

Case ID	Glomerular cells				Tubular cells		Interstitial cells		Peritubular capillary cells		Arterial and arteriolar vessels			
	Podocytes		Parietal cells								Endothelial cells		Smooth muscle cells	
H07-13445	+	ND	++	ND	+	ND	+	ND	++	ND	++	ND	+	ND
	+	+++	++	++ / +++	+	++	+	+/++	++	+++	++	+++	+	+++
H04-4366	+++	++	+++	+++	++	+++	++	++	++	++	+	+	+	+
	+++	+++	+++	+++	++	++	++	+++	++	+++	+	+++	+	+++
H05-9169	++	+	+	++	+/++	+++	++	+	++	-	NS	NS	NS	NS
	++	+++	+	+++	+/++	+	++	+++	++	+++	NS	+++	NS	+++
H05-6791	+++	++	+++	++	+	+++	++	-	++	-	++	+	+	-
	+++	+++	+++	+++	+	+++	++	+	++	++	++	+	+	+++
H05-7176	+	+	++	++	+/++	++/+++	+/++	+	+/++	+	+	+	++	+
	+	+++	++	+++	+/++	+++	+/++	+++	+/++	+	+	+++	++	+++
H99-4183	+	-	++	+/++	+/++	++	+	-	+	-	+	-	+	-
	+	++	++	+++	+/++	+++	+	++	+	++	+	++	+	+++
H05-9180	+	+	+	+	+	+++	+	+	+	+	-	+	+	+
	+	+	+	+++	+	+	+	-	+	+	-	-	+	++
H03-3708	NS	NS	NS	NS	+	+++	+	-	+	+	NS	NS	NS	NS
	NS	++	NS	++	+	+	+	-	+	-	NS	+	NS	+++
H05-6994	NS	NS	NS	NS	+	+++	+	-	-	-	+	-	+	-
	NS	+	NS	+++	+	+	+	-	-	-	+	NS	+	+
H05-9092	-	+/++	-	++	+	+++	-	+/++	-	+/++	-	+/++	-	+
	-	-	-	-	+	-	-	-	-	-	-	-	-	-

Left upper quadrant: semi-quantification of immunohistochemical Gb3 staining. Immunostaining was scored semi-quantitatively according to the proportion of affected cells of each type: "–" no staining, "+" staining of <1/3 of cells, "++" staining of 1/3–2/3 of cells and "+++" staining of >2/3 of cells. "Controls" (autopsy specimens) were all tissue negative, except for "+" for tubular cells.

Right upper quadrant: semi-quantification of immunohistochemical lysosomal-associated membrane protein 2. Immunostaining was scored semi-quantitatively according to the relative average of the staining intensity of cells of each type: "–" absent, "+" weak, "++" moderate and "+++" strong.

Left and right lower quadrants: comparison of the semi-quantification of Gb3 immunostaining with the semi-quantification of glycosphingolipid inclusions in semi-thin cuts, according to their prevalence per kidney cell type. Left: paraffin-embedded LM sections, immunohistochemically stained with an anti-Gb3 monoclonal antibody. Right: semi-thin plastic embedded sections, stained with toluidine blue or methylene blue. Gb3 staining and GSL deposits scored semi-quantitatively according to the proportion of affected cells of each type: "–" no staining, "+" staining of <1/3 of cells, "++" staining of 1/3–2/3 of cells, "+++" staining of >2/3 of cells

NS cell type not sampled in the biopsy section, *ND* not done

diagnostic data of the patient cohort are summarised in Table 2. One female who had a *GLA* mutation (p.R118C) associated with a mild clinical phenotype had no histopathological or biochemical evidence of Fabry nephropathy. All others had severe FD mutations as evaluated by disease severity and/or minimal residual α-galactosidase activity in the males [1, 2].

Gb3 immunoreactivity

Table 3 and Fig. 1 summarise the immunohistochemical features and semi-quantification of Gb3 deposits in study biopsies, as well as in autopsy control specimens. In three cases, there were no glomeruli and/or arterial and arteriolar vessels available in the biopsy section for scoring. The carrier of mutation p.R118C showed Gb3 immunoreactivity only in a few tubular cells, a pattern similar to that observed in autopsy control specimens.

Glomerular cells All biopsies of patients carrying severe FD mutations which had glomeruli available for scoring (n=7; five males, including the boy) showed Gb3 deposits in podocytes and in parietal epithelial cells (Fig. 1a). In these males, there were no significant correlations between the extent of Gb3 immunoreactivity and either age, degree of proteinuria or CKD stage.

Tubular cells All patients showed Gb3 immunoreactivity in the tubular epithelium with a rather variable pattern of Gb3 immunoreactivity, either involvement of all cells in some

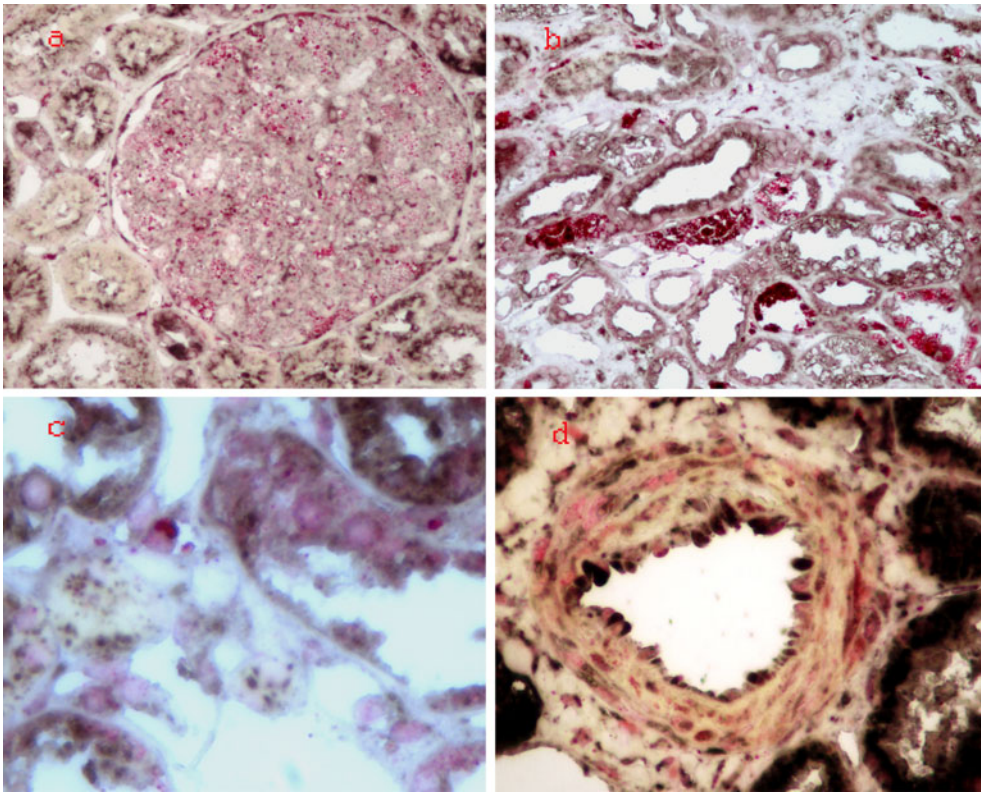

Fig. 1 Gb3 immunoreactivity on different kidney cell types. Gb3 (bright red precipitate)/LAMP2 (crisp brown precipitate) double immunohistochemistry. Magnification × 200 (**a**, **b**), ×600 (**c**), ×400 (**d**). **a** Glomerulus showing extensive Gb3 immunoreactivity, particularly in podocytes and parietal epithelial cells. Some interstitial cells are also stained. **b** Tubulointerstitial area showing variable degrees of Gb3 immunoreactivity among different tubules: In a few tubules, all the epithelial cells have Gb3 deposits while others have faint or no visible Gb3 immunoreactivity. Some of the peritubular capillaries are dilated and have Gb3 deposits in the endothelium. **c** Higher magnification of an interstitial area showing strong Gb3 immunoreactivity within an endothelial cell of a peritubular capillary. **d** Arterial vessel showing Gb3 immunoreactivity both in endothelial and smooth muscle cells

tubules or only of a few cells in other tubules (Fig. 1b). Tubular Gb3 deposits were relatively more abundant in patients with moderate/severe proteinuria (three males, one female). In the remainder, tubular Gb3 immunoreactivity was present only in a minority of cells, which was not different from the autopsy control specimens or the carrier of mutation p.R118C.

Interstitial cells Gb3 deposits were found in at least a few interstitial cells in all patients carrying severe FD mutations (Fig. 1a) but not in autopsy control specimens or in the carrier of mutation p.R118C.

Peritubular capillary cells With the notable exception of the 50-year-old woman, all patients carrying severe FD mutations showed Gb3 deposits in at least a few peritubular capillary cells (Fig. 1c). Such deposits were not found in the autopsy control specimens or in the carrier of mutation p.R118C.

Arterial and/or arteriolar vessels All evaluable biopsies of patients carrying severe FD mutations (n=7; four males, including the boy) showed Gb3 immunoreactivity in endothelial and/or smooth muscle cells (Fig. 1d). In one of the females, Gb3 immunoreactivity was identified only in smooth muscle cells. No Gb3 immunoreactivity was observed in these vessels in autopsy control specimens or in the carrier of mutation p.R118C.

LAMP2 immunoreactivity

Table 3 summarises the LAMP2 immunoreactivity data per kidney cell type in the adult patients (n=8; four males) carrying severe FD mutations and in the heterozygous carrier of mutation p.R118C. Linear (membrane-like) and punctiform LAMP2 immunoreactivity was identified in all types of kidney cells (Fig. 2a–d). Expression varied from high in tubular cells, variably in apical (Fig. 2b) or basal, or in both locations; intermediate in parietal glomerular epithelial cells; intermediate to low in podocytes (Fig. 2a) or low or absent in interstitial, peritubular capillary endothelial, arterial/arteriolar endothelial and smooth muscle cells (Fig. 2a–c). No meaningful associations could be identified between LAMP2 immunoreactivity and any demographic or clinical variables.

Relation between immunohistochemical detection of Gb3 and LAMP2

In all kidney cell compartments, Gb3 deposits were visible either co-localising with or independent of LAMP2 immunoreactivity (Figs. 2d and 3a–d). Three different (co-)

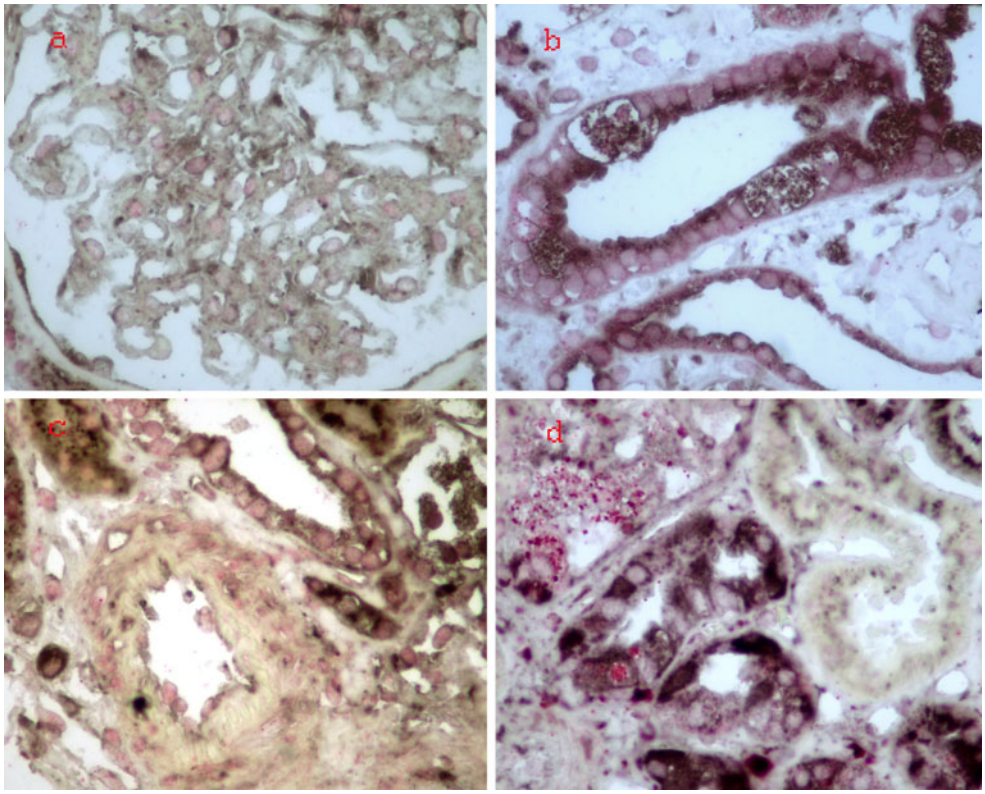

Fig. 2 LAMP2 immunoreactivity on different kidney cell types. Gb3 (bright red precipitate)/LAMP2 (crisp brown precipitate) double immunohistochemistry. Magnification × 400. **a** Glomerulus showing diffuse LAMP2 immunoreactivity in parietal epithelial cells. In podocytes, the distribution of LAMP2 immunoreactivity is limited to a few cells. **b** Tubules showing LAMP2 immunoreactivity in most cells, localised predominantly to the apical pole of the epithelium. Strong LAMP2 immunoreactivity is also seen in the endothelial cells of some of the peritubular capillaries. **c** Arteriole showing weak LAMP2 immunoreactivity in a few reactive endothelial cells. **d** Gb3 immunoreactivity in tubular cells and in podocytes. In one of the tubular epithelial cells, Gb3 deposits appear to be aggregated within a vacuole and surrounded by linear LAMP2 immunoreactivity. In podocytes (*upper left corner*) Gb3 deposits seem to be freely distributed within the cytoplasm, not co-localising with LAMP2 immunoreactivity

staining patterns could be identified, which were particularly evident in podocytes and tubular cells: (1) granular Gb3 staining surrounded by linear LAMP2 staining (Fig. 3a); (2) both Gb3 and LAMP2 staining, either in scattered or diffuse patterns, but topographically independent within the same cells (Fig. 3b) and (3) isolated Gb3 staining (Fig. 3c). No meaningful associations could be identified between the expression of LAMP2 immunoreactivity and the density of Gb3 deposits on the different kidney cell types.

Immunohistochemical detection of Gb3 as compared to histological identification of GSL deposits on semi-thin sections

We have compared the immunohistochemical semi-quantification of Gb3 per kidney cell type to the histological assessment of GSL inclusions on toluidine blue- or methylene blue-stained plastic-embedded EM scout sections (Table 3). In general, the scorings of the prevalence per different kidney cell types and/or the amount of GSL deposits identified on the ST sections were higher than the corresponding scorings of Gb3 immunoreactivity. These differences were particularly obvious on the glomerular epithelial and on the arterial/arteriolar vascular endothelial and smooth muscle cells (Fig. 4a–d). In three females carrying severe FD mutations, the immunohistochemical method allowed the identification of cytoplasmic Gb3 accumulation on kidney cells where GSL inclusions were not seen on the ST sections, specifically on interstitial cells and endothelial cells of peritubular capillaries. The female carrier of mutation p.R118C had no visible GSL deposits on the ST sections but showed Gb3 immunoreactivity on a small proportion of tubular cells. Gb3 was immunohistochemically detected on all kidney cell types that had GSL inclusions visible on the semi-thin sections.

Discussion

The most characteristic finding on routine LM of kidney biopsies of Fabry patients is the vacuolization of affected cells, especially of podocytes, parietal epithelial cells of Bowman's capsule, distal tubular and smooth muscle cells

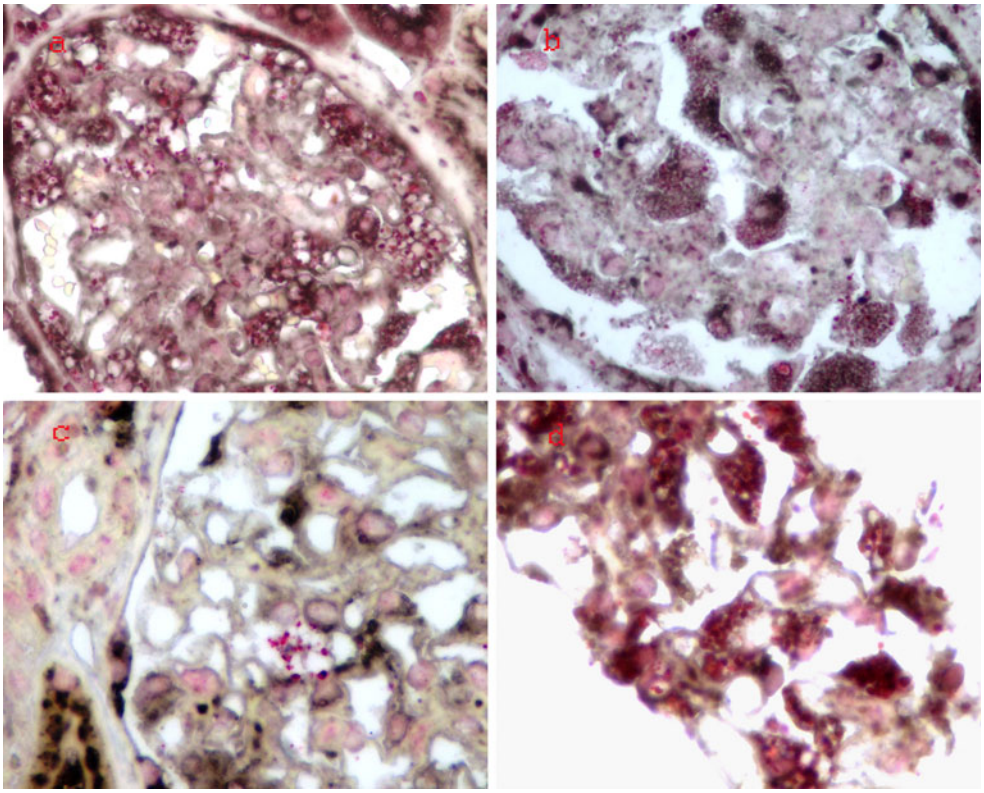

Fig. 3 Topographical relations between Gb3 and LAMP2 immunostaining. Gb3 (bright red precipitate)/LAMP2 (crisp brown precipitate) double immunohistochemistry. Magnification × 400 (**a**, **b**), ×600 (**c**, **d**). **a** In this glomerulus, granular Gb3 deposits within podocyte vacuoles are surrounded by linear LAMP2 staining ("fried egg" or "owl eye" pattern). **b** Gb3 immunostaining within podocytes additionally appears as granular or punctiform cytoplasmic deposits topographically unrelated to LAMP2 immunostaining. **c** Glomerulus showing granular Gb3 deposits in rare podocytes with no evidence of LAMP2 immunoreactivity. **d** Gb3 deposits seemingly breaking into the glomerular urinary space

[6, 16–20]. The vacuoles are histological artifacts resulting from removal of GSL deposits during clearing and paraffin embedding of the tissue. Cytoplasmic vacuolization is a non-specific feature of several other, often more prevalent kidney diseases [8–10], and although the pattern of cellular involvement may be suggestive of FD, the diagnosis of Fabry nephropathy can be overlooked on routine LM evaluation.

Gb3 and galabiosylceramide, the main GSL that accumulate in the kidneys of Fabry patients [21], are amphipathic molecules. The ceramide moiety is lipophilic and soluble in non-polar solvents, while the oligosaccharide chains are hydrophilic and may remain within the vacuoles in tissue sections routinely processed for LM. These residual carbohydrates can be non-specifically identified as argyrophilic granules in methenamine silver-stained [18, 22] and in PAS-stained (Valbuena, personal observation) [1] FFPE tissue.

Using murine monoclonal antibodies [13] formerly employed for immunohistochemical staining of Gb3 in FFPE skin biopsies [23], Askari et al. [15] have demonstrated the presence of residual Gb3 immunoreactivity in glomeruli, tubules, interstitial cells and blood vessels in FFPE kidney tissue sections of a deceased adult male with FD. With the same anti-Gb3 monoclonal antibody as primary antibody, we have now shown that immunostaining of Gb3 using standard immunohistochemical procedures can be helpful for the specific diagnosis of Fabry nephropathy, even in archive kidney tissue specimens routinely processed for LM study.

Gb3 and galabiosylceramide are cell surface receptors for the B-subunit of Shiga-toxins (Verotoxins) [24] and are both intrinsically expressed in the human kidney with the highest expression levels observed in cortical tubular epithelial cells, but also occurring in podocytes, mesangial cells and endothelium of renal vessels, including the microvasculature [25–28]. This constitutive expression of Gb3 in the kidney could hinder the specificity of immunostaining for the diagnosis of Fabry nephropathy. However, the staining of Gb3 in kidney tissue is temperature sensitive, becoming erratic, weak and indistinct unless the samples are kept continuously refrigerated (≤4°C). Indeed, kidney sections stained at room temperature had ~90% reduction in staining intensity [25]. Therefore, our immunohistochemical protocol was carried out at room temperature. In such conditions, ≤1% of tubular cortical cells of tissue negative control samples displayed faint Gb3 immunostaining and none of the other parenchymatous kidney cell types bound any anti-Gb3 antibodies at all. An identical Gb3 immunostaining pattern was observed in the female carrying the *GLA* p.R118C mutation.

In males, Gb3 immunostaining was seen in all cells types sampled in each biopsy specimen (Table 3), glomerular epithelial cells being most extensively involved. In comparison to males, females had smaller proportions of cells of each type that stained with the anti-Gb3 monoclonal antibody, which is consistent with the expected effect of X-chromosome inactivation [29].

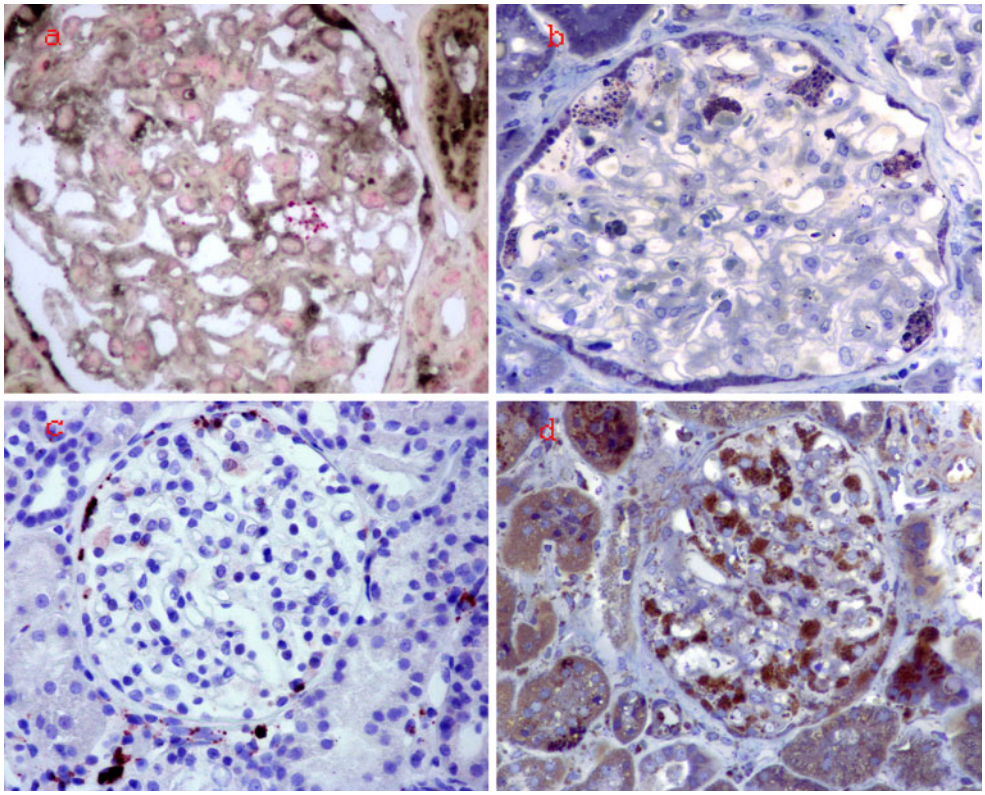

Fig. 4 Comparison of Gb3 immunostaining with glycosphigolipid histological identification in semi-thin sections. Gb3 (bright red precipitate)/LAMP2 (crisp brown precipitate) double immunohistochemistry (**a**); toluidine blue-stained semi-thin section (**b**); Gb3 (crisp brown precipitate) immunohistochemistry (**c**); toluidine blue-stained semi-thin section (**d**). Magnification×400 (**a**, **b**), ×600 (**c**, **d**). Case H05-9180. **a** Glomerulus showing granular Gb3 immunoreactivity in the cytoplasm of a single podocyte. **b** Glomerulus showing cytoplasmic glycosphingolipid inclusions in all parietal epithelial cells and in several podocytes. Case H07-13445. **c** Glomerulus showing strong Gb3 immunoreactivity in some of the parietal epithelial cells and weak staining of a few podocytes. Gb3 deposits are also visible in some interstitial cells but none of the tubular cells is Gb3 immunoreactive. **d** Large amounts of glycosphingolipid inclusions are present in most of the glomerular parietal epithelial cells and podocytes and in many interstitial and peritubular capillary cells. Glycosphingolipids are also visible in endothelial and smooth muscle cells of an arteriole. Tubular cells contain significantly lesser amounts of glycosphingolipid inclusions

With the exception of the interstitial and peritubular capillary endothelial cells, the extent of involvement of each kidney cell type, whether evaluated immunohistochemically by Gb3 staining or in EM scout sections by GSL inclusions, was closely correlated (Table 3). However, the prevalence of affected cells estimated by immunohistochemistry was lower for most cell types, particularly glomerular epithelial cells and vascular endothelial and smooth muscle cells of arteries and arterioles. Apart from removal of GSL by the histological procedure, an additional explanation for the difference in relative methodological sensitivity might be that GSL inclusions identified in ST sections may also contain galabiosylceramide, which is not recognized by the anti-Gb3 monoclonal antibody [13]. In females, the immunohistochemical approach was apparently more sensitive to detect Gb3 accumulation in interstitial cells (Table 3), but an alternative explanation is the tissue patching effect of X-chromosome inactivation [30].

We performed double Gb3 and LAMP2 immunostaining to analyse whether Gb3 could also be demonstrated in extralysosomal locations in kidney cells of Fabry patients. Testing that hypothesis was the aim of a previous study [15] that used immunofluorescence to identify the subcellular localisation of Gb3 in Fabry kidney cells; Gb3 was found to be widely distributed in other cellular structures, co-localising with lysosomal, endoplasmic reticulum and nuclear markers [15]. That study used LAMP1 as the lysosomal marker, and incubation with the anti-LAMP1 primary antibody was the first step in the immunofluorescence protocol. Although our finding that Gb3 could be detected in kidney cells not co-localising with LAMP2 is in agreement with their results, the same criticisms made to that study [31] also apply to our histological protocol.

LAMP2 immunostaining allowed an estimation of the relative abundance of lysosomes in each kidney cell type. The largest amounts of anti-LAMP2 antibody binding were

seen in the tubular epithelial cells followed by the parietal glomerular epithelial cells and podocytes. The observation of Gb3 deposits scattered in the cytoplasm of glomerular epithelial cells not co-localising with the lysosomal marker is in agreement with the postulate that rupture of Gb3 overloaded lysosomes into the cytoplasm might be involved in the pathogenesis of glomerular sclerotic lesions of Fabry nephropathy [16]. Of note, peritubular capillary cells and vascular endothelial and smooth muscle cells, which are thought to be critically involved in the pathogenesis of renal complications of FD [6, 17, 20], at most stained faintly with the lysosomal marker. The double immunostaining resulted in loss of cellular contours and the different types of tubular epithelial, mesangial and glomerular capillary endothelial cells could not be discriminated in some cases. This limits its usefulness in diagnostic pathology and research.

In conclusion, immunohistochemical staining of Gb3 is a relatively simple and specific diagnostic method for FD in the routine LM study of kidney biopsies, which can be used even for retrospective diagnosis of Fabry nephropathy in archive paraffin blocks, particularly when cell vacuolization is a prominent finding. Furthermore, it allows the exclusion of the diagnosis of Fabry nephropathy in patients carrying *GLA* mutations associated with high residual enzyme activity.

Acknowledgements We thank David Warnock, M.D. for critically reviewing and commenting the protocol and results of this study and Hans Ebels, M.D. for the invaluable assistance in the text editing of the manuscript.

Conflict of interest statement Carmen Valbuena was a recipient of a non-restricted research grant from Genzyme Portugal. All authors declare that they have no conflicts of interest.

References

1. Desnick RJ, Ioannou YA, Eng CM (2001) α-Galactosidase A deficiency: Fabry disease. In: Scriver CR, Beaudet AL, Sly WS et al (eds) The metabolic and molecular bases of inherited disease, 8th edn. McGraw Hill, New York, pp 3733–3774
2. Zarate YA, Hopkin RJ (2008) Fabry's disease. Lancet 372:1427–1435
3. Wilcox WR, Oliveira JP, Hopkin RJ et al (2008) Females with Fabry disease frequently have major organ involvement: lessons from the Fabry Registry. Mol Genet Metab 93:112–128
4. Scriba K (1950) Zur Pathogenese des Angiokeratoma corporis diffusum Fabry mit cardio vasorenalem symptomenkomplex. Verhandlg Deutsch Path GesellschVerhandlg Deutsch Path Gesellsch 34:221–226
5. Henry EW, Rally CR (1963) The renal lesion in angiokeratoma corporis diffusum (Fabry's disease). Canad Med Ass J 89:206–213
6. Gubler MC, Lenoir G, Grunfeld JP et al (1978) Early renal changes in hemizygous and heterozygous patients with Fabry's disease. Kidney Int 13:223–235
7. Faraggiana T, Churg J, Grishman E et al (1981) Light- and electron-microscopic histochemistry of Fabry's disease. Am J Pathol 103:247–262
8. Finn SL, Bernstein J (2006) Renal disease caused by familial metabolic and hematologic disease. In: Jennette JC, Olson JL, Schwartz MM, Silva FG (eds) Heptinstall's pathology of the kidney, 6th edn. Lippincott Williams and Wilkins, Philadelphia, pp 1200–1256
9. Gubler MC, Heidet L, Antignac C (2006) Alport's syndrome, thin basement membrane nephropathy, Nail–Patella syndrome, and type III collagen glomerulopathy. In: Jennette JC, Olson JL, Schwartz MM, Silva FG (eds) Heptinstall's pathology of the kidney, 6th edn. Lippincott Williams and Wilkins, Philadelphia, pp 488–517
10. Olson JL (2006) The nephrotic syndrome and minimal change disease. In: Jennette JC, Olson JL, Schwartz MM, Silva FG (eds) Heptinstall's pathology of the kidney, 6th edn. Lippincott Williams and Wilkins, Philadelphia, pp 126–155
11. Sessa A, Toson A, Nebuloni M et al (2002) Renal ultrastructural findings in Anderson–Fabry disease. J Nephrol 15:109–112
12. Savi M, Olivetti G, Neri TM et al (1977) Clinical, histopathological, and biochemical findings in Fabry's disease. A case report and family study. Arch Pathol Lab Med 101:536–539
13. Kotani M, Kawashima I, Ozawa H et al (1994) Generation of one set of murine monoclonal antibodies specific for globo-series glycolipids: evidence for differential distribution of the glycolipids in rat small intestine. Arch Biochem Biophys 310:89–96
14. Fukushima M, Tsuchiyama Y, Nakato T et al (1995) A female heterozygous patient with Fabry's disease with renal accumulation of trihexosylceramide detected with a monoclonal antibody. Am J Kidney Dis 26:952–955
15. Askari H, Kaneski CR, Semino-Mora C et al (2007) Cellular and tissue localization of globotriaosylceramide in Fabry disease. Virchows Arch 451:823–834
16. Valbuena C, Carvalho E, Bustorff M et al (2008) Kidney biopsy findings in heterozygous Fabry disease females with early nephropathy. Virchows Arch 453:329–338
17. Alroy J, Sabnis S, Kopp JB (2002) Renal pathology in Fabry disease. J Am Soc Nephrol 13(Suppl 2):S134–S138
18. Fischer EG, Moore MJ, Lager DJ (2006) Fabry disease: a morphologic study of 11 cases. Mod Pathol 19:1295–1301
19. Fogo AB, Bostad L, Svarstad E et al (2010) Scoring system for renal pathology in Fabry disease: report of the International Study Group of Fabry Nephropathy (ISGFN). Nephrol Dial Transplant 25:2168–2177
20. Sessa A, Meroni M, Battini G et al (2003) Renal involvement in Anderson–Fabry disease. J Nephrol 16:310–313
21. Sweeley CC, Klionsky B (1963) Fabry's disease: classification as a sphingolipidosis and partial characterization of a novel glycolipid. J Biol Chem 238:3148–3150
22. Oliveira JP, Valbuena C, Baldaia Moreira A et al (2008) Splenomegaly, hypersplenism and peripheral blood cytopaenias in patients with classical Anderson–Fabry disease. Virchows Arch 453:291–300
23. Kanekura T, Fukushige T, Kanda A et al (2005) Immunoelectron-microscopic detection of globotriaosylceramide accumulated in the skin of patients with Fabry disease. Br J Dermatol 153:544–548
24. Cohen A, Hannigan GE, Williams BR et al (1987) Roles of globotriosyl- and galabiosylceramide in verotoxin binding and high affinity interferon receptor. J Biol Chem 262:17088–17091
25. Ergonul Z, Clayton F, Fogo AB et al (2003) Shigatoxin-1 binding and receptor expression in human kidneys do not change with age. Pediatr Nephrol 18:246–253
26. Hughes AK, Stricklett PK, Kohan DE (1998) Cytotoxic effect of Shiga toxin-1 on human proximal tubule cells. Kidney Int 54:426–437
27. Hughes AK, Stricklett PK, Schmid D et al (2000) Cytotoxic effect of Shiga toxin-1 on human glomerular epithelial cells. Kidney Int 57:2350–2359

28. Taguchi T, Uchida H, Kiyokawa N et al (1998) Verotoxins induce apoptosis in human renal tubular epithelium derived cells. Kidney Int 53:1681–1688
29. Migeon BR (2006) The role of X inactivation and cellular mosaicism in women's health and sex-specific diseases. JAMA 295:1428–1433
30. Novelli M, Cossu A, Oukrif D et al (2003) X-inactivation patch size in human female tissue confounds the assessment of tumor clonality. Proc Natl Acad Sci USA 100:3311–3314
31. Elleder M (2008) Cellular and tissue localization of globotriaosylceramide in Fabry disease. Virchows Arch 452(705):707–708

Virchows Arch (2012) 460:223–224
DOI 10.1007/s00428-012-1196-0

ERRATUM

Erratum to: Immunohistochemical diagnosis of Fabry nephropathy and localisation of globotriaosylceramide deposits in paraffin-embedded kidney tissue sections

Carmen Valbuena · Dina Leitão · Fátima Carneiro · João Paulo Oliveira

Published online: 22 January 2012
© Springer-Verlag 2012

Erratum to: Virchows Arch
DOI: 10.1007/s00428-011-1182-y

The original version of the above mentioned manuscript, unfortunately, contained a mistake. Table 1 was published with the wrong version.

The authors very much regret their error.

The following is the updated version of Table 1.

The online version of the original article can be found at http://dx.doi.org/10.1007/s00428-011-1182-y.

C. Valbuena (✉) · F. Carneiro
Department of Pathology, Hospital São João,
Alameda Prof. Hernâni Monteiro,
4200-319 Porto, Portugal
e-mail: valbuena@med.up.pt

C. Valbuena · F. Carneiro · J. P. Oliveira
Faculty of Medicine, University of Porto (FMUP),
Porto, Portugal

D. Leitão · F. Carneiro
Department of Pathology, Institute of Molecular Pathology
and Immunology of the University of Porto (IPATIMUP),
Porto, Portugal

C. Valbuena · J. P. Oliveira
Department of Nephrology and Unit of Research & Development
in Nephrology (FCT-725), Hospital São João,
Porto, Portugal

J. P. Oliveira
Department of Human Genetics, Faculty of Medicine,
University of Porto,
Porto, Portugal

Table 1 Medical diseases affecting the kidney parenchyma, with histological vacuolization of cells [8–10]

Disease	Podocytes	Mesangial cells	Glomerular capillary endothelium	Proximal tubular cells	Distal tubular cells	Interstitial cells	Vascular smooth-muscle cells	Vascular endothelium
Aspartylglycosaminuria	+							
Fabry disease	+	+	+		+	+	+	+
Fucosidosis	+							
Gaucher disease						+		
Glycogen storage disease type I				+	+			
GM1 gangliosidosis	+	+						
Hurler's disease	+			+				
I-cell disease	+			+				
LCAT deficiency		+	+			+	+	+
Lipoprotein glomerulopathy						+		
Mannosidosis	+							
Metachromatic leukodystrophy				+	+			
Nephrosialidosis	+			+	+	+		+
Neuronal ceroid lipofuscinosis	+		+	+	+			
Niemann-Pick disease	+		+	+	+	+		
Sandhoff disease	+			+				
Type III hyperlipoproteinemia		+						
Alport disease						+		
Nephrotic range proteinuria	+					+		
Minimal change disease				+	+	+		

GM1: monosialotetrahexosylganglioside. LCAT: Lecithin:cholesterol acyltransferase. "+" vacuolization present

Virchows Arch (2012) 460:225–229
DOI 10.1007/s00428-011-1186-7

CASE REPORT

Primary IgG4-related lymphadenopathy with prominent granulomatous inflammation and reactivation of Epstein–Barr virus

Emiko Takahashi · Masaru Kojima · Mizuki Kobayashi · Atsuko Kitamura · Toyoharu Yokoi · Kazuo Hara · Shigeo Nakamura

Received: 4 November 2011 / Accepted: 14 December 2011 / Published online: 17 January 2012
© Springer-Verlag 2011

Abstract We report a unique case of primary IgG4-related lymphadenopathy showing prominent granulomatous inflammation and Epstein–Barr virus (EBV) reactivation. Involved lymph nodes showed an expanded interfollicular zone with prominent granulomatous inflammation, including a predominance of epithelioid macrophages and occasional Langhans multinucleated giant cells. Bundles of spindle cells were also observed. Intermingled with the granulomatous inflammation were numerous mature plasma cells, eosinophils, and neutrophils. The percentage of IgG4+/IgG+ plasma cells was markedly elevated (70%), along with raised serum IgG4 levels. The plasma cells did not show immunoglobulin light-chain restriction. EBV-positive lymphocytes were scattered throughout the paracortical areas. Corticosteroid treatment was very effective. IgG4-related lymphadenopathy has a broad histological spectrum and might be misdiagnosed due to other conditions which morphologically closely resemble it. The correct diagnosis is important in view of the remarkable response to steroid therapy.

E. Takahashi (✉) · M. Kobayashi · A. Kitamura · T. Yokoi · K. Hara
Department of Pathology, Aichi Medical University Hospital, Nagakute, Japan
e-mail: emikot@aichi-med-u.ac.jp

M. Kojima
Department of Anatomic Diagnostic Pathology, Dokkyo University School of Medicine, Mibu, Japan

S. Nakamura
Department of Pathology and Laboratory Medicine, Nagoya University Hospital, Nagoya, Japan

Keywords IgG4-related lymphadenopathy · IgG4-related disease · Granulomatous inflammation · Epstein−Barr virus · Reactivation of Epstein−Barr virus

Introduction

IgG4-related sclerosing disease is a recently recognized syndrome characterized by mass-forming lesions in exocrine glands and extranodal tissues due to lymphoplasmacytic infiltrates and sclerosis, an increased number of IgG4+ plasma cells in the tissue involved, and a raised serum IgG4 level. The morphological features of affected lymph nodes have also been reported. Five histological subtypes have been described, including Castleman's disease-like morphology, reactive follicular hyperplasia, interfollicular plasmacytosis and immunoblasts, progressive transformation of germinal center-like morphology, and nodal inflammatory pseudotumor (IPT)-like morphology [1–4].

We report a unique case of IgG4-related lymphadenopathy showing prominent granulomatous inflammation and Epstein–Barr virus (EBV) reactivation. We also discuss other conditions that may bear morphological resemblance IgG4-related lymphadenopathy.

Clinical history

A 60-year-old woman presented with swelling of the bilateral postauricular region accompanied by regional pain that was resolved in 1 week. Computed tomography revealed generalized lymphadenopathy (cervical, supraclavicular, axillary, mediastinal, abdomen, pelvic, paraaortic, and inguinal, up to 3 cm). Extranodal lesions were not found. The enlarged lymph

nodes showed increased uptake of fluorodeoxy-D-glucose on positron emission tomography.

Laboratory findings revealed mild anemia and hypocomplementemia with a hemoglobin level of 10.9 g/dL (normal range 11.4–14.8 g/dL), a C3 level of 37.9 mg/dL (normal range 65.0–135.0 mg/dL), and a C4 level of 2 mg/dL (normal range 13.0–35.0 mg/dL). Soluble interleukin-2 receptor (sIL-2R) levels were elevated (1,740 U/mL; normal range 145–519 U/mL). Also elevated were serum IgG levels (4,776 mg/dL; normal range 870–1,700 mg/dL) and IgG4 levels (1,330 mg/dL; normal range 4.8–105 mg/dL). Serum IgM levels, IgA levels, lactate dehydrogenase (LDH) levels, and C-reactive protein (CRP) levels were all within normal limits. Although tests for anti-DNA antibodies and antinuclear antibodies were positive, the patient did not show any symptoms of autoimmune disease such as systemic lupus erythematosus. EBV serology showed elevation of IgG anti-VCA and IgG anti-EBNA (9.5 and 3.5, respectively, determined by ELISA). The IgM anti-VCA was negative, indicative of past infection. Biopsies of the enlarged cervical and inguinal lymph nodes were performed.

Upon a diagnosis of IgG4-related lymphadenopathy on a lymph node biopsy, the patient was started on oral prednisolone at 20 mg/day, which resulted in a very good response. Prednisolone dosage was tapered gradually to 3 mg/day, and the lymph node lesions remained well under control.

Materials and methods

Clinical information was obtained from the patient record. Lymph nodes were fixed in formalin, processed, and embedded in paraffin. For light microscopic examination, the sections were stained with hematoxylin–eosin. Immunohistochemical staining was performed on formalin-fixed paraffin-embedded tissue sections using the Roche-automated immunostaining detection system (Roche, Basel, Switzerland). Color was developed by the streptavidin–biotin–peroxidase technique using 3′-diaminobenzidine as the chromogen. The following antibodies were applied: anti-IgG (IgG, Predilute, Signet, Dedham, MA, USA), anti-IgG4 (HP6025, 1:500, Zymed, San Francisco, CA, USA), anti-α-smooth muscle actin (1A4, 1:50, DAKO, Carpinteria, CA, USA), anti-desmin (D33, 1:50, DAKO), anti-CD21 (1F8, 1:20, DAKO), anti-CNA.42 (CNA.42, 1:50, DAKO), anti-CD1a (O10, Predilute, Beckman Coulter, Brea, CA, USA), anti-S100 (S100, 1:500, DAKO), anti-CD68 (KP-1, 1:50, DAKO), anti-IL-6 (10C12, 1:50, Leica Biosystems, Laboratories Ltd., Newcastle Upon Tyne, UK), anti-HHV-8 (13B10, 1:50, Leica Biosystems), anti-LMP1 (CS1, CS2, CS3, and CS4, 1:200, Novocastra, Newcastle, UK), and anti-EBNA2 (Abcam, 1:50, Cambridge, UK). For IgG, CD68, and LMP1, the slides were pretreated with protease. For IgG4, desmin, CD1a, HHV-8, EBNA2, CD21, and CAN.42, the slides were pretreated with heat-induced epitope retrieval. EBV small ribonucleic acids were demonstrated on formalin-fixed paraffin-embedded sections by in situ hybridization (ISH), using EBV-encoded small nuclear early region (EBER) oligonucleotides. Briefly, a DAKO hybridization kit was used with a cocktail of fluorescein isothiocyanate (FITC)-labeled EBER oligonucleotides (one oligonucleotide corresponding to EBER1 and the other to EBER2, both 30 bases long; DAKO A/S code Y017). Hybridized probe was detected using a mouse monoclonal anti-FITC (M878) and a Vectastain ABC Kit (Vector, Burlingame, CA, USA). RNase A or DNase I pretreatment was applied as negative control, and EBER-positive Hodgkin lymphoma was used as positive control.

Results

Pathological findings

Histologically, the cervical lymph node architecture was distorted by an expanded interfollicular zone, with hyperplastic and regressive follicles scattered in the cortex (Fig. 1a). Small nodules with interfollicular involvement were seen in the inguinal lymph node. The interfollicular zone and sinuses showed a prominent granulomatous inflammation, with a predominance of epithelioid macrophages and some Langhans multinucleated giant cells and dendritic cells, extending beyond the capsule into the fat (Fig. 1b). Bundles of spindle cells with long attenuated cytoplasmic processes and round to oval nuclei were also seen (Fig. 1c). Intermingled with the granulomatous inflammation were mature plasma cells, small lymphocytes, eosinophils, and neutrophils (Fig. 1d). Coagulative necrosis was not seen. Other interfollicular areas were moderately to densely infiltrated by mature plasma cells, eosinophils, neutrophils, immunoblasts, plasmacytoid cells, small and medium-sized lymphocytes, histiocytes, and few Hodgkin cell-like cells, accompanied by arborizing high endothelial venules. The lymph nodes did not exhibit obliterative phlebitis.

Immunohistochemical studies and in situ hybridization

Immunohistochemical studies demonstrated a large number of IgG-positive cells. The percentage of IgG4+/IgG+plasma cells was 70%, and the absolute number of IgG4+ cells exceeded 50/high power field, fulfilling the histological criteria for IgG4-related sclerosing disease as proposed by Cheuk and Chan [3] (Fig. 2a, b). The majority of IgG4-positive cells were located in interfollicular areas, although some were observed in the intrafollicular areas. The plasma

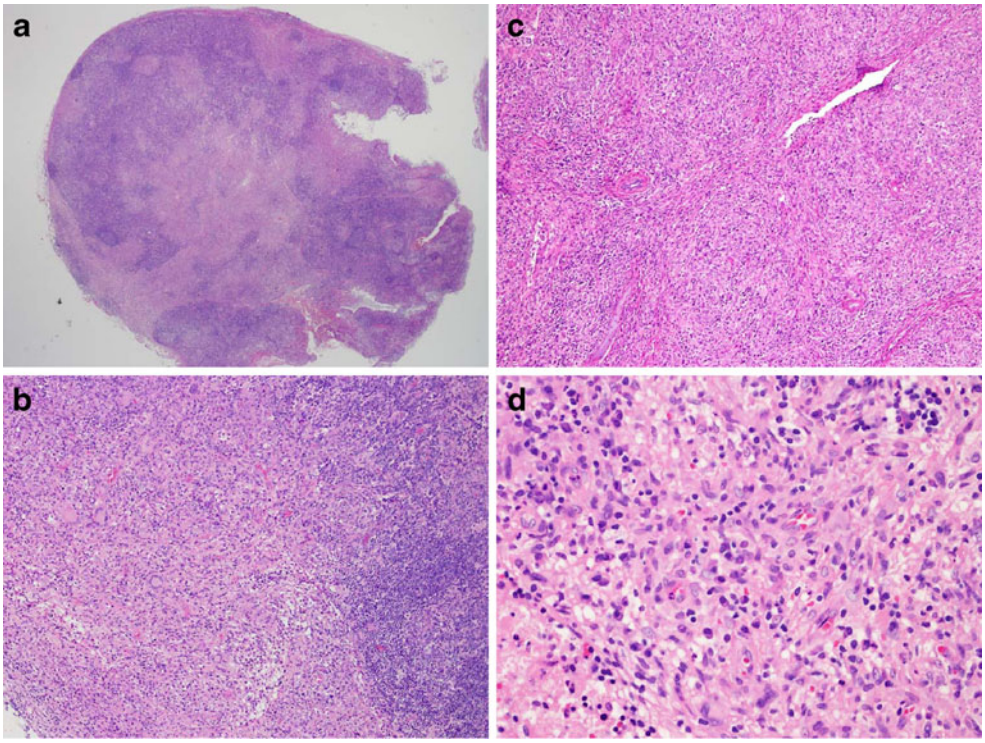

Fig. 1 Morphological features of a lymph node biopsy specimen. **a** Lymph node architecture is distorted by an expanded interfollicular zone with prominent granulomatous inflammation (hematoxylin and eosin; original magnification× 12.5). **b** Granulomatous inflammation comprises epithelioid macrophages with scattered Langhans multinucleated giant cells (hematoxylin and eosin; original magnification×100). **c** Bundles of spindle cells with long attenuated cytoplasmic processes and round to oval nuclei (hematoxylin and eosin; original magnification× 100). **d** Intermingled with the granulomatous inflammation were mature plasma cells, small lymphocytes, eosinophils, and neutrophils (hematoxylin and eosin; original magnification×400)

cells did not show immunoglobulin light chain restriction. Spindle cells were positive for α-smooth muscle actin and negative for desmin, CD21, and CNA.42, indicating a myofibroblast phenotype. CD68 staining revealed a population of histiocytes and also highlighted some spindle cells. S-100 staining showed scattered interdigitating dendritic cells and also staining of some spindle cells. No IL-6-positive cells or HHV-8-positive cells were found. Special stains for organisms, including Fite-Faraco stain, periodic acid-Schiff stain, and Grocott methenamine silver stain, were all negative. ISH-EBER-positive lymphoid cells with small-sized nuclei were scattered throughout the paracortical area, although some EBV+ cells were medium-sized to large lymphocytes [334 EBV+ cells/0.5 cm^2 (up to 36/mm^2)] (Fig. 2c). EBER-positive cells were negative for LMP1 and EBNA2.

Discussion

At least five histological subtypes of IgG4-related lymphadenopathy have been reported [1–4]. To the best of our knowledge, this is the first report of primary IgG4-related lymphadenopathy showing prominent granulomatous inflammation and EBV reactivation.

Our patient shared clinical similarities with other reported IgG4-related lymphadenopathy cases, i.e., middle aged to elderly age group, generalized lymphadenopathy, absence of fever, anemia, raised serum IgG levels, elevation of serum sIL-2R, normal serum LDH, presence of autoantibodies, as well as a good response to steroid therapy [1–3]. Our case did not show concomitant extranodal lesions, corresponding to group C as proposed by Cheuk et al. [2], i.e., primary IgG4-related lymphadenopathy. However, extranodal lesions can develop during the clinical course, and its diagnosis is helpful for clinical follow-up.

Histologically, the patient needed to be distinguished from infectious or non-infectious lymphadenitis with granulomatous inflammation, IPT of the lymph node, interdigitating dendritic cell sarcoma, follicular dendritic cell sarcoma, and age-related EBV-associated reactive lymphoid hyperplasia.

Granulomatous inflammation of lymph nodes is observed in a wide variety of disease conditions including infectious diseases (viral, fungal mycobacterial, bacterial, and parasitic/protozoal), malignancy associated (carcinoma, melanoma, and lymphoma), and systemic disorders (autoimmune disease and primary granulomatous disease) [5]. The absence of organisms, elevated CRP levels, leukocytosis, and systemic symptoms such as fever in our patient ruled out infection. A lack of its signs and symptoms eliminated the possibility of autoimmune disease. Absence of clinical or histological evidence of malignancy or of a primary granulomatous disease, such as sarcoidosis, ruled out these diagnoses.

Our patient showed histological findings similar to those of histological stage I or II of IPT of the lymph node, which manifests as small nodules with partial lymph node involvement or marked distortion of the lymph node connective tissue framework due to a polymorphous inflammatory infiltration and myofibroblast proliferation with a storiform growth

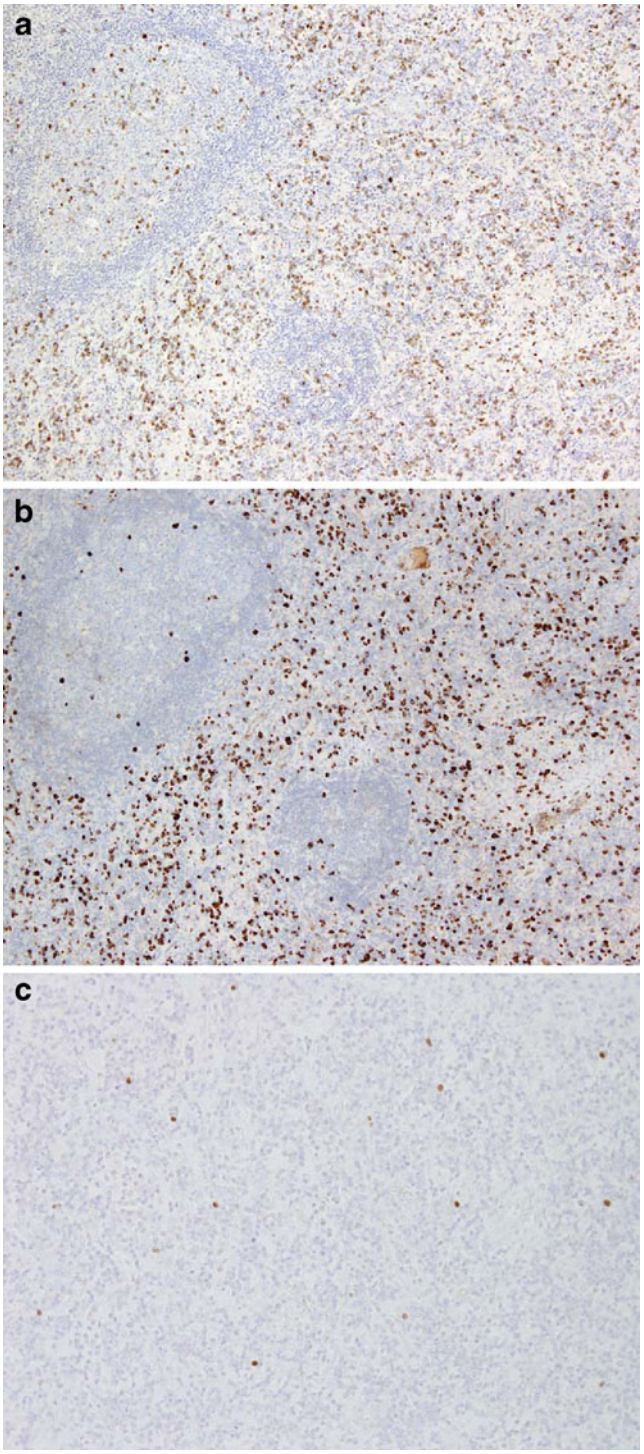

Fig. 2 Immunohistochemical and in situ hybridization study of a lymph node biopsy specimen. **a** Immunohistochemical study shows a large number of IgG-positive cells (original magnification×100). **b** IgG4-positive plasma cells (70% of all IgG-positive plasma cells); absolute number of IgG4-positive cells exceeds 50/high power field (original magnification×100). **c** EBER-positive lymphoid cells are scattered in the paracortical area (original magnification×200)

pattern [6, 7]. IPT of the lymph node with granulomatous inflammation with multinucleated giant cells has been described but generally with involvement of only one lymph node group and constitutional symptoms such as fever [6]. In addition, immunostaining for IgG and IgG4 as well as presence of eosinophils helped in differentiating between the two disorders. IPT-like IgG4-related lymphadenopathy reported by Sato et al. [1] bears histological similarity to histological stage III of IPT, implying that every histological stage of IPT could be a differential diagnosis of IgG4-related lymphadenopathy.

In our case, the differential with interdigitating dendritic cell sarcoma or follicular dendritic cell sarcoma needed to be made in view of the paracortical and interfollicular proliferation of spindle cells admixed with a lymphoid infiltrate. The lack of S-100-positive cells in our case excluded interdigitating dendritic cell sarcoma. Follicular dendritic cell sarcoma was ruled out in view of the absence of entire replacement of lymph node parenchyma by spindle cell proliferation and of CD21 and CNA.42 expressing cells.

Interestingly, scattered EBER-positive lymphocytes have occasionally been found in IgG4-related lymphadenopathy (E.T. and M.K., personal communication, 2011). In a study on latent EBV infection in healthy individuals, hyperplastic lymph nodes, obtained from patients without clinically known dysfunction of the immune system, generally fewer than 200 cells/0.5 cm^2 EBER-positive cells were found [8]. EBV+ small lymphocytes were almost exclusively localized to extrafollicular areas [8]. The relatively higher number of EBER+ cells and the presence of autoantibodies in our patient suggested immunological dysfunction. We hypothesize that the number of EBV+ lymphocytes is influenced by the immune status of the host.

Age-related EBV-associated reactive lymphoid hyperplasia, i.e., the reactive lesion within the spectrum of age-related EBV-associated lymphoproliferative disorders (AR-EBVLPD), could be another differential diagnosis in our patient [9]. Dojcinov et al. [9] recently documented 31 patients over 45 years of age with age-related EBV+ reactive lymphoid hyperplasia, 26% of which presented with generalized lymphadenopathy, characterized by a varying degree of plasma cell hyperplasia, epithelioid granulomas, and eosinophilic infiltrate in the paracortical areas and high EBV count (mean, 34.3/mm^2; range, 0.43–247.4/mm^2) [9]. Histologically, differentiating IgG4-related lymphadenopathy from AR-EBVLPD can be a problem. In our experience (unpublished work), IgG4+ plasma cells do occur in AR-EBVLPD (in two of eight examined cases) but in low numbers, not fulfilling the diagnostic criteria for IgG4-related disease.

In conclusion, we report a case of primary IgG4-related lymphadenopathy with prominent granulomatous inflammation and EBV reactivation. In a case of unexplained lymphadenopathy with increased plasma cells with eosinophils,

immunostaining for IgG4 and IgG may help in reaching a final diagnosis which is important in view of the favorable response to steroid therapy of these cases.

Acknowledgments The authors acknowledge the technical assistance of Kaneko Sakurai, Eriko Wada, Mitsunori Sato, Junji Sano, and Yoshimi Mizuno.

Conflict of interest We declare that we have no conflict of interest.

References

1. Sato Y, Notohara K, Kojima M, Takata K, Masaki Y, Yoshino T (2010) IgG4-related disease: historical overview and pathology of hematological disorders. Pathol Int 60:247–258
2. Cheuk W, Yuen HKL, Chu SYY, Shiu EKW, Lam LK, Chan JKC (2008) Lymphadenopathy of IgG4-related sclerosing disease. Am J Surg Pathol 32:671–681
3. Cheuk W, Chan JKC (2010) IgG4-related sclerosing disease: a critical appraisal of an evolving clinicopathologic entity. Adv Anat Pathol 17:303–332
4. Kojima M, Miyazaki S, Takada S, Kashiwabara K, Igarashi T, Nakamura S (2008) Lymphoplasmacytic infiltrate of regional lymph nodes in Küttner's tumor (chronic sclerosing sialadenitis): a report of 3 cases. Int J Surg Pathol 16:263–268
5. Armed forces institute of Pathology (2009) Granulomatous inflammation. In: O'malley DP, George TL, Orazi A, Abbondanzo SI (eds) Benign and reactive conditions of lymph node and spleen. American Registry of Pathology, Washington, pp 119–125
6. Kojima M, Nakamura S, Shimizu K, Hosomura Y, Ohno Y, Itoh H, Yamane N, Yoshida K, Masawa N (2001) Inflammatory pseudotumor of lymph nodes: clinicopathological study of 11 Japanese cases. Int J Surg Pathol 9:207–214
7. Moran CA, Suster S, Abbondanzo SL (1996) Inflammatory pseudotumor of lymph nodes: a study of 25 cases with emphasis on morphological heterogeneity. Hum Pathol 28:332–338
8. Niedobitek G, Herbst H, Young LS, Brooks L, Masucci MG, Crocker J, Rickinson AB, Stein H (1992) Patterns of Epstein–Barr virus infection in Non-neoplastic lymphoid tissue. Blood 79:2520–2526
9. Dojcinov SD, Venkataraman G, Pittaluga S, Wlodarska I, Schrager JA, Raffeld M, Hills RK, Jaffe ES (2011) Age-related EBV-associated lymphoproliferative disorders in the Western population: a spectrum of reactive lymphoid hyperplasia and lymphoma. Blood 117:4726–4735

Virchows Arch (2012) 460:231–235
DOI 10.1007/s00428-011-1189-4

CASE REPORT

Pseudolymphomatous luetic lymphadenitis associated with B cell clonality

Marianna Salemme · Simona Fisogni · Roberto Giardini · Daniela Medicina · William Vermi · Fabio Facchetti

Received: 4 August 2011 / Revised: 6 December 2011 / Accepted: 26 December 2011 / Published online: 19 January 2012
© Springer-Verlag 2012

Introduction

Syphilis is a sexually transmitted disease that can display heterogeneous clinical and pathological manifestations, in keeping with its definition as to "the great mimic" [1]. Recently, an outbreak of the infection has been noticed in several countries; a phenomenon that has been partially explained by migratory fluxes from areas with high rate of infection [1, 2].

Luetic lymphadenitis is a common histological manifestation of *Treponema pallidum* infection [3] especially in the primary and in the secondary stages of the disease. Histological hallmarks are represented by pronounced follicular hyperplasia associated with plasmacytosis, granulomas, and capsular fibrosis [3–5]. Recently, an inflammatory pseudotumor reaction pattern has been found to be part of the spectrum of the disease [3].

Here we report a case of luetic lymphadenitis presenting with hitherto unreported features consisting of multiple large lymphoid nodules, strongly suggesting a lymphomatous process. A diagnosis of lymphoma was initially supported by the detection of a B cell clone on flow cytometry and polymerase chain reaction (PCR) analysis. Lues adds to the causes of nodal inflammatory processes that may mimic lymphomas, including the occurrence of B cell clonality likely induced by the infection [4–6]. High rate of alert in cases of lymphoid proliferations with unusual features should prompt to consider the possibility of *T. pallidum* infection and to perform immunohistochemical analysis to detect the pathogen.

M. Salemme · S. Fisogni · D. Medicina · W. Vermi · F. Facchetti (✉)
Department of Pathology, University-Spedali Civili Brescia, 25123 Brescia, Italy
e-mail: facchett@med.unibs.it

R. Giardini
Department of Pathology, Istituti Ospitalieri Cremona, 26100 Cremona, Italy

Clinical history

A 36-year-old male has presented with an asymptomatic isolated cervical mass since few months. A 5×2×2.5-cm lymph node was surgically removed; after histological diagnosis of luetic lymphadenitis, serology for syphilis was performed and resulted positive. The patient was subsequently treated with a single dose of intramuscular benzathine penicillin (2.4 million units). Five months later all serological parameters regarding the infection were negative and the patient was considered definitely recovered.

Materials and methods

A minute unfixed part of the node was immediately submitted for flow and molecular analysis; the remaining was fixed in formalin and embedded in paraffin for morphological, immunohistochemical, fluorescence in situ hybridization, and molecular analyses.

Immunohistochemistry

Four-micron tissue sections were stained for the following antigens: BCL2 (Dako, Glostrup, Denmark), CD3 (Thermo Scientific, Fremont, CA, USA), CD5 (Novocastra Laboratories, Newcastle upon Tyne, UK), CD20 (Dako, Glostrup, Denmark), CD21 (Thermo Scientific), CD23 (Thermo Scientific), CD30 (Dako), CD35 (Dako), CD68/PGM-1 (Dako),

CD163 (Thermo Scientific), BCL2 (Dako), Clusterin (Novocastra), IgD (Dako), programmed cell death 1 (a costimulatory molecule strongly expressed on follicular T helper cells; kindly provided by Dr. T. Marafioti, London), T cell leukemia/lymphoma protein 1A (stains B cells and especially mantle B lymphocytes in normal tissues; Medical & Biological Laboratories, Naka-ku Nagaya, Japan), *Bartonella henselae* (Abcam, Cambridge, UK), and *T. pallidum* (Biocare Medical, Concord, CA, USA). Images were taken with the Olympus BX60 microscope using a DP-70 Olympus digital camera (Olympus).

Fluorescent-in-situ hybridization

Fluorescent-in-situ hybridization (FISH) analysis for the t (14;18) translocation was performed on paraffin sections using the break apart (Dako) and dual fusion (Abbot Molecular, USA) probes; both procedures were performed according to the manufacturer's indications.

Polymerase chain reaction

Genomic DNA was extracted from fresh tissue and paraffin sections using QIAamp DNA Tissue kits (Qiagen, Hilden, Germany). On the fresh tissue specimen, the B cell lymphoma molecular diagnosis kit (Nanogen, Milan, Italy) was applied, amplifying through a semi-nested PCR technique the FR2/J fragment (240–260 bp). On paraffin sections, we applied the multiplex PCR assay for the identification of clonal rearrangements of the immunoglobulin heavy and kappa light chain genes (InVivoScribe Technologies, San Diego, CA, USA), according to the BIOMED-2 protocol [7, 8]. All tests were performed on six distinct tissue blocks of the same lymph node; all these blocks showed similar histological features. The analyses were at least duplicated on the same extracted DNA.

A clonal rearrangement was defined as the presence on the electropherogram of a peak falling within the expected size range and whose amplitude is at least three times that of the third largest peak in the polyclonal background; a peak was defined as dominant when it clearly exceeded the amplitude of adjacent neighboring peaks.

Results

On histology (Fig. 1a–c), the nodal parenchyma was effaced by multiple large nodules associated with marked follicular hyperplasia; the nodules were four to ten times larger than reactive follicles. They were composed of small mature lymphocytes that were heterogeneously distributed in the center of the nodules and formed a peripheral rim; intermingled with the small lymphocytes variable numbers of spindle cells, histiocytes, neutrophils and plasma cells were found, which occasionally formed pale areas within the nodules. Some intranodular vessels were permeated by the infiltrate, but fibrinoid necrosis or obvious vasculitis was absent; granulomas were not evident. The capsule showed focal fibrosis with a sparse inflammatory infiltrate including plasma cells. Mitoses, necrosis, or atypical cells were undetectable.

On immunohistochemistry (Fig. 1d–f) the small lymphocytes were predominantly represented by B cells with a mantle cell phenotype (CD20+IgD+TCL1+), admixed with fewer CD3+CD5+ T cells that included in variable proportions PD1+ follicular T helper cells; immunostain for CD68+ and CD163+ highlighted the macrophage component of the nodules, while anti-follicular dendritic cell markers (CD21, CD23, CD35, and clusterin) did not identify positive cells within the nodules, in contrast to the associated secondary B follicles. These follicles exhibited extremely hyperplastic germinal centers which, in keeping with their reactive features, lacked BCL2 expression and did not show *BCL2* rearrangement on FISH analysis.

Immunohistochemistry for *B. henselae* was negative, while anti-*T. pallidum* immunostain showed huge numbers of spirochetes within the large nodules, with clustering around blood vessels; rare spirochetes were observed in the capsule. Flow cytometry performed on the fresh tissue fragment revealed a small fractions (18%) of CD10+CD20+ B cells with kappa light chain restriction, while PCR analysis showed a monoclonal rearrangement of the immunoglobulin heavy chain gene of 230 bp on a polyclonal background (not shown).

We extended the molecular analysis on additional six paraffin blocks and found clonal or dominant peaks of identical size for the FR1/JH, FR2/JH, and FR3/JH targets of the immunoglobulin heavy chain gene (313, 247, and 106 bp, respectively). Only in one block a clonal peak was identified for all three targets, while the others revealed a combination of patterns, including the polyclonal (Fig. 2, Table 1). Interestingly, a minor peak of the same molecular weight of the clonal/dominant counterpart was frequently observed even in the polyclonal electropherograms, indicating that a clonal B cell population was widely distributed, albeit in different proportions, throughout the entire lymph node. The analysis of the immunoglobulin kappa light chain gene regularly showed a polyclonal pattern.

Discussion

We report a case of luetic lymphadenitis showing hitherto unreported features consisting of multiple large lymphoid nodules composed of numerous mantle B cells associated with follicular T helper cells and strongly mimicking a

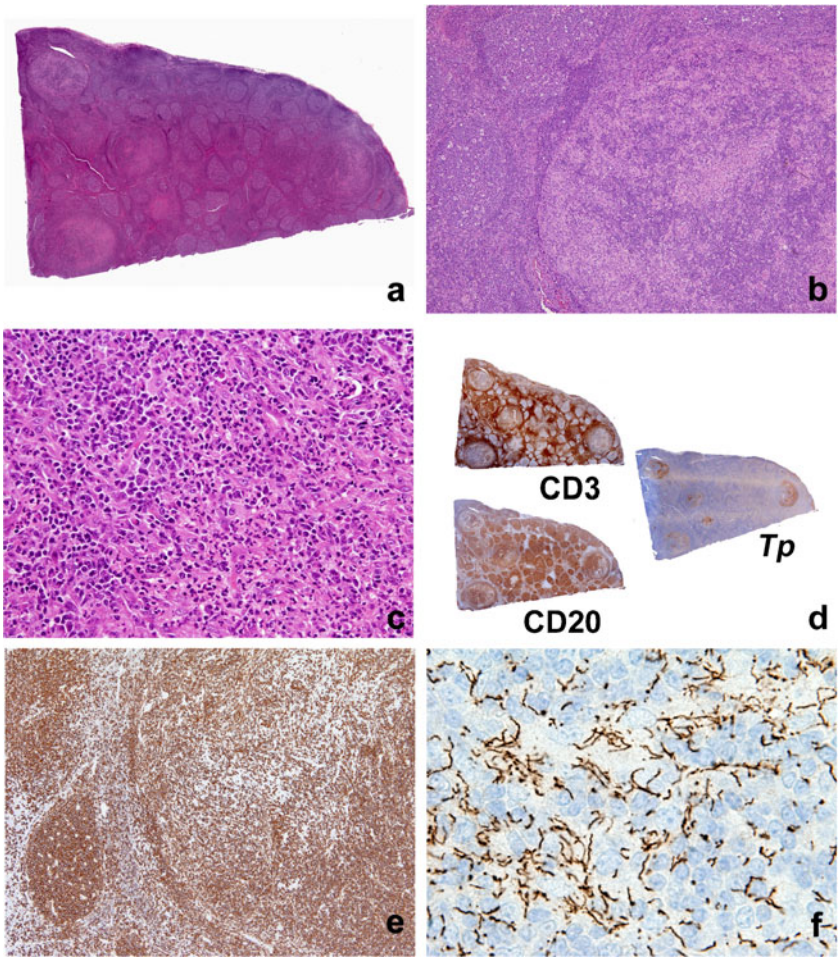

Fig. 1 Luetic lymphadenitis: full section view shows multiple large nodules associated with pronounced follicular hyperplasia (**a**). The nodules contain variable proportions of small lymphocytes and pale areas (**b**), which on higher magnification show a mixture of lymphocytes, macrophages, polymorphs, and plasma cells (**c**). Immunostains for *CD3*, *CD20*, and *Treponema pallidum* (*Tp*) performed on serial sections demonstrate that the large nodules contain numerous lymphocytes with a predominant B cell phenotype and huge numbers of spirochetes (**d**). **e**, **f** Highlight the high content of small CD20+ B cells and show the spirochetes within the nodules

lymphomatous proliferation. In particular, the possibility of nodular lymphocyte predominant or classical lymphocyte-rich Hodgkin lymphoma was considered; however, the lack of atypical cells within the nodules and the association with a polymorphous population of inflammatory cells suggested these nodules most likely represented an unusual reactive process. This hypothesis was also sustained by the coexistence of a prominent follicular hyperplasia.

On the basis of some similarities of the cellular composition of the nodules with the inflammatory pseudotumor-like reaction recently reported in cases of luetic lymphadenitis [3], the search of *T. pallidum* by immunohistochemistry was performed and showed huge numbers of spirochetes within the nodules, suggesting that they represented the principal site of infection. Remarkably, these nodules were composed of numerous small B lymphocytes with a mantle cell phenotype, but no germinal center reaction was noticed and no follicular dendritic cells were detected by different markers. Since sepsis-like syndrome has been shown to induce profound depletion of follicular dendritic cells and lack of B cell maturation [9], it is tempting to speculate that the colonization of *T. pallidum* of primary follicles and the associated inflammatory cells could be able to inhibit the differentiation of follicular dendritic cells and the germinal center cell reaction within the nodules. In keeping with this observation, the associated reactive B follicles were totally devoid of spirochetes, as previously found [3].

At the preliminary work out of the case, flow cytometric and molecular analysis performed on a small portion of fresh tissue addressed towards a clonal B cell proliferation that, however, was not sustained by morphology. The molecular analysis was subsequently extended on six multiple paraffin tissue blocks obtained from the same lymph node and confirmed the occurrence of a clonal B cell population. In fact, the heavy chain genes (FR1/JH, FR2/JH, and FR3/JH) were clonally rearranged, as revealed by "clonal" or "dominant" peaks of the same molecular weight occurring in the different blocks. In contrast, the kappa light chain gene rearrangement was polyclonal. Several studies have demonstrated that clonal B cell populations can be identified in different lymphoid and nonlymphoid tissues involved by antigen-driven proliferations of B cells associated with pathogens, such as HIV [5], hepatitis C virus [10], *Borrelia burgdorferi* [11], herpes virus [12], Epstein–Barr virus, *Cytomegalovirus*, and *Tropheryma whippelii* [13]. In addition,

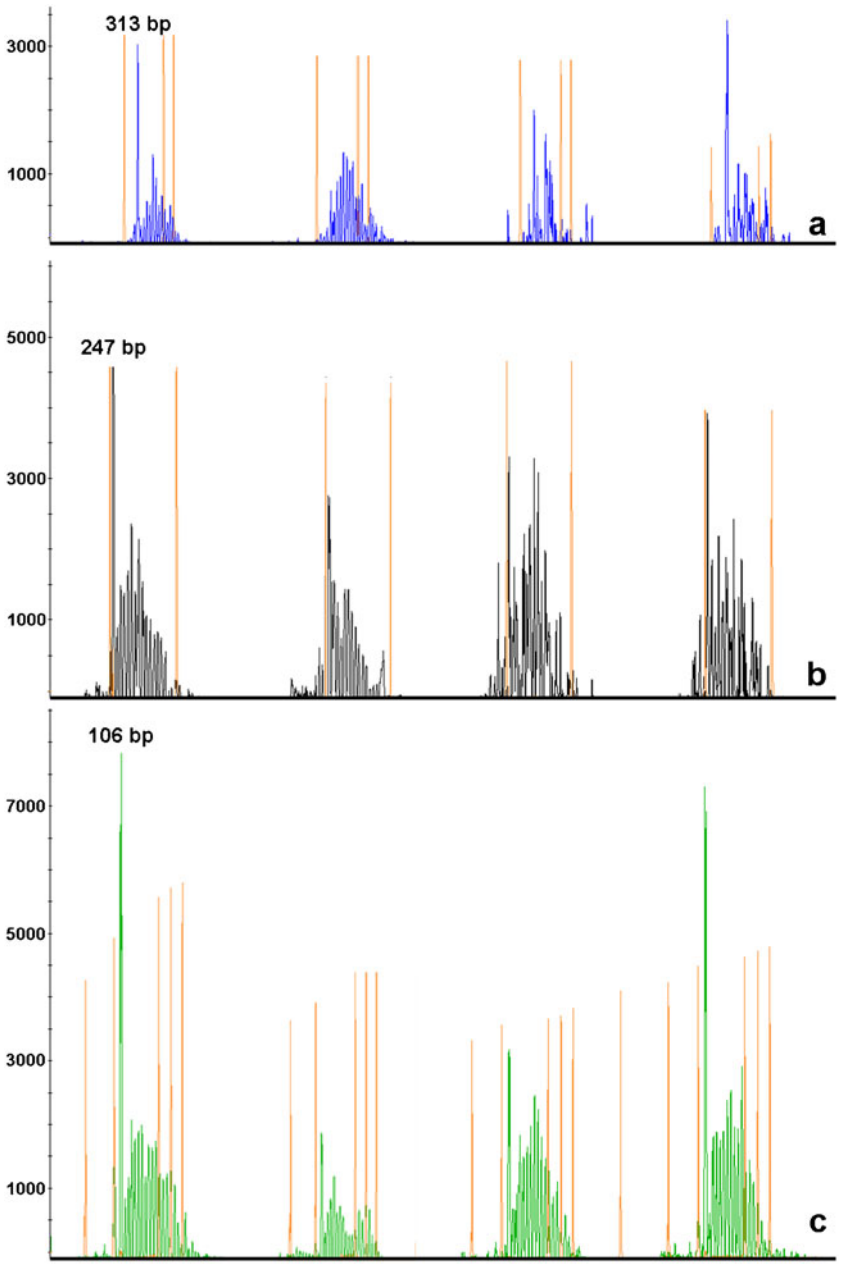

Fig. 2 Electropherograms of PCR analysis for the FR1/JH (**a**), FR2/JH (**b**), and FR3/JH (**c**) targets of the immunoglobulin heavy chain gene in four distinct paraffin tissue blocks (*from left to right*: BL-1, BL-2, BL-3, and BL-4). Except for BL1 that show a clonal peak in all three assays (313, 247, and 106 bp, respectively), the other blocks reveal a combination of patterns, including the dominant peak or the polyclonal pattern. Note that a peak of the same molecular weight of the clonal/dominant counterpart is recognizable in the polyclonal background in BL-3 for FR1/JH an FR2/JH. Ladder is represented by *yellow bars*

Kussick et al. reported young patients developing reactive lymphadenitis showing follicular hyperplasia and containing a fraction of clonal follicular B cells, detected by either flow and gene rearrangement analysis [5]. In keeping with these observations, the present study further highlights that the interpretation of lymphoid clonality should be strictly performed in the contest of morphology to reduce the risk of misdiagnosis [14].

Table 1 Results of the PCR analysis for rearrangements of the immunoglobulin heavy and light chain genes performed on six different paraffin tissue blocks (BL) of the same lymph node

PCR Target	BL-1	BL-2	BL-3	BL-4	BL-5	BL-6
FR1-JH	C (313 bp)	P	P	C (313 bp)	P	P
FR2-JH	C (247 bp)	D (247 bp)	P	D (247 bp)	C (247 bp)	P
FR3-JH	C (106 bp)	D (106 bp)	D (106 bp)	C (106 bp)	C (106 bp)	D (106 bp)
IGK (Vk-Jk)	P	P	np	np	np	np
IGK (Vk-Intron-KdE)	P	P	np	np	np	np

C clonal, *D* presence of a dominant peak, *P* polyclonal, *np* not performed

Acknowledgments The authors thank Mrs. Cristina Rossini, Wilma Pellegrini, Paola Bossini and Laura Fappani for their technical skills; Dr. Luisa Pecoroni (Department of Immunohematology, Istituti Ospitalieri di Cremona) kindly provided data on flow and molecular analyses on fresh tissue.

Conflict of interest statement We declare that we have no conflict of interest.

References

1. Daskalakis D (2008) Syphilis: continuing public health and diagnostic challenges. Curr HIV/AIDS Rep 5(2):72–77
2. Nicoll A, Hamers FF (2002) Are trends in HIV, gonorrhoea, and syphilis worsening in western Europe? BMJ 324:1324–1327
3. Facchetti F, Incardona P, Lonardi S, Fisogni S, Legrenzi L, Chioda C, Ponzoni M, Chiodera PL (2009) Nodal inflammatory pseudotumor caused by luetic infection. Am J Surg Pathol 33:447–453
4. Hartsock RJ, Halling LW, King FM (1970) Luetic lymphadenitis: a clinical and histologic study of 20 cases. Am J Clin Pathol 53:304–314
5. Kussick SJ, Kalnoski M, Braziel RM, Wood BL (2004) Prominent clonal B-cell populations identified by flow cytometry in histologically reactive lymphoid proliferations. Am J Clin Pathol 121:464–472
6. Simmers WC (1978) The lymphoreticular system. In: Simmers WC (ed) Systemic pathology, IIth edn. Churchill Livingstone, Edinburg, pp 611–617
7. van Dongen JJ, Langerak AW, Bruggemann M, Evans PA, Hummel M, Lavender FL, Delabesse E, Davi F, Schuuring E, Garcia-Sanz R, van Krieken JH, Droese J, Gonzalez D, Bastard C, White HE, Spaargaren M, Gonzalez M, Parreira A, Smith JL, Morgan GJ, Kneba M, Macintyre EA (2003) Design and standardization of PCR primers and protocols for detection of clonal immunoglobulin and T-cell receptor gene recombinations in suspect lymphoproliferations: report of the BIOMED-2 Concerted Action BMH4-CT98-3936. Leukemia 17:2257–2317
8. van Krieken JH, Langerak AW, Macintyre EA, Kneba M, Hodges E, Sanz RG, Morgan GJ, Parreira A, Molina TJ, Cabecadas J, Gaulard P, Jasani B, Garcia JF, Ott M, Hannsmann ML, Berger F, Hummel M, Davi F, Bruggemann M, Lavender FL, Schuuring E, Evans PA, White H, Salles G, Groenen PJ, Gameiro P, Pott C, Dongen JJ (2007) Improved reliability of lymphoma diagnostics via PCR-based clonality testing: report of the BIOMED-2 Concerted Action BHM4-CT98-3936. Leukemia 21:201–206
9. Chatterjee S, Lardinois O, Bhattacharjee S, Tucker J, Corbett J, Deterding L, Ehrenshaft M, M GB, Mason RP (2011) Oxidative stress induces protein and DNA radical formation in follicular dendritic cells of the germinal center and modulates its cell death patterns in late sepsis. Free Radic Biol Med 50:988-99.
10. Magalini AR, Facchetti F, Salvi L, Fontana L, Puoti M, Scarpa A (1998) Clonality of B-cells in portal lymphoid infiltrates of HCV-infected livers. J Pathol 185:86–90
11. Boer A, Tirumalae R, Bresch M, Falk TM (2008) Pseudoclonality in cutaneous pseudolymphomas: a pitfall in interpretation of rearrangement studies. Br J Dermatol 159:394–402
12. Sanchez JL, Mendez JA, Palacio R (1981) Cutaneous pseudolymphoma at the site of resolving herpes zoster. Arch Dermatol 117:377
13. Wang S, Ernst LM, Smith BR, Tallini G, Howe JG, Crouch J, Cooper DL (2003) Systemic *Tropheryma whippleii* infection associated with monoclonal B-cell proliferation: a *Helicobacter pylori*-type pathogenesis? Arch Pathol Lab Med 127:1619–1622
14. Chan JK, Kwong YL (2010) Common misdiagnoses in lymphomas and avoidance strategies. Lancet Oncol 11:579–588

Virchows Arch (2012) 460:237–249
DOI 10.1007/s00428-012-1203-5

REVIEW AND PERSPECTIVES

Ovarian carcinomas: five distinct diseases with different origins, genetic alterations, and clinicopathological features

Jaime Prat

Received: 23 November 2011 / Revised: 22 January 2012 / Accepted: 24 January 2012 / Published online: 10 February 2012
© Springer-Verlag 2012

Abstract Malignant epithelial tumors (carcinomas) are the most common ovarian cancers and also the most lethal gynecological malignancies. Based on histopathology and molecular genetic alterations, ovarian carcinomas are divided into five main types (high-grade serous (70%), endometrioid (10%), clear cell (10%), mucinous (3%), and low-grade serous carcinomas (<5%)) that account for over 95% of cases. These types are essentially distinct diseases, as indicated by differences in epidemiological and genetic risk factors, precursor lesions, patterns of spread, and molecular events during oncogenesis, response to chemotherapy, and prognosis. For a successful specific treatment, reproducible histopathological diagnosis of the tumor cell type is critical. The five tumor types are morphologically diverse and resemble carcinomas of the uterus. Actually, recent investigations have demonstrated that a significant number of cancers, traditionally thought to be primary ovarian tumors (particularly serous, endometrioid, and clear cell carcinomas), originate in the fallopian tube and the endometrium and involve the ovary secondarily. This review summarizes recent advances in the molecular pathology which have greatly improved our understanding of the biology of ovarian carcinoma and are also relevant to patient management.

Keywords Ovary · Carcinomas · Histopathological types · Molecular genetics · TP53 · BRCA · KRAS · PTEN · ARID1A · HNF-1beta · PIK3CA · CTNNB1

J. Prat (✉)
Department of Pathology, Hospital de la Santa Creu i Sant Pau,
Autonomous University of Barcelona,
Sant Quinti 87-89,
08041 Barcelona, Spain
e-mail: jprat@santpau.cat

Epithelial ovarian tumors are heterogeneous neoplasms which are primarily classified according to cell type into serous, mucinous, endometrioid, clear cell, transitional, and squamous cell tumors [1, 2]. Parenthetically, none of these cells are found in the normal ovary and their development has long been attributed to mullerian "neometaplasia" of the ovarian surface epithelium (mesothelium). More importantly, these tumors are further subdivided into benign, borderline (intermediate), and malignant (carcinoma) depending upon the degree of cell proliferation and nuclear atypia, and the presence or absence of stromal invasion [1, 2].

Borderline tumors show epithelial proliferation greater than that seen in their benign counterparts and variable nuclear atypia; however, in contrast to carcinomas, there is absence of stromal invasion, and their prognosis is much better than that of carcinomas. In spite of the lack of ovarian stromal invasion, serous borderline tumors, particularly those with exophytic growth, can implant on peritoneal surfaces and, rarely (about 10% of peritoneal implants), progress to low-grade serous carcinoma (LGSC) and invade the underlying tissues. The biologic behavior of invasive peritoneal implants is similar to that of LGSC. However, the lack of stromal invasion in the primary borderline ovarian tumor justifies designating the associated (frequently superficial) peritoneal lesions as *implants* rather than metastasis [1, 2]. In contrast, LGSC is usually associated with peritoneal carcinomatosis [3].

Malignant epithelial tumors (carcinomas) are the most common ovarian cancers accounting for 90% of cases [1, 2]. Although traditionally referred to as a single entity, ovarian cancer is not a homogeneous disease but rather a group of diseases, each with different morphology and

biologic behavior. Compared to breast cancer, ovarian cancer is ten times less frequent, yet is associated with a much greater number of deaths, as 75% of patients present with advanced (stage III) tumors experience recurrence after surgery and chemotherapy and most, ultimately, die of the disease. Globally, it accounts for over 100,000 women's deaths per year, constitutes the fifth most frequent cause of cancer death in women in the Western world, and is the most lethal gynecological cancer [4]. Early diagnosis has been unsuccessful.

Unlike colorectal carcinoma, a progression model for ovarian carcinoma has not been described. In spite of being an oversimplified model, defining colorectal cancer as a linear sequence of mutations has served as a working guide and has allowed for a better understanding of tumor progression from premalignant lesions to invasive carcinoma [5]. The clinical benefit of this includes the successful screening, early detection, and treatment of colon cancer. Conversely, the origins of ovarian cancer are only now being elucidated, and thus it remains the most aggressive gynecologic malignancy.

Currently, however, based on histopathology, immunohistochemistry, and molecular genetic analysis, at least five main types of ovarian carcinomas are identified: high-grade serous carcinomas (HGSC) (70%), endometrioid carcinomas (EC) (10%), clear cell carcinomas (CCC) (10%), mucinous carcinomas (MC) (3 %), and LGSC (<5%) [6] (Table 1) (Fig. 1). These tumors account for 98% of ovarian carcinomas, can be reproducibly diagnosed by light microscopy, and are inherently different diseases, as indicated by differences in epidemiological and genetic risk factors, precursor lesions, patterns of spread, molecular events during oncogenesis, response to chemotherapy, and prognosis.

In the era of personalized cancer medicine, reproducible histopathological diagnosis of tumor cell type is a *sine qua non* condition for successful treatment. For instance, it has been found that different tumor types respond differently to chemotherapy. The poor response rate of clear cell carcinomas (15%) contrasts notably with that of high-grade serous carcinomas (80%), resulting in a lower 5-year survival for clear cell compared with high-grade serous carcinoma in patients with advanced stage tumors (20% versus 30%) [7, 8]. The clear cell and mucinous types, in particular, are candidates for clinical trials to identify more active therapy than what is presently used [9]. Furthermore, the biomarker expression profile within a given type is consistent across stage [10]. Thus, early and advanced stage ovarian carcinomas differ primarily based on histological type, while, within a type there is no difference in biomarker expression between early and advanced stage tumors [9].

The fact that one tumor type (high-grade serous carcinomas) accounts for over two-thirds of cases, it does not justify classifying ovarian carcinomas into only two types, lumping together the other four (endometrioid, clear cell, mucinous, and low-grade serous carcinomas) as "type 1 carcinomas" [11]. In fact, the latter tumors are clinically, morphologically, and molecularly distinct diseases that individually bear resemblance neither to high-grade serous carcinomas nor to each other. Thus, classifying ovarian carcinomas into just two types ("types I and II") [11] is artificial and limits progress in understanding the biology or improving the management of the less common types of ovarian carcinomas.

As indicated above, benign counterparts of the cells of ovarian carcinomas are not found in the normal ovary. The tumor cells were thought to derive exclusively from the surface epithelium (mesothelium) and epithelial inclusion cysts through a process of mullerian "neometaplasia"; thus, they would resemble morphologically the epithelia of the fallopian tube, endometrium, or endocervix. Although the mesothelial origin cannot be excluded, there is now compelling evidence that a number of what have been thought to be primary ovarian cancers are actually originated in other pelvic organs and involve the ovary secondarily. In fact, it has been proposed that HGSC arise from precursor epithelial lesions in the distal fimbriated end of the fallopian tube [12–18], whereas endometrioid and clear cell carcinomas originate from ovarian endometriosis (Fig. 2) [19, 20]. This review summarizes recent advances in the molecular pathology which have greatly improved our understanding of the

Table 1 Ovarian carcinoma: clinical and molecular features of the five most common types

	HGSC	LGSC	MC	EC	CCC
Risk factors	*BRCA1/2*	?	?	HNPCC	?
Precursor lesions	Tubal intraepithelial carcinoma	Serous borderline tumor	cystadenoma/ borderline tumor?	Atypical endometriosis	Atypical endometriosis
Pattern of spread	Very early transcoelomic spread	Transcoelomic spread	Usually confined to ovary	Usually confined to pelvis	Usually confined to pelvis
Molecular abnormalities	*BRCA*, *p53*	*BRAF*, *KRAS*	*KRAS*, *HER2*	*PTEN ARID1A*	HNF1 *ARID1A*
Chemosensitivity	High	Intermediate	Low	High	Low
Prognosis	Poor	Intermediate	Favorable	Favorable	Intermediate

HGSC High-grade serous carcinoma, *LGSC* Low-grade serous carcinoma, *MC* Mucinous carcinoma, *EC* Endometrioid carcinoma, *CCC* Clear cell carcinoma, *HNPCC* Hereditary non-polyposis colorectal carcinoma

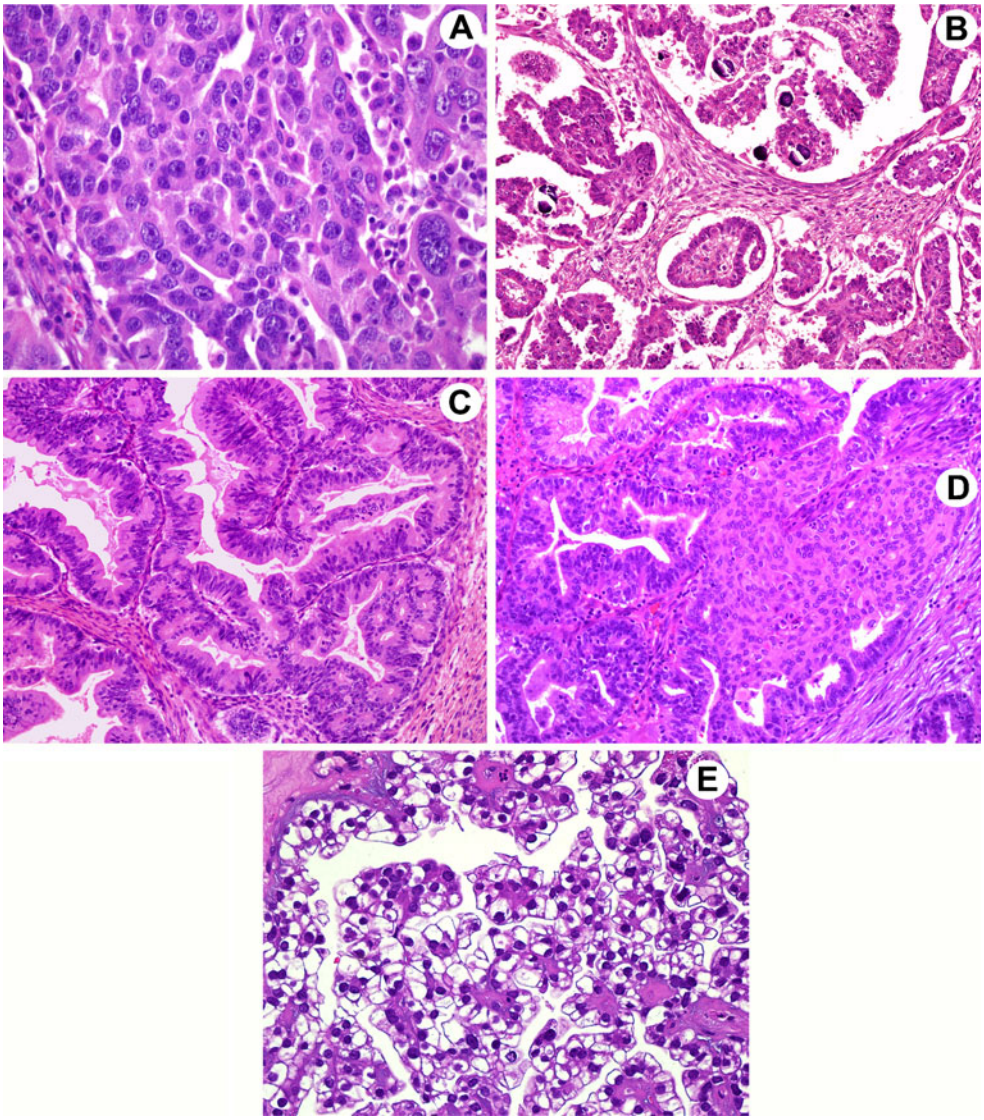

Fig. 1 Representative examples of the five main types of ovarian carcinoma, which together account for 98% of cases: **a** High-grade serous carcinoma; **b** Low-grade serous carcinoma; **c** Mucinous carcinoma; **d** Endometrioid carcinoma; and **e** Clear cell carcinoma

biology of ovarian carcinoma and are also relevant to patient management.

Serous carcinomas

It is now accepted that high-grade serous carcinoma and low-grade serous carcinoma are fundamentally different tumor types, and consequently, different diseases [20]. LGSCs are associated, in most cases, with a serous borderline component, carry *KRAS* and *BRAF* mutations, and are unrelated to *TP53* mutations and *BRCA* abnormalities [21, 22]. In contrast, HGSCs are not associated with serous borderline tumors and typically exhibit *TP53* mutations and *BRCA* abnormalities. However, it has been recently shown that both tumor types may derive from fallopian tube precursor lesions (tubal intraepithelial carcinoma (TIC)) [12–18] (Fig. 3) or fallopian tube epithelium (endosalpingiosis) in a significant number of cases [23, 24].

High-grade serous carcinomas

HGSCs are the most common ovarian carcinomas and most patients present with advanced stage disease (approximately 80%); tumors confined to the ovary at diagnosis are distinctly uncommon (<10%).

Microscopically, HGSCs show papillary and solid growth with slit-like glandular lumens. The tumor cells are typically of intermediate size, with scattered bizarre mononuclear giant cells exhibiting prominent nucleoli (Fig. 1a). In contrast to LGSCs, these tumors show more than 3-fold variation in nuclear size. Although nuclear features are the chief criterion for distinguishing between HGSC and LGSC,

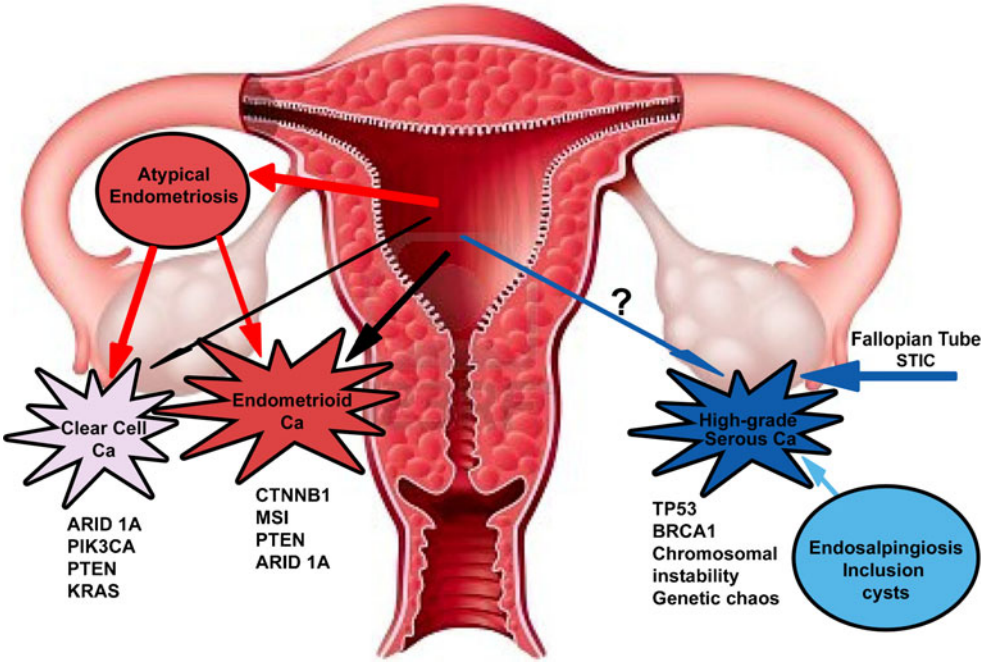

Fig. 2 Classification of gynecological cancers based on origin and mutations

the mitotic activity can be used in cases with equivocal degrees of nuclear pleomorphism; mitotic activity greater than 12/10 high-power microscopic fields (HPF) favors a diagnosis of HGSC [6, 25]. In these tumors, mitotic activity is often several times higher than the diagnostic threshold and is associated with abundant apoptotic bodies. High-grade and predominantly solid carcinomas showing serous differentiation, even in a minority of the tumor, should be classified as HGSC (rather than mixed serous/undifferentiated). To date, no underlying molecular differences between these tumors and pure HGSC have been detected [26].

Most HGSCs immunoreact for p53, BRCA1, WT1, and p16. They also exhibit a high proliferation index as indicated by an increased nuclear expression of Ki-67. Only strong and diffuse p53 and p16 reactions should be considered positive. Nuclear WT1 reaction occurs in approximately 80% of cases of HGSC and LGSC but in less than 5% of ovarian carcinomas of other types [10, 27, 28]. Estrogen receptor (ER) is expressed in approximately two thirds of cases of HGSC and is also expressed in LGSCs and ECs but is negative in almost all CCCs and MCs [28].

The traditional view that HGSC arise exclusively from ovarian surface epithelium or epithelial inclusion cysts has been recently challenged by the identification, in women with *BRCA1* or *BRCA2* germline mutations, of TIC in the distal fimbriated end of the fallopian tube as the probable precursor of advanced HGSC [12, 13, 16]. Cytologically, the cells of TIC show secretory differentiation [16] and resemble those of HGSC (Fig. 3a). They lack cilia and show nuclear enlargement, hyperchromasia, loss of polarity, prominent nucleoli, and mitotic figures. TIC shows strong immunoreaction for HMFG2, an antibody that recognizes mucin 1, and Stathmin 1, both markers of secretory cells, suggesting that these cells are the target for malignant transformation [16, 29]. TIC also shows immunohistochemical evidence of double-stranded DNA damage, as indicated by nuclear staining for gamma-H2AX [18]. Like HGSC, TIC diffusely and strongly expresses p53 (Fig. 3b) and the Ki-67 proliferation index is usually markedly elevated (Fig. 3c) (mean labeling index, 72%; range: 40–95%) [18]. p16 and WT-1 may also be expressed. Furthermore, the finding of identical *TP53* mutations in both TIC and concomitant tumors classified as ovarian in origin [15] indicates a clonal relationship between them and suggests that the distal fallopian tube (fimbria) is an important site for the initiation of HGSC. Nevertheless, implantation of tubal-type epithelium into the ovary (endosalpingiosis) or mesothelial surface invaginations (inclusion cysts) may explain the origin of those HGSC lacking TIC. In such cases, the primary tumor would appear to originate from the ovary. Currently, the relative proportion of HGSC of ovarian and tubal derivation is unknown mainly because the growth of tumor in advanced stage cancers conceals the primary site. However, extensive examination of the fallopian tubes from 55 consecutive cases of HGSC (ovarian, tubal, or pelvic) revealed involvement of the endosalpinx in 70% and TIC in approximately 50% of the cases [15].

Women with germline mutations in *BRCA1* or *BRCA2* have a 30%–70% risk of developing ovarian cancer by the age of 70, mainly HGSC [30]. Carcinomas arising in patients with germline *BRCA1* or *BRCA2* mutations are almost invariably of high-grade serous type. *BRCA1* and *BRCA2* are essential components of the homologous recombination DNA system required to repair DNA double-strand breaks (DSB) [31]. Like *TP53* mutations, *BRCA* inactivation seems

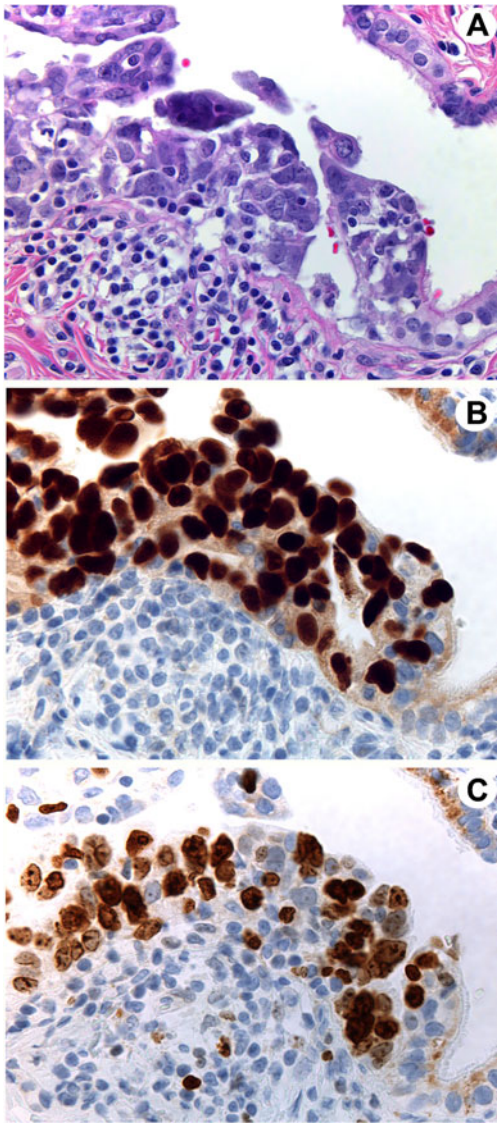

Fig. 3 Tubal intraepithelial carcinoma **(a).** Immunostaining for p53 and Ki-67 are shown as (**b**) and (**c**), respectively. Note the abrupt transition from benign tubal epithelium to a region with marked cytological atypia, diffuse strong p53 immunoreactivity, and increased proliferation index

to be a consistent genetic alteration of HGSC. Besides germline mutation, inactivation of the BRCA pathway may result from somatic mutation in either *BRCA1* or *BRCA2* [32], or promoter hypermethylation in *BRCA1* [33].

The discovery of TICs in risk-reducing salpingo-oophorectomy (RRSO) specimens from women with known *BRCA* mutations and/or a strong family history of ovarian cancer has resulted in extensive research into the role of the fallopian tube in pelvic serous carcinogenesis [12–18]. Early studies revealed small foci of strongly p53-immunoreactive cells in largely histologically normal fallopian tube epithelium [16]. These foci, which predominate in the distal portion of the fallopian tube, have been designated "p53 signatures". Like TIC, p53 signatures are comprised exclusively of secretory cells (at least 12 consecutive immunoreactive cells), and the majority exhibit evidence of DNA damage by immunoreaction for gamma-H2AX [16, 18]. They are more frequent and multifocal in tubes with TIC and, in some cases, can be identified in direct continuity with TIC. About 57% of p53 signatures contain *TP53* mutations [16]; however, Ki-67 proliferation index is low (mean, 3%). p53 signatures probably represent early clonal expansion short of neoplastic proliferation [34] and, surprisingly, are found in both women with and without *BRCA1* or *BRCA2* mutations at the same frequency (10–38% versus 17–33%, respectively) [16]; should BRCA loss have caused p53 signature foci, one would expect a much higher frequency in women with germline mutations in *BRCA1* or *BRCA2*, but this does not occur [16]. Thus, *TP53* mutation is an early event in the genesis of HGSC, occurring in p53 signature foci and leading to TIC in the distal fallopian tube. *BRCA1* mutation also occurs early in the development of TIC but after TP53 mutation [34]. It is possible that germline mutations of *BRCA1* act as a promoter for the development of TIC [17].

Jarboe et al. have described a morphologic continuum of epithelial changes taking place in the distal fallopian tube [18]. The transition is as follows: normal fallopian tube epithelium, overexpression of p53, serous tubal intraepithelial carcinoma (STIC), and finally, invasive serous carcinoma. Clonality of the precursor cells in both the so-called p53 signature and STICs are the strongest support for the fimbriated end of the fallopian tube as a site of origin for HGSC [14]. Concentration of *TP53* mutant lesions in the distal fallopian tube suggests a vulnerability of these cells to DNA damage. In fact, the secretory cells of the tubal epithelium have a limited ability to repair DNA DSB, as shown by the persistence of gamma-H2AX immunoreactive foci after DNA damage [35]. This might explain why this tissue seems to be especially sensitive to inactivating *BRCA* mutations.

The protocol for Sectioning and Extensively Examining the Fimbriated End (SEE-FIM protocol) was developed for processing RRSO [14]. According to this protocol, the entire tube is initially fixed for at least 4 h to prevent denuding of the mucosal epithelial cells. Then, the fimbriated end is amputated from the proximal tube and sectioned longitudinally into multiple (at least four) sections and the entire tube is submitted for histologic review. With more extensive sectioning of these specimens, an increased rate of detection of early cancer (up to 17%) can be obtained [36].

Although a significant number of HGSC may not arise from the ovary, and the term "ovarian cancer" would not be pathogenetically precise in every case, ovarian involvement is the rule in almost all cases. Furthermore, in view of the rarity of HGSC associated with tubal tumor masses, it is unlikely that all HGSC originate in the fallopian tube. Thus,

the term HGSC of ovary should be kept until the different origins of the ovarian tumors are better understood. Terms like "mullerian" or "pelvic" would create confusion for patients, physicians, and medical investigators.

A pathogenetic model that includes the stages of initiation and progression of HGSC is essential for an effective screening and treatment that takes into account biomarkers of early tumorigenesis. The model described by Bowtell [34] (Fig. 4) proposes that the sequence of primary events were as follows: early p53 loss followed by BRCA loss, leading to deficiency in homologous recombination repair of DSB, which triggers chromosomal instability (genetic chaos) and widespread copy number changes [34, 37, 38]. Secondary and tertiary events then cause global changes in gene expression followed by mutations to facilitate tumor evolution. Importantly, this model suggests early loss of p53 and BRCA. Once chromosomal instability is set up by mutation in *TP53* and *BRCA* inactivation, gene copy number is the major determinant of progression of HGSC [34]. Potential biomarkers or therapeutic targets must consider the driver mutations and events that occur before the full development of carcinoma, when a multitude of mutations and copy number alterations occur to configure each individual tumor.

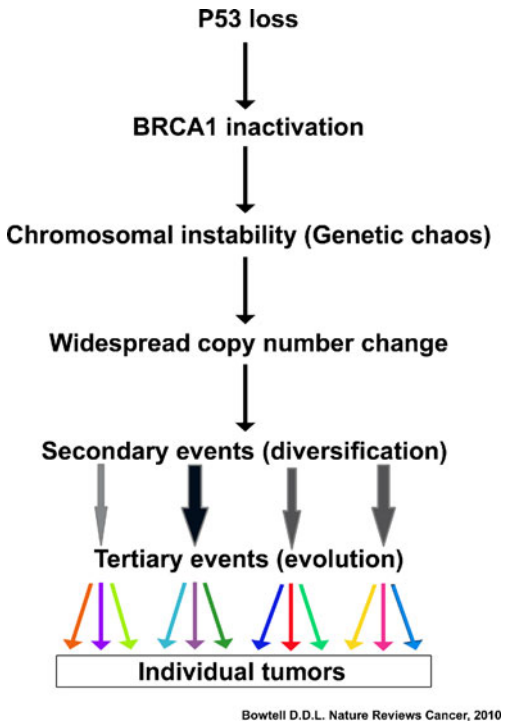

Fig. 4 Initiation and progression of high-grade serous ovarian cancer. This model proposes that the sequence of primary events were as follows: early p53 loss followed by BRCA loss, leading to deficiency in homologous recombination repair (HRR) of DSB, which triggers chromosomal instability (genetic chaos) and widespread copy number changes. Copy number change can be a driver of molecular subtype specification and results in global changes in gene expression. Subsequent mutations facilitate tumor progression. Modified from DD Bowtell [34]

Concerning heterogeneity of HGSC, we have recently described two molecular subtypes of this tumor based on distinct patterns of expression of genes involved in the PI3K–AKT pathway [39]. Expression of active caspase-3 in the tumor stroma (lymphocytes and macrophages) was associated with good prognosis and response to chemotherapy. Furthermore, co-expression of caspase-3 and X-linked inhibitor of apoptosis (XIAP) identified high-grade serous carcinomas with better prognosis. These findings indicate that there are different biological subtypes of HGSC.

After primary surgical debulking, most (70–80%) HGSCs show a response to platinum/taxane chemotherapy, but the majority of patients will subsequently experience a recurrence, at which point cure is not possible [8]. Recently, PARP inhibitors that target loss of BRCA function and inability to repair double-strand breaks in DNA have been used [40, 41].

Low-grade serous carcinomas

LGSCs are uncommon and account for less than 5% of all cases of ovarian carcinoma [42]. They frequently have a noninvasive serous borderline component (with or without micropapillary pattern) and most likely represent progression of serous borderline tumors beyond microinvasion. Whereas the presence of small foci of LGSC in an ovarian borderline tumor is associated with an excellent prognosis, patients with advanced stage disease fare less favorably. Nevertheless, the disease usually follows a relatively indolent course.

Microscopically, LGSCs show small papillae of tumor cells exhibiting uniform nuclei within variable amounts of hyalinized stroma, which often contains psammoma bodies (Fig. 1b). Uniformity of the nuclei is the principal criterion for distinguishing between LGSC and HGSC, with less than threefold variability [25]. This distinction has been shown to be highly reproducible [43]. Tumors showing nuclei of intermediate size often have *TP53* mutations and should be classified as HGSC [44]. LGSC rarely progress to high-grade tumors.

The biomarker expression profile of LGSC is similar to that of their high-grade counterparts. Only Ki-67 immunoreaction differs significantly between the two tumor types, with median Ki-67 labeling index of 2.5% in LGSC versus 22.4% in HGSC [10]. *BRAF* or *KRAS* mutations are present in LGSCs (38% and 19%, respectively). [21, 45]. LGSCs do not show chromosomal instability and lack the complex genetic abnormalities seen in HGSCs. LGSCs are not associated with BRCA germline mutations.

With regard to the distinction between LGSC and serous borderline tumor, micropapillarity, by itself, is not sufficient to warrant a diagnosis of carcinoma in the absence of invasion. If there are invasive foci measuring less than 10 mm^2, the tumor is considered to be borderline with microinvasion [46]. Tumors with larger invasive components are classified as LGSC. Histopathologically, invasive peritoneal implants and LGSC are identical lesions which are only distinguished by the timing of the disease and the volume of the tumor. Whereas invasive implants are early superficial lesions of microscopic or small macroscopic size (≤1–2 cm), LGSC frequently presents as bulky disease [3]. Although the independent origin of the invasive peritoneal implants associated with ovarian SBT cannot be completely excluded, we have recently demonstrated identical *BRAF* and *KRAS* mutations as well as identical LOH in a series of ovarian SBT and peritoneal implants. Such findings support a monoclonal origin of these tumors and the secondary nature of the implants [47].

The response rate to conventional therapy for LGSC is difficult to determine because this tumor type has only recently been recognized and existing data may reflect case series that include some cases of HGSC. Data from series of patients with serous borderline tumors who experience a recurrence as carcinoma, indicate that, in most cases, LGSC do not respond to conventional ovarian carcinoma chemotherapy [48].

Mucinous carcinomas

Mucinous tumors account for 10–15% of all primary ovarian tumors; however, approximately 80% are benign and most of the remainder are borderline tumors. If metastases to the ovary, particularly from the gastrointestinal tract, are carefully excluded, only 3–4% of ovarian carcinomas are of mucinous type. The cells of MCs may resemble those of the gastric pylorus, intestine, or endocervix [1, 2]; nevertheless, the vast majority of these tumors show gastrointestinal differentiation (Fig. 1c). The origin of these tumors is unknown. Large size (>13 cm) and unilaterality are features suggestive of a primary MC, while metastases are typically smaller and bilateral. Primary MCs of the ovary are usually confined to the ovary, without ovarian surface involvement or pseudomyxoma peritonei.

Malignant mucinous ovarian tumors are often heterogeneous. Benign-appearing, borderline, noninvasive carcinoma, and invasive components may coexist within an individual tumor and suggest tumor progression from benign to borderline and from borderline to carcinoma. Therefore, extensive sampling for histological examination is necessary [49]. The category of mucinous borderline tumor with intraepithelial carcinoma is used for those tumors that lack obvious stromal invasion but show areas, less than 10 mm^2, where the cytological features of the tumor cells are unequivocally malignant [50]. Mucinous borderline tumors with intraepithelial carcinoma have a very low risk of recurrence, of less than 5% [51].

Recently, MCs have been divided into two categories: (a) an *expansile* type without obvious stromal invasion, but exhibiting back-to-back or complex malignant glands with minimal or no intervening stroma, and exceeding 10 mm^2 in area (>3 mm in each of two linear dimensions) (Fig. 1c); and (b) an *infiltrative* type, showing evident stromal invasion in the form of glands, cell clusters, or individual cells, disorderly infiltrating the stroma and frequently associated with a desmoplastic stromal reaction [49, 50]. The expansile pattern of growth has also been referred to as the "noninvasive", "intraglandular", [52] or "confluent glandular" [53] pattern and is associated with a more favorable prognosis than the infiltrative pattern. A histopathological feature unique to mucinous tumors is the occasional finding of mural nodules of anaplastic carcinoma or high-grade sarcoma. When such nodules are localized in the wall of an unruptured cyst, the prognosis may be favorable, but such tumors may recur and do so as the anaplastic component [49, 54].

The gene expression profile of MCs differs from those of serous, endometrioid, and clear cell carcinomas [55]. As expected, MCs have genes that encode markers of intestinal differentiation such as *CDX2* and *KRAS*. *KRAS* mutations, which are an early event in mucinous tumorigenesis, are frequent in ovarian MCs [56]. Primary ovarian mucinous tumors are almost always (up to 80%) immunoreactive for cytokeratin 7 (CK7) whereas colorectal adenocarcinomas are usually CK7 negative [57]. Ovarian MCs are immunoreactive for CK20 in 65% of cases, but the reaction is typically weak and focal; staining for CDX-2 (nuclear immunoreaction) is similar [58]. In contrast, colorectal adenocarcinomas are diffusely and strongly reactive for CK20 and CDX-2. Loss of Dpc4 immunoreactivity occurs in almost 50% of metastatic carcinomas of the pancreas, whereas most primary ovarian MCs are focally or diffusely positive [59]. Human papilloma virus (HPV) DNA assessment may be helpful for distinguishing mucinous adenocarcinoma of the cervix metastatic to the ovary from a primary ovarian MC. p16 expression is also a reliable surrogate marker for HPV [60]. MCs are uniformly negative for ER and WT1, in contrast to endometrioid (ER+) and serous (ER+and WT1+) carcinomas.

Endometrioid carcinomas

Endometrioid tumors of the ovary closely mimic their uterine counterparts. ECs account for 10% of all ovarian carcinomas, occur most frequently in women of perimenopausal

age, and most are found at an early stage [1]. The ovarian tumors are bilateral in 28% of cases and are associated in 15–20% of cases with carcinoma of the endometrium [2, 61]. Most ECs are low-grade adenocarcinomas and seem to arise from endometriotic cysts. Up to 42% of cases have evidence of ipsilateral ovarian or pelvic endometriosis [1, 2]. Squamous differentiation occurs in 50% of cases [1] (Fig.1d). In contrast, high-grade ECs are morphologically indistinguishable from HGSCs and often express WT1. Gene expression profiling is also similar, suggesting that high-grade EC is not a distinct tumor type [62].

It has been recognized that atypical endometriosis is the precursor lesion of endometrioid and clear cell carcinomas of the ovary, and a direct transition from ovarian atypical endometriosis to endometrioid or clear cell carcinomas has been described in 15–32% of cases [63] (Fig. 5). In cases of ovarian endometrioid carcinoma associated with endometriosis, common genetic alterations have been encountered in the adjacent endometriosis, atypical endometriosis, and adenocarcinoma [64]. In mice harboring *KRAS* mutations that result in the development of benign lesions reminiscent of endometriosis, deletion of *PTEN* leads to the induction of invasive endometrioid carcinoma [65]. These results indicate that inactivation of tumor suppressor genes such as *PTEN* may represent early events in the malignant transformation of endometriosis [20].

With the recent discovery of AT-rich interactive domain 1A gene (*ARID1A*) mutations in endometrioid and clear cell carcinomas as well as in adjacent endometriosis, there is renewed interest in the molecular events that occur in precursor lesions [66]. *ARID1A* is a component of the SWI–SNF-A complex, a large, multiprotein chromatin remodeling complex which is known to both enhance and repress transcription [67]. It behaves as a tumor suppressor gene. BAF250 protein, encoded by *ARID1A*, plays a crucial role in chromatin remodeling. The question has been raised whether endometriotic lesions should be analyzed for expression of BAF250. Also, if patients with endometriotic lesions that show loss of expression should be viewed as being at high risk for the development of CCC or endometrioid ovarian cancers [68].

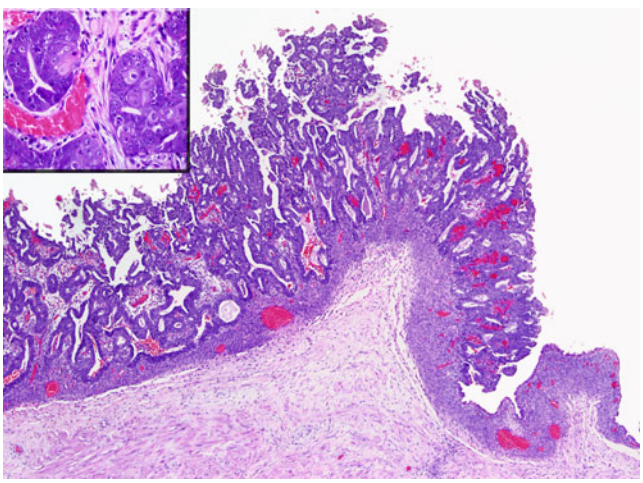

Fig. 5 Endometrioid carcinoma arising from endometriosis. The *inset* shows squamous differentiation

Somatic mutations of the beta-catenin (*CTNNB1*) and *PTEN* genes are the most common genetic abnormalities identified in ovarian ECs [19, 69, 70]. Compared with uterine ECs, ovarian ECs have a similar frequency of beta-catenin abnormalities but lower rate of microsatellite instability (MI) and *PTEN* alterations [70]. *CTNNB1* mutations, which occur in 38%–50% of cases, are associated with squamous differentiation, low tumor grade, and favorable outcome [71]. Mutations have been described in exon 3 (codons 32, 33, 37, and 41) and involve the phosphorylation sequence for glycogen synthase kinase 3-beta. These mutations probably render a fraction of cellular beta-catenin insensitive to APC-mediated downregulation and are responsible for its accumulation in the nuclei of the tumor cells. Beta-catenin is immunohistochemically detectable in carcinoma cells in more than 80% of the cases.

PTEN inactivation results in activation of the PI3K-AKT signaling pathway that inhibits apoptosis. *PTEN* is mutated in approximately 20% of ovarian ECs and in 46% of those with 10q23 LOH. *PTEN* mutations occur between exons 3 and 8. The finding of LOH at 10q23 and somatic *PTEN* mutations in endometriotic cysts adjacent to ECs with similar genetic alterations provides additional evidence for the precursor role of endometriosis in ovarian carcinogenesis [20]. An alternative mechanism for activation of the PI3K signaling in ECs is through activating mutations of *PIK3CA*, which encodes the p110 catalytic subunit of PI3K. *PIK3CA* mutations in exons 9 and 20 have been identified in 20% of ovarian ECs and CCCs but in only 2% of HGSC [72]. *PIK3CA* mutations are associated with adverse prognostic parameters [73, 74].

ECs are the types most commonly encountered in patients with hereditary non-polyposis colon cancer syndrome. The reported frequency of MI in ovarian ECs ranges from 12.5% to 19% [75, 76]. Like endometrial carcinomas, ovarian ECs with MI follow the same process of MLH-1 promoter methylation and frameshift mutations at coding mononucleotide repeat microsatellites [70]. ECs are immunoreactive for vimentin, cytokeratins (CK7, 97%; CK20, 13%), epithelial membrane antigen, and estrogen and progesterone receptors. Immunoreaction for alpha-inhibin, WT-1, and calretinin are negative in most ECs. The median Ki-67 labeling index for endometrioid is 8.2% [10].

Simultaneous carcinomas of the uterine corpus and ovary occur in 15–20% of ovarian tumors and in approximately 5% of uterine tumors [2]. Both tumors are of endometrioid type in the majority of cases. In addition to prognostic

implications, accurate diagnosis as independent primaries or metastases is necessary for appropriate staging and treatment. Assessment of conventional pathological features including tumor size, histological type and grade, pattern of tumor growth, vascular invasion, and coexisting atypical hyperplasia or endometriosis allows the distinction between primary and metastatic tumors in most cases [2]. Occasionally, however, the differential diagnosis can be difficult or impossible as the tumors may show overlapping features [2]. In such cases, patient follow-up is the single most conclusive factor, but ancillary techniques may help to establish the correct diagnosis.

Clonality analysis using LOH and gene mutation is useful in the distinction of independent primary carcinomas from metastatic carcinomas, provided the diagnosis does not rely exclusively on a single molecular result and the molecular data are interpreted in the light of appropriate clinical and pathologic findings [61]. According to a recent study [61], the frequency of molecular alterations in both independent and metastatic tumors, including MI and *PTEN* mutations, is higher than that observed in single sporadic tumors. Nuclear immunoreactivities for β-catenin and *CTNNB1* mutations were restricted to independent uterine and ovarian tumors and were absent in metastatic tumors. These findings correlated with the clinical outcome [61].

EC is the type of ovarian carcinoma with the most favorable prognosis. Although their lower grade and lower stage account for much of the favorable prognosis, responsiveness to chemotherapy may also be a contributory factor.

Clear cell carcinomas

CCCs account for approximately 10% of ovarian carcinomas and patients typically present with stage 1 or 2 disease. Tumors are rarely bilateral. CCCs are associated with an unfavorable prognosis when they present at advanced stage [77]. As with EC, there is an association with endometriosis, and CCCs associated with endometriosis have a favorable prognosis [78].

The presence of clear cells alone is not sufficient for a diagnosis of CCC, as cells with clear cytoplasm can be seen in HGSC and EC. Besides the characteristic clear or hobnail cells with eccentric, rounded, and bulbous nuclei, the diagnosis is based on the following architectural and cytological findings: (a) multiple complex papillae; (b) densely hyaline basement membrane material expanding the cores of the papillae (Fig. 1e); and (c) hyaline bodies, which are present in approximately 25% of cases. Mitoses are less frequent than in other types of ovarian carcinomas (usually less than 5 /10 HPFs).

CCCs lack the *BRCA* abnormalities, chromosomal instability, or complex karyotypes of HGSC [79]. Recently, it has been found that nearly half the CCCs (46–57%) carry *ARID1A* mutations and lack BAF250 protein [66]. In two cases, *ARID1A* mutations and loss of BAF250a expression were found in the tumor and adjacent endometriosis but not in distant endometriosis. This finding suggests that *ARID1A* inactivation occurs early during malignant transformation of endometriosis [66]. CCCs are usually positive for HNF1-beta (>90%) and are negative for ER and WT1 in more than 95% of cases [10, 28].

Hepatocyte nuclear factor-1beta (HNF-1beta) is upregulated in ovarian clear cell tumors, including benign, borderline tumors, and carcinomas [80]. This transcription factor facilitates glycogen synthesis and is expressed in mid-to-late secretory and gestational endometrium (Arias–Stella reaction) [80], atypical and inflammatory endometriosis, and clear cell carcinoma [80]. HNF-1beta regulates several specific genes of clear cell carcinoma, including dipeptidyl peptidase IV (glycogen synthesis), osteopontin (progesterone-regulated endometrial secretory protein), angiotensin converting enzyme 2 (ferritin induction, iron deposition, antiapoptosis), annexin 4 (paclitaxel resistance), and *UGT1A1* (detoxification) [81]. Thus, HNF-1beta appears to play an important role in the pathogenesis and behavior of clear cell carcinoma.

The RHO GTPase family of proteins is involved in tumor progression through cytoskeleton regulation [82]. Compared with HGSCs, CDC42 mRNA levels are significantly lower in CCCs. In contrast, the expression of Rho GDP dissociation inhibitor gamma (ARHGDIG) mRNA is higher in CCCs than HGSCs. In patients with clear cell carcinoma, high expression of ARHGDIG mRNA is associated with low stage, fewer recurrences, and better survival [83]. Thus, RHO GTPase inhibition could explain the fact that clear cell carcinomas of the ovary are found at stage I in about 25% of cases.

CCCs are less likely to respond to chemotherapy than HGSCs [8]. The reported differences in response rates (15–45%) may reflect inclusion of HGSC with clear cell change in some case series. Whereas highly proliferative cells that lack the ability to repair double-stranded DNA (i.e., HGSC cells) show sensitivity to platinum-based chemotherapy, the less proliferative, genomically stable cells of CCC are less sensitive to platinum compounds [84].

Mixed epithelial tumors

As noted previously, if tumors with an undifferentiated component are classified based on the areas showing a recognizable growth pattern, they usually will end up classified as HGSC. Most tumors considered in the past to be mixed high-grade serous/endometrioid, high-grade serous/clear cell, or high-grade serous/transitional cell are, based on

molecular studies, better classified as HGSC. One of the most common mixed epithelial carcinomas of ovary are EC/CCC. These tumors are often associated with endometriosis and, based on the presence of a CCC component, it is appropriate to consider them high-grade carcinomas.

Conclusions

The five main types of ovarian carcinoma (in descending order of frequency: HGSC, CCC, EC, MC, and LGSC) account for 98% of ovarian carcinomas, can be reproducibly diagnosed, and are inherently different diseases, as indicated by differences in risk factors, molecular genetic abnormalities, natural history, and response to chemotherapy. Even if HGSC comprise 70% of the total, lumping the other four types together for classifying ovarian carcinomas into just two types ("types I and II") is artificial and limits progress in understanding the biology or improving the treatment of the less common types of ovarian carcinomas. For a successful type-specific treatment of ovarian carcinoma, reproducible histopathological diagnosis of the tumor cell type is critical.

Even if a mesothelial origin cannot be excluded, there is compelling evidence that a significant number of cases of HGSC originate in the distal fallopian tube. The identification of a precursor lesion (TIC) within the fallopian tube fimbria opens new ways for prevention in the general population. Given that a significant number of "ovarian cancers" originate in the fallopian tube, removal during surgery of the fallopian tubes while keeping the hormone producing ovaries in place would prevent the adverse effects of early menopause such as osteoporosis or vasomotor symptoms.

Although endometriosis is essentially a benign disease, it does exhibit some features reminiscent of malignancy such as metastatic potential and monoclonality. Whereas the incidence of malignant tumors arising from ovarian endometriosis is minimal, the incidence of endometriosis in women with ovarian cancer is more significant. It has been recognized that atypical endometriosis is the precursor lesion of EC and CCC of the ovary and a direct transition from ovarian atypical endometriosis to EC or CCC has been described. The question has been raised whether the finding in endometriotic lesions of the genetic alterations frequently encountered in EC and CCC should be interpreted as evidence of high risk of malignant transformation.

Conflicts of interest The author declares that there are no conflicts of interest

References

1. Prat J (2004) Pathology of the ovary. Saunders, Philadelphia
2. Lee KR, Tavassoli FA, Prat J et al (2003) Surface epithelial-stromal tumours (Ch 2: tumours of the ovary and peritoneum). In: Tavassoli FA, Devilee P (eds) World Health Organization classification of tumours: pathology and genetics of tumours of the breast and female genital organs. IARC Press, Lyon, pp 117–145
3. Shvartsman HS, Sun CC, Bodurka CC, Mahajan V, Crispens M, Lu KH, Deavers MT, Malpica A, Silva EG, Gershenson DM (2007) Comparison of the clinical behavior of newly diagnosed stages II–IV low-grade serous carcinoma of the ovary with that of serous ovarian tumors of low malignant potential that recur as low-grade serous carcinoma. Gynecol Oncol 105:625–629
4. Stewart BW, Kleihues P (2003). World Cancer Report (IARC Press)
5. Jass JR (2006) Colorectal cancer: a multipathway disease. Crit Rev Oncog 12:273–287
6. Gilks CB, Prat J (2009) Ovarian carcinoma pathology and genetics: recent advances. Hum Pathol 40:1213–1223
7. Takano M, Kikuchi Y, Yaegashi N, Kuzuya K, Ueki M, Tsuda H, Suzuki M, Kigawa J, Takeuchi S, Tsuda H, Moriya T, Sugiyama T (2006) Clear cell carcinoma of the ovary: a retrospective multicentre experience of 254 patients with complete surgical staging. Br J Cancer 94:1369–1374
8. du Bois A, Lück HJ, Meier W, Adams HP, Möbus V, Costa S, Bauknecht T, Richter B, Warm M, Schröder W, Olbricht S, Nitz U, Jackisch C, Emons G, Wagner U, Kuhn W, Pfisterer J (2003) A randomized clinical trial of cisplatin/paclitaxel versus carboplatin/paclitaxel as first-line treatment of ovarian cancer. J Natl Cancer Inst 95:1320–1329
9. Fountain J, Trimble E, Birrer MJ (2006) Summary and discussion of session recommendations. Gynecol Oncol 103:S23–S25
10. Köbel M, Kalloger SE, Boyd N, McKinney S, Mehl E, Palmer C, Leung S, Bowen NJ, Ionescu DN, Rajput A, Prentice LM, Miller D, Santos J, Swenerton K, Gilks CB, Huntsman D (2008) Ovarian carcinoma subtypes are different diseases: implications for biomarker studies. PLoS Med 5:e232
11. Kurman RJ, Shih IM (2010) The origin and pathogenesis of epithelial ovarian cancer: a proposed unifying theory. Am J Surg Pathol 34:433–443
12. Piek JM, van Diest PJ, Zweemer RP, Jansen JW, Poort-Keesom RJ, Menko FH, Gille JJ, Jongsma AP, Pals G, Kenemans P, Verheijen RH (2001) Dysplastic changes in prophylactically removed fallopian tubes of women predisposed to developing ovarian cancer. J Pathol 195:451–456
13. Piek JM, van Diest PJ, Zweemer RP, Kenemans P, Verheijen RH (2001) Tubal ligation and risk of ovarian cancer. Lancet 358:844
14. Medeiros F, Muto MG, Lee Y, Elvin JA, Callahan MJ, Feltmate C, Garber JE, Cramer DW, Crum CP (2006) The tubal fimbria is a preferred site for early adenocarcinoma in women with familial ovarian cancer syndrome. Am J Surg Pathol 30:230–236
15. Kindelberger DW, Lee Y, Miron A, Hirsch MS, Feltmate C, Medeiros F, Callahan MJ, Garner EO, Gordon RW, Birch C, Berkowitz RS, Muto MG, Crum CP (2007) Intraepithelial carcinoma of the fimbria and pelvic serous carcinoma: evidence for a causal relationship. Am J Surg Pathol 31:161–169
16. Lee Y, Miron A, Drapkin R, Nucci MR, Medeiros F, Saleemuddin A, Garber J, Birch C, Mou H, Gordon RW, Cramer DW, McKeon FD, Crum CP (2007) A candidate precursor to serous carcinoma that originates in the distal fallopian tube. J Pathol 211:26–35
17. Folkins AK, Jarboe EA, Saleemuddin A, Lee Y, Callahan MJ, Drapkin R, Garber JE, Muto MG, Tworoger S, Crum CP (2008) A candidate precursor to pelvic serous cancer (p53 signature) and

its prevalence in ovaries and fallopian tubes from women with *BRCA* mutations. Gynecol Oncol 109:168–173
18. Jarboe E, Folkins A, Nucci MR, Kindelberger D, Drapkin R, Miron A, Lee Y, Crum CP (2008) Serous carcinogenesis in the fallopian tube: a descriptive classification. Int J Gynecol Pathol 27:1–9
19. Obata K, Morland SJ, Watson RH, Hitchcock A, Chenevix-Trench G, Thomas EJ, Campbell IG (1998) Frequent *PTEN/MMAC* mutations in endometrioid but not serous or mucinous epithelial ovarian tumors. Cancer Res 58:2095–2097
20. Sato N, Tsunoda H, Nishida M, Morishita Y, Takimoto Y, Kubo T, Noguchi M (2000) Loss of heterozygosity on 10q23.3 and mutation of the tumor suppressor gene *PTEN* in benign endometrial cyst of the ovary: possible sequence progression from benign endometrial cyst to endometrioid carcinoma and clear cell carcinoma of the ovary. Cancer Res 60:7052–7056
21. Singer G, Oldt R 3rd, Cohen Y, Wang BG, Sidransky D, Kurman RJ, IeM S (2003) Mutations in *BRAF* and *KRAS* characterize the development of low-grade ovarian serous carcinoma. J Nat Cancer Inst 95:484–486
22. Singer G, Stöhr R, Cope L, Dehari R, Hartmann A, Cao DF, Wang TL, Kurman RJ, IeM S (2005) Patterns of p53 mutations separate ovarian serous borderline tumors and low- and high-grade carcinomas and provide support for a new model of ovarian carcinogenesis. Am J Surg Pathol 29:218–224
23. Laury AR, Ning G, Quick CM, Nucci MR, Parast MM, McKeon FD, Xian W, Crum CP (2011) Fallopian tube correlates of serous borderline tumors. Am J Surg Pathol 35:1759–1765
24. Kurman RJ, Vang R, Junge J, Hannibal CG, Kjaer SK, Shih Ie M (2011) Papillary tubal hyperplasia: the putative precursor of ovarian atypical proliferative (borderline) serous tumors, noninvasive implants, and endosalpingiosis. Am J Surg Pathol 35:1605–1614
25. Malpica A, Deavers MT, Lu K, Bodurka DC, Atkinson EN, Gershenson DM, Silva EG (2004) Grading ovarian serous carcinoma using a two-tier system. Am J Surg Pathol 28:496–504
26. Gilks CB, Ionescu DN, Kalloger SE, Köbel M, Irving J, Clarke B, Santos J, Le N, Moravan V, Swenerton K (2008) Tumor cell type can be reproducibly diagnosed and is of independent prognostic significance in patients with maximally debulked ovarian carcinoma. Hum Pathol 39:1239–1251
27. Al-Hussaini M, Stockman A, Foster H, Mc Cluggage WG (2004) WT-1 assists in distinguishing ovarian from uterine serous carcinoma and in distinguishing between serous and endometrioid ovarian carcinoma. Histopathology 44:109–105
28. Köbel M, Kalloger SE, Carrick J, Huntsman D, Asad H, Oliva E, Ewanowich CA, Soslow RA, Gilks CB (2009) A limited panel of immunomarkers can reliably distinguish between clear cell and high-grade serous carcinoma of the ovary. Am J Surg Pathol 33:14–21
29. Karst AM, Levanon K, Duraisamy S, Liu JF, Hirsch MS, Hecht JL, Drapkin R (2011) Stathmin 1, a marker of PI3K pathway activation and regulator of microtubule dynamics, is expressed in early pelvic serous carcinomas. Gynecol Oncol 123:5–12
30. Risch HA, McLaughlin JR, Cole DE, Rosen B, Bradley L, Fan I, Tang J, Li S, Zhang S, Shaw PA, Narod SA (2006) Population *BRCA1* and *BRCA2* mutation frequencies and cancer penetrances: a kin-cohort study in Ontario, Canada. J Natl Cancer Inst 98:1694–1706
31. Venkitaraman AR (2009) Linking the cellular functions of *BRCA* genes to cancer pathogenesis and treatment. Annu Rev Pathol 4:461–487
32. Geisler JP, Hatterman-Zogg MA, Rathe JA, Buller RE (2002) Frequency of *BRCA1* dysfunction in ovarian cancer. J Natl Cancer Inst 94:61–67
33. Esteller M, Silva JM, Dominguez G, Bonilla F, Matias-Guiu X, Lerma E, Prat J, Harkes I, Repasky EA, Gabrielson E, Schutte M, Baylin SB, Herman JG (2000) Promoter hypermethylation is a cause of *BRCA1* inactivation in sporadic breast and ovarian tumors. J Natl Cancer Inst 92:564–569
34. Bowtell DD (2010) The genesis and evolution of high-grade serous ovarian cancer. Nat Rev Cancer 10:803–808
35. Levanon K, Ng V, Piao HY, Zhang Y, Chang MC, Roh MH, Kindelberger DW, Hirsch MS, Crum CP, Marto JA, Drapkin R (2010) Primary ex vivo cultures of human fallopian tube epithelium as a model for serous ovarian carcinogenesis. Oncogene 29:1103–1113
36. Powell CB, Kenley E, Chen LM, Crawford B, McLennan J, Zaloudek C, Komaromy M, Beattie M, Ziegler J (2005) Risk-reducing salpingo-oophorectomy in *BRCA* mutation carriers: role of serial sectioning in the detection of occult malignancy. J Clin Oncol 23:127–132
37. Pothuri B, Leitao MM, Levine DA, Viale A, Olshen AB, Arroyo C, Bogomolniy F, Olvera N, Lin O, Soslow RA, Robson ME, Offit K, Barakat RR, Boyd J (2010) Genetic analysis of the early natural history of epithelial ovarian carcinoma. PLoS One 5:e10358
38. Norquist BM, Garcia RL, Allison KH, Jokinen CH, Kernochan LE, Pizzi CC, Barrow BJ, Goff BA, Swisher EM (2010) The molecular pathogenesis of hereditary ovarian carcinoma: alterations in the tubal epithelium of women with *BRCA1* and *BRCA2* mutations. Cancer 116:5261–5271
39. Espinosa I, Catasus L, Canet B, D'Angelo E, Muñoz J, Prat J (2011) Gene expression analysis identifies two groups of ovarian high-grade serous carcinomas with different prognosis. Mod Pathol 24:846–854
40. Farmer H, McCabe N, Lord CJ, Tutt AN, Johnson DA, Richardson TB, Santarosa M, Dillon KJ, Hickson I, Knights C, Martin NM, Jackson SP, Smith GC, Ashworth A (2005) Targeting the DNA repair defectin BRCA mutant cells as a therapeutic strategy. Nature 434:917–921
41. Tutt AN, Lord CJ, McCabe N, Farmer H, Turner N, Martin NM, Jackson SP, Smith GC, Ashworth A (2005) Exploiting the DNA repair defectin BRCA mutant cells in the design of new therapeutic strategies for cancer. Cold Spring Harb Symp Quant Biol 70:139–148
42. Gershenson DM, Sun CC, Lu KH, Coleman RL, Sood AK, Malpica A, Deavers MT, Silva EG, Bodurka DC (2006) Clinical behavior of stage II–IV low-grade serous carcinoma of the ovary. Obstet Gynecol 108:361–368
43. Malpica A, Deavers MT, Tornos C, Kurman RJ, Soslow R, Seidman JD, Munsell MF, Gaertner E, Frishberg D, Silva EG (2007) Inter-observer and intraobserver variability of a two-tier system for grading ovarian serous carcinoma. Am J Surg Pathol 31:1203–1208
44. Ayhan A, Kurman RJ, Yemelyanova A, Vang R, Logani S, Seidman JD, IeM S (2009) Defining the cut-point between low- and high-grade ovarian serous carcinomas: a clinicopathologic and molecular genetic analysis. Am J Surg Pathol 33:1220–1224
45. Jones S, Wang T-L, Kurman RJ, Nakayama K, Velculescu VE, Vogelstein B, Kinzler KW, Papadopoulos N, Shih I-M (2012) Low-grade serous carcinomas of the ovary contain very few point mutations. J Pathol 226:413–420
46. Bell DA, Longacre TA, Prat J, Kohn EC, Soslow RA, Ellenson LH, Malpica A, Stoler MH, Kurman RJ (2004) Serous borderline (low malignant potential, atypical proliferative) ovarian tumors: workshop perspectives. Hum Pathol 35:934–948
47. Sieben NL, Roemen GMJM, Oosting J, Fleuren GJ, van Engeland M, Prat J (2006) Clonal analysis favours a monoclonal origin for serous borderline tumours with peritoneal implants. J Pathol 210:405–411
48. Crispens MA, Bodurka D, Deavers M, Lu K, Silva EG, Gershenson DM (2002) Response and survival in patients with progressive or

recurrent serous ovarian tumors of low malignant potential. Obstet Gynecol 99:3–10
49. Rodriguez IM, Prat J (2002) Mucinous tumors of the ovary: a clinicopathologic analysis of 75 borderline tumors (of intestinal type) and carcinomas. Am J Surg Pathol 26:139–152
50. Lee KR, Scully RE (2000) Mucinous tumors of the ovary—A clinicopathologic study of 196 borderline tumors (of intestinal type) and carcinomas, including an evaluation of 11 cases with "pseudomyxomaperitonei". Am J Surg Pathol 24:1447–1464
51. Silverberg SG, Bell DA, Kurman RJ, Seidman JD, Prat J, Ronnett BM, Copeland L, Silva E, Gorstein F, Young RH (2004) Borderline ovarian tumors: key points and workshop summary. Hum Pathol 35:910–917
52. Hoerl HD, Hart WR (1998) Primary ovarian mucinous cystadenocarcinomas: a clinicopathologic study of 49 cases with long term follow-up. Am J Surg Pathol 22:1449–1462
53. Riopel MA, Ronnett BM, Kurman RJ (1999) Evaluation of diagnostic criteria and behavior of ovarian intestinal-type mucinous tumors. Atypical proliferative (borderline) tumors and intraepithelial, microinvasive, invasive and metastatic carcinomas. Am J Surg Pathol 23:617–635
54. Provenza C, Young RH, Prat J (2008) Anaplastic carcinoma in mucinous ovarian tumors: a clinicopathologic study of 34 cases emphasizing the crucial impact of stage on prognosis, their histologic spectrum, and overlap with sarcoma-like mural nodules. Am J Surg Pathol 32:383–389
55. Heinzelmann-Schwarz VA, Gardiner-Garden M, Henshall SM, Scurry JP, Scolyer RA, Smith AN, Bali A, Vanden Bergh P, Baron-Hay S, Scott C, Fink D, Hacker NF, Sutherland RL, O'Brien PM (2006) A distinct molecular profile associated with mucinous epithelial ovarian cancer. Br J Cancer 94:904–91353
56. Cuatrecasas M, Villanueva A, Matias-Guiu X, Prat J (1997) *K-ras* mutations in mucinous ovarian tumors. A clinicopathologic and molecular study of 95 cases. Cancer 79:1581–1586
57. Park SY, Kim HS, Hong EK, Kim WH (2002) Expression of cytokeratins 7 and 20 in primary carcinomas of the stomach and colorectum and their value in the differential diagnosis of metastatic carcinomas to the ovary. Hum Pathol 33:1078–1085
58. Vang R, Gown AM, Wu LS, Barry TS, Wheeler DT, Yemelyanova A, Seidman JD, Ronnett BM (2006) Immunohistochemical expression ofCDX2 in primary ovarian mucinous tumors and metastatic mucinous carcinomas involving the ovary: comparison with CK20 and correlation with coordinate expression of CK7. Mod Pathol 19:1421–1428
59. Ji H, Isacson C, Seidman J, Kurman RJ, Ronnett BM (2002) Cytokeratins 7and 20, Dpc4, and MUC5AC in the distinction of metastatic mucinous carcinomas in the ovary from primary ovarian mucinous tumors: Dpc4assists in identifying metastatic pancreatic carcinomas. Int J Gynecol Pathol 21:391–400
60. Ronnett BM, Yemelyanova AV, Vang R, Gilks CB, Miller D, Gravitt PE, Kurman RJ (2008) Endocervical adenocarcinomas with ovarian metastases: analysis of 29 cases with emphasis on minimally invasive cervical tumors and the ability of the metastases to simulate primary ovarian neoplasms. Am J Surg Pathol 32:1835–1853
61. Irving JA, Catasús L, Gallardo A, Bussaglia E, Romero M, Matias-Guiu X, Prat J (2005) Synchronous endometrioid carcinomas of the uterine corpus and ovary: alterations in the beta-catenin (*CTNNB1*) pathway are associated with independent primary tumors and favorable prognosis. Hum Pathol 36:605–619
62. Tothill RW, Tinker AV, George J, Brown R, Fox SB, Lade S, Johnson DS, Trivett MK, Etemadmoghadam D, Locandro B, Traficante N, Fereday S, Hung JA, Chiew YE, Haviv I, Australian Ovarian Cancer Study Group, Gertig D, DeFazio A, Bowtell D (2008) Novel molecular subtypes of serous and endometrioid ovarian cancer linked to clinical outcome. Clin Cancer Res 14:5198–5208
63. Sainz de la Cuesta R, Eichhorn JH, Rice LW, Fuller AF Jr, Nikrui N, Goff BA (1996) Histologic transformation of benign endometriosis to early epithelial ovarian cancer. Gynecol Oncol 60:238–244
64. Jiang X, Morland SJ, Hitchcock A, Thomas EJ, Campbell IG (1998) Allelotyping of endometriosis with adjacent ovarian carcinoma reveals evidence of a common lineage. Cancer Res 58:1707–1712
65. Dinulescu DM, Ince TA, Quade BJ, Shafer SA, Crowley D, Jacks T (2005) Role of K-ras and *PTEN* in the development of mouse models of endometriosis and endometrioid ovarian cancer. Nat Med 11:63–70
66. Wiegand KC, Shah SP, Al-Agha OM, Zhao Y, Tse K, Zeng T, Senz J, McConechy MK, Anglesio MS, Kalloger SE, Yang W, Heravi-Moussavi A, Giuliany R, Chow C, Fee J, Zayed A, Prentice L, Melnyk N, Turashvili G, Delaney AD, Madore J, Yip S, McPherson AW, Ha G, Bell L, Fereday S, Tam A, Galletta L, Tonin PN, Provencher D, Miller D, Jones SJ, Moore RA, Morin GB, Oloumi A, Boyd N, Aparicio SA, Shih Ie M, Mes-Masson AM, Bowtell DD, Hirst M, Gilks B, Marra MA, Huntsman DG (2010) *ARID1A* mutations in endometriosis-associated ovarian carcinomas. N Engl J Med 363:1532–1543
67. Lemon B, Inouye C, King DS, Tjian R (2001) Selectivity of chromatin-remodelling cofactors for ligand-activated transcription. Nature 414:924–928
68. Birrer MJ (2010) The origin of ovarian cancer—is it getting clearer? N Engl J Med 363:1574–1575
69. Palacios J, Gamallo C (1998) Mutations in the beta-catenin gene (*CTNNB1*) in endometrioid ovarian carcinomas. Cancer Res 58:1344–1347
70. Catasús L, Bussaglia E, Rodriguez I, Gallardo A, Pons C, Irving JA, Prat J (2004) Molecular genetic alterations in endometrioid carcinomas of the ovary: similar frequency of beta-catenin abnormalities but lower rate of microsatellite instability and *PTEN* alterations than in uterine endometrioid carcinomas. Hum Pathol 35:1360–1368
71. Gamallo C, Palacios J, Moreno G, Calvo de Mora J, Suárez A, Armas A (1999) Beta-catenin expression pattern in stage I and II ovarian carcinomas: relationship withbeta-catenin gene mutations, clinicopathological features, and clinical outcome. Am J Pathol 155:527–536
72. Campbell IG, Russell SE, Choong DY, Montgomery KG, Ciavarella ML, Hooi CS, Cristiano BE, Pearson RB, Phillips WA (2004) Mutation of the *PIK3CA* gene in ovarian and breast cancer. Cancer Res 64:7678–7681
73. Catasus L, Gallardo A, Cuatrecasas M, Prat J (2008) PIK3CA mutations in the kinase domain (exon 20) of uterine endometrial adenocarcinomas are associated with adverse prognostic parameters. Mod Pathol 21:131–139
74. Willner J, Wurz K, Allison KH, Galic V, Garcia RL, Goff BA, Swisher EM (2007) Alternate molecular genetic pathways in ovarian carcinomas of common histological types. Hum Pathol 38:607–613
75. Gras E, Catasus L, Argüelles R, Moreno-Bueno G, Palacios J, Gamallo C, Matias-Guiu X, Prat J (2001) Microsatellite instability, MLH-1 promoter hypermethylation, and frameshift mutations at coding mononucleotide repeat microsatellites in ovarian tumors. Cancer 92:2829–2836
76. Moreno-Bueno G, Gamallo C, Perez-Gallego L, Calvo de Mora J, Suarez A, Palacios J (2001) Beta-catenin expression pattern, beta-catenin gene mutations, and microsatellite instability in endometrioid ovarian carcinomas and synchronous endometrial carcinomas. Diagn Mol Pathol 10:116–122
77. Sugiyama T, Kamura T, Kigawa J, Terakawa N, Kikuchi Y, Kita T, Suzuki M, Sato I, Taguchi K (2000) Clinical characteristics of clear cell carcinoma of the ovary: a distinct histologic type with poor

prognosis and resistance to platinum based chemotherapy. Cancer 88:2584–2589
78. Komiyama S, Aoki D, Tominaga E, Susumu N, Udagawa Y, Nozawa S (1999) Prognosis of Japanese patients with ovarian clear cell carcinoma associated with pelvic endometriosis: clinicopathologic evaluation. Gynecol Oncol 72:342–346
79. Press JZ, De Luca A, Boyd N, Young S, Troussard A, Ridge Y, Kaurah P, Kalloger SE, Blood KA, Smith M, Spellman PT, Wang Y, Miller DM, Horsman D, Faham M, Gilks CB, Gray J, Huntsman DG (2008) Ovarian carcinomas with genetic and epigenetic *BRCA1* loss have distinct molecular abnormalities. BMC Cancer 8:17
80. Kato N, Sasou S, Motoyama T (2006) Expression of hepatocyte nuclear factor-1beta (HNF-1beta) in clear cell tumors and endometriosis of the ovary. Mod Pathol 19:83–89
81. Kobayashi H, Yamada Y, Kanayama S, Furukawa N, Noguchi T, Haruta S, Yoshida S, Sakata M, Sado T, Oi H (2009) The role of hepatocyte nuclear factor-1beta in the pathogenesis of clear cell carcinoma of the ovary. Int J Gynecol Cancer 19:471–479
82. Horiuchi A, Imai T, Wang C, Ohira S, Feng Y, Nikaido T, Konishi I (2003) Upregulation of small GTPases, RhoA and RhoC, is associated with tumor progression in ovarian carcinoma. Lab Invest 83:861–870
83. Canet B, Pons C, Espinosa I, Prat J (2011) Ovarian clear cell carcinomas: RHO GTPases may contribute to explain their singular biologic behavior. Hum Pathol 42:833–839
84. Itamochi H, Kigawa J, Sugiyama T, Kikuchi Y, Suzuki M, Terakawa N (2002) Low proliferation activity may be associated with chemoresistance in clear cell carcinoma of the ovary. Obstet Gynecol 100:281–287

Virchows Arch (2012) 460:251–259
DOI 10.1007/s00428-012-1204-4

ORIGINAL ARTICLE

Decentral gene expression analysis for ER+/Her2− breast cancer: results of a proficiency testing program for the EndoPredict assay

Carsten Denkert · Ralf Kronenwett · Werner Schlake · Kerstin Bohmann · Roland Penzel · Karsten E. Weber · Heinz Höfler · Ulrich Lehmann · Peter Schirmacher · Katja Specht · Margaretha Rudas · Hans-Heinrich Kreipe · Peter Schraml · Gudrun Schlake · Zsuzsanna Bago-Horvath · Frank Tiecke · Zsuzsanna Varga · Holger Moch · Marcus Schmidt · Judith Prinzler · Dontscho Kerjaschki · Bruno Valentin Sinn · Berit Maria Müller · Martin Filipits · Christoph Petry · Manfred Dietel

Received: 7 November 2011 / Revised: 1 January 2012 / Accepted: 25 January 2012 / Published online: 28 February 2012
© The Author(s) 2012. This article is published with open access at Springerlink.com

Abstract Gene expression profiles provide important information about the biology of breast tumors and can be used to develop prognostic tests. However, the implementation of quantitative RNA-based testing in routine molecular pathology has not been accomplished, so far. The EndoPredict assay has recently been described as a quantitative RT-PCR-based multigene expression test to identify a subgroup of hormone–receptor-positive tumors that have an excellent prognosis with endocrine therapy only. To transfer this test from bench to bedside, it is essential to evaluate the test–performance in a multicenter setting in different molecular pathology laboratories. In this study, we have evaluated the EndoPredict (EP) assay in seven different molecular pathology laboratories in Germany, Austria, and Switzerland. A

C. Denkert (✉) · J. Prinzler · B. V. Sinn · B. M. Müller · M. Dietel
Institute of Pathology, Charité Hospital,
Campus Mitte, Schumannstr. 20/21,
10117 Berlin, Germany
e-mail: carsten.denkert@charite.de

R. Kronenwett · K. Bohmann · K. E. Weber · C. Petry
Sividon Diagnostics GmbH,
50829 Cologne, Germany

W. Schlake · G. Schlake · F. Tiecke
Institute of Pathology,
45879 Gelsenkirchen, Germany

R. Penzel · P. Schirmacher
Institute of Pathology, University of Heidelberg,
69120 Heidelberg, Germany

H. Höfler · K. Specht
Institute of Pathology and Pathological Anatomy,
Technical University of Munich,
81675 Munich, Germany

U. Lehmann · H.-H. Kreipe
Institute of Pathology, Medizinische Hochschule Hannover,
30625 Hannover, Germany

M. Rudas · Z. Bago-Horvath · D. Kerjaschki
Institute of Pathology, Medical University of Vienna,
1090 Vienna, Austria

P. Schraml · Z. Varga · H. Moch
Institute of Surgical Pathology, University Hospital Zurich,
8091 Zurich, Switzerland

M. Schmidt
Department of Gynecology and Obstetrics, University of Mainz,
Mainz, Germany

M. Filipits
Institute of Cancer Research, Medical University of Vienna,
1090 Vienna, Austria

set of ten formalin-fixed paraffin-embedded tumors was tested in the different labs, and the variance and accuracy of the EndoPredict assays were determined using predefined reference values. Extraction of a sufficient amount of RNA and generation of a valid EP score was possible for all 70 study samples (100%). The EP scores measured by the individual participants showed an excellent correlation with the reference values, respectively, as reflected by Pearson correlation coefficients ranging from 0.987 to 0.999. The Pearson correlation coefficient of all values compared to the reference value was 0.994. All laboratories determined EP scores for all samples differing not more than 1.0 score units from the pre-defined references. All samples were assigned to the correct EP risk group, resulting in a sensitivity and specificity of 100%, a concordance of 100%, and a kappa of 1.0. Taken together, the EndoPredict test could be successfully implemented in all seven participating laboratories and is feasible for reliable decentralized assessment of gene expression in luminal breast cancer.

Keywords Breast cancer · Prognosis · mRNA · Quality control

Introduction

The success of individualized cancer therapy critically depends on reliable molecular biomarker assays that identify those tumors that have a particular good response to a defined treatment.

In the last years, molecular assays for prediction of therapy response have been established in colon cancer and non-small cell lung cancer. These assays are based on retrospective evaluation of clinical trials that had been performed to evaluate new therapeutic approaches [1, 2]. It has been shown that determination of *EGFR* and *KRAS* mutations in formalin-fixed paraffin-embedded (FFPE) tissues can be performed reliably in the routine molecular pathology laboratory [3, 4].

While this approach is now routine for colorectal and lung cancer, the molecular characterization of breast cancer in the pathology institutes is largely based on immunohistochemical evaluation of hormone receptors and HER2 [5, 6]. However, one central clinical question in breast cancer is the identification of those tumors that have an excellent outcome with endocrine therapy alone—a task which cannot be accomplished by standard immunohistochemistry.

It has been shown in several studies that gene expression analysis can identify subgroups of breast tumors with good outcome under endocrine therapy [7–10]. Based on these observations, molecular assays have been developed that are currently performed centralized in reference laboratories in Europe [11] and the USA [12, 13]. These assays provide useful information for treatment strategies; however, they are not linked to the histopathology workflow in the local pathology laboratory. As most of the tissue-derived information is generated in clinical pathology laboratories, it would improve the acceptance of the new technologies if the molecular assay would be available in each pathology institute that diagnoses the breast cancer cases anyway.

We have recently described a quantitative reverse transcription polymerase chain reaction (RT-qPCR)-based molecular assay that uses routine FFPE tissue samples and identifies a subgroup of breast cancer cases that have an excellent prognosis if treated with endocrine therapy alone, without additional chemotherapy [14]. The assay measures the expression of eight functional genes and three normalization genes as well as the presence of genomic DNA to calculate the EndoPredict score (EP score) ranging from 0 to 15. Using the validated cutoff value of 5, patients can be classified into low or high risk for the occurrence of distant recurrence under endocrine therapy. The molecular score can subsequently be combined with the nodal status and the tumor size to calculate the integrated molecular and clinical risk score (EPclin). The EPclin score is superior over the EP score as the outcome of breast cancer cannot be predicted optimally by gene expression data alone [14]. Clinical parameters reflecting the size and the dissemination status of the tumor are not necessarily reflected by tumor RNA expression.

The EndoPredict score had been generated in a cohort of 964 ER-positive, HER2-negative tumors. After transfer to the RT-qPCR platform, the test was validated independently in two separate clinical cohorts, the ABCSG-6 (n=378), and the ABCSG-8 (n=1,324) cohort [14]. This validation approach resulted in a level of evidence of 1 according to the classification scheme for biomarker studies that has been suggested by Simon et al. [15].

The next and essential step would be to transfer this molecular testing system to the individual clinical pathology laboratories. In this study, we report the results of the proficiency testing program, which show that the EndoPredict test can be executed reliably and de-centralized in molecular–pathological laboratories. Aim of the study was to evaluate the performance of the test in the different molecular pathology laboratories and to determine the number of laboratories that have implemented the EndoPredict test successfully.

Methods

Materials and study logistics Ten-micrometer sections of ten FFPE breast cancer tumor blocks were shipped to the seven participating laboratories: Institute of Pathology, Charité Hospital, Berlin; Institute of Pathology, Gelsenkirchen,

Germany; Institute of Pathology, Medizinische Hochschule Hannover, Germany; Institute of Pathology, University of Heidelberg, Germany; Institute of Pathology and Pathological Anatomy, Technical University of Munich, Germany; Institute of Pathology, Medizinische Universität Wien, Vienna, Austria; and Institute of Surgical Pathology, University Hospital Zurich, Switzerland. Selection criteria for these institutions were (1) experience in high-volume diagnostic molecular pathology and breast pathology, (2) localization in different countries (Germany, Austria, or Switzerland); (3) different organizational structure (university hospital or large specialized private institution). The pathological data of the tumors are shown in Table 1, the steps for development of the EndoPredict assay and the workflow of the study are incorporated in Fig. 1.

Adjacent sections were used for histopathological quality control to ensure that the sample used for the molecular analysis contains at least 30% of tumor tissue. The range of tumor content of the samples was 30–80%, mean tumor content 63%.

For each block, a reference EP score was generated in Sividon's laboratory by measurement of four further sections of each tumor. The reference values were calculated as means of these four replicate measurements. The range of the EP scores of the ten tumors was from 2.7 to 12.1. For this analytical evaluation of the EndoPredict assay, the samples were chosen to cover the range of possible EP scores.

These reference EP scores were not provided to the study participants until the study was completed and were only used for the final analysis. A random unique number identified each section; the association between an individual section, and the block of origin was unknown to the study participants.

Pre-specified analysis plan Study aims and statistical analysis plan were defined prospectively. The primary aim of the study was to determine the number of pathology laboratories that have implemented the EndoPredict assay successfully. For a successful implementation, it was required that the absolute difference between the local EP score and the reference EP score was below 1.0 EP units for at least nine of ten samples. The predefined secondary aims are shown in Table 2. In the event that the analysis could not be completed due to technical reasons or out-of-specification controls the laboratory could ask for replacement sections. The total number of replacement sections and the number of repeated plates were recorded.

RNA isolation from FFPE tissue Total RNA was extracted from one FFPE tissue section of each of the ten FFPE tumor blocks, respectively, using a silica-coated magnetic bead-based method developed by Siemens Healthcare Diagnostics (Marburg, Germany) as published previously [16–19]. The method was either performed manually or automatically, depending on the robotic equipment available at each site. DNA-free total RNA from one FFPE section was finally eluted with 100 μl of elution buffer. For the assessment of DNA contamination in the respective RNA extract, an HBB-DNA-specific qPCR was included in the EndoPredict assay. Samples were considered to be substantially free of DNA when Ct values above 38 were detected. In case of DNA contamination, samples were manually re-digested by DNase I treatment.

Gene expression analysis using RT-qPCR Expression of eight genes-of-interest (*AZGP1*, *BIRC5*, *DHCR7*, *IL6ST*, *MGP*, *RBBP8*, *STC2*, *UBE2C*), three normalization genes (*CALM2*, *OAZ1*, *RPL37A*) as well as the amount of residual genomic DNA (HBB) were assessed by the EndoPredict® assay (Sividon Diagnostics, Cologne, Germany). This assay is configured on a 96-well plate containing primers and FAM/TAMRA-labeled probes dried into the wells. Each EndoPredict plate contains PCR assays for two tumor samples as well as one positive and one negative control for each gene. Genes were measured in triplicates as a necessary means to control for PCR imprecision and to enable outlier

Table 1 Clinicopathological parameters

Sample ID	Tumor content (%)	Grade	pT stage	pN stage	ER (%)	PR (%)
A	60	2	pT2	pN0	100	60
B	75	2	pT2	pN0(sn)	90	10
C	65	3	pT2(m)	pN2a	95	40
D	80	1	pT2	pN0	Pos.	n.d.
E	65	2	pT1c	pN0	100	0
F	75	2	pT2	pN0(sn)	Pos.	n.d.
G	30	1	pT2	pN1mi	100	30
H	70	3	pT2	pN2a	90	80
I	60	2	pT2	pN3a	90	8
J	75	2	pT3(m)	pN1a	95	0

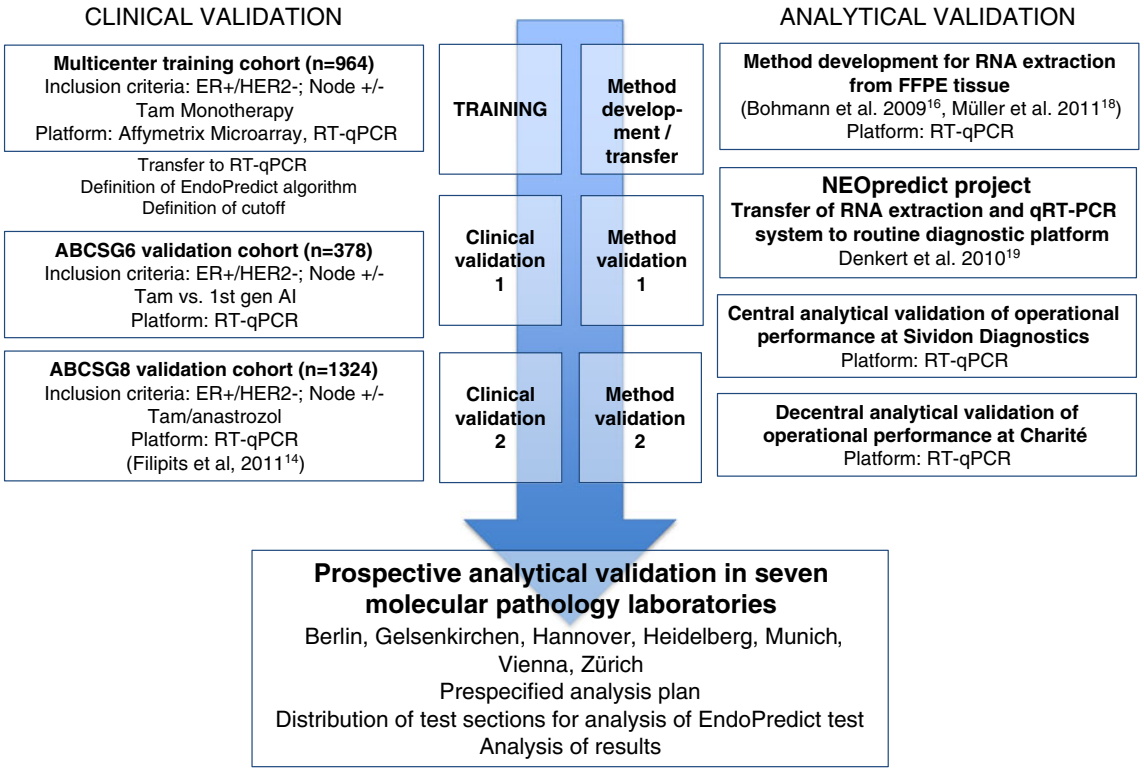

Fig. 1 Workflow of sequential validation of the EndoPredict assay and the interlaboratory quality assurance (*ER* estrogen receptor)

removal. Sequences of primers and probes were published previously [14]. Gene expression was assessed by one-step RT-qPCR using the SuperScript III PLATINUM One-Step Quantitative RT-PCR System with ROX (Invitrogen,

Table 2 Predefined study aims and summary of the results

		Results
Primary aim		
	Determine the number of participating laboratories that successfully implement the EndoPredict test. A successful implementation is achieved if the absolute difference between EP scores determined in the laboratory and the corresponding reference EP scores is below 1.0 EP score units for at least 9 of the 10 samples.	100% (7 of 7)
Secondary aims		
1.	Determine the number and ratio of sections for which the EP score was successfully measured (across all blocks and laboratories).	98.6% (69 of 70)
2.	Determine the (mean) standard deviation of EP scores between laboratories (including one result per block from Sividon). Results per block are summarized by averaging the corresponding variances.	0.25 score units (1.7% of EP score range)
3.	Determine the number and ratio of EP scores deviating more than 2.0 EP score units from the reference EP score across all blocks and laboratories (outliers). The same analysis will be done for deviations of more than 1.0 and 0.5 EP score units.	Deviation of more than 2.0 units: 0 of 70 samples Deviation of more than 1.0 units: 0 of 70 samples (one sample had a deviation of exact 1.0 score unit) Deviation of more than 0.5 units: 10 of 70 samples (14%)
4.	Calculate the Pearson correlation coefficient between the reference EP scores and the EP scores reported by the participating laboratories (across all blocks and laboratories).	0.994
5.	Calculate the EP classes from the EP scores. Determine the number and ratio of EP classes discordant to the corresponding reference EP classes across all blocks for each laboratory (across all laboratories). Also, report contingency table, kappa statistics, sensitivity, and specificity.	All EP classes were calculated correctly, resulting in a sensitivity and specificity of 100% and a kappa of 1.0.

Karlsruhe, Germany) according to manufacturer's instructions in a VERSANT® kPCR Molecular System (Siemens Healthcare Diagnostics) with 30 min at 50°C, 2 min at 95°C followed by 40 cycles of 15 s at 95°C and 30 s at 60°C. Mastermix containing 1 µl sample RNA for each well was added to the respective wells. As positive controls of RT-qPCR assays a standardized reference RNA (Stratagene qPCR Human Reference Total RNA, Agilent Technologies, Waldbronn, Germany) was tested for each gene on each plate. As positive control for HBB–DNA PCR assay Human Genomic DNA (Roche Applied Bioscience, Mannheim, Germany) was used. For exclusion of contamination no-template-controls were assessed in parallel as well. Detection of outliers which were defined by a difference of more than three "noise model"-predicted standard deviations from the other replicates, relative expression levels of each gene of interest as well as EP scores were calculated as described previously [14] using a web-based implementation to process analytical PCR results into EP scores which can be found at http://forschung.medizin.uni-mainz.de/epreport/. The amount of input RNA was assessed by the EndoPredict assay using the mean of the Ct values of the three normalization genes as surrogate. RNA input was considered as sufficient if the mean of the ct values of *CALM2*, *OAZ1* and *RPL37A* of a tumor sample was below 28. Before the start of the proficiency testing program, each participant performed a pre-defined analytical validation of the performance characteristics of the EndoPredict assay.

Evaluation of study results After completion of the PCR, for each sample, analytical data (raw data of PCR run), calculated EP score as well as classification into low or high risk of distant metastasis were reported to Sividon and to Charité, who performed the data analysis according to the pre-defined analysis plan. After completion of the study, summary results and reference EP scores were disclosed to all participants.

Results

Successful implementation of the EndoPredict assay—primary study aim The EndoPredict test could be successfully implemented in all seven participating laboratories. As defined in the study plan, a successful implementation was achieved, if the absolute difference between EP scores determined in the participating laboratory and the corresponding reference EP scores was below 1.0 EP score units for at least nine of the ten samples. Six of the seven laboratories have reached a difference below 1.0 score units for all ten samples. One laboratory had differences below 1.0 score units for nine of ten samples and a difference of exactly 1.0 score unit for a single sample.

Therefore, the EP scores of 69 of the 70 measurements were correct with respect to the reference value and one was just at the pre-specified cutoff. For the EP score, the results of the individual measurements are shown in Fig. 2. As shown in Fig. 3, there was a high concordance in the analysis of the different genes in the seven laboratories. The EndoPredict score is arranged as a linear combination of eight genes for increased robustness. Three genes (*BIRC5*, *DHCR7*, *UBE2C*) are positively associated with the EP score, the other genes (*AZGP1*, *IL6ST*, *MGP*, *RBBP8*, *STC2*) yield to a smaller score the higher they are expressed. For details on the biological interpretation of the genes, see supplementary appendix in Filipits et al. [14].

Variation, correlation and concordance of results—secondary study aims The results of the analysis of the secondary study aims are shown in Table 2. Extraction of a sufficient amount of RNA and generation of a valid EP score was possible for all 70 study samples (100%); it was not required to ship any extra tissue sections for additional measurements. For four of the 70 samples (two EndoPredict plates), the RT-qPCR analysis had to be repeated. This was due to an instrument problem and one positive control that was out of the prespecified range. Averaging the corresponding variances per tumor block, the mean standard deviation of all 80 measurements (70 decentral measurements and ten central reference values) in ten tumor blocks was 0.25 score units. Eighty-six percent of the samples had a difference between local analysis and central reference value of 0.5 score units or less. The EP scores measured by the individual participants showed an excellent correlation with the reference values, respectively, as reflected by Pearson correlation coefficients ranging from 0.987 to 0.999 (Fig. 4). The Pearson

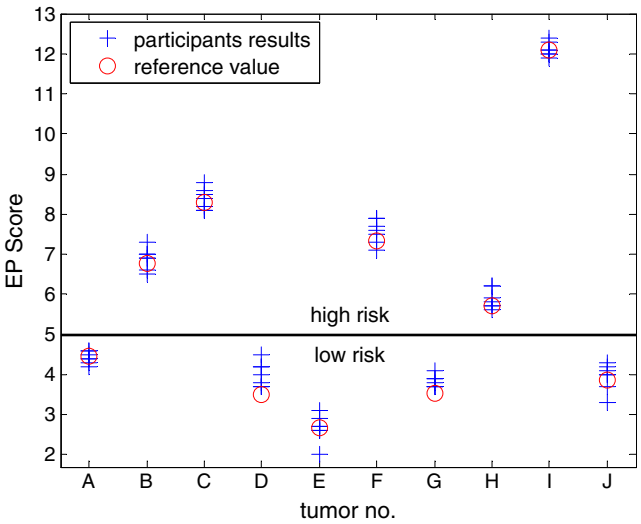

Fig. 2 Results of the decentral measurement of 70 tumor samples from ten different tumors. The central reference value is marked in *red*, the *blue* labels represent the seven different measurements at the seven institutes of pathology

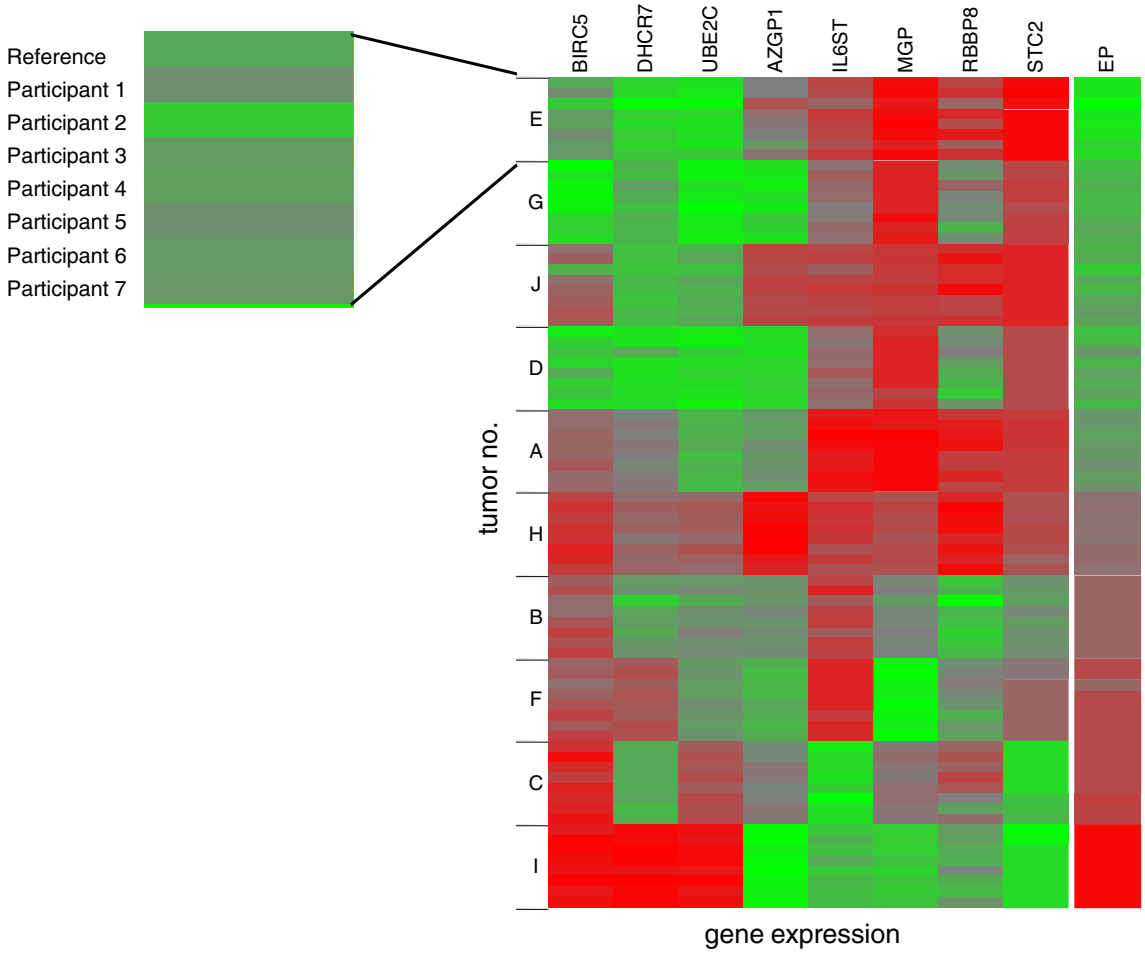

Fig. 3 Cluster analysis of the results of the RT-qPCR in the different centers. The EndoPredict score is shown on the *right*

correlation coefficient of all values compared to the reference value was 0.994. All samples were assigned to the correct EP risk group, resulting in a sensitivity and specificity of 100%, a concordance of 100%, and a kappa of 1.0.

Discussion

In this study, we have tested the EndoPredict assay in seven different molecular pathology laboratories in Germany, Austria, and Switzerland. All laboratories fulfilled the pre-specified quality criteria and are thus qualified to run the test. For 69 of 70 samples, the quantitative EP score was measured correctly with an EP score deviation of less than 1.0 score units. Only one sample had a deviation of exactly 1.0 score unit and missed the pre-specified threshold marginally. Nevertheless, all 70 samples were assigned to the correct EP risk group (low risk or high risk).

The data demonstrate that the EndoPredict assay is a reproducible and easy-to-perform prognostic multigene expression test, which can easily be included in the routine workflow of patient care in breast cancer centers. The decentral use of the EndoPredict assay, a unique feature which has not been shown for other RNA-based multigene expression tests so far, has several advantages in comparison to centralized diagnostic services. The analysis can be integrated into the regular diagnostic workflow and the clinic–diagnostic setup in the setting of established local tumor boards with a clear interdisciplinary communication strategy. Moreover, the local pathologist can select optimal FFPE tumor material for this complex multigene assay ensuring high-quality on-site testing. Since no shipping of tumor material is necessary and the EndoPredict assay can be performed within one working day, results are promptly available for clinical decision making. Therefore, the EndoPredict assay is different from the Recurrence Score [20], which is based on an assessment in a central laboratory as well as the UPA/PAI assay [21], which requires fresh-frozen tissue.

It should be noted, however, that despite the excellent results of this proficiency testing, the standardized evaluation of quantitative RNA markers is not an easy and

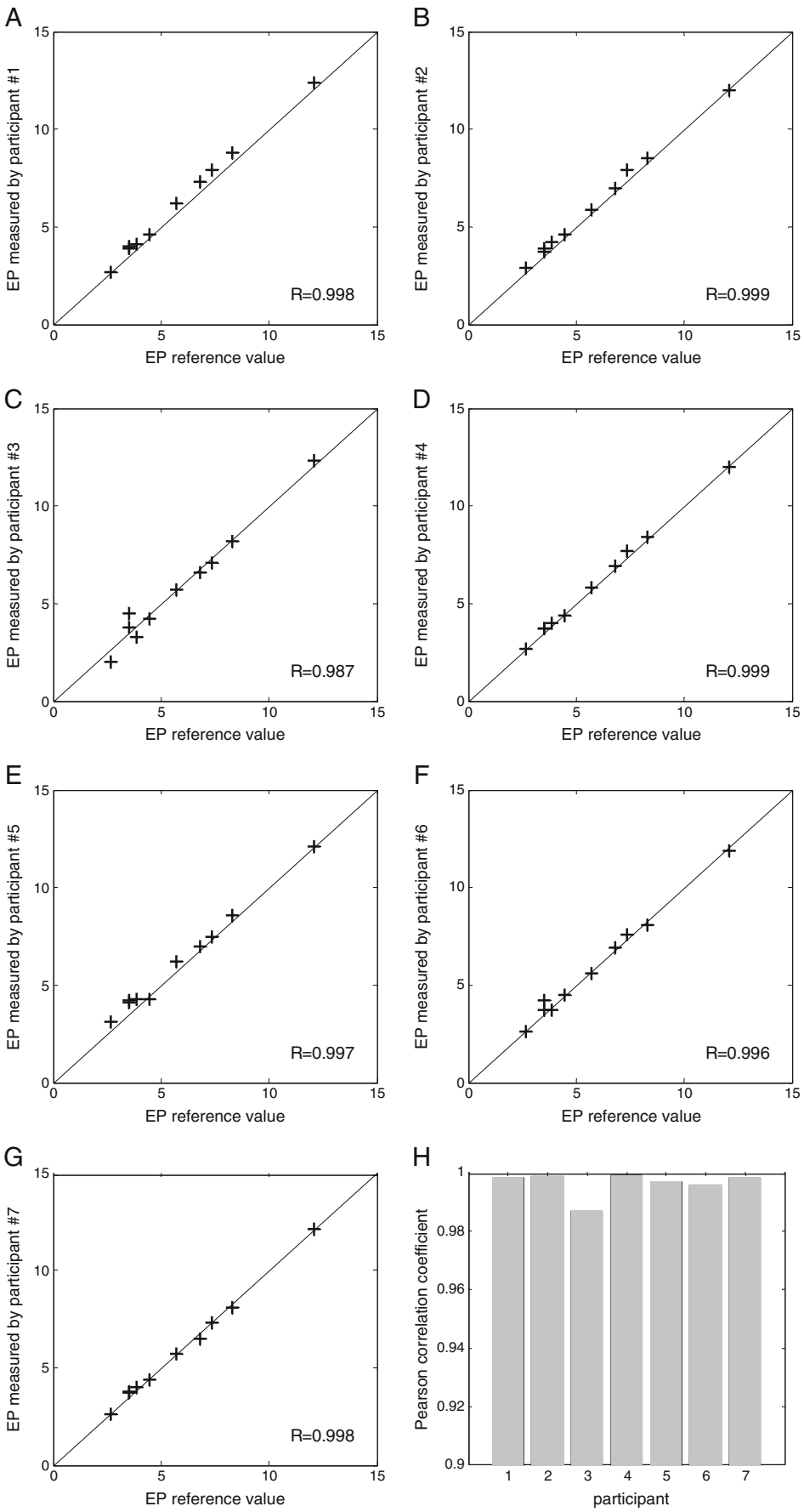

Fig. 4 Correlation analysis of the EndoPredict test results in the seven different pathology laboratories. **a–g** Results of the individual laboratories. **h** Pearson correlation coefficients

straightforward task. The essential elements are highly standardized reagents and controls including intensive lot-to-lot quality controls of 96-well plates coated with primers and probes as well as precisely pre-defined and technically validated limits of positive controls for quantitative RT-qPCR. Moreover, quality control was performed for individual genes-of-interest using a "noise model," previously constructed from an independent large data set of replicate measurements [14]. The "noise model" estimates the variance of replicate-to-replicate noise from the Ct value and identifies and removes outliers within replicates. Outlier detection and removal in a complex test based on normalized expressions of several genes is crucial since outliers occur frequently and is possible only if at least three replicates for each gene are measured. Using two replicates only raises the portion of invalid test outcomes significantly, leading to a high number of repetitions of the whole EP test. Using one replicate only does not allow to detect outliers resulting in incorrect EP test results. A further reason for the robust decentral performance of the EndoPredict assay was the use of a standardized qPCR system as well as a reproducible technique to isolate RNA from FFPE tissue, which was extensively evaluated for RNA biomarker testing in previous studies [16, 18]. Finally, each participant performed a pre-defined analytical validation of the performance characteristics of the EndoPredict assay before proficiency testing.

The current evaluation needs to be continued to include other centers and additional samples to control for variation in molecular pathology laboratory standard operating procedures in different institutions and regions, and a validation programme for this is currently in preparation. While in our study, all 70 samples were assigned to the correct EP risk group; it should be mentioned that risk group assignment might vary for those samples with an EP score within 0.5 score units (2 SD) near the cutoff. In this situation, the estimated risk of distant metastasis, which is reported as a continuous parameter, might be useful for the interpretation of results. This study shows that RT-qPCR-based quantitative multigene expression analysis of FFPE tissue samples including algorithmic analysis is feasible in a decentral multicenter setting in diagnostic pathology laboratories. This opens the door for a new generation of molecular diagnostic tests in breast cancer that might add relevant information to the standard immunohistochemistry approach without being confined to globally centralized reference laboratories.

Acknowledgments We would like to thank Manuela Averdick, Britta Beyer, Nicole Bleuel, Angelika Bönisch, Angelika Brüntgens, Susanne Dettwiler, Franziska Haufe, Tina Holper, Ines Koch, Tanja Ropers, Claudia Roth, Elisa Schipper, Petra Wachs, Claudia Windbergs for their excellent technical assistance and Martina Eickmann for her editorial assistance. Part of this work was funded by the German Ministry of Science and Technology (BMBF) in the NEOpredict project (Project number 01ES0725).

Conflict of interest statement CD, RK, KB, KEW, CP, and MD are founders of Sividon Diagnostics.

Open Access This article is distributed under the terms of the Creative Commons Attribution License which permits any use, distribution, and reproduction in any medium, provided the original author(s) and the source are credited.

References

1. Allegra CJ, Jessup JM, Somerfield MR, Hamilton SR, Hammond EH, Hayes DF, McAllister PK, Morton RF, Schilsky RL (2009) American Society of Clinical Oncology provisional clinical opinion: testing for KRAS gene mutations in patients with metastatic colorectal carcinoma to predict response to anti-epidermal growth factor receptor monoclonal antibody therapy. J Clin Oncol 27:2091–2096
2. Siena S, Sartore-Bianchi A, Di Nicolantonio F, Balfour J, Bardelli A (2009) Biomarkers predicting clinical outcome of epidermal growth factor receptor-targeted therapy in metastatic colorectal cancer. J Natl Cancer Inst 101:1308–24
3. Penzel R, Sers C, Chen Y, Lehmann-Mühlenhoff U, Merkelbach-Bruse S, Jung A, Kirchner T, Büttner R, Kreipe HH, Petersen I, Dietel M, Schirmacher P (2011) EGFR mutation detection in NSCLC—assessment of diagnostic application and recommendations of the German Panel for Mutation Testing in NSCLC. Virchows Arch 458:95–98
4. Weichert W, Schewe C, Lehmann A, Sers C, Denkert C, Budczies J, Stenzinger A, Joos H, Landt O, Heiser V, Röcken C, Dietel M (2010) KRAS genotyping of paraffin-embedded colorectal cancer tissue in routine diagnostics: comparison of methods and impact of histology. J Mol Diagn 12:35–42
5. Hammond ME, Hayes DF, Wolff AC, Mangu PB, Temin S (2010) American Society of Clinical Oncology/College of American pathologists guideline recommendations for immunohistochemical testing of estrogen and progesterone receptors in breast cancer. J Oncol Pract 6:195–197
6. Wolff AC, Hammond ME, Schwartz JN et al (2007) American Society of Clinical Oncology/College of American Pathologists guideline recommendations for human epidermal growth factor receptor 2 testing in breast cancer. J Clin Oncol 25:118–45
7. Paik S, Shak S, Tang G, Kim C, Baker J, Cronin M, Baehner FL, Walker MG, Watson D, Park T, Hiller W, Fisher ER, Wickerham DL, Bryant J, Wolmark N (2004) A multigene assay to predict recurrence of tamoxifen-treated, node-negative breast cancer. N Engl J Med 351:2817–2826
8. van't Veer LJ, Dai H, van de Vijver MJ, He YD, Hart AA, Mao M, Peterse HL, van der Kooy K, Marton MJ, Witteveen AT, Schreiber GJ, Kerkhoven RM, Roberts C, Linsley PS, Bernards R, Friend SH, Veer LJ, Dai H, van de Vijver MJ, He YD, Hart AA, Mao M, Peterse HL, van der Kooy K, Marton MJ, Witteveen AT, Schreiber GJ, Kerkhoven RM, Roberts C, Linsley PS, Bernards R, Friend SH (2002) Gene expression profiling predicts clinical outcome of breast cancer. Nature 415:530–536
9. van de Vijver MJ, He YD, van't Veer LJ, Dai H, Hart AA, Voskuil DW, Schreiber GJ, Peterse JL, Roberts C, Marton MJ, Parrish M, Atsma D, Witteveen A, Glas A, Delahaye L, van der Velde T, Bartelink H, Rodenhuis S, Rutgers ET, Friend SH, Bernards R (2002) A gene-expression signature as a predictor of survival in breastcancer. N Engl J Med 347:1999–2009

10. Sotiriou C, Pusztai L (2009) Gene-expression signatures in breast cancer. N Engl J Med 360:790–800
11. Glas AM, Floore A, Delahaye LJ, Witteveen AT, Pover RC, Bakx N, Lahti-Domenici JS, Bruinsma TJ, Warmoes MO, Bernards R, Wessels LF, Van't Veer LJ (2006) Converting a breast cancer microarray signature into a high-throughput diagnostic test. BMC Genomics 7:278
12. Cronin M, Sangli C, Liu ML, Pho M, Dutta D, Nguyen A, Jeong J, Wu J, Langone KC, Watson D (2007) Analytical validation of the oncotype DX genomic diagnostic test for recurrence prognosis and therapeutic response prediction in node-negative, estrogen receptor-positive breast cancer. Clin Chem 53:1084–1091
13. Sparano JA, Paik S (2008) Development of the 21-gene assay and its application in clinical practice and clinical trials. J Clin Oncol 26:721–728
14. Filipits M, Rudas M, Jakesz R, Dubsky P, Fitzal F, Singer CF, Dietze O, Greil R, Jelen A, Sevelda P, Freibauer C, Müller V, Jänicke F, Schmidt M, Kölbl H, Rody A, Kaufmann M, Schroth W, Brauch H, Schwab M, Fritz P, Weber KE, Feder IS, Hennig G, Kronenwett R, Gehrmann M, Gnant M, EP Investigators (2011) A new molecular predictor of distant recurrence in ER-positive, HER2-negative breast cancer adds independent information to conventional clinical risk factors. Clin Cancer Res 17:6012–6020
15. Simon RM, Paik S, Hayes DF (2009) Use of archived specimens in evaluation of prognostic and predictive biomarkers. J Natl Cancer Inst 101:1–7
16. Bohmann K, Hennig G, Rogel U et al (2009) RNA extraction from archival formalin-fixed paraffin-embedded tissue: a comparison of manual, semiautomated, and fully automated purification methods. Clin Chem 55:1719–1727
17. Hennig G, Gehrmann M, Stropp U, Brauch H, Fritz P, Eichelbaum M, Schwab M, Schroth W (2010) Automated extraction of DNA and RNA from a single formalin-fixed paraffin-embedded tissue section for analysis of both single-nucleotide polymorphisms and mRNA expression. Clin Chem 56:1845–1853
18. Müller BM, Kronenwett R, Hennig G et al (2011) Quantitative determination of estrogen receptor, progesterone receptor, and HER2 mRNA in formalin-fixed paraffin-embedded tissue—a new option for predictive biomarker assessment in breast cancer. Diagn Mol Pathol 20:1–10
19. Denkert C, Loibl S, Noske A, Roller M, Müller BM, Komor M, Budczies J, Darb-Esfahani S, Kronenwett R, Hanusch C, von Törne C, Weichert W, Engels K, Solbach C, Schrader I, Dietel M, von Minckwitz G (2010) Tumor-associated lymphocytes as an independent predictor of response to neoadjuvant chemotherapy in breast cancer. J Clin Oncol 28:105–113
20. Paik S, Shak S, Tang G, Kim C, Baker J, Cronin M, Baehner FL, Walker MG, Watson D, Park T, Hiller W, Fisher ER, Wickerham DL, Bryant J, Wolmark N (2004) A multigene assay to predict recurrence of tamoxifen-treated, node-negative breast cancer. N Engl J Med 351(27):2817–2826
21. Zemzoum I, Kates RE, Ross JS, Dettmar P, Dutta M, Henrichs C, Yurdseven S, Höfler H, Kiechle M, Schmitt M, Harbeck N (2003) Invasion factors uPA/PAI-1 and HER2 status provide independent and complementary information on patient outcome in node-negative breast cancer. J Clin Oncol 21(6):1022–1028

Virchows Arch (2012) 460:261–270
DOI 10.1007/s00428-012-1195-1

ORIGINAL ARTICLE

Comparative tight junction protein expressions in colonic Crohn's disease, ulcerative colitis, and tuberculosis: a new perspective

Prasenjit Das · Pooja Goswami · Tapash K. Das · Tapas Nag · Vishnubhatla Sreenivas · Vineet Ahuja · Subrat K. Panda · Siddhartha Datta Gupta · Govind K. Makharia

Received: 9 December 2011 / Revised: 31 December 2011 / Accepted: 11 January 2012 / Published online: 2 February 2012
© Springer-Verlag 2012

Abstract We intended to see the pattern of TJ protein expression along with ultrastructural changes in colonic biopsies from patients with Crohn's disease (CD), ulcerative colitis (UC), and tuberculosis (cTB). Colonic biopsies from 11 patients with active CD and ten patients each with active UC and untreated cTB were taken along with biopsies from six patients with irritable bowel syndrome as controls. These were evaluated for expression pattern of key TJ proteins which included claudin-2 as TJ pore-forming protein, claudin-4 as pore-sealing protein, ZO-1 as scaffold protein, and occludin as TJ protein related to cell migration and polarity. Claudin-2 expression was upregulated along the whole length of intercellular junction (ICJ) in biopsies from patients with active CD and UC in comparison to the biopsies from cTB patients and controls, where its expression was limited to the uppermost part of ICJ. There was reduced expression of ZO-1 in UC, CD, and cTB. On transmission electron microscopic examination, the pentalaminar structure of TJs was destroyed in patients with CD and UC but no significant change was seen in those with cTB and in controls. The expression of claudin-2 was distinctly different in active CD and UC in comparison to its expression pattern in patients with cTB and in controls. The redistribution of claudin-2 expression was in accordance with the TJ ultrastructural changes in patients with UC, CD, and cTB. Altered claudin-2 expression, along with destroyed TJs, may result in loss of selective permeability in patients with UC and CD.

Keywords Colon · Crohn's disease · Ulcerative colitis · Immunohistochemistry · Colonic tuberculosis · Tight junction proteins · Ultrastructure

This paper was presented in the Asia Pacific Digestive Week 2010 in Kuala Lumpur, Malaysia. The abstract was published in *Journal of Gastroenterology and Hepatology* (*J Gastroenterol Hepatol* 2010; 25 (Suppl 2): A12).

P. Das · S. K. Panda · S. D. Gupta
Department of Pathology, All India Institute of Medical Sciences, Ansari Nagar New Delhi 110029, India

P. Goswami · V. Ahuja · G. K. Makharia (✉)
Department of Gastroenterology and Human Nutrition, All India Institute of Medical Sciences, Ansari Nagar New Delhi 110029, India
e-mail: govindmakharia@gmail.com

G. K. Makharia
e-mail: govindmakharia@aiims.ac.in

T. K. Das · T. Nag
Department of Anatomy, All India Institute of Medical Sciences, Ansari Nagar New Delhi 110029, India

V. Sreenivas
Department of Biostatistics, All India Institute of Medical Sciences, Ansari Nagar New Delhi 110029, India

Introduction

The lumen of the colon is an enormous reservoir of microbes and other potentially toxic microbial products which, upon gaining access to the lamina propria, activate the mucosal immune system. This interaction does not always take place due to the presence of an effective intestinal epithelial barrier. Normally, the luminal and the mucosal compartments communicate via a paracellular pathway, a well-guarded channel in between two adjacent enterocytes. The tight junction (TJ) is

the most effective and uppermost guard in this paracellular pathway, followed from the apical to the basal side of the cell by the intermediate junctions, desmosomes, gap junctions, and intercellular folds, all of which contribute to maintaining selective permeability. In chronic colitis, this barrier gets compromised and harmful toxic substances from the intestinal lumen enter the intra-epithelial compartment to initiate a disease [1–3]. The TJ (also called zonula occludens) is a continuous, circumferential band-like structure situated at the junction of the apical and the baso-lateral membrane of the enterocytes [2, 3]. As yet, although more than 40 different TJ constituent proteins have been identified including the transcellular *filament proteins* such as occludin, junctional adhesion molecules, claudins (a family of 20 different proteins), and *co-polymerizing scaffold protein molecule* such as Zo-1, only a few specific functions have been identified. While claudin-2 creates pores in the paracellular junction, claudin-4 seals/blocks these pores. Zo-1 is possibly related to the maintenance of cell polarity, while occludins are linked to cell migration functions [4–6] (Fig. 1). A complex harmonious interaction among all these proteins is responsible for the maintenance of paracellular selective permeability [3].

In published studies, the inflammatory cytokines, especially IL-1, IL-3, IL-4, tumor necrosis factor (TNF)-α, and interferon (IFN)-γ, have been shown to be responsible for TJ protein alterations [7–12]. The aim of the present study was to examine the expression patterns of key TJ proteins in different chronic colonic inflammatory conditions, where inflammatory cytokines are in abundance, in comparison with the expression patterns observed in biopsies from control patients.

Patients and methods

Patients

Eleven patients with active Crohn's disease (CD) and ten patients each with ulcerative colitis (UC) and untreated colonic tuberculosis (cTB) were included in this study. The diagnosis of CD was based on the criteria laid down by the European Crohn's and Colitis Organization guidelines. The diagnosis of UC was also based on a combination of clinical, endoscopic, and histological characteristics. The diagnosis of colonic tuberculosis was made on the basis of characteristic clinical features (abdominal pain, constipation, and/or diarrhea, constitutional symptoms, intestinal obstruction), endoscopic findings (ileo-caecal area involvement, ulcerations, nodularity, and strictures), histological features (presence of granulomas), and based on the results of microbiological test, as presence of acid-fast bacilli on Ziehl Neelsen stain or polymerase chain reaction for bacterial DNA (Paustian's criteria with Logan's modification) [13, 14]. The disease activity was assessed using the Crohn's Disease Activity Index (CDAI) and Ulcerative Colitis Disease Activity Index (UCDAI). The mean UCDAI and CDAI were 9 and 248, respectively, for the patients included in this study. Of all patients, colonoscopic biopsies were taken from the ulcerative mucosal lesions and sent for histopathological and immunohistochemical studies. Patients with UC and CD in clinical remission and those with cTB that had been exposed to anti-tubercular drugs were excluded from the study.

Controls

Six patients with irritable bowel syndrome, in whom neither organic lesions nor abnormalities were identified upon biochemical and colonoscopic examination, were included as controls. Multiple biopsies were taken from recto-sigmoid junction.

Histological examination

Technique of slide preparation

After preparation of the paraffin blocks, 4-μm-thick sections were cut on glass slides and sections were stained by

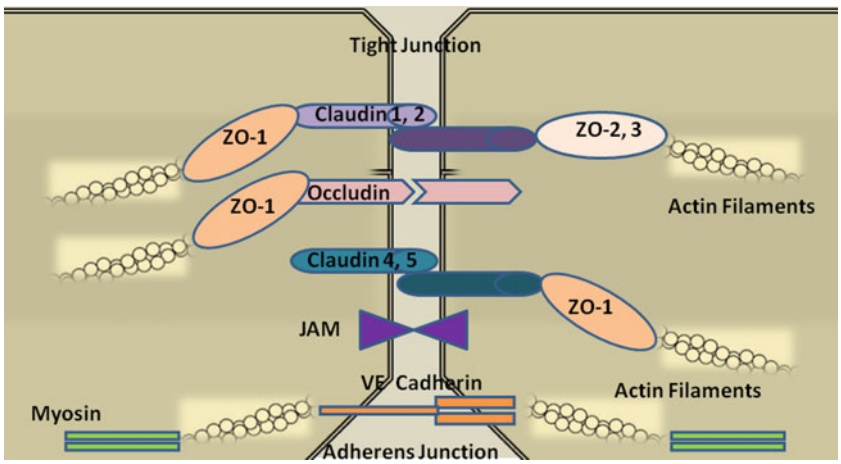

Fig. 1 Schematic diagram showing the molecular structure of tight junction and the relationship between the transmembrane and scaffold proteins

hematoxylin and eosin (H&E) stain to analyze the histopathological parameters semi-quantitatively for the following parameters: architectural changes, *crypt* abnormalities, status of lamina propria, sub-mucosal inflammation, and presence of macro/microgranuloma.

Immunohistochemistry

For IHC, sections from paraffin blocks of colonic biopsies of CD, UC, and cTB were deparaffinised and rehydrated, followed by suitable antigen retrieval (boiling in 0.01 M citrate buffer, EDTA buffer for claudin-2 and -4, respectively, and proteolytic retrieval for ZO-1 and occludin). Endogenous peroxidase was blocked by 3% H_2O_2 in methanol for 15–20 min. Non-specific antibody binding sites were blocked with 5% bovine serum albumin for 15 min. Then, the sections were incubated with monoclonal antibodies (Zymed, San Francisco, CA, USA) against ZO-1 (1:20), claudin-2 (1:50), claudin-4 (1:400), and occludin (1:20) and incubated overnight. Thereafter, the slides were incubated with universal secondary antibody (DAKO, Envision Real System, Denmark) for an hour. Immunodetection was done using DAB as chromogen and H_2O_2 as substrate, followed by counter-staining with hematoxylin. As negative control, primary antibody was not added for some stainings. The stained smears and tissue sections were analyzed by a pathologist with a special interest in this field. The pathologist was blinded about the groups of the biopsies.

Interpretation technique

When at least 5% of the epithelial cells displayed distinct immune-staining, this was considered positive. The stain distribution was semi-quantified as 0—negative (<5% area), 1—very focal (≥5% but <20% surface area), 2—focal (21–50% surface area), and 3—diffuse (>50% surface area). The exact location of staining in the enterocytes was noted as: 1—surface, 2—intercellular junction (ICJ) upper one third, 3—ICJ middle one third, 4—ICJ lower one third, 5—full ICJ, and six-cell cytoplasm.

Transmission electron microscopy

Transmission electron microscopy (TEM) was performed in cases where adequate biopsy fragments were taken and could be spared for gluteraldehyde fixation. Finally, TEM could be performed in three biopsies each from subjects with CD, UC, cTB, and controls. Small fragments of colonic biopsies, measuring 1–2 mm^2 were primarily fixed in 2.5% gluteraldehyde made with 0.1 M sodium phosphate buffer (pH=7.4). OsO_4 (1% solution) was used as a secondary fixative to fix the lipid components. After fixation and adequate dehydration, the tissues were infiltrated by epoxy resin and embedding was done in beam capsules. To polymerize the embedded block, tissue specimens were kept at 40°C to 50°C overnight. After adequate polymerization and washings, to check the presence of desirable colonic mucosa and *crypt*s, ultrathin sections were cut (60–90 nm). These sections were placed on a copper grid with a 300 mesh size and stained with a double staining method of uranyl acetate and lead citrate. The stained sections were observed in a Morgagni 268D transmission electron microscope (Fei Company, The Netherlands) at an operating voltage of 80 kV. Images were digitally acquired using a CCD camera (Megaview III, Fei Company).

Statistical analyses

Statistical analysis was done using Stata-10 data analysis statistical software (StataCorp). All different parameters were compared among four patient groups (UC, CD, cTB, and controls) using Fisher's exact test. Continuous variables, such as age, granulomas size, etc., were compared using one-way analyses of variance, followed by multiple comparisons by Bonferroni corrections.

Results

The mean age (± SD) of patients with CD, UC, and cTB were 30.9±12, 33±10, and 28.8±13 years, respectively.

Status of key TJ proteins

Pattern of expression of TJ markers in control biopsies

Claudin-2 was expressed in the upper third of the intercellular junction (ICJ), both in mucosal surface and in *crypt* epithelium. Nuclei were negative.

Claudin-4 was expressed along the entire ICJ of the colonocytes. Nuclei were negative.

ZO-1 was expressed at the surface of luminal and *crypt* epithelium, more intense in the crypts than on luminal epithelial cells. Occasionally, nuclear expression of ZO-1 was noted. Occludin was expressed at ICJ at the luminal surface, as well as in the cytoplasm and nuclei of epithelial cells.

All these markers were seen to be expressed diffusely in the colonic biopsies (Fig. 2).

Pattern of expression of TJ markers in colonic biopsies in inflammatory disease

Claudin-2 expression was focal in all disease groups [CD (54.5%), UC (20%), and cTB (50%) in comparison to

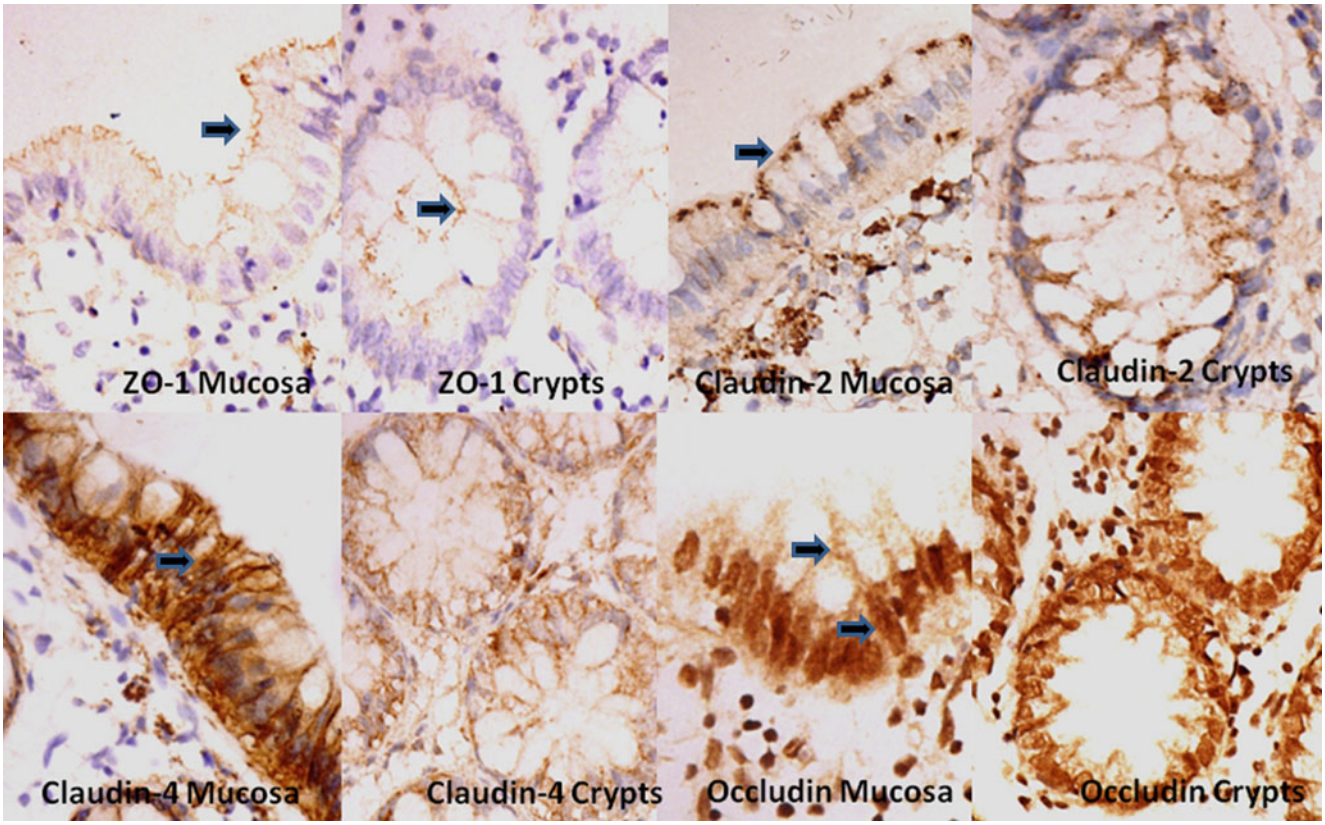

Fig. 2 Normal pattern of TJ marker protein expression in control colonic biopsies. ZO-1 expression was seen at the mucosal surface of both colonic mucosal epithelium and *crypt*s (*arrow*; IHC (Zo-1)×600). In both mucosal epithelium and *crypt*s, claudin-2 expression was noted in the upper one third part of ICJ (*arrow*; IHC (claudin-2)×600). Claudin-4 expression was noted along the whole length of ICJ (*arrow*) as well as in colonocytes cytoplasm (IHC (claudin-4)×600). Occludin expression was identified in the ICJ (*arrow*), in the cell cytoplasm, and in the cell nuclei (*arrow*) of both mucosal epithelium and in *crypt*s (IHC (occludin)×600)

control biopsies (100%) (p=0.002)]. The pattern of expression differed between biopsies from cTB and control subjects on the one hand and from CD and UC on the other. While in cTB and control biopsies claudin-2 expression was noted only in the upper one third of the ICJ, in CD and UC expression this was along the full ICJ (54.5% CD, 100% of UC, and 10% of cTB; $p \leq 0.01$). In *crypt* epithelia claudin-2 was expressed along the entire ICJ in 72.3% CD, 80% UC, and 10% cTB ($p \leq 0.01$; Table 1; Fig. 3).

Claudin-4 expression was lower in luminal epithelium in inflammatory mucosa in comparison to control mucosa [18.2% CD, none in UC, and 10% cTB biopsies ($p \leq 0.01$)]. A similar pattern of expression was also noted in the *crypt* epithelium [0% in CD, 20% in UC, and 30% in cTB in comparison to 100% diffuse strong expression in control biopsies ($p \leq 0.01$)]. Expression was limited to the lower one third portion of ICJ in 63.6% of CD, 50% of UC, and 40% of cTB ($p \leq 0.01$). Claudin-4 expression was not significantly different between cTB, UC, and CD (Table 1; Fig. 4g–l).

Zo-1 expression was diffuse on the luminal surface epithelium in control biopsies but in all disease groups its expression was focal [27% of patients with CD, 70% of patients with UC, and 70% of patients with cTB (p=0.32)]. Similarly, in *crypt* epithelium, Zo-1 expression was also focal [72.7% in CD, 70% in UC, and 60% in cTB in comparison to control biopsies (p=0.6)]. Expression was not significantly different between the luminal surface and *crypt* epithelium or between the cTB and CD–UC group (p=0.2) (Table 1; Fig. 4a–f).

Occludin expression was not significantly different in CD, UC, and cTB biopsies as compared to control biopsies. Consistent expression of occludin was noted on luminal surface and *crypt* epithelium and nuclei (Table 1).

Histopathological findings in different disease groups

Variable histopathological changes were identified in the biopsies examined. Architectural distortion of mucosal glands was noted in 54.5% of CD, in 70% of UC, and in 50% of cTB; significant mucosal epithelial damage was noted in 54.5% CD, in 70% UC, and in 90% cTB. Granulomas were most frequently seen in cTB (100%), while in 63.6% of biopsies from patients with CD microgranulomas (<100 μm) were noted. In none of the biopsies from UC patients in our series

Table 1 Expression of key tight junction proteins in colonic biopsies from patients with CD, UC, and cTB

Site		Parameters	CD	UC	cTB	*P* value
ZO-1	Mucosal surface	Distribution	27%	70%	70%	NS
		Intensity	Strong	Strong	Strong	NS
		Site of expression	Surface	Surface	Surface	NS
	Crypt surface	Distribution	73%	70%	60%	NS
		Intensity	Strong	Strong	Strong	NS
		Site of expression	Surface	Surface	Surface	NS
Claudin-2	Mucosal surface	Distribution	75%	60%	30%	0.02
		Intensity	91%	70%	80%	0.05
		Site of expression	55% full ICJ	100% full ICJ	Uppermost ICJ	0.01
	Crypt surface	Distribution	55%	50%	40%	NS
		Intensity	Strong	80%	70%	NS
		Site of expression	72% full ICJ	80% full ICJ	Uppermost ICJ	0.01
Claudin-4	Mucosal surface	Distribution	18%	0%	10%	0.01
		Intensity	18%	50%	50%	0.02
		Site of expression	64% lower one third ICJ	50% lower one third ICJ	40% lower one third ICJ	0.01
	Crypt surface	Distribution	0%	30%	20%	0.01
		Intensity	0%	30%	20%	0.01
		Site of expression	0%	30% lower one third ICJ	20% lower one third ICJ	0.01
Occludin	Mucosal surface	Distribution	55%	100%	50%	NS
		Intensity	55%	Strong	60%	NS
		Site of expression	73% full ICJ	Full ICJ	90% full ICJ	NS
	Crypt surface	Distribution	64%	100%	50%	NS
		Intensity	64%	Strong	60%	NS
		Site of expression	73% full ICJ	Full ICJ	90% full ICJ	NS

NS statistically not significant

were granulomas found. Granulomas >200 μm (80% in cTB vs. 18.1% in CD and 0% in UC; $p=0$) or more than five granulomas in a single slide were more frequently associated with cTB (60% vs. 9% in CD and 0% in UC; $p=0.004$). Necrotizing granulomas were also significantly more frequent in cTB than in CD or UC (80% vs. 18.18% in CD and 0% in UC; $p=0$). Histologically active cryptitis or crypt abscesses were noted in all three diseases (CD-cryptitis 27.2%; crypt abscess 18.1%; UC-cryptitis 20%; crypt abscess-40% and in cTB-cryptitis-30%; crypt abscess-in none). Dense mononuclear lamina propria inflammatory infiltrate was noted in 55% of CD and in all biopsies from UC and cTB patients. Polymorphs in substantial density were more prominently seen in colonic biopsies from UC (50%) than in biopsies from CD (18.18%) and cTB (20%) patients. Disproportionately heavy sub-mucosal inflammation was however significantly higher in TB (80%) patients than in CD (18.1%) or UC (10%).

We compared the expression pattern of various TJ proteins in different disease groups with different grades of histopathological changes; no statistically significant associations were found.

Ultra-structural changes in IBD vs. cTB

In the control colonic biopsies, ultrastructurally, the TJ was identified as the narrowest and uppermost part of ICJ (Fig. 5, arrow). On higher magnification, it was seen as a pentalaminar structure formed by two layers of cell membrane on both sides and a linear electron-dense lamina in the center (Fig. 5 (inset)). Below the TJ, the ICJ was subsequently formed by the intermediate junction, desmosomes, gap junctions, and intercellular folds from top to bottom as shown in Fig. 5.

In cTB, apoptotic changes were found among colonocytes, including cytoplasmic and nuclear vesiculation, loss of cytoplasmic glycogen, dilatation of cytoplasmic organelles, and central nuclear chromatin clearing. However, the TJ and its pentalaminar structures were intact. The other components of ICJ as described earlier were also normal in these patients. In contrast, in UC and CD there were significant alterations of TJ ultra-structure in the form of dilatation and destruction of the pentalaminar structure, along with dilatation of gap junctions and intercellular folds and multiplication of desmosomes (Table 2; Fig. 6a–d, e–h; CD and UC and cTB, respectively). Though there were ultrastructural

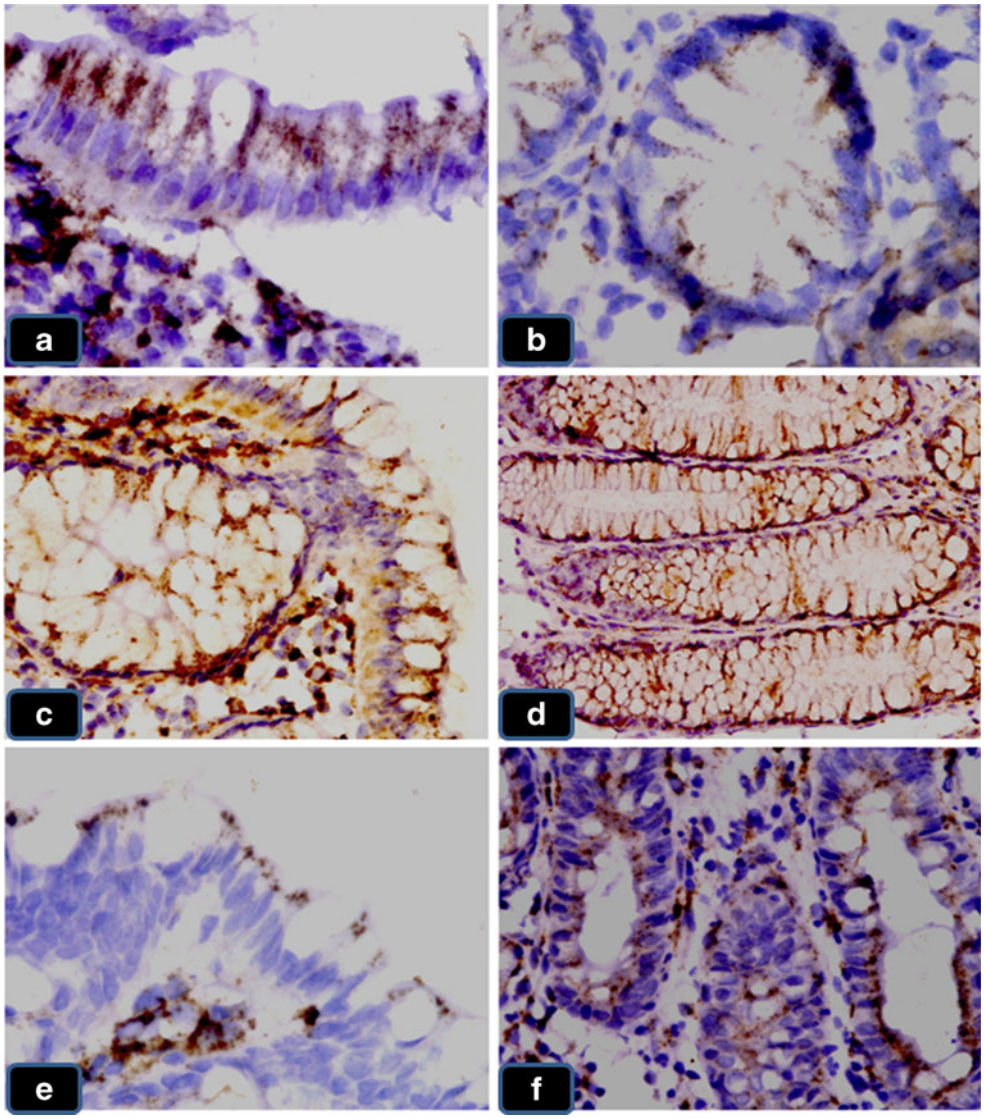

Fig. 3 Redistribution of claudin-2 expression along the whole length of ICJ in the mucosal and *crypt* epithelium in CD and UC (*arrow*) as compared to the cTB where the claudin-2 expression was noted only at the upper one third of ICJ (*arrow*). IHC (claudin-2), **a**, **b**—CD, **c**, **d**—UC, **e**, **f**—cTB –200

differences between cTB and UC-CD, no significant differences were identified between CD and UC.

Discussion

In this observational study, we highlight the differences in the expression of tight junction proteins in patients with cTB and colonic UC and CD. Our final goal was to see the expression patterns of different TJ proteins in intestinal pre- and post-treatment biopsies and to correlate those findings with functional and ultrastructural alterations. The different pattern of expression of claudin-2, a key pore-forming TJ protein, in patients with cTB, UC, and CD suggests that it is involved in the pathophysiology of these diseases. In previous studies, increased intestinal permeability has been shown in 60–80% of patients with CD (both active and recurrent) but not in cTB [11, 12].

As stated previously claudin-2 is responsible for forming pores in the TJs, while claudin-4 is a pore-sealing protein. The claudins consist of fourfold trans-membrane domains, which are quite dissimilar to occludin [3]. Though occludin has not been directly linked with the maintenance of pores, they are believed to maintain the enterocyte polarity and indirectly maintain the pores by forming hetero-polymers with different claudin proteins [15–17]. In this study, we found claudin-2 expression along the whole length of the ICJ and decreased expression of claudin-4 in patients with UC and CD. These changes may be co-responsible for diarrhea in these patients. In patients with cTB, while there was no difference in claudin-2 distribution as compared with that of controls', there was reduction in the expression of claudin-4. The persistence of a normal expression of claudin-2 in patients with cTB may explain the finding of normal intestinal permeability in patients with cTB as reported earlier [12]. As claudin-2 protein is mostly responsible for

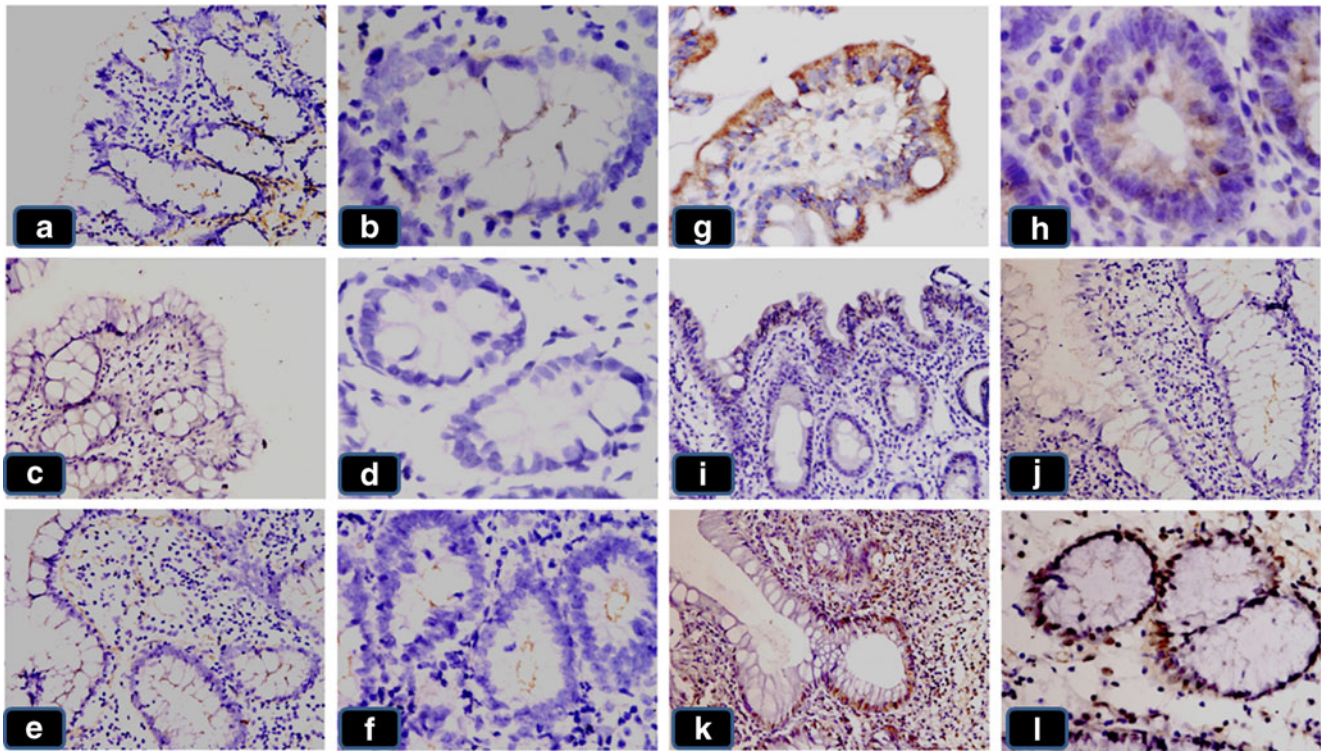

Fig. 4 Photomicrographs showing under-expression of ZO-1 in colonic CD (IHC (ZO-1), **a**, **b**×200), ulcerative colitis (IHC (ZO-1); **c**, **d**×200) and colonic tuberculosis (IHC (ZO-1), **e**, **f**×200) in comparison to the expression pattern in control biopsies where the expression was noted diffusely over the mucosal and crypt mucosa. **g**–**l** Marked reduction of claudin-4 stain distribution and intensity in colonic CD and UC and in cTB in comparison to the control biopsies. Only the focal expression of claudin-4 expression can be noted in the lower one third of ICJ in CD, UC, and cTB (IHC (claudin-4), **g**, **h**—CD, **i**, **j**—UC, **k**, **l**—cTB×200)

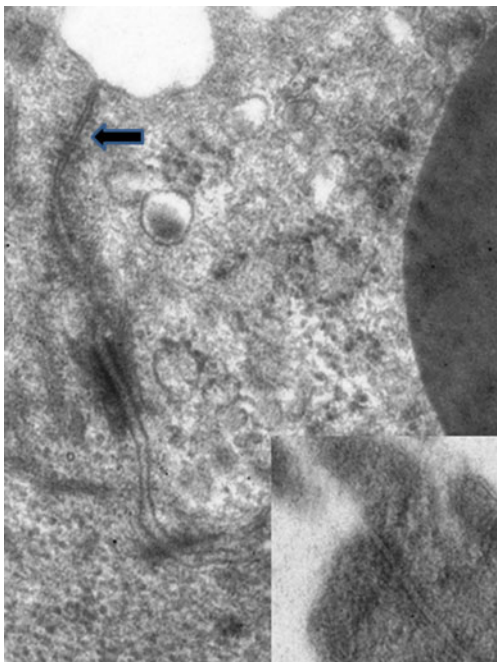

Fig. 5 Transmission electron micrograph from the control colon biopsy shows a paracellular pathway, with the tight junction situated at the top of it (*arrow*). The *inset* shows the pentalaminar structure of tight junction, comprising of cell membranes of two adjacent colonocytes and an electron-dense lamina in the center (EM×30,000; *inset*, $\times 10^5$)

trans-cellular ion transport as, e.g., Ca^{++}, Mg^{++}, etc., upregulation of this TJ protein along the full ICJ (Fig. 3) may explain the increased ionic and fluid transport across the colonic epithelium in patients with IBD.

The transmembrane hetero-polymer claudin and occludin proteins connect with the cytoplasmic actin–myosin filaments by the scaffold protein ZO-1 (Fig. 1). In the present study, we found reduced expression of ZO-1 (though not statistically significant) in all the three disease groups, more prominently in CD, in comparison to the control biopsies. It has been postulated that in chronic inflammatory conditions of the intestine, the released cytokines, specially NF-κB,

Table 2 Ultrastructural changes in colonic biopsies of patients with IBD (CD, UC) and cTB

TJ abnormalities	Colonic IBD	cTB
TJ integrity	Lost—destruction, dilatation	Maintained
TJ diameter	Increased	Maintained
TJ length	Not altered	Not altered
Penta-laminar structure	Often destroyed	Maintained
Intermediate junction	Not altered	Not altered
Desmosomes	Multiplication in UC	Not altered
Gap junctions	Often vesicular dilatation	Not altered

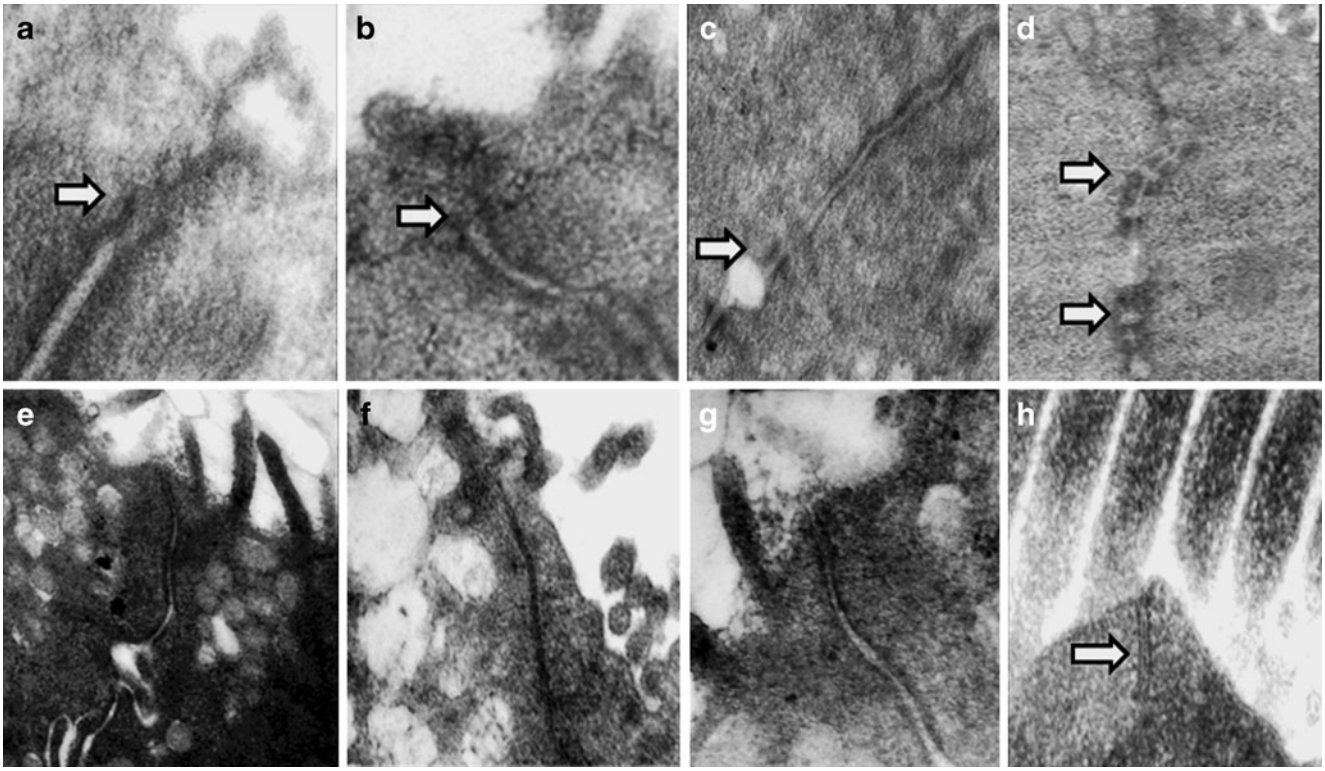

Fig. 6 Electron photomicrographs from the patients with CD and UC show varying degrees of saccular dilatation (**a**, ×120,000), destruction of pentalaminar structure (**b**, ×100,000), dilatation of gap junction (**c**, ×30,000), and multiplication of inter-cellular desmosomes (**d**, ×30,000). Photomicrographs of TEM of colon biopsies from cTB patients show the disorganization of microvilli (**e**, ×30,000), apoptotic changes (**f**, ×30,000) and a normal pentalaminar structure (**g**, **h**, ×30,000)

result in the redistribution of ZO-1 away from the ICJs [18–24]. Others observed over-expression of ZO-1 [23], which is contradictory to our findings. Among the different claudin proteins, over-expression of claudin-2 and -4 has been identified in gastrointestinal carcinomas [25–28]. In contrast to our findings, the increased expression of claudin-4 in patients with IBD has been described [29]. A correlation was also found between the levels of claudin-4 expression and the grade of inflammatory cell infiltrate [28]. We did not find any correlation between severity of inflammation (mild, moderate, or severe inflammation) and the degree of alteration in TJ protein expression. Prasad et al., in line with the present study, also identified reduced expression of claudin-4 in patients with UC [30].

As there were no alterations in occludin expression in any of these disease groups, we hypothesize that occludin may not be directly linked with the pathophysiological changes in these diseases. In occludin knock-out mouse models, it was noticed that occludin cannot only maintain selective permeability. Occludin appears to interact, directly or indirectly, with claudins and is accommodated in between the long strands of claudin-1 and claudin-2 proteins [31–34]. Its specific role in IBD could not be established from this observational study [35–37]. A few studies show an association of increased trans-epithelial electrical resistance in mammalian epithelial cells with increased occludin level [35, 38–40].

Although we did not perform immune-electron microscopical examination for localization of these proteins at ultrastructural level, the TEM showed normal TJs in biopsies of patients with cTB and variable alterations of TJ architecture and integrity of its pentalaminar structure in those with CD and UC. In patients with CD and UC, there were other changes of the paracellular junction components also. The immunohistochemical and ultrastructural findings suggest that TJs are not altered in patients with cTB, while they are altered and become leaky in patients with UC and CD.

Conclusions

In patients with CD and UC, while there was expression of the pore-forming protein claudin-2 along the whole length of the ICJ, the expression of pore-sealing protein claudin-4 was reduced. In patients with colonic TB, there was reduced expression of claudin-4 but the expression of claudin-2 remained unchanged. Ultrastructurally, while the pentalaminar structure of TJ was destroyed in patients with UC in CD, no significant alteration was observed in those with cTB. Altered claudin-2 expression, along with destroyed TJs,

may result in loss of selective permeability in patients with UC and CD. A differential expression pattern of claudin-2 in colonic UC and CD and cTB opens up a new perspective in the pathogenesis of these diseases, which must be further investigated.

Conflict of interest The authors declare no conflicts of interest.

References

1. Mariscal LG, Betanzos A, Nava P, Jaramillo BE (2003) Tight junction proteins. Prog Biophy Mol Biol 81(1):1–44
2. Unno N, Fink MP (1998) Intestinal epithelial hyper permeability mechanisms and relevance to disease. Gastroenterol Clinics North Am 27(2):289–307
3. Förster C (2008) Tight junctions and the modulation of barrier function in disease. Histochem Cell Biol 130(1):55–70
4. Oshima T, Laroux FS, Coe LL, Morise Z, Kawachi S, Bauer P, Grisham MB, Specian RD, Carter P, Jennings S, Granger DN, Joh T, Alexander JS (2001) Interferon-gamma and interleukin-10 reciprocally regulate endothelial junction integrity and barrier function. Microvasc Res 61:130–143
5. Youakim A, Ahdieh M (1999) Interferon-gamma decreases barrier function in T84 cells by reducing ZO-1 levels and disrupting apical actin. Am J Physiol 276:G1279–G1288
6. Hollander D (1993) Permeability in Crohn's disease: altered barrier functions in healthy relatives? Gastroenterology 104:1848–1851
7. Peeters M, Geypens B, Claus D, Nevens H, Ghoos Y, Verbeke G, Baert F, Vermeire S, Vlitienck S, Rutgreets P (1997) Clustering of increased small intestinal permeability in families with Crohn's disease. Gastroenterology 113:802–807
8. Nusrat A, Parkos CA, Verkade P, Foley CS, Liang TW, Innis-Whitehouse W, Eastburn KK, Madara JL (2000) Tight junctions are membrane microdomains. J Cell Sci 113:1771–1781
9. Zeissig S, Burgel N, Gunzel D, Richter J, Mankertz J, Wahnschaffe U, Kroesen AJ, Zeitz M, Fromm M, Schulzke JD (2007) Changes in expression and distribution of claudin 2, 5 and 8 lead to discontinuous tight junctions and barrier dysfunction in active Crohn's disease. Gut 56:61–72
10. Weber CR, Turner JR (2007) Inflammatory bowel disease: is it really just another break in the wall? Gut 56:6–8
11. Benjamin J, Makharia GK, Ahuja V, Kalaivani M, Joshi YK (2008) Intestinal permeability and its association with the patient and disease characteristics in Crohn's disease. World J Gastroenterol 14(9):1399–1405
12. Wallaert B, Colombel JF, Adenis A, Marchandise X, Hallgren R, Janin A, Tonnel AB (1992) Increased intestinal permeability in active pulmonary sarcoidosis. Am Rev Respir Dis 145(6):1440–1445
13. Paustian FF (1995) Tuberculosis of the intestine. In: Bockus HL (ed) Bockus castroenterology, vol 4, 5th edn. Saunders, Philadelphia, p 3304
14. Logan VSCD (1969) Anorectal tuberculosis. Proc R Soc Med 62:1227–1230
15. Ando-Akatsuka Y, Saitou M, Hirase T, Kishi M, Sakakibara A, Itoh M, Yonemura S, Furuse M, Tsukita S (1996) Interspecies diversity of the occludin sequence: cDNA cloning of human, mouse, dog, and rat–kangaroo homologues. J Cell Biol 133:43–47
16. Furuse M, Fujita K, Hiiragi T, Fujimoto K, Tsukita S (1998) Claudin- 1 and -2: novel integral membrane proteins localizing at tight junctions with no sequence similarity to occludin. J Cell Biol 141:1539–1550
17. Tsukita S, Furuse M, Itoh M (2001) Multifunctional strands in tight junctions. Nat Rev Mol Cell Biol 2:285–293
18. Ma TY, Iwamoto GK, Hoa NT, Akotia V, Pedram A, Boivin MA, Said HM (2004) TNF-alpha-induced increase in intestinal epithelial tight junction permeability requires NF-kappa B activation. Am J Physiol 286:G367–G376
19. MacDonald TT, Hutchings P, Choy MY, Murch S, Cooke A (1990) Tumour necrosis factor-alpha and interferon-gamma production measured at the single cell level in normal and inflamed human intestine. Clin Exp Immunol 81:301–305
20. Ye D, Ma I, Ma TY (2006) Molecular mechanism of tumor necrosis factor-alpha modulation of intestinal epithelial tight junction barrier. Am J Physiol Gastrointest Liver Physiol 290:G496–G504
21. Mankertz J, Tavalali S, Schmitz H, Mankertz A, Riecken EO, Fromm M, Schulzke JD (2000) Expression from the human occludin promoter is affected by tumor necrosis factor alpha and interferon gamma. J Cell Sci 113:2085–2090
22. Sapone A, de Magistris L, Pietzak M, Clemente MG, Tripathi A, Cucca F, Lampis R, Kryszak D, Cartenì M, Generoso M, Iafusco D, Prisco F, Laghi F, Riegler G, Carratu R, Counts D, Fasano A (2006) Zonulin upregulation is associated with increased gut permeability in subjects with type 1 diabetes and their relatives. Diabetes 55(5):1443–1449
23. Fasano A, Uzzau S, Fiore C, Margaret K (1997) The enterotoxic effect of zonula occludens toxin (Zot) on rabbit small intestine involves the paracellular pathway. Gastroenterology 112:839–846
24. Marinaro M, Fasano A, De Magistris MT (2003) Zonula occludens toxin acts as an adjuvant through different mucosal routes and induces protective immune responses. Infect Immun 71(4):1897–1902
25. Schneeberger EE, Lynch RD (2004) The tight junction: a multifunctional complex. Am J Physiol Cell Physiol 86:C1213–C1228
26. Ebnet K (2008) Organization of multiprotein complexes at cell–cell junctions. Histochem Cell Biol Histochem Cell Biol 130(1):1–20
27. Németh Z, Szász AM, Tátrai P, Németh J, Gyorffy H, Somorácz A, Szíjártó A, Kupcsulik P, Kiss A, Schaff Z (2009) Claudin-1, -2, -3, -4, -7, -8 and -10 protein expression in biliary tract cancers. J Histochem Cytochem 57:2113–2121
28. Soler AP, Miller RD, Laughlin KV, Card NZ, Klurfeld DM, Mullin JM (1999) Increased tight junctional permeability is associated with the development of colon cancer. Carcinogenesis 20:1425–1431
29. Weber CR, Nalle SC, Tretiakova M, Rubin DT, Turner JR (2008) Claudin-1 and claudin-2 expression is elevated in inflammatory bowel disease and may contribute to early neoplastic transformation. Lab Invest 88:1110–1120
30. Prasad S, Mingrino R, Kaukinen K, Hayes KL, Powell RM, MacDonald TT, Collins JE (2005) Inflammatory processes has differential effects on claudins 2, 3 and 4 in colonic epithelial cells. Lab Invest 85:1139–1162
31. Shao L, Serrano D, Mayer L (2001) The role of epithelial cells in immune regulation in the gut. Semin Immunol 13:163–176
32. Furuse M, Fujimoto K, Sato N, Hirase T, Tsukita S, Tsukita S (1996) Over-expression of occludin, a tight junction-associated integral membrane protein, induces the formation of intracellular multi-lamellar bodies bearing tight junction-like structures. J Cell Sci 109:429–435
33. Saitou M, Fujimoto K, Doi Y, Schulzke JD, Fromm M, Takano H, Noda T, Tsukita S (1998) Occludin-deficient embryonic stem cells can differentiate into polarized epithelial cells bearing tight junctions. J Cell Biol 141:397–408
34. Furuse M, Sasaki H, Fujimoto K, Tsukita S (1998) A single gene product, claudin-1 or -2, reconstitutes tight junction strands and recruits occludin in fibroblasts. J Cell Biol 143:391–401

35. Furuse M, Sasaki H, Tsukita S (1999) Manner of interaction of heterogeneous claudin species within and between tight junction strands. J Cell Biol 147:891–903
36. Balda MS, Whitney JA, Flores C, González S, Cereijido M, Matter K (1996) Functional dissociation of paracellular permeability and trans-epithelial electrical resistance and disruption of the apical–basolateral intramembrane diffusion barrier by expression of a mutant tight junction membrane protein. J Cell Biol 134:1031–1049
37. McCarthy M, Skare IB, Stankewich MC, Furuse M, Tsulita S, Rogers RA, Lynch RD, Schneeberger EE (1996) Occludin is a functional component of the tight junction. J Cell Sci 109:2287–2298
38. Bamforth SD, Kniesel U, Wolburg H, Engelhardt B, Risau W (1999) A dominant mutant of occludin disrupts tight junction structure and function. J Cell Sci 112:1879–1888
39. Saitou M, Furuse M, Sasaki H, Schulzke JD, Fromm M, Takano H, Nodall T, Tsukita S (2000) Complex phenotype of mice lacking occludin, a component of tight junction strands. Mol Biol Cell 11:4131–4142
40. Furuse M, Hirase T, Itoh M, Nagafuchi A, Yonemura S, Tsukita S, Tsukita S (1993) Occludin: a novel integral membrane protein localizing at tight junctions. J Cell Biol 123:1777–1788

Virchows Arch (2012) 460:271–279
DOI 10.1007/s00428-012-1201-7

ORIGINAL ARTICLE

SOX9 expression and its methylation status in gastric cancer

Minhua Sun · Hiroshi Uozaki · Rumi Hino · Akiko Kunita · Aya Shinozaki · Tetsuo Ushiku · Takashi Hibiya · Kimiko Takeshita · Maya Isogai · Kenzo Takada · Masashi Fukayama

Received: 6 June 2011 / Revised: 11 January 2012 / Accepted: 22 January 2012 / Published online: 14 February 2012
© Springer-Verlag 2012

Abstract SOX9 is a member of the SOX [Sry-related high-mobility group (HMG) box] family and is required for the development and differentiation of multiple cell lineages. To clarify the significance of SOX9 in gastric carcinoma (GC), immunohistochemical expression of SOX9 and the CpG island methylation status of *SOX9* were evaluated and compared with clinicopathological factors including overall survival. SOX9 expression was immunohistochemically evaluated in 382 GC tumors and the methylation status was examined in 121 GC tumors. SOX9 expression and its methylation status in six GC cell lines, their Epstein–Barr virus (EBV)-infected cell lines, and two EBV-associated GC cell lines was also examined. The SOX9 expression increased from non-neoplastic mucosa to early cancer. High expression of SOX9 was seen in 212 cases (56%). SOX9 expression was inversely related to advanced tumor stage, vessel infiltration, nodal metastasis, and EBV infection. Fifty-eight (48%) of 121 GC tumors had a methylated promoter in GC and the methylated status was related to low expression. The expression and methylation status were not related to prognosis. Three of six cell lines had increased methylation through EBV infection and decreased SOX9 expression. Upregulation of SOX9 is related to GC development. Downregulation by promoter methylation is related to GC progression and EBV infection. SOX9 is closely related to GC carcinogenesis and EBV-associated GC carcinogenesis.

Keywords SOX9 · Gastric cancer · Epstein–Barr virus · Immunohistochemistry · CpG island methylation

M. Sun · H. Uozaki (✉) · R. Hino · A. Kunita · A. Shinozaki · T. Ushiku · T. Hibiya · K. Takeshita · M. Isogai · M. Fukayama
Department of Pathology, Graduate School of Medicine,
The University of Tokyo,
7-3-1 Hongo, Bunkyo-ku,
Tokyo 113-0033, Japan
e-mail: uozaki-tky@umin.ac.jp

K. Takada
Department of Tumor Virology, Institute for Genetic Medicine,
Hokkaido University,
Sapporo, Japan

Introduction

Gastric carcinoma (GC) is the second most common cause of cancer-related mortality in the world, and occurs commonly in Eastern Asia. *Helicobacter pylori* and Epstein–Barr virus (EBV) are widely disseminated agents in the pathogenesis of GC [1]. Recently, the correlation between anomalous expression of transcription factors, such as SOXs, CDXs, and GATAs, and carcinogenesis has attracted extensive research attention in various cancers, including gastric cancer [2–4].

The SOX family has been identified through their homology to the high-mobility group (HMG) box of sex-determining region Y, and encodes transcription factors that bind to DNA through a HMG domain and play critical roles in cell fate determination, differentiation, and proliferation [5]. SOX9 belongs to the subgroup of the *SOX* E family, which is a key regulator of developmental processes, including male sex determination, chondrogenesis, neurogenesis, and neural crest development [6–9]. Heterozygous SOX9 mutations are the cause of the human disease campomelic dysplasia, a form of dwarfism characterized by extreme cartilage and bone malformation, which is frequently associated with XY sex reversal [10]. The major targets of SOX9 have been identified during chondrogenesis, including type-II collagen (Col2a1) and type XI collagen gene (Col11a2),

and anti-Mullerian hormone (also known as Müllerian-inhibiting substance) [11]. SOX9 is additionally essential for gastrointestinal tract development. SOX9 expression in intestinal crypt cells is regulated by the Wnt/β-catenin signaling pathway [12], which has been identified as one of the key pathways in the initiation and development of colorectal cancer and in gastrulation and morphogenesis and maintenance of crypt stem cell self-renewal.

EBV-associated GC has been identified in the last two decades. It is a distinct subgroup of GC, comprising about 10% of all cases of GC [1]. EBV-associated GC exhibits global and nonrandom DNA hypermethylation of the promoter regions of various cancer-associated genes [13]. This high activity of CpG island methylation is referred to as the CpG island methylator phenotype (CIMP), and EBV-associated GC is usually included in cases of CIMP-high GC.

Recent studies have shown the emerging role of SOX9 in cancer [14, 15]. To our knowledge, no studies have shown the clinical significance of SOX9 expression and CpG island methylation in gastric cancer. Here, we conducted comprehensive immunohistochemical analysis of SOX9 expression at the protein level in cases of gastric cancer and precancerous lesions. Next, we examined the SOX9 expression and methylation status in GC cell lines. We revealed the role of SOX9 in GC, comparing the status and clinicopathological data.

Materials and methods

Patients and samples

Three hundred eighty-two primary gastric carcinoma tissues (39 EBV-associated and 343 EBV-negative GCs; 28–90 years old; 274 males and 108 females) were examined in our immunohistochemical study. They were obtained from GC patients who had undergone surgery at the University of Tokyo Hospital, from 1990 to 2008.

Tissue arrays were constructed from formalin-fixed and paraffin-embedded blocks of GC tissues. Briefly, two columns of 2 mm in diameter from each representative GC block were used for construction of tissue arrays. Additionally, three adenomas and six non-neoplastic gastric tissues, including three cases of intestinal metaplasia, were retrieved. All blocks were sectioned in 4 μm slices and stained. One hundred twenty-one frozen samples of GC were used to analyze the SOX9 methylation status. One hundred eight cases were examined both in the immunohistochemical study and in the methylation status analysis.

All GCs were histologically evaluated according to the Japanese Classification of Gastric Carcinoma and Lauren's classification [16, 17]. The presence of EBV in the carcinoma tissues was evaluated by in situ hybridization (ISH) targeting EBV-encoded small RNA (EBER-ISH) with an EBER-RNA probe (DakoCytomation).

Immunohistochemical analysis

All specimens were deparaffinized, rehydrated, and underwent an antigen retrieval procedure and 10 min of autoclaving in citrate buffer pH 6.0. Immunohistochemical staining with a rabbit polyclonal SOX9 antibody (1:3,000 dilution; Millipore) was applied to the sections using LSAB2 kit (Dako) and visualized with DAB. For negative controls, the primary antibodies were replaced with a PBS solution. Normal testis was used as SOX9-positive controls.

Evaluation of immunohistochemical staining data

Both the intensity of immunohistochemical staining of SOX9 and proportion of stained epithelial cells were evaluated according to a previous study [18]. The percentages of positive tumor cells were scored using the following scale: 0, no staining or <5%; 1, 5–25%; 2, 26–50%; 3, 51–75%; 4, >75%. The intensity of SOX9 staining was scored as 0, none; 1, weak; 2, intermediate; or 3, strong. The percentage of positivity of the tumor cells, and staining intensity were multiplied to generate the immunoreactive score (IS) for each tumor specimen. All samples were separately examined by two pathologists (M.S. and H.U.). We interpreted IS 0–5 as low expression and over 5 as high expression.

GC cell lines

We studied six GC cell lines (MKN1, MKN7, MKN74, TMK1, AGS, and NUGC3), and two EBV-associated GC cell line (SNU719 and KT [19]). We made six EBV-infected GC cell lines from six GC cell lines with recombinant EBV using the cell-to-cell contact method [20, 21].

Western blot analysis

The cells were lysed in a lysis buffer consisting of 20 mM Tris-HCl (pH 7.5), 150 mM NaCl, 5 mM EDTA, 1% NP40, 50 mM NaF, 0.1%SDS, 1 mM phenylmethylsulfonyl fluoride, and protein inhibitor cocktail (Sigma-Aldrich). Typically, 30 μg of the protein was loaded per lane and was first separated on a 10% sodium dodecyl sulfate–polyacrylamide gel and then electrophoretically transferred to a polyvinylidene fluoride (PVDF) membrane. The PVDF membrane was incubated with the primary SOX9 antibody overnight at 4°C, followed by a peroxidase-linked secondary antibody (GE Healthcare UK Ltd., Buckinghamshire, UK) for 1 h at room temperature. Enhanced chemiluminescence western blotting detection system (GE Healthcare UK Ltd.) was used for the detection.

RNA extraction and semiquantitative Reverse transcription-PCR

Total RNA was isolated with Trizol reagent (Life Technologies, Carlsbad, CA) and reverse transcribed with a Super Script III First-Strand Synthesis System (Life Technologies). PCR amplification was carried out using the Platinum GeneAmp PCR System 9700 (Life Technologies) with specific oligonucleotide primer sequences as follows: *SOX9* sense primer, 5′-AGTACCCGCACTTGCACAAC-3′ and 5′-CGTTCTTCACCGACTTCCTC-3′; *GAPDH* sense 5′-GAAGGTGAAGGTCGGAGTC-3′ and antisense 5′-GAAGATGGTGATGGGATTTC-3′. We amplified *SOX9* and *GAPDH* with 28 cycles of PCR and electrophoresed the products. cDNA of a colorectal cancer cell line, SW480, was used as a positive control.

DNA extraction and methylation-specific PCR

DNA was extracted from the cultured cell lines and 121 frozen primary GC samples using a DNeasy Tissue kit (Qiagen). All GC samples were specimens surgically resected at the University of Tokyo Hospital from 2003 to 2008. DNA was modified by the bisulfite reaction using an EpiTect Bisulfite kit (Qiagen). The methylation status of the SOX9 promoter region was determined by methylation-specific PCR (MSP) using bisulfite-modified DNA. We used MSP primers which were previously reported in a preliminary study [22], but it did not amplify DNA efficiently and did not correlate with the expression. We therefore designed new MSP primers for the SOX9 gene between −1,000 and +500 of the transpription start site. New primers were established using Methyl Primer Express software v1.0 (Applied Biosystems) and were confirmed to amplify bisulfite-treated DNA controls efficiently. It spanned a region of approximately 300 bp immediately downstream of the transcription start site. Primer sequences of SOX9 for methylated alleles were as follows: forward 5′-TGTTTCGTATTCGGGTAGTC-3′ and reverse 5′-CCTACTCGTCGATCATCTTC-3′ (+265–+415 region from the transcription start site); those for unmethylated alleles were: forward 5′-GTTTGTTTTGTATTTGGGTAGTT-3′ and reverse 5′-CCTTCTCCTACTCATCAATCATC-3′. DNA from gastric cancer cells treated in vitro with a CpG methyltransferase (M.SssI) (New England Biolabs Inc.) was used as a positive control for methylated alleles. DNA amplified with a GenomiPhi V2 DNA Amplification kit (GE Healthcare Life Sciences) was used as a positive control for unmethylated alleles; no template control was included in each experiment. PCR products were electrophoresed in 2% agarose gels. MSP experiments were performed at least in triplicate. Additionally, five CIMP markers, *LOX*, *HRASLS*, *FLNc*, *HAND1*, and *TM*, are examined as our previous study [23]. CIMP-N, CIMP-I, and CIMP-H status were determined by the number of methylated genes (0, 1–3, and 4–5, respectively).

Some cell lines are further examined with bisulfite sequencing, using primers, 5′-TTTTTTTTTTTTTTTTTTTTAATTYGTTT-3′ and 5′-AAAAACTTATCCTCCTCRCTCT-3′, which amplifies 447 bp products (+135–+581 region from the transcription start site), including 45 CpG sites.

Statistical analysis

Statistical analyses were performed using chi-square tests, Fisher's exact test, or the Mann–Whitney *U* test. Overall survival was calculated from the day of surgery. Survival was analyzed with the Kaplan–Meier method and examined by the Wilcoxon test. Differences were considered significant when $P<0.05$. This study was approved by our institutional review board (No. 710).

Results

SOX9 expression in normal epithelium, intestinal metaplasia, and adenoma

In normal gastric epithelium, SOX9 positivity was nuclear and was observed in the proliferative zone of the glands (Fig. 1). In intestinal metaplasia, the lower part of the crypt was positive for SOX9 and was identical to the proliferating zone of intestinal metaplasia. Gastric adenomas showed extensive SOX9 positivity with uniform positivity from the lower to upper zone of crypts.

SOX9 expression in GC

Examples of SOX9 immunostaining of GC are shown in Fig. 1. The distribution of SOX9-IS was as follows: Score 0 $N=33$, 1 $N=5$, 2 $N=40$, 3 $N=40$, 4 $N=52$, 6 $N=87$, 8 $N=48$, 9 $N=31$, 12 $N=46$. Two hundred twelve tumors (56%) showed high expression. Figure 1d, e shows examples of SOX9 positivity.

The correlation of SOX9 expression with clinicopathological parameters in gastric cancer patients is summarized in Table 1. SOX9 was more frequently expressed in the middle or lower part of the stomach ($P=0.002$). SOX9 low expression was related to many clinicopathological factors, including tumor advanced stage, vessel infiltration, nodal metastasis, and EBV infection.

SOX9 expression was not related to the overall prognosis of GC (Fig. 2a, $P=0.365$).

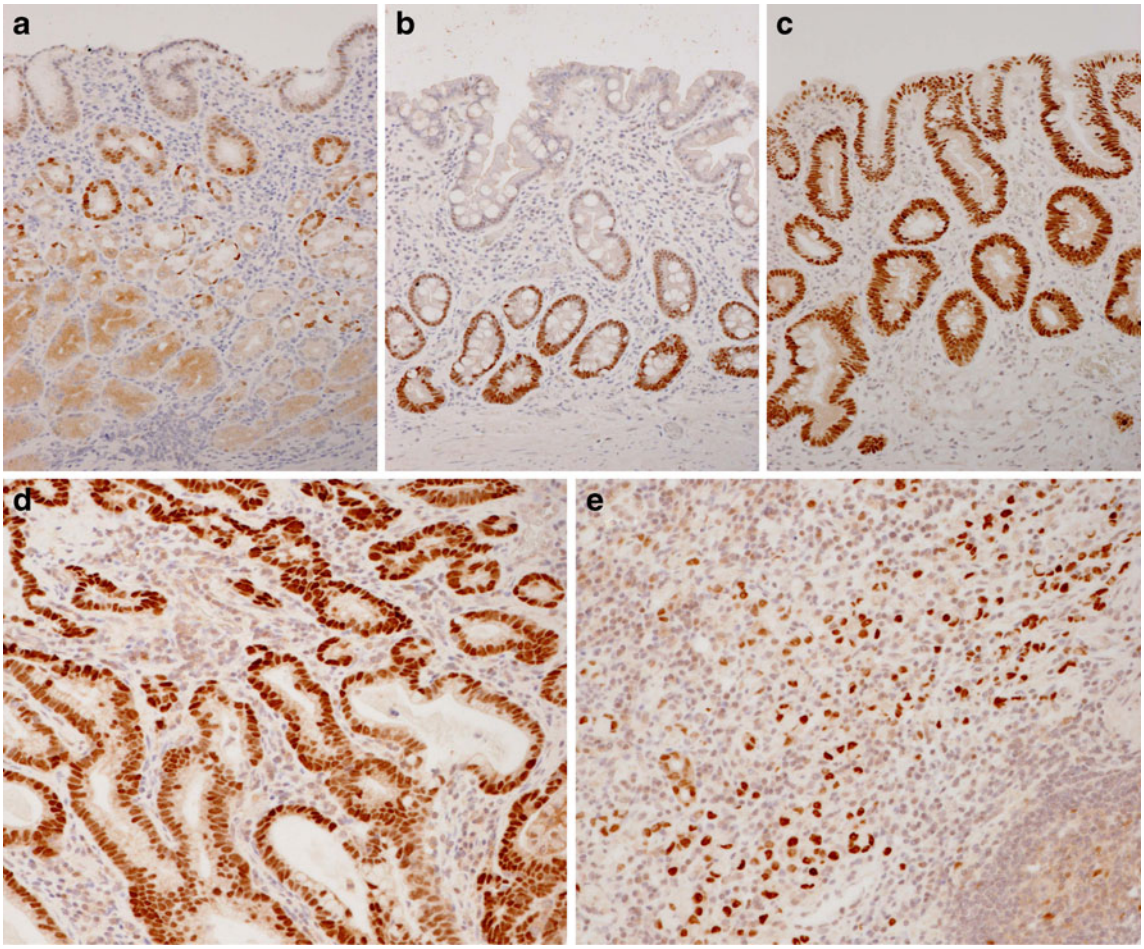

Fig. 1 SOX9 expression and immunohistochemical stain of normal epithelium (**a**), intestinal metaplasia (**b**), gastric adenoma (**c**), and gastric carcinoma (**d**, **e**). **a**–**c** shows an increase of SOX9 positivity during early carcinogenesis of GC. **d** Percentage score 4 and intensity score 3, IS 12. **e** Percentage score 3, intensity score 2, IS 6

SOX9 methylation status in GC and its relation with clinicopathological factors

Fifty-eight tumors (47.9%) from 121 samples were methylated in the MSP study (Fig. 3a, b). Methylated tumors showed more frequent low expression of SOX9 immunohistochemistry (29/50 58% vs unmethylated 20/58 34.5%, P=0.014). Among 121 samples, CIMP-H was 28, CIMP-I was 75, and CIMP-N was 10. SOX9 methylation status was not related to the CIMP status (P=0.758).

Table 1 The relationship between SOX9 expression and clinicopathological factors

Clinicopathological factors	Sox9		*P* value
	+	–	
Age (year old)	64.6±11.0	63.7±12.4	0.446
Gender (male/female)	148/64	126/44	0.353
Tumor size (cm)	47.2±33.9	57.7±37.0	0.004
Location (U/M/L)	40/101/71	59/60/51	0.002
Clinic stage (early/advanced)	123/88	68/102	0.0003
Lauren's classification (intestinal/diffuse)	111/101	77/93	0.170
Lymphatic invasion (positive/negative)	68/144	89/81	<0.0001
Venous infiltration (positive/negative)	85/127	98/72	0.0006
Nodal metastasis (positive/negative)	62/133	84/83	0.0003
EBV infection (positive/negative)	6/206	33/137	<0.0001

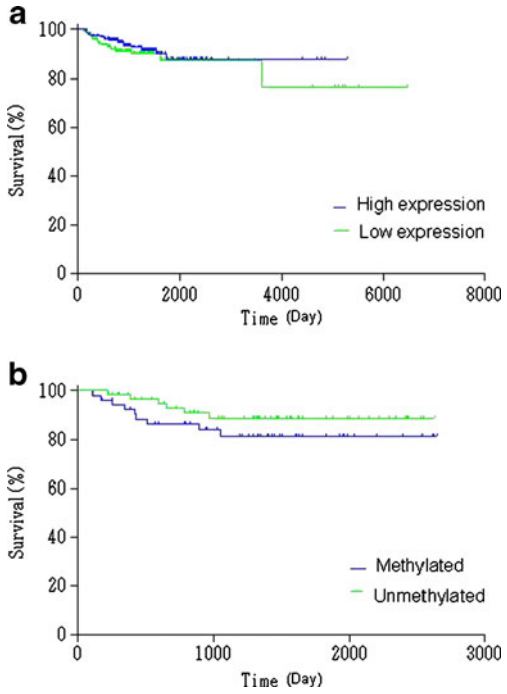

Fig. 2 **a** Overall survival curve by SOX9 immunohistochemical expression. SOX9 low expression group showed slightly poor prognosis, but the difference was not significant (P=0.365). **b** Survival curve by SOX9 methylation status. Methylated SOX9 group showed mildly poor prognosis, but it was not significant (P=0.211)

The relation between the SOX9 methylation status and clinicopathological factors is summarized in Table 2. EBVaGC included significantly more SOX9-methylated GC (P=0.041), which showed more venous infiltration and nodal involvement (P=0.045, 0.008). Methylated SOX9 did not show a significant difference in prognosis (P=0.211, Fig. 2b).

SOX9 CpG island hypermethylation and its association with transcriptional gene silencing in GC cell lines

Since our studies demonstrated that SOX9 was frequently lost in some GC cases and was more markedly lost in EBV-associated GCs, we examined whether these abnormalities were observed in vitro. First, by means of semiquantitative reverse transcription (RT)-PCR and Western blot analysis, we investigated SOX9 expression in six GC cell lines and their EBV-infected cell lines and also in two EBV-associated GC cell lines, SNU-719 and KT tumor (Fig. 3c, d). The SOX9 transcript expression pattern is almost consistent with the results of Western blot analysis. The levels of *SOX9* mRNA expression differed among original GC cell lines: MKN-1 and KT did not exhibit *SOX9* expression. MKN7 and TMK1 expressed *SOX9* faintly. MKN74 and SNU-719 showed moderate expression. AGS and NUGC-3 exhibited high expression. Downregulation of SOX9 was observed markedly in 4 EBV-infected GC cell lines (MKN1-EBV, MKN7-EBV, TMK1-EBV, NUGC3-EBV); however, MKN74 and AGS did not change their SOX9 expression through EBV infection.

Next, the methylation status of *SOX9* promoter was evaluated by MSP in these cell lines (Fig. 3d). All the cells show U genes and some shows M genes. It means that the cell lines showing M genes have heterogenously methylated. CpG methylation rose in three GC cell lines; MKN7, TMK1, and NUGC3, through EBV infection. Two originally EBV-associated GC cell lines, SNU0719 and KT, showed methylated *SOX9* promoter. EBV-MKN7, EBV-NUGC3, and KT showed downregulated SOX9 expression. MKN7 and NUGC3 with/without EBV were further evaluated by bisulfite sequence (Fig. 4a). MKN7-EBV, which was M in MSP, shows almost complete methylation in the CpGs around the MSP site, whereas MKN7 showed few methylation. NUGC3-EBV also show many methylated sites, but a clone with few methylation was revealed among five clones.

To further confirm that SOX9 expression-loss was caused by promoter methylation, MKN-7 and MKN7-EBV were incubated with 3 μM 5-aza-2′-deoxycytidine (5-Aza). This treatment restored *SOX9* expression in MKN7-EBV in a quantitive real time RT-PCR study with same primers used in the semiquantitive RT-PCR study (Fig. 4b). On the other hand, MKN7 did not increase SOX9 expression after 5-Aza treatment. This result shows that *SOX9* was repressed by methylation in MKN7-EBV.

Discussion

SOX9 is involved in the development of various organs, including the nervous system [24], cartilage [25], prostate [26], testis [27], and the pyloric region of the stomach [28]. In the digestive tract, SOX9 is essential for Paneth cell differentiation [29, 30] and represses CDX2 and MUC2 [12]. There are a few reports of SOX9 expression in gastrointestinal cancers. Among GC, SOX9 is related to the intestinal type [31]. SOX9 was downregulated in colonic cancer [32]. We investigated SOX9 expression and methylation status in GC in detail in this study.

SOX9 and GC carcinogenesis

Our results showed that SOX9 was expressed in a two-stage pattern during the whole metaplasia-adenoma early-advanced carcinoma sequence of the stomach. Firstly, the increase of SOX9 occurred at the normal-metaplasia-adenoma transition. Secondly, we found that SOX9 decreased during the progression from early to advanced GC.

SOX9 was expressed more in intestinal metaplasia and adenoma. We additionally compared SOX9 expression with

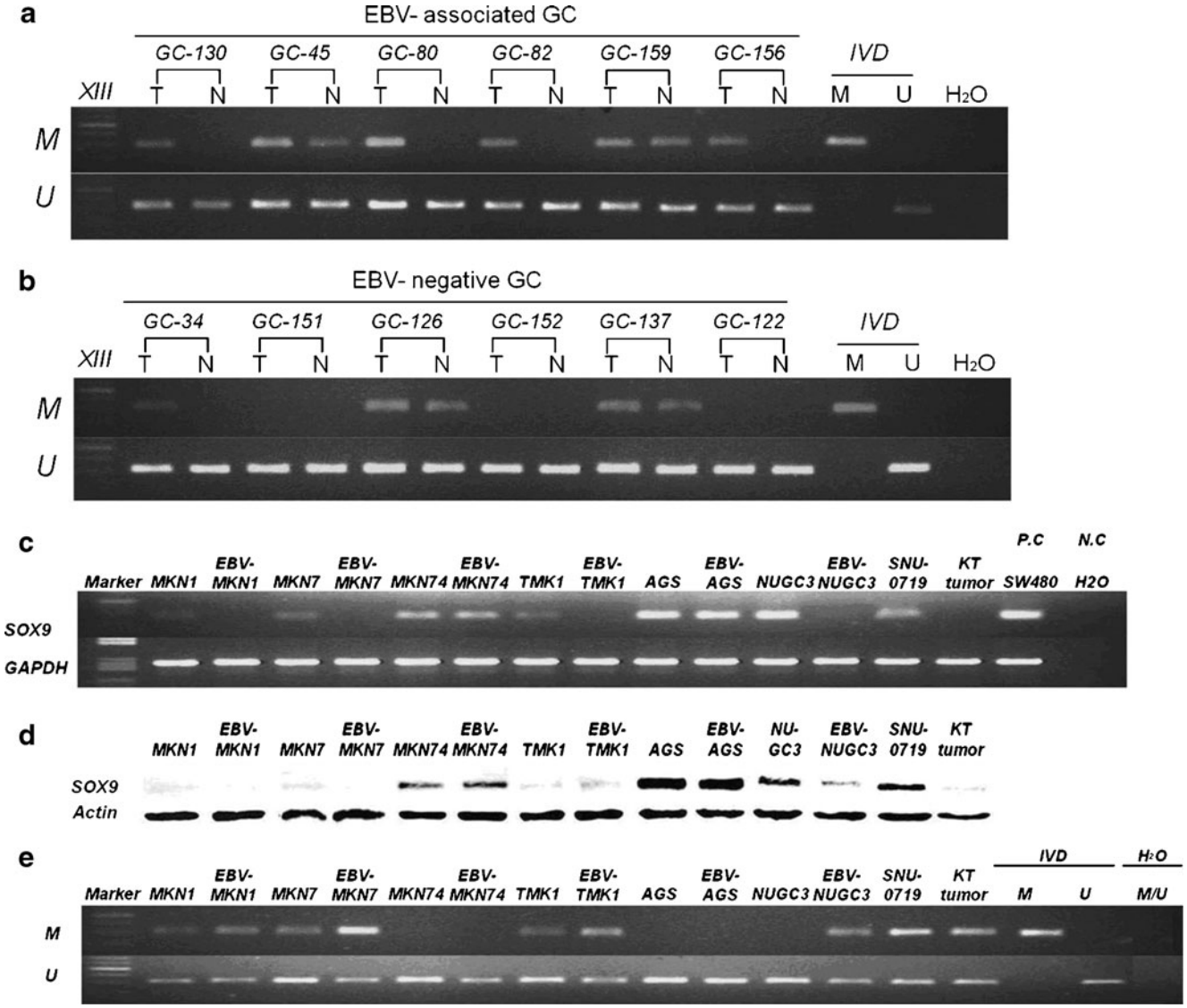

Fig. 3 Methylation status of SOX9 CpG islands and SOX9 expression in surgical samples and cell lines. **a** MSP results of EBV-associated GC. Tumors (*T*) and their corresponding non-neoplastic tissues (*N*) were examined. Unmethylated (*lanes U*) and methylated (*lanes M*) MSP products were displayed on 2% agarose gels. *IVD* in vitro-methylated control. Six out of 7 EBV-associated GC showed methylated SOX9 promoters. **b** MSP results in EBV-negative GC. Fifty-one out of 114 EBV-negative GC showed methylated SOX9 promoters. **c** RT-PCR analysis of SOX9 expression in GC cell lines and their EBV-infected cell lines. GAPDH transcripts were used as transcript controls. The levels of SOX9 mRNA expression differed among original GC cell lines. Downregulation of SOX9 was observed markedly in 4 EBV-infected GC cell lines (*MKN1-EBV, MKN7-EBV, TMK1-EBV, NUGC3-EBV*). **d** Western blot analysis of GC cell lines. Actin was used as a control. The results were almost concordant with immunohistochemical results. **e** MSP analysis of the SOX9 promoter in GC cell lines. The hypermethylated cell lines, *MKN7-EBV, TMK1-EBV*, and *NUGC3-EBV*, showed relatively low transcript and protein expression of SOX9 compared to the original cell lines

CDX2 expression in 378 tumors which were used in our previous study [2]. SOX9 was related to CDX2 expression ($P<0.0001$, chi-square test). SOX9 is reported to regulate CDX2 and MUC2 in the intestine [12]. Further study is needed to know whether the same regulation by SOX9 is working in GC as in the intestine.

SOX9 is reported as a tumorigenic gene in lung cancer [33], and prostatic cancer [15, 34], but inhibits melanoma [35]. High SOX9 expression is related to poor prognosis in colon cancer [14] and breast cancer [36]. SOX9 overexpression in colon cancer is associated with constituent β-catenin activation [12], which has been implicated in the initiation and progression of many types of cancer [37]. Sonic hedgehog signaling can maintain SOX9 overexpression in skin tumors [38]. Insulin receptor substrate-1 can modulate the number of SOX9 positive cells in intestinal crypts [39].

Table 2 Comparison of SOX9 methylation status with clinicopathological characteristics

Clinicopathological factors	M	U	*P* value
Age (year old)	64.9±12.1	62.0±12.9	0.220
Gender (male/female)	37/18	42/19	0.855
Tumor size (cm)	5.6±3.3	5.0±3.3	0.332
Tumor location (U/M/L)	14/18/22	14/29/17	0.234
Tumor stage (early/advanced)	18/39	28/35	0.148
Lauren's classification (intestinal/diffuse)	22/33	26/35	0.774
Lymphatic infiltration (negative/positive)	24/31	37/24	0.067
Venous infiltration (negative/positive)	17/38	30/31	0.045
Nodal metastasis (negative/positive)	23/29	42/19	0.008
EBV infection (negative/positive)	51/6	63/1	0.041

However, much work needs to be done on the regulatory mechanism of SOX9 expression in gastric carcinogenesis.

We revealed that SOX9 is related to the development of GC, but it decreases through the progression of GC and does not affect overall survival. We hypothesized that SOX9 assists the development of GC in the early stage by accelerating cell cycle or reducing apoptosis, and that SOX9 is not essential in the progression or invasion of GC and is decreased and methylated gradually due to a disturbance of methylation separately from CIMP-type methylation. CDX2 shows almost the same expression pattern in GC progression [2]. SOX9 might be expressed in parallel with CDX2, which increases during tumorigenesis through intestinal metaplasia but then is lost as the tumor grade increases and the tumor becomes less differentiated. SOX9 has many functions in development and signaling pathways. Further studies are needed to reveal which function of SOX9 assists in the development of GC.

We have demonstrated that the expression of SOX9 decreased in half of all gastric cancer tissues. Although the importance of genetic mutation in carcinogenesis has long been recognized, DNA methylation is also a powerful mechanism for the suppression of gene activity. To date, many genes, such as $p16^{INK4a}$, *MGMT*, *APC*, and *hMLH1*, have been shown to be inactivated by hypermethylation in gastric cancers [40]. *SOX9* promoter was reported to be methylated in bladder cancer [22], whereas *SOX9* methylation in GC has not been reported previously. We tried the previously reported MSP primers first [22], but the MSP results were not related to immunohistochemical expression of SOX9, so we settled new primers for SOX9 methylation. In this study, we found that *SOX9* methylation was detected in 47% of GCs and correlated with the low expression of SOX9 protein. We classified GC into 3 groups: intramucosal GC, GC invading submucosa, and GC invading the muscular layer or deeper. The rate of methylated SOX9 tumors increased and SOX9 expression gradually decreased through the depth of GC invasion. These data strongly suggest that the decrease of SOX9 expression in advanced GC is related to the epigenetic suppression of SOX9 during invasion.

Survival analysis revealed that GC with SOX9 low expression and methylated *SOX9* showed slightly poorer prognosis, but the differences were not statistically significant. Our GC cases had few metastases, so the prognosis was relatively better than the average prognosis of GC; however, the bias of our GC cases might eradicate this difference. Further study is essential to clarify the prognostic value of SOX9 in GC.

SOX9 and EBV-associated GC

SOX9 protein was downregulated in EBV-associated GC specimens. We found that more *SOX9* methylation in gastric cancer samples from patients with EBV infection (86%, 6/7) was detected than in those without EBV infection (45%, 51/114, P=0.041). EBV-associated GC exhibits global and nonrandom DNA methylation of the promoter regions of various cancer-associated genes and is included in CIMP-H, whereas CIMP-H GC and SOX9 methylation was not related. SOX9 is one of the methylated genes in EBV-associated GC, which shows more methylated genes than CIMP-H GC. EBV-associated GC is a group of distinct GC with more methylated genes.

SOX9 methylation was induced by EBV infection in vitro. Four of 6 GC cell lines increased the methylation of *SOX9* promoter through infection. It was confirmed by bisulfite sequence in MKN7 and NUGC3 cells. NUGC3-EBV showed an almost unmethylated sequence among 5 clones. It was not clear whether EBV did not infect all the cells or both alleles. It might be clarified by bisulfite sequencing from a single cell, but degeneration of DNA in bisulfite treatment and efficacy of amplification using PCR primers are severe difficulties in the trial.

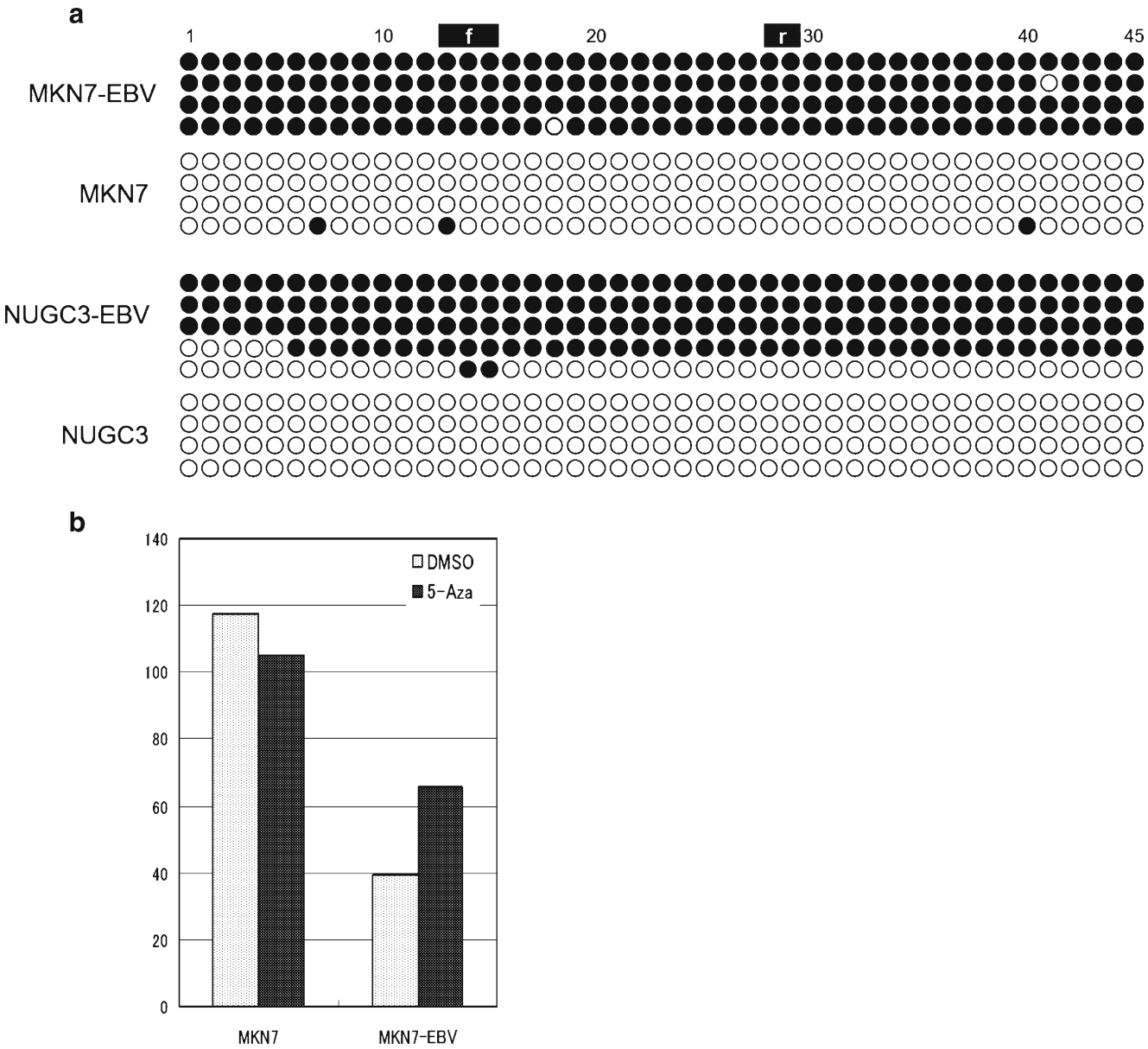

Fig. 4 Confirmation of methylation status of *SOX9*. **a** Bisulfite sequence of *SOX9* exon1 region including MSP primer sites (13–15, 28–29). The *numbers* show CpGs in the examined region (+135–+581 region from the transcription start site). *Filled circles* show methylated CpG and *open circles* show unmethylated CpG. MKN7-EBV has been almost fully methylated, but NUGC3-EBV was heterogenously methylated. **b** *SOX9* expression per 1,000 copies of *GAPDH* are shown. 5-Aza treatment of *MKN7/MKN7-EBV*. *MKN7* did not increase *SOX9* expression by 5-Aza treatment, but *MKN7-EBV* increased *SOX9* after 5-Aza treatment. *SOX9* was repressed by methylation in MKN7-EBV

In summary, SOX9 expression is increased in the development of GC and decreased through its progression. The increase might be related to intestinal character of GC and influence proliferation of GC cells via Wnt/β-catenin signaling pathway. SOX9 expression was inversely related to vessel infiltration and nodal metastasis. SOX9 negativity might be a marker for using anti-angiogenesis drugs in GC treatment. Methylation of *SOX9* promoter increased through progression and was the cause of SOX9 suppression in advanced cancer. SOX9 does not affect overall prognosis. *SOX9* methylation is also related to EBV-associated GC, which shows low expression of SOX9. SOX9 is closely related to GC carcinogenesis.

Acknowledgment This study was supported by grants-in-aid for scientific research on priority areas (20249022, 20590337) and the Global COE Research Program "Comprehensive center of education and research for chemical biology of the diseases" from the Ministry of Education, Culture, Sports, Science and Technology of Japan.

Conflicts of interest We declare that we have no conflicts of interest.

References

1. Uozaki H, Fukayama M (2008) Epstein–Barr virus and gastric carcinoma—viral carcinogenesis through epigenetic mechanisms. Int J Clin Exp Pathol 1:198–216
2. Uozaki H, Barua RR, Sun M et al (2011) Transcriptional factor typing with SOX2, HNF4aP1, and CDX2 closely relates to tumor invasion and Epstein–Barr virus status in gastric cancer. Int J Clin Exp Pathol 4:230–240
3. Park DY, Srivastava A, Kim GH et al (2010) CDX2 expression in the intestinal-type gastric epithelial neoplasia: frequency and significance. Mod Pathol 23:54–61
4. Haveri H, Westerholm-Ormio M, Lindfors K et al (2008) Transcription factors GATA-4 and GATA-6 in normal and neoplastic human gastrointestinal mucosa. BMC Gastroenterol 8:9
5. Lefebvre V, Dumitriu B, Penzo-Mendez A et al (2007) Control of cell fate and differentiation by Sry-related high-mobility-group box (Sox) transcription factors. Int J Biochem Cell Biol 39:2195–2214
6. Kent J, Wheatley SC, Andrews JE et al (1996) A male-specific role for SOX9 in vertebrate sex determination. Development 122:2813–2822
7. Lefebvre V, Huang W, Harley VR et al (1997) SOX9 is a potent activator of the chondrocyte-specific enhancer of the pro alpha1(II) collagen gene. Mol Cell Biol 17:2336–2346
8. Stolt CC, Lommes P, Sock E et al (2003) The Sox9 transcription factor determines glial fate choice in the developing spinal cord. Genes Dev 17:1677–1689
9. Perez-Alcala S, Nieto MA, Barbas JA (2004) LSox5 regulates RhoB expression in the neural tube and promotes generation of the neural crest. Development 131:4455–4465
10. Foster JW, Dominguez-Steglich MA, Guioli S et al (1994) Campomelic dysplasia and autosomal sex reversal caused by mutations in an SRY-related gene. Nature 372:525–530
11. De Santa BP, Bonneaud N, Boizet B et al (1998) Direct interaction of SRY-related protein SOX9 and steroidogenic factor 1 regulates transcription of the human anti-Mullerian hormone gene. Mol Cell Biol 18:6653–6665
12. Blache P, van de Wetering M, Duluc I et al (2004) SOX9 is an intestine crypt transcription factor, is regulated by the Wnt pathway, and represses the CDX2 and MUC2 genes. J Cell Biol 166:37–47
13. Fukayama M, Hino R, Uozaki H (2008) Epstein–Barr virus and gastric carcinoma: virus–host interactions leading to carcinoma. Cancer Sci 99:1726–1733
14. Lu B, Fang Y, Xu J et al (2008) Analysis of SOX9 expression in colorectal cancer. Am J Clin Pathol 130:897–904
15. Thomsen MK, Ambroisine L, Wynn S et al (2010) SOX9 elevation in the prostate promotes proliferation and cooperates with PTEN loss to drive tumor formation. Cancer Res 70:979–987
16. Japanese Gastric Cancer Association (1998) Japanese classification of gastric carcinoma—2nd English edition. Gastric Cancer 1:10–24
17. Lauren P (1965) The two histological main types of gastric carcinoma. Diffuse and so-called intestinal type carcinoma. An attempt at histoclinical classification. Acta Pathol Microbiol Scand 64:31–49
18. Sinicrope FA, Ruan SB, Cleary KR et al (1995) bcl-2 and p53 oncoprotein expression during colorectal tumorigenesis. Cancer Res 55:237–241
19. Iwasaki Y, Chong JM, Hayashi Y et al (1998) Establishment and characterization of a human Epstein–Barr virus-associated gastric carcinoma in SCID mice. J Virol 72:8321–8326
20. Imai S, Nishikawa J, Takada K (1998) Cell-to-cell contact as an efficient mode of Epstein–Barr virus infection of diverse human epithelial cells. J Virol 72:4371–4378
21. Shimizu N, Yoshiyama H, Takada K (1996) Clonal propagation of Epstein–Barr virus (EBV) recombinants in EBV-negative Akata cells. J Virol 70:7260–7263
22. Aleman A, Adrien L, Lopez-Serra L et al (2008) Identification of DNA hypermethylation of SOX9 in association with bladder cancer progression using CpG microarrays. Br J Cancer 98:466–473
23. Chang MS, Uozaki H, Chong JM et al (2006) CpG island methylation status in gastric carcinoma with and without infection of Epstein–Barr virus. Clin Cancer Res 12:2995–3002
24. Stolt CC, Wegner M (2010) SoxE function in vertebrate nervous system development. Int J Biochem Cell Biol 42:437–440
25. Akiyama H (2008) Control of chondrogenesis by the transcription factor Sox9. Mod Rheumatol 18:213–219
26. Thomsen MK, Francis JC, Swain A (2008) The role of Sox9 in prostate development. Differentiation 76:728–735
27. Barrionuevo F, Scherer G (2010) SOX E genes: SOX9 and SOX8 in mammalian testis development. Int J Biochem Cell Biol 42:433–436
28. Moniot B, Biau S, Faure S et al (2004) SOX9 specifies the pyloric sphincter epithelium through mesenchymal-epithelial signals. Development 131:3795–3804
29. Mori-Akiyama Y, van den Born M, van Es JH et al (2007) SOX9 is required for the differentiation of paneth cells in the intestinal epithelium. Gastroenterology 133:539–546
30. Bastide P, Darido C, Pannequin J et al (2007) Sox9 regulates cell proliferation and is required for Paneth cell differentiation in the intestinal epithelium. J Cell Biol 178:635–648
31. Yasui W, Oue N, Sentani K et al (2009) Transcriptome dissection of gastric cancer: identification of novel diagnostic and therapeutic targets from pathology specimens. Pathol Int 59:121–136
32. Chen Y, Zhang Y-Z, Zhou Z-G et al (2006) Identification of differently expressed genes in human colorectal adenocarcinoma. World J Gastroenterol 12:1025–1032
33. Jiang SS, Fang W-T, Hou Y-H et al (2010) Upregulation of SOX9 in lung adenocarcinoma and its involvement in the regulation of cell growth and tumorigenicity. Clin Cancer Res 16:4363–4373
34. Wang H, Leav I, Ibaragi S et al (2008) SOX9 is expressed in human fetal prostate epithelium and enhances prostate cancer invasion. Cancer Res 68:1625–1630
35. Passeron T, Valencia JC, Namiki T et al (2009) Upregulation of SOX9 inhibits the growth of human and mouse melanomas and restores their sensitivity to retinoic acid. J Clin Invest 119:954–963
36. Chakravarty G, Moroz K, Makridakis NM et al (2011) Prognostic significance of cytoplasmic SOX9 in invasive ductal carcinoma and metastatic breast cancer. Exp Biol Med (Maywood) 236:145–155
37. Clevers H (2006) Wnt/beta-catenin signaling in development and disease. Cell 127:469–480
38. Vidal VP, Ortonne N, Schedl A (2008) SOX9 expression is a general marker of basal cell carcinoma and adnexal-related neoplasms. J Cutan Pathol 35:373–379
39. Ramocki NM, Wilkins HR, Magness ST et al (2008) Insulin receptor substrate-1 deficiency promotes apoptosis in the putative intestinal crypt stem cell region, limits Apcmin/+ tumors, and regulates Sox9. Endocrinology 149:261–267
40. Choi IS, Wu TT (2005) Epigenetic alterations in gastric carcinogenesis. Cell Res 15:247–254

Virchows Arch (2012) 460:281–289
DOI 10.1007/s00428-012-1212-4

ORIGINAL ARTICLE

Clinicopathologic study of mixed adenoneuroendocrine carcinomas of hepatobiliary organs

Kenichi Harada · Yasunori Sato · Hiroko Ikeda · Hsu Maylee · Saya Igarashi · Atsushi Okamura · Shinji Masuda · Yasuni Nakanuma

Received: 4 August 2011 / Revised: 21 December 2011 / Accepted: 8 February 2012 / Published online: 23 February 2012
© Springer-Verlag 2012

Abstract Neuroendocrine neoplasms in hepatobiliary organs are very rare, but several cases of mixed adenoneuroendocrine carcinoma (MANEC) have been reported. In this study, we characterized the neuroendocrine component of biliary MANEC. A total of 274 cases of biliary cancer including 17 intrahepatic cholangiocarcinomas (CCs), 15 hepatic hilar CCs without preceding hepatobiliary disease, 55 hepatic hilar CCs with hepatolithiasis, 49 gallbladder cancers, 53 extrahepatic CCs, and 85 hepatocellular carcinomas were examined for a neuroendocrine component using immunohistochemistry with neuroendocrine markers (chromogranin A and synaptophysin). In the MANEC cases, in addition to a close histological examination, the proliferative activity and the expression of somatostatin receptor 2A were also evaluated. In addition to an ordinary adenocarcinoma, a neuroendocrine component occupying more than 30% of the entire tumor was also found in 4% (2/55 cases) of hepatic hilar cholangiocarcinomas with hepatolithiasis, 10% (5/49 cases) of gallbladder cancers, and 4% (2/53 cases) of extrahepatic cholangiocarcinomas, but not in the intrahepatic cholangiocarcinomas, hilar cholangiocarcinomas without preceding hepatobiliary disease, and hepatocellular carcinomas. Two cases were positive for somatostatin receptor 2A. The adenocarcinoma components were predominately located at the surface of the tumors, and the majority of stromal and vascular invasion and lymph node metastasis involved neuroendocrine components, showing the features of neuroendocrine tumor G2 or neuroendocrine carcinomas (NECs). NEC components showed higher proliferative activity on Ki67 immunostaining, compared to the adenocarcinoma components. Biliary MANECs are found in hepatic hilar cholangiocarcinomas with hepatolithiasis, gallbladder cancers, and extrahepatic cholangiocarcinomas and show a characteristic histology. Since the neuroendocrine component in biliary MANEC defines the prognosis, it is important to identify it and consider the indications for adjunctive therapy with somatostatin analogues.

Keywords Neuroendocrine neoplasm · Cholangiocarcinoma · Mixed adenoneuroendocrine carcinoma · Somatostatin analogue

K. Harada (✉) · Y. Sato · H. Maylee · S. Igarashi · A. Okamura · Y. Nakanuma
Department of Human Pathology,
Kanazawa University Graduate School of Medicine,
Kanazawa 920-8640, Japan
e-mail: kenichih@med.kanazawa-u.ac.jp

H. Ikeda
Division of Pathology, Kanazawa University Hospital,
Kanazawa, Japan

S. Masuda
Department of Pathology, Kouseiren Takaoka Hospital,
Takaoka, Japan

Introduction

Neuroendocrine neoplasms including carcinoid tumors are commonly found in several organs including the pancreas and the gastrointestinal tract. The World Health Organization (WHO) classification (2000) [1] has been widely used to categorize neuroendocrine tumors (NETs) for all anatomical sites, and NETs are histologically and biologically classed as well-differentiated neuroendocrine tumors, well-differentiated neuroendocrine carcinomas (NECs; low grade malignancy), poorly differentiated neuroendocrine carcinomas (high grade malignancy), and mixed exocrine–endocrine carcinomas [2,

3]. The European Neuroendocrine Tumor Society (ENETS) has recently proposed two complementary classification tools: a grading classification and a site-specific staging system [4]. The recent WHO classification (2010) [5, 6], moreover, strengthens the appreciation of three concepts: tumor heterogeneity, tumor differentiation, and malignancy. According to the WHO classification (2010), neuroendocrine neoplasms in the digestive system, including the gallbladder and the extrahepatic bile ducts, are classed as NET G1 (carcinoid, mitotic count of <2 per 10 high powder fields (HPF) and/or ≤2% Ki67 index), NET G2 (mitotic count 2–20 per 10 HPF and/or 3–20% Ki67 index), NET G3 (neuroendocrine carcinoma, mitotic count of >20 per 10 HPF and/or >20% Ki67 index), and mixed adenoneuroendocrine carcinoma (MANEC). This classification reflects the prognosis of patients with neuroendocrine neoplasms as well as biologic potential and is based on the general pathological findings such as tumor size, differentiation, mitotic index, perineural or vascular invasion, metastasis, and local invasion to muscular propria (gastrointestinal tracts) and adjacent organs [2, 3]. Typical carcinoids showing benign behavior and atypical carcinoids showing malignant features are equated with NET G1 and NET G2, respectively. NEC includes small cell carcinoma and large cell neuroendocrine carcinoma (LCNEC) considered as homologous to the pulmonary counterpart [2, 3].

Neuroendocrine cells and tumors are characterized by the expression of markers such as chromogranin A and synaptophysin and the production of hormonal substances including serotonin, gastrin, and somatostatin. However, because some neuroendocrine neoplasms lack distinct or functional hormones, a functional classification is of little value. Recently, it was demonstrated that somatostatin analogues such as SOM230 and octreotide are the best therapeutic option for neuroendocrine neoplasms, because they reduce hormone-related symptoms and also have antitumor effects [7, 8]. A neuroendocrine neoplasm demonstrated to possess the receptor for somatostatin (SSTR) is a good candidate for treatment with a somatostatin analogue. Therefore, the pathological differentiation and diagnosis of neuroendocrine neoplasms is important for chemotherapy after the resection of a tumor [7]. Tumors originating from the intrahepatic and extrahepatic biliary trees are mostly malignant carcinomas, in particular adenocarcinomas, irrespective of their etiology. Physiologically, a few neuroendocrine cells resembling enterochromaffin-like cells exist in the biliary tree, particularly in the large bile ducts and peribiliary glands of the hepatic hilus [9], but cases of neuroendocrine neoplasms in hepatobiliary organs are extremely rare. Carcinoids of the gallbladder and the extrahepatic biliary tract represent 0.2 and 0.01% of all carcinoids, respectively [1].

To date, several cases of hepatobiliary neuroendocrine neoplasms, mostly biliary adenocarcinomas accompanying a neuroendocrine component (MANEC), have been reported [10–14], but the neuroendocrine component in biliary MANEC is not well characterized. In this study, we surveyed neuroendocrine neoplasms in hepatobiliary tumors and characterized hepatobiliary MANEC. Our final aim was to assess the clinicopathological significance of neuroendocrine components in hepatobiliary MANEC including the prognosis after the surgical resection of tumors.

Materials and methods

Patients and tissue preparations

A total of 274 cases of biliary cancer including 17 intrahepatic cholangiocarcinomas (CCs), 15 hepatic hilar CCs without preceding hepatobiliary disease, 55 hepatic hilar CCs with hepatolithiasis, 49 gallbladder cancers, 53 extrahepatic CCs, and 85 hepatocellular carcinomas (HCCs) were examined in this study. All materials were surgically resected hepatobiliary specimens retrieved from the surgical files of our laboratories and affiliated hospitals. These tissue specimens containing tumorous lesions were immediately fixed in 10% neutral buffered formalin and embedded in paraffin. Several 4-μm-thick sections were prepared from each paraffin-embedded block and either routinely stained for histologic evaluation or processed for immunohistochemical analysis.

Immunohistochemistry

Using representative cancerous sections from each case and also cases involving neuroendocrine neoplasms, all sections including lymph nodes were prepared for pathological diagnosis, and the immunohistochemical staining of neuroendocrine markers (chromogranin A and synaptophysin) was performed for surveying the presence of neuroendocrine neoplasms. Moreover, in cases involving neuroendocrine neoplasms, a cell proliferative marker (Ki67) and SSTR type 2A (SSTR2A) were also immunostained to examine the cell kinetics as a marker of malignancy and the indications for treatment with somatostatin analogues.

Deparaffinized and rehydrated sections were pretreated for antigen retrieval prior to staining (Table 1). Following endogenous peroxidase blocking and incubation in normal goat serum (1:10; Vector Lab, Burlingame, CA) for 20 min, these sections were incubated at 4°C overnight with the primary antibodies (Table 1) and then at room temperature for 1 h with goat anti-mouse or anti-rabbit immunoglobulins conjugated to a peroxidase-labeled dextran polymer (Envision, Dako Japan). After a benzidine reaction, sections were weakly counterstained with hematoxylin. As a negative control, non-immune serum was used for the primary antibody. This procedure consistently resulted in no staining.

Table 1 Primary antibodies used in this study

Antibody	Concentration	Antigen retrieval	Supplier
Chromogranin A (Ms)	0.5 μg/ml	No treatment	Dako Japan[a]
Synaptophysin (Ms)	5 μg/ml	MW(citrate buffer)	Dako Japan[a]
Ki67 (Ms)	0.22 μg/ml	MW(EDTA buffer)	Dako Japan[a]
SSTR2A (Rb)	diluted 1:1000	AC(citrate buffer)	Gramsch Laboratories[b]

Ms mouse monoclonal, *Rb* rabbit polyclonal, *AC* autoclaved, *MW* microwave

[a] Tokyo, Japan

[b] Schwabhausen, Germany

Examination of hepatobiliary neuroendocrine neoplasms

Chromogranin A- and/or synaptophysin-positive cells were evaluated as neuroendocrine cells, and a neuroendocrine neoplasm was basically defined as a well- to poorly differentiated tumor composed of cells with features similar to those of the normal gut endocrine cell, showing the diffuse and distinct staining for chromogranin A and/or synaptophysin [5]. The grading for neuroendocrine neoplasms (NET G1, G2, or G3; NEC) was performed on the basis of morphological criteria, and the assessment of the proliferative fraction according to the ENETS scheme [4]. We established a Ki67 labeling index as a percentage of 2,000 cells counted in the area of strongest nuclear labeling and mitotic count per 10 HPF by evaluating at least 50 HPF. In MANEC cases, at least 30% of the main lesion excluding any broad invasive area had to be made up of either component for this definition to apply [5], and the following pathological features were also examined: tumor size, gross classification (mass forming, periductal infiltrating, or intraductal growth), depth of invasion (lymphatic, vascular, and perineural invasion; present or absent, and if present, its histology), and lymph node metastasis (present or absent, and if present, its histology).

Results

Staining pattern of chromogranin A and synaptophysin

Hepatobiliary tumors merely contain cells positive for the neuroendocrine marker chromogranin A or synaptophysin. However, in some biliary tumors, the positive cells were scattered and sometimes clustered within tumors and extended within the biliary epithelium of adjacent nonneoplastic bile ducts (Fig. 1). Some neuroendocrine cells resembling enterochromaffin-like cells morphologically were also found (Fig. 1). The scattering and/or clustering of these neuroendocrine cells was found in 12 of 55 hepatic hilar CCs with hepatolithiasis, 19 of 49 gallbladder cancers, and 13 of 53 extrahepatic CCs, but not in HCCs, intrahepatic CCs, or hepatic hilar CCs without preceding hepatobiliary disease (Table 2).

Clinicopathological features of the neuroendocrine component in hepatobiliary MANEC

No cases of HCC, intrahepatic CC, and hepatic hilar CC without preceding hepatobiliary disease included neuroendocrine

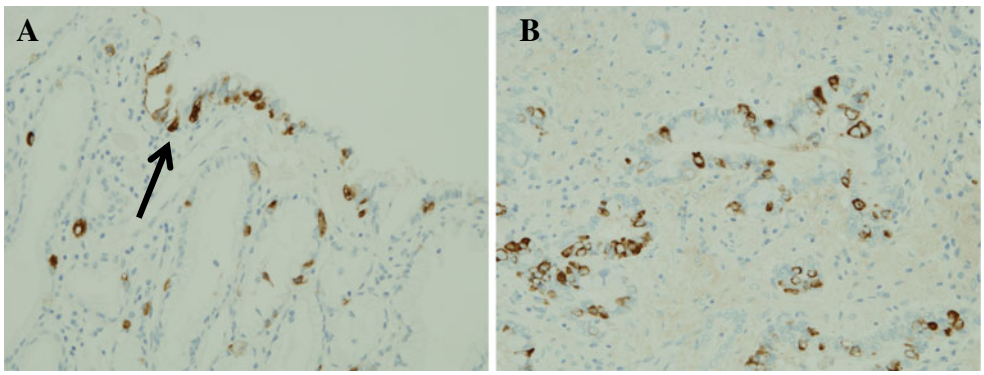

Fig. 1 Immunohistochemistry for chromogranin A. Chromogranin A-immunoreactive neuroendocrine cells are scattered in the nonneoplastic biliary epithelium of gallbladder cancer (**a**) and adenocarcinoma of extrahepatic cholangiocarcinoma (**b**). Some neuroendocrine cells resembling enterochromaffin-like cells morphology, which show a triangular shape and are located in the basement membrane, are also found (*arrow*). Original magnification, ×200

components. In contrast, hepatic hilar CC with hepatolithiasis, gallbladder cancer, and extrahepatic CC accompanied neuroendocrine components in addition to the ordinary adenocarcinoma in 4, 10, and 4% of cases, respectively (Table 2). A summary of a total of nine cases of biliary MANEC found in this study is shown in Table 3. As shown in Figs. 2, 3 and 4, representative findings of these MANEC cases showed that the adenocarcinoma component was located at the surface of tumors, and the majority of the stromal invasion including vascular invasion and lymph node metastasis involved neuroendocrine components. These components were NET G2 or NEC, and the tumor cells of which had a round- or oval-shaped nucleus and "salt-and-pepper" pattern of nuclear chromatin, which are the general characteristics of neuroendocrine cells. NET G1 was not found in any cases (Table 3). Cases of NEC showed the morphological features of small cell carcinoma or large cell neuroendocrine carcinoma, broadly typical of lung cancer. In biliary MANEC, the components showing the deepest invasion were neuroendocrine neoplasms, and vascular and perineural invasion also involved neuroendocrine components. Moreover, several other characteristics were evident as follows. The NEC (LCNEC) component in case 1 had widespread necrosis. In case 2 which composed of a uniformly well-differentiated tubular adenocarcinoma, a neuroendocrine marker-positive tubular component was also found in an invasive area (Fig. 5). Although the Ki67 index was less than 2%, the NET in case 2 was categorized as NET G2 according to the morphology and mitotic index. The Ki67 index in case 3 was less than 20%, but this case was regarded as NEC in consideration of the small cell carcinoma-like morphology with necrosis and mitotic index. The NEC component in case 4 had the highest proliferative activity among the biliary MANEC cases examined in this study. The Ki67 index in case 5 was less than 2%, but this tumor was regarded as NET G2 based on morphology and the mitotic index (Fig. 2). In case 6, the NEC component (small cell carcinoma) had conspicuous necrosis (Fig. 3), and the ordinary adenocarcinoma as well as NEC component also showed distinct stromal and vascular invasion. The NEC component (LCNEC) in case 7 had widespread necrosis. Cases 8 and 9 were MANEC cases arising from the preceding hepatolithiasis, and the NEC component (LCNEC) in case 9 clearly had necrosis.

Immunohistochemistry revealed that Ki67-positive cells were scattered in the neuroendocrine component as well as ordinary adenocarcinoma, and in particular, many positive tumor cells were found in NEC (Fig. 6). Quantitative evaluation also confirmed that the NEC component constantly showed high proliferative activity, compared with the adenocarcinoma component in each case (Fig. 6). SSTR2A expression was found in the cytoplasm and membrane of tumor cells of the adenocarcinoma and neuroendocrine components. However, significant membranous expression [7] was restricted to the neuroendocrine component, and two cases of biliary MANEC clearly expressed SSTR2A with a NEC histology (Fig. 7 and Table 3).

Discussion

Several cases of hepatobiliary neuroendocrine neoplasms including carcinoid tumors have been reported, but most involve hepatic carcinoids or biliary neuroendocrine neoplasms arising from or accompanying ordinary adenocarcinomas, mostly in patients with gallbladder cancer and extrahepatic CC [10–14]. One case of hepatic NET G1 (carcinoid tumor), but not pure biliary neuroendocrine neoplasms without ordinary CC, has been registered in our laboratories and affiliated hospitals. In this study, we primarily surveyed the presence of neuroendocrine neoplasms in hepatobiliary tumors (CC and HCC) using immunohistochemistry for chromogranin A and synaptophysin. CD56 (NCAM) is also used as a neuroendocrine marker, but biliary epithelial cells in intrahepatic small bile ducts, particularly bile ductules, and their tumors are positive for CD56 [15]. Therefore, CD56 is not suitable for the identification of neuroendocrine neoplasms in biliary tumors. Consequently, as for intrahepatic neuroendocrine neoplasms, no cases of HCC or intrahepatic CC accompanying neuroendocrine neoplasms were found in this study, though one case of hepatic carcinoid was registered in our files. This finding is very interesting when considering the tumorigenesis

Table 2 Frequency of neuroendocrine cells and neoplasms in hepatobiliary tumors

Original diagnosis	Neuroendocrine components	
	Neuroendocrine cell positive/total cases	Neuroendocrine neoplasm positive/total cases
Intrahepatic CC	0/17 (0%)	0/17 (0%)
Hepatic hilar CC without preceding hepatobiliary diseases	0/15 (0%)	0/15 (0%)
Hepatic hilar CC associated with hepatolithiasis	12/55 (22%)	2/55 (4%)
Gallbladder cancer	19/49 (39%)	5/49 (10%)
Extrahepatic CC	13/53 (25%)	2/53 (4%)
Hepatocellular carcinoma	0/85 (0%)	0/85 (0%)

CC cholangiocarcinoma

Table 3 Cases of biliary MANEC

	Case 1	Case 2	Case 3	Case 4	Case 5	Case 6	Case 7	Case 8	Case 9
Age (years), gender	60, male	80, female	70, female	70, female	70, female	60, female	50, female	60, male	70, female
Location	Extrahepatic bile duct	Extrahepatic bile duct	Gallbladder	Gallbladder	Gallbladder	Gallbladder	Gallbladder	Hepatic hilum	Hepatic hilum
Precursor lesion			Cholecystolithiasis		Cholecystolithiasis	Cholecystolithiasis		Hepatolithiasis	Hepatolithiasis
Tumor size	2.2×1.5 cm	1.5×1.2 cm	3.5×2.5 cm	4.5×1.0 cm	4.5×2.5 cm	1.5×1.5 cm	15×12 cm	>2.5 cm	>2.8 cm
Gross classification	Mass forming	Mass forming	Mass forming	Mass forming	Mass forming	Mass forming	Mass forming	Mass forming	Mass forming
Histology of adenocarcinoma	Pap-wel	Wel	Wel	Pap-wel	Wel	Pap-wel	Wel	Wel	Wel
Histology of NET	NEC, LCNEC	NET G2, adenocarcinoma-like	NEC, small cell carcinoma	NEC, LCNEC	NET G2, atypical carcinoid	NEC, small cell carcinoma	NEC, LCNEC	NET G2, atypical carcinoid	NEC, LCNEC
Intensity of neuroendocrine marker	+	++	++	+	++	+	+	+	+
Mitotic index of NET (mitotic count/10 HPF)	53	7	59	137	4	95	42	15	76
Ki67 index of NET (%)	22.3	1.2	12.3	32.3	0.5	28.5	15.1	3.8	35.2
Depth of invasion (histology)	Exposure from serosa (NET)	Invasion to pancreas (NET)	Invasion to liver, (NET)	Exposure from serosa (NET)	Invasion to duodenum (NET)	Subserosa (adenocarcinoma)	Invasion to liver, (NET)	Unspecified	Unspecified
Lymphatic invasion (histology)	+ (NET)	+ (NET)	+ (NET)	+ (NET)	+ (NET)	+ (NET and adenocarcinoma)	+ (NET)	+ (NET)	+ (NET)
Vascular invasion (histology)	+ (NET)	+ (NET)	+ (NET)	+ (NET)	−	+ (NET and adenocarcinoma)	+ (NET)	−	−
Perineural invasion (histology)	+ (NET)	+ (NET)	+ (NET)	−	+ (NET)	+ (NET)	+ (NET)	−	−
Lymph node metastasis (histology)	+ (NET)	−	+ (NET)	−	−	+ (NET and adenocarcinoma)	+ (NET)	Unspecified	Unspecified
SSTR2A in NET	+	−	−	−	−	−	+	−	−

NET G2 and NEC (WHO classification 2010)

MANEC mixed adenoneuroendocrine carcinoma, *Pap* papillary adenocarcinoma, *Wel* well-differentiated adenocarcinoma, *NET* neuroendocrine tumor, *NEC* neuroendocrine carcinoma, *LCNEC* large cell neuroendocrine carcinoma, *HPF* high powder field

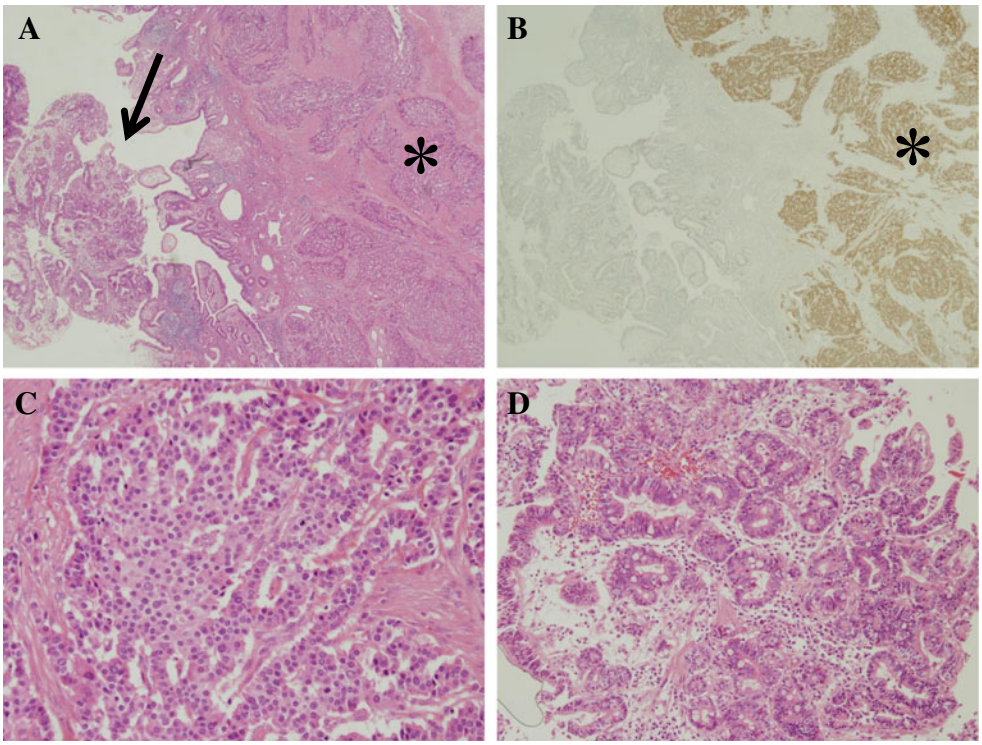

Fig. 2 Gallbladder cancer with neuroendocrine tumor G2 (WHO classification 2010) (case 5 in Table 3). Although the surface of the tumor is an ordinary adenocarcinoma (**a**, *arrow*; higher magnification, **d**), the invasive component shows a different histology and chromogranin A positivity (**a** and **b**, *asterisk*). Tumors show a trabecular pattern and consist of small monotonous cells with mild atypia, indicating atypical carcinoid (**c**). (**a**, **b**, and **d**) are hematoxylin and eosin (H&E) staining. (**b**) Immunohistochemistry for chromogranin A. Original magnification, ×20 (**a** and **b**), ×200 (**c**), and×100 (**d**)

of intrahepatic neuroendocrine neoplasms such as hepatic carcinoid, and intrahepatic neuroendocrine neoplasms are unlikely to originate from hepatocytes, cholangiocytes in intrahepatic small bile ducts, and their carcinomas (HCC and intrahepatic CC). Therefore, an association between hepatic stem cells, that is, multipotential progenitor cells possessing the ability to differentiate into various cell types including neuroendocrine cells, and heterotopic neuroendocrine tissue possibly remains in the tumorigenesis of hepatic neuroendocrine neoplasms. In contrast, the proliferation of neuroendocrine cells and the presence of biliary neuroendocrine neoplasms accompanied by biliary adenocarcinoma were found in hepatic hilar CC with hepatolithiasis in addition to gallbladder cancer and extrahepatic CC. This finding is also of interest when considering the tumorigenesis of biliary neuroendocrine neoplasms and suggests that the preceding chronic inflammation, particularly lithiasis-associated inflammation, and the accidental proliferation of neuroendocrine cells are closely associated with the histogenesis of biliary neuroendocrine neoplasms. The absence of cases of hepatic hilar CC without preceding hepatobiliary disease supports this speculation. As for the incidence, among biliary cancers, gallbladder cancers most often accompany neuroendocrine neoplasms in 10% (5/49) of cases. In this study, we surveyed the cases of

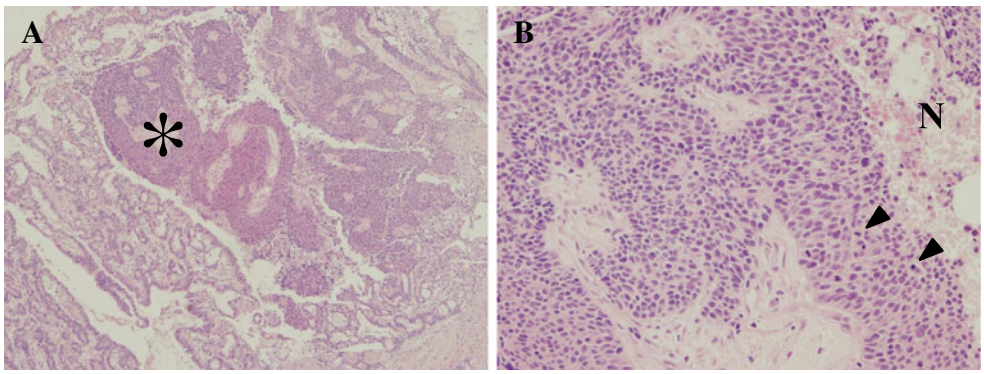

Fig. 3 Gallbladder cancer with neuroendocrine carcinoma (WHO classification 2010) (case 6 in Table 3). A solid component is found within the adenocarcinoma area (**a**, *asterisk*). The solid part consists of intermediate-sized round cells with nuclear molding and scanty cytoplasm resembling a small cell carcinoma of the lung (**b**). Several mitoses (*arrowheads*) and necrosis are found (**b**). Original magnification, ×20 (**a**) and×400 (**b**)

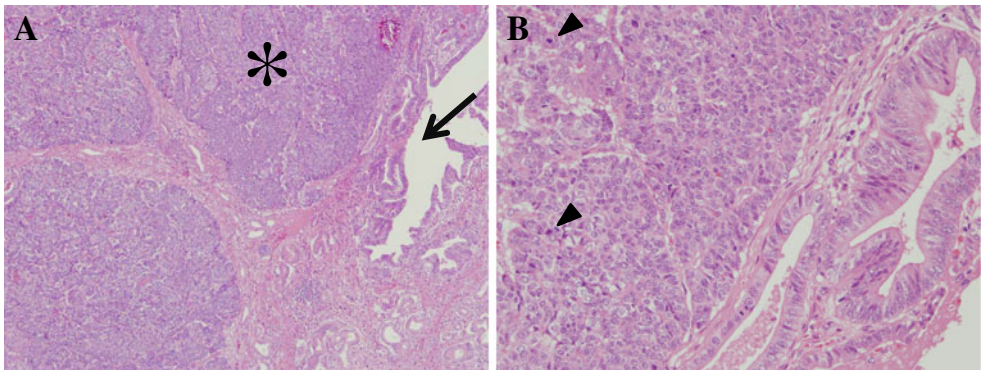

Fig. 4 Hepatic hilar cholangiocarcinoma associated with hepatolithiasis accompanying neuroendocrine carcinoma (WHO classification 2010) (case 9 in Table 3). An ordinary adenocarcinoma (**a**, *arrow*) is found in the lumen of a hepatic hilar bile duct, but the proliferating invasive nest shows solid sheets (**a**, *asterisk*). The latter part consists of uniform and large-sized tumor cells resembling a large cell neuroendocrine carcinoma of the lung (**b**). *Arrowheads* denote mitoses. Original magnification, ×20 (**a**) and×400 (**b**)

biliary cancer and collected MANEC cases from affiliated hospitals which specialize in hepatobiliary diseases. Therefore, the possibility of a high incidence compared with that in the general population could not be excluded. However, we recently encountered additional two cases of MANEC in the gallbladder after completing this study (not included herein). Moreover, cases originally diagnosed as a poorly differentiated component (case 4) or an ordinary adenocarcinoma component (case 2) were included in the biliary MANEC cases found in this study. Therefore, we speculate that biliary MANEC cases are not that rare. Pathologists should take into account the presence of a neuroendocrine component during the pathological diagnosis of biliary cancers.

In the new WHO classification system, neuroendocrine neoplasms in the digestive system are classed as NET G1 including carcinoid tumor, NET G2, and NEC [5]. This classification also applies to biliary neuroendocrine neoplasms [6], but NET G1 was not found in any neuroendocrine components of biliary MANEC morphologically. All neuroendocrine components of biliary MANEC found in this study belonged to NET G2 or NEC. The malignant grade of neuroendocrine neoplasms is generally based on the size of the tumor and cell kinetics (Ki67 labeling index) in addition to tumor morphology [2, 3], but there is still no broadly accepted definition of malignant grade in biliary neuroendocrine neoplasms. Because all neuroendocrine components were found

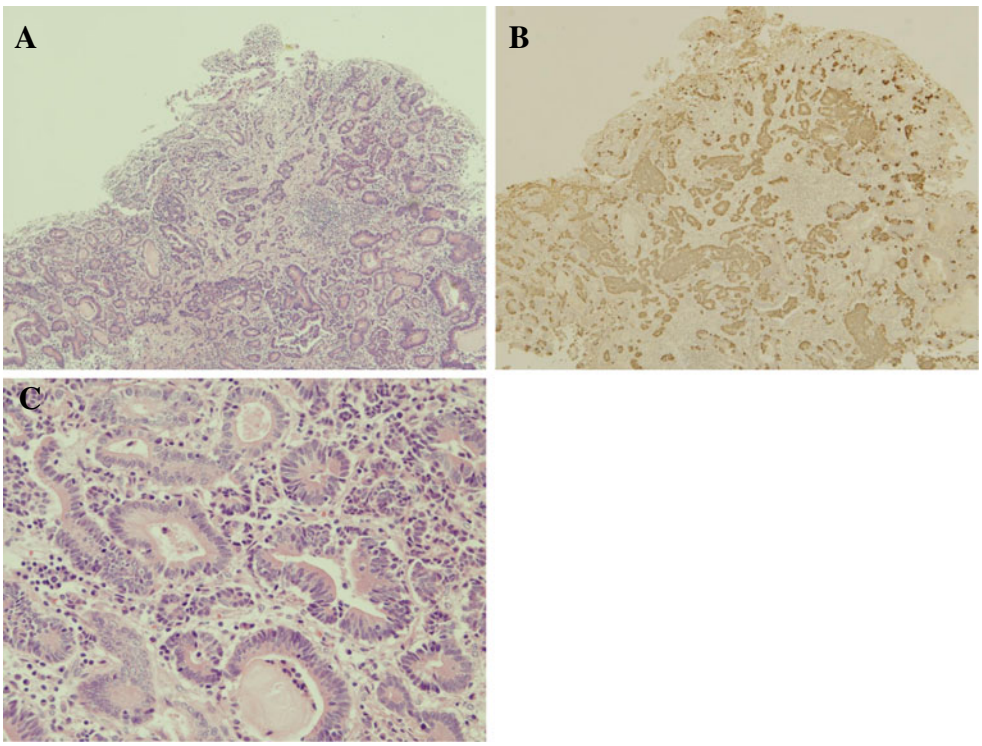

Fig. 5 Extrahepatic cholangiocarcinoma with neuroendocrine tumor G2 (WHO classification 2010), showing adenocarcinoma morphology (case 2 in Table 3). The tumor is histologically an ordinary adenocarcinoma (**a** and **c**), but diffusely positive for chromogranin A except at the surface (**b**). (**a** and **c**) H&E staining. (**b**) Immunohistochemistry for chromogranin A. Original magnification, ×20 (**a** and **b**) and×200 (**c**)

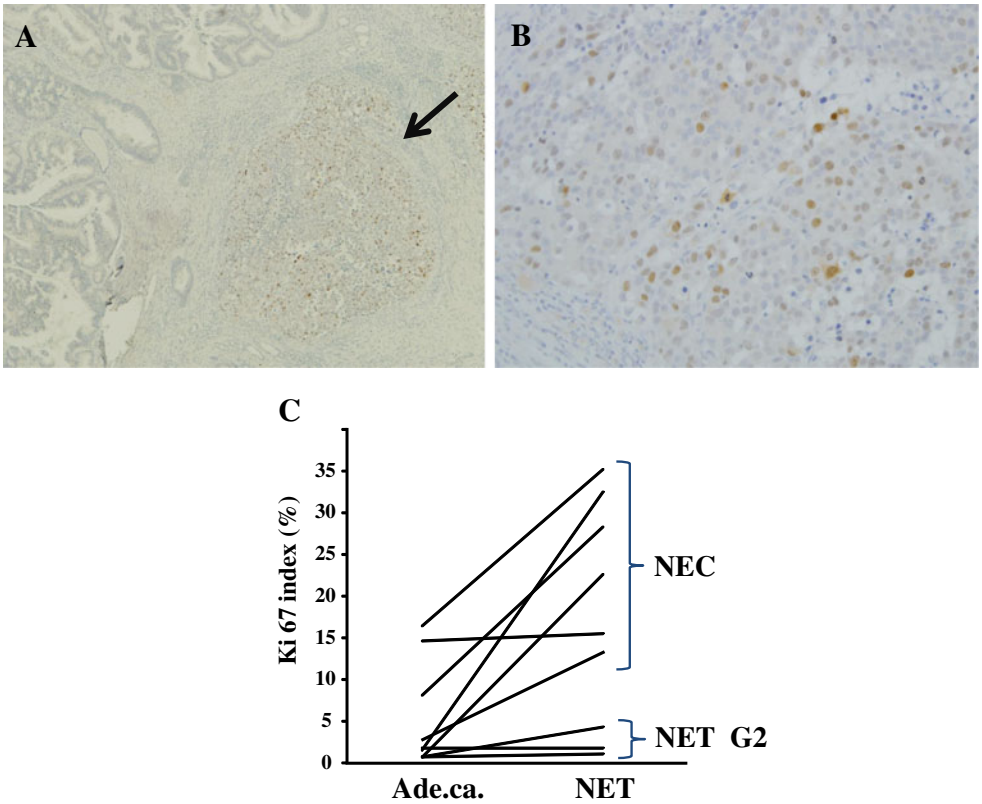

Fig. 6 Comparative analysis of cell kinetics between adenocarcinomas and neuroendocrine neoplasms. Many Ki67-positive cells are found within the neuroendocrine carcinoma (large cell neuroendocrine carcinoma type) (WHO classification 2010) (**a**, *arrow*; and **b**), but rarely in adenocarcinomas (**a**, *upper left*). In two cases of neuroendocrine tumor G2 (WHO classification 2010), there is no significant difference in the percentage of Ki67-positive cells (Ki67 index) between adenocarcinoma and NET G2, but in other all cases, particularly NEC, the indices are increased in the neuroendocrine components (**c**). Immunohistochemistry for Ki67 (**a** and **b**). Original magnification, ×20 (**a**) and×100 (**b**)

in the invasive areas of biliary MANEC, it is difficult to define them by the size of a sole neuroendocrine component. However, in this study, neuroendocrine components of biliary MANEC could be classified according to morphology and cell kinetics, that is, NET G2 and NEC show different levels of cell proliferation. Ki67 indices of NEC were constantly higher than those of NET G2 and also those of background adenocarcinoma components. This finding suggests that NET G2 and NEC could be distinguished by morphological atypia and proliferating activity without information on the size of neuroendocrine components in biliary MANEC. It is speculated that biliary tumors containing NEC have a poor prognosis based on histological evaluation. We tried to confirm this using a Kaplan–Maier analysis, but the number of biliary MANECs was too small. Moreover, because the prognosis of biliary tumors appreciably differed with the location in the biliary tree, it was difficult to comprehensively analyze the biliary MANECs found in this study.

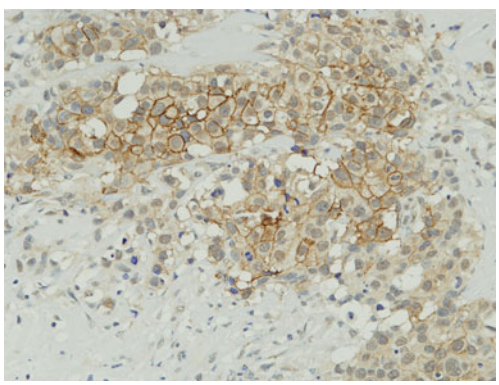

Fig. 7 Somatostatin receptor 2A-positive case (case 1 in Table 3). An intense membranous pattern is found in tumor cells (large cell neuroendocrine carcinoma type). Immunohistochemistry for SSTR2A. Original magnification, ×400

This study revealed that biliary MANECs showed a very characteristic histology, that is, the surface of the tumor was an ordinary adenocarcinoma, and the neuroendocrine component was located in an area of vascular and perineural invasion, and lymph node metastasis always involved neuroendocrine components. Moreover, the NEC component showed high proliferative activity compared with the adenocarcinoma component, suggesting that neuroendocrine components, particularly NEC, in biliary MANEC could prescribe the prognosis. Among the biliary MANECs examined in this study, two cases showed the expression of SSTR2A in NEC, which is a good indication for the use of somatostatin analogues as adjunctive therapy after surgery.

In this study, HCC, intrahepatic CC, and hepatic hilar CC without preceding hepatobiliary disease contained no neuroendocrine components, but some cases of hepatic hilar CC with hepatolithiasis, gallbladder cancer, and extrahepatic CC had neuroendocrine components, and some of which were a high grade malignancy such as neuroendocrine neoplasm and

SSTR2A-positive NEC. Pathologists must be aware of the poor prognosis and of cases indicating the need for adjunct therapy including somatostatin analogues after surgical resection.

Conflict of interest statement The authors have no conflicts of interest to declare.

References

1. Capella C, Solcia E, Sobin L, Arnold R (2000) Endocrine tumors of the gallbladder and extrahepatic bile ducts. In: Hamilton S, Aaltonen L (eds) WHO classification of tumors of the digestive system; World Health Organization of Tumors. IARC, Lyon, pp 214–216
2. Kloppel G, Perren A, Heitz PU (2004) The gastroenteropancreatic neuroendocrine cell system and its tumors: the WHO classification. Ann N Y Acad Sci 1014:13–27
3. Kloppel G (2007) Tumour biology and histopathology of neuroendocrine tumours. Best Pract Res Clin Endocrinol Metab 21:15–31
4. Rindi G, Kloppel G, Alhman H et al (2006) TNM staging of foregut (neuro) endocrine tumors: a consensus proposal including a grading system. Virchows Arch 449:395–401
5. Rindi G, Klimstra DS, Arnold R et al (2010) Nomenclature and classification of neuroendocrine neoplasms of the digestive system. In: Bosman FT, Carneiro F, Hruban RH, Theise ND (eds) WHO classification of tumors of the digestive system; World Health Organization of Tumors, 4th edn. IARC, Lyon, pp 13–14
6. Komminoth P, Arnold R, Capella C et al (2010) Neuroendocrine neoplasms of the gallbladder and extrahepatic bile ducts. In: Bosman FT, Carneiro F, Hruban RH, Theise ND (eds) WHO classification of tumors of the digestive system; World Health Organization of Tumors, 4th edn. IARC, Lyon, pp 274–276
7. Volante M, Brizzi MP, Faggiano A et al (2007) Somatostatin receptor type 2A immunohistochemistry in neuroendocrine tumors: a proposal of scoring system correlated with somatostatin receptor scintigraphy. Mod Pathol 20:1172–1182
8. Oberg KE, Reubi JC, Kwekkeboom DJ, Krenning EP (2010) Role of somatostatins in gastroenteropancreatic neuroendocrine tumor development and therapy. Gastroenterology 139:742–753
9. Kurumaya H, Ohta G, Nakanuma Y (1989) Endocrine cells in the intrahepatic biliary tree in normal livers and hepatolithiasis. Arch Pathol Lab Med 113:143–147
10. Tsuchiya A, Endo Y, Yazawa T et al (2006) Adenoendocrine cell carcinoma of the gallbladder: report of a case. Surg Today 36:849–852
11. Nesi G, Lombardi A, Batignani G et al (2006) Well-differentiated endocrine tumor of the distal common bile duct: a case study and literature review. Virchows Arch 449:104–111
12. Squillaci S, Marchione R, Piccolomini M et al (2010) Well-differentiated neuroendocrine carcinoma (malignant carcinoid) of the extrahepatic biliary tract: report of two cases and literature review. Apmis 118:543–556
13. Shimizu T, Tajiri T, Akimaru K et al (2006) Combined neuroendocrine cell carcinoma and adenocarcinoma of the gallbladder: report of a case. J Nippon Med Sch 73:101–105
14. Kuraoka K, Taniyama K, Fujitaka T et al (2003) Small cell carcinoma of the extrahepatic bile duct: case report and immunohistochemical analysis. Pathol Int 53:887–891
15. Kozaka K, Fujii T, Harada K et al (2007) A subgroup of intrahepatic cholangiocarcinoma with an infiltrating replacement growth pattern and a resemblance to reactive proliferating bile ductules: 'bile ductular carcinoma'. Histopathology 51:390–400

Virchows Arch (2012) 460:291–298
DOI 10.1007/s00428-012-1202-6

ORIGINAL ARTICLE

Aspects of liver pathology in adult patients with *MDR3/ABCB4* gene mutations

Dominique Wendum · Véronique Barbu · Olivier Rosmorduc · Lionel Arrivé · Jean-François Fléjou · Raoul Poupon

Received: 17 August 2011 / Revised: 18 January 2012 / Accepted: 24 January 2012 / Published online: 14 February 2012
© Springer-Verlag 2012

Abstract The aims of this study were to describe the histological liver lesions in adult patients with *MDR3/ ABCB4* mutation and to study the usefulness of MDR3 immunostaining as a diagnostic tool. All adult patients from our institution with an *MDR3/ABCB4* mutation and a liver histology were included (n=13). Eleven patients had a single heterozygous gene mutation and two patients had two heterozygous mutations. Two patients had no liver lesions. Eight patients had a mild ductular reaction and portal fibrosis. One patient had a few fibrous septa and two patients had biliary cirrhosis. In three cases intraductal lipid crystals were identified. Two patients had biliary fibroobliterative lesions with no sclerosing cholangitis on cholangiography. Biliary dysplasia was identified in hepatectomy specimens from two patients, one of whom developed an intrahepatic cholangiocarcinoma. One patient with biliary cirrhosis developed a hepatocellular carcinoma. MDR3 immunostainings performed on formalin-fixed paraffin-embedded sections showed a strong canalicular staining in all patients except in one. To conclude, the predominant histological features were ductular reaction with no or mild fibrosis without cholangitis. Liver lesions previously unreported in association with *MDR3/ABCB4* gene mutations (biliary dysplasia, cholangiocarcinoma, small duct sclerosing cholangitis) were also found. Lipid crystals in bile ducts may be suggestive of *MDR3/ABCB4* mutation. MDR3 immunostaining on formalin-fixed paraffin-embedded sections does not seem to be sensitive for the diagnosis of heterozygous *MDR3/ABCB4* mutations.

Keywords Liver pathology · *MDR3/ABCB4* gene · Immunohistochemistry

D. Wendum · J.-F. Fléjou
Service d'Anatomie Pathologique, APHP, Hôpital St Antoine,
75012 Paris, France

V. Barbu
Service de Biochimie, APHP, Hôpital St Antoine,
75012 Paris, France

O. Rosmorduc · R. Poupon
Service d'Hépatologie, APHP, Hôpital St Antoine,
75012 Paris, France

L. Arrivé
Service d'imagerie médicale, APHP, Hôpital St Antoine,
75012 Paris, France

D. Wendum · V. Barbu · O. Rosmorduc · L. Arrivé · J.-F. Fléjou · R. Poupon
Université Pierre et Marie Curie, UPMC,
Univ Paris06,
75005 Paris, France

D. Wendum · V. Barbu · O. Rosmorduc
INSERM, UMR_S938, CdR Saint-Antoine,
75012 Paris, France

D. Wendum (✉)
Service d'Anatomie et Cytologie Pathologiques,
Hôpital St Antoine,
184, rue du Faubourg St Antoine,
75571 Paris Cedex 12, France
e-mail: dominique.wendum@sat.aphp.fr

Introduction

Multidrug resistance P-glycoprotein 3 (MDR3) is a membranous protein expressed at the apical pole of hepatocytes and encoded by the *ABCB4/MDR3* gene located on chromosome 7. It has a floppase activity and is able to flop phosphatidyl choline from the inner to the outer leaflet of the canalicular cytoplasmic membrane of hepatocytes. At the outer leaflet, phosphatidyl choline is available for extraction into bile by bile acids [1].

Several liver diseases are known to be associated with *MDR3/ABCB4* mutations [2]. In human pathology, mutations of both alleles of the *MDR3/ABCB4* gene are associated with type 3 progressive familial intrahepatic cholestasis (PFIC-3) which is a pediatric disease. In adults, biliary cirrhosis with ductopenia has been described as well as several other liver diseases such as low phospholipid-associated cholelithiasis syndrome (LPAC syndrome), intrahepatic cholestasis of pregnancy, drug-induced cholestasis, and "unexplained" chronic cholestasis [3–7].

The mouse equivalent of MDR3 protein is called "mdr2". Knockout mice for *Abcb4 gene* (mdr2 −/−) develop biliary lesions that are considered the equivalent of sclerosing cholangitis, with ductular reaction and fibrosis, and the later possible development of hepatocellular carcinoma [8, 9]. However, in humans, there is no evidence of an association between primary sclerosing cholangitis and MDR3 deficiency [10, 11], and as yet, no hepatocellular carcinoma associated with MDR3 deficiency has been described.

While the clinical spectrum of liver disease associated with MDR3 deficiency is an ongoing work in progress and, thus, relatively well described, the histopathological appearances are less clear and found in scattered reports in the literature. Moreover, the use of MDR3 immunohistochemistry to diagnose MDR3 deficiency appears promising. Indeed, patients with PFIC-3 and patients with heterozygous mutations frequently appear to have reduced or even absent MDR3 canalicular expression on immunostainings [6, 12, 13].

For this reasons, the aim of the present study was to describe the histological patterns and lesions observed in a series of adult patients with *MDR3/ABCB4* mutation-associated liver disease and to assess the usefulness of MDR3 immunostaining as a putative diagnostic or screening tool to assess MDR3 deficiency.

Patients, materials, and methods

Patients

At our institution, all adult patients, defined as those at least 18 years at the time of their first symptoms, with an *MDR3/ABCB4* gene mutation identified by gene analysis before 2010, and who have had a liver sampling with histopathological analysis were included. *MDR3/ABCB4* gene analysis was mostly performed in patients with biliary disease (hepatolithiasis, recurrent cholangitis, or biliary pain) associated with intrahepatic hyperechogenic foci on ultrasound examination. Some of them had all of the clinical characteristics associated with the LPAC syndrome (biliary symptoms before the age of 40 and recurrence of the symptoms after cholecystectomy and intrahepatic microlithiasis or intrahepatic hyperechogenic foci on ultrasound examination, with a normal cholangiography) [14]. Other conditions prompting *MDR3/ABCB4* gene analysis were the so-called "unexplained chronic anicteric cholestasis" (chronic cholestasis in the absence of heavy alcohol intake, drug intake, viral hepatitis B or C, serum antimitochondrial type M2 antibodies, p-ANCA antibodies, and antinuclear antibodies), drug-induced cholestasis, or intrahepatic cholestasis of pregnancy. All clinical and radiological data were retrospectively analyzed.

MDR3/ABCB4 gene analysis

MDR3/ABCB4 gene sequencing was performed as previously described [6]. Briefly, genomic DNA was obtained from peripheral blood cells using standard procedures. A Polymerase chain reaction amplification using specific primers and DNA sequencing of exons 2–28 and all spliced junctions were performed. Identification and localization of the *MDR3/ABCB4* gene sequence variations were assessed by sequence comparison with SeqScape software (Applied Biosystems, v2.5).

Histological analysis

Retrospective histological analyses were performed blindly by one pathologist specialized in hepatopathology (DW), with no knowledge of the clinical and radiological data, and no knowledge of the type of mutation. All samples were formalin-fixed and paraffin-embedded, and stained with hematoxylin–eosin and Sirius red. The following lesions were systematically assessed: portal and periportal fibrosis using the METAVIR semiquantitative scale (F0, no fibrosis; F1, portal/periportal fibrosis with no septa; F2, periportal fibrosis with few septa; F3, periportal fibrosis with numerous septa; and F4, cirrhosis), portal inflammation, bile duct lesions (fibroobliterative bile duct lesion, lymphocytic destructive cholangitis, acute cholangitis, and periductal edema), ductular reaction, ductopenia, biliary dysplasia, bilirubinostasis, and the presence of intraluminal material in the bile ducts. Ductopenia was defined as the absence of interlobular bile duct in more than 50% of the portal tracts in a liver biopsy with at least ten portal tracts. Biliary dysplasia (biliary intraepithelial neoplasia (Bil IN)) was diagnosed and graded according to published criteria [15].

MDR3 immunostaining

For immunohistochemical staining, formalin-fixed, paraffin-embedded 4-μm sections were cut. The sections were pretreated in a water bath with EDTA buffer (10 mM, pH 8) for 30 min. An anti-MDR3 mouse monoclonal antibody (clone P3II-26, Chemicon International) was used. The primary antibody was detected using a BOND™ Polymer Refine Detection Kit (DS9800) with a BOND-MAX autostainer

(Vision Biosystems, Leica Microsystems). Briefly a poly-HRP (horseradish peroxidase) anti-mouse IgG was applied, followed by a diaminobenzidine chromogen substrate. The sections were counterstained with hematoxylin.

Liver sections of several patients without *MDR3/ABCB4* mutation assessed by gene analysis were used as positive control (two patients with chronic unexplained cholestasis and two patients with the LPAC syndrome). The negative control was by omission of the primary antibody. We used an anti-CD10 monoclonal antibody (Novocastra) to check canalicular tissue reactivity.

Results

Thirteen patients (five men, eight women) who had undergone *MDR3/ABCB4* gene analysis had a gene mutation and also a liver sampling with a histopathological analysis (eight needle liver biopsies, two wedge biopsies, two partial hepatectomy specimens, and one total hepatectomy with subsequent orthotopic liver transplantation). All the biopsies contained more than ten portal tracts. Immunohistochemistry was performed in all patients except two, whose biopsies had insufficient material into the paraffin block. A positive canalicular staining with an anti-CD10 antibody was observed in all the cases, confirming the immunoreactivity of the samples.

All patients also underwent ultrasound examination and all except one underwent cholangiography (magnetic resonance cholangiography in 11 cases and intraoperative cholangiography in one case). The main clinical, biological, radiological data for each patient are presented in Table 1. Genomic data are summarized in Table 2.

Based on clinical and radiological findings, four groups of patients were defined. The first group (patients 1–4, two women, two men) referred here as the "LPAC group" had the complete LPAC syndrome: biliary symptoms before the age of 40 and recurrence of the symptoms after cholecystectomy and intrahepatic microlithiasis or intrahepatic hyperechogenic foci, with a normal cholangiography [14]. Their main histopathological features were mild portal inflammation, mild periportal ductular reaction, and mild periportal fibrosis without fibrous septa (Fig. 1a). In two biopsies, a periductal edema was seen around an interlobular bile duct. In one of these two, the epithelial bile duct lining was disrupted by a needle-shaped empty space that could suggest a cholesterol crystal deposit. In this first group, all the patients had a single heterozygous *MDR3/ABCB4* gene mutation, with two of them being deleterious frame shift mutations. Immunohistochemistry performed in two cases (patients no. 3 and 4) showed a diffuse intense canalicular staining similar to the staining found in controls (Fig. 2a, b).

The second group (patient no. 5 to 8, two women and two men) had hepatolithiasis and suffered of recurrent cholangitis associated with localized large spindle-shaped biliary dilatations and bile stones on cholangiography. On cholangiography, bile duct dilatation was not associated with strictures and there was no pattern of sclerosing cholangitis. Within this group, three of the four patients (patient no. 6, 7, and 8) have been included in a previous study [16]. On the liver samples, there was a periportal fibrosis with a few septa in only one case. There was also a mild mononuclear portal inflammatory infiltrate and a mild ductular reaction. In two cases a pattern of sclerosing cholangitis with typical fibroobliterative bile duct lesions was seen (Fig. 1d). Of note, in these two cases the liver biopsy was not performed in the liver area with bile duct dilatation. In two cases an intraductal cholesterol crystal could be identified (Fig. 1b). On the hepatectomy specimen, moderate bile duct dysplasia (Bil IN-2) was identified in large and septal bile ducts. In this group, two patients had a single heterozygous *MDR3/ABCB4* mutation and two patients (patient no. 6 and 8) had two heterozygous *MDR3/ABCB4* mutations. For one patient (patient no. 6), it could be demonstrated that there was one mutation on each allele (compound heterozygous patient). Immunohistochemical analysis of MDR3 protein showed a faint staining in one patient (patient no. 8) (Fig. 2c). On the other samples, the staining had a diffuse and strong canalicular pattern.

The third group of patients (patient no. 9 and 10, two women) had hepatolithiasis with several episodes of cholangitis with features of sclerosing cholangitis on magnetic resonance cholangiography. One patient developed biliary cirrhosis with a marked ductular reaction. The other patient had a mild periportal fibrosis with mild ductular reaction. In the latter, moderate biliary dysplasia (Bil IN-2) was identified in large bile ducts. Of note this patient (patient no. 10) developed a pure intrahepatic cholangiocarcinoma 1 year after the first partial hepatectomy (Fig. 3a, b). Both patients had a heterozygous *MDR3/ABCB4* mutation. Immunohistochemical staining of MDR3 had a diffuse and strong canalicular pattern.

The fourth group of patients is heterogeneous and gathers together patients with miscellaneous symptoms. Two patients had unexplained cholestasis with elevated serum aminotransferase with normal magnetic resonance cholangiography. Concerning these two patients, one had a normal liver biopsy and the other had a mild ductular reaction with ductopenia (Fig. 1c). The last patient had a decompensated biliary cirrhosis leading to liver transplantation. On the liver specimen, there was a pattern of biliary cirrhosis with marked bilirubinostasis and ductular reaction. A 4-cm liver macronodule was identified on the explanted liver with areas of well-differentiated hepatocellular carcinoma with bile production (liver plates more than three cells width with an altered reticulin framework and glypican-3 expression) (Fig. 3c–f). The genetic analysis showed heterozygous *MDR3/ABCB4* mutations in all three cases. MDR3 immunohistochemistry showed, in all these cases, a moderate to strong diffuse canalicular staining.

Table 1 Main clinical, radiological, and histopathological data for each patient

Patient, no./gender/age[a] (years)	Clinical data	Radiological data	Liver sample	Histology (hematoxylin–eosin and Sirius red stainings)
1/M/26	Complete LPAC syndrome	Normal MR cholangiography	Wedge biopsy	F1, mild ductular reaction, periductal edema
2/M/46	Complete LPAC syndrome	Normal MR cholangiography	Needle biopsy	No lesion
3/F/43	Complete LPAC syndrome	Normal intraoperative cholangiography	Wedge biopsy	F1, mild ductular reaction
4/F/31	Complete LPAC syndrome, ICP	Normal MR cholangiography	Needle biopsy	F1, mild ductular reaction, periductal edema, intraductal cholesterol crystal
5/F/53	Recurrent cholangitis	Spindle-shaped bile duct dilatation without stenosis or sclerosing cholangitis	Needle biopsy	F1, mild ductular reaction
6/F/24	Recurrent cholangitis	Spindle-shaped bile duct dilatation without stenosis or sclerosing cholangitis	Needle biopsy	F1, mild ductular reaction, sclerosing cholangitis, intraductal cholesterol crystal
7/M/50	Recurrent cholangitis	Spindle-shaped bile duct dilatation without stenosis or sclerosing cholangitis	Needle biopsy	F2, mild ductular reaction, sclerosing cholangitis
8/M/57	Recurrent cholangitis	Spindle-shaped bile duct dilatation without stenosis or sclerosing cholangitis	Partial Hepatectomy	F1, mild ductular reaction, biliary dysplasia, intraductal cholesterol crystal
9/F/63	Recurrent cholangitis	Sclerosing cholangitis	Needle biopsy	Biliary cirrhosis, periductal edema
10/F/54	Recurrent cholangitis, cholangiocarcinoma	Sclerosing cholangitis	Partial hepatectomy	F1, mild ductular reaction, steatosis, biliary dysplasia, cholangiocarcinoma
11/M/47	Unexplained cholestasis and elevated aminotransferase	Normal MR cholangiography	Needle biopsy	No lesion
12/F/34	Unexplained cholestasis and elevated aminotransferase ICP	Normal MR cholangiography	Needle biopsy	F1, mild ductular, ductopenia
13/F/55	Biliary cirrhosis, ICP	Not performed	Total hepatectomy	Biliary cirrhosis, macronodule with well-differentiated hepatocellular carcinoma

LPAC low phospholipid-associated cholelithiasis, *ICP* intrahepatic cholestasis of pregnancy, *F1* periportal fibrosis without septa, *F2* periportal fibrosis with a few septa

[a] At the time of liver sampling

Table 2 *MDR3/ABCB4* gene mutations in our patients

Patients no.	Location and nucleotide change	Effect on protein	Status of variant	Mutation category
1	c.1328dup	p.Arg444Glu fsX4, truncating	Heterozygous	Insertion
2	c.1584 G > C	p.Glu528Asp	Heterozygous	Missense
3	c.101 C > T	p.Thr34Met	Heterozygous	Missense
4	c.1553delT	p.Leu518Tyr fsX16, truncating	Heterozygous	Deletion
5	c.139 C > G	p.Arg 47 Gly	Heterozygous	Missense
6	c.1217 G > A	p.Arg 406 Gln	Heterozygous	Missense
	c.140 G > A	p.Arg47Gln	Heterozygous, compound	Missense
7	c.857 C > T	p.Ala 286 Val	Heterozygous	Missense
8	c.2324 C > T	p.Thr775Met	Heterozygous	Missense
	c.2836 G > A	p.Ala946Thr	Heterozygous	Missense
9	c.523A > G	p.Thr175Ala	Heterozygous	Missense
10	c.1005 + 5 G > A	p.?	Heterozygous	Splicing
11	c.523A > G	p.Thr175Ala	Heterozygous	Missense
12	c.959 C > T	Ser 320 Phe	Heterozygous	Missense
13	c.959 C > T	Ser 320 Phe	Heterozygous	Missense

For *MDR3/ABCB4* mutation effect on protein, the mutated codon number is indicated as well as the resultant change of the encoded amino acid. In the case of patient 10, the mutation was an alternative splicing sequence variation. For patient no. 8, we could not determine if the two mutations were on the same allele or one on each allele (compound heterozygous). ABCB4 gene mutations found in patients nos 1, 2, 7, 8, 9, 11, 12, and 13 have been already described in the literature [14, 25]

Discussion

The aim of this study was to describe the histopathological features associated with *MDR3/ABCB4* gene mutations in adult patients in order to clarify and specify the possible histological patterns and find aspects suggestive of *MDR3/ABCB4* mutations.

Limitations of this study were that it only reflected a small subgroup of symptomatic patients. And although the number of liver specimens was quite low, we found various lesions. The main histological pattern was a mild ductular reaction with a few portal inflammatory mononuclear cells and a mild periportal fibrosis. This was consistent with previous reports [3, 6].

These mild and nonspecific lesions were sometimes accompanied with bile duct lesions: periductular edema, sclerosing cholangitis, and presence of intraductal cholesterol crystals. Intraductal crystals were rarely seen in liver needle biopsies (in two cases in our study and also in one case in the study of Ziol et al.). This lesion could be a clue to suggest an *MDR3/ABCB4* mutation. Indeed, *MDR3/ABCB4* mutation leads to a defect into the hepatic transport and biliary secretion of phospholipids with increased cholesterol saturation in bile. This increased cholesterol saturation favors cholesterol precipitation

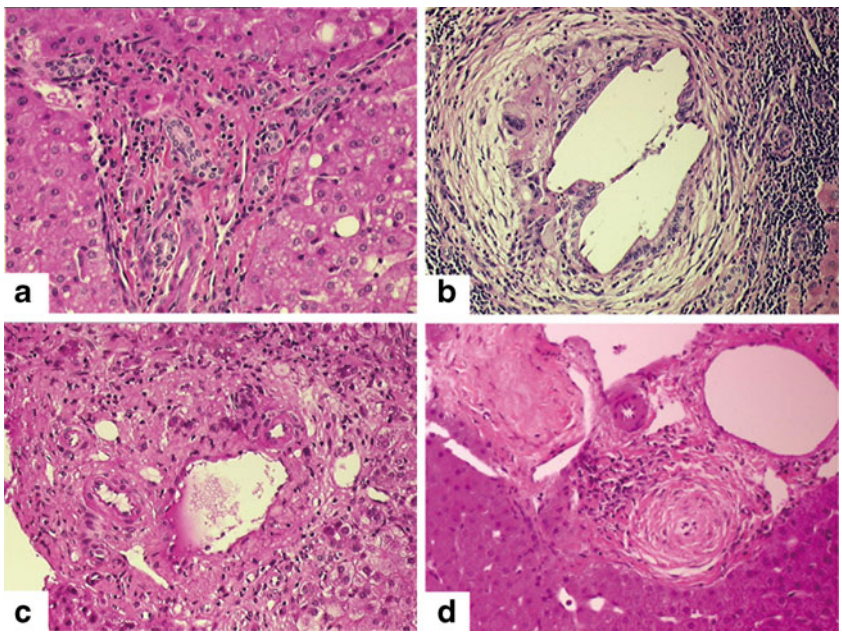

Fig. 1 Liver lesions in adult patients with MDR3 deficiency (*MDR3/ABCB4* mutation). **a** mild ductular reaction with periportal fibrosis; **b** Intraductal cholesterol crystals; **c** portal tract without bile ducts in a patient with ductopenia; **d** fibroobliterative lesion of an interlobular bile duct (sclerosing cholangitis)

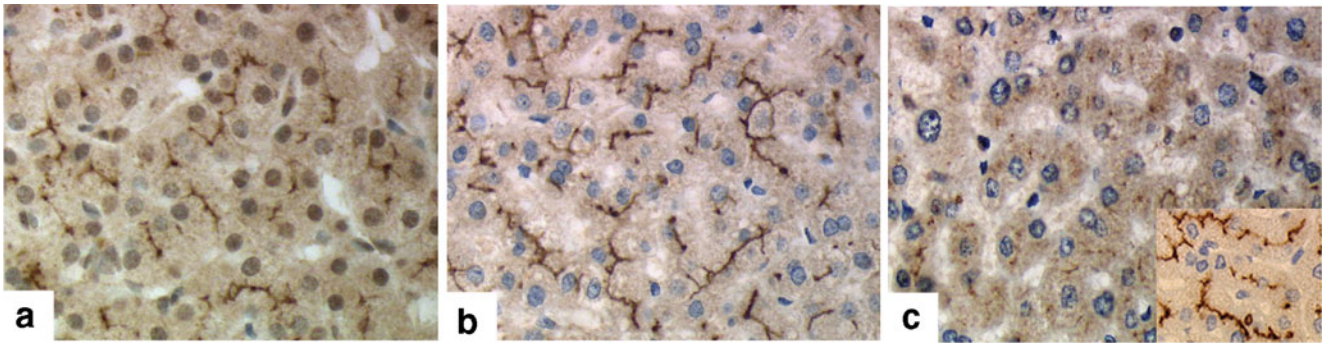

Fig. 2 MDR3 immunostainings on formalin-fixed paraffin-embedded sections: **a** diffuse and strong canalicular staining in a patient with low phospholipid-associated cholelithiasis without *MDR3/ABCB4* gene mutation; **b** diffuse and strong canalicular staining in a patient with a heterozygous mutation (patient no. 3); **c** weak and incomplete staining in a patient with two heterozygous *MDR3/ABCB4* mutations. *Inset*: canalicular staining with an anti-CD10 antibody used as positive control for antigenic preservation of the tissue (patient no. 8)

that can be seen as hyperechogenic foci on ultrasound examination [17, 18]. The histological equivalent of these hyperechogenic foci is probably these lipid crystals that can be seen on a liver biopsy. Although suggestive, this lesion is probably not specific because cholesterol precipitation can occur in the absence of *MDR3/ABCB4* mutation. Indeed, in the series of Rosmorduc et al. only 56% of the patients with a complete LPAC syndrome had a *MDR3/ABCB4* gene mutation [14]. Other biliary lesions that were described in this study were periductal edema and sclerosing cholangitis. Fibroobliterative lesions of interlobular bile ducts were seen in two patients. Interestingly these two patients had MDR3 deficiency with large spindle-shaped bile duct dilatations filled with gallstones. This pattern recently described was not associated with radiological sclerosing cholangitis or bile strictures. Therefore, these fibroobliterative biliary lesions correspond to small duct sclerosing cholangitis. Of note, the biopsies were not performed into the liver area with bile duct dilatation. Whereas sclerosing

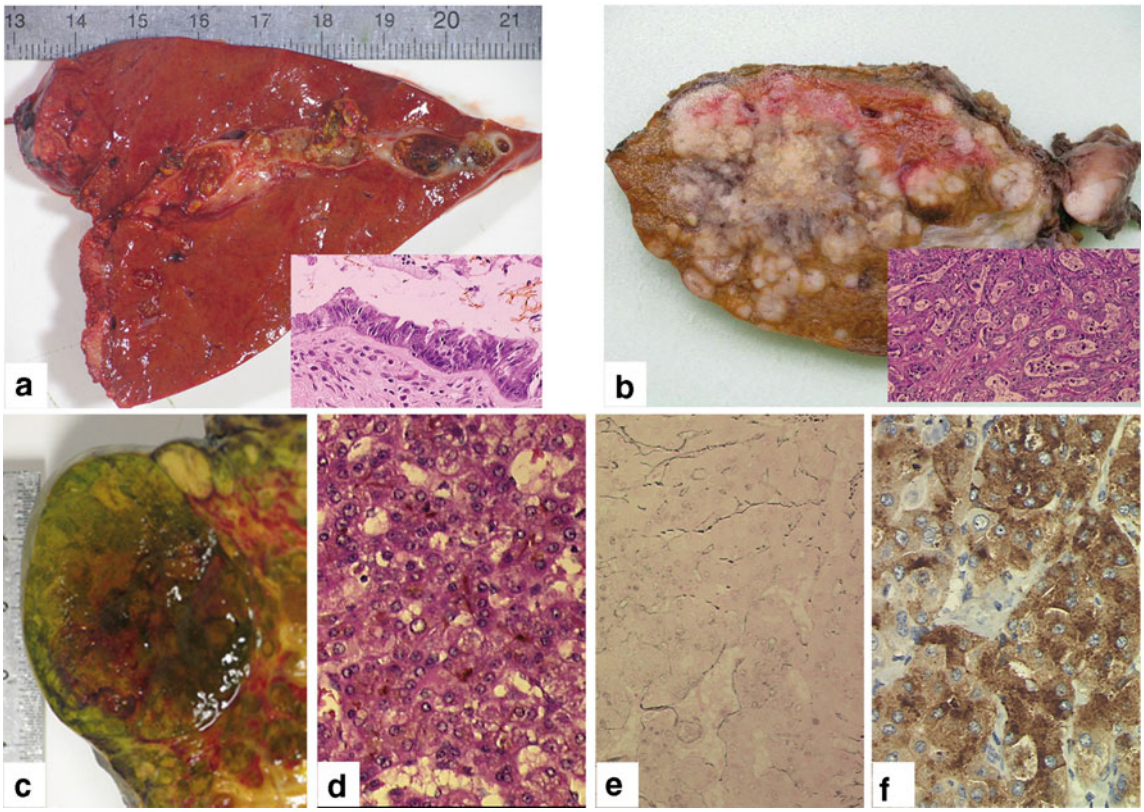

Fig. 3 **a** Hepatolithiasis (macroscopy) with biliary dysplasia (*inset*); **b** the patient developed 1 year later an intrahepatic cholangiocarcinoma (macroscopy, *inset*: microscopy) (patient no. 10); **c** biliary cirrhosis with a 4-cm macronodule (macroscopy) corresponding to a well-differentiated hepatocellular carcinoma with bile production (**d**), with loss of the reticulin framework (**e**), and glypican-3 expression (**f**) (patient no. 13)

cholangitis (intra and extrahepatic) is the main feature in mdr2 knockout mice, MDR3 deficiency seems not to be involved in primary sclerosing cholangitis in humans [10]. In this series we showed for the first time that small duct sclerosing cholangitis can be seen in some patients with MDR3 deficiency. These small duct fibroobliterative lesions could be secondary to the intrahepatic microscopic stones (cholesterol precipitation), recurrent cholangitis, or could also be due to a direct toxic effect of bile acids on the biliary cells [14, 19].

In this series we also found biliary dysplasia (grade 2 biliary intraepithelial neoplasia/Bil IN-2) in large bile and septal ducts in hepatectomy specimens in two patients who suffered of hepatolithiasis with recurrent cholangitis. In one case, the patient developed 1 year later an intrahepatic cholangiocarcinoma in the remaining liver. This is the first case of intrahepatic cholangiocarcinoma reported in the literature associated with MDR3 deficiency. Biliary dysplasia may occur in the bile duct of patients suffering from hepatolithiasis which is well known to predispose for the development of cholangiocarcinoma. However cholangiocarcinoma associated with cholesterol hepatolithiasis seems to be rare [20–22]. Biliary dysplasia and cholangiocarcinoma associated with cholesterol gallstones with MDR3 deficiency could be related to bile duct chronic inflammation or to the toxic bile concept—because MDR3 deficiency induces low phosphatidylcholine concentrations into bile, micelles have an abnormal structure and bile acids which have toxic properties are more prone to be in contact with cholangiocytes. Further studies are needed to clarify the role of MDR3 deficiency in biliary dysplasia or cholangiocarcinoma development.

In our series, we also found several lesions that have already been described such as the mild ductular reaction, biliary cirrhosis, and ductopenia [5, 7]. We also observed a case of biliary cirrhosis with hepatocellular carcinoma, which is already known to be associated with mdr2 mutations in mice [8] but not described yet in humans. Here also, further studies are needed to asses if MDR3 deficiency is a risk factor for hepatocellular carcinoma development in humans.

In this study, we evaluated the use of MDR3 immunohistochemical staining in order to diagnose *MDR3/ABCB4* mutations because the histological aspects associated with *MDR3/ABCB4* mutations are nonspecific. Indeed, MDR3 immunostaining on frozen sections is used for PFIC-3 patients and can show a complete absence of canalicular staining, a faint or sometimes a normal canalicular staining [4, 23]. Some studies showed that patients with heterozygous *MDR3/ABCB4* mutations seem to have a reduced or absent MDR3 canalicular expression on immunostainings on frozen sections without antigen retrieval [4, 6, 12]. We found that MDR3 immunostaining on paraffin section was not efficient to diagnose heterozygous *MDR3/ABCB4* mutations. Indeed, in our series all the patients with a single heterozygous *MDR3/ABCB4* mutation had a strong diffuse canalicular staining, even patient no. 4 with a deleterious heterozygous frameshift mutation. This immunostaining pattern in heterozygous patients, identical to the pattern observed in patients without *MD3/ABCB4* mutation, could be related to the remaining normal allele in case of heterozygous patients because, with antigen retrieval, immunohistochemistry is a very sensitive technique. In accordance with this, immunostaining for patient no. 4 with a heterozygous deleterious mutation that leads to a truncated protein before the 629th amino acid was also strong, diffuse, and canalicular. Indeed, the antibody we used in this study is directed against amino acids 629–692 of the MDR3 human protein; therefore, it theoretically does not recognize the truncated protein produced by the mutated allele in this patient. The other normal existing allele might be sufficient to give a normal appearing staining. The normal immunostaining pattern in patients with heterozygous *MDR3/ABCB4* mutations could also be related to mutations leading to a functional defect with normal protein localization [24] (JL Delaunay, personal communication).

Finally, antigen retrieval may also give rise to antigen modification and possible false-positive results. However, one patient, who had two heterozygous *MDR3/ABCB4* mutations, had a faint staining although the mutations were not localized in the part of the protein recognized with the antibody. For this case, a lack of tissue reactivity does not seem to be involved because CD10 canalicular immunostaining was strong and continuous. Accordingly, MDR3 immunohistochemistry on paraffin section cannot be used to rule out an *MDR3/ABCB4* mutation—a normal canalicular staining does not exclude MDR3 deficiency as already described [4, 12, 23]. Immunohistochemistry can be performed but only a negative or faint staining is informative. Moreover, immunohistochemistry on formalin-fixed paraffin-embedded material does not seem to be sensitive enough because, in our series, a faint staining was observed in only one case (double heterozygous patient, patient no. 8).

To summarize, in this series, we described a panel of histological lesions associated with *MDR3/ABCB4* mutations in adult patients. In addition to the lesions already described in the literature, we observed lesions that have not been reported yet (biliary dysplasia with later development of a cholangiocarcinoma, hepatocellular carcinoma, and small duct sclerosing cholangitis). Although rare, we also showed that the presence of lipid crystals in the interlobular bile duct can be seen on biopsies and although probably not specific, this could suggest a *MDR3/ABCB4* mutation. Finally, in our series MDR3 immunostaining on formalin-fixed and paraffin-embedded sections did not seem to be a useful tool to diagnose heterozygous *MDR3/ABCB4* mutations.

Conflicts of interest The authors have no conflict of interest to declare.

References

1. Oude Elferink RP, Paulusma CC (2007) Function and pathophysiological importance of ABCB4 (MDR3 P-glycoprotein). Pflugers Arch 453:601–610
2. Davit-Spraul A, Gonzales E, Baussan C, Jacquemin E (2009) Progressive familial intrahepatic cholestasis. Orphanet J Rare Dis 4:1
3. Rosmorduc O, Hermelin B, Poupon R (2001) MDR3 gene defect in adults with symptomatic intrahepatic and gallbladder cholesterol cholelithiasis. Gastroenterology 120:1459–1467
4. Jacquemin E, De Vree JM, Cresteil D, Sokal EM, Sturm E, Dumont M, Scheffer GL, Paul M, Burdelski M, Bosma PJ, Bernard O, Hadchouel M, Elferink RP (2001) The wide spectrum of multidrug resistance 3 deficiency: from neonatal cholestasis to cirrhosis of adulthood. Gastroenterology 120:1448–1458
5. Gotthardt D, Runz H, Keitel V, Fischer C, Flechtenmacher C, Wirtenberger M, Weiss KH, Imparato S, Braun A, Hemminki K, Stremmel W, Ruschendorf F, Stiehl A, Kubitz R, Burwinkel B, Schirmacher P, Knisely AS, Zschocke J, Sauer P (2008) A mutation in the canalicular phospholipid transporter gene, ABCB4, is associated with cholestasis, ductopenia, and cirrhosis in adults. Hepatology 48:1157–1166
6. Ziol M, Barbu V, Rosmorduc O, Frassati-Biaggi A, Barget N, Hermelin B, Scheffer GL, Bennouna S, Trinchet JC, Beaugrand M, Ganne-Carrie N (2008) ABCB4 heterozygous gene mutations associated with fibrosing cholestatic liver disease in adults. Gastroenterology 135:131–141
7. Poupon R, Barbu V, Chamouard P, Wendum D, Rosmorduc O, Housset C (2010) Combined features of low phospholipid-associated cholelithiasis and progressive familial intrahepatic cholestasis 3. Liver Int 30:327–331
8. Mauad TH, van Nieuwkerk CM, Dingemans KP, Smit JJ, Schinkel AH, Notenboom RG, van den Bergh Weerman MA, Verkruisen RP, Groen AK, Oude Elferink RP et al (1994) Mice with homozygous disruption of the mdr2 P-glycoprotein gene. A novel animal model for studies of nonsuppurative inflammatory cholangitis and hepatocarcinogenesis. Am J Pathol 145:1237–1245
9. Fickert P, Fuchsbichler A, Wagner M, Zollner G, Kaser A, Tilg H, Krause R, Lammert F, Langner C, Zatloukal K, Marschall HU, Denk H, Trauner M (2004) Regurgitation of bile acids from leaky bile ducts causes sclerosing cholangitis in Mdr2 (Abcb4) knockout mice. Gastroenterology 127:261–274
10. Pauli-Magnus C, Kerb R, Fattinger K, Lang T, Anwald B, Kullak-Ublick GA, Beuers U, Meier PJ (2004) BSEP and MDR3 haplotype structure in healthy Caucasians, primary biliary cirrhosis and primary sclerosing cholangitis. Hepatology 39:779–791
11. Rosmorduc O, Hermelin B, Boelle PY, Poupon RE, Poupon R, Chazouilleres O (2004) ABCB4 gene mutations and primary sclerosing cholangitis. Gastroenterology 126:1220–1222, author reply 1222-1223
12. Davit-Spraul A, Gonzales E, Baussan C, Jacquemin E (2010) The spectrum of liver diseases related to ABCB4 gene mutations: pathophysiology and clinical aspects. Semin Liver Dis 30:134–146
13. Colombo C, Vajro P, Degiorgio D, Coviello DA, Costantino L, Tornillo L, Motta V, Consonni D, Maggiore G (2011) Clinical features and genotype-phenotype correlations in children with progressive familial intrahepatic cholestasis type 3 related to ABCB4 mutations. J Pediatr Gastroenterol Nutr 52:73–83
14. Rosmorduc O, Hermelin B, Boelle PY, Parc R, Taboury J, Poupon R (2003) ABCB4 gene mutation-associated cholelithiasis in adults. Gastroenterology 125:452–459
15. Zen Y, Adsay NV, Bardadin K, Colombari R, Ferrell L, Haga H, Hong SM, Hytiroglou P, Kloppel G, Lauwers GY, van Leeuwen DJ, Notohara K, Oshima K, Quaglia A, Sasaki M, Sessa F, Suriawinata A, Tsui W, Atomi Y, Nakanuma Y (2007) Biliary intraepithelial neoplasia: an international interobserver agreement study and proposal for diagnostic criteria. Mod Pathol 20:701–709
16. Poupon R, Arrive L, Rosmorduc O (2010) The cholangiographic features of severe forms of ABCB4/MDR3 deficiency-associated cholangiopathy in adults. Gastroenterol Clin Biol 34:380–387
17. Carey MC (1978) Critical tables for calculating the cholesterol saturation of native bile. J Lipid Res 19:945–955
18. Shoda J, Oda K, Suzuki H, Sugiyama Y, Ito K, Cohen DE, Feng L, Kamiya J, Nimura Y, Miyazaki H, Kano M, Matsuzaki Y, Tanaka N (2001) Etiologic significance of defects in cholesterol, phospholipid, and bile acid metabolism in the liver of patients with intrahepatic calculi. Hepatology 33:1194–1205
19. Trauner M, Fickert P, Wagner M (2007) MDR3 (ABCB4) defects: a paradigm for the genetics of adult cholestatic syndromes. Semin Liver Dis 27:77–98
20. Kawakami H, Kuwatani M, Onodera M, Hirano S, Kondo S, Nakanishi Y, Itoh T, Asaka M (2007) Primary cholesterol hepatolithiasis associated with cholangiocellular carcinoma: a case report and literature review. Intern Med 46:1191–1196
21. Shaib Y, El-Serag HB (2004) The epidemiology of cholangiocarcinoma. Semin Liver Dis 24:115–125
22. Shoda J, Tanaka N, Osuga T (2003) Hepatolithiasis—epidemiology and pathogenesis update. Front Biosci 8:e398–e409
23. Keitel V, Burdelski M, Warskulat U, Kuhlkamp T, Keppler D, Haussinger D, Kubitz R (2005) Expression and localization of hepatobiliary transport proteins in progressive familial intrahepatic cholestasis. Hepatology 41:1160–1172
24. Delaunay JL, Durand-Schneider AM, Delautier D, Rada A, Gautherot J, Jacquemin E, Ait-Slimane T, Maurice M (2009) A missense mutation in ABCB4 gene involved in progressive familial intrahepatic cholestasis type 3 leads to a folding defect that can be rescued by low temperature. Hepatology 49:1218–1227
25. Degiorgio D, Colombo C, Seia M, Porcaro L, Costantino L, Zazzeron L, Bordo D, Coviello DA (2007) Molecular characterization and structural implications of 25 new ABCB4 mutations in progressive familial intrahepatic cholestasis type 3 (PFIC3). Eur J Hum Genet 15:1230–1238

Virchows Arch (2012) 460:299–308
DOI 10.1007/s00428-012-1194-2

ORIGINAL ARTICLE

Phenotyping of pulmonary carcinoids and a Ki-67-based grading approach

Tina Zahel · Sabine Krysa · Esther Herpel · Albrecht Stenzinger · Benjamin Goeppert · Peter Schirmacher · Hans Hoffmann · Philipp A. Schnabel · Arne Warth

Received: 22 August 2011 / Revised: 11 December 2011 / Accepted: 10 January 2012 / Published online: 1 February 2012
© Springer-Verlag 2012

Abstract Pulmonary carcinoids (PC) are separated into typical (TC) and atypical carcinoids (ATC). However, the biological behavior cannot be reliably predicted, and in small biopsies differential diagnosis can be challenging. To provide a basis for a grading approach, we analyzed mitoses and the proliferative index (PI; Ki-67) of 200 PC specimens (TC: $n=114$; ATC: $n=86$). To define suitable diagnostic and to screen for putative therapeutic markers, CD56, CD57, CD99, CD117, TTF-1, synaptophysin, chromogranin A, CK 18, KL-1, epidermal growth factor receptor (EGFR), human epidermal growth factor receptor 2 (Her-2/neu), somatostatin receptor subtype 2A (SSTR2A), thymidylate synthase (TS), and excision repair cross-complementation group 1 (ERCC-1) expression was analyzed. A combination of synaptophysin and cytokeratins is the most sensitive marker panel for PC with unclear histomorphology. Predictive phenotyping revealed that SSTR2A is expressed in >80% of all PC and may be used both, as a diagnostic marker for imaging approaches and as a predictive marker for octreotide-based therapies. We introduced a grading system distinguishing between PC with low and highly aggressive biological behavior similar to the grading system for gastrointestinal neuroendocrine tumors. The system is superior to the classical separation into TC and ATC. This study indicates that PI in addition to mitotic count may improve prediction of the biological behavior of PC and should be validated in prospective studies.

Keywords Pulmonary carcinoids · Immunomarkers · Grading · Prognosis · Biological behavior · Diagnostic marker

T. Zahel · E. Herpel · A. Stenzinger · B. Goeppert · P. Schirmacher · P. A. Schnabel · A. Warth (✉)
Institute for Pathology, University Hospital Heidelberg,
Im Neuenheimer Feld 220/221,
69120 Heidelberg, Germany
e-mail: arne.warth@med.uni-heidelberg.de

S. Krysa · H. Hoffmann
Department of Thoracic Surgery, Thoraxklinik Heidelberg,
Heidelberg, Germany

Introduction

Lung cancer is the leading cause of cancer-related mortality [1]. Besides highly aggressive small cell (SCLC) and large cell neuroendocrine carcinomas (LCNEC), the spectrum of neuroendocrine tumors of the lungs includes carcinoids, which are considered tumors of intermediate malignancy. According to the World Health Organization (WHO) classification [2], pulmonary carcinoids (PC) are subdivided into typical carcinoids (TC) and atypical carcinoids (ATC). The distinction is based on histological criteria; less than two mitoses per 2 mm^2 and absence of necrosis qualifies for TC and ≥ two to ten mitoses or presence of necrosis is diagnostic for ATC [2]. In small tumor samples, the differential diagnosis to SCLC, LCNEC, adenocarcinomas, and paragangliomas can be challenging.

PC patients usually have a good prognosis. However, these tumors harbor the potential to invade, metastasize, and the biological behavior is not reliably predictable. Lymph node metastases of PC occur in 10–15% [3, 4]; distant metastases are reported in less than 5% [5, 6]. Five-year survival for TC and ATC is 87–100% and 61–88%, respectively [7, 8]. Thus, it is essential to distinguish between PC with a low malignant course and those that progress [9]. We recently demonstrated that analyses of chromosomal instability [4] and S100 protein-positive sustentacular cells [10] may be helpful in this regard. However, it is well known that the proliferative index (PI) is a useful

predictor of the biological behavior of many tumors [11]. A recent grading proposal for gastrointestinal neuroendocrine tumors, formerly designated as carcinoids, therefore introduced a grading system based on PI and mitotic count to better predict the biological behavior of these entities [12], while a grading system has not been established for PC yet.

To provide an integrated approach of PC typing, prognostic evaluation, and prediction, we performed a screening for diagnostic immunomarkers and selected markers with a putative therapeutic significance (epidermal growth factor receptor (EGFR), human epidermal growth factor receptor 2 (Her-2/neu), somatostatin receptor subtype 2A (SSTR2A), thymidylate synthase (TS), and excision repair cross-complementation group 1 (ERCC-1)) and aimed to test for a grading system for PC that optimizes distinction of tumors with low and highly aggressive biological behavior.

Material and methods

Patient data and tumor specimens

Resection material from all PC patients who underwent surgery in the Thoraxklinik Heidelberg, Germany between January 1986 and December 2008 were collected. Usage of the tissue was approved by the local ethics committee (no. 206/2005). Clinical data (birth, sex, age at primary tumor surgery, location of tumor, lymph node and distant metastases, overall survival, tumor recurrence, and cause of death) were collected from the files of the Institute of Pathology, University Hospital Heidelberg, Germany and the Thoraxklinik. Complete data were available for 193 out of 200 included specimens. A reclassification of all specimens was done according to the criteria of the current WHO classification; besides the classical histomorphology, expression of cytokeratins and neuroendocrine markers are considered the diagnostic gold standard [2]. Large cell neuroendocrine carcinomas were thoroughly excluded by histomorphological analyses; this is also reflected by the low number of deaths in the final PC cohort (see below). The paraffin blocks were used for TMA construction; HE-stained full-section slides of each tumor were analyzed to select regions with high tumor cell content (>50%). A TMA machine (AlphaMetrix Biotech, Rödermark, Germany) was used to extract tandem 1 mm cylindrical core samples from each tissue donor block in regions with high, viable tumor cell content. Two core biopsies of each specimen were placed on the recipient blocks in order to address potential tumor heterogeneity, which is usually rather low in carcinoids. Immunohistochemical analyses were based on the average of both cores. Prior to tissue core extraction, immunohistochemical stains of full-slide sections for Ki-67 were performed from the same tissue block in order to determine the mean and maximum ("hot spot") proliferative rate of each tumor.

Immunohistochemistry and evaluation

Immunohistochemical staining was performed according to a standardized protocol with commercially available and well-established antibodies (Table 1). The TMA slides were deparaffinized and pretreated with an antigen-retrieval buffer (pH 6.0 or 9.0; DAKO, Hamburg, Germany). Subsequent steps were carried out in an immunostaining device (DAKO Techmate 500plus). Incubation of the primary antibody was 40 min at room temperature. The immunostaining protocol was based on the avidin–biotin peroxidase principle using AEC as the chromogen and hematoxylin for counterstaining. EGFR staining was done using the EGFR pharm Dx kit (DAKO) according to the manufacturer's instructions. For negative controls, primary antibodies were omitted. All stained TMA slides were analyzed using semiquantitative scoring systems (Table 1). Cases were excluded when the tissue was uninterpretable (e.g., no tumor cells, folded tissue cores) or when both tissue cores were lost during the staining procedure. To determine the mean PI of each case, only regions with high tumor cell content on full-slide sections were used. At least 100 tumor cells/HPF were manually counted in four different regions (4×100) by two pathologists together using a double-headed microscope. Respective percentages were calculated. For the maximum (max) PI, areas with the highest numbers of Ki-67-stained cells (hot spot) were selected.

Statistical analysis

Subgroups and grading criteria were compared using Fisher's exact and chi-square tests. For histopathological and clinical analyses, Pearson's correlation was applied. Only two-sided p values <0.05 were considered significant. Statistical analyses were performed using Excel 2003 (Microsoft, Redmond, WA, USA) and Prism 5 (GraphPad Software, LaJolla, CA, USA).

Results

Clinicopathologic parameters

Two hundred resected PC specimens could be evaluated. One hundred fourteen (57%) tumors were classified as TC, 86 (43%) as ATC. In TC, the mean number of mitoses (standard deviation) was 0.7 (±0.5; range ≤1) and in ATC 2.7 (±1.5; range 2–10), respectively. Nineteen ATC (22.1% from all ATC) displayed focal necrosis. Fifty-five out of 86 ATC presented with only two mitoses, six of these with

Table 1 Antibodies and semiquantitative immunoreactivity scores employed in this study

Antibody	Pretreatment	Dilution	Clone	Supplier	Score	Reference
Ki-67	ph 6	1:200	MIB-1	DakoCytomation, Copenhagen, Denmark	Proliferative index	Skov et al. [11]
Synaptophysin	ph 9	1:400	27 G12	Novocastra Laboratories, Newcastle upon Tyne, UK	Staining intensity×number of positive cells	Lyda et al. [36]
CD56 (NCAM)	ph 6	1:50	1B6	Novocastra	Staining intensity:	
Chromogranin	ph 9	1:5000	A0430	DakoCytomation	0=no staining	
CD57 (Leu-7)	ph 6	1:50	HNK-1	Becton Dickinson, San Jose, CA, USA	1 = low	
					2 = moderate	
CK18	ph 9	1:150	DC10	DakoCytomation	3 = high intensity	
KL-1	ph 9	1:200	1918	Immunotech, Marseille, France	Number of positive cells:	
					0 = no staining	
TTF-1	ph 9	1:100	8G7G3/1	DakoCytomation	1=1–2%	
CD99	ph 6	1:25	MIC2 12E7	DakoCytomation	2=3–20%	
CD117 (c-kit)	ph 6	1:50	A4502	DakoCytomation	3=20–50%	
EGFR	–	–	2–18 C9	DakoCytomation	4=>50%	
Her-2/neu	ph 6	1:100	C-erB-2	DakoCytomation	0—no staining or <10% of membranes	Kyoda et al. [37]
					1+—very low staining intensity of membrane; >10% of parts of membrane	
					2+—low to medium intensity >10%; circumferential staining	
					3+—high intensity staining >10%; circumferential	
ERCC-1	ph 6	1:50	8F1	ThermoScientific, Fremont, CA, USA	Staining intensity × number of positive cells	Skov et al. [11]
					Staining intensity: see above	
					Number of positive cells:	
					0=0%	
					0.1=1–<10%	
					0.5=10–<50%	
					1.0=≥50%	
SSTR	ph 6	1:500	SSTR2A	BioTrend GmBH, Köln, Germany	0 = no staining	Volante et al. [27]
					1 = pure cytoplasmic staining, focal or diffuse	
					2 = membranous reactivity in <50% tumor cells; irrespective of cytoplasmic staining	
					3 = circumferential membranous reactivity	
TS	ph 9	1:8,000	TS 106	Invitrogen, Carlsbad, CA, USA	Staining intensity × number of positive cells (in percent)	Righi et al. [38]
					Staining intensity: see above	
					Number of positive cells: 0–100%	

necrosis. The high number of ATC is likely a consequence of previously performed studies using PC tissue [4, 10], leaving sparse/no further material for this study, especially from the usually smaller TC. However, similar TC/ATC ratios were also reported in other large PC series [13, 14]. More than 50% of all PC were stage IA tumors; all stage IV tumors (n=5) were ATC. Lymph node metastases were more frequently present in TC than ATC (25.2% TC vs. 13.4% AC; p=0.0476), but distant metastases were more frequently found in ATC than in TC (13.4% vs. 1.8%; p=0.0023). At the closure of this study, 178 patients were still alive. Seven patients had died of tumor-related causes; 8 patients had died of other reasons. Patients with a tumor-related death were 6.9 years older than the average PC

patient, 5 were male, and the maximum tumor diameter was 17.6 mm larger on average. Neither age, gender, stage, tumor location nor tumor size was significantly different between TC and ATC. Clinical data of all analyzed tumors are given in Table 2.

Cytokeratins and markers for neuroendocrine differentiation are expressed in the majority of pulmonary carcinoids

To comparatively analyze all WHO-suggested diagnostic immunomarkers [2] for PC phenotyping in one large cohort, we analyzed the expression of synaptophysin, chromogranin A, CD56, CD57, CK18, KL-1, TTF-1, CD117, and CD99 in all specimens. Furthermore, we screened all PC for the expression of Her-2/neu, EGFR, ERCC-1, SSTR2A, and TS, known biomarkers for tumor-specific therapies of non-small cell lung cancer, in order to identify candidates potentially susceptible for therapeutic approaches (Figs. 1 and 2; Table 3). Almost all specimens expressed pan-cytokeratins (KL-1; 98.7%) and CK18 (98.8%), confirming the epithelial nature of the disease. The few specimens negative for the analyzed cytokeratins expressed at least one neuroendocrine marker. Among the neuroendocrine markers, synaptophysin was expressed in 97% of PC with a mean immunoreactivity score (IRS) of 11.7 in ATC and 10.9 in TC. Chromogranin A (97%), CD56 (90%), and CD57 (74%) were also frequently expressed, but staining intensities were only moderate compared to synaptophysin. CD117 immunoreactivity was more frequently detected in ATC (80%) than in TC (65.1%; $p=0.052$; borderline significant). CD99 expression was only seen in <10% of all PC. Notably, nuclear TTF-1 expression was evident in >70% of all PC (TC 73%; ATC 77%). Thus, cytokeratins and markers for neuroendocrine differentiation are highly sensitive for PC.

Fig. 1 Semiquantitative immunoreactivity scores of all analyzed diagnostic immunomarkers. *p* values are based on the correlations between positive-stained atypical (*ATC*) and typical carcinoids (*TC*) for each marker. The *y*-axis depicts positively stained specimens (in percent), the *x*-axis immunoreactive scores, ranging from 0–12 ▶

A grading approach for pulmonary carcinoids

The current classification system separates TC and ATC on the basis of mitotic count and necrosis to distinguish between more aggressive tumors and tumors with a better outcome. In contrast to other neuroendocrine neoplasms, a grading system for PC is not established yet. Thus, we aimed to analyze to which extent mitoses and/or PI of PC is associated with an aggressive phenotype (lymph node and/or distant metastases, death). In the analyzed cohort, a significant correlation was found between mitotic count and distant metastases ($p=0.0009$), between mitotic count and

Table 2 Clinicopathological features in typical and atypical carcinoids

Patient characteristics		Total ($n=193$)	TC ($n=111$)	ATC ($n=82$)
Age (years)	Mean, SD	53.8±14.4	53.0±14.6	54.9±14.3
	Range	14–82	14–80	19–82
Gender	Male	76 (39.4%)	44 (39.6%)	32 (39.0%)
	Female	117 (60.6%)	67 (60.4%)	50 (61.0%)
Stage; total $n=139$;TC $n=77$; AC $n=62$	IA	79 (56.8%)	48 (62.3%)	31 (50%)
	IB	21 (15.1%)	8 (10.3%)	13 (21%)
	IIA	24 (17.2%)	16 (20.8%)	8 (12.9%)
	IIB	2 (1.4%)	0	2 (3.2%)
	IIIA	8 (5.8%)	5 (6.4%)	3 (4.8%)
	IIIB	0	0	0
	IV	5 (3.6%)	0	5 (8.1%)
Tumor location	Right	119 (61.7%)	73 (65.8%)	46 (56.1%)
	Left	74 (38.3%)	38 (34.2%)	36 (43.9%)
	Central	38 (19.7%)	22 (19.9%)	16 (19.5%)
	Peripheral	155 (80.3%)	89 (80.1%)	66 (80.5%)
Tumor size (mm) $n=139$	Mean	28.2±19.1	25.7±18.0	30.1±17.0
	Range	2–120	2–120	4–120
Follow up (months)	Mean	73.2±66.6	70.9±64.5	76.7±69.8
	Range	0.5–253	1–253	0.5–246
Metastases	Lymph node	39 (20.2%)	28 (25.2%)	11 (13.4%)
	Distant	13 (6.7%)	2 (1.8%)	11 (13.4%)
Dead (tumor-related)		7 (3.6%)	2 (1.8%)	5 (6.1%)

Retrospective evaluation for clinicopathological features in 193 patients

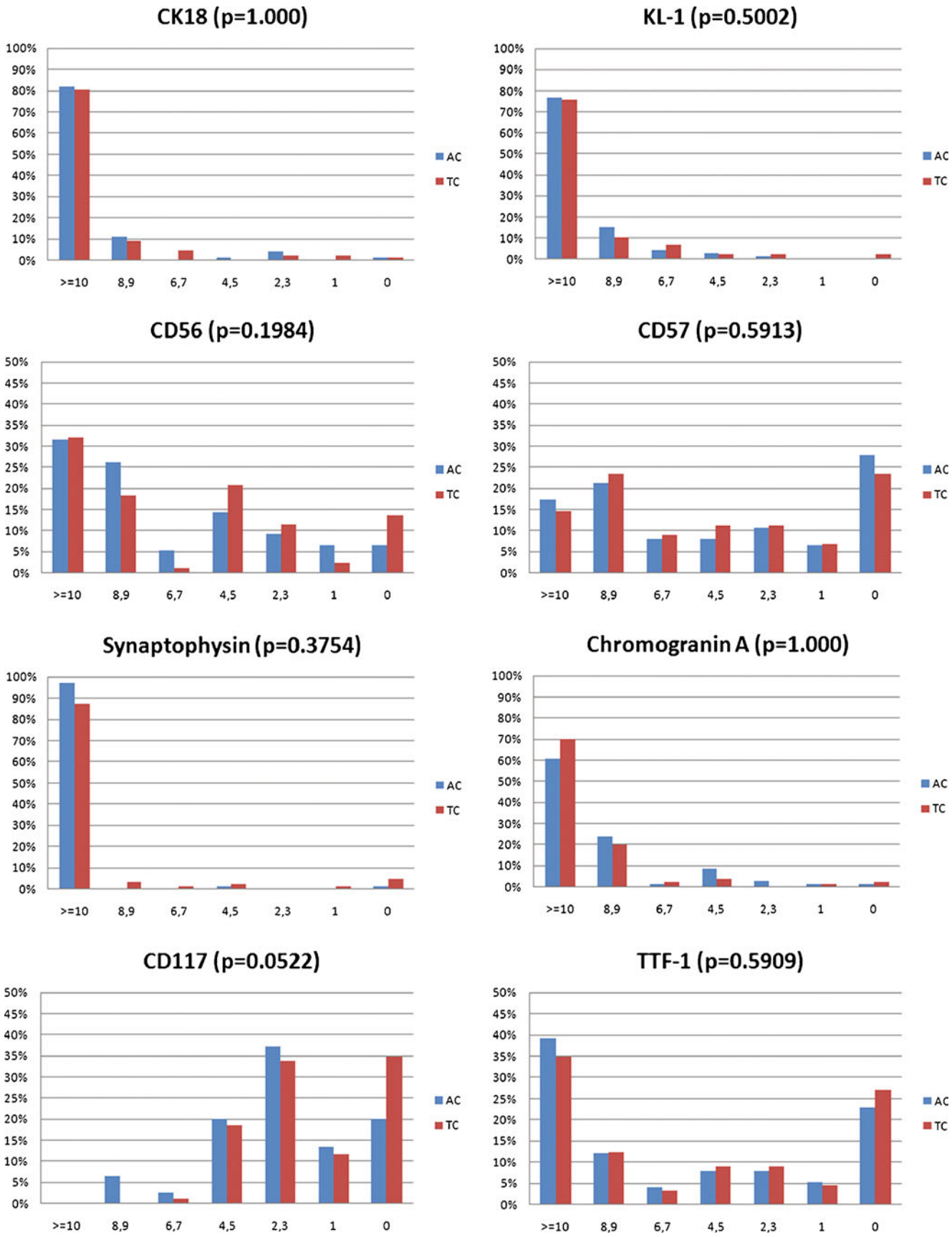
CK18 (p=1.000)
KL-1 (p=0.5002)
CD56 (p=0.1984)
CD57 (p=0.5913)
Synaptophysin (p=0.3754)
Chromogranin A (p=1.000)
CD117 (p=0.0522)
TTF-1 (p=0.5909)
AC
TC
>=10
8,9
6,7
4,5
2,3
1
0

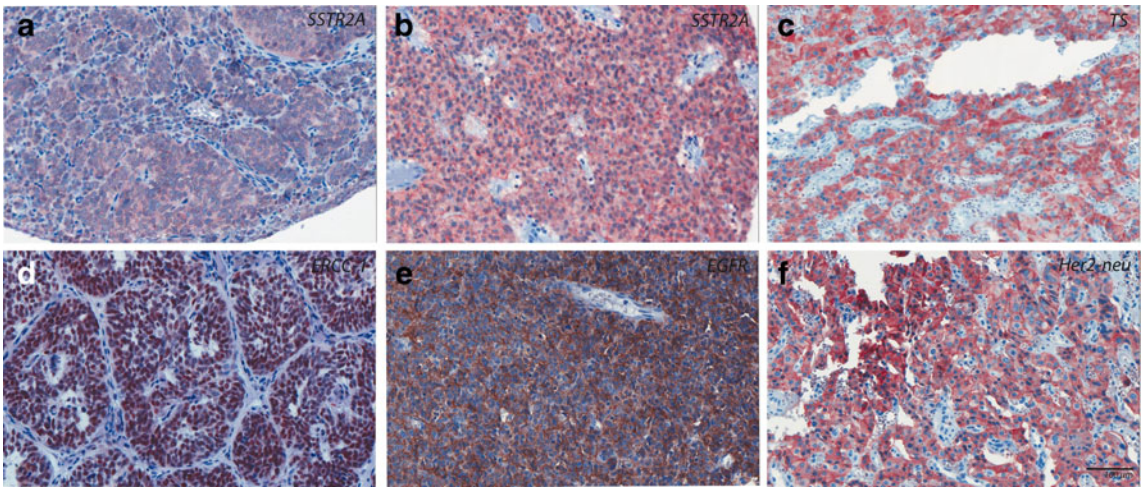

Fig. 2 Expression of putative predictive markers in typical and atypical pulmonary carcinoids. **a** Weak cytoplasmatic staining for SSTR2A without membranous reactivity, score 1, in a typical carcinoid. **b** Strong cytoplasmatic as well as membranous (including circumferential) staining in more than 50% of tumor cells, score 3, against SSTR2A in a typical carcinoid. **c** Intense cytoplasmatic and partial nuclear staining, score 270, against TS in an atypical carcinoid in almost all tumor cells. **d** Strong nuclear staining against ERCC-1 in almost all tumor cells, score 3.0, in an atypical carcinoid. **e** Strong membranous staining for EGFR in more than half of the tumor cells, score 12, in an atypical carcinoid. **f** Moderate membranous, circumferential staining in more than 10% of tumor cells, score 2+, against Her2/neu in an atypical carcinoid (all magnifications×200)

tumor stage (p=0.0467), and between mitotic count and patient death (p=0.0196), thus principally confirming the prognostic value of mitotic count. Mean PI was 1.8% (±1.7%) and max PI 2.5% (±2.5%) in TC and 3.7% (±4.8%) and 5.8% (±7.6%) in ATC, respectively. The PI of TC and ATC was statistically significantly different for both, mean and max PI (p<0.0001). Furthermore, there were significant correlations between increased PI and the following criteria (mean/max PI): large tumor size (p=0.0459/0.0212), advanced stage (stage III/IV; p=0.0131/0.0018), positive nodal status (p=0.0606/0.0319), and distant metastases (p=0.0063/0.0005).

Therefore, we tried to test for a PC-specific grading system based on both factors. We used the established grading system for gastrointestinal neuroendocrine tumors [12] and grouped all PC according to the respective criteria. Only G1 (< two mitoses per 2 mm² and/or Ki-67 index ≤2%) and G2 (2–20 mitoses per 2 mm² and Ki-67 index between 3–20%) criteria could be applied to the PC cohort because mitotic count was never higher than ten, a basic requirement

Table 3 Expression of all analyzed markers in typical (TC) and atypical (ATC) carcinoids

Marker	Interpretable cases	Positive cases	Mean scores ATC	Mean scores TC
Synapthophysin	161 (80.5%)	156 (96.9%)	11.7±1.7	10.9±3.1
Chromogranin A	151 (75.5%)	147 (97.3%)	9.7±3.3	10.3±2.6
CD56	163 (81.5%)	146 (89.6%)	6.8±4.0	6.5±4.5
CD57	164 (82%)	122 (74.4%)	4.8±4.2	4.9±4.0
CK18	160 (80%)	158 (98.8%)	10.8±2.7	10.7±2.8
KL-1	159 (79.5%)	157 (98.7%)	10.8±2.3	10.3±3.0
CD117	161 (80.5%)	116 (72.0%)	2.6±2.1	1.8±1.6
TTF-1	163 (81.5%)	122 (74.8%)	6.5±5.0	6.0±5.0
CD99	162 (81%)	10 (6.1%)	0.3±1.2	0.2±0.9
Her-2/neu	159 (79.5%)	6 (3.8%)	0.1±0.4	0.01±0.1
EGFR	161 (80.5%)	18 (11%)	0.8±2.4	0.5±1.6
ERCC-1	159 (79.5%)	68 (42.7%)	0.4±0.9	0.4±0.7
TS	166 (83%)	16 (9.6%)	11.9±45.4	2.9±12.5
SSTR2A	147 (73.5%)	119 (80.9%)	1.1±0.8	1.0±0.7

for G3 in this system. Eighty-two patients were classified as G1 and 111 as G2 tumors. When comparing G1 and G2 PC, G2 tumors were 4.5 mm larger in size, patients with G2 tumors developed 16 times more distant metastases (p=0.0007), and seven times more patients died due to tumor-related complications (p=0.2428). The presence of lymph node metastases was similar in both groups. Comparison of the grading system for gastrointestinal neuroendocrine tumors (G1/G2) to the TC/ATC classification system revealed that 72.3% more patients with G2 tumors developed lymph node metastases, 18.2% more distant metastases, and 20.0% more died, when compared to ATC. A direct comparison of the traditional TC/ATC classification and the applied grading system for gastrointestinal neuroendocrine carcinomas is given in Fig. 3.

Predictive phenotyping of pulmonary carcinoids: SSTR2A and EGFR may be used for therapeutic approaches in progressive PC

Besides challenges in the differential diagnosis and in a reliable grading of PC, advanced tumor stages may require chemotherapy. To narrow-in on respective PC phenotypes suitable for the application of more tumor-specific therapies, we performed a screening for putative useful biomarkers. More than 80% of all PC displayed SSTR2A expression (Fig. 2), a potential marker for octreotide-based diagnostic and therapeutic approaches. ERCC-1, a potentially predictive marker for platinum-based therapies in non-small cell lung cancer, was expressed in almost 50% of all specimens. EGFR and Her2/neu were only expressed in a few cases (18 and 6 cases, respectively). TS was the only marker with expression differences in the subgroups; however, significance was not reached (p=0.2929) because of the overall low number of positive cases. The positive TC specimens (6.9%) presented with an average IRS (range 0–300) from 54.2±29.9 and the positive ATC (12.6%) with an average IRS of 104.0±90.0. Two ATC demonstrated highest expression levels (265 and 285). Of note, overall positive EGFR immunoreactivity significantly correlated with a positive nodal status (p=0.0431) and distant metastases (p<0.0001) in all specimens.

Discussion

In this study, we aimed to provide comprehensive data of PC phenotyping and prognostic/predictive analyses. For the first time, we applied the grading system for gastrointestinal neuroendocrine tumors to PC. Evaluation of PI in addition to mitotic count may serve as an additional prognostic factor for PC. Furthermore, we performed a diagnostic and predictive phenotyping of PC investigating all WHO recommended diagnostic immunomarkers in a large cohort of PC as well as selected markers with a putative therapeutic relevance.

While synaptophysin, chromogranin, CD56, and cytokeratins are established routine markers [2], the most sensitive markers for PC have not been defined yet. Although most PC are well diagnosed on the basis of morphological criteria, immunostaining may be relevant in those cases where only sparse tumor material is available (i.e., diagnostic biopsies). We demonstrate that synaptophysin, chromogranin, and cytokeratins, although not specific, are highly sensitive markers for PC. Synaptophysin in combination with pan-cytokeratins is the most useful marker panel for these constellations, whereas CD57, CD99, and CD117 are of inferior diagnostic value. These results are in line with the latest Delphic Consensus Process, indicating that chromogranin A and synaptophysin are the most valuable two markers to be used in routine diagnostics [15]. Even though specificity of cytokeratins is limited, stainings may be used in critical cases in addition to synaptophysin because they were expressed in nearly all (99%) carcinoids. TTF-1 has been recommended to detect the primary site in metastatic disease in the lung [15]. Expression of TTF-1 in PC is reported with 0–80% in TC and 0–100% in ATC [16–20].

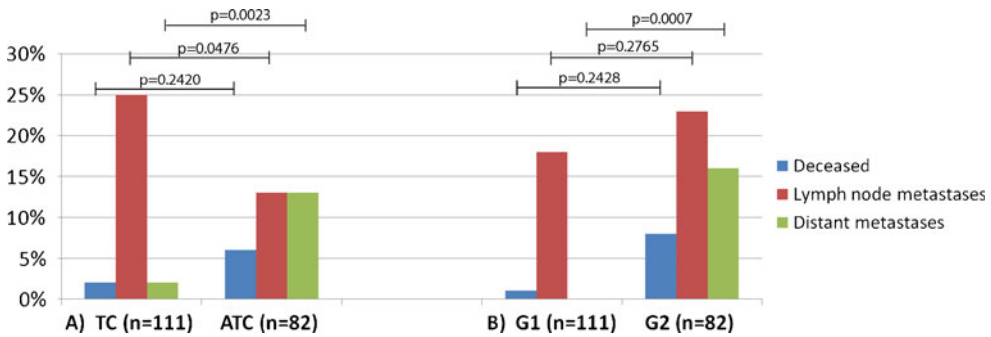

Fig. 3 Comparison of the current WHO classification system for pulmonary carcinoids (**A**) with the grading system for gastrointestinal neuroendocrine tumors (**B**). The *bar diagram* depicts the differences between the two systems, emphasizing aggressiveness of G2 tumors. *p* values demonstrate the differences between the separated groups (TC and ATC; G1 and G2) in each category associated with malignancy (lymph node metastases, distant metastases, and death), respectively

These diverging numbers may be a result of different scoring systems. Some studies applied scoring systems with a 5–10% cutoff for immunoreactive cells [18–20], which results in a lower percentage rate of positive cases compared to studies which even considered few stained cells as positive. The reported differences of TTF-1 positivity in PC could also be attributed to different staining protocols, antibody concentrations, and the selection of cases. In our series, TC and ATC were tested positive for TTF-1 in 73% and 77%, respectively, with an established antibody clone frequently tested in round robin tests (www.nordicq.org). However, since TTF-1 is also expressed in other neuroendocrine neoplasms [16], it is no strong argument for a primary pulmonary neoplasm in the differential diagnosis of primary PC and metastases of morphologically similar neuroendocrine neoplasms. The herein presented comprehensive diagnostic marker assessment may be helpful for the differential diagnostic setting.

Besides diagnostic histomorphological and immunohistochemical PC phenotyping, a reliable subtyping of PC is of utmost importance in order to select tumors with a high risk of metastases and an aggressive biological behavior. Skov et al. [11] recently discussed the diagnostic and prognostic value of Ki-67 count and suggested PI inclusion into the histopathological definition of neuroendocrine tumors in general. In our study, compared to mitotic count, PI showed a more significant correlation with advanced tumor stage and distant metastases, and additionally, PI correlated significantly with a larger tumor size and a positive nodal status. However, mitotic count better predicted patient death. With the applied grading system, patients with G1 tumors developed lymph node metastases in 18% and none developed distant metastases; 1% in this group died. In G2 tumors 23% developed lymph node and 16% distant metastases and 8% of the patients died of tumor-related causes. Based on p values (Fig. 3), compared to the TC/ATC classification, differences between lymph node metastases were more distinct and patients with G2 tumors developed significantly more distant metastases compared to those with G1 tumors. Thus, an additional criterion like PI may be helpful to more precisely separate tumors with an aggressive biological behavior. Although already state of the art in routine diagnostics [12, 21], problems with reproducibility of Ki-67 evaluation have been described over the past years [15, 22]. Different staining protocols and varying methods of interpretation of Ki-67 count have led to high interlaboratory variability [22, 23]. To reduce this center-to-center variability, reference standards for Ki-67 staining and evaluation still need to be established. Interpretation methods range from estimating the number of positive cells by "eyeballing" over different counting techniques to computer-assisted automated analysis [23]. In contrast to eyeballing, manual counting in hot spot regions yields lower interobserver variability. Further, it is more precise than automated analysis, which tends to overestimate Ki-67 count due to proliferating lymphoid cells [23, 24]. As outlined by Hsu and colleagues [2], application of standardized reagents, retrieval methods, and detection systems in combination with standardized analysis render Ki-67 as an important and reliable factor in the prognostic setting of many tumors including pulmonary carcinoids. Moreover, the cutoff criteria which best separate low-grade specimens from moderate- or high-grade specimens will have to be validated in further studies of large PC cohorts.

Advanced, non-resectable, or metastasized PC specimens may require chemotherapy. No clear guidelines have been set for chemotherapy regimens in PC so far. Commonly used agents including interferon-α, platinum- or etoposid-based agents, streptozotocin, and 5-fluorouracil have partially been successful [25]. Whereas targeted therapies are becoming the standard for non-small cell lung cancer, only limited information on the usefulness of clinically well-established therapeutic targets and predictive biomarkers for PC is available so far. Few small studies have investigated the expression of SSTR2A [26, 27] and known biomarkers for pulmonary neoplasms like EGFR [28], Her-2/neu [29], ERCC-1 [11], and TS [30] in PC. Somatostatin receptors are increasingly used as targets for both diagnostic procedures and targeted treatment strategies and have been described as putative predictive markers for octreotide-based therapies [31]. The diagnostic and therapeutic effect depends on the level of individual receptor subtype expression [32]. Somatostatin analogues, synthetic somatostatin octapeptide derivates like octreotide and lanreotide, as well as ^{111}In-labeled somatostatin analogues (scintigraphy) and ^{68}Ga-DOTATOC (PET), preferably bind to SSTR2 [33, 34], which was expressed in >80% of all specimens in this study. Volante et al. [27] reported positive immunoreactivity in 76% (n=17) and Righi et al. [26] in 34% TC (n=41), 70% TC with metastases (n=27), and 51% ATC (n=73). They concluded that SSTR2A status correlates with metastatic propensity in PCs. In this cohort, there was no correlation of SSTR2A expression with either lymph node or distant metastases. However, it may be worth to validate the therapeutic value of SSTR2A expression for octreotide-based therapies for PC. Our data indicate that the majority of PC may be susceptible for SSTR-based scintigraphy, a helpful diagnostic and follow-up tool for early and specific detection of tumor recurrence.

Only few PC specimens expressed EGFR and Her-2/neu. EGFR expression was higher in patients with advanced disease, a positive nodal status, and distant metastases. Further studies are required to determine if PC patients may benefit from tyrosine kinase inhibition in non-resectable constellations. ERCC-1 expression was preferentially detected in PC with distant metastases and increased proliferative activity, which is likely a consequence of its

main functions in DNA repair. Therefore, platinum-based chemotherapies [25] may represent an option for tumors in advanced stages without overexpression of ERCC-1. Other chemotherapy regimens, partially effective in PC, include 5-fluorouracil (5-FU), which functions in the inhibition of TS [30, 35]. In neuroendocrine tumors, increased TS expression levels (especially in the highest tertile) have been associated with decreased response rates to 5-FU treatment, making TS a potential predictive marker in the selection of patients susceptible for therapy. Notably, overall TS expression was higher in ATC than in TC but only two ATC presented with TS expression levels in the highest tertile. Positive TC specimens only showed low to medium staining intensities.

In conclusion, we demonstrate that pan-cytokeratin and neuroendocrine markers are useful diagnostic panels with a high sensitivity for PC. In addition to PC phenotyping, prognostic assessment based on mitotic count and proliferative index allows an optimized prediction of the biological behavior of PC and thus the patients' outcome compared to the classification into TC and ATC. The findings of this study should be validated in other large series of PC.

Acknowledgments We gratefully acknowledge Ms Bettina Walter (tissue bank of the National Center for Tumor Diseases Heidelberg) and Jennifer Schmitt for excellent technical support.

Conflict of interest The authors declare that they have no conflict of interest.

References

1. Jemal A, Siegel R, Xu J, Ward E (2010) Cancer statistics, 2010. CA Cancer J Clin 60(5):277–300. doi:10.3322/caac.20073
2. Travis WD (ed) (2004) WHO classification of tumours: pathology and genetics of tumours of the lung, pleura, thymus and heart, 1st edn. IARC, Lyon
3. Rekhtman N (2010) Neuroendocrine tumors of the lung: an update. Arch Pathol Lab Med 134(11):1628–1638. doi:10.1043/2009-0583-RAR.1
4. Warth A, Herpel E, Krysa S, Hoffmann H, Schnabel PA, Schirmacher P, Mechtersheimer G, Blaker H (2009) Chromosomal instability is more frequent in metastasized than in non-metastasized pulmonary carcinoids but is not a reliable predictor of metastatic potential. Exp Mol Med 41(5):349–353. doi:10.3858/emm.2009.41.5.039
5. Ducrocq X, Thomas P, Massard G, Barsotti P, Giudicelli R, Fuentes P, Wihlm JM (1998) Operative risk and prognostic factors of typical bronchial carcinoid tumors. Ann Thorac Surg 65 (5):1410–1414. doi:S0003497598000836
6. Warren WH, Gould VE, Faber LP, Kittle CF, Memoli VA (1985) Neuroendocrine neoplasms of the bronchopulmonary tract. A classification of the spectrum of carcinoid to small cell carcinoma and intervening variants. J Thorac Cardiovasc Surg 89(6):819–825
7. Fink G, Krelbaum T, Yellin A, Bendayan D, Saute M, Glazer M, Kramer MR (2001) Pulmonary carcinoid: presentation, diagnosis, and outcome in 142 cases in Israel and review of 640 cases from the literature. Chest 119(6):1647–1651
8. Travis WD (2010) Advances in neuroendocrine lung tumors. Ann Oncol 21(Suppl 7):vii65–vii71. doi:10.1093/annonc/mdq380
9. Hage R, de la Riviere AB, Seldenrijk CA, van den Bosch JM (2003) Update in pulmonary carcinoid tumors: a review article. Ann Surg Oncol 10(6):697–704
10. Warth A, Krysa S, Zahel T, Hoffmann H, Schirmacher P, Schnabel PA, Herpel E (2010) S100 protein positive sustentacular cells in pulmonary carcinoids and thoracic paragangliomas: differential diagnostic and prognostic evaluation. Pathologe 31(5):379–384. doi:10.1007/s00292-010-1293-2
11. Skov BG, Holm B, Erreboe A, Skov T, Mellemgaard A (2010) ERCC1 and Ki67 in small cell lung carcinoma and other neuroendocrine tumors of the lung: distribution and impact on survival. J Thorac Oncol 5(4):453–459. doi:10.1097/JTO.0b013e3181ca063b
12. Rindi G, Kloppel G, Alhman H, Caplin M, Couvelard A, de Herder WW, Erikssson B, Falchetti A, Falconi M, Komminoth P, Korner M, Lopes JM, McNicol AM, Nilsson O, Perren A, Scarpa A, Scoazec JY, Wiedenmann B (2006) TNM staging of foregut (neuro)endocrine tumors: a consensus proposal including a grading system. Virchows Arch 449(4):395–401. doi:10.1007/s00428-006-0250-1
13. Travis WD, Rush W, Flieder DB, Falk R, Fleming MV, Gal AA, Koss MN (1998) Survival analysis of 200 pulmonary neuroendocrine tumors with clarification of criteria for atypical carcinoid and its separation from typical carcinoid. Am J Surg Pathol 22(8):934–944
14. Skuladottir H, Hirsch FR, Hansen HH, Olsen JH (2002) Pulmonary neuroendocrine tumors: incidence and prognosis of histological subtypes. A population-based study in Denmark. Lung Cancer 37(2):127–135
15. Klimstra DS, Modlin IR, Adsay NV, Chetty R, Deshpande V, Gonen M, Jensen RT, Kidd M, Kulke MH, Lloyd RV, Moran C, Moss SF, Oberg K, O'Toole D, Rindi G, Robert ME, Suster S, Tang LH, Tzen CY, Washington MK, Wiedenmann B, Yao J (2010) Pathology reporting of neuroendocrine tumors: application of the Delphic consensus process to the development of a minimum pathology data set. Am J Surg Pathol 34(3):300–313. doi:10.1097/PAS.0b013e3181ce1447
16. Oliveira AM, Tazelaar HD, Myers JL, Erickson LA, Lloyd RV (2001) Thyroid transcription factor-1 distinguishes metastatic pulmonary from well-differentiated neuroendocrine tumors of other sites. Am J Surg Pathol 25(6):815–819
17. Folpe AL, Gown AM, Lamps LW, Garcia R, Dail DH, Zarbo RJ, Schmidt RA (1999) Thyroid transcription factor-1: immunohistochemical evaluation in pulmonary neuroendocrine tumors. Mod Pathol 12(1):5–8
18. Sturm N, Rossi G, Lantuejoul S, Papotti M, Frachon S, Claraz C, Brichon PY, Brambilla C, Brambilla E (2002) Expression of thyroid transcription factor-1 in the spectrum of neuroendocrine cell lung proliferations with special interest in carcinoids. Hum Pathol 33(2):175–182
19. Du EZ, Goldstraw P, Zacharias J, Tiffet O, Craig PJ, Nicholson AG, Weidner N, Yi ES (2004) TTF-1 expression is specific for lung primary in typical and atypical carcinoids: TTF-1-positive carcinoids are predominantly in peripheral location. Hum Pathol 35(7):825–831
20. La Rosa S, Chiaravalli AM, Placidi C, Papanikolaou N, Cerati M, Capella C (2010) TTF1 expression in normal lung neuroendocrine cells and related tumors: immunohistochemical study comparing two different monoclonal antibodies. Virchows Arch 457(4):497–507. doi:10.1007/s00428-010-0954-0
21. Rindi G, Kloppel G, Couvelard A, Komminoth P, Korner M, Lopes JM, McNicol AM, Nilsson O, Perren A, Scarpa A, Scoazec JY, Wiedenmann B (2007) TNM staging of midgut and hindgut (neuro) endocrine tumors: a consensus proposal including a grading system. Virchows Arch 451(4):757–762. doi:10.1007/s00428-007-0452-1
22. Mengel M, von Wasielewski R, Wiese B, Rudiger T, Muller-Hermelink HK, Kreipe H (2002) Inter-laboratory and inter-observer reproducibility of immunohistochemical assessment of

the Ki-67 labelling index in a large multi-centre trial. J Pathol 198 (3):292–299. doi:10.1002/path.1218
23. Hsu CY, Ho DM, Yang CF, Chiang H (2003) Interobserver reproducibility of MIB-1 labeling index in astrocytic tumors using different counting methods. Mod Pathol 16(9):951–957. doi:10.1097/01.MP.0000084631.64279.BC
24. Dhall D (2009) Interobserver variability in assessing Ki67 proliferative index in gastrointestinal well-differentiated neuroendocrine neoplasms. Mod Pathol 22:116A
25. Kosmidis PA (2004) Treatment of carcinoid of the lung. Curr Opin Oncol 16(2):146–149
26. Righi L, Volante M, Tavaglione V, Bille A, Daniele L, Angusti T, Inzani F, Pelosi G, Rindi G, Papotti M (2010) Somatostatin receptor tissue distribution in lung neuroendocrine tumours: a clinicopathologic and immunohistochemical study of 218 'clinically aggressive' cases. Ann Oncol 21(3):548–555. doi:10.1093/annonc/mdp334
27. Volante M, Brizzi MP, Faggiano A, La Rosa S, Rapa I, Ferrero A, Mansueto G, Righi L, Garancini S, Capella C, De Rosa G, Dogliotti L, Colao A, Papotti M (2007) Somatostatin receptor type 2A immunohistochemistry in neuroendocrine tumors: a proposal of scoring system correlated with somatostatin receptor scintigraphy. Mod Pathol 20(11):1172–1182. doi:10.1038/modpathol.3800954
28. Rusch VW, Klimstra DS, Venkatraman ES (1996) Molecular markers help characterize neuroendocrine lung tumors. Ann Thorac Surg 62(3):798–809, discussion 809-710
29. Rickman OB, Vohra PK, Sanyal B, Vrana JA, Aubry MC, Wigle DA, Thomas CF Jr (2009) Analysis of ErbB receptors in pulmonary carcinoid tumors. Clin Cancer Res 15(10):3315–3324. doi:10.1158/1078-0432.CCR-08-2549
30. Ceppi P, Volante M, Ferrero A, Righi L, Rapa I, Rosas R, Berruti A, Dogliotti L, Scagliotti GV, Papotti M (2008) Thymidylate synthase expression in gastroenteropancreatic and pulmonary neuroendocrine tumors. Clin Cancer Res 14(4):1059–1064. doi:10.1158/1078-0432.CCR-07-1513
31. Oberg K, Norheim I, Theodorsson E (1991) Treatment of malignant midgut carcinoid tumours with a long-acting somatostatin analogue octreotide. Acta Oncol 30(4):503–507
32. Divisi D, Crisci R (2005) Carcinoid tumors of the lung and multimodal therapy. Thorac Cardiovasc Surg 53(3):168–172. doi:10.1055/s-2005-837539
33. Nilsson O, Kolby L, Wangberg B, Wigander A, Billig H, William-Olsson L, Fjalling M, Forssell-Aronsson E, Ahlman H (1998) Comparative studies on the expression of somatostatin receptor subtypes, outcome of octreotide scintigraphy and response to octreotide treatment in patients with carcinoid tumours. Br J Cancer 77(4):632–637
34. Haug AR, Auernhammer CJ, Wangler B, Schmidt GP, Uebleis C, Goke B, Cumming P, Bartenstein P, Tiling R, Hacker M (2010) 68Ga-DOTATATE PET/CT for the early prediction of response to somatostatin receptor-mediated radionuclide therapy in patients with well-differentiated neuroendocrine tumors. J Nucl Med 51 (9):1349–1356. doi:10.2967/jnumed.110.075002
35. Bajetta E, Catena L, Procopio G, De Dosso S, Bichisao E, Ferrari L, Martinetti A, Platania M, Verzoni E, Formisano B, Bajetta R (2007) Are capecitabine and oxaliplatin (XELOX) suitable treatments for progressing low-grade and high-grade neuroendocrine tumours? Cancer Chemother Pharmacol 59(5):637–642. doi:10.1007/s00280-006-0306-6
36. Lyda MH, Weiss LM (2000) Immunoreactivity for epithelial and neuroendocrine antibodies are useful in the differential diagnosis of lung carcinomas. Hum Pathol 31(8):980–987. doi:10.1053/hupa.2000.9076
37. Kyoda S, Kinoshita S, Takeyama H, Uchida K, Morikawa T (2008) HER-2 protein overexpression in metastatic breast carcinoma found at autopsy. Jpn J Clin Oncol 38(11):743–747. doi:10.1093/jjco/hyn103
38. Righi L, Papotti MG, Ceppi P, Bille A, Bacillo E, Molinaro L, Ruffini E, Scagliotti GV, Selvaggi G (2010) Thymidylate synthase but not excision repair cross-complementation group 1 tumor expression predicts outcome in patients with malignant pleural mesothelioma treated with pemetrexed-based chemotherapy. J Clin Oncol 28(9):1534–1539. doi:10.1200/JCO.2009.25.9275

Virchows Arch (2012) 460:309–318
DOI 10.1007/s00428-011-1173-z

ORIGINAL ARTICLE

Sudden cardiac death caused by coronary vasculitis

Katsuya Norita · Sofia V. de Noronha · Mary N. Sheppard

Received: 18 August 2011 / Revised: 25 October 2011 / Accepted: 8 November 2011 / Published online: 4 February 2012
© Springer-Verlag 2012

Abstract Coronary vasculitis is a rare and diagnostically challenging cause of sudden cardiac death (SCD). There are currently no large-scale series on this rare entity. A retrospective non-case–control observational study of SCD with coronary vasculitis referred to a tertiary cardiac pathology referral centre at the National Heart and Lung Institute at the Royal Brompton Hospital between 1996 and 2010 was completed. Ten cases of SCD with coronary artery vasculitis were retrieved from a database of 1,980 SCD cases (0.5%) with a 1:1 male/female ratio; median age was 39 years and range 15–71 years. Six deaths occurred in hospital following symptoms or cardiac arrest in the community; the remaining died at rest at home (n=4). Appearances ranged from aneurysms of the coronary artery to occlusive lesions mimicking atheroma or masses imitating tumour. Types of vasculitis detected were: eosinophilic (n=5), two associated with Churg–Strauss syndrome; lymphoplasmacytic vasculitis (n=4); and idiopathic giant cell arteritis (n=1). This study shows coronary vasculitis as a rare cause of SCD with a variable macroscopic and microscopic presentation that pathologists need to be aware of.

Keywords Coronary artery disease · Churg Strauss · Sudden cardiac death · Vasculitis

This study was carried out with ethical approval from Brompton, Harefield and National Heart and Lung Institute REC: 07/Q0404/9.

K. Norita
Imperial College London,
London, UK

S. V. de Noronha · M. N. Sheppard
CRY Centre for Cardiac Pathology, Imperial College London,
London, UK

M. N. Sheppard (✉)
CRY Centre for Cardiac Pathology,
Department of Histopathology,
Royal Brompton and Harefield NHS Foundation Trust Hospital,
Sydney Street,
London SW3 6NP, UK
e-mail: m.sheppard@rbht.nhs.uk

Introduction

Cardiovascular disease remains the single most common cause of natural death in developed nations with an incidence of 1 in 1,000 [1]. The majority of adult sudden cardiac death (SCD) is attributed to atherosclerotic coronary artery disease with predominance in older people [2]. Non-atherosclerotic coronary causes of sudden death are far less common and include coronary vasculitis often reported as case studies. The most recent review on coronary vasculitis, dating from 1987, cited infections, associations with Takayasu's arteritis (TA), Kawasaki disease (KD) in children, collagen vascular disease, hypersensitivity arteritis, Churg–Strauss syndrome (CSS) and Wegener's granulomatosis as the most common forms of vasculitis affecting the coronary arteries [3].

Most reported cases of coronary vasculitis are of TA [4] and KD in children [5, 6]. Coronary vasculitis can occur as an isolated entity or as a manifestation of systemic diseases such as CSS [7], systemic lupus erythematosus (SLE) [8], rheumatoid arthritis (RA) [9], ankylosing spondylitis [10, 11] or Behçet's disease [12]. Eosinophilic and lymphoplasmacytic vasculitis are commonly associated with RA or SLE. Neutrophilic inflammatory infiltrate can be associated with Wegener's granulomatosis [13] and giant cell arteritis (GCA) can occur as part of systemic disease involving the temporal artery [14].

There are currently no large-scale series of SCD associated with isolated coronary vasculitis. We present 10 such cases retrieved over a period of 15 years from our database of 1,980 hearts. We aim to investigate the demographics, any relevant medical history and the cardiac pathology involved.

Methods

Between January 1995 and 2010, 10 with vasculitis out of a total 1,980 cases of SCD were referred to our tertiary referral cardiac pathology centre and the Royal Brompton Hospital. The database includes cases aged 1–95 years.

Pathological analysis of all hearts was performed by MNS with the consent of the coroner and the family of the deceased. The majority of referrals were histological slides (n=8), and macroscopic examination of the heart was performed in two cases. Slides for microscopic examination were stained with haematoxylin and eosin stain for identification of inflammatory infiltrate, and elastic Van Gieson stain was used to visualise elastin fibres and myocardial fibrosis.

The age, sex, circumstances of death and past medical history were obtained for each patient from the referring pathologist and/or coroner. Due to the sudden and unexpected nature of the deaths, all patients underwent a toxicology screen in accordance with the coroner's mandate.

We defined SCD as an unexpected death occurring generally within 1–24 h of onset of symptoms [15]. Coronary vasculitis refers to vasculitis found in the coronary vessels and not noted in vessels in other parts of the body by the referring pathologist.

Results

Table 1 lists 10 cases of SCD with coronary vasculitis. An equal distribution by gender was found, with a mean age of 40.7±18.3, range 15–71 years. Over half of the deaths occurred in a hospital following symptoms or cardiac arrest in the community (n=6), the remaining died at rest, at home (n=4).

History

The five eosinophilic cases included a history of asthma with either peripheral eosinophilia and chest infections or nasal polyectomy (n=2), peripheral eosinophilia alone (n=1), or no relevant medical history (n=2). The lymphoplasmacytic cases had history of elevated erythrocyte sedimentation rate, IgGλ paraproteinaemia with finding of an inflammatory pseudotumour in the kidney at autopsy (n=1), syncope (n=1), obesity (n=1) or chest pain (n=1). The giant cell case had no relevant history other than shortness of breath (n=1). None had a diagnosis of vasculitis prior to their sudden death (Table 1).

Macroscopic findings

The whole heart and ascending aorta were available for examination by MNS in only two cases (cases 7 and 10). Slides were available from the coronaries and underlying myocardium in the remaining cases, and sampling of the aorta was only available in three of these cases (see Table 1). The temporal artery was not sampled at autopsy in any of the cases.

Two of the eosinophilic vasculitis cases had aneurysmal dilatation of the proximal epicardial coronary arteries, the largest size being 3 cm with thrombus (Fig. 1) with diffuse thickening elsewhere throughout the epicardial vessels. The other three eosinophilic vasculitis cases showed significant thickening and narrowing of the epicardial coronary arteries but no dilatation or thrombosis. Samples of a lung lymph node, spleen and bone marrow were available in two out of the five eosinophilic cases (cases 1 and 5, Table 1).

Among the lymphoplasmacytic cases (cases 6–9, Table 1), all had diffuse narrowing of the epicardial vessels. Case 6 also showed thrombosis in all three epicardial vessels. Additionally a white elastic firm mass extended along the coronary arteries in two cases (7 and 8) including the carotids (case 7) (Fig. 2a). There was also aortic thickening. Upon sectioning, the coronary arteries appeared to be almost completely occluded by this mass (Fig. 2b). No samples of tissue or blood vessels were available from the rest of the body in each case.

The giant cell vasculitis case (case 10) had diffuse narrowing of the coronaries with thickening of the ascending aorta. No samples of tissue or blood vessels were available from the rest of the body in this case.

Microscopic findings

The coronary vasculitides were characterised as eosinophilic vasculitis (n=5), lymphoplasmacytic vasculitis (n=4) and giant cell vasculitis (n=1).

Eosinophilic

All of the five eosinophilic vasculitis cases (cases 1–5) showed variation in vessel and myocardial involvement. Eosinophils were predominantly present in the intima and adventitia of the epicardial vessels with marked intimal thickening and narrowing. There were very few eosinophils in the media which was spared along with the internal and

Table 1 Summary of results

Case no.	Sex	Age	Medical history	Sampled organs/ vessels	Macroscopic features (CA ad aorta)	Macroscopic features (heart)	Vessels involved	Myocardial findings	Aorta	Other organs	Type of vasculitis
1	F	40	Retrosternal pain, ECG ectopics, eosoniphilia	Coronary arteries, myocardium, LV, lung, bone marrow, spleen	Aneurysmal dilatation of proximal RCA and LCA with thrombosis	Unknown	LCA, RCA	Focal collections of eosinophils, diffuse fibrosis of LV	Unknown	Eosinophils in lungs, bone marrow, spleen	Eosinophilic vasculitis
2	M	44	IgA nephropathy, hypertension, chest pain	Coronary arteries only	Severe narrowing RCA distally and LAD proximally	LVH (528 g)	RCA, LCA	Unknown	Unknown	Unknown	Eosinophilic vasculitis
3	F	37	Chest pain, no previous disease	Coronary arteries, myocardium	Pinhole narrowing of LAD	Scarring in LV	LAD	Fibrous scar in anterior wall of LV	Unknown	Unknown	Eosinophilic vasculitis
4	M	50	Asthma, chest infection, eosoniphilia	Coronary arteries, myocardium	Aneurysmal dilatation of LMS and LAD	Heavy and dilated (700 g)	LMS, LAD	Left ventricular subendocardial fibrosis with eosinophils	Unknown	Unknown	Eosinophilic vasculitis, Churg–Strauss syndrome
5	M	31	Asthma, nasal polyectomy	Coronary arteries, myocardium, LV, lung, liver, kidney, brain	Narrowing of all coronary arteries	Scarring in LV (425 g)	LCA, CX, RCA	Marked subendocardial fibrosis; few eosinophils	Unknown	Lungs: granulomatous inflammation, asthmatic changes; granulomas in lymph node	Eosinophilic vasculitis, Churg–Strauss syndrome
6	M	71	High ESR and IgG lambda paraproteinaemia	Coronary arteries, myocardium, lymph nodes, kidney	Narrowing with thrombosis in all coronary arteries	Unknown	LCA, CX, RCA	Acute infarction	Unknown	Inflammation in kidney	Lymphoplasmacytic vasculitis
7	F	15	Syncope	Coronary arteries, myocardium, LV and RV, aorta, carotid vessels	Coronary arteries and aortic arch unusually firm with tumour-like masses expanding along the course of the epicardial vessels, significant narrowing	Scarring in LV (289.35 g)	LAD, CX, RCA, aortic arch	Inflammation into underlying myocardium, myocardial fibrosis, healing granulation tissue in anterior LV	Lymphoplasmacytic infiltrate in intima and adventitia	Unknown	Lymphoplasmacytic vasculitis (IgG4 vasculitis?)
8	M	28	BMI 30.3 (obese)	Coronary arteries, myocardium, LV, aorta	Thick rim of fibrous tissue around LAD, fibrous tissue around aortic wall	Normal (343 g)	LCA, RCA, aorta	Infiltrate extends slightly into smaller intramural vessels, LV fibrosis	Lymphoplasmacytic infiltrate adventitia and media	Unknown	Lymphoplasmacytic vasculitis (IgG4 vasculitis?)
9	F	68	Hypertension, abnormal ECG and recurrent symptoms chest pain, 10 months	Coronary arteries, mycardium	Extensive concentric thickening of left coronary artery with narrowing	LVH, LV infarction (508 g)	LCA, RCA	Areas of old and new infarction in LV	Unknown	Unknown	Lymphoplasmacytic vasculitis
10	F	23	Shortness of breath	Coronary arteries, myocardium, aorta	Fibrosis around coronary ostia extending around aorta,markedly thickened intima of proximal coronary arteries	Normal (285 g)	LCA, RCA	Dense fibrosis	Lymphoplasmacytic infiltrate giant cells	Unknown	Idiopathic giant cell arteritis

CA coronary artery, *CX* circumflex, *ESR* erythrocyte sedimentation rate, *LAD* left anterior descending, *LCA* left coronary artery, *LMS* left main stem, *LV* left ventricle, *LVH* left ventricular hypertrophy, *RCA* right coronary artery, *RV* right ventricle

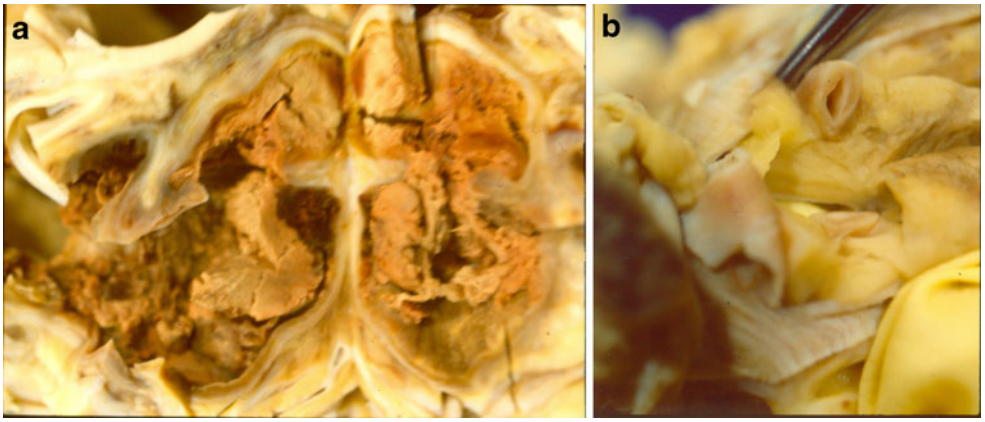

Fig. 1 **a**. Aneurysm of the left main coronary artery measuring 3 cm in diameter, in which there is a thickened wall. The lumen is full of thrombus which is occluding the vessel, resulting in sudden death. **b**. A distal left anterior descending coronary artery showing diffuse thickening of the wall

external elastic laminae (Fig. 3). There were skip lesions where parts of the vessel wall were not as affected or even normal with no evidence of blood clot or medial dissection in these areas of the coronary vessel wall. In cases 2 and 3, the adventitial inflammation was much more prominent with eosinophilic abscesses noted (Fig. 4). There were also areas of eosinophilic and granulomatous inflammation with epithelioid and small giant cells within the media of the vessels with focal necrosis in both of the cases (Fig. 5).

The eosinophils extended out into the peri- or epicardial fat and also focally into the underlying myocardium in three cases (cases 1, 4 and 5) as an interstitial infiltrate extending throughout the wall but lessening towards the subendocardium. Associated with this was fibrosis in the left ventricle throughout the wall in cases 1 and 3 and subendocardial in cases 4 and 5. In case 5 there was focal eosinophilic vasculitis of smaller intramural muscular coronary arteries. However no granulomas or abscesses were seen in the intramural coronary vessels. The smaller coronaries show eosinophils around the vessels but do not show a significant vasculitis or capillaritis. The fibrosis in the ventricle could be due to vasculitis with vessel narrowing or be a direct effect from the eosinophils within the myocardium. There was no evidence of dissection or blood clot in the media of the coronary arteries and all vessels showed involvement of all three layers not just the adventitia which one would expect with dissection.

Vasculitis was not detected in samples of lung, lymph node, spleen and bone marrow in two out of five eosinophilic cases. Case 1 showed excess eosinophils in the interstitium of the lung, spleen and bone marrow. Case 5 had severe asthmatic changes in the major airways with focal eosinophilic pneumonia within the alveoli. Well-defined granulomas were identified around the blood vessels but not in the airways. These granulomas consisted of multinucleate giant cells with epithelioid cells but no eosinophils. Granulomas were also detected within intrapulmonary lymph nodes. Eosinophilic abscesses were absent in the lungs. Sections of the aorta were not available for examination in all five cases.

Lymphoplasmacytic

Lymphoplasmacytic infiltration was present in all three layers of the coronary arterial wall. There was a circumferential

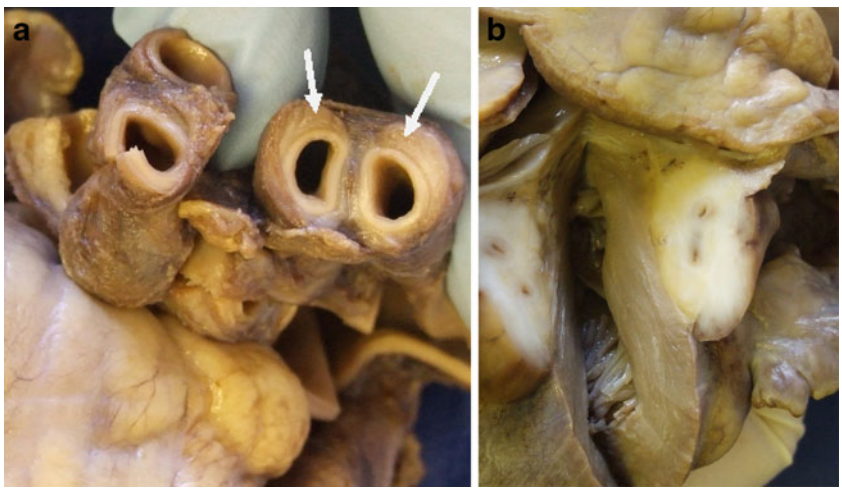

Fig. 2 **a**. Head and neck vessels show diffuse thickening of the vessel wall with pale areas of firm tissue in the adventitia and extending around the vessels (*arrows*). **b.** Narrowing of the right coronary artery and vein with diffuse pale firm thickening around the vessels mimicking a mass. Note infiltration of the underlying myocardium

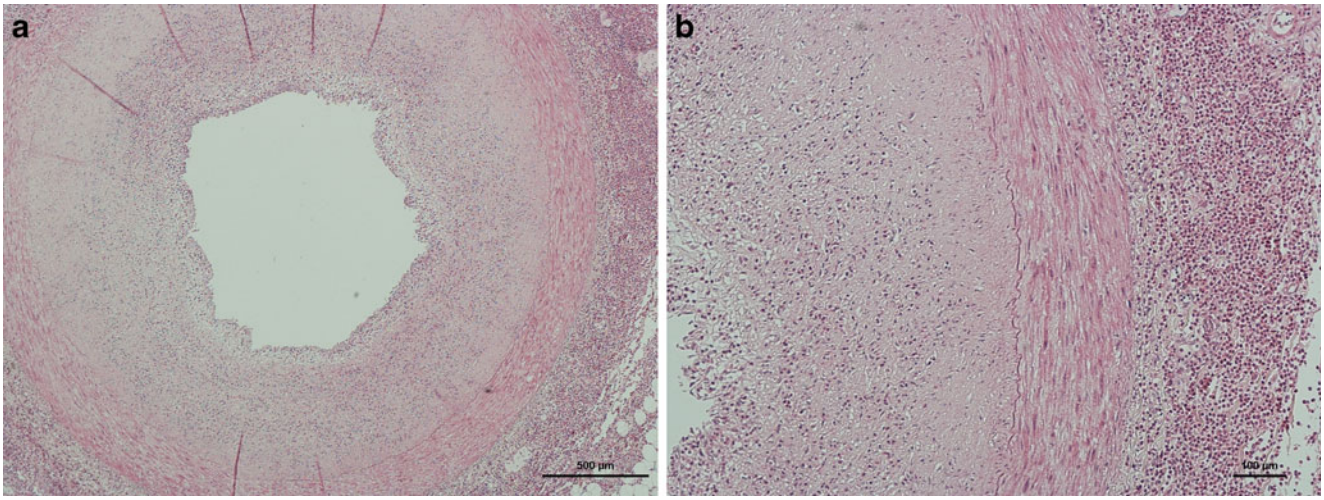

Fig. 3 Eosinophils present mainly in the adventitia of the epicardial vessels and also in the intima. Note the media is spared

expansion of both the coronary and carotid artery adventitia by fibrous tissue, with compression of the media and almost complete obliteration of the arterial lumen. Inflammation extended to the epicardial fat (Fig. 6). The cells were mainly lymphocytes admixed with smaller numbers of plasma cells. There was focal destruction of the internal and external elastic laminae with extensive fibrosis admixed with the inflammatory cells in the adventitia of the coronary arteries of all cases forming a mass around the vessel (Fig. 7). In case 6 there was an occlusive thrombus within the lumen of the epicardial coronary artery. No atheroma was noted in any of the vessels. Cases 7 and 8 had involvement of the aortic outer media and adventitia by the chronic inflammation with lymphocytes and plasma cells along the vasa vasorum of the media in keeping with lymphoplasmacytic aortitis.

The lymphoplasmacytic inflammation extended slightly into the underlying myocardium in cases 7 and 8 but did not go beyond the outer epicardium and followed intramural vessels in case 8. There was no intramural coronary artery vasculitis. Acute and chronic myocardial infarction was noted in all the lymphoplasmacytic vasculitis cases with no lymphoplasmacytic inflammation in these areas. Thus the damage is most likely due to narrowing of the epicardial vessels. Case 6 had an inflammatory myofibroblastic tumour reported by the referring pathologist in the kidney with no vasculitis.

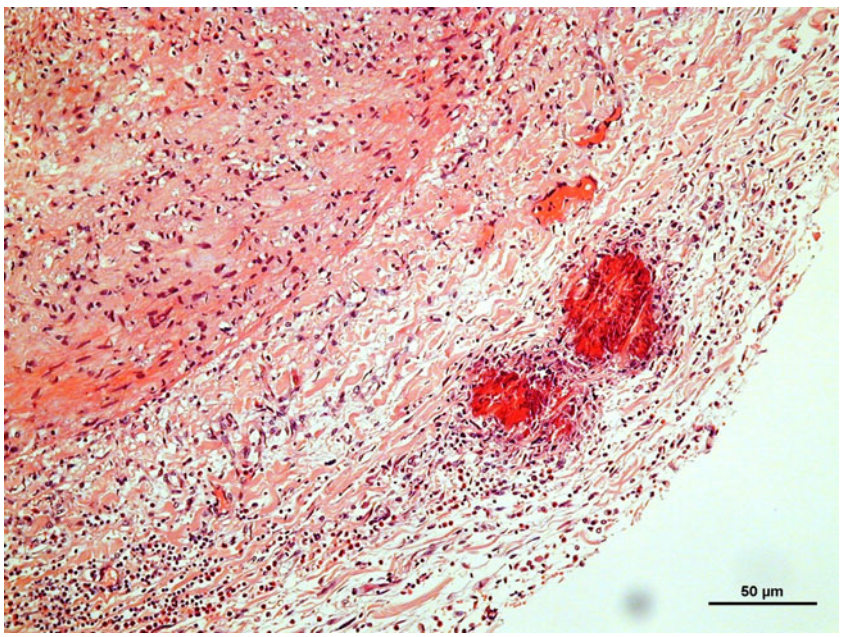

Fig. 4 Prominent adventitial inflammation with eosinophilic abscesses noted in the epicardial fat surrounding the blood vessels

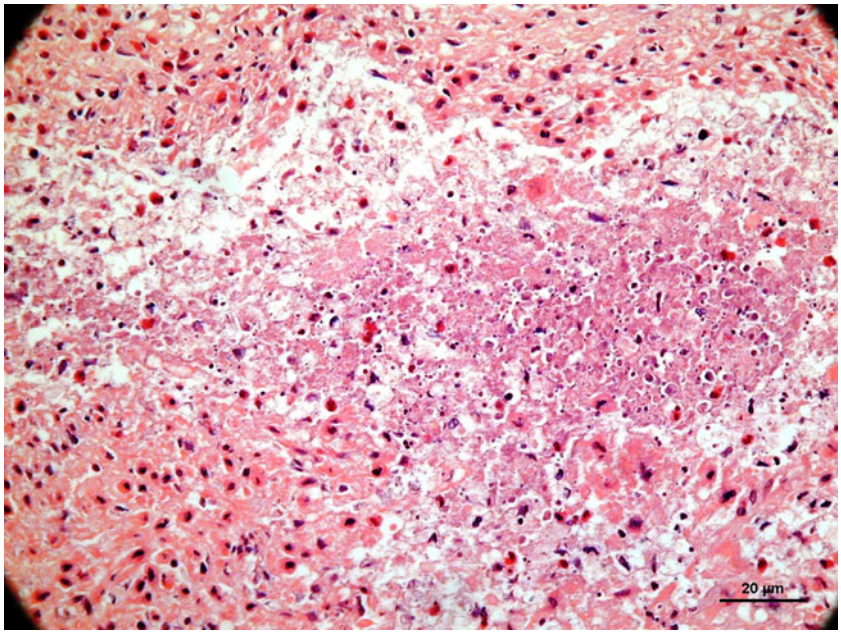

Fig. 5 Eosinophilic and granulomatous inflammation with epithelioid and small giant cells within the media of the vessels with focal necrosis

Giant cell

In case 10 there was giant cell vasculitis with involvement of both the coronary arteries and the aorta with giant cells (Fig. 8). Giant cell vasculitis consisted of giant cells at the external elastic lamina of the vessels with scattered lymphocytes and epithelioid cells. In the aorta there was classic giant cell inflammation in the media around the elastic laminae. Myocardium showed dense fibrosis.

Discussion

Our study highlights the coronary artery vasculitis and SCD in all age groups with a rare incidence of 0.5% in our SCD database. Six cases from a previous study are included in this paper [16]. The pathological presentation of this disease is highly variable. None of these cases had evidence of the classic systemic vasculitides. This study demonstrates the eosinophilic, lymphoplasmacytic and giant cell types of coronary artery vasculitis.

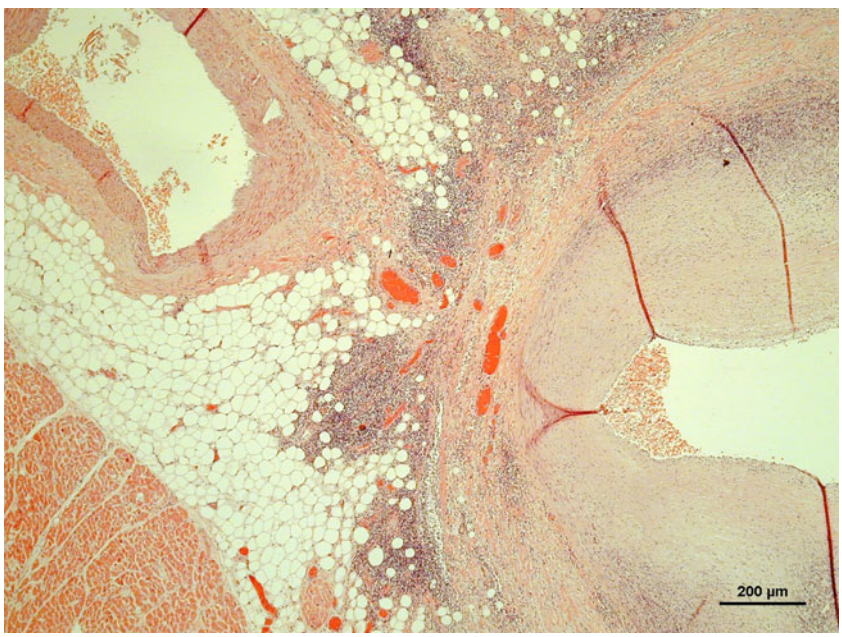

Fig. 6 Lymphocytic inflammation extending into epicardial fat

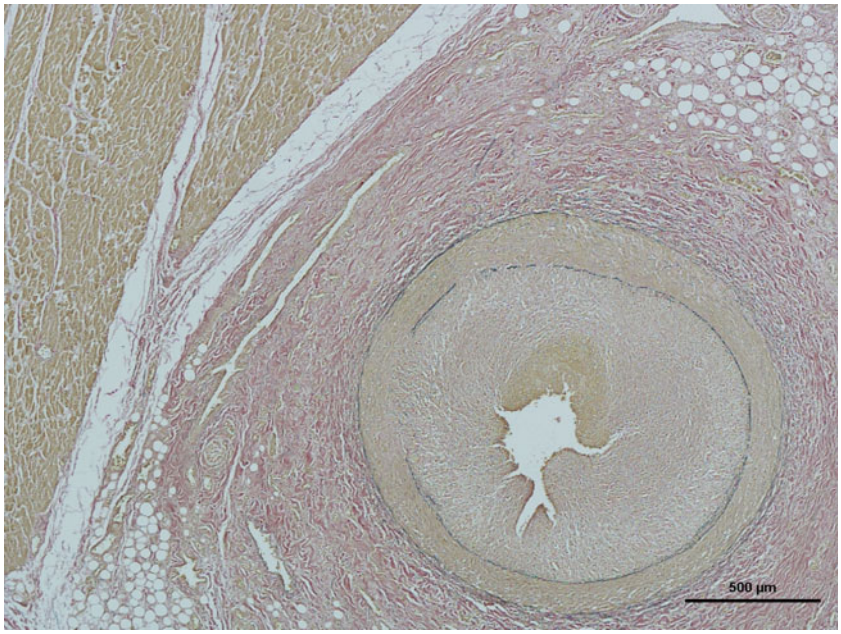

Fig. 7 Epicardial coronary arteries showing fibroblastic proliferation in the intima with destruction of the elastic lamina

Eosinophilic vasculitis

This was the most common vasculitis of the coronary arteries in our series. Eosinophilic vasculitis is often associated with CSS where asthma, eosinophilia, pulmonary infiltrates and vasculitis are needed for the diagnosis. Isolated forms of eosinophilic arteritis are rare [17–21]. All our cases presented with vasculitis in the epicardial coronary arteries, with little or no intramural coronary artery involvement. Only three of our cases had a previous history pointing to allergy and eosinophilia, two of whom had coronary aneurysms, which is often associated with systemic vasculitides [22, 23]. Coronary aneurysms are rarely associated with CSS, and there are very few reports in the literature [24]. Myocardial fibrosis was prominent in all cases where the myocardium was examined, with or without eosinophilic infiltrate. Fibrosis particularly in the subendocardium is associated with eosinophils and is

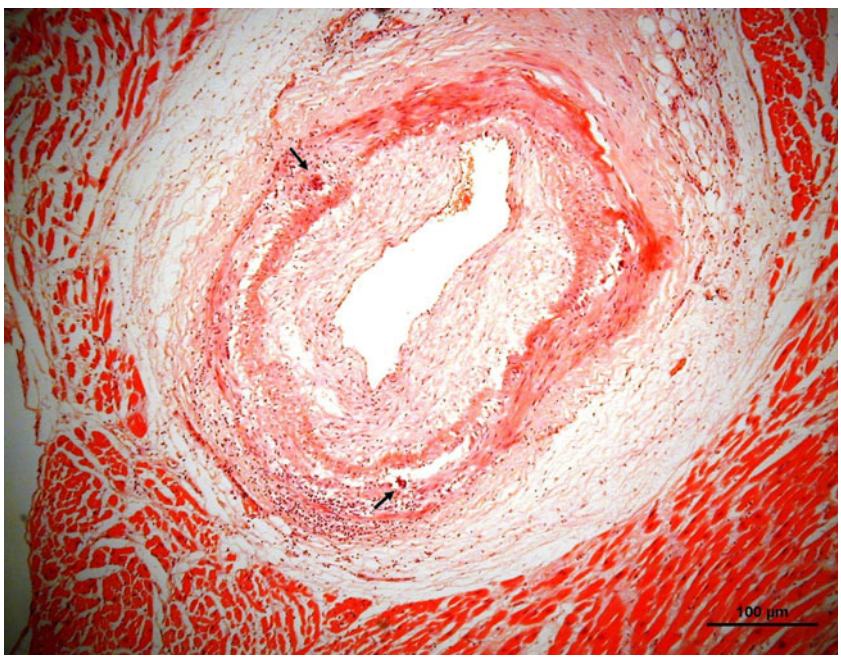

Fig. 8 Giant cell vasculitis in a coronary artery with giant cells in the vessel media (*arrows*)

linked to the release of granular proteins from the cytoplasm of the cells [25]. Heart lesions directly attributable to CSS are frequent, severe and underestimated as demonstrated in a recent French study [26].

Case 2 was associated with IgA nephropathy which is usually reported as a localised form of Henoch–Schönlein purpura but has not been reported with eosinophilic vasculitis. We do not know of any other vascular involvement, particularly the aorta.

The major differential diagnosis is spontaneous dissection. This usually manifests as intramural blood clot and does not give rise to aneurysms or diffuse coronary arterial wall thickening. There was no evidence of dissection or blood clot in the media of the coronary arteries macroscopically or microscopically, and all vessels showed involvement of all three layers and not just the adventitia which one would expect with dissection [27]. In addition normal parts of the coronary arterial wall seen in the eosinophilic vasculitis cases did not contain blood clot or medial dissection.

Lymphoplasmacytic vasculitis

The type of vasculitis most reported in the literature is that with lymphocytic infiltration [28]. All our cases had diffuse thickening of the coronary arteries with narrowing and with firm tissue around the vessels resembling tumour-like masses in two cases. This has been reported in the past as an inflammatory pseudotumour (IPT), so called due to its tumour-like appearance around the blood vessels macroscopically [29]. IPT was additionally detected in the kidney of one of these patients who suffered IgG paraproteinaemia which is associated with chronic inflammatory processes and IgG4-related disease. The latter is also linked to lymphoplasmacytic aortitis [30]. We found aortic involvement at both the macroscopic and microscopic levels in two cases. However systemic involvement could be underestimated since no other vessels were sampled at autopsy in the other cases. Lymphoplasmacytic aortitis is an established entity often linked to IgG4 disease [31]. Thus isolated lymphoplasmacytic vasculitis of the coronaries is rare and sampling of the aorta is essential in all cases. It is interesting that none of cases had a history of rheumatoid arthritis, systemic lupus erythematosus or other collagen vascular disease, which are classic diseases associated with lymphoplasmacytic vasculitis [3, 8, 9].

Myocardial infarction from coronary vasculitis is a cause of death in such patients [32] and we found both old and recent infarction in all our cases. The major differential for lymphoplasmacytic coronary artery vasculitis is lymphoplasmacytic response to atheroma in older patients. All stages of atherosclerotic plaques are characterised by an inflammatory component, in which T lymphocytes and macrophages orchestrate lesion progression and destabilisation. At the extreme end of this process plaque rupture occurs, which may manifest clinically as an acute coronary syndrome [33]. None of our cases had atheroma in their vessels and the response was throughout the wall. The thrombosis noted in one case was overlying intimal inflammation with no lipid deposition or rupture.

Idiopathic giant cell arteritis

GCA is a systemic medium- and large-vessel vasculitis, also known as temporal arteritis due to its common manifestation in the temporal artery [34]. Additional vascular manifestations include stroke, aortic aneurysm or dissection and aortic rupture [35]. Cardiac deaths from GCA are usually as a result of aortic involvement, and deaths from coronary GCA are rare [3]. Our case of idiopathic GCA did show involvement of the aorta suggesting that giant cell vasculitis of the coronaries is usually linked to aortitis. GCA is almost exclusively a disease of individuals over the age of 50 [34], while our case was a 23-year-old female. The differential diagnosis would be TA, as it is known to be more common than GCA in this age group [36]. However with the only previous medical history being shortness of breath prior to death and with no abnormalities of the aorta, carotid or subclavian vessels mentioned at autopsy, there is little evidence to support this.

Diagnostic difficulties

Identification of coronary vasculitis prior to death is difficult as symptoms may be extremely variable as illustrated by our 10 cases. We have previously published on vasculitis causing surgical challenges [37]. Coronary vasculitis is generally only found post-mortem, and even then diagnosis is not always accurate if insufficient material is taken at autopsy as our cases illustrate. There were only two cases where the whole heart was referred for examination. The sampling of tissue in other cases was often insufficient for a definitive diagnosis, with the involvement of other blood vessels largely unknown. In a cardiac referral where vasculitis is suspected, referring pathologists are advised to examine sufficient samples of blood vessels throughout the body, particularly the aorta and the temporal artery to ensure that important features are not missed in the process of diagnosis. Thus while involvement of the coronary vessels may be prominent as in all our cases, lack of sampling of other vessels/tissues indicates that isolated involvement of the coronary vessels cannot be definitively reported in this study.

Other vascular diseases may mimic vasculitis. Idiopathic arterial calcification of infancy has been misdiagnosed as

arteritis, only to be corrected later when the disease was observed in a sibling [38–41]. Inflammation secondary to atheroma can also be misdiagnosed as vasculitis [42], which can be quite florid in older patients with calcification. None of our cases fell into these categories.

Limitations

Due to the selective nature of the referrals to the CRY Centre for Cardiac Pathology in the Royal Brompton Hospital, this study may not be representative of vasculitis cases in the general UK population. Kawasaki disease is the second most common acquired cause of childhood vasculitis in England, yet none of our cases show this. This may be due to the good prognosis of the disease, as the mortality of Kawasaki patients is around 1–2%.

Conclusion

Our study demonstrates the macroscopic and microscopic variations in the presentation of coronary vasculitis, and its role in SCD. This remains a difficult field for pathologists and clinicians in terms of disease aetiology and diagnosis. More research is required to understand the immunopathological nature of coronary vasculitis including specific genetic predispositions and the influence environmental exposures. Pathologists should investigate thoroughly the histology of coronary arteries of patients who suffer a SCD and be aware of the differential diagnosis of non-atherosclerotic coronary disease.

Acknowledgements We wish to thank the Pathological Society of Great Britain and Ireland (Grant Reference No: UE 2011/07/48) and the charity Cardiac Risk in the Young (CRY) UK for funding KN and SVN, respectively.

Conflicts of interest KN is a biomedical graduate from Imperial College London. SVN is a research fellow funded by the charity CRY. MNS has received a research grant from CRY. The authors declare that they have no conflict of interest.

References

1. Chugh SS, Reinier K, Teodorescu C, Evanado A, Kehr E, Al SM, Mariani R, Gunson K, Jui J (2008) Epidemiology of sudden cardiac death: clinical and research implications. Prog Cardiovasc Dis 51:213–228
2. Thomas AC, Knapman PA, Krikler DM, Davies MJ (1988) Community study of the causes of "natural" sudden death. BMJ 297:1453–1456
3. Lie JT (1987) Coronary vasculitis. A review in the current scheme of classification of vasculitis. Arch Pathol Lab Med 111:224–233
4. Soto ME, Espinola N, Flores-Suarez LF, Reyes PA (2008) Takayasu arteritis: clinical features in 110 Mexican mestizo patients and cardiovascular impact on survival and prognosis. Clin Exp Rheumatol 26:S9–S15
5. Ashrafi AH, Wang J, Stockwell CA, Lloyd D, McAlvin JB, Russo P, Shehata BM (2007) Kawasaki disease: four case reports of cardiopathy with an institutional and literature review. Pediatr Dev Pathol 10:491–499
6. Caballero-Mora FJ, Alonso-Martin B, Tamariz-Martel-Moreno A, Cano-Fernandez J, Sanchez-Bayle M (2011) Kawasaki disease in 76 patients. Risk factors for coronary artery aneurysms. An Pediatr (Barc) 74(4):232–238
7. Dennert RM, Van Paassen P, Schalla S, Kuznetsova T, Alzand BS, Staessen JA, Velthuis S, Crijns HJ, Tervaert JW, Heymans S (2010) Cardiac involvement in Churg–Strauss syndrome. Arthritis Rheum 62:627–634
8. Calamia KT, Balabanova M (2004) Vasculitis in systemic lupus erythematosus. Clin Dermatol 22:148–156
9. Morris PB, Imber MJ, Heinsimer JA, Hlatky MA, Reimer KA (1986) Rheumatoid arthritis and coronary arteritis. Am J Cardiol 57:689–690
10. Soomro H, Armstrong M, Graham EM, Stanford MR (2006) Sudden loss of vision caused by a vasculitic ophthalmic artery occlusion in a patient with ankylosing spondylitis and Crohn's disease. Br J Ophthalmol 90:1438
11. Yalcindag FN, Kahraman S, Batioglu F, Ozdemir O (2006) Occlusive retinal vasculitis in a patient with ankylosing spondylitis. Eye 20:733–735
12. Van der Wal AC (2007) Coronary artery pathology. Heart 93:1484–1489
13. Mukhopadhyay S, Hensley RG, Tazelaar HD (2010) Cardiac involvement in Wegener granulomatosis diagnosed at autopsy. Cardiovasc Pathol 19:312–315
14. Sendino A, Barbado FJ, Gonzalez-Anglada I, Anton E, Lopez-Barea F, Vazquez JJ (1992) Temporal arteritis: a form of systemic panarteritis. Ann Rheum Dis 51:1082–1084
15. Wannamethee G, Shaper AG, Macfarlane PW, Walker M (1995) Risk factors for sudden cardiac death in middle-aged British men. Circulation 91:1749–1756
16. Hill SF, Sheppard MN (2010) Non-atherosclerotic coronary artery disease associated with sudden cardiac death. Heart 96:1119–1125
17. Arena V, Valerio L, Arena E, De-Giorgio F, Stigliano E, Monego G, Capelli A (2010) Isolated eosinophilic coronary arteritis. J Clin Pathol 63:469–471
18. Ceresa F, Sansone F, Attisani M, Rinaldi M (2009) Images in cardio-thoracic surgery. Spontaneous coronary dissection due to isolated eosinophilic arteritis as a cause of urgent heart transplantation. Eur J Cardiothorac Surg 36:767
19. Lepper PM, Koenig W, Moller P, Perner S (2005) A case of sudden cardiac death due to isolated eosinophilic coronary arteritis. Chest 128:1047–1050
20. Lie JT, Bayardo RJ (1989) Isolated eosinophilic coronary arteritis and eosinophilic myocarditis. A limited form of Churg–Strauss syndrome. Arch Pathol Lab Med 113:199–201
21. Taira K, Tsunoda R, Watanabe T, Fujino A, Ogyu A, Ashikawa K (2005) An autopsy case of isolated eosinophilic coronary periarteritis: a limited form of Churg–Strauss syndrome or a new entity? Intern Med 44:586–589
22. Mukhtyar C, Brogan P, Luqmani R (2009) Cardiovascular involvement in primary systemic vasculitis. Best Pract Res Clin Rheumatol 23:419–428
23. Canino-Rodriguez A, Cox RA (2008) Giant coronary aneurysms in a young adult patient with Kawasaki disease. P R Health Sci J 27:382–386
24. Drogue M, Vergnon JM, Wintzer B, Antoine JC, Malquarti V (1993) Prinzmetal's angina pectoris revealing aneurysm of the right coronary artery during evolution of Churg–Strauss syndrome. Chest 103:978

25. Eicher JC, Bonnotte B, L'huillier I, Cottin Y, Potard D, Abou TJ, Muller G, Guy H, Tent JP, Wolf JE (2009) Cardiovascular manifestations of eosinophilia: clinical and echocardiographic presentation. Rev Med Interne 30:1011–1019
26. Vinit J, Bielefeld P, Muller G, Pfitzenmeyer P, Bonniaud P, Lorcerie B, Besancenot JF (2010) Heart involvement in Churg–Strauss syndrome: retrospective study in French Burgundy population in past 10 years. Eur J Intern Med 21:341–346
27. Desai S, Sheppard MN (2010) Sudden cardiac death: look closely at the coronaries for spontaneous dissection which can be missed. A study of 9 cases. Am J Forensic Med Pathol. doi:10.1097/PAF.0b013e3181e29598
28. Shimizu M, Okada T, Kobayashi S, Yamamoto Y, Takahashi H, Kawata M, Nakamura T (2003) Multiple coronary aneurysms resulting from isolated coronary vasculitis in an elderly patient. Circ J 67:637–639
29. Rose AG, McCormick S, Cooper K, Titus JL (1996) Inflammatory pseudotumor (plasma cell granuloma) of the heart. Report of two cases and literature review. Arch Pathol Lab Med 120:549–554
30. Hurst NP, Smith W, Henderson DR (1987) IgG (kappa) paraproteinaemia and arthritis. Br J Rheumatol 26:142–146
31. Stone JH, Khosroshahi A, Deshpande V, Stone JR (2010) IgG4-related systemic disease accounts for a significant proportion of thoracic lymphoplasmacytic aortitis cases. Arthritis Care Res (Hoboken) 62:316–322
32. Takayanagi M, Haraoka H, Kikuchi H, Hirohata S (2003) Myocardial infarction caused by rheumatoid vasculitis: histological evidence of the involvement of T lymphocytes. Rheumatol Int 23:315–318
33. Higuchi ML, Gutierrez PS, Bezerra HG, Palomino SA, Aiello VD, Silvestre JM, Libby P, Ramires JA (2002) Comparison between adventitial and intimal inflammation of ruptured and nonruptured atherosclerotic plaques in human coronary arteries. Arq Bras Cardiol 79:20–24
34. Weyand CM, Goronzy JJ (2002) Pathogenic mechanisms in giant cell arteritis. Cleve Clin J Med 69(2):SII28–SII32
35. Eberhardt RT, Dhadly M (2007) Giant cell arteritis: diagnosis, management, and cardiovascular implications. Cardiol Rev 15:55–61
36. Gulati A, Bagga A (2010) Large vessel vasculitis. Pediatr Nephrol 25:1037–1048
37. Jansen M, Saleh S, Bolster M, O'Donnell A, Ahern T, Spence L, Sheppard MN, Burke L (2010) Thoracic vasculitis presenting as surgical problems. Virchows Arch 456:91–96
38. Lie JT (1985) Arteritis or idiopathic arterial calcification of infancy [letter]. Hum Pathol 16:1178–1179
39. Knisely AS (1986) Idiopathic arterial calcification of infancy. Hum Pathol 17:534
40. Barlow JF, Fraser B, Carter GA (1985) Aortitis and large vessel arteritis in a newborn. Hum Pathol 16:427–429
41. Anderson KA, Burbach JA, Fenton LJ, Jaqua RA, Barlow JF (1985) Idiopathic arterial calcification of infancy in newborn siblings with unusual light and electron microscopic manifestations. Arch Pathol Lab Med 109:838–842
42. Kedar R, Eisen A, Dovrish Z, Hadari R, Lew S, Amital H (2009) Isolated coronary vasculitis as a cause of unexpected sudden death. Isr Med Assoc J 11:769–770

Virchows Arch (2012) 460:319–325
DOI 10.1007/s00428-012-1208-0

ORIGINAL ARTICLE

Diagnostic value of neutrophil gelatinase-associated lipocalin (NGAL) immunoexpression in follicular-patterned lesions of the thyroid gland

Valeria Barresi · Enrica Vitarelli · Luca Reggiani Bonetti · Giovanni Tuccari · Gaetano Barresi

Received: 14 December 2011 / Revised: 13 January 2012 / Accepted: 31 January 2012 / Published online: 28 February 2012
© Springer-Verlag 2012

Abstract Neutrophil gelatinase-associated lipocalin (NGAL) is a protein which participates in iron trafficking and which is involved in cancerogenesis and cancer progression. Since its over-expression has been documented in thyroid malignancies in comparison to thyroid normal gland, in the present study, we aimed to determine whether the evaluation of NGAL immunoexpression may be of help in the differential diagnosis of follicular-patterned thyroid lesions. Our additional aim was to test the possible interference of endogenous biotin on the immunohistochemical findings. Thus, all the immunohistochemical procedures, carried out with labeled streptavidin biotin method, were doubly performed, with or without the preliminary inhibition of endogenous biotin. No NGAL staining was found in the normal thyroid gland nor in the nodular colloid goiters or in Hashimoto's thyroiditis. NGAL expression appeared to be significantly more frequent in the malignant tumors in comparison to benign ones ($P<0.000001$). Even more, NGAL expression appeared to be specific (specificity 93%) for carcinoma and represented a sensitive method (sensitivity 84%), with high negative (88%) and positive (94%) predictive values, as well as high diagnostic accuracy (88%), in the identification of follicular-patterned thyroid malignant tumors. The specificity, positive predictive value and diagnostic accuracy lowered when biotin was not preliminary inhibited, due to the presence of false positives among benign Hürthle cell tumors. In conclusion, the immunohistochemical detection of NGAL may be helpful in the differential diagnosis between malignant and benign follicular-patterned lesions of the thyroid. The use of biotin free system or the preliminary biotin inhibition is warranted for the detection of NGAL in thyroid samples, especially when dealing with Hürthle cell tumors.

Keywords NGAL · Thyroid · Differential diagnosis · Biotin

Dedicated to my father, Gaetano Barresi, who left us on the 14th of February 2012, a great researcher, but above all a great man.

V. Barresi · E. Vitarelli · G. Tuccari · G. Barresi
Department of Human Pathology, University of Messina, Messina, Italy

L. Reggiani Bonetti
Department of Laboratory Integrated Activities, Anatomic Pathology and Legal Medicine, University of Modena and Reggio Emilia, Modena, Italy

V. Barresi (✉)
Department of Human Pathology, Policlinico Universitario G. Martino, Pad D, Via Consolare Valeria, 98125 Messina, Italy
e-mail: vbarresi@unime.it

Introduction

Neutrophil gelatinase-associated lipocalin (NGAL), also known as neu-related lipocalin (NRL), oncogene 24p3, uterocalin and lipocalin 2 (LCN2), is a 25 KDa protein which participates in iron trafficking [1]. In particular, it increases the cytoplasmic levels of this mineral by capturing and transporting the iron particles to the inner cell after interaction with specific membrane receptors (24p3, megalin) [2].

Following the demonstration that NGAL is over-expressed in several human malignancies [3–8] and that its synthesis is induced by the same factors that promote the development of cancer [9], the involvement of NGAL in tumorigenesis was suggested. Specifically, NGAL seems to take part to cancerogenesis by favoring iron uptake from the extracellular space within the malignant cells, a fundamental process for the maintenance of neoplastic cell multiplication [10, 11]. Even more,

NGAL may induce cancer progression through the (positive) modulation of matrix metallo-proteinase-9 (MMP-9), an enzyme which degrades the basement membranes and extracellular matrix and enables the neoplastic cell invasion [12]. Finally, NGAL may also increase the invasiveness of cancer cells by decreasing E-cadherin-mediated cell–cell adhesion through an iron-dependent mechanism [13].

Several histotypes of thyroid carcinoma, including follicular, papillary and anaplastic, were demonstrated to over-express NGAL at both the m-RNA and protein levels [4] and NGAL was shown to favor the survival of thyroid cancer cells through its ability to bind iron and transport it into the cells [4]. Even more, our group recently showed, in a small series of thyroid tumors that the expression of NGAL is significantly more frequent in malignant tumors in comparison to benign ones [14].

In the present study, we analyzed the immunohistochemical expression of NGAL in a larger cohort of follicular-patterned lesions of the thyroid gland, including benign and malignant tumors, as well as nodular goiters and Hashimoto's thyroiditis, with the aim to determine whether the evaluation of NGAL immunoexpression may be of help in the differential diagnosis of benign versus malignant thyroid follicular pathologic conditions.

For the immunohistochemical investigation of thyroid diseases, it is very important to choose an optimal visualization method and an appropriate quality control, as it was shown that the presence of endogenous biotin in benign and malignant follicular cells may determine false positive immunohistochemical results [15, 16]. Widely used and highly sensitive immunohistochemical methods, such as the labeled streptavidin biotin (LSAB) method, based on the high affinity of streptavidin and biotin, may lead to non-specific reactions in paraffin-embedded material, caused by the interaction between streptavidin and endogenous biotin. Our additional aim in the present study was to test the possible interference of endogenous biotin on the immunohistochemical findings when the widely used method LSAB is applied for NGAL detection in thyroid samples. Thus, all the immunohistochemical procedures, carried out with LSAB method, were doubly performed, with or without the preliminary inhibition of endogenous biotin.

Materials and methods

Seventy-two surgical specimens of primary thyroid tumors, obtained from an equal number of patients (47 female and 25 male patients; age range 20–78 years; mean age: 48.6 years) were retrieved from our files and the tested for NGAL immunohistochemical expression. Tumors were classified according to the World Health Organization classification system criteria [17] into 25 follicular adenomas (FA), 14 Hürthle cell adenomas (HA), 2 atypical adenomas (AA), 10 minimally invasive follicular carcinomas (MIFC), 10 widely invasive follicular carcinomas (WIFC), 3 Hürthle cell follicular carcinomas (HC), and 8 follicular variant papillary carcinomas (FVPC). Among MIFC, five displayed capsular and vascular invasion (Table 1: cases 56, 57, 59, 60, 62), while the remaining five were characterized by only capsular invasion.

NGAL immuno-expression was also analyzed in the thyroid parenchyma adjacent to the tumors, as well as in samples from 4 nodular colloid goiters and from 6 Hashimoto's thyroiditis (Table 1).

All cases had been formalin fixed and paraffin embedded. For each case, 4 μm thick sections were cut from the corresponding paraffin block for the subsequent immunohistochemical study.

All the experiments were carried out twice, with the preliminary use of biotin blocking system (Dako Cytomation, Glostrup, Denmark) or not. The endogenous peroxidase activity was blocked with 0.1% H_2O_2 in methanol for 20 min., then normal sheep serum was applied for 30 min to prevent unspecific adherence of serum proteins. Sections were successively incubated at 4°C overnight with the primary antibody against NGAL (Santa Cruz Biotechnology, Santa Cruz, CA; w.d. 1:100). The bound primary antibody was visualized by using the LSAB kit (Dako Cytomation, Glostrup, Denmark) according to the manufacturer's instructions. To reveal the immunostaining, the sections were incubated in darkness for 10 min. with 3-3′ diaminobenzidine tetra hydrochloride (Dako Cytomation, Glostrup, Denmark), in the amount of 100 mg in 200 ml 0.03% hydrogen peroxide in phosphate-buffered saline solution (PBS). Nuclear counterstaining was performed by Mayer's haemalum.Proximal tubules within samples of normal renal parenchyma were used as positive controls for the immunoreactions [5].

The assessment of immuno-stained section was performed by two independent pathologists (V.B. and G.B.), blinded to the clinico-pathological data. NGAL expression was based on the presence of cytoplasmic and membranous staining. The intensity of staining (IS) was graded as (0) negative, (1) weak, (2) moderate, (3) strong; the area of staining positivity (ASP), recorded as percentage of neoplastic positive cells, was assessed by following values, 0 (≤ 10%), 1 (11–25%), 2 (26–50%), 3 (51–75%), 4 (>75%), according to the procedure previously described [5, 7]. Then, an intensity-distribution (ID) score was generated for each case by multiplying the values of IS and ASP. Cases displaying an ID score 0 were considered as negative for NGAL.

Fisher exact test was performed to assess the statistical correlations between NGAL expression and the type (benign vs. malignant) of the tumors. The ID scores obtained when the immunoreactions were carried out by the preliminary biotin inhibition was considered for the statistical analysis. A probability (P) value less than 0.05 was considered to be statistically significant. Data were analyzed using the SPSS package version 6.1.3 (SPSS Inc., Chicago, IL, USA).

Table 1 Clinico-pathological features and NGAL immunohistochemical expression in neoplastic and non-neoplastic thyroid lesions

Case	Sex	Age	Diagnosis	NGAL ID score (p.b.i.)	NGAL ID score (a.b.i.)
1	M	69	NG	0	0
2	F	69	NG	0	0
3	F	58	NG	0	0
4	M	45	NG	0	0
5	F	47	HT	0	0
6	F	44	HT	0	0
7	F	39	HT	0	0
8	F	32	HT	0	0
9	M	48	HT	0	0
10	F	37	HT	0	0
11	F	48	FA	0	0
12	M	60	FA	0	0
13	F	63	FA	0	0
14	M	61	FA	0	0
15	M	64	FA	1	1
16	M	46	FA	0	0
17	F	40	FA	0	0
18	M	52	FA	0	0
19	M	45	FA	0	0
20	M	35	FA	0	0
21	M	31	FA	0	0
22	M	57	FA	0	0
23	M	37	FA	0	0
24	F	70	FA	0	0
25	F	50	FA	0	0
26	F	21	FA	0	0
27	M	47	FA	0	0
28	F	33	FA	0	0
29	M	27	FA	0	0
30	F	32	FA	0	0
31	F	50	FA	0	1
32	M	34	FA	0	0
33	F	54	FA	0	0
34	F	20	FA	0	0
35	F	33	FA	0	0
36	M	32	HA	0	0
37	F	66	HA	0	0
38	F	20	HA	0	0
39	F	69	HA	0	2
40	M	63	HA	0	2
41	F	64	HA	0	2
42	F	35	HA	1	4
43	F	40	HA	0	0
44	F	60	HA	0	0
45	F	29	HA	0	2
46	F	40	HA	0	4
47	M	43	HA	0	2
48	M	35	HA	0	4
49	F	26	HA	1	8
50	F	48	AA	0	0
51	F	35	AA	0	0
52	F	40	MIFC	8	8
53	F	49	MIFC	12	12
54	F	56	MIFC	8	8
55	F	58	MIFC	8	8
56	F	49	MIFC	4	4
57	F	45	MIFC	4	4
58	M	50	MIFC	8	8
59	F	47	MIFC	2	2
60	M	42	MIFC	0	0
61	F	56	MIFC	4	4
62	M	55	WIFC	0	0
63	F	65	WIFC	8	8
64	F	78	WIFC	1	1
65	F	54	WIFC	12	12
66	F	52	WIFC	8	8
67	F	46	WIFC	8	8
68	F	62	WIFC	12	12
69	M	55	WIFC	8	8
70	F	51	WIFC	4	4
71	F	67	WIFC	12	12
72	F	32	HC	8	8
73	F	38	HC	8	8
74	M	42	HC	8	8
75	F	43	FVPC	8	8
76	M	40	FVPC	0	0
77	M	71	FVPC	2	2
78	F	66	FVPC	3	3
79	F	38	FVPC	12	12
80	F	77	FVPC	4	4
81	M	52	FVPC	0	0
82	F	71	FVPC	0	0

M male, *F* female, *NG* nodular goiter, *HT* Hashimoto's thyroiditis, *FA* follicular adenoma, *HA* Hürthle cell adenoma, *AA* atypical adenoma, *MIFC* minimally invasive follicular carcinoma, *WIFC* widely invasive follicular carcinoma, *FVPC* follicular variant of papillary carcinoma, *P. b.i.* prelimary biotin inhibition, *A.b.i.* absence of biotin inhibition

The percent of malignant lesions with positive staining for NGAL of the total malignant lesions (sensitivity), the percent of unstained benign lesions of the total benign lesions (specificity), the percent of malignant lesions with positive staining of the total lesions with positive staining (positive predictive value), and the percent of benign lesions with negative staining to NGAL of the total lesions with

negative staining (negative predictive value) were calculated. The diagnostic accuracy (true positive+true negative/all positive+all negative) of NGAL staining was also assessed.

Results

The clinico-pathological characteristics as well as NGAL immunohistochemical expression of the analyzed thyroid samples are summarized in Table 1.

No NGAL staining was observed in the follicular cells of the thyroid parenchyma adjacent to the analyzed tumors nor in the four samples of nodular colloid goiters or in the six Hashimoto's thyroiditis (Fig. 1) submitted to the immunohistochemical analysis.

In the neoplastic samples, different findings were achieved depending on the preliminary inhibition of endogenous biotin (Table 1). Indeed, when biotin was not inhibited, NGAL staining was evidenced in 37 out of the 72 thyroid tumors included in the cohort, and, specifically, in 2/25 (8%) of FA, in 9/14 (64%) HA, in 9/10 (90%) of MIFC, in 9/10 (90%) of WIFC, in 5/8 (62%) of FVPC, in 3/3 (100%) of HC. Following preliminary biotin inhibition, 29/72 tumors stained positively for NGAL; in particular, no staining was evidenced in seven HA and in one FA, which had shown a positive reaction when endogenous biotin had not been inhibited (Fig. 2). In the two HA still showing NGAL stain, ID score was significantly lower than that revealed in the absence of biotin inhibition. In the FA and HA which were NGAL positive even following biotin inhibition, staining was weak (1+) and involved 20% of neoplastic cells (Table 1).

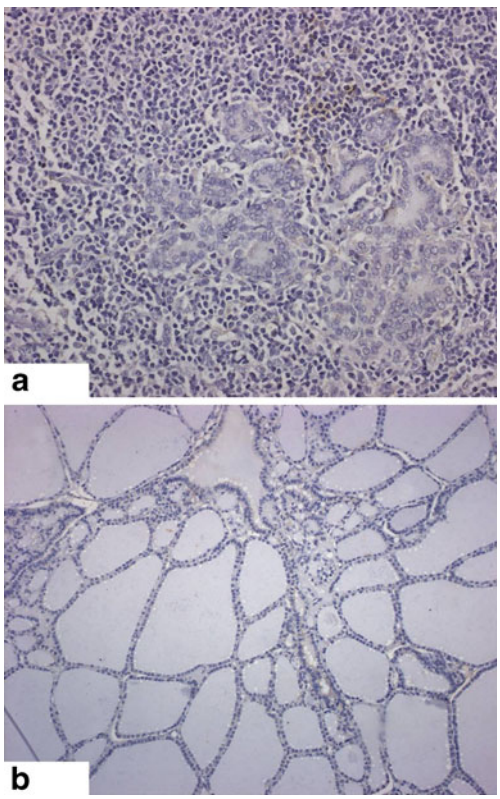

Fig. 1 Absence of NGAL staining in (**a**) follicular cells with nuclear clearing in Hashimoto's thyroiditis (NGAL stain; original magnification, ×200) and in (**b**) follicles of nodular colloid goiter (NGAL stain; original magnification, ×100)

In the HC, in all but two positive MIFC (cases no. 61 and 63) and in all but two WIFC (cases 66 and 72), NGAL labelling was widespread and involved the majority of the neoplastic cells (Table 1). In MIFC no. 61 and 63 (Table 1), NGAL immunostaining was limited to the neoplastic cells at the capsular infiltrative front.

With reference to positive FVPC, two were stained by anti-NGAL antibody in 100% of cells, while in three cases, labelling was found in 50% or less of the neoplastic cells.

At the statistical analysis through Fisher exact test, NGAL expression appeared to be significantly more frequent in the malignant tumors in comparison to benign ones ($P<0.000001$) (Fig. 3).

NGAL expression was specific (specificity 93%) for carcinoma, though specificity decreased to 73% when biotin was not preliminary inhibited. The probability that a malignant thyroid tumor expressed NGAL (sensitivity) was 84%. The probability that a positive NGAL thyroid neoplasia was a carcinoma (positive predictive value) was 94%; it lowered to 70% in the absence of biotin inhibition. The probability that a negative tumor was a benign one (negative predictive value) was 88%. The diagnostic accuracy of NGAL expression in the differential diagnosis between benign and malignant follicular-patterned thyroid tumors was 88%; it lowered to 77% in the absence of preliminary biotin inhibition.

Discussion

One of the major controversies in surgical pathology relates to the diagnosis of follicular-patterned lesions of the thyroid gland [18]. Controversy mainly involves the differential diagnosis of follicular adenoma, follicular carcinoma (FC), and follicular variant of papillary carcinoma [18]. The root cause for the controversy surrounding the diagnosis of thyroid tumors with follicular architecture is the lack of totally reproducible diagnostic criteria for these lesions. In the World Health Organization (WHO) classification, FC of the thyroid is defined as a malignant epithelial tumour showing follicular cell differentiation and lacking the diagnostic nuclear features of papillary thyroid carcinoma [17]. Thus, the diagnosis of FC is based on the presence of invasion through the capsule and/or invasion into the blood vessels. These criteria, though posing few problems in cases of WIFC, may lead to inter-observer variation among pathologists in the discrimination of minimally invasive (or encapsulated) carcinoma from adenoma [19]. Also, since

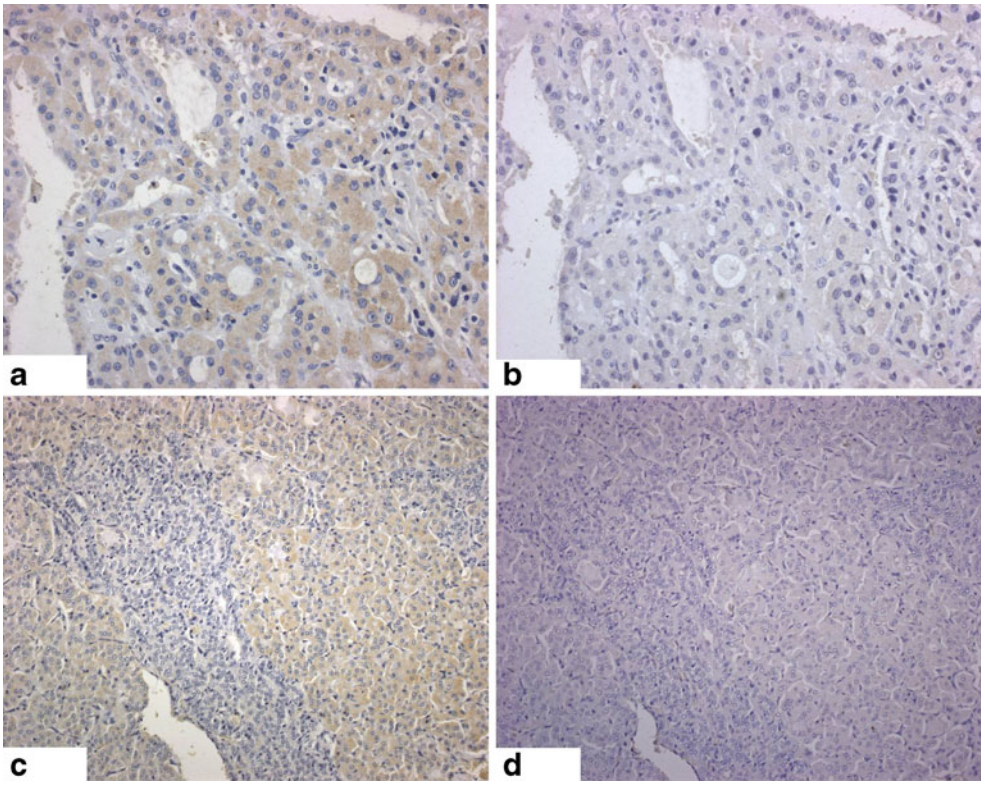

Fig. 2 NGAL staining in Hürthle cell adenoma (**a** absence of biotin inhibition; **b** preliminary biotin inhibition; NGAL stain; original magnification, ×200) and follicular adenoma (**c** absence of biotin inhibition; **b** preliminary biotin inhibition; NGAL stain; original magnification, ×100)

the differential diagnosis of the FVPC from FA or FC resides mainly on the nuclear features of the neoplastic cells [17], the discrimination of FVPC may be challenging when the nuclear features of papillary carcinoma are not well developed or are only focally expressed [20]. The actual extent of the diagnostic dilemma involving follicular-patterned thyroid tumors is demonstrated by the large number of papers in the literature aimed at finding more objective markers, able to discriminate among

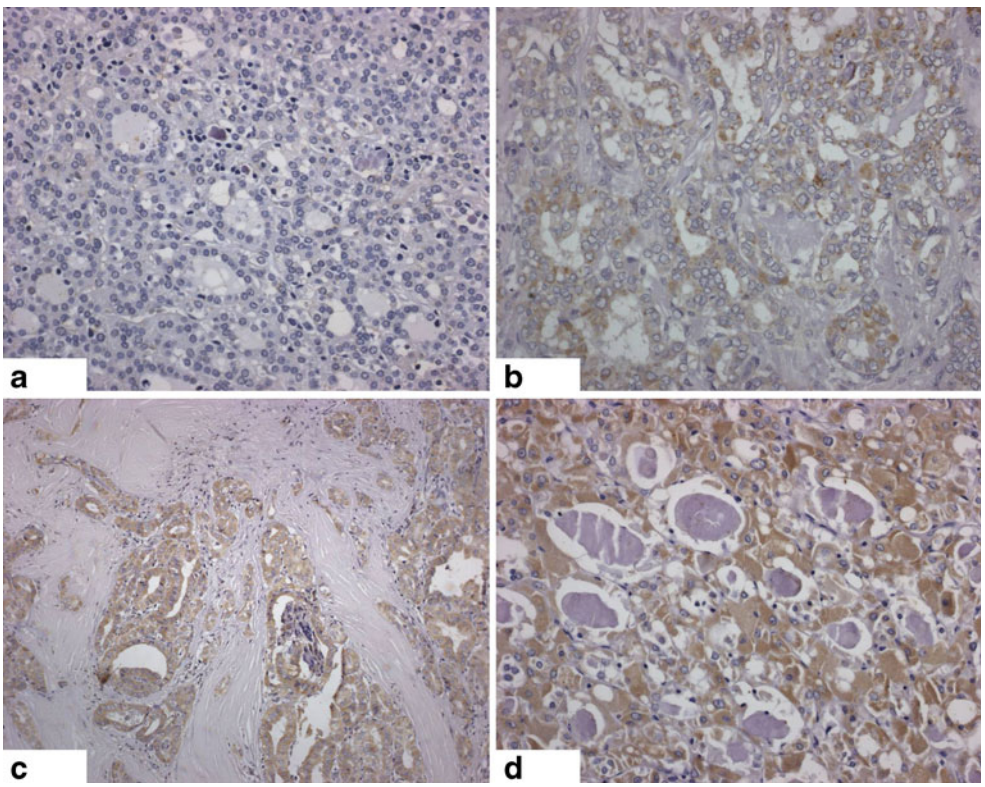

Fig. 3 **a** Absence of NGAL immuno-expression in follicular adenoma (NGAL stain; preliminary biotin inhibition; original magnification, ×200). NGAL staining in the neoplastic cells of **b** papillary carcinoma follicular variant (FVPC) (NGAL stain; preliminary biotin inhibition; original magnification, ×200), **c** widely invasive follicular carcinoma (WIFC) (NGAL stain; preliminary biotin inhibition; original magnification, ×100), and **d** Hürthle cell carcinoma (WIFC) (NGAL stain; preliminary biotin inhibition; original magnification, ×200)

these entities [21–30]. The diagnostic value of galectin-3, HBME-1, cytokeratin-19 and matrix-metallo proteinases (MMP), or that of proliferation markers such as MCM2 and Ki-67, as additional tools for the differential diagnosis of thyroid tumors was investigated [21–30]. The findings were generally encouraging and promising although some studies demonstrated inconclusive or conflicting results [21–30].

Our group recently showed, in a small series of thyroid tumors, follicular-patterned or not, that the expression of NGAL is found with a significantly higher frequency in malignant tumors in comparison to benign ones [14]. In the present study, we analyzed NGAL immunohistochemical expression in a larger cohort including only follicular-patterned lesions, neoplastic or not, of the thyroid gland.

In line with the findings reported by Iannetti et al. [4], we did not evidence any NGAL immuno-staining in the thyroid parenchyma adjacent to the analyzed tumors nor in the colloid nodular goiters or in the Hashimoto's thyroiditis. The evidence that all the lesions which stained positively for NGAL belonged to the tumoral group, supports the hypothesis that NGAL is involved in the tumorigenesis and progression of thyroid cancer, as already suggested [4]. NGAL immuno-expression was detected in 84% of malignant tumors and in 7% of benign ones. The preferential expression of NGAL in malignant thyroid tumors in comparison to benign ones is not surprising since it may lead to the acquisition of invasive potential, which differentiate thyroid follicular adenomas from carcinomas. Indeed, it has been shown that NGAL may enhance the invasiveness of neoplastic cell by the positive regulation of the activity of MMP-9, an enzyme which degrades the basement membranes and extracellular matrix, thus liberating vascular endothelial growth factor (VEGF), and enabling angiogenesis, invasion and metastasis [12, 31, 32]. Specifically, NGAL can protect MMP-9 from proteolytic degradation by forming the NGAL/MMP-9 complex. This would trigger an enhancement of the enzymatic activity of MMP-9 and explain the enhanced tumoral invasiveness and diffusion associated with NGAL overexpression [12]. Besides, the presence of the NGAL/MMP-9 complex was demonstrated in malignant thyroid cells, though its function has been not fully clarified [4]. Nevertheless, NGAL may also increase the invasiveness of cancer cells by decreasing E-cadherin-mediated cell–cell adhesion through an iron-dependent mechanism [13].

In our analysis, different findings were obtained if the endogenous biotin was inhibited preliminary to the immunohistochemical procedures or not. Indeed eight more benign tumors, including seven Hürthle cell adenomas and one follicular adenoma, showed NGAL expression when endogenous biotin was not preliminary inhibited. The possible explanation for such discrepancy comes from the knowledge that Hürthle cells are rich in endogenous biotin, which may provide false positive results in Hürthle cell tumors if biotin-based detection systems are used. Since the presence of biotin has been also documented in follicular adenomas, follicular carcinomas, and papillary carcinoma [15, 16, 22], the use of biotin-free systems appears to be extremely relevant when immunohistochemistry is performed in thyroid lesions. The artifacts due to the presence of endogenous biotin are known to be markedly enhanced when heat-induced procedures for antigen retrieval are carried out during immunohistochemical protocols [33]. In the present analysis, the majority of false positives involved Hürthle adenomas. We may speculate that, since no antigen retrieval procedure is needed for the immunohistochemical detection of NGAL, artifacts were limited to cells containing high quantity of biotin, such as Hürthle cells.

The significantly higher frequency ($P<0.000001$) of NGAL immuno-expression which we found in malignant follicular-patterned thyroid tumors in comparison to benign ones may be of use in the differential diagnosis of these lesions. Indeed, NGAL expression appeared to be specific (specificity 93%) for carcinoma and represented a sensitive method (sensitivity 84%), with high negative (88%) and positive (94%) predictive values, as well as high diagnostic accuracy (88%), in the identification of follicular-patterned thyroid malignant tumors; nevertheless, it is noteworthy that the specificity, positive predictive value and diagnostic accuracy lowered when biotin inhibition was not preliminary performed.

The evaluation of NGAL immunoexpression might be particularly useful in order to differentiate benign and malignant encapsulated follicular tumors of the thyroid, i.e., for the differential diagnosis of MIFC from FA, as well as for the distinction between HA and minimally invasive HC. Though the nuclear clearing represents one of the hallmarks of papillary carcinoma, it maybe also present in the follicular cells in thyroiditis, or as a reactive change or an artefact of tissue processing [34]; thus, the presence of NGAL staining in FVPC may help in the differential diagnosis towards benign conditions showing clear nuclei. By contrast, the evaluation of NGAL staining appears to be helpless to distinguish FVPC from WIFC, as both display cytoplasmic NGAL labelling.

In conclusion, our findings show that the immunohistochemical detection of NGAL may be helpful in the differential diagnosis between malignant and benign follicular-patterned lesions of the thyroid. The LSAB method appeared to ensure the specificity, positive predictive value and diagnostic accuracy of NGAL as a marker of malignant lesions, when the preliminary inhibition of endogenous biotin was carried out. Thus, the use of biotin free system or the preliminary biotin inhibition is warranted for the detection of NGAL in thyroid samples, especially when dealing with Hürthle cell tumors, though in the absence of heat induced antigen retrieval procedures.

Conflict of interest statement We declare that we have no conflict of interest.

References

1. Yang J, Goetz D, Li JY et al (2002) An iron delivery pathway mediated by a lipocalin. Mol Cell 10:1045–1056
2. Goetz DH, Willie ST, Arme RS et al (2000) Ligand preference inferred from the structure of neutrophil gelatinase associated lipocalin. Biochemistry 39:1935–1941
3. Bauer M, Eickhoff JC, Gould MN et al (2008) Neutrophil gelatinase- associated lipocalin (NGAL) is a predictor of poor prognosis in human primary breast cancer. Breast Cancer Res Treat 108:389–397
4. Iannetti A, Pacifico F, Acquaviva R et al (2008) The neutrophil gelatinase-associated lipocalin (NGAL), a NF-kappaB-regulated gene, is a survival factor for thyroid neoplastic cells. Proc Natl Acad Sci U S A 105:14058–14063
5. Barresi V, Ieni A, Bolignano D et al (2010) Neutrophil gelatinase-associated lipocalin immunoexpression in renal tumors: correlation with histotype and histological grade. Oncol Rep 24:305–310
6. Barresi V, Lucianò R, Vitarelli E et al (2010) Neutrophil gelatinase-associated lipocalin immunoexpression in colorectal carcinoma: a stage-specific prognostic factor? Oncol Lett 1:1089–1096
7. Barresi V, Tuccari G, Barresi G (2010) NGAL immunohistochemical expression in brain primary and metastatic tumors. Clin Neuropathol 29:317–322
8. Barresi V, Di Gregorio C, Regiani-Bonetti L et al (2011) Neutrophil gelatinase-associated lipocalin (NGAL): a new prognostic marker in stage I colorectal carcinoma? Hum Pathol 42:1720–1726
9. Bratt T (2000) Lipocalins and cancer. Biochim Biophys Acta 1482:318–326
10. Devireddy LR, Gazin C, Zhu X et al (2005) A cell-surface receptor for lipocalin 24p3 selectively mediates apoptosis and iron uptake. Cell 23:1293–1305
11. Le NT, Richardson DR (2002) The role of iron in cell cycle progression and the proliferation of neoplastic cells. Biochim Biophys Acta 1603:3146
12. Yan L, Borregaard N, Kjeldsen L et al (2001) The high molecular weight urinary matrix metalloproteinase (MMP) activity is a complex of gelatinase B/MMP-9 and neutrophil gelatinase-associated lipocalin (NGAL). Modulation of MMP-9 activity by NGAL. J Biol Chem 276:37258–37265
13. Hu L, Hittelman W, Lu T et al (2009) NGAL decreases E-cadherin-mediated cell–cell adhesion and increases cell motility and invasion through Rac1 in colon carcinoma cells. Lab Invest 89:531–548
14. Barresi V, Ieni A, Tuccari G et al (2012) Neutrophil gelatinase-associated lipocalin (NGAL) immunohistochemical expression in follicular cell-derived thyroid tumors: a novel diagnostic tool? Histol Histopathol (in press)
15. Bussolati G, Gugliotta P, Volante M et al (1997) Retrieved endogenous biotin: a novel marker and a potential pitfall in diagnostic immunohistochemistry. Histopathology 31:400–407
16. Nikiel B, Chekan M, Jarzab M et al (2009) Endogenous avidin biotin activity (EABA) in thyroid pathology: immunohistochemical study. Thyroid Res 2:5
17. De Lellis RA, Lloyd RV, Heitz PU et al (2004) Pathology and genetics of tumours of endocrine organs. IARC Press, Lyon
18. Livolsi VA, Baloch ZW (2011) Follicular-patterned tumors of the thyroid: the battle of benign vs. malignant vs. so-called uncertain. Endocr Pathol 22:184–189
19. Hirokawa M, Carney JA, Goellner JR et al (2002) Observer variation of encapsulated follicular lesions of the thyroid gland. Am J Surg Pathol 26:1508–1514
20. Elsheikh TM, Asa SL, Chan JK et al (2008) Interobserver and intraobserver variation among experts in the diagnosis of thyroid follicular lesions with borderline nuclear features of papillary carcinoma. Am J Clin Pathol 130:736–744
21. Sahoo S, Hoda SA, Rosai J et al (2001) Cytokeratin 19 immunoreactivity in the diagnosis of papillary thyroid carcinoma: a note of caution. Am J Clin Pathol 116:696–702
22. Herrmann ME, LiVolsi VA, Pasha TL et al (2002) Immunohistochemical expression of galectin-3 in benign and malignant thyroid lesions. Arch Pathol Lab Med 126:710–713
23. Erickson LA, Lloyd RV (2004) Practical markers used in the diagnosis of endocrine tumors. Adv Anat Pathol 11:175–189
24. Prasad ML, Pellegata NS, Huang Y et al (2005) Galectin-3, fibronectin-1, CITED-1, HBME1 and cytokeratin-19 immunohistochemistry is useful for the differential diagnosis of thyroid tumors. Mod Pathol 18:48–57
25. Cho Mar K, Eimoto T, Tateyama H et al (2006) Expression of matrix metalloproteinases in benign and malignant follicular thyroid lesions. Histopathology 48:286–294
26. Cho Mar K, Eimoto T, Nagaya S et al (2006) Cell proliferation marker MCM2, but not Ki67, is helpful for distinguishing between minimally invasive follicular carcinoma and follicular adenoma of the thyroid. Histopathology 48:801–807
27. Barroeta JE, Baloch ZW, Lal P et al (2006) Diagnostic value of differential expression of CK19, Galectin-3, HBME-1, ERK, RET, and p16 in benign and malignant follicular-derived lesions of the thyroid: an immunohistochemical tissue microarray analysis. Endocr Pathol 17:225–234
28. El Demellawy D, Nasr A, Alowami S (2008) Application of CD56, P63 and CK19 immunohistochemistry in the diagnosis of papillary carcinoma of the thyroid. Diagn Pathol 3:5
29. Buergy D, Weber T, Maurer GD et al (2009) Urokinase receptor, MMP-1 and MMP-9 are markers to differentiate prognosis, adenoma and carcinoma in thyroid malignancies. Int J Cancer 125:894–901
30. Saleh HA, Jin B, Barnwell J et al (2010) Utility of immunohistochemical markers in differentiating benign from malignant follicular-derived thyroid nodules. Diagn Pathol 26:5–9
31. Fernandez CA, Yan L, Louis G et al (2005) The matrix metalloproteinase-9/neutrophil gelatinase associated lipocalin complex plays a role in breast tumor growth and is present in the urine of breast cancer patients. Clin Cancer Res 11:5390–5395
32. Lee S, Jilani SM, Nikolova GV et al (2005) Processing of VEGF-A by matrix metalloproteinases regulates bioavailability and vascular patterning in tumors. J Cell Biol 169:681–691
33. Kim SH, Jung KC, Shin YK et al (2002) The enhanced reactivity of endogenous biotin-like molecules by antigen retrieval procedures and signal amplification with tyramine. Histochem J 34:97–103
34. Rosai J, Kuhn E, Carcangiu ML (2006) Pitfalls in thyroid tumour pathology. Histopathology 49:107–120

Virchows Arch (2012) 460:327–334
DOI 10.1007/s00428-012-1198-y

ORIGINAL ARTICLE

Histological and clinical characteristics of malignant giant cell tumor of bone

Lihua Gong · Weifeng Liu · Xiaoqi Sun · Constantin Sajdik · Xinxia Tian · Xiaohui Niu · XiaoYuan Huang

Received: 11 July 2011 / Revised: 12 January 2012 / Accepted: 19 January 2012 / Published online: 17 February 2012
© Springer-Verlag 2012

Abstract Malignant giant cell tumors of bone (MGCTB) are rare, and the diagnosis can be difficult due to the occurrence of a variety of malignant tumors containing giant cells. To better understand its clinicopathological features, we have reviewed our experience with 17 cases of MGCTB. Five cases were primary malignant giant cell tumor of bone (PMGCTB), and 12 cases were giant cell tumors of bone initially diagnosed as benign but malignant in a recurrent lesion (secondary MGCTB, SMGCTB). The patients included six women and 11 men (age ranged from 17 to 52 years; mean, 30.5 years). The tumor arose in the femur (six cases), the tibia (seven cases), the humerus (three cases), and the fibula (one case). Microscopically, PMGCTB showed both conventional giant cell tumor and malignant sarcoma features. SMGCTB were initially diagnosed as conventional giant cell tumor of bone, the recurrent lesion showing malignant features. Histologically, the malignant components included osteosarcoma (11 cases), undifferentiated high-grade pleomorphic sarcoma (two cases), and fibrosarcoma (four cases). SMGCTB cases showed strong expression of p53. Follow-up information revealed that four patients died of lung metastasis, two patients are alive with lung metastases, and 11 patients are alive without tumor. MGCTB should be considered as a high-grade sarcoma. It must be distinguished from GCTB and other malignant tumors containing giant cells. p53 might play a role in the malignant transformation of GCTB.

Keywords Malignancy · Giant cell · Bone tumor · Osteosarcoma · Fibrosarcoma · Undifferentiated high-grade pleomorphic sarcoma

L. Gong (✉) · X. Sun · X. Huang
Department of Pathology, Beijing Jishuitan Hospital,
Fourth Medical College of Peking University,
Teaching Hospital of Tsinghua University,
31 Xinjiekou East Street, Xicheng District,
Beijing 100035, China
e-mail: Lhgong2005@126.com

W. Liu · X. Niu
Department of Orthopedic Oncology, Beijing Jishuitan Hospital,
Fourth Medical College of Peking University,
Teaching Hospital of Tsinghua University,
Beijing, China

C. Sajdik
Department of Gynaecology and Gynaecological Oncology,
Medical University of Vienna,
Vienna, Austria

X. Tian
Department of Pathology,
Peking University Health Science Center,
Beijing, China

Introduction

Giant cell tumor of bone (GCTB) is a benign and locally aggressive neoplasm that is composed of sheets of mononuclear cells interspersed with uniformly distributed large, osteoclast-like giant cells [1]. Malignant giant cell tumor of bone (MGCTB) is a high-grade sarcoma diagnosed either at the onset in a giant cell tumor of bone (primary MGCTB or PMGCTB) or at the site of a recurrent lesion, previously diagnosed as a conventional giant cell tumor of bone (secondary MGCTB or SMGCTB) [1, 2]. The high-grade sarcoma component of PMGCTB often exists side by side with histologically benign GCTB components. SMGCTB occurs after surgery, radiotherapy, or both. It occurs more frequently than PMGCTB [2, 3]. MGCTB is uncommon and accounts for 1.8–7% of all GCTBs [4, 5]. It can be confused with other malignant lesions containing giant cells, such as osteosarcoma, fibrosarcoma, and undifferentiated high-

grade pleomorphic sarcoma (UPS). To better understand the characteristics of MGCTB and the features that distinguish it from other malignant bone tumors, we report the clinicopathological features of 17 such cases.

Materials and methods

Seventeen cases were retrieved from the surgical pathology files between 1990 and 2010 in the Department of Pathology in Beijing Jishuitan Hospital, Beijing. In all cases, the tissues derived from surgical operation in the Department of Orthopedic Oncology were fixed in neutral buffered formalin and processed routinely with paraffin embedding. The sections were prepared and stained with hematoxylin and eosin. The histopathological features were reviewed by three pathologists. Clinical and radiological information was obtained from the electronic medical records and the surgeons. Immunohistochemistry was performed by an automated immunostainer (Autostainer 720, Labvision) using standard heat-induced epitope retrieval and an avidin–biotin–peroxidase complex method. Antibodies against the following antigens were used: p53, p16, vimentin, desmin, CD68, SMA, and myogenin. Appropriate positive and negative controls were included with each batch of staining (Table 3). This study was approved by the Ethics Committee of the Beijing Jishuitan Hospital.

Results

Clinical features

The patient series included six women and 11 men, with an age range from 17 to 52 years (mean age, 30.5 years). In the PMGCTB group (five cases), one case was from a female patient, and four cases were from male patients, whose ages ranged from 18 to 47 years (mean age, 29.2 years). In the SMGCTB group (12 cases), five cases were from female patients and seven cases were from male patients, whose ages ranged from 17 to 52 years (mean age, 30 years). The tumors involved the proximal tibia (two cases), distal tibia (one case), and proximal femur (two cases) in the PMGCTB, and distal femur (four cases), proximal tibia (four cases), proximal humerus (one case), distal humerus (one case), graft humerus (one case), and fibula (one case) in SMGCTB (Tables 1 and 2). None of the patients reported a history of prior radiation treatment.

Radiologic features

The radiologic features of the PMGCTB were similar to those of conventional GCTB: osteolytic lesions with well-circumscribed margins in the epiphyses of long bones (Fig. 1). In a few cases, cortical breakthrough, with or without soft tissue mass, was seen on plain

Table 1 Clinical summary of PMGCTB

Case	Age (years)	Sex	Site	Histology	Outcome (time in months)
1	18	M	Proximal femur	Fibrosarcoma	NER (79)
2	21	M	Proximal tibia	Osteosarcoma	NER (55)
3	40	M	Proximal tibia	Osteosarcoma	NER (28)
4	47	M	Distal tibia	Fibrosarcoma	Lung metastasis (8)
5	20	F	Proximal femur	Fibrosarcoma	NER (12)

NER no evidence of recurrence

Table 2 Clinical summary of SMGCTB

Case	Age (years)	Sex	Site	Histology	Outcome (time in months)
6	21	F	Proximal humerus	UPS	Died (54)
7	52	M	Proximal tibia	Osteosarcoma	NER (203)
8	45	M	Proximal tibia	Osteosarcoma	Died of lung metastasis (84)
9	25	F	Distal femur	Osteosarcoma	NER (36)
10	17	M	Distal humerus	Osteosarcoma	NER (19)
11	29	M	Proximal tibia	UPS	Died of lung metastasis (24)
12	29	F	Distal femur	Osteosarcoma	Died of lung metastasis (100)
13	40	F	Distal femur	Osteosarcoma	NER (221)
14	21	M	Distal femur	Osteosarcoma	NER (22)
15	27	F	Proximal fibula	Osteosarcoma	NER (37)
16	33	M	Proximal tibia	Osteosarcoma	Lung metastasis (112)
17	34	M	Graft humerus	Osteosarcoma	NER (28)

NER no evidence of recurrence

Fig. 1 PMGCTB (case 4). Anteroposterior radiograph of left tibia shows an eccentric and osteolytic lesion. The lesion is well demarcated on the metaphysis of the distal tibia

films. In SMGCTB, the initial radiographic appearance was similar to that of conventional GCTB (Fig. 4a). The radiographic appearance of SMGCTB showed more aggressive features, with a less distinct margin of the lesion and more prominent sclerotic components. Cortical breakthrough and soft tissue mass formation were more common in these cases (Fig. 4b).

Gross features

The gross features of PMGCTB did not differ from those of GCTB. The tissue was soft and brown, and some areas were gray red to gray white because of hemorrhage and fibrosis; cyst formation and a thin bone shell were also often found. The tumor tissue of SMGCTB was white and soft; in some areas, it appeared randomly granular, suggesting the production of osteoid. The tumor transgressed the cortex and extended into the soft tissue in some cases.

Histologic features

In PMGCTB, the conventional GCTB features were prominent (Figs. 2a and 3a). The multinuclear giant cells were sparsely spread in the ovoid/round or spindle mononuclear stromal cells. The number of nuclei of giant cells ranged from 50 to 100, and the nuclei of the osteoclasts were similar to those of the stromal cells. The cytoplasm of stromal cells was ill defined, and mitotic figures were present, but atypical mitosis was not found. In addition to the GCTB characteristics, malignant features were also present. In our study, three cases showed fibrosarcoma characteristics and two cases features of osteosarcoma. In the fibrosarcoma component, tumor cells were densely arranged in long intersecting fascicles, and storiform areas were found (Fig. 2b). The cells had hyperchromatic nuclei with variably prominent nucleoli. Mitotic activity was almost always present, and atypical mitosis could also be found. Malignant

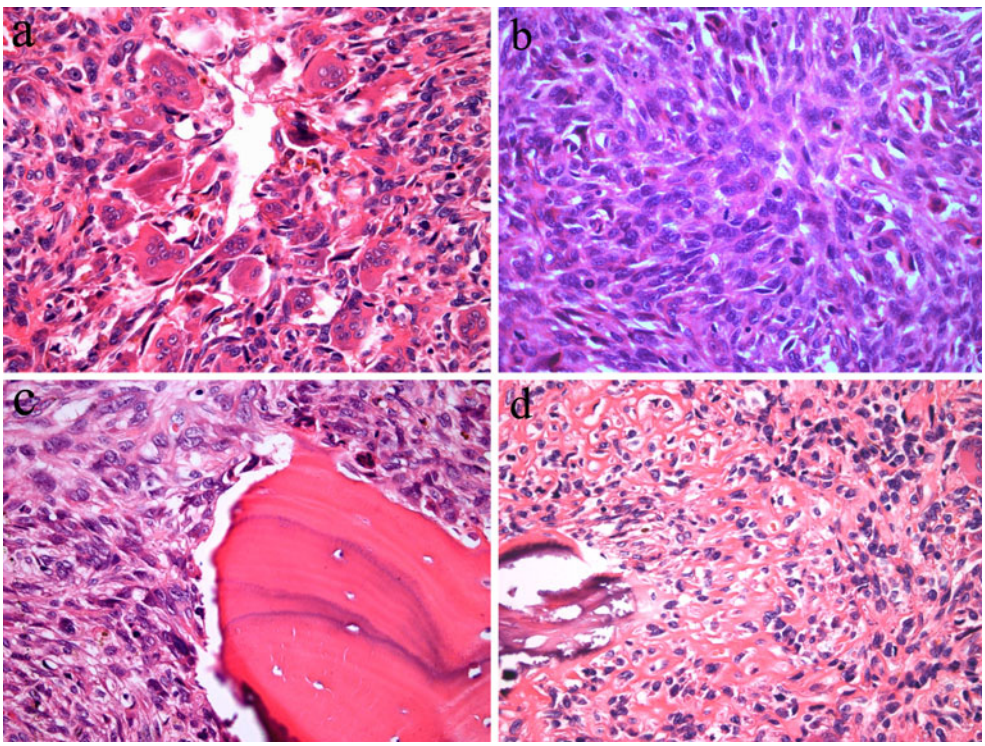

Fig. 2 PMGCTB (case 4). **a** The characteristic giant cell tumor area. **b** The spindle cell sarcoma area showing active motitic activity. **c** The spindle cell sarcoma invading into the normal bone cortex. **d** The extracellular eosinophilic collagen mimic the osteoid

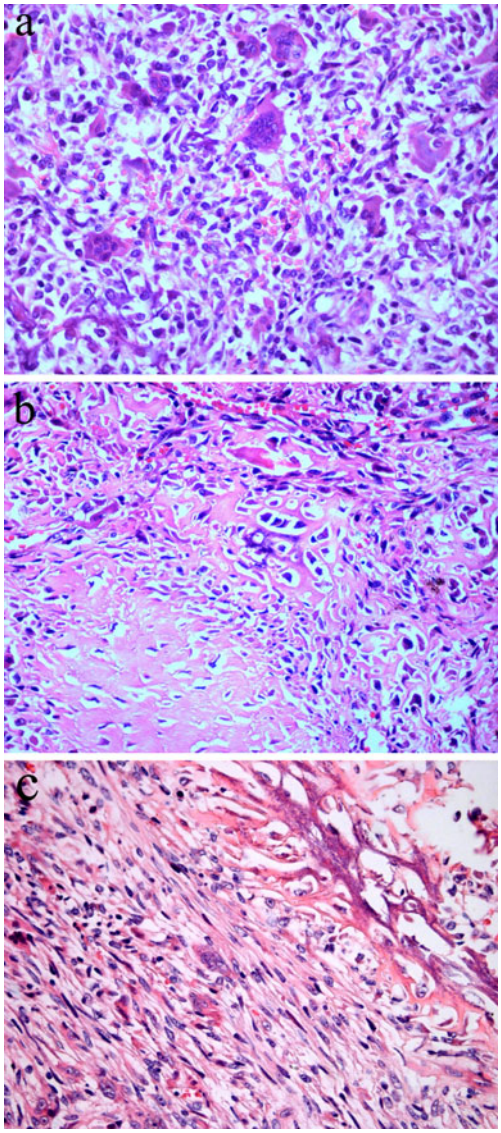

Fig. 3 PMGCTB (case 2). **a** The characteristic giant cell tumor area. **b** The osteosarcoma. **c** The residual giant cell tumor adjacent to the osteosarcoma area

spindle cells could be found infiltrating the normal bone trabecula (Fig. 2c). In the osteosarcoma component, the cells were highly anaplastic and pleomorphic with large hyperchromatic nuclei. Necessary characteristic for a diagnosis of osteosarcoma was the production of osteoid by malignant tumor cells: dense, pink, and amorphous intercellular material to be distinguished from non-osseous collagen (Fig. 3b). Collagen was linear and fibrillar, appearing around tumor cells without atypia or other malignant features found in osteosarcoma cells (Fig. 2d). In neighboring osteosarcoma areas, residual giant cell tumor areas were found (Fig. 3c).

In the cases of PMGCTB, between conventional giant cell tumor areas and high-grade malignant sarcoma, a distinct line of demarcation as described in the WHO classification [6] was not observed. The tumor gradually transited from the giant cell tumor area to the malignant area. In the transitional zone, the number of giant cells decreased, and the number of mononuclear cells increased. The mononuclear cells were arranged more densely and their shape changed to spindle, nuclear atypia appeared, and finally the characteristics of a high-grade malignant tumor (Fig. 4).

For SMGCTB, the initial lesions were conventional GCTB without evidence of malignancy. After one or more recurrences, the histological characteristics became malignant. We found one case with fibrosarcoma similar to conventional fibrosarcoma. Histological features of two cases were similar to UPS, with striking cytological atypia and nuclear pleomorphism, frequent and occasionally atypical mitotic figures. Some tumor cells showed prominent eosinophilic cytoplasm resembling rhabdomyosarcoma (Fig. 5b). Immunohistochemical stains showed reactivity for CD68 and vimentin, while stains for other antigens were negative, confirming a diagnosis of UPS and excluding rhabdomyosarcoma and leiomyosarcoma. Staining for p16 was negative in both UPS and original GCTB lesions (Fig. 8). p53 was diffusely positive in the nuclei of tumor cells in UPS, but expressed only focally and weakly in original GCTB lesions (Fig. 9; Table 3).

Nine cases of SMGCTB were osteosarcoma. In one case, uniform undifferentiated small round cells constituted the major malignant component (Fig. 6c); other areas showed a chondroid matrix (Fig. 6b) as in mesenchymal chondrosarcoma, but osteoid formation by markedly atypical tumor cells confirmed the diagnosis (Fig. 6a). Another case of osteosarcoma showed areas of aneurysmal bone cyst-like

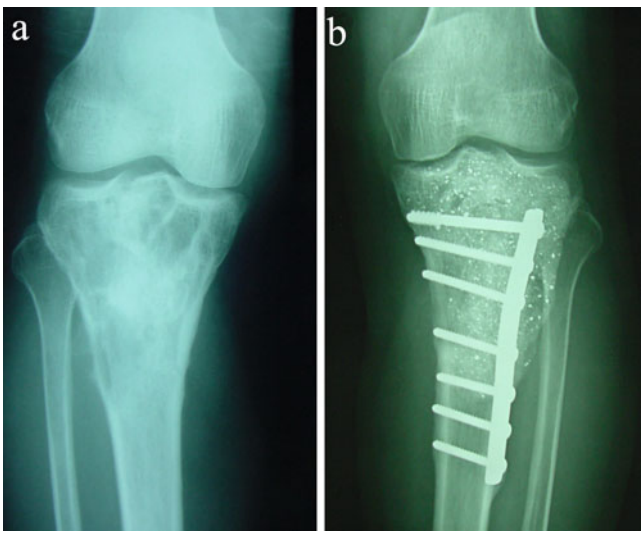

Fig. 4 SMGCTB (case 7). **a** Anteroposterior radiograph of proximal tibia shows a conventional giant cell tumor appearance. **b** Anteroposterior radiograph made 4 years after curettage and bone graft shows osteolysis and ossification changes indicating tumor recurrence

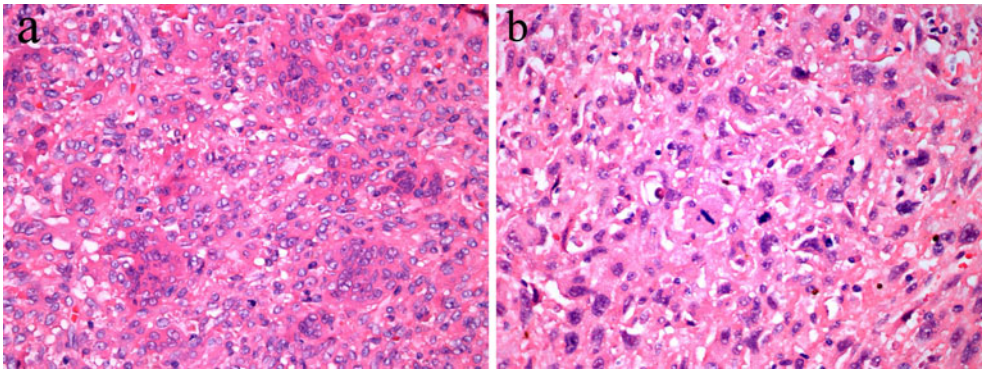

Fig. 5 SMGCTB (case 9). **a** The remnant giant call tumor from the initial lesion. **b** The high-grade undifferentiated pleomorphic sarcoma in the recurrent lesion

structure (Fig. 7), and one case invaded into the soft tissue and nerve fibers.

A remnant of conventional GCTB was found in four of 11 cases (Fig. 5a), suggesting the diagnosis of SMGCT. In cases without GCTB areas, the combination of malignant features in the recurrent lesion with the histopathology of the original conventional CGTB justified the diagnosis of SMGCTB. SMGCTB can occur after surgery or radiation therapy. In our hospital, radiation therapy was not used, so all of our 12 SMGCTB cases occurred without irradiation (Fig. 8).

Prognosis

The patients had been followed up for 8 to 221 months. One patient with PMGCTB had developed lung metastasis but is alive after 8 months follow-up. The remaining four patients with PMGCTB showed no evidence of recurrence. One patient with SMGCTB died of UPS. Four patients with SMGCTB developed lung metastasis, of whom three patients died. The remaining seven patients with SMGCTB showed no evidence of recurrence (Fig. 9).

Table 3 Antibodies used for immunohistochemical staining

Antigen	Antibody	Source	type	Dilution
p53	D0-7	Leica	Monoclonal antibody	1:100
p16	G175-405	Zymed	Monoclonal antibody	working fluid
vimentin	V9	Leica	Monoclonal antibody	1:500
desmin	ZC18	Zymed	Monoclonal antibody	Working fluid
CD68	PG-MI	Zymed	Monoclonal antibody	1:400
SMA	1A4	DAKO	Monoclonal antibody	1:300
Myogenin	F5D	DAKO	Monoclonal antibody	1:200

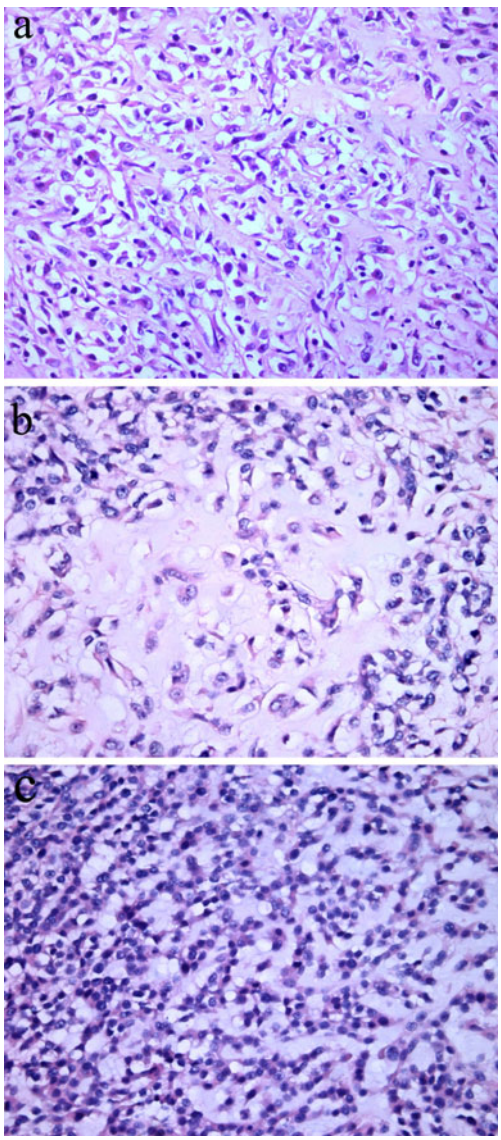

Fig. 6 SMGCTB (case 14). **a** The typical osteosarcoma structure. **b** Some areas show the chondrosarcoma features with mucoid chondroid matrix. **c** Densely arranged small cells without definite differentiation

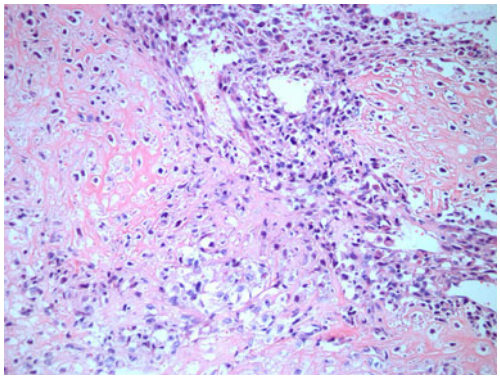

Fig. 7 SMGCTB (case 12). The osteosarcoma with aneurysmal bone cyst structure

Discussion

GCTB was originally described by Jaffe et al. and Lichtenstein et al. They classified GCTB into three categories: grade I (benign) without appreciable atypia of stromal cells, few mitoses, none abnormal; grade II (intermediate) with stromal cells showing only slight or more marked atypia, but not enough to justify a diagnosis of malignancy; and grade III (malignant) with obvious features of malignancy [7, 8]. However, this grading system is difficult to apply in practice and is unable to predict the clinical behavior and prognosis of this tumor [9]. Thus, this grade system is not used any more.

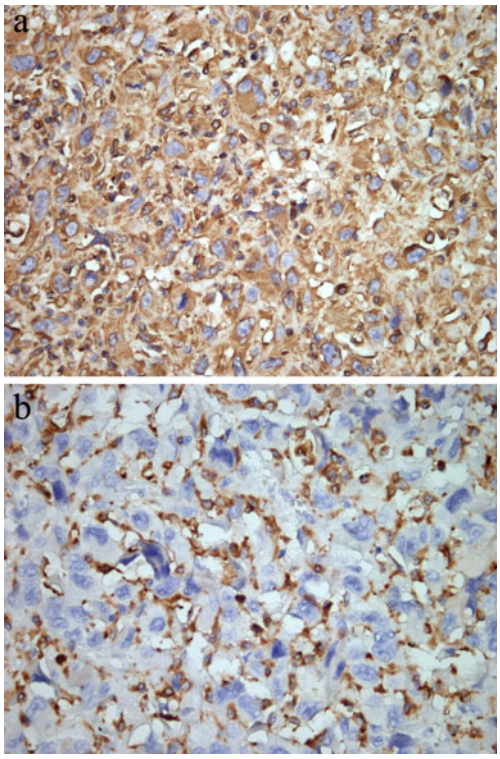

Fig. 8 Expression of vimentin (**a**) and CD68 (**b**) in SMGCTB

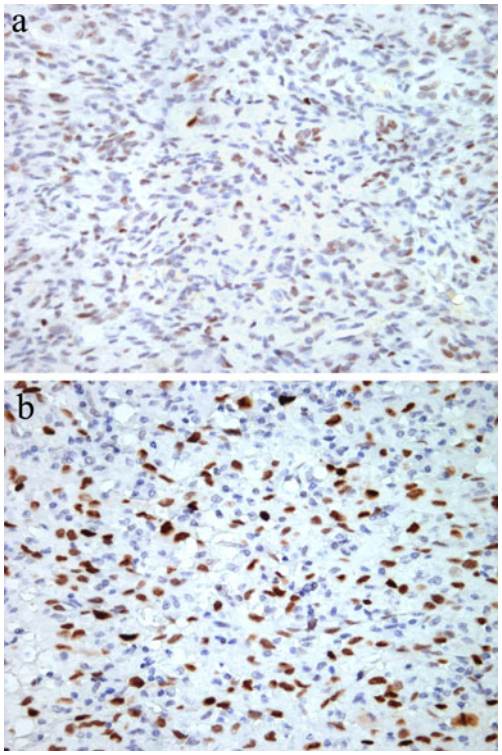

Fig. 9 Expression of p53 in GCTB (**a**) and SMGCTB (**b**)

In Jaffe's grade system, grade III represents malignant GCTB. The nomenclature and diagnostic criteria of malignant GCTB were further elaborated by Hutter et al. and Dalin et al. [10, 11]: Malignant GCTB is a sarcoma either in a pre-existing GCTB or in conjunction with it. Their term malignant GCTB included several types of giant-cell-rich tumor, such as osteosarcoma, UPS, metastatic or recurrent GCTB, and de novo malignant transformation of formerly conventional GCTB [3, 12]. To better describe malignant GCTB, Unni [2] introduced the name "malignancy in giant cell tumor" and subdivided it into primary and secondary malignancy in GCTB. The PMGCTB are those lesions in which a high-grade sarcoma component is present de novo in conjunction with GCTB, while SMGCTB is a high-grade sarcoma occurring as a recurrent lesion at the site of previously treated GCTB. According to this definition, PMGCTB and SMGCTB must include a high-grade sarcoma component. Some lesions need to be differentiated from MGCTB. Some features of GCTB do not justify a diagnosis of MGCTB. This can be pseudoanaplasia in the GCTB [22]. In addition, hemorrhage and necrosis are not uncommon in GCTB. The mononuclear stromal cells adjacent to the hemorrhage and necrosis show mild nuclear atypia, with enlarged and hyperchromatic or condensed hyperchromatic nuclei because of pyknosis. In some areas, only densely arranged mildly atypical spindle cells occur without giant cells, features insufficient to classify the lesion as malignant (similar to grade II as Jaffe described). Mitotic activity may

be increased but without pathological mitosis. None of these features justify classification of the lesion as malignant. Reactive bone formation is often found at the border of the tumor. It is more regular and mature than malignant osteoid, and it is surrounded by mature osteoblasts, features that help to distinguish them from osteosarcoma cells. Furthermore, MGCTB needs to be differentiated from other malignant tumors containing giant cells such as osteosarcoma and UPS. Sufficient sampling to explore the GCTB features is helpful to distinguish it from the PMGCTB and other malignant tumors. The key points to differentiate between SMGCTB and other malignant tumors are the GCTB history and the recurrence information.

Histologically, in MGCTB, the reported sarcoma types include fibrosarcoma [15, 16], osteosarcoma [17, 18], UPS [19], and undifferentiated sarcoma [20]. In our cases, the malignant components included fibrosarcoma, osteosarcoma (one case with undifferentiated component), and UPS.

In SMGCTB, the original diagnosis is GCTB, but the recurrent secondary tumor is malignant. In some cases, residual giant cell tumor elements can also be found, justifying a diagnosis of SMGCTB. In other cases, the patient's hospital history needs to be investigated to make the diagnosis of SMGCTB. In our cases, osteosarcoma was the major malignant tumor type. Sakkers et al. [21] proposed a theory about the malignant transformation of GCTB treated by curettage and bone grafting, stating that in this situation, the reparative proliferation occurring at the border of the dead bone might serve as a nidus for the formation of a malignant tumor. Currently, curettage and bone grafting constitute the routine surgical treatment of GCTB, and this may also be the element that favors malignant transformation.

Regarding the immunophenotype, the giant cells express RANK, CD51, and CD33 but are negative for CD14. The mononuclear cells express RANK, CD51, CD33, and CD14 [26, 27]. These cells are believed to derive from blood monocyte-macrophage lineage cells and infiltrate the tumor by chemotactic factors secreted by spindle-shaped stromal cells [28, 29]. GCTB is frequently regarded as a polyclonal tumor. Cytogenetically, telomeric associations are the most common chromosomal aberrations [30], but other genetic alterations have been reported. Moskovszky et al. found an elevated number of individual-cell aneusomies in recurrent GCTB compared with nonrecurrent cases. Eusomic polysomy has been seen in several tetraploid nonrecurrent cases, and balanced aneusomy has been found more frequently in diploid recurrent than in diploid nonrecurrent cases. These findings suggest that chromosomal abnormalities superimposed on telomeric associations might be responsible for the aggressive behavior of GCTB [31]. The expression of proteins involved in cell cycle regulation/oncogenesis, such as p53, p63, ki-67, cyclinD1, or Bcl-2, are not predictive for the clinical behaviour of GCTB [32]. We found the expression of p53 in UPS stronger than that in original GCTB, which suggests that it may play a role in the malignant transformation of GCTB.

Clinical and radiographic information are of limited value for the diagnosis of MGCTB, especially for PMGCTB. According to Compannacci et al. [13] radiographic features allow grading of the GCTB as three types: quiescent (type I), active (type II), and aggressive (type III). Clinically aggressive behavior of GCTB has suggested a surgical staging system with stages 1–3, respectively, representing the clinically latent, active, and aggressive forms of GCTB [14]. However, these stages do not correspond to histological benign or malignant features. In our study, five cases were diagnosed as PMGCTB by histology, while the clinical and radiographic features suggested a diagnosis of benign GCTB.

As in another study, we found MGCTB often to involve the distal femur and tibia [23]. The preponderance of gender is controversial in different cohorts. In our study and in another report [4], there is a male preponderance, but in other reports, a female preponderance was described [23]. The age distribution in MGCTB reports also varies. In our study, the mean age was younger than what was reported earlier [4].

The prognosis of MGCTB is still indefinite because of its rareness and short follow-up of MGCTB. Most reports consider the prognosis as poor, and most of the patients die rapidly [24]. Anract et al. [6] reported poor prognosis of MGCTB with a 5-year survival of 50%, despite the combination of surgery and chemotherapy. Similar to the report of Nascimento et al. [25], we found PMGCTB to have a better prognosis than SMGCTB. However, Anract et al. [6] observed equally poor outcomes in PMGCTB and SMGCTB.

In summary, we report a series of cases of MGCTB and describe its histological characteristics. Because of its rareness, the diagnosis should be made carefully, and the lesion should be differentiated from other primary malignant sarcomas. Genetic abnormalities and other factors related to malignant transformation should be further investigated.

Conflict of interest There is no conflict of interest in our study.

References

1. Reed R, Bareyce SS, Sciot R (2002) Giant cell tumour. In: Fletcher CD, Unni KK, Mertens F (eds) World Health Organization Classification of Tumours. Pathology and Genetics of Tumours of Soft Tissue and Bone. IARC, Lyon, pp 309–312

2. Unni KK (1996) Dalin's bone tumors-general aspects and data on 11,087 cases, 5th edn. Lippincott-Raven, Philadelphia, pp 263–287
3. Marui T, Yamamoto T, Yoshihara H et al (2001) De novo malignant transformation of giant cell tumor of bone. Skeletal Radiol 30:104–108
4. Bertoni F, Bacchini P, Staals EL (2003) Malignancy in giant cell tumor of bone. Cancer 97:2520–2529
5. Rock MG, Sim FH, Unni KK et al (1986) Secondary malignant giant-cell tumor of bone. Clinicopathological assessment of nineteen patients. J Bone Joint Surg Am 68:1073–1079
6. Anract P, De Pinieux G, Cottias P et al (1998) Malignant giant-cell tumours of bone. Clinico-pathological types and prognosis: a review of 29 cases. Int Orthop 22:19–26
7. Jaffe HL, Lichtenstein L, Portis RB (1940) Giant cell tumor of bone. Its pathologic appearance, grading, supposed variants and treatment. Arch Pathol 30:993–1031
8. Lichtenstein L (1972) Bone tumors, 4th edn. Mosby, St. Louis, pp 135–165
9. Sanerkin NG (1980) Malignancy, aggressiveness, and recurrence in giant cell tumor of bone. Cancer 46:1641–1649
10. Dahlin DC, Cupps RE, Johnson EW Jr (1970) Giant-cell tumor: a study of 195 cases. Cancer 25:1061–1070
11. Hutter RV, Worcester JN Jr, Francis KC et al (1962) Benign and malignant giant cell tumors of bone. A clinicopathological analysis of the natural history of the disease. Cancer 15:653–690
12. Mirra MJ (1989) De novo malignant transformation of giant cell tumor of bone. Bone tumous: clinical, radiologic, and pathologic correlations. Lea & Febiger, Philadelphia, pp 941–1020
13. Campanacci M, Baldini N, Boriani S et al (1987) Giant-cell tumor of bone. J Bone Joint Surg Am 69:106–114
14. Present D, Bertoni F, Hudson T et al (1986) The correlation between the radiologic staging studies and histopathologic findings in aggressive stage 3 giant cell tumor of bone. Cancer 57:237–244
15. Boriani S, Sudanese A, Baldini N et al (1986) Sarcomatous degeneration of giant cell tumors. Ital J Orthop Traumatol 12:191–199
16. Gitelis S, Wang JW, Quast M et al (1989) Recurrence of a giant-cell tumor with malignant transformation to a fibrosarcoma twenty-five years after primary treatment. A case report. J Bone Joint Surg Am 71:757–761
17. Kenan S, Abdelwahab IF, Klein MJ et al (1995) Case report 863. Osteosarcoma associated with giant cell tumor. Skeletal Radiol 24:55–58
18. Brien EW, Mirra JM, Kessler S et al (1997) Benign giant cell tumor of bone with osteosarcomatous transformation ("dedifferentiated" primary malignant GCT): report of two cases. Skeletal Radiol 26:246–255
19. Ortiz-Cruz EJ, Quinn RH, Fanburg JC et al (1995) Late development of a malignant fibrous histiocytoma at the site of a giant cell tumor. Clin Orthop Relat Res 318:199–204
20. Zhu XZ, Steiner GC (1990) Malignant giant cell tumor of bone: malignant transformation of a benign giant cell tumor treated by surgery. Bull Hosp Jt Dis Orthop Inst 50:169–176
21. Sakkers RJ, van der Heul RO, Kroon HM et al (1997) Late malignant transformation of a benign giant-cell tumor of bone. A case report. J Bone Joint Surg Am 79:259–262
22. Layfield LJ, Bentley RC, Mirra JM (1999) Pseudoanaplastic giant cell tumor of bone. Arch Pathol Lab Med 123:163–166
23. Domovitov SV, Healey JH (2010) Primary malignant giant-cell tumor of bone has high survival rate. Ann Surg Oncol 17:694–701
24. Karamanakos PN, Jaaskelainen JE, Alafuzoff I et al (2010) Malignant giant cell tumor in the posterior fossa of a neonate. J Neurosurg Pediatr 5:277–282
25. Nascimento AG, Huvos AG (1979) Primary malignant giant cell tumor of bone: a study of eight cases and review of the literature. Cancer 44:1393–1402
26. Forsyth RG, De Boeck G, Baelde JJ et al (2009) CD33(+)CD14(−) Phenotype is characteristic of multinuclear osteoclastlike cells in giant cell tumor of bone. J Bone Miner Res 24:70–77
27. Maggiani F, Forsyth R, Hogendoorn PCW et al (2011) The immunophenotype of osteoclasts and macrophage polykaryons. J Clin Pathol 64:701–705
28. Zheng MH, Robbins P, Xu J et al (2001) The histogenesis of giant cell tumour of bone: A model of interaction between neoplastic cells and osteoclasts. Histol Histopathol 16:297–307
29. Lau YS, Sabokbar A, Gibbons CL et al (2005) Phenotypic and molecular studies of giant cell tumours of bone and soft tissue. Hum Pathol 36:945–954
30. Forsyth RG, De Boeck G, Bekaert S et al (2008) Telomere biology in giant cell tumour of bone. J Pathol 214:555–563
31. Moskovszky L, Szuhai K, Krenács T et al (2009) Genomic instability in giant cell tumor of bone. A study of 52 cases using DNA ploidy, relocalization FISH, and array-CGH analysis GENES. Chromosomes Cancer 48:468–479
32. Alberghini M, Kliskey K, Krenacs T et al (2010) Morphological and immunophenotypic featuresof primary and metastatic giant cell tumour of bone. Virchows Arch 456:97–103

Virchows Arch (2012) 460:335–342
DOI 10.1007/s00428-012-1206-2

ORIGINAL ARTICLE

Dedifferentiated peripheral chondrosarcoma: a clinicopathologic, immunohistochemical, and molecular analysis of four cases

Alessandro Franchi · Gianna Baroni · Iacopo Sardi · Laura Giunti · Rodolfo Capanna · Domenico Campanacci

Received: 14 November 2011 / Revised: 17 January 2012 / Accepted: 31 January 2012 / Published online: 16 February 2012
© Springer-Verlag 2012

Abstract Peripheral dedifferentiated chondrosarcoma (DCS) is an exceedingly rare aggressive surface bone neoplasm in which a high-grade sarcoma arises within an osteochondroma. Four such examples were identified in our files, representing 11.1% of all DCS treated at our hospital in the years 1995–2010, and were the object of the present study. The patients were two men and two women ranging in age between 30 and 64 years, with tumors located in the pelvis ($n = 2$), in the scapula ($n = 1$), and the tibia ($n = 1$). Radiologically, there was evidence of a preexisting osteochondroma associated with aggressive osteolytic areas at the base and periphery of the exostosis, extending to the bone segment of origin and to the soft tissues. Immunohistochemical analysis of cell cycle regulators showed consistent loss in the expression of p16 and overexpression of cyclin D1, and to a lesser extent of RB and p53, in the anaplastic compartments of peripheral DCS in comparison with the well-differentiated cartilaginous components, while no significant expression of MDM2 was observed in any of the cases studied. Moreover, PDGFRα was absent in both tumor components, and PDGF-Rβ was strongly and diffusely positive in all the cases. Finally, no mutations were identified in exons 4–9 of the TP53 gene in both cases, showing positivity for p53 in the anaplastic component. In conclusion, our study shows that alterations of genes implicated in the regulation of the G1 to the S phase cell cycle checkpoint contribute to the process of dedifferentiation in peripheral secondary chondrosarcoma (CS), although the molecular mechanisms seem at least in part to differ from those involved in the process of dedifferentiation of central CS. PDGFRβ could represent a potential target for treatments with receptor tyrosine kinase inhibitors in peripheral DCS.

Keywords Dedifferentiated chondrosarcoma · Peripheral · Immunohistochemistry · Cell cycle regulators · p53 gene · PDGF receptors

A. Franchi (✉) · G. Baroni
Division of Anatomic Pathology, Department of Critical Care Medicine and Surgery, University of Florence Medical School,
Viale G.B. Morgagni 85,
50134 Florence, Italy
e-mail: franchi@unifi.it

I. Sardi · L. Giunti
Division of Onco-Haematology,
Azienda Ospedaliera Universitaria Meyer,
Florence, Italy

R. Capanna · D. Campanacci
Division of Orthopedic Oncology,
Azienda Ospedaliera Universitaria Careggi,
Florence, Italy

Introduction

Dedifferentiated chondrosarcoma (DCS) is a well-known entity defined as a well-differentiated cartilage tumor juxtaposed with abrupt transition to a high-grade non-cartilaginous sarcoma. The process of dedifferentiation usually takes place in central chondromas or low-grade secondary chondrosarcoma (CS), but in rare instances, a high-grade non-cartilaginous sarcoma may originate in a low-grade peripheral CS secondary to a preexisting osteochondroma [1, 2]. The incidence of peripheral DCS has ranged between 8.9% and 13.7% of all DCS [1, 3], and they approximately represented 5.5% of all cases of CS arising in preexisting exostoses [2]. Tumors occurred both in patients with multiple hereditary exostoses (multiple osteochondromas) or in

preexisting osteochondromas, the most common location being the pelvis [2]. Dedifferentiation takes place either synchronously, when both components are present side by side in the same lesion, or metachronously, when a high-grade sarcoma is diagnosed at the same site of a previously excised osteochondroma or secondary peripheral CS [2]. Overall, the prognosis is poor, although a better cure rate has been obtained with a combination of surgery and chemotherapy [2].

In the attempt to further characterize the clinicopathologic features of these rare tumors, here, we describe the features of four cases of peripheral DCS arising in osteochondroma. Moreover, we carried out an analysis of the status of a number of regulators involved in the G1-S checkpoint, including p53, MDM-2, cyclin D1, p16, and RB oncoproteins, to determine whether aberrations of these regulatory pathways may be involved in the process of dedifferentiation in these tumors. Finally, we studied the expression of PDGF receptors α and β, which have recently been identified as possibly implicated in the growth of CS, in both tumor components.

Materials and methods

Patients

Thirty-six patients diagnosed with DCS in the years 1995–2010 were identified in the files of the Section of Anatomic Pathology of the Department of Critical Care Medicine and Surgery, University of Florence. Of these, four tumors (11.1%) had developed in a preexisting osteochondroma. Patient charts, radiographs, histological slides, and paraffin blocks were retrieved in each case. Patient details are summarized in Table 1.

Immunohistochemistry

A panel of well-characterized antibodies was used, which included mouse monoclonal antibodies to p53 (clone DO-7, pre-diluted; Ventana Medical Systems, Inc., Tucson, AZ), MDM-2 (clone IF2; Histo-Line Laboratories, Milan, Italy), p16 (clone 16P04, pre-diluted; Cell Marque), RB (clone 1F8, 1:50 dilution; NeoMarkers, Fremont, CA), cyclin D1 (clone SP4, pre-diluted; Ventana Medical Systems, Inc.), PDGFRα (sc-338, 1:200 dilution; Santa Cruz Biotechnology, Santa Cruz, CA), and PDGFRβ (sc-339, 1:100 dilution; Santa Cruz Biotechnology).

Immunohistochemistry was performed using a Ventana BenchMark® XT automated staining system (Ventana Medical Systems). For antigen retrieval, slides were heated with Cell Conditioning Solution 1 (CC1) for 30 min. Endogenous biotin was blocked with the appropriate kit. Primary antibodies against p53, p16, and cyclin D1 were then applied for 32 min at 37°C in a BenchMark® XT stainer and revealed with the iVIEW DAB detection kit, yielding a brown reaction product. After the staining run was complete, the slides were removed from the autostainer, counterstained with hematoxylin, dehydrated, and mounted with permanent mounting medium.

For RB, PDGFRα, and PDGFRβ immunohistochemical analyses, antigen retrieval was routinely performed in thermostat bath, PT Link Dako, at 97°C with EDTA (pH 9.0) for 15 min. The sections were placed in the Dako Autostainer Link 48 (Dako, Glostrup, Denmark) and the primary antibodies then applied for 60 min at 20°C. Bound antibodies were visualized using the Envision™ FLEX and DAB with chromogen.

For negative controls, primary antibodies were substituted with PBS.

TP53 gene sequencing

Ten serial sections (thickness, 5 μm) were obtained from one paraffin-embedded tissue block from the lesions of patients 2 and 4. Tissue fragments were microdissected using stereomicroscopic visualization from blank deparaffinized slides in order to separate the chondrogenic and

Table 1 Summary of the clinicopathologic features of four cases of dedifferentiated peripheral chondrosarcomas

Patient	Age	Sex	Site	Chondrogenic component	Anaplastic component	Treatment	Outcome
1	64	F	Proximal tibia	G2	Osteosarcoma	Resection and reconstruction with modular prosthesis	Lost at follow-up
2	33	M	Pelvis (iliac wing)	G1	Undifferentiated pleomorphic sarcoma	Wedge resection without reconstruction	Lost at follow-up
3	30	F	Pelvis (anterior pelvic arch)	G1	Undifferentiated pleomorphic sarcoma	Anterior pelvic arch resection without reconstruction. Local recurrence treated with resection and modular prosthesis	Local recurrence on femoral head after 8 months. Synchronous inguinal lymph node and L4 metastasis
4	55	M	Scapula	G1	Undifferentiated pleomorphic sarcoma	Partial scapular resection	Multiple local recurrences and pulmonary metastases after 4 months

dedifferentiated areas of the tumor. Post-microdissected slides were evaluated to confirm accurate sample microdissection. DNA was extracted from the microdissected paraffin-embedded tissues using a manual protocol [4]. Polymerase chain reaction (PCR) primers for exons 4–9, encoding the DNA-binding domain of the TP53 gene, were designed to obtain fragments of no more than 300 bp. Amplification reactions were performed with 60 ng of DNA, 10 ng of each primer, 200 μM dNTPs, 1× PCR reaction buffer, and 2.5 U Taq polymerase in a final volume of 25 μl. PCR products were sequenced directly on both strands using an ABI PRISM 3130XL Genetic Analyzer (Perkin-Elmer Applied Biosystems, Foster City, CA, USA).

Results

Clinical features

The clinical features of the patients, including treatment and follow-up, are summarized in Table 1. The patients were two men and two women ranging in age between 30 and 64 years. No patient was affected by multiple hereditary exostoses (multiple osteochondromas). Three patients reported a mass present for several years (4, 9, and 30, respectively), with recent (2–24 months) increase in dimension and onset of pain in one instance. Two lesions were located in the pelvis, one in the scapula, and one in the tibia. Radiologically, there was evidence of a preexisting osteochondroma consisting of a large lesion arising on the bone surface with irregular peripheric calcifications and ossifications, associated with aggressive osteolytic areas at the base and periphery of the exostosis, extending to the bone segment of origin. A soft tissue mass could be detected by CT scan or MRI (Fig. 1).

Histopathology

Histologically, all tumors had the characteristic biphasic pattern of dedifferentiated CS and appeared to originate from a preexisting osteochondroma (synchronous dedifferentiation). The cartilaginous component consisted of areas of well-differentiated grade 1 CS in three lesions and grade 2 in the remaining one, with diffuse aspects of calcification and ossification. The dedifferentiated component showed features of a high-grade fibroblastic osteosarcoma in patient 1 (Fig. 2), while it consisted of a high-grade undifferentiated pleomorphic sarcoma in the other three cases (Figs. 3, 4 and 5).

Immunohistochemistry

The results of the immunohistochemical studies are summarized in Table 2 and illustrated in Fig. 6.

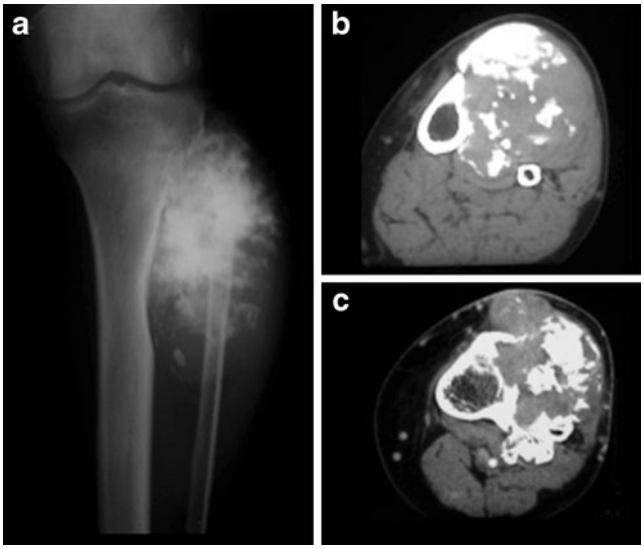

Fig. 1 Sixty-four-year-old woman (patient 1) with history of proximal tibia osteochondroma. She complained of recent progressive swelling and pain. **a** Antero-posterior radiographic view showed a cauliflower-shaped mass, with ossification and calcifications, arising from the proximal tibia and scalloping the lateral cortex of the tibia from outside. **b**, **c** The CT scan confirmed the base of implant of the preexisting osteochondroma on the tibia showing the typical extroflession of the cortex. Diffuse and irregular osteolysis of the ossifications within the mass, aggressive erosion of the external surface of the tibial cortex, and the presence of a soft tissue mass were signs of aggressiveness consistent with dedifferentiation

Overall, dedifferentiation was consistently accompanied by the loss of p16 nuclear expression since this protein was expressed in the chondrogenic component but not in the anaplastic component in all the cases. In addition, RB positivity was observed in the anaplastic component in three of four cases, while this oncoprotein was not detectable in the chondrogenic areas. Diffuse cyclin D1 nuclear immunoreactivity was present in the high-grade anaplastic component of all cases, while only one lesion displayed focal positivity in well-differentiated cartilaginous areas. On the other hand, there was a limited difference in the expression of p53 in the two components since it was detected in the anaplastic component in only two of four cases, while the chondrosarcomatous areas were negative. Finally, no significant expression of MDM2 was observed in any of the cases studied. While PDGFRα was absent in both tumor components of dedifferentiated peripheral chondrosarcomas, PDGFRβ was strongly and diffusely positive in all the cases.

For comparison, we immunostained a series of ten central conventional chondrosarcomas (six grade 1, three grade 2, and one grade 3). All these tumors stained diffusely for p16, RB1, PDGFRα, and PDGFRβ, while p53 and cyclin D1 were expressed only in one grade 2 and in the grade 3 chondrosarcomas. MDM2 was negative in all cases.

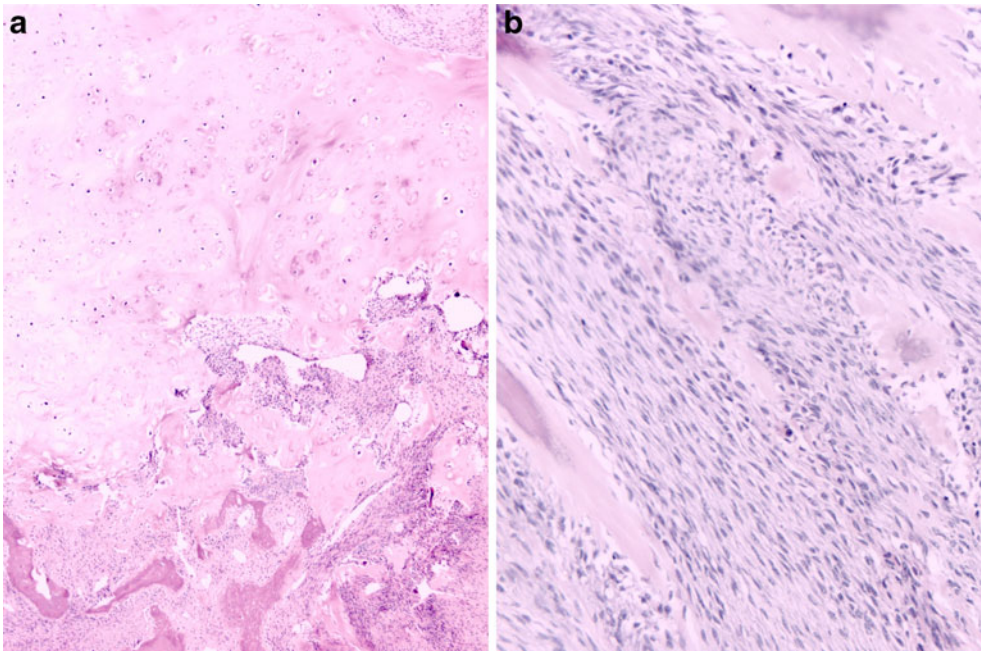

Fig. 2 In patient 1, the high-grade component of the lesion showed histological features of fibroblastic osteosarcoma. **a** Low-power view of the lesion with both low-grade and high-grade components. **b** High-power view of the osteosarcomatous component

TP53 gene status

Both cases showing positivity for p53 in the anaplastic component were analyzed for the status of exons 4–9 of the TP53 gene. In case 4, we were able to analyze both the chondrogenic and the anaplastic components, while in case 2 we succeeded in amplifying and screening mutations only in samples from the anaplastic component. PCR amplification and subsequent DNA sequencing revealed no mutations in the exons examined.

Discussion

The present report confirms that approximately 10% of DCS occur at the bone surface, developing in a peripheral CS ex-osteochondroma. The most commonly affected sites are the pelvis and the long bones of the lower leg (femur and tibia), reflecting the distribution of secondary peripheral CS [1, 2]. The age at presentation is lower than in central DCS, and the most common presenting sign is a recent increase in a mass that had been present for several years. At imaging, the typical features of a peripheral CS are associated with signs of local aggressiveness consisting in diffuse and irregular osteolysis within the mass or at the base of implant and the presence of tumor extension in the soft tissues.

At variance with central DCS, the high-grade component of peripheral DCS more often showed a histological appearance of a high-grade spindle cell and pleomorphic sarcoma, variably classified as fibrosarcoma or malignant fibrous histiocytoma. However, immunohistochemical analysis demonstrated the frequent expression of myogenic markers, including actins and desmin, in the high-grade anaplastic component [5].

The development of metastatic disease is a frequent event which is associated with a dismal prognosis. The treatment of choice is surgery with wide margins, but some benefit in overall survival has been reported when patients presenting with localized disease were treated with a combination of surgery and chemotherapy [2].

The biology of the process of dedifferentiation occurring in CS has been studied more in depth in central lesions, while only limited information is available regarding the molecular characterization of peripheral DCS. Inactivation of the EXT1 and/or the EXT2 genes is a well-known event in the development of osteochondromas [6], but it is likely not involved in the pathogenesis of secondary peripheral CS [7]. An immunohistochemical analysis of cell signaling pathways that are known to have an important role in normal chondrocyte proliferation showed that the FGF signaling pathway is more frequently active than in the chondrogenic component of conventional secondary peripheral CS, whereas PTHLH signaling seems to be low/downregulated [5]. This suggests that these changes may be of importance in the transformation of CS toward DCS. Moreover, a comparison between the chondrogenic and anaplastic components showed relevant differences in the expression of molecules related to cell cycle regulation, such as cyclin D1 and p53 [5]. Abnormalities in the checkpoints controlling cell cycle contribute to tumorigenesis and progression in several human malignancies; therefore, in the present study, we further explored the status of other players involved in the control of the G1/S checkpoint. We observed a consistent difference in the

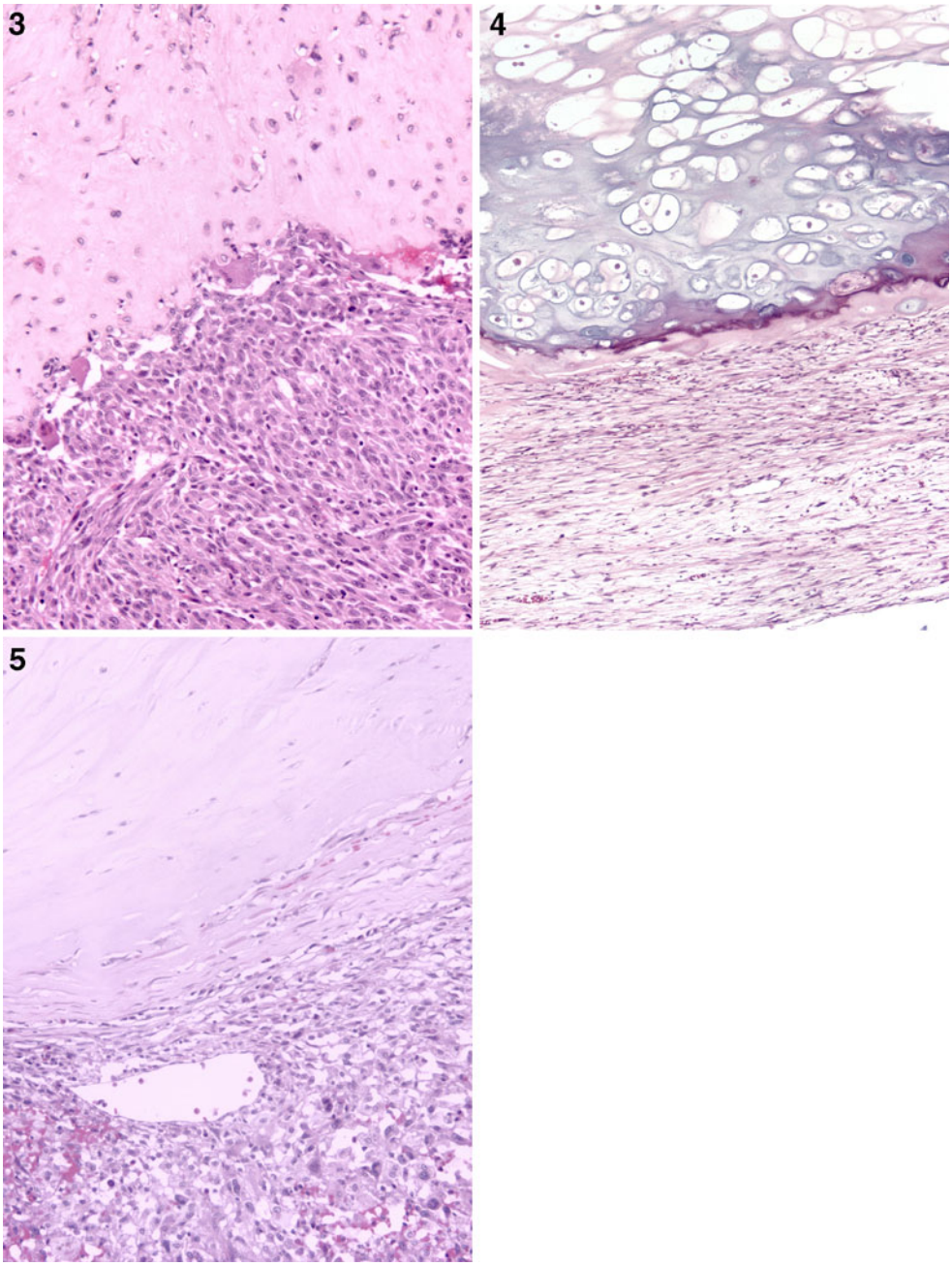

Figs. 3–5 In the remaining patients, the tumor consisted of a low-grade well-differentiated chondrosarcoma (*top*) and a high-grade pleomorphic sarcoma (*bottom*). There is a sharp separation between the two components

expression of p16 and cyclin D1, and to a lesser extent of RB and p53, between the well-differentiated and anaplastic compartments of peripheral DCS.

According to our results and to previous reports, it appears that the molecular abnormalities present in peripheral DCS differ from those occurring in central DCS.

Table 2 Summary of the results of the immunohistochemical studies

Pt	P53		MDM-2		P16		RB		Cyclin D1		PDGF-R α		PDGF-R β	
	CC	AC	CC	AC	CC	AC	CC	AC	CC	AC	CC	AC	CC	AC
1	−	−	−	−	+	−	−	−	−	+	−	−	+	+
2	−	+	−	−	+	−	−	+	−	−	−	−	+	+
3	−	−	−	−	+	−	−	+	−	+	−	−	+	+
4	−	+	−	−	+	−	−	+	−	+	−	−	+	+

CC chondrogenic component, *AC* anaplastic component

Indeed, several studies have shown that the process of dedifferentiation taking place in central CS is consistently accompanied by an alteration of the p53 pathway. Strong nuclear immunostaining has been observed in the high-grade non-cartilaginous component, but not in the low-grade cartilaginous one [8–10]. In addition, point mutations of the p53 gene have been identified in the high-grade component of central DCS, and this has also been associated with LOH at 17p [8, 10–12]. In one case, a p53 mutation consisting of a 6-bp deletion starting at the second base of codon 250 in exon 7 was detected in both the cartilaginous and the anaplastic components [11].

At partial variance with these findings, in the present study, we observed that two of the four tumors (50%) showed immunohistochemical positivity in the anaplastic component, but molecular analysis did not reveal any alteration of exons 4–9 of the TP53 gene in these cases. A discordance between the results of immunohistochemical analysis showing p53 positivity and those of DNA analysis showing no detectable gene alterations has been repeatedly reported with variable frequency in bone and soft tissue sarcomas [13–16]. Several mechanisms are known to be involved in the stabilization of wild-type p53 protein resulting in nuclear accumulation and immunohistochemical

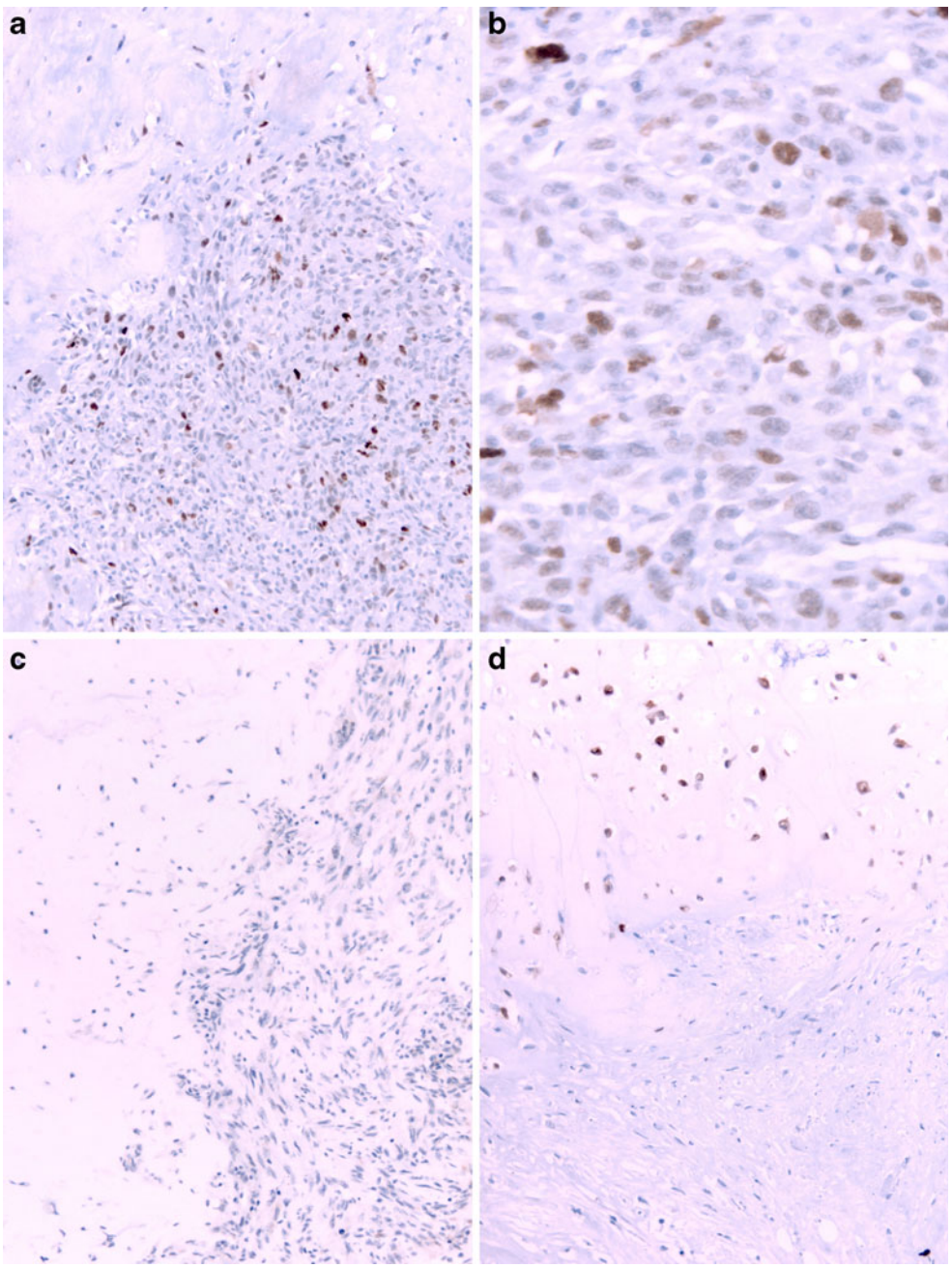

Fig. 6 Representative images of the immunohistochemical stains from case 4. Nuclear positivity for p53 is visible only in the anaplastic component of the tumor (*bottom*), while the well-differentiated chondrosarcomatous areas are negative (*top*) (**a**). A higher power detail of the immunostaining for p53 in the high-grade component is shown in **b**. Similarly, RB (**e**) and cyclin D1 (**f**) were present in the anaplastic component of the lesion (*bottom*), while the well-differentiated component was negative (*top*). P16 (**d**) was detectable only in the well-differentiated chondrosarcomatous areas (*top*) and not in the high-grade sarcaomatous areas (*bottom*). MDM2 (**c**) and PDGFRα (**g**) were negative in both components, while PDGFRβ was intensely and diffusely positive (**h**)

Fig. 6 (continued)

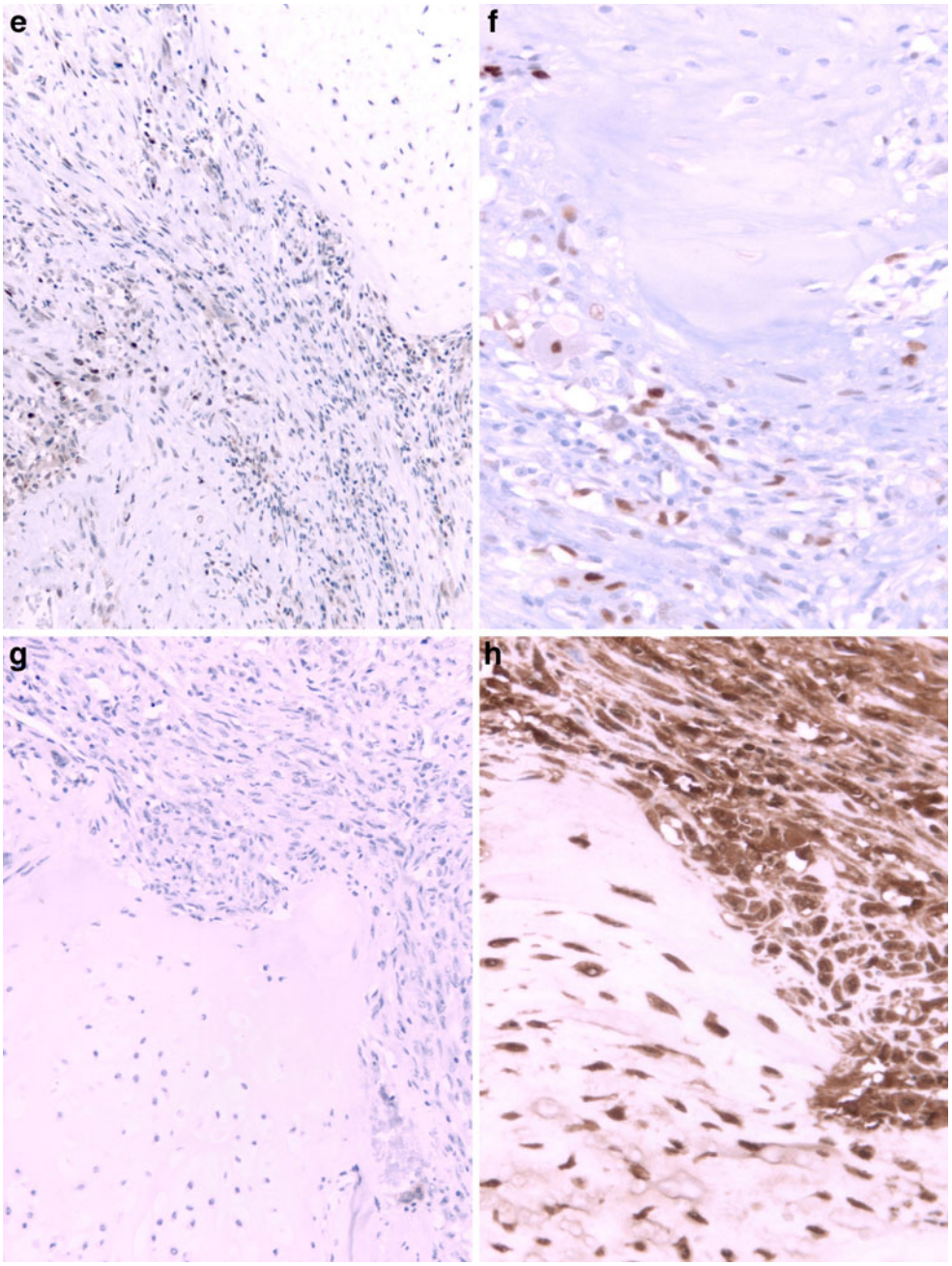

positivity, including DNA damage in cells and binding to viral oncogene products or to the MDM2 gene product [17]. This latter mechanism, however, seems to be unlikely in peripheral DCS since we did not observe any significant immunoreactivity for MDM2 in our series. Therefore, although the number of cases analyzed is small, the data obtained indicate that a molecular alteration of the p53 gene is unlikely to be involved in the growth and dedifferentiation of peripheral CS arising in osteochondromas. However, we cannot exclude the presence of TP53 mutations outside exons that were screened in this study.

Other molecular abnormalities previously identified in central DCS include genetic and epigenetic alterations of other genes involved in cell cycle control, including the RB p16INK4, FHIT, and E-cadherin genes [18, 19]. Interestingly, p16INK4 promoter methylation was observed in both the low-grade and the high-grade compartments of central DCS, while in our study, p16 expression was maintained in the well-differentiated component of the tumor. Therefore, inactivation of cell cycle genes involved in the G1/S arrest seems to be an early event in the development of central DCS, while it appears to occur later in the process of dedifferentiation of peripheral CS.

Recent studies [20, 21] have investigated the status of platelet-derived growth factor (PDGF) receptors and their ligands in conventional CS as they could represent possible

candidates for molecular therapies with receptor tyrosine kinase (RTK) inhibitors. The immunohistochemical and biochemical analyses showed that CS co-expressed PDGFRα and PDGFRβ, with the latter showing greater protein expression and phosphorylation levels. Conversely, no activating mutations were found [21]. These findings are in keeping with the existence of an autocrine/paracrine loop which could play an important role in the development of conventional central CS. To our knowledge, the status of PDGFRs has not been previously investigated in DCS. In the present study, all four cases of peripheral DCS were intensely and diffusely positive for PDGFRβ in both components, while PDGFRα was not detectable. These findings may suggest that PDGFRβ could represent a potential target for treatments with RTK inhibitors in peripheral DCS.

In summary, our study shows that alterations of genes implicated in the regulation of the G1 to the S phase cell cycle checkpoint contribute to the process of dedifferentiation in peripheral secondary CS, although the molecular mechanisms seem at least in part to differ from those involved in the process of dedifferentiation of central CS.

Conflict of interest statement We declare that we have no conflict of interest.

References

1. Bertoni F, Present D, Bacchini P, Picci P, Pignatti G, Gherlinzoni F, Campanacci M (1989) Dedifferentiated peripheral chondrosarcomas. A report of seven cases. Cancer 63:2054–2059
2. Staals EL, Bacchini P, Mercuri M, Bertoni F (2007) Dedifferentiated chondrosarcomas arising in preexisting osteochondromas. J Bone Joint Surg Am 89:987–993
3. Frassica FJ, Unni KK, Beabout JW, Sim FH (1986) Dedifferentiated chondrosarcoma. A report of the clinicopathological features and treatment of seventy-eight cases. J Bone Joint Surg Am 68:1197–1205
4. Coombs NJ, Gough AC, Primrose JN (1999) Optimisation of DNA and RNA extraction from archival formalin-fixed tissue. Nucleic Acids Res 27:e12
5. Rozeman LB, de Bruijn IH, Bacchini P, Staals EL, Bertoni F, Bovée JV, Hogendoorn PC (2009) Dedifferentiated peripheral chondrosarcomas: regulation of EXT-downstream molecules and differentiation-related genes. Mod Pathol 22:1489–1498
6. Bovée JVMG, Cleton-Jansen AM, Wuyts W, Caethoven G, Taminiau AH, Bakker E, Van Hul W, Cornelisse CJ, Hogendoorn PC (1999) EXT mutation analysis and loss of heterozygosity in sporadic and hereditary osteochondromas and secondary chondrosarcomas. Am J Hum Genet 65:689–698
7. de Andrea CE, Reijnders CM, Kroon HM, de Jong D, Hogendoorn PC, Szuhai K, Bovée JV (2012) Secondary peripheral chondrosarcoma evolving from osteochondroma as a result of outgrowth of cells with functional EXT. Oncogene. doi:10.1038/onc.2011.311
8. Wadayama B, Toguchida J, Yamaguchi T, Sasaki MS, Yamamuro T (1993) p53 expression and its relationship to DNA alterations in bone and soft tissue sarcomas. Br J Cancer 68:1134–1139
9. Simms WW, Ordonez NG, Johnston D, Ayala AG, Czerniak B (1995) p53 expression in dedifferentiated chondrosarcoma. Cancer 76:223–227
10. Terek RM, Healey JH, Garin-Chesa P, Mak S, Huvos A, Albino AP (1998) p53 mutations in chondrosarcoma. Diagn Mol Pathol 7:51–56
11. Bovée JV, Cleton-Jansen AM, Rosenberg C, Taminiau AH, Cornelisse CJ, Hogendoorn PC (1999) Molecular genetic characterization of both components of a dedifferentiated chondrosarcoma, with implications for its histogenesis. J Pathol 189:454–462
12. Grote HJ, Schneider-Stock R, Neumann W, Roessner A (2000) Mutation of p53 with loss of heterozygosity in the osteosarcomatous component of a dedifferentiated chondrosarcoma. Virchows Arch 436:494–497
13. Cordon-Cardo C, Latres E, Drobnjak M, Oliva MR, Pollack D, Woodruff JM, Marechal V, Chen J, Brennan MF, Levine AJ (1994) Molecular abnormalities of mdm2 and p53 genes in adult soft tissue sarcomas. Cancer Res 54:794–799
14. Mousses S, McAuley L, Bell RS, Kandel R, Andrulis IL (1996) Molecular and immunohistochemical identification of p53 alterations in bone and soft tissue sarcomas. Mod Pathol 9:1–6
15. Yoo J, Lee HK, Kang CS, Park WS, Lee JY, Shim SI (1997) p53 gene mutations and p53 protein expression in human soft tissue sarcomas. Arch Pathol Lab Med 121:395–399
16. Taubert H, Würl P, Bache M, Meye A, Berger D, Holzhausen HJ, Hinze R, Schmidt H, Rath FW (1998) The p53 gene in soft tissue sarcomas: prognostic value of DNA sequencing versus immunohistochemistry. Anticancer Res 18:183–187
17. Momand J, Zambetti GP, Olson DC, George D, Levine AJ (1992) The mdm-2 oncogene product forms a complex with the p53 protein and inhibits p53-mediated transactivation. Cell 69:1237–1245
18. Yamaguchi T, Toguchida J, Wadayama B, Kanoe H, Nakayama T, Ishizaki K, Ikenaga M, Kotoura Y, Sasaki MS (1996) Loss of heterozygosity and tumor suppressor gene mutations in chondrosarcomas. Anticancer Res 16:2009–2015
19. Röpke M, Boltze C, Neumann HW, Roessner A, Schneider-Stock R (2003) Genetic and epigenetic alterations in tumor progression in a dedifferentiated chondrosarcoma. Pathol Res Pract 199:437–444
20. Sulzbacher I, Birner P, Trieb K, Mühlbauer M, Lang S, Chott A (2001) Platelet-derived growth factor-alpha receptor expression supports the growth of conventional chondrosarcoma and is associated with adverse outcome. Am J Surg Pathol 25:1520–1527
21. Lagonigro MS, Tamborini E, Negri T, Staurengo S, Dagrada GP, Miselli F, Gabanti E, Greco A, Casali PG, Carbone A, Pierotti MA, Pilotti S (2006) PDGFRalpha, PDGFRbeta and KIT expression/activation in conventional chondrosarcoma. J Pathol 208:615–623

Virchows Arch (2012) 460:343–352
DOI 10.1007/s00428-011-1187-6

ORIGINAL ARTICLE

Immunohistochemical marker panel differentiates between the three most common subtypes of renal cell carcinoma independent from histomorphologic criteria

B. Walter · A. Hartmann · F. Hofstädter · K. Junker · H. Moch · S. Bertz · S. Denzinger · W. Otto · M. Gajda · C. G. Stoehr

Received: 13 October 2011 / Revised: 7 December 2011 / Accepted: 20 December 2011 / Published online: 17 February 2012
© Springer-Verlag 2012

Abstract To develop a reliable immunohistochemical marker panel differentiating between the three most common renal cell carcinoma (RCC) subtypes without inclusion of histomorphologic criteria we investigated protein expression of vimentin, glutathione S-transferase alpha (GST-α), CD10, CD117 (C-KIT), carbonic anhydrase 2 (CAII), parvalbumin, alpha-methyl-CoA-racemase (AMACR), and cytokeratin-19 (CK 19) in 65 age and stage matched trios of clear cell carcinoma, papillary renal carcinoma and chromophobe renal carcinoma using tissue microarrays. All markers displayed significant differential expression among the subtypes ($p<0.001$) except CAII ($p=0.192$). According to positive (LR+) and negative (LR−) likelihood ratio, six markers (CD10, GST-α, AMACR, CK19, C-KIT and arvalbumin) demonstrated acceptable or good values to detect certain subtypes of RCC, but failed in terms of ruling out the respective subtypes. Based on the individual performance of these six markers, we combined them and reviewed each single case: LR+ for detection of clear cell RCC considerably increased by application of the six marker panel, but did not exceed 10. LR− was still >0.1; in case of papillary RCC LR+ rose beyond 10, but LR− remained >0.1. LR+ for recognition of chromophobe RCC rose far beyond 10, but LR− remained >0.1. Thus, the panel can reliably recognize two main RCC subtypes without inclusion of histomorphologic features. Further improvement is needed for consistent detection of clear cell RCC and for dependably ruling out all three main subtypes as well as identification of rare variants and benign lesions like oncocytoma.

Keywords Renal cell carcinoma · Subtype differentiation · Renal mass biopsy · Immunohistochemistry

B. Walter
Department of Urology, Friedrich Alexander University, Erlangen, Germany

A. Hartmann · S. Bertz · C. G. Stoehr
Institute of Pathology, Friedrich Alexander University, Erlangen, Germany

F. Hofstädter
Institute of Pathology, University of Regensburg, Regensburg, Germany

K. Junker
Department of Urology, Jena University Hospital, Jena, Germany

H. Moch
Institute of Pathology, University of Zurich, Zurich, Switzerland

S. Denzinger · W. Otto
Department of Urology, University of Regensburg, Regensburg, Germany

M. Gajda
Institute of Pathology, Jena University Hospital, Jena, Germany

B. Walter (✉)
Department of Urology, University Hospital Erlangen, 91054 Erlangen, Germany
e-mail: bernhard.walter@uk-erlangen.de

Introduction

Renal neoplasms comprise several distinct clinicopathologic entities with potential prognostic and therapeutic differences. More than 95% of clinically significant lesions can be diagnosed as one of the common subtypes of renal epithelial tumors: clear cell renal cell carcinoma (cc-RCC), papillary

RCC (pp-RCC) and chromophobe (cp-RCC) [1]. These distinct types of renal tumors may have overlapping morphological features including variable cytoplasmic staining and architectural patterns, making diagnosis sometimes challenging [2]. Considering the increasing role for percutaneous biopsy procedures in the management of solid renal masses, differentiation between the three subtypes has become still more difficult and subjective in many cases [3, 4]. In these small biopsies, the entire range of cytoarchitectural features may not be fully represented. Each of these three carcinoma subtypes is accompanied by the expression of a certain spectrum of antigens that can be detected immunohistologically. The list of candidate genes has expanded considerably in the recent past and several molecular markers have been investigated to optimize subtype differentiation in RCC [2, 5]. We found GST-α and CD10 as commonly quoted markers for clear cell RCC, CK-19 and AMACR for papillary RCC and C-KIT Parvalbumin plus Vimentin for chromophobe RCC.

cc-RCC is frequently associated with high expression of GST-α [6, 7] and CD10 [8–12]. Both markers are already in use to differentiate the most common subtypes in RCC [5, 11, 13]. Furthermpre, lack of expression for C-KIT [14, 15] and Parvalbumin [5, 16] in connection with cc-RCC histology is discussed as a typical feature of this subtype. Subtype specific markers in terms of pp-RCC by contrast are not as pronounced. High AMACR expression is seen both in pp-RCC and cc-RCC [17, 18]. Although CK 19 was reported to display strong positivity in pp-RCC specimens [19], validation is still lacking. Lack of immunoreactivity for C-KIT and Parvalbumin is also a typical characteristic of pp-RCC [16, 20–22] while chromophobe (cp) RCC was repeatedly shown to be associated with highest expression of both markers: Sensitivity was consistently reported to be about 100% (C-KIT [15, 21–23], parvalbumin [16, 24–26]). Vice versa loss of expression for Vimentin is referred to as a distinguishing marker for cp-RCC and specificity is reported to be about 80–100% in the literature [24, 25, 27]. CA-2 expression in RCC was found to be highly sensitive in terms of chromophobe RCC in one of the earliest gene array profile studies [28]. However, further publications analyzing CA-2 immunostaining in RCC tissue specimens are lacking.

Our objective was to investigate the selected markers as a panel in an adequate case numbers of the three RCC main subtypes. Depending on the generated sensitivity and specificity for each examined marker we were searching for a marker panel allowing the differentiation of the three RCC subtypes with a maximum of likelihood and a minimum of markers. For this purpose, we constructed a tissue microarray containing 65 cc-RCC, pp-RCC and cp-RCC specimens, respectively. All cases were matched regarding age, grade and tumor stage leading to a comprehensive study cohort for all tumor subytpes.

Materials and methods

Clinical data

A total of 65 age-, stage-, grade- and gender-matched trios of each clear cell, papillary and chromophobe RCC were retrieved from archives of three pathology institutes (Table 1). Patients with familial RCC syndromes (e.g., von Hippel–Lindau disease) were excluded. All cases were reviewed by two experienced uropathologists (A.H. and H.M.) according to the 2004 WHO classification and 2002 UICC TNM system. A consensus of the histopathological classification was reached for all cases. Cases with questionable histology or other histopathological entities were excluded from the study.

Immunohistochemistry

A Tissue Micro Array (TMA) of representative areas from formalin-fixed, paraffin-embedded tumor material was established as described previously [29]. Briefly, suitable areas with representative tumor were marked on standard haematoxylin and eosin (H&E)-stained sections, punched out of the paraffin block and inserted into a recipient block. The punch diameter was 1.5 mm. The freshly cut 5-μm sections of the resulting blocks underwent strictly synchronous treatment throughout all staining procedures. After deparaffinization, rehydration and microwave treatment according to standard procedures, staining with primary monoclonal antibodies to AMACR (Dako M361,1:10), Vimentin (Dako M0725, 1:50; no microwave treatment), Cytokeratin 19 (Dako M0888, 1:100) and CD117 (Dako A4502, 1:200) were performed on a Ventana Nexes immunohistochemistry device. The antibodies to GST-α (Acris Antibodies BP144, 1:50), CAII (Santa Cruz Biotechnology

Table 1 Patient's tumor characteristics

RCC subtype	Clear cell	Papillary	Chromophobe
Total number (*n*)	65	65	65
pT1a	24	24	24
pT1b	18	18	18
pT2	10	10	10
pT3a	8	8	8
pT3b	5	5	5
pN2	2	2	2
G1 (Fuhrman)	44	44	44
G2 (Fuhrman)	14	14	14
G3 (Fuhrman)	7	7	7
Male Pat.	39	48	30
Female pat.	26	17	35
Median pat. age	66 (25–88)	66 (26–85)	66 (36–84)

sc25596, 1:50), Parvalbumin (Abcam, ab11427, 2 μg/ml) and CD10 (Novocastra NCL-L-CD10-270, dilution: 1.25) were used together with the Envison + Dual Link System HRP detection (Dako). Hale's colloidal iron staining was performed using Muller–Mowry staining method [30].

Evaluation of immunoreactivity was performed in accordance to previously published studies using an approach incorporating staining intensity as well as amount of stained cells or nuclei.

AMACR staining was negative if intensity was not exceeding weak staining in at least 5% of tumor cells. When at least 5%, but not more than 50%, of cells were stained weakly, moderately or strongly, this was considered focal positive. When more than 50% of cells were stained weakly, moderately or strongly, the case was rated diffusely positive. Vimentin and Parvalbumin staining were negative if less than 30% of cells demonstrated cytoplasmic reactivity or staining was not more than moderate. Only strong staining in at least 30% of cells was considered positive. CK-19 staining was negative if no peroxidase reaction was observed. Weak reactivity or moderate to strong staining in less than 30% of cells was rated weakly positive, while moderate to strong staining in at least 30% was considered as strong positivity. CD117 was rated positive if weak staining was exceeding 50% of cells or reactivity was at least moderate. GST-α staining was negative if no reactivity was observed. If less than 30% of cells stained or staining was weak, the case was rated weakly positive. When these criteria were exceeded, staining was considered as strongly positive. CD10 staining was considered positive if a minimum of 2% of cells demonstrated at least weak membranous staining. CA-II staining was considered positive when moderate and strong immunoreaction was present in at least 10% cells and considered negative when no or weak staining was present.

Scoring of the immunohistochemical data was done by two Uro-Pathologists (A.H. and H.M.) who had no knowledge of the clinical data.

Statistical analysis

Statistical analyses were completed using SPSS version 15.0 (SPSS, Chicago, IL). Values of $p<0.05$ were considered significant. Exact χ^2 tests were used to study the statistical association between the three groups.

Results

Of the 195 tumor specimens on the array, 159 to 176 could be successfully analysed for the respective stainings. Non-informative spots in the majority of cases resulted from missing tissue or tumor cells.

GST-α staining resulted in strong positivity in 93.8% (60/64) cc-RCC tumors. This was in contrast to papillary and chromophobe tumors, which expressed GST-α in 44.1% (26/59) or 19.6% (9/46) of cases. This differential expression was significant ($p<0.001$).

In total, 77.8% (42/54) of the cc-RCC specimens were marked by strong CD10 reactivity, while pp-RCC tumors stained positive in 51.8% (27/56) and cp-RCC tumors displayed reactivity in 29.5% (13/44). These subtype specific differences again reached statistical significance ($p<0.001$). Sensitivity and specificity resulted in positive likelihood ratio (LR+) for diagnosis of cc-RCC using GST-α that was below 10 (1.9); for CD10, it was 2.8. LR− for exclusion of cc-RCC was 0.4 for GST-α and 0.1 for CD10 (Fig. 1).

Diffuse AMACR staining was observed in 27.0% (17/63) of the cc-RCC tumors and in 34.1% (15/44) of the cp-RCC specimens, while papillary carcinomas displayed diffuse staining pattern in 88.3% (53/60). Overall, 74.6% (47/63) pp-RCC tumors were strongly positive for CK-19. In contrast, only 15.4% (10/65) cc-RCC tumors and 23.9% (10/43) cp-RCC tumors were CK-19 positive. Subtype specific differences for CK-19 reached statistical significance ($p<0.001$). LR+ for diagnosis of pp-RCC by AMACR dropped below 10 (2.9), as it did for diagnosis pp-RCC tumors by CK19 (4.0). LR− for exclusion of pp-RCC was 0.3 for AMACR and 0.2 for CK-19 (Fig. 2).

Overall, 76.1% (35/46) of the cp-RCC tumors stained C-KIT positive. In contrast, only 4.8% (3/63) pp-RCC tumors expressed C-KIT, and all 60 (100%) cc-RCC specimens were C-KIT negative. These staining differences were highly significant ($p<0.001$). Parvalbumin expression was positive in 87.8% (35/45) of the cp-RCC tumors, while 78.2% (43/55) pp-RCC tumors and all 62 cc-RCC (100%) were Parvalbumin negative; these observations were also statistically significant ($p<0.0001$).

LR+ for diagnosis of cp-RCC by C-KIT reached a value high that exceeded 10 (34.7), but dropped below 10 for detection of cp-RCC by Parvalbumin (7.5). LR− for exclusion of cp-RCC by C-KIT was 0.2, as well as by Parvalbumin (0.2) (Fig. 3).

Vimentin negative tumors were found in 95.7% (44/46) of the cp-RCC cases, while cc-RCC tumors expressed Vimentin in 35.9% (23/64) and pp-RCC tumors in 38.7% (24/64). This differential expression was significant ($p<0.05$). Sensitivity and specificity resulted in LR+ of 8.8 and LR− of 0.8 (Fig. 4).

Carboanhydrase II staining was present in 79.7% (51/64) of cc-RCC cases and 81% (47/58) pp-RCC tumors. It was noted that 92.9% (39/42) of the cp-RCC tumors displayed positive CA-2 reaction. Significance for differential expression failed ($p=0.5$), and sensitivity and specificity resulted in LR+ far below 10 and LR− >0.1 (Fig. 4).

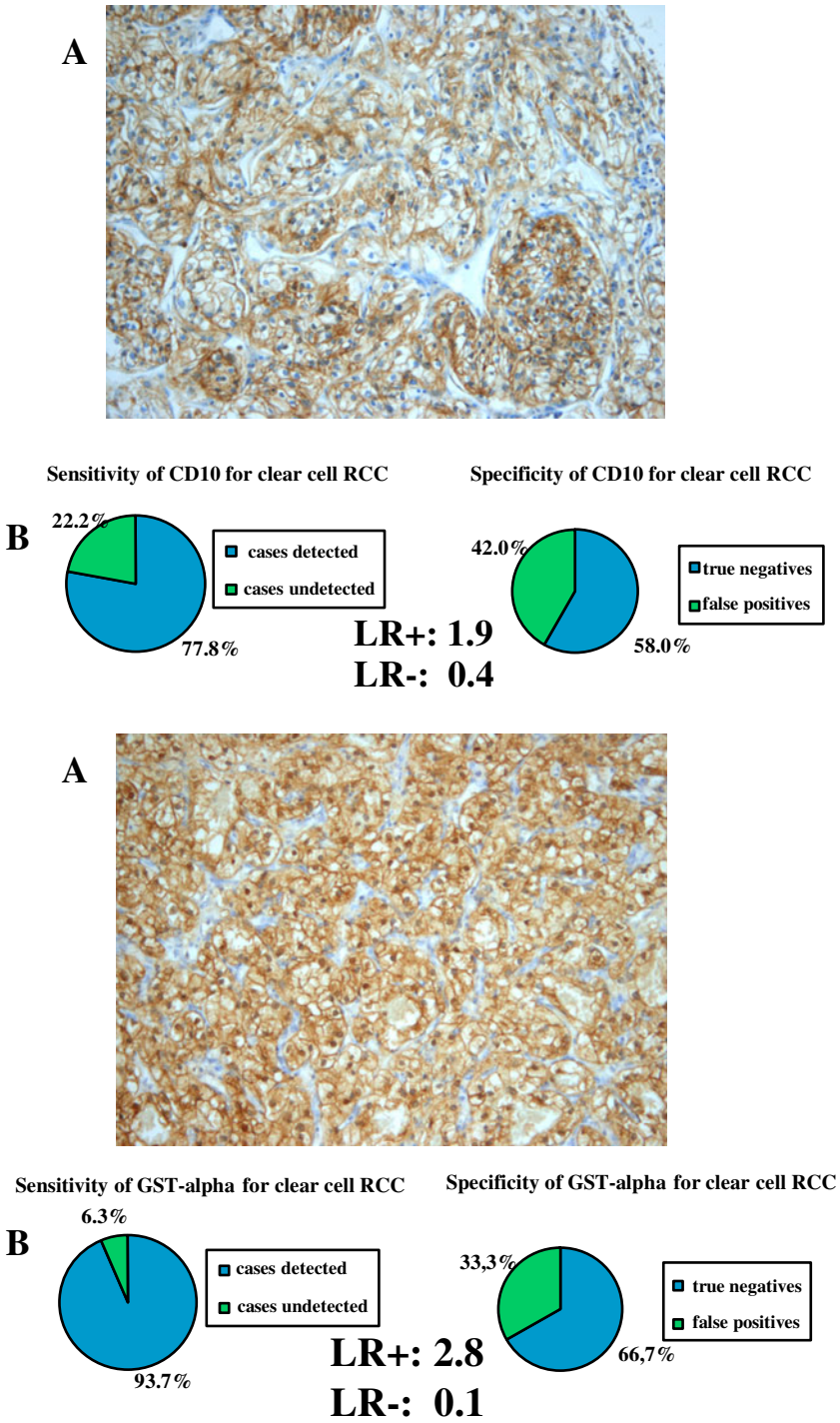

Fig. 1 GST-α and CD10 performance as potential markers to diagnose clear cell RCC. **a** CD10 and GST-alpha positive cc-RCC tumors. **b** Sensitivity and specificity resulted in LR+ <10 and LR- >0.1 for both markers

Hale's colloidal iron staining resulted in strong positivity in only 31.2% (20/64) cp-RCC tumors. This was in contrast to papillary and clear cell tumors, which were negative for Hale colloidal iron. This differential expression was significant ($p<$ 0.001). LR+ for detection of cp-RCC by Hale iron was 2.4. LR− for exclusion of cp-RCC by colloidal iron was 0.43.

Based on the performances of the markers for the detection of one subtype, we combined a marker set containing CD10, GST-α, AMACR, CK19, C-KIT and Parvalbumin and reviewed each case. Vimentin and CA-II were excluded due to their insufficient positive and negative likelihood ratios. To develop a six-marker panel algorithm, positive staining for each marker was scored +1 for the respective subtype. Accordingly, each RCC specimen was assigned the subtype with the highest score (Table 2). This way, 80.9% (148/183) of RCC cases could be assigned to one certain subtype.

As a result of this individual case analysis, LR+ for detection of clear cell RCC was increased by application

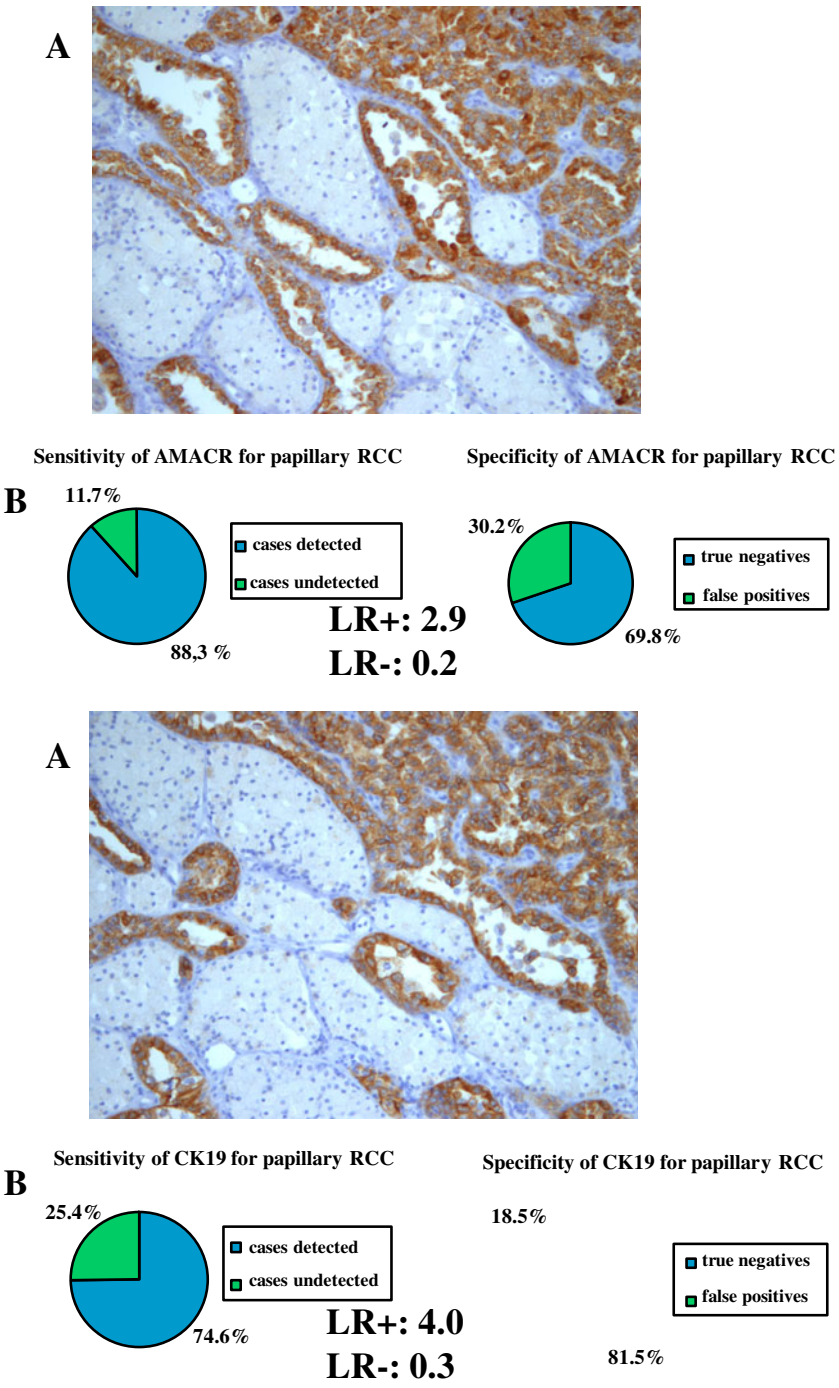

Fig. 2 AMACR and CK 19 performance as potential markers to diagnose papillary RCC. **a** AMACR and CK-19 positive pp-RCC tumors. **b** Sensitivity and specificity resulted in LR+ <10 and LR- >0.1 for both markers

of the six marker panel, but did not exceed 10 (7.4) and LR− remained >0.1 (0.3) (Fig. 5). The panel increased the LR+ for pp-RCC beyond 10 (17.7), thereby detecting papillary histology with high reliability; because of a LR− was still >0.1 (0.4), it cannot be used to definitely rule out this subtype. The panel enhanced LR+ for detection of cp-RCC far beyond 10 (30.2), but as LR− remains >0.1 (0.4), it cannot be used to rule out cp-RCC reliably. For this subtype, the panel performed slightly inferior to C-KIT alone.

Discussion

In the age of individual therapy, the approach to percutaneous image-guided RCC biopsy procedures plays an expanded role. However, difficulties in histopathological interpretation of the biopsy specimens—i.e., estimation of nuclear grading or correct classification of the certain RCC subtype—are reported in the literature [3, 31, 32]. As a result, various models have been proposed to simulate needle biopsy procedures for solid renal masses [33, 34]. We

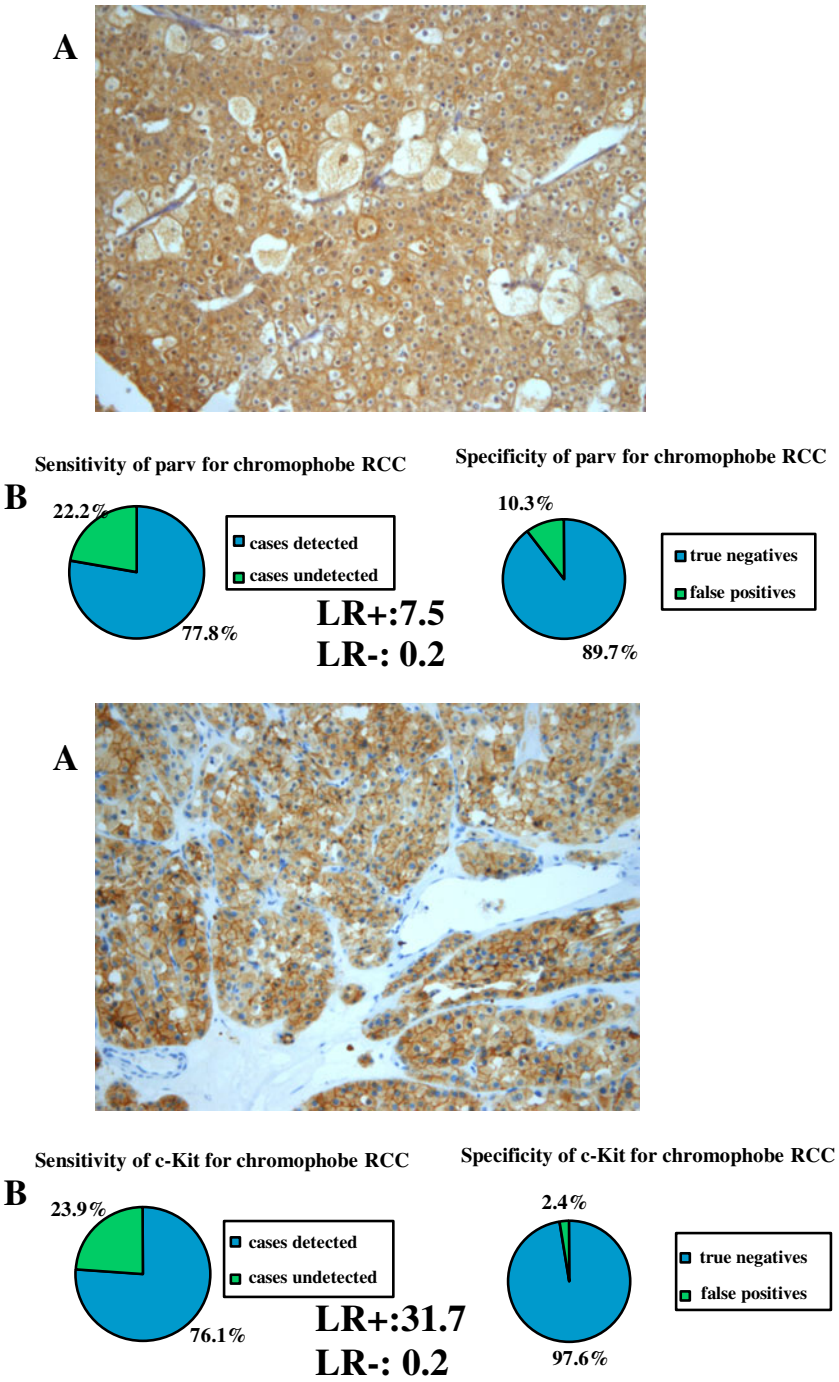

Fig. 3 C-KIT and parvalbumin performance as potential markers to diagnose chromophobe RCC. **a** Parvalbumin and C-KIT positive cp-RCC specimens. **b** Sensitivity for C-KIT resulted in LR+ >10; Specificity resulted in LR- >0.1 for both markers

applied a 1.5-mm punch needle for constructing a TMA, thereby mimicking the percutaneous biopsy technique. In this way, each core unit reflects a core conformation comparable to a Trucat needle biopsy core. Thus, the aim was to be able to differentiate between the three RCC main subtypes with a maximum of confidence and using a minimum of markers.

Several studies were dedicated to the development of a suitable immunohistochemistry panel to facilitate RCC subtype diagnosis. Yin-Goen et al. [35] describe 13 different immunomarkers, each of them highly specifically expressed in a particular RCC subtype. Takahashi et al. [36] proposed a classification model for kidney tumors using eight biomarkers based on previous gene expression profiling studies. Zhou et al. [11] used an immunohistochemistry set including 11 biomarkers differentiating not only clear cell and chromophobe RCC, but also papillary RCC type I from type II. Bazille et al. [37] reduced the marker panel from ten to only three biomarkers, which distinguished the different tumor subtypes in 79% of the cases. Similarly, Geramizadeh et al. [38] decreased

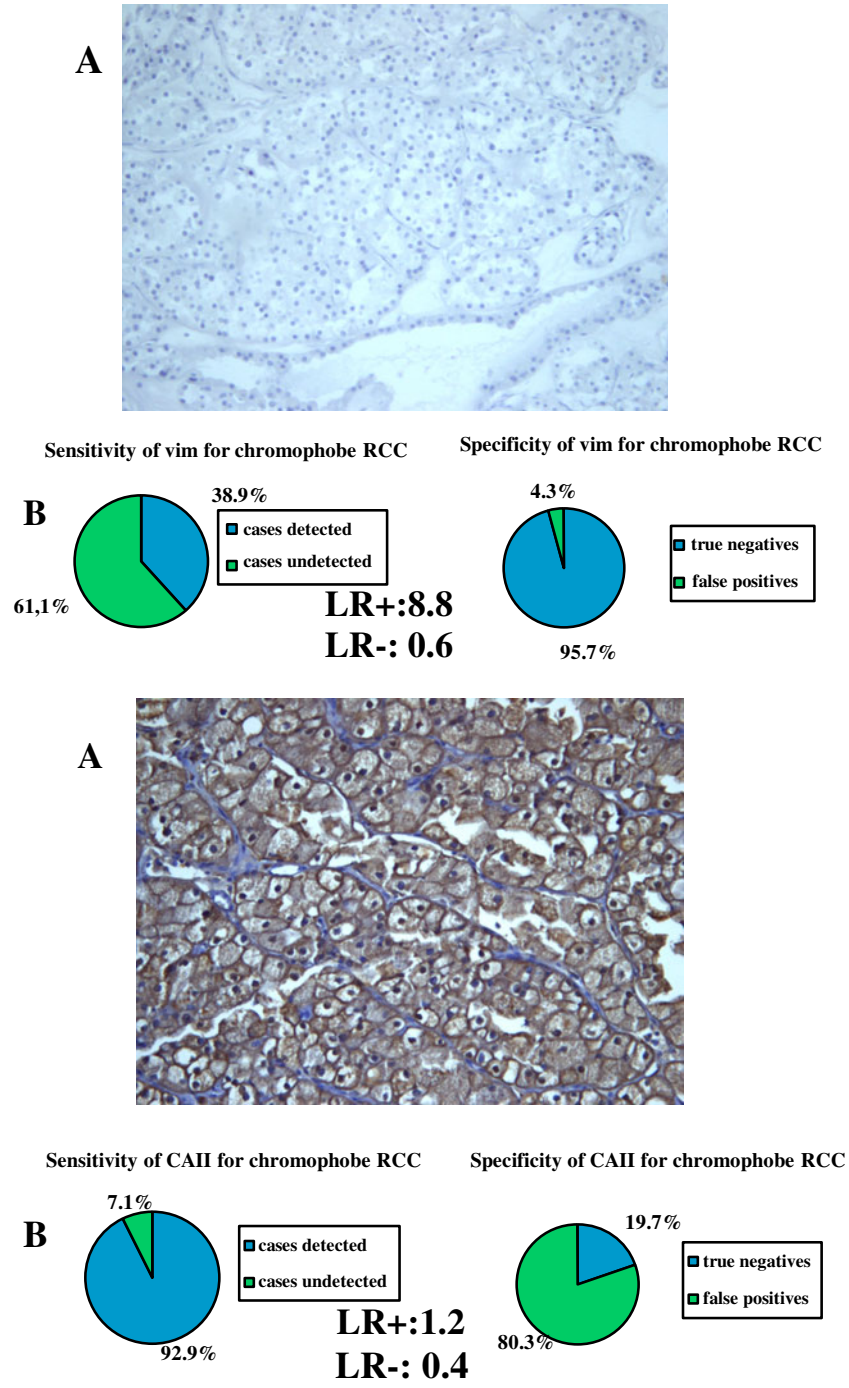

Fig. 4 Vimentin and CA-II performance as potential markers to differentiate chromophobe RCC. **a** CA-II and Vimentin positive cp-RCC specimens. **b** Sensitivity and specificity for both markers resulted in LR+ <10 and LR- >0.1

Table 2 Review of the six marker combination for each single specimen; positive staining for each marker scored +1 for the respective subtype

Positivity	CD10	GST-α	AMACR	ck19	c-Kit	Parvalbumin
Clear cell	+1	+1	0	0	0	0
Papillary	0	0	+1	+1	0	0
Chromophobe	0	0	0	0	+1	+1

the number of their marker set from ten primary candidates to five markers, which allowed them to determine the correct subtype in the majority of the analysed RCC specimens. Remarkably, the sensitivity and specificity rates of the examined markers vary widely from study to study. Moreover, some of the studies are underpowered in the case of papillary and—particularly—chromophobe subtype specimens.

Generally, GST-α, CD10, AMACR, CK-19 and Vimentin were found to be differentially expressed in the three

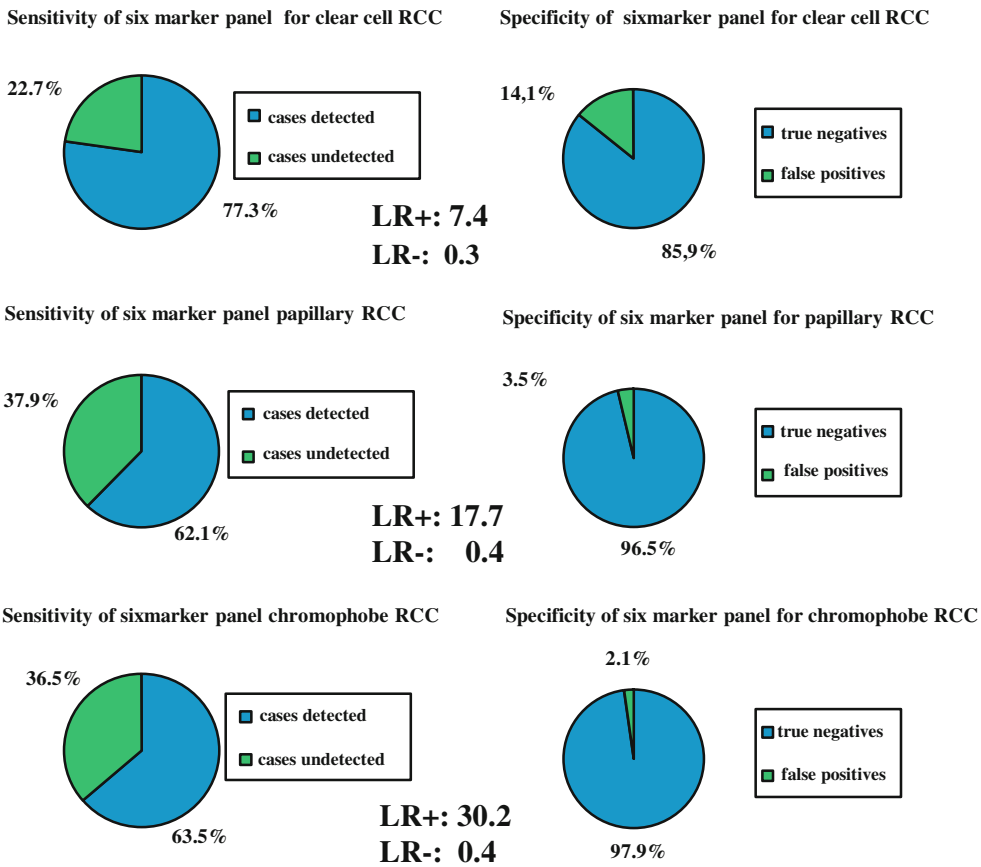

Fig. 5 Likelihood ratio positive (LR+) and likelihood ratio negative (LR−) for each of the three main subtypes utilizing the six marker panel

RCC main subtypes as described in the literature, although the differences between the subtypes were occasionally not as pronounced. For example, sensitivity for GST-α and CD-10 in terms of cc-RCC was comparable to the published data [6–10, 13]; however, a number of pp-RCC and cp-RCC tumors expressed GST-α and CD10, respectively. Consequently, specificity of these markers was affected and lower than that reported in earlier studies [7, 13, 15]. This might be attributed to the increased number of papillary and especially chromophobe RCC tumors in our study [8–10, 14, 25].

Another aspect concerns the TMA technology itself: due to possible heterogeneity within tumors, the use of one core per unit within the TMA may not fully represent the respective tumor as a whole. Antigen expression as demonstrated by a single tumor core might depend on its location within the tumor and not fully represent expression within the dominating histologic subtype.

The two papillary RCC associated markers, AMACR and CK19, demonstrated comparable sensitivity as in published data, but specificity of AMACR [17, 18] was impaired by positivity in non-papillary RCC tumors. Screening the literature for CK-19 expression in RCC, we encountered two relevant publications [19, 36] in this context. Despite the low case numbers, the authors found CK19 expression in pp-RCC tumors as well as in non pp-RCC tumors comparable to our findings. A potential future value for CK 19 was reported by Mertz et al. [39], who identified two distinct molecular subtypes of cc-RCC with prognostic relevance. These were defined by different CK19 (and CK7) expression. Thus, the variability observed for CK expression in cc-RCC can be explained by genetic heterogeneity.

Lack of Vimentin expression in chromophobe RCC histology is quite specific and reported for almost 100% of the chromophobe RCC cases in literature [15, 27]. Our analysis —95% of the examined tumors were Vimentin negative— corresponded well to these findings. However, Vimentin is also one of our markers, which displayed expression deviant from literature: We detected Vimentin staining in both papillary (40.2%) and clear cell (37.5%) RCC only in a subset of tumors compared to earlier reports, in which Vimentin expression both for cc-RCC and pp-RCC is reported to be up to100% [15, 19, 24, 27].

As noted above, Parvalbumin- and C-KIT expression is characterized as specific attribute of chromophobe RCC. Although our findings verified this observation, both markers are reported to be expressed to a higher extent in literature, reaching values up to100% for C-KIT [20–23] and Parvalbumin [7, 16]. However, LR+ for detection of cp-RCC by C-KIT was still 34.7. In contrast, the LR+ of Hale's colloidal iron staining was considerably worse. Thus, the

value of colloidal iron as a reliable marker for detection of chromophobe RCC cases is still on discussion [40].

Our analyses further confirmed the results of former investigations showing total lack of C-KIT [21–23] and Parvalbumin [16] in cc-RCC tumors as well as in pp-RCC tumors [16, 20–22].

In one of the earliest gene signature reports, CA-2 was identified as a potential marker for the differential diagnosis of chromophobe RCC [28]. However, the number of cases for the different subtypes was low. Our findings demonstrated high expression of CA II in all three RCC subtypes and consequently poor specificity, arguing against a utility of this marker for differential diagnosis of RCC.

After exclusion of Vimentin and CA-2, six immunohistochemical markers remained for the revision of all 183 RCC cases to simulate a diagnostic needle biopsy algorithm differentiating between the three RCC main subtypes without considering histopathology. As a result of this individual case review, the panel reliably detected two main RCC subtypes without inclusion of cytoarchitectural features, but failed to carry out a reliable detection of clear cell histology and to reliably rule out all three main subtypes.

Further limitations of our study are the lack of clear cell RCC cases comprised entirely or predominately of cells with eosinophilic cytoplasm as well as oncoctomas extending the differential diagnosis in tumors with eosinophilic cytoplasm beyond carcinoma.

Although there are several antigens that can be employed to separate oncocytoma from clear-cell RCC with eosinophilic cells and the eosinophilic variant of chromophobe RCC, immunohistochemical stains in these two tumors show substantial overlap. Thus, parvalbumin and C-kit, for example, are usually positive in both tumor entities. A recent update addresses to this issue proposing a three marker panel including C-KIT, CK 7 and PAX2, which has been reported to discriminate between oncocytoma and ch-RCC, to separate the four most common RCCs with eosinophilic cytoplasm reliably [41].

However, the present report highlights several important key points: With the investigation of 65 age-, grade- and stage-matched trios of clear cell, papillary and chromophobe renal carcinoma, this series comprises—to our knowledge—the largest and most homogeneous patient cohort studied so far. Moreover, scoring all punched biopsy cores without knowledge of the clinical data was the foundation for the design of a diagnostic algorithm imitating the potential difficulties in interpretation of a percutaneous needle biopsy.

All six markers are currently used as part of the daily routine in our immunohistochemistry laboratory unit; therefore, the panel enables cost-efficient and fast RCC subtype differentiation.

Our marker panel is a clear advancement in terms of immunohistochemistry application for RCC subtype differentiation. However, it needs further revisions, as shown by the relatively low specificity of values. Currently, further markers are evaluated for refinement of the panel.

Acknowledgements The authors thank Rudolf Jung and Nina Niessl for excellent technical assistance.

Conflict of interest There is no financial support or conflict of interest involved in this work.

References

1. Lopez-Beltran A, Scarpelli M, Montironi R, Kirkali Z (2006) 2004 WHO classification of the renal tumors of the adults. Eur Urol 49 (5):798–805
2. Skinnider BF, Amin M (2005) An immunohistochemical approach to the differential diagnosis of renal tumors. Semin Diagn Pathol 22(1):51–68
3. Kümmerlin I, Smedts F, Horn T, Algaba F, Trias I, de la Rosette J (2009) Diagnostic problems in the subtyping of renal tumors encountered by five pathologists. Pathol Res Pract 205(1):27–34
4. Shannon BA, Cohen RJ, de Bruto H, Davies RJ (2008) The value of preoperative needle core biopsy for diagnosing benign lesions among small, incidentally detected renal masses. J Urol 180 (4):1257–1261
5. Martignoni G, Brunelli M, Gobbo S, Remo A, Ficarra V, Cossu-Rocca P, Pea M, Chilosi M, Menestrina F, Cheng L (2007) Role of molecular markers in diagnosis and prognosis of renal cell carcinoma. Anal Quant Cytol Histol 29(1):41–49
6. Grignon DJ, Abdel-Malak M, Mertens WC, Sakr WA, Shepherd RR (1994) Glutathione S-transferase expression in renal cell carcinoma: a new marker or differentiation. Mod Pathol 7(2):186–189
7. Chuang S-T, Chu P, Sugimura J, Tretiakova MS, Papavero V, Wang K, Tan MH, Lin F, Teh BT, Yang XJ (2005) Overexpression of glutathione S-transferase α in clear cell renal cell carcinoma. Am J Clin Pathol 123:421–429
8. Pan C-C, Chen PC-H, Ho DM-T (2004) The diagnostic utility of MOC31, BerEP4, RCC marker and CD 10 in the classification of renal cell carcinoma and renal oncocytoma: an immunohistochemical analysis of 328 cases. Histopathology 45:452–459
9. Avery AK, Beckstead J, Renshaw AA, Corless CL (2000) Use of antibodies to RCC and CD 10 in the differential diagnosis of renal neoplasms. Am J Surg Pathol 24:203–210
10. Martignoni G, Pea M, Brunelli M, Chilosi M, Zamó A, Bertaso M, Cossu-Rocca P, Eble JN, Mikuz G, Puppa G, Badoual C, Ficarra V, Novella G, Bonetti F (2004) CD 10 is expressed in a subset of chromophobe renal cell carcinomas. Mod Pathol 17:1455–1463
11. Zhou M, Roma A, Magi-Galluzzi C (2005) The usefulness of immunohistochemical markers in the differential diagnosis of renal neoplasms. Clin Lab Med 25:247–257
12. Dahinden C, Ingold B, Wild P, Boysen G, Luu VD, Montani M, Kristiansen G, Sulser T, Buhlmann P, Moch H, Schraml P (2010) Mining tissue microarray data to uncover combinations of biomarker expression patterns that improve intermediate staging and grading of clear cell renal cell cancer. Clin Cancer Res 16(1):88–98
13. Takahashi M, Yang XJ, Sugimura J, Backdahl J, Tretiakova M, Qian CN, Gray SG, Knapp R, Anema J, Kahnoski R, Nicol D, Vogelzang NJ, Furge KA, Kanayama H, Kagawa S, Teh BT (2003) Molecular subclassification of kidney tumors and the discovery of new diagnostic markers. Oncogene 22(43):6810–6818
14. Wang H-Y, Mills SE (2005) KIT and RCC ere useful in distinguishing chromophobe renal cell carcinoma from the granular variant of clear cell renal cell carcinoma. Am J Surg Pathol 29:640–646

15. Liu L, Qian J, Singh H, Meiers I, Zhou X, Bostwick DG (2007) Immunohistochemical analysis of chromophobe renal cell carcinoma, renal oncocytoma, and clear cell carcinoma. Arch Pathol Lab Med 131:1290–1297
16. Martignoni G, Pea M, Chilosi M, Brunelli M, Scarpa A, Colato C, Tardanico R, Zamboni G, Bonetti F (2001) Parvalbumin is constantly expressed in chromophobe renal carcinoma. Mod Pathol 14:760–767
17. Molinié V, Balaton A, Rotman S, Mansouri D, De Pinieux I, Homsi T, Guillou L (2005) Alpha-methyl CoA racemase expression in renal cell carcinomas. Hum Pathol 37:698–703
18. Tretiakova MS, Sahoo S, Takahashi M, Turkyilmaz M, Vogelzang NJ, Lin F, Krausz T, Teh BT, Yang XJ (2004) Expression of alpha-methylacyl-CoA racemase in papillary renal cell carcinoma. Am J Surg Pathol 28:69–76
19. Skinnider BF, Folpe AL, Hennigar RA, Lim SD, Cohen C, Tamboli P, Young A, de Peralta-Venturina M, Amin MB (2005) Distribution of cytokeratins and vimentin in adult renal neoplasms and normal renal tissue: potential utility of a cytokeratin antibody panel in the differential diagnosis of renal tumors. Am J Surg Pathol 29:747–754
20. Memeo L, Jhang J, Assaad AM, Mckiernan JM, Murty VVVS, Hibshoosh H, Tong G-X, Mansukhani MM (2007) Immunohistochemical analysis for cytokeratin 7, KIT, and PAX2: value in the differential diagnosis of chromophobe cell carcinoma. Am J Clin Pathol 127:225–229
21. Pan C-C, Chen PC-H, Chiang H (2004) Overexpression of KIT (CD 117) in chromophobe renal cell carcinoma and renal oncocytoma. Am J Clin Pathol 121:878–883
22. Petit A, Castillo M, Santos M, Mellado B, Alcover JB, Mallofré C (2004) KIT Expression in chromophobe renal cell carcinoma: comparative immunohisto-chemical analysis of KIT expression in different renal cell neoplasms. Am J Surg Pathol 28:676–678
23. Huo L, Sugimura J, Tretiakova MS, Patton KT, Gupta R, Popov B, Laskin WB, Yeldandi A, Teh BT, Yang XJ (2005) C-kit expression in renal oncocytomas and chromophobe renal cell carcinomas. Hum Pathol 36:262–268
24. Young AN, de Oliveira Salles PG, Lim SD, Cohen C, Petros JA, Marshall FF, Neish AS, Amin MB (2003) Beta defensin-1, parvalbumin, and vimentin: a panel of diagnostic immunohistochemical markers for renal tumors derived from gene expression profiling studies using cDNA microarrays. Am J Surg Pathol 27:199–205
25. Abrahams NA, MacLennan GT, Khoury JD, Ormsby AH, Tamboli P, Doglioni C, Schumacher B, Tickoo SK (2004) Chromophobe renal cell carcinoma: a comparative study of histological, immunohistochemical and ultrastructural features using high throughput tissue microarray. Histopathology 45:593–602
26. Adley BP, Papavero V, Sugimura J, Teh BT, Yang XJ (2006) Diagnostic value of cytokeratin 7 and parvalbumin in differentiating chromophobe renal cell carcinoma from renal oncocytoma. Anal Quant Cytol Histol 28:228–236
27. Khoury JD, Abrahams NA, Levin HS, MacLennan GT (2002) The utility of epithelial membrane antigen and vimentin in the diagnosis of chromophobe renal cell carcinoma. Ann Diagn Pathol 6:154–158
28. Young AN, Amin MB, Moreno CS, Lim SD, Cohen C, Petros JA, Marshall FF, Neish AS (2001) Expression profiling of renal epithelial neoplasms. A method for tumor classification and discovery of diagnostic molecular markers. Am J Pathol 158:1639–1651
29. Bubendorf L, Nocito A, Moch H, Sauter G (2005) Tissue microarray (TMA) technology: miniaturized pathology archives for high-throughput in situ studies. J Pathol 195:72–79
30. Skinnider BF, Jones EC (1999) Renal oncocytoma and chromophobe renal cell carcinoma. A comparison of colloidal iron staining and electron microscopy. Am J Clin Pathol 111:796–803
31. Blumenfeld AJ, Guru K, Fuchs GJ, Kim HL (2010) Percutaneous biopsy of renal cell carcinoma underestimates nuclear grade. Urology 76(3):610–613
32. Schmidbauer J, Remzi M, Memarsadeghi M, Haitel A, Klingler HC, Katzenbeisser D, Wiener H, Marberger M (2008) Diagnostic accuracy of computed tomography-guided percutaneous biopsy of renal masses. Eur Urol 53(5):1003–1011
33. Reichelt O, Gajda M, Chyhrai A, Wunderlich H, Junker K, Schubert J (2007) XY ultrasound-guided biopsy of homogeneous solid renal masses. Eur Urol 52(5):1421–1426
34. Brown CL, Hartman RP, Dzyubak OP, Takahashi N, Kawashima A, McCollough CH, Bruesewitz MR, Primak AM, Fletcher JG (2009) Dual-energy CT iodine overlay technique for characterization of renal masses as cyst or solid: a phantom feasibility study. Eur Radiol 19(5):1289–1295
35. Yin-Goen Q, Dale J, Yang WL, Phan J, Moffitt R, Petros JA, Datta MW, Amin MB, Wang MD, Young AN (2006) Advances in molecular classification of renal neoplasms. Histol Histopathol 21:325–339
36. Takahashi M, Teh BT, Kanayama HO (2006) Elucidation of the molecular signatures of renal cell carcinoma by gene expression profiling. J Med Investig 53(1–2):9–19
37. Bazille C, Allory Y, Molinié V, Vieillefond A, Cochand-Priollet B, Cussenot O, Callard P, Sibony M (2004) Immunohistochemical characterisation of the main histologic subtypes of epithelial renal tumours on tissue-microarrays. Study of 310 cases. Ann Pathol 24 (5):395–406
38. Geramizadeh B, Ravanshad M, Rahsaz M (2008) Useful markers for differential diagnosis of oncocytoma, chromophobe renal cell carcinoma and conventional renal cell carcinoma. Indian J Pathol Microbiol 51(2):167–171
39. Mertz KD, Demichelis F, Sboner A, Hirsch MS, Dal Cin P, Struckmann K, Storz M, Scherrer S, Schmid DM, Strebel RT, Probst-Hensch NM, Gerstein M, Moch H, Rubin MA (2008) Association of cytokeratin 7 and 19 expression with genomic stability and favorable prognosis in clear cell renal cell cancer. Int J Cancer 123(3):569–576
40. Amin MB, Paner GP, Alvarado-Cabrero I, Young AN, Stricker HJ, Lyles RH, Moch H (2008) Chromophobe renal cell carcinoma: histomorphologic characteristics and evaluation of conventional pathologic prognostic parameters in 145 cases. Am J Surg Pathol 32(12):1822–1823
41. Bhalodia A, Bonsib SM (2010) Renal neoplasms: an update on immunohistochemical and histochemical features. Dako.com. Special Stains Education. Guide Chapter 26

Virchows Arch (2012) 460:353–356
DOI 10.1007/s00428-012-1211-5

CASE REPORT

Urothelial carcinoma of the renal pelvis with simultaneous trophoblastic and malignant clear cell endodermal-type differentiation

Ovidiu Preda · Alis Dema · Mihaela Iacob · Pablo Goyenaga · Isabel Dulcey · José Aneiros Fernández · Francisco F. Nogales

Received: 23 January 2012 / Accepted: 6 February 2012 / Published online: 24 February 2012
© Springer-Verlag 2012

Embryonal-type differentiations in urothelial neoplasms are uncommon [1, 2]. These frequently underdiagnosed phenomena may include either the presence of trophoblastic areas or, even more rarely, admixed yolk sac tumour patterns (YST) [2]. We present for the first time the association of both trophoblastic and malignant endodermal-type elements within an aggressive high-grade urothelial carcinoma (HGUC). Due to the presence of the endodermal component, which had cells with a prominent clear cytoplasm, a differential diagnosis with other papillary and clear cell renal neoplasms was necessary.

Paper presented at the 23rd Congress of the european Society of Pathology. Helsinki, Finland, August 27-September 1, 2011

O. Preda
MasterDiagnostica,
Granada, Spain

P. Goyenaga · I. Dulcey · J. Aneiros Fernández · F. F. Nogales (✉)
Department of Pathology, San Cecilio University Hospital,
E-18012 Granada, Spain
e-mail: fnogales@ugr.es

A. Dema
Victor Babeş University of Medicine and Pharmacy,
Timisoara, Romania

M. Iacob
Department of Emergency County Hospital,
Timisoara, Romania

Clinical history

A 47-year-old male presented with intense pain in the lumbar region. Seventeen years previously, he had been treated for a non-seminomatous testicular tumour with lung and liver metastases. He eventually underwent a right orchidectomy followed by platinum-based chemotherapy. Follow-up showed only residual mature teratomatous tissue in the biopsy material from the remaining testicle.

On his recent admission, elevated levels of serum β-hCG of 9,897.06 mUI/ml (normal 0–2.6 mUI/ml) and a lactate dehydrogenase of 1,280 U/L (normal 0–480 U/l) were found. Serum α-foetoprotein (AFP) was negative. A CT scan showed a large, ill-defined retroperitoneal mass involving the left kidney and ureter. There was marked infiltration of the psoas, and lung and vertebral metastases were prominent. No lesions were detected in the left testicle after both clinical and ultrasonographical exploration. A left ureteronephrectomy with resection of the surrounding tissues was performed. Patient refused chemo- or radiotherapy and 18 months after diagnosis is alive but has a large residual mass and pulmonary metastases.

Materials and methods

The ureteronephrectomy specimen was bivalved and fixed overnight in 10% buffered formalin and routinely processed. Seven tissue blocks were taken, and H&E-stained sections were analysed. Immunohistochemistry was performed on representative sections with the antibodies shown in Table 1.

Table 1 Antibodies used in this study

Antibody	Clone	Vendor
AFP	Polyclonal	DAKO, Glostrup, Denmark
Glypican 3	1G12	Bio Mosaics, Burlington, VT
SALL4	Sc-101147	Santa Cruz Biotechnology, Inc
CDX2	AMT 28	MasterDiagnostica, Granada
HepPar-1	OCH1E5	DAKO, Glostrup, Denmark
β-hCG	polyclonal	DAKO, Glostrup, Denmark
hPL	polyclonal	MasterDiagnostica, Granada
α-Inhibin	R1	DAKO, Glostrup, Denmark
Cytokeratin 20	K_s20.8	DAKO, Glostrup, Denmark
Cytokeratin 7	Ovtl 12/30	DAKO, Glostrup, Denmark
p63	4A4	MasterDiagnostica, Granada

Results

The nephrectomy specimen showed a dilated pelvis harbouring a solid 6×4.7-cm mass which infiltrated the adjoining kidney parenchyma, perirenal fat and the psoas muscle. Microscopically, a solid HGUC originating from the pelvis had numerous scattered syncytiotrophoblasts, which were also present in the numerous tumour emboli (Fig. 1a). In close transition with the urothelial tumour (Fig. 1b), a complex tubulopapillary neoplasm lined by tall, vacuolated, clear, atypical cells (Fig. 1c) was seen protruding into the pelvic space.

Immunohistochemical markers differentiated the cytokeratin 7 (CK7) and p63-positive (Fig. 2a) urothelial component from the trophoblastic cells which were positive for β-hCG, α-inhibin (Fig. 2b) and human placental lactogen (hPL). In contrast, the clear cell tubulopapillary cells had a characteristic primitive endodermal immunophenotype positive for glypican 3 (GLY3), CDX-2 and SALL4 (Fig. 3a–c) which, however, failed to stain for AFP, a fact which precluded a diagnosis of glandular yolk sac tumour. Cytokeratin 20 and HepPar-1 were negative.

Discussion

The capacity of urothelial carcinomas to differentiate into various cell lineages is well recognized. Amongst others, glandular, squamous, neuroendocrine and lymphoepithelioma-like patterns are relatively frequent in the bladder [1].

The rare trophoblastic differentiation in transitional tumours represents a variant of carcinomas associated with a poor prognosis [1, 3, 4]. Immunohistochemistry performed in the present case demonstrated the coexistence of atypical transitional cells with a characteristic CK7 and p63 positivity showing both syncytio- and intermediate trophoblastic differentiations, the former positive for β-hCG and α-inhibin and the latter for hPL. This highly specific immunophenotype helped to differentiate this variant of urothelial carcinoma from other giant cell-containing tumours [1].

This case also showed the concomitant presence of a clear cell tubulopapillary growth that merged with the urothelial neoplasm. This aberrant component had a characteristic primitive endodermal immunophenotype which was positive to SALL4, a stem cell marker [5],

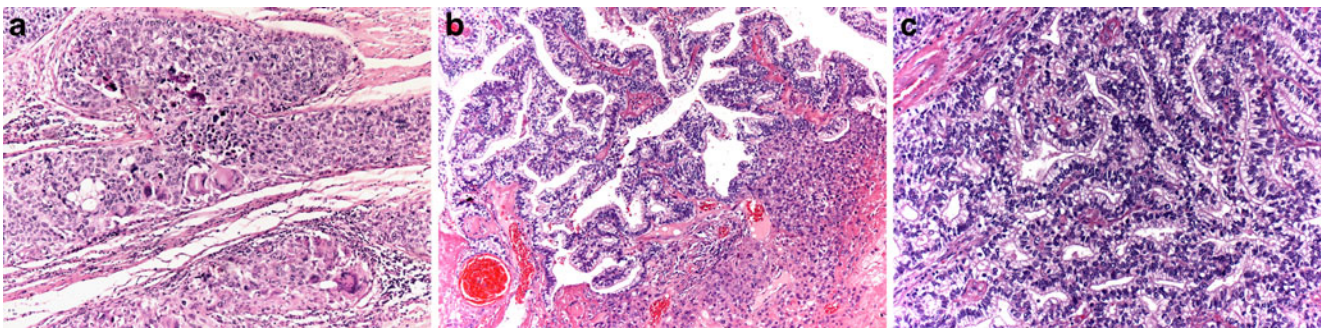

Fig. 1 Pelvic urothelial tumour with abundant syncytiotrophoblasts (**a**), merging with a tubulopapillary growth (**b**) lined by cells with prominent clear cytoplasm (**c**)

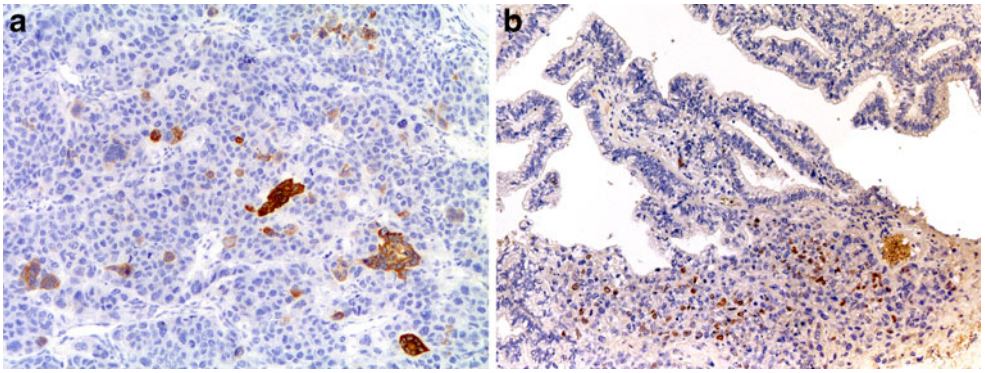

Fig. 2 Trophoblastic component of urothelial tumour is positive for α-inhibin (**a**). p63 positivity in urothelial neoplasm (**b**) contrasts with its negativity in the clear cell areas

and to GLY3, a marker for both yolk sac and liver cell tumours [6]. Both antibodies are always co-expressed in yolk sac tumours [7].

The primitive malignant endodermal or YST-type differentiation may be present in somatic, non-embryonal tumours of the female genital tract [8, 9], although it can also develop in the sinonasal area, stomach, colon, etc., where it is also associated with both high-grade tumours and a poor prognosis [7]. In the urinary tract, this association has been reported in rare, isolated cases of AFP-producing adeno- or transitional cell carcinomas and demonstrated by AFP stains only. Histologically, these cases consistently reveal the presence of a distinctive vacuolated epithelium with a characteristic AFP-positive immunophenotype [2]. The higher sensitivity of recently introduced antibodies such GLY3 [6] and SALL4 [5] has facilitated the demonstration of areas of primitive endodermal differentiation (YST) [7] present in various mixed tumours. In our case, tubulopapillary areas showed an incomplete primitive endodermal phenotype due to presence of a strong GLY3 and SALL4 positivity in the absence of AFP staining, a more specific but less sensitive marker of endodermal differentiation [6]. Furthermore, CDX2, an intestinal type differentiation marker [10], was also positive in our case, supporting an intestinal differentiation in the malignant primitive endodermal component [7, 11]. This immunophenotype helped to differentiate the endodermal tubulopapillary areas from both clear cell renal cell carcinoma (negative for CK7 and p63 but positive for renal cell carcinoma marker, vimentin and CD10) and from the newly introduced entity of tubulopapillary clear cell carcinoma (positive for CK7 and vimentin but negative for CD10, alpha-methyl CoA racemase and renal cell carcinoma marker) [12, 13].

Simultaneous placental and endodermal-type differentiations have not been previously reported in association with transitional cell carcinomas. The non-germ cell origin of some embryonal-type tumours, arising from somatic type neoplasms, has been recently reviewed [7], and an origin from pluripotent malignant stem cells present in the somatic tumour has been proposed [14]. We believe that the relationship of this complex renal tumour with the previous testicular tumour is coincidental, as there was a successful response to chemotherapy with no short-term recurrence; furthermore, the present lesion showed an intimate admixture of somatic and embryonal histological patterns reflecting tumour heterogeneity rather than a metastasis.

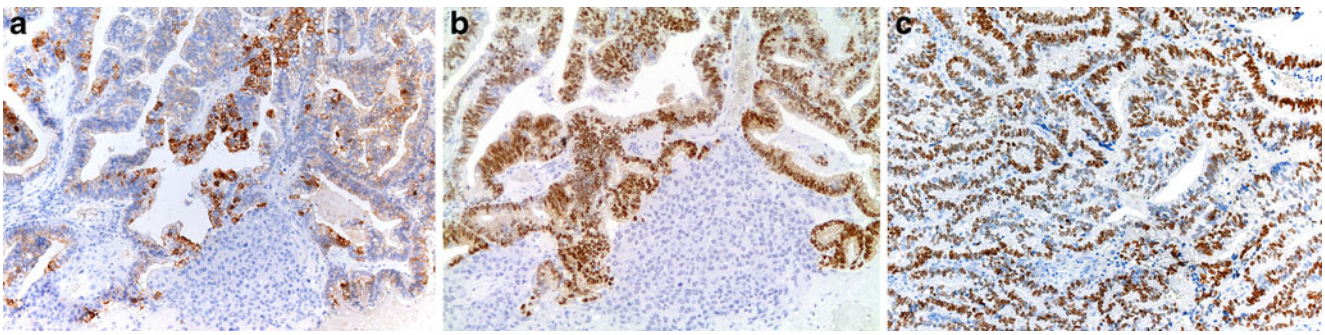

Fig. 3 Clear cell tubulopapillary areas with a primitive endodermal phenotype are positive for GLY3 (**a**), CDX2 (**b**) and SALL4 (**c**)

Conflict of interest None.

References

1. Shanks JH, Iczkowski KA (2009) Divergent differentiation in urothelial carcinoma and other bladder cancer subtypes with selected mimics. Histopathology 54:885–900. doi:10.1111/j.1365-2559.2008.03167.x
2. El-Bahrawy M (2011) alpha-Fetoprotein-producing non-germ cell tumors of the urological system. Rev Urol 13:14–19
3. Amin MB (2009) Histological variants of urothelial carcinoma: diagnostic, therapeutic and prognostic implications. Mod Pathol 22 (Suppl 2):S96–S118. doi:10.1038/modpathol.2009.26
4. Jenkins BJ, Martin JE, Baithun SI, Zuk RJ, Oliver RT, Blandy JP (1990) Prediction of response to radiotherapy in invasive bladder cancer. Br J Urol 65:345–348
5. Wang F, Liu A, Peng Y, Rakheja D, Wei L, Xue D, Allan RW, Molberg KH, Li J, Cao D (2009) Diagnostic utility of SALL4 in extragonadal yolk sac tumors: an immunohistochemical study of 59 cases with comparison to placental-like alkaline phosphatase, alpha-fetoprotein, and glypican-3. Am J Surg Pathol 33:1529–1539. doi:10.1097/PAS.0b013e3181ad25d5
6. Preda O, Nicolae A, Aneiros-Fernandez J, Borda A, Nogales FF (2011) Glypican 3 is a sensitive, but not a specific, marker for the diagnosis of yolk sac tumours. Histopathology 58:312–314. doi:10.1111/j.1365-2559.2010.03735.x, author reply 314–315
7. Nogales FF, Preda O, Nicolae A (2011) Yolk sac tumours revisited. A review of their many faces and names. Histopathology. doi:10.1111/j.1365-2559.2011.03889.x
8. Rutgers JL, Young RH, Scully RE (1987) Ovarian yolk sac tumor arising from an endometrioid carcinoma. Hum Pathol 18:1296–1299
9. Nogales FF, Bergeron C, Carvia RE, Alvaro T, Fulwood HR (1996) Ovarian endometrioid tumors with yolk sac tumor component, an unusual form of ovarian neoplasm, Analysis of six cases. Am J Surg Pathol 20:1056–1066
10. De Lott LB, Morrison C, Suster S, Cohn DE, Frankel WL (2005) CDX2 is a useful marker of intestinal-type differentiation: a tissue microarray-based study of 629 tumors from various sites. Arch Pathol Lab Med 129:1100–1105. doi:10.1043/1543-2165(2005)129[1100:CIAUMO]2.0.CO;2
11. Bing Z, Pasha T, Tomaszewski JE, Zhang P (2009) CDX2 expression in yolk sac component of testicular germ cell tumors. Int J Surg Pathol 17:373–377. doi:10.1177/1066896909338598
12. Aydin H, Chen L, Cheng L, Vaziri S, He H, Ganapathi R, Delahunt B, Magi-Galluzzi C, Zhou M (2010) Clear cell tubulopapillary renal cell carcinoma: a study of 36 distinctive low-grade epithelial tumors of the kidney. Am J Surg Pathol 34:1608–1621. doi:10.1097/PAS.0b013e3181f2ee0b
13. Gobbo S, Eble JN, Grignon DJ, Martignoni G, MacLennan GT, Shah RB, Zhang S, Brunelli M, Cheng L (2008) Clear cell papillary renal cell carcinoma: a distinct histopathologic and molecular genetic entity. Am J Surg Pathol 32:1239–1245. doi:10.1097/PAS.0b013e318164bcbb
14. Garcia-Galvis OF, Cabrera-Ozoria C, Fernandez JA, Stolnicu S, Nogales FF (2008) Malignant Mullerian mixed tumor of the ovary associated with yolk sac tumor, neuroepithelial and trophoblastic differentiation (teratoid carcinosarcoma). Int J Gynecol Pathol 27:515–520. doi:10.1097/PGP.0b013e31817b06c7

Virchows Arch (2012) 460:357–360
DOI 10.1007/s00428-012-1207-1

CASE REPORT

Visceral leishmaniasis in a patient with AIDS: early pathological diagnosis using conventional histology, PCR and electron microscopy is the key for adequate treatment

Albrecht Stenzinger · Johannes Nemeth · Frederick Klauschen · Christiane Schewe · Axel-Michael Ladhoff · Alexander Muckenhuber · Mariana Schürmann · Dirk Schürmann · Wilko Weichert

Received: 17 November 2011 / Accepted: 31 January 2012 / Published online: 16 February 2012
© Springer-Verlag 2012

Introduction

Leishmaniasis is a disease caused by protozoa that are transmitted by female sand flies (*Phlebotomus*) from either animals to humans (zoonosis) or from humans to humans (anthroponosis). Currently, approximately 30 sand fly species and 21 different *Leishmania* species are known, which reside as promastigotes in the gut of the arthropod. Once being inoculated via the skin and internalized in host macrophages and dendritic cells, the promastigotes transform to amastigotes and eventually disseminate via the lymph and blood system [1].

With respect to the organ primarily affected, leishmaniasis comprises four different syndromes: cutaneous leishmaniasis, mucocutaneous leishmaniasis, visceral leishmaniasis (VL; kalar-azar: Hindi for 'black fever') and a cutaneous form, which may occur after visceral leishmaniasis (post-kala-azar leishmaniasis—PKDL) [1]. Due to its systemic manifestations, visceral leishmaniasis is a potentially fatal disease with approximately 50,000 deaths per year and an estimated incidence of approx. 500,000/year. This mortality rate in parasitic diseases is second after malaria [2].

After 2–6 months of incubation, VL shows a panel of symptoms including fever, chills, fatigue, weight loss and tiredness. These symptoms are accompanied by hepato- and splenomegaly and sometimes lymphadenopathy and anaemia. However, as our case shows, immunocompromised patients may not present with the full picture of symptoms and manifestations may be atypically localized [2, 3].

Clinical history

A 49-year-old male, originally from the Dominican Republic, presented with loss of appetite, unspecific gastric discomfort and changes of bowel habits. His past medical history included infection with human immunodeficiency virus (HIV) with a CD4 lymphocyte nadir of 36/μl, approximately 2 years ago and

Electronic supplementary material The online version of this article (doi:10.1007/s00428-012-1207-1) contains supplementary material, which is available to authorized users.

A. Stenzinger (✉) · A. Muckenhuber · W. Weichert
Institute of Pathology, University Hospital Heidelberg,
Im Neuenheimer Feld 220/221,
69120 Heidelberg, Germany
e-mail: albrecht.stenzinger@med.uni-heidelberg.de

J. Nemeth
Department of Infectious Diseases, University Hospital Zurich,
Zurich, Switzerland

F. Klauschen · C. Schewe · A.-M. Ladhoff
Institute of Pathology, Charité—University Medicine Berlin,
Campus Mitte,
Berlin, Germany

M. Schürmann · D. Schürmann
Department of Infectious Diseases and Lung Diseases,
Charité—University Medicine Berlin,
Campus Virchow,
Berlin, Germany

multiple AIDS-defining diseases, including generalized *Mycobacterium avium* infection, cerebral toxoplasmosis, *Pneumocystis jiroveci* pneumonia, optic neuritis and generalized Herpes simplex infection. Moreover, he underwent nephrectomy for renal carcinoma 15 years ago. His current treatment regimen for HIV infection, chronic *M. avium* infection and toxoplasmosis included lopinavir/ritonavir, lamivudin, abacavir, clarithromycin, myambutol, folate and sulfadoxin/pyrimethamin.

Physical examination was unremarkable except for a slightly enlarged spleen. Laboratory tests showed long-standing chronic anaemia and chronic kidney failure. The CD4 lymphocyte count at this time point was 95/μl. Stool specimens were negative for microspora and cryptospora. Abdominal ultrasound confirmed splenomegaly without any further abnormalities. Gastroscopy revealed patchy, erythematous infiltrates in gastric mucosa and in the duodenum. Sampling for histological examination was performed.

Materials and methods

Electron microscopy

Tissue samples were fixed by immersion with 2.5% glutaraldehyde in 0.1 M phosphate buffer, pH 7.3, postfixed with 1% osmium tetroxide in the same buffer, processed through graded solutions of methanol and propylene oxide, and embedded in epoxy resin according to standard procedures. Resin blocks were ultrathin sectioned, stained with uranyl acetate and lead citrate, and examined on a Zeiss EM 10 electron microscope operating at 60 kV.

Polymerase chain reaction

For PCR analysis, a thermocycler from Biometra (Biometra Trio T3000) with Thermoprime Plus DNA Polymerase was used. For the detection of the ssurRNA Gen (small subunit rRNA coding gen of *Leishmania donovani*) the following primers were used: P1: 5′-TTA GAC CGC ACC AAG ACG AAC T-3′ sense (nucleotides 1158 – 1178) and P2: 5′-GGG TGT CAT CGT TTG CAG TGT G-3′ antisense (nucleotides 1264–1284) resulting in an amplicon of 126 bp. For the detection of *Leishmania* kinetoplast DNA (kDNA minicircle) the following primers were used: P1: 5′- GTG GGG GAG GGG CGT TCT-3′ and P2: 5′- ATT TTA CAC CAA CCC CCA GTT-3′ resulting in an amplicon of 120 bp.

Results and clinical course

Histological examination revealed dense subepithelial infiltrates of macrophages with dot-like microorganisms in the lamina propria of the stomach and the descending duodenum (Fig. 1). The microorganisms were found to be PAS negative but to contrast well in Giemsa staining. Examination of bone marrow trephines showed a similar histological picture with a dense/scattered infiltrate of pathogen-containing macrophages.

Electron microscopy eventually unravelled the nature of these microorganisms. As exemplified by Fig. 2a, b, we detected intracellulary located round to ovoid protozoa with a size of 2–4 μm. The amastigotes consisted of a doubled outer membrane, an oval nucleus and perinuclear kinetoplasts.

DNA was extracted from the formalin-fixed, paraffin-embedded biopsy specimens to perform a PCR with specific primer sets for a DNA sequence of the ssurRNA gene as well as for kinetoplast minicircle DNA as described elsewhere [4–6]. Matching the morphological results, DNA of *L. donovani* was found (Fig. 2c, d).

After confirming infection with *L. donovani*, treatment with amphotericin B was initiated, resulting in clinical improvement. However, treatment and the following prophylaxis were complicated by worsening kidney function, which led to low-dose amphotericin B treatment and, later on, to the use of miltefosine. Disappointingly, treatment failure was confirmed after 2 years by still detectable *Leishmania*, both in gastric mucosa and bone marrow. Based on two reports, the patient was then changed to fluconazole and allopurinol.

At the moment, the patient is being treated for HIV infection, chronic *M. avium* infection, toxoplasmosis and chronic visceral leishmaniosis. Given the circumstances, he is in relatively good physical condition, but further therapy remains challenging.

Discussion

Leishmaniasis is a well-known opportunistic infection in HIV-positive patients and is regarded as AIDS-defining disease in Africa only [2]. In vitro data suggest that leishmaniasis in HIV patients chronically activates the immune system and increases the viral load, thereby accelerating AIDS progression while HIV-mediated compromising of the immune system abets protozoan reproduction [1].

In HIV patients, symptoms caused by leishmaniasis are often non-specific. Particularly, splenomegaly is less often observed and coinfections may hamper diagnosis. Some case series point to the fact that VL in HIV-coinfected patients is often associated with atypical localizations [7, 8]. Our case also showed an unusual gastrointestinal manifestation of leishmaniasis.

The clinical course and prognosis of VL–HIV-coinfected patients differ considerably from those without HIV infection. Characteristically relapse risk and mortality are very high [3, 9]. Moreover therapy-related toxicity is significantly increased. With the highly active antiretroviral therapy (HAART) regimen being introduced in 1995, a significant reduction in the incidence of symptomatic VL in Europe was observed. For

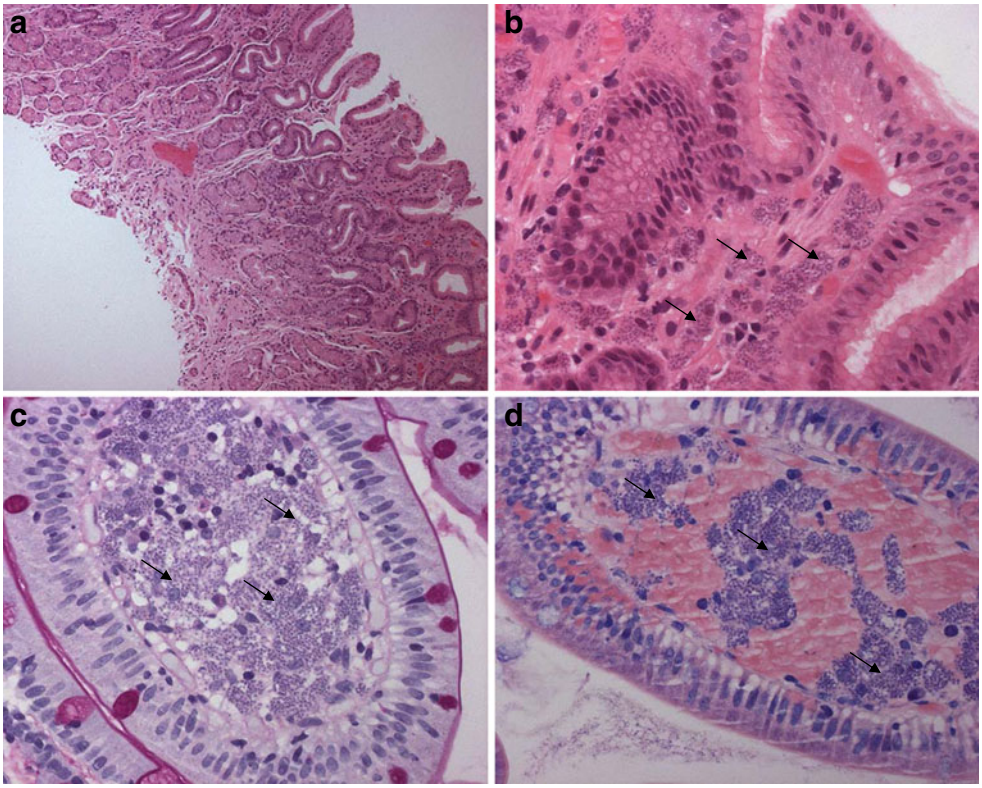

Fig. 1 Histological examination: **a** gastric mucosa (HE staining), low power view; **b** aggregates of *Leishmania* in macrophages of the gastric mucosa (*arrows*). Aggregates of *Leishmania* in macrophages of duodenal mucosa (*arrows*): **c** PAS staining and **d** Giemsa staining

patients receiving no HAART therapy, a high relapse risk was reported [1, 2]. With respect to relapse and recovery rate, our case clearly underlines the adverse effect of HIV coinfection in VL patients.

For the diagnosis of leishmaniasis in HIV-positive patients, microscopy of bone marrow aspirates/trephines or of biopsies of other localizations is the current gold standard. While sensitivity ranges from 67% to 94%, specificity is very high, but both quality numbers are intimately linked to the diagnostic expertise of the pathologist. Cell cultures from spleen or bone marrow biopsies also allow for the diagnosis of leishmaniasis with a relatively high sensitivity [1, 2]. Serological tests play a

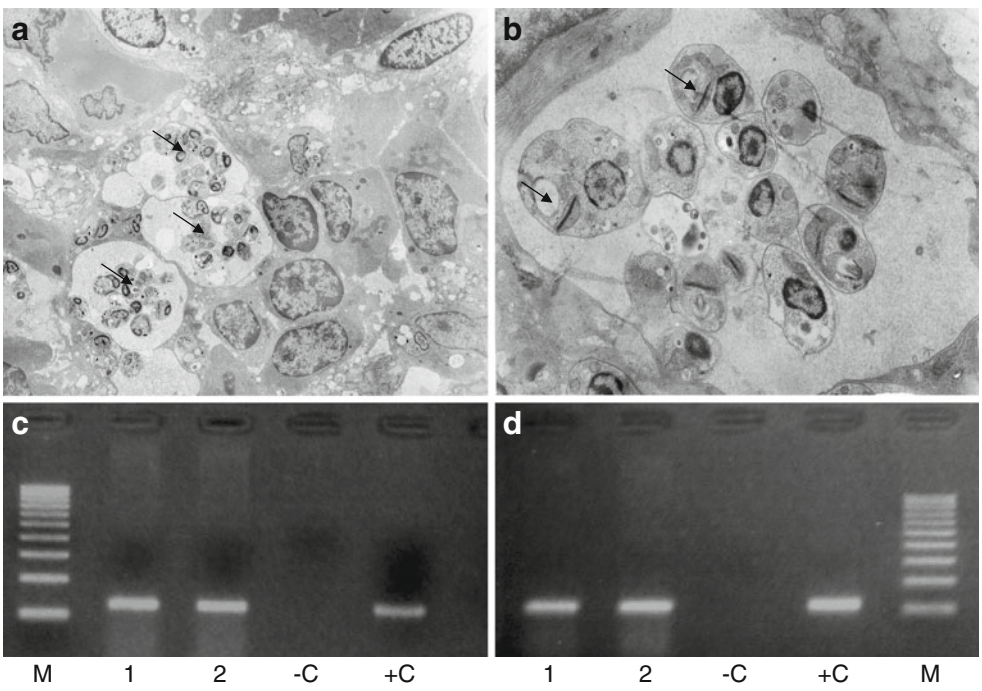

Fig. 2 Electron microscopy of leishmania in gastric (**a**) and duodenal (**b**) mucosa. PCR-based analysis of formalin-fixed, paraffin-embedded biopsies of the duodenum (agarose gel of PCR products). *Lanes 1 and 2* kDNA amplicon (126 bp, **c**), *lanes 1 and 2* SSUr-gene amplicon (120 bp, **d**). *M* marker, *−C* negative control, *+C* positive control

minor role in HIV-coinfected patients since approx. 40% of these patients display negative antibody titres. PCR-based analysis of bone marrow and blood specimens show a high sensitivity in this patient collective but is predominantly reserved for continuous monitoring of the clinical course [2, 4, 5, 10].

The case presented here supports these data. Serological tests were negative. Only histological analysis by the pathologist led to a successful diagnosis and paved the way for further clinical treatment. To allow for disease monitoring, this diagnostic approach was accompanied by a specific PCR analysis.

In 2007, the WHO suggested a diagnostic algorithm, which aims at improving and accelerating the diagnosis of leishmaniasis. Here, conventional microscopy and PCR-based analysis are considered as pivotal [2].

With respect to therapy, VL–HIV-coinfected patients have limited treatment options as opposed to patients without HIV infection. There are some therapy studies, which set out to prove the efficacy of several drugs, but the interpretation of the results is somewhat limited with respect to data quality. For HIV-coinfected patients, data are sparse and comparison of the results is hampered due to country-specific patient collectives and pathogenic agents [1–3]. Since the relapse frequency is high, secondary prophylaxis is of major importance [2, 9]. In conclusion, our case illustrates that an opportunistic VL with atypical gastrointestinal localization should be considered in HIV-positive patients with accordant symptoms and that a fast pathological diagnosis, merely based on morphology, is crucial for patients and clinical colleagues.

Conflict of interest The authors declare no conflict of interest.

References

1. Alvar J, Cañavate C, Gutiérrez-Solar B, Jiménez M, Laguna F, López-Vélez R, Molina R, Moreno J (1997) Leishmania and human immunodeficiency virus coinfection: the first 10 years. Clin Microbiol Rev 10:298–319
2. Alvar J, Aparicio P, Aseffa A, Den Boer M, Cañavate C, Dedet JP, Gradoni L, Ter Horst R, López-Vélez R, Moreno J (2008) The relationship between leishmaniasis and AIDS: the second 10 years. Clin Microbiol Rev 21:334–359
3. Chappuis F, Sundar S, Hailu A, Ghalib H, Rijal S, Peeling RW, Alvar J, Boelaert M (2007) Visceral leishmaniasis: what are the needs for diagnosis, treatment and control? Nat Rev Microbiol 5:873–882
4. Lasky T, Miko TL, Negesse Y, Solbach W, Röllinghoff M, Frommel D (1995) Detection of cutaneous *Leishmania* infection in paraffin-embedded skin biopsies using the polymerase chain reaction. Trans Royal Soc Trop Med Hyg 89:273–275
5. Rogers MR, Popper SJ, Wirth DF (1990) Amplification of kinetoplast DNA as a tool in the detection and diagnosis of *Leishmania*. Exp Parasitol 71:267–275
6. Costa JM, Durnand R, Denieu M, Rivollett D, Izri M, Houin R, Vidaud M, Bretagne S (1996) PCR-linked immunosorbent assay for diagnosis of *Leishmaniasis* in human immunodeficiency virus-infected patients. J Clin Microbiol 34:1831–1833
7. Laguna F, García-Samaniego J, Soriano V, Valencia E, Redondo C, Alonso MJ, González-Lahoz JM (1994) Gastrointestinal leishmaniasis in human immunodeficiency virus-infected patients: report of five cases and review. Clin Infect Dis 19:48–53
8. Rosenthal E, Marty P, del Giudice P, Pradier C, Ceppi C, Gastaut JA, Le Fichoux Y, Cassuto JP (2000) HIV and *Leishmania* coinfection: a review of 91 cases with focus on atypical locations of *Leishmania*. Clin Infect Dis 31:1093–1095
9. van Griensven J, Balasegaram M, Meheus F, Alvar J, Lynen L, Boelaert M (2010) Combination therapy for visceral leishmaniasis. Lancet Infect Dis 10:184–194
10. Schönian G, Nasereddin A, Dinse N, Schweynoch C, Schallig HD, Presber W, Jaffe CL (2003) PCR diagnosis and characterization of *Leishmania* in local and imported clinical samples. Diagn Microbiol Infect Dis 47:349–358

Virchows Arch (2012) 460:361
DOI 10.1007/s00428-012-1229-8

INVITED EDITORIAL

Pathology in Africa: back to basics

Pieter J. Slootweg

Received: 13 March 2012 / Accepted: 14 March 2012 / Published online: 29 March 2012
© The Author(s) 2012. This article is published with open access at Springerlink.com

In this issue, Berezowski et al. describe their experience as volunteers in a pathology laboratory in Malawi. It is not a surprise that the case mix they were confronted with differs greatly from what is seen in the daily practice of the majority of diagnostic pathology laboratories: almost half of the cases consisting of nonneoplastic lesions and within the group of neoplasias are a large proportion of pediatric cases, which would be rather unusual for a pathology laboratory in the northern hemisphere.

Not only the nature of cases is different but also the stage of development and size of the lesions that are submitted for pathological examination. Tourists on safari trips to Africa usually want to see the big five: lion, leopard, rhino, elephant, and buffalo. Getting to see them requires some luck and effort and this wish is not always fulfilled. It does not take much effort for the volunteering pathologist to encounter her or his own version of the big five: very large uterine fibroids, goiters, ovarian tumors, breast cancers, and lesions sometimes weighing several kilograms.

However, it is not only the difference in the type of lesion and their size that makes a stay in an African pathology laboratory such a rewarding experience. Working there in fact means practicing pathology as it was done where most of us reside not that long ago: before immunohistochemistry and molecular pathology entered the scene. It encompasses looking at slides that quite often are slightly or even quite a bit thicker than the 3 or 4 μm we are accustomed to. There is no room for postponing of decisions by ordering time-consuming additional stains: the diagnosis has to be made on a few or even just one single hematoxylin and eosin-stained slide. Diagnostic skill and acumen that tend to languish in an environment where a brown deposit usually is considered to be more decisive for diagnosis than careful morphological analysis are brought to new life when one is left with nothing else than a microscope of moderate quality, a pair of eyes, and experience.

An issue only briefly alluded to by Berezowski et al. but requiring a little bit more reflection is whether in that setting histopathological examination plays any role in patient management. Quite often, patients are treated without prior biopsy or, in case their specimens are submitted for pathological examination, have already left the hospital and returned to their villages somewhere in a remote area before the pathology report has arrived on the clinician's desk. This precludes any guidance of treatment by pathological analysis, either preoperatively on the basis of a biopsy or postoperatively through examination of a resection specimen.

Therefore, if pathology is to play any role in guiding daily patient care under sub-Saharan African conditions and resources, it should provide a cheap and quick diagnosis—requirements that obviously can be met by diagnostic cytology. Any volunteering pathologist should master this area and should preferably also be capable of performing FNAs, as this allows not only rapid diagnosis and valuable clinical correlations but also offers an opportunity for personal contacts with less privileged people whose daily lives are much more difficult than ours. This experience may make us more humble and lenient in handling the small inconveniences we all regularly encounter in either our private or professional lives.

P. J. Slootweg (✉)
Department of Pathology,
Radboud University Nijmegen Medical Center,
P.O. Box 9101, 6500 HB, Nijmegen, Netherlands
e-mail: p.slootweg@pathol.umcn.nl

P. J. Slootweg
Department of Pathology, Kilimanjaro Christian Medical Center,
Moshi, Tanzania

Open Access This article is distributed under the terms of the Creative Commons Attribution License which permits any use, distribution, and reproduction in any medium, provided the original author(s) and the source are credited.

Virchows Arch (2012) 460:363–370
DOI 10.1007/s00428-012-1217-z

ORIGINAL ARTICLE

Surgical pathology in sub-Saharan Africa—volunteering in Malawi

Sabina Berezowska · Tamiwe Tomoka · Steve Kamiza · Danny A. Milner Jr. · Rupert Langer

Received: 9 February 2012 / Accepted: 22 February 2012 / Published online: 10 March 2012
© Springer-Verlag 2012

Abstract The breadth of material found in surgical pathology services in African countries differs from the common spectrum of "the West". We report our experience of a voluntary work in the pathology departments of Blantyre and Lilongwe, Malawi. During a 6-week period, 405 cases (378 histology and 27 cytology cases) were processed. The vast majority showed significant pathological findings (n=369; 91.1 %): 175 cases (47.4 %) were non-tumoral conditions with predominance of inflammatory lesions, e.g., schistosomiasis (n=11) and tuberculosis (n=11). There were 39 (10.6 %) benign tumors or tumor-like lesions. Intraepithelial neoplasia of the cervix uteri dominated among premalignant conditions (n=15; 4.1 %). The large group of malignancies (n=140; 37.9 %) comprised 11 pediatric tumors (e.g., rhabdomyosarcoma, small blue round cell tumors) and 129 adult tumors. Among women (n=76), squamous cell carcinomas (SCCs) of the cervix uteri predominated (n=25; 32.9 %), followed by breast carcinomas (n=12; 15.8 %) and esophageal SCC (n=9; 11.8 %). Males (n=53) most often showed SCC of the esophagus (n=9; 17.0 %) and of the urinary bladder (n=7; 13.2 %). Lymphomas (n=7) and Kaposi's sarcomas (n=6) were less frequent. Differences compared to the western world include the character of the conditions in general, the spectrum of inflammatory lesions, and the young age of adult tumor patients (median 45 years; range 18–87 years). Providing pathology service in a low-resource country may be handicapped by lack of personnel, inadequate material resources, or insufficient infrastructure. Rotating volunteers offer a bridge for capacity building of both personnel and the local medical service; in addition, the volunteer's horizons are broadened professionally and personally.

Keywords Pathology · Low-resource country · Africa

Electronic supplementary material The online version of this article (doi:10.1007/s00428-012-1217-z) contains supplementary material, which is available to authorized users.

S. Berezowska · R. Langer (✉)
Institute of Pathology, University of Bern,
Murtenstr 31,
3010 Bern, Switzerland
e-mail: rupert.langer@pathology.unibe.ch

T. Tomoka · S. Kamiza
Department of Histopathology, College of Medicine,
University of Malawi,
Blantyre, Malawi

D. A. Milner Jr.
Department of Pathology, Brigham and Women's Hospital,
Boston, MA, USA

R. Langer
Institute of Pathology, Technische Universität München,
Munich, Germany

Introduction

Providing pathology service in low-resource countries is challenging due to the lack of trained personal and technical equipment and inefficient infrastructure (e.g., transportation, communication, etc.) [1–3]. The latter of these can be built quickly when money, demand, and motivation are available; the former (i.e., personnel) requires time for training which creates gaps. The challenge of providing high-quality pathological services in Africa is limited by the number of available well-trained and skilled pathologists in a particular country or medical unit. When indigenous highly skilled pathologists are available, they may often be so few in number that the overwhelming challenges of providing medical education, pathology service, and government/

administrative responsibilities hinder their day to day sign-out ability. When a low-resource pathology unit has the opportunity to add staff to their system, they are still faced with the gap between the arrivals of the new team members. One system to overcome this problem which can serve as a temporary bridge while building the required capacity with indigenous pathologists is a rotating volunteer system. This provides qualified pathologist who can insure continuity, establish turn-around-time goals, and train local medical staff in the best methods for tissue collection for both histology and cytology.

Malawi is a small country in southeast Africa bordered by Tanzania in the north and northeast, Zambia in the west, and Mozambique in the southeast and southwest. It is one of the smallest but most densely populated counties in subequatorial Africa with a population of currently around 16 million inhabitants, of whom the vast majority lives in rural areas. Malawi belongs to the poorest countries in the world with around 40 % of Malawians living below the international poverty line. The economy is essentially agricultural, and tobacco accounts for 70 % of Malawi's export earnings, followed by tea and sugar—all mainly grown by smallholder farmers. The country is heavily dependent on foreign aid, which represents half of its gross domestic product [4].

Like most sub-Saharan countries, Malawi suffers from a high burden of HIV, with an estimated prevalence of 15 % for the age group between 15 and 49 years. Tuberculosis and malaria are common [5, 6]. Major efforts to establish and improve Malawi's health care system are in process, e.g., offering the main health services free of charge. Life expectancy has successfully improved from less than 40 years in 2000 to 52.2 years in 2009 [4].

In Malawi, there are currently two functioning government-run pathology laboratories situated in the University of Malawi College of Medicine in Blantyre (serving the majority of the country's hospitals) and at the Kamuzu Central Hospital in Lilongwe (Malawi's capital). There are four fully certified pathologists. One of them does forensic postmortems only and one retired pathologist is providing service for the Lilongwe lab. The remaining two (TT and KS) are working at the College of Medicine. Being faculty members, they are also heavily involved in administrative and academic duties. Two local residents are currently abroad and two more are beginning their residency in 2012. All residents are trained in South Africa over a 4-year period, as special education for pathology residents is currently not available in Malawi.

In July 2011, a structured support project for the pathology service of Malawi was initiated by Danny Milner from the Department of Pathology, Brigham and Women's Hospital, Boston, USA, in association with the Partners in Health [7]. The aim of the Pathologists for Malawi Project (which uses the well-established model provided by the long-time operating organization "Pathologists Overseas") is to provide continuous on-site support by volunteer pathologists until local pathology residents finish their training abroad, thereby shortening turnover times, avoiding larger backloads, but also creating an intellectual and cultural exchange between local and foreign pathologists. Here, we report our individual experience of a 6-week voluntary work in the pathology departments of Blantyre and Lilongwe, Malawi, between November and December 2011.

Materials and methods

Pathology laboratories in Blantyre and Lilongwe

The Department of Histopathology in Blantyre is part of the College of Medicine of Malawi and provides diagnostic service for the large Queen Elisabeth Central Hospital in Blantyre and for at least 20 additional hospitals of Blantyre and the rest of the country. The annual workload reaches around 3,000 cases for histological examination (estimated to be approximately 10 % of the actual potential caseload for the country). Moreover, the department provides pathology service for a large number of scientific projects, mostly coordinated from abroad.

In Lilongwe, the histopathologic laboratory is located within the area of the Kamuzu Central Hospital (KCH), the capital's largest clinic. The lab is set up and financed by the University of North Carolina (UNC), which is running a large research center on the campus. Before the UNC-sponsored lab was constructed, there were approximately 150 cases per year from KCH. In the first 6 months of operation, 700 diagnostic cases processed, creating a projected caseload of ~1,500 cases annually (a tenfold increase). Because there is no on-site permanent pathologist in Lilongwe, the slides are produced at KCH but then have to be sent to Blantyre for reading and signing-out by Professor George Liomba, the retired former head of the Blantyre Department of Histopathology. Both laboratories (Blantyre and Lilongwe) are fully functional, equipped with embedding processors, microtomes, and automatic staining machines. At present, hematoxylin and eosin (H&E), periodic acid-Schiff, and Ziehl–Neelsen (ZN) stains are available. Both labs plan to implement further special histochemical and basic immunohistochemical stains. There are expert technicians on both sites, and additional staff is going to be trained during the next years.

Pathology volunteers

The work of volunteering pathologist mainly consists of providing diagnostic service, which results in immediate support for the local pathologists. Furthermore, there is a

possibility to assist in teaching of the forthcoming pathology residents (e.g., grossing and histology, preparing teaching slides), technicians, and clinicians (e.g., performing fine needle aspirations). The volunteers are self-funded but housing is provided by Danny Milner and the UNC.

Time period reported

The reported cases encompass our diagnostic workload (SB and RL) during a 6-week period between November and December 2011 while working as volunteering pathologists in Malawi—4 weeks in Blantyre and 2 weeks in Lilongwe.

Results

A total of 405 cases were processed and reviewed, encompassing 378 histology specimens (139 biopsies, 133 excisions and curettages, and 106 resection specimens) and 27 cytology cases. The Blantyre load included 326 cases, while 79 cases were seen in Lilongwe. The majority of cases (n=120, 29.6 %) were from gynecological sites (uterus, ovary, and breast), followed by gastrointestinal cases (n=73; 18 %; esophagus and colon). An overview about the distribution of the various sites is given in Fig. 1. Most cases showed significant pathological findings. In some of the 26 cases lacking pathological changes, the clinical diagnosis of a tumor (e.g., stenosing esophageal cancer) implied insufficient sampling. The cases with pathological findings consisted of 175 (47.4 %) non-tumoral conditions, 39 (10.6 %) benign tumors or tumor-like lesions, 15 (4.1 %) premalignant changes, and 140 (37.9 %) malignant tumors. Ten cases (six of them cytology) were technically unsatisfactory.

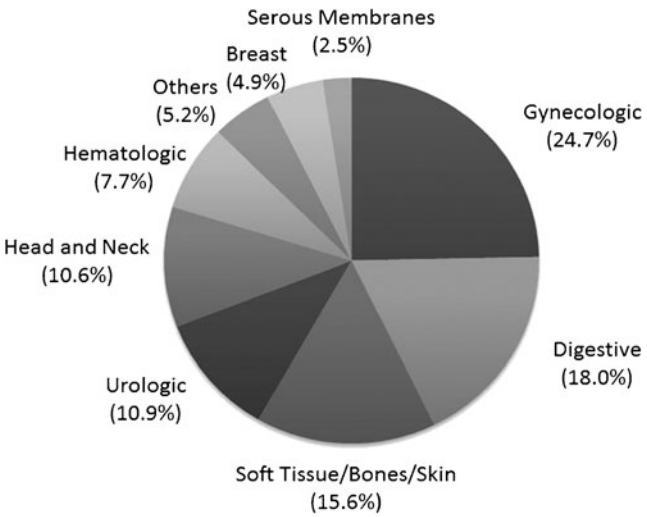

Fig. 1 Topographical distribution of cases

Macroscopic and histologic pictures of some examples of the cases are given in Fig. 2. A complete list of all cases is provided as Electronic supplemental material.

Benign conditions

Eighty-nine cases (22.0 %) showed only degenerative or functional changes, like disorders of pregnancy (ectopic pregnancies or missed abortions), Hirschsprung's disease (n=4), cysts, hyperplastic conditions, or fibrosis. Inflammatory conditions as main diagnosis were found in 94 cases (25.5 %); the most frequent sites being soft tissue, cervix, uteri, and appendix. Unspecific inflammation was acute (n=32) or chronic or chronic granulating (n=39). Twenty-three inflammatory cases showed specific histomorphological findings. Schistosomiasis (n=10) was an additional finding in four malignant cases. There were two cases of a cysticercosis. Eleven cases were consistent with tuberculosis. However, only one of them could be confirmed by demonstration of acid-fast bacilli in a ZN staining, resulting in the need for correlation with microbiological cultures.

Benign tumors and tumor-like lesions

Among the benign tumors, there were 15 epithelial neoplasms, e.g., benign salivary gland tumors like pleomorphic adenomas and ovarian tumors like granulosa cell tumors. Within the group of benign mesenchymal tumors or tumor-like lesions, there were leiomyomas of the uterus, hemangiomas, and spindle cell proliferations of unknown lineage, which could not be finally classified due to lack of immunohistochemistry.

Premalignant lesions

The vast majority of premalignant lesions consisted of cervical intraepithelial neoplasia (CIN I–III), diagnosed in cervical biopsies, excisions, and three hysterectomy specimens. Two cases showed squamous cell dysplasia of the conjunctiva.

Malignant tumors

Among the malignant cases were 11 pediatric tumors (patients under 18 years): three cases of small blue round cell tumors (not otherwise classifiable), two retinoblastomas, two cases consistent with rhabdomyosarcoma, and two Kaposi's sarcomas. The large group of adult malignant tumors consisted of 76 cases (58.9 %) from female patients and 53 cases (41.1 %) from male patients. The most frequent malignancies among women were cervical squamous cell carcinomas (SCCs; n=25; 32.9% of all female malignancies), followed by breast carcinomas (n=12; 15.8 %), esophageal

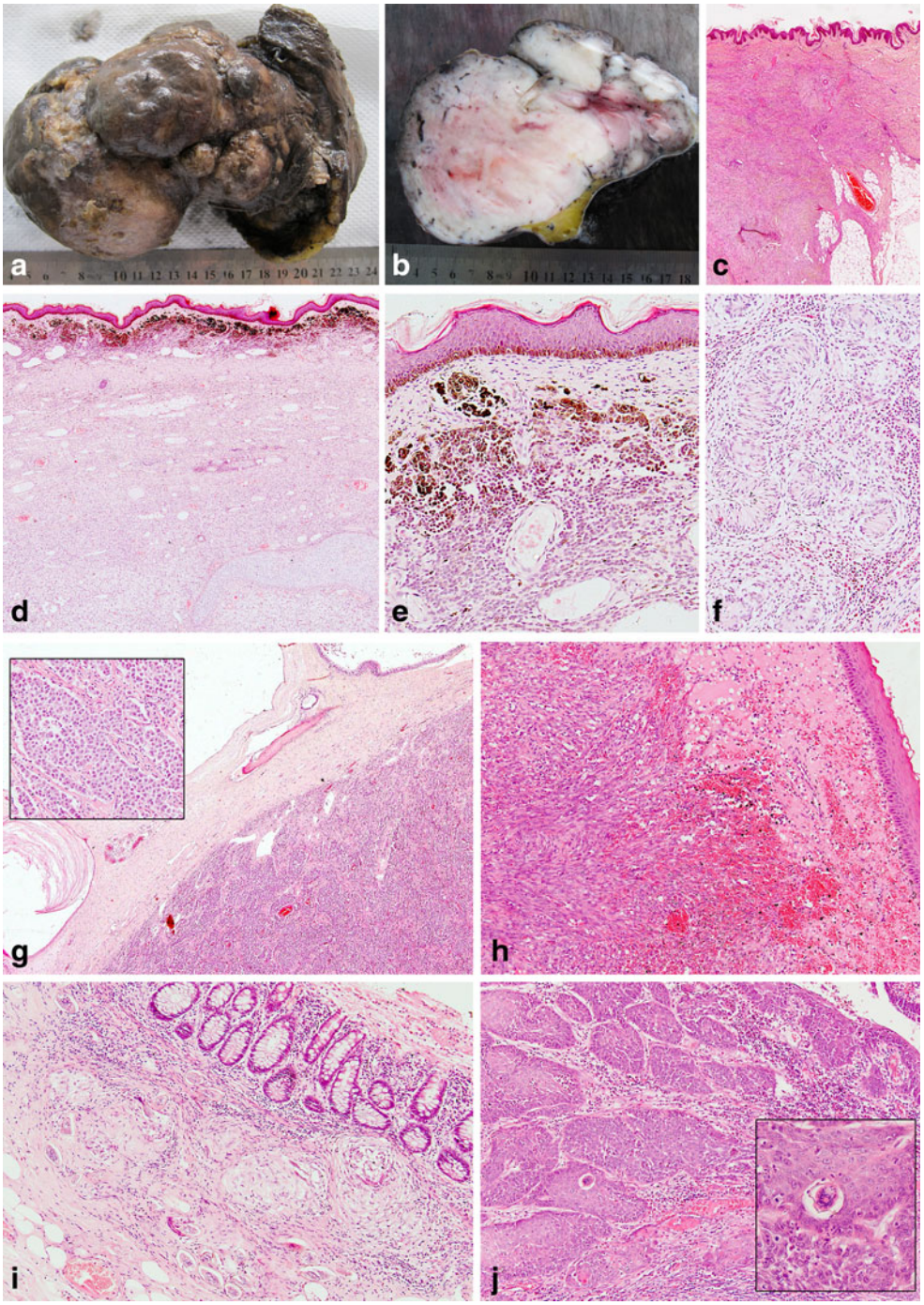

Fig. 2 Examples of cases. **a–c** Very large dermatofibrosarcoma protuberance of the abdominal wall (15-year-old male). **a** Macroscopic top view. **b** Macroscopic cut surface. **c** Histology (H&E; ×2.5). **d–f** Giant dermal nevus with underlying large diffuse neurofibroma (1-year-old girl). **d** Overview (H&E; ×2.5)—note chondroid metaplasia (*right angle*). **e** Dermal nevus (H&E, ×10). **f** Wagner–Meissner bodies within diffuse neurofibroma (H&E, ×10). **g** Collision of a mature teratoma and a dysgerminoma in the ovary (18-year-old female; H&E, ×2.5; *inset*, magnification of dysgerminoma). **h** Kaposi's sarcoma of the tonsil region (39-year-old female; H&E, ×10). **i** Colon specimen with granulomatous inflammation in the submucosa due to schistosomiasis (13-year-old girl, with the clinical diagnosis of Hirschsprung's disease; H&E, ×20). **j** Squamous cell carcinoma of the urinary bladder (39-year-old male; H&E, ×20) with schistosoma eggs (*inset*, magnification)

SCC (n=9; 11.8 %), and ovarian carcinomas (n=7; 9.2 %). Within the group of males, the most frequent malignant tumors were esophageal SCC (n=9; 17.0 %) and SCC of the urinary bladder (n=7; 13.2 %). The median age of adult cancer patients was 43.5 years for females (range, 18–87 years) and 52 years for males (range, 24–82 years). Of note, the overall percentage of Kaposi's sarcomas and lymphomas was relatively low, with only six cases (4.3 %) and seven cases (5 %), respectively. Other tumors, like laryngeal carcinoma, skin cancer, or intestinal cancers were comparably rare. Metastatic disease was found in ten cases (7.1 %), comprising two metastases of primary gastric cancer and eight metastases without known primary. An overview of the most frequently seen adult malignancies is given in Tables 1 and 2.

Among the rare or unexpected tumors were (a) a high-grade sarcoma with rhabdoid features from a 23-year-old female, presenting as a large abdominal mass, (b) a soft tissue manifestation (clinical information) of a chondrosarcoma with extension into the musculus iliopsoas from a 22-year-old woman, (c) a dysgerminoma of the ovary of an 18-

Table 1 Most frequently seen adult female malignancies

Site	No.	Percentage	Median age (min–max)
Cervix uteri	23	31.9	42 (28–70)
Breast	11	15.3	50 (29–60)
Esophagus	9	12.5	40 (32–57)
Skin	5	6.9	46 (32–70)
Ovaries	5	6.9	28 (18–52)
Lymphomas	3	4.2	30 (27–50)
Total adult female malignancies	72	100	43 (18–87)

year-old female with a simultaneous mature teratoma, (d) a gigantic dermatofibrosarcoma protuberance from a 15-year-old boy (without fibrosarcomatous areas), and (e) three cases of malignant melanoma. A number of tumors could not be finally classified due to the inability to determine the tumor's lineage due to the lack of additional immunohistochemical stains or molecular diagnostics (e.g., for the determination of specific translocations).

Discussion

In low-resource medicine, it is not uncommon for pathologists to be only rarely involved in the diagnostic process during the treatment of patients—in benign or malignant conditions alike. Patients are treated either without a pathologic or laboratory diagnosis based on clinical suspicion alone or are not treated at all. Pathology service in developing countries is complicated by insufficient infrastructural conditions and the lack of specialized personnel and technical equipment [1–3]. Thus, tissue may be submitted for histopathological examinations just in case of clinically highly relevant questions. And even in these cases, clinicians may be faced with long turnover times—often exceeding many months—and the provision of differential diagnoses only, especially in those instances when special additional methods would be mandatory to solve the case.

Table 2 Most frequently seen adult male malignancies

Site	No.	Percentage	Median age (min–max)
Esophagus	9	18	55 (27–79)
Bladder	7	14	39 (28–82)
Soft tissue	5	10	54 (30–76)
Lymphomas	4	8	36 (24–60)
Larynx	4	8	50 (26–76)
Skin	3	6	40 (25–61)
Prostate	3	6	72 (60–76)
Total adult male malignancies	50	100	52 (24–82)

During the 6 weeks, we had the opportunity to gain insight into the diagnostic spectrum of a typical histopathological laboratory in sub-Saharan Africa. A comparison with statistics of a previous year showed that the variety of our cases is representative of the average distribution and character of the annual workload. The majority of biopsies and excisions received consisted of quantitatively adequate, well-preserved tissue, enabling high-quality histomorphology. Fixation of larger resection specimens was sometimes unsatisfactory; however, this did not impede diagnosis. In contrast, fine needle aspiration (FNA), which represents a much simpler technique requiring far fewer resources, failed to provide satisfactory diagnostic material in many cases of our series. This coincides with similar observations from other low-resource countries and highlights the necessity for FNA training facilities.

Probably due to the low rate of submitted specimens mentioned above, the number of cases with significant pathologic findings was remarkably high as compared to a western world pathology laboratory—in particular the percentage of malignancies (34.5 vs. 19.2 % in the Institute of Pathology, Technische Universität München, Germany, during the same time period). It is important to keep in mind that therefore our case series cannot be used to estimate prevalence. Milner et al. are currently preparing a 10-year retrospective paper which covers a full pathoepidemiological assessment of Malawi's pathology from 1997 to 2007.

Communicable diseases, e.g., malaria, HIV, and tuberculosis (including HIV-associated), represent a major cause of morbidity and mortality in central and southeast Africa [5, 6, 8–10]. In accordance, a significant number of cases were histomorphologically most consistent with tuberculosis or atypical mycobacterial infection. This was seen in about half of the lymph nodes sent in for examination, but also at various other sites like soft tissue or joints. Using ZN staining, the presence of acid-fast bacilli could be confirmed in only one of those cases. However, the ZN results are most probably false negative due to suboptimal staining procedures, as reported by others in similar settings [11].

Another very interesting finding was the frequency of schistosomiasis, which is widespread in Malawi like in other African countries [12, 13]. In our cases, schistosoma eggs causing inflammation were found at various sites, e.g., the cervix uteri, the urinary bladder (some as additional finding to carcinoma), or in the appendix, causing an acute perforating appendicitis. Of note, schistosomiasis was the definite histopathological diagnosis in a colon segment of a 13-year-old girl, which was removed with the clinical diagnosis of Hirschsprung's disease, and in a hysterectomy specimen resected due to the clinical impression of a cervical carcinoma. The majority of inflammatory lesions, although

representing 25 % of the caseload, however, failed to present specific etiologic findings.

In the large group of tumoral conditions, the number of malignant and premalignant cases dominated over benign conditions. Most benign tumors were soft tissue tumors, e.g., leiomyomas of the uterus. There were some rare findings, like a lipofibromatosis/fibrous hamartoma of infancy or a large diffuse neurofibroma underlying a giant dermal nevus, as well as two peripheral ossifying fibromas in the oral cavity.

Although in a number of cases a definitive diagnosis could not be performed due to lack of ancillary techniques, we could at least estimate the dignity in all these cases or provide the most probable differential diagnoses according to the histomorphological picture. Apart from the soft tissue tumors, we also saw a considerable number of benign salivary gland tumors, mainly pleomorphic adenomas (n=6). This is consistent with the observation of the high incidence of salivary gland tumors among African people [14].

Most of the pediatric cases were malignant. Among them are two retinoblastomas and two rhabdomyosarcomas—one of them representing a recurrent case with current "small round cell tumor" morphology. Of note, there were three other cases of small round cell tumors; one of them probably a hematolyphoid malignancy. Unfortunately, the lack of ancillary techniques impeded a definitive diagnosis.

Within the adult malignant cases, the high frequency of SCC of the cervix uteri and intraepithelial precursor lesions reflects the incidence of HPV-induced cervical cancer as the leading malignancy of women in Malawi and most other African countries [15–17]. Cervical cancer has been shown to have a strong association with HIV as a co-driving factor [18]. Unfortunately, the HIV status was only very inconstantly provided in the clinical submission forms, rendering a reliable analysis in this regard fairly impossible. Schistosomiasis of the cervix uteri was relatively common (n=3), and one case showed concomitant SCC. An etiologic correlation has not yet been sufficiently investigated.

A striking finding was the high percentage of malignant squamous lesions at various other sites, like the esophagus, the urinary bladder, or the conjunctiva. Esophageal squamous cell carcinomas were observed in both females and males, in a relatively high frequency and with a low median patient age (45 years). This represents a marked difference as compared to western countries [16]. Several previous studies have highlighted the differing carcinogenesis of esophageal cancer in high-incidence areas like Southeast Asia or Southern Africa [16, 19, 20]. A number of nutritional or environmental factors have been identified—varying dependent on the geographic area investigated [21, 22]. HPV and/or HIV also may have major impact on esophageal carcinogenesis in these countries [23]. However, larger studies with comprehensive epidemiologic and molecular genetic investigations are still missing in this field.

Conjunctival squamous cell carcinoma is also known to occur with increased frequency in Africa. This is likely related to sun exposure and possibly aggravated by viral infections as HIV; however, the exact etiology of this tumor remains unknown [24].

SCC of the bladder is known to be strongly associated with infections by *Schistosoma haematobium* [12, 16]. In fact, the presence of parasite eggs was directly demonstrated in one case of SCC of the bladder and in one case with epithelial changes indefinite for dysplasia. Among the other cases, identification of schistosoma eggs was impeded by extensive tissue infiltration by the SCC.

The incidence of breast cancer in Africa is reported to be increasing, although it still remains less frequent than in western countries. In our collection of cases, mammary carcinomas accounted for 15 % of all female malignancies. Breast cancer in Africa has been shown to be unusually aggressive and to affect women at a relatively young age [16, 25–28]. In our collection, however, only two carcinomas were grade III tumors using the Elston and Ellis grading system, and all were specified as invasive ductal (NOS)—some of them with an intraductal component. Regarding the age distribution, five women were 40 years and younger, which could be expected in accordance with the data mentioned above. Interestingly, we saw one case of a male breast cancer, which was already described to occur relatively frequently in this part of Africa [29]. Finally, consistent with the low incidence of lung, colorectal, gastric, and prostatic cancers in sub-Saharan Africa [16], we only had three intestinal carcinomas (one of them a carcinoma of the small intestine), three gastric carcinomas or metastases of gastric carcinomas, four prostate carcinomas, and no lung malignancy.

An interesting finding was our low percentage of Kaposi's sarcomas, which are described to occur in a frequency of around 20 % in female and 50 % in male cancer patients in east Africa [16, 17]. Similarly, albeit in lower extent, the frequency of lymphomas among our cases did not reach the expected numbers. This probably represents either sampling bias during our short visit, clinical acumen at making the diagnosis without biopsy, and/or the fact that fewer than 20 % of malignancy diagnoses are being confirmed by laboratory methods (histology, cytology, or hematology) [30].

Unequivocal clinical findings of malignant tumors, like Kaposi's sarcoma in HIV patients or Burkitt's lymphoma in the clinical setting of a rapidly growing mass in association with a dramatic clinical worsening, do not necessarily warrant histopathologic confirmation in the setting of low-resource medicine. The usual therapy of Kaposi's sarcoma consists of antiviral treatment plus a trial and error application of chemotherapy, if available, and diagnosis is confirmed by response [31]. For Burkitt's lymphoma, a rapid

histopathologic diagnosis would be required, which could be provided only in a very small number of cases [32, 33]. Therefore, treatment is initiated on clinical diagnosis alone.

One has to consider that this is also true in many other cases: even a diagnosis of malignancy would not change therapy due to the lack of adequate therapeutic options. However, in many low-resource countries, medical service improves slowly but steadily as countries progress to higher economic status [34]. Surgical and nonsurgical treatment of oncologic diseases is performed (we saw a case of a breast cancer with the previous history of neoadjuvant chemotherapy). Therefore, adequate pathology services can lead to the recognition of pathology as an integral part of a multidisciplinary healthcare setting. An example is the consensus guideline on breast health care in low-resource and middle-resource countries of the Breast Health Global Initiative, which requires a pathologic diagnosis before the initiation of treatment [35]. Providing pathology service in low-resource countries therefore not only challenges pathologists with difficult working conditions and extraordinary and rare cases, but also provides patient access to better, tailored, and potentially even curative therapies.

There are several modes of support for pathology services: One may be support of already existing laboratories, like the pathologists for Malawi project does, providing immediate load relief for local physicians or covering them during professional education periods. Laboratories, which have been closed due to breakdown of technical equipment and lack of pathologists, can be reestablished [36], and exchange programs can help in forming local pathologists [1]. Teaching clinicians about what can be expected from a pathologic diagnosis can be very helpful, as well as training in performing biopsies and FNAs—the most useful technique in low-resource settings. The immediate feedback given by the pathologists about the quality of the tissue or smears is most often a first, but very important, step for improving quality [37].

Apart from activities by individuals, there are a few organizations, which are coordinating support for pathology in low-resource countries: “Pathologists overseas” (contact: hoenecke57@gmail.com) has been active for almost 20 years [38]. “Pathologists and technicians in favor of developing countries” is a working group within the European Society of Pathology, which mainly consists of members of the Italian organization “Patologi Oltre Frontiera” (www.patologioltrefrontiera.it). They have already performed and are currently conducting several projects in African and Asian countries, e.g., the implementation of telepathology in combination with training of local physicians [11].

In summary, our volunteering work gave us a broad insight into the spectrum of diseases that pathologists can expect in sub-Saharan countries [39, 40] and the challenges that pathology is faced with in low-resource settings. While working as volunteering pathologists, both a rich cultural and an intellectually stimulating professional experience can be achieved, at the same time providing a much needed and appreciated diagnostic service.

Acknowledgments The authors thank Kingsley Makwakwa and Fred Chimzimu for excellent technical assistance, and Rob Krysiak and our housekeeper Naomi for taking care of us during our stay in Lilongwe and Blantyre, respectively. We also like to thank Heinz Hoenecke (Pathologists Overseas) for bringing us in contact with the Pathologists for Malawi Project. Furthermore, we thank Katja Specht, MD for expert reevaluation of some tricky cases back at home.

Conflict of interest The authors declare no conflict of interest.

References

1. Adeyi OA (2011) Pathology services in developing countries—the West African experience. Arch Pathol Lab Med 135(2):183–186. doi:10.1043/2008-0432-CCR.1
2. Benediktsson H, Whitelaw J, Roy I (2007) Pathology services in developing countries: a challenge. Arch Pathol Lab Med 131 (11):1636–1639. doi:10.1043/1543-2165(2007)131[1636:psidca]2.0.co;2
3. Rambau PF (2011) Pathology practice in a resource-poor setting: Mwanza, Tanzania. Arch Pathol Lab Med 135(2):191–193. doi:10.1043/1543-2165-135.2.191
4. Wikipedia (2012) Malawi. http://en.wikipedia.org/wiki/Malawi. Accessed 10 Jan 2012
5. Mathers CD, Loncar D (2006) Projections of global mortality and burden of disease from 2002 to 2030. PLoS Med 3(11):e442. doi:10.1371/journal.pmed.0030442
6. Mhalu FS (2005) Burden of diseases in poor resource countries: meeting the challenges of combating HIV/AIDS, tuberculosis and malaria. Tanzan Health Res Bull 7(3):179–184
7. Carlson JW, Lyon E, Walton D, Foo WC, Sievers AC, Shulman LN, Farmer P, Nose V, Milner DA Jr (2010) Partners in pathology: a collaborative model to bring pathology to resource poor settings. Am J Surg Pathol 34(1):118–123. doi:10.1097/PAS.0b013e3181c17fe6
8. Jones LA, Chilton JA, Hajek RA, Iammarino NK, Laufman L (2006) Between and within: international perspectives on cancer and health disparities. J Clin Oncol 24(14):2204–2208. doi:10.1200/jco.2005.05.1813
9. Zachariah R, Ford N, Philips M, Lynch S, Massaquoi M, Janssens V, Harries AD (2009) Task shifting in HIV/AIDS: opportunities, challenges and proposed actions for sub-Saharan Africa. Trans R Soc Trop Med Hyg 103(6):549–558
10. WHO (2011) Global tuberculosis control 2011. http://www.who.int/gho/mdg/diseases/hiv/en/index.html. World Health Organization, Geneva, Switzerland http://www.who.int/tb/publications/global_report/2011/gtbr11_full.pdf
11. Pagni F, Bono F, Di Bella C, Faravelli A, Cappellini A (2011) Virtual surgical pathology in underdeveloped countries: the Zambia project. Arch Pathol Lab Med 135(2):215–219. doi:10.1043/1543-2165-135.2.215
12. Ross AGP, Bartley PB, Sleigh AC, Olds GR, Li Y, Williams GM, McManus DP (2002) Schistosomiasis. N Engl J Med 346 (16):1212–1220. doi:10.1056/NEJMra012396
13. Steinmann P, Keiser J, Bos R, Tanner M, Utzinger J (2006) Schistosomiasis and water resources development: systematic

review, meta-analysis, and estimates of people at risk. Lancet Infect Dis 6(7):411–425. doi:10.1016/S1473-3099(06)70521-7
14. Masanja MI, Kalyanyama BM, Simon EN (2003) Salivary gland tumours in Tanzania. East Afr Med J 80(8):429–434
15. Anorlu RI (2008) Cervical cancer: the sub-Saharan African perspective. Reprod Health Matters 16(32):41–49
16. Jemal A, Bray F, Center MM, Ferlay J, Ward E, Forman D (2011) Global cancer statistics. CA Cancer J Clin 61(2):69–90. doi:10.3322/caac.20107
17. Parkin DM, Sitas F, Chirenje M, Stein L, Abratt R, Wabinga H (2008) Part I: cancer in indigenous africans—burden, distribution, and trends. Lancet Oncol 9(7):683–692. doi:10.1016/s1470-2045(08)70175-x
18. Chirenje ZM (2005) HIV and cancer of the cervix. Best Pract Res Clin Obstet Gynaecol 19(2):269–276
19. Hendricks D, Parker MI (2002) Oesophageal cancer in Africa. IUBMB Life 53(4–5):263–268. doi:10.1080/15216540212643
20. Walker ARP, Adam F, Walker J, Walker BF (2002) Cancer of the oesophagus in Africans in sub-Saharan Africa: any hopes for its control? Eur J Cancer Prev 11(5):413–418
21. Sammon AM (2007) Carcinogens and endemic squamous cancer of the oesophagus in Transkei, South Africa. Environmental initiation is the dominant factor; tobacco or other carcinogens of low potency or concentration are sufficient for carcinogenesis in the predisposed mucosa. Med Hypotheses 69(1):125–131
22. Sammon AM, Iputo JE (2006) Maize meal predisposes to endemic squamous cancer of the oesophagus in Africa: breakdown of esterified linoleic acid to the free form in stored meal leads to increased intragastric PGE2 production and a low-acid reflux. Med Hypotheses 67(6):1431–1436
23. Patel K, Mining S, Wakhisi J, Gheit T, Tommasino M, Martel-Planche G, Hainaut P, Abedi-Ardekani B (2011) TP53 mutations, human papilloma virus DNA and inflammation markers in esophageal squamous cell carcinoma from the Rift Valley, a high-incidence area in Kenya. BMC Res Notes 4:469. doi:10.1186/1756-0500-4-469
24. Orem J, Otieno MW, Remick SC (2004) AIDS-associated cancer in developing nations. Curr Opin Oncol 16(5):468–476
25. Fregene A, Newman LA (2005) Breast cancer in sub-Saharan Africa: how does it relate to breast cancer in African-American women? Cancer 103(8):1540–1550. doi:10.1002/cncr.20978
26. Burson AM, Soliman AS, Ngoma TA, Mwaiselage J, Ogweyo P, Eissa MS, Dey S, Merajver SD (2010) Clinical and epidemiologic profile of breast cancer in Tanzania. Breast Dis 31(1):33–41
27. Rambau PF, Chalya PL, Manyama MM, Jackson KJ (2011) Pathological features of breast cancer seen in Northwestern Tanzania: a nine years retrospective study. BMC Res Notes 4:214. doi:10.1186/1756-0500-4-214
28. Roy I, Othieno E (2011) Breast carcinoma in Uganda: microscopic study and receptor profile of 45 cases. Arch Pathol Lab Med 135 (2):194–199. doi:10.1043/2008-0421-sor1.1
29. Ravandi-Kashani F, Hayes TG (1998) Male breast cancer: a review of the literature. Eur J Cancer 34(9):1341–1347 (Oxford, England: 1990)
30. Msyamboza KP, Dzamalala C, Mdokwe C, Kamiza S, Lemerani M, Dzowela T, Kathyola D, Parkin DM (2011) Burden of cancer in Malawi; common types, incidence and trends 2007–2010: national population based cancer registry. Paper presented at the 15th College of Medicine Research Dissemination Conference, Blantyre, Malawi, 15th November 2011
31. Krown SE (2011) Treatment strategies for Kaposi sarcoma in sub-Saharan Africa: challenges and opportunities. Curr Opin Oncol 23 (5):463–468, 410.1097/CCO.1090b1013e328349428d
32. Ogwang MD, Zhao W, Ayers LW, Mbulaiteye SM (2011) Accuracy of Burkitt lymphoma diagnosis in constrained pathology settings: importance to epidemiology. Arch Pathol Lab Med 135 (4):445–450. doi:10.1043/2009-0443-ep.1
33. Naresh KN, Ibrahim HAH, Lazzi S, Rince P, Onorati M, Ambrosio MR, Bilhou-Nabera C, Amen F, Reid A, Mawanda M, Calbi V, Ogwang M, Rogena E, Byakika B, Sayed S, Moshi E, Mwakigonja A, Raphael M, Magrath I, Leoncini L (2011) Diagnosis of Burkitt lymphoma using an algorithmic approach—applicable in both resource-poor and resource-rich countries. Br J Haematol 154 (6):770–776. doi:10.1111/j.1365-2141.2011.08771.x
34. Farmer P, Frenk J, Knaul FM, Shulman LN, Alleyne G, Armstrong L, Atun R, Blayney D, Chen L, Feachem R, Gospodarowicz M, Gralow J, Gupta S, Langer A, Lob-Levyt J, Neal C, Mbewu A, Mired D, Piot P, Reddy KS, Sachs JD, Sarhan M, Seffrin JR (2010) Expansion of cancer care and control in countries of low and middle income: a call to action. Lancet 376(9747):1186–1193. doi:10.1016/s0140-6736(10)61152-x
35. Anderson BO, Cazap E, El Saghir NS, Yip CH, Khaled HM, Otero IV, Adebamowo CA, Badwe RA, Harford JB (2011) Optimisation of breast cancer management in low-resource and middle-resource countries: executive summary of the Breast Health Global Initiative consensus, 2010. Lancet Oncol 12(4):387–398. doi:10.1016/S1470-2045(11)70031-6
36. Stalsberg H, Awuah B, Ibarra JA, Nsiah-Asare A (2008) Re-establishing a surgical pathology service in Kumasi, Ghana: case report and discussion of barriers and key elements of a successful collaboration between low- and high-resource countries. Cancer 113(8 Suppl):2338–2346. doi:10.1002/cncr.23830
37. Guggisberg K, Okorie C, Khalil M (2011) Cytopathology including fine-needle aspiration in sub-Saharan Africa: a Cameroon experience. Arch Pathol Lab Med 135(2):200–206. doi:10.1043/1543-2165-135.2.200
38. Hoenecke H, Lee V, Roy I (2011) Pathologists overseas: coordinating volunteer pathology services for 19 years. Arch Pathol Lab Med 135(2):173–178. doi:10.1043/2008-0450-sor1.1
39. Bowa K, Wood C, Chao A, Chintu C, Mudenda V, Chikwenya M (2009) A review of the epidemiology of cancers at the University Teaching Hospital, Lusaka, Zambia. Trop Dr 39(1):5–7. doi:10.1258/td.2008.070450
40. Hutt MS, Spencer H (1982) Histopathology services for developing countries. Br Med J (Clin Res Ed) 285(6351):1327–1329

Virchows Arch (2012) 460:371–377
DOI 10.1007/s00428-012-1215-1

ORIGINAL ARTICLE

Deregulation of a distinct set of microRNAs is associated with transformation of gastritis into MALT lymphoma

Christoph Thorns · Johannes Kuba · Veronica Bernard · Andrea Senft · Silke Szymczak · Alfred C. Feller · Heinz-Wolfram Bernd

Received: 27 December 2011 / Revised: 6 February 2012 / Accepted: 16 February 2012 / Published online: 7 March 2012
© Springer-Verlag 2012

Abstract The mechanisms underlying the transformation from chronic *Helicobacter pylori* gastritis to gastric extranodal marginal zone lymphoma (MALT lymphoma) are poorly understood. This study aims to identify microRNAs that might be involved in the process of neoplastic transformation. We generated microRNA signatures by RT-PCR in 68 gastric biopsy samples representing normal mucosa, gastritis, suspicious lymphoid infiltrates, and overt MALT lymphoma according to Wotherspoon criteria. Analyses revealed a total of 41 microRNAs that were significantly upregulated (n=33) or downregulated (n=8) in succession from normal mucosa to gastritis and to MALT lymphoma. While some of these merely reflect the presence of lymphocytes (e.g. miR-566 and miR-212) or *H. pylori* infection (e.g. miR-155 and let7f), a distinct set of five microRNAs (miR-150, miR-550, miR-124a, miR-518b and miR-539) was shown to be differentially expressed in gastritis as opposed to MALT lymphoma. This differential expression might therefore indicate a central role of these microRNAs in the process of malignant transformation.

C. Thorns · J. Kuba · V. Bernard · A. C. Feller · H.-W. Bernd
Institut für Pathologie und Referenzzentrum für Hämatopathologie und Lymphknotendiagnostik, Universitätsklinikum Schleswig-Holstein, Campus Lübeck, Universität zu Lübeck, Lübeck, Germany

A. Senft · S. Szymczak
Institut für Medizinische Biometrie und Statistik, Universität zu Lübeck, Lübeck, Germany

H.-W. Bernd (✉)
Institut für Pathologie und Referenzzentrum für Hämatopathologie und Lymphknotendiagnostik, Universitätsklinikum Schleswig-Holstein, Campus Lübeck, Ratzeburger Allee 160, 23538 Lübeck, Germany
e-mail: heinz-wolfram.bernd@uksh.de

Keywords MicroRNA · Gastritis · MALT lymphoma · Malignant transformation

Introduction

Extranodal marginal zone lymphomas (MALT lymphomas) are rare, low-grade B cell lymphomas of the mucosa-associated lymphatic tissue with an annual incidence of less than 1:100,000 [1]. Most frequently, they are diagnosed in the stomach, but they do occur in other sites (e.g. lung, skin, ocular adnexa). In the stomach, most cases of MALT lymphomas are associated with a *Helicobacter pylori*-positive gastritis, and eradication of *H. pylori* can induce remissions [2]. Different chromosomal abnormalities have been described in gastric MALT lymphoma. The most frequent translocation in this lymphoma subtype *t*(11;18)(q21;q21) involves the MALT1 gene locus and is associated with a resistance to *H. pylori* eradication therapy [3]. The histological diagnosis of MALT lymphoma can be challenging, and the use of a score based on data from Wotherspoon and colleagues (Table 1) is encouraged [4, 5]. Detection of a B cell clone in Wotherspoon scores 3 and 4 is regarded as diagnostic for MALT lymphoma [6].

MicroRNAs are short non-coding RNAs that can modulate gene expression on a post-transcriptional level. Binding of a microRNA to the 3′-untranslated region of the mRNA leads to inhibition of the translational process or degradation of the mRNA. Importantly, one mRNA sequence can generally be targeted by multiple microRNAs, and one microRNA generally has multiple mRNA targets. Plenty of data suggest that microRNAs are crucially involved in fundamental cellular processes like proliferation and apoptosis. Therefore, microRNAs can function as "oncomirs" or tumour suppressor microRNAs, and deregulation of microRNAs has been described for many neoplasms [7].

Table 1 Histology score to assess lymphoid infiltrates in gastric mucosa, based on data from Wotherspoon et al. [4, 5]

Score	Histology	Interpretation
0	Few plasma cells, no lymphoid follicles	Normal mucosa
1	Clusters of lymphocytes, no lymphoid follicles, no lymphoepithelial lesions	Gastritis
2	Lymphoid follicles with mantle zone and plasma cells, no lymphoepithelial lesions	Follicular gastritis
3	Lymphoid follicles surrounded by small lymphocytes diffusely infiltrating the lamina propria with occasional intraepithelial B cells	Suspicious, probably reactive
4	Lymphoid follicles surrounded by marginal zone cells that diffusely infiltrate the lamina propria with lymphoepithelial lesions	Suspicious, probably lymphoma
5	Dense diffuse infiltrate with prominent lymphoepithelial lesions	Lymphoma

Although the link between *H. pylori*-associated gastritis and MALT lymphoma is well established, the mechanisms that promote the development from normal mucosa to gastritis and ultimately lymphoma are not well understood. In this study, we analysed the microRNA expression signatures of gastric biopsies with lesions corresponding to Wotherspoon scores 0 to 5 to identify microRNAs which might be involved in the process of neoplastic transformation.

Material and methods

The study has been approved by the local ethics committee. Gastric biopsies were identified in the database of the pathology department (University of Lübeck). All cases were re-evaluated and scored according to the histology score depicted in Table 1. Immunohistochemistry was used to verify or exclude lymphoepithelial lesions in scores 2 to 5, and clonality was assessed by immunohistochemical staining for immunoglobulin light chains and/or by polymerase chain reactions (PCR) of the immunoglobulin heavy chain gene locus according to the BIOMED2 protocol [8]. All lymphoma samples were analysed by fluorescence in situ hybridisation for a translocation of the MALT1 gene locus using the dual colour break apart probe for LSI MALT1 (18q21) from Abbott (IL, USA). Cases with prominent intestinal metaplasia, severe granulocytic infiltration or ulceration were excluded to minimize changes in microRNA expression not caused by the lymphoid proliferation. To ensure that an appropriate amount of lymphoid infiltrate was analysed, we evaluated control sections before and after obtaining sections for nucleic acid extraction. A number of 1,250 lymphoid cells per high power filed (0.24 mm²) was regarded as sufficient.

MicroRNA expression signatures were generated for a total of 68 cases (score 0, 14; score 1, 10; score 2, 11; score 3, 11; score 4, 10; score 5, 12) as described previously [9]. Briefly, the RecoverAll kit (Ambion, Austin, TX, USA) was used for RNA extraction from four 20-μm sections of formalin-fixed, paraffin-embedded tissues. The TaqMan® universal PCR master mix, No AmpErase® UNG-kit and TaqMan® microRNA reverse transcription kit from Applied Biosystems (Foster City, CA, USA) were used for cDNA synthesis and quantitative PCR. The reactions were performed in a 384-well format for 376 different microRNAs. The profiles were measured on the LightCycler® 480 instrument (Roche, Basel, Switzerland).

MicroRNA expression data were normalized using quantile normalization. Cases with more than 45% missing values (CT value=40) were excluded (n=3). Likewise, microRNAs with more than 50% missing values (CT value=40) were excluded (n=103). To identify microRNAs with increasing or decreasing expression values in biopsies with increasing Wotherspoon scores, Jonckheere–Terpstra trend tests (R-package "clinfun" R version 2.11.1) were performed. These analyses were also performed for Wotherspoon scores 2 to 5. To compare expression values of microRNAs in gastritis (Wotherspoon scores 1 and 2, and polyclonal 3 and 4) and lymphomas (monoclonal scores 3, 4 and 5), Wilcoxon–Mann–Whitney tests were used. P values of both analyses were separately adjusted for multiple testing using the Bonferroni method. A P value <0.000183 was regarded significant. All statistical analyses were performed using the statistical software R (R version 2.11.1).

Results

Clonality among ambiguous lesions and lymphomas

Clonality analyses of Wotherspoon scores 3, 4 and 5 by means of immunohistochemistry for light chains kappa and lambda and by PCR for the immunoglobulin heavy chain gene locus according to the BIOMED2 protocol revealed monoclonal results in 1 (9%), 5 (50%) and 12 cases (100%), respectively. In one score 3 lesion, the PCR was equivocal.

microRNA expression patterns in Wotherspoon scores 0 to 5

Gastric biopsies with different Wotherspoon scores showed different microRNA signatures. In total, 41 microRNAs showed an increasing or decreasing expression level from

score 0 to 5 ($P \leq 1.80 \times 10^{-4}$, Table 2). Eight microRNAs showed decreasing expression levels (e.g. miR-182, $P = 2.25 \times 10^{-8}$, Fig. 1), whereas 33 microRNAs showed increasing expression levels (e.g. miR-150, $P = 1.19 \times 10^{-11}$, Fig. 2). Some of these show a linear increase (e.g. miR-150, Fig. 2) while others seem to be switched on in gastritis (Wotherspoon score 1) and remain on a very similar level through scores 2 to 5 (e.g. miR-566, Fig. 3). The latter expression pattern most likely reflects the physiologic expression in lymphocytes, as comparison to expression of

Table 2 MicroRNAs with increasing or decreasing expression levels during the transition from Wotherspoon scores 0 to 5 and corresponding unadjusted *P* values as well as median differences of Wotherspoon groups 0 and 5 with its confidence intervals at 95% level

microRNA	Median difference	Confidence interval	Adjusted *P* value	Unadjusted *P* value
Increasing expression				
miR-150	3.482	[3.132, 3.938]	3.25×10^{-9}	1.19×10^{-11}
miR-518b	2.677	[1.905, 3.572]	5.07×10^{-8}	1.86×10^{-10}
miR-566	3.015	[2.149, 4.869]	7.01×10^{-8}	2.57×10^{-10}
miR-142.3p	5.033	[3.647, 6.159]	9.441×10^{-8}	3.46×10^{-10}
miR-142.5p	2.848	[2.247, 3.543]	1.47×10^{-6}	5.38×10^{-9}
miR-494	3.633	[2.186, 4.328]	2.16×10^{-6}	7.90×10^{-9}
miR-575	2.344	[1.598, 3.127]	9.40×10^{-6}	3.44×10^{-9}
miR-198	1.934	[1.188, 2.659]	1.72×10^{-5}	6.31×10^{-8}
miR-138	3.447	[2.642, 4.600]	2.46×10^{-5}	9.01×10^{-8}
miR-572	2.561	[1.787, 3.144]	4.49×10^{-5}	1.65×10^{-7}
miR-124a	2.242	[1.434, 3.340]	5.33×10^{-5}	1.95×10^{-7}
miR-519d	2.722	[1.867, 3.622]	8.29×10^{-5}	3.04×10^{-7}
miR-155	5.468	[4.166, 6.827]	1.77×10^{-4}	6.47×10^{-7}
miR-202	1.558	[0.840, 2.195]	1.77×10^{-4}	6.47×10^{-7}
miR-188	1.810	[1.011, 2.675]	1.99×10^{-4}	7.29×10^{-7}
miR-584	2.186	[1.327, 3.177]	6.82×10^{-4}	2.50×10^{-6}
miR-612	2.643	[1.868, 4.294]	8.24×10^{-4}	3.02×10^{-6}
miR-596	1.260	[0.794, 1.837]	1.44×10^{-3}	5.28×10^{-6}
miR-346	2.344	[1.293, 3.368]	2.18×10^{-3}	7.99×10^{-6}
miR-550	1.430	[0.774, 1.949]	2.94×10^{-3}	1.08×10^{-5}
miR-100	1.198	[0.806, 1.518]	3.63×10^{-3}	1.33×10^{-5}
miR-199a	1.496	[0.778, 2.128]	7.87×10^{-3}	2.88×10^{-5}
miR-601	1.485	[0.825, 2.296]	1.29×10^{-2}	4.73×10^{-5}
miR-342	1.280	[0.729, 1.908]	1.35×10^{-2}	4.96×10^{-5}
miR-604	1.399	[0.827, 1.971]	1.54×10^{-2}	5.63×10^{-5}
miR-149	1.011	[0.451, 1.457]	2.45×10^{-2}	8.99×10^{-5}
miR-549	1.677	[0.705, 2.469]	2.60×10^{-2}	9.52×10^{-5}
miR-212	1.014	[0.508, 2.485]	3.17×10^{-2}	1.16×10^{-4}
miR-361	1.543	[0.615, 2.093]	3.41×10^{-2}	1.25×10^{-4}
miR-492	1.777	[0.566, 2.792]	3.64×10^{-2}	1.33×10^{-4}
miR-23b	1.376	[0.614, 1.887]	4.49×10^{-2}	1.64×10^{-4}
miR-565	1.891	[1.021, 3.077]	4.92×10^{-2}	1.80×10^{-4}
Decreasing expression				
Let7f	−1.199	[−1.825, −0.657]	4.70×10^{-2}	1.72×10^{-4}
miR-182	−1.766	[−2.336, −1.129]	6.12×10^{-6}	2.24×10^{-8}
miR-375	−2.192	[−2.904, −1.589]	2.01×10^{-5}	7.35×10^{-8}
miR-335	−1.947	[−2.665, −1.138]	1.16×10^{-4}	4.24×10^{-7}
miR-429	−2.423	[−3.292, −1.572]	1.88×10^{-4}	6.87×10^{-7}
miR-153	−2.573	[−3.804, −1.443]	3.31×10^{-4}	1.21×10^{-6}
miR-135a	−2.310	[−3.299, −1.416]	5.26×10^{-4}	1.93×10^{-6}
miR-148a	−2.061	[−3.157, −0.875]	9.88×10^{-3}	3.62×10^{-5}
miR-7	−3.588	[−5.098, −1.283]	1.69×10^{-2}	6.17×10^{-5}

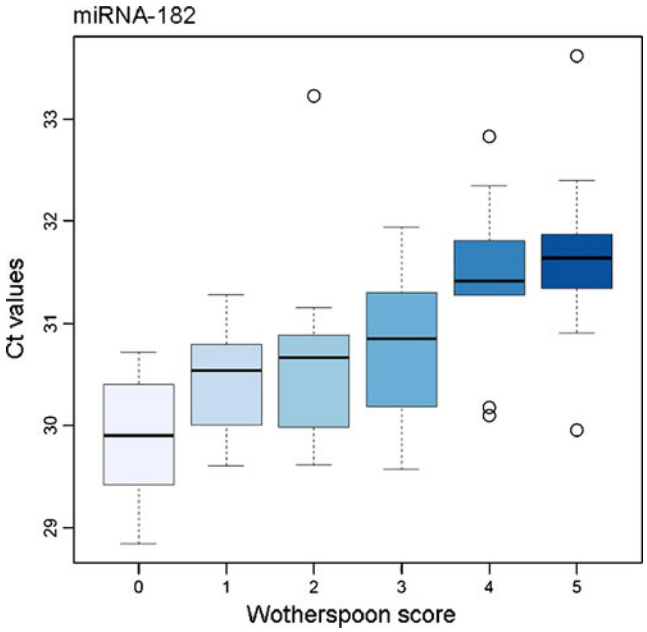

Fig. 1 The *box plot* illustrates the expression level of microRNA-182, which shows a gradual decrease from Wotherspoon lesion 0 to 5 (a lower ct value means a higher microRNA expression level and vice versa)

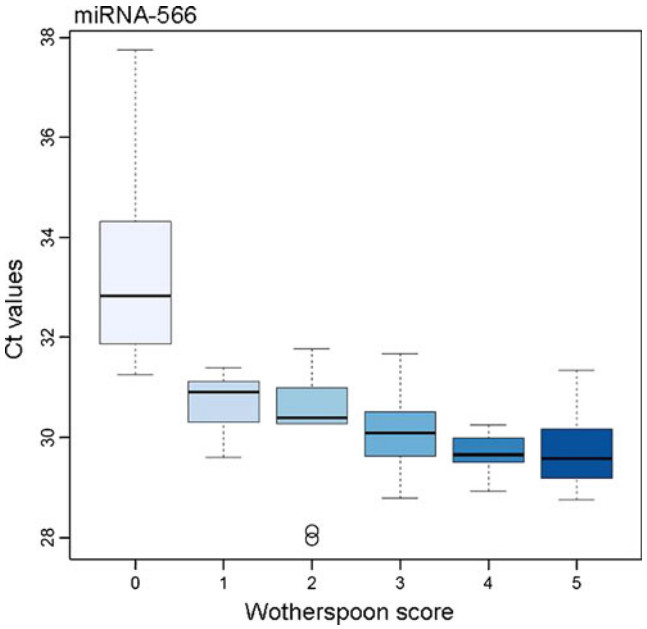

Fig. 3 Illustration of the expression level of microRNA-566 showing a marked increase from normal gastric mucosa (Wotherspoon score 0) to gastritis (Wotherspoon score 1), but only minor differences across Wotherspoon scores 2 to 5 (a lower ct value means a higher microRNA expression level and vice versa)

miR-566 and miR-212 in reactive lymph nodes showed very similar expression levels (data not shown). This is corroborated by the finding that only miR-150, miR-142-5p and miR-539 showed a steady increase or decrease in Wotherspoon scores 2–5 that was significant ($P=3.03\times10^{-5}$, 1.17×10^{-6} and 7.97×10^{-5}, respectively).

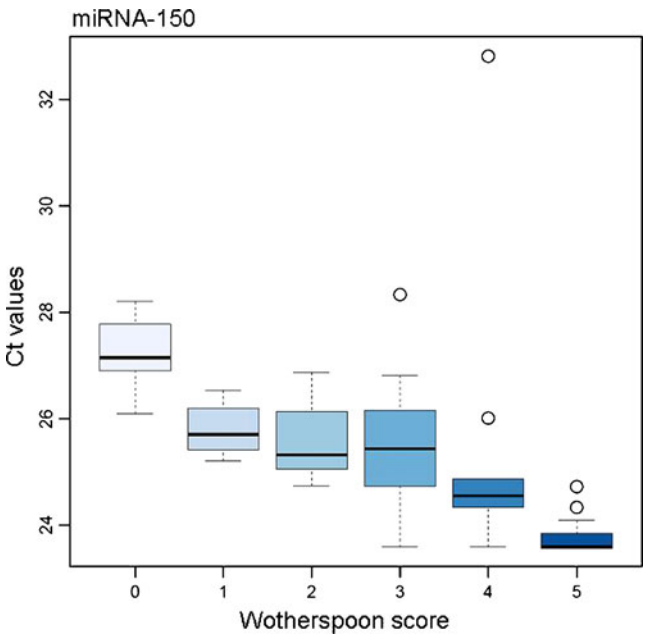

Fig. 2 Illustration of the expression level of microRNA-150 showing a gradual increase from Wotherspoon lesion 0 to 5 (a lower ct value means a higher microRNA expression level and vice versa)

MALT lymphomas are characterized by deregulation of five microRNAs

Comparison of MALT lymphomas (Wotherspoon score 5 and monoclonal scores 3 and 4) to gastritis (Wotherspoon scores 1 and 2, and polyclonal 3, 4) revealed five microRNAs to be differentially expressed after adjusting for multiple testing ($P\leq1.37\times10^{-4}$, Table 3). miR-150, miR-550, miR-124a and miR-518b were overexpressed in lymphoma samples, whereas miR-539 was downregulated in MALT lymphoma. Of note, the expression of miR-539 was not linear decreasing from Wotherspoon scores 0 to 5, but showed an undulating pattern with low expression levels in normal mucosa and lymphomas and higher expression in gastritis (data not shown).

Analyses of lymphoma samples for a translocation of the MALT1 gene locus by FISH revealed only three cases with a translocation. Therefore, the low number of cases harbouring such a translocation precluded statistical analyses.

Discussion

The morphological diagnosis of MALT lymphoma is hampered by overlapping histological features with advanced chronic *H. pylori*-induced gastritis. The histology score based on data from Wotherspoon and colleagues (Table 1) has certainly improved the diagnostic accuracy, but still

Table 3 Differentially expressed microRNAs in MALT lymphomas compared to gastritis and corresponding unadjusted *P* values as well as median differences with its confidence intervals at 95% level

microRNA	Median difference	Confidence interval	Adjusted *P* value	Unadjusted *P* value
miR-150	1.467	[1.030, 1.976]	3.36×10^{-3}	1.21×10^{-5}
miR-550	0.921	[0.521, 1.265]	7.01×10^{-3}	2.54×10^{-5}
miR-124a	1.556	[0.935, 2.052]	1.51×10^{-2}	5.44×10^{-5}
miR-518b	1.213	[0.584, 1.714]	2.77×10^{-2}	9.95×10^{-5}
miR-539	−1.117	[−1.667, −0.500]	3.81×10^{-2}	1.37×10^{-4}

includes the ambiguous categories 3 (probably reactive) and 4 (probably lymphoma). This missing accuracy has been complicated by descriptions of monoclonal B cells in benign lymphoid proliferations with variable frequencies [10, 11]. In this regard, Wuendisch and colleagues described B cell monoclonality with low incidence even in Wotherspoon score 1 (1/24) and with high incidence in Wotherspoon score 2, 3 and 4 (5/21, 4/14, 8/23) [12]. However, using standardized PCR protocols like the Biomed-2 protocol [8], B cell monoclonality in reactive lymphoid proliferations is a rare event, and it is thus now accepted to classify the ambiguous Wotherspoon scores 3 and 4 as MALT lymphoma if B cell monoclonality is established [6]. Even though it is possible in this way to separate gastritis and lymphoma for diagnostic purposes, the transition from *H. pylori*-induced gastritis to MALT lymphoma is most likely not a single-step event but rather a multi-step development, and the different histology scores may merely reflect different stages of this development. This would be in accordance with our finding of a linear or close to linear deregulation of several microRNAs in lesions representing Wotherspoon scores 0 to 5, including overexpression of potential oncogenic microRNAs like miR-494 [13] and downregulation of potential tumour suppressor microRNAs like miR-182 [14, 15]. However, it must be kept in mind that the increasing expression of at least some microRNAs in higher Wotherspoon scores might be merely reflecting an increasing number of lymphoid cells.

Overexpression of miR-155 and downregulation of let7f are caused by infection with *H. pylori*, as has been previously shown [16–18]. The role of *H. pylori*-induced miR-155 expression and let7f silencing may represent, however, already an important step to lymphoma development, since we have found miR-155 to be strongly overexpressed in diffuse large B cell lymphomas and follicular lymphomas [9]. The high levels of miR-155 are of special interest in this setting, since high expression of miR-155 has been described to be associated with NF-kappaB activation [19], a pathway which is also activated in MALT lymphomas [reviewed in 20]. In contrast, the let7 family has tumour suppressor activities and is downregulated in several tumours [21–24]. Let7f has been shown to inhibit gastric cancer invasion and metastasis potentially through the targeting of MYH9 [25].

It is generally accepted to classify Wotherspoon scores 3 and 4 as MALT lymphoma if the B cells are monoclonal [7]. Therefore, B cell clonality is a prerequisite to differentiate certain reactive from neoplastic lymphoid proliferations in the stomach, irrespective of the potential responsiveness to eradication of the causing infectious agent. Consequently, we compared microRNA signatures of polyclonal gastritis to monoclonal cases of the ambiguous categories 3 and 4 as well as overt lymphomas (score 5) and found a set of five microRNAs that were differentially expressed in gastritis and lymphoma ($P\leq1.37\times10^{-4}$). Of these, four were overexpressed in lymphoma (miR-150, miR-550, miR-124a, miR-518b), whereas only one (miR-539) was downregulated in lymphoma to an expression level that was comparable to normal gastric mucosa. Of note, the increase of miR-150 and decrease of miR-539 remained significant when the Jonckheere–Terpstra test was limited to Wotherspoon scores 2–5.

The increased expression of miR-150 and miR-124a is remarkable, since these microRNAs are generally known as tumour suppressor microRNAs in the hematopoietic system and therefore would be expected to be downregulated in lymphomas. miR-150 is crucial in the differentiation of B and T cells and is regularly expressed in lymphocytes. In a previous study, we could show that miR-150 is downregulated in diffuse large B cell lymphoma, but not in follicular lymphoma [9]. Decreased expression of miR-150 has been described in mantle cell lymphoma [26] and NK/T cell lymphoma [27]. In contrast to low miR-150 levels in lymphatic tumours, high expression has been described in gastric cancer [28]. It may be that the function of miR-150 as oncogenic or tumour suppressor microRNA essentially depends on the localization of the respective neoplasm. Moreover, recent data indicate interaction between Notch3 and NF-kappaB [29], and Notch3 is targeted by miR-150 [30].

The published data on the expression of miR-124a solely report on decreased expression in tumours (haematological tumours, medulloblastoma, oral squamous cell carcinoma, cervical cancer and hepatocellular carcinoma), mainly through epigenetic silencing [31–36]. However, IκBζ is a target of miR-124a, and IκBζ inhibits the transcriptional activity of NF-kappaB [37]. Therefore, overexpression of miR-124a may activate the NF-kappaB pathway, potentially in liaison with miR-155. Of note, Craig and colleagues [38] recently described miR-203 as differentially expressed in MALT lymphomas through epigenetic silencing. In our series, miR-203 was also downregulated in Wotherspoon

scores 1 to 5, but the difference was not statistically significant after adjusting for multiple testing (P=0.0058).

In conclusion, gastric extranodal marginal zone lymphomas and the precursor lesions show distinct microRNA signatures. Firstly, differentially expressed microRNAs reflect regular expression in the infiltrating lymphocytes (e.g. miR-556 and miR-212); others are the result of *H. pylori* infection (e.g. miR-155 and let7f). The upregulation of potential oncogenic microRNAs (miR-494) and silencing of potential tumour suppressor miRNAs (miR-182) seem to be part of a multi-step lymphomagenesis. Secondly, the final step from gastritis to a monoclonal B cell lymphoma is associated with the deregulation of a distinct set of microRNAs (miR-150, miR-124a, miR-550, miR-518b and miR-539). Future studies will have to clarify further the precise mechanisms by which these miRNAs may promote malignant transformation. This may build the basis for the development of new sophisticated therapeutic approaches.

Acknowledgments This work was supported by "Deutsche Forschungsgemeinschaft" grant no. TH 813/4-1 to C.T.

Conflict of interest The authors declare that there are no financial or other potential conflicts relevant to the manuscript.

References

1. Ulrich A, Fischbach W, Blettner M (2002) Incidence of gastric B-cell lymphomas: a population-based study in Germany. Ann Oncol 13:1120–1127
2. Fischbach W, Goebeler-Klove ME, Dragosics B et al (2004) Long term outcome of patients with gastric marginal zone B cell lymphoma of mucosa associated lymphoid tissue (MALT) following exclusive *Helicobacter pylori* eradication: experience from a large prospective series. Gut 53:34–37
3. Liu H, Ruskon-Fourmestraux A, Lavergne-Slove A et al (2001) Resistance of t(11;18) positive gastric mucosa-associated lymphoid tissue lymphoma to *Helicobacter pylori* eradication therapy. Lancet 357:39–40
4. Wotherspoon A, Ortiz-Hidalgo C, Falzon MR et al (1991) *Helicobacter pylori* associated gastritis and primary B-cell gastric lymphoma. Lancet 338:1175–1176
5. Isaacson PG (2010) Extranodal marginal zone lymphoma: MALT lymphoma. In: Jaffe ES, Harris NL, Vardiman JW, Campo E, Arber DA (eds) Hematopathology, 1st edn. Saunders/Elsevier, Philadelphia, pp 291–305
6. Hummel M, Oeschger S, Barth TFE et al (2006) Wotherspoon criteria combined with B cell clonality analysis by advanced polymerase chain reaction technology discriminates covert gastric marginal zone lymphoma from chronic gastritis. Gut 55:782–787
7. Kasinski AL, Slack FJ (2011) Epigenetics and genetics. MicroRNAs en route to the clinic: progress in validating and targeting microRNAs for cancer therapy. Nat Rev Cancer 11:849–864
8. van Dongen JJ, Langerak AW, Bruggemann M et al (2003) Design and standardization of PCR primers and protocols for detection of clonal immunoglobulin and T-cell receptor gene recombinations in suspect lymphoproliferations: report of the BIOMED-2 Concerted Action BMH4-CT98-3936. Leukemia 17:2257–2317
9. Roehle A, Hoefig KP, Repsilber D et al (2008) MicroRNA expression signatures characterize diffuse large B-cell lymphomas and follicular lymphomas. Br J Haematol 142:732–744
10. Torcalivics E, Cherwitz DL, Jessurun J et al (1997) B-cell gene rearrangement in benign and malignant lymphoid proliferations of mucosa-associated lymphoid tissue and lymph node. Hum Pathol 28:166–173
11. Miyamoto M, Hamura K, Hiyama T et al (2001) High incidence of B-cell monoclonality in follicular gastritis: a possible association between follicular gastritis and MALT lymphoma. Virchows Arch 438:232–237
12. Wundisch T, Neubauer A, Stolte M et al (2003) B-cell monoclonality is associated with lymphoid follicles in gastritis. Am J Surg Pathol 27:882–887
13. Liu L, Jiang Y, Zhang H et al (2010) Overexpressed miR-494 down-regulates PTEN gene expression in cells transformed by anti-benzo(a)pyrene-trans-7,8-dihydrodiol-9,10-epoxide. Life Sci 86:192–198
14. Zhang L, Liu T, Huang Y et al (2011) microRNA-182 inhibits the proliferation and invasion of human lung adenocarcinoma cells through its effect on human cortical actin-associated protein. Int J Mol Med 28:381–388
15. Sun Y, Fang R, Li C et al (2010) Hsa-mir-182 suppresses lung tumorigenesis through down regulation of RGS17 expression in vitro. Biochem Biophys Res Commun 396:501–507
16. Xiao B, Liu Z, Li B-S et al (2009) Induction of microRNA-155 during *Helicobacter pylori* infection and its negative regulatory role in the inflammatory response. J Infect Dis 200:916–925
17. Fehri LF, Koch M, Belogolova E et al (2010) *Helicobacter pylori* induces miR-155 in T cells in a cAMP-Foxp3-dependent manner. PLoS One 5:e9500
18. Matsushima K, Isomoto H, Inoue N et al (2011) MicroRNA signatures in *Helicobacter pylori*-infected gastric mucosa. Int J Cancer 128:361–370
19. Rai D, Karanti S, Jung I et al (2008) Coordinated expression of microRNA-155 and predicted target genes in diffuse large B-cell lymphoma. Cancer Genet Cytogenet 181:8–15
20. Du M-Q (2011) MALT-lymphoma: many roads to nuclear factor-kb activation. Histopathology 58:26–38
21. Esquela-Kerscher A, Trang P, Wiggins JF et al (2008) The let-7 microRNA reduces tumor growth in mouse models of lung cancer. Cell Cycle 7:759–764
22. Schultz J, Lorenz P, Gross G et al (2008) MicroRNA let-7b targets important cell cycle molecules in malignant melanoma cells and interferes with anchorage-independent growth. Cell Res 18:549–557
23. Yu F, Yao H, Zhu P et al (2007) let-7 regulates self renewal and tumorigenicity of breast cancer cells. Cell 131:1109–1123
24. Sampson VB, Rong NH, Han J et al (2007) MicroRNA let-7a down-regulates MYC and reverts MYC-induced growth in Burkitt lymphoma cells. Cancer Res 67:9762–9770
25. Liang S, He L, Zhao X et al (2011) MicroRNA let-7f inhibits tumor invasion and metastasis by targeting MYH9 in human gastric cancer. PLoS One 6:e18409
26. Zhao JJ, Lin J, Lwin T et al (2010) microRNA expression profile and identification of miR-29 as a prognostic marker and pathogenetic factor by targeting CDK6 in mantle cell lymphoma. Blood 115:2630–2639
27. Watanabe A, Tagawa H, Yamashita J et al (2011) The role of microRNA-150 as a tumor suppressor in malignant lymphoma. Leukemia 25:1324–1334
28. Wu Q, Jin H, Yang Z et al (2010) MiR-150 promotes gastric cancer proliferation by negatively regulating the pro-apoptotic gene EGR2. Biochem Biophys Res Commun 392:340–345
29. Barbarulo A, Grazioli P, Campese AF et al (2011) Notch3 and canonical NF-kappaB signaling pathways cooperatively regulate Foxp3 transcription. J Immunol 186:6199–6206

30. Ghisi M, Corradin A, Basso K et al (2011) Modulation of microRNA expression in human T-cell development: targeting of NOTCH3 by miR-150. Blood 117:7053–7062
31. Li KK, Pang JC, Ching AK et al (2009) miR-124 is frequently down-regulated in medulloblastoma and is a negative regulator of SLC16A1. Hum Pathol 40:1234–1243
32. Zheng F, Liao YJ, Cai MY et al (2011) The putative tumour suppressor microRNA-124 modulates hepatocellular carcinoma cell aggressiveness by repressing ROCK2 and EZH2. Gut 61:278–289
33. Wong KY, So CC, Loong F et al (2011) Epigenetic inactivation of the miR-124-1 in haematological malignancies. PLoS One 6:e19027
34. Hunt S, Jones AV, Hinsley EE et al (2011) MicroRNA-124 suppresses oral squamous cell carcinoma motility by targeting ITGB1. FEBS Lett 585:187–192
35. Wilting SM, van Boerdonk RA, Henken FE et al (2010) Methylation-mediated silencing and tumour suppressive function of hsa-miR-124 in cervical cancer. Mol Cancer 9:167
36. Furuta M, Kozaki KI, Tanaka S et al (2010) miR-124 and miR-203 are epigenetically silenced tumor-suppressive microRNAs in hepatocellular carcinoma. Carcinogenesis 31:766–776
37. Lindenblatt C, Schulze-Osthoff K, Totzke G (2009) IkappaB-zeta expression is regulated by miR-124a. Cell Cycle 8:2019–2023
38. Craig VJ, Cogliatti SB, Rehrauer H et al (2011) Epigenetic silencing of microRNA-203 dysregulates ABL1 expression and drives *Helicobacter*-associated gastric lymphomagenesis. Cancer Res 71:3616–3624

Virchows Arch (2012) 460:379–387
DOI 10.1007/s00428-012-1199-x

ORIGINAL ARTICLE

Etiological factors in primary hepatic B-cell lymphoma

Kanta Kikuma · Jiro Watanabe · Yumi Oshiro · Tatsuo Shimogama · Yumi Honda · Seiichi Okamura · Koichi Higaki · Naokuni Uike · Tetsuro Soda · Seiya Momosaki · Tadaaki Yokota · Satoshi Toyoshima · Morishige Takeshita

Received: 12 November 2011 / Revised: 8 January 2012 / Accepted: 19 January 2012 / Published online: 7 March 2012
© The Author(s) 2012. This article is published with open access at Springerlink.com

Abstract Sixty-four cases of malignant lymphoma involving the liver were examined. Of these, 20 cases were histologically confirmed to be primary hepatic B-cell lymphoma. Twelve of these 20 cases were diffuse large B-cell lymphoma (DLBCL) and eight cases were mucosa-associated lymphoid tissue (MALT) lymphoma. Of the 12 cases of DLBCL, six were immunohistologically positive for CD10 and/or Bcl6 (indicating a germinal center phenotype), six were positive for Bcl2, and five were positive for CD25. Eight of the 12 DLBCL cases (66.7%) and two of the eight MALT lymphoma cases (25%) had serum anti-hepatitis C virus (HCV) antibodies and HCV RNA. The incidence of HCV infection was significantly higher in the hepatic DLBCL cases than in systemic intravascular large B-cell cases with liver involvement (one of 11 cases, 9.1%) and T/NK-cell lymphoma cases (one of 19 cases, 5.3%) ($p<0.01$ for both). Two hepatic DLBCL cases (16.7%) had rheumatoid arthritis treated with methotrexate, and four MALT lymphoma cases (50%) had Sjögren's syndrome, primary biliary cirrhosis, or autoimmune hepatitis; one case in each of these two groups was complicated by chronic HCV-seropositive hepatitis. Although primary hepatic lymphoma is rare, persistent inflammatory processes associated with HCV infection or autoimmune disease may play independent roles in the lymphomagenesis of hepatic B cells.

K. Kikuma · T. Soda · M. Takeshita (✉)
Departments of Pathology and Internal Medicine,
Faculty of Medicine,
Fukuoka University,
Nanakuma 7-45-1, Johnan-ku,
Fukuoka, Japan
e-mail: m-take@adm.fukuoka-u.ac.jp

J. Watanabe
Pathological Laboratory, National Organization Kokura Hospital,
Harugaoko 10-1, Kokura minmi-ku,
Kitakyushu, Japan

Y. Oshiro
Pathological Laboratory, Matsuyama Red-Cross Hospital,
Bunkyo-cho, 1-1,
Matsuyama, Japan

T. Shimogama
Pathological Laboratory, Nihon Steel Yawata Memorial Hospital,
Horunomachi 1-1-1, Yawata nishi-ku,
Kitakyushu, Japan

Y. Honda
Pathological Laboratory, Kumamoto University Hospital,
Honjyo 1-1-1,
Kumamoto, Japan

S. Okamura · S. Momosaki
Hematology Laboratory and Pathological Laboratory,
National Organization Kyushu Medical Center,
Jigyohama 1-8-1, Chuo-ku,
Fukuoka, Japan

K. Higaki
Pathological Laboratory, Saint Mary Hospital,
Tsufukumotomachi 422,
Kurume, Japan

N. Uike
Hematology Laboratory,
National Organization Kyushu Cancer Center,
Notamo 3-1-1, Minami-ku,
Fukuoka, Japan

T. Yokota
Pathological Laboratory, Kokura Memorial Hospital,
Kisencho 1-1, Kokura kita-ku,
Kitakyushu, Japan

S. Toyoshima
Pathological Laboratory, Municipal Kitakyushu Medical Center,
Bashaku 2-1-1, Kokura kita-ku,
Kitakyushu, Japan

Keywords Liver · Malignant lymphoma · HCV · Autoimmune disease

Introduction

B-cell lymphoma in hepatitis C virus (HCV)-seropositive patients frequently presents with extranodal disease in the bone marrow, major salivary glands, or spleen [1, 2]. Although diffuse large B-cell lymphoma (DLBCL) is frequent in HCV-seropositive B-cell lymphoma patients, a significantly higher incidence of lymphoplasmacytic lymphoma than HCV-negative B-cell lymphoma has been reported (43 of 257 cases, 16.7% versus 91 of 1118 cases, 8%; $p<0.01$) [3]. Hermine et al. [4] described nine French HCV-seropositive cases of splenic marginal zone lymphoma with monoclonal IgM and polyclonal IgG (type II) cryoglobulinemia, and reported that all these cases showed loss of serum HCV RNA and complete remission of lymphoma after treatment with interferon-α and ribavirin. HCV infection and associated type II cryoglobulinemia may induce B-cell lymphoid neoplasia.

The HCV core protein has been shown to induce proliferation of human B-cell lines through up-regulation of specific B-cell-related genes and reduction in apoptosis [5, 6]. The levels of the activation-induced cytidine deaminase protein and gene, which provide a key enzyme for somatic hypermutation of germinal center (GC) B cells, were dramatically increased in peripheral blood B cells in patients with HCV-seropositive hepatitis [7]. HCV transgenic mice expressing the full HCV genome in B cells showed a high incidence of CD25 [interleukin-2α receptor (IL2αR)]-positive DLBCL as well as elevated serum levels of IL2αR [8]. HCV infection may play a role in the multistep mechanism of lymphomagenesis in peripheral B cells.

Ramos-Casals et al. [9] reported 25 cases of B-cell lymphoma with HCV infection and Sjögren's syndrome (SS), which showed frequent type II cryoglobulinemia (80%), extranodal tumor invasion (60%) including in the liver (16%), mucosa-associated lymphoid tissue (MALT) lymphoma (44%), and DLBCL (24%). Primary biliary cirrhosis (PBC) has been reported to occasionally be complicated by HCV infection (14 of 170 cases, 8.2%), but not by lymphoma [10]. Autoimmune disease with or without HCV infection may play a role in primary hepatic lymphoma.

Primary hepatic B-cell lymphoma is rare, representing 0.06% of all non-Hodgkin's lymphoma [11]. Page et al. [11] reported 23 cases of primary hepatic DLBCL and one of MALT lymphoma, of which six of the 10 examined DLBCL cases (60%) had HCV infection. Persistent HCV infection often complicates cases of primary hepatic DLBCL. We selected 20 cases of primary hepatic B-cell lymphoma from an area of Japan in which HCV infection is endemic. Of these, eight of 12 DLBCL cases (66.7%) and two of eight MALT lymphoma cases (25%) had serum anti-HCV antibodies and HCV RNA, and six DLBCL cases and four MALT lymphoma cases had autoimmune disease. We examined clinicopathological characteristics and etiological factors in patients with primary hepatic B-cell lymphoma, especially cases with HCV infection and autoimmune disease.

Materials and methods

Case selection

We reviewed the 5220 cases of malignant lymphoma in our register from 1995 to 2010, and included the 64 cases with histologically confirmed liver involvement at initial presentation in this study. Primary hepatic B-cell lymphoma was defined as extranodal lymphoma of the liver, with the bulk of the disease localized to this site [12]. Contiguous lymph node and perihepatic metastasis may be seen in primary hepatic B-cell lymphoma, as in gastrointestinal extranodal B-cell lymphoma [13, 14]. Histological diagnosis was according to the World Health Organization classification [13]. Twenty of 5,220 cases (0.4%) had clinical stage I or II primary hepatic lymphoma without superficial lymphadenopathy. The other 44 cases with liver involvement had malignant lymphoma with systemic or secondary intrahepatic tumor invasion as well as extrahepatic tumors or superficial nodal invasion. These 44 cases were used as a control group, comprising 22 cases of systemic B-cell lymphoma [12 cases of intravascular large B-cell lymphoma (IVLBCL) and 10 cases of DLBCL] and 22 cases of T/NK-cell lymphoma (nine cases of hepatosplenic T-cell lymphoma, seven cases of adult T-cell leukemia/lymphoma (ATL/L), four cases of aggressive NK-cell leukemia/lymphoma, and two cases of other T-cell lymphoma). In an additional control study, the seven cases of primary hepatic reactive lymphoid hyperplasia [14] were also examined to check for HCV infection and autoimmune disease.

The clinical and laboratory findings, treatment, and prognosis of patients presenting to ten hospitals were examined. Tumor stages were classified according to the modified Ann Arbor staging system [15].

Examination for HCV and HBV infections

Serum samples were screened for HCV infection by measuring anti-HCV antibody levels using the second generation enzyme-linked immunosorbent assay (ELISA) technique (Abbott Laboratories, Chicago, IL, USA). If positive, a PCR-based technique (PCR Amplicor; Roche, Branchburg, NJ, USA) was used to detect HCV RNA. The HCV core genotype was determined using PCR-based techniques (SMI test HCV genotyping kit; Sumitomo Metals,

Osaka, Japan), which identified six genotypes according to the Simmonds classification: 1A, 1B, 2A, 2B, 3A, and 3B. HBV surface (HBs) and envelope (HBe) antigens were detected using an ELISA kit (Abbott Laboratories, Abbott Park, IL, USA) [16].

Histology and immunohistology

Biopsy and surgical specimens were fixed with 20% formalin, embedded in paraffin, and stained with hematoxylin and eosin. The hepatic lesions of all 71 cases were examined histologically, including 16 autopsy cases (two primary hepatic DLBCL cases, two IVLBCL cases, and 12 T/NK-cell lymphoma cases). Immunohistological examination was performed by applying a panel of monoclonal and polyclonal antibodies to formalin-fixed tumor samples using the ChemMate Envision method (DakoCytomation, Glostrup, Denmark), and the peroxidase color reaction was developed using diaminobenzidine as the substrate. Antibody, clone, and source were as follows: CD3 (PS1, Novocastra, UK), CD5 (4C7, Novocastra), CD10 (56C6, Novocastra), CD20 (L26, Dako, USA), CD23 (1B23, Novocastra), IL2α receptor (CD25, 4C9, Novocastra), CD30 (BerH2, Dako), Bcl1 (5D4, IBL, Japan), Bcl2 (124, Dako), Bcl6 (P1F6, Novocastra), multiple myeloma 1 (MUM1p, Dako), anti-HBs antigen (ZCH16, Nichirei, Japan), and IgG4 (HP6026, Zymed, USA).

In situ hybridization for detection of Epstein–Barr virus-encoded RNA (EBER)

Deparaffinized tissue sections were digested with proteinase K and hybridized in a solution of 50% formamide containing fluorescein isothiocyanate (FITC)-labeled EBER oligonucleotides using a Dako hybridization kit (DakoCytomation, Glostrup, Denmark). Hybridization products were detected using rabbit anti-FITC antibody, then incubated with ChemMate Envision and colored with DAB.

Statistical analyses

Univariate analyses were performed using the chi-square and Fisher's tests to determine differences between the two malignant lymphoma groups. Fifty-four node-based DLBCL cases and 445 colon cancer cases admitted to the National Kyushu Medical Center were selected for examination of HCV and HBV infections as a control group. Prognosis was determined by calculating the cumulative survival time of 53 cases using the Kaplan–Meier method and was analyzed using the log-rank and generalized Wilcoxon tests.

Selection of 36 previously reported primary hepatic B-cell lymphoma cases

Sixteen primary DLBCL cases and 20 MALT lymphoma cases, which had each been described in detail, were selected from 27 reports in the English literature from 1990 to 2010 [17–42]. The clinical and histological details of these 36 cases were determined from the reported findings by the corresponding laboratory.

Results

Clinical findings, laboratory data, and outcomes

The clinical data at initial presentation of the 20 cases of primary hepatic lymphoma, 44 cases of systemic B- and T/NK-cell lymphoma with liver involvement, and seven cases of reactive lymphoid hyperplasia are shown in Table 1. Twelve cases had primary hepatic DLBCL. Eight of these 12 cases (66.7%) had serum anti-HCV antibodies, and HCV RNA was detected in all six of these cases examined. Two of these cases were infected with genotype 1b and two with genotype 2a. The prevalence of anti-HCV antibody positivity was significantly higher in DLBCL cases (66.7%) than in cases of systemic IVLBCL (one of 11, 9.1%), systemic T/NK-cell lymphoma (one of 19, 5.3%), nodal DLBCL (five of 54, 9.3%), and colon cancer (23 of 445, 5.2%) ($p<0.01$). Two other DLBCL cases (16.7%) had HBs and HBe antigens, but this prevalence was not significantly higher than in cases of systemic IVLBCL (one of 11, 9.1%), nodal DLBCL (one of 54, 1.9%), or colon cancer (seven of 445, 1.6%). Eight cases had primary hepatic MALT lymphoma. Two of these cases (25%) were positive for serum anti-HCV antibodies and HCV RNA, and were infected with genotype 1b. This HCV prevalence was not significantly higher than in the other four tumor groups described above. In the other two groups of patients with systemic B-cell lymphoma, five of the ten DLBCL cases (50%) had anti-HCV antibodies. One case (14.3%) with reactive lymphoid hyperplasia had HCV infection. There were no cases with co-infection of HCV and HBV.

Detailed clinicopathological findings of the primary hepatic and systemic B-cell lymphoma cases are shown in Table 2. Of the cases with primary hepatic DLBCL, five had chronic hepatitis, three had liver cirrhosis, and one had chronic hepatitis and hepatocellular carcinoma. The remaining case was an HCV carrier. Two cases had rheumatoid arthritis which had been treated with methotrexate for 7 and 10 years, respectively, and one case had chronic HCV hepatitis. Seven cases were classified as clinical stage I and five were classified as II1 or II2. Combined chemotherapy was administered in nine cases. The five cases who underwent rituximab plus cytotoxic treatment were alive

Table 1 Initial clinical data of 71 cases of liver-involving lymphoproliferative disease

No. of cases	Age (mean)	M/F	Histological type: no. of cases	Anti-HCV Ab	HBs, e Ag	Anti-HTLV-1 Ab
Primary hepatic B-cell lymphoma						
20	64 years old	10:2	DLBCL: 12	8 (66.7%)	2 (16.7%)	1 (8.3%)
		3:5	MALT: 8	2 (25%)	1 (12.5%)	0/5 (0)
Total		13:7		10 (50%)	3 (15%)	1/17 (5.9%)
Liver-involving systemic B-cell lymphoma						
22	67 years old	7:5	IVLBCL: 12	1/11 (9.1%)	1/11 (9.1%)	1/10 (10%)
		5:5	DLBCL: 10	5 (50%)	1 (10%)	0/7 (0)
Total		12:10		6/21 (29%)	2/21 (9.5%)	1/17 (5.9%)
Liver-involving systematic T/NK-cell lymphoma						
22	55 years old	17:5		1/19 (5.3%)	0/19 (0)	7/21 (33.3%)
Reactive lymphoid hyperplasia						
7	61 years old	0:7		1(14.3%)	0 (0)	0 (0)

/: positive/examined cases. *HCV* hepatitis C virus, *HB* hepatitis B, *HTLV* human T-cell lymphotropic virus, *DLBCL* diffuse large B-cell lymphoma, *MALT* mucosa-associated lymphoid tissue, *IVLBCL* intravascular large B-cell lymphoma

and well at 21 to 72 months after treatment initiation, while three of the four cases who received only cytotoxic treatment died of disease with extrahepatic tumor invasion. The median survival time of these nine treated cases was 27 months, and the 5-year overall survival rate was 44%. Two cases did not receive cytotoxic treatment and died of hepatic failure. Limited intrahepatic lymphoma was found at autopsy. The remaining case was lost to follow-up after 3 months.

All eight cases of primary hepatic MALT lymphoma had a single hepatic tumor (Fig. 1). Two cases had SS, one had SS and PBC, and one had autoimmune hepatitis. All these cases received surgery and/or cytotoxic treatment with or without rituximab, and were alive and well at 5 to 84 months after treatment initiation. Their median survival time was longer than 84 months, which was significantly longer than that of primary hepatic DLBCL cases ($p<0.05$) (Fig. 2).

In cases of systemic lymphoma with liver involvement, only one of 12 IVLBCL cases (8.3%) had systemic lupus erythematosus. The prevalence of autoimmune disease was significantly lower in IVLBCL cases than in primary hepatic lymphoma cases (six of 20 cases, 30%; $p<0.05$). The median survival time of the seven IVLBCL cases for which this information was available was 6 months, which was significantly shorter than in primary hepatic DLBCL cases ($p<0.01$). Of the ten cases with systemic DLBCL, four patients with anti-HCV antibodies died of disease within 6 months. The median survival time of these ten cases was 13 months, which was significantly shorter than in primary hepatic DLBCL cases ($p<0.05$). Of the 22 cases of systemic T/NK-cell lymphoma, one case with T-LGL leukemia (5.3%) had PBC. One case with reactive lymphoid hyperplasia (14.3%) was complicated by PBC.

Table 2 Detailed clinicopathological findings and prognosis in 42 of liver-involving B-cell lymphoma

Histological type	Clinical stage	Liver disease			Hepatic tumors			Complication	Median survival (months)
	I/II/III/IV	CH	LC	HCC	Single	Multiple	Diffuse		
Primary hepatic B-cell lymphoma									
DLBCL: 12	7/5/0//0	5	3	1	8	4	0	RA: 2	27
MALT: 8	8/0/0//0	3	1	1	8	0	0	SS: 2, PBC: 1[a], AH: 1	>84
Total: 20	15/5/0//0	8	4	2	16	4	0	6	
Liver-involving systemic B-cell lymphoma									
IVLBCL: 12	0/0/0//12	1	0	0	0	0	12	SLE: 1	6
DLBCL: 10	0/0/0//10	5	0	0	2	8	0	0	13
Total 22	0/0/0//22	6	0	0	2	8	12	1	

DLBCL diffuse large B-cell lymphoma, *MALT* mucosa-associated lymphoid tissue, *IVLBCL* intravascular large B-cell lymphoma, *CH* chronic hepatitis, *LC* liver cirrhosis, *HCC* hepatocellular carcinoma, *RA* rheumatoid arthritis, *SS* Sjögren's syndrome, *PBC* primary biliary cirrhosis, *AH* autoimmune hepatitis, *SLE* systemic lupus erythematosus

[a] One patient complicates PBC and SS

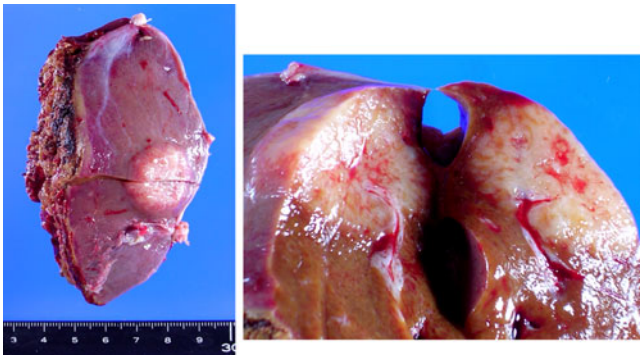

Fig. 1 Macroscopic appearance of a primary hepatic MALT lymphoma without HCV infection. A whitish nodular tumor is seen in the liver

Histological and immunohistological findings

The immunohistological characteristics of the primary hepatic and systemic B-cell lymphoma cases are shown in Table 3. Demarcated tumors were detected histologically in all of the cases of primary hepatic DLBCL and MALT lymphoma (Fig. 3), and no intrasinusoidal tumor invasion was found. A few atrophic reactive lymph follicles were detected in the tumors of all 20 cases. The lymphoma cells in the 12 primary hepatic DLBCL cases were positive for the following antigens (number of positive cases, % of total): CD10 (4, 33.3%), Bcl2 (6, 50%), Bcl6 (5, 41.7%), MUM1 (5, 41.7%), and CD25 (5, 41.7%) (Fig. 4a–c). Six cases had a GC B-cell phenotype. Three cases were CD5-positive and Bcl1-negative. In situ hybridization indicated nuclear EBER signals in two primary hepatic DLBCL cases (16.7%) which were complicated by rheumatic arthritis (Fig. 4d).

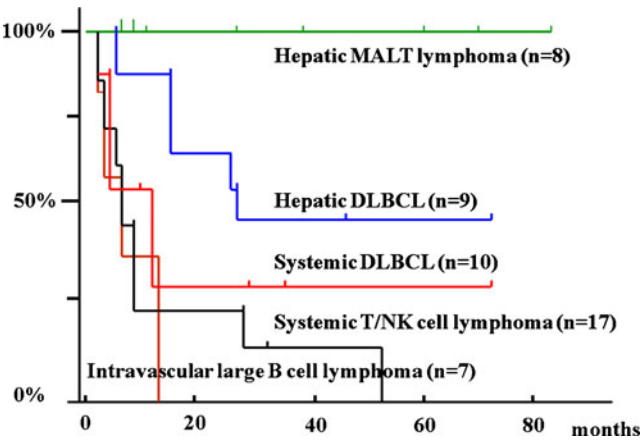

Fig. 2 Actuarial survival curves of cases of primary hepatic DLBCL and MALT lymphoma, intravascular and systemic large B-cell lymphoma, and systemic T/NK-cell lymphoma with liver involvement. Primary hepatic MALT lymphoma cases have a significantly better prognosis than primary hepatic DLBCL cases ($p<0.05$). Primary hepatic DLBCL cases have a significantly better prognosis than cases of intravascular large B-cell lymphoma, systemic DLBCL, and systemic T/NK-cell lymphoma ($p<0.01$ or <0.05)

The lymphoma cells of all eight MALT lymphoma cases were positive for Bcl2 and negative for CD5, CD23, CD10, Bcl6, MUM1, and CD25. No positive reaction to HBs antigen (ZCH16) was detected in the lymphoma cells of the three primary lymphoma cases who were HBs-antigen seropositive. No increase in IgG4-positive plasma cells was detected in any cases of hepatic DLBCL, MALT lymphoma, or reactive lymphoid hyperplasia.

Of the systemic B-cell lymphoma cases, all 12 IVLBCL cases had an intrasinusoidal growth pattern of lymphoma cells, and ten cases (83.3%) had MUM1-positive lymphoma cells. Eight of ten systemic DLBCL cases (80%) were positive for MUM1 and three cases (33.3%) were positive for CD25.

Findings of 36 previously reported of primary hepatic B-cell lymphoma cases

Sixteen of the previously reported cases were DLBCL and 20 cases were MALT lymphoma [17–42]. Of the 16 DLBCL cases, nine (56.3%) were HCV-seropositive and four (25%) were HBV-seropositive. Only one DLBCL case had both HCV infection and SS. The median survival time of the ten DLBCL cases examined was 48 months. Nine of the 20 MALT lymphoma cases (45%) were HCV-seropositive and two cases (10%) were HBV-seropositive. Three MALT lymphoma cases had PBC, one had SS, and one had both PBC and SS, and these five cases (25%) did not have HCV nor HBV infection. The median survival time of the 18 MALT lymphoma cases for which this information was available was 65 months, which was significantly longer than in the above-reported ten DLBCL cases ($p<0.05$).

Discussion

The prevalence of HCV infection was significantly higher in the 12 primary hepatic DLBCL cases examined (66.7%) than in the systemic lymphoma cases with liver involvement, as well as in the other two control groups ($p<0.01$). Two MALT lymphoma cases examined (25%) had chronic HCV-positive hepatitis. Bronowicki et al. [43] reported HCV infection in four of 21 primary hepatic DLBCL cases (19%), but no HCV infection in three MALT lymphoma cases. Among the previously reported cases [17–42], nine of 16 primary hepatic DLBCL cases (56.3%) and nine of 20 MALT lymphoma cases (45%) had HCV infection. Although the prevalence of HCV infection was low in the MALT lymphoma cases that we examined, our results are consistent with those of other reports [11, 43] examining the relationship between HCV infection and primary hepatic DLBCL. Intracytoplasmic HCV RNA signals have been detected in hepatocytes, mononuclear cells, and lymph

Table 3 Immunohistological findings and Epstein–Barr virus infection in 42 cases of liver-involving B-cell lymphoma

Histological type	CD5	CD10	Bcl2	Bcl6	MUM1	CD25	EBERs
Primary hepatic B-cell lymphoma							
DLBCL: 12	3 (25%)	4 (33.3%)	6 (50%)	5 (41.7%)	5 (41.7%)	5 (41.7%)	2 (16.7%)
MALT: 8	0/7 (0)	0 (0)	8 (100%)	0/6 (0)	0 (0)	0 (0)	0 (0)
Liver-involving systemic B-cell lymphoma							
IVLBCL: 12	3/10 (30%)	0/11 (0)	8/10 (80%)	1/10 (10%)	10 (83.3%)	2 (16.7%)	0 (0)
DLBCL: 10	1/9 (11.1%)	1 (10%)	8/9 (88.9%)	2/9 (22.2%)	8 (80%)	3/9 (33.3%)	0 (0)

/: positive/examined cases. *EBERs* Epstein–Barr encoded RNAs, *DLBCL* diffuse large B-cell lymphoma, *MALT* mucosa-associated lymphoid tissue, *IVLBCL* intravascular large B-cell lymphoma

follicles in the liver of HCV-seropositive cases by PCR and in situ hybridization [44]. Sung et al. [45] established a cell line of an HCV-seropositive B-cell lymphoma, from which they extracted HCV viral particles with which they were able to infect other B-cell lines as well as hepatocytes. Kasama et al. [8] demonstrated expression of the full HCV genome in B cells of HCV transgenic mice, and 25% of these mice progressed to DLBCL within 600 days after birth. These reports support the theory that HCV can infect reactive and neoplastic B cells, and that persistent HCV infection may induce primary hepatic as well as other organ B-cell lymphoma.

Of the eight HCV-seropositive primary hepatic DLBCL cases examined, five were classified as CD10- and/or Bcl6-positive GC B-cell phenotype. Expression of Bcl2 and CD25 (IL2αR) was detected in the lymphoma cells of four of these eight DLBCL cases. HCV infection has been reported to cause an approximately 5- to 10-fold increase in the mutation frequency of the Bcl6 gene in peripheral blood mononuclear cells, B-cell lymphoma cells, and their cell lines [46]. Zuckerman et al. [47] reported a significantly higher incidence of Bcl2 gene translocation in peripheral blood cells in cases with HCV-seropositive hepatitis, compared with HCV-negative controls ($p<0.01$). Machida et al. [48] demonstrated that disruption of interferon regulatory factor 1 in HCV-infected mice increased serum IL-2 and Bcl2 expression in lymphocytes, and induced a high incidence of B-cell lymphoma. As well as inducing anti-apoptotic Bcl2 and transcription factors such as Bcl6, IL-2 may activate cytokine signaling via CD25 (IL2αR) in HCV-infected B cells [49]. Thus, lymphomagenesis may occur via a multistep mechanism in HCV-infected GC and non-GC B cells, even in the liver.

We found that two cases of primary hepatic DLBCL (16.7%) had rheumatoid arthritis treated with methotrexate. Although there were no reports of complications in these two cases, they were consistent with iatrogenic immunodeficiency-associated lymphoproliferative disorder [13]. Four of the eight cases of MALT lymphoma (50%) were complicated by PBC and/or SS or autoimmune hepatitis. Of these six cases with autoimmune disease, one case each of DLBCL and MALT lymphoma had chronic HCV hepatitis. Of the 36 previously

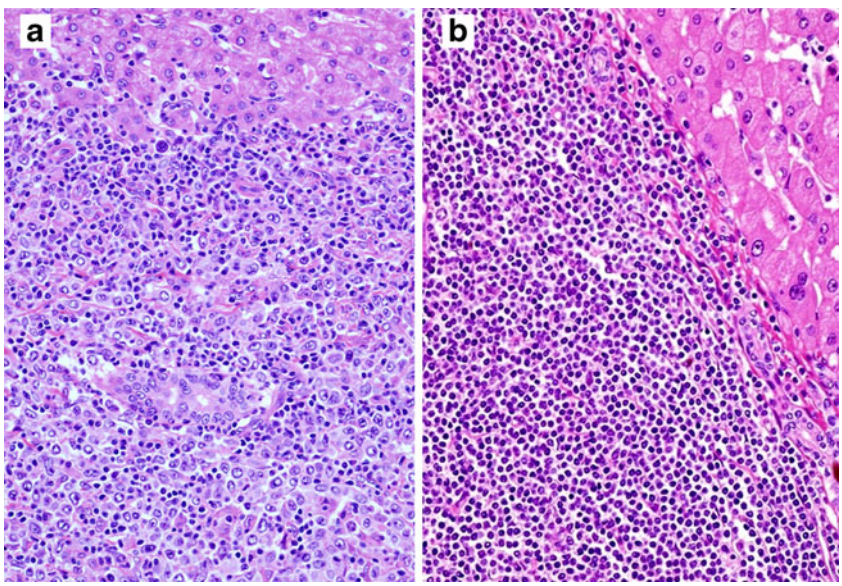

Fig. 3 Histological appearance of primary hepatic DLBCL (**a**) and MALT lymphoma (**b**) in HCV-seropositive cases (hematoxylin and eosin staining, ×400). In the DLBCL case, many small lymphocytes are seen among large lymphoid cells

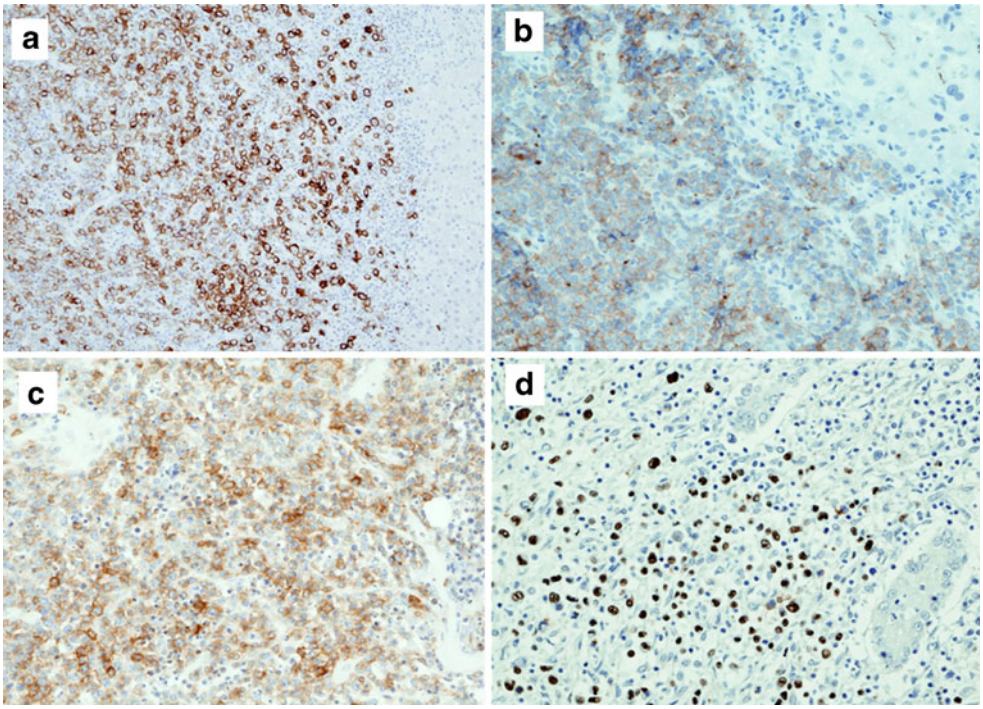

Fig. 4 HCV-seropositive primary hepatic DLBCL. **a, b, c** Immunoperoxidase staining. **d** In situ hybridization, ×200. **a** Many CD20-positive large lymphoid cells show a diffuse infiltrating pattern. **b** CD10-positive large lymphoid cells are diffusely distributed. Bile canaliculi have focal weak CD10-positivity in the upper right hepatic lobule. **c** Large lymphoid cells are positive for CD25. **d** Many nuclear EBER signals are detected in medium-sized and large lymphoid cells. Two bile ducts on the right are preserved

reported cases examined [17–42], one primary hepatic DLBCL case and five MALT lymphoma cases (total 16.7%) were complicated by PBC and/or SS. Of these, only one DLBCL case had HCV infection. In Europe, SS occurs frequently in HCV-seropositive patients with type II cryoglobulinemia, which is highly suggestive of a prodromal stage of extranodal low-grade B-cell lymphoma [50, 51]. There is great geographic heterogeneity in the prevalence of type II cryoglobulinemia in HCV-seropositive cases, with type II cryoglobulinemia occurring more commonly in Southern Europe (40–60% of HCV-seropositive cases) [52]. In Japan, type III cryoglobulinemia was found in 23 of 65 HCV-seropositive cases (35.4%), but type II cryoglobulinemia was found in only one case (1.5%) [53]. Japanese lymphoplasmacytic and MALT lymphoma cases also had a low incidence of HCV infection compared with DLBCL cases [16]. These findings support the view that primary hepatic lymphoma, especially MALT lymphoma, can occur in cases of autoimmune disease independently of HCV infection and type II cryoglobulinemia in Japan.

The present study also demonstrated that HBV or EBV infection, which are important etiological factors for tumorigenesis, were a minor complication of primary hepatic B-cell lymphoma cases. Hepatic reactive lymphoid hyperplasia and IgG4-positive plasma cells have also been reported to have no direct relationship with HCV infection, autoimmune disease, or primary hepatic B-cell lymphoma [15, 54]. Although HCV infection and autoimmune disease were frequent in Japanese cases of primary hepatic B-cell lymphoma, they were mostly found independently of each other. However, primary hepatic lymphoma is rare, even in the primarily HCV-infected liver [11, 43]. Marcucci et al. [55] proposed multifactorial models for lymphomagenesis in HCV-seropositive cases, suggesting that lymphomagenesis was caused by both HCV infection and additional factors such as other receptors (CD81 and others), EBV co-infection, and environmental factors. The reasons for lymphoma being rare in the liver may be related to localized lymphoid reactions in the portal area and to specific cytotoxic immune reactions of pit (NK) cells in HCV infection [56]. Further studies are necessary to clarify the reasons for the low incidence of primary hepatic lymphoma and the mechanisms of lymphomagenesis in HCV infection.

The 5-year survival rate of the nine primary hepatic DLBCL cases we examined was 43%, and the five cases receiving rituximab plus cytotoxic treatment were alive and well at the time of writing. A French lymphoma study demonstrated that 24 HCV-seropositive systemic DLBCL cases had a significantly worse overall 2-year survival rate (56%) than 72 HCV-negative DLBCL cases (80%), after matching for age and prognostic factors ($p=0.02$) [57]. However, four reported primary hepatic DLBCL cases had a good prognosis after cytotoxic treatment with or without rituximab [58]. Antiviral treatment after cytotoxic treatment also contributed to a significantly longer disease-free survival period in 69 HCV-seropositive B-cell lymphoma cases ($p<0.05$) [59]. These data strongly suggest that rituximab plus cytotoxic treatment followed by antiviral treatment may result in an improved clinical outcome in primary hepatic and systemic HCV-seropositive DLBCL cases.

Acknowledgments This study was supported in part by a grant (No. 066007) from the Central Research Institute of Fukuoka University. We are grateful to Akiko Ogami, Tomomi Okabe, Kaori Saga, Akiko Ishiguro, and Tomoko Fukushige for their excellent technical assistance.

Competing interests The authors declare that they have no competing financial interests and have no conflicts of interest to disclose.

Open Access This article is distributed under the terms of the Creative Commons Attribution License which permits any use, distribution, and reproduction in any medium, provided the original author(s) and the source are credited.

References

1. Arcaini L, Paulli M, Boveri E, Vallisa D, Bernuzzi P et al (2004) Splenic and nodal marginal zone lymphomas are indolent disorders at high hepatitis C virus seroprevalence with distinct presenting features but similar morphologic and phenotypic profiles. Cancer 100:107–115
2. Viswanatha DS, Dogan A (2007) Hepatitis C virus and lymphoma. J Clin Pathol 60:1378–1383
3. Libra M, Polesel J, Russo AE, V De Re, Cina D et al (2010) Extrahepatic disorders of HCV infection: a distinct entity of B-cell neoplasia? Int J Oncol 36:1331–1340
4. Hermine O, Lefrere F, Bronowicki JP, Mariette X, Jondeau K et al (2002) Regression of splenic lymphoma with villous lymphocytes after treatment of hepatitis C virus infection. N Engl J Med 347:89–97
5. Feldmann G, Nischalke HD, Nattermann J, Banas B, Berg T et al (2006) Induction of interleukin-6 by hepatitis C virus core protein in hepatitis C-associated mixed cryoglobulinemia and B-cell non-Hodgkin's lymphoma. Clin Cancer Res 12:4491–4498
6. Wu C, Budhu A, Chen S, Zhou X, Popescu NC, Valerie K, Wang XW (2006) Effect of hepatitis C virus core protein on the molecular profiling of human B lymphocytes. Mol Med 12:47–53
7. Ito M, Murakami K, Suzuki T, Mochida K, Suzuki M et al (2010) Enhanced expression of lymphomagenesis-related genes in peripheral blood B cells of chronic hepatitis C patients. Clin Immunol 135:459–465
8. Kasama Y, Sekiguchi S, Saito M, Tanaka K, Satoh M et al (2010) Persistent expression of full genome of hepatitis C virus in B cells induces spontaneous development of B-cell lymphomas in vivo. Blood 116:4926–4933
9. Ramos-Casals M, Civita L, Vita S, Solans R, Luppi M et al (2007) Characterization of B cell lymphoma in patients with Sjögren's syndrome and hepatitis C virus infection. Arth Rheumatol 57:161–170
10. Floreani A, Baragiotta A, Leone MG, Baldo V, Naccarato R (2003) Primary biliary cirrhosis and hepatitis C virus infection. Am J Gastroenterol 98:2757–2762
11. Page RD, Romaguera JE, Osborne B, Medeiros LJ, Rodriguez J et al (2001) Primary hepatic lymphoma: favorable outcome after combination chemotherapy. Cancer 92:2023–2029
12. Bosman FT, Carneiro F, Hruban RH, Theise ND (2010) WHO classification of tumours of the digestive system. IARC, Lyon, pp 239–240
13. Swerdlow SH, Campo E, Harris NL, Jaffe ES, Peleri SA et al (2008) WHO classification of tumours of haematopoietic and lymphoid tissues. IARC, Lyon
14. Willenbrock K, Kriener S, Oeschger S, Hansmann ML (2006) Nodular lymphoid hyperplasia of the liver with simultaneous focal nodular hyperplasia and hemangioma. Virchows Arch 448:223–227
15. d'Amore F, Coiffier B, Crowther D, Crowther D, Gospodarowicz M et al (1994) Report on a workshop convened to discuss the pathological and staging classifications of gastrointestinal tract lymphoma. Ann Oncol 5:397–400
16. Takeshita M, Sakai H, Okamura S, Higaki K, Oshiro Y et al (2006) Prevalence of hepatitis C virus infection in cases of B-cell lymphoma in Japan. Histopathology 48:189–198
17. Ascoli V, Lo Coco F, Artini M, Levrero M, Martelli M, Negro F (1998) Extranodal lymphomas associated with hepatitis C virus infection. Am J Clin Pathol 109:600–609
18. Chowla A, Malhi-Chowla N, Chidambaram A, Surick B (1999) Primary hepatic lymphoma in hepatitis C. Am Surg 65:881–883
19. Doi H, Horiike N, Hiraoka A, Koizumi Y, Yamamoto Y et al (2008) Primary hepatic marginal zone B cell lymphoma of mucosa-associated lymphoid tissue type. Int J Hematol 88:418–423
20. Eom D-W, Huh JR, Kang YK, Lee YS, Yu E (2004) Clinicopathological features of eight Korean cases of primary hepatic lymphoma. Pathol Int 54:830–836
21. Gockel HR, Heidemann J, Lugering A, Mesters RM, Parwaersch R et al (2005) Stable remission after administration of rituximab in a patient with primary hepatic marginal zone B-cell lymphoma. Eur J Haematol 74:445–447
22. Hayashi H, Ohtani H, Ueda T, Yamaguchi J, Izawa K et al (2006) Primary hepatic lymphoma with spindle cell components. Virchows Arch 449:591–596
23. Iida T, Iwahashi M, Nakamura M, Nakamori M, Yokoyama S et al (2007) Primary hepatic low-grade B-cell lymphoma of MALT associated with *Helicobacter pylori* infection. Hepatogastroenterology 54:1898–1901
24. Maes M, Depardieu C, Dargent JL, Hermans M, Verhaeghe JL et al (1997) Primary low-grade B-cell lymphoma of MALT-type occurring in the liver. J Hepatol 27:922–927
25. Mahjoub WK, Chaumette-Planckaert MT, Penas EMM, Dierlamm J et al (2008) Primary hepatic lymphoma of mucosa-associated lymphoid tissue type. Int J Surg Pathol 16:301–307
26. Matano S, Nakamura S, Annen Y, Hattori N, Kiyohara K et al (1998) Primary hepatic lymphoma in a patient with chronic hepatitis B. Am J Gastroenterol 93:2301–2302
27. Mizorogi F, Hiramoto J, Nozato A, Takekuma Y, Nagayama K et al (2000) Hepatitis C virus infection in patients with B-cell non-Hodgkin's lymphoma. Int Med 39:112–117
28. Mizuno S, Isaji S, Tabata M, Uemoto S, Imai H, Shiraki K (2002) Hepatic mucosa-associated lymphoid tissue (MALT) lymphoma associated with hepatitis C. J Hepatol 37:872–873
29. Mohler M, Gutzler F, Kallinowski B, Goeser T, Stremmel W (1997) Primary hepatic high-grade non-Hodgkin's lymphoma and chronic hepatitis C infection. Diagn Dis Sci 42:2241–2245
30. Murakami J, Fukushima N, Ueno H, Saito T, Watanabe T et al (2002) Primary hepatic low-grade B-cell lymphoma of the mucosa-associated lymphoid tissue type. Hematology 75:1431–1439
31. Orrego M, Guo L, Reeder C, De Petris G, Balan V et al (2005) Hepatic B-cell non-Hodgkin's lymphoma of MALT type in the liver explant of a patient with chronic hepatitis C infection. Liver Transpl 11:796–799
32. Prabhu RM, Medeiros LJ, Kumar D, Drachenbery CI, Papadimitriou JC et al (1998) Primary hepatic low-grade B-cell lymphoma of mucosa-associated lymphoid tissue (MALT) associated with primary biliary cirrhosis. Mod Pathol 11:404–410
33. Rubin-Brandt L, Brundler M-A, Kerl K, Negro F, Nador RG et al (1999) Primary hepatic diffuse large B cell lymphoma in a patient with chronic hepatitis C. Am J Surg Pathol 23:1124–1130

34. Sato S, Masuda T, Oikawa H, Satoh T, Suzuki Y et al (1999) Primary hepatic lymphoma associated with primary biliary cirrhosis. Am J Gastroenterol 94:1669–1673
35. Takeshima F, Kunisaki M, Aritomi T, Osabe M, Akama F et al (2004) Hepatic mucosa-associated lymphoid tissue lymphoma and hepatocellular carcinoma in a patient with hepatitis B virus infection. J Clin Gastroenterol 38:823–826
36. Tsuruta S, Enjoji M, Nakamuta M, Makihata T, Kotoh K, Sakai H, Ando B, Nawata H (2002) Primary hepatic lymphoma in a patient with Sjögren's syndrome. J Gastroenterol 37:129–132
37. Yago K, Shimada H, Itoh M, Ooba N, Itoh K et al (2002) Primary low-grade B-cell lymphoma of mucosa-associated lymphoid tissue (MALT)-type of the liver in a patient with hepatitis C virus infection. Leuk Lymphoma 43:1497–1500
38. Ye MQ, Suriawinata A, Black C, Min AD, Strauchen J, Thung SN (2000) Primary hepatic marginal zone B-cell lymphoma of mucosa-associated lymphoid tissue type in a patient with primary biliary cirrhosis. Arch Pathol Lab Med 124:604–608
39. Masood A, Kairouz S, Hudhud KH, Hegazi AZ, Banu A, Gupta NC (2009) Primary non-Hodgkin lymphoma of liver. Curr Oncol 16:74–77
40. Delshad SD, Ahdoot JJ, Portocarrero DJ (2010) Primary hepatic lymphoma. Clin Gastroenterol Hepatol 8:e49–e50
41. Nakayama S, Yokote T, Kobayashi K, Hirata Y, Akioka T et al (2010) Primary hepatic MALT lymphoma associated with primary biliary cirrhosis. Leuk Res 34:e17–e20
42. Oda Y, Kou T, Watanabe M, Sakuma Y, Taguchi N et al (2010) Regression of B-cell lymphoma of the liver with hepatitis C virus infection after treatment with pegylated interferon-α and ribavirin. Dig Dis Sci 55:1791–1793
43. Bronowicki JP, Bineau C, Feugier P, Hermine O, Brousse N et al (2003) Primary lymphoma of the liver. Hepatology 37:781–787
44. Alzahrani AJ, Vallely PJ, McMahon RFT (2002) Development of a novel nested in situ PCR–ISH method for detection of hepatitis C virus RNA in liver tissue. J Virol Methods 99:53–61
45. Sung VMH, Shimodaira S, Doughty AL, Piccio GR, Can H et al (2003) Establishment of B-cell lymphoma cell lines persistently infected with hepatitis C virus in vivo and in vitro. J Virol 77:2134–2146
46. Machida K, Cheng KTN, Sung VMH, Shimodaira S, Lindsay KL et al (2004) Hepatitis C virus induces a mutator phenotype: enhanced mutations of immunoglobulin and protooncogenes. Proc Natl Acad Sci USA 101:4262–4267
47. Zuckerman E, Zuckerman T, Sahar D, Streichman S, Attias D et al (2001) The effect of antiviral therapy on t(14;18) translocation and immunoglobulin gene rearrangement in patients with chronic hepatitis C virus infection. Blood 97:1555–1559
48. Machida K, Tsukiyama-Kohara K, Sekiguchi S, Seike E, Tóne S et al (2009) Hepatitis C virus and disruption of interferon signaling promote lymphoproliferation via type II CD95 and interleukins. Gastroenterology 137:285–296
49. Takeshita M, Sakai H, Okamura S, Oshiro Y, Higaki K et al (2005) Splenic large B-cell lymphoma in patients with hepatitis C virus infection. Human Pathol 36:878–885
50. De Re V, Pavan A, Sansonno S, Sansonno D, Racanelli V (2009) Clonal CD27+, CD19+ B cell expansion through inhibition of FC gamma IIR in HCV(+) cryoglobulinemic patients. Ann N Y Acad Sci 1173:326–333
51. De Re V, Caggiar L, Monti G, Libra M, Spina M et al (2010) HLA DR-DQ combination associated with the increased risk of developing human HCV-seropositive non-Hodgkin's lymphoma is related to the type II mixed cryoglobulinemia. Tissue Antigens 75:127–135
52. Saadoun D, Landau DA, Calabrese LH, Cacoub PP (2007) Hepatitis-associated mixed cryoglobulinemia. Rheumatology 46:1234–1242
53. Tanaka K, Aiyama T, Imai J, Morishita Y, Fukatsu T, Kakumu S (1995) Serum cryoglobulinemia and chronic hepatitis C virus disease among Japanese patients. Am J Gastroenterol 90:1847–1852
54. Zen Y, Fujii T, Sato Y, Masuda S, Naganuma Y (2007) Pathological classification of hepatic inflammatory pseudotumor with respect to IgG4-related disease. Mod Pathol 20:884–894
55. Marcucci F, Mele A (2011) Hepatitis viruses and non-Hodgkin lymphoma. Blood 117:1792–1798
56. Bonorino P, Ramzan M, Camous X, Dufeu-Duchesne T, Thélu MA et al (2009) Fine characterization of intrahepatic NK cells expressing natural killer receptors in chronic hepatitis B and C. J Hepatol 51:458–467
57. Besson C, Canioni D, Lepage E, Pol S, Morel P et al (2006) Characteristics and outcome of diffuse large B-cell lymphoma in hepatitis C virus-positive patients in LNH 93 and LNH 98 groupe d'Etude des lymphomes de l'Adulte Programs. J Clin Oncol 24:953–960
58. De Renzo A, Perna F, Persico M, Notaro R, Mainolfi C et al (2008) Excellent prognosis and prevalence of HCV infection of primary hepatic and splenic non-Hodgkin's lymphoma. Eur J Haematol 81:51–57
59. La Mura V, De Renzo A, Perna R, D'Agostino D, Masarone M et al (2008) Antiviral therapy after complete response to chemotherapy could be efficacious in HCV-seropositive non-Hodgkin's lymphoma. J Hepatol 49:557–563

Virchows Arch (2012) 460:389–397
DOI 10.1007/s00428-012-1216-0

ORIGINAL ARTICLE

Keratin 8 variants are associated with cryptogenic hepatitis

Mario Zierden · Arndt-Hendrik Penner · Manuel Montesinos-Rongen · Maren Weferling · Uta Drebber · Judith Stift · Jochen W. U. Fries · Margarete Odenthal · Stephan Rosenkranz · Hans-Peter Dienes

Received: 17 August 2011 / Revised: 13 February 2012 / Accepted: 22 February 2012 / Published online: 15 March 2012
© Springer-Verlag 2012

Abstract Keratins 8 and 18 (K8 and K18) are the cytoskeletal intermediate filament proteins of adult hepatocytes. Murine models indicate that mutations in the K8- and K18-encoding genes predispose to liver injury. Moreover, studies showed an association of K8/K18 variants with human acute and chronic liver diseases. However, only little is known about a putative association of K8/K18 variants with cryptogenic hepatitis, a frequent liver disease of enigmatic etiology, often necessitating liver transplantation. Therefore, we analyzed whether K8 variants associate with cryptogenic hepatitis in a German cohort of patients in comparison to control blood bank donors. Genomic DNA isolated from liver biopsies of cryptogenic hepatitis patients or peripheral blood of healthy donors was analyzed for K8 variants by PCR amplification and direct DNA sequencing. We identified 8 novel heterozygous or homozygous amino acid-altering K8 variants in 5 of 62 cryptogenic hepatitis patients (8.1 %) and in none of 67 controls (P=0.02). Previously described K8 variants p.G62C and p.R341H were found at similar incidence in cryptogenic hepatitis patients and controls. Hence, they were considered as polymorphisms not associated with liver disease progression. In conclusion, previously undescribed K8 variants associate with cryptogenic hepatitis in a German cohort of patients, possibly predisposing carriers to the development of liver disease.

Keywords Cryptogenic liver disease · Genetic predisposition to disease · Genetic variation · Keratin 8 · Mutation detection

Mario Zierden and Arndt-Hendrik Penner contributed equally to this work.

M. Zierden (✉) · A.-H. Penner · M. Weferling · U. Drebber · J. W. U. Fries · M. Odenthal · H.-P. Dienes
Institute for Pathology, University Hospital of Cologne, 50924 Cologne, Germany
e-mail: mario.zierden@uni-koeln.de

M. Zierden · S. Rosenkranz
Center for Molecular Medicine Cologne (CMMC), University of Cologne, 50931 Cologne, Germany

M. Montesinos-Rongen
Department of Neuropathology, University Hospital of Cologne, 50924 Cologne, Germany

J. Stift
Clinical Institute of Pathology, Medical University of Vienna, Vienna, Austria

M. Zierden · S. Rosenkranz
Department III of Internal Medicine, University Hospital of Cologne, 50937 Cologne, Germany

Introduction

Intermediate filaments (IFs) represent one of the main cytoskeletal elements found in mammalian cells. Keratins (K) are the largest subgroup of IFs, classified as acidic type I (K9–28, K31–40) and neutral–basic type II (K1–8, K71–86) proteins [1]. Epithelial cells express at least one type I and one type II keratin that form heteropolymeric IFs. In simple (single-layered) epithelia found in the pancreas, liver, and intestine, K8 and K18 are primarily expressed with variable levels of K7, K19, and K20 [2, 3]. However, adult hepatocytes express K8 and K18 proteins exclusively [3].

Murine models indicate that K8 and K18 provide hepatoprotection against mechanical and toxic liver damage [3]. For example, K8-deficient C57BL/6 mice show embryonic lethality due to liver hemorrhage, while K8-deficient FVB/

N mice develop mild hepatitis, increased hepatocyte fragility, and susceptibility to hepatocyte apoptosis [4–6]. Moreover, transgenic mice that overexpress a human K8 variant are predisposed to hepatocyte apoptosis and liver injury [7]. Likewise, mice overexpressing a human K18 mutant exhibit mild chronic hepatitis in association with hepatocyte fragility and increased susceptibility to liver injury [8, 9]. Collectively, these data suggest that K8 and K18 mutations predispose or cause liver diseases.

Human studies demonstrated an association of K8/K18 mutations with various end-stage liver diseases as well as with disease progression during chronic hepatitis C and primary biliary cirrhosis, an autoimmune cholestatic liver disease [10–14]. Furthermore, K8/K18 variants confer a risk of developing acute liver failure [15]. However, only little is known about a potential association of K8/K18 mutations with cryptogenic hepatitis, a liver disease that is diagnosed only after extensive evaluation has excluded all known etiologies [16]. Cryptogenic hepatitis has a prevalence of approximately 10 % among patients with chronic liver diseases, frequently requiring liver transplantation upon progression to cirrhosis [17]. In a US-American cohort, K8 p.Y54H, p.G62C, p.R341H, and p.R454C as well as K18 p.H128L heterozygous variants were reported in 7 of 68 (10.3 %) cryptogenic cirrhosis patients in comparison to 13 of 349 blood bank controls (3.7 %; $P=0.03$) [10, 11, 13]. In contrast, a German study suggests that the frequencies of K8 mutations are similar in 61 cryptogenic cirrhosis patients to those in controls (1.6 versus 1.9 %, respectively) [18]. The reasons for the observed discrepancies could include the limited analysis of the K8 variants p.Y54H and p.G62C in the latter study only as well as possible population differences. Therefore, we investigated whether K8 mutations in three of eight exonic regions, covering all K8 variants previously found in cryptogenic cirrhosis and more than 95 % of K8 variants found in various acute and chronic liver diseases [10–15], associate with cryptogenic hepatitis in a German cohort of 62 patients in comparison to 67 control blood bank donors. We identified 8 previously undescribed heterozygous and homozygous amino acid-altering K8 variants in 5 of 62 cryptogenic hepatitis patients (8.1 %) and in none of 67 controls ($P=0.02$). Notably, previously described K8 variants p.G62C and p.R341H were found at similar incidence in both cohorts. Hence, they were considered as genetic alterations not associated with liver disease progression.

Patients and methods

Cryptogenic hepatitis patients and controls

A cohort of liver biopsies from German patients referred to the Institute of Pathology with liver disease of uncertain etiology were selected and cryptogenic hepatitis was diagnosed according to the following criteria: seronegativity for hepatitis A, B, and C and of markers of autoimmune hepatitis (AIH), primary biliary cirrhosis, and primary sclerosing cholangitis, negative history for alcohol, drugs, hepatotoxins, diabetes mellitus, inflammatory bowel disease, blood transfusions, and hepatocellular carcinoma, elevation of liver enzymes aspartate aminotransferase (AST) and/or alanine aminotransferase (ALT) indicating liver cell damage. Metabolic diseases as hereditary hemochromatosis, Wilson's disease, and alpha-1 antitrypsin deficiency were excluded by biochemical tests and liver histopathology. In addition, liver biopsies were tested for Epstein–Barr virus DNA, cytomegalovirus DNA, and hepatitis E virus RNA by PCR. Body mass index, fasting serum glucose, and lipid profiles were generally not available and were thus not analyzed.

Randomly selected 67 healthy German donors with normal liver function tests including ALT (<35 IU/L), AST (<35 IU/L), γ-glutamyltransferase (γ-GT) (<40 IU/L), alkaline phosphatase (AP) (≤105 IU/L), and total bilirubin concentration (<1.1 mg/dL) provided peripheral blood to the blood bank of the University Hospital of Cologne.

This study was approved by local ethic committees of human experimentation. Informed consent was provided in accordance with the Helsinki Declaration of 1975.

Histological examination of liver biopsy specimens

Histopathology was evaluated and scored independently by two experienced liver pathologists (U.D. and H.-P.D.). The scoring system according to Desmet was used to quantify the grade of inflammatory activity (grade 1–4) and stage of fibrosis (grade 0–4) [19]. In addition, biopsies were scored for the grade of steatosis (grade 0–3 with grade 0, ≤5 % of hepatocytes containing fat; grade 1, 6–33 %; grade 2, 34–65 %; grade 3, ≥66 %), ballooned hepatocytes, Mallory–Denk bodies, interface hepatitis, and plasma cell infiltration. Histological steatosis of grade 1–3 in the absence or presence of necroinflammatory activity, hepatocyte ballooning degeneration, and Mallory–Denk bodies led to the diagnosis of nonalcoholic fatty liver disease (NAFLD) or nonalcoholic steatohepatitis [20–22], respectively, and thus to the exclusion from the study.

PCR amplification of K8 exons 1, 6, and 8 and direct DNA sequencing

Genomic DNA was isolated from liver biopsies of cryptogenic hepatitis patients or peripheral blood of healthy donors by using the QIAamp DNA FFPE Tissue Kit (Qiagen, Hilden, Germany) or NucleoSpin Blood XL Kit (Macherey-Nagel, Düren, Germany) according to manufacturer's instructions, respectively. Genomic DNA was analyzed for K8 variants in three of eight exonic regions by

seminested PCR amplification using Platinum Taq DNA Polymerase (Invitrogen, Karlsruhe, Germany) and intron-spanning primers specific for K8 exons 1, 6, and 8 (K8.1for, 5′-CGAGTGGGCAGCAGCAACTTTCG-3′; K8.1rev1, 5′-ATGTGCATAGGGACCGGGACTACCAG-3′; K8.1rev2, 5′-CACCTTGTCTATGAAGGAGGCAAAC-3′; K8.6for, 5′-GAGAAGGCATACCCAACCTGAC-3′; K8.6rev1, 5′-GGCCAGCTTGACGTTCATCAGC-3′; K8.6rev2, 5′-CTCCAGCTCGGACAACTTGGC-3′; K8.8for, 5′-CTTCTGTACTCATGTGGCTACCTCTG-3′; K8.8rev1, 5′-GCTGCCGCAGCTGTTCACTTGG-3′; K8.8rev2, 5′-GACGTCAGAGGACTCAGACAC-3′) followed by direct bidirectional DNA sequencing covering the exonic regions coding for K8 amino acids G48-N100, R328-N350, and G421-L473 and thereby comprising the K8 variant hot spots [10–15]. Primers were designed according to the genomic K8 sequence NG_008402.1, and K8 variants were assigned based on the mRNA sequence NM_002273.3. Amino acids are depicted by the one-letter symbols according to the K8 protein sequence NP_002264.1.

Table 1 K8 variants in cryptogenic hepatitis patients and controls

K8 variants		Number of K8 variant carriers from		
Nucleotide	**Amino acid**	**Cryptogenic hepatitis cohort (n = 62)**		**Blood bank controls (n = 67)**
c.287G>T[a,b]	p.G62C[a,b]	1		2
c.[287G>T]+[287G>T][a,b]	p.[G62C]+[G62C][a,b]	1		0
c.[299G>A]+[299G>A]	*p.[V66I]+[V66I]*	*1*		*0*
c.296G>A	*p.A65T*	*1*	*1 carrier*	*0*
c.[332G>A(+)333T>A]	*p.V77?*	*1*		*0*
c.365C>T	*p.R88C*	*1*		*0*
c.1125G>A[a,c]	p.R341H[a,c]	2 = 1 + 1		2
c.1395C>T	*p.T431I*	*1*		*0*
c.1439G>A	*p.G446S*	*1*	*1 carrier*	*0*
c.1455C>T	*p.S451F*	*1*		*0*
c.[1464G>A]+[1464G>A]	*p.[R454H]+[R454H]*	*1*		*0*
Number of carriers with any K8 variant		8/62 (12.9%)		4/67 (5.9%)
Number of carriers with K8 variants excluding polymorphisms p.G62C and p.R341H		*5/62 (8.1%)*		*0/67 (0%)*

P=0.02 (when comparing the number of carriers with K8 variants in cryptogenic hepatitis cohort versus control cohort upon exclusion of polymorphisms p.G62C and p.R341H)

[a] Variants considered as polymorphisms not associated with liver disease because they were found at a similar incidence in cryptogenic hepatitis patients compared with the control cohort

[b] Reference SNP cluster report: rs11554495

[c] Reference SNP cluster report: rs57422427

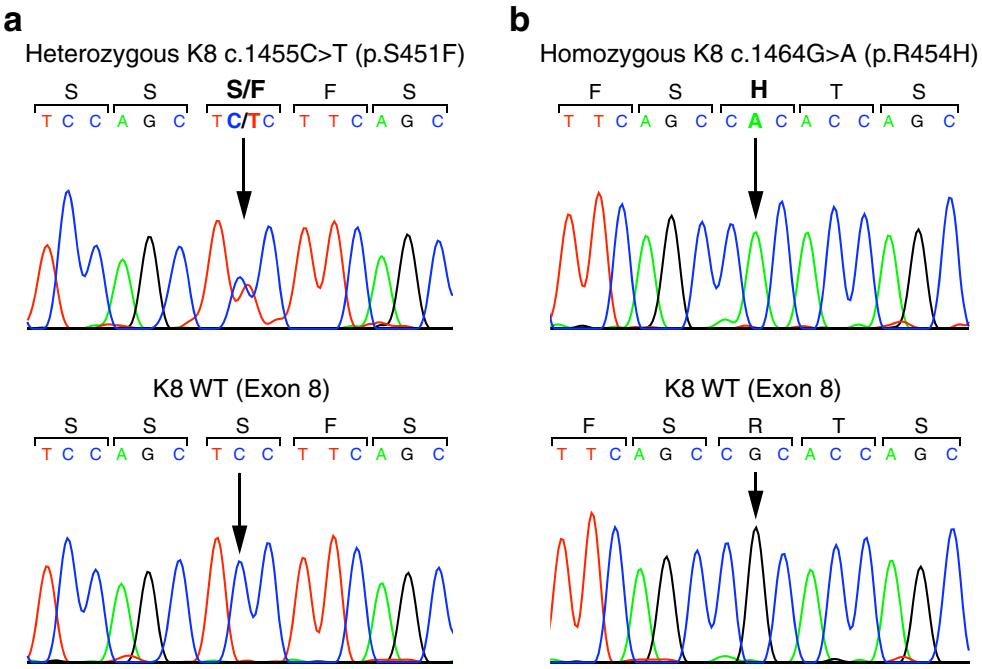

Fig. 1 Identification of K8 variants in patients with cryptogenic hepatitis and in blood bank donors. Genomic DNA was isolated from liver biopsies of cryptogenic hepatitis patients or from peripheral blood of healthy donors, and individual K8 exonic regions were amplified by PCR and then analyzed by direct bidirectional sequencing. K8 variants were assigned based on the mRNA sequence NM_002273.3. The novel **a** heterozygous c.1455C>T (p.S451F) and **b** homozygous c.1464G>A (p.R454H) K8 exon 8 variants from cryptogenic hepatitis patients are depicted in comparison to their corresponding wild-type (*WT*) blood bank donor sample

Statistical evaluation

Two-tailed Fisher's exact test was used to evaluate statistical significance between the K8 variant frequency of the cryptogenic hepatitis patients group and of the control cohort or for comparison of categorical variables between groups of patients. Differences between laboratory values of patient groups were evaluated by ANOVA. *P* values <0.05 were considered significant.

Results

Of 62 cryptogenic hepatitis patients, 8 (12.9 %) harbored any K8 amino acid-altering mutation including the previously described p.G62C and p.R341H (2 carriers each (6.5 % in total)) (Table 1). Since the latter mutations were observed with similar frequencies in 67 healthy blood donors as well (2 carriers each (6.0 % in total)), they were considered as polymorphisms rather than pathogenic mutations associated with liver disease (the latter are rendered in italics in Table 1). Upon exclusion of polymorphisms, 5 of 62 (8.1 %) cryptogenic hepatitis patients carried K8 variants in comparison to none of the controls (P=0.02). Interestingly, we identified six novel heterozygous amino acid-changing K8 variants and two homozygous K8 variants in five cryptogenic hepatitis patients (Table 1; Fig. 1) that were not described previously. Three patients had single and two had compound variants (Table 1).

K8 variant carriers were predominantly female (P=0.049) and displayed a low-level hepatitis or hepatitis

Table 2 Demographic and laboratory characteristics of cryptogenic hepatitis patients

	K8 variant carrier		
	No (n=57)	Yes (n=5)	All (n=62)
Age	53.5±15.4 (18–84)	53.8±18.4 (19–73)	53.5±15.7 (18–84)
Gender, M/F	39/18	1/4	40/22
ALT	214.5±369.4 (6–1,600)	528.8±780.4 (19–2,065)	241.6±430.1 (6–2,065)
AST	218.4±340.1 (10–1,659)	671.8±959.7 (31–2,580)	257.5±448.7 (10–2,580)
Γ-GT	154.9±233.5 (9–1,533)	144.6±98.3 (17–232)	153.9±224.6 (9–1,533)
AP	235.0±225.5 (57–1,570)	185.4±52.5 (117–270)	230.0±214.9 (57–1,570)
Bilirubin	2.8±4.7 (0.3–25.6)	4.3±6.6 (0.5–17.5)	2.9±5.0 (0.3–25.6)

Values for ALT, AST, γ-GT, AP, and age are depicted as international units per liter and years, respectively, and bilirubin levels are displayed as milligrams per deciliter. Data are presented as the mean±standard deviation and the range of values in parenthesis. Comparison of demographic and laboratory values between groups of patients with or without K8 variants revealed no significant differences except for gender (P=0.049) and AST (P=0.03)

Table 3 Liver enzyme profiles of cryptogenic hepatitis patients with (n=5) or without (n=57) novel K8 amino acid variants

K8 variant carrier	Low-level hepatitis[a]	Hepatitis[b]	Cholestatic[c]
No	30 (52.6 %)	16 (28.1 %)	11 (19.3 %)
Yes	3 (60 %)	2 (40 %)	0

Comparison of categorical values between groups of patients revealed no significant differences

[a] Low-level hepatitis enzyme profile: ALT<4×upper limit, AP<1.5×upper limit

[b] Hepatitis enzyme pattern: ALT>4×upper limit, ALT>AST, AP<1.5×upper limit, ALT>AP

[c] Cholestatic enzyme profile: AP>1.5×upper limit, AP/ALT>1.5, AP>γ-GT

enzyme profile with a tendency for higher ALT levels and with significantly higher AST levels than cryptogenic hepatitis patients without K8 variants (P=0.03) (Tables 2, 3, and 4). Liver biopsies from K8 variant carriers displayed chronic hepatitis of mild or moderate necroinflammatory activity (grade 2 or 3) with lobular focal hepatocyte necroses or nonzonal multifocal necroses. Additionally, they were characterized by mild or moderate fibrosis (stage 1 or 2) and the absence of fatty change of hepatocytes (steatosis grade 0), Mallory–Denk bodies, hepatocyte ballooning degeneration, and plasma cell infiltration (Tables 4 and 5; Fig. 2). In summary, no specific histological features associated with the novel K8 variants in liver biopsy specimens.

Discussion

Our results show an overrepresentation of K8 variants in German patients with cryptogenic hepatitis in comparison to healthy blood bank donors (8.1 versus 0 %; P=0.02), implicating K8 mutations as genetic risk factors for developing liver disease.

The observed association of K8 variants with cryptogenic hepatitis is in line with a US-American study by Ku et al. reporting K8 variants in 7 of 68 (10.3 %) cryptogenic cirrhosis patients in comparison to 13 variant carriers of 349 controls (3.7 %; P=0.03) [10, 11, 13]. However, we found that K8 mutations p.G62C and p.R341H present with similar frequencies in cryptogenic hepatitis patients and controls (3.2 % each versus 3.0 % each; P=1.0). Therefore, we classified these as polymorphisms rather than as disease-associated variants, being in partial contrast to the latter study. Ku et al. described p.G62C (3 of 68 patients; 4.4 %) as the most common of all K8 variants including p.R341H (1 of 68 patients; 1.5 %) found in cryptogenic cirrhosis patients in comparison to 0.3 % (P=0.02) and 2.9 % (P=1.0) carriers in the control cohort, respectively [10, 11, 13]. Even though p.R341H and p.G62C are the most and second most common K8 variants in white US-American and European acute and chronic liver disease patients [3, 12–15] and transgenic mice support a role for the human p.G62C K8 mutant in predisposition to liver injury [7], the frequencies of p.G62C and p.R341H K8 mutations varies in European control populations from 0.4 to 3.8 % or is presumably about 1.5 %, respectively [14, 23]. Thus, the discrepancies between our study and previous studies by Ku et al. might be due to different genetic backgrounds in the patient and control populations investigated. Furthermore, differences in the analyzed patient cohorts might contribute to the observed discrepancies because Ku et al. investigated cryptogenic cirrhosis patients requiring liver transplantation [10, 11, 13], whereas our cryptogenic hepatitis patient cohort was characterized by a relatively even distribution of all stages of fibrosis, including 14 patients without fibrosis (22.6 %; stage 0) and 9 cirrhosis patients (14.5 %; stage 4) (Table 5).

Table 4 Demographic, laboratory, and liver histopathological characteristics of cryptogenic hepatitis patients carrying novel K8 amino acid variants

Patient no.	Age (years)	Sex	K8 amino acid variants carried	Grading	Staging	Liver enzyme profile
06	54	F	p.A65T p.V77? p.R88C	2	2	Low-level hepatitis[a]
19	62	F	p.[V66I]+[V66I]	2	1	Low-level hepatitis[a]
28	19	F	p.G446S p.S451F	2	1	Low-level hepatitis[a]
35	73	M	p.[R454H]+[R454H]	3	2	Hepatitis[b]
47	61	F	p.T431I	3	2	Hepatitis[b]

Liver biopsies from K8 variant carriers showed no fatty infiltration (steatosis grade 0), Mallory–Denk bodies, ballooned hepatocytes, or plasma cell infiltration

[a] Low-level hepatitis enzyme profile: ALT<4×upper limit, AP<1.5×upper limit

[b] Hepatitis enzyme pattern: ALT>4×upper limit, ALT>AST, AP<1.5×upper limit, ALT>AP

Table 5 Histological scoring of liver biopsies from cryptogenic hepatitis patients with (n=5) or without (n=57) novel K8 amino acid variants for grading and staging

	K8 variant carrier	0	1	2	3	4
Grading	No	0	27 (47.4 %)	21 (36.8 %)	8 (14.0 %)	1 (1.8 %)
	Yes	0	0	3 (60 %)	2 (40 %)	0
Staging	No	14 (22.6 %)	18 (29.0 %)	14 (22.6 %)	7 (11.3 %)	9 (14.5 %)
	Yes	0	2 (40 %)	3 (60 %)	0	0

None of the liver biopsies showed fatty infiltration of more than 5 % of the hepatocytes (steatosis grade 0). Comparison of categorical values between groups of patients revealed no significant differences

The observed association of K8 variants with cryptogenic hepatitis is in contrast to a previous German report suggesting that K8 variant frequencies are similar in cryptogenic cirrhosis patients and controls [18]. The discrepancies between both studies are readily explained by the limited analysis of K8 mutations p.Y54H and p.G62C only by Halangk et al. that identified 1 variant carrier among 61 cryptogenic cirrhosis patients (p.G62C; 1.6 %) in contrast to 12 p.G62C and 1 p.Y54H carriers among 679 control subjects (1.9 % in total; P=1.0) [18]. Seemingly contradictory results by an Austrian report that identified 2 p.G62C carriers among 15 patients with cryptogenic liver disease (13.3 %) and 1 carrier among 45 controls (2.2 %; P=0.15) [24] might be caused by the

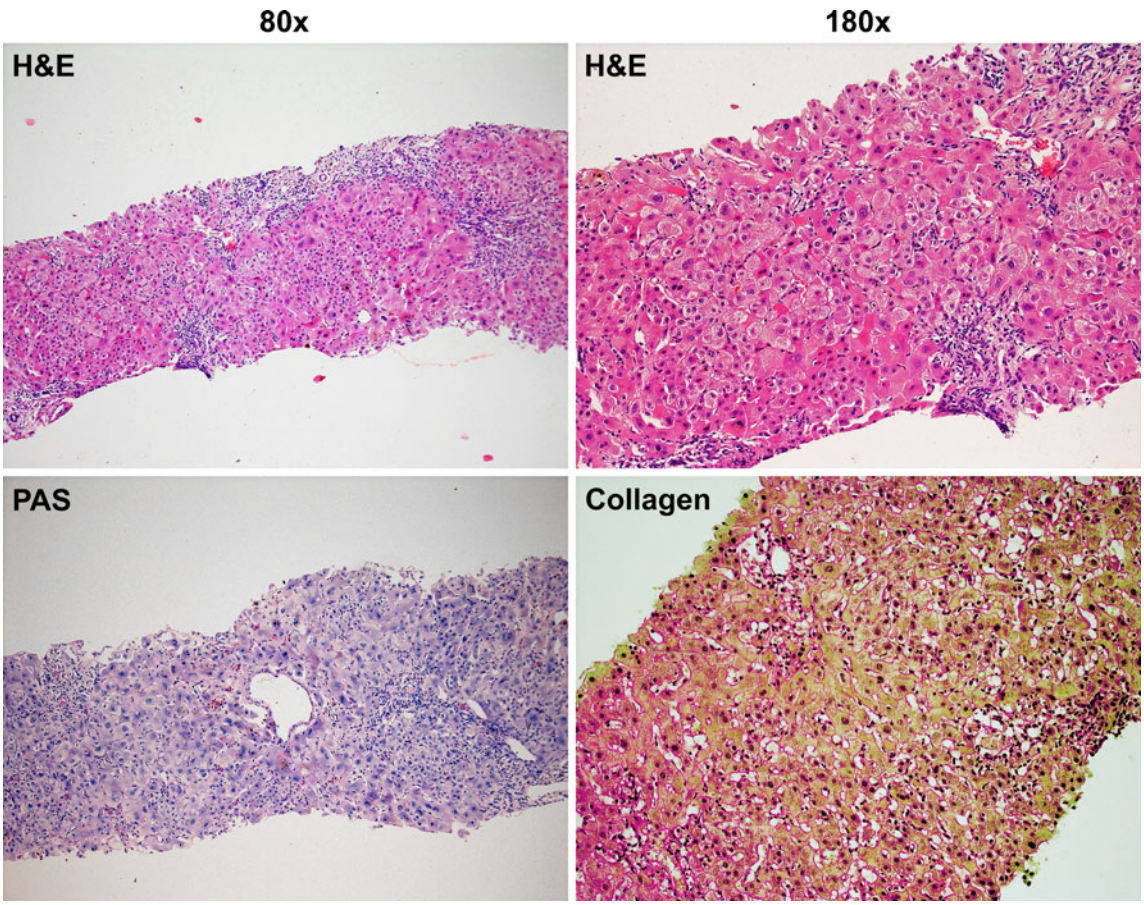

Fig. 2 Representative liver histopathology from a cryptogenic hepatitis patient carrying a novel K8 amino acid variant. Liver biopsy from cryptogenic hepatitis patient no. 35 carrying a homozygous p.R454H K8 variant shows chronic hepatitis with severe inflammatory activity (grade 3), spotty necrosis, and foci of confluent necrosis with mild portal and septal fibrosis (stage 2). There is no fat, no Mallory–Denk bodies, no hepatocyte ballooning, and no perisinusoidal fibrosis. Liver sections were stained with H&E, for glycogen and polysaccharides by periodic acid-Schiff (PAS) staining (*pink*), or for collagen fibers by van Gieson staining (*red*)

small number of patients investigated and the inherent imprecision of the latter study.

Apart from this, cryptogenic hepatitis is diagnosed in the absence of a standardized set of criteria only after comprehensive exclusion of all known etiologies [16]. Hence, its perception and character may differ between our and previous studies due to possible differences in the used diagnostic tools and the lifestyle of patients. Recent studies have implicated NAFLD and AIH as a likely diagnosis in a major fraction of cryptogenic hepatitis patients [16, 25, 26]. Although we were not able to exclude all risk factors of NAFLD like excess weight, obesity, and metabolic syndrome [16, 20], neither disease should underlie the cryptogenic hepatitis diagnosed in our patients. In fact, histological steatosis of more than 5 % of hepatocytes or the presence of typical autoantibodies, hypergammaglobulinemia, and interface hepatitis with a predominantly lymphoplasmacytic necroinflammatory infiltrate as the hallmarks of NAFLD or AIH [20, 27], respectively, led to the exclusion from this study. In addition, none of the cirrhotic patients in whom characteristic histological features of steatosis or AIH possibly have disappeared due to progressive fibrosis carried any K8 mutation (Table 5). Thus, neither NAFLD nor AIH could have significantly influenced the incidence of K8 mutations in our cryptogenic hepatitis cohort. In contrast, due to its high prevalence in developed countries and its often asymptomatic course [20], NAFLD presumably has been present in our control group of blood bank donors. However, its presence in the control group and simultaneous absence in the patient group unlikely accounts for the similar frequencies of K8 mutations p.G62C and p.R341H (about 3 % each) observed in both cohorts of our study. Moreover, previous studies by Ku et al. utilizing control blood bank donors as well should have been similarly affected by NAFLD, but observed a significant difference in the p.G62C variant frequency between patients and controls (4.4 versus 0.3 %; P=0.02) [10, 11, 13]. Finally, NAFLD and AIH have been associated with different genetic variants, but none of the diseases was found to be associated with K8 mutations [20, 28–30], making a putative contribution of these disorders to K8 mutation frequencies observed in cryptogenic hepatitis and control cohorts even more unlikely.

Importantly, we identified six novel heterozygous amino acid-altering K8 variants including p.A65T, p.V77?, p.R88C, p.T431I, p.G446S, and p.S451F as well as, for the first time, two homozygous K8 variants including p.V66I and p.R454H in cryptogenic hepatitis patients that have not been previously found and were absent from the control cohort (Table 1; Fig. 1). Among the affected K8 amino acids, p.T431, p.S451, and p.R454 as well as p.A65, p.V66, and p.R88 are conserved or highly conserved within the K8 C-terminal tail and N-terminal head protein domains across human, dog, rat, mouse, and zebra fish species,

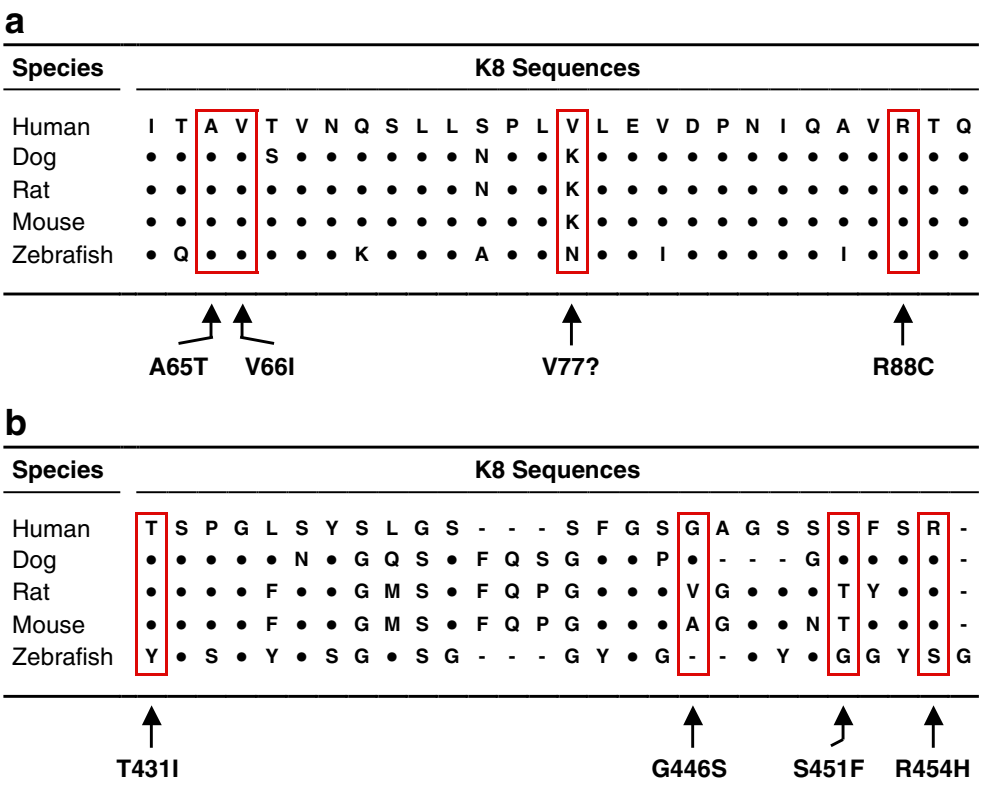

Fig. 3 K8 amino acid conservation across species. **a** and **b** The K8 amino acid sequence surrounding the variants p.A65T, p.V66I, p.V77?, and p.R88C as well as p.T431I, p.G446S, p.S451F, and p.R454H. *Dots* indicate conservation of residues in comparison with the human K8 sequence, whereas *dashes* represent gaps in order to optimize sequence alignment

respectively (Fig. 3). Among these, K8 p.A65T, p.K88C, p.S451F, and p.T431I are nonconservative amino acid substitutions. Thus, the majority of K8 amino acid substitutions identified in cryptogenic hepatitis patients are at residues that are conserved through evolution. Evolutionary conservation suggests that these K8 variants may be of biological relevance for protein structure, integrity, and function, such as their major role as cytoprotectors providing mechanical integrity and apoptosis protection to hepatocytes, e.g., by contributing to appropriate positioning and function of organelles as well as serving as a phosphate sponge to absorb undesirable stress-activated protein kinase substrate phosphorylation [3, 7].

Interestingly, we observed a low-level hepatitis or hepatitis enzyme pattern in K8 variant carriers as well as a significant association of K8 variants with higher AST levels (mean values, 671.8 versus 218.4 IU/L; P=0.03). This was accompanied by a nonsignificant trend for higher ALT levels (mean values, 528.8 versus 214.5 IU/L; P=0.123) and higher grade of inflammatory activity (mean grade, 2.4 versus 1.7; P=0.055) than in cryptogenic hepatitis noncarriers of K8 variants (Tables 2 and 5; data not shown). These previously undescribed characteristics may indicate an augmented inflammatory activity causing increased hepatocellular damage in K8 variant carriers among cryptogenic hepatitis patients. However, we neither found any specific histological changes in liver biopsies of K8 variant carriers like Mallory–Denk bodies, ground glass hepatocytes, and hepatocyte ballooning degeneration nor observed an association or trend with/for a higher stage of fibrosis (Fig. 2; Tables 4 and 5) that would support an injury-promoting role for the identified keratin variants in hepatocytes at the level of light microscopy. Nevertheless, the number of cryptogenic hepatitis patients carrying K8 variants remains low, making a reliable association of K8 variants with laboratory and liver histopathological features difficult at this stage. Thus, the biological consequences of the newly identified K8 variants including p.S451F (removing a K8 phosphorylation site conserved among species as S or T; Fig. 3; based on the K8 protein sequence NP_002264.1) and particularly those of the homozygous mutations for developing liver diseases remain to be elucidated.

In summary, we identified novel amino acid-altering K8 variants that associate with cryptogenic hepatitis in a German cohort of patients, possibly predisposing carriers to the development of liver disease.

Acknowledgments The authors thank E. Kühnen, C. Stock, and C. Dorloff for the excellent technical assistance. This work was supported by the Maria-Pesch and the Moritz Foundation.

Conflict of interest The authors declare that they have no conflict of interest.

References

1. Schweizer J, Bowden PE, Coulombe PA, Langbein L, Lane EB, Magin TM, Maltais L, Omary MB, Parry DA, Rogers MA, Wright MW (2006) New consensus nomenclature for mammalian keratins. J Cell Biol 174(2):169–174
2. Moll R, Franke WW, Schiller DL, Geiger B, Krepler R (1982) The catalog of human cytokeratins: patterns of expression in normal epithelia, tumors and cultured cells. Cell 31(1):11–24
3. Omary MB, Ku NO, Strnad P, Hanada S (2009) Toward unraveling the complexity of simple epithelial keratins in human disease. J Clin Invest 119(7):1794–1805
4. Baribault H, Price J, Miyai K, Oshima RG (1993) Mid-gestational lethality in mice lacking keratin 8. Genes Dev 7(7A):1191–1202
5. Baribault H, Penner J, Iozzo RV, Wilson-Heiner M (1994) Colorectal hyperplasia and inflammation in keratin 8-deficient FVB/N mice. Genes Dev 8(24):2964–2973
6. Loranger A, Duclos S, Grenier A, Price J, Wilson-Heiner M, Baribault H, Marceau N (1997) Simple epithelium keratins are required for maintenance of hepatocyte integrity. Am J Pathol 151(6):1673–1683
7. Ku NO, Omary MB (2006) A disease- and phosphorylation-related nonmechanical function for keratin 8. J Cell Biol 174(1):115–125
8. Ku NO, Michie S, Oshima RG, Omary MB (1995) Chronic hepatitis, hepatocyte fragility, and increased soluble phosphoglycokeratins in transgenic mice expressing a keratin 18 conserved arginine mutant. J Cell Biol 131(5):1303–1314
9. Ku NO, Michie SA, Soetikno RM, Resurreccion EZ, Broome RL, Oshima RG, Omary MB (1996) Susceptibility to hepatotoxicity in transgenic mice that express a dominant-negative human keratin 18 mutant. J Clin Invest 98(4):1034–1046
10. Ku NO, Gish R, Wright TL, Omary MB (2001) Keratin 8 mutations in patients with cryptogenic liver disease. N Engl J Med 344 (21):1580–1587
11. Ku NO, Darling JM, Krams SM, Esquivel CO, Keeffe EB, Sibley RK, Lee YM, Wright TL, Omary MB (2003) Keratin 8 and 18 mutations are risk factors for developing liver disease of multiple etiologies. Proc Natl Acad Sci U S A 100(10):6063–6068
12. Strnad P, Lienau TC, Tao GZ, Lazzeroni LC, Stickel F, Schuppan D, Omary MB (2006) Keratin variants associate with progression of fibrosis during chronic hepatitis C infection. Hepatology 43 (6):1354–1363
13. Ku NO, Lim JK, Krams SM, Esquivel CO, Keeffe EB, Wright TL, Parry DA, Omary MB (2005) Keratins as susceptibility genes for end-stage liver disease. Gastroenterology 129(3):885–893
14. Zhong B, Strnad P, Selmi C, Invernizzi P, Tao GZ, Caleffi A, Chen M, Bianchi I, Podda M, Pietrangelo A, Gershwin ME, Omary MB (2009) Keratin variants are overrepresented in primary biliary cirrhosis and associate with disease severity. Hepatology 50(2):546–554
15. Strnad P, Zhou Q, Hanada S, Lazzeroni LC, Zhong BH, So P, Davern TJ, Lee WM, Omary MB (2010) Keratin variants predispose to acute liver failure and adverse outcome: race and ethnic associations. Gastroenterology 139(3):828–835, 835.e1–835.e3
16. Czaja AJ (2011) Cryptogenic chronic hepatitis and its changing guise in adults. Dig Dis Sci 56(12):4321–4338
17. Nair S, Verma S, Thuluvath PJ (2002) Obesity and its effect on survival in patients undergoing orthotopic liver transplantation in the United States. Hepatology 35(1):105–109
18. Halangk J, Berg T, Puhl G, Mueller T, Nickel R, Kage A, Landt O, Luck W, Wiedenmann B, Neuhaus P, Witt H (2004) Keratin 8 Y54H and G62C mutations are not associated with liver disease. J Med Genet 41(7):e92
19. Desmet VJ, Gerber M, Hoofnagle JH, Manns M, Scheuer PJ (1994) Classification of chronic hepatitis: diagnosis, grading and staging. Hepatology 19(6):1513–1520

20. Cohen JC, Horton JD, Hobbs HH (2011) Human fatty liver disease: old questions and new insights. Science 332(6037):1519–1523
21. Brunt EM (2001) Nonalcoholic steatohepatitis: definition and pathology. Semin Liver Dis 21(1):3–16
22. Czaja AJ, Carpenter HA (2007) Optimizing diagnosis from the medical liver biopsy. Clin Gastroenterol Hepatol 5(8):898–907
23. Treiber M, Schulz HU, Landt O, Drenth JP, Castellani C, Real FX, Akar N, Ammann RW, Bargetzi M, Bhatia E, Demaine AG, Battagia C, Kingsnorth A, O'Reilly D, Truninger K, Koudova M, Spicak J, Cerny M, Menzel HJ, Moral P, Pignatti PF, Romanelli MG, Rickards O, De Stefano GF, Zarnescu NO et al (2006) Keratin 8 sequence variants in patients with pancreatitis and pancreatic cancer. J Mol Med 84(12):1015–1022
24. Schoniger-Hekele M, Petermann D, Muller C (2006) Mutation of keratin 8 in patients with liver disease. J Gastroenterol Hepatol 21 (9):1466–1469
25. Maheshwari A, Thuluvath PJ (2006) Cryptogenic cirrhosis and NAFLD: are they related? Am J Gastroenterol 101(3):664–668
26. Heringlake S, Schutte A, Flemming P, Schmiegel W, Manns MP, Tillmann HL (2009) Presumed cryptogenic liver disease in Germany: high prevalence of autoantibody-negative autoimmune hepatitis, low prevalence of NASH, no evidence for occult viral etiology. Z Gastroenterol 47(5):417–423
27. Alvarez F, Berg PA, Bianchi FB, Bianchi L, Burroughs AK, Cancado EL, Chapman RW, Cooksley WG, Czaja AJ, Desmet VJ, Donaldson PT, Eddleston AL, Fainboim L, Heathcote J, Homberg JC, Hoofnagle JH, Kakumu S, Krawitt EL, Mackay IR, MacSween RN, Maddrey WC, Manns MP, McFarlane IG, Buschenfelde KH Meyer zum, Zeniya M et al (1999) International Autoimmune Hepatitis Group Report: review of criteria for diagnosis of autoimmune hepatitis. J Hepatol 31(5):929–938
28. Speliotes EK, Yerges-Armstrong LM, Wu J, Hernaez R, Kim LJ, Palmer CD, Gudnason V, Eiriksdottir G, Garcia ME, Launer LJ, Nalls MA, Clark JM, Mitchell BD, Shuldiner AR, Butler JL, Tomas M, Hoffmann U, Hwang SJ, Massaro JM, O'Donnell CJ, Sahani DV, Salomaa V, Schadt EE, Schwartz SM, Siscovick DS et al (2011) Genome-wide association analysis identifies variants associated with nonalcoholic fatty liver disease that have distinct effects on metabolic traits. PLoS Genet 7(3):e1001324
29. Czaja AJ (2008) Genetic factors affecting the occurrence, clinical phenotype, and outcome of autoimmune hepatitis. Clin Gastroenterol Hepatol 6(4):379–388
30. Strassburg CP (2010) Autoimmune hepatitis. Best Pract Res Clin Gastroenterol 24(5):667–682

Virchows Arch (2012) 460:399–406
DOI 10.1007/s00428-012-1214-2

ORIGINAL ARTICLE

Fetal liver calcifications: an autopsy study

Debora Kidron · Reuven Sharony

Received: 14 December 2011 / Revised: 6 February 2012 / Accepted: 16 February 2012 / Published online: 4 March 2012
© Springer-Verlag 2012

Abstract Fetal liver calcifications are occasionally found in fetal autopsies. However, the incidence, associated findings, clinical significance, and presumed pathogenesis of fetal liver calcifications are not well documented. This study analyzed the characteristics and significance of fetal liver calcifications found on fetal autopsies. Cases of fetal liver calcifications were collected from a fetal autopsy database. Their clinical and pathological characteristics were analyzed in comparison to the remaining cases in the database. Thirty-five cases (4.2%) of fetal liver calcifications were found among 827 consecutive fetal autopsies that had been performed in our hospital during the 16-year period from January 1, 1994 through December 31, 2009. Twenty-nine cases had nodular calcifications, predominantly subcapsular. Calcification in portal spaces and porta hepatis were present in six cases. Twenty cases were missed abortions and intrauterine fetal death. Missed abortion at or earlier than 23 weeks had significantly more subcutaneous edema and other evidence of circulatory abnormalities. Calcifications in older fetuses (>23 weeks) were located more commonly in portal spaces and in other organs. Fetal liver calcification is an incidental finding during autopsies. The significance of fetal liver calcifications has to be assessed in combination with other clinical and pathological parameters, including location and number of the lesions, signs of circulatory compromise, and abnormalities of placenta, umbilical cord, and fetal malformations. Fetal liver calcifications are commonly associated with conditions related to impaired circulation, including umbilical cord abnormalities and subcutaneous edema. We suggest that fetal liver calcifications might attest to circulatory compromise preceding death, especially if subcutaneous edema is present and even when no other abnormal findings are seen.

Keywords Calcifications · Liver · Fetal · Edema · Intrauterine fetal death · Termination of pregnancy · Autopsy

D. Kidron (✉)
The Department of Pathology, Meir Medical Center,
Kfar Saba, Israel, affiliated with Sackler Faculty of Medicine,
Tel Aviv University,
59 Tchernichovsky St,
Kfar Saba 44281, Israel
e-mail: dkidron@clalit.org.il

R. Sharony
The Genetics Institute, Meir Medical Center,
Kfar Saba, Israel, affiliated with Sackler Faculty of Medicine,
Tel Aviv University,
Tel Aviv 44281, Israel

R. Sharony
Department of Obstetrics and Gynecology,
Meir Medical Center, Kfar Saba, Israel,
affiliated with Sackler Faculty of Medicine,
Tel Aviv University,
Tel Aviv 44281, Israel

Introduction

Fetal liver calcifications are occasionally found in histologic sections of fetal autopsies. While many morphological features are obscured by autolysis in histological sections of the liver, fetal liver calcifications can be visualized regardless of the degree of autolysis. Although fetal liver calcifications seen by imaging techniques are reported, the incidence of histologic fetal liver calcifications, associated pathological features, and the clinical settings are not well documented [1, 2].

Since the finding of fetal liver calcifications on autopsy is abnormal, we hypothesized that it might provide clues to fetal morbidity and demise. The purpose of this study was to

analyze the characteristics and significance of fetal liver calcifications found on autopsy.

Methods and materials

This study included 827 consecutive and comprehensive fetal autopsies, which were performed at the Unit of Perinatal Pathology at Meir Medical Center, Kfar Saba, Israel, from January 1, 1994 through December 31, 2009, following intrauterine demise, spontaneous abortion, or termination of pregnancy for genetic or sonographic abnormalities. Written parental consent was given in all cases. Autopsy procedures followed routine protocols [3, 4] and included detailed examinations of the fetuses and placentas. Regardless of the degree of autolysis, the liver was grossly inspected, weighed, and sliced. Representative sections of both lobes were taken for histological evaluation. In cases of gross abnormality, the liver was further sampled for histology and stained with Von-Kossa, Masson trichrome, Prussian blue, and additional histochemical and immunohistochemical stains, as needed.

Autopsy findings, including gross and histological abnormalities of fetuses and placentas together with clinical information, were recorded in a database. The characteristics of fetuses with fetal liver calcifications were compared with those of the control group, composed of all other cases in the database. The gestational age was clinically determined, according to last menstrual period. First trimester ultrasound measurements were used if there was a discrepancy of more than 9 days.

The cases were divided according to the limit of viability, using 23 weeks as the cut-off value. Fetal demise after 23 weeks of gestation was termed intrauterine fetal death (IUFD). Demise at or prior to 23 weeks was considered a missed abortion (MA).

Statistical analysis

Chi-square and Fisher's exact test were used to compare the incidence of pregnancy complications between the study and the control groups. Odds ratios were calculated to assess the risk of the outcome. A p value of <0.05 was considered significant.

Results

Liver calcifications were found in 35 of 827 (4.2%) consecutive fetal autopsy cases. Male/female ratio was 1.06 (18/17). The clinical features and pathological findings are listed in Table 1. The cases were categorized according to gestational age, method of pregnancy termination (i.e., MA, IUFD, or termination of pregnancy [TOP]), growth, malformations, umbilical cord findings, and placental abnormalities (Table 2). Thirty-three cases were singleton fetuses and two were from two separate twin pairs.

Morphological features of fetal liver calcifications

Fetal liver calcifications appeared in nodules (29 cases), in portal spaces (5 cases), and in the porta hepatis (1 case). Nodular liver calcifications were predominantly located directly beneath the liver capsule (Fig. 1a). However, a thin rim of liver parenchyma separated the calcification from the liver capsule in several cases (Fig. 1b). Calcifications were surrounded by fibrosis (Fig. 1c). Occasionally, the calcification extended deeper or was located deeper, unrelated to the liver capsule (Fig. 1d). Fetal liver calcifications contained minimal to no iron. In some cases, they occurred individually or in small clusters (Fig. 1a) and were numerous in others. Diameters of calcified nodules ranged from 0.1 to 0.5 mm.

Portal calcifications were minute, numerous, and located predominantly in or around the portal veins (Fig. 2a, b). All five cases with portal calcifications were aborted in an advanced stage of pregnancy (26–38 weeks), in contrast to subcapsular calcifications which were found mainly in missed abortions (<23 weeks). Three fetuses were IUFD, and the remaining two were terminated due to genetic abnormalities. Three fetuses had calcifications in other abdominal organs and viscera; two were IUFD.

A single case with calcification in the porta hepatis was associated with gall bladder agenesis. In this case, the extrahepatic bile ducts were patent.

Early versus late abortion

Twenty-six of the 35 cases with fetal liver calcifications (74%) were found at or prior to 23 weeks of gestation (Table 2). These pregnancies were considered MA and the fetuses had significantly more subcutaneous edema than similar fetuses in the control group ($p<0.001$). Older fetuses (>23 weeks) had more calcifications elsewhere compared to the control group ($p<0.001$).

No statistically significant differences were found in the incidence of IUGR, malformations, chorioamnionitis, umbilical cord, and placental abnormalities between fetal liver calcifications cases from early or late abortions. In addition, no differences in these parameters were found between cases with fetal liver calcifications and other autopsy cases.

Spontaneous demise versus TOP

Twenty of 35 cases (57%) died in utero (MA/IUFD) compared to 31% in the other autopsy cases ($p<0.001$; Table 3).

Table 1 Clinical features and pathological findings in 35 cases of fetal liver calcifications

Case no.	Liver calcification	Week	Gender	Clinical diagnosis	Autopsy diagnosis	Growth	Additional autopsy findings	Umbilical cord	Placental abnormalities
1	Nodular, multiple	15	M	MA 13/15 weeks	Cystic hygroma, dilated right brain ventricle	SGA			VE
2	SC, hematoma	16	M	MA, post reduction of twin B for TOF	A—edema, B—Tetralogy of Fallot	AGA	E subcutaneous (A)		
3	SC, multiple	16	M	MA, Rh incompatibility	Villous edema	AGA	E generalized subcutaneous		VE
4	SC, focal	17	F	TOP, right renal agenesis, SUA, oligohydramnios	MCA: ASD, VSD, arthrogryposis, Meckel's diverticulum, intestinal malrotation	AGA	NE	VI, SUA	Perivillous fibrin depositions
5	SC, focal	17	M	MA	Placental abnormalities: maternal floor fibrin thrombi	AGA	E subcutaneous		Maternal floor fibrin thrombi, plasma cell deciduitis
6	SC, multiple	17	F	MA	c/w cord strangulation	AGA	E head	Flattened segment	
7	SC, focal and fibrosis	17	M	MA	Fetal vascular obliterative changes	AGA	E scalp	Long hypercoiled	
8	SC and intrahepatic, delicate	18	M	MA (twin B)	Twin-twin transfusion, villous edema	SGA	E generalized	VI, SUA	VE
9	SC, multiple	18	M	TOP, posterior urethral valve	Obstructive uropathy sequence	SGA			Large, edematous villi with irregular outlines
10	SC	18	F	MA	Thin segment of hypercoiled, umbilical cord	SGA	E subcutaneous	Hypercoiled, thin segment, thrombi in UV	
11	SC, agenesis of gall bladder	18	F	TOP, multiple anomalies	Cloacal dysgenesis sequence	AGA		Hypoplasia of one umbilical artery	
12	Nodular, extensive	18	M	MA 18/14 weeks	c/w entanglement and strangulation of cord, calcification in diaphragm	AGA	Calcifications—diaphragm, epididymis, perinephric	E, cord around neck and leg	E, hypercellularity, calcifications
13	Perivascular, lobular	18	F	MA 18/13 weeks	Chronic histiocytic intervillositis, extensive	SGA			
14	SC, multiple	19	F	MA 19/14 weeks	VSD	SGA	NE.	VI, SUA	
15	SC, focal, fibrotic nodule	19	F	TOP, trisomy 21	TOF	AGA			
16	SC, multiple	19	M	TOP, suspected bowel obstruction	Multiple jejunal atresia	AGA			
17	Bile ductules proliferation, coagulative necrosis	19	M	TOP, prune belli syndrome	MCA: prune belli syndrome, foreshortened right leg	AGA	Ascites		
18	SC, focal	20	M	MA	Hemosiderin in placental membranes	AGA	NE.		

Table 1 (continued)

Case no.	Liver calcification	Week	Gender	Clinical diagnosis	Autopsy diagnosis	Growth	Additional autopsy findings	Umbilical cord	Placental abnormalities
19	SC	20	F	MA 20/14 weeks	A-IUGR, thin placenta	SGA	NE.		Decidual vasculopathy, acute atherosis
20	SC, multiple	20	F	TOP, periventricular echogenicity, right club foot	Massive perivillous fibrin depositions	SGA			Perivillous fibrin, Abundant fibrin
21	SC, multiple	21	M	MA	A-IUGR, excessive spiraling, hemosiderin	SGA	NE.	E, excessive spiraling, constriction	Calcifications of vessels
22	SC, multiple	21	M	TOP, MCA, triploidy	MCA, AV canal, hypoplastic cerebellum, anal atresia	SGA	A-IUGR		Small villi
23	SC, nodular	22	F	TOP, hydrops, cystic hygroma, elevated MSAFP, oligohydramnios	Coarctation of aorta, hypoplasia of lungs	SGA	E, ascites, cystic hygroma		
24	Nodular, focal (left lobe)	22	F	TOP, acrocephaly, skin folds, scoliosis, banana sign	Myelomeningocele T3-L5, Arnold Chiari type II	SGA			Variable-sized villi
25	SC, focal	22	F	MA	Umbilical blood flow restriction	AGA		Umbilical arteries—uneven, hemorrhage	Avascular villi
26	Intrahepatic, nodular, large mutiple	23	F	MA 23/17 weeks	Fibrinoid necrosis, infarcts, hypermaturity	SGA			Hypermaturity severe extensive, infarcts <5%
27	In sinuses	24	F	IUFD, severe PET	A-IUGR	SGA			
28	SC, focal, fibrosis	25	M	TOP, frontal bossing, polyhydramnios, syndactyly	MCA, consistent with Van Den Ende-Gupta syndrome	AGA		Recent hemorrhages, phlebitis	
29	Portal spaces, multiple	26	M	TOP, 5p deletion	MCA: neuroblastic heterotopias in cerebellum, Persistent left superior vena cava, hypoplasia of kidneys	AGA			
30	Portal tract, focal	30	F	IUFD, previous IUFD at 35 w	Villitis, high grade, IUGR	SGA	Pleural and pericardial effusion		Villitis, lymphocytic, high grade
31	Porta hepatis, atresia of gall bladder	30	M	TOP, non-visualized gall bladder	Atresia of gall bladder	AGA			
32	Focal and fibrosis	31	M	TOP, microcephaly	Microcephaly, polymicrogyria, calcified focal dysplasia of vermis	AGA			Avascular villi
33	Portal tracts around hillus	31	F	TOP, fragile X syndrome	Focal cerebellar neuronal dysplasia, periadrenal calcifications	LGA	Calcifications—periadrenal		

Table 1 (continued)

Case no.	Liver calcification	Week	Gender	Clinical diagnosis	Autopsy diagnosis	Growth	Additional autopsy findings	Umbilical cord	Placental abnormalities
34	Portal	35	F	IUFD	Organomegaly, calcification in adrenals	AGA			Delayed villous maturation, villous calcifications
35	Portal veins	38	M	IUFD	Tear in umbilical artery, intestinal malrotation, vascular calcifications in stomach	LGA			
SC—subcapsular	M—male		MA—missed abortion	MCA—multiple congenital anomalies		SGA—small for gestational age	E—edema	SUA—single umbilical cord	VE—villous edema
	F—female		TOP—termination of pregnancy	A—IUGR asymmetric intrauterine growth retardation		AGA—adequate for gestational age	NE—nuchal edema	UV—umbilical vein	
			IUFD—intrauterine fetal death			LGA—large for gestational age		VI—velamentous insertion	
			PET—preeclamptic toxemia						

MA/IUFD Twelve of 20 cases had an abnormality related to fetal circulation (including various abnormalities of umbilical cord, cardiac abnormalities, donor twin in twin-to-twin transfusion, and Rh incompatibility). Eight cases had placental abnormalities, including features of placental underperfusion, villitis of unknown etiology, and chronic histiocytic intervillositis.

TOP was carried out in 15 of 35 cases. The indications for TOP were malformations (11 cases, detailed in Table 3) and chromosomal abnormalities (four cases: triploidy, monosomy X, trisomy 21, 5p deletion).

Discussion

Tissue calcifications are formed by accumulation of calcium salts with small amounts of other mineral salts. Dystrophic calcification occurs at sites of previously damaged tissue, whereas metastatic calcification is secondary to hypercalcemia. Hypercalcemia also exacerbates dystrophic calcification [5]. Fetal calcium levels are consistently higher than maternal calcium levels [6]. Although calcification takes place under physiologic conditions, e.g., in the fetal pituitary gland [7], it is considered predominantly dystrophic. Possibly, damaged fetal tissue rapidly calcifies under conditions of high calcium and low pH [8]. The unique vascular supply of the fetal liver derives from the hepatic artery and the portal vein. The portal vein receives highly oxygenated blood through the umbilical vein. This pattern creates local and temporal variation in oxygen tension.

We hypothesized that the deposition of calcium salts and their location in the fetal liver are affected by several factors, including (a) circulatory compromise and (b) gestational age.

(a) Circulatory compromise (i.e., constricted flow in the umbilical vein or impaired cardiac function) plays a role in the deposition of calcium in the liver due to sluggish circulation, rapid variations in oxygen tension, elevated CO_2, and low pH. These conditions are probably accentuated in the periphery of the liver. This might explain the predominant subcapsular location of fetal liver calcifications. The association between fetal liver calcifications and impaired circulation is strengthened by the observation that 17/35 (49%) cases in our series had abnormalities related to fetal circulation (including 11 cases of umbilical cord abnormalities and 6 cases of cardiac malformations). Moreover, edema (subcutaneous, nuchal, or in placental villi) commonly found in the autopsies, is another reflection of circulatory abnormalities.

Table 2 A comparison of clinical and pathological features between the study group (fetal liver calcifications) and control (other autopsy cases) before and after 23 weeks of gestation, considered as the limit of viability

Characteristic	Study group		Control group		Total		*p* Study vs. Control	*p* Study vs. Control	Odds ratio
	≤23 weeks	>23 weeks	≤23 weeks	>23 weeks	Study	Control	≤23 weeks	>23 weeks	
Total	26	9	410	382	35	792			
Missed abortion/IUFD	16	4	87	161	19	248	<0.001	0.890	5.063*
Subcutaneous edema	14	1	81	9	15	90	<0.001	0.100	4.739*
Calcifications in other sites	1	4	1	3	5	4	0.801	<0.001	63.167**
IUGR	12	3	124	109	14	233	0.089	0.678	
Malformations	9	5	199	162	14	361	0.168	0.431	
Umbilical cord problem	10	1	125	138	11	263	0.394	0.390	
Chorioamnionitis	1	0	85	55	1	140	0.480	0.219	
Edematous placental villi	5	0	46	23	5	69	0.071	0.448	

Odds ratios were calculated for characteristics showing significant statistical differences: *≤23 weeks, **>23 weeks

(b) Since pH increases with gestational age [9], we assume that the pathophysiologic conditions during the second trimester differ from those of the third trimester. The relatively acidotic conditions, which prevail in the periphery of the liver during the second trimester, facilitate the deposition of calcium salts. In contrast, all cases of portal calcification were seen in fetuses from the later stages of pregnancy (26–38 weeks). Presumably, older fetuses differ from younger fetuses in terms of tendency for coagulation and vascular obliteration.

Fifty-seven percent of fetuses died in utero and the remaining pregnancies were terminated. This suggests that fetal liver calcifications in and of themselves do not affect short-term viability. Nevertheless, the odds ratio for intrauterine death of fetal liver calcifications cases was significantly higher than that of the remaining autopsy cases. Therefore, fetal liver calcifications are markers of abnormalities that eventually interfere with long-term intrauterine survival.

Calcifications in a fetus can be recognized by ultrasound, X-ray, and in histologic tissue sections. While

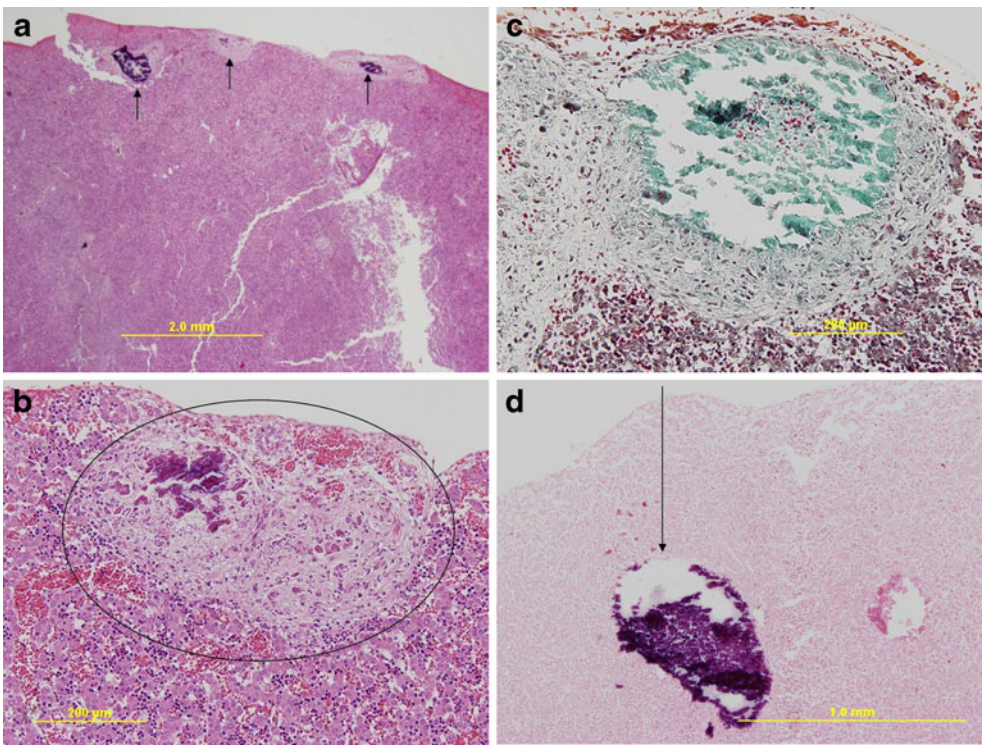

Fig. 1 **a** Several nodular calcifications located underneath the liver capsule. **b** Calcifications separated by a thin rim of liver parenchyma. **c** Calcifications surrounded by fibrosis (Masson trichrome stain). **d** Calcification located deeper in the liver, unrelated to the liver capsule

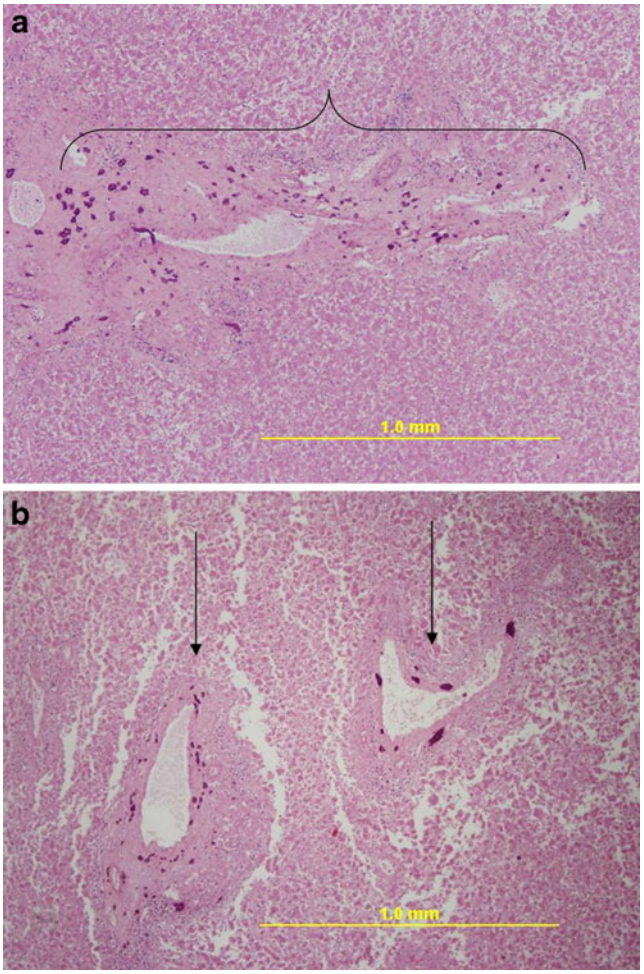

Fig. 2 **a** Portal calcifications—minute numerous liver calcifications in the portal space. **b** Multiple liver calcifications located predominantly around portal vein

calcifications as small as several microns may be identified on histologic sections, imaging techniques detect calcifications that are 10^3 times larger, i.e., several millimeters in size. Thus, calcification seen on ultrasound or X-ray images is probably a different entity. The incidence of fetal liver calcifications detected by ultrasound was 0.6% (14 of 24,600 fetuses scanned between 15 and 26 weeks of gestation) [1].

The incidence of fetal liver calcifications detected by X-ray in spontaneous abortions was 2.2% (33 fetuses out of 1,500) [2]. The higher incidence of calcifications per histology in autopsy cases (4.2%) seems to be attributed to the fact that histologic calcifications represent a different phenomenon.

Of note is the fact that although fetal liver hematomas were associated with fetuses with chorioamnionitis, such an association was not found among our patients. This fact probably attests to the different pathogenesis of fetal liver hematomas and fetal liver calcifications [10].

The focus of this study was fetal liver calcifications found in microscopic sections in fetal autopsy. A fetal autopsy is performed to describe the entire spectrum of malformations and to search for the cause of intrauterine death or impaired development. The overall interpretation depends on the sum of the various findings, including abnormalities of the fetus (intrauterine growth, edema, features suggesting circulatory impairment, and specific malformations), placenta, and umbilical cord. We suggest that fetal liver calcifications can denote circulatory compromise preceding death, especially if subcutaneous edema is present and even when no other findings are seen.

In conclusion, fetal liver calcifications are incidentally found in autopsies and are easily seen in histological sections, regardless of the degree of autolysis. The significance of fetal liver calcifications has to be assessed in combination with other clinical and pathological parameters. These parameters include location and number of the calcifications, fetal malformations, and abnormalities of the placenta and umbilical cord. Signs of circulatory compromise, such as edema, cardiac, and umbilical cord abnormalities should be given special attention.

Table 3 Features associated with fetal liver calcifications in cases with IUFD vs. TOP

Associated features	IUFD	TOP	Total
Number	20	15	35
Weeks gestation	15–38	16–31	
IUGR	10	5	15
Findings associated with circulatory problems			
Subcutaneous edema	14	1	15
Umbilical cord abnormalities	9	2	
Single umbilical artery	2	2	4
Velamentous insertion	2	1	3
Abnormal twisting	6	0	6
Severe placental abnormalities	6	1	7
Maternal underperfusion	6	5	11
Inflammatory lesions	2	0	2
Avascular villi	1	2	3
Villous edema	4	1	5
Malformations			
Congenital heart disease	1	5	6
Genitourinary abnormalities	0	4	4
Central nervous system	0	2	2
Intestinal malrotation	1	6	7
Agenesis of gall bladder	0	2	2
Gastrointestinal atresia	0	2	2
Multiple congenital anomalies	2	7	9
Calcification in other fetal sites	3	2	5
Known chromosomal abnormalities	0	4	4

Conflict of interest The authors declare that they have no conflict of interest. This study was not supported by outside funding.

References

1. Bronshtein M, Blazer S (1995) Prenatal diagnosis of liver calcifications. Obstet Gynecol 86:739–743
2. Hawass ND, El-Badawi MG, Fatani JA, Al-Mashary A, Makanjoula D, Edress YB (1990) Foetal hepatic calcification. Pediatr Radiol 20:528–535
3. Bove KE (1997) Practice guidelines for autopsy pathology: the perinatal and pediatric autopsy. Autopsy Committee of the College of American Pathologists. Arch Pathol Lab Med 121:368–376
4. Macpherson TA, Valdes Dapena M (1998) The perinatal autopsy. In: Wigglesworth JS, Singer D (eds) Perinatal pathology. WB Saunders, Philadelphia, pp 93–122
5. Kumar V, Abbas AK, Fausto N, Aster JC (2010) Cellular responses to stress and toxic insults: adaptation, injury, and death. In: Kumar V, Abbas AK, Fausto N, Aster JC (eds) Robbins and Cotran pathologic basis of disease, 8th edn. Saunders Elsevier, Philadelphia, pp 38–39
6. Reitz RE, Daane TA, Woods JR, Weinstein RI (1977) Calcium, magnesium, phosphorus, and parathyroid hormone interrelationship in pregnancy and newborn infants. Obstet Gynecol 50:701–705
7. Groisman GM, Kerner H, Polak-Charcon S (1996) Calcified concretions in the anterior pituitary gland of the fetus and the newborn: a light and electron miscroscopic study. Hum Pathol 27:1139–1143
8. Nguyen DL, Leonard JC (1986) Ischemic hepatic necrosis: a cause of fetal liver calcification. AJR 147:596–597
9. Soothill PW, Nicolaides HN, Rodeck CH, Campbell S (1986) Effect of gestational age on fetal and intervillous blood gas and acid–base values in human pregnancy. Fetal Therapy 1:168–175
10. Singer DB, Neave C, Oyer CE, Pinar H (1999) Hepatic subcapsular hematomas in fetuses and neonatal infants. Pediatr Dev Pathol 2:215–220

Virchows Arch (2012) 460:407–414
DOI 10.1007/s00428-012-1219-x

ORIGINAL ARTICLE

Optimized algorithm for Sanger sequencing-based *EGFR* mutation analyses in NSCLC biopsies

Arne Warth · Roland Penzel · Regine Brandt · Christine Sers · Jürgen R. Fischer · Michael Thomas · Felix J. F. Herth · Manfred Dietel · Peter Schirmacher · Hendrik Bläker

Received: 26 September 2011 / Revised: 16 January 2012 / Accepted: 23 February 2012 / Published online: 15 March 2012
© Springer-Verlag 2012

Abstract Pulmonary adenocarcinoma patients harboring *EGFR* mutations can benefit from tyrosine kinase inhibitor therapy. Reliable molecular analyses and precise pathological reporting of the *EGFR* mutational status are factors essential for patient treatment and outcome. More than 70 % of all *EGFR* mutation analyses are performed on non-small cell lung cancer (NSCLC) biopsies. However, biopsies may not be sufficient for mutation analysis due to low tumor content and admixture with non-neoplastic cells. To define the minimal concentration of tumor cells required for reliable *EGFR* mutational diagnostics by Sanger sequencing and to develop an algorithm for routine diagnostics on biopsy material, we determined total numbers of tumor and non-tumor cells, calculated the tumor cell concentration and serially diluted DNA from *EGFR*-mutated NSCLC by adding DNA of non-tumor cells from the same section. A counted tumor cell concentration of 30 %, which refers to a histologically estimated concentration of 40 %, is necessary for reliable detection of all mutations. Based on these data, we developed an algorithm for evidence-based *EGFR* mutation analysis by Sanger sequencing in biopsy specimens, which was subsequently applied to 461 diagnostic cases. Optimized diagnostic testing results in 80 % reliable *EGFR* mutation analyses of biopsy specimens, while in 20 % of cases re-biopsies had to be recommended.

Keywords EGFR · Mutation analyses · Sanger sequencing · Detection limit · Non-small cell lung cancer · Biopsy

Arne Warth and Roland Penzel contributed equally.

A. Warth · R. Penzel · R. Brandt · P. Schirmacher · H. Bläker (✉)
Institute of Pathology, University Hospital Heidelberg,
Im Neuenheimer Feld 220/221,
69120, Heidelberg, Germany
e-mail: hendrik_blaeker@med.uni-heidelberg.de

C. Sers · M. Dietel · H. Bläker
Institute of Pathology, Charité,
Berlin, Germany

J. R. Fischer
Department of Thoracic Oncology, Klinik Löwenstein,
Löwenstein, Germany

M. Thomas
Department of Thoracic Oncology, Thoraxklinik Heidelberg,
Heidelberg, Germany

F. J. F. Herth
Department of Pneumology and Critical Care Medicine,
Thoraxklinik Heidelberg,
Heidelberg, Germany

Present Address:
H. Bläker
Institute of Pathology, University Hospital Charité,
Campus Mitte, Charitéplatz 1,
10117, Berlin, Germany

Introduction

Lung cancer is the leading cause of cancer-related mortality in the developed countries [1] and non-small cell lung cancer (NSCLC) accounts for more than 80 % of all lung cancers. In NSCLC, epidermal growth factor receptor (*EGFR*) mutations are associated with responsiveness to tyrosine kinase inhibitors [2, 3]. Recent data showed that patients with pulmonary adenocarcinomas harboring activating *EGFR* mutations treated with a TKI (especially gefitinib) have a significantly better progression-free survival compared to carboplatin-paclitaxel treatment [4], while an adverse effect was seen in patients without *EGFR* mutations. Thus, reliable molecular analysis and precise pathological reporting of the *EGFR* mutational status are factors

determining the patient treatment and outcome. Initially, diagnostic *EGFR* mutation analyses were performed in surgically resected specimens, which yielded sufficient tumor tissue for DNA extraction. However, since gefitinib received market authorization for primary, non-resectable NSCLC, more than 70 % of all *EGFR* mutation analyses are performed on biopsies or cytological specimens of NSCLCs today. *EGFR* mutations are heterogeneous; according to the COSMIC database (http://www.sanger.ac.uk/genetics/CGP/cosmic/), more than 250 different *EGFR* mutations have been reported up to now. For reliable results and thus optimal benefit for the patient, it is important to (1) define the minimal tumor cell concentration required in a biopsy specimen for a reliable result of the chosen type of analysis (i.e., ARMS, Sanger sequencing, pyrosequencing), (2) standardize the processing of samples, and (3) generate evidence-based reporting on *EGFR* mutations [5].

In this study, we aimed to identify the minimal percentage of tumor cells needed for reliable diagnostic Sanger sequencing-based *EGFR* mutation analyses, the most commonly used mutation analysis technique, in routine biopsies in order to provide an algorithm for a consistent evaluation and reporting of the results. To this end, we counted as well as histologically estimated the number of *EGFR*-mutated NSCLC cells isolated from paraffin sections submitted for *EGFR* mutation analysis by Sanger sequencing. We show that the threshold for reliable results is 30 % when counted and 40 % when estimated. Based on these data, we have developed an algorithm for evidence-based *EGFR* mutation analysis and reporting in biopsy specimens, which we applied to a large cohort of consecutive diagnostic cases. These data provide an evidence-based rationale for routine diagnostic evaluation of *EGFR* mutations in clinical samples.

Material and methods

Tumor samples and analytical probes

For analysis of the minimally required tumor cell concentration for Sanger sequencing analysis, we selected four NSCLC resection specimens with known *EGFR* mutation status (deletions $n=2$; point mutation L858R $n=2$; Table 1, case 1–4). Use of the tissue was approved by the local ethics committee (No. 206/2005). Serial sections from paraffin blocks of each case containing both neoplastic and non-neoplastic tissue were cut, and one section was H&E stained in order to define two regions of interest of approximately 1 cm^2 (ROI1 and ROI2) for each case. ROI1 consisted of a tumor area with a high number and concentration of tumor cells while for ROI2 a non-neoplastic area of lung tissue with a high cell density was chosen. These ROIs were removed from unstained serial sections under microscopic control by manual microdissection, using a glass needle, and further processed for mutation analysis. Subsequently, the slide was stained. A picture of the area removed was overlaid to the primary H&E section using a ScanScope CS System and ImageScope (both Aperio Technologies, Vista, CA, USA) which allows counting all neoplastic (ROI1) and non-neoplastic cells (ROI1 and 2) isolated from the ROIs. As almost all non-neoplastic

Table 1 Counted cell numbers of neoplastic and non-neoplastic cells in the selected regions of interest

Case	Mutation	DNA concentration/counted cell number non-neoplastic ROI2 (ng/µl)	DNA concentration/ counted cell number tumor ROI1 (ng/µl)	Counted cell number non-neoplastic cells in tumor ROI1	Percentage of tumor cells in ROI1 (%)	Estimated tumor cell concentration (%) ROI1				
						P1	P2	P3	P4	Mean
1	Deletion *Not ampfified*	5.7/13,895	12.0/16,210	15,181	52	50	75	60	65	62.5
2	Point Mutation *Not amplified*	5.5/7,693	23.6/14,009	15,184	48	50	40	50	60	50
3	Deletion *Amplified*	22.4/169,943	11.2/12,697	10,086	56	75	80	70	65	72.5
4	Point mutation *Not amplified*	4.0/23,499	5.0/9,825	10,248	49	75	75	55	55	65
5	Deletion *Amplified*	n.a.	n.a.	18,442	2.2	2	10	5	5	5.5

Data of all NSCLC for which the tumor cell concentration was determined and both neoplastic and non-neoplastic cells were manually counted to define the absolute tumor cell concentration

ROI1 =region of interest 1 (tumor area with highest tumor cell concentration)

ROI2=region of interest 2 (non-neoplastic tissue)

P = pathologist

and NSCLC cells contain a single nucleus, any nucleus was considered to represent one cell. The number of nuclei was counted by visual examination of high resolution images.

Fluorescence in-situ hybridization

Amplification of the mutated *EGFR* allele in NSCLC can result in overrepresentation of the mutated *EGFR* copy in comparison to the wild type allele. In carcinomas with an amplified mutated *EGFR* allele, a mutation can be detected on lower tumor cell concentrations. To define thresholds for reliable detection, we therefore decided to investigate the carcinomas for *EGFR* amplification. Deparaffinized 5 μm serial sections were used for *EGFR* fluorescence in-situ hybridization (FISH) analysis with the LSI *EGFR*/CEP 7 Dual Color Probe (Vysis; Abbott Laboratories, Illinois, U.S. A.) following the manufacturer's protocols. The stained slides were analyzed for *EGFR* amplification according to standardized criteria [6].

DNA extraction and Sanger sequencing

Extraction of genomic DNA was performed by proteinase K digestion and fully automated purification using a QIASymphony SP (Qiagen, Hilden, Germany). The DNA content was measured using a NanoDrop (Thermo Scientific, Wilmington, USA). For PCR amplification of *EGFR*, the following primers were used: 5′-gctgaggtgacccttgtctc-3′ (Exon 18 forward), 5′-acagcttgcaaggactctgg-3′ (Exon 18 reverse); 5′-gctggtaacatccacccaga-3′ (Exon 19 forward), 5′-gagaaaaggtgggcctgag-3′ (Exon 19 reverse); 5′-catgtgcccctccttctg-3′ (Exon 20 forward), 5′-gatcctggctcctatctcc-3′ (Exon 20 reverse), 5′-cctcacagcagggtcttctc-3′ (Exon 21 forward), 5′-cctggtgtcaggaaaatgct-3′ (Exon 21 reverse). Exon 1 of *KRAS* was amplified with the following primers: 5′-gtgtgacatgttctaatatagtca-3′ (Exon 1 forward) and 5′-gaatggtcctgcaccagtaa-3′ (Exon 1 reverse). Direct sequencing of the PCR amplicons was carried out for both strands on an 3500 Genetic Analyzer (Applied Biosystems by Life Technologies Corporation) using the BigDye® Terminator v1.1 Cycle Sequencing Kit (Applied Biosystems by Life Technologies Corporation).

Dilution analysis to determine the minimum tumor cell concentration allowing reliable *EGFR* analysis

To determine the minimum tumor cell concentration allowing reliable mutation analysis by Sanger sequencing, each tumor-derived DNA sample was serially diluted with DNA extracted from corresponding non-neoplastic tissue based upon the counted number of non-neoplastic cells from the same tissue block, to obtain a final tumor cell concentration of: 50 %, 40 %, 30 %, 20 %, 10 %, and 5 %. The tumor DNA concentration (ROI1) was calculated by dividing the DNA concentration by the total number of counted cells and multiplication by the counted number of tumor cells. Tumor cell DNA was then serially diltuted by adding the calculated DNA amount from cells of ROI2. Prior to cell counting, four experienced pathologists visually estimated the tumor cell concentration in the ROIs. For comparison of the counted cell numbers with the estimated cell numbers, arithmetic mean values were used (Table 1).

In one *EGFR*-mutated tumor with only few tumor cells, the tumor cell concentration was determined by counting of neoplastic and non-neoplastic cells in a single ROI using a ScanScope CS System and ImageScope (Table 1, case number 5).

Development of EGFR mutation analysis algorithm and its diagnostic application

Based on the experimental studies on the tumors above, the resulting diagnostic algorithm (Fig. 3) was applied to a total of 461 consecutive biopsy specimens referred to the Institute of Pathology Heidelberg for molecular pathology diagnosis.

Results

Detection limit for *EGFR* mutation analysis according to the *EGFR* amplification status established by FISH

Of the five cases chosen for tumor cell counting, FISH analysis revealed 3 without and 2 with an *EGFR* gene amplification (see Table 1). Dilution experiments as outlined above showed that the detection limit of *EGFR* mutations in small NSCLC biopsy specimens depends on the type of the mutation. For point mutations without *EGFR* amplification, a counted tumor cell concentration of 30 % allowed reliable mutation detection, but lower tumor cell concentrations did not (Fig. 1).

For complex mutations in non-amplified cases, as frequently observed in exon 19, the detection limit for *EGFR* mutations was a counted tumor cell concentration of 10–20 % (Fig. 2). That this is lower than for samples with point mutations is due to the sequence overlay as a consequence of the frame shift, which is easier to detect than point mutations, mainly due to the high amplitude of the last base of the mutated allele, which becomes evident even at lower concentrations of the mutant allele. When the FISH analysis showed the *EGFR* locus to be amplified, the increased concentration of the mutated *EGFR* allele resulted in even lower tumor cell concentration limits as compared to non-amplified cases (Table 1; cases number 3 and 5).

Given that exact cell counting of large areas of tissue is not feasible under real-time diagnostic conditions, we next determined to what extent the results of cell number

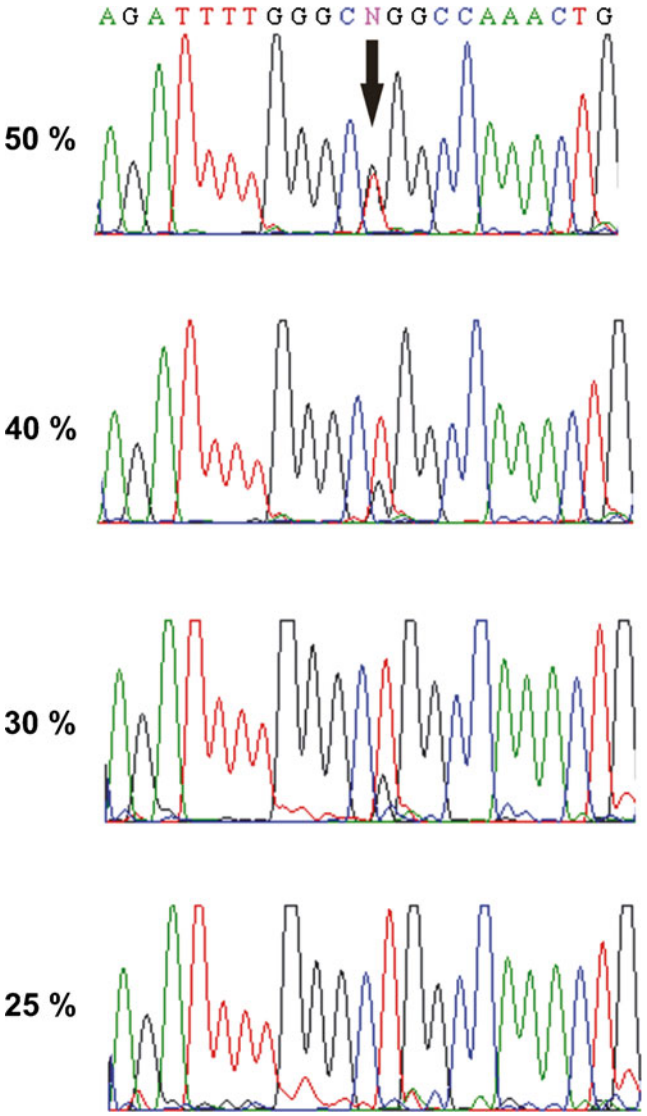

Fig. 1 Sanger sequencing of *EGFR* point mutations (not amplified). Tumor-derived DNA was diluted with non-neoplastic DNA from the same patient as outlined under "Materials and methods". Note that the peak of the mutated allele (*arrow*) is reliably detectable with a tumor cell concentration up to 30 %

counting corresponded to those of visual assessment. Four experienced histopathologists performed visual assessment individually, and this generally resulted in an over-estimation of the tumor cell concentration by 10 % to 20 % (Table 1). Therefore, dividing the result of visual assessment by 1.2–1.3 results in values which correspond with a counted cell number of 30 %. The tumor cell concentration of 40 % by visual assessment therefore describes the lower detection limit.

Generation of an algorithm for routine *EGFR* mutation analysis and reporting

Based on the determined detection limit for *EGFR* mutations by Sanger sequencing we aimed to develop an algorithm for performing and reporting diagnostic analysis of NSCLC biopsies and cytological specimens (Fig. 3). If the estimated tumor cell concentration was equal to or exceeded 40 %, the result of the *EGFR* mutation analysis was reported as reliable and when an *EGFR* mutation was found a statement concerning TKI sensitivity was added (according to [7] or the Somatic Mutations in Epidermal Growth Factor Receptor DataBase; www.somaticmutations-egfr.info/index.html). When the estimated tumor cell concentration was lower than 40 %, an *EGFR* analysis was nonetheless performed. When a mutation was detected, mutations were reported as described above. When no *EGFR* mutation was detected, we additionally analyzed the specimens for *KRAS* mutations. This analysis was chosen for three reasons. Firstly, for *KRAS* DNA sequencing in other cancers, the analytical sensitivity is reported to be 10 % to 30 % of mutant *KRAS* alleles in a background of wild-type alleles [8–10]. Secondly, *KRAS* is frequently affected by point mutations without gene amplification, especially in pulmonary adenocarcinomas (5–40 % [11–13]). As *KRAS* mutations occur regularly, detection of a *KRAS* mutation would imply that any *EGFR* mutation should also be detectable in that tumor sample. Finally, *KRAS* and *EGFR* mutations are almost always mutually exclusive in NSCLC [14], implying that a *KRAS* mutated tumor is highly unlikely to also have an *EGFR* mutation. Therefore, *KRAS* mutated samples with an estimated tumor cell concentration <40 % were reported as negative for *EGFR* mutation. When neither an *EGFR* nor a *KRAS* mutation was detected in a specimen with an estimated tumor cell concentration lower than 40 %, the result was reported as not reliable, and additional tumor sampling was recommended.

Diagnostic application of the *EGFR* mutation analysis and reporting algorithm

This algorithm was tested in daily practice for all NSCLC biopsy specimens analyzed over a period of 6 months in the Institute for Pathology, University Hospital Heidelberg, Germany. Biopsy specimens (461) were received for *EGFR* analysis. Nine cases were excluded since the sample contained no tumor cells (drop-out rate 1.99 %), leaving 452 cases for *EGFR* mutation analyses. An *EGFR* mutation was detected in 58 tumors. Specimens with a tumor cell concentration >40 % (n=322; 71.2 % of all cases) harbored 45 mutations (13.9 %; 26 point mutations (57.8 %); 19 complex mutations (42.2%)). Specimens with a tumor cell concentration <40 % (n=130; 28.8 % of all cases) harbored 13 mutations (10 %; 6 point mutations (46.2 %); 7 complex mutations (53.8 %)). The 117 specimens (25.9 % of all cases) with a tumor cell concentration <40 % and without a detectable *EGFR* mutation were subsequently subjected to *KRAS* mutation analysis, of which 34 specimens were *KRAS*

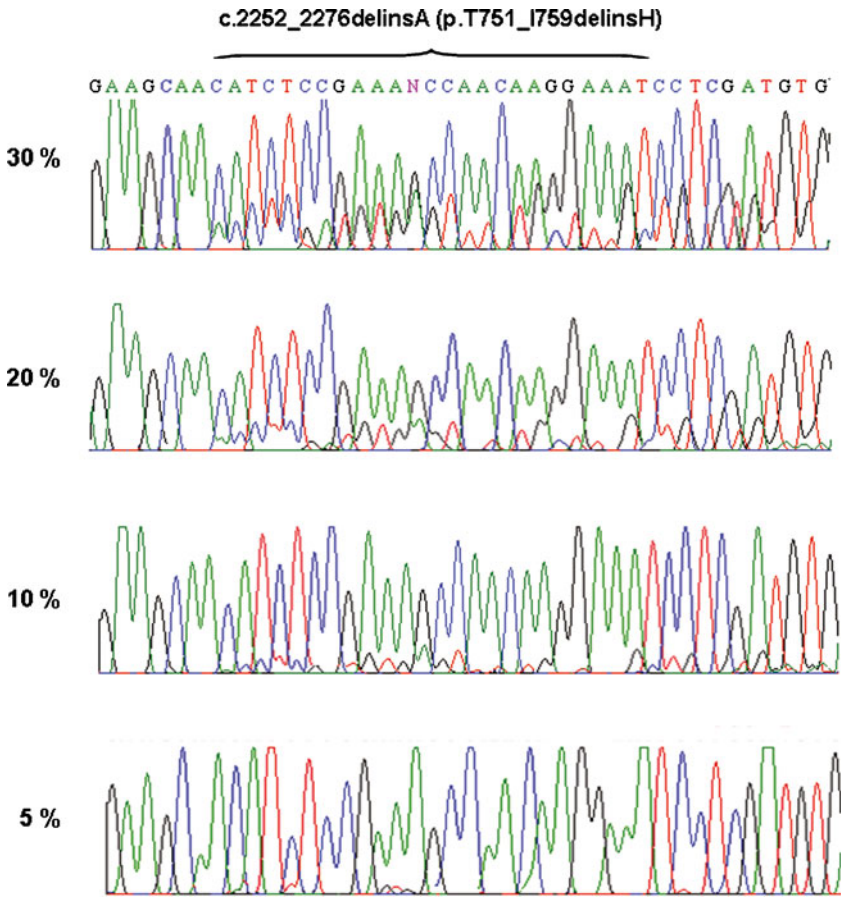

Fig. 2 Sanger sequencing of complex *EGFR* mutations (deletion; not amplified). Tumor-derived DNA was diluted with non-neoplastic DNA from the same patient as outlined under "Materials and methods". Note that complex mutations can be reliably detected with tumor cell concentrations up to 10 %

mutated. Thus, for 83 specimens out of all analyzed specimens (18.4%), the *EGFR* mutation analysis was reported as unreliable.

Discussion

There are only few recommendations concerning standardized processing, analysis, and reporting of *EGFR* mutation analyses in NSCLC biopsy or cytological specimens [5] and practically validated, evidence-based data concerning thresholds of tumor cell concentration for reliable analysis by Sanger sequencing are lacking. Thus, we established detection limits for reliable mutation analyses and developed and evaluated a reporting algorithm with defined consequences for the clinical diagnostic setting (Fig. 3).

Sanger sequencing is the main and standard technology used for *EGFR* mutation analysis with a potential specificity of 100 %. It is a non-biased technology able to detect all *EGFR* mutations; its primary methodological disadvantage is its relatively low sensitivity. To define detection limits of any molecular method, in vitro settings with optimal DNA quality are frequently used. However, conditions in diagnostic molecular pathology practice are different. Tissue processing (formalin fixation and paraffin embedding) and tissue sectioning conditions vary between samples with potentially significant effects on DNA quality. Whereas cell number and DNA quantity were very homogenous in cases 1, 2, and 4, DNA extraction from case 3 had a low yield considering the high number of cells; this may be due to poor fixation or DNA degradation. Evidently, to obtain a sufficient amount of DNA of sufficient quality a sample size with a sufficient number of cells and with well preserved DNA is necessary. The amount of tissue is normally not an issue in molecular pathology, since even from small biopsy samples, normally a sufficient amount of DNA can be extracted. For detection limits of Sanger sequencing, one therefore has to consider additional factors influencing the results of the analysis in comparison with, e.g., cell culture-based dilution experiments. Commercially available kits recognize several types of *EGFR* mutations with high sensitivity for specific mutations, but a large number of *EGFR* mutations cannot be detected by these methods. A recent quality-controlled multicenter study revealed that 32 % of NSCLC carrying activating *EGFR* mutations (notably even 38 % of the complex exon 19 mutations) as detected by Sanger sequencing would have been missed by commercially available PCR tests [15]. Thus, Sanger sequencing is currently the standard for routine diagnostic *EGFR* mutation analyses for paraffin-embedded specimens in most institutions.

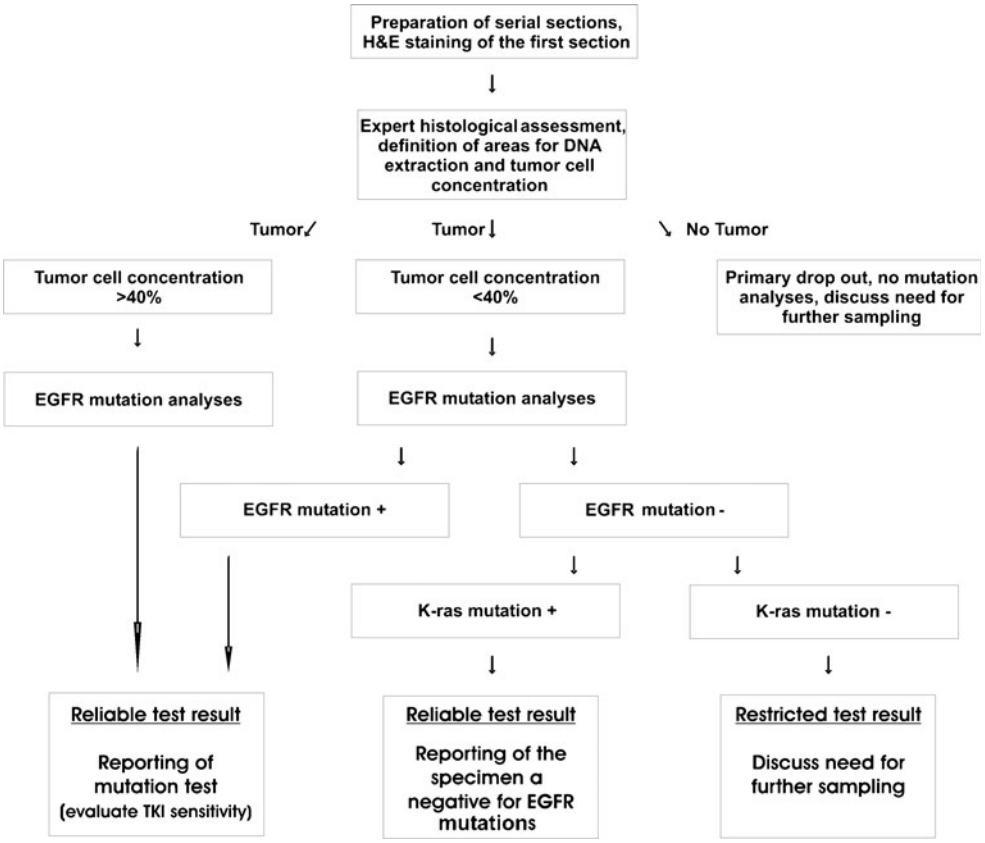

Fig. 3 Diagnostic algorithm for EGFR mutation analyses in non-small cell lung cancer biopsies by Sanger sequencing

The newly established algorithm was applied to a consecutive single institution series of 461 NSCLC specimens over a time span of 6 months (Table 2). We show that the defined cut-off for reliable analyses of 40 % tumor cell concentration estimated on H&E stain is applicable to daily diagnostic practice. However, mutations may also be detected in samples with tumor cell concentrations <40 % (see for example Table 1, case 5). The cut-off of 40 % tumor cells merely indicates that with Sanger sequencing the *EGFR* mutation analysis is reliable. Based on the histomorphologically estimated tumor cell concentration alone the majority (~71 %) of all cases could be classified as reliable. With molecular *EGFR* mutation analysis and subsequent, complementary *KRAS* mutation analysis in *EGFR* mutation negative (wild type or not detectable) cases, the total number of unreliable cases can be reduced to ~18 %. Thus, more than 80 % of all NSCLC biopsy specimens can be reliably analyzed for predictive mutation analyses, limiting to <20 % the cases for which re-biopsies may be recommended. Several methods exist which allow for mutation detection way beyond the sensitivity threshold of Sanger sequencing. Sanger sequencing, however, is a well established, very robust and cost effective technique. Moreover, it should be kept in mind that sensitivity is a problem in a minority of cases. Nevertheless, before re-biopsies are recommended, one may also consider applying more sensitive

Table 2 Diagnostic *EGFR* mutation analyses by Sanger sequencing in 452 consecutive tumor containing NSCLC biopsy cases

EGFR mutation analyses of 452 specimens according to the established algorithm							
Reliable TCC >40 % (*n*=322; ~71 %)			Not reliable TCC <40 % (*n*=130; ~29 %)				
EGFR wt (*n*=277)	*EGFR* mutation (*n*=45)		*EGFR* mutation (*n*=13)		*EGFR* wt (*n*=117)		
	Complex mutations (*n*=19)	Point mutations (*n*=26)	Complex mutations (*n*=7)	Point mutations (*n*=6)	*KRAS* mutation (*n*=34)	*EGFR* wt (*n*=83)	
n=369/452 (~82 %)						*n*=83/452 (~18 %)	

diagnostic methods for detection of *EGFR* mutations, e.g., pyrosequencing, RNA-based sequencing, or enrichment/suppression of wt sequences.

Whereas we could detect *EGFR* mutations in ~14 % of all specimens with a tumor cell concentration exceeding 40 %, this was only possible in 10 % of the specimens with tumor cell concentration below 40 %. The relative detection rate of point mutations in specimens with a tumor cell concentration >40 % (~71 total) and <40 % (~29 % total) was ~58 % and 46 %, whereas the relative detection rate of complex mutations was ~42 % and ~54 %, respectively. The 4 % lower detection rate of *EGFR* mutations in the small group of NSCLC biopsies with <40 % tumor cell concentration is largely a consequence of missed point mutations due to sparse tumor material of presumably non-amplified cases, which underlines the reliability of our experimentally evaluated cut-off of 40 % tumor cell concentration. A switch of the percentages from point mutations to complex mutations in samples with <40 % tumor cell concentration must be expected due to the fact that complex mutations are easier to detect (see Fig. 2). Subsequent mutation analyses of *B-RAF* or EML4-ALK translocations will further reduce the percentage of cases with unreliable results, since these alterations are currently considered to be mutually exclusive with *EGFR* mutations [16]. Furthermore, ARMS or yet other experimental methods [17–22] with a putative higher sensitivity for the detection of *EGFR* mutations than Sanger sequencing may be used subsequently in such settings.

Our experimentally defined and in diagnostic routine validated algorithm can in principle be used analogously for other driver mutations or candidates for targeted therapies of NSCLC, e.g. *KRAS* mutations. However, a priori validation in other clinicopathological settings in which only little tumor material is available and therapeutic decisions depend on reliable mutation analyses by Sanger sequencing is required. This would be the case for example, for *c-kit* mutation analyses in biopsies of non-resectable gastro-intestinal stromal tumors (GIST) or *B-RAF* mutation analyses in small samples of melanoma tissue.

According to our results, we suggest the following criteria for standardized, evidence-based *EGFR* mutation analyses in addition to recently published consensus recommendations for *EGFR* mutation testing in NSCLC [5]:

- NSCLC biopsy specimens should be processed in serial sections. The first section should be used for an H&E stain in order to define appropriate regions with highest tumor cell concentration. Subsequent sections are used for histochemical and/or immunohistochemical stains if necessary for diagnostic reasons and DNA extraction.
- The evidence-based upper detection limit for reliable diagnostic *EGFR* mutation analyses by Sanger sequencing in NSCLC biopsy or cytological specimens is a counted or tumor cell concentration of 30 % or an estimated concentration of 40 %.
- *EGFR* mutation analyses should always be performed when tumor cells are detectable in corresponding H&E sections since the detection limit is low for complex mutations and cases with *EGFR* mutations and simultaneous *EGFR* gene amplification.
- In *EGFR* mutation, negative specimens with a low tumor cell concentration (<40 %) analyses for complementary and (indirectly confirmatory) genomic alterations, e.g., *KRAS*, should be performed in order to minimize the rate of specimens with results of restricted reliability. With this strategy, one may demonstrate that mutations are detectable in a given case and the presence of complementary driver mutations like *KRAS*, *B-RAF*, or subsequently EML4-ALK translocations largely excludes the presence of *EGFR* mutations.
- Mutation analyses of specimens with an estimated tumor cell concentration of >40 % or detectable *EGFR* or *KRAS* mutations should be reported as definitively reliable.
- Mutation analyses of specimens with an estimated tumor cell concentration of <40 % without detectable *EGFR* or *KRAS* mutations should be reported but labelled as unreliable and further sampling should be recommended.

In conclusion, our experimentally defined algorithm was validated in the clinical diagnostic setting. It allowed reducing the number of samples of restricted reliability below 20 %. It represents an evidence-based diagnostic algorithm for standardized, timely, and comprehensive clinical diagnostic *EGFR* mutation testing. New specific diagnostic challenges and areas for future improvement are specifically outlined, which will lead to future optimization.

Acknowledgements This study was supported by a research grant from Astra Zeneca. We gratefully acknowledge Wilko Weichert and Wilfried Roth for estimating tumor cell concentrations.

Conflict of interest statement We declare that we have no conflict of interest.

References

1. Jemal A, Siegel R, Ward E, Hao Y, Xu J, Thun MJ (2009) Cancer statistics, 2009. CA Cancer J Clin 59:225–249
2. Rosell R, Moran T, Queralt C, Porta R, Cardenal F, Camps C, Majem M, Lopez-Vivanco G, Isla D, Provencio M, Insa A, Massuti B, Gonzalez-Larriba JL, Paz-Ares L, Bover I, Garcia-Campelo R, Moreno MA, Catot S, Rolfo C, Reguart N, Palmero R, Sanchez JM, Bastus R, Mayo C, Bertran-Alamillo J, Molina MA, Sanchez JJ, Taron M (2009) Screening for epidermal growth factor receptor mutations in lung cancer. N Engl J Med 361:958–967

3. Fischer JR, Haffner U, Dietrich GM, Spahlinger B, Geiger D, Lahm H (2005) Non-small-cell lung cancer third-line therapy with gefitinib. Pneumologie 59:321–327
4. Maemondo M, Inoue A, Kobayashi K, Sugawara S, Oizumi S, Isobe H, Gemma A, Harada M, Yoshizawa H, Kinoshita I, Fujita Y, Okinaga S, Hirano H, Yoshimori K, Harada T, Ogura T, Ando M, Miyazawa H, Tanaka T, Saijo Y, Hagiwara K, Morita S, Nukiwa T (2010) Gefitinib or chemotherapy for non-small-cell lung cancer with mutated EGFR. N Engl J Med 362:2380–2388
5. Pirker R, Herth FJ, Kerr KM, Filipits M, Taron M, Gandara D, Hirsch FR, Grunenwald D, Popper H, Smit E, Dietel M, Marchetti A, Manegold C, Schirmacher P, Thomas M, Rosell R, Cappuzzo F, Stahel R (2010) Consensus for EGFR mutation testing in non-small cell lung cancer: results from a European workshop. J Thorac Oncol 5:1706–1713
6. Varella-Garcia M (2006) Stratification of non-small cell lung cancer patients for therapy with epidermal growth factor receptor inhibitors: the EGFR fluorescence in situ hybridization assay. Diagn Pathol 1:19
7. Sharma SV, Bell DW, Settleman J, Haber DA (2007) Epidermal growth factor receptor mutations in lung cancer. Nat Rev Cancer 7:169–181
8. Li J, Wang L, Mamon H, Kulke MH, Berbeco R, Makrigiorgos GM (2008) Replacing PCR with COLD-PCR enriches variant DNA sequences and redefines the sensitivity of genetic testing. Nat Med 14:579–584
9. Ogino S, Kawasaki T, Brahmandam M, Yan L, Cantor M, Namgyal C, Mino-Kenudson M, Lauwers GY, Loda M, Fuchs CS (2005) Sensitive sequencing method for KRAS mutation detection by pyrosequencing. J Mol Diagn 7:413–421
10. Tsiatis AC, Norris-Kirby A, Rich RG, Hafez MJ, Gocke CD, Eshleman JR, Murphy KM (2010) Comparison of Sanger sequencing, pyrosequencing, and melting curve analysis for the detection of KRAS mutations: diagnostic and clinical implications. J Mol Diagn 12:425–432
11. Okudela K, Woo T, Kitamura H (2010) KRAS gene mutations in lung cancer: particulars established and issues unresolved. Pathol Int 60:651–660
12. Riely GJ, Kris MG, Rosenbaum D, Marks J, Li A, Chitale DA, Nafa K, Riedel ER, Hsu M, Pao W, Miller VA, Ladanyi M (2008) Frequency and distinctive spectrum of KRAS mutations in never smokers with lung adenocarcinoma. Clin Cancer Res 14:5731–5734
13. Riely GJ, Marks J, Pao W (2009) KRAS mutations in non-small cell lung cancer. Proc Am Thorac Soc 6:201–205
14. Suda K, Tomizawa K, Mitsudomi T (2010) Biological and clinical significance of KRAS mutations in lung cancer: an oncogenic driver that contrasts with EGFR mutation. Cancer Metastasis Rev 29:49–60
15. Penzel R, Sers C, Chen Y, Lehmann-Muhlenhoff U, Merkelbach-Bruse S, Jung A, Kirchner T, Buttner R, Kreipe HH, Petersen I, Dietel M, Schirmacher P (2011) EGFR mutation detection in NSCLC—assessment of diagnostic application and recommendations of the German panel for mutation testing in NSCLC. Virchows Arch 458:95–98
16. Tam IY, Chung LP, Suen WS, Wang E, Wong MC, Ho KK, Lam WK, Chiu SW, Girard L, Minna JD, Gazdar AF, Wong MP (2006) Distinct epidermal growth factor receptor and KRAS mutation patterns in non-small cell lung cancer patients with different tobacco exposure and clinicopathologic features. Clin Cancer Res 12:1647–1653
17. Molina-Vila MA, Bertran-Alamillo J, Reguart N, Taron M, Castella E, Llatjos M, Costa C, Mayo C, Pradas A, Queralt C, Botia M, Perez-Cano M, Carrasco E, Tomas M, Mate JL, Moran T, Rosell R (2008) A sensitive method for detecting EGFR mutations in non-small cell lung cancer samples with few tumor cells. J Thorac Oncol 3:1224–1235
18. Do H, Dobrovic A (2009) Limited copy number-high resolution melting (LCN-HRM) enables the detection and identification by sequencing of low level mutations in cancer biopsies. Mol Cancer 8:82
19. Fassina A, Gazziero A, Zardo D, Corradin M, Aldighieri E, Rossi GP (2009) Detection of EGFR and KRAS mutations on transthoracic needle aspiration of lung nodules by high resolution melting analysis. J Clin Pathol 62:1096–1102
20. Morinaga R, Okamoto I, Fujita Y, Arao T, Sekijima M, Nishio K, Ito H, Fukuoka M, Kadota J, Nakagawa K (2008) Association of epidermal growth factor receptor (EGFR) gene mutations with EGFR amplification in advanced non-small cell lung cancer. Cancer Sci 99:2455–2460
21. Marchetti A, Martella C, Felicioni L, Barassi F, Salvatore S, Chella A, Camplese PP, Iarussi T, Mucilli F, Mezzetti A, Cuccurullo F, Sacco R, Buttitta F (2005) EGFR mutations in non-small-cell lung cancer: analysis of a large series of cases and development of a rapid and sensitive method for diagnostic screening with potential implications on pharmacologic treatment. J Clin Oncol 23:857–865
22. Pao W, Ladanyi M (2007) Epidermal growth factor receptor mutation testing in lung cancer: searching for the ideal method. Clin Cancer Res 13:4954–4955

Virchows Arch (2012) 460:415–421
DOI 10.1007/s00428-012-1223-1

ORIGINAL ARTICLE

Human achaete-scute homolog-1 expression in neuroendocrine breast carcinoma

Luisella Righi · Ida Rapa · Arianna Votta · Mauro Papotti · Anna Sapino

Received: 9 November 2011 / Revised: 27 February 2012 / Accepted: 5 March 2012 / Published online: 16 March 2012
© Springer-Verlag 2012

Abstract Neuroendocrine (NE) breast carcinoma is defined by morphological features similar to those of NE tumors of other organs and NE marker expression in at least 50 % of neoplastic cells. However, a NE morphology may be observed even in breast carcinomas lacking NE markers. Human achaete-scute homolog-1 (hASH-1) is a transcription factor that plays a key role in the regulation of mammalian neural and NE cell development and has been identified in several human NE tumors. The aim of this study was to investigate hASH-1 expression in human breast cancers. hASH-1 expression was evaluated in 482 consecutive non-NE invasive breast carcinomas, in a series of 84 breast cancers with >50 % NE marker expression (*high NE differentiation*) and 21 carcinomas with NE histology but negative or focally (<50 %) positive for NE markers (*low NE differentiation*). hASH-1 protein was evaluated by a specific monoclonal antibody using immunohistochemistry and gene expression by real-time polymerase chain reaction. None of the non-NE invasive breast carcinomas expressed hASH-1 at any levels. hASH-1 was expressed in tumor cell nuclei of 63 and 38 % of cases with high and low NE differentiation, respectively. Strong correlation with protein and gene expression levels was observed ($p<0.0001$). hASH-1 expression was correlated to a low mitotic count ($p=0.02$) and a low Ki67 proliferative index ($p=0.0062$). hASH-1 expression occurs in breast cancers with NE differentiation regardless of the extent of the NE cell population, and it is restricted to a subset of tumor cells having a low proliferative potential.

Keywords Breast cancer · hASH1 · Neuroendocrine phenotype · Chromogranin · Synaptophysin

L. Righi · I. Rapa · A. Votta · M. Papotti
Department of Clinical and Biological Sciences,
University of Turin at San Luigi Hospital,
Orbassano, Turin, Italy

A. Sapino
Department of Biomedical Sciences and Human Oncology,
University of Turin,
Turin, Italy

L. Righi (✉)
Department of Clinical and Biological Sciences, Pathology Unit,
University of Turin al San Luigi Hospital,
Regione Gonzole 10,
10143 Orbassano, Turin, Italy
e-mail: luisella.righi@unito.it

Introduction

Primary neuroendocrine (NE) breast carcinomas, which were originally described in 1977 by Cubilla and Woodruff [1], are rare breast tumors (2–5 %) [2] with controversial diagnostic criteria and clinical outcomes [3, 4]. In the last edition of the Armed Forces Institute of Pathology (AFIP) fascicle on breast tumors [5], NE tumors are defined just by morphology as "neoplasms that are histologically characterized by a solid, trabecular or glandular arrangement of cells, which may also form pseudorosettes or tubulo-acinar structures." In 2003, NE carcinomas were instead defined by the World Health Organization (WHO) as a specific histological type of breast cancer exhibiting morphological features similar to those of NE tumors of other sites and expressing a NE marker in at least 50 % of neoplastic cells [2]. Following this definition, breast cancers of the usual type having less than 50 % of tumor cells stained by a NE marker were excluded from the NE subtype category. Recently, López-Bonet and co-workers showed that only 0.5 % of a large series of 1,368 infiltrating breast tumors fulfilled histopathological and immunohistochemical patterns compatible with NE breast

cancer as defined by the WHO classification [6]. Conversely, using the presence of scattered NE cells in invasive duct carcinoma not otherwise specified or in other carcinoma subtypes as a diagnostic criterion, the incidence could increase to up to 20 % of breast cancers [7]. Indeed, the definition of "endocrine" cells as cells expressing NE markers by immunohistochemistry (IHC) is partial and potentially misleading, since IHC staining reveals stored antigens and does not consider cell functionality with peptide release [8]. On the other hand, truly "endocrine" cells might store hormonal peptides, but below the threshold of IHC sensitivity. In addition, the most sensitive and specific marker of NE differentiation in breast cancer has not been established yet. Classically, chromogranin A (CGA) and/or synaptophysin (SYP) expression are considered the most appropriate NE markers [2, 9, 10] and have been associated with the ultrastructural localization in tumor cells of neurosecretory dense core granules and presynaptic clear vesicles, respectively [11]. Other NE markers are less sensitive and specific, and new molecules are under investigation.

Human achaete-scute homolog-1 (hASH-1) is a member of the basic helix–loop–helix (bHLH) family of transcription factors [12], which have been identified as key regulators of mammalian neural development, promoting the lineage commitment of cell progenitors in the central and peripheral nervous system [13–16]. In addition, hASH-1 is essential for the development of several types of non-neoplastic NE cells [17], including those of the lung [18]. These cells were suggested to play an important role in the early regulation of pulmonary epithelial development by functioning as stem cells [19]. hASH-1 is highly expressed in malignant tumors with neural or NE phenotype, such as neuroblastoma [20], medullary carcinoma of the thyroid [21], neuroendocrine neoplasms of the gastrointestinal tract [22], and small cell lung carcinoma (SCLC) [18, 19]. Recently, hASH-1 was found in cell lines of SCLC, carcinoid, and non-SCLC with NE features, confirming that hASH-1 is an early controller of NE differentiation in lung neoplasms [23]. Moreover, our group [24] and other researchers [25] have demonstrated that hASH-1 expression is correlated with NE differentiation in prostate adenocarcinomas, especially those submitted to androgen deprivation therapy. In addition, hASH-1 transfection of prostate cancer cell lines induces production of CGA as shown by mRNA and protein detection [24]. In breast cancer, the single report dealing with hASH-1 investigated the function of Hes-6, another member of the bHLH family, in T47D and MCF-7 breast cancer cell lines (both expressing estrogen receptor-alpha) [26]. Hes-6 transfection in such cells followed by treatment with 17-beta-estradiol, the most potent sex hormone that mediates proliferative effects in breast cancer cells, was able to modulate hASH-1 expression levels. However, to our knowledge, the real role of hASH-1 in breast cancer has never been investigated nor is the mechanism driving NE differentiation in breast cancer fully understood.

The aims of the present study were to investigate if the hASH-1 gene and protein are expressed in breast cancer tissues and to correlate the expression levels with the NE differentiation.

Materials and methods

Case selection To evaluate whether hASH-1 protein is expressed in breast cancer, a consecutive series of 482 invasive carcinomas was tested by IHC on tissue microarrays. All cases were reviewed to identify NE morphological features, as defined by AFIP [5], and to select areas suitable for the construction of tissue microarrays. For the study purpose, tumors reported by Capella [27] as hypercellular or type B mucinous carcinomas were considered as breast cancers with NE morphology. In addition, hASH-1 protein and gene expression were evaluated in a series of 84 highly selected NE breast carcinomas with >50 % NE marker expression (according to the 2003 WHO classification [2]), here defined as tumors with "high NE differentiation" and in 21 breast carcinomas with a clear-cut NE morphology (according to the 2009 AFIP fascicle definition) [5], but negative or only focally positive (<50 %) for NE markers (tumors with "low NE differentiation"), collected from 1985 to 2010 at the pathology divisions of San Giovanni Battista and San Luigi hospitals of the University of Turin.

Immunohistochemistry NE differentiation was tested using primary monoclonal antibodies to CGA (mouse, clone LK2H10, diluted 1/800; NeoMarkers, Fremont, CA, USA) and SYP (rabbit, clone SP11, diluted 1/100, Thermo Fisher Scientific, Fremont, CA, USA). hASH-1 protein expression was assessed using a monoclonal antibody (clone 24B72D11.1, diluted 1/150; BD Biosciences, San Jose, CA, USA). Endogenous peroxidase activity was blocked by absolute methanol and 0.3 % hydrogen peroxide for 15 min. Heat-induced antigen retrieval was performed in a pressure cooker at 95 °C for 5 min in citrate buffer at pH 6.0. Immunoreactions were revealed by a dextran-chain (biotin-free) detection system (EnVision; DakoCytomation, Glostrup, Denmark) using 3,3′-diaminobenzidine (DAB; Dako) as a chromogen.

A case of SCLC was used as a positive control for all of the antibodies. Negative controls were obtained by omitting the primary antibodies in the IHC reactions. For hASH-1, the percentage of nuclear staining of invasive breast cancer cells was assessed independently by two of the authors (LR, IR) regardless of the staining intensity, and the results were categorized into four groups: score 0=no staining, score 1=≤10 % of positive tumor cells, score 2=11–50 %, and score 3=>50 % of positive tumor cells.

Double immunohistochemical procedure To determine whether hASH-1 positive cells were actively participating in NE differentiation and neoplastic growth, double staining was performed to test the co-expression of hASH-1 and NE markers, as well as of hASH-1 and Ki67. After the antigen-retrieval procedure (see above), sections were incubated overnight at 4 °C with monoclonal 24B72D11.1 to hASH-1, and the reaction was revealed by EnVision detection system (Dako) and DAB as a chromogen. The sections were then incubated for 5 min at room temperature in 1 N HCl, washed in TBS buffer, and incubated for 40 min at room temperature with CGA or SYP primary antibodies (at the above conditions) or with Ki67 (clone MIB-1, diluted 1/200, Dako), followed by pre-diluted Dako-En Vision-Polymer AP mouse/rabbit antibody. Finally, the immune reactions were detected using Vector Blue Alkaline Phosphatase substrate kit and were mounted in glycerol. Nuclear hASH-1 was detected as a brown stain, while CGA and SYP or Ki67 appeared as a blue cytoplasmic or nuclear stain, respectively. For nuclear markers, the co-localization of two antigens in the same cell was rarely detected and in any case demonstrated by an overlapped brown–blue stain in the same nucleus.

Real-time polymerase chain reaction analysis RNA isolation and cDNA synthesis were performed from formalin-fixed, paraffin-embedded tissues of the tumors with "high and low NE differentiation" as previously described [28] and in 20 out of 482 non-NE carcinomas. Relative cDNA quantification of *hASH-1* and *β-actin* (internal reference gene) was performed using a fluorescence-based real-time (RT) detection method, as previously described [29]. Tests were conducted in duplicate, and the comparative Ct method was employed. To normalize the measurements across samples, the ΔCt value of the control calibrator (Stratagene, La Jolla, CA, USA) was subtracted from each ΔCt to obtain the ΔΔCt values, which were converted into the relative expression level using the following formula: $2^{-\Delta\Delta Ct}$. The sequences of primers and probes used for *hASH-1* and *β-actin* have been previously reported [24]. The expression of transcripts was examined by quantitative RT polymerase chain reaction (PCR), as previously described [30], and the observed levels quantified as unitless values.

Statistical analysis To identify significant associations between continuous and dichotomous variables such as age, sex, and tumor stage, the Mann–Whitney *U* test or Kruskal–Wallis was used, and correlations between gene or protein expression and clinicopathological variables were analyzed by the chi-square or Fisher test, using Bonferroni's correction for multiple comparisons. Spearman's test was employed to correlate protein and gene expression. Survival analysis was performed by Kaplan–Meier curves and the significance verified by log rank. Univariate analyses of survival were carried out using the Cox proportional-hazard model. The level of significance was set at $p=0.05$. All tests were performed using GraphPad software version 5.0.

Results

hASH-1 protein expression Three of the 482 consecutive invasive breast cancer showed some NE morphological features. None had hASH-1 protein expression.

The clinicopathological features of patients having tumors with high or low NE differentiation are summarized in Table 1. hASH-1 protein expression was detected in 53 (63 %) of the 84 cancers with high NE differentiation. In particular, 20 cases (38 %) were classified as score 1, 25 (47 %) were categorized as score 2, and 8 cases (15 %) were labeled as score 3 (Fig. 1). In situ carcinomas had hASH-1 expression always concordant with the associated invasive component, while no reactivity was observed in non-neoplastic breast lobules and ducts.

hASH-1 immunoreactivity was found in 8 out of 21 (38 %) breast cancers with low NE differentiation, including three cases with NE morphology only (one type B mucinous carcinoma and two carcinomas with solid-cohesive patterns) and five with focal NE differentiation (one small cell and four solid-cohesive carcinomas, focally expressing CGA or SYP). The different percentage of hASH-1-expressing cells in tumors with high versus those with low NE differentiation was of borderline statistical significance ($p=0.05$, Fisher's exact test).

No correlation between hASH-1 protein expression and any of the NE markers was found, nor with age, morphological type, size, nodal status, metastases, presence of an in situ component, or survival status. On the contrary, in the 84 cancers with high NE differentiation, a trend of significant correlation was found between high hASH-1 protein expression and low histological grade, either considering the three tumor grades separately (chi-square, $p=0.071$) or comparing hASH-1 levels in differentiated (G1 and G2) versus poorly differentiated (G3) tumors (chi-square, $p=0.067$). In addition, a significant correlation was observed between hASH-1 expression and low mitotic count (chi-square, $p=0.02$, using the mean value of 20 mitoses/10 high-power fields as cutoff; Fig. 2a) and low Ki67 proliferative index (chi-square, $p=0.0062$, using the mean value of 20 % positive nuclei as cutoff; Fig. 2b).

Co-localization studies To investigate the possible co-localization of hASH-1 with NE or proliferation markers, double immunohistochemical stains were performed. The co-localization of hASH-1 (nuclear staining) and CGA or SYP (cytoplasmic staining) was detected in a large fraction

Table 1 Clinicopathological features of 84 breast cancers with "high NE differentiation" (NE markers >50 %, WHO 2003 [2]) and of 21 breast cancers with "low NE differentiation" (NE morphology and/or NE markers <50 %)

Characteristics	Tumor with "high NE differentiation"	Tumor with "low NE differentiation"
Median age (range)	69 years (27–93)	67 years (44–87)
Presence of an in situ component	29/84 (35 %)	7/21 (33 %)
Histological grade [37]		
G1	20/84 (24 %)	8/21 (38 %)
G2	44/84 (52 %)	7/21 (33 %)
G3	20/84 (24 %)	6/21 (29 %)
pT1	34/67 (51 %)	7/15 (47 %)
pT2	24/67 (36 %)	6/15 (40 %)
pT3-4	9/67 (13 %)	2/15 (13 %)
pN0	29/50 (58 %)	10/14 (71 %)
pN+	21/50 (42 %)	4/14 (29 %)
hASH-1 protein expression	53/84 (63 %)	8/21 (38 %)
CGA expression (range)	60/84 (71 %) (0–95)	6/21 (29 %) (0–30)
SYP expression (range)	65/84 (77 %) (0–98)	4/21 (19 %) (0–40)
Mean Ki67 index (range)	20% (1–80)	28% (3–80)
Median survival (months)	117	Undetermined
NED/DOC	50/66 (75 %)	14/18 (78 %)
AWD/DOD	16/66 (25 %)	4/18 (22 %)

NE neuroendocrine, *WHO* World Health Organization, *G* grade, *hASH-1* human achaete-scute homolog-1, *CGA* chromogranin A, *SYP* synaptophysin, *NED* no evidence of disease, *DOC* died of other causes, *AWD* alive with disease, *DOD* died of disease

of the tumor cell population. On the contrary, a mutually exclusive nuclear localization of hASH-1 and Ki67 was the most common occurrence, co-localization (characterized by an overlapped brown–blue nuclear stain) being an extremely rare observation (Fig. 3).

hASH-1 gene expression None of the 20 non-NE invasive breast carcinomas successfully submitted to RNA extraction and RT-PCR expressed *hASH-1* mRNA. RNA isolation was successful in 47 out of 84 carcinomas with "high NE differentiation." *hASH-1* mRNA levels had a median unitless

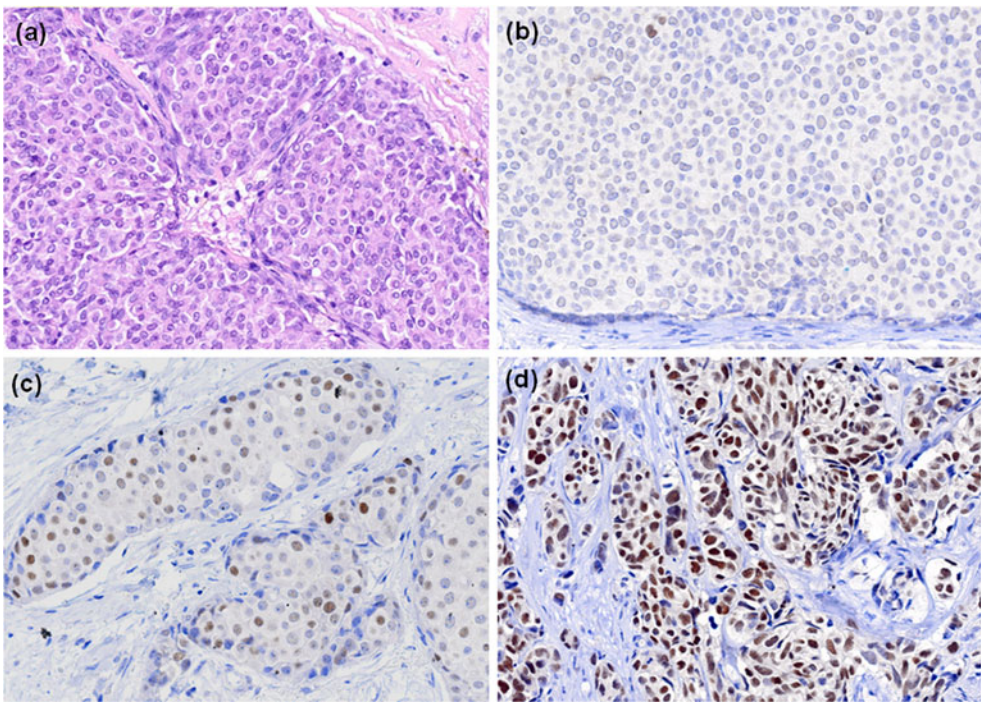

Fig. 1 Human ASH-1 immunohistochemical expression in tumors with high NE differentiation. **a** Solid growth pattern (hematoxylin & eosin, ×20). **b** hASH-1 nuclear expression score 1. **c** hASH-1 nuclear expression score 2. **d** hASH-1 nuclear expression score 3 (see scoring in Materials and methods, immunoperoxidase, ×20)

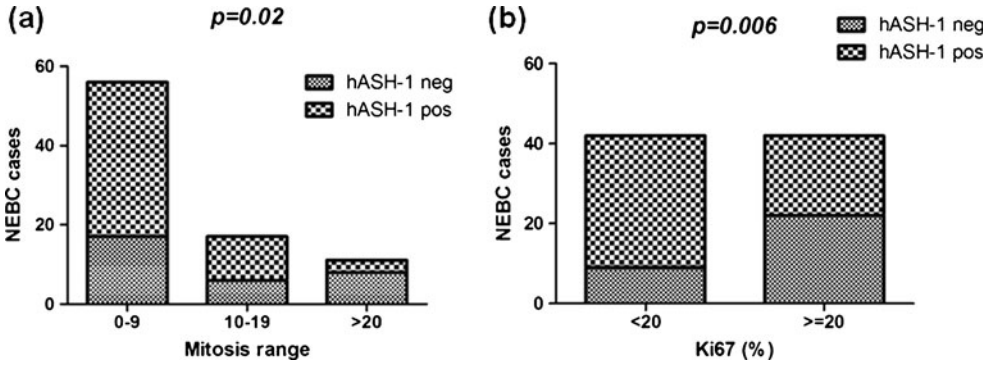

Fig. 2 Distribution of hASH-1 protein expression in 84 tumors with high NE differentiation as a function of **a** the mitotic index (number of mitoses/10 high-power fields, according to Elston–Ellis grading system ranges [37]) and **b** the Ki67 proliferative index (using the mean value of 20 % as a cutoff)

value of 187.8 (range, 0.1–12006.0). A good correlation between total *hASH-1* gene and protein expression was found ($p<0.0001$, chi-square test, Fig. 4a). One case only (6 %) of the 16 negative cases at the protein level displayed high *hASH-1* mRNA expression (414.8 unitless ratio) at the PCR analysis. A strong correlation between *hASH-1* mRNA level and protein expression by IHC was observed (Kruskal–Wallis test, $p<0.0001$, Fig. 4b).

In the series of 21 carcinomas with low NE differentiation (NE morphology and/or focal NE marker expression), RNA was successfully extracted in seven (33 %) cases only (two solid cohesive, four mucinous, and one small cell carcinoma). In these few cases, a good correlation of *hASH-1* gene versus protein expression was observed. Interestingly, the single hASH-1 immunohistochemically positive case of small cell carcinoma (having 10 % CGA reactivity in the absence of SYP expression) also contained high mRNA expression levels. Conversely, the other six cases neither had detectable hASH-1 mRNA nor hASH-1 immunoreactivity in tumor cells (Fig. 5). In the current series, no correlation between survival and hASH expression (at neither protein nor mRNA levels) was found.

Discussion

In the present study, we demonstrated that hASH-1, a bHLH transcription factor which drives neural cell development in fetal life [31], and NE differentiation in several cancers [32] was expressed to various extents in NE breast cancers. Conversely, no hASH-1 protein or mRNA was ever detected in a large series of non-NE invasive breast cancers. To our knowledge, this is the first report of hASH-1 expression in primary breast cancers. Specifically, two thirds (63 %) of breast cancers with high NE differentiation expressed hASH-1 at the protein level, with good correlation with

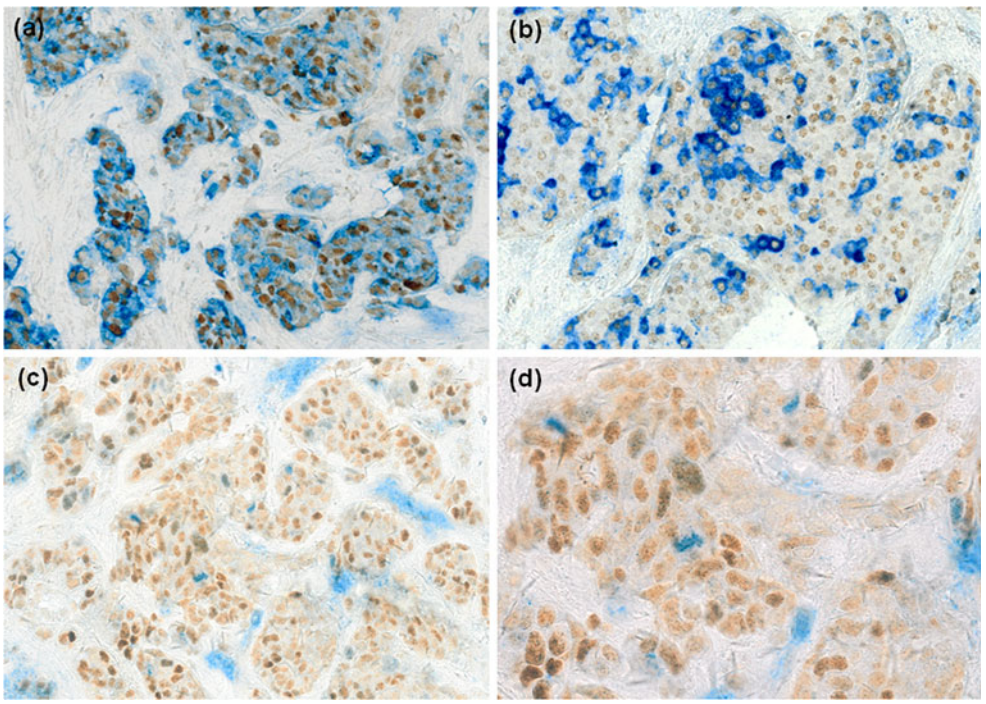

Fig. 3 Tumor with high NE differentiation submitted to a double immunohistochemical staining for hASH-1 (*brown*) followed by **a** CGA (*blue*), **b** SYP (*blue*), or **c, d** Ki67 (*blue*) (sequential immunoperoxidase and immunoalkaline phosphatase; **a**, **b**, **c** ×20, **d** ×40)

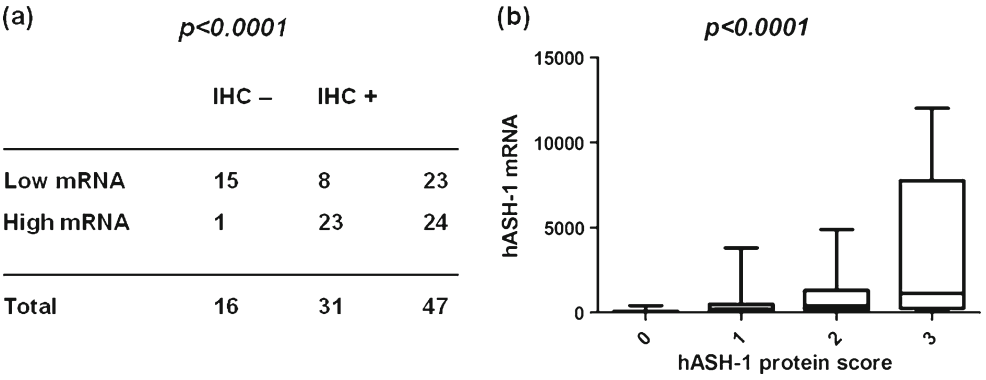

Fig. 4 Correlation between hASH-1 gene and protein expression in 47 tumors with high NE differentiation as a function of **a** total hASH-1 or **b** hASH-1 scored reactivity

mRNA levels. A further evidence of the role of hASH-1 in NE differentiated breast carcinoma is the presence of either protein or mRNA in one third of cases that possessed focal NE marker expression or NE morphology only, as defined by the recent AFIP fascicle on breast tumors [5]. This latter condition has been investigated in the lung, where rare poorly differentiated carcinomas of the large cell type displayed morphologically clear-cut NE features, but lacked NE marker expression [33]. The authors labeled these tumors as "carcinoma with NE morphology" and left the pathogenesis and nature of these carcinomas open for debate. In the same organ, Miki and Linnoila [23] reported that six of their ten hASH-1-positive non-small cell lung carcinomas lacked NE marker expression and suggested that a hASH-1-only reactivity might represent a primitive NE phenotype. Similar events might occur in the breast, where solid-cohesive patterns strongly resemble the organoid pattern of NE tumors, but generally lack NE marker expression and may focally express hASH-1. This indicates that the diagnostic criterion proposed by the 2003 WHO classification [2] for NE breast carcinomas (requiring NE marker expression in at least 50 % of tumor cells) may be arbitrary, and common mechanisms likely drive the induction of NE morphology, regardless of the extent of traditional NE marker expression. We have previously shown in breast tumors with morphological NE features the co-expression of NE and apocrine markers suggesting the possibility of an uncommitted stem cell capable of differentiating towards both lineages [34]. The role of regulatory factors that drive NE differentiation in breast tumors has never been studied. hASH-1 may have such a role in the transition from classical exocrine to the rare NE differentiated carcinoma. As a matter of fact, we showed that hASH-1 was not only expressed in a relatively wide proportion of invasive cancer expressing high levels of NE markers, but also in the associated in situ component, while it was never expressed in normal breast ducts, nor in ductal or lobular cancer. It has been suggested that hASH-1 modulates currently unknown downstream targets essential for the NE commitment, probably related to the Notch/HES signaling pathway [35]. In this line, the early activation of hASH-1 in NE differentiated (or committed) cells may not go in parallel with the expression of CGA and/or SYP and/or other markers, since the secretory machinery of NE products may be delayed along the NE differentiation process. We have previously shown that cells of well-differentiated NE tumors maintain a multidifferentiation capacity, whereas those of poorly differentiated carcinomas do not show this ability [34]. hASH-1 expression was associated to low tumor grade and low proliferative activity in NE breast cancers. On the other hand, the upstream downregulatory role of HES-1 on hASH-1 expression and function could explain the presence of final NE differentiation in the absence of hASH-1 detection. [36].

In conclusion, rather than prognostic, the interest of hASH-1 expression in breast cancer is restricted to the understanding of developmental mechanisms of combined exocrine and NE breast carcinomas, with possible future therapeutic implications.

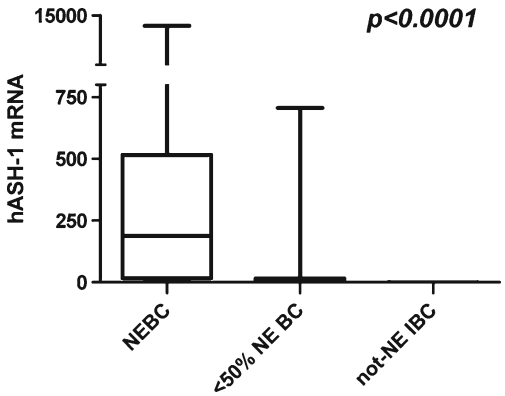

Fig. 5 Distribution of *hASH-1* mRNA expression in the different breast cancer series

Conflict of interest The authors do not have any conflicts of interest to declare with regard to the current study.

References

1. Cubilla AL, Woodruff JM (1977) Primary carcinoid tumor of the breast. A report of eight patients. Am J Surg Pathol 1:283–292
2. Ellis P, Schnitt SJ, Sastre-Garau X (2003) Invasive breast carcinoma. In: Tavassoli FA, Devilee P (eds) Tumours of the breast and female genital organs. Pathology and genetics. World Health Organization Classification of Tumours. IARC Press, Lyon
3. Righi L, Sapino A, Marchio C, Papotti M, Bussolati G (2010) Neuroendocrine differentiation in breast cancer: established facts and unresolved problems. Semin Diagn Pathol 27(1):69–76
4. Wei B, Ding T, Xing Y, Wei W, Tian Z, Tang F, Abraham S, Nayeemuddin K, Hunt K, Wu Y (2010) Invasive neuroendocrine carcinoma of the breast: a distinctive subtype of aggressive mammary carcinoma. Cancer 116(19):4463–4473. doi:10.1002/cncr.25352
5. Tavassoli F, Eusebi V (2009) AFIP atlas of tumor pathology. Armed Forces Institute of Pathology, Washington DC
6. Lopez-Bonet E, Alonso-Ruano M, Barraza G, Vazquez-Martin A, Bernado L, Menendez JA (2008) Solid neuroendocrine breast carcinomas: incidence, clinico-pathological features and immunohistochemical profiling. Oncol Rep 20(6):1369–1374
7. Miremadi A, Pinder SE, Lee AH, Bell JA, Paish EC, Wencyk P, Elston CW, Nicholson RI, Blamey RW, Robertson JF, Ellis IO (2002) Neuroendocrine differentiation and prognosis in breast adenocarcinoma. Histopathology 40(3):215–222
8. Sapino A, Bussolati G (2002) Is detection of endocrine cells in breast adenocarcinoma of diagnostic and clinical significance? Histopathology 40(3):211–214
9. Sapino A, Righi L, Cassoni P, Papotti M, Pietribiasi F, Bussolati G (2000) Expression of the neuroendocrine phenotype in carcinomas of the breast. Semin Diagn Pathol 17(2):127–137
10. Moriya T, Kanomata N, Kozuka Y, Fukumoto M, Iwachido N, Hata S, Takahashi Y, Miura H, Ishida K, Watanabe M (2009) Usefulness of immunohistochemistry for differential diagnosis between benign and malignant breast lesions. Breast Cancer 16(3):173–178
11. Capella C, Usellini L, Papotti M, Macri L, Finzi G, Eusebi V, Bussolati G (1990) Ultrastructural features of neuroendocrine differentiated carcinomas of the breast. Ultrastruct Pathol 14(4):321–334
12. Massari ME, Murre C (2000) Helix-loop-helix proteins: regulators of transcription in eucaryotic organisms. Mol Cell Biol 20(2):429–440
13. Casarosa S, Fode C, Guillemot F (1999) Mash1 regulates neurogenesis in the ventral telencephalon. Development 126(3):525–534
14. Guillemot F, Joyner AL (1993) Dynamic expression of the murine Achaete-Scute homologue Mash-1 in the developing nervous system. Mech Dev 42(3):171–185
15. Huber K, Bruhl B, Guillemot F, Olson EN, Ernsberger U, Unsicker K (2002) Development of chromaffin cells depends on MASH1 function. Development 129(20):4729–4738
16. Tomita K, Nakanishi S, Guillemot F, Kageyama R (1996) Mash1 promotes neuronal differentiation in the retina. Genes Cells 1 (8):765–774
17. Hirsch MR, Tiveron MC, Guillemot F, Brunet JF, Goridis C (1998) Control of noradrenergic differentiation and Phox2a expression by MASH1 in the central and peripheral nervous system. Development 125(4):599–608
18. Borges M, Linnoila RI, van de Velde HJ, Chen H, Nelkin BD, Mabry M, Baylin SB, Ball DW (1997) An achaete-scute homologue essential for neuroendocrine differentiation in the lung. Nature 386(6627):852–855
19. Osada H, Tomida S, Yatabe Y, Tatematsu Y, Takeuchi T, Murakami H, Kondo Y, Sekido Y, Takahashi T (2008) Roles of achaete-scute homologue 1 in DKK1 and E-cadherin repression and neuroendocrine differentiation in lung cancer. Cancer Res 68(6):1647–1655
20. Rostomily RC, Bermingham-McDonogh O, Berger MS, Tapscott SJ, Reh TA, Olson JM (1997) Expression of neurogenic basic helix-loop-helix genes in primitive neuroectodermal tumors. Cancer Res 57(16):3526–3531
21. Ball DW, Azzoli CG, Baylin SB, Chi D, Dou S, Donis-Keller H, Cumaraswamy A, Borges M, Nelkin BD (1993) Identification of a human achaete-scute homolog highly expressed in neuroendocrine tumors. Proc Natl Acad Sci USA 90(12):5648–5652
22. Shida T, Furuya M, Nikaido T, Kishimoto T, Koda K, Oda K, Nakatani Y, Miyazaki M, Ishikura H (2005) Aberrant expression of human achaete-scute homologue gene 1 in the gastrointestinal neuroendocrine carcinomas. Clin Cancer Res 11(2 Pt 1):450–458
23. Miki M, Ball DW, Linnoila RI (2011) Insights into the achaete-scute homolog-1 gene (hASH1) in normal and neoplastic human lung. Lung cancer (Amsterdam, Netherlands). doi:10.1016/j.lungcan.2011.05.019
24. Rapa I, Ceppi P, Bollito E, Rosas R, Cappia S, Bacillo E, Porpiglia F, Berruti A, Papotti M, Volante M (2008) Human ASH1 expression in prostate cancer with neuroendocrine differentiation. Mod Pathol 21(6):700–707
25. Vias M, Massie CE, East P, Scott H, Warren A, Zhou Z, Nikitin AY, Neal DE, Mills IG (2008) Pro-neural transcription factors as cancer markers. BMC Med Genomics 1:17. doi:10.1186/1755-8794-1-17
26. Hartman J, Lam EW, Gustafsson JA, Strom A (2009) Hes-6, an inhibitor of Hes-1, is regulated by 17beta-estradiol and promotes breast cancer cell proliferation. Breast Cancer Res 11(6):R79. doi:10.1186/bcr2446
27. Capella C, Eusebi V, Mann B, Azzopardi JG (1980) Endocrine differentiation in mucoid carcinoma of the breast. Histopathology 4(6):613–630
28. Ceppi P, Volante M, Saviozzi S, Rapa I, Novello S, Cambieri A, Lo Iacono M, Cappia S, Papotti M, Scagliotti GV (2006) Squamous cell carcinoma of the lung compared with other histotypes shows higher messenger RNA and protein levels for thymidylate synthase. Cancer 107(7):1589–1596
29. Heid CA, Stevens J, Livak KJ, Williams PM (1996) Real time quantitative PCR. Genome Res 6(10):986–994
30. Righi L, Papotti MG, Ceppi P, Bille A, Bacillo E, Molinaro L, Ruffini E, Scagliotti GV, Selvaggi G (2010) Thymidylate synthase but not excision repair cross-complementation group 1 tumor expression predicts outcome in patients with malignant pleural mesothelioma treated with pemetrexed-based chemotherapy. J Clin Oncol 28(9):1534–1539. doi:10.1200/JCO.2009.25.9275
31. Guillemot F, Lo LC, Johnson JE, Auerbach A, Anderson DJ, Joyner AL (1993) Mammalian achaete-scute homolog 1 is required for the early development of olfactory and autonomic neurons. Cell 75(3):463–476
32. Linnoila RI, Zhao B, DeMayo JL, Nelkin BD, Baylin SB, DeMayo FJ, Ball DW (2000) Constitutive achaete-scute homologue-1 promotes airway dysplasia and lung neuroendocrine tumors in transgenic mice. Cancer Res 60(15):4005–4009
33. Iyoda A, Hiroshima K, Toyozaki T, Haga Y, Fujisawa T, Ohwada H (2001) Clinical characterization of pulmonary large cell neuroendocrine carcinoma and large cell carcinoma with neuroendocrine morphology. Cancer 91(11):1992–2000
34. Sapino A, Righi L, Cassoni P, Papotti M, Gugliotta P, Bussolati G (2001) Expression of apocrine differentiation markers in neuroendocrine breast carcinomas of aged women. Mod Pathol 14(8):768–776
35. Ball DW (2004) Achaete-scute homolog-1 and Notch in lung neuroendocrine development and cancer. Cancer Lett 204(2):159–169
36. Axelson H (2004) The Notch signaling cascade in neuroblastoma: role of the basic helix-loop-helix proteins HASH-1 and HES-1. Cancer Lett 204(2):171–178. doi:10.1016/S0304-3835(03)00453-1
37. Elston CW, Ellis IO (1991) Pathological prognostic factors in breast cancer. I. The value of histological grade in breast cancer: experience from a large study with long-term follow-up. Histopathology 19(5):403–410

Virchows Arch (2012) 460:423–427
DOI 10.1007/s00428-012-1209-z

ORIGINAL ARTICLE

Expression of KRT7 and WT1 differentiates precursor lesions of Wilms' tumours from those of papillary renal cell tumours and mucinous tubular and spindle cell carcinomas

Adrianna Szponar · Gyula Kovacs

Received: 5 August 2011 / Revised: 22 November 2011 / Accepted: 31 January 2012 / Published online: 2 March 2012
© Springer-Verlag 2012

Abstract Wilms' tumours (WT) and adult papillary renal cell tumours (pRCT) are associated with precursor lesions of embryonic origin. The aim of this study was to analyse the expression of WT1, KRT7, KRT8, KRT18 and KRT19 genes by immunohistochemistry in 74 precursor lesions associated with WTs, pRCTs and mucinous tubular and spindle cell carcinomas (MTSCC). All precursor lesions associated with Wilms' tumours were positive for WT1, whereas all precursor lesions in pRCT and MTSCC-bearing kidneys were negative. None of the WT-associated lesions were positive for KRT7, but 69–80% of lesions associated with pRCTs and MTSCCs were positive for KRT7. KRT8, KRT18 and KRT19 were found to be expressed in 80–100% of all types of precursor lesions. Our findings indicate that the precursor lesions analysed in this study are committed in an early stage of cellular differentiation to the development of either Wilms' tumours or papillary RCTs and MTSCCs.

Keywords Precursor lesions · KRT7 · WT1 · Wilms' tumour · Papillary renal cell tumour

Introduction

Papillary renal cell tumours (pRCT) are characterised by trisomies of chromosome 7 and 17 and mutation/overexpression of the MET and overexpression of the HNF1B genes, respectively [1–3]. Papillary RCTs have an excellent prognosis, around 90% of the patients with pRCTs are alive 5 years after the diagnosis [4]. Although pRCTs account only for 10% of renal cell cancers in surgical series, the number of small papillary lesions accompanying clinically recognized tumours is much higher than that of all other types of renal tumours together. It is generally believed that pRCTs develop from the adult renal tubular system [5, 6]. However, we have suggested that pRCTs develop from partially differentiated nephrogenic rests and the cellular characteristics of tumours correspond to the level of cellular differentiation of the precursor lesions [7].

The latter hypothesis is supported by observations that both sporadic and familial pRCTs are associated with a high number of microscopic nephrogenic rest-like lesions, their number being significantly higher in hereditary cases. On average, 42 small tubulary and papillary precursor lesions were detected in the kidneys with sporadic pRCTs whereas only 0.4 such lesions per kidney were found in association with conventional renal cell carcinoma [8]. In hereditary cases the estimated number of microscopic tubulopapillary lesions and small tumours ranges from 1,100 to 3,400 per kidney [9].

The link between embryonal rests and Wilms' tumour has already been established [10]. Interestingly, pRCTs and Wilms' tumours share also some genetic characteristics. Trisomies of chromosomes 7, 8, 12, 17 and 20, which are specific alterations in pRCTs, have also been found in 20% to 38% of Wilms' tumours [1, 11]. Based on the genetic and histological analyses, we suggest that not only Wilms' tumours but also pRCT arises from blastemal cells persisting after cessation of the kidney development in the 36th week of gestation [7]. Although the vast majority of these lesions regress during the first years of life, some of them progress into a Wilms' tumour and others may persist for decades and may develop a clinically recognised pRCT in adult [4, 10].

A. Szponar · G. Kovacs
Medical Faculty, Ruprecht-Karls University,
Heidelberg, Germany

G. Kovacs (✉)
Department of Laboratory Medicine, Medical School,
University of Pecs,
Szigeti str. 12,
7624 Pecs, Hungary
e-mail: gyula.kovacs@urz.uni-heidelberg.de

Whether Wilms' tumours and pRCTs arise from common precursor lesions and their phenotype is simply governed by the genetic changes acquired during tumourigenesis, or they develop from distinct types of precursor lesions is not yet known. To answer this question, we have analysed such precursor lesions for the expression of the WT1 gene as well as of KRT7, KRT8, KRT18 and KRT19.

Materials and methods

Tissue samples

We performed a comprehensive analysis of two kidneys bearing Wilms' tumours, seven kidneys with pRCTs and one kidney with a mucinous tubular and spindle cell carcinoma (MTSCC), which were totally included in hundreds of paraffin blocks. H&E-stained slides were scored for precursor lesions, and ten slides of 4 μm thickness were cut from each paraffin block containing a precursor lesion. The first and tenth slides were stained with H&E to check the occurrence and location of the lesions, whereas slides 2–6 were used for immunohistochemical staining. The rest was dipped in liquid paraffin and stored for further analysis. We have also included in this study two paraffin blocks from six Wilms' tumours; two of them contained one and two nephrogenic rests as well. Paraffin blocks of foetal and adult kidneys were used as positive control and to localize the proteins in normal kidneys. The collection and use of all tissue samples for this study was approved by the ethics committee of the University of Heidelberg and University of Pecs, Hungary.

Immunohistochemistry

The tissue sections were deparaffinised with xylene. Antigen retrieval was performed by boiling the tissues in 10 mM citrate buffer pH 6.0 in 2100 Retriever according to the standard programme. Endogenous peroxidase activity was quenched with 0.3% hydrogen peroxide. The non-specific binding was blocked with 10% goat serum (Dako, Hamburg, Germany) in 1% BSA in TBS by incubation for 2 h at room temperature. The following primary antibody diluted in 1% BSA in TBS was used: mouse anti-KRT7 (1:50; Abcam, Cambridge, UK; cat. no. ab9021, clone RCK105), rabbit anti-KRT8 (1:200; Thermo Fisher Scientific, Schwerte, Germany; cat. no. RB-9095), mouse anti-CK18 (1:500; Thermo Fisher Scientific; cat no. MS-142), rabbit anti-KRT19 (1:100; Dako; cat no. ab15463) and mouse anti-WT1 (1:50; Dako; cat no. M3561, clone 6F-H2). Incubation was overnight at 4°C. Next the sections were incubated for 1 h at room temperature with anti-rabbit secondary HRP-conjugated antibody, and the reaction was developed by applying AEC substrate for HRP (Dako). The tissue sections were counterstained by immersing in Mayer's haemalaun solution (Merck, Darmstadt, Germany), mounted with aqueous permanent mounting medium Ultramount (Dako) and cover-slipped with Pertex (Medite GmbH, Burgdorf, Germany).

Results

We found an average of 42 precursor lesions per kidney in association with papillary RCTs, 9 precursor lesions in the kidney with MTSSC, and 17 and 8 nephrogenic rests in the two kidneys with Wilms' tumour, respectively. We have analysed 5 foetal and 5 adult kidneys, 21 nephrogenic rests associated with Wilms' tumour, 48 lesions associated with pRCT and 5 lesions detected in a single kidney with MTSCC by immunohistochemistry (Table 1). During a GenChip analysis of end-stage kidneys, we found that KRT7 and KRT19 were overexpressed in proliferating cells of cysts and tubulopapillary lesions (unpublished data). KRT7 was specifically expressed in papillary precursor lesions and pRCTs arising in such kidneys. We also selected KRT8 and KRT18 for this study because they are characteristic for single-layered epithelia such as the kidney tubular system. We analysed WT1 because of its role in the embryonal development of the kidney. Because some slides in deeper cuts did not contain more precursor lesions and we carried out the WT1 analysis as the last step, we have the results for all antibodies in 17 nephrogenic rests, 5 precursors for MTSCC and 39 precursor lesions associated with pRCTs (Table 1).

The normal kidney parenchyma surrounding the precursor lesions was used as positive control. Each specimen revealed specific staining of normal tubular and glomerular

Table 1 Summary of immunohistochemical analysis of precursor lesions for Wilms' tumour, MTSCC and papillary RCT

Precursors for	KRT7	KRT8	KRT18	KRT19	WT1
Wilms' tumour	0% (0/21)	81% (17/21)	100% (20/20)	95% (19/20)	100% (17/17)
MTSCC	80% (4/5)	80% (4/5)	100% (5/5)	100% (5/5)	0% (0/5)
Papillary RCT	69% (31/45)	100% (45/45)	100% (43/43)	94% (45/48)	0% (0/39)

KRT keratin, *WT1* Wilms' tumour 1 gene, *MTSCC* mucinous tubular and spindle cell carcinoma, *RCT* renal cell tumour

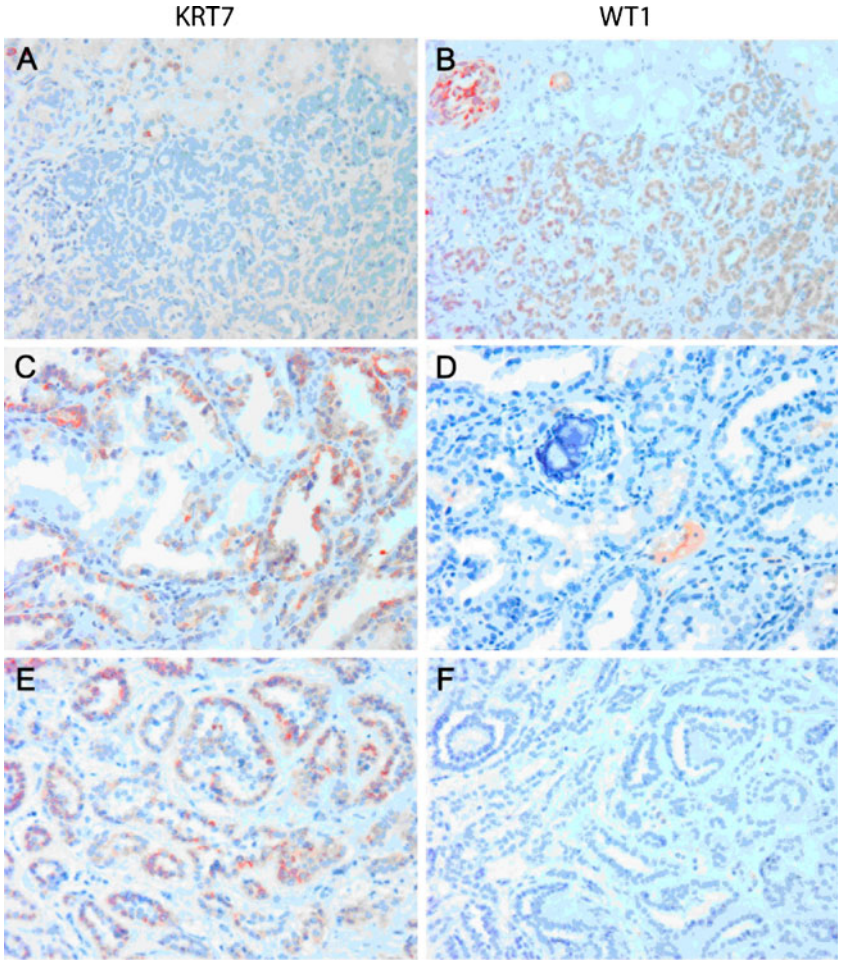

Fig. 1 Immunohistochemical staining of KRT7 and WT1 in precursor lesions associated with Wilms' tumour, MTSCC and pRCT. **a** A tubular/solid growing nephrogenic rest observed in a kidney with Wilms' tumour show a negative staining for KRT7. Note the characteristic scattered immunoreactivity in cells of distal convoluted tubuli. **b** Strong nuclear staining for WT1 of the same nephrogenic rest. Staining of a glomerulus in the *right corner* serves as an internal control. **c** KRT7 staining of a papillary precursor lesion associated with a pRCT. **d** The same lesion is negative for WT1. **e** Scattered staining of cells with the KRT7 antibody in a tubulopapillary precursor lesion associated with a clinically recognized MTSCC. **f** The same lesion is negative for the WT1 antibody. All pictures are of the same magnification

cells known to be positive for a given antibody. Positive cytoplasmic staining with KRT8 and KRT18 antibody was seen in 80–100% of the precursor lesions associated with pRCTs, MTSCC and Wilms' tumour (Table 1). We have also found strong expression of KRT19 in 94–100% of all types of precursor lesions. Of interest, KRT7 was expressed in 69% and 80% of the precursor lesions associated with pRCTs and MTSCCs, respectively, whereas none of the 21 nephrogenic rests associated with Wilms' tumour stained (Fig. 1).

WT1 protein was localized exclusively in cells of the glomeruli in foetal and adult kidneys. A strong although in

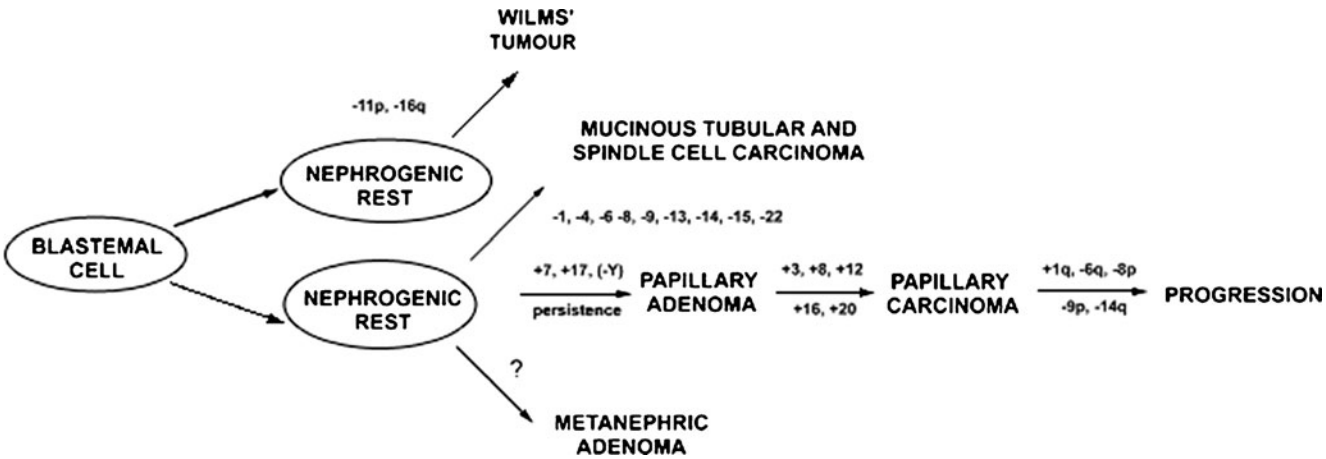

Fig. 2 A model for development of Wilms' tumour and adult kidney tumours from precursor lesions of embryonal origin and their characteristic genetic alterations

some cases only scattered nuclear staining was seen in each of the 17 nephrogenic rests associated with Wilms' tumour (100%), whereas none of the 39 and 5 precursor lesions associated with pRCTs and the MTSCC showed a positive reaction with the WT1 antibody. Examples are shown in Fig. 1.

Discussion

WT recapitulates the embryonal kidney development and may consist of blastemal cells as well as of tubular and papillary structures resembling all parts of the mature tubular system including collecting ducts, and also of glomeruloid bodies [10, 12]. MTSCC, contrary to its official name, shows infrequently mucinous changes. The vast majority of MTSCC cells resemble those of the Henle loop, but sometimes, they differentiate into cells with more abundant cytoplasm corresponding to other parts of the tubulary system or grow in papillary formations [13]. In pRCTs solid, tubulary and papillary structures of small blastema-like cells towards large differentiated cells resembling mature proximal tubular cells may be seen [14]. Metanephric adenomas (MAs) display small tubular structures or sometimes papillary structures of small, undifferentiated blastema-like cells frequently seen in hyperplastic nephrogenic rests and in some areas of Wilms' tumours. Based on the cellular characteristics, it has been suggested that MA may represent a mature, benign counterpart of WT [15]. Thus, Wilms' tumour, MA as well as MTSCC and pRCT display morphological variations corresponding to delayed tubular/glomerular differentiation of blastemal cells, albeit at different degree and cellular direction.

We have analysed the expression of KRT7, KRT8, KRT18, KRT19 and WT1 to characterize the precursor lesions associated with Wilms' tumour, pRCT and MTSCC. As expected, KRT8 and KRT18, characteristic for single-layered epithelia such as the kidney tubulary system, were expressed in normal kidneys and all types of precursor lesions. KRT7 immunostaining was restricted to single cells of distal tubuli in foetal and adult kidneys. The positive staining in some small proliferating tubuli or cell groups in scarred tissue under the renal capsule suggests that KRT7-positive cells may serve as functional stem cells in regenerating kidneys. KRT19, which was expressed in distal tubuli of foetal and adult kidneys, has already been described as putative marker of epidermal stem cells [16]. The coexpression of type II basic cytokeratin KRT7 and type I acidic cytokeratin KRT19 in developing kidneys and in the vast majority of precursor lesions indicates that forming a new type of intermediate filaments by copolymerization may play an important role in the increased plasticity of cells in developing kidneys and precursor lesions.

The WT1 gene, which encodes a transcription factor with four zinc finger DNA-binding motif, shows a variable stage-specific expression in the developing kidney. All precursor lesions of Wilms' tumours expressed the WT1 gene. Of interest, WT1 was negative in hyperplastic nephrogenic rests but positive in surrounding nephrogenic rest. Seven of the eight Wilms' tumours showed diffuse or scattered immunoreactivity for WT1.

We have suggested previously that Wilms' tumour, pRCT and MTSCC may develop from embryonal rests or persisting embryonal rest-like structures [4]. Our recent finding that all nephrogenic rests associated with Wilms' tumour show nuclear immunoreactivity for WT1, but are negative for KRT7 and that precursor lesions for pRCTs and MTSCCs are positive for KRT7 but negative for WT1 indicates that two types of precursor lesions exist corresponding with distinct developmental stages. One is associated with the development of Wilms' tumour and the other with the development of pRCT and MTSCC (Fig. 2). We believe that the two types of precursor lesions are committed at their earlier stage of differentiation to the development of distinct types of tumours, which are then marked by a characteristic although sometimes overlapping phenotype. However, as we indicated in Fig. 2, the genetic changes identify unequivocally each type of tumour [4, 14, 17].

Acknowledgements This study was supported by a grant from the German Research Council.

Conflict of interest Nothing to declare.

References

1. Kovacs G (1989) Papillary renal cell carcinoma: a morphologic and cytogenetic study of 11 cases. Am J Pathol 34:27–34
2. Schmidt L, Duh FM, Chen F, Kishida T, Glenn G, Choyke P et al (1997) Germline and somatic mutations in the tyrosine kinase domain of the MET proto-oncogene in papillary renal carcinomas. Nat Genet 16:68–73
3. Szponar A, Yusenko MV, Kuiper R, van Kessel AG, Kovacs G (2011) Genomic profiling of papillary renal cell tumours identifies small regions of DNA alterations: a possible role of HNF1B in tumour development. Histopathology 58:934–943
4. Szponar A, Zubakov D, Pawlak J, Jauch A, Kovacs G (2009) Three genetic developmental stages of papillary renal cell tumours: duplication of chromosome 1q marks fatal progression. Int J Cancer 124:2071–2076
5. Reuter VE, Tickoo SK (2004) Adult renal tumors. In: Mills SE (ed) Sternberg's diagnostic surgical pathology, 4th edn. Lippincott Williams & Wilkins, Philadelphia, p 1956
6. Skinnider BF, Folpe AL, Hennigar RA, Lim SD, Cohen C, Tamboli P, Young A, de Peralta-Venturina M, Amin MB (2005) Distributions of cytokeratins and vimentin and adult renal neoplasms and normal renal tissue. Potential utility of a cytokeratin antibody panel in the differential diagnosis of renal tumors. Am J Surg Pathol 29:747–754

7. Kovacs G (1993) Molecular cytogenetics of renal cell tumors. Adv Cancer Res 62:89–124
8. Kovacs G, Kovacs A (1993) Parenchymal abnormalities associated with papillary renal cell tumors. J Urol Path 1:301–312
9. Ornstein DK, Lubensky IA, Venzon D, Zbar B, Linehan WM, Walther MM (2000) Prevalence of microscopic tumors in normal appearing renal parenchyma of patients with hereditary papillary renal cancer. J Urol 163:431–433
10. Beckwith JB, Kiviat NB, Bonadio JF (1990) Nephrogenic rests, nephroblastomatosis, and the pathogenesis of Wilms' tumor. Pediatr Pathol 10:1–36
11. Kaneko Y, Homma C, Maseki N, Sakurai M, Hata J (1991) Correlation of chromosome abnormalities with histological and clinical feature in Wilms' and other childhood renal tumors. Cancer Res 51:5937–5942
12. Stupar Z, Chi S, Veszpremi B, Koesters R, Stallmach P, Geng J-G, Kovacs G (2007) Wilms' tumour may develop from impaired differentiation of the ureteric bud as well. Histopathology 51:265–268
13. Rakozy C, Schmahl GE, Bogner S, Störkel S (2002) Low-grade tubular-mucinous renal neoplasms: morphologic, immunohistochemical, and genetic features. Mod Pathol 15:1162–1171
14. Balint I, Szponar A, Jauch A, Kovacs G (2009) Trisomy 7 and 17 mark papillary renal cell tumours irrespectively of variation of the phenotype. J Clin Pathol 62:892–895
15. Henniger RA, Beckwith JB (1992) Nephrogenic adenofibroma. A novel kidney tumor of young people. Am J Surg Pathol 16:325–334
16. Commo S, Gaillard O, Bernard BA (2000) The human hair follicle contains two distinct K19 positive compartments in the outer root sheath: a unifying hypothesis for stem cell reservoir? Differentiation 66:157–164
17. Natrajan R, Williams RD, Hing SN et al (2006) Array CGH profiling of favourable histology Wilms tumours reveals novel gains and losses associated with relapse. J Pathol 210:49–58

Virchows Arch (2012) 460:429–435
DOI 10.1007/s00428-012-1213-3

ORIGINAL ARTICLE

A spectrum of morphologic lesions of focal segmental glomerulosclerosis by Columbia criteria in human immunodeficiency virus infection

Shane M. Meehan · Lisa Kim · Anthony Chang

Received: 10 November 2011 / Revised: 2 February 2012 / Accepted: 16 February 2012 / Published online: 3 March 2012
© Springer-Verlag 2012

Abstract The Columbia working classification of focal segmental glomerulosclerosis (FSGS) identifies five types of glomerular lesions, designated collapsing (COLL), cellular (CELL), glomerular tip lesion (GTL), perihilar (PH), and not otherwise specified (NOS) variant lesions. FSGS COLL and non-collapsing variants of FSGS are described in human immunodeficiency virus (HIV)-associated kidney disease. This study examined the range and relationships of Columbia-type segmental sclerosing lesions in biopsies from patients with HIV infection. We identified 47 renal biopsies from 46 patients with HIV infection obtained over an 8-year period. Twenty-seven biopsies from 26 patients had FSGS. Sixteen biopsies had FSGS COLL (59.3%), 3 had CELL (11.1%), 5 had NOS (18.5%), 2 had PH (7.4%), and 1 had GTL (3.7%) by the Columbia classification. Biopsies had more than one type of Columbia FSGS lesion in 63% and one type in 37%. Single types of FSGS lesions were identified in eight of eight biopsies with ≤10 glomeruli. Combinations of lesions were observed in 17 of 19 (89.5%) with >10 glomeruli, and the coincidence of COLL, CELL, and NOS lesions was not random. NOS, COLL, and CELL morphologic lesions of FSGS frequently coexist in kidney biopsies from HIV+ patients. Combined patterns of FSGS suggest that lesions identified by Columbia criteria may be part of a spectrum of responses to injury in the setting of HIV infection.

Keywords HIV infection · Focal segmental glomerulosclerosis · Collapsing glomerulopathy

S. M. Meehan (✉) · L. Kim · A. Chang
Department of Pathology,
University of Chicago,
5841 South Maryland Ave,
Chicago, IL 60637, USA
e-mail: shane.meehan@uchospitals.edu

Introduction

The Columbia system of classification of focal segmental glomerulosclerosis (FSGS) is a working classification designed to divide a morphologically heterogenous group of primary glomerulopathies into clinically and pathologically meaningful subgroups [1–3]. Five categories of FSGS, designated collapsing (COLL), cellular (CELL), glomerular tip lesion (GTL), perihilar (PH), and not otherwise specified (NOS) variants are defined. These variants are categorized by the recognition of specific morphologic FSGS lesions using defined criteria. However, certain structural FSGS lesions predominate over others for final classification in the Columbia system [1]. COLL preempts other FSGS variants. GTL requires exclusion of COLL; CELL requires exclusion of COLL and GTL lesions; PH requires exclusion of COLL, GTL, and CELL; and NOS requires exclusion of the other four lesions for final Columbia classification.

Prior studies have noted heterogeneity of Columbia structural lesions of FSGS in the same renal biopsy specimen [1, 4]. It is uncertain whether FSGS morphological lesions reflect differences in pathogenesis or severity of injury to the glomeruli or different stages in the histologic evolution of segmental sclerosis [1]. It has been hypothesized that heterogenous FSGS lesions may reflect patterns of injury at particular points in time [5]. The possibility that primary FSGS morphologic lesions described in the Columbia classification are inter-related has been suggested; however, detailed analyses are not available [5–7]. The possibility that differences in clinical outcome may be the result of intervention at different time points in the evolution of a single disease process has not been disproven. In a study that predated the Columbia classification system, cellular lesions of FSGS, most likely a combination of FSGS COLL and CELL, were compared with scarred FSGS lesions [7].

The patients with cellular lesions had shorter duration of the nephrotic syndrome and more severe proteinuria than those with segmental scars. The authors also noted frequent coexistence of cellular and scarred lesions in the same glomeruli or in different glomeruli in the same biopsy specimen.

Studies of the progression of FSGS lesions in serial kidney biopsies are limited. One study of FSGS GTL presented features of serial biopsies from patients treated with steroids or other immunosuppressives [8]. GTL transformed to "multiple" lesions in serial biopsies obtained at intervals of 11 months to more than 12 years. The "multiple" lesions are consistent with CELL or NOS lesions in the Columbia system. A few patients showed regression of GTL lesions with small tuft adhesions at the tubular pole. Another study of GTL described progression to CELL and NOS lesions in serial biopsies of three patients [9]. The findings of these studies suggest a possible histogenetic relationship between GTL and NOS or CELL. Some studies suggest that CELL and GTL lesions are observed in biopsies obtained earlier in the course of disease than those with COLL and NOS lesions [4, 9]. Stokes et al. observed combinations of CELL, GTL, and NOS lesions in earlier biopsies. Biopsies with COLL also had CELL, PH, and NOS lesions and were obtained after patients had been symptomatic for longer periods [9].

Morphologic heterogeneity of glomerular lesions is well recognized in diagnostic renal biopsies. Injured and normal-appearing tissue structures are often encountered side by side, despite a strong likelihood of exposure to similar harbingers of injury. A morphologic spectrum of glomerular lesions may be apparent in some biopsy samples. To explore the heterogeneity of FSGS, we studied the spectrum of structural FSGS lesions, as defined in the Columbia system [1], in biopsies from patients with human immunodeficiency virus (HIV) infection, with and without classical lesions of HIV-associated nephropathy [10].

Materials and methods

Pathology files from 2003 to 2010 were searched for kidney biopsies from patients with HIV infection. Infection was verified by identification of anti-HIV 1 or 2 antibodies by enzyme immunoassay or Western blot assay, and by identification of HIV DNA in plasma by polymerase chain reaction assay. Clinical and laboratory data were collected retrospectively from medical records.

Two-micron paraffin sections, numbering 18 to more than 30, were stained using hematoxylin and eosin, periodic acid–Schiff, and Jones methenamine silver methods. Sections were examined by light and electron microscopy. Direct immunofluorescence staining for IgG, IgA, IgM, C3, C1q, kappa and lambda light chains, and fibrinogen was performed in each instance (rabbit polyclonal antibodies, dilution 1:20 for each; Dako, Carpinteria, CA, USA). For electron microscopy, tissue was fixed in 2.5% glutaraldehyde in 0.1% Millonig's phosphate buffer, washed and post-fixed in 1% osmium tetroxide, dehydrated, and mounted in Epon resin. Ultrathin sections were stained on copper palladium grids using uranyl acetate and lead citrate. Stained sections were viewed and photographed using a Phillips CM-10 transmission electron microscope (Phillips Systems, Andover, MA, USA).

Forty-seven kidney biopsies were obtained from 46 HIV+ patients over an 8-year period (2003–2010). The biopsy diagnoses are given in Table 1. Twenty-seven biopsies from 26 patients had FSGS. All of these biopsies were evaluated for the presence of morphologic types of FSGS. Five categories of FSGS, designated COLL, CELL, GTL, PH, and NOS variants are defined in the Columbia system [1]. COLL is characterized by segmental or global collapse of the glomerular tuft, wrinkling of the glomerular basement membrane, hypertrophy, and hyperplasia of the podocytes. CELL is characterized by endocapillary hypercellularity with capillary luminal occlusion, foam cells, and karyorrhexis, involving at least 25% of the glomerular tuft. Lesions may affect any segment of the glomerular tuft and may be associated with hypertrophy and hyperplasia of the podocytes. GTL lesions are characterized by segmental hypercellularity or sclerosis involving the outer 25% of the glomerular tuft, with or without adhesions, adjacent to the tubular pole. PH lesions are characterized by perihilar hyalinosis or sclerosis in more than 50% of glomeruli with FSGS lesions, with or without segmental adhesions and glomerulomegaly. NOS lesions are characterized by segmental consolidation of the tuft by increased extracellular

Table 1 Diagnoses in kidney biopsies from HIV+ patients

Diagnosis	*N*
Focal segmental glomerulosclerosis	
-Collapsing	16
-Cellular	3
-Glomerular tip lesion	1
-Not otherwise specified (NOS)	5
-Perihilar	2
IgA nephropathy	3
Membranoproliferative GN	1
Immune complex GN, NOS	2
Tubulointerstitial nephritis	4
Acute tubular necrosis or injury	1
Diabetic nephropathy	3
Arterionephrosclerosis	3
End stage kidney disease, NOS	3
Total	47

matrix with capillary obliteration and segmental capillary wall collapse without podocyte hyperplasia.

The average age at biopsy was 39 years (range, 16–57 years). The group had 10 females and 16 males. Twenty-one patients were African–American, 4 were Caucasian, and 2 were Hispanic. The median serum creatinine at biopsy was 3.8 mg/dl (range, 0.9–14 mg/dl). Daily urinary protein excretion had a median value of 5.3 g/24 h (range, 0.5–20 g/24 h). The salient clinical findings are summarized in Table 2. All patients with FSGS COLL were African–American (16 of 21 AA patients in the study group). Patients had known HIV infection for months to years before the index kidney biopsies were obtained. Nine patients had received antiviral agents from months to years before the biopsy.

To investigate interobserver reproducibility of FSGS classification, three pathologists evaluated photographic images of 23 lesions from the study biopsies. The images consisted of representative lesions stained by standard periodic acid–Schiff or Jones methenamine silver methods. Photographic images were chosen for this portion of the study to ensure that each observer classified the same data set. The kappa statistic was calculated as a measure of interobserver reproducibility of Columbia structural FSGS lesions. Comparisons between groups were made using the Mann–Whitney *U* test, and odds ratios were determined using the Fisher exact test.

Results

Twenty-seven biopsies from 26 patients had glomerular morphologic lesions of FSGS (Fig. 1). The biopsies with FSGS had a mean of 15.8 glomeruli (range, 3–34). FSGS lesions were observed in an average of 35.4% of glomeruli (range, 9.4–94.4%) and global glomerular sclerosis in an average of 23.6% of the glomeruli (5 with 0% and 22 with a range of 5.6–68.8%).

Columbia variants of FSGS in HIV-positive patients

Using predefined criteria, we determined kappa values for interobserver reproducibility of Columbia morphologic lesions of FSGS. Multirater kappa values were 0.65 between individuals. Agreement between 3 observers occurred in 13 (56.5%). Two of three observers agreed in 21 of 23 examples (91.3%). Greatest disagreement related to classification of CELL, COLL, and NOS FSGS in 10 examples. Disagreement occurred in distinction of COLL v NOS (n=4, 40%), COLL v CELL (n=3, 30%), CELL v NOS (n=2, 20%), and in COLL v CELL v NOS (n=1, 10%). After consensus was reached, it was determined that 27 biopsies with FSGS had lesions classifiable as Columbia categories COLL (n=16, 59.3%), CELL (n=3, 11.1%), GTL (n=1, 3.7%), NOS (n=5, 18.5%), and PH (n=2, 7.4%).

Additional pathologic findings are summarized in Table 3. Glomeruli also had segmental or global capillary collapse without visceral epithelial hyperplasia in 10 and mild mesangial hyperplasia in 9 biopsies with COLL. Acute tubular injury was evident in 23, tubulointerstitial nephritis in 19, and tubular microcysts in 16 biopsies. One case with COLL had subepithelial and mesangial immune deposits containing IgG and C3, consistent with membranous glomerulopathy, and five had mesangial IgM and C3 deposits. One of three biopsies with FSGS CELL had mesangial IgA deposits, consistent with mesangial IgA nephropathy. One biopsy with FSGS NOS had diffuse mesangial sclerosis with focal nodular mesangial sclerosis, consistent with diabetic glomerulopathy. Biopsies with FSGS COLL had moderate or severe arterial or arteriolar sclerosis in 6 of 16, compared with 5 of 11 biopsies with non-collapsing FSGS, p=0.7. Mesangial IgM and C3 deposits were evident by immunofluorescence microscopy in two of five with FSGS NOS and in one of two with FSGS PH. Electron microscopy was performed on 26 biopsies. Nineteen of 26 biopsies had endothelial tubuloreticular inclusions in glomeruli. Twenty five of 26 had effacement of the podocytes (19 global and 6 segmental). Six patients were known to have received highly active antiretroviral therapy before the index biopsies; however, no differences in morphology were apparent in these biopsies.

Table 4 shows the proportions of FSGS morphologic lesions by Columbia criteria in the biopsy cohort (n=27). Involvement of 50% or less of the glomeruli by segmental sclerosis was seen in 20 biopsies, and 7 biopsies had >50% of glomeruli with such lesions. The mean proportion of

Table 2 Clinical findings in HIV+ patients with FSGS (n=26)

FSGS type	*N*	Age (years)	Gender	Race	Antiviral Rx	Serum Cr (mg/dl)	Proteinuria (g/day)
COLL	16	37.4 (24–57)	7 F:9 M	16 AA	4	7.5 (2.3–14)	7.3 (2.8–10.8)
CELL	3	44.3 (31–52)	0 F:3 M	2 AA, 1 H	1	3.1 (1.6–6)	7.1 (0.5–15)
GTL	1	39	1 F:0 M	1 C	1	1.4	2.5
NOS	4	38 (15–48)	1 F:3 M	3 AA, 1 C	2	1.6 (0.9–2.2)	7 (2–20)
PH	2	41, 43	1 F:1 M	1 C, 1 H	1	1.4, 2	3, 20

F female, *M* male, *AA* African–American, *H* Hispanic, *C* Caucasian

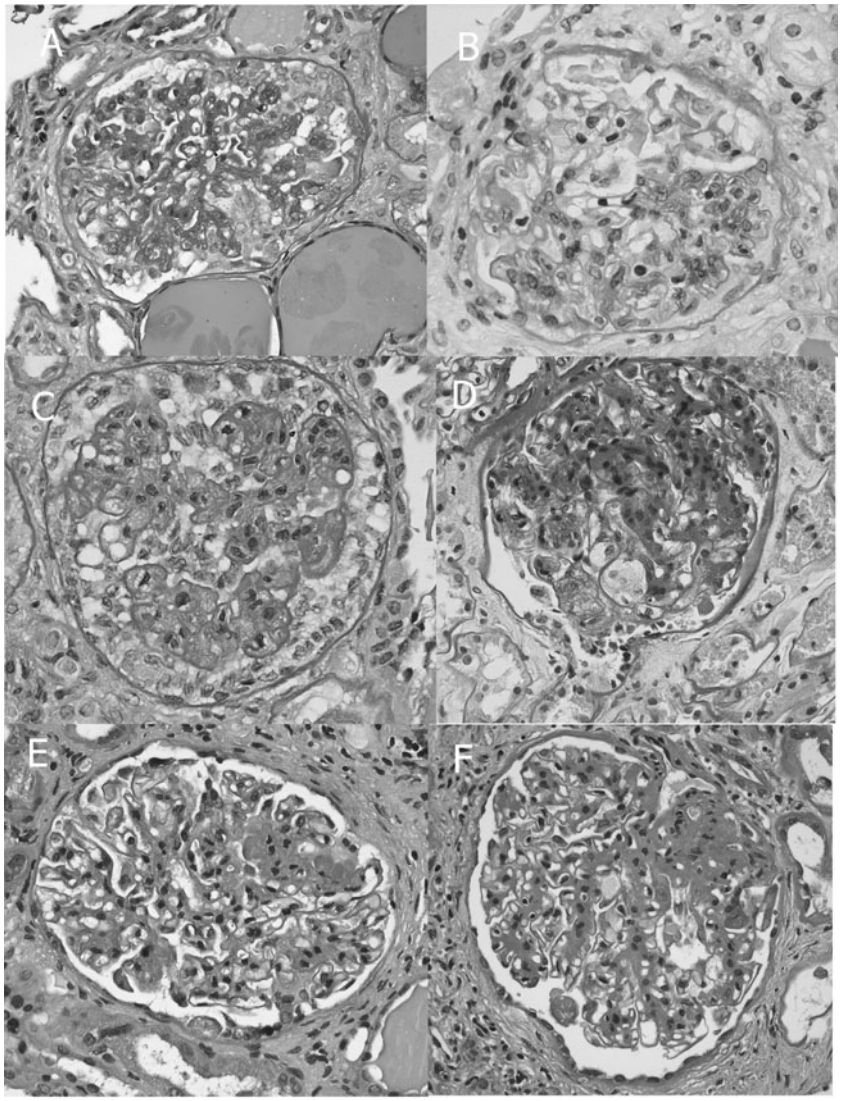

Fig. 1 Morphologic spectrum of glomerular lesions in biopsies from HIV+ patients. **a** Collapsing glomerulopathy with capillary collapse and visceral epithelial hyperplasia affecting mainly the right side of the tuft. **b** Cellular FSGS affecting the tuft segment at 3 o′ clock. This was not associated with the opening of the proximal tubule and is thus distinguished from the tip lesion. **c** Another example of a cellular lesion with endocapillary hypercellularity, increased matrix, and prominence of the visceral and parietal epithelium. The presence of endocapillary hypercellularity helps distinguish this from the collapsing lesion. **d** Glomerular tip lesion with foam cell accumulation and mesangial hypercellularity. **e** FSGS not otherwise specified with segmental solidification, hyalinization, podocyte bridging, and periglomerular fibrosis. **f** Perihilar segmental sclerosis, with adhesion, mesangial sclerosis, and mild hypercellularity

glomeruli with COLL lesions exceeded the proportion with NOS by a factor of 2.6 and exceeded the proportion with CELL by a factor 7.25. CELL was evident in <20% of glomeruli and NOS in <50% of glomeruli in any sample.

Table 5 outlines the frequency of single and mixed FSGS lesions in each biopsy for the entire cohort.

Ten biopsies (37%) had only one type of FSGS lesion, and 17 (63%) had more than one Columbia FSGS lesion.

Table 3 Summary of additional pathologic findings in biopsies from HIV+ patients with FSGS (n=27)

FSGS type	*N*	IF	EM		Tubulointerstitial and vascular lesions				
			TRI	FPE	TMC	TIN	Fibrosis	TA	As/Aos
COLL	16	1 cw IgG 5 mes IgM+C3	13	13 glob 1 seg	11	14	10	10	10
CELL	3	1 mes IgA	3	3 glob	3	2	3	3	3
GTL	1	Negative	0	1 glob	0	0	0	0	1
NOS	5	2 mes IgM+C3	1	5 seg	1	2	3	2	4
PH	2	1 mes IgM+C3	1	2 glob	1	1	1	1	2

IF immunofluorescence, *EM* electron microscopy, *cw* capillary wall, *mes* mesangium, *TRI* tubuloreticular inclusions, *FPE* foot process effacement, *TMC* tubular microcysts, *TIN* tubulointerstitial nephritis, *Fibrosis* interstitial fibrosis, *TA* tubular atrophy, *As* arteriosclerosis, *Aos* arteriolosclerosis, *seg* segmental, *glob* global

Table 4 Proportions of glomeruli with FSGS lesions by Columbia categories

FSGS type	*N*	Total glomeruli	GGS %	COLL %	CELL %	GTL %	NOS %	PH %
COLL	16	18	25	29	4	0	11	1
		3–34	0–69	3–94	0–19	0	0–47	0–9
CELL	3	24	38	0	4	0	15	3
		18–30	11–65	0	3–6	0	7–22	0–9
GTL	1	13	15.4	0	7.7	7.7	0	0
NOS	5	8	14.3	0	0	0	33.3	1.8
		3–14	0–44	0	0	0	13–44	0–7
PH	2	5.5	12.5	0	0	0	0	29.1
		3–8	0–25	0	0	0	0	25–33

Values given as mean and range

GGS global glomerular sclerosis

Biopsies with single FSGS lesions had fewer glomeruli (median single lesions, 8.2, v mixed lesions, 20.2, $p=0.0003$). Eight of 8 biopsies with 10 glomeruli or less had single types of FSGS lesions, compared with only 2 of 19 biopsies (10.5%) with more than 10 glomeruli, $p=0.00005$. If biopsies with 10 glomeruli or less are arbitrarily excluded, on the basis of limited sample size, the odds of finding a single type of FSGS decreases to 0.105 (2 of 19), and the odds of finding mixed lesions increases to 0.895 (17 of 19).

Heterogeneity of FSGS in biopsy samples with more than 10 glomeruli

In the group with more than 10 glomeruli (range, 11–34 glomeruli; $n=19$ biopsies), 14 had COLL, 3 had CELL, and 1 each had GTL and NOS variants by the Columbia system. FSGS COLL had tubular microcysts in 9, tubulointerstitial nephritis and acute tubular injury in 14, diffuse podocyte effacement in 12 (of 13 with data), and endothelial tubuloreticular inclusions in 12. Non-collapsing FSGS ($n=5$) had tubular microcysts in three, tubular injury and inflammation in four, diffuse podocyte effacement in four, and tubuloreticular inclusions in three.

Table 6 describes the frequency of association of morphologic FSGS lesions with each other and with other FSGS types in these 19 biopsies. The diagonal is the frequency of occurrence of only a single type of FSGS lesion. Two biopsies had diffuse COLL only. The value predicted for each cell of the diagonal in Table 6 is given by $n(\text{row})\times n(\text{column})/N$ (sum of the rows or columns, which are equal). The expected value of 18.9 (27%) is significantly greater than the observed value of 2 (1%), $p<0.0001$.

Of 17 biopsies with mixed lesions, 10 (58.8%) had NOS + COLL, 8 (47%) had NOS + CELL, and 5 (26.3%) had NOS + COLL + CELL. Eleven of 14 with COLL (78.6%) and 3 of 3 with CELL (100%) had at least one glomerulus with an NOS FSGS lesion in the same biopsy. Twelve of 14 COLL (85.7%) had more than one FSGS lesion. Eleven of 12 with mixed types of FSGS had COLL + NOS (91.7%). Six of 12 had COLL + CELL (50%), and 4 of these 6 had COLL + CELL + NOS.

To determine the significance of the associations, we compared the observed and expected frequencies of FSGS lesions in the group with more than 10 glomeruli. COLL FSGS lesions were evident in 83 (22.1%), CELL in 16 (4.25%), GTL in 1 (0.3%), NOS in 42 (11.2%), and PH in 5 (1.3%) of this sample of glomeruli ($n=376$) from 19 biopsies. The expected random frequency of coincidence of FSGS lesions, assuming independence, for COLL and CELL is 9%, COLL and NOS 24%, and CELL and NOS 5% in a theoretical sample of 19 biopsies, each with 20 glomeruli. These values are significantly less than the observed respective values of 32% (6 of 19), 53% (10 of 19), and 42% (8 of 19) in the study group, $p<0.0001$. The expected random coincidence of COLL + CELL + NOS is 1%, significantly less than the observed value of 26.3% (5 of 19), $p<0.0001$.

Table 5 FSGS lesions in each Columbia category

Columbia FSGS type	FSGS lesions		Mixed lesions		
	1 type	>1 type			
COLL	4	12	NOS (66.7%)	CELL (41.6%)	PH (13.3%)
CELL	0	3	NOS (100%)	PH (25%)	
GTL	0	1	CELL (100%)		
NOS	4	1	PH (25%)		
PH	2	0			

Table 6 Matrix of association of Columbia morphologic FSGS types (n=19)

FSGS types	N'	Biopsies with FSGS morphologic subtypes (# (%))				
		COLL	CELL	GTL	NOS	PH
COLL	14	2 (14)	6 (43)	0 (0)	11 (78.6)	2 (14)
CELL	10	6 (0)	0 (0)	1 (10)	8 (80)	2 (20)
GTL	1	0 (0)	1 (100)	0 (0)	0 (0)	0 (0)
NOS	15	11 (73)	8 (53)	0 (0)	0 (0)	4 (27)
PH	4	2(50)	2(50)	0 (0)	4 (100)	0 (0)

N' number of biopsies with Columbia morphologic FSGS lesion in 1 or more glomeruli from 19 biopsy samples with more than 10 glomeruli. Numbers expected in diagonal by chance=n(row)×n(col)/N row or column total=18.9/70 (0.27) v observed 2/70 (0.03), p<0.0001

Discussion

The Columbia classification system describes morphologic criteria for different types of lesions of FSGS and recognizes that considerable variation of FSGS lesions may exist between glomeruli in the same biopsy [1–4]. The biologic meaning of heterogeneity of Columbia FSGS lesions is unknown, and the determination of the frequency of association of these lesions is central to this study. FSGS of each variant recognized in the Columbia system was evident in our cohort of HIV+ patients, the most frequent, COLL, and the least frequent, GTL. Adequate sampling of the glomerular population affects classification of glomerular diseases in general [11], and it is hardly surprising that the smaller biopsy samples in our series yielded only one type of FSGS lesion, whereas multiple lesions were observed in larger samples. This observation suggests that in most instances, single lesion types are the result of sampling error. Larger samples had mixed FSGS lesions in nearly 90% of instances. Only two biopsies with larger samples of glomeruli had diffuse collapsing FSGS, without other types of FSGS lesions. Mixed FSGS lesions were observed with greater frequency than expected by chance, since most FSGS lesions, with the exception of COLL, were uncommonly present in the pooled total glomerular population. COLL, CELL, and NOS were most commonly associated. The association of COLL and NOS was frequent, and biopsies with COLL and CELL frequently had NOS lesions in the same sample. Other studies have described collapsing and non-collapsing FSGS in biopsies of HIV+ patients [12, 13]. One study described the non-collapsing FSGS as FSGS NOS [12]. The details of interglomerular heterogeneity in these biopsy cohorts were not described.

It has been suggested that there are at least three possible explanations of the observed concurrence of different FSGS morphologic lesions [1, 7]. The first is sequential injury where cellular lesions (i.e., COLL, CELL, or GTL) evolve to segmental and global glomerular scars (i.e., NOS and global sclerosis). Alternatively, cellular and sclerosing FSGS lesions may be part of a spectrum of responses to glomerular injury caused by the same mechanism, with scars representing a response to more severe glomerular injury. The process of development of scars is uncertain by this hypothesis; however, cellular lesions could possibly resolve with healing, and scars remain. This could partially explain the development of NOS lesions but leaves their relationship to cellular lesions unexplained. The third possibility is that the lesions are non-specific responses to injury, caused by unrelated mechanisms, and their coincidence in biopsies may reflect a limited range of responses of the glomerulus to injury. Non-random combinations of COLL, CELL, and NOS in HIV+ kidneys in this study support the idea of a spectrum or sequence of injury. Our observation of non-random association of these FSGS lesions argues against the possibility of a non-specific response to injury, given the low probability of chance association.

Variation in identification of FSGS lesions could contribute to lesional heterogeneity and can be subjective or objective. Subjective variation is the different interpretation of the same morphologic features by different observers, so features such as hypercellularity, capillary collapse, and sclerosis may be interpreted differently by different observers and give rise to diagnostic discrepancies. Objective variation is the application of different criteria for identification of a histologic lesion, leading to different conclusions by different observers [14]. Interpretive variation of these types may complicate identification and quantification of FSGS lesions. Discrepancies in classification of FSGS lesions in this study were most common in the categories with the highest degree of observed association (i.e., COLL, CELL, and NOS). The difficulty in distinction of these lesions may reflect objective and/or subjective variation in interpretation or perhaps a seamless transformation from one morphologic type to another, making clear discrimination of lesions by light microscopy problematic in some instances. If indeed there is seamless transformation of these lesions, this would argue in favor of phases in the evolution of FSGS lesions. We attempted to minimize objective variation by strict adherence to morphologic criteria outlined in the Columbia working classification [1].

The heterogenous pattern of FSGS lesions observed in this and other studies of HIV-infected patients [12, 13] suggests a histopathogenetic spectrum of injury in this disease. It seems apparent that FSGS NOS is a common pathway to development of global glomerular sclerosis. The frequent concurrence of Columbia FSGS morphologic lesions in biopsy samples in HIV infection indicates a non-random association of these lesions; however, our data do not give insight to the biologic nature of this association.

These lesions may represent related or unrelated morphologic stages, or a spectrum of injury, in the evolution of glomerular sclerosis in this form of secondary FSGS.

Conflict of interest We declare that we have no conflict of interest.

References

1. D'Agati VD, Fogo AB, Bruijn JA, Jennette JC (2004) Pathologic classification of focal segmental glomerulosclerosis: a working proposal. Am J Kidney Dis 43:368–382
2. D'Agati VD (2003) Pathologic classification of focal segmental glomerulosclerosis. Semin Nephrol 23:117–134
3. D'Agati VD (1994) The many masks of focal segmental glomerulosclerosis. Kidney Int 46:1223–1241
4. Stokes MB, Valeri AM, Markowitz GS, D'Agati VD (2006) Cellular focal segmental glomerulosclerosis: clinical and pathologic features. Kidney Int 70:1783–1792
5. Pollack MR (2003) Inherited podocytopathies: FSGS and nephrotic syndrome from a genetic viewpoint. J Am Soc Nephrol 13:3016–3023
6. Meyrier A (2005) Mechanisms of disease: focal segmental glomerulosclerosis. Nature Clin Pract 1:44–54
7. Schwartz MM, Lewis EJ (1985) Focal segmental glomerular sclerosis: the cellular lesion. Kidney Int 28:968–974
8. Howie AJ, Pankhurst T, Sarioglu S, Turhan N, Adu D (2005) Evolution of nephrotic associated focal segmental glomerulosclerosis and relation to the glomerular tip lesion. Kidney Int 67:987–1001
9. Stokes MB, Markowitz G, Lin J, Valeri AM, D'Agati VD (2004) Glomerular tip lesion: a distinct entity within the minimal change disease/focal segmental glomerulosclerosis disease spectrum. Kidney Int 65:1690–1702
10. D'Agati VD, Suh J-L, Carbone L, Cheng J-T, Appel G (1989) Pathology of HIV-associated nephropathy: a detailed morphologic and comparative study. Kidney Int 35:1358–1370
11. Corwin HL, Schwartz MM, Lewis EJ (1988) The importance of sample size in the interpretation of the renal biopsy. Am J Nephrol 8:85–89
12. Nebuloni M, Barbiano di Belgioso G, Genderini A, Tosoni A, Landriana N, Hidempergher M, Zerbi P, Vago L (2009) Glomerular lesions in HIV positive patients: a 20 year biopsy experience from Northern Italy. Clin Nephrol 72:38–45
13. Berliner AR, Fine DM, Lucas GM, Hazifur Rahman M, Racusen LC, Scheel PJ, Atta MG (2008) Observations on a cohort of HIV infected patients undergoing native renal biopsy. Am J Nephrol 28:478–486
14. Latour M, Amin MB, Billis A, Egevad L, Grignon DJ, Humphrey PA, Reuter VE, Sakr WA, Srigley JR, Wheeler TM, Yang XJ, Epstein JI (2008) Grading of invasive cribriform carcinoma on prostate needle biopsy. Am J Surg Pathol 32:1532–1539

Virchows Arch (2012) 460:437–438
DOI 10.1007/s00428-012-1218-y

LETTER TO THE EDITOR

Urinary bladder chondroma

Carmen M. Perrino · Kamal S. Pohar · Debra L. Zynger

Received: 10 February 2012 / Accepted: 22 February 2012 / Published online: 7 March 2012
© Springer-Verlag 2012

Dear Editor,

Soft tissue chondromas are rare tumors that most often occur in the fingers, less commonly in the hands and feet, and rarely in other areas of the body [1]. There has been one previously reported extraskeletal chondroma of the urinary bladder, which occurred in a patient with no prior urologic history [2].

A 62-year-old female presented with dysuria, frequency, nocturia, lower abdominal pain, and constipation that had been worsening over the past 4 years. Cystoscopy showed patchy inflammation and erythema, especially pronounced caudad to the right ureteral orifice. Bladder biopsy demonstrated microinvasive high-grade urothelial carcinoma. Cystoscopy with transurethral resection was performed 1.5 months after diagnosis. The prior biopsy site was visualized and resected. In addition, a solid, subepithelial 3-cm mass inconsistent with urothelial carcinoma was seen on the anterior bladder wall. Microscopic examination of the mass revealed a well-circumscribed nodule of mature hyaline cartilage within the lamina propria, surrounded by dense fibrous tissue (Fig. 1a) characterized by sparse, bland-appearing, single cells in the lacunae on a smooth, pale blue, myxoid background with rare calcifications (Fig. 1b). The lesion immunohistochemically expressed S100 (Fig. 1c) and vimentin but was negative for AE1/3, p53, and Ki-67. No urothelial tumor was present. After transurethral resection, the patient completed 6 weeks of intravesical instillation induction Bacillus Calmette–Guerin chemotherapy followed by cystoscopy that failed to demonstrate recurrent tumor.

The bladder chondroma we have described is the second case in the literature. The first published bladder chondroma occurred in a 63-year-old female without previous urologic complaints who presented with pain in her left iliac fossa [2]. Cystoscopy identified a submucosal mass on the ventral dome of the bladder that was treated with transurethral resection [2]. The histologic and immunohistochemical features were similar to our findings with bland, mature hyaline cartilage positive for S100 and vimentin and negative using AE1/3, p53, and Ki-67 [2]. Our case is unique because the bladder chondroma was diagnosed in a patient with a recent diagnosis of high-grade urothelial carcinoma. It is

C. M. Perrino · D. L. Zynger (✉)
Department of Pathology,
The Ohio State University Medical Center,
E-401 Doan Hall, 410 W 10th Ave,
Columbus, OH 43210, USA
e-mail: debra.zynger@osumc.edu

K. S. Pohar
Department of Urology,
The Ohio State University Medical Center,
E-401 Doan Hall, 410 W 10th Ave,
Columbus, OH 43210, USA

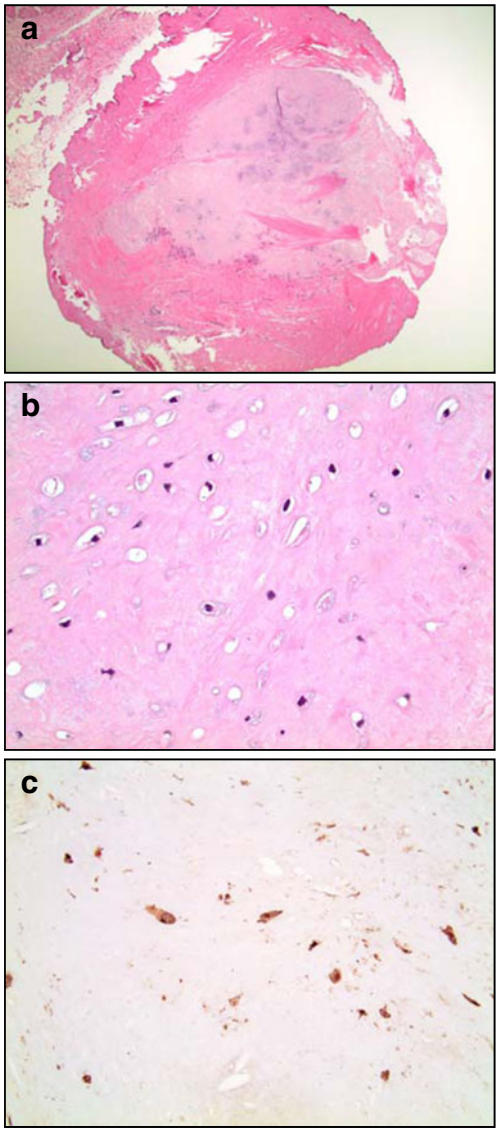

Fig. 1 **a** A well-circumscribed nodule consisting of mature hyaline cartilage surrounded by fibrous tissue embedded in the lamina propria of the bladder (×4). **b** Bland-appearing cells in the lacunae are evident on a pale blue, myxoid background (×40). **c** Diffuse positivity for S100 immunohistochemical stain (×20)

interesting to note that both patients were female and of similar age, although it is not possible to make conclusions regarding demographics as only two patients have been reported.

The origin of extraskeletal chondromas as a clonal neoplasm versus a reactive process has been debated. Cytogenetic analysis of extraskeletal chondromas has identified various chromosomal abnormalities including monosomy of 6, rearrangement of 11, trisomy 11, and translocations of X [3–5]. However, there is still controversy due to the small number of demonstrated clonal abnormalities, the lack of consistent genetic findings, and the fact that several chondromas were not found to have a clonal mutation [4]. In addition to chondroma, there are rare reports of chondrosarcoma within the bladder with the relationship between these two entities currently unknown.

Pathologists should be aware that bladder chondroma is a possible diagnostic entity for a subepithelial chondroid mass. Further cases of bladder chondroma will need to be studied to understand the context in which they occur.

References

1. Nayler S, Heim S (2002) Soft tissue chondroma. In: Fletcher CDM, Unni KK, Mertens F (eds) Pathology and genetics of tumours of soft tissue and bone. IARC Press, Lyon, pp 180–181
2. Pauwels CF, Van den Broecke C, Demeyer JM, De Potter CR (1998) Chondroma of the bladder. Virchows Arch 432:299–300
3. Cin PD, Qi H, Sciot R, Van Den Berghe H (1991) Involvement of chromosomes 6 and 11 in a soft tissue chondroma. Cancer Genet Cytogenet 93:177–178
4. Mandahl N, Heim S, Arheden K, Rydholm A, Willen H, Mitelman F (1990) Chromosomal rearrangements in chondromatous tumors. Cancer 65:242–248
5. Teyssier JR (1987) Nonrandom chromosomal changes in human solid tumors: application of an improved culture method. J Natl Cancer Inst 79:1189–1198

Virchows Arch (2012) 460:439–446
DOI 10.1007/s00428-012-1220-4

ORIGINAL ARTICLE

E2F-1 is overexpressed and pro-apoptotic in human hepatocellular carcinoma

Marina Palaiologou · John Koskinas · Menelaos Karanikolas · Evangelia Fatourou · Dina G. Tiniakos

Received: 18 September 2011 / Revised: 30 January 2012 / Accepted: 27 February 2012 / Published online: 27 March 2012
© Springer-Verlag 2012

Abstract E2F-1 is a transcription factor involved in DNA synthesis and repair, cell proliferation, and apoptosis. Hyposphorylated pRb represses E2F-1 action in early G1 phase, while in late G1, pRb hyperphosphorylation leads to E2F-1 release and activation. In vitro studies have shown that E2F-1 may act either as oncogene or as tumor suppressor gene. We evaluated immunohistochemical expression of E2F-1 protein in chronic viral liver disease and hepatocellular carcinoma (HCC) and correlated this with clinicopathological parameters, cell proliferation, apoptosis, and the expression of E2F-1-regulators, pRb, and phospho-pRb (Ser795). In liver biopsies from 30 patients with chronic viral hepatitis, including 22 with cirrhosis without HCC, and 57 with cirrhosis with HCC, E2F-1 expression was assessed by immunohistochemistry. In chronic hepatitis and cirrhosis, hepatocytes and cholangiocytes demonstrated mild cytoplasmic and/or nuclear membrane E2F-1 immunostaining. In contrast, all HCC (100%) showed strong nuclear E2F-1 immunostaining, with or without membrane accentuation, while a minority demonstrated additional moderate cytoplasmic immunostaining. Abnormally low pRb and phospho-pRb expression was seen in 70% and 67.9% of HCC, respectively. In HCC, nuclear E2F-1 expression was inversely correlated with phospho-pRb expression ($p=0.001$) and positively related to tumor apoptotic index ($p=0.025$). No significant correlation was found between E2F-1 expression and patient demographics, HCC etiology, tumor grade, pRb, p53 expression, or cell proliferation. In conclusion, we show that the increased expression of E2F-1 protein in human HCC is correlated with enhanced tumor cell apoptosis supporting a pro-apoptotic role of E2F-1 in human HCC.

Keywords Hepatocellular carcinoma · E2F-1 · pRb · Phospho(Ser795)-pRb · Apoptosis

M. Palaiologou, BSc, and Dr. J. Koskinas, MD, PhD, contributed equally to this work.

Electronic supplementary material The online version of this article (doi:10.1007/s00428-012-1220-4) contains supplementary material, which is available to authorized users.

M. Palaiologou · D. G. Tiniakos (✉)
Laboratory of Histology and Embryology, Medical School,
National and Kapodistrian University of Athens,
75 M. Asias str, Goudi,
Athens 11527, Greece
e-mail: dtiniak@med.uoa.gr

J. Koskinas
2nd Academic Department of Internal Medicine,
Hippokration General Hospital, Medical School,
National and Kapodistrian University of Athens,
Athens, Greece

M. Karanikolas
Department of Anesthesiology,
Washington University School of Medicine,
Saint Louis, MO, USA

E. Fatourou
Liver Transplant Unit, King's College Hospital,
London, UK

Introduction

Hepatocellular carcinoma (HCC) is the sixth most common cancer globally and the third leading cause of cancer death [1, 2]. The major risk factors for HCC development are chronic hepatitis B virus (HBV) and hepatitis C virus (HCV) infections, as they are implicated in 80% of HCC cases worldwide, while the remainder 20% are attributed to alcohol abuse, dietary

aflatoxin, nonalcoholic fatty liver disease, hemochromatosis, and other metabolic disorders [2]. The mechanisms underlying malignant transformation of HBV-infected or HCV-infected hepatocytes have not yet been fully clarified [3]. However, deregulation of cell cycle control is involved in the multistep process of hepatocarcinogenesis [4, 5]. In chronic viral hepatitis B and C, there is a loss of balance between cell survival and cell death, and during hepatocarcinogenesis, this confers autonomy from regulatory signals to the neoplastic cell [4].

Pathways governing the transition from G1-phase to S-phase of the cell cycle are frequent targets of carcinogenic events. A key regulator for the G1-phase to S-phase transition is the transcription factor E2F-1 [5, 6]. E2F-1 induces expression of a wide spectrum of genes implicated in a variety of cellular functions such as cell cycle control, DNA replication, apoptosis, and DNA damage response [7]. Hyposphorylated Rb protein (pRb) represses E2F-1 action in early G1 phase by binding to it. In late G1phase, phosphorylation of pRb (phospho-pRb) on serine residues (Ser375, Ser795, etc.) induced by cyclin-dependent kinase (CDK)4/CDK6–cyclin D and CDK2–cyclin E complexes, releases E2F-1 from pRb, which activates it [6].

In vitro and in vivo studies in mouse models have shown that E2F-1 may have a dual behavior acting either as an oncogene, promoting cell proliferation or as a tumor suppressor gene, promoting apoptosis [6, 7]. In human malignancies, E2F-1 is equally pleiotropic, its actual function depending on the specific cellular context: oncogene in some tumors, i.e., nonsmall cell lung carcinoma and tumor suppressor in other tumors, i.e., colonic adenocarcinoma [8, 9].

Few reports have been published regarding E2F-1 expression in HCC. In a transgenic mouse model, in which E2F-1 was overexpressed in the liver, it displayed both oncogenic and tumor-suppressive properties [10]. The oncogenic activity of E2F-1 was most evident during the preneoplastic stages and was reflected in early increase of cell proliferative activity. However, in this model, slow but persistant escalation of apoptotic cell death converted E2F-1 from a positive to a negative regulator of tumor growth, leading to a delay of malignant transformation [10]. E2F-1 has also been shown to inhibit c-*myc*-initiated apoptosis, indicating that it may act as an anti-apoptotic factor in human and rodent HCC [11]. In human HCC increased E2F-1 mRNA and protein expression has been reported [12, 13]. To the best of our knowledge, whether E2F-1 is oncogenic or tumor suppressing in human HCC has not been elucidated as yet.

To clarify the role of E2F-1 in human hepatocarcinogenesis, we examined E2F-1 expression by immunohistochemistry in chronic viral hepatitis and HCC and assessed its relationship to clinicopathological parameters, tumor cell proliferation, and apoptosis. Furthermore, since pRb and p53 pathways are known to affect E2F-1 activity, the results were correlated with the expression of pRb/phospho-pRb and p53.

Materials and methods

Liver specimens

Liver needle biopsies from 30 patients with chronic viral (HBV or HCV) hepatitis (including 22 with cirrhosis but without HCC) and from 57 patients with cirrhosis and HCC, followed up according established protocols at "Hippocration" General Hospital (Athens, Greece), were used in this study. Table 1 shows patients' demographics and pathological data. In six patients with presumed HCC, directed biopsies were obtained both from the suspected nodule seen on imaging and from liver tissue distant from the nodule. None of the patients had a history of alcohol consumption and all were HIV-negative. Normal adult liver tissue ($n=5$) from surgical specimens of hepatic resection for benign tumors was also assessed for E2F-1 expression. The study was performed in accordance with National Bioethical Standards and ethical standards of the revised Helsinki Declaration of World Medical Association (2000). Appropriate consent for use of anonymised archival tissue for research was obtained in each case.

Histological diagnosis of cirrhosis and HCC was based on universally accepted criteria [14, 15]. Chronic hepatitis lesions were graded for necroinflammatory activity and staged for fibrosis using Ishak's scoring system [16]. HCC were graded according to nuclear features of tumor cells using a four-tier system (I–IV) [17].

Immunohistochemistry

Tissue E2F-1 expression was evaluated by immunohistochemistry. To indirectly assess the activity of E2F-1 in HCC samples, we also examined by immunohistochemistry the expression of its regulator proteins pRb and phospho-pRb. Apoptosis of neoplastic hepatocytes was assessed by using a caspase-cleaved keratin 18 fragment (neoepitope M30)-specific antibody. Ki-67 labeling index (LI) and p53 immunohistochemical status of the cases included in this study had been previously identified by our group [18].

Formalin-fixed, paraffin-embedded 4-μm-thick serial tissue sections of each case were heated at 60°C, deparaffinized in xylene, rehydrated in graded ethanol, and then washed in Tris buffered saline. Immunohistochemistry for E2F-1 was performed using an indirect streptavidin biotin peroxidise method, as previously described, with the addition of an endogenous biotin blocking step (Avidin biotin blocking kit, BioGenex, San Ramon, CA, USA) [8]. The Novolynk Polymer Detection System Kit (Novocastra Laboratories–Menarini, Athens, Greece) was used to immunostain sections with pRb-, phospho-pRb-, and neoepitope M30-specific antibodies. Table 2 shows the source, origin, antigen retrieval method, dilution, duration of incubation, and source of primary antibodies used. 3′,3′-Diaminobenzidine tetrahydrochloride (Sigma, St. Louis,

Table 1 Summary of patients' clinicopathological data

	Number	Male sex	Median age (range)	HBV chronic infection	HCV chronic infection	Cirrhosis
Chronic hepatitis	30	21	51 (39–65)	16	14	22
HCC	57	45	59 (49–70)	40	17	57
Grade						
I	5					
II	27					
III	23					
IV	2					

MO, USA) was used as chromogen, and hematoxylin for counterstaining.

In negative control sections of each case, the primary antibody was replaced with nonimmune diluent (RE7133, Novocastra Laboratories, UK) compatible with the immunohistochemical kit used. Sections of nonsmall cell lung carcinoma with known positive E2F-1, pRb/phospho-pRb status [8, 9], and of a liver biopsy with ischemic hepatitis and high apoptotic index (AI) were used as positive controls for E2F-1, pRb/phospho-pRb, and M30 immunostaining, respectively.

Evaluation of immunohistochemical staining

Immunostained sections were evaluated by two observers (MP and DT) at a double-headed microscope. The LI values for E2F-1, pRb, and phospho-pRb were determined as the percentage of hepatocytes (cases of chronic hepatitis–cirrhosis) or tumor cells (cases of HCC) with strictly nuclear immunopositivity, after counting an average of 500 cells per case at ×40 magnification. Cytoplasmic immunoreactivity was scored for intensity (mild, moderate, strong) and, in cases of cirrhosis adjacent to HCC and HCC samples, the percentage of positive cells was also established. HCC samples were divided in two categories according to pRb immunohistochemical expression: normal when pRb LI was >90% and abnormal when there was absence of nuclear staining in ≥10% of tumor cells [8]. HCC with normal pRb expression were considered also normal for phospho-pRb expression if more than 10% of tumor nuclei was phospho-pRb-positive (phospho-pRb LI ≥10%) [19]. In HCC, M30 AI was determined as the percentage of M30-positive tumor cells after counting an average of 500 cells/case at ×40 magnification.

Statistical analysis

The SPSS v. 17 statistical software package (SPSS, Chicago, IL) was used for all data analysis. The Kolmogorov–Smirnov test was used to assess normality of data distribution. Because none of the variables of interest (E2F-1, pRb, phospho-pRb LI, and M30 AI) were normally distributed, data were analyzed with nonparametric tests. Continuous data were compared with the Mann–Whitney *U* test, whereas correlations between variables with continuous data were assessed with Spearman's ρ. Statistical associations were considered significant for p values less than 0.05.

Results

E2F-1 status and relation to clinicopathological parameters and cell proliferation

Hepatocytes and bile duct cells in normal liver showed mild cytoplasmic and/or nuclear membrane E2F-1 immunoexpression. Mononuclear and endothelial cells showed nuclear E2F-1-

Table 2 Specificity, origin, antigen retrieval method, working dilution, duration of incubation, and source of antibodies used in the immunohistochemical study

Antibody specificity	Origin	Antigen retrieval method	Dilution	Incubation	Source
E2F-1 Rb-binding domain p60	Mouse, clone KH95	1 mM EDTA, pH 8.0 steamer, 30 min	1:100	Overnight, 4°C	Santa Cruz Biotechnologies-Bioanalytica (Athens, Greece)
pRb	Mouse, clone IF8	Citrate buffer pH 6.0 MW, 20 min	1:50	Overnight, 4°C	Santa Cruz Biotechnologies-Bioanalytica (Athens, Greece)
Phospho-pRb(Ser795)	Goat	Citrate buffer pH 6.0 MW, 20 min	1:50	Overnight, 4°C	Santa Cruz Biotechnologies-Bioanalytica (Athens, Greece)
M30 neopitope	Mouse	Citrate buffer pH 6.0 MW, 20 min	1:40	Overnight, 4°C	Roche Diagnostics (Manheim, Germany)

EDTA ethylenediaminetetraacetic acid solution, *MW* microwave

specific immunostaining and served as internal E2F-1-positive control.

In all cases of chronic hepatitis (Fig. 1a) and cirrhosis (with or without HCC; Fig. 1d), most hepatocytes and bile duct cells demonstrated mild granular cytoplasmic and/or nuclear membrane E2F-1 immunoreactivity. No nuclear E2F-1 immunostaining was seen in non-neoplastic liver parenchyma. In some cases of cirrhosis ductular cells at the septal–parenchymal interphase displayed strong cytoplasmic E2F-1 immunostaining, in contrast to the majority of periseptal hepatocytes that were negative or showed mild cytoplasmic immunoreactivity.

All HCC (100%) exhibited strong nuclear E2F-1 immunostaining with or without nuclear membrane accentuation (Figs. 1c, 2a, and 3a). E2F-1 LI ranged from 5% to 100% with a median value of 30% and a mean value of 44.8±38.8% (Table 3). In 16 HCC (9.1%), moderate cytoplasmic E2F-1 immunostaining was additionally noted in some neoplastic cells (Table 3).

In our previous study of the same HCC cohort, cell proliferation index Ki-67 LI was significantly higher in HCC compared to adjacent cirrhotic parenchyma and correlated positively with histological tumor grade [18]. There was no significant correlation of Ki-67 LI, age and sex of HCC patients, viral etiology, or tumor grade with E2F-1 LI.

Relationship of E2F-1 status to AI in HCC

The mean M30 AI of HCC was 3.5±3.9% (median 2.0%, range 0.3–16.3%; Figs. 2d and 3d; Table 3). There was a positive, highly significant correlation between E2F-1 LI and AI (Spearman ρ=0.557, p=0.025). This result was sustained in subgroups of HCC with normal pRb and HCC with abnormal phospho-pRB expression (Spearman ρ=0.975, p=0.005, and ρ=0.855, p=0.007, respectively). Evaluation of E2F-1 expression and M30 immunostaining in serial sections of HCC samples showed a topographical relation between E2F-1 and M30 immunoreactivity with increased AI (Fig. 2d) in HCC exhibiting high E2F-1 LI (Fig. 2a) and decreased AI (Fig. 3d) in HCC with low E2F-1 LI (Fig. 3a). There was no correlation between HCC AI and tumor grade.

Relationship of E2F-1 status to pRb and p53 immumohistochemical expression

We examined expression of E2F-1 regulator proteins pRb and phospho-pRb in our HCC cases and adjacent cirrhotic parenchyma. Kupffer cells and bile duct cells in non-neoplastic liver parenchyma adjacent to HCC showing normal nuclear pRb expression served as internal positive control. In a majority of

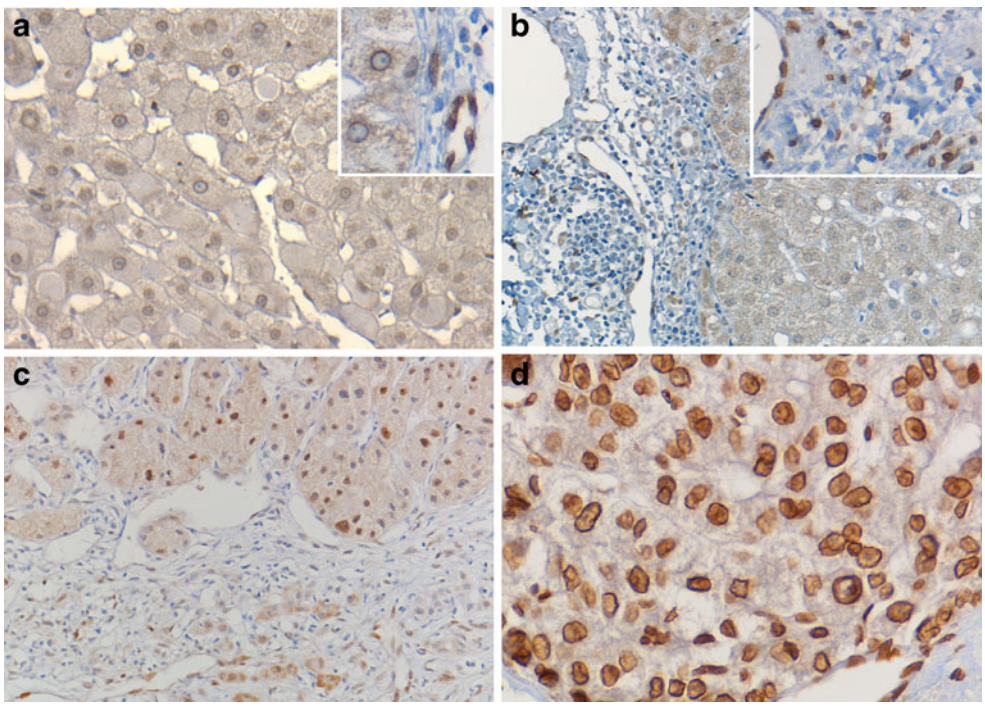

Fig. 1 **a** Chronic hepatitis B. Nuclear membrane E2F-1 immunostaining in most hepatocytes. Several ground-glass hepatocytes are present, ×100. *Inset* shows a periportal hepatocyte with nuclear membrane E2F-1 immunostaining in contrast to nuclear E2F1 immunostaining in endothelial cells of a portal vessel, ×400. **b** Chronic hepatitis C. Cytoplasmic E2F-1 immunoreactivity in hepatocytes; mononuclear and endothelial cells in this photo, as well as in the *inset*, show nuclear E2F-1 immunoreactivity serving as internal positive control, ×100 and ×400. **c** HCC grade 2 with nuclear E2F-1 immunostaining in most tumor cells. Ductules and entrapped hepatocytes in fibrous capsule show granular cytoplasmic E2F-1 immunostaining, ×100. **d** HCC grade 2, with nuclear E2F1-specific immunoreactivity in all tumor cells. Nuclear membrane accentuation of E2F-1 immunostaining is evident, ×200

Table 3 Immunohistochemical expression and LI values of E2F-1, pRB, phospho-pRb, and AI in cirrhosis adjacent to HCC and in HCC

	E2F-1 cytoplasmic % Median (range) mean±SD	E2F-1 nuclear %, LI Median (range) mean±SD	pRb % normal, LI Median (range) mean±SD	Phospho-pRb % normal, LI Median (range) mean±SD	M30 AI Median (range) mean±SD
Cirrhosis-adjacent to HCC (n=6)	100	0	16.67	0	
	15 (5-100)	0 (0-0)	16 (0-90)	0 (0-1)	0.375 (0.06-0.8)
	38.3±32.9	0	28.67±32.9	0.17±0.41	0.38±0.29
HCC (n=57)	16	100	30	22.1	
	0 (0–90)	30 (5–100)	32.5 (0–90)	1 (0–50)	2.05 (0.3–16.34)
	5.2±18.28	44.8±38.8*,**	39.85±37.64	12.32±18.21**,***	3.49±3.94*,***

LI Labeling index, *AI* apoptotic index, *SD* standard deviation

$^{*}p$=0.025, significant positive correlation ρ=0.557; $^{**}p$=0.001, significant inverse correlation ρ=−0.693; $^{***}p$=0.013, significant negative correlation ρ=−0.623

cases of cirrhosis, the liver tissue adjacent to HCC (five out of six, 83.33%), showed abnormal pRb expression (pRb LI median 16%, mean 28.67±32.9%, range 0–90%). In all but one of these cases, abnormal pRb was also noted in the adjacent HCC. In one case, cirrhotic parenchyma showed normal pRb expression in contrast to adjacent HCC where pRb expression was abnormal. All cases of cirrhosis adjacent to HCC were phospho-pRb-negative (phospho-pRb LI median 0%, range 0–1%, mean 0.17±0.41%; Table 3).

Abnormal expression of pRb and phospho-pRb was noted in 70% and 67.9% of HCC, respectively (Fig. 2b, c), while 30 % and 32.1% of HCC showed normal pRb (Fig. 3b) and phospho-pRb (Fig. 3c) expression, respectively (Table 3). Phospho-pRb LI <10% was noted in the majority of HCC (66.6%) that showed normal pRb expression, indicating hypophospho-pRb. Phospho-pRb LI was inversely correlated with E2F-1 LI (Spearman ρ=−0.693, p=0.001), while there was no significant correlation between E2F-1 LI and pRb LI (Spearman ρ=-0.111, p=0.652). A strongly significant negative correlation was observed between phospho-pRb expression and M30 AI (Spearman ρ=−0.623, p=0.013), while pRB expression showed no relation to M30 AI. There was no correlation between pRb and phospho-pRb expression (Spearman ρ=−0.012, p=0.96). No significant correlation was

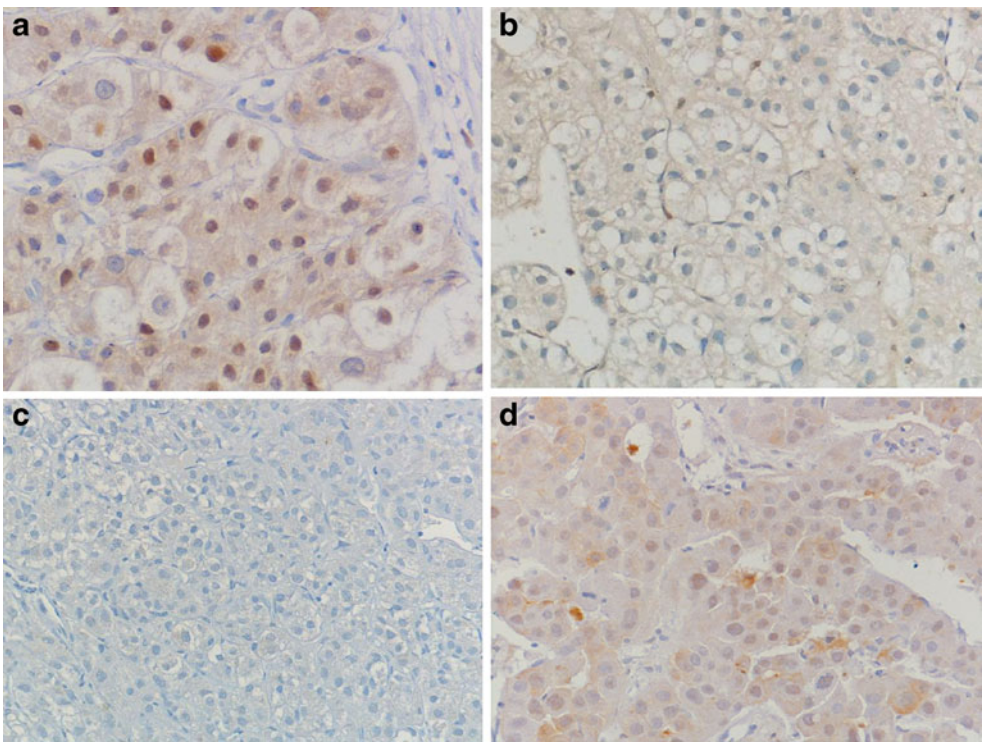

Fig. 2 HCC grade 2, showing: **a** high nuclear E2F-1 immunoreactivity in the majority of tumor cells (LI 95%), ×200; **b** abnormal pRb immunostaining (LI 0%), ×100; **c** abnormal phospho-pRb immunoexpression (LI 0%), indicating that E2F-1 may be free and active, ×100; and **d** high apoptotic index with many tumor cells showing membranous and/or cytoplasmic M30-positive immunoreactivity, ×200

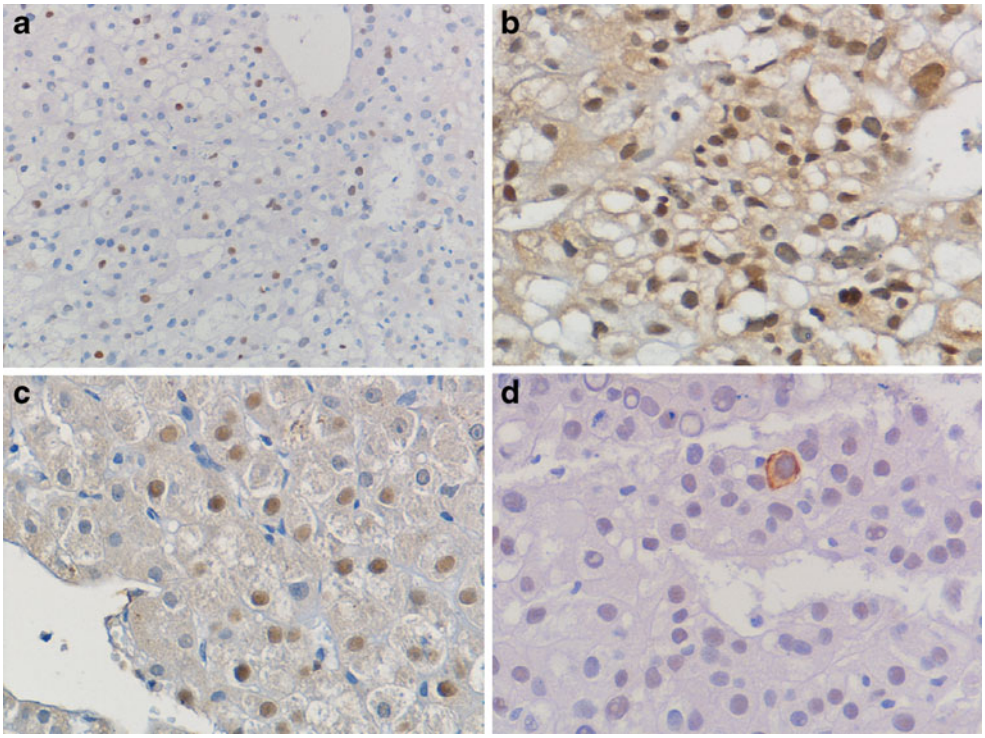

Fig. 3 HBV-related HCC grade 2–3, showing: **a** low nuclear E2F-1 immunoreactivity (LI 10 %), ×100; **b** normal pRb expression in the nuclei of most tumor cells, ×200; **c** phospho-pRb expression in many tumor cells, indicating that pRb is phosphorylated and E2F-1 may be active, ×200; and **d** low AI with one tumor cell showing M30-positive cytoplasmic immunostaining (AI 1.56%), ×200

found between pRb or phospho-pRb expression and patients' age and sex, viral etiology of underlying chronic liver disease and tumor grade ($p>0.05$).

We have previously shown in this set of HCC, that 30 out of 57 cases (53%) were p53 immunopositive. All p53-positive cases had >10% positive tumor cell nuclei [18]. There was no correlation between E2F-1 and p53 immunohistochemical status in HCC.

Discussion

In the present study, we have shown that E2F-1 protein expression is increased in HCC as compared to adjacent cirrhotic liver parenchyma. E2F-1 immunohistochemical expression was correlated with increased tumor cell apoptosis, suggesting that E2F-1 may have an oncosuppressor role in HCC. An apoptosis promoting tumor suppressor role for E2F-1 has also been demonstrated in adenocarcinoma of Barrett esophagus, in carcinomas of colon, prostate, and bladder, and more recently, in osteosarcoma [8, 9, 20–22]. In contrast, E2F-1 appears to act as an oncogene, promoting tumor growth, in lung cancer, esophageal squamous cell carcinoma, and carcinomas of the breast, pancreas, and ovary [9, 23, 24].

Our results are corroborated by those of a study of 46 HCC from Singapore, in which 64% of HCC showed increased E2F-1 expression [13]. At the mRNA level, E2F-1 has been reported to be overexpressed in 41 HCC from Japan [12] and in 50 HCC, most of which were of Chinese origin [11]. In the latter study, it was shown, in a transgenic mouse HCC model, that E2F-1 inhibits c-Myc-initiated apoptosis through induction of the PIK3CA/Akt/mTOR and c-Myb/Cox-2 survival pathways [11]. Furthermore, suppression of E2F-1-dependent apoptosis in human HCC was reported to be an indicator of poor prognosis [11]. In contrast, we show that nuclear E2F-1 expression is positively correlated with tumor AI [25]. This is partly in accordance with the dual, oncogenic, and tumor-suppressing, behavior of E2F-1 as reported in a transgenic mouse model in which E2F-1 was overexpressed in the liver [10]. The oncogenic activity of E2F-1 in that model was mostly evident during the preneoplastic stages and was mediated by early upregulation of cell proliferation. However, slow but persistant escalation of apoptotic cell death may have converted E2F-1 from a positive to a negative regulator of tumor growth [10].

E2F-1 may promote apoptosis through both p53-dependent and p53-independent signaling pathways [5]. To study apoptosis in HCC, we have used the apoptotic marker M30 that binds to fragments of keratin 18 cleaved by caspase 6, an effector of both pathways [25]. In the previous immunohistochemical study of the same cohort, we showed lack of p53 nuclear staining in cirrhosis in the absence of HCC, but it was present in 30% of cases of cirrhosis adjacent to HCC and in 53 % of HCC [18]. In the present study, all HCC cases showed increased nuclear E2F-1 immunostaining, independent of p53 status or tumor grade, indicating that, in HCC p53, immunohistochemical expression is not related to E2F-1 expression.

E2F-1 overexpression in human HCC might be attributted to gene amplification as has been shown in metastatic liver tumors [26]. Increased E2F-1 levels may also be the result of

the disruption of its self-inhibitory loop [5]. This presupposes that E2F-1 is transcriptionally active, and to demonstrate this in our HCC samples, we examined the immunoexpression of its regulator proteins pRb and phospho-pRb. The decreased expression of both pRb and phospho-pRb suggests that E2F-1 might be transcriptionally active. We found abnormal pRb expression in 70% and decreased of phospho-pRb in 68% of HCC. Decreased pRb expression has been previously reported in HCC [13, 27–29] in 13–58% of the cases [13, 29]. Loss of phospho-pRb expression has been previously detected in 37% of HCC [13].

We did not find any correlation between increased E2F-1 expression and HBV or HCV etiology of HCC. However, increasing evidence links HBV and HCV proteins with E2F-1 and pRb cellular function and HCC development. HBV X (HB_X) protein induces the p38MAPKα pathway leading to pRb phosphorylation and consequently to E2F-1 activation [30]. Contradictory results exist regarding HCV implication in E2F-1/pRb function in hepatocarcinogenesis, although most studies are in favor of E2F-1 upregulation and activation by HCV proteins [31].

We found only nuclear E2F-1-specific immunohistochemical staining in most HCC cases, while only in a minority of HCC additional cytoplasmic immunostaining was seen in tumor cells. Cytoplasmic E2F-1 immunolocalization was seen in hepatocytes and bile duct cells in non-neoplastic liver parenchyma. Cytoplasmic E2F-1 immunostaining might reflect heterodimerization of E2F-1 with a splice variant of DRTF-1 polypeptide 2 (DP-2), a transcription factor with significant homology with E2Fs that affects E2F subcelular localization [32].

The limitations of our study include the use of needle biopsy specimens, resulting in reduced availability of tissue in some cases, and the investigation of E2F-1 expression at the protein level only. However, one of the main strengths of our work is the correlation of E2F-1 expression with tumor cell kinetic parameters at the tissue level in serial sections enabling their concurrent in vivo evaluation in HCC. This allowed us to show, for the first time, a pro-apoptotic action of E2F-1 in human HCC.

E2F-1 expression in HCC and its role in hepatocarcinogenesis may have useful clinical implications. The importance of E2F-1 activation and overexpression as a marker of poor patient prognosis in HCC has already been reported [11] and remains to be confirmed in large clinicopathological studies. Furthermore, overexpression of E2F-1 has been shown to exert tumor-suppressor activity in selectively targeted subcutaneous xenograft tumors, introducing adenoviral vectors expressing E2F-1 as a new therapeutic approach through gene therapy of HCC [33].

In conclusion, our observations at the tissue level demonstrate that E2F-1 is overexpressed and may promote apoptosis in human HCC. The E2F-1's regulatory pRb/phospho-Ser795pRb pathway is frequently defective in HCC, indicating that in most cases E2F-1 exists in its active form. Further studies using a larger number of cases with follow-up data are needed to confirm our results and characterize the prognostic significance of E2F-1 expression in human HCC.

Acknowledgments We gratefully acknowledge the support of "Kapodistrias" Research Program, Special Accounts Research Fund 70/4/6549, National and Kapodistrian University of Athens (NKUoA), Greece. We thank Prof. V. Gorgoulis, Laboratory of Histology and Embryology, NKUoA, Greece for helpful insights, suggestions, and critical review of the manuscript and Dr. A. Kotsinas, Laboratory of Histology and Embryology, NKUoA, Greece, for his support during the experimental part of the study. The technical expertise of Ms. Kalliopi Apostolopoulou is appreciated.

Conflict of interest None

References

1. Parkin DM, Bray F, Ferlay J, Pisani P (2005) Global cancer statistics, 2002. CA Cancer J Clin 55(2):74–108
2. Ferlay J, Shin HR, Bray F, Forman D, Mathers C, Parkin DM (2010) Estimates of worldwide burden of cancer in 2008: GLOBOCAN 2008. Int J Cancer 127:2893–2917. doi:10.1002/ijc.25516
3. Tan A, Yeh SH, Liu CJ, Cheung C, Chen PJ (2008) Viral hepatocarcinogenesis: from infection to cancer. Liver Int 28:175–188. doi:10.1111/j.1478-3231.2007.01652.x
4. Wong CM, Ng IOL (2008) Molecular pathogenesis of hepatocellular carcinoma. Liver Int 28:160–174. doi:10.1111/j.1478-3231.2007.01637.x
5. Hallstrom TC, Nevins JR (2009) Balancing the decision of cell proliferation and cell fate. Cell Cycle 15:532–535. doi:10.4161/cc.8.4.7609
6. Tsantoulis PK, Gorgoulis VG (2005) Involvement of E2F transcription factor family in cancer. Eur J Cancer 41:2403–2414. doi:10.1016/j.ejca.2005.08.005
7. Polager S, Ginsberg D (2008) E2F—at the crossroads of life and death. Trends Cell Biol 18:528–536. doi:10.1016/j.tcb.2008.08.003
8. Gorgoulis VG, Zacharatos P, Mariatos M et al (2002) Transcription factor E2F-1 acts as a growth-promoting factor and is associated with adverse prognosis in non-small cell lung carcinoma. J Pathol 198:142–156. doi:10.1002/path.1121
9. Zacharatos P, Kotsinas A, Evangelou K et al (2004) Distinct expression patterns of the transcription factor E2F-1 in relation to tumour growth parameters in common human carcinomas. J Pathol 203:744–753. doi:10.1002/path.1582
10. Conner AE, Lemmer RE, Omori M et al (2000) Dual functions of E2F-1 in a transgenic mouse model of liver carcinogenesis. Oncogene 19:5054–5562
11. Ladu S, Cabisi DF, Conner EA, Farina M, Factor VM, Thorgeirsson SS (2008) E2F1 inhibits c-Myc driven apoptosis via PIK3CA/Akt/mTOR and COX-2 in a mouse model of human liver cancer. Gastroenterology 135:1322–1332. doi:10.1053/j.gastro.2008.07.012
12. Nakajima T, Yasui K, Zen K et al (2008) Activation of B-Myb by E2F1 in hepatocellular carcinoma. Hepatol Res 38:886–895. doi:10.1111/j.1872-034X.2008.00324.x
13. Huynh H, Do PT, Nguyen TH et al (2004) (2004) Extracellular signal-regulated kinase induces cyclin D1 and Cdk-2 expression and phosphorylation of retinoblastoma in hepatocellular carcinoma. Int J Oncol 25:1839–1847
14. Anthony PP, Ishak K, Nayak NC (1978) The morphology of cirrhosis. J Clin Pathol 31:395–414

15. Bosman TF, Carneiro F, Hruban HR, Theise DN (2010) WHO classification of tumours of the digestive system. IARC Press, Lyon, pp 205–216
16. Ishak K, Baptista A, Bianchi L, Callea F (1995) Histological grading and staging of chronic hepatitis. J Hepatol 22:696–699
17. Ishak KG, Goodman ZD, Stocker JT (2001) Tumors of the liver and intrahepatic bile ducts. In: Atlas of tumor pathology, 3rd series, Fascicle 31. AFIP, Washington, DC, pp 219–220
18. Koskinas J, Petraki K, Kavantzas N et al (2005) Hepatic expression of the proliferative marker Ki67 and p53 protein in HBV or HCV cirrhosis in relation to dysplastic liver cell changes and hepatocellular carcinoma. J Viral Hepat 12:635–641. doi:10.1111/j.1365-2893.2005.00635.x
19. Roesch A, Becker B, Meyer S et al (2005) Overexpression and hyperphosphorylation of retinoblastoma protein in the progression of malignant melanoma. Mod Pathol 18:565–572. doi:10.1038/modpathol.3800324
20. Yamazaki M, Hasegawa M, Ohaka I et al (2005) Increased E2F-1 expression via tumour cell proliferation and decreased apoptosis are correlated with adverse prognosis in patients with squamous cell carcinoma of the oesophagus. J Clin Pathol 58:904–910
21. Yamazaki K, Yajima T, Nagao T (2003) Expression of transcription factor E2F-1 in pancreatic ductal carcinoma: an immunohistochemical study. Pathol Res Pract 199:23–28
22. Suh DS, Yoon MS, Choi KU, Kim JY (2008) Significance of E2F-1 overexpression in epithelial ovarian cancer. Int J Gynecol Cancer 18:492–498
23. Evangelou K, Kotsinas A, Mariolis-Sapsakos T et al (2008) E2F-1 overexpression correlates with decreased proliferation and better prognosis in adenocarcinomas of Barrett oesophagus. J Clin Pathol 65:601–605
24. Liontos M, Niforou K, Velimezi G et al (2009) Modulation of the E2F1-driven cancer cell fate by DNA damage response machinery and potential E2F1 targets in osteosarcoma. Am J Pathol 175:376–391. doi:10.2353/ajpath.2009.081160
25. Grassi A, Susca M, Ferri S et al (2004) Detection of the M30 neoepitope as a new tool to quantify liver apoptosis. Am J Clin Pathol 121:211–219. doi:10.1309/UK621LFJ4FX07KDE
26. Iwamoto M, Benerjee D, Menon LG et al (2004) Overexpression of the E2F-1 in lung and liver metastasis of human colon cancer is associated with gene amplification. Cancer Biol Ther 3:395–399. doi:10.4161/cbt.3.4.733
27. Azechi H, Nishida N, Fukuda Y et al (2001) Disruption of the p16/cyclin D1/retinoblastoma protein pathway in the majority of human hepatocellular carcinomas. Oncology 60:346–354. doi:10.1159/000058531
28. Liu K, Lei XZ, Zhao LS et al (2005) Tissue microarray for high-throughput analysis of gene expression profiles in hepatocellular carcinoma. World J Gastroenterol 11:1369–1372
29. Tan L, Fu X-Y, Liu S-Q et al (2005) Expression of $p28^{GANK}$ and its correlation with RB in human hepatocellular carcinoma. Liver Int 25:667–676. doi:10.1111/j.1478-3231.2005.01003.x
30. Wang WH, Hullinger RL, Andrisani OM (2008) Hepatitis B virus X protein via the p38MAPK pathway induces E2F1 release and ATR kinase activation mediating p53 apoptosis. J Biol Chem 283:25455–2567. doi:10.1074/jbc.M801934200
31. Machida K, Liu JC, McNamara G et al (2009) Hepatitis C virus causes uncoupling of mitotic checkpoint and chromosomal polyploidy through the Rb pathway. J Virol 83:12590–12600. doi:10.1128/JVI.02643-08
32. de la Luna S, Burden M, Lee C et al (1996) Nuclear accumulation of the E2F heterodimer regulated by subunit composition and alternative splicing of a nuclear localization signal. J Cell Sci 109:1717–1726
33. Roh V, Laemmle A, Von Holzen U et al (2008) Dual induction of PKR with E2F-1 and IFN-alpha to enhance gene therapy against hepatocellular carcinoma. Cancer Gene Ther 15:636–644. doi:10.1038/cgt.2008.34

Virchows Arch (2012) 460:447–453
DOI 10.1007/s00428-012-1210-6

ORIGINAL ARTICLE

Increased CD133 expression after preoperative chemoradiotherapy in rectal cancers other than mucin-rich tumors

Chih-Hung Lin · Wan-Tzu Chen · Chia-Hsing Liu · Hung-Pei Tsai · Chun-Chieh Wu · Chee-Yin Chai

Received: 13 December 2011 / Revised: 18 January 2012 / Accepted: 31 January 2012 / Published online: 28 March 2012
© Springer-Verlag 2012

Abstract This study is to characterize the sequential change in CD133 expression after preoperative chemoradiotherapy (CRT) in rectal cancer and its impact on postoperative prognosis. Forty-one patients with rectal cancer who had received CRT before surgery were selected retrospectively. In each case, immunohistochemical analysis was performed to compare CD133 expression in biopsy specimens taken before and after CRT. After CRT, CD133 expression was significantly increased in 14 (34%) patients, mildly increased in 25 (61%), and decreased in 2 (5%). However, no mucin-rich tumors showed high CD133 expression before or after CRT ($p<0.001$). Disease-free survival and overall survival were significantly poorer in patients with significantly increased CD133 ($p=0.049$ and $p=0.038$, respectively). Increased CD133 after CRT is a significant prognostic factor in rectal cancer patients treated with preoperative CRT and surgical resection. CD133 might be an essential cancer stem cell marker.

Keywords Cancer stem cell · CD133 · Chemoradiotherapy · Rectal cancer

Chun-Chieh Wu and Chee-Yin Chai contributed equally to this work.

C.-H. Lin · W.-T. Chen · C.-H. Liu · C.-C. Wu (✉) · C.-Y. Chai (✉)
Department of Pathology, Kaohsiung Medical University Hospital, No.100, Tzyou 1st Road, Kaohsiung 807, Taiwan
e-mail: lazzz_wu@yahoo.com.tw
e-mail: cychai@kmu.edu.tw

H.-P. Tsai · C.-Y. Chai
Graduate Institute of Medicine, College of Medicine, Kaohsiung Medical University, Kaohsiung, Taiwan

C.-Y. Chai
Department of Pathology, College of Medicine, Kaohsiung Medical University, Kaohsiung, Taiwan

Introduction

Colorectal cancer is a leading cause of cancer-related death both globally and in Taiwan. Before surgical intervention for rectal cancer or colon cancer in the sigmoid region, fluorouracil-based neo-adjuvant chemotherapy is often combined with local radiotherapy to improve survival, especially in advanced stages of the disease. Although new chemotherapeutic drugs appear promising, no single treatment is consistently curative. The emerging cancer stem cell concept has elucidated possible mechanisms of resistance to current therapeutic modalities for treating solid tumors such as those in colorectal cancer [1–5]. Accumulating evidence also supports the hypothesis that cancer stem cells have a major role in cancer progression. These so-called cancer stem cells are not only capable of self-renewal and initiation of tumor growth, they are also resistant to conventional cytotoxic chemotherapeutic agents. Some researchers hypothesize that using these agents to target actively proliferating tumor cells enables the escape of cancer stem cell subpopulations in which proliferation is relatively slower. According to this theory, the selection advantage of cancer stem cells increases their population after standard chemoradiotherapy (CRT) [1].

The CD133 cell surface transmembrane glycoprotein, also known as prominin-1, is among the most intensively studied cancer stem cell markers in solid tumors, including colorectal cancer [1, 6–8]. In both colorectal cancer and normal colon crypts, this cell surface marker is expressed on the luminal surface and in the cytoplasm of intraluminal cells [6, 9]. In vitro studies show that, after 5-fluorouracil (5-FU) treatment, colon cancer cells that express CD133 have a higher resistance

compared to CD133-negative cells [10]. Colorectal cancers with CD133 expression are also reportedly associated with resistance to chemotherapy and poor prognosis [11]. In rectal cancer, CD133 is more commonly expressed in tumors after CRT, in comparison with non-CRT tumors [9]. Recent studies show that, in patients who receive CRT treatment before surgery for rectal cancer, CD133 expression is associated with tumor regrowth and distant recurrence after CRT, but not with overall survival [12]. Our study of rectal cancer patients compared the difference of CD133 expression before and after preoperative CRT and tested CD133 expression for correlations with clinical outcome after surgical resection.

Materials and methods

Patients and specimens

Forty-one patients who had received CRT before undergoing surgery for rectal cancer at this institution were retrospectively selected. Medical records were reviewed, and clinicopathological data were documented. All selected cases received colonoscopic biopsy for histopathological diagnosis before CRT. For the accuracy of diagnosis and avoiding the need for re-biopsy, multiple sites of the tumor were sampled and areas of necrosis were avoided. All the biopsy samples contained at least three tissue fragments, each representing a different location of the tumor. Each fragment of tumor tissue was at least 0.1 cm in diameter. The CRT regimen included two cycles of 5-FU-based chemotherapy given on a continuous intravenous route, with concurrent 20–45 Gy pelvic radiotherapy, followed by resection. The patients with complete regression were excluded. The time interval between pre-CRT biopsy and surgery was 2 to 4 months. The patients were followed up for at least 18 months or until death. All specimens were fixed in formalin and embedded in paraffin. This work was approved by the ethics committee of the Kaohsiung Medical University Hospital (KMUH-IRB-20110084).

Histopathology

The archival slides and histopathological parameters were reviewed by two independent pathologists (C.H. Lin and C. Y. Chai). The biopsy samples with an inadequately small amount of tumor were excluded. The histopathological parameters included tumor grade, depth of tumor invasion, nodal metastasis, lymphovascular and perineural invasion, and tumor regression. The post-CRT staging was performed according to the AJCC Cancer Staging Manual (seventh edition). Tumor regression was graded as follows: grade 0, no regression; grade 1, minor regression (dominant tumor mass with obvious fibrosis in ≤25% of the tumor mass); grade 2, moderate regression (dominant tumor mass with obvious fibrosis in 26% to 50% of the tumor mass); and grade 3, good regression (> 50% tumor regression).

Immunohistochemical staining

Four-micrometer thick sections were serially cut from the formalin-fixed paraffin-embedded tissue blocks. Tissue sections were de-paraffinized, rehydrated, and pretreated by autoclave for antigen retrieval. In each section, endogenous peroxidase was blocked by 5 min incubation in 3% hydrogen peroxide. The sections were incubated with primary antibody CD133 (Biocare Medical, Concord, CA, USA), CDX-2 (BioGenex, San Ramon, CA, USA), or Ki-67 (DAKO, Glostrup, Denmark) at room temperature for 1 h. The Dako REAL EnVision Detection System-HRP (Dako, Denmark) was then applied for 30 min. Finally, the sections were incubated in 3′3-diaminobenzidine for 5 min, counterstained with Mayer hematoxylin, and mounted. Negative controls were obtained by replacing the primary antibody with non-immune serum.

Scoring for protein expression and comparison of pre- and post-CRT specimens

The CD133 expression was scored in terms of staining intensity, percentage of positive cancer cells, and staining pattern. A score of 0 indicated a complete absence of staining. A score of 1 indicated weak luminal surface staining in <50% tumor cells. A score of 2 indicated weak luminal surface staining in >50% tumor cells or strong luminal surface and intraluminal cell staining in <50% tumor cells. A score of 3 indicated strong labeling on luminal surfaces, intraluminal cells, and cytoplasm in >50% tumor cells. A score of 0 or 1 for CD133 expression was considered low, and a score of 2 or 3 was considered high. A significant increase in the CD133 expression was defined as an increase of two or more points between before and after CRT.

Statistical analysis

Chi-square test was used to compare clinicopathological features between tumors with and without marked increased of CD133 after CRT. The difference in the CD133 expression between tumors with abundant mucin production and other histological types was also examined by chi-square test. Disease-free survival was calculated from the date of surgery to the date of disease recurrence or metastasis. Overall survival was calculated from date of surgery to date of death or last follow-up. Survival was evaluated by Kaplan–Meier method. The log-rank test was used to compare the cumulative survival durations in the patient groups. All statistical analyses were performed using the SPSS package (version 14.0 for Windows, SPSS, USA).

Results

Clinicopathological features and difference of CD133 expression

Table 1 summarizes the clinicopathological features of 41 patients and lists differences in CD133 expression before and after CRT. The difference in CD133 expression was significantly lower in poorly differentiated histology ($p<0.01$). Other clinicopathological features, including age, gender, stage, depth of tumor invasion, nodal metastasis, perineural invasion, and tumor regression, were not significantly correlated with the difference in the CD133 expression.

Increased CD133 expression in subset of rectal cancer after concurrent CRT

Figure 1 shows representative immunohistochemical stains for CD133 in matched pre-CRT biopsy and post-CRT resection. As in previous works, the CD133 expression was localized to the luminal surfaces and intraluminal cells of invasive glandular structures. CD133 expression was assessed before and after CRT in 41 rectal adenocarcinoma patients. After CRT, expression was significantly increased in 14 (34%), mildly increased in 25 (61%), and decreased in 2 (5%). When grouped together, 27 (66%) of 41 showed high CD133 expression in post-CRT tumors, which is consistent with the literature [9]. Five post-CRT tumors with scores of 2 or 3 were also stained with CDX-2 and Ki-67 to characterize the proliferative activity and differentiation of CD133-positive cells. The tumor nests with CD133 overexpression showed less CDX-2 expression and lower Ki-67 proliferation indices compared to those without CD133 expression, suggesting that CD133-positive cells are less differentiated and less proliferative (Fig. 2).

Low CD133 expression is associated with mucin-rich phenotype and degree of differentiation after CRT

Out of 41 cases with abundant mucin production, ten showed prominent mucin pools and islands of cancerous cells with mucinous histotype of >50% of the tumor area. None of these ten cases showed high CD133 expression before or after chemotherapy, and two had an expression score of 1 at post-chemotherapy resection. Neither of the two showed CD133 expression staining in pre-CRT biopsy, although mucin production was low in the biopsy specimen. CD133 expression after CRT was negatively correlated with the mucin-rich phenotype ($p<0.001$). Moreover, the CD133 expression after CRT was also negatively correlated with the degree of differentiation (well/moderately vs poorly differentiated, $p<0.01$).

Table 1 Correlation between clinicopathologic features and change in CD133 expression after chemoradiotherapy (CRT)

		Marked CD133 increase after CRT	Minor change of CD133 after CRT	*p* value
n		14	27	
Age (mean±SD)		62.21±10.29	63.33±13.19	1.00
Gender	Male:female	10:4	16:11	0.51
Differentiation	Well/moderately	14	16	<0.01
	Poor	0	11	
Depth of tumor (ypT1 + ypT2 vs ypT3 + ypT4)	T1	0	1	0.45
	T2	2	7	
	T3	12	16	
	T4	0	3	
Lymph node metastasis	Negative	8	17	0.75
	Positive	6	10	
Distant metastasis	Negative	12	25	0.60
	Positive	2	2	
Post-CRT AJCC stage (stage I + II vs III + IV)	I	2	6	0.35
	II	4	10	
	III	6	9	
	IV	2	2	
Perineural invasion	Negative	10	21	0.71
	Positive	4	6	
Lymphovascular invasion	Negative	12	22	1.00
	Positive	2	5	
Regression (score 0+1 vs 2+3)	Negative	6	10	0.75
	Positive	8	17	

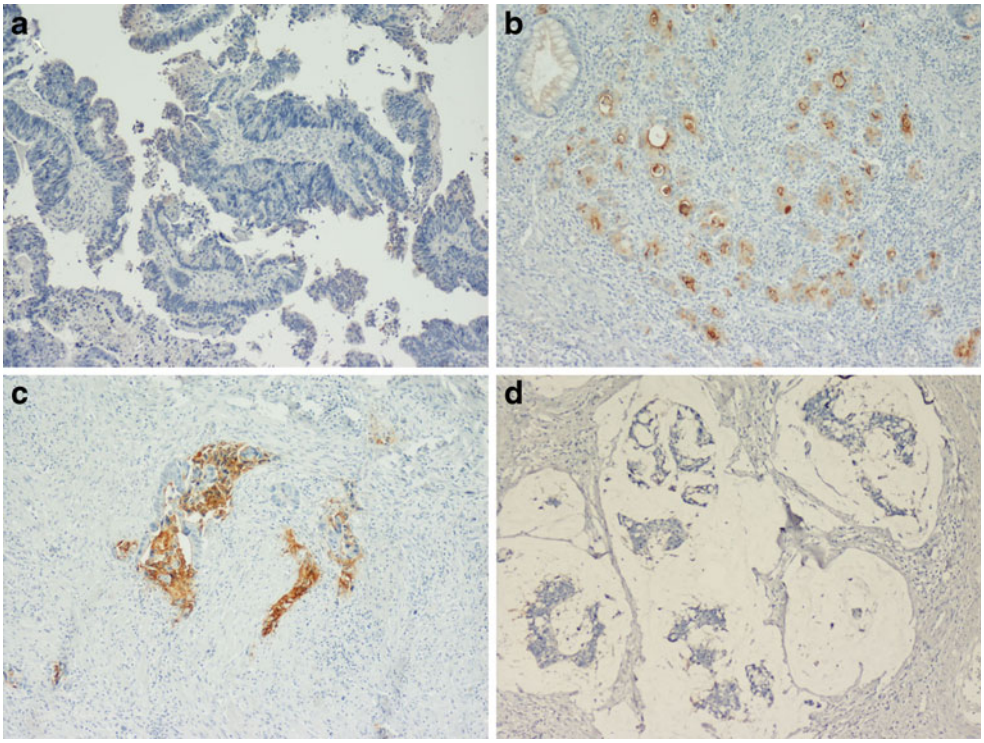

Fig. 1 Immunohistochemistry of a representative case showing significantly increased CD133 expression after preoperative CRT. **a** Biopsy results showing no CD133 expression before CRT (score 0); **b**, **c** CD133 expression after CRT in resection specimen of the same tumor. Luminal surfaces (**b**) and intraluminal cells (**c**) showing prominent staining. In contrast, CD133 expression is low in mucin-producing tumors (**d**)

Prognosis is associated with increased CD133 expression after CRT

To understand how CD133 expression affects the prognosis of rectal cancer after CRT, survival was compared between patients with and without significantly increased CD133. The survival analysis excluded two patients lost to follow-up. Since tumors with abundant mucin production represent a unique group in terms of CD133 expression, the prognostic implications of CD133 overexpression after CRT were analyzed in the subgroup of cases without significant mucin production. The comparison of the overall population showed that patients with significantly increased CD133 had significantly lower disease-free survival (p=0.049) and overall survival (p=0.038) compared to those without increased CD133 expression (Fig. 3a, b). When only tumors without abundant mucin production were included (29 cases), prognosis was significantly poorer in terms of both disease-free survival (p=0.007) and overall survival (p=0.010) in tumors showing significantly increased CD133 after CRT (Fig. 3c, d).

When only post-CRT specimens were considered, however, prognosis did not significantly differ between tumors with high and low CD133 expression (p=0.899 for disease-free survival and p=0.874). Therefore, the difference in CD133 expression after CRT is a more reliable prognostic indicator compared to CD133 expression measured at only one point.

Discussion

The important role of cancer stem cells has been demonstrated in several solid organ tumors in recent years. Like normal

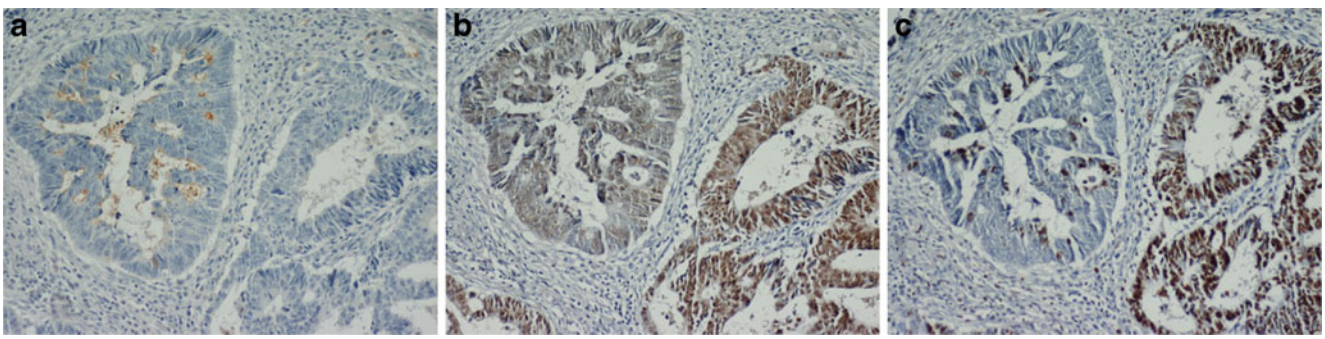

Fig. 2 Decreased CDX-2 and Ki-67 expression in CD133-positive area. Immunostaining results for serial section of the same field are shown. The left side of the glandular structure shows expression of CD133 (**a**) and decreased expressions of CDX-2 (**b**) and Ki-67 (**c**) in comparison with other CD133-negative glands

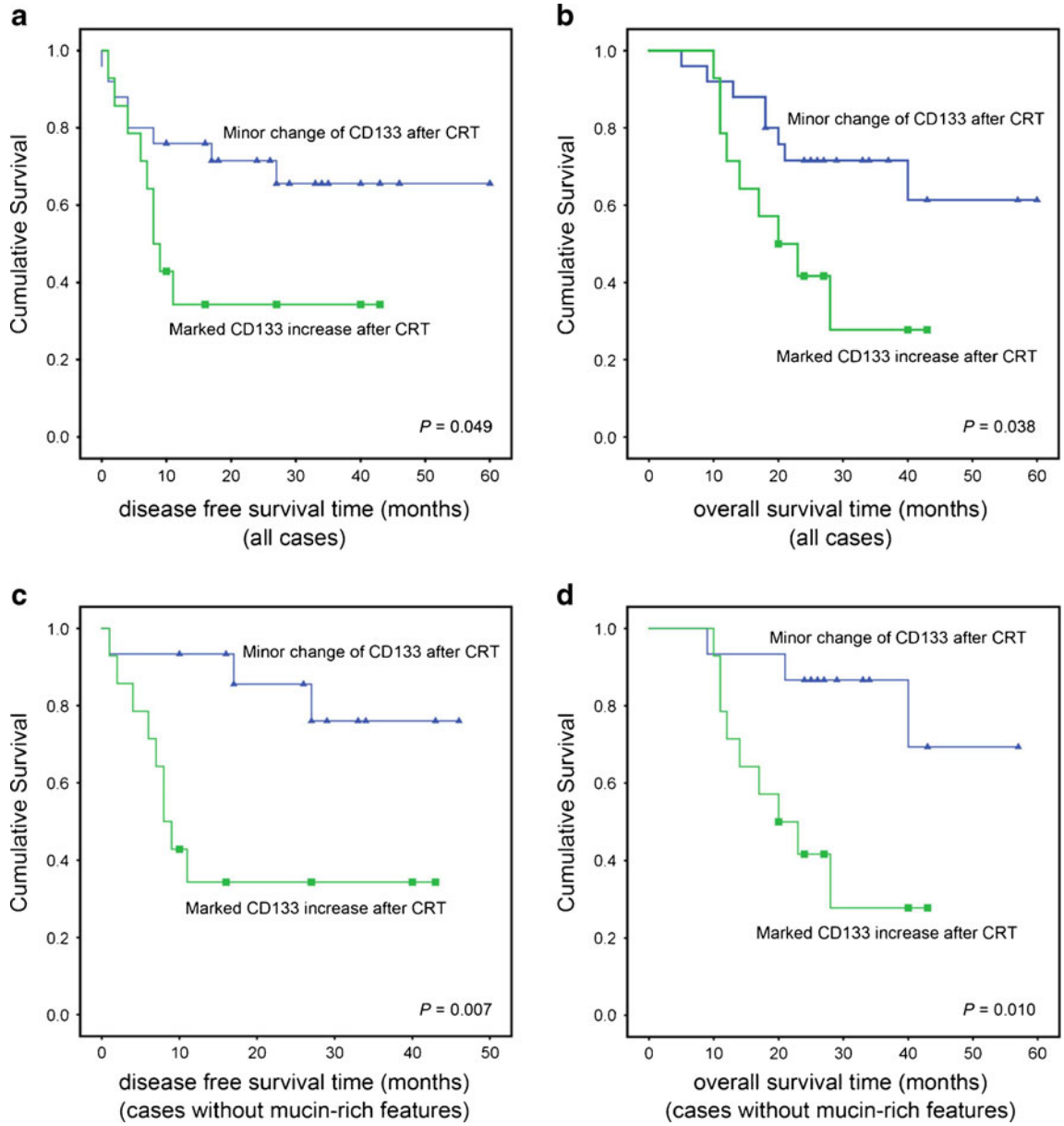

Fig. 3 Correlations between the difference of CD133 expression after CRT and **a** disease-free survival (39 cases); **b** overall survival (39 cases); **c** disease-free survival in cases without mucin-rich phenotype (29 cases); **d** overall survival in cases without mucin-rich phenotype (29 cases)

stem cells, cancer stem cells are capable of self-renewal, tumor initiation, growth, invasion, and metastasis. Because they divide more slowly compared to other cells, cancer stem cells are believed to be more resistant to most current chemotherapies that target rapidly proliferating tumor cells [1–5].

The CD133 is among the most intensively studied cancer stem cell markers in solid tumors, including colorectal cancer. Accumulating data from in vitro and in vivo studies suggest that CD133-positive cells are putative cancer stem cells in colorectal cancers [3, 8, 13]. Mouse studies show that tumors can be induced by injection of CD133-positive colorectal cancer cells [3]. Clinical studies show that elevated CD133 expression is associated with poor prognosis [14, 15]. In rectal cancer, CD133 overexpression is much more common after CRT [9]. Moreover, tumors with high CD133 expression predict non-responsiveness to standard CRT in colorectal cancer [11]. Additionally, CD133 expression is an important prognostic factor in rectal cancer after preoperative CRT [16]. A colorectal cancer cell line model established to evaluate the long-term stability of resistance to 5-FU, which is an important component of standard chemotherapy for colon cancer, showed that 5 FU-resistant cell clones had a CD133-positive phenotype [17]. However, no studies have performed a paired comparison of CD133 expression before and after CRT in a single population of rectal cancer patients. The current analysis of colorectal cancer patients before and after CRT provides

further evidence of increased CD133-positive cells after CRT and suggests that these cells may have a key role in tumor recurrence or metastasis after standard treatment. The reduced differentiation marker (CDX-2) and proliferative activity (Ki-67) observed in some areas of these CD133-positive cells also suggest that their properties resemble those of cancer stem cells. This phenomenon is consistent with two previous works showing an inverse association between CD133 expression and CK20 expression [6, 11]. Notably, however, not all CD133-positive cells showed a decreased CDX-2 or Ki-67 labeling index. We postulate that not all CD133-positive cells are true cancer stem cells, which implies that not all of these cells are CRT-resistant. Subpopulations might exist in these CD133-positive cells. Moreover, the difference in CD133 expression before and after CRT is a more reliable predictive factor compared to expression measured at a single point. The abundance of CD133-positive tumor cells may result from their increased survival capacity since these cells are highly resistant to standard CRT. Another possibility is that CD133-positive cells propagate during tumor progression. The presence of either or both of these conditions would increase the rate of recurrence or metastasis.

The marked difference of CD133 was found more often in the ypT3 plus ypT4 group than tumors with ypT1 plus ypT2 (38% vs 20%). However, the post-CRT difference in CD133 expression was not significantly related to the ypT status ($p=0.45$). We assume that some of these tumors are at higher post-CRT stage because more chemoradiotherapy-resistant cancer cells are present in the remaining tumors after CRT. The proportion of CD133-positive cancer stem cells and post-CRT stage might be interconnected, both being related to patient outcome.

The unique immunostaining pattern of CD133 in colorectal cancers is well documented in the literature. CD133 is typically expressed on luminal surfaces and in the intraluminal cell in malignant glandular structures. In rare cases, the expression exhibits a cytoplasmic pattern, especially in rectal cancers after CRT [9]. Proliferation and regrowth after CRT reportedly exhibits a spherical structure. Two cases in the current study revealed cytoplasmic staining but no spherical structure or association with proliferation. Interestingly, some colorectal cancer studies report much lower CD133 expression in poorly differentiated tumors than in well-differentiated tumors [18], whereas others report that CD133 expression has no correlation with differentiation [11, 12, 19]. The current study also revealed a significant negative association between CD133 expression and differentiation. Furthermore, no tumors with abundant mucin production showed overexpression of CD133, even in gland-forming areas (data not shown). Additionally, pre-CRT biopsy of tissues from the same tumors invariably showed low CD133 expression. An earlier study of intraductal papillary mucinous neoplasms similarly reported the absence of CD133 expression in mucin-producing epithelial cells and carcinoma cells [20]. Thus, a mucin-producing phenotype may carry intrinsic properties that inhibit CD133 expression.

In the previous studies of CD133 expression in colorectal cancer, most authors selected 10% cut-off value to define positivity [18]. However, we deemed this positive–negative approach not suitable for the present study. The difference in CD133 expression was very conspicuous between pre-CRT and post-CRT specimens. If the pre-CRT specimen showed 10% weak luminal surface staining and the post-CRT specimen showed 90% strong luminal and intraluminal staining, both would be regarded as "positive" based on the 10% criteria. This would lead to misinterpretation: no difference before and after CRT. Therefore, we developed a new scoring system to take both staining intensity and proportion of positive tumor cells into consideration to demonstrate the difference of CD133 expression after CRT.

Although the mechanism whereby CD133 contributes to resistance to chemotherapy or radiotherapy is not fully understood at the molecular level or cellular level, recent studies provide some clues. In glioblastoma, radiation exposure elevates the activity of chk1 and chk2 molecules that participate in the DNA damage check point response in CD133-positive cells but not in CD133-negative cells [1]. The Wnt signaling pathway has also been implicated in the 5-FU resistance of CD133-positive colon cancer cells [10]. Hypoxia-inducible factor-1α gene expression is also known to have an inverse correlation with CD133 expression in rectal cancers after CRT [12]. Activation of the Akt and MAPK pathways is higher in CD133-positive cells. Inhibited activity of Akt and Erk1/2 substantially reduces the clonogenic growth of CD133-positive cells [21]. These accumulating data suggest a potential therapeutic target for putative CD133-positive cancer stem cells. Molecules for reducing CD133-positive cells have also been developed [22].

In conclusion, CD133 expression is increased after standard CRT in rectal cancer, but not in those showing abundant mucinous histology. Our finding that increased CD133 after CRT is a significant prognostic indicator in rectal cancer patients treated with preoperative CRT and surgical resection provides further evidence that CD133 is a potential cancer stem cell marker in colorectal cancer. However, the precise therapeutic value of targeting CD133 for treating colorectal cancers remains to be determined.

Conflict of interest We declare that we have no conflict of interest.

References

1. Bao S, Wu Q, McLendon RE, Hao Y, Shi Q, Hjelmeland AB, Dewhirst MW, Bigner DD, Rich JN (2006) Glioma stem cells

promote radioresistance by preferential activation of the DNA damage response. Nature 444:756–760
2. Jordan CT, Guzman ML, Noble M (2006) Cancer stem cells. N Engl J Med 355:1253–1261
3. O'Brien CA, Pollett A, Gallinger S, Dick JE (2007) A human colon cancer cell capable of initiating tumour growth in immunodeficient mice. Nature 445:106–110
4. Todaro M, Francipane MG, Medema JP, Stassi G (2010) Colon cancer stem cells: promise of targeted therapy. Gastroenterology 138:2151–2162
5. Ward RJ, Dirks PB (2007) Cancer stem cells: at the headwaters of tumor development. Annu Rev Pathol 2:175–189
6. Horst D, Kriegl L, Engel J, Kirchner T, Jung A (2008) CD133 expression is an independent prognostic marker for low survival in colorectal cancer. Br J Cancer 99:1285–1289
7. Horst D, Kriegl L, Engel J, Kirchner T, Jung A (2009) Prognostic significance of the cancer stem cell markers CD133, CD44, and CD166 in colorectal cancer. Cancer Invest 27:844–850
8. Ricci-Vitiani L, Lombardi DG, Pilozzi E, Biffoni M, Todaro M, Peschle C, De Maria R (2007) Identification and expansion of human colon-cancer-initiating cells. Nature 445:111–115
9. Saigusa S, Tanaka K, Toiyama Y, Yokoe T, Okugawa Y, Kawamoto A, Yasuda H, Morimoto Y, Fujikawa H, Inoue Y, Miki C, Kusunoki M (2010) Immunohistochemical features of CD133 expression: association with resistance to chemoradiotherapy in rectal cancer. Oncol Rep 24:345–350
10. Deng YH, Pu XX, Pu MJ, Huang JX, Zhou JM, Lin TY, Lin EH (2010) 5-Fluorouracil up regulates the activity of Wnt signaling pathway in CD133-positive colon cancer stem-like cells. Chin J Cancer 29:810–815
11. Ong CW, Kim LG, Kong HH, Low LY, Iacopetta B, Soong R, Salto-Tellez M (2010) CD133 expression predicts for non-response to chemotherapy in colorectal cancer. Mod Pathol 23:450–457
12. Saigusa S, Tanaka K, Toiyama Y, Yokoe T, Okugawa Y, Koike Y, Fujikawa H, Inoue Y, Miki C, Kusunoki M (2011) Clinical significance of CD133 and hypoxia inducible factor-1alpha gene expression in rectal cancer after preoperative chemoradiotherapy. Clin Oncol (R Coll Radiol) 23:323–332
13. Haraguchi N, Ohkuma M, Sakashita H, Matsuzaki S, Tanaka F, Mimori K, Kamohara Y, Inoue H, Mori M (2008) CD133+ CD44+ population efficiently enriches colon cancer initiating cells. Ann Surg Oncol 15:2927–2933
14. Nakamura K, Iinuma H, Aoyagi Y, Shibuya H, Watanabe T (2010) Predictive value of cancer stem-like cells and cancer-associated genetic markers for peritoneal recurrence of colorectal cancer in patients after curative surgery. Oncology 78:309–315
15. Xi HQ, Zhao P (2011) Clinicopathological significance and prognostic value of EphA3 and CD133 expression in colorectal carcinoma. J Clin Pathol 64:498–503
16. Kojima M, Ishii G, Atsumi N, Nishizawa Y, Saito N, Ochiai A (2010) CD133 expression in rectal cancer after preoperative chemoradiotherapy. Cancer Sci 101:906–912
17. Tentes IK, Schmidt WM, Krupitza G, Steger GG, Mikulits W, Kortsaris A, Mader RM (2010) Long-term persistence of acquired resistance to 5-fluorouracil in the colon cancer cell line SW620. Exp Cell Res 316:3172–3181
18. Kojima M, Ishii G, Atsumi N, Fujii S, Saito N, Ochiai A (2008) Immunohistochemical detection of CD133 expression in colorectal cancer: a clinicopathological study. Cancer Sci 99:1578–1583
19. Saigusa S, Tanaka K, Toiyama Y, Yokoe T, Okugawa Y, Ioue Y, Miki C, Kusunoki M (2009) Correlation of CD133, OCT4, and SOX2 in rectal cancer and their association with distant recurrence after chemoradiotherapy. Ann Surg Oncol 16:3488–3498
20. Shimizu K, Itoh T, Shimizu M, Ku Y, Hori Y (2009) CD133 expression pattern distinguishes intraductal papillary mucinous neoplasms from ductal adenocarcinomas of the pancreas. Pancreas 38:e207–e214
21. Wang YK, Zhu YL, Qiu FM, Zhang T, Chen ZG, Zheng S, Huang J (2010) Activation of Akt and MAPK pathways enhances the tumorigenicity of CD133+ primary colon cancer cells. Carcinogenesis 31:1376–1380
22. Dong TT, Zhou HM, Wang LL, Feng B, Lv B, Zheng MH (2011) Salinomycin selectively targets 'CD133 +' cell subpopulations and decreases malignant traits in colorectal cancer lines. Ann Surg Oncol 18:1797–1804

Virchows Arch (2012) 460:455–465
DOI 10.1007/s00428-012-1232-0

ORIGINAL ARTICLE

An improved image analysis method for cell counting lends credibility to the prognostic significance of T cells in colorectal cancer

Juha P. Väyrynen · Juha O. Vornanen · Sara Sajanti · Jan P. Böhm · Anne Tuomisto · Markus J. Mäkinen

Received: 2 November 2011 / Revised: 2 February 2012 / Accepted: 26 March 2012 / Published online: 24 April 2012
© Springer-Verlag 2012

Abstract Numerous immunohistochemically detectable proteins, such as immune cell surface (CD) proteins, vascular endothelial growth factor, and matrix metalloproteinases, have been proposed as potential prognostic markers in colorectal cancer (CRC) and other malignancies. However, the lack of reproducibility has been a major problem in validating the clinical use of such markers, and this has been attributed to insufficiently robust methods used in immunohistochemical staining or its assessment. In this study, we assessed how computer-assisted image analysis might contribute to the reliable assessment of positive area percentage and immune cell density in CRC specimens, and subsequently, we applied the computer-assisted cell counting method in assessing the prognostic value of T cell infiltration in CRC. The computer-assisted analysis methods were based on separating hematoxylin and diaminobenzidine color layers and then applying a brightness threshold using open source image analysis software ImageJ. We found that computer-based analysis results in a more reproducible assessment of the immune positive area percentage than visual semiquantitative estimation. Computer-assisted immune cell counting was rapid to perform and accurate (Pearson $r>0.96$ with exact manual cell counts). Moreover, the computer-assisted determination of peritumoral and stromal T cell density had independent prognostic value. Our results suggest that computer-assisted image analysis, utilizing freely available image analysis software, provides a valuable alternative to semiquantitative assessment of immunohistochemical results in cancer research, as well as in clinical practice. The advantages of using computer-assisted analysis include objectivity, accuracy, reproducibility, and time efficiency. This study supports the prognostic value of assessing T cell infiltration in CRC.

Keywords Immunohistochemistry · Computer-assisted image analysis · Molecular marker · Colorectal cancer · T cell · Prognosis

Introduction

Immunohistochemistry is used both for research and diagnostic pathology. Numerous proteins have been identified as prognostic and predictive markers in different malignancies, and some are in clinical use, including estrogen receptor (ER) and HER-2 oncogene in breast cancer [1]. The discovery of new molecular markers is largely based on improved understanding of the pathogenesis of cancer, and most markers are related to the hallmarks of cancer, which include sustaining proliferative signaling, evading growth suppressors and apoptosis, inducing angiogenesis, and acquiring an optimal inflammatory environment [2]. In the years to come, large numbers of new molecular prognostic markers for different cancers will be discovered, and accuracy in the analysis of immunohistochemistry is essential to ensure the reproducibility of the results [3, 4].

Colorectal cancer (CRC) is one of the most common malignancies and an important cause of cancer death in the western world [5]. TNM stage is the most important prognostic

Electronic supplementary material The online version of this article (doi:10.1007/s00428-012-1232-0) contains supplementary material, which is available to authorized users.

J. P. Väyrynen · J. O. Vornanen · S. Sajanti · A. Tuomisto · M. J. Mäkinen (✉)
Department of Pathology, University of Oulu,
POB 5000, 90014 Oulu, Finland
e-mail: markus.makinen@oulu.fi

J. P. Böhm
Department of Pathology, Jyväskylä Central Hospital,
Jyväskylä, Finland

factor, and immunohistochemical markers are currently rarely used in clinical practice [3, 6]. In CRC, vascular endothelial growth factor (VEGF) [7, 8], epidermal growth factor receptor [7, 9], and matrix metalloproteinases [10] have been proposed as markers. In addition to the properties of the cancer cells, more and more attention has also recently been paid to the tumor–stroma interactions [2, 11]. In this context, one of the prognostic factors for CRC, frequently studied immunohistochemically, is immune cell infiltration. The cancer immunosurveillance hypothesis states that cancer cells can be recognized and eliminated by the immune system [12], and accordingly, increased numbers of different peri- and intratumoral immune cells have been associated with better survival in CRC [13–17]. Notably, T cells have been shown to have high prognostic value in several studies [13, 15, 18, 19].

One of the biggest problems in validating new molecular prognostic markers has been the lack of reproducibility between studies, which is related to the different methods used for analyzing the immunohistochemically stained sections [3, 4]. Often, predetermined cutoff scores or categorizations are used [16, 20], which might lead to false-negative results as to the prognostic value, as well as to problems in comparing the results of individual studies [3, 4]. Also, semiquantitative methods based on estimating the percentage of positive cells in intervals of, e.g., 5 %, have been used, which have been found reasonably accurate in assessing the expression of proteins such as p53 and VEGF [21]. Moreover, computer-based methods are increasingly being utilized [13, 22, 23] and have been shown highly accurate in several applications [23, 24]. In this study, we intended to examine the availability and the functionality of freely available computer-assisted solutions to aid the accuracy in the analysis of immunohistochemistry. We first describe a free computer-based analyzing method for positive area percentage evaluation and cell counting and test its validity. We also use automated computer-assisted cell counting for assessing the prognostic value of T cell infiltration in CRC.

Materials and methods

Patients

This study was based on an earlier described cohort of 466 patients who underwent an operation for colorectal cancer between the years 1986 and 1996 in Oulu University Hospital [25]. The clinical data on the patients were collected from case records, and 60-month follow-up data for 386 patients were provided by the Finnish Cancer Registry. For this study, 235 (60.9 %) of these 386 cases with follow-up data were selected (Table 1). The study was performed in accordance with the standards of the Ethics Committee of Oulu University Hospital.

Table 1 Patient characteristics

Colorectal cancer	235 (100 %)
Age, mean (SD)	68.0 (10.7)
Sex	
Male	118 (50.2 %)
Female	117 (49.8 %)
Tumor location	
Proximal colon	78 (33.2 %)
Distal colon	66 (28.1 %)
Rectum	91 (38.7 %)
TNM stage	
Stage I	42 (17.9 %)
Stage II	99 (42.1 %)
Stage III	61 (26.0 %)
Stage IV	33 (14.0 %)
WHO grade	
Grade 1	53 (22.6 %)
Grade 2	142 (60.4 %)
Grade 3	40 (17.0 %)

The study was based on an earlier described cohort of 386 colorectal cancer patients with follow-up data of which a group of 235 patients was selected for this study. The included patients showed no significant differences in mean age and the distribution of sex, tumor location, stage, and grade with the original cohort of 386 patients

Samples from surgical specimens had been fixed in 10 % buffered formalin and embedded in paraffin. Five-micrometer sections had been cut and stained with hematoxylin and eosin. The staging of the tumors was performed according to TNM6 [26], and WHO histological grading [27] was used. Tumor budding was evaluated as present or absent [25].

CD3 and FoxP3 immunohistochemistry

For immunohistochemistry, 3.5-μm sections were cut from the retrieved paraffin blocks, deparaffinized in xylene, and rehydrated through graded alcohols. Antigen retrieval was performed in a microwave oven with Tris–EDTA, pH 9.0 (800 W for 2 min, 150 W for 15 min). After neutralizing endogenous peroxidase activity, the sections were incubated at room temperature with either mouse monoclonal CD3 antibody (clone PS1; Leica Biosystems, Newcastle, UK) diluent (1:50) for 30 min or mouse monoclonal FoxP3 antibody (clone 236A/E7, Abcam, Cambridge, UK) diluent (1:100) for 30 min. Bound antibodies were detected using the EnVision™ system (Dako, Copenhagen, Denmark). Diaminobenzidine (DAB) was used as the chromogen and hematoxylin as the counterstain.

Image capturing

The images were captured with an Olympus DP25 camera (Olympus, Center Valley, PA) attached to a Nikon Eclipse E600 microscope (Nikon, Tokyo, Japan) equipped with a ×20 objective. The image format was TIFF with a resolution of 2,560×1,920 pixels. For validation purposes, one series of images for T cell counting was also obtained with a

Nikon Coolpix 4500 camera attached to a Leitz Ortholux II microscope (Leitz, Wetzlar, Germany) using a ×40 objective, JPEG format, and a resolution of 2,272×1,704 pixels.

For positive area percentage estimation, we utilized CD3 staining and 40 lymphoid follicles around the tumors of five different CRC patients, as well as FoxP3 staining and 31 lymphoid follicles from the same patients. Each follicle was photographed once. For immune cell counting, CD3 staining was used, and a median of five (range, 2–11) images were obtained from the invasive front of the tumors (peritumorally) and a median of four (range, 2–7) from the stromal parts of the tumors (intratumorally) representing an average immune cell reaction. Peritumoral T cells of 34 randomly selected cases were used in testing the validity of the automated computer-based cell counting method, while all 235 cases were included in the survival analysis.

Manual analysis of the sections

The manual area percentage estimations were performed semiquantitatively using intervals of 5 % for CD3 and 0.5 % for FoxP3. The manual cell counting was performed on the captured images by ticking off the counted cells. Four observers, who were blinded for the other results, participated in the evaluations (observer 1, JPV; observer 2, JOV; observer 3, SS; observer 4, JPB).

Computer-assisted image analysis

The computer-assisted image analyses were conducted using a Java-based open source image processing software ImageJ v1.44 [28]. The methods were based on three common functions (Fig. 1). First, the rolling ball method was used in background subtraction [29], after which the image was divided into separate color layers by color deconvolution plugin [30] with a built-in vector for separating hematoxylin and DAB. Next, the DAB image was processed using the Threshold tool of ImageJ, which creates a binary mask of the stained area based on its brightness.

Besides these common procedures, the Freehand selections tool and Analyze particles tool of ImageJ were used in the area percentage estimation process (Fig. 2). Universal threshold values for each series were used, and each observer determined the desired threshold level using about five randomly selected images of the series. The cell counting method consisted of six phases: rolling ball background subtraction, color deconvolution, brightness threshold, Gaussian blur, watershed segmentation [31], and analyze particles tool (Fig. 3). The commands were recorded in as a macro for ImageJ enabling a continuous, automated analysis of the images by the program. All the observers used a value of "3" for Gaussian blur and "0.20" for cell circularity, since those require few adjustments when using different equipment and when counting different cell types. Instead, the optimal brightness threshold levels and cell size settings are dependent on the size of the cells and the equipment used, and therefore, each researcher manually determined the desired values using five to ten randomly selected images from the series. A macro and example images for both cell counting and positive area percentage estimation are provided in the Supplementary material.

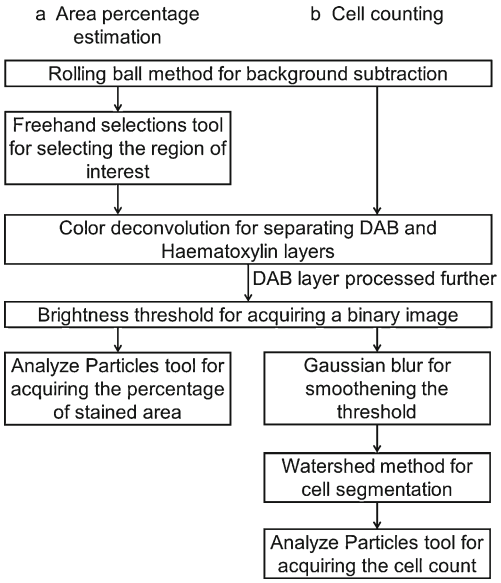

Fig. 1 Flowcharts of the two applications of the computer-based analysis of immunohistochemistry presented in this article

Statistical analyses

Normally distributed continuous variables are presented as mean (standard deviation), whereas other continuous variables are presented as median (interquartile range). Intra- and interobserver correlations between different analysis methods are presented as Pearson correlation coefficients (r). Receiver operating characteristics (ROC) analysis in randomly selected 160 of all 325 (49.2 %) patients from the material was used to determine optimal cutoff scores of CD3 density for discriminating survivors from non-survivors. The Kaplan–Meier method and log-rank test were utilized in the univariate survival analyses, and Cox's proportional hazards regression models were used to analyze the independent prognostic significance of T cell infiltration. Cancer-specific survival was measured. The statistical analyses were conducted using statistical analysis software IBM SPSS Statistics 19 (IBM, Chicago, IL). In all the tests, a two-tailed, exact p value less than 0.05 was considered statistically significant.

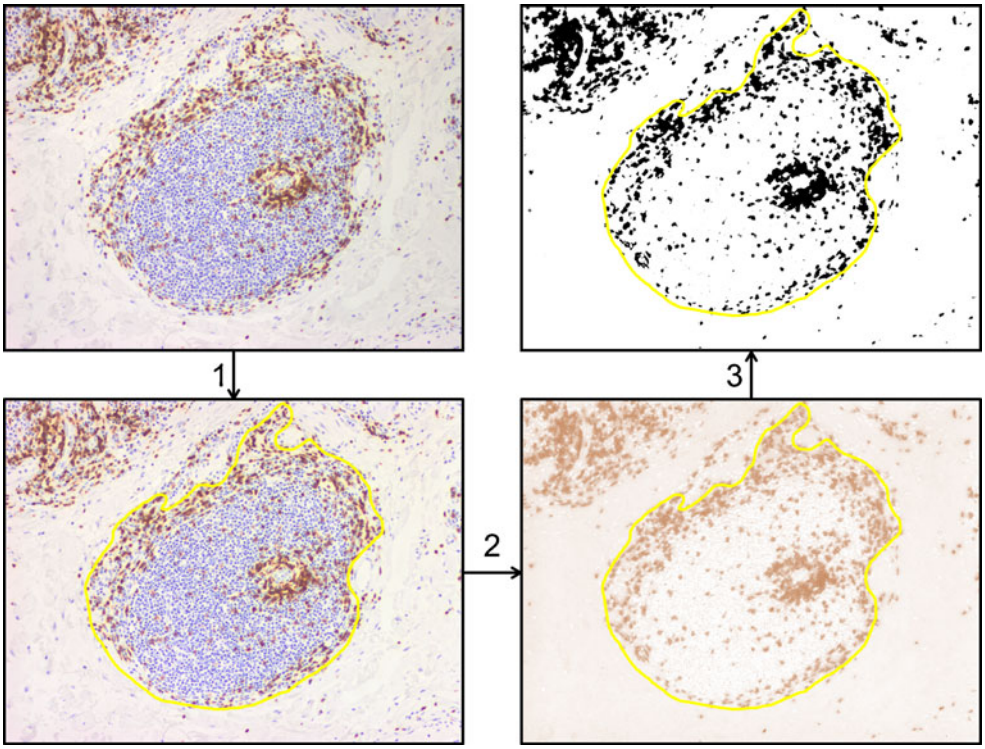

Fig. 2 Example of the computer-assisted evaluation of positive area percentage. The image features a lymphoid follicle with CD3 staining. ×10 magnification. *1* Rolling ball method for background subtraction and freehand selections tool for selecting margins of the lymphoid follicle. *2* Color deconvolution for separating DAB layer. *3* Brightness threshold for acquiring a binary image. The percentage of black pixels within the selected area was counted by the Analyze particles tool and was found to be 16 % in this example

Results

Positive area percentage

The $CD3^+$ area percentage, determined using the computer-assisted method, in the 40 lymphoid follicles varied from 8.6 to 65.0 % (median, 31.85 %). The results acquired by different researchers using ImageJ had a nearly perfect correlation with each other (Pearson r=0.982–0.991) (Table 2, Fig. 4a), indicating an excellent reproducibility of the analysis. The minor variation was related to the determination of the margins of the lymphoid follicles. The threshold levels

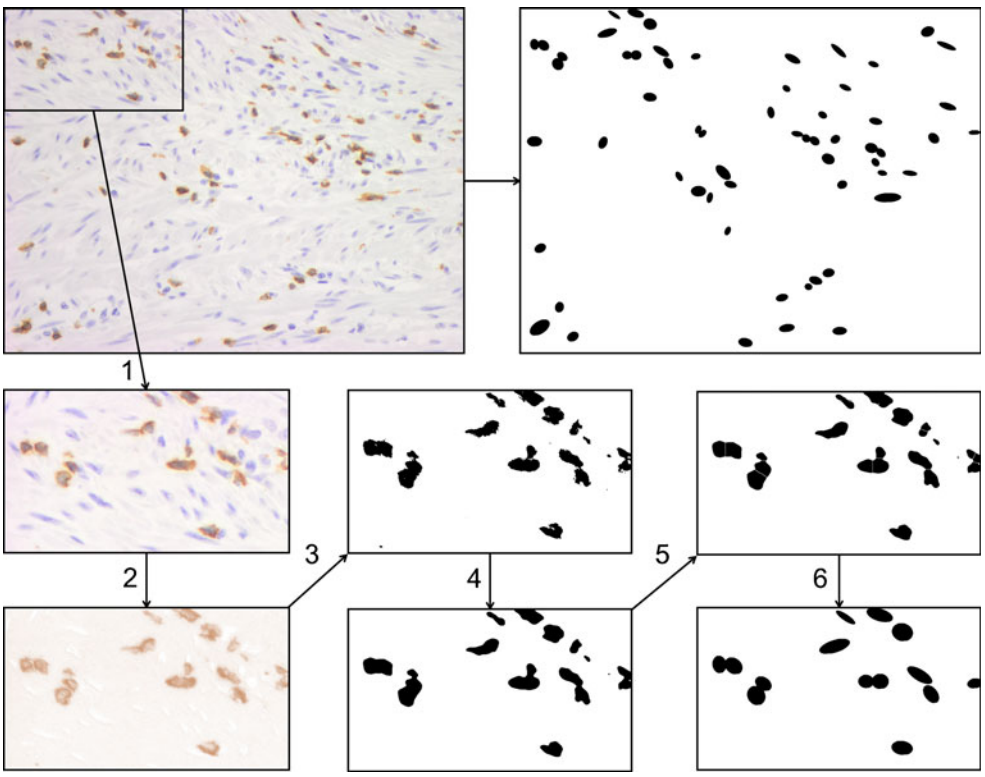

Fig. 3 Example of the automated computer-based cell counting. The image presents peritumoral T cells (CD3 staining). ×20 magnification. In this example, the framed part of the image is inspected in more detail to allow a better visualization of the structures. *1* Rolling ball method for background subtraction. *2* Color deconvolution for the separation of DAB layer. *3* Brightness threshold for the acquisition of a binary image. *4* Gaussian blur for smoothening of the threshold. *5* Watershed method for the segmentation of cells touching each other. *6* Analyze particles function for finding out the cell count. The cells were recognized based on their size and circularity. In this example image, an ellipse is shown for each counted cell

Table 2 Medians, interquartile ranges, and Pearson correlation coefficients for the positive area percentages estimated by different researchers and analysis methods

Series 1, 40 lymphoid follicles with CD3 staining							
Analyzer	JPV, computer	JPV, computer 2	JOV, computer	SS, computer	JPV, manual	JOV, manual	SS, manual
Median (%)	33.1	33.7	31.4	30.1	25.0	37.5	35.0
Interquartile range (%)	23.3–46.3	21.4–45.0	20.6–41.4	19.6–42.3	20.0–50.0	21.3–50.0	20.0–40.0
Pearson correlation coefficient							
JPV, computer		0.991	0.984	0.990	0.912	0.865	0.793
JPV, computer 2			0.982	0.989	0.911	0.884	0.794
JOV, computer				0.985	0.896	0.867	0.821
SS, computer					0.901	0.869	0.812
JPV, manual						0.864	0.790
JOV, manual							0.777
Series 2, 31 lymphoid follicles with FoxP3 staining							
Analyzer	JPV, computer	JPV, computer 2	JOV, computer	SS, computer	JPV, manual	JOV, manual	SS, manual
Median (%)	1.4	1.8	1.7	1.8	1.5	2.5	1.5
Interquartile range (%)	0.8–2.3	1.2–3.0	0.9–2.7	1.1–2.8	1.0–3.0	1.0–4.0	1.0–3.0
Pearson correlation coefficient							
JPV, computer		0.993	0.975	0.987	0.799	0.868	0.912
JPV, computer 2			0.971	0.987	0.795	0.856	0.920
JOV, computer				0.959	0.750	0.827	0.905
SS, computer					0.812	0.860	0.921
JPV, manual						0.863	0.795
JOV, manual							0.847

The evaluations are named by the initials of the photographer/analyzer (e.g. JPV), the analysis method (computer, computer-assisted; manual, manual semiquantitative), and if needed, a number to distinguish multiple evaluations of one type. The computer-assisted analysis was performed as depicted in Figs. 1 and 2, whereas the manual estimations were done semiquantitatively using intervals of 5 % (CD3) or 0.5 % (FoxP3)

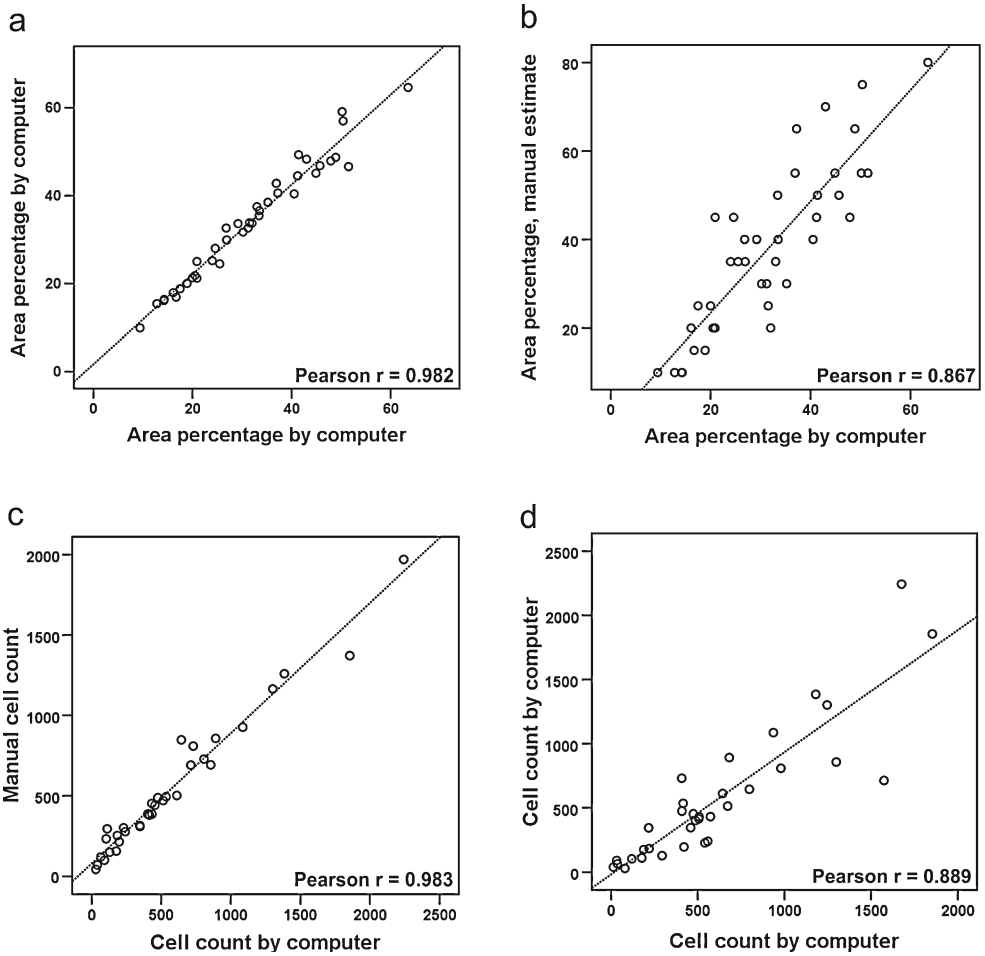

Fig. 4 Reproducibility and the accuracy of the computer-assisted immunohistochemistry analysis methods. **a**, **b** Positive area percentage evaluation ($CD3^+$ area in lymphoid follicles). **a** Example of the correlation between the results of computer-assisted analysis by different researchers (JOV computer, JPV computer 2). **b** Example of the correlation between the computer-assisted evaluation and the manual estimation from the same researcher (JOV computer, JOV manual). **c**, **d** Cell counting (peritumoral $CD3^+$ T cells). **c** Example of the correlation between cell counts by manual counting and computer-based analysis (JPV computer 1, JPV manual 1). **d** Example of the correlation between automated cell counts from different image series (JOV computer 2, JPV computer 1). The abbreviations (e.g. JOV computer 1) denote initials of the analyzer, analysis method (computer, computer-assisted; manual), and, if needed, a number to distinguish multiple evaluations of one type (Tables 2 and 3)

set by different researchers ranged from 151 (SS) to 160 (JPV), causing only marginal differences in the median and interquartile range (IQR) scores of different researchers. Also, manual semiquantitative estimations achieved an excellent correlation with each other as well as with the computer-assisted analysis (Pearson r=0.777–0.912) (Fig. 4b). However, the correlations were still considerably lower than in the computer-assisted analysis, and also, the median and IQR scores showed a lot more variation. Another set of 31 lymphoid follicles with FoxP3 staining (positive area percentage ranging from 0.6 to 6.3 %) was also included in the study, and the results of the reproducibility were comparable to the first set of lymphoid follicles with CD3 staining (Table 2).

Immune cell counting

Peritumoral $CD3^+$ T cell densities ranged from 1.8 to 2,243 cells/mm^2 (median, 471 cells/mm^2) in the 34 CRC cases used in testing the validity of the cell counting method. The automated cell counting method achieved an almost perfect correlation with manual cell counting from the same images (Pearson r=0.960–0.987) (Table 3, Fig. 4c). Unlike the semiquantitative estimation used in the previous section of the study, manual cell counting can be considered accurate when performed thoroughly [4]. Therefore, these high correlations between the manual cell counts and the counts yielded by the computer-assisted method support the accuracy of the automated counting. The slight variation was found to be a result of either weakly positive immunoreaction in the T cells or background staining. Different image series from the same sections were included in the study to see the effect of photographed tumor location selections on the cell counts and thus evaluate the overall reproducibility of the immune cell assessment for each case. Although more variation was observed, the correlations with other series were still excellent (Pearson r=0.832–0.934) (Fig. 4d), indicating that the number of images captured for each case was sufficient. The results acquired with the older equipment and in another institution (Jyväskylä Central Hospital, Department of Pathology, Jyväskylä, Finland) were also comparable. The time consumption of the cell counting methods was measured using 20 randomly selected images; observer 1 (JPV) averaged 42.05 s/image (0.46 s/cell) in manual counting, and observer 2 (JOV) averaged 49.9 s/image (0.54 s/cell) in manual counting. Regardless of

Table 3 Medians, interquartile ranges, and Pearson correlation coefficients for T cell counts acquired by different researchers and cell counting methods

Analyzer	JPV, computer 1	JPV, manual 1	JOV, computer 2	JPV, computer 2	JPB, computer 2	JOV, manual 2	JPV, manual 2	JPV, computer 3	JPV, computer 4
Image series	1	1	2	2	2	2	2	3	4
Photographer	JPV	JPV	JOV	JOV	JOV	JOV	JOV	JPV	JPV
Median (cells/mm^2)	432.3	413.8	497.1	616.6	706.4	448.4	531.1	554.3	509.9
Interquartile range (cells/mm^2)	182.0–749.6	249.2–748.3	218.7–831.8	291.9–1,123.4	340.7-1,257.7	248.0–592.3	227.3–868.4	353.0–1,015.9	261.4–1,142.5
Pearson correlation coefficient									
JPV, computer 1		0.983	0.889	0.866	0.848	0.876	0.899	0.911	0.922
JPV, manual 1			0.862	0.847	0.832	0.859	0.885	0.900	0.923
JOV, computer 2				0.994	0.983	0.979	0.986	0.844	0.918
JPV, computer 2					0.996	0.975	0.987	0.846	0.923
JPB, computer 2						0.960	0.975	0.836	0.912
JOV, manual 2							0.973	0.843	0.899
JPV, manual 2								0.868	0.934
JPV, computer 3									0.910

The evaluations are named by the initials of the analyzer (e.g. JPV), the analysis method (computer, computer-assisted automated; manual), and image series number. Image series 1, 2, and 3 were captured with Olympus DP25, whereas image series 4 was captured with Nikon Coolpix 4500. Automated cell counting was performed as depicted in Figs. 1 and 3. Manual analysis was conducted by ticking off the cells from the corresponding images. All the values are based on 34 colorectal cancer cases

the observer, the automated cell counting macro averaged 6.75 s/image (0.07 s/cell).

In the final part of the study, we determined the peritumoral and stromal CD3$^+$ T cell density of all 235 CRC patients using the automated cell counting procedure. No method-related issues were encountered during the analysis. First, the survival effect of CD3 densities was determined in univariate analyses (Fig. 5). ROC analysis was used to set optimal cutoff scores for CD3 density in discriminating survivors from non-survivors (Fig. 5a), and optimal values were 590 CD3$^+$ cells/mm^2 at the invasive front and 475 CD3$^+$ cells/mm^2 in the tumor stroma. T cells at the invasive front had a slightly higher area under the curve than stromal T cells (0.651 vs. 0.624). Kaplan–Meier curves showed that higher T cell counts on both locations associated with better survival (Fig. 5b and c). We decided to combine these scores into a three-tiered "CD3 overall" variable, where "low-grade" denoted low grade on both invasive front and stroma, "average" denoted high grade in either invasive front or stroma, and "high-grade" denoted high grade on both invasive front and stroma (Fig. 5d). High grade on both locations was observed to be a requirement for better survival, and thus, classes "average" and "low-grade" were combined for the later analyses. This new classification was found to strongly associate with disease-specific survival in stages I–IV (Fig. 5e), as well as in stages I–III (Fig. 5f). Cox's proportional hazards regression analysis was used to study the independent prognostic value of T cell infiltration, and in our material, the 2-grade overall CD3 density was found to be an independent prognostic factor in both stages I–IV (Table 4) and I–III (Table 5).

Discussion

This study provides knowledge on the availability and the functionality of free computer-based analyzing methods for immunohistochemistry. Our modification, based on separating DAB and hematoxylin color layers and then applying a brightness threshold, was accurate in estimating the percentage of the area with a positive immunoreaction and in counting positive cells and thus in assessing both follicular and non-follicular inflammatory infiltrate in CRC specimens. Moreover, automated image analysis was suitable for the analysis of large volumes of CRC cases in terms of the amount of time it took. Accurate measurements of stromal and peritumoral T cell densities by automated analysis were found to have independent prognostic value in CRC in our material.

Our five-phased method for assessing the percentage of positive area was tested in estimating the percentage of the area containing T cells (antigen CD3) and regulatory T cells (FoxP3) in CRC-associated lymphoid aggregates. The

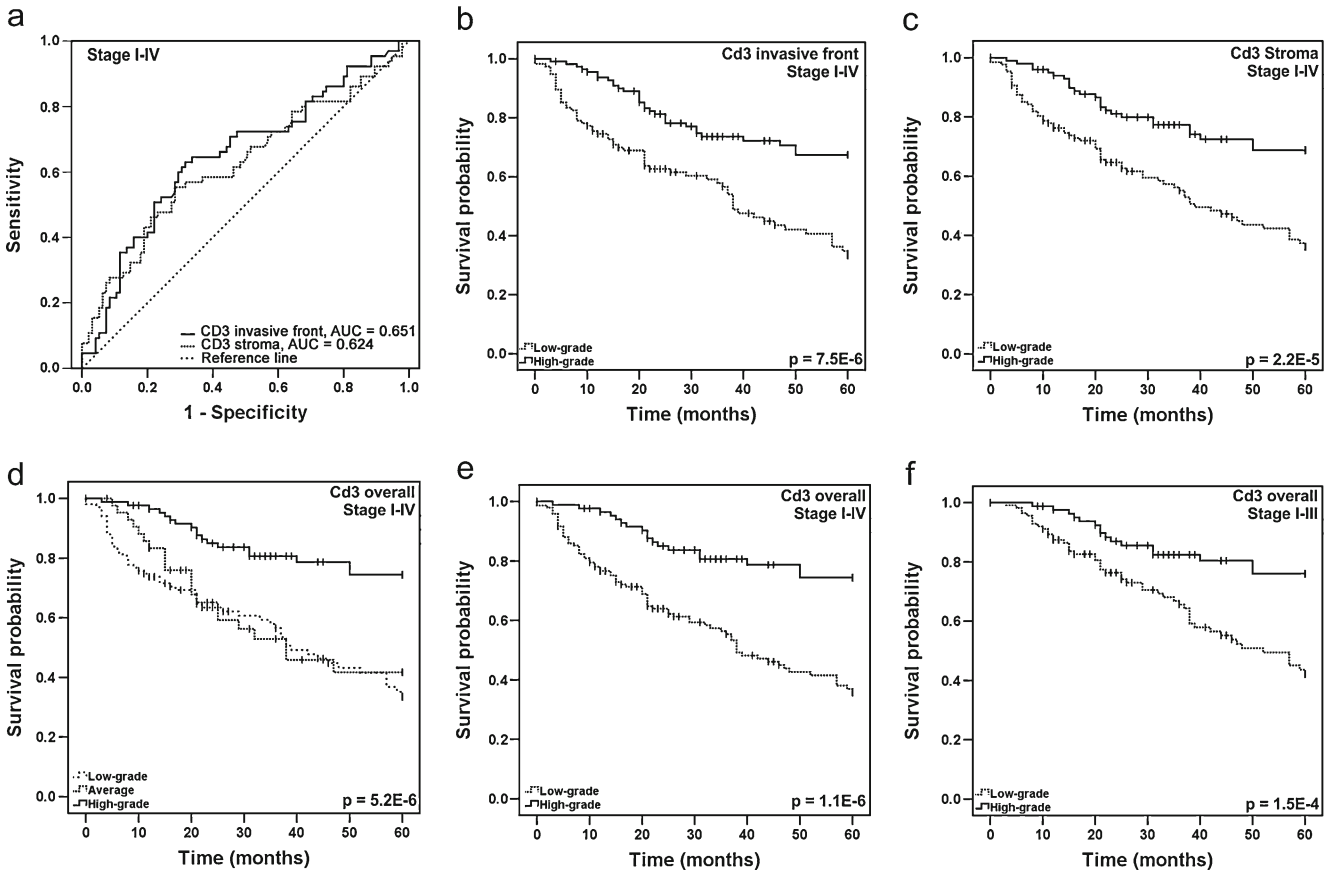

Fig. 5 Prognostic significance of T cell infiltration in colorectal cancer. **a** ROC curves for discriminating survivors from non-survivors. The curves were used in classifying the cell densities into high grade and low grade for the survival analyses. **b–f** Kaplan–Meier curves for the effect of T cell infiltration on disease-specific survival. High-grade T cell infiltration on both the invasive front (**b**) and the stromal parts (**c**) of the tumor associated with better survival. In overall T cell infiltration (**d**), "low-grade" denotes low grade on both invasive front and stroma, "average" denotes high grade in either invasive front or stroma, and "high-grade" denotes high grade on both invasive front and stroma. High grade on both locations was a requirement for the survival effect, and thus, classes "average" and "low-grade" were combined for **e** and **f**. High-grade overall T cell infiltration was a strong predictor of survival in stages I–IV (**e**) as well as in stages I–III (**f**). All the *p* values are for log-rank test

Table 4 Cox's proportional hazards regression analysis for the independent prognostic significance of CD3 cell density in stage I–IV colorectal cancer

	Hazard ratio	95 % CI	*p* value
Depth of invasion (T1–2 vs. T3–4)	2.51	1.06–5.93	0.036
Nodal metastases (N0 vs. N1–2)	2.21	1.35–3.60	1.5E-3
Distant metastases (M0 vs. M1)	3.99	2.38–6.65	1.4E-8
WHO grade (1–2 vs. 3)	1.80	1.07–3.03	0.028
Tumor location (colon vs. rectum)	1.56	1.02–2.38	0.041
Tumor budding (no vs. yes)	2.67	1.72–4.17	1.4E-5
CD3 cell density (low grade vs. high grade)	0.49	0.28–0.85	0.011

The model represents disease-specific survival and is based on 235 patients. It was constructed using the backward conditional method restricting the model to statistically significant variables. Considered variables included T class, N class, M class, grade, age, sex, tumor location, tumor budding, and overall CD3 density

method could have a wide variety of other applications in evaluating the percentage of tumor cells expressing certain cytoplasmic proteins. We compared the computer-based method with a manual semiquantitative analysis method utilizing percentage intervals. Supporting earlier reports on its functionality [21], the semiquantitative method also showed an excellent reproducibility in the assessment of the composition of the lymphoid follicles especially in the higher percentages, but did not reach the nearly perfect level of reproducibility and accuracy of the computer-assisted method. Therefore, the more exact computer-assisted area percentage estimation could be especially helpful when the variation between cases is small.

In this study, we used immune cell counting as a comprehensively studied example of the application of computer-based image analysis. Earlier, several different methods have been utilized in assessing immune cell infiltration in CRC specimens, each having a number of

Table 5 Cox's proportional hazards regression analysis for the independent prognostic significance of CD3 cell density in stage I–III colorectal cancer

	Hazard ratio	95 % CI	*p* value
Depth of invasion (T1–2 vs. T3–4)	2.55	1.08–6.03	0.033
Nodal metastases (N0 vs. N1–2)	2.14	1.25–3.65	5.3E−3
Tumor location (colon vs. rectum)	1.75	1.01–2.84	0.025
Tumor budding (no vs. yes)	2.16	1.27–3.65	4.3E−3
CD3 cell density (low grade vs. high grade)	0.46	0.25–0.82	9.2E−3

The model represents disease-specific survival and is based on 202 patients. It was constructed using the backward conditional method restricting the model to statistically significant variables. Considered variables included T class, N class, grade, age, sex, tumor location, tumor budding, and overall CD3 density

advantages and disadvantages (Table 6). Manual evaluation with two- to four-tiered categorical variables has been commonly used and is quick to perform [16, 18, 32, 33], but these assessments are subjective, and the lack of continuous variables also limits the applicability of statistical methods including correlation analyses, ROC analysis, and linear regression and can lead to difficulties in comparing the results of different studies [4, 34]. Manual cell counting from captured images is exact, and we used it as a method to compare with automated computer-based cell counting. We found that cell counts determined by automated cell counting had a nearly perfect correlation with the manual cell counts from the same images, highlighting the accuracy of the automated counting method. One significant advantage of the automated counting was time efficiency, since it was 85 % faster than average manual counting. As an example, analysis of our 235 CRC cases (each with an average of ten images) would take the fastest manually counting individual 27.4 h while the computer would finish the task in about 4.4 h. Moreover, computer-assisted counting needs only to be supervised whereas manual counting is strenuous, and the rate of manual analysis of immunohistochemistry has been shown to decrease when large series have to be assessed [35], yet increasing the time savings achieved by automated analysis. Instead, time saving is less significant if the number of cases is small or the number of infiltrating immune cells is low.

In the final part of this study, we addressed the potential prognostic role of T cells in CRC. Intense overall T cell infiltrate, as determined by automated computer-aided image analysis, was found to have independent prognostic value in our material, in agreement with results published earlier [13, 36]. Still, at least three studies report only a tendency towards better survival for tumors with higher T cell counts, lacking statistical significance on multivariate analysis [22, 32, 33]. However, in two of these studies, the categorical nature of the collected data could have contributed to the non-significant result [32, 33], stressing the importance of avoiding arbitrary predetermined classification of variables in the study of potential tumor markers. In all, our study added convincing evidence of the positive prognostic value of T cells in CRC, and the clinical value of assessing immune cell infiltrate in CRC will likely be further clarified in the coming years [37].

Since the late 1980s when the first methods were described [38], the precision and the advantages of commercially available computer-based platforms for the analysis of immunohistochemistry have been shown in a number of studies [24, 35]. However, the availability of these automated analysis machines is still limited due to high cost. Therefore, freely available solutions such as the color layer separation and brightness threshold-based methods that we describe here represent a viable chance to improve the

Table 6 Pros and cons of some of the methods used in analyzing immune cell infiltration in colorectal cancer

Computer-assisted using ImageJ	Computer-assisted commercial	Manual counting from captured images	Manual counting without image capturing	Manual evaluation utilizing 2–4 categories
Pros:				
Provides continuous variables	Provides continuous variables	Provides continuous variables	Provides continuous variables	Time efficiency
Exactness	Exactness	Exactness		
Objectivity	Objectivity			
Time efficiency	Time efficiency			
	Technical support from the manufacturer			
Cons:				
Potential errors related to incorrect calibration	Potential errors related to incorrect calibration	Potential errors related to subjectivity	Potential errors related to subjectivity	Potential errors related to subjectivity
	Costs	Time consumption	Inaccuracy in higher cell counts	Does not provide continuous variables

exactness of the analysis of immunohistochemistry. When adapting new analysis methods, their potential sources of error need to be identified. In our data, the minor differences in the cell counts by the computer-aided method and manual counting from the same images were due to either excessive background staining or a weakly positive immunoreaction, and these need to be noted when employing the methods in subsequent studies. Also stable staining protocols and image capturing conditions are needed to allow balanced and accurate automated analysis. Furthermore, valid selection of brightness threshold limits, Gaussian blur, and cell size and circularity are of importance.

Also, the percentage of the nuclei with a positive immunoreaction can be estimated using image analysis based on separating hematoxylin and DAB color layers and applying a brightness threshold, and we have tested a slightly modified version of the cell counting macro (i.e., after color deconvolution, the rest of the described phases of the cell counting method applied to both DAB and hematoxylin layers) in the analysis of ER, progesterone receptor (PR), and Ki-67 in breast cancer (data not shown). Also, in this application, the results were accurate, but the nuclei of stromal fibroblasts and inflammatory cells were in some cases difficult to distinguish from the negative nuclei of breast cancer cells in the hematoxylin layer. Therefore, additional calibrations for brightness threshold and cell size were required for each cancer case limiting the time-saving advantages of the method compared to manual nuclei counting. Moreover, a plugin for ImageJ called ImmunoRatio has recently been developed and proven to be accurate in the analysis of ER, PR, and Ki-67 [39], and thus, we did not include positive nuclei percentage evaluation in this study. Compared to the methods we described, ImmunoRatio plugin includes some additional elements like blankfield correction for uneven illumination, which, if needed, can also be easily added to the methods we used because of the high modality of ImageJ. In this study, we aimed to keep the described methods as straightforward as possible without sacrificing accuracy. The methods indeed achieved excellent reproducibility, while the reasons behind the methods remained easy to understand and they were easy to use. Furthermore, since the methods consist of only a few basic functions, image analysis based on the same approaches can also be carried out using other freely available image analysis programs like CellProfiler [40].

In conclusion, our results suggest that computer-assisted image analysis based on separating DAB and hematoxylin layers and applying a brightness threshold provides a good, freely available alternative to the traditional methods of analyzing immunohistochemical sections in cancer research, as well as in clinical practice. In positive area percentage evaluation, the advantages of using computer-based analysis included objectivity, exactness, and reproducibility, whereas automated cell counting also saved significant amounts of time in the analysis of a series of cancer cases.

Acknowledgments We express our sincere gratitude to Ms. Riitta Vuento for her substantial assistance in the preparation of the study material. This work was supported by grants from the Academy of Finland, Emil Aaltonen Foundation, Finnish Cancer Foundation, and Northern Finland Cancer Foundation.

Conflict of interest The authors declare that they have no conflict of interest.

References

1. Taneja P, Maglic D, Kai F, Zhu S, Kendig RD, Fry EA, Inoue K (2010) Classical and novel prognostic markers for breast cancer and their clinical significance. Clin Med Insights Oncol 4:15–34
2. Hanahan D, Weinberg RA (2011) Hallmarks of cancer: the next generation. Cell 144:646–674
3. Zlobec I, Lugli A (2008) Prognostic and predictive factors in colorectal cancer. J Clin Pathol 61:561–569
4. Walker RA (2006) Quantification of immunohistochemistry—issues concerning methods, utility and semiquantitative assessment I. Histopathology 49:406–410
5. Jemal A, Siegel R, Ward E, Hao Y, Xu J, Thun MJ (2009) Cancer statistics, 2009. CA Cancer J Clin 59:225–249
6. Puppa G, Sonzogni A, Colombari R, Pelosi G (2010) TNM staging system of colorectal carcinoma: a critical appraisal of challenging issues. Arch Pathol Lab Med 134:837–852
7. Zlobec I, Vuong T, Compton CC, Lugli A, Michel RP, Hayashi S, Jass JR (2008) Combined analysis of VEGF and EGFR predicts complete tumour response in rectal cancer treated with preoperative radiotherapy. Br J Cancer 98:450–456
8. Zafirellis K, Agrogiannis G, Zachaki A, Gravani K, Karameris A, Kombouras C (2008) Prognostic significance of VEGF expression evaluated by quantitative immunohistochemical analysis in colorectal cancer. J Surg Res 147:99–107
9. Rego RL, Foster NR, Smyrk TC, Le M, O'Connell MJ, Sargent DJ, Windschitl H, Sinicrope FA (2010) Prognostic effect of activated EGFR expression in human colon carcinomas: comparison with EGFR status. Br J Cancer 102:165–172
10. Curran S, Dundas SR, Buxton J, Leeman MF, Ramsay R, Murray GI (2004) Matrix metalloproteinase/tissue inhibitors of matrix metalloproteinase phenotype identifies poor prognosis colorectal cancers. Clin Cancer Res 10:8229–8234
11. de Visser KE, Eichten A, Coussens LM (2006) Paradoxical roles of the immune system during cancer development. Nat Rev Cancer 6:24–37
12. Schreiber RD, Old LJ, Smyth MJ (2011) Cancer immunoediting: integrating immunity's roles in cancer suppression and promotion. Science 331:1565–1570
13. Galon J, Costes A, Sanchez-Cabo F, Kirilovsky A, Mlecnik B, Lagorce-Pages C, Tosolini M, Camus M, Berger A, Wind P, Zinzindohoue F, Bruneval P, Cugnenc PH, Trajanoski Z, Fridman WH, Pages F (2006) Type, density, and location of immune cells within human colorectal tumors predict clinical outcome. Science 313:1960–1964
14. Klintrup K, Makinen JM, Kauppila S, Vare PO, Melkko J, Tuominen H, Tuppurainen K, Makela J, Karttunen TJ, Makinen MJ (2005) Inflammation and prognosis in colorectal cancer. Eur J Cancer 41:2645–2654
15. Simpson JA, Al-Attar A, Watson NF, Scholefield JH, Ilyas M, Durrant LG (2010) Intratumoral T cell infiltration, MHC class I

and STAT1 as biomarkers of good prognosis in colorectal cancer. Gut 59:926–933
16. Forssell J, Oberg A, Henriksson ML, Stenling R, Jung A, Palmqvist R (2007) High macrophage infiltration along the tumor front correlates with improved survival in colon cancer. Clin Cancer Res 13:1472–1479
17. Zlobec I, Lugli A (2009) Invasive front of colorectal cancer: dynamic interface of pro-/anti-tumor factors. World J Gastroenterol 15:5898–5906
18. Naito Y, Saito K, Shiiba K, Ohuchi A, Saigenji K, Nagura H, Ohtani H (1998) CD8+ T cells infiltrated within cancer cell nests as a prognostic factor in human colorectal cancer. Cancer Res 58:3491–3494
19. Lugli A, Karamitopoulou E, Panayiotides I, Karakitsos P, Rallis G, Peros G, Iezzi G, Spagnoli G, Bihl M, Terracciano L, Zlobec I (2009) CD8+ lymphocytes/tumour-budding index: an independent prognostic factor representing a 'pro-/anti-tumour' approach to tumour host interaction in colorectal cancer. Br J Cancer 101:1382–1392
20. Doger FK, Meteoglu I, Tuncyurek P, Okyay P, Cevikel H (2006) Does the EGFR and VEGF expression predict the prognosis in colon cancer? Eur Surg Res 38:540–544
21. Zlobec I, Steele R, Michel RP, Compton CC, Lugli A, Jass JR (2006) Scoring of p53, VEGF, Bcl-2 and APAF-1 immunohistochemistry and interobserver reliability in colorectal cancer. Mod Pathol 19:1236–1242
22. Nosho K, Baba Y, Tanaka N, Shima K, Hayashi M, Meyerhardt JA, Giovannucci E, Dranoff G, Fuchs CS, Ogino S (2010) Tumour-infiltrating T-cell subsets, molecular changes in colorectal cancer, and prognosis: cohort study and literature review. J Pathol 222:350–366
23. Taylor CR, Levenson RM (2006) Quantification of immunohistochemistry—issues concerning methods, utility and semiquantitative assessment II. Histopathology 49:411–424
24. Gokhale S, Rosen D, Sneige N, Diaz LK, Resetkova E, Sahin A, Liu J, Albarracin CT (2007) Assessment of two automated imaging systems in evaluating estrogen receptor status in breast carcinoma. Appl Immunohistochem Mol Morphol 15:451–455
25. Horkko TT, Klintrup K, Makinen JM, Napankangas JB, Tuominen HJ, Makela J, Karttunen TJ, Makinen MJ (2006) Budding invasive margin and prognosis in colorectal cancer—no direct association with beta-catenin expression. Eur J Cancer 42:964–971
26. Sobin LH, Wittekind C (2002) TNM classification of malignant tumours, 6th edn. Wiley-Liss, New York
27. Hamilton SR, Vogelstein B, Kudo S, Riboli E, Nakamura S, Hainaut P, Rubio CA, Sobin LH, Fogt F, Winawer SJ, Goldgar DE, Jass JR (2000) Carsinoma of the colon and rectum. In: Hamilton SR, Aaltonen LA (eds) World Health Organization classification of tumours. Pathology and genetics of tumours of the digestive system. IARC Press, Lyon, pp 103–143
28. Abramoff MD, Magelhaes PJ, Ram SJ (2004) Image processing with ImageJ. Biophotonics International 11:36–42
29. Sternberg SR (1983) Biomedical image processing. IEEE Computer 16:22–34
30. Ruifrok AC, Johnston DA (2001) Quantification of histochemical staining by color deconvolution. Anal Quant Cytol Histol 23:291–299
31. Beucher S, Meyer F (1993) The morphological approach to segmentation: the watershed transformation. In: Dougherty ER (ed) Mathematical morphology in image processing, 1st edn. Marcel Dekker, New York, pp 433–481
32. Takemoto N, Konishi F, Yamashita K, Kojima M, Furukawa T, Miyakura Y, Shitoh K, Nagai H (2004) The correlation of microsatellite instability and tumor-infiltrating lymphocytes in hereditary non-polyposis colorectal cancer (HNPCC) and sporadic colorectal cancers: the significance of different types of lymphocyte infiltration. Jpn J Clin Oncol 34:90–98
33. Deschoolmeester V, Baay M, Van Marck E, Weyler J, Vermeulen P, Lardon F, Vermorken JB (2010) Tumor infiltrating lymphocytes: an intriguing player in the survival of colorectal cancer patients. BMC Immunol 11:19
34. Zlobec I, Steele R, Terracciano L, Jass JR, Lugli A (2007) Selecting immunohistochemical cut-off scores for novel biomarkers of progression and survival in colorectal cancer. J Clin Pathol 60:1112–1116
35. Ong CW, Kim LG, Kong HH, Low LY, Wang TT, Supriya S, Kathiresan M, Soong R, Salto-Tellez M (2010) Computer-assisted pathological immunohistochemistry scoring is more time-effective than conventional scoring, but provides no analytical advantage. Histopathology 56:523–529
36. Dahlin AM, Henriksson ML, Van Guelpen B, Stenling R, Oberg A, Rutegard J, Palmqvist R (2011) Colorectal cancer prognosis depends on T-cell infiltration and molecular characteristics of the tumor. Mod Pathol 24:671–682
37. Pages F, Galon J, Dieu-Nosjean MC, Tartour E, Sautes-Fridman C, Fridman WH (2010) Immune infiltration in human tumors: a prognostic factor that should not be ignored. Oncogene 29:1093–1102
38. Bacus S, Flowers JL, Press MF, Bacus JW, McCarty KS Jr (1988) The evaluation of estrogen receptor in primary breast carcinoma by computer-assisted image analysis. Am J Clin Pathol 90:233–239
39. Tuominen VJ, Ruotoistenmaki S, Viitanen A, Jumppanen M, Isola J (2010) ImmunoRatio: a publicly available web application for quantitative image analysis of estrogen receptor (ER), progesterone receptor (PR), and Ki-67. Breast Cancer Res 12:R56
40. Lamprecht MR, Sabatini DM, Carpenter AE (2007) Cell Profiler: free, versatile software for automated biological image analysis. Biotechniques 42:71–75

Virchows Arch (2012) 460:467–472
DOI 10.1007/s00428-012-1225-z

ORIGINAL ARTICLE

Nonsebaceous lymphadenoma of salivary glands: proposed development from intraparotid lymph nodes and risk of misdiagnosis

Christoph Weiler · Abbas Agaimy · Pamela Zengel · Johannes Zenk · Thomas Kirchner · Stephan Ihrler

Received: 26 September 2011 / Revised: 20 December 2011 / Accepted: 13 March 2012 / Published online: 4 April 2012
© Springer-Verlag 2012

Abstract Nonsebaceous lymphadenoma (NSLA) is a rare benign salivary gland tumor composed of lymphoid and epithelial components. By definition, the epithelial component lacks sebaceous differentiation and instead displays a wide range of histological differentiation. In this study, we have collected nine cases of NSLA to characterize their histological and immunohistochemical profiles. The samples were histologically reviewed and immunohistochemical stains for CK5/6, CK7, CK14, CK18, p63, and Ki67 performed. Patients were six males and three females (mean age, 50 years). All tumors were located in the parotid gland and showed intimate intermingling of lymphoid tissue with islands or strands of epithelium with a wide spectrum of histological differentiation. The immunohistochemical profiles mirrored the epithelial differentiation; hence, areas with basaloid or lymphoepithelial differentiation strongly expressed CK5/6, CK14, and p63, while areas with ductal differentiation showed strong positivity for CK18/CK7 and CK5/6/CK14/p63 in luminal and basal cell layers, respectively. A hilus structure with salivary inclusions or D2-40 (podoplanin)-positive marginal sinus was identifiable in four and nine of the cases, respectively, supporting origin within intra-/periparotid lymph nodes. Six cases were initially misdiagnosed as other benign (n=4) or malignant tumors (n=2). Our study on the second largest series of NSLA reported to date provides strong evidence that NSLA belongs to the group of salivary gland tumors that pathogenetically develop from embryonic salivary gland inclusions in intra-/periparotid lymph nodes. Knowledge of the wide histological spectrum of this rare and presumably underreported tumor is important in order to avoid misdiagnosis, particularly as malignant tumor.

Keywords Nonsebaceous lymphadenoma · Salivary gland · Parotid gland · Pathogenesis · Lymph node

C. Weiler (✉) · T. Kirchner · S. Ihrler
Institute of Pathology, Ludwig Maximilian University,
Thalkirchnerstraße 36,
D-80337 München, Germany
e-mail: christoph.weiler@lrz.uni-muenchen.de

A. Agaimy
Institute of Pathology, University Hospital Erlangen,
Erlangen, Germany

P. Zengel
Department of Otorhinolaryngology, Head and Neck Surgery,
Grosshadern Medical Center, Ludwig Maximilian University,
Munich, Germany

J. Zenk
Department of Otorhinolaryngology, Head and Neck Surgery,
University Hospital Erlangen,
Erlangen, Germany

S. Ihrler
Laboratory for Dermatohistology and Oral pathology,
Munich, Germany

C. Weiler
Amedes MVZ for Gynecology and Pathology,
Maximilianstraße 38,
80539 Munich, Germany

Introduction

Since the first description of a case designated as 'nonsebaceous lymphadenoma' (NSLA) in 1991 by Auclair et al. [1], a total of 17 cases of this rare entity have been described, mostly as single case reports or small case series [2–11]. NSLA was officially recognized as a separate tumor entity by the World Health Organization's (WHO) classification in 2005 [12], distinct from the more common sebaceous lymphadenoma. NSLA is defined as a benign salivary tumor,

composed of intimately intermingled lymphoid and epithelial components, the latter being devoid of sebaceous, oncocytic, clear cell, and mucinous differentiation [3, 7, 9, 10, 12, 13]. During the revision of this article, a large series of salivary gland lymphadenoma (n=33) including 11 cases of NSLA was published [13]. Thus, the nine cases described in our study represent the second largest series to date of this rare salivary gland tumor, increasing the total number of reported cases to 37 cases in the English literature.

Analogous to Warthin's tumor, a pathogenetic development of NSLA from intraparotid lymph nodes harboring embryonic salivary gland inclusions has been proposed [2, 8, 13] but refuted by the majority of authors [3, 4, 6, 7, 9–11]. The present findings represent arguments for a pathogenetic development of NSLA from intraparotid lymph nodes. Knowledge of this rare tumor entity is important, as misdiagnosis occurs frequently.

Material and methods

Material

Seven cases were retrieved from the records of the Institute of Pathology, Ludwig Maximilian University, Munich and the Institute of Pathology, University Hospital Erlangen and two cases from the consultation files of one of the authors (SI). The investigation was undertaken according to the guidelines of the local research ethics committee.

Methods

The specimens were fixed in 4% buffered formaldehyde, embedded in low melting point paraffin wax (Vogel, Germany) and cut into serial sections of 4 μm. Antibodies for p63 (BC4A4, Biocare Medical, USA/dilution 1:100), pancytokeratin (Lu-5, Biocare Medical, USA/dilution 1:500), cytokeratin (CK) subtype 7 (Ks7.18, Progen, Germany/dilution 1:500), CK14 (MCA890, Serotec, Germany/dilution 1:400), CK18 (Ks18.04, Progen, Germany/dilution 1:450), CK5/6 (D5/16 B4, Roche Tissue Diagnostics Basel, Switzerland/dilution 1:50), and the proliferation-associated antigen Ki67 (MIB1, Dako, Germany/dilution 1:50) were applied as described in previous investigations by our group [14, 15]. For MIB1, the alkaline phosphatase–antialkaline phosphatase (APAAP) method was used (APAAP-ChemMate, Dako, Germany). For the other antibodies, an avidin–biotin–peroxidase complex (ABC) method was applied (ABC kit, Vector, UK). Because of the high level of endogenous biotin, especially in eosinophilic cells of salivary glands, a biotin-blocking system (Biotin-Blocking System X0590, Dako, Germany) was added to the ABC method.

Results

Clinical and histological data are summarized in Table 1. The cases included six males and three females aged between 40 and 65 years with a mean age of 50 years. A parotid mass was the presenting symptom in all cases, and none of the patients had clinical evidence of Sjögren syndrome or human immunodeficiency virus (HIV) infection. In two cases, a positive and in three cases, a negative smoking history was found. However, in four cases (including two referral cases) information regarding smoking history was not available. All tumors were located in the region of parotid glands. Surgical excision was complete in all cases. There was no reported recurrence in any of the cases. The tumor size ranged from 1.2 to 3.5 cm with an average of 2.0 cm. All tumors were macroscopically and microscopically well circumscribed and surrounded by a thin fibrous capsule (Fig. 1). Histologically, they showed intimate intermingling of organoid lymphoid tissue with islands and strands of epithelium, the latter comprising 20% to 70% of the whole tumor area (Fig. 2a, b, d, e, f, g).

The lymphoid component showed characteristics of lymph nodes. A hilus structure with embryonic inclusion of salivary gland parenchyma was clearly identifiable in four cases, equivalent to a typical hilus structure of intraparotid lymph nodes (Fig. 2a, b, d, e, f, g). Although most lesions completely replaced the lymph nodelike structure (Fig. 2a, b), two tumors showed clear-cut residual lymphoid tissue adjacent to the tumor (Fig. 2d, e). Reactive-type lymphoid follicles were present with variable frequency in all cases. Marginal sinus structures with D2-40 (podoplanin)-positive lymph vessels consistent with a lymph node sinus were present in all cases (Fig. 2c).

Sebaceous, oncocytic, clear cell or mucinous differentiation of the epithelial component was lacking in all cases. Five of the nine cases showed multiple small- to medium-sized cysts of up to 8 mm in the epithelial islands (Fig. 1 and Fig. 2a, b, f, g). Both epithelial and lymphoid components showed no evidence of cytological atypia and a lack of increased mitotic or proliferative activity (Ki67 index <10%).

The epithelial component showed a wide variety of histological differentiation with dominant basaloid differentiation in three cases (Fig. 3a), diffuse intraepithelial distribution of lymphocytes equivalent to lymphoepithelial differentiation in four cases (Fig. 3d), and dominant ductal or cribriform differentiation in two cases (Fig. 3g). The type of epithelial differentiation correlated with the expression pattern of immunohistological markers: Tumors or areas with dominant basaloid or lymphoepithelial differentiation showed strong reaction to CK5/6, CK14, and p63 with absence or minor expression of CK18/CK7 in suprabasal layers (Fig. 3b, c, e, f). Tumors or areas with dominant ductal differentiation showed strong positivity for CK18/

Table 1 Clinical and histomorphological data of nine cases of nonsebaceous lymphadenoma

	Sex/age	Size (mm)	Histological differentiation	Suprabasal cell layers: CK5/6 (+CK14, p63)	Suprabasal cell layers: CK18/7	Cysts (mm)	Epithelial component in %	LN-hilus	Original diagnosis
1	f/40	12	Ductal	−	+	Yes (3)	50	Yes	Lymph node metastasis of adenocarcinoma
2	m/65	35	Basaloid	+	−	No	60	Yes	Nonsebaceous lymphadenoma
3	m/62	15	Basaloid/ductal	+	(+)	Yes (3)	50	Yes	Warthin's tumor
4	m/51	23	Lymphoepithelial	+	(+)	Yes (8)	20	No	Metaplastic Warthin's tumor
5	m/50	14	Lymphoepithelial	+	(+)	Yes (8)	70	No	Cystic benign lymphoepithelial lesion
6	m/62	35	Basaloid/lymphoepithelial	+	−	Yes (4)	50	No	Lymphoepithelial carcinoma
7	f/65	22	Ductal	−	+	No	70	No	Sebaceous lymphadenoma
8	f/51	17	Lymphoepithelial	+	−	No	30	No	Nonsebaceous lymphadenoma
9	m/47	15	Lymphoepithelial	(+)	(+)	No	40	Yes	Nonsebaceous lymphadenoma

f female, *m* male, *LN* lymph node

CK7 in suprabasal cell layers and positivity for CK5/6, CK14, and p63 restricted to the basal cell layer (Fig. 3h, i). The original diagnosis was NSLA in three cases. Six cases were initially mislabelled as other types of benign salivary tumors in three cases, cystic lymphoepithelial lesion in one case, and malignant salivary tumor in two cases (Table 1).

Discussion

This study, based on the second largest series of the recently recognized entity of NSLA reported to date, supports the previous notion that the epithelial component is characterized by a broad spectrum of histological differentiation, ranging from basaloid to lymphoepithelial and ductal [3, 4, 6, 7]. Presumably developing from a common basal cell component, this diverse epithelial differentiation seems to represent a neoplastic counterpart to diverse reactive metaplasias (such as lymphoepithelial metaplasia and basal cell hyperplasia), which develop from basal cells of regular striated ducts, as described by our group [14, 16]. Kang et al. [17] had suggested a separation of this rare entity into cases with ductal differentiation in sensu strictu 'Nonsebaceous lymphadenoma' and cases with basaloid or lymphoepithelial differentiation in 'nonsebaceous lymphoepithelioma'. Considering the rarity of this tumor entity and the broad and overlapping spectrum of the histological epithelial differentiation, we, however, strongly support to regard all cases as part of a common tumor entity comprising a heterogeneous spectrum of epithelial differentiation including a variable degree of cystic transformation.

Analogous to Warthin's tumor, pathogenetic development of NSLA from embryonic salivary inclusions in intra-/periparotid lymph nodes has been proposed [2, 8, 13]. However, this theory did not achieve wide acceptance and has been refuted by the majority of authors, who instead regard the lymphoid component as reactive tumor-associated lymphoid tissue [3, 4, 6, 7, 9–11]. Our finding of an unequivocal hilus structure with embryonic parenchymal inclusions in four of the nine cases (Fig. 2), in conjunction with frequent secondary follicles and lymph vessels within marginal sinus structures demonstrated in all cases (Fig. 2c), represent, in our view, strong arguments for a pathogenetic development of NSLA from embryonic salivary inclusions in intra- or periparotid lymph nodes.

Hilus structures were not detectable in five of the nine tumors, which can be attributed to incomplete tumor sampling and/or to effacement of hilus structures by the expanding tumor. A respective development of a Warthin's tumor

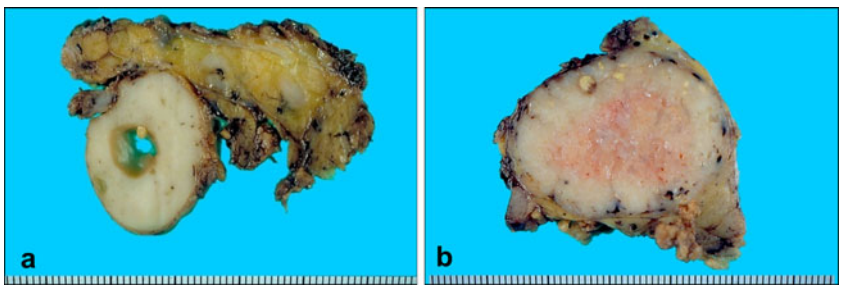

Fig. 1 Macroscopic image of two cases of nonsebaceous lymphadenoma (NSLA) with well delineated border and gray-whitish cut surface that displayed both solid areas and large (**a**) or small (**b**) cystic components

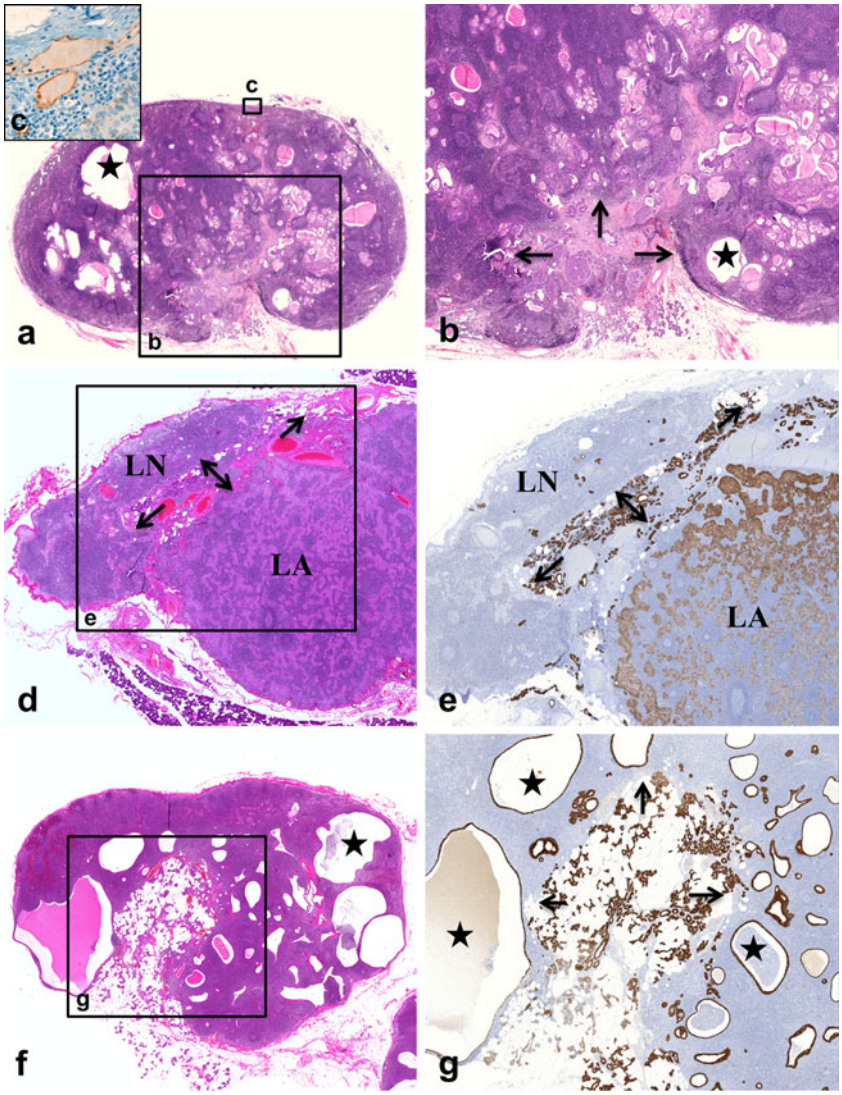

Fig. 2 **a**–**c** Case no. 1 with minor cystic component (*star*) and unequivocal preserved hilus structure (**a**) with inclusion of salivary parenchyma (**b**: *arrows*); podoplanin-positive lymph vessels in marginal sinus (**c**); **d**, **e** case no. 2 with a preserved portion of a lymph node (*LN*) on the left, adjacent hilus with inclusion of salivary parenchyma (*arrows*) and NSLA on the right; no cystic component (**e** pan-keratin); **f**, **g** case no. 3 with intense cystic components (*star*) and unequivocal hilus structure (*arrows*; **g**: pan-keratin); magnification: **a**×6, **b**×10, **c**×1,000, **d**×4, **e**×5, **f**×4.5, **g**×10

from intraparotid lymph nodes was first postulated by Bernier and Bhaskar in 1958 [18] and is now generally accepted [19, 20] even though hilus structures can be demonstrated in only a minority of mostly small and incipient Warthin's tumors. An analogous histogenetic pathogenesis has been proposed for sebaceous lympadenoma [21, 22]. The proposed development from intra- or periglandular lymph nodes is further supported by the fact that Warthin's tumor, sebaceous lymphadenoma, and NSLA are almost invariably restricted to parotid glands [12, 20], which exclusively harbor intra- and periglandular lymph nodes. However, this constellation presumably does not represent a pure intranodal epithelial tumor growth, but an intimate immunological relationship of the epithelial and lymphatic components within this combined lymphoepithelial type of tumor.

It is highly likely that this rare tumor entity is more frequent than the data suggest, as it is easily confused with a series of other benign and malignant tumor entities. In contrast to the usually straightforward diagnosis of sebaceous lymphadenoma, misdiagnosis of NSLA has been repeatedly reported [4, 7] and is attributable to a lack of familiarity with this rare tumor entity as well as to the heterogeneous spectrum of lymphoepithelial, basaloid, or ductal epithelial differentiation seen in NSLA, which results in an unusually wide spectrum of both benign and malignant differential diagnoses.

Six of our nine cases were initially misdiagnosed, with three cases having been misdiagnosed as other types of benign salivary tumors without clinical consequence, one case as reactive sialadenitis, and two cases as carcinoma (Table 1). Due to imprecise diagnostic criteria, so-called benign lymphoepithelial lesion represents one lesion that is at risk to be confused with NSLA, which occurred in one of our cases. The basaloid type of NSLA might be misinterpreted as basal cell adenoma within a lymph node. However, the basaloid nests of NSLA are loosely arranged within the lymphoid background and lack prominent PAS-positive basal membranelike material. A serious misinterpretation in our series was a lymph node

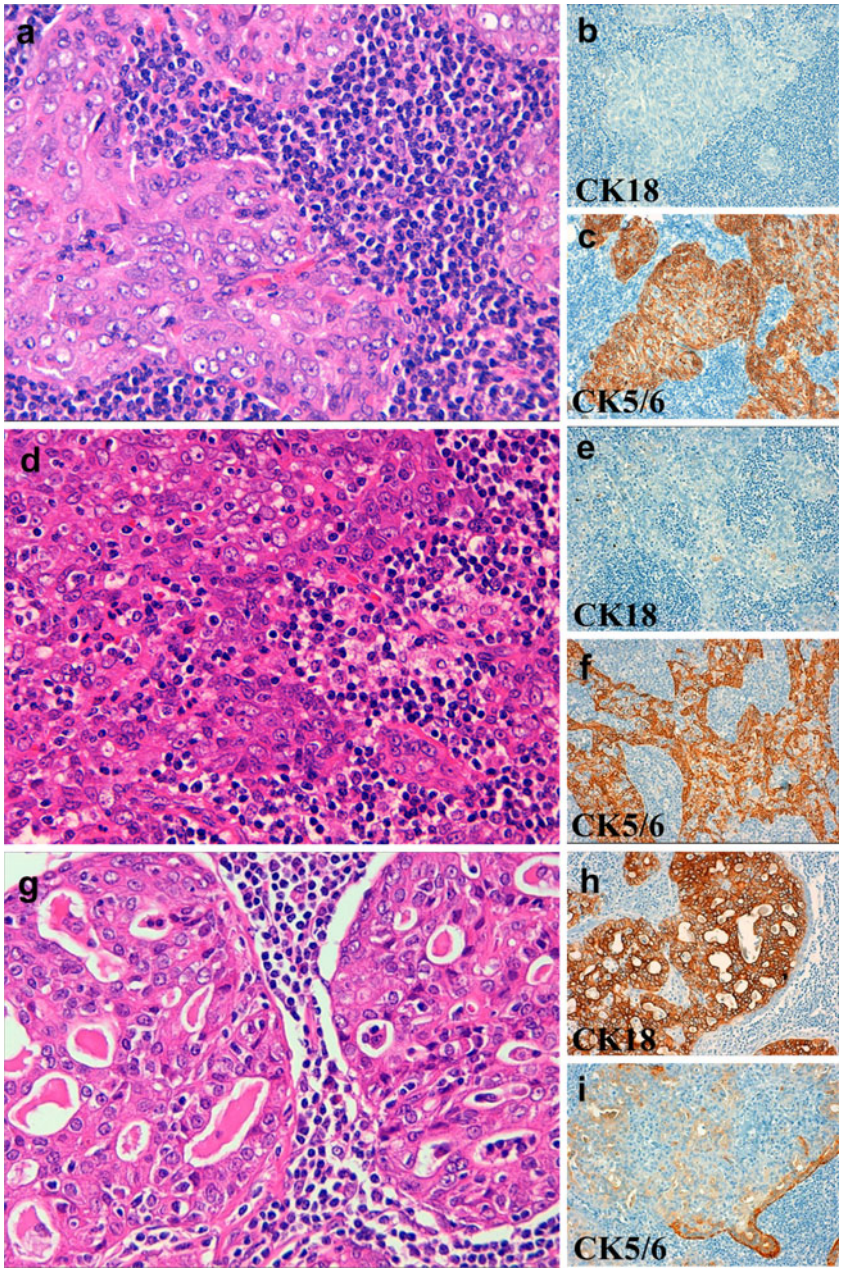

Fig. 3 **a**–**c** Case no. 2 with basaloid epithelial differentiation, corresponding to strong overall positivity for CK5/6 (**c**) and negativity for CK18 (**b**); **d**–**f** case no. 6 with lymphoepithelial differentiation with abundant intraepithelial lymphocytes and identical immunoreactive pattern as in **b** and **c** (**e**, **f**); **g**–**i** case no. 7 with ductal epithelial differentiation with positivity for CK18 in suprabasal layers (**h**) and positivity for CK5/6 restricted to basal cells (**i**); magnification: **a**, **d**, **g**×800; **b**, **c**, **e**, **f**, **h**, **i**×400

metastasis from a well-differentiated adenocarcinoma, which led to an uneventful search for a suspected primary carcinoma (Fig. 2a, b). Another serious misinterpretation was lymphoepithelial carcinoma, which, in contrast to NSLA, is characterized by blunt tumor infiltration, significant proliferation, and other features of frank malignancy. Finally, NSLA has to be distinguished from microscopic embryonal salivary tissue inclusions within intra- or periparotid lymph nodes, which may show a minor degree of reactive hyperplasia and cyst development.

During the revision of this article, another slightly larger series of 11 cases of NSLA was published [13]. Although their investigation and ours share many equivalent findings especially with regard to intranodal location in four cases, there are noteworthy differences: Two of their 11 cases showed focal keratinization, a feature that was absent in our cases. The mean age was one decade higher than in our series, and they found a dominant female predominance (4:1) in contrast to a male predominance (3:1) in our series. The findings in these two large series indicate that the clinicopathological features of NSLA are rather heterogeneous with wide variation with respect to histology, age, and gender distribution.

In summary, we report the second largest case series of NSLA illustrating that this rare lesion belongs to the group of salivary gland tumors that pathogenetically develop from embryonic salivary inclusions in intra- or periparotid lymph nodes. Similar to Warthin's tumor, the exact mechanisms driving the

tumorigenesis of NSLA from intranodal salivary inclusions remains currently obscure. The prognosis of NSLA is excellent with no reported recurrences. Knowledge of this rare and probably under-recognized lymphoepithelial tumor entity and familiarity with its heterogeneous spectrum of epithelial differentiation is important in order to avoid misdiagnosis, especially as malignant tumor with inappropriate overtreatment.

Acknowledgments This investigation is supported by a grant of "Wissenschaftliches Herausgeberkollegium der Münchener Medizinischen Wochenschrift e.V."

References

1. Auclair PL, Ellis GL, Gnepp DR (1991) Other benign epithelial neoplasms. In: Ellis GL, Auclair PL, Gnepp DR (eds) "Surgical pathology of the salivary glands". Saunders, Philadelphia, PA
2. Kwon GY, Kim EJ, Go JH (2002) Lymphadenoma arising in the parotid gland: a case report. Yonsei Med J 43:536–538
3. Ma J, Chan JK, Chow CW, Orell SR (2002) Lymphadenoma: a report of three cases of an uncommon salivary gland neoplasm. Histopathology 41:342–350
4. Bos I, Meyer S, Merz H (2004) Lymphadenoma of the parotid gland without sebaceous differentiation. Immunohistochemical investigations. Pathologe 25:73–78
5. Chang JY, Hsiao CH (2004) Lymphadenoma lacking sebaceous differentiation in the parotid gland. J Formos Med Assoc 103:459–462
6. Musthyala NB, Low SE, Seneviratne RH (2004) Lymphadenoma of the salivary gland: a rare tumour. J Clin Pathol 57:1007
7. Dardick I, Thomas MJ (2008) Lymphadenoma of parotid gland: two additional cases and a literature review. Oral Surg Oral Med Oral Pathol Oral Radiol Endod 105:491–494
8. Castelino-Prabhu S, Li QK, Ali SZ (2010) Nonsebaceous lymphadenoma of the parotid gland: cytopathologic findings and differential diagnosis. Diagn Cytopathol 38:137–140
9. Gallego L, Junquera L, Fresno MF (2009) Non-sebaceous lymphadenoma of the parotid gland: immunohistochemical study and DNA ploidy analysis. Oral Surg Oral Med Oral Pathol Oral Radiol Endod 107:555–558
10. Yang S, Chen X, Wang L, Zhang J (2007) Non-sebaceous lymphadenoma of the salivary gland: case report with immunohistochemical investigation. Virchows Arch 450:595–599
11. Auclair PL (1994) Tumor-associated lymphoid proliferation in the parotid gland. A potential diagnostic pitfall. Oral Surg Oral Med Oral Pathol 77:19–26
12. Gnepp DR, Cheuk W, Chan JKC, Nagao T (2005) Lymphadenomas: sebaceous and non-sebaceous. In: "Pathology and genetics of head and neck tumours". IARC, Lyon, France
13. Seethala RR, Thompson LD, Gnepp DR, Barnes EL, Skalova A, Montone K, Kane S, Lewis JS, Jr., Solomon LW, Simpson RH, Khan A, Prasad ML (2012) Lymphadenoma of the salivary gland: clinicopathological and immunohistochemical analysis of 33 tumors. Mod Pathol 25(1):26–35
14. Ihrler S, Zietz C, Sendelhofert A, Lang S, Blasenbreu-Vogt S, Lohrs U (2002) A morphogenetic concept of salivary duct regeneration and metaplasia. Virchows Arch 440:519–526
15. Ihrler S, Weiler C, Hirschmann A, Sendelhofert A, Lang S, Guntinas-Lichius O, Arnold G, Zietz C, Harrison JD (2007) Intraductal carcinoma is the precursor of carcinoma ex pleomorphic adenoma and is often associated with dysfunctional p53. Histopathology 51:362–371
16. Ihrler S, Zietz C, Sendelhofert A, Riederer A, Lohrs U (1999) Lymphoepithelial duct lesions in Sjogren-type sialadenitis. Virchows Arch 434:315–323
17. Kang J, Kim SY, Cho KJ (2008) Lymphadenoma of the salivary gland: a novel classification based on immunohistochemical comparison of benign and malignant lymphoepithelial neoplasms. Basic Appl Pathol 1:18–22
18. Bernier JL, Bhaskar SN (1958) Lymphoepithelial lesions of salivary glands; histogenesis and classification based on 186 cases. Cancer 11:1156–1179
19. Kleinsasser O, Klein HJ, Steinbach E, Hubner G (1966) Oncocytic adenoma-like hyperplasia, adenolymphoma and oncocytoma of the salivary glands. Arch Klin Exp Ohren Nasen Kehlkopfheilkd 186:317–336
20. Seifert G (1997) Primary salivary gland tumors in lymph nodes of the parotid gland. Report of 3 cases and review of the literature. Pathologe 18:141–146
21. Gnepp DR, Brannon R (1984) Sebaceous neoplasms of salivary gland origin. Report of 21 cases. Cancer 53:2155–2170
22. Majeed M, Murray B, Hume W, Makura Z (2008) Sebaceous lymphadenoma of the parotid gland. Dentomaxillofac Radiol 37:300–304

Virchows Arch (2012) 460:473–480
DOI 10.1007/s00428-012-1224-0

ORIGINAL ARTICLE

Intraepithelially entrapped blood vessels in oral carcinoma in-situ

Akinori Funayama · Satoshi Maruyama · Manabu Yamazaki · Kamal Al-Eryani · Susumu Shingaki · Chikara Saito · Jun Cheng · Takashi Saku

Received: 23 October 2011 / Revised: 26 December 2011 / Accepted: 30 January 2012 / Published online: 5 April 2012
© Springer-Verlag 2012

Abstract It can be difficult to make a certain diagnosis in case of an oral borderline malignant lesion on hematoxylin–eosin-stained sections only. Furthermore, assessment of surgical margins of borderline lesions is difficult with the naked eye. We set out to determine the topographical distribution of capillary blood vessels within the epithelial zone and to assess its use as an aid for histopathological diagnosis and a framework for clinical assessment of lesional margins using optical techniques, such as narrow-band imaging (NBI) endoscopy. Capillary blood vessels entrapped in the epithelial compartment, which we have designated as intraepithelially entrapped blood vessels (IEBVs), were examined for their frequency, location, and shape in normal mucosa, dysplasia, and carcinoma in-situ (CIS) of the tongue using immunohistochemistry for CD31 and type IV collagen. When counted per unit length of epithelial surface, IEBVs increased in number significantly in CIS (5.6±2.8), which was two times more than in normal (1.9±1.6) and dysplastic (2.4±1.5) epithelia. In addition, IEBVs in CIS had compressed shapes with occasional obstruction or collapse with hemorrhage and were arranged perpendicular to and extending up to the epithelial surface. These characteristic IEBVs in CIS were considered to be generated by complex expansion of rete ridges due to carcinoma cell proliferation within the limited epithelial space determined by the basement membrane. The recognition of IEBVs was helpful in the differential diagnosis of oral CIS, and the present data provide a valuable frame of reference for detecting oral CIS areas using such NBI-based optical devices.

Keywords Carcinoma in-situ · CD31 · Epithelial dysplasia · Intraepithelial blood vessels · Narrow-band imaging endoscopy · Oral mucosa · Type IV collagen

A. Funayama · M. Yamazaki · K. Al-Eryani · J. Cheng · T. Saku (✉)
Division of Oral Pathology, Department of Tissue Regeneration and Reconstruction, Niigata University Graduate School of Medical and Dental Sciences,
2-5274 Gakkocho-dori, Chuo-ku,
Niigata 951-8514, Japan
e-mail: tsaku@dent.niigata-u.ac.jp

A. Funayama · S. Shingaki · C. Saito
Division of Reconstructive Surgery for Oral and Maxillofacial Region, Department of Tissue Regeneration and Reconstruction, Niigata University Graduate School of Medical and Dental Sciences,
Niigata, Japan

S. Maruyama · T. Saku
Oral Pathology Section, Department of Surgical Pathology, Niigata University Hospital,
Niigata, Japan

Introduction

The recent increase in the incidence of oral cancers seems to be partly due to an increase in superficial-type cancers [1], which usually form lesional complexes of borderline malignancy, including epithelial dysplasia and carcinoma in-situ (CIS) [2]. For surgical intervention of these borderline lesional complexes, design and setting of surgical margins are important factors. However, the histopathological evaluation of surgical margins in frozen sections during surgery or in surgical specimens after surgery is not always performed on the basis of objective criteria. The WHO classification, which was first published in 1971 [3] and revised twice in 1997 [4] and 2005 [5], has been considered to be a world-wide diagnostic standard on which reporting pathologists have depended. However, it is still difficult for

pathologists to make objective differential diagnoses only on histological characteristics of hematoxylin–eosin (HE)-stained sections, as proposed in the WHO book [5]. Therefore, more definite and characteristic features, which can be objectively recognized, are needed.

To this end, we have developed a differential diagnostic method using immunohistochemistry for keratin subtypes, Ki-67 and podoplanin, which recognizes the degree of differentiation of keratinocytes and the positioning of the cell proliferating center, respectively [2, 6, 7]. This combined immunohistochemical method has enabled us to objectively distinguish CIS from dysplasia. We have also recognized a category of epithelial dysplasia with a characteristic two-phase appearance as a precursor to CIS [2]. The two-phase appearance is generated by the contrasting layers of basaloid cells in the lower half and keratinized cells in the upper half of the epithelium [8–10]. The lower half basaloid cells are Ki-67-positive, and they lack E-cadherin due to hypermethylation of its gene promoter region but show nuclear translocation of β-catenin [11]. In addition, an intercellular deposit of perlecan [12, 13] with enhanced expression levels of MMP-7 [13], podoplanin [7], or Wnt target molecules [11] has been demonstrated in the lower half of two-phase dysplasia. Based on these lines of evidence, it is now possible to clearly separate CIS from epithelial dysplasia.

Since we started to apply this method to daily diagnostic activities, we have noticed that small vessels are often engulfed in the epithelial layer of these borderline lesions, especially in CIS foci. Therefore, we wanted to elucidate the significance of these vascular channels within these epithelial lesions, because there have been no investigations on microvasculature entrapped within proliferative epithelium of lesions that are not yet invasive. In oral cancer, angiogenesis in the neoplastic stroma has been considered particularly important in characterizing individual cases, as neovascularization is one of the critical events that determines tumor growth and metastasis and has been regarded as a prognostic factor [14, 15]. As a measure of angiogenesis in histological sections, the distribution of microvessel density (MVD) has been widely used [16, 17]. On the other hand, microvascular architecture in the pre-invasive stages of oral mucosal neoplasia has not yet been investigated nor attracted any attention, though some devices, such as narrow-band imaging (NBI), to visualize abnormal microvascular patterns in mucosal neoplasms, have entered into practical use [18–20].

In this study, we have applied immunohistochemistry for CD31 and type IV collagen to demonstrate the presence of blood vessels within the epithelial layer of oral premalignant neoplastic lesions. Using anti-CD31, vascular endothelial cells were visualized, and vascular basement membranes were stained using anti-type IV collagen antibodies. Our aim was to compare the distribution of microvasculature in normal and dysplastic epithelia and CIS of the oral mucosa to determine whether their recognition does improve our diagnostic precision and whether these immunohistochemical methods could be an additional aid for discriminating between CIS and dysplasia.

Materials and methods

Materials

A total of 64 surgical specimens from the lateral side of the tongue mucosa, which had been surgically removed between 2002 and 2008 due to invasive squamous cell carcinoma (SCC) or CIS, were selected from the surgical pathology files in the Division of Oral Pathology, Niigata University Graduate School of Medical and Dental Sciences. The specimens contained regions of epithelial dysplasia and/or normal epithelium in addition to SCC/CIS. In 284 tissue sections of 64 specimens, 50 foci each of CIS and epithelial dysplasia, and 30 of normal epithelium were investigated. The samples were restricted to those from the lateral surface of the tongue, because the shape and thickness of the oral mucosal epithelia differ depending on the area of provenance. Normal epithelium from the lateral surface of the tongue shows independent rete ridges, contrary to those from the dorsal surface epithelium, which are not as flat and small as those in the sublingual region or on the floor of the mouth. In addition, normal epithelium was also defined by the presence of a lamina propria without fibrosis. All specimens were routinely fixed in 10 % formalin and embedded in paraffin. Serial 4-μm sections were cut from paraffin blocks. One set of the sections was stained with HE and was used for reevaluation of the histological diagnosis, and the other sets were used for immunohistochemistry. The experimental protocol for analyzing surgical materials was reviewed and approved by the Ethical Board of Niigata University Graduate School of Medical and Dental Sciences (Oral Life Science).

Antibodies

A mouse monoclonal antibody against human CD31 (clone JC-70A, IgG_1, Dako, Glostrup, Denmark, diluted at 1:40) was used for demonstrating vascular endothelial cells. Rabbit polyclonal antibodies against human collagen type IV (type IV) were obtained from Cappel Laboratories (IgG, Cochranville, OH, USA, diluted at 1:100) and used for revealing vascular basement membranes.

Immunohistochemistry

Serial tissue sections were deparaffinized and subjected to standard immunohistochemical techniques using the Envision+/HRP system (Dako). After deparaffinization and

hydration, sections were rinsed in 0.01 M phosphate buffered saline (PBS, pH 7.4). To retrieve CD31 epitopes, sections were treated with 0.1% (w/v) trypsin (type II; Sigma Chemical Co., St. Louis, MO, USA) in 0.05 M Tris-HCl (pH 7.6) containing 1% $CaCl_2$ for 30 min at 37°C. For type IV collagen staining, the sections were digested with 4 mg/ml pepsin (Sigma) in 0.01 M HCl for 30 min at 37°C. After pre-treatment, the sections were rinsed again in PBS and then treated with 0.3% hydrogen peroxide in methanol for 30 min at room temperature to block endogenous peroxidase activity. After rinsing in PBS containing 0.5% skim milk and 0.05% Triton X-100 (T-PBS), the sections were incubated with 5% milk protein in T-PBS for 1 h at room temperature to block non-specific protein binding sites. After incubation with the primary antibodies overnight at 4°C, the sections were rinsed in T-PBS and then treated with polymer-immune complexes for 1 h at room temperature. After rinsing with T-PBS, the peroxidase reaction product was visualized by incubation with 0.02% 3,3'-diaminobenzimine (Dohjindo Laboratories, Kumamoto, Japan) in 0.05 M Tris-HCl (pH 7.6) containing 0.005% hydrogen peroxide. Finally, the sections were counterstained with hematoxylin. For control study, the primary antibodies were replaced with pre-immune mouse IgG_1 or rabbit IgG. Three-dimensional reconstruction of vascular patterns was not attempted in our material.

Histopathological evaluation

HE-stained sections were evaluated by three pathologists independently according to WHO 2005 criteria [5]. Histopathological diagnoses included normal epithelium, epithelial dysplasia (mild and moderate), CIS, and SCC. For the diagnosis of CIS, the criteria are described elsewhere [2, 6, 7]. In this approach, severe epithelial dysplasia according to the WHO criteria is classified as CIS. For the differential diagnosis between CIS and (mild and moderate) dysplasia, immunohistochemical profiles for Ki-67 [2, 6, 7], K13 [2, 6], K17 [6], K19 [2], and podoplanin [7] were employed.

Evaluation of intraepithelially entrapped blood vessels and the shape of rete ridges

The total number of intraepithelial blood vessels (IEBVs) was counted per mm surface unit length, and the average number was calculated per diagnostic category. In addition, the following parameters were analyzed to characterize rete ridge shapes: the shortest distance between the IEBVs closest to the surface (red circle, Fig. 1) and the epithelial surface (value A, Fig. 1), the maximum length of the rete ridge containing IEBVs (value B, Fig. 1), and the length of the basement membrane delimiting the rete ridges per mm of surface epithelial length (value C, blue line, Fig. 1). An average value was calculated for parameter for each diagnostic category. To determine relative position of IEBVs relative to the epithelial layer, ratios of the A/B values mentioned previously were calculated for each diagnostic category. To assess the degree of indentation of the rete ridges, the ratios of epithelial thickness between the shortest (value D, Fig. 1) and the longest (value E, Fig. 1) rete ridges with and without IEBVs were calculated (value D/E). All measurements were performed on an Olympus BX2 microscope equipped with an Olympus FX-380 digital video camera at × 60 magnification (× 1.5 camera and × 40 objective lenses) and operated with image analysis software FLVFS-LS, Ver.1.11 (Olympus Inc., Tokyo, Japan).

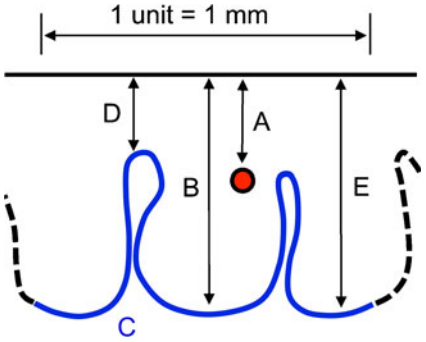

Fig. 1 Schematic indication of measuring objects in the epithelial layer used for quantitative analyses of intraepithelially entrapped blood vessels (IEBVs). *A* shortest distance between the top position of IEBVs and the epithelial surface, *B* maximum thickness of the rete process which include intraepithelially entrapped blood vessels IEBVs, *C* curve length of rete ridges at the basement membrane level per mm of surface epithelium, *D* shortest rete process regardless of the absence or presence of IEBVs, *E* longest rete process regardless of the absence or presence of IEBVs

Statistical analysis

The number and location of IEBVs, as well as the thickness and shape of rete ridges, were compared between normal and dysplastic epithelia and CIS. Statistical significance was assessed using the Scheffe's F test of independence with Statcel 3, an Excel 2007 add-on (Seiun Inc., OMS Publishing, Tokorozawa, Japan). Differences with a $P<0.05$ were considered to be statistically significant.

Results

Evaluation of intraepithelially entrapped blood vessels

Panels in Fig. 2 were prepared at the same magnification for simple comparison of the epithelial thickness and blood vasculature between normal and dysplastic epithelia and CIS. In normal mucosa, which was defined by the presence

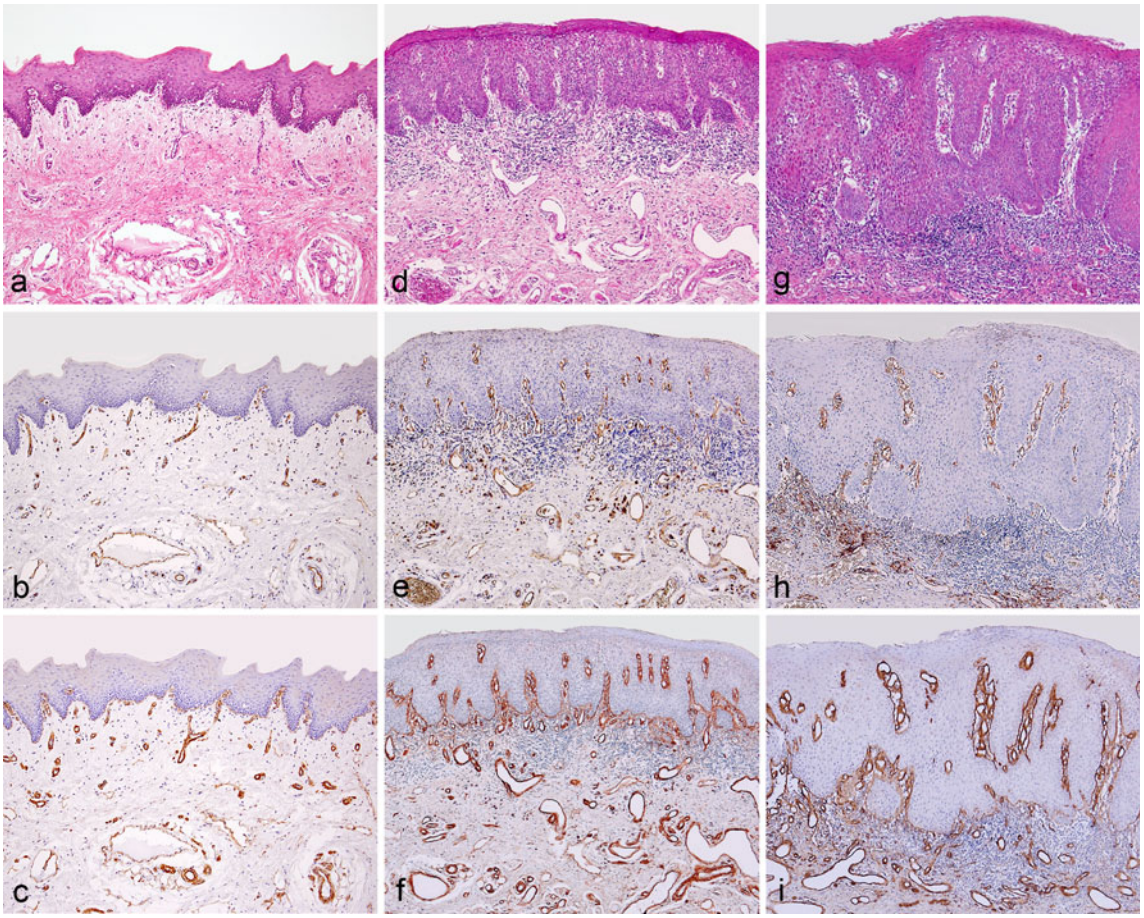

Fig. 2 Comparative immunohistochemical demonstration of blood vessels between normal and dysplastic epithelia and carcinoma in-situ of the tongue mucosa. **a**–**c** Normal epithelia, left column. **d**–**f** Moderate dysplasia, middle column. **g**–**i** Carcinoma in-situ, right column. **a**, **d**, and **g** HE stain, upper layer. **b**, **e**, and **h** Immunoperoxidase stain for CD31, middle layer. **c**, **f**, and **i** Immunoperoxidase stain for type IV collagen, lower layer. Hematoxylin counterstain, ×100. In normal epithelium (**a**), CD31-immunopositive (**b**) and type IV collagen-immunopositive (**c**) blood vessels were scattered in the lamina propria and the submucosal layer. Normal mucosa was defined by the presence of the lamina propria with loose connective tissue but without fibrosis. Type IV collagen immunohistochemistry showed vessel wall differences between capillaries and venules, in addition to the epithelial basement membrane (**c**). There were no blood vessels within the epithelium. In epithelial dysplasia (**d**), the distribution of blood vessels extended further into the range of the epithelial layer (**e**, **f**). In carcinoma in-situ (CIS) (**g**), blood vessels were involved along narrow connective tissue papillae (**h**, **i**), compressed in shape and arranged perpendicular to the epithelial surface. IEBVs appear to be isolated, but might be in continuity with blood vessels in the connective tissue papillae. IEBVs were most striking in CIS (**h**, **i**)

of lamina propria with loose connective tissue but without fibrosis (Fig. 2a), blood vessels demonstrated by immunohistochemistry for CD31 (Fig. 2b) and type IV (Fig. 2c) were scattered in the lamina propria and the submucosal layer. Type IV collagen immunohistochemistry outlined both vascular and epithelial basement membranes. Vascular wall thickness variations were also discernible by type IV collagen positive smooth muscle basement membranes (Fig. 2c). Blood vessels were scarce within the epithelial zone, although some were occasionally observed perpendicular to the epithelial surface in fan-shaped connective tissue papillae. These blood vessels were sometimes cross sectioned and seemed to be isolated within the epithelial layer. These were designated as intraepithelial blood vessels (IEBVs). In epithelial dysplasia (Fig. 2d), IEBVs were increased in number, and their shape at cross section was basically round, as seen in normal epithelium (Fig. 2e, f).

However, in CIS (Fig. 2g), IEBVs were observed much more frequently (Fig. 2h, i) with an average number per mm of epithelium of 5.6±2.8 compared to that of normal (1.9±1.6) ($P<0.01$) and dysplastic (2.4±1.5) ($P<0.01$) epithelia (Fig. 4a). In addition, the shape and architecture of IEBVs in CIS were different from those seen in normal or dysplastic epithelia: They were irregularly compressed, distorted, and elongated in shape, and perpendicular to the epithelial surface.

Figure 3 shows the variability of IEBV in CIS. While IEBVs were surrounded by connective tissue in normal and dysplastic epithelia (Fig. 2), those in CIS appeared to be directly surrounded by epithelial cells and frequently located in the vicinity of the epithelial surface (Fig. 3a–d). In basaloid-

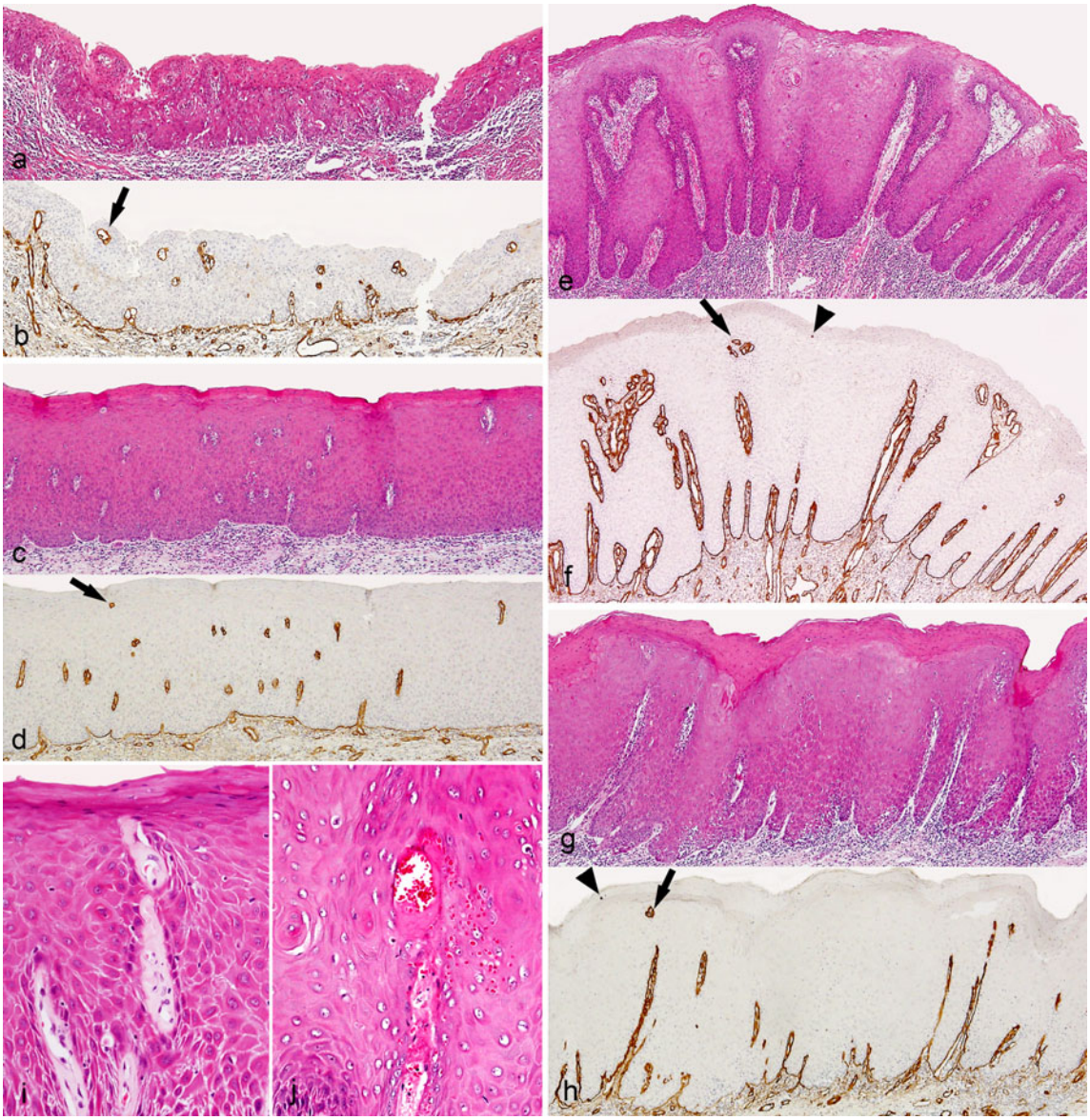

Fig. 3 Variation of IEBVs in CIS of the tongue. **a**, **b** Cross section of intraepithelial blood vessels (IEBVs) in basaloid CIS. **c**–**h** IEBVs in well-differentiated or acanthotic CIS. **i**, **j** High power views of IEBVs in CIS. **a**, **c**, **e**, **g**, **i**, and **j** HE stain, immunoperoxidase stains for type IV collagen (**b**, **d**, and **f**) and for CD31 (**h**), hematoxylin counterstain. **a**, **b**×100. **c**, **d**×80. **e**–**h**×50. **i**, **j**×400. IEBVs in CIS shown by immunohistochemical staining for type IV collagen (**b**, **d**, and **f**) and CD31 (**h**). They were sometimes continuous with blood vessels in the subepithelial connective tissue (**f**, **h**) but sometimes isolated within the epithelial layer (**b**, **d**). Isolated patterns resulted from cross sectioning of capillaries, and such capillaries were frequently located in the vicinity of the epithelial surface (**b**, **d**, **f**, and **h**; *arrows*). The generation process of IEBVs was most easily recognized in panel sets **e**, **f** and **g**, **h**: With an expansive growth of CIS cells, the surrounding connective tissue papillae became narrow, leaving only IEBVs. Occasionally, IEBVs were collapsed, resulting in dot-like staining (**f**, **h**; *arrowheads*). The perivascular space in the papillae often became hyaline with atrophic changes of endothelial cells (**i**). There were also hemorrhagic foci arising from collapsed IEBVs, extravasating red cells in the intercellular space of CIS cells (**j**)

type CIS in which the epithelial layer was less thick (Fig. 3a), IEBVs with open lumina were located in the upper part of the epithelial layer (Fig. 3b, arrow). With expansive growth of CIS cells, limited by the basement membrane, the rete ridges tended to be fused (Fig. 3c), and the perivascular connective tissue was reduced in volume, leaving only IEBVs, which gave an impression that IEBVs were directly facing epithelial cells (Fig. 3d, arrows). When CIS rete ridges were long and broad (Fig. 3e, g), IEBVs were positioned perpendicular and close to the surface (Fig. 3f, h, arrows), and collapsed or closed IEBVs resulted in a dot-like staining pattern for CD31 and type IV collagen (Fig. 3f, h, arrowheads). The perivascular space in the papillae often became hyaline with endothelial cell atrophy (Fig. 3i). Hemorrhagic foci arising from collapsed IEBVs and extravasating red cells spread into the intercellular space of CIS cells (Fig. 3j) were also noted.

Characterization of CIS rete ridges

The curve length of rete ridges along the basement membrane per unit width (1 mm) (value C, Fig. 1) was longer in CIS (2.25±0.67 mm) than in epithelial dysplasia (1.43±0.30 mm) ($P<0.01$) or in normal epithelium (1.35±0.25 mm) ($P<0.01$) (Fig. 4b), indicating larger rete ridge surface in CIS and more complex in shape. In order to examine the relationship between the occurrence of IEBVs and the epithelial thickness, the distance between the top position of IEBVs and the epithelial surface was determined (value A, Fig. 1). This appeared to be longer in CIS (192±102 μm) than in dysplasia (104±61 μm) or normal epithelium (76±20 μm) ($P<0.01$) (Fig. 4c), but rete ridges containing IEBVs (value B, Fig. 1) were thicker in CIS (491±212 μm) than in dysplasia (237±105 μm) ($P<0.01$) and normal epithelium (165±31 μm) ($P<0.01$) (Fig. 4d).

We also determined the relative position of IEBVs within the epithelial layer (value A/B, Fig. 1). This was shorter in CIS (0.38±0.09) than in dysplasia (0.43±0.07) or normal epithelium (0.44±0.09) ($P<0.05$) (Fig. 4e). The indenting pattern of rete ridges (value D/E, Fig. 1) was similar between the three diagnostic categories (Fig. 4f), indicating that IEBVs are not produced by simple interdigitation of rete ridges and connective tissue papillae.

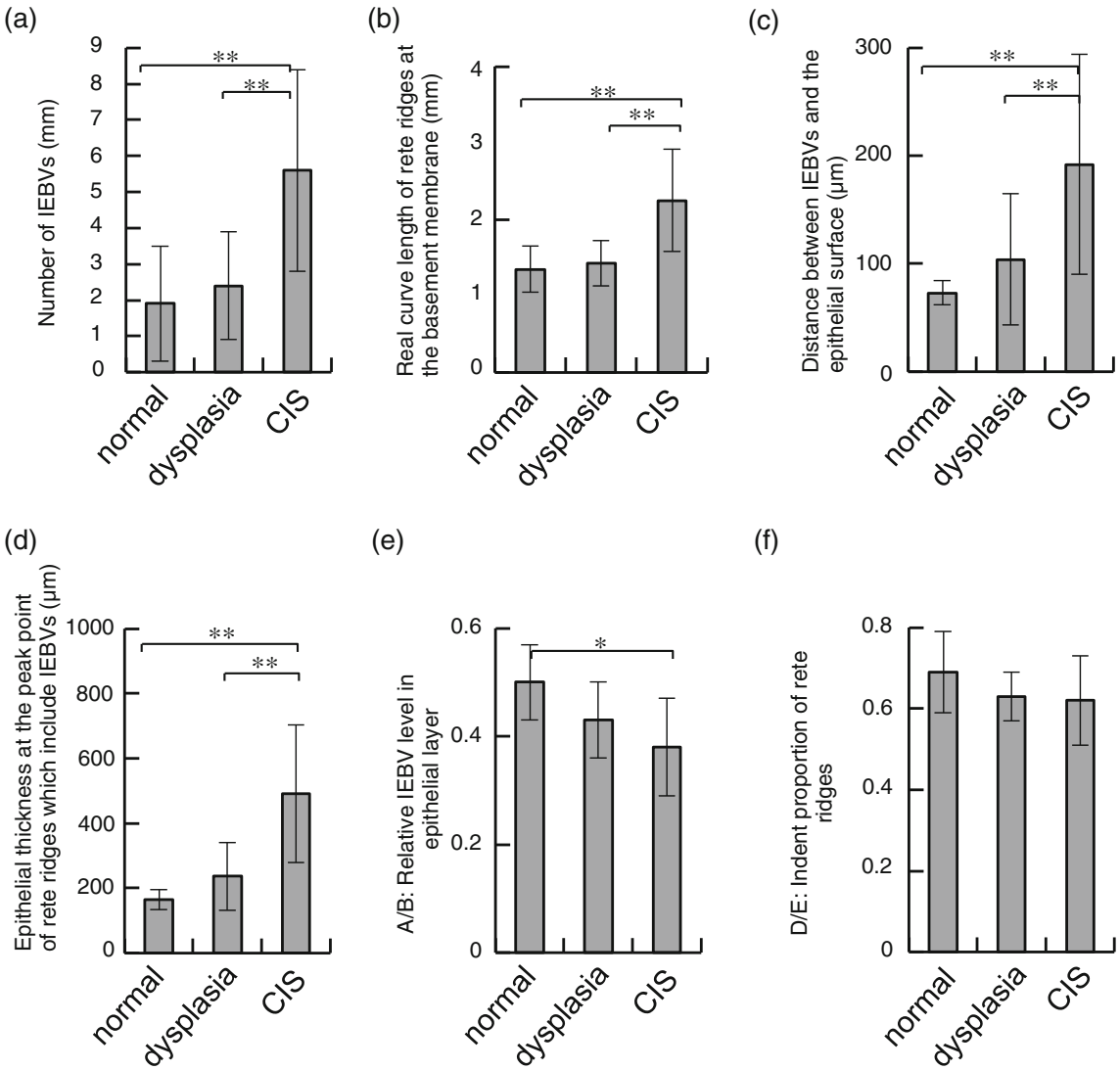

Fig. 4 Quantitative analysis of IEBVs in comparison with rete ridge shapes in oral mucosal epithelia from normal and dysplastic epithelia to carcinoma in-situ. **a** Average number of IEBVs per unit length of surface epithelium, **b** length of rete ridges at the basement membrane level per millimeter of surface epithelium, **c** shortest distance between the top position of IEBVs and the epithelial surface, **d** thicknesses of the rete process including IEBVs, **e** average ratios of A/B values, indicating relative positioning levels of IEBVs within the epithelial layer, and **f** average ratios of epithelial thickness between the bottom point (shortest) and at the peak point (longest) of rete ridges, indicating the degree of indentation of rete ridges, D/E. *$P<0.05$; **$P<0.01$

Discussion

We are the first to show in this study that in oral CIS blood vessels are intraepithelially entrapped, and we have proposed to call these IEBVs. IEBVs were clearly visualized using immunohistochemistry for CD31 and type IV collagen, and their presence was highest in CIS of the oral mucosa, in which the IEBV shape and location were closely related to the shape of CIS rete ridges. The number of IEBVs was significantly higher in CIS than in normal or dysplastic epithelia. We consider that this tendency for the number of IEBVs in CIS to increase is associated with the accelerated proliferation of carcinoma cells. The shape of CIS rete ridges was expansive or elongated, presumably due to compression as a result of space limitation by the basement membrane. IEBVs in CIS were located perpendicular to the epithelial surface and distorted in shape in narrow connective tissue papillae between expanded rete ridges. Based on morphometric analysis of the relationship between the distribution mode of IEBVs and the shape of rete ridges, we consider IEBVs to be generated by entrapment of capillary vessels of the lamina propria. The recognition of IEBVs has proven very useful in the differential diagnosis of oral CIS from non-neoplastic lesions, even though the use of HE staining and immunohistochemistry for cellular differentiation and cell proliferation [2, 6, 7] remains essential for the diagnosis of CIS.

Blood supply is an essential infrastructure of solid tumors for growth and dissemination [15, 21, 22]. In the tumor stroma, blood vessels are induced from pre-existing blood vessels [21] or from circulating monocytes [22] due to activation and migration of endothelial cells by angiogenic growth factors, such as vascular endothelial growth factor or basic fibroblast growth factor, which are produced and released from tumor cells and stromal cells, as well as from endothelial precursor cells, followed by their directional migration towards the tumor and tube formation with extracellular matrix remodeling [23]. In order to characterize neoplastic angiogenesis in tissue samples, most investigations have focused on the number of microvessels in the lesion, expressed as microvessel density (MVD) usually through immunohistochemical detection of endothelial cell-specific antigens such as CD31, CD34, von Willebrand factor, and CD105 [14, 17, 24–26]. MVD is positively correlated with metastasis and clinical behavior of cancer [27], although the relationship between angiogenesis and prognosis in head and neck cancers remains controversial [26, 28, 29]. MVD in the underlying stroma has been shown to increase with increasing grade of cervical intraepithelial neoplasia [16]. In bronchial mucosa, MVD was examined in dysplastic or metaplastic lesions by Keith et al., who proposed a disease entity of angiogenic squamous dysplasia (ASD) [30]. For oral epithelial dysplasia or CIS, there have been no reports on microvascular patterns or MVD.

We intended to objectively characterize IEBVs, with the intention to assess their use for daily diagnosis of CIS. We showed curve distances of CIS rete ridges to be longer than those of dysplastic and normal epithelia, implying that CIS rete ridges are larger than those in normal or dysplastic epithelia. The increased number of IEBVs in CIS can be explained by complex elongation and expansion of rete ridges. The shortest relative positioning of IEBVs in rete ridges of CIS indicates that the CIS IEBVs are generated by proliferation of rete ridges and not a sectioning artifact. IEBVs have not been reported previously and neither has morphometric analysis of rete ridge shapes of oral epithelium [31, 32].

NBI, a novel, non-invasive diagnostic approach using optical devices, has been established to visualize abnormal epithelial microvascular patterns and detect abnormal angiogenesis in the clinical diagnosis of squamous cell carcinoma, especially in case of superficial carcinoma of the oropharynx and hypopharynx [18, 19] or oral cavity [20], or of the esophageal [33], gastric [34], and colorectal [35] mucosa. The NBI system is combined with medical endoscopy by using narrow-band illumination created with three optical interference filters (415±30 μm, 445±30 μm, 450±30 μm) to detect erythrocytic hemoglobin, of which the absorption band is 415 nm [36]. Using NBI endoscopy, capillaries near the mucosal surface can be clearly detected. These studies have suggested that capillaries penetrate into the epithelium in superficial mucosal cancers, but a detailed description of the corresponding microvascular histology has never been published. Based upon our study, we consider that the abnormal capillaries in superficial neoplasms of the oropharynx or esophagus, visualized by the NBI method, are identical to what we have observed in terms of IEBVs of oral CIS in the present study, although their abnormal shapes or architecture were not fully analyzed in our two-dimensional study. For more detailed morphology of IEBVs, a three-dimensional analysis should be conducted. However, the present data provide a frame of reference for vascular patterns in oral CIS using such NBI-based optical devices.

Acknowledgments This work was supported in part by Grants-in-Aid for Scientific Research from the Japan Society for the Promotion of Science and from the Ministry of Education, Culture, Sports, Science and Technology, Japan.

Conflicts of interest We declare that we have no conflicts of interest.

References

1. Franceschi S, Bodoli E, Herrero R, Munoz N (2000) Comparison of cancers of the oral cavity and pharynx worldwide: etiological clues. Oral Oncol 36:106–115

2. Kobayashi T, Maruyama S, Cheng J, Ida-Yonemochi H, Yagi M, Takagi R, Saku T (2010) Histopathological varieties of oral carcinoma in situ: diagnosis aided by immunohistochemistry dealing with the second basal cell layer as the proliferating center of oral mucosal epithelia. Pathol Int 60:156–166
3. Wahi PN, Cohen B, Luthra UK, Torloni H (1971) Histological typing of oral and oropharyngeal tumours. World Health Organization International Histological Classification of Tumors. World Health Organization, Geneva, pp 15–23
4. Pindborg JJ, Reichart PA, Smith CJ, van der Waal I (1997) Histological typing of cancer and precancer of the oral mucosa. World Health Organization International Histological Classification of Tumors, 2nd edn. Springer, Berlin, pp 21–29
5. Gale N, Piclch BZ, Sidransky D et al (2005) Epithelial precursor lesions. In: Barnes L, Evson JW, Reichart P, Sidransky D (eds) Pathology and genetics of head and neck tumours. World Health Organization Classification of Tumours. IARC Press, Lyon, pp 177–179
6. Mikami T, Cheng J, Maruyama S, Kobayashi T, Funayama A, Yamazaki M, Adeola HA, Wu L, Shingaki S, Saito C, Saku T (2011) Emergence of keratin 17 vs. loss of keratin 13: their reciprocal immunohistochemical profiles in oral carcinoma in situ. Oral Oncol 47:497–503
7. Funayama A, Cheng J, Maruyama S, Yamazaki M, Kobayashi T, Syafriadi M, Kundu S, Shingaki S, Saito C, Saku T (2011) Enhanced expressions of podoplanin in oral carcinomas in-situ and squamous cell carcinomas. Pathobiology 78:171–180
8. Syafriadi M, Cheng J, Jen KY, Ida-Yonemochi H, Suzuki M, Saku T (2005) Two-phase appearance of oral epithelial dysplasia resulting from focal proliferation of parabasal cells and apoptosis of prickle cells. J Oral Pathol Med 34:140–149
9. Takeda T, Sugihara K, Hirayama Y et al (2006) Immunohistological evaluation of Ki-67, p63, CK19 and p53 expression in oral epithelial dysplasias. J Oral Pathol Med 35:369–375
10. Pavlova I, Williams M, El-Naggar A et al (2008) Understanding the biological basis of autofluorescence imaging for oral cancer detection: high-resolution fluorescence microscopy in viable tissue. Clin Cancer Res 14:2396–2404
11. Alvarado CG, Maruyama S, Cheng J, Ida-Yonemochi H, Kobayashi T, Yamazaki M, Takagi R, Saku T (2011) Nuclear translocation of β-catenin synchronized with loss of E-cadherin in oral epithelial dysplasia with a characteristic two-phase appearance. Histopathology 59:283–291
12. Ikarashi T, Ida-Yonemochi H, Ohshiro K, Cheng J, Saku T (2004) Intraepithelial expression of perlecan, a basement membrane-type heparan sulfate proteoglycan reflects dysplastic changes of the oral mucosal epithelium. J Oral Pathol Med 33:87–95
13. Tilakaratne WM, Kobayashi T, Ida-Yonemochi H, Swelam W, Yamazaki M, Shahidul AM, Maruyama S, Cheng J, Saku T (2009) Matrix metalloproteinase 7 and perlecan in oral epithelial dysplasia and carcinoma in situ: an aid for histopathologic recognition of their cell proliferation centers. J Oral Pathol Med 38:348–355
14. Kademani D, Lewis JT, Lamb DH, Rallis DJ, Harrington JR (2009) Angiogenesis and CD34 expression as a predictor of recurrence in oral squamous cell carcinoma. J Oral Maxillofac Surg 67:1800–1805
15. Hannen EJ, Riediger D (2004) The quantification of angiogenesis in relation to metastasis in oral cancer: a review. Int J Oral Maxillafac Surg 33:2–7
16. Dobbs SP, Hewett PW, Johnson IR, Carmichael J, Murray JC (1997) Angiogenesis is associated with vascular endothelial growth factor expression in cervical intraepithelial neoplasia. Br J Cancer 76:1410–1415
17. Che N, Zhao XL, Sun T et al (2011) The role of Twist 1 in hepatocellular carcinoma angiogenesis: a clinical study. Hum Pathol 42:840–847
18. Muto M, Nakane M, Katada C et al (2004) Squamous cell carcinoma in situ at oropharyngeal and hypopharygeal mucosal site. Cancer 101:1375–1381
19. Matsuba H, Katada C, Masaki T et al (2011) Diagnosis of extent of advanced oropharyngeal cancers by narrow band imaging with magnifying endoscopy. Laryngoscope 121:753–759
20. Takano JH, Yakushiji T, Kamiyama I, et al (2010) Detecting early oral cancer: narrowband imaging system observation of the oral mucosa microvasculature. Int J Oral Maxillofac Surg 39:208–213
21. Nikitenko LL (2008) Vascular endothelium in cancer. Cell Tissue Res 335:223–240
22. Murdoch C, Muthana M, Coffelt SB, Lewis CE (2008) The role of myeloid cells in the promotion of tumour angiogenesis. Nat Rev Cancer 8:618–631
23. Swelam W, Ida-Yonemochi H, Saku T (2005) Angiogenesis in mucous retention cyst: a human in-vivo-like model of endothelial cell differentiation in mucous substrate. J Oral Pathol Med 34:30–38
24. Weidner N (1995) Intratumor microvessel density as a prognostic factor in cancer. Am J Pathol 147:9–19
25. Vermeulen PB, Gasparini G, Fox SB et al (1996) Quantification of angiogenesis in solid human tumors: an international consensus on the methodology and criteria of evaluation. Eur J Cancer 32:2474–2484
26. Martonea T, Rossoa P, Alberaa R et al (2005) Prognostic relevance of CD105+ microvessel density in HNSCC patient outcome. Oral Oncol 41:147–155
27. Meert A-P, Paesmans M, Martin1 B et al (2002) The role of microvessel density on the survival of patients with lung cancer: a systematic review of the literature with meta-analysis. Brit J Cancer 87:694-701
28. Tae K, El-Naggar AK, Yoo E et al (2000) Expression of vascular endothelial growth factor and microvessel density in head and neck tumorigenesis. Clin Cancer Res 6:2821–2828
29. Li C, Shintani S, Terakado N et al (2005) Microvessel density and expression of vascular endothelial growth factor, basic fibroblast growth factor, and platelet-derived endothelial growth factor in oral squamous cell carcinomas. Int J Oral Maxillofac Surg 34:559–565
30. Keith RL, Miller YE, Gemmill RM et al (2000) Angiogenic squamous dysplasia in bronchi of individuals at high risk for lung cancer. Clin Cancer Res 6:1616–1625
31. Krutchkoff DJ, Eisengerg E, Anderson C (1991) Dysplasia of oral mucosa: a unified approach to proper evaluation. Mod Pathol 4:113–119
32. Abu Eid R, Sawair F, Landini G, Saku T (2012) Age and the architecture of oral mucosa. Age (Dordr). doi:10.1007/s11357-011-9261-1
33. Kara MA, Bergman JJ (2006) Autofluorescence imaging and narrow-band imaging for the detection of early neoplasia in patients with Barrett's esophagus. Endoscopy 38:627–631
34. Yasuda K (2006) Early gastric cancer: diagnosis, treatment techniques and outcomes. Eur J Gastroenterol Hepatol 18: 839–845
35. Oba S, Tanaka S, Sano Y, Oka S, Chayama K (2011) Current status of narrow-band imaging magnifying colonoscopy for colorectal neoplasia in Japan. Digestion 83:167–172
36. Muto M, Katada C, Sano Y, Yoshida S (2005) Narrow band imaging: a new diagnostic approach to visualize angiogenesis in superficial neoplasia. Clin Gastroenterol Hepatol 3:S16–20

Virchows Arch (2012) 460:481–487
DOI 10.1007/s00428-012-1227-x

ORIGINAL ARTICLE

Epithelial to mesenchymal transition in cutaneous squamous cell carcinoma is correlated with COX-2 expression but not with the presence of stromal macrophages or CD10-expressing cells

Tae Jung Jang

Received: 14 December 2011 / Revised: 16 February 2012 / Accepted: 13 March 2012 / Published online: 30 March 2012
© Springer-Verlag 2012

Abstract Epithelial to mesenchymal transition (EMT) is an intricate process by which epithelial cells loose epithelial characteristics and acquire a mesenchymal-like phenotype. EMT and cyclooxygenase 2 (COX-2) expression are related to tumor invasion and metastasis. The tumor microenvironment plays a major role in tumor progression and the induction of EMT. Here, we investigated the relationship between EMT and COX-2 expression as well as tumor-associated macrophages (TAM) and CD10-positive stromal cells during the development of cutaneous squamous neoplastic lesion. We performed immunohistochemical staining for vimentin, E-cadherin, β-catenin, COX-2, CD68, and CD10 in 41 cases of squamous cell cancers (SCC), 20 of Bowen's disease, 30 of actinic keratosis, and 30 samples of normal skin. SCC cells showed significantly increased vimentin expression and reduced expression of membranous E-cadherin and β-catenin compared with cells in precursor lesions and in normal skin. COX-2 expression was also markedly increased in SCC cells. E-cadherin expression was positively correlated with β-catenin expression and inversely correlated with COX-2 expression in SCC cells. The number of TAM and CD10-positive stromal cells increased from the normal skin to precursor lesions and SCC cells. The number of TAM and of CD10-positive stromal cells did not correlate with the expression of E-cadherin, β-catenin, COX-2, and vimentin in SCC cells. We suggest that cutaneous SCC cells show EMT, which appears to be correlated with COX-2 expression but not with stromal CD10 expression and TAM.

T. J. Jang (✉)
Department of Pathology,
Dongguk University College of Medicine,
Sukjang-dong 707,
Gyeongju, Gyeongbuk 780-714, South Korea
e-mail: taejung@mail.dongguk.ac.kr

Keywords Skin squamous cell cancer · Epithelial to mesenchymal transition · Cyclooxygenase 2 · CD10 · Tumor-associated macrophages

Introduction

Cell–cell adhesion mediated by E-cadherin is required for the maintenance of epithelial tissue architecture in adult organisms [1]. Loss of E-cadherin expression is observed during the later stages of carcinogenesis [2]. This loss of E-cadherin expression occurring in carcinogenesis can take place through gene mutations, hypermethylation of its promoter, or transcriptional repression [3] and is accompanied by a loss of epithelial characteristics and the acquisition of mesenchymal properties, a process often referred to as the epithelial to mesenchymal transition (EMT) [2]. During EMT, carcinoma cells become more motile and invasive by acquiring characteristics similar to embryonic mesenchymal cells, which allow them to penetrate into the surrounding stroma [4]. E-cadherin expression has been reported to be decreased in cutaneous squamous cell cancer (SCC) and its premalignant lesions [5–7]. β-catenin is bound to membrane-associated E-cadherin and is essential for its correct intracellular localization and function [8]. Decreased membranous E-cadherin releases β-catenin which then can translocate to the nucleus. Nuclear β-catenin activates genes involved in cell proliferation and invasive growth [9]. Nuclear expression of β-catenin has also been demonstrated in cutaneous SCC and premalignant lesions [5, 7, 10].

Cyclooxygenase 2 (COX-2) expression is transiently induced by proinflammatory cytokines and growth factors. Prostaglandin E_2 (PGE_2) plays a role in carcinogenesis, inducing immunosuppression, inhibiting apoptosis, increasing

the metastatic potential of epithelial cells, and promoting angiogenesis [11, 12]. COX-2 expression has been found to be increased in skin SCC and in precursor lesions [13–16]. Tsujii and DuBois have demonstrated that COX-2 overexpression occurs together with inactivation of E-cadherin [11]. It has been reported that loss of E-cadherin occurs during UV-induced SCC progression via PGE_2–EP2 signaling pathway [17]. COX-2-dependent PGE_2 in lung cancer cells reduces E-cadherin expression via transcription repressors such as zinc finger E-box-binding homeobox 1 (ZEB1) and Snail [18].

The communication between tumor cells and tumor stroma, composed of noncellular components and nonneoplastic cells such as a variety of different immune cells including lymphocytes and tumor-associated macrophages (TAM), endothelial cells, cancer-associated fibroblasts, and mesenchymal stem cells, plays an important role in cancer progression and metastasis [19, 20]. TAMs can promote tumor growth, invasion, metastasis, and activate tumor-promoting genes in cancer cells [21, 22]. A recent paper reported that TNF-α produced in TAM induced Snail promoter activity and EMT in MCF-7 breast cancer cells [23]. The number of TAM was higher in cutaneous SCC and Bowen's disease (BD) than in precancerous lesions [24]. CD10, a 90- to 110-kDa cell surface zinc-dependent metalloprotease expressed in the peritumoral fibroblast-like stromal cells in the invasion front of various cancers [25–28], was reported to be increased in cutaneous SCC compared with precancerous lesions [24]. The aim of this study was to investigate the relationship between EMT and COX-2 expression of tumor cells as well as the presence of TAM and CD10-positive cells in cutaneous SCC and its precursor lesions by immunohistochemistry.

Materials and methods

Patients and tissue samples

Ninety-one patients with actinic keratosis (AK), BD, or SCC treated at Dongguk University Gyeongju Hospital between 2008 and 2011 were enrolled in this study. Normal skin (NS) was defined as histologically normal peritumoral skin that was separated by at least 4 mm of unaffected skin from the SCC. The characteristics of the study subjects are summarized in Table 1. Of the 30 cases of AK, 20 cases showed low-grade dysplasia and 10 cases high-grade dysplasia. Low-grade dysplasia was defined by atypical keratinocytes situated mostly in lower half of epidermis and high-grade dysplasia by atypical keratinocytes in more than half of the thickness of the epidermis, but insufficient to be considered as squamous cell carcinoma in situ. None of the patients received radiotherapy or chemotherapy before diagnosis. Biopsy specimens were fixed in 10 % neutral-buffered formalin for 12 h and were embedded in paraffin. If multiple biopsy samples were present for each patient, we selected only one representative tissue sample.

Table 1 Characteristics of patients

	Number of cases	Age distribution	Gender (male/female)
Squamous cell cancer	41	95~45	11/30
Bowen's disease	20	82~53	10/10
Actinic keratosis with high grade	10	82~60	5/5
Actinic keratosis with low grade	20	83~58	5/15
Normal skin	30	95~69	7/23

Immunohistochemistry

Tissue sections (4 μm) were spread on poly-L-lysine-coated slides, immersed in three changes of xylene, and rehydrated using a graded series of alcohol. Antigen retrieval was routinely performed by immersing the sections in 0.01 M citrate buffer (pH 6.0) in a pressure cooker and autoclaving for 15 min. Endogenous peroxidase activity was blocked with 3 % hydrogen peroxide for 15 min, and then, the sections were incubated with primary antibody for 2 h at room temperature. The primary antibodies used were anti-COX-2 (1:500; Cayman Chemical, Ann Arbor, MI, USA), anti-E-cadherin (1:1,000, Transduction Laboratories, Lexington, KY, USA), anti-β-catenin (1:500, Transduction Laboratories), anti-CD68 (DAKO, Santa Barbara, CA, USA), anti-CD10 (DAKO), and anti-vimentin (DAKO). Staining was achieved with an EnVision kit (DAKO), and immunoreactvity was developed with 3,3′-diaminobenzidine tetrahydrochloride (Zymed Laboratories, Inc., South San Francisco, CA, USA) as a chromogen. The sections were counterstained for 3 min with Meyer's hematoxylin. As a negative control, rabbit or mouse IgG isotype was used instead of the primary antibody. As a positive control, a tissue section of colonic adenocarcinoma was used. The expression for epithelial COX-2 and vimentin was evaluated by assessing the percentage of positive cells, rated as negative (0–5 %) or positive (>5 %). Membranous expression of E-cadherin and β-catenin was rated according to the proportion of positive cells and classified into positive (>90 %) or focal loss (0–90 %). Expression of CD68 and CD10 in peritumoral stromal cells was graded as none (0), weak (1), moderate (2), or strong (3) based on the number of positive cells (CD68) or staining area (CD10).

Statistical analysis

Chi-square test, one-way ANOVA, *t* test, and Pearson correlation coefficient were used. Statistical significance was

assumed if a p value was less than 0.05. Data were expressed as mean±standard error of mean.

Results

We evaluated immunohistochemical staining for vimentin, E-cadherin, and β-catenin in the lesional cells of cutaneous SCC, its precursor lesions, and NS in order to examine EMT. As shown in Fig. 1, NS, AK, and BD showed normal membranous expression of E-cadherin and β-catenin, and did not reveal vimentin expression, whereas in SCC the cells showed marked loss of membranous expression of E-cadherin and β-catenin, in combination with cytoplasmic vimentin expression. However, we did not detect cytoplasmic or nuclear β-catenin expression in SCC with loss of membranous β-catenin expression. This immunohistochemical staining pattern in SCC was not associated with clinicopathological parameters such as gender, age, tumor site, and tumor differentiation (data not shown). Expression of vimentin in epithelial cells occurred in 51 % (21 out of 41) of SCC but in 0 % in BD, AK, and NS. Focal loss of E-cadherin expression was found in 46 % (19 out of 41) of SCC, 0 % of BD, 10 % (1 out of 10) of AK with high-grade dysplasia, 10 % (2 out of 20) of AK with low-grade dysplasia, and 0 % of NS. Focal loss of membranous β-catenin staining was noted in 41 % (17 out of 41) of SCC, 15 % (3 out of 20) of BD, 10 % (1 out of 10) of AK with high-grade dysplasia, and 0 % of AK with low-grade dysplasia and NS. Expression of EMT-related markers was significantly higher in SCC compared with premalignant lesions and NS ($p<0.05$). In SCC there was a significant correlation between the expression of E-cadherin and of β-catenin ($p=0.001$).

COX-2 expression was not found in NS and BD (Fig. 2), whereas in SCC perinuclear cytoplasmic COX-2 expression was noted in 46 % (19 out of 41) compared to 7 % (2 out of 30) in AK. COX-2 expression was significantly higher in SCC than in precursors and NS ($p<0.05$). An inverse

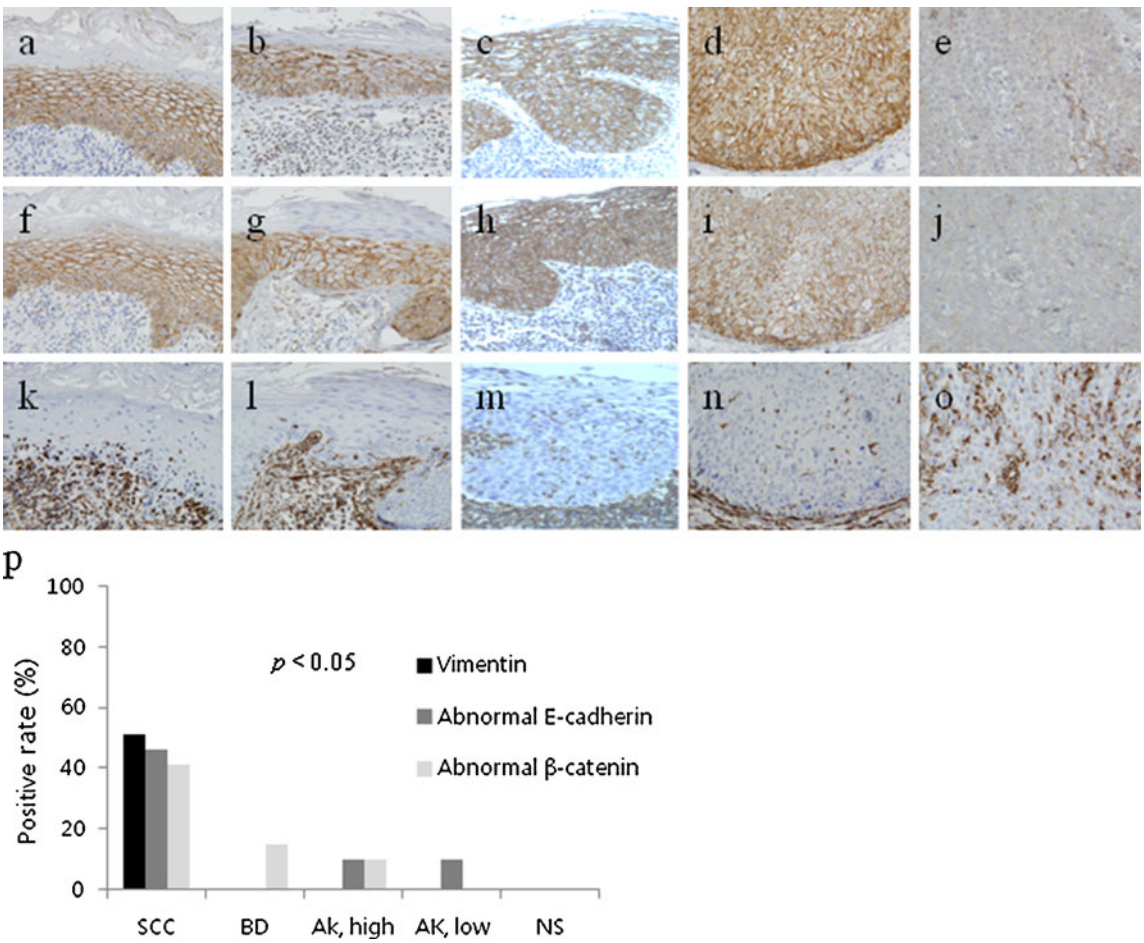

Fig. 1 Immunohistochemical staining of E-cadherin (**a**–**e**), β-catenin (**f**–**j**), and vimentin (**k**–**o**) in NS (**a**, **f**, **k**), AK with low grade (**b**, **g**, **l**), AK with high grade (**c**, **h**, **m**), BD (**d**, **i**, **n**), and SCC (**e**, **j**, **o**). SCC showed loss of membranous expression of E-cadherin and β-catenin, and cytoplasmic vimentin expression, whereas other lesions showed membranous expression of E-cadherin and β-catenin, and did not reveal vimentin expression. **p** Abnormal expression of E-cadherin and β-catenin, and vimentin expression significantly occurred in SCC compared with premalignant lesions and NS ($p<0.05$). **a**–**o** ×400

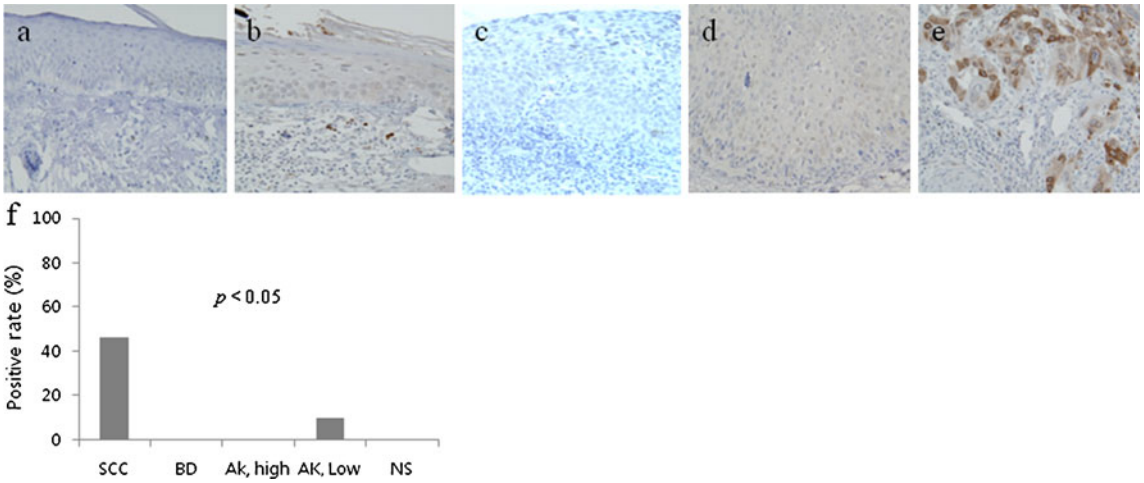

Fig. 2 Immunohistochemical staining of COX-2 in NS (**a**), AK with low grade (**b**), AK with high grade (**c**), BD (**d**), and SCC (**e**). SCC showed perinuclear cytoplasmic COX-2 expression, whereas other lesions did not reveal COX-2. **f** COX-2 expression was significantly higher in SCC than in precursors and NS ($p<0.05$). **a**–**e** ×400

correlation was found between the expression of COX-2 and E-cadherin in a variety of tumors [18, 29]. We found COX-2 expression in 68 % (13 out of 19) of SCC with focal loss of E-cadherin and in 22 % (6 out of 22) of SCC with normal expression of E-cadherin ($p=0.008$).

We examined TAM and CD10-positive stromal cells in cutaneous tumors and NS. As shown in Fig. 3, the score of TAM was 2.2±0.1 in SCC, 2.0±0.2 in BD, 1.8±0.2 in AK with high-grade dysplasia, 1.7±0.2 in AK with low-grade dysplasia, and 0.2±0.1 in NS, and the score of CD10-positive stromal cells was 2.0±0.1 in SCC, 1.4±0.2 in BD, 1.0±0.1 in AK with high dysplasia, and 0.9±0.1 in AK with low dysplasia and 0 in NS. TAM were significantly more numerous in SCC compared with AK and NS ($p<0.05$). Stromal CD10 expression was significantly higher in SCC and precursor lesions than in NS ($p<0.05$). In addition, there was a significant positive correlation between TAM and CD10-positive stromal cells in neoplastic lesions and NS ($R^2=0.607$, $p<0.001$).We evaluated the relation between tumor stromal cells and the expression of E-cadherin, β-catenin, vimentin, and COX-2 in all neoplastic lesions. As shown in Table 2, TAM was not correlated with the expression of any of these proteins, whereas CD10-positive stromal cells significantly correlated with focal loss

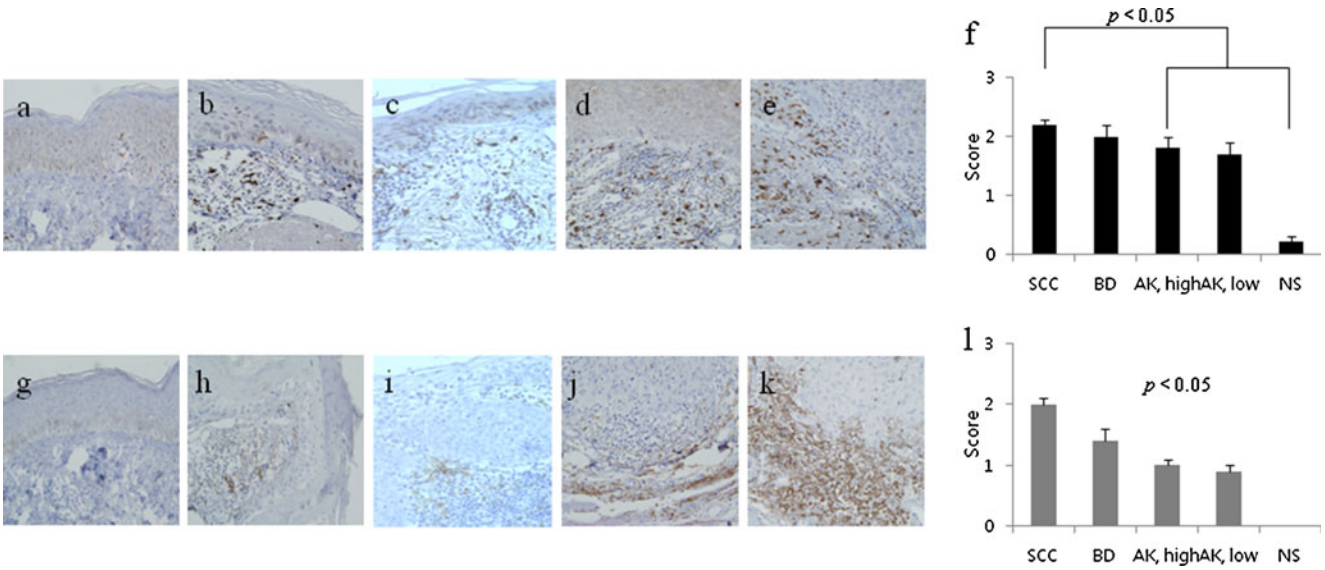

Fig. 3 Immunohistochemical staining of CD68 (**a**–**e**) and CD10 (**g**–**k**) in NS (**a**, **g**), AK with low grade (**b**, **h**), AK with high grade (**c**, **i**), BD (**d**, **j**), and SCC (**e**, **k**). TAM infiltrated in the lesions of AK, BD, and SCC, whereas it did not infiltrate in the area of NS. **f** TAM was significantly increased in SCC compared with AK and NS ($p<0.05$). Stromal CD10 expression was noted in AK, BD, and SCC, but not in NS. **l** Stromal D10 expression significantly and sequentially increased from NS to SCC and precursors ($p<0.05$). **a**–**e** and **g**–**k** ×400

Table 2 Relation between stromal cells such as CD68 and CD10 and expression of vimentin, E-cadherin, β-catenin, and COX-2 in tumor cells of overall squamous neoplastic lesions

		CD68	CD10
Vimentin	Negative (70)	2.0±0.1	1.4±0.1
	Positive (21)	2.3±0.1	2.1±0.1*
E-cadherin	Normal (69)	2.0±0.1	1.4±0.1
	Abnormal (22)	2.3±0.2	1.8±0.2
β-Catenin	Normal (70)	2.0±0.1	1.4±0.1
	Abnormal (22)	2.3±0.2	1.9±0.1**
COX-2	Negative (70)	2.0±0.1	1.4±0.2
	Positive (21)	2.1±0.2	2.1±0.2*

*p value <0.01; **p value <0.05

of expression of β-catenin, and of expression of COX-2 and vimentin in lesional cells, respectively ($p<0.05$), but not in SCC alone.

Discussion

In this present study, we show that in cutaneous SCC the expression of vimentin and COX-2 is induced, focal loss of membranous expression of E-cadherin and β-catenin are correlated, as well as induction of COX-2 expression is associated with focal loss of E-cadherin expression. In addition, TAM and stromal CD10 expression increased from NS to SCC and precursor lesions; however, there was no significant correlation with the expression of E-cadherin, β-catenin, COX-2, and vimentin in SCC.

EMT is an intricate process by which epithelial cells loose epithelial characteristics and acquire a mesenchymal-like phenotype. This dramatic phenotypic change involves the loss of E-cadherin, induction of mesenchymal markers such as vimentin and fibronectin, as well as extracellular matrix remodeling enzymes [2]. EMT plays important roles not only in the morphogenesis but also in wound healing, tissue fibrosis, and cancer progression. The present study showed that vimentin expression and abnormal expression of E-cadherin and β-catenin significantly occurred in SCC compared with precursors and NS, suggesting that EMT occurs late in cutaneous squamous cell carcinogenesis, closely associated with tumor invasion. This result is compatible with a previous study showing that membranous E-cadherin expression was reduced only in SCC but not in precursor lesions [30]. However, other studies showed that although abnormal expression of E-cadherin and β-catenin is common in SCC, they can also observed in intraepithelial squamous neoplastic lesions [5, 7]. Further studies are to be performed to clarify the onset time of EMT during the development of cutaneous SCC. We found no correlation between induction of vimentin expression and foal loss of E-cadherin expression, indicating that these processes are not strictly coregulated.

Transcriptional repression is a predominant mechanism controlling the expression of E-cadherin in most carcinomas [31]. E-cadherin repressors are the Snail family, the basic helix–loop–helix factors E47 and Twist, and the ZEB1 and Smad-interacting protein 1 [4, 32]. Induction of PGE_2 represses E-cadherin expression through the induction of Snail and ZEB1 in non-small cell lung cancer and colon cancer [18, 33, 34]. Ectopic expression of COX-2 in or PGE_2 treatment of bladder cancer cells reduces E-cadherin expression [29]. Recently it was found that E-cadherin expression is inhibited via the PGE_2–EP2 signaling pathway during ultraviolet-induced cutaneous squamous cell carcinoma progression [17]. We found COX-2 expression to be significantly correlated with focal loss of E-cadherin in SCC. Overall, an inverse correlation has been demonstrated between the expression of COX-2 and of E-cadherin in a variety of tumors, including cutaneous SCC.

β-catenin is bound to the cytoplasmic domain of E-cadherin, in which it enables E-cadherin to function as a cell–cell adhesion molecule and mediates the interplay of adherens junction molecules with the actin cytoskeleton [8]. Aberrations of E-cadherin expression lead to the translocation of β-catenin to cytoplasm and nucleus from cell membrane. Cytosolic β-catenin is rapidly eliminated by the proteasome, but inappropriate activation of the Wnt signaling pathway can inhibit degradation of cytosolic β-catenin, allowing it to enter the cell nucleus and bind to transcription factors, which eventually activate genes involved in cell proliferation [19]. In the present study, membranous β-catenin expression was markedly reduced in SCC and closely correlated with focal loss of E-cadherin expression. However, cytoplasmic or nuclear β-catenin expression was not detected in SCC. Previous studies also showed that marked reduction of membranous β-catenin expression is frequently observed in SCC compared with precursor lesions and significantly correlated with reduced E-cadherin [5, 10, 35]. A β-catenin gene mutation responsible for nuclear or cytoplasmic β-catenin accumulation was found in only pilomatricoma and but not in BD and SCC [36, 37]. A previous study found that in BD β-catenin is diffusely expressed in the nuclei and cytoplasm [35], and a defect or mutation in β-catenin was suggested. However, this finding has not been confirmed. Overall, these results suggest that the Wnt signaling pathway does not play a role in the development of cutaneous SCC.

Tumor microenvironment includes the total functional and structural constellation of neoplastic and nonneoplastic cells as well as extracellular components, including cytokines, chemokines, and growth factors that may be derived from either the neoplastic or the nonneoplastic

cells [38]. It is well established that the tumor microenvironment plays a major role in the tumor progression and induces EMT [19, 20, 38]. In the present study, CD10-positive stromal cells were nearly absent in NS, whereas its number significantly increased from AK to BD and SCC. CD10 expression in tumor-associated stromal cells has been described in several tumors including cutaneous SCC [24–28]. Stromal CD10 expression has been found to be induced in the dermis during wound healing [39]. Inflammatory and healing processes accompany tumor cell invasion of surrounding tissue. It thus appears that stromal CD10 expression may be induced by the local inflammatory process in malignant tumors [24]. CD10 is assumed to create a tumor microenvironment that facilitates cancer cell invasion and metastasis due to the structural similarity of CD10 to matrix metalloproteinases (MMPs) [40]. In the present study, stromal CD10 expression correlated with vimentin expression of tumor cells in all neoplastic lesions, suggesting that CD10 plays a role in the induction of EMT. Stromal CD10 expression and vimentin expression were markedly increased in SCC compared with precursor lesions. In SCC, however, CD10 and vimentin were not correlated. Data in the literature to this effect have not been found either. Additional studies need to be performed to elucidate the role of CD10 in EMT in tumors. TAM resemble M2 macrophages and are generally thought to promote tumor progression because of their inability to induce T cell activation along with the release of protumorigenic factors such as transforming growth factor-β1 (TGF-β1), interleukin-10, proangiogenic factors and MMPs [41]. Our finding that TAM are more prevalent in cutaneous SCC than in AK is in keeping with this concept and is also in accordance with recently published data [24]. TGF-β1 produced by TAM induces tumor EMT through a Smad-dependent transcriptional pathway and a Smad-independent transcriptional pathway [42]. TAM also increases angiogenesis and invasion via COX-2-dependent release of basic fibroblast growth factor and vascular endothelial growth factor-A and MMP-9 in basal cell carcinoma cells [43]. However, we did not detect any correlation between TAM and expression of EMT markers or COX-2 expression. Taken together, CD10 and TAM seem to be involved in the development of cutaneous SCC, but the mechanisms are to be further clarified.

In conclusion, in cutaneous SCC, expression of EMT markers correlated with COX-2 expression. Stromal CD10 expression and TAM are involved in the development of cutaneous SCC.

Conflict of interest I declare that I have no conflict of interest.

References

1. Vleminckx K, Kemler R (1999) Cadherins and tissue formation: integrating adhesion and signaling. Bioessays 21:211–220
2. Thiery JP (2002) Epithelial-mesenchymal transitions in tumour progression. Nat Rev Cancer 2:442–454
3. Hirohashi S (1998) Inactivation of the E-cadherin-mediated cell adhesion system in human cancer. Am J Pathol 153:333–339
4. Guarino M, Rubino B, Ballabio G (2007) The role of epithelial-mesenchymal transition in cancer pathology. Pathology 39:305–318
5. Papadavid E, Pignatelli M, Zakynthinos S, Krausz T, Chu AC (2002) Abnormal immunoreactivity of the E-cadherin/catenin (alpha-, beta-, and gamma-) complex in premalignant and malignant non-melanocytic skin tumours. J Pathol 196:154–162
6. Czech W, Krutmann J, Herrejnetcht K, Schopf E, Kapp A (1993) Human cell adhesion molecule uvomorulin is differentially expressed in various skin tumors. J Cutan Pathol 20:168–172
7. Lyakhovitsky A, Barzilai A, Fogel M, Trau H, Huszar M (2004) Expression of e-cadherin and beta-catenin in cutaneous squamous cell carcinoma and its precursors. Am J Dermatopathol 26:372–378
8. Barth AI, Näthke IS, Nelson WJ (1997) Cadherins, catenins and APC protein: interplay between cytoskeletal complexes and signaling pathways. Curr Opin Cell Biol 9:683–690
9. Brembeck FH, Rosário M, Birchmeier W (2006) Balancing cell adhesion and Wnt signaling, the key role of beta-catenin. Curr Opin Genet Dev 16:51–59
10. Brasanac D, Boricic I, Todorovic V, Tomanovic N, Radojevic S (2005) Cyclin A and beta-catenin expression in actinic keratosis, Bowen's disease and invasive squamous cell carcinoma of the skin. Br J Dermatol 153:1166–1175
11. Tsujii M, DuBois RN (1995) Alterations in cellular adhesion and apoptosis in epithelial cells overexpressing prostaglandin endoperoxide synthase 2. Cell 83:493–501
12. Tsujii M, Kawano S, DuBois RN (1997) Cyclooxyenase-2 expression in human colon cancer cells increases metastatic potential. Proc Natl Acad Sci U S A 94:3336–3340
13. Nijsten T, Colpaert CG, Vermeulen PB, Harris AL, Van Marck E, Lambert J (2004) Cyclooxygenase-2 expression and angiogenesis in squamous cell carcinoma of the skin and its precursors: a paired immunohistochemical study of 35 cases. Br J Dermatol 151:837–845
14. Muller-Decker K, Reinerth G, Krieg P et al (1999) Prostaglandin-H synthase isozyme expression in normal and neoplastic skin. Int J Cancer 82:648–656
15. Kagoura M, Toyoda M, Matsui C et al (2001) Immunohistochemical expression of cyclooxygenase-2 in skin cancers. J Cutan Pathol 28:298–302
16. Denkert C, Kobel M, Berger S et al (2001) Expression of cyclooxygenase 2 in human malignant melanoma. Cancer Res 61:303–308
17. Brouxhon S, Kyrkanides S, O'Banion MK et al (2007) Sequential down-regulation of E-cadherin with squamous cell carcinoma progression: loss of E-cadherin via a prostaglandin E_2-EP_2-dependent posttranslational mechanism. Cancer Res 67:7654–7664
18. Dohadwala M, Yang SC, Luo J et al (2006) Cyclooxygenase-2-dependent regulation of E-cadherin: prostaglandin E_2 induces transcriptional repressors ZEB1 and snail in non-small cell lung cancer. Cancer Res 66:5338–5345
19. Jing Y, Han Z, Zhang S, Liu Y, Wei L (2011) Epithelial-mesenchymal transition in tumor microenvironment. Cell Biosci 1:29
20. Ungefroren H, Sebens S, Seidl D, Lehnert H, Hass R (2011) Interaction of tumor cells with the microenvironment. Cell Commun Signal 9:18

21. Chen JJ, Lin YC, Yao PL et al (2005) Tumor associated macrophages: the double-edged sword in cancer progression. J Clin Oncol 23:953–964
22. Lewis CE, Pollard JW (2006) Distinct role of macrophages in different tumor microenvironments. Cancer Res 66:605–612
23. Dong R, Wang Q, He XL, Chu YK, Lu JG, Ma QJ (2007) Role of nuclear factor kappa B and reactive oxygen species in the tumor necrosis factor-alpha induced epithelial-mesenchymal transition of MCF-7 cells. Braz J Med Biol Res 40:1071–1078
24. Takahara M, Chen S, Kido M et al (2009) Stromal CD10 expression, as well as increased dermal macrophages and decreased Langerhans cells, are associated with malignant transformation of keratinocytes. J Cutan Pathol 36:668–674
25. Albrecht M, Gillen S, Wilhelm B et al (2002) Expression, localization and activity of neutral endopeptidase in cultured cells of benign prostatic hyperplasia and prostate cancer. J Urol 168:336–342
26. Iwaya K, Ogawa H, Izumi M et al (2002) Stromal expression of CD10 in invasive breast carcinoma: a new predictor of clinical outcome. Virchows Arch 440:589–593
27. Kesse-Adu R, Shousha S (2004) Myoepithelial markers are expressed in at least 29% of oestrogen receptor negative invasive breast carcinoma. Mod Pathol 17:646–652
28. Ogawa H, Iwaya K, Izumi M et al (2002) Expression of CD10 by stromal cells during colorectal tumor development. Hum Pathol 33:806–811
29. Jang TJ, Cha WH, Lee KS (2010) Reciprocal correlation between the expression of cyclooxygenase-2 and E-cadherin in human bladder transitional cell carcinomas. Virchows Arch 457:319–328
30. Fuller LC, Allen MH, Montesu M, Barker JN, MacDonald DM (1996) Expression of E-cadherin in human epidermal non-melanoma cutaneous tumours. Br J Dermatol 134:28–32
31. Park SH, Cheung LW, Wong AS, Leung PC (2008) Estrogen regulates Snail and Slug in the down-regulation of E-cadherin and induces metastatic potential of ovarian cancer cells through estrogen receptor alpha. Mol Endocrinol 22:2085–2098
32. Peinado H, Portillo F, Cano A (2004) Transcriptional regulation of cadherins during development and carcinogenesis. Int J Dev Biol 48:365–375
33. Jang TJ (2009) Cyclooxgenase-2 expression is related to the epithelial-to-mesenchymal transition in human colon cancers. Yon Med J 50:818–824
34. Mann JR, Backlund MG, Buchanan FG et al (2006) Repression of prostaglandin dehydrogenase by epidermal growth factor and snail increases prostaglandin E_2 and promotes cancer progression. Cancer Res 66:6649–6656
35. Fukumaru K, Yoshii N, Kanzaki T, Kanekura T (2007) Immunohistochemical comparison of beta-catenin expression by human normal epidermis and epidermal tumors. J Dermatol 34:746–753
36. Moreno-Bueno G, Gamallo C, Perez-Gallego L et al (2001) β-catenin expression in pilomatrixomas. Relationship with β-catenin gene mutations and comparison with β-catenin expression in normal hair follicles. Br J Dermatol 145:576–581
37. Doglioni C, Piccinin S, Demontis S et al (2003) Alterations of β-catenin pathway in non-melanoma skin tumors. Loss of α-ABC nuclear reactivity correlates with the presence of β-catenin gene mutation. Am J Pathol 163:2277–2287
38. Ruiter D, Bogenrieder T, Elder D, Herlyn M (2002) Melanoma-stroma interactions: structural and functional aspects. Lancet Oncol 3:35–43
39. Olerud JE, Usui ML, Seckin D et al (1999) Neutral endopeptidase expression and distribution in human skin and wounds. J Invest Dermatol 112:873–881
40. Basset P, Wolf C, Rouyer N, Bellocq JP, Rio MC, Chambon P (1994) Stromelysin-3 in stromal tissue as a control factor in breast cancer behavior. Cancer 74:1045–1049
41. Sica A, Larghi P, Mancino A et al (2008) Macrophage polarization in tumour progression. Sem Cancer Biol 18:349–355
42. Kalluri R, Weinberg RA (2009) The basics of epithelial-mesenchymal transition. J Clin Invest 119:1420–1428
43. Tjiu JW, Chen JS, Shun CT (2009) Tumor-associated macrophage-induced invasion and angiogenesis of human basal cell carcinoma cells by cyclooxygenase-2 induction. J Invest Dermatol 129:1016–1025

Virchows Arch (2012) 460:489–495
DOI 10.1007/s00428-012-1226-y

ORIGINAL ARTICLE

Subgross breast pathology in the twenty-first century

William A. Smith · James J. Going

Received: 15 November 2011 / Revised: 7 March 2012 / Accepted: 13 March 2012 / Published online: 30 March 2012
© Springer-Verlag 2012

Abstract Subgross studies on breast morphology in cleared thick sections are informative, but lengthy protocols could clash with diagnostic timescales and interfere with immunohistochemistry (IHC) or molecular analysis. We sought to speed up staining and tissue clearing to improve compatibility with diagnostic needs without detriment to histology or other assays. Thick sections (2–3 mm) of normal human breast tissue and whole mouse mammary glands were stained with alum-carmine, aceto-carmine, Harris's haematoxylin, cresyl violet, neutral red, thionin, 4',6-diamidino-2-phenylindole (DAPI), ethidium bromide (EB), or propidium iodide (PI) and cleared in xylene (refractive index ν=1.50), benzyl alcohol/benzyl benzoate (BABB; ν=1.59), xylene–BABB (X-BABB), thiodiglycol (2,2′-thiodiethanol, ν=1.52) or anethole (ν=1.56). Tissue was then paraffin embedded for IHC for ER, PR, E-cadherin, CD31 or cytokeratin 7. Haematoxylin and alum-carmine are excellent non-fluorescent subgross stains giving strong nuclear staining and minimal background. DAPI and EB permeate thick sections poorly but PI penetrates well, with a high signal-to-noise ratio after clearing in BABB or X-BABB. Other clearing agents were less effective, including thiodiglycol. Anethole's unpleasant odour precluded further evaluation. All evaluated clearing agents preserved comparable immunoreactivity for all markers. PI is a promising stain for subgross breast studies, compatible with BABB clearing. The hope that the water-miscible thioalcohol, thiodiglycol, might accelerate tissue clearing was not realised. There is scope for further streamlining to make subgross techniques more acceptable in combined research/diagnostic settings.

Keywords Breast · Subgross · Anatomy · Visualisation · Parenchyma

W. A. Smith · J. J. Going (✉)
Department of Pathology, Glasgow Royal Infirmary,
Castle Street,
Glasgow G4 OSF, UK
e-mail: going@udcf.gla.ac.uk

W. A. Smith · J. J. Going
Institute of Cancer Sciences, College of Medicine,
Veterinary and Life Sciences, University of Glasgow,
Glasgow, UK

Introduction

Cancer develops from native epithelium of the breast via complex pathways. Some breast cancer precursors [1] are histologically distinctive, but cancer-promoting mutations do not always confer any definite morphological phenotype [2]: Lahkani et al. [3, 4] showed identical genetic abnormalities in carcinomas and normal-looking cancer-adjacent breast tissue, and neither TP53 mutations in Li-Fraumeni syndrome nor BRCA1 or 2 mutations have any *obligatory* mammary phenotype, although atypical epithelial proliferations are more common in women with BRCA mutations [5].

Investigating pre-malignancy in the human breast is hindered by its anatomical complexity. Fifteen to 30 or more distinct lobes [6], each with one central (lactiferous) duct, ramify extensively from the nipple, to end in myriad terminal ducts and lobules (TDLU) [7]. For 30 or 40 years, the TDLU have been regarded as the likely source of breast cancer [8], but this view has been challenged [4, 7].

In particular, the *sick lobe* hypothesis (Tot et al.) [4, 7] suggests that an entire lobe can be at increased risk of malignancy. Such a lobe 'sick' ab initio could be built by the daughters of one cell which had acquired a cancer-promoting mutation before thelarche, or even during foetal life. Just as one cell can reconstitute an entire mammary gland in a cleared mouse mammary fat pad [9], daughter cells carrying the same

mutation could increase the risk of neoplastic transformation throughout a whole lobe. Alternatively, 'supercompetitor' cells could infiltrate or displace normal epithelium throughout an entire lobe, placing it at increased risk of cancer [4, 7].

The sick lobe hypothesis naturally directs our thoughts towards lobe-orientated diagnosis and therapy. Ablation of a sick lobe could reduce local recurrence by eliminating a field of genetically abnormal high-risk cells [4, 7], but effective endoductal diagnosis and treatment [10, 11] will require improved knowledge of mammary lobe biology and its role in mammary carcinogenesis.

Unfortunately, breast lobes are invisible with current breast imaging and conventional histology, and 3D reconstruction from thin histological sections is prohibitively laborious [12]. This limitation is less stringent with classical subgross technique, which allows branching ducts to be traced through serial thick tissue sections which have been stained and cleared, allowing lobes to be visualised [13]—a requirement for testing the sick lobe hypothesis [10, 11].

Drawbacks of classical subgross technique limit its application in diagnostic settings. Lengthy fixation, staining, dehydration and clearing are incompatible with time pressures on examination of clinical specimens [14]. Haematoxylin is an excellent subgross stain but requires regressive destaining in acid–alcohol which may limit compatibility with modern molecular pathology and immunohistochemistry. Methyl salicylate, a traditional clearing agent, is a toxic and malodorous irritant.

We sought to make it easier to combine subgross examination of human breast tissue for research with diagnostic histopathology. DNA-specific fluorescent dyes could minimise background staining and allow confocal or multiphoton imaging [15] while retaining compatibility with immunohistochemical and molecular analysis. Dye-compatible water-miscible clearing agents like 2,2′-thiodiethanol could reduce processing times by eliminating lengthy dehydrating and clearing in multiple successive reagents [16, 17] and reduce dependency on detrimental reagents like methyl salicylate.

Materials and methods

Tissue samples Normal human breast tissue surplus to diagnostic needs was from women undergoing reduction mammoplasty at Glasgow Royal Infirmary, with ethical approval for an anonymised study following histological exclusion of pathology. Surplus mice from Glasgow University animal house were killed by cervical dislocation in accordance with Schedule 1 of the Animals (Scientific Procedures) Act 1986 and Home Office requirements [18]. Isolated fourth inguinal mammary glands of each mouse (Rasmussen et al.) [19] were mounted on glass slides and fixed in 4 % neutral-buffered formaldehyde.

Preliminary stain analysis Candidate stains (in aqueous solution unless otherwise stated) were applied to 3-μm sections of formalin-fixed, paraffin-embedded human breast tissue. Tissue sections on silanised slides were de-paraffinized in xylene, rehydrated through graded ethanol to deionised water and rinsed in phosphate-buffered saline (PBS) (pH 7.4) before staining as follows:

Harris's haematoxylin for 2 min: Sections rinsed in deionised water were destained in acid–alcohol, blued in Scott's tap water substitute, rinsed in running tap water, dehydrated through graded ethanol and air dried.

Alum-carmine (carmine 0.2 %, aluminium potassium sulphate 0.5 %) for 15 min: Stained sections were rinsed in distilled water, dehydrated through graded ethanol and air dried.

Aceto-carmine (carmine 0.5 % in 45 % acetic acid), for 2 min: Stained sections were rinsed with deionised water, differentiated in 96 % ethanol, dehydrated in 100 % ethanol and air dried.

Cresyl violet (0.2 %), for 5 min: Stained sections were rinsed with deionised water, differentiated in Nissl differentiator, dehydrated in 100 % ethanol and air dried.

Neutral red (0.2 % in 80 % ethanol), for 2 min: Stained sections were then rinsed in deionised water, dipped briefly in 70 % ethanol, further differentiated in 95 % ethanol, dehydrated in 100 % ethanol and air dried.

Thionin (1 % in 25 % ethanol), for 15 min: Stained sections were rinsed in deionised water, differentiated in 95 % ethanol, dehydrated in 100 % ethanol and air dried.

4',6-Diamidino-2-phenylindole (DAPI) (300 μl/100 ng/ml) was pipetted onto the section with a coverslip promoting even distribution. Sections were incubated in the dark for 30 min to prevent photobleaching, the coverslip removed, rinsed with deionised water and air dried.

Ethidium bromide (300 μl of 0.1 μg/ml) was pipetted onto the section for 30 min under a coverslip in the dark, then rinsed with deionised water and air dried.

Propidium iodide (300 μl of 1.5 μM) was pipetted directly onto the section for 30 min under a coverslip in the dark, then rinsed with deionised water and air dried.

Air-dried sections were mounted and coverslipped in potential clearing agents including benzyl alcohol/benzyl benzoate 1:2 (BABB), 97 % thiodiethanol (TDE), xylene/Pertex or Vectashield and sealed with nail varnish.

Slides except those stained with fluorescent labels were viewed by white light microscopy (Olympus-BX51) to assess staining and compatibility with clearing agents. A standard H&E slide was used as a morphology control. All the stained slides were subsequently viewed using an Olympus-BX61 fluorescent microscope to evaluate nuclear staining and persistence of fluorescence in xylene/Pertex, BABB or TDE.

Subgross staining Nuclear stains giving low stromal background in preliminary analysis were further tested by staining subgross sections of breast tissue (25×15×~2–3 mm) washed in running water (15 min) to remove excess formaldehyde. Standard subgross staining in Harris's haematoxylin (1 h) was carried out as a control [20]. Stained thick sections were washed in running water (1 h), destained in 2 % acid–alcohol (1 h), washed in running water (30 min) and then dehydrated through graded ethanol: 95 %, 1×3 h; 99 %, 2×3 h; and 100 % 2×4 h, before clearing.

Alum-carmine is a slow-penetrating dye, thus human and mouse tissues require overnight staining [19]. Various dilutions and staining times were evaluated for cresyl violet, neutral red [15] and thionin, and as described by Samoilov and Chebyshev [21], simultaneous postfixation and thionin staining were attempted using various dilutions of thionin and formaldehyde.

Three different staining protocols were tested with DAPI, ethidium bromide and propidium iodide. The first (Landau et al.) [15] involved defatting tissue in acetone (1 h) prior to overnight staining in 50 % glycerol/PBS containing 10 μg/ml of propidium iodide, ethidium bromide or DAPI. Tissues were then destained in 50 % glycerol/PBS for 1 h and dehydrated in 75 % glycerol/PBS (1×1 h) and 100 % glycerol (1×1 h).

Alternatively, sections were stained overnight with 10 μg/ml of propidium iodide, ethidium bromide or DAPI in PBS before dehydration. This protocol omitted defatting in acetone prior to staining. Thirdly, samples were dehydrated and cleared in xylene prior to staining in BABB containing 10 μg/ml of either propidium iodide, ethidium bromide or DAPI to assess simultaneous staining and clearing.

Dehydration Stained subgross and whole-mount sections rinsed in water were dehydrated through graded ethanol. Samples stained in alum-carmine were used to investigate dehydration protocols. Samples variously underwent prolonged dehydration through multiple ethanol concentrations 30, 50, 70, 85, 90, 95 (×2) and 100 % (×2) or shorter protocols that omitted weaker concentrations (70, 90, 95 and 100 % ×2) or used more widely spaced ethanol concentrations (30, 50, 70, and 100 % ×2). The samples spent 15 min in each dilution. Effective dehydration was indicated by a complete absence of brownish water stains in cleared tissues.

Clearing Agents investigated included xylene, BABB and 2,2′-thiodiethanol, which is water-miscible, so tissues cleared in this agent should not require dehydration through ethanol. Thiodiethanol clearing used increasing concentrations for 15-min intervals—10, 25, 50 and 97 % ×2—to minimise osmotic effects [16].

Specimens for clearing in BABB or xylene must be completely dehydrated, since neither agent is water-miscible. Incomplete dehydration causes brownish stains after clearing and reduces transparency. Dehydrated samples cleared in 100 % xylene or BABB (2×1 h) were placed in fresh clearing agent overnight. Samples containing water after clearing were returned to 100 % alcohol (15 min) and then re-cleared. Sequential clearing with xylene and BABB was investigated by clearing samples in xylene then BABB overnight. In some experiments, acetone and Tween-20 were used as tissue defatting agents before staining.

Measuring transparency To compare the quality of clearing, we devised a technique allowing quantification of transparency (Fig. 1). Individual lines of a photographic resolution chart seen through the tissue at a standard distance become harder to resolve as their spacing decreases or the distance (z) between chart and tissue section increases. Greater transparency allows more closely spaced lines to be resolved. The samples were tested with z=0, 15 or 30 mm. Resolution of lines with pitch<0.45 mm^{-1} at z=30 mm was regarded as satisfactory.

Analysis of subgross morphology Immersed subgross sections in 100 mm glass Petri dishes were viewed with an Olympus-SZ11 stereoscopic dissecting microscope equipped with an Olympus-E450 digital SLR camera. The samples stained with fluorescent dyes were viewed with the microscope on an ultraviolet gel transilluminator (UVP-TL33).

Immunohistochemistry and histology After subgross imaging and data collection, tissues were rehydrated and processed to paraffin wax. Blocks representing useful stains and clearing agents were chosen to investigate compatibility with subsequent immunohistochemical analysis. Blocks of fixed but not otherwise treated tissue were included as a control.

Paraffin sections (4 μ) were mounted on silanised slides and baked at 60 °C (2 h). Immunohistochemistry was performed with established laboratory protocols. Five antigens were chosen: oestrogen receptor (clone 6F11/2, Vector Laboratories); progesterone receptor (clone PgR-636, Dako); cell adhesion molecule E-cadherin (clone NCH-38, Dako); endothelial marker CD31 (clone JC70A, Dako); and luminal marker cytokeratin 7 (clone OV-TL12/30, Dako), plus a negative control. A section from each block was also processed for H&E staining.

Results

Determination of candidate dyes for subgross application Harris's haematoxylin and alum-carmine both gave excellent subgross staining, with little background. Aceto-carmine stained nuclei but with a high background staining

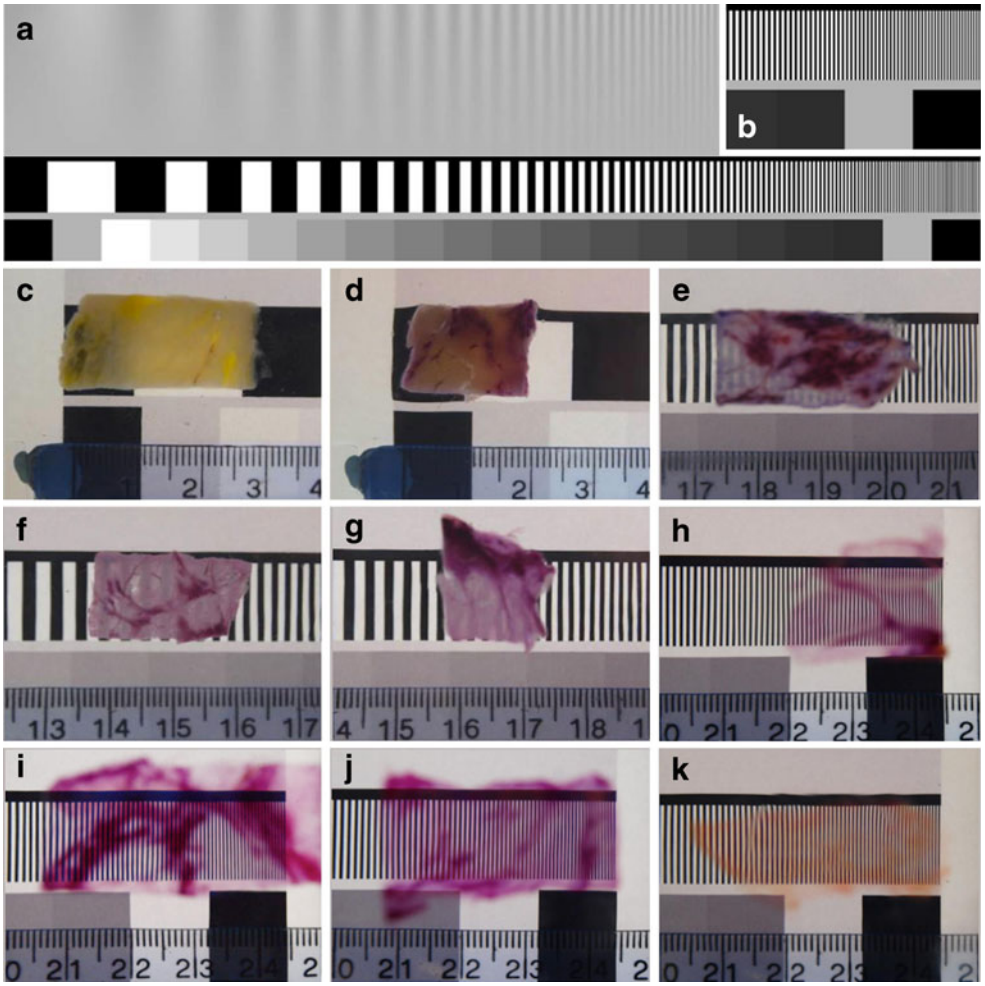

Fig. 1 Assessing transparency. **a**, **b** A photographic resolution chart was used to evaluate transparency. **b** A detail of part of the chart with line spacing ~0.45 mm^{-1}. Clear resolution of these lines with the distance between tissue and chart (z)=30 mm demonstrated satisfactory transparency. **c**, **d** Neither glycerol (**c**) nor thiodiethanol cleared tissues to any significant degree (z=0 mm). **e**–**g** Although better, none of these portions of breast tissue has cleated satisfactorily in xylene (z=15 mm). **h**–**k** Complete clearing of breast tissue is achieved in BABB (**h**, **i**) and xylene–BABB (**j**, **k**) (z=30 mm)

and was not applied to subsequent subgross analyses. Cresyl violet and neutral red showed selective staining of nuclei with slightly more background staining than the haematoxylin. Thionin stained nuclei with low background, comparable to haematoxylin (Fig. 2)

DAPI, ethidium bromide and propidium iodide yielded strong blue, orange or red nuclear fluorescence. Minimal background suggested that any of these dyes might be suitable in a subgross application. All three stains were equally compatible with xylene/Pertex, BABB and thiodiethanol with little photobleaching and fluorescent signals comparable with the sections mounted in Vectashield.

Preliminary experiments suggested the most promising candidates dyes for subgross staining are haematoxylin, alum-carmine, DAPI, ethidium bromide and propidium iodide. Cresyl violet, neutral red and thionin were less encouraging.

Optimal dehydration All three dehydration protocols were equally effective and the shortest was adopted.

Application to subgross staining Neutral red, thionin and cresyl violet all stained nuclei in subgross sections but with heavy background, independent of concentration. Destaining failed to improve signal-to-noise ratio in human tissue, unlike mouse mammary glands. Exposure to thionin during postfixation failed to stain nuclei.

The established subgross stains, haematoxylin and alum-carmine gave excellent signal-to-noise ratios. DAPI and ethidium bromide failed to penetrate human breast tissue, with fluorescent nuclear staining on the surface only of thick sections. Propidium iodide stained nuclei throughout tissues with minimal background or autofluorescence. Staining from BABB failed with all the three fluorescent dyes.

Clearing and transparency Xylene clearing was only moderately effective. No tissues achieved entirely satisfactory transparency, with a maximum z=15 mm. Thin areas of mouse mammary gland could be visualised.

BABB is a superlative clearing agent. Where good specific staining has been achieved, BABB achieves high transparency in fatty and dense collagenous tissues, optimising visualisation. It cannot compensate for poor staining. Best of all was sequential the xylene–BABB processing,

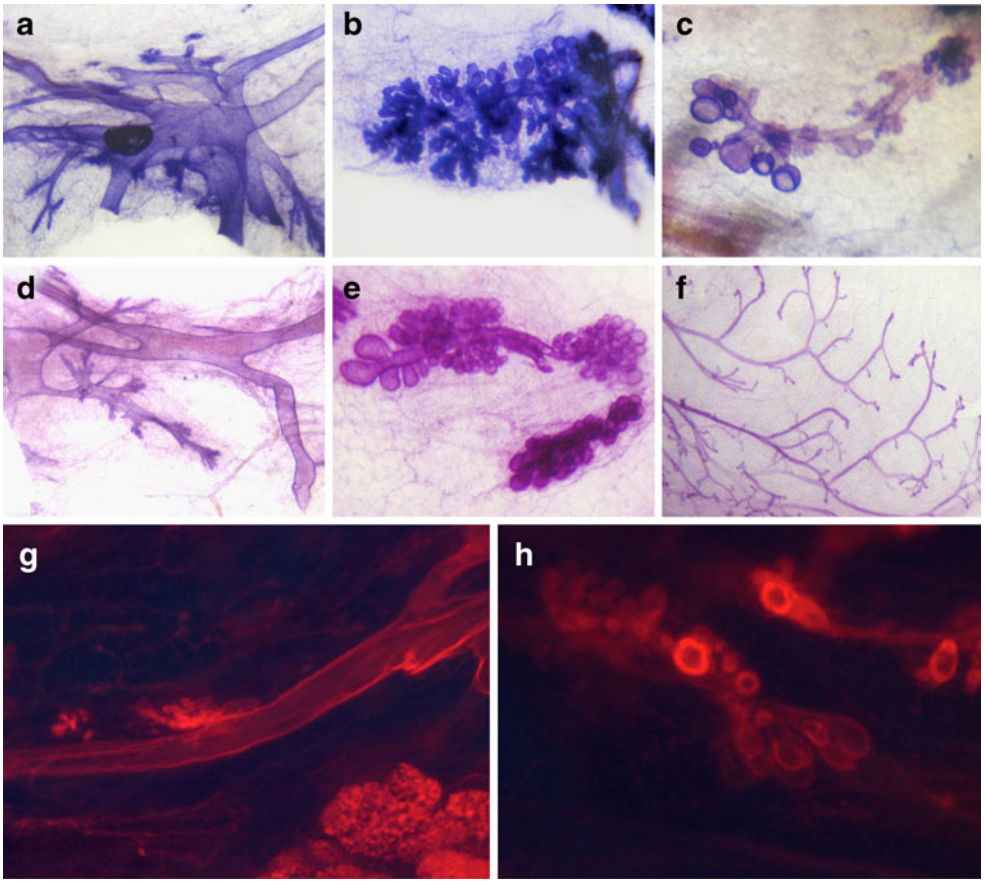

Fig. 2 Subgross morphology with different stains. **a**–**c** Human breast tissue stained with haematoxylin: **a** branching ducts; **b**, **c** lobules. **d**, **e** Human breast tissue stained with alum-carmine: **d** branching ducts and atrophic lobules; **e** small lobules. **f** Whole mount of mouse mammary gland stained with alum-carmine, showing ductal branching and terminal end buds. **g**, **h** Human breast tissue stained with propidium iodide, showing ducts and lobules

although this subtle difference was not quantifiable using the transparency measuring technique. Xylene–BABB also cleared more quickly than BABB alone.

Thiodiethanol failed as a clearing agent in mouse and human mammary tissues, probably as it has limited capacity to extract lipids which BABB and xylene achieve easily. Following tissue defatting in acetone or Tween-20, thiodiethanol performed slightly better but not well enough, despite achieving some measurable transparency. Glycerol likewise failed to clear samples sufficiently.

Compatibility with immunohistochemistry All five marker molecules (oestrogen receptor and progesterone receptors; E-cadherin; cytokeratin 7 and CD31) remained strongly detectable in all samples, giving comparable results to the control section, even after several weeks. Tissue clearing using xylene, BABB and TDE appears to have no detectable impact on immunohistochemical staining, nor does prior staining with alum-carmine, propidium iodide or haematoxylin. All negative controls were appropriately negative.

Compatibility with histology Following subgross analyses, the samples were processed for histology and standard H&E slides to assess compatibility of subgross processing with morphological preservation. All sections showed morphology including nuclear detail comparable to conventionally processed H&E sections of the same tissues.

Discussion

Spalteholz technique Tissue clearing, introduced by Werner Spalteholz [22], inspired H.G. Wells' *The Invisible Man* [23]. Substitution of tissue interstitial fluid with organic solvents of high-refractive index reduces light scattering and a high transparency is achievable [24]. Spalteholz technique has been used extensively in the study of vascular networks injected with India ink [25] and was the foundation of breast subgross studies pioneered by Dabelow [26]. Small numbers of recent human breast subgross studies may reflect the difficulty of combining molecular and subgross work, which this study attempts to address. This project aimed to speed up subgross examination of human and mouse mammary gland tissues, improve staining and avoid protocols detrimental to immunohistochemistry and molecular analysis.

Tissue clearing We had high hopes for 2,2′-thiodiethanol. This relatively non-toxic, water-miscible thioalcohol was recently introduced into confocal microscopy as a mounting medium compatible with many fluorescent markers [16,

17]. It was hoped that direct clearing in TDE would be quicker than classical techniques of dehydration in alcohol and transfer through intermediate solvents to the final clearing agent. Unfortunately, TDE was not effective in comparison with traditional protocols which extract most tissue lipids, increasing transparency. Alternative defatting agents (acetone and Tween-20) did not achieve high transparency when followed by TDE.

BABB was highly effective, and with minimal odour, it is pleasanter to use than the methyl salicylate [27]. The odour of methyl salicylate easily becomes overpowering, and like all salicylates, it is toxic [28]. Odour is not trivial: another candidate clearing agent was anethole (refractive index 1.57), but the supply we obtained had an unpleasant odour which excluded it from practical considerations [29].

Measuring transparency The use of a photo resolution chart to measure transparency distinguished samples of low, moderate and high transparency, but visual inspection did not detect subtle differences between highly transparent samples (x>240 mm, z=30 mm), such as tissues cleared in BABB alone or xylene–BABB. If necessary, a small difference might be quantifiable by techniques designed to assess corneal transparency [30].

Tissue stability and morphological preservation Tissues undergo some distortion and shrinkage in clearing agents, potentially affecting subsequent mapping [27]. Tissues cleared in xylene alone shrank little but did harden with some distortion. In contrast, samples in BABB alone were soft and delicate with a tendency to tear without gentle handling. Sequential clearing with xylene and BABB minimised hardening caused by xylene and the fragility caused by BABB, producing samples with little shrinkage or distortion, flexible yet firm, ideal for subgross imaging. Samples did not deteriorate or undergo bleaching on extended storage (months) in xylene or BABB or thiodiethanol.

Tissue staining Haematoxylin and alum-carmine have long been used for subgross and whole-mount preparations. Both dyes gave excellent nuclear staining with minimal background, as one would wish, but alum-carmine staining is prolonged and haematoxylin requires destaining in acid–alcohol, which might be detrimental to immunohistochemical or molecular analysis, although immunoreactivity of all five chosen molecules was retained in haematoxylin-stained subgross tissue subsequently processed for histology.

Cresyl violet, neutral red or thionin all suffered from excessive background staining and none of these dyes gave any nuclear fluorescence. Despite a previous study describing reddish-orange fluorescence of carmine-stained nuclei in cell smears [31], we were unable to demonstrate such fluorescence in human breast tissue, even in water-mounted tissue.

DAPI, ethidium bromide and propidium iodide have been applied to murine whole-mount studies [17] but DAPI and ethidium bromide penetrate poorly into thick sections of human breast tissue. In contrast, propidium iodide stained thick sections of human breast tissue throughout, yielding selective nuclear fluorescence. Low-level stromal autofluorescence did not interfere with clear visualisation of ducts and lobules.

Simultaneous staining of thick sections with propidium iodide and clearing in BABB was unsuccessful (as were equivalent experiments with ethidium bromide and DAPI), with fluorescence being observed only at the periphery of the sections despite transparency being achieved. The compatibility of propidium iodide with subsequent immunohistochemistry for all five markers makes this stain a promising candidate for future study: it is clearly important to demonstrate that clinically important assays are not adversely affected by specimen-processing procedures including subgross protocols.

Future work Improvements in subgross methodology are clearly possible and could facilitate novel integrated morphological and molecular studies in mammary biology. The preservation of epitopes recognised by several different monoclonal antibodies is encouraging and a logical extension would be to demonstrate adequate preservation of DNA and RNA. Compatibility of BABB with propidium iodide fluorescence is valuable for the possibilities it suggests for visualising breast parenchyma on a large scale and as a tool for investigating recent hypotheses about mammary carcinogenesis including ‘sick lobe’ theories [4, 7]. The ultimate goal is nothing less than complete visualisation of all the parenchyma in a breast with detailed structural correlation and molecular analysis [32, 33]. The potential of thiodiethanol as a clearing agent may not have been fully evaluated and further work in this area could be of value.

Acknowledgments This work was supported by the School of Medicine of the University of Glasgow.

Conflict of interest We declare no conflicts of interest.

References

1. Larson PS, De Las Morenas A, Cerda SR, Bennett SR, Cupples LA, Rosenberg CL (2006) Quantitative analysis of allele imbalance supports atypical ductal hyperplasia lesions as direct breast cancer precursors. J Pathol 209:307–316
2. Heaphy CM, Griffith JK, Bisoffi M (2009) Mammary field cancerization: molecular evidence and clinical importance. Breast Cancer Res Treat 118:229–239
3. Lakhani SR, Chaggar R, Davies S et al (1999) Genetic alterations in “normal” luminal and myoepithelial cells of the breast. J Pathol 189:496–503

4. Tot T (2007) The theory of the sick lobe and the possible consequence. Int J Surg Pathol 15:369–375
5. Kauff ND, Brogi E, Lauren S, Pathak DR, Borgen PI, Hudis CA, Offit K, Robson ME (2003) Epithelial lesions in prophylactic mastectomy specimens from women with BRCA mutations. Cancer 97:1601–1608
6. Going JJ, Moffat DF (2004) Escaping from Flatland: clinical and biological aspects of human mammary duct anatomy in three dimensions. J Pathol 203:538–544
7. Tot T (2005) DCIS, cytokeratins, and the theory of the sick lobe. Virchows Archiv 447:1–8
8. Wellings SR, Jensen HM, Marcum RG (1975) An atlas of subgross pathology of the human breast with special reference to possible precancerous lesions. J Natl Cancer Inst 55:231–273
9. Kordon EC, Smith GH (1998) An entire functional mammary gland may comprise the progeny from a single cell. Development 125:1921–1930
10. Love SM, Barsky SH (1996) Breast-duct endoscopy to study stages of cancerous breast disease. Lancet 348:997–999
11. Murata S, Kominsky SL, Vali M et al (2006) Ductal access for prevention and therapy of mammary tumours. Cancer Res 66:638–645
12. Going JJ, Mohun TJ (2006) Human breast duct anatomy, the "sick lobe" hypothesis and intraductal approaches to breast cancer. Breast Cancer Res Treat 97:285–291
13. Going JJ, Moffat DF (1996) Three dimensional anatomy of complete duct systems in human breast: pathological and development implications. J Clin Pathol 49:48–52
14. Armstrong JS, Davies JD, Hronkova B (1992) Backprocessing paraffin wax blocks for subgross examination. J Clin Pathol 45:1116–1117
15. Landau JD, Visbal AP, Lewis MT (2009) Methods for preparing fluorescent and neutral red stained whole mounts of mouse mammary glands. J Mammary Gland Biol Neoplasia 14:411–415
16. Staudt T, Lang MC, Medda R, Engelhardt J, Hell SW (2007) 2,2′-Thiodiethanol: a new water-soluble mounting medium for high resolution optical microscopy. Microsc Res Tech 70:1–9
17. Appleton PL, Quyn AJ, Swift S, Nathke I (2009) Preparation of wholemount mouse intestine for high-resolution three dimensional imaging using two-photon microscopy. J Microsc 234:196–204
18. Animals (Scientific Procedures) Act 1986, Sch 1.
19. Rasmussen SB, Young LJT, Smith GH (2000) Preparing mammary gland whole mounts from mice. In: Margot MI, Bonnie BA (eds) Methods in mammary gland biology and cancer research. Kluwer Academic, New York, pp 75–85
20. Manton SL, Ferguson DJ, Anderson TJ (1981) An automated technique for the rapid processing breast tissue for subgross examination. J Clin Pathol 34:1189–1191
21. Samoilov VI, Chebyshev AP (1964) Whole mount preparations of rat and mouse mammary glands. Bulletin Exp Biol Med 58:1468–1469
22. Steinke H, Wolff W (2001) A modified Spalteholz technique with preservation of the histology. Ann Anat 183:91–95
23. Wells HG (1897) The invisible man. Pearson, London
24. Smith RM, Matiukas A, Zemlin CW, Pertsov AM (2008) Nondestructive optical determination of fiber organisation in intact myocardial wall. Microsc Res Technique 71:510–516
25. Cassot F, Lauwers F, Lorthois S, Puwanarajah P, Cances-Lauwers V, Duvernoy H (2010) Branching patterns for arterioles and venules of the human cerebral cortex. Brain Res 1313:62–78
26. Dabelow A (1957) Die Milchdrüse. In: Mollendorf WV, Bragmann W (eds) Handbuch der mikroskopischen Anatomie des Menshcen. Springer, Berlin, pp 1–277
27. Zucker RM (2006) Whole insect and mammalian embryo imaging with confocal microscopy: morphology and apotosis. Cytometry A 69:1143–1152
28. Howard MD, Cann M, Henry MS, Verhulst L (1958) The salicylate problem with special reference to methyl salicylate. J Paediatrics 53:271–276
29. Haberman J (1948) Clearing brain tissue with anethole. Biotech Histochem 23:143–144
30. Jain S, Khoury JM, Chamon W, Azar DT (1995) Corneal light scattering after laser in situ keratomileusis and photorefractive keratectomy. Am J Ophthalmol 120:532–534
31. Stockert JC, Llorente AR, Castillo PD, Gomez A (1990) Chromatin fluorescence after carmine staining. Biotech Histochem 65:299–302
32. Megalooikonomou V, Barnathan M, Kontos D, Bakic PR, Maidment ADA (2009) A representation and classification scheme for tree-like structures in medical images: analyzing the branching pattern of ductal trees in X-ray galactograms. IEEE Transactions Med Imaging 28:487–493
33. Clarke GM, Peressotti C, Constantinou P, Hosseinzadeh D, Martel A, Yaffe MJ (2011) Increasing specimen coverage using digital whole-mount breast pathology: implementation, clinical feasibility and application in research. Computerized MedicalImaging and Graphics 35:531–541

Virchows Arch (2012) 460:497–504
DOI 10.1007/s00428-012-1200-8

ORIGINAL ARTICLE

Loss of heterozygosity on chromosome 16q suggests malignancy in core needle biopsy specimens of intraductal papillary breast lesions

Miwa Yoshida · Hitoshi Tsuda · Sohei Yamamoto · Takayuki Kinoshita · Sadako Akashi-Tanaka · Takashi Hojo · Takashi Fukutomi

Received: 10 August 2011 / Revised: 16 December 2011 / Accepted: 23 January 2012 / Published online: 4 April 2012
© Springer-Verlag 2012

Abstract It is often difficult to make a definitive diagnosis of papillary breast lesions using core needle biopsy (CNB) specimens. We studied loss of heterozygosity (LOH) on chromosome 16q in order to assess its diagnostic use for papillary breast lesions in CNB specimens. Of 25 patients with intraductal papillary breast tumors, we extracted DNA from paired samples of tumor cells from CNB specimens and non-tumor cells from subsequent excision specimens and analyzed LOH at the D16S419 and D16S514 loci on chromosome 16q. LOH analysis results were compared with final diagnoses based on pathological features of the resected specimens. On the CNB specimens, 21 tumors were histologically diagnosed as indeterminate or suspicious for malignancy, while four tumors were unambiguously malignant. Of the 21 indeterminate or suspicious tumors, 11 were finally diagnosed as benign and ten as malignant, and on these, LOH analyses were informative for 8 of the 11 benign tumors and 7 of the 10 malignant tumors. LOH was also informative on two of the four tumors unambiguously malignant on CNB. None of the eight informative benign tumors showed LOH on 16q. Six of the eleven informative malignant tumors showed LOH on 16q. LOH on 16q was significantly different between CNB specimens of benign and malignant intraductal papillary tumors (P=0.007). Analysis of LOH on 16q may be helpful in making a definitive diagnosis in cases of papillary breast lesions, in both excised and CNB specimens.

Keywords Loss of heterozygosity · Breast · Papilloma · Papillary carcinoma · Core needle biopsy

M. Yoshida · H. Tsuda (✉)
Division of Diagnostic Pathology,
National Cancer Center Hospital,
5-1-1 Tsukiji, Chuo-ku,
Tokyo 104-0045, Japan
e-mail: hstsuda@ncc.co.jp

M. Yoshida · T. Fukutomi
Division of Breast and Endocrine Surgery,
Aichi Medical University,
21 Nagakute-cho, Aichi-gun,
Aichi 480-1195, Japan

S. Yamamoto
Department of Basic Pathology,
National Defense Medical College,
3-2 Namiki, Tokorozawa,
Saitama 359-8513, Japan

T. Kinoshita · S. Akashi-Tanaka · T. Hojo
Division of Breast Surgery, National Cancer Center Hospital,
5-1-1 Tsukiji, Chuo-ku,
Tokyo 104-0045, Japan

Introduction

Preoperative diagnosis of intraductal papillary tumors of the breast is challenging because of the difficulty of differentiating intraductal papillary carcinoma from intraductal papilloma. It is very difficult to diagnose the biological nature of these tumors based on mammography and ultrasonography, unless there is evidence of massive tumor invasion or rapid growth. Although image-guided core needle biopsy (CNB) is a highly reliable method of diagnosing breast lesions, it is often difficult to differentiate between intraductal papillary lesions based on routine pathological examination of CNB specimens. This difficulty arises because intraductal papillary carcinomas tend to be well differentiated, and CNB specimens do not always include a section with pathognomonic features. Therefore, a final diagnosis

can often be made only by histological examination of the surgically resected specimen.

A number of genetic and chromosomal alterations have been identified in sporadic breast carcinomas, and their clinical implications have been investigated. Loss of heterozygosity (LOH) on chromosomes 16q and 17p are frequent in both invasive carcinoma and ductal carcinoma in situ (DCIS), irrespective of differences in the histological types and grades [1–8]. Several studies have reported a striking difference in the incidence of LOH on 16q between DCIS and intraductal papilloma [1, 5, 7] and have suggested that analysis of LOH on chromosome 16q could be helpful in the differential diagnosis of intraductal papillary tumors. In a previous study, we used Southern blot analysis to examine LOH on 16q in intracystic papillary tumors using DNA isolated from frozen, paired, surgically resected samples of tumor and non-tumor tissues [7]. More recently, we reported a polymerase chain reaction (PCR)-based LOH analysis technique using DNA isolated from paraffin-embedded tumor samples [9, 10]. In the study we report here, we used this PCR-based approach to assess its diagnostic utility on CNB specimens of indeterminate or suspicious intraductal papillary breast lesions.

Materials and methods

Samples

We selected tumor samples of 25 women with a preoperative diagnosis of intraductal papillary breast tumor by image-guided CNB, who had undergone surgical resection between 2005 and 2008, from the pathology computer database at the National Cancer Center Hospital, Japan. Image-guided CNB had been performed under sonographic guidance using either a 14-gauge needle or an 11-gauge vacuum-assisted biopsy probe. Twenty-one tumors had been diagnosed as indeterminate or suspicious for malignancy based on the pathological features of the CNB specimens and the lesions had been surgically resected for definitive histological diagnosis. The remaining four tumors had been unambiguously diagnosed as DCIS. The research protocol was approved by the Ethics Committee of the National Cancer Center Hospital, Japan. All patients gave written informed consent for use of their specimens in the study.

Histological criteria of intraductal papillary tumors

The diagnosis of intraductal papillary tumor was based on the presence of epithelial proliferations supported by fibrovascular stalks, with or without an intervening myoepithelial cell layer [11, 12]. All of the hematoxylin and eosin (H&E)-stained slides of the CNB and resected specimens were retrieved and reviewed for diagnostic consistency by the authors using published criteria.

The Japanese reporting form for cytology and core needle biopsy [13] was used to review the CNB specimens. This reporting form records findings and a judgment of whether the specimen is adequate or inadequate. Adequate specimens are categorized as normal or benign, indeterminate, suspicious for malignancy, or malignant.

Intraductal papillary tumors were diagnosed as benign or malignant using the following histological criteria of cytological and structural features [11, 14]. Papillomas or benign papillary tumors were diagnosed in cases showing an arborescent structure composed of fibrovascular stalks covered by a layer of myoepithelial cells with overlying epithelial cells. Intraductal papillary carcinomas or malignant papillary tumors were usually large papillary lesions (mean 2 cm, range 0.4–10 cm) located within a large cystic duct, with thin fibrovascular stalks devoid of a myoepithelial cell layer and a neoplastic epithelial cell population with characteristics of low-grade DCIS. Cases of "papilloma with atypia" with focal atypical epithelial proliferation and low-grade nuclei [15] were categorized as indeterminate in CNB specimens and as benign in resected specimens. For cases in which it was difficult to distinguish between benign and malignant tumors, the diagnosis was made by assessing the architectural features and visualizing the myoepithelial cell layer with immunohistochemical staining. Final diagnosis was made by pathological examination of the excision specimens.

Microdissection of paraffin-embedded tissues and DNA extraction

For all 25 patients, we extracted DNA from paired samples of intraductal papillary tumor cells from CNB specimens and non-tumor cells (normal mammary glands or lymph nodes) from surgically resected specimens, as previously described [9, 10]. Formalin-fixed and paraffin-embedded tissue sections, 5 to 10 μm thick, were cut using a microtome. Sections mounted on PEN foil slides were deparaffinized in xylene for 5 min (twice) and rehydrated using a descending series of ethanol concentrations as follows: 100% for 30 s (twice), 95% for 30 s (twice), 70% for 10 s, and distilled water for 10 s. The sections were stained with Meyer's hematoxylin, washed with water, and then stained with eosin for 1 min (H&E stain). The slides were dehydrated with 100% ethanol, placed in xylene for 10 min, and air-dried. Specific cells of interest were microdissected and selected using a Leica LMD 6000 system in accordance with the manufacturer's instructions (Leica, Narishige Micromanipulator, Wetzlar, Germany). The microdissected cells were placed in 50 μl proteinase K solution (5 mg/ml proteinase K in 10 mM Tris–HCl, 1 mM EDTA, pH 8.0, 1% Tween 20) and incubated for 36–48 h at 55°C. The

proteinase K was inactivated by incubating the samples at 95°C for 10 min, and then subjected to standard phenol-chloroform extraction and ethanol precipitation in the presence of glycogen. The pellets were resuspended in distilled water and the concentration was adjusted to 0.01 μg/μl. The extracted DNA samples were stored at 4°C until further use.

Selection of polymorphic markers

The chromosomal regions and markers used were D16S419 (16q12.2) and D16S514 (16q21). The following primer sequences were used for PCR amplification:

D16S419	Forward	5′-ATT TTT AAG GAA TGT AAA GNA CAC A-3′
	Reverse	5′-GAC GTT AGA CCA GGA GTC AG-3′
D16S514	Forward	5′-CTA TCC ACT CAC TTT CCA GG-3′
	Reverse	5′-TCC CAC TGA TCA TCT TCT C-3′

We selected polymorphic markers located on chromosome 16q based on the following criteria: (1) the markers were localized to regions with frequent DNA polymorphisms and with frequent LOH events reported in intraductal papillary carcinomas, notably low-grade DCIS [1–5, 7, 16], and (2) the amplified fragments were <250 bp, indicating that they could be successfully amplified using DNA from formalin-fixed tissues. Forward and reverse primer pairs for oligonucleotide polymorphic markers corresponding to the sequences retrieved from the UniSTS database (http://www.ncbi.nlm.nih.gov/unists) were synthesized and purchased from Perkin-Elmer (Applied Biosystems, Foster City, CA, USA). The 5′ ends of the forward primers were labeled with 6-carboxyfluorescein (6-FAM).

PCR

Genomic DNA was PCR amplified in a 25-μl reaction mixture containing 2 μl DNA solution corresponding to 20 ng genomic DNA, 0.4 pmol/μl of each primer, and 1× TaqMan Universal PCR Master Mix (Applied Biosystems) using a GeneAmp® PCR system 9600 (Applied Biosystems). The typical PCR cycling conditions included 2 min incubation at 50°C and 10 min denaturation at 95°C, followed by 40 cycles at 95°C for 15 s and 60°C for 1 min. An

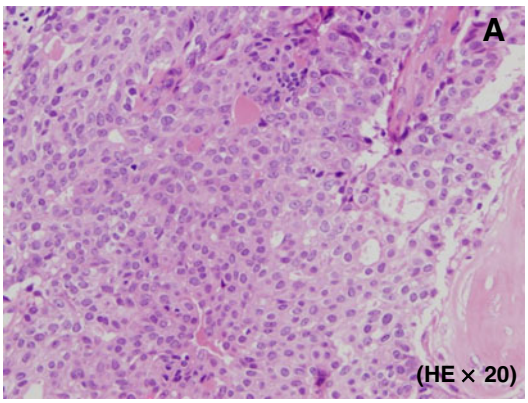

$$\frac{\text{Allele 2 peak height (T)} / \text{Allele 1 peak height (T)}}{\text{Allele 2 peak height (N)} / \text{Allele 1 peak height (N)}} = \frac{\text{Allele 2 peak height (T)} \times \text{Allele 1 peak height (N)}}{\text{Allele 2 peak height (N)} \times \text{Allele 1 peak height (T)}} = \frac{3266 \times 7891}{2749 \times 8266} = 1.13\ (0.6 - 1.4) \rightarrow \text{Negative for 16q LOH}$$

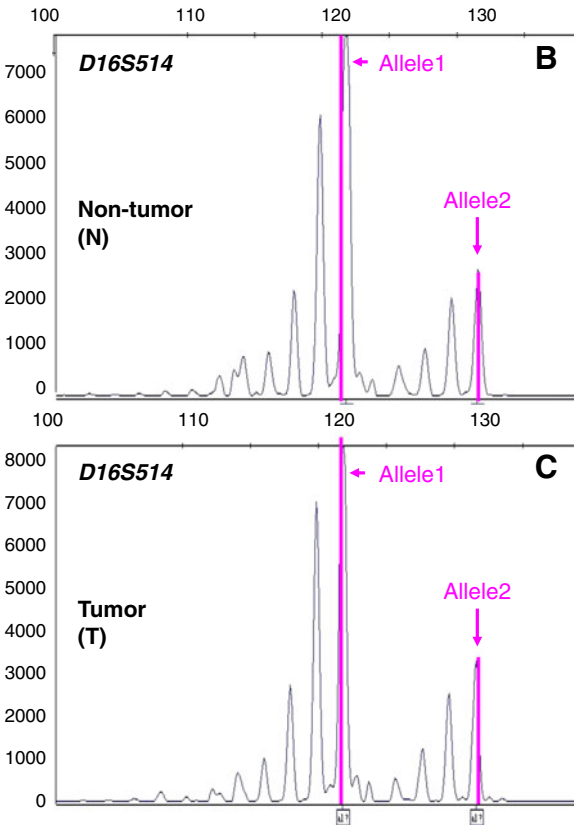

Fig. 1 Analysis of loss of heterozygosity (LOH) in an intraductal papillary tumor (case 4). **a** Based on the pathological features of the excised specimen, the tumor was diagnosed as intraductal papilloma. **b** Electrophoretogram showing constitutional heterozygosity (alleles 1 and 2) at the D16S514 locus in non-tumor DNA. The horizontal axis indicates the size of the DNA fragments (bp), and the vertical axis indicates signal intensity. **c**. Electrophoretogram showing retention of heterozygosity (alleles 1 and 2) at the D16S514 locus in tumor DNA. The axes are the same as in **b**

elongation step at 72°C for 10 min was added to the final cycle. Aliquots of the PCR products were then mixed with size standard and formamide, denatured, and run on an ABI 3130 automated capillary electrophoresis DNA sequencer (Applied Biosystems). The quantity and the quality of the DNA fragments amplified by PCR were confirmed by agarose gel electrophoresis. As a positive control, we used DNA isolated from formalin-fixed, paraffin-embedded tissues of five breast carcinomas in which LOH on 16q had already been detected by Southern blot analysis of fresh frozen tissues [17]. As a negative control, PCR was performed without template DNA.

Assessment of allele loss

The amplified products were assessed for peak height and area using Gene Mapper software (version 3.7; Applied Biosystems). Non-cancerous DNA samples with two different amplified bands were defined as informative cases for LOH analysis. The presence of LOH was determined in accordance with the manufacturer's criteria. LOH was considered to exist if the ratio of the peak heights, which was calculated with the following formula, was <0.6 or >1.4: [peak height of the affected allele (allele A) of the tumor× peak height of the unaffected allele (allele B) of normal cells]/[peak height of allele A of normal cells×peak height of allele B of tumor cells] (Figs. 1 and 2) [17]. If the ratio of the peak height was 0.6 and 1.4 according to the formula, the case was judged to have retention of heterozygosity or absence of LOH.

When the results were questionable, PCR amplification and LOH analysis were performed at least twice to obtain equivalent results. Results were considered non-informative when the normal tissue was constitutionally homozygous and were not evaluated when the tissue lysates were not amplified, that is, PCR was unsuccessful. When either D16S419 or D16S514 showed LOH, the tumor was considered to have LOH. The LOH analysis results were compared with the final diagnoses based on the pathological features of the surgically resected specimens.

Statistical analyses

The χ^2 test was used to determine differences between the benign and malignant groups of intraductal papillary tumors. Differences of $P<0.05$ were considered statistically

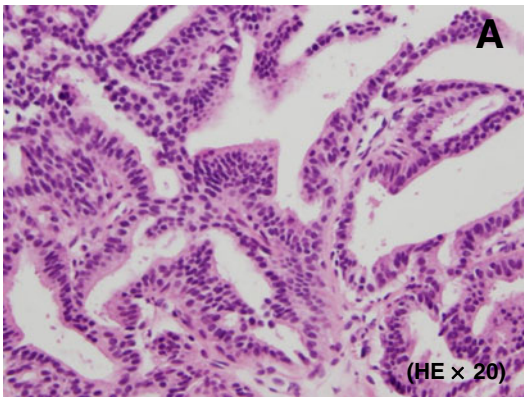

$$\frac{\text{Allele 2 peak height (T)} / \text{Allele 1 peak height (T)}}{\text{Allele 2 peak height (N)} / \text{Allele 1 peak height (N)}}$$

$$= \frac{\text{Allele 2 peak height (T)} \times \text{Allele 1 peak height (N)}}{\text{Allele 2 peak height (N)} \times \text{Allele 1 peak height (T)}}$$

$$= \frac{760 \times 8161}{4052 \times 8530}$$

$$= 0.18\ (< 0.6,\ 1.4 <) \rightarrow \text{Positive for 16q LOH}$$

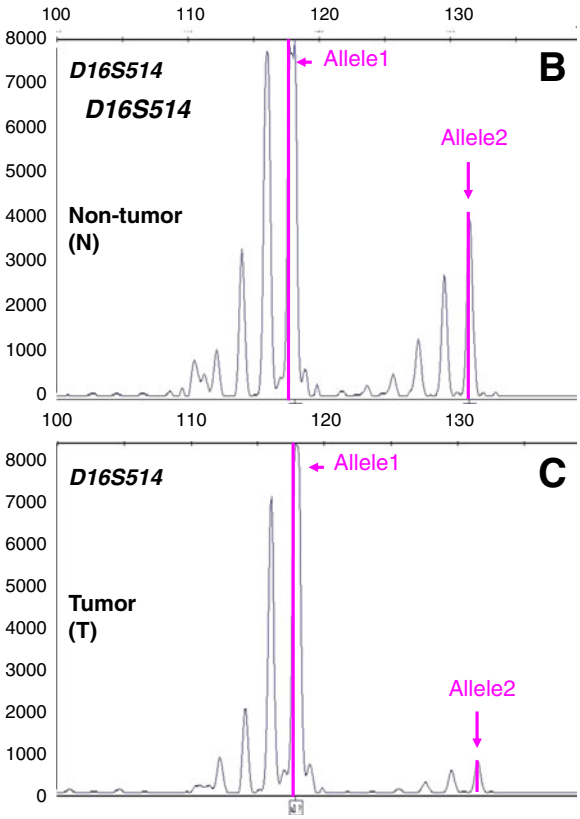

Fig. 2 Analysis of loss of heterozygosity (LOH) in an intraductal papillary carcinoma (case 15). **a** Based on the pathological features of the excised specimen, the tumor was diagnosed as intraductal papillary carcinoma. **b** Electrophoretogram showing constitutional heterozygosity (alleles 1 and 2) at the D16S514 locus in non-tumor DNA. **c** Electrophoretogram showing loss of heterozygosity (loss of allele 2) at the D16S514 locus in tumor DNA

significant. PASW statistics 17 (SPSS, Inc., Chicago, IL, USA) was used for all statistical analyses.

Results

Of the 21 indeterminate or suspicious intraductal papillary tumors, 11 were finally diagnosed as benign and 10 as malignant by microscopic examination of surgically resected specimens (Table 1). The first clinical sign was nipple discharge in 8 (38%) and a palpable mass in 4 (19%) of the 21 cases. Sonographic findings of the papillary lesions included a well-defined solid mass in nine cases (43%), a cystic lesion with solid components in five (24%), and duct dilatation with solid components in seven (33%). Multiple papillary lesions were found in seven cases (33%). The median tumor size on imaging was 1.9 cm (range 0.6–4.0 cm). There were no significant differences in clinical or imaging findings between lesions finally diagnosed as malignant on excisional biopsy specimens and those finally diagnosed as benign (Table 1). Thirteen (62%) of the 21 lesions were biopsied using a 14-gauge needle, and 8 (38%) were biopsied using an 11-gauge vacuum-assisted biopsy probe. The type of percutaneous biopsy was not correlated with postoperative conversion of histopathological diagnosis.

Table 2 shows the final histological diagnoses and 16q LOH results of CNB specimens for each of the 25 intraductal papillary tumors. Eight of the 11 benign tumors were informative, and none of these cases showed LOH on 16q. Nine of the 14 malignant tumors were informative, and these showed frequent LOH on 16q. Out of the total of 25 papillary tumors, seven were considered non-informative (constitutional homozygosity) and one was not evaluated after PCR was unsuccessful. As representative results, case 4 in which 16q LOH was negative is shown in Fig. 1 and case 15 in which 16q LOH was positive is shown in Fig. 2. Case 4 was finally diagnosed as papilloma based on the pathological features of the resected specimen. Figure 1b, c show two peaks of alleles in both the non-tumor and tumor DNA. The ratio of allele 2 peak height to allele 1 peak height in the tumor DNA divided by the ratio in the normal DNA was 1.13.

Table 1 Clinical and imaging findings in papillary breast lesions

	Total (n=21)	Final histological diagnosis		P value
		Benign (n=11)	Malignant (n=10)	
First clinical sign				
Nipple discharge	4 (19%)	1	3	0.14
Palpable mass	8 (38%)	4	4	
None	9 (43%)	6	3	
Sonographic findings				
Well-defined solid mass	9 (43%)	4	5	0.31
Cystic lesion with solid components	4 (19%)	2	2	
Duct dilatation with solid components	8 (38%)	5	3	
Mean tumor size on imaging (cm)	1.9±1.0 (0.6–4.0)	1.8±1.0 (0.6–3.0)	2.1±1.1 (0.6–4.0)	0.49
Number of lesions on imaging				
Multiple	7 (33%)	2	5	0.14
Solitary	14 (67%)	9	5	
Method of percutaneous biopsy				
Core needle biopsy (14-gauge)	13 (62%)	8	5	0.27
Vacuum-assisted biopsy (11-gauge)	8 (38%)	3	5	

Table 2 Final histological diagnoses of surgically resected specimens and 16q loss of heterozygosity (LOH) analysis results in core needle (CNB) specimens of papillary breast lesions

Case no.	Final histological diagnosis	Retained alleles on 16q	
		D16S419	*D16S514*
1	Benign	□	□
2	Benign	□	□
3	Benign	□	NI[a]
4	Benign	□	□
5	Benign	NE[b]	NI
6	Benign	□	□
7	Benign	□	NI
8	Benign	NE	□
9	Benign	NE	NI
10	Benign	□	NI
11	Benign	MSI[c]	NI
12	Malignant	■	■
13	Malignant	NI	NI
14	Malignant	NI	NI
15	Malignant	NI	■
16	Malignant	□	■
17	Malignant	□	□
18	Malignant	NI	MSI
19	Malignant	■	□
20	Malignant	□	□
21	Malignant	NI	□
22	Malignant (positive control)	NE	NE
23	Malignant (positive control)	NI	■
24	Malignant (positive control)	NI	■
25	Malignant (positive control)	NI	NI

Filled square loss of heterozygosity (LOH); *empty square* constitutional heterozygosity

NI[a] : not informative (constitutional homozygosity) NE[b] : not evaluated (PCR was unsuccessful)

MSI[c] : microsatellite instability

Therefore, this tumor was considered negative for LOH on 16q. On the other hand, case 15 (Fig. 2) was histologically diagnosed as low-grade DCIS or intraductal papillary carcinoma in the surgically resected specimen. Figure 2b, c shows a difference in the allele 2 peak heights between the normal and tumor DNA, and the ratio of allele 2 peak height to allele 1 peak height in the tumor DNA divided by the ratio in the normal DNA was 0.18. Therefore, this tumor was considered positive for LOH on 16q.

As shown in Table 3, 6 of the 11 (55%) informative malignant tumors showed LOH on 16q, whereas LOH was not detected in benign tumors. The incidence of 16q LOH in CNB specimens of intraductal papillary tumors was significantly different between benign and malignant tumors (P=0.007). Of three malignant tumors which were negative for LOH on 16q, two were histologically diagnosed as intraductal papillary carcinoma associated with papilloma in the surgically resected specimens.

Discussion

The aim of this study was to evaluate the use of LOH on chromosome 16q to make a final diagnosis in case of an indeterminate or suspicous intraductal papillary tumor in a CNB specimen. We found a statistically significant difference in the incidence of 16q LOH between of benign and malignant intraductal papillary tumors on CNB specimens. The results of the present study suggest that analysis of LOH on 16q may be helpful for making a definitive diagnosis of an indeterminate or suspicious papillary breast lesion in CNB and surgically resected specimens.

In our previous studies, we examined LOH on 16q in intracystic papillary tumors by Southern blot analysis using frozen tissue samples [3, 5] and determined that the incidence of LOH on 16q is strikingly different between cases of DCIS and papilloma [1, 7]. In the present study, we performed PCR-based LOH analysis using DNA isolated from formalin-fixed, paraffin-embedded samples from CNB specimens of intraductal papillary tumors. Although we used a different technique and different type of samples than in previous studies, we show that the incidence of 16q LOH is significantly different between CNB specimens of benign and malignant intraductal papillary tumors.

In the present study, LOH was detected at either16q12.2 or 16q21 in 6 of 11 malignant tumors (55%), whereas LOH was not detected in histologically benign tumors. Similarly, our previous data on intracystic papillary breast tumors showed that 12 of 17 intracystic papillary adenocarcinomas (71%) had LOH on 16q, whereas none of 11 intraductal papillomas had this genetic alteration [1]. Di Cristofano et al. [5] documented LOH at locus 16q23.1–16q24.1 in 7 of 11 malignant samples (63.6%), whereas none of the four informative benign samples appeared to be altered. Taken together, LOH on 16q has high specificity and positive predictive value for the diagnosis of malignancy in intraductal papillary tumors of the breast.

None of the benign papillary lesions we examined in any of our studies, including the eight papillomas in the present study, revealed LOH on 16q. In contrast, Di Cristofano et al. [5] found LOH on 16q in benign papillary lesions, with LOH at locus 16q21.1–16q22.2 detected in both malignant and benign lesions, and at 16q23.3–16q24.1 detected only in malignant lesions. Based on these results, the authors concluded that these differences might be due to the use of the novel molecular marker D16S310 which targets 16q21.1–16q22.2, which putatively contains a tumor suppressor gene involved in the genesis/progression of breast carcinomas.

We propose that the differences between results can be explained by the cellular heterogeneity of the intraductal papillary lesions. Atypical proliferative breast lesions are thought to be precursors of breast carcinomas and have frequently been shown to have LOH on 16q [18, 19].

Table 3 Incidence of loss of heterozygosity (LOH) on 16q in core needle biopsy (CNB) specimens of papillary breast lesions

Final histological diagnosis	Number of cases (%)					
	Chromosome 16q				Total	P-value
	LOH		Constitutional heterozygosity		(Informative)	
Benign	0	(0)	8	(100)	8	0.007
Malignant	4	(57)	3	(43)	7	
Malignant (positive control)	2	(100)	0	(0)	2	

Atypical proliferative lesions and carcinomas are considered to be clones and probably originated from a field within these clones [19]. “Atypical papilloma” or “papilloma with atypia” is defined as papilloma with a proliferation of epithelial cells that have cytological and architectural features consistent with atypical ductal hyperplasia (ADH). Page et al. [15] further refined these terms and used atypical papilloma when the ADH focus involved 3 mm or less of the papillary lesion and the term minor DCIS lesion when the atypical focus involved more than 3 mm of the papillary lesion. These definitions were applied to the surgically resected specimens in the present study. In contrast, Tavassoli [20] suggested using the term atypical papilloma if the area of ADH occupies less than 33% of the papillary lesion, and the term carcinoma arising in a papilloma when the area of ADH occupies 33–90% of the papillary lesion. The ratio of atypical epithelial cells to total epithelial cells may have influenced the LOH analysis results.

Papillary lesions in CNB specimens are diagnosed as benign, atypical (indeterminate), suspicious for malignancy, or definitely malignant based on their pathologic features. Papillary lesions which are histologically diagnosed as definitely malignant must be treated as breast carcinomas. Papillary lesions with atypia, i.e., lesions that are histologically diagnosed as indeterminate or suspicious for malignancy in CNB specimens, need to be resected to determine if there is a more significant lesion [21]. Based on the results of our study, we propose that papillary lesions in CNB specimens that are histologically diagnosed as indeterminate or suspicious for malignancy and show LOH on 16q should also be treated as carcinoma. However, absence of LOH on 16q occurred in both papillomas and papillary carcinomas, and the predictive value of absence of LOH for a benign lesion was only 73%. In lesions in CNB judged as indeterminate or suspicious for malignancy, absence of LOH on 16q therefore has no diagnostic significance.

It is still controversial whether lesions diagnosed as papilloma without atypia by CNB need to be resected. From a pathological review of 19 papillary lesions with postoperative conversion from nonmalignant to malignant, Cheng et al. [22] concluded that the causes of diagnostic conversion were borderline atypical lesions (47%), sampling problems (32%), interpretation errors (16%), and an inadequate sample (5%). Based on the results of the present study, we cannot give clear guidelines for the management of papillomas without atypia based on LOH on 16q, but we consider that analysis of LOH on 16q in CNB specimens with an adequate amount of tumor tissue could reduce interpretation errors and be helpful in determining whether a papilloma without atypia needs to be resected.

The following limitations of the present study are worth discussing. First, results of analysis of LOH on 16q are not sufficiently sensitive for detection of malignancy. Absence of LOH cannot guarantee a benign lesion. Second, the number of cases examined in the present study is small. Third, we did not consider the possibility of intratumor heterogeneity, e.g., cases of carcinoma arising within papilloma. To our knowledge, this is nevertheless the first report which confirms that the incidence of LOH on 16q is significantly different between CNB specimens of benign and malignant intraductal papillary tumors. In conclusion, analysis of LOH on 16q may be helpful in making a definitive diagnosis in cases of papillary breast lesions, in both excised and CNB specimens.

Acknowledgments We thank Ms. Kozue Suzuki (Basic Pathology, National Defense Medical College), Sachiko Miura, M.T. and Chizu Kina, M.T. (Department of Pathology and Clinical Laboratories, National Cancer Center Hospital) for technical assistance. This work was presented at the 7th Biennial Meeting of the Asian Breast Cancer Society held on October 8 to 10, 2009 in Seoul, Korea.

Funding This work was supported in part by a Grant-in-Aid for Cancer Research [5] and in part by a Grant-in-Aid for Scientific Research from the Ministry of Health, Labour and Welfare of Japan.

Conflict of interest The authors declare that they have no conflicts of interest.

References

1. Tsuda H, Uei Y, Fukutomi T, Hirohashi S (1994) Different incidence of loss of heterozygosity on chromosome 16q between intraductal papilloma and intracystic papillary carcinoma of the breast. Jpn J Cancer Res 85(10):992–996
2. Chen T, Sahin A, Aldaz CM (1996) Deletion map of chromosome 16q in ductal carcinoma in situ of the breast: refining a putative tumor suppressor gene region. Cancer Res 56(24):5605–5609
3. Fujii H, Szumel R, Marsh C, Zhou W, Gabrielson E (1996) Genetic progression, histological grade, and allelic loss in ductal carcinoma in situ of the breast. Cancer Res 56(22):5260–5265
4. Vos CB, ter Haar NT, Rosenberg C, Peterse JL, Cleton-Jansen AM, Cornelisse CJ, van de Vijver MJ (1999) Genetic alterations on chromosome 16 and 17 are important features of ductal carcinoma in situ of the breast and are associated with histologic type. Br J Cancer 81(8):1410–1418
5. Di Cristofano C, Mrad K, Zavaglia K, Bertacca G, Aretini P, Cipollini G, Bevilacqua G, Ben Romdhane K, Cavazzana A (2005) Papillary lesions of the breast: a molecular progression? Breast Cancer Res Treat 90(1):71–76
6. Radford DM, Fair KL, Phillips NJ, Ritter JH, Steinbrueck T, Holt MS, Donis-Keller H (1995) Allelotyping of ductal carcinoma in situ of the breast: deletion of loci on 8p, 13q, 16q, 17p and 17q. Cancer Res 55(15):3399–3405
7. Tsuda H, Fukutomi T, Hirohashi S (1995) Pattern of gene alterations in intraductal breast neoplasms associated with histological type and grade. Clin Cancer Res 1(3):261–267
8. Tsuda H, Callen DF, Fukutomi T, Nakamura Y, Hirohashi S (1994) Allele loss on chromosome 16q24.2-qter occurs frequently in breast cancers irrespectively of differences in phenotype and extent of spread. Cancer Res 54(2):513–517

9. Yamamoto S, Tsuda H, Takano M, Hase K, Tamai S, Matsubara O (2008) Clear-cell adenofibroma can be a clonal precursor for clear-cell adenocarcinoma of the ovary: a possible alternative ovarian clear-cell carcinogenic pathway. J Pathol 216(1):103–110
10. Yoshida M, Mouri Y, Yamamoto S, Yorozuya K, Fujii K, Nakano S, Fukutomi T, Hara K, Tsuda H (2010) Intracystic invasive papillary carcinoma of the male breast with analyses of loss of heterozygosity on chromosome 16q. Breast Cancer 17(2):146–150
11. Tavassoli FA, Devilee P (eds) (2003) Pathology and genetics of tumours of the breast and female genital organs. World Health Organization Classification of Tumours. IARC Press, Lyon
12. Rosen PP (2009) Papillary Carcinoma. In: Rosen PP (ed) Rosen's breast pathology, 3rd edn. Lippincott Williams & Wilkins, Philadelphia, pp 423–448
13. Tsuchiya S, Akiyama F, Moriya T, Tsuda H, Umemura S, Katayama Y, Ishihara A, Inai Y, Itoh H, Kitamura T (2009) A new reporting form for breast cytology. Breast Cancer 16(3):202–206
14. Kraus FT, Neubecker RD (1962) The differential diagnosis of papillary tumors of the breast. Cancer 15:444–455
15. Page DL, Salhany KE, Jensen RA, Dupont WD (1996) Subsequent breast carcinoma risk after biopsy with atypia in a breast papilloma. Cancer 78(2):258–266
16. Cleton-Jansen AM, Moerland EW, Kuipers-Dijkshoorn NJ, Callen DF, Sutherland GR, Hansen B, Devilee P, Cornelisse CJ (1994) At least two different regions are involved in allelic imbalance on chromosome arm 16q in breast cancer. Genes Chromosome Cancer 9(2):101–107
17. Niederacher D, Picard F, van Roeyen C, An HX, Bender HG, Beckmann MW (1997) Patterns of allelic loss on chromosome 17 in sporadic breast carcinomas detected by fluorescent-labeled microsatellite analysis. Genes Chromosome Cancer 18(3):181–192
18. Lakhani SR, Collins N, Stratton MR, Sloane JP (1995) Atypical ductal hyperplasia of the breast: clonal proliferation with loss of heterozygosity on chromosomes 16q and 17p. J Clin Pathol 48 (7):611–615
19. Tsuda H, Takarabe T, Akashi-Tanaka S, Fukutomi T, Hirohashi S (2001) Pattern of chromosome 6q loss differs between an atypical proliferative lesion and an intraductal or invasive ductal carcinoma occurring subsequently in the same area of the breast. Mod Pathol 14(5):382–388
20. Tavassoli FA (1999) Papillary lesions. In: Tavassoli FA (ed) Pathology of the breast, 2nd edn. Appleton and Lange, Stamford, pp 325–372
21. Ibarra JA (2006) Papillary lesions of the breast. Breast J 12 (3):237–251
22. Cheng TY, Chen CM, Lee MY, Lin KJ, Hung CF, Yang PS, Yu BL, Yang CE, Tsai TJ, Lin CW (2009) Risk factors associated with conversion from nonmalignant to malignant diagnosis after surgical excision of breast papillary lesions. Ann Surg Oncol 16 (12):3375–3379

Virchows Arch (2012) 460:505–513
DOI 10.1007/s00428-012-1228-9

ORIGINAL ARTICLE

HMGA2 protein expression in ovarian serous carcinoma effusions, primary tumors, and solid metastases

Thea Eline Hetland · Arild Holth · Janne Kærn · Vivi Ann Flørenes · Claes G. Tropé · Ben Davidson

Received: 5 February 2012 / Revised: 5 March 2012 / Accepted: 13 March 2012 / Published online: 4 April 2012
© Springer-Verlag 2012

Abstract The objective of this study was to analyze the expression and clinical role of the high mobility group AT hook (HMGA) protein in advanced-stage serous ovarian carcinoma. HMGA2 protein expression was investigated in 199 effusions and in 50 patient-matched primary tumors and solid metastases using immunohistochemistry. Results were analyzed for association with clinicopathologic parameters, including chemotherapy response, and survival. HMGA2 was expressed in tumor cells in 94.5 %, 96 %, and 90 % of specimens, respectively. There was no difference in HMGA2 expression between patient-matched samples from different anatomic sites ($p>0.3$). HMGA2 expression in chemo-naïve samples was significantly higher in older patients ($p=0.006$, $p=0.01$, and $p=0.005$ for effusions, primary tumors, and solid metastases, respectively). No association was found with residual disease volume. Furthermore, HMGA2 expression was not associated with FIGO stage ($p>0.2$), except in chemo-naïve effusions ($n=106$, $p=0.016$). There was no difference in HMGA2 expression between chemo-naïve samples and samples obtained post-chemotherapy in effusions ($p=0.2$) or primary tumors ($p=0.1$). However, solid metastases obtained after chemotherapy exposure had higher HMGA2 expression compared with chemo-naïve samples ($p=0.032$). HMGA2 expression was unrelated to chemotherapy response or survival. However, it was directly related to protein expression of the previously studied cancer stem cell marker Nestin ($p=0.01$) and the gap junction protein claudin-7 ($p=0.02$) and inversely related to the mRNA level of the E-cadherin repressor *SIP1* ($p=0.02$). This study provides evidence that HMGA2 is universally expressed in advanced-stage ovarian serous carcinoma irrespective of anatomic site, suggesting that HMGA2 may have a clinical role as therapeutic target.

Keywords Ovarian carcinomas · Effusions · Metastasis · HMGA2 · Survival

T. E. Hetland · J. Kærn · C. G. Tropé
Department of Gynecologic Oncology, Oslo University Hospital, Norwegian Radium Hospital,
0424 Oslo, Norway

A. Holth · V. A. Flørenes · B. Davidson
Division of Pathology, Oslo University Hospital, Norwegian Radium Hospital,
0424 Oslo, Norway

C. G. Tropé · B. Davidson
Institute of Clinical Medicine, Faculty of Medicine, University of Oslo,
0424 Oslo, Norway

V. A. Flørenes
Faculty of Health Sciences, Oslo University College,
0130 Oslo, Norway

B. Davidson (✉)
Division of Pathology, Norwegian Radium Hospital, Oslo University Hospital,
Montebello,
0310 Oslo, Norway
e-mail: bend@medisin.uio.no

Introduction

Ovarian cancer is the most lethal gynecologic malignancy and one of the major causes of death from cancer among women in the Western world. Two thirds of the patients are diagnosed with advanced disease, and the majority will recur after primary treatment. The 5-year survival rate is only 29 % for stage IIIc and 13 % for stage IV disease [1]. Standard primary treatment is surgery and carboplatin/

paclitaxel chemotherapy [2], with residual tumor volume after surgery being the most important factor affecting survival [3, 4]. In recurrent disease, patients with progression-free survival (PFS) of >6 months are defined as platinum-sensitive and receive platinum-based therapy [2, 5]. Patients with PFS of ≤6 months are defined as platinum-resistant and will receive non-platinum agents such as weekly paclitaxel, liposomal doxorubicin, gemcitabine, topotecan, or anti-hormonal treatment. Fifteen to twenty percent of patients are platinum-resistant from the beginning, and most patients develop resistance after repeated lines of therapy. So far, no study has shown survival benefit for any chemotherapy agent in resistant disease [6]. Thus, identifying molecular markers that are central to the underlying biology of the disease is important in order to design future treatment that may improve survival and/or circumvent chemoresistance.

HMGA2, a high mobility group AT hook (HMGA) protein, belongs to a family of non-histone nuclear proteins involved in chromatin remodeling and gene transcription. The protein is characterized by three DNA binding domains (AT-hooks) and an acidic carboxy-terminal tail. High levels of expression are observed in almost all tissues during embryogenesis, but, in differentiated adult tissues, it is undetectable or very low. HMGA2 is an important regulator of a variety of biological processes including cell growth, proliferation, differentiation, and death [7]. HMGA2 becomes over-expressed in many cancers, including ovarian cancer [8, 9]. High-grade serous ovarian carcinomas (OC) and carcinosarcomas were reported to have increased HMGA2 expression compared with other types of ovarian cancer [9]. In microarray gene expression analysis of serous and endometrioid OC, high-grade serous tumors with a more mesenchymal phenotype, termed the C5 subtype, had higher HMGA2 expression compared with other subgroups [10]. HMGA2 is regulated by the let-7 microRNA family, and it was recently demonstrated that the C5 OC subtype was associated with the let-7/HMGA2 pathway [11].

Advanced disease (FIGO stage III-IV) is recognized by widespread intraperitoneal metastasis, including malignant serous effusions within the peritoneal cavity. Pleural effusions constitute the most frequent site of distant metastasis (FIGO stage IV disease) [12]. HMGA2 overexpression in solid OC tumors has been previously described in several studies [9, 11, 13–16]. However, to the best of our knowledge, there are at present no reports regarding HMGA2 expression in effusions.

HMGA2 may be involved in the response to chemotherapy. HMGA2-expressing cells are proposed to have increased sensitivity to double-strand DNA breaks caused by chemotherapy, such as platinum, and radiation [8]. Artificial addition of HMGA2 to cancer unresponsive to such damage may cause tumor cells to respond to treatment. On the other hand, as HMGA2 overexpression is a feature of malignant, but not normal cells, silencing of HMGA2 may represent a therapeutic approach, as suggested by an in vitro study of OC cells [17].

Previous studies by our group have demonstrated that several cancer-related molecules are differentially expressed in OC at different anatomic sites, as well as in chemo-naïve samples compared with samples obtained after exposure to chemotherapy [12]. The present study is the first analysis of HMGA2 expression in metastatic fluids from a large group of advanced serous OC patients. We additionally compared HMGA2 expression in effusions and patient-matched primary tumors and solid metastases, as well as in pre- vs. post-chemotherapy specimens. The association with clinicopathologic parameters, including chemotherapy response and survival, was analyzed, as was the association with previously studied markers related to microRNA-processing machinery, the cancer stem cell phenotype, and epithelial-to-mesenchymal transition (EMT).

Materials and methods

Patients and material

Specimens and clinical data were obtained from the Department of Gynecologic Oncology, Norwegian Radium Hospital, Oslo University Hospital. Informed consent was obtained according to national Norwegian and international guidelines. Study approval was given by the Regional Committee for Medical Research Ethics in Norway. Clinicopathologic data are detailed in Table 1. The Johns Hopkins grading system, dividing serous tumors into low- and high-grade tumors, was used [18].

Effusions Fresh non-fixed malignant peritoneal (n=161) and pleural (n=38) effusions were obtained from 199 patients diagnosed with serous carcinoma. Peritoneal and pleural effusions were thus not patient-matched. Of the 199 patients, 159 were diagnosed with OC, 31 with primary peritoneal carcinomas, and nine with tubal carcinoma. Due to their closely linked histogenesis and phenotype, these tumors will all be referred to as serous OC henceforth. We present a highly selected group, including patients with serous OC and FIGO stage IIIc (n=119) or IV (n=80) disease. One hundred and eleven patients had primary surgery; 70 received neoadjuvant chemotherapy with interval debulking surgery, and 18 patients only received chemotherapy. One hundred and six samples were obtained prior to chemotherapy administration, and 93 were obtained after chemotherapy treatment, at interval debulking surgery (n=22), or at recurrent disease (n=71). The majority of

Table 1 Clinicopathologic parameters of the study cohort

Parameter		Number of patients[a]
Age		23–88 years (mean=62)
Histological grade	Low	10 (1)
	High	164 (46)
	NA[b]	25 (3)
FIGO stage	IIIc	119 (29)
	IV[c]	80 (21)
Residual disease	0 cm	24 (6)
	0–1 cm	63 (18)
	>1 cm	93 (26)
	NA[d]	19
Chemoresponse at diagnosis	Complete response	101 (29)
	Partial response	43 (9)
	Stable disease	16 (2)
	Progressive disease	27 (3)
	NE[e]	12 (7)

[a] Parentheses: numbers of patients among the 50 patients with matching biopsies

[b] *NA*=non available, including effusions from inoperable patients where biopsy was too small for grading (n=12) and patients operated on in other hospitals, for which the primary tumor could not be accessed for assessment of grade (n=13)

[c] In FIGO stage IV disease, 63 (17) patients were classified due to pleural metastases and 16 (four) patients had distant metastases in other locations. One patient had stage IV disease with unspecified metastasis site

[d] Eighteen patients only received chemotherapy treatment, and one patient had missing information

[e] *NE*=not evaluable disease response after chemotherapy treatment because of normalized CA-125 after primary surgery (n=7) or missing CA-125 information (n=5)

patients (n=195) received platinum-based therapy, and 156 patients received platinum/paclitaxel combination treatment. Effusions were submitted for routine diagnostic purposes during 1998–2006 and were processed immediately after tapping. Cell blocks were prepared from all effusions using the thrombin clot method. Remaining material, when available, was fresh-frozen. Diagnoses were established using morphology and immunohistochemistry [19].

Surgical specimens Patient-matched specimens from the primary ovarian tumor and a solid metastatic site (44 from the omentum, four peritoneal, two intestinal) were available for 50 of the 199 patients. Twenty-nine samples were chemo-naïve, and 21 samples were obtained after chemotherapy treatment. Forty-eight of these patients received platinum-based therapy, and 45 patients received platinum/paclitaxel combination treatment. The omental biopsy was chosen when patients had metastatic biopsies from more than one site. Hematoxylin-and-eosin-stained sections from these tumors were reviewed by a gynecopathologist (BD) in order to establish tumor type and histological grade.

Immunohistochemistry

Formalin-fixed paraffin-embedded sections were analyzed for protein expression of HMGA2 using the FLEX+system (Dako A/S, Glostrup, Denmark). All slides were deparaffinized and rehydrated prior to pretreatment to unmask epitopes and subsequently treated with 0.03 % H_2O_2 for 5 min to block endogenous peroxidase. The sections were incubated with HMGA2 mAb (GenWay Biotech. Inc, San Diego, CA) diluted 1:500 for 30 min at room temperature and then incubated with a secondary antibody for an additional 30 min. Visualization was achieved using 3′3-diaminobenzidine tetrahydrochloride substrate and hematoxylin counterstaining. Positive controls consisted of a serous OC that was shown to express the protein in a pilot study. Negative controls consisted of sections that underwent similar staining procedures with a nonrelevant rabbit IgG1 (Sigma-Aldrich, St Louis, MO).

Staining was considered positive when localized to the nucleus. Staining extent was scored on a scale of 0–4, as follows—0=no staining, 1=1–5 %, 2=6–25 %, 3=26–75 %, 4=76–100 % stained tumor cells. All specimens contained at least 100 tumor cells.

Scoring was performed by two observers (BD and TEH), both blinded to clinical data. The inter- and intra-observer concordance was >90 %. Discrepant cases were generally of one scoring level and easily settled in consensus meetings.

Statistical analysis

Statistical analysis was performed applying the SPSS-PC package (version 18.0, Chicago, IL). Probability of <0.05 was considered statistically significant. Analysis of the association between HMGA2 expression and anatomic site was executed using the Wilcoxon signed rank test. Analyses of the association between HMGA2 expression and clinicopathologic parameters were undertaken using the Mann–Whitney U test. Clinicopathologic parameters were grouped as follows: age, ≤60 vs. >60 years; effusion site, peritoneal vs. pleural; FIGO stage, IIIc vs. IV; chemotherapy status, pre- vs. post-chemotherapy specimens; residual disease volume (≤1 vs. >1 cm); response to chemotherapy, complete vs. partial response/stable disease/progression. The association with histological grade was not studied in view of the small number of patients (n=10) with low-grade tumors. PFS and overall survival (OS) were calculated from the date of the last chemotherapy treatment/diagnosis to the date of recurrence/death or last follow-up (08/11/2011), respectively. Univariate survival analyses of PFS and OS were executed using the Kaplan–Meier method and log-rank test. Platinum

resistance was defined as PFS≤6 months according to guidelines published by the Gynecologic Oncology Group [20], and progressive disease or recurrence was evaluated by the RECIST criteria [21]. Expression categories in survival analyses were clustered as high vs. low based on immunohistochemistry (IHC) score of 0–2 vs. 3–4.

Results

HMGA2 is equally expressed in primary serous OC, their solid metastases and metastatic effusions

IHC analysis of 199 metastatic effusions with 50 patient-matched primary tumors and solid metastases demonstrated HMGA2 expression in the tumor cells in 94.5 %, 96 %, and 90 % of specimens, respectively (Fig. 1). Staining extent is detailed in Table 2. HMGA2 expression was equally expressed in patient-matched samples from the different sites (effusions vs. primary samples, $p=0.4$; effusions vs. metastatic samples, $p=0.3$; primary tumors vs. metastatic samples, $p=0.7$). HMGA2 expression did not differ between serous OC cells in peritoneal and pleural effusions ($p=0.5$), or between different metastatic sample sites ($p=0.8$). No association between HMGA2 expression and primary diagnosis was seen (effusion, $p=0.8$; primary tumor samples, $p=0.1$; solid metastases, $p=0.1$).

HMGA2 expression is significantly associated with age

HMGA2 expression in the entire effusion series ($n=199$) was significantly higher in patients >60 years old ($p=0.002$). However, in sub-analyses, this finding retained its significance only for the patients with chemo-naïve specimens ($n=106$, $p=0.006$; Table 3) and those with specimens obtained after neoadjuvant chemotherapy ($n=22$, $p=0.046$),

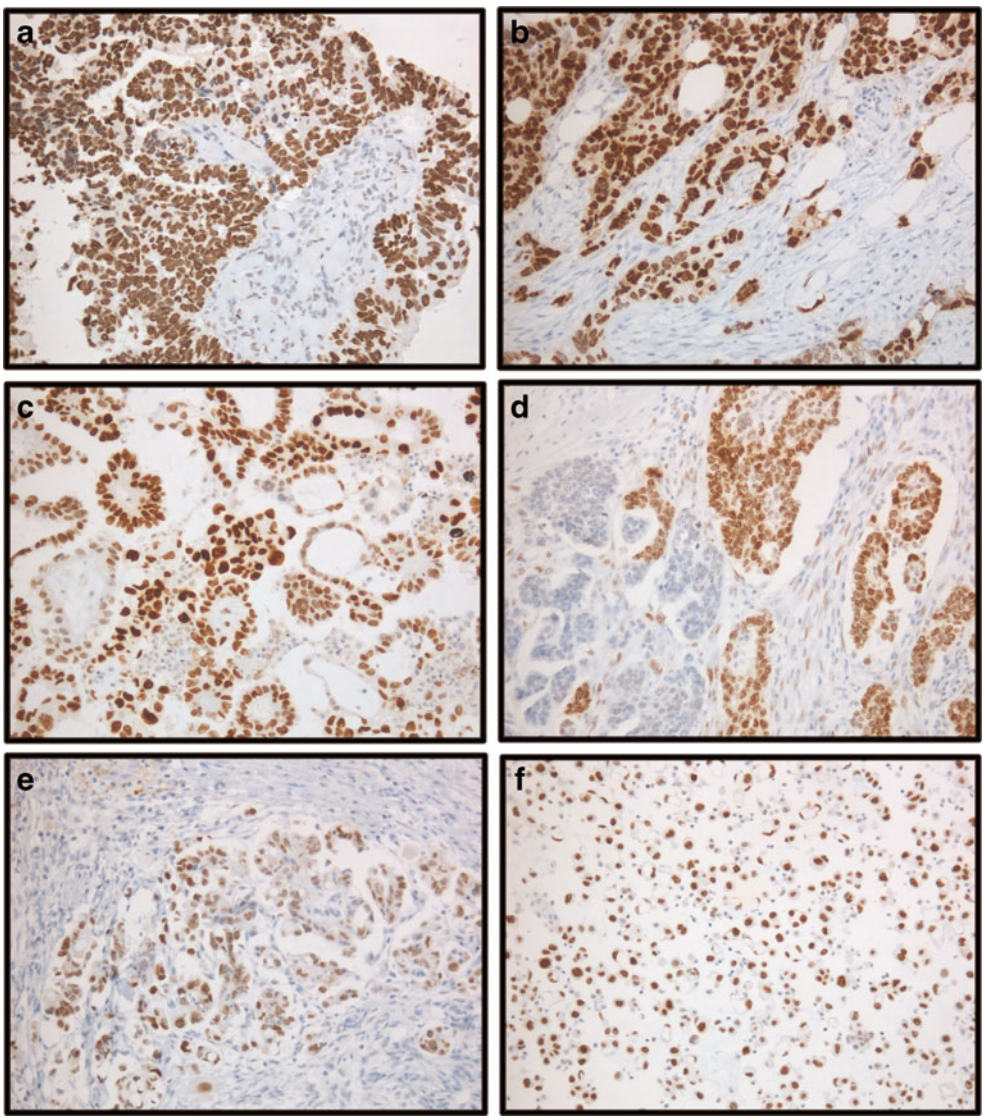

Fig. 1 Examples of HMGA2 immunostaining in primary and metastatic serous ovarian carcinoma. **a**–**c** Patient-matched specimens consisting of the ovary (**a**), omentum (**b**), and effusion (**c**), all with nuclear staining in the majority of carcinoma cells; (**d**–**f**) Additional examples of HMGA2 expression in the primary ovarian carcinoma (**d**), colon metastasis (**e**), and effusion (**f**)

Table 2 HMGA2 protein expression

Sample site	Staining extent (percentage of positive cells)					Total
	0 %	1–5 %	6–25 %	26–75 %	76–100 %	
Effusions	11 (5.5)	29 (14.6)	21 (10.6)	47 (23.6)	91 (45.7)	199 (100)
Primary tumors	2 (4)	8 (16)	7 (14)	15 (30)	18 (36)	50 (100)
Solid metastases	5 (10)	5 (10)	7 (14)	15 (30)	18 (36)	50 (100)

whereas no association was found between age and HMGA2 expression in samples obtained in recurrent disease (n=71, p=0.4). In primary biopsies (n=50), HMGA2 expression was also associated with older age in chemo-naïve samples (n=29, p=0.010; Table 3) but not in samples obtained after chemotherapy exposure (n=21, p=0.7). A similar association was found for metastatic samples (chemo-naïve, n=29, p=0.005; [Table 3]; after chemotherapy exposure, n=21, p=0.8).

No association was found between HMGA2 expression and residual disease volume (effusions, p=0.5; primary tumors, p=0.6; solid metastases, p=0.3). Chemotherapy exposure did not alter the results. Furthermore, HMGA2 expression was not associated with FIGO stage (p>0.2), except in sub-analysis of chemo-naïve effusions, in which specimens from FIGO stage IV patients had significantly higher HMGA2 expression (n=106, p=0.016). Though not analyzed statistically, low-grade serous OC specimens had staining extent that was comparable to high-grade serous OC, with 10/10 effusions staining for HMGA2, of which 7/10 had score=4 staining.

HMGA2, chemotherapy exposure, and response

There was no difference in HMGA2 expression between chemo-naïve samples and samples obtained after chemotherapy in primary samples (p=0.1) or metastatic effusions (p=0.2). However, solid metastatic samples obtained after chemotherapy exposure had higher HMGA2 expression compared with chemo-naïve samples (p=0.032).

Table 3 The association between HMGA2 expression and age in chemo-naïve samples

Sample site	Age	Staining extent (% cells)		P value (Mann–Whitney U test)
		≤25 %	>25 %	
Effusions (n=106)	≤60 years	16	28	0.006
	>60 years	15	47	
Primary tumors (n=29)	≤60 years	9	4	0.010
	>60 years	3	13	
Solid metastases (n=29)	≤60 years	9	4	0.005
	>60 years	5	11	

HMGA2 expression was not associated with platinum resistance or response to primary treatment (p>0.1). Analyses of HMGA2 expression with respect to chemotherapy exposure or exposure to different chemotherapy regimes, e.g., patients receiving platinum with or without paclitaxel combination, did not alter the results (data not shown).

HMGA2 and survival

Median PFS was 7 months (range, 0–103 months) and median OS was 28 months (range, 1–110 months) for all patients. At last follow up, 186 patients were dead of disease; eight patients were alive with disease, and four patients were disease-free. One patient died of treatment complications. No association was seen between HMGA2 expression and PFS or OS in effusions (p=0.5 and p=0.9, respectively), primary tumors (p=0.7 and p=0.5, respectively) or metastatic samples (p=0.1 and p=0.5, respectively). The results were not altered by sub-analyses with respect to chemotherapy exposure (data not shown).

Analysis of the association between HMGA2 expression, markers of EMT, the microRNA-processing machinery, and cancer stem cell (CSC) markers

HMGA2 is regulated by the let-7 microRNA family and is a postulated marker of EMT and CSC. We therefore studied the potential association between its presence and expression of several markers related to these processes that have been previously studied in our effusion material, including E-cadherin and its transcriptional repressors Snail, Slug, and Sip1 [22, 23], matrix metalloproteinase-2 (MMP-2) [22], claudin-1, 3-, 4-, and −7 [24], and Pak1 [25], all related to EMT; the miRNA-processing machinery proteins Ago1 and Dicer [26]; and the CSC-related molecules Notch3 [27] and Nestin [28]. A minimum of 30 specimens was required for each comparative analysis. HMGA2 expression was directly related to Nestin (p=0.01) and claudin-7 (p=0.02) protein expression and inversely related to *SIP1* mRNA level (p=0.02), the other analyses yielding no significant findings (Table 4).

Table 4 The association between HMGA2 protein expression, markers of epithelial–mesenchymal transition (EMT), and cancer stem cells (CSC) and the microRNA-processing machinery

References	Molecule	Expression level	Method	No.	*P* value (Mann–Whitney *U* test)
22	E-cadherin	mRNA	RT-PCR[a]	32	0.77
22	Snail	mRNA	RT-PCR	32	0.11
22	Slug	mRNA	RT-PCR	32	0.40
22	SIP1	mRNA	RT-PCR	32	0.02[b]
22	MMP-2	mRNA	RT-PCR	32	0.08
23	Snail	Protein	Western blotting	31	0.12
24	Claudin-1	Protein	IHC	101	0.25
24	Claudin-3	Protein	IHC	101	0.07
24	Claudin-4	Protein	IHC	101	0.09
24	Claudin-7	Protein	IHC	101	0.02[b]
25	Pak1	Protein	IHC	94	0.71
26	Ago1	Protein	IHC	37	0.18
26	Dicer	Protein	IHC	37	0.15
27	Notch3	mRNA	qPCR	41	0.65
28	Nestin	Protein	IHC	167	0.01

IHC immunohistochemistry, *qPCR* quantitative PCR

[a]Semi-quantitative

[b]Direct association to nestin and claudin-7, inverse to SIP1

Discussion

The aim of this study was to analyze HMGA2 expression in serous OC effusions, of which a subset had patient-matched primary ovarian tumors and solid metastases. We additionally evaluated the association between HMGA2 expression and prognostic/predictive factors, including chemotherapy resistance and clinical outcome, while considering whether or not the patients had received chemotherapy at the time of specimen sampling.

The present study is the first to demonstrate HMGA2 expression in metastatic serous OC cells in effusions and compare it to other disease sites. HMGA2 expression was comparable in effusion specimens, primary tumors, and solid metastases, with 90–96 % of tumors being positive and 66–69 % showing ≥25 % expression in tumor cells at the three anatomic sites. This may suggest that HMGA2 expression is a universal marker for serous OC tumor cells, with consistent expression throughout disease progression. This is in contrast to previous studies by our group, in which several cancer-related molecules were differentially expressed at different anatomic sites, as well as in chemo-naïve samples compared with samples obtained after exposure to chemotherapy [12].

In agreement with our findings, Shell and colleagues [14] found no significant difference in HMGA2 expression between primary tumors and patient-matched omental or peritoneal metastases. They demonstrated that HMGA2 overexpression was upregulated early on transformation of ovarian epithelial cells by examining different stages of OC. These data indicate that HMGA2 expression is a marker for early tumor progression, and not metastasis, as supported by others [13]. Furthermore, IHC analysis of precursor lesions in 24 serous intraepithelial tubal carcinomas found HMGA2 overexpression in 75 % of the cases, suggesting that HMGA2 might be a valuable marker in the detection of early stage disease [16].

In the present study, there was variable expression between samples, although there was no statistical difference between the anatomic sites. OC carcinoma subtypes (serous, clear cell, endometrioid, and mucinous) are recognized as different diseases with variable expression of biomarkers [29], and we therefore included only patients with serous histology in our cohort. However, the presence of additional subtypes within the serous type [10, 11] may explain the inter-sample variation.

It is suggested that metastatic disease may be caused by spread of a small population of cells with stem cell characteristics, referred to as CSC. Protein expression of HMGA2 and the CSC marker nestin were directly associated in effusions of the 167 patients included both in the present and a previous study [28]. These findings may suggest that cells expressing HMGA2 are a less differentiated tumor type with stem cell-like characteristics, as suggested by others [11, 30]. Other postulated stem cell markers, including CD44 [31] and Oct3/4 (unpublished results) are similarly widely expressed in serous OC cells in effusions. However, the number of patients matching the present cohort was too small for analyses of their association with HMGA2.

Patients of age >60 years in our cohort had higher HMGA2 expression than younger patients. In contrast, it has been postulated that stem cell self-renewal capacity declines with age, caused by age-associated loss of HMGA2, possibly by induction of let-7b [32]. However, the findings in our study were only significant for chemo-naïve samples, and when both HMGA2 expression and age were dichotomized, the

association was only significant for solid samples (data not shown). The biological explanation and clinical relevance of HMGA2 expression in association with age is yet to be understood.

In recent years, extensive research has been directed at studying the phenomenon termed EMT, during which carcinoma cells lose their epithelial characteristics and gain mesenchymal ones, with increased motility and invasive capacity, resulting in aggressive clinical behavior [33, 34]. However, previous studies by our group suggest that OC effusions do not follow the classical model of EMT, as they have higher E-cadherin expression and lower levels of its transcriptional repressors, such as Snail and Slug, compared with primary tumors [23, 35]. Analyzing patients that were included both in the present and the previous studies indicated that HMGA2 protein expression and mRNA expression of the E-cadherin repressor SIP1 in effusions are inversely related, whereas a trend for direct association was observed between HMGA2 and Snail. Others have proposed Snail to be the master effector downstream of HMGA2 for induction of EMT through E-cadherin repression [36] and several studies have shown an inverse relationship between HMGA2 and E-cadherin [8, 10, 14]. Although no association was found between HMGA2 protein expression and E-cadherin mRNA levels in our series, this may be related to the small number of cases in this analysis. We are currently expanding this series, with focus on E-cadherin and N-cadherin protein expression, in order to better define the relationship between HMGA2 and EMT markers in serous OC effusions.

In our series, all analyses were executed with respect to chemotherapy exposure. HMGA2 expression was demonstrated in the majority of both pre- and post-chemotherapy serous OC samples, suggesting that HMGA2 expression in effusions may not be considerably altered by chemotherapy. On the other hand, solid metastatic samples had higher HMGA2 expression after exposure to chemotherapy compared with chemo-naïve samples, and the association with age was only seen for chemo-naïve samples. This may indicate that serous OC cells at different anatomic sites react differently to chemotherapy and that chemotherapy somehow alters HMGA2 expression. Previous studies have been inconclusive. HMGA2 has been linked to enhanced sensitivity to DNA damaging agents, such as platinum and radiation [7]. In contrast, the in vitro study by Wu et al. [15] indicates an increase in chemoresistance in the presence of HMGA2, and Let-7 is suggested to sensitize cancer cells to platinum and induce resistance to paclitaxel [37]. The role of HMGA2 in chemotherapy resistance therefore remains unclear.

By including only FIGO stage IIIc-IV disease and serous histology, we present a highly selected cohort of patients with similar prognosis, and our results indicate that HMGA2 is not a predictor of clinical outcome. This is in contrast to observations for several other cancer types [8]. Furthermore, Shell et al. [14] observed that high HMGA2 expression was significantly associated with poor PFS in IHC analysis of 100 ovarian cancer patients. However, the authors included both FIGO stage II-IV patients and several histological subtypes, and both parameters were predictors of survival in univariate analysis. In our series, FIGO stage was a predictor of survival in univariate analyses for all patients with effusions ($p=0.008$) but not in the 50 patients with solid samples ($p=0.2$), probably due to the fact that most patients who were diagnosed with stage IV disease had isolated pleural effusion without solid distant metastases. The clinical outcome of these patients is comparable to that of patients diagnosed at FIGO stage IIIc. There was no difference in HMGA2 expression between FIGO stage IIIc and IV disease, except in sub-analysis of chemo-naïve effusions, where patients with FIGO stage IV had higher HMGA2 expression than FIGO stage IIIc. However, no difference in HMGA2 expression between samples from pleural effusions (from stage IV patients) and ascites ($p=0.7$) was observed.

In summary, this study provides evidence that HMGA2 is universally expressed along tumor progression in advanced-stage serous OC. Identification of molecular markers that are associated with the clinical behavior of serous OC is likely to impact the treatment of this disease in the future and hopefully contribute to increased survival. The recognition of HMGA2 protein in ascites and pleural fluids may have clinical relevance, as these samples are easily obtained for analysis, when surgery is not indicated. Additional research is necessary in order to evaluate whether HMGA2 may differentiate serous OC from other cancers affecting the serosal cavities and thus have a diagnostic role as well. Targeting HMGA2 may present a promising approach to eradicate systemic cancer, as recently discussed [17], as the differential expression of HMGA2 in neoplastic cells and in normal cells should allow for high specificity and low toxicity.

Financial acknowledgment This work was supported by the Inger and John Fredriksen Foundation for Ovarian Cancer Research, the Norwegian Cancer Society, and the Research Foundation at the Norwegian Radium Hospital. Thea Eline Hetland is the recipient of a PhD scholarship from the Health Region South-Eastern Norway.

Conflict of interest statement We declare that we have no conflict of interest.

References

1. Heintz AP, Odicino F, Maisonneuve P, Beller U, Benedet JL, Creasman WT, Ngan HY, Pecorelli S (2003) Carcinoma of the ovary. Int J Gynaecol Obstet 83(Suppl 1):135–166

2. Cannistra SA (2004) Cancer of the ovary. N Engl J Med 351:2519–2529
3. Bristow RE, Tomacruz RS, Armstrong DK, Trimble EL, Montz FJ (2002) Survival effect of maximal cytoreductive surgery for advanced ovarian carcinoma during the platinum era: a meta-analysis. J Clin Oncol 20:1248–1259
4. Vergote I, Trope CG, Amant F, Kristensen GB, Ehlen T, Johnson N, Verheijen RH, van der Burg ME, Lacave AJ, Panici PB, Kenter GG, Casado A, Mendiola C, Coens C, Verleye L, Stuart GC, Pecorelli S, Reed NS, European Organization for Research and Treatment of Cancer-Gynaecological Cancer Group; NCIC Clinical Trials Group (2010) Neoadjuvant chemotherapy or primary surgery in stage IIIC or IV ovarian cancer. N Engl J Med 363:943–953
5. Pujade-Lauraine E, Mahner S, Kaern J, Gebski V, Heywood M, Vasey P, Reinthaller A, Vergote I, Pignata S, Ferrero A (2009) A randomized, phase III study of carboplatin and pegylated liposomal doxorubicin versus carboplatin and paclitaxel in relapsed platinum-sensitive ovarian cancer (OC): CALYPSO study of the Gynecologic Cancer Intergroup (GCIG) J Clin Oncol 27:18 s (suppl; abstr LBA5509).
6. Harter P, Hilpert F, Mahner S, Heitz F, Pfisterer J, du Bois A (2010) Systemic therapy in recurrent ovarian cancer: current treatment options and new drugs. Expert Rev Anticancer Ther 10:81–88
7. Cleynen I, Van De Ven WJ (2008) The HMGA proteins: a myriad of functions (review). Int J Oncol 32:289–305
8. Fedele M, Fusco A (2010) HMGA and cancer. Biochim Biophys Acta 1799:48–54
9. Mahajan A, Liu Z, Gellert L, Zou X, Yang G, Lee P, Yang X, Wei JJ (2010) HMGA2: a biomarker significantly overexpressed in high-grade ovarian serous carcinoma. Mod Pathol 23:673–681
10. Tothill RW, Tinker AV, George J, Brown R, Fox SB, Lade S, Johnson DS, Trivett MK, Etemadmoghadam D, Locandro B, Traficante N, Fereday S, Hung JA, Chiew YE, Haviv I, Australian Ovarian Cancer Study Group, Gertig D, DeFazio A, Bowtell DD (2008) Novel molecular subtypes of serous and endometrioid ovarian cancer linked to clinical outcome. Clin Cancer Res 14(5198)
11. Helland Å, Anglesio MS, George J, Cowin PA, Johnstone CN, House CM, Sheppard KE, Etemadmoghadam D, Melnyk N, Rustgi AK, Phillips WA, Johnsen H, Holm R, Kristensen GB, Birrer MJ, Group Australian Ovarian Cancer Study, Pearson RB, Børresen-Dale AL, Huntsman DG, deFazio A, Creighton CJ, Smyth GK, Bowtell DD (2011) Deregulation of MYCN, LIN28B and LET7 in a molecular subtype of aggressive high-grade serous ovarian cancers. PLoS One 6:e18064
12. Davidson B (2007) Biological characteristics of cancers involving the serosal cavities. Crit Rev Oncog 13:189–227
13. Park SM, Shell S, Radjabi AR, Schickel R, Feig C, Boyerinas B, Dinulescu DM, Lengyel E, Peter ME (2007) Let-7 prevents early cancer progression by suppressing expression of the embryonic gene HMGA2. Cell Cycle 6:2585–2590
14. Shell S, Park SM, Radjabi AR, Schickel R, Kistner EO, Jewell DA, Feig C, Lengyel E, Peter ME (2007) Let-7 expression defines two differentiation stages of cancer. Proc Natl Acad Sci U S A 104:11400–11405
15. Wu J, Liu Z, Shao C, Gong Y, Hernando E, Lee P, Narita M, Muller W, Liu J, Wei JJ (2011) HMGA2 overexpression-induced ovarian surface epithelial transformation is mediated though regulation of EMT genes. Cancer Res 71:349–359
16. Wei JJ, Wu J, Luan C, Yeldandi A, Lee P, Keh P, Liu J (2010) HMGA2: a potential biomarker complement to P53 for detection of early-stage high-grade papillary serous carcinoma in fallopian tubes. Am J Surg Pathol 34:18–26
17. Malek A, Bakhidze E, Noske A, Sers C, Aigner A, Schäfer R, Tchernitsa O (2008) HMGA2 gene is a promising target for ovarian cancer silencing therapy. Int J Cancer 123:348–356
18. Vang R, Shih IeM, Kurman RJ (2009) Ovarian low-grade and high-grade serous carcinoma: pathogenesis, clinicopathologic and molecular biologic features, and diagnostic problems. Adv Anat Pathol 16:267–282
19. Davidson B, Nielsen S, Christensen J, Asschenfeldt P, Berner A, Risberg B, Johansen P (2001) The role of desmin and N-cadherin in effusion cytology: a comparative study using established markers of mesothelial and epithelial cells. Am J Surg Pathol 25:1405–1412
20. Thigpen JT, Blessing JA, Ball H, Hummel SJ, Barrett RJ (1994) Phase II trial of paclitaxel in patients with progressive ovarian carcinoma after platinum-based chemotherapy: a Gynecologic Oncology Group study. J Clin Oncol 12:1748–1753
21. Therasse P, Arbuck SG, Eisenhauer EA, Wanders J, Kaplan RS, Rubinstein L, Verweij J, Van Glabbeke M, van Oosterom AT, Christian MC, Gwyther SG (2000) New guidelines to evaluate the response to treatment in solid tumors. European Organization for Research and Treatment of Cancer, National Cancer Institute of the United States, National Cancer Institute of Canada. J Natl Cancer Inst 92:205–216
22. Elloul S, Elstrand MB, Nesland JM, Tropé CG, Kvalheim G, Goldberg I, Reich R, Davidson B (2005) Snail, Slug, and Smad-interacting protein 1 as novel parameters of disease aggressiveness in metastatic ovarian and breast carcinoma. Cancer 103:1631–1643
23. Elloul S, Silins I, Tropé CG, Benshushan A, Davidson B, Reich R (2006) Expression of E-cadherin transcriptional regulators in ovarian carcinoma. Virchows Arch 449:520–528
24. Kleinberg L, Holth A, Trope' CG, Reich R, Davidson B (2008) Claudin upregulation in ovarian carcinoma effusions is associated with poor survival. Hum Pathol 39:747–757
25. Davidson B, Shih IM, Wang TL (2008) Different clinical roles for p21-activated kinase-1 in primary and recurrent ovarian carcinoma. Hum Pathol 39:1630–1636
26. Vaksman O, Tuft Stavnes H, Kærn J, Trope' CG, Davidson B, Reich R (2011) miRNA profiling along tumor progression in ovarian carcinoma. J Cell Mol Med 15:1593–1602
27. Park JT, Chen X, Tropè CG, Davidson B, IeM S, Wang TL (2010) Notch3 overexpression is related to the recurrence of ovarian cancer and confers resistance to carboplatin. Am J Pathol 177:1087–1094
28. Hetland TE, Hellesylt E, Flørenes AV, Tropé C, Davidson B, Kærn J (2011) Class III β-tubulin expression in advanced state serous ovarian carcinoma effusions is associated with poor survival and primary chemoresistance. Hum Pathol 42:1019–1026
29. Köbel M, Kalloger SE, Boyd N, McKinney S, Mehl E, Palmer C, Leung S, Bowen NJ, Ionescu DN, Rajput A, Prentice LM, Miller D, Santos J, Swenerton K, Gilks CB, Huntsman D (2008) Ovarian carcinoma subtypes are different diseases: implications for biomarker studies. PLoS Med 5:e232
30. Yu F, Yao H, Zhu P, Zhang X, Pan Q, Gong C, Huang Y, Hu X, Su F, Lieberman J, Song E (2007) Let-7 regulates self renewal and tumorigenicity of breast cancer cells. Cell 131:1109–1123
31. Berner HS, Davidson B, Berner A, Risberg B, Kristensen GB, Trope CG, Van de Putte G, Nesland JM (2000) Expression of CD44 in effusions of patients diagnosed with serous ovarian carcinoma - diagnostic and prognostic implications. Clin Exp Metastasis 18:197–202
32. Tzatsos A, Bardeesy N (2008) Ink4a/Arf regulation by let-7b and Hmga2: a genetic pathway governing stem cell aging. Cell Stem Cell 3:469–470
33. Thiery JP, Acloque H, Huang RY, Nieto MA (2009) Epithelial–mesenchymal transitions in development and disease. Cell 139:871–890
34. Kalluri R, Weinberg RA (2009) The basics of epithelial–mesenchymal transition. J Clin Invest 119:1420–1428

35. Davidson B, Berner A, Nesland JM, Risberg B, Berner HS, Tropè CG, Kristensen GB, Bryne M, Ann Florenes V (2000) E-cadherin and alpha-, beta-, and gamma-catenin protein expression is up-regulated in ovarian carcinoma cells in serous effusions. J Pathol 192:460–469
36. Thuault S, Tan EJ, Peinado H, Cano A, Heldin CH, Moustakas A (2008) HMGA2 and Smads co-regulate SNAIL1 expression during induction of epithelial-to-mesenchymal transition. J Biol Chem 283:33437–33446
37. Lu L, Schwartz P, Scarampi L, Rutherford T, Canuto EM, Yu H, Katsaros D (2011) MicroRNA let-7a: a potential marker for selection of paclitaxel in ovarian cancer management. Gynecol Oncol 122:366–371

Virchows Arch (2012) 460:515–523
DOI 10.1007/s00428-012-1230-2

ORIGINAL ARTICLE

NSCLC and the alternative pathway of NF-κB: uncovering an unknown relation

Fotinos-Ioannis D. Dimitrakopoulos · Anna G. Antonacopoulou · Anastasia Kottorou · Helen Vlotinou · Nikolaos D. Panagopoulos · Dimitrios Dougenis · Chrisoula Scopa · Helen Papadaki · Haralabos P. Kalofonos

Received: 3 January 2012 / Accepted: 23 March 2012 / Published online: 5 May 2012
© Springer-Verlag 2012

Abstract Lung cancer is the leading cause of cancer-related deaths worldwide. Although our knowledge on the pathobiology of the disease has increased in the last decades, the prognosis of lung cancer patients has hardly changed. Many signaling pathways are implicated in lung carcinogenesis, but the role of the alternative pathway of nuclear factor kappa-light-chain-enhancer of activated B cells (NF-κB) in lung cancer pathogenesis and progression has not been investigated. The aim of our study was to investigate the role of this pathway in non-small cell lung cancer (NSCLC) patients. NF-κB2 and RelB protein expression was retrospectively assessed by immunohistochemistry in tissue samples from 109 NSCLC patients. RelB and NF-κB2 protein levels differed between tumors and adjacent nonneoplastic lung parenchyma. Cytoplasmic immunoreactivity of NF-κB2 and RelB was correlated with tumor stage ($p=0.03$ and $p=0.016$, respectively). In addition, cytoplasmic NF-κB2 levels were related to tumor grade ($p=0.046$). Expression of RelB in the cytoplasm was tumor histologic type-specific, with squamous cell carcinomas having the highest protein levels. Nuclear expression of RelB and NF-κB2 differed between tumor and nonneoplastic tissues, possibly indicating activation of the alternative pathway of NF-κB in cancer cells. Moreover, lymph node metastasis was related to nuclear NF-κB2 expression in tumor cells. The deregulation of the alternative NF-κB pathway in NSCLC could play a role in the development and progression of the disease.

Keywords NF-κB2 · p52 · RelB · Lung cancer · NSCLC

F.-I. D. Dimitrakopoulos · A. G. Antonacopoulou · A. Kottorou · H. P. Kalofonos
Molecular Oncology Laboratory, Division of Oncology, Department of Internal Medicine, Medical School, University of Patras, Patras, Greece

H. Vlotinou · C. Scopa
Department of Pathology, Medical School, University of Patras, Patras, Greece

N. D. Panagopoulos · D. Dougenis
Department of Cardiothoracic Surgery, Medical School, University of Patras, Patras, Greece

H. Papadaki
Department of Anatomy, Medical School, University of Patras, Patras, Greece

H. P. Kalofonos (✉)
Division of Oncology, Department of Medicine, Medical School, University of Patras, Rion, Patras 26504, Greece
e-mail: kalofonos@upatras.gr

Introduction

Primary tumors of the lung were rare until the beginning of the twentieth century [1, 2]. At present, lung cancer is the first cause of cancer-related deaths in both sexes (30 % in males, 26 % in females) in the USA and worldwide [3, 4]. Non-small cell lung cancer (NSCLC) and small cell lung cancer are the two major clinical lung cancer subtypes. The majority (85 %) of lung carcinomas are NSCLC (squamous cell carcinoma, adenocarcinoma, and large cell carcinoma) [4]. The current therapeutic approaches, which include surgical resection, platinum-based doublet chemotherapy, radiotherapy, and targeted therapies, rarely cure the disease, and the overall survival rate remains low at approximately 15 % [5].

In the last decades, there has been an expansion of knowledge relating to the pathobiology of malignant epithelial lung tumors, but the prognosis of the disease has little changed.

Although a wide spectrum of genes and proteins has been studied in human lung cancer, it remains unclear whether the alternative nuclear factor kappa-light-chain-enhancer of activated B cells (NF-κB) pathway can promote tumorigenesis or change the tumor progression. At present, it is well documented that NF-κB has a pleiotropic function by binding to discrete DNA sequences in promoters and enhancers.

The family of NF-κB transcriptional regulators consists of seven members p105/p50 (NF-κB1), p100/p52 (NF-κB2), p65 (RelA), RelB, c-Rel, which are encoded by five genes (NF-κB1, NF-κB2, RELA, RELB, and c-REL) [6, 7]. NF-κB1 and NF-κB2 encode the precursor proteins p105 and p100, which are proteasomaly cleaved to give rise to the functional molecules p50 and p52, respectively [7, 8]. The NF-κB family gives rise to two major signaling pathways, the classical and the alternative. In the alternative pathway, two of the central players are p100/p52 and RelB. As only the Rel family members carry a carboxy-terminal transcriptional activating domain, which is a positive regulator of gene expression, a heterodimer between p100/p52 and RelB must form in order to bind to promoters and enhancers [8, 9].

Until recently, the role of NF-κBs and their signaling pathways has been thought to be limited to coordinating the innate and adaptive immune responses. Their role in cancer development has not been elucidated, although it is now documented that NF-κB is a major factor linking inflammation and carcinogenesis [10, 11]. Moreover, NF-κB is a central player in virus-associated carcinogenesis [12]. In many types of cancer, not only in hematological but also in solid malignancies, e.g., melanoma, breast, prostate, ovarian, pancreatic, colon, head and neck, renal, bladder, liver, astrocytoma, glioblastoma, and thyroid, NF-κB family members exhibit elevated activity [13, 14]. In lung cancer, only p50 and p65 have been studied, while little is known about the role of the alternative pathway of NF-κB in lung carcinogenesis and the progression of the disease [15–17].

Methods

Tissue specimens

This study was carried out according to the principles and after the approval of the Committee on Research and Ethics and the Scientific Committee of the University Hospital of Patras, Greece. The study comprised 109 formalin-fixed paraffin-embedded (FFPE) lung tissue specimens of invasive NSCLCs including adjacent nonneoplastic lung parenchyma, retrieved from the archives of the Laboratory of Pathology of the University Hospital of Patras. All cases were surgically managed at the University Hospital of Patras Medical School between 2005 and 2008.

Clinicopathological information was obtained from the pathology reports and is given in Table 1. Sixty (n=60) samples were squamous cell carcinomas, 38 (n=38) were adenocarcinomas, and 8 (n=8) were large cell carcinomas. The majority of patients were men (90.9 %) with a mean age of 67 years (range, 46–81 years). The pathological stage was defined according to the primary pathology reports. All stages were represented with the majority of samples equally distributed between stages I, II, and III. The tumor grade was (2 %) grade 1, (49 %) grade 2, and (43 %) grade 3, respectively. Lymph node status was known for 102 patients. Fifty percent of them had lymph node metastatic disease. First- and second-year survival rates were available in 101 of the 109 patients. Moreover, the regional relapse status in the 2-year observational period was known for 29 patients (11 relapsed).

Table 1 Clinicopathological characteristics of NSCLC patients

Age (years): median (range)	67 (46–81)
Gender: no. (%)	109
Male	99 (90.8 %)
Female	10 (9.2 %)
Site	109
Left lung	51 (46.8 %)
Right lung	58 (53.2 %)
Histology: no. (%)	106
Squamous	60 (56.6 %)
Adenocarcinoma	38 (35.8 %)
Large carcinoma	8 (7.5 %)
Stage: no. (%)	103
0	1 (1.0 %)
I	35 (34.0 %)
II	32 (31.1 %)
III	31 (30.1 %)
IV	4 (3.9 %)
Grade: no. (%)	100
I	2 (2.0 %)
II	49 (49.0 %)
III	43 (43.0 %)
IV	6 (6.0 %)
Maximum diameter (cm): mean (range)	104
	5.39 (1.50–21)
Lymph node infiltration: no. (%)	102
No	51 (50.0 %)
Yes	51 (50.0 %)
Survival (2 years): no. (%)	101
Death	35 (31.8 %)
Alive	66 (60.0 %)
Relapse (2 years): no. (%)	29
No	18 (62.1 %)
Yes	11 (37.9 %)

Immunohistochemical analysis

Four-micrometer sections from FFPE tissue specimens were deparaffinised in xylene and rehydrated in a series of graded alcohols. The sections were then pre-treated in a microwave oven, and peroxidase activity was blocked with 3 % hydrogen peroxide for 20 min, followed by incubation with an appropriate protein blocking solution. Primary antibodies used were mouse monoclonal anti-NF-κB2 (dilution 1:500, clone: C-4, sc-7386, Santa Cruz) and rabbit polyclonal antibody against ReB (dilution 1:100, clone: C-19, sc-226, Santa Cruz). Detection was performed using the Envision detection kit (DAKO) according to the manufacturer's instructions. Diaminobenzidine was used as the chromogen for visualization. Sections were counterstained with Harris' hematoxylin solution, dehydrated, and mounted. To test for specificity, the procedure was repeated in consecutive sections substituting the anti-NF-κB2 and anti-RelB antibodies with protein blocking solution.

Evaluation of immunohistochemistry

All slides were assessed by one pathologist (H.P.) and one investigator (F.D.) independently and blinded to the case. The histological type and tumor grade were confirmed according to the 2004 WHO classification of lung tumors [18]. Cases with staining in >10 % of cells were considered positive. Immunohistochemical reactivity was graded on a scale of 0–3 according to the intensity of the staining, and the percentage of immunopositive cells as follows: 0, no staining or <10 % positive cells; 1, weak staining in >10 % of cells or moderate staining in 10–70 % of cells; 2, moderate staining in >70 % of cells or strong staining in 10–70 % of cells; and 3, strong staining in >70 % of cells. NFkB2 and RelB expression in cancer cells was categorized in three groups (high vs medium vs low) using as a cutoff point the 33rd and 66th percentiles [19]. The intensity and distribution of the NF-κB2 and RelB signal were the parameters used to estimate NF-κB2 and RelB expression. The total score for each slide was the sum of the intensity and distribution (between 0 and 6). Per tissue section, the more representative areas were selected using low-power fields (magnification ×10). The accurate quantification was performed on high-power fields (magnification ×40). Microphotographs were obtained using a Nikon DXM 1200C digital camera mounted on a Nikon Eclipse 80i microscope and ACT-1C software (Nikon Instruments Inc., Melville, NY, USA).

Statistical analysis

Statistical analysis was performed with the Statistical Package for Social Sciences version 17 (SPSS, Chicago, IL, USA). Possible associations between NF-κB and RelB protein expression with the clinicopathological parameters of the tumors were evaluated with the Kruskal–Wallis or the Mann–Whitney tests for ordinal variables and χ^2 test for nominal variables. Spearman's correlations were used to assess associations between variables. Survival rates were estimated using the Kaplan–Meier method and then compared with the log rank test. Cox regression analysis was used to assess the role of the two NF-κB molecules as prognostic factors. For all comparisons, statistical significance was defined as $p<0.05$.

Results

RelB and NF-κB2 protein levels differ between NSCLC and control tissue

The association of NF-κB2 and RelB expression with the clinicopathological characteristics is listed in Tables 2 and 3, respectively. As shown in Fig. 1a–f, immunoreactivity of NF-κB2 and RelB in epithelial cells was cytoplasmic and nuclear in all NSCLC histological subtypes. Cytoplasmic expression of NF-κB2 and RelB was observed in 96.3 and 81.7 % of the tumor specimens, respectively, in contrast to 10 % of tumor-adjacent nonneoplastic tissue (Fig. 2a–b). Moreover, expression levels were higher in tumor cells than in nonneoplastic tissue ($p<0.001$ for both molecules). Regarding nuclear staining, it was noted exclusively in tumor specimens. Approximately half (48.6 %) of the tumor specimens were positive for RelB and 15.7 % for NF-κB2. However, concurrent expression of these molecules was detected only in 12.1 % of cases.

NF-κB2 and RelB expression is correlated with the tumor stage

Cytoplasmic NF-κB2 expression in tumor cells was related to disease stage ($p=0.03$). More specifically, NF-κB2 levels were higher in stages II and III and lower in stages I and IV, with the metastatic stage having the lowest score. Likewise, cytoplasmic RelB levels were lower at stage IV compared to stages I to III ($p=0.016$). In contrast, nuclear NF-κB2 (p52) and RelB expression was similar across stages ($p=0.178$ and $p=0.10$, respectively).

Regional lymph node infiltration is associated with NF-κB2 nuclear expression levels

Lymph node metastasis was found to be related to NF-κB2 expression in the nucleus of primary site tumor cells. That is, the nuclear NF-κB2 protein levels were higher in tumor cells of patients without lymph node metastasis ($p=0.044$). However, no association was detected between NF-κB2 cytoplasmic expression and lymph node positivity. RelB expression, whether cytoplasmic or nuclear, was independent of lymph node metastatic frequency.

Table 2 NF-κB2 protein expression and clinicopathological parameters

Parameters		*N*	NFkB2 protein expression in:									
			Cytoplasm				*p*	Nucleus				*p*
			0–3, *n* (%)	4, *n* (%)	5, *n* (%)	6, *n* (%)		0–3, *n* (%)	4, *n* (%)	5, *n* (%)	6, *n* (%)	
Tissue	Neoplastic	108	11 (10.2)	18 (16.7)	23 (21.3)	56 (51.9)		105 (97.2)	3 (2.8)	0 (0)	0 (0)	
Gender	Male	98	9 (9.2)	16 (16.3)	20 (20.4)	53 (54.1)	0.139	95 (96.9)	3 (3.1)	0 (0)	0 (0)	0.839
	Female	10	2 (20.0)	2 (20.0)	3 (33.3)	3 (33.3)		10 (100.0)	0 (0)	0 (0)	0 (0)	
Primary site	Left lung	45	6(13.3)	8 (17.8)	7 (15.6)	24 (53.3)	0.197	42 (93.3)	3 (6.7)	0 (0)	0 (0)	0.307
	Right lung	51	2 (3.9)	7 (13.7)	13 (25.5)	29 (56.9)		51 (100)	0 (0)	0 (0)	0 (0)	
Stage	I	31	3 (9.7)	6 (19.4)	7 (22.6)	15 (48.4)	0.030	30 (96.8)	1 (3.2)	0 (0)	0 (0)	0.178
	II	28	2 (7.1)	1 (3.6)	7 (25.0)	18 (64.3)		27 (93.2)	1 (3.6)	0 (0)	0 (0)	
	III	26	1 (3.8)	4 (15.4)	4 (15.4)	17 (65.4)		26 (100)	0 (0)	0 (0)	0 (0)	
	IV	3	1 (33.3)	1 (33.3)	1 (33.3)	0 (0)		3 (100)	0 (0)	0 (0)	0 (0)	
Lymph nodes	Positive	45	3 (6.7)	6 (13.3)	10 (22.2)	26 (57.8)	0.680	45 (100)	0 (0)	0 (0)	0 (0)	0.044
	Negative	46	4 (8.7)	8 (17.4)	10 (21.7)	24 (52.2)		44 (95.7)	2 (4.3)	0 (0)	0 (0)	
Maximum diameter	< Median	45	3 (6.8)	6 (13.3)	10 (22.2)	26 (57.8)	0.700	44 (97.8)	1 (2.2)	0 (0)	0 (0)	0.260
	≥Median	46	4 (0)	8 (4.0)	10 (36.0)	24 (60.0)		45 (97.8)	1 (2.2)	0 (0)	0 (0)	
Age	<Median	53	5 (9.4)	10 (18.9)	11 (20.1)	27 (51.9)	0.826	51 (98.1)	2 (1.9)	0 (0)	0 (0)	0.284
	≥Median	54	5 (9.3)	8 (14.8)	12 (22.2)	29 (53.7)		53 (98.1)	1 (1.9)	0 (0)	0 (0)	
Histology	Squamous	48	2 (4.2)	8 (16.7)	7 (14.6)	31 (64.6)	0.489	47 (97.9)	1 (2.1)	0 (0)	0 (0)	0.261
	Adenocarcinoma	38	9 (23.7)	3 (7.9)	12 (31.6)	14 (36.8)		38 (100.0)	0 (0)	0 (0)	0 (0)	
	Large cell	8	0 (0)	2 (25.0)	2 (25.0)	4 (50.0)		7 (87.5)	1 (12.5)	0 (0)	0 (0)	
Smoking	≤80 pack-years	10	1 (10.0)	0 (0)	3 (30.0)	6 (60.0)	0.892	10 (100)	0 (0)	0 (0)	0 (0)	0.424
	>80 pack-years	9	2 (22.2)	1 (11.1)	2 (22.2)	4 (44.4)		9 (100.0)	0 (0)	0 (0)	0 (0)	
Relapse	No	18	2 (11.1)	1 (5.6)	3 (16.7)	12 (66.6)	0.348	18 (100.0)	0 (0)	0 (0)	0 (0)	0.201
	Yes	11	1 (9.1)	1 (9.1)	4 (36.4)	5 (45.4)		11 (100.0)	0 (0)	0 (0)	0 (0)	
Survival 2 years	Dead	35	4 (11.4)	5 (14.3)	7 (20.0)	19 (54.3)	0.416	34 (97.2)	1 (2.8)	0 (0)	0 (0)	0.493
	Alive	65	7 (10.8)	10 (15.4)	14 (21.5)	34 (52.3)		64 (98.5)	1 (1.5)	0 (0)	0 (0)	
Differentiation	Well	2	0 (0)	0 (0)	0 (0)	2 (100.0)	0.168	2 (100.0)	0 (0)	0 (0)	0 (0)	0.115
	Moderate	47	2 (4.3)	9 (19.2)	7 (14.9)	29 (61.6)		46 (97.8)	1 (2.2)	0 (0)	0 (0)	
	Poor	49	6 (12.2)	8 (16.3)	15 (30.6)	20 (40.8)		48 (98.0)	1 (2.0)	0 (0)	0 (0)	

Table 3 RelB protein expression and clinicopathological parameters

Parameters		*N*	RelB protein expression in:								
			Cytoplasm				*p*	Nucleus			*p*
			0–3, *n* (%)	4, *n* (%)	5, *n* (%)	6, *n* (%)		0–3, *n* (%)	4, *n* (%)	5, *n* (%)	6, *n* (%)	
Tissue	Neoplastic	109	45 (41.3)	41 (37.6)	17 (15.6)	6 (5.5)		96 (88.1)	9 (8.3)	4 (3.7)	0 (0)	
Gender	Male	100	40 (40.0)	38 (38.0)	17 (17.0)	5 (5.0)	0.640	88 (88.0)	7 (7.0)	4 (4.0)	0 (0)	0.481
	Female	9	5 (55.6)	3 (33.3)	0 (0)	1 (11.1)		7 (77.8)	2 (22.2)	0 (0)	0 (0)	
Primary site	Left lung	47	18 (38.3)	20 (42.6)	6 (12.8)	3 (6.4)	0.776	40 (85.1)	6 (12.8)	1 (2.1)	0 (0)	0.556
	Right lung	51	25 (49.0)	14 (27.5)	9 (17.5)	3 (5.9)		46 (90.2)	2 (3.9)	3 (5.9)	0 (0)	
Stage	I	32	15 (46.9)	9 (28.1)	5 (15.6)	3 (9.4)	0.016	26 (81.2)	4 (12.5)	2 (6.3)	0 (0)	0.101
	II	29	15 (51.7)	12 (41.4)	1 (3.4)	1 (3.4)		27 (93.2)	1 (3.4)	1 (3.4)	0 (0)	
	III	26	6 (23.1)	9 (34.6)	9 (34.6)	2 (7.7)		24 (92.3)	2 (7.7)	0 (0)	0 (0)	
	IV	3	2 (66.7)	1 (33.3)	0 (0)	0 (0)		1 (33.3)	1 (33.3)	1 (33.3)	0 (0)	
Lymph nodes	Positive	46	19 (41.3)	18 (39.1)	7 (15.2)	2 (4.3)	0.947	41 (89.1)	4 (8.7)	1 (2.2)	0 (0)	0.959
	Negative	47	20 (42.6)	16 (34.0)	7 (14.9)	4 (8.5)		40 (85.1)	4 (8.5)	3 (6.4)	0 (0)	
Maximum diameter	≤Median	46	15 (32.6)	21 (45.7)	6 (13.0)	4 (8.7)	0.394	40 (87.0)	4 (8.7)	2 (4.3)	0 (0)	0.891
	>Median	46	25 (54.3)	11 (23.9)	8 (17.4)	2 (4.3)		44 (95.7)	3 (6.5)	1 (2.2)	0 (0)	
Age	<Median	54	22 (40.8)	22 (40.8)	9 (16.7)	1 (1.9)	0.259	49 (90.1)	2 (3.8)	3 (5.6)	0 (0)	0.842
	≥Median	53	23 (43.4)	17 (32.1)	8 (15.1)	5 (9.4)		45 (84.0)	7 (13.2)	1 (1.9)	0 (0)	
Histology	Squamous	52	14 (26.9)	18 (34.6)	13 (25.0)	6 (11.6)	0.008	48 (92.4)	2 (3.8)	2 (3.8)	0 (0)	0.066
	Adenocarcinoma	38	23 (60.5)	14 (36.8)	1 (2.6)	0 (0)		32 (84.2)	4 (10.4)	2 (0)	0 (0)	
	Large cell	8	4 (50.0)	2 (25.0)	1 (12.5)	1 (12.5)		8 (100)	0 (0)	0 (0)	0 (0)	
Smoking	≤80 pack-years	9	1 (11.1)	3 (33.3)	4 (44.4)	1 (11.1)	0.415	8 (0)	1 (0.0)	0 (0)	0 (0)	0.809
	>80 pack-years	10	3 (30.0)	5 (50.0)	2 (20.0)	0 (0)		9 (90.0)	1 (10.0)	0 (0)	0 (0)	
Relapse	No	18	4 (22.2)	9 (50.0)	3 (16.6)	2 (11.2)	0.379	16 (88.9)	2 (11.1)	0 (0)	0 (0)	0.352
	Yes	11	6 (54.5)	3 (22.3)	2 (18.2)	0 (0)		11 (100.0)	0 (0)	0 (0)	0 (0)	
Survival 2 years	Dead	35	15 (42.9)	8 (22.9)	9 (25.7)	3 (8.5)	0.101	32 (91.4)	3 (8.6)	0 (0)	0 (0)	0.608
	Alive	65	24 (36.9)	30 (46.2)	8 (12.3)	3 (4.6)		57 (87.7)	5 (7.7)	3 (4.6)	0 (0)	
Differentiation	Well	2	1 (50.0)	0 (0)	1 (50.0)	0 (0)	0.813	2 (100.0)	0 (0)	0 (0)	0 (0)	0.896
	Moderate	49	17 (34.6)	22 (44.9)	5 (10.2)	4 (8.2)		44 (89.8)	3 (6.1)	2 (4.1)	0 (0)	
	Poor	48	19 (39.6)	15 (31.25)	7 (14.6)	3 (6.25)		41 (85.4)	5 (10.4)	2 (4.2)	0 (0)	

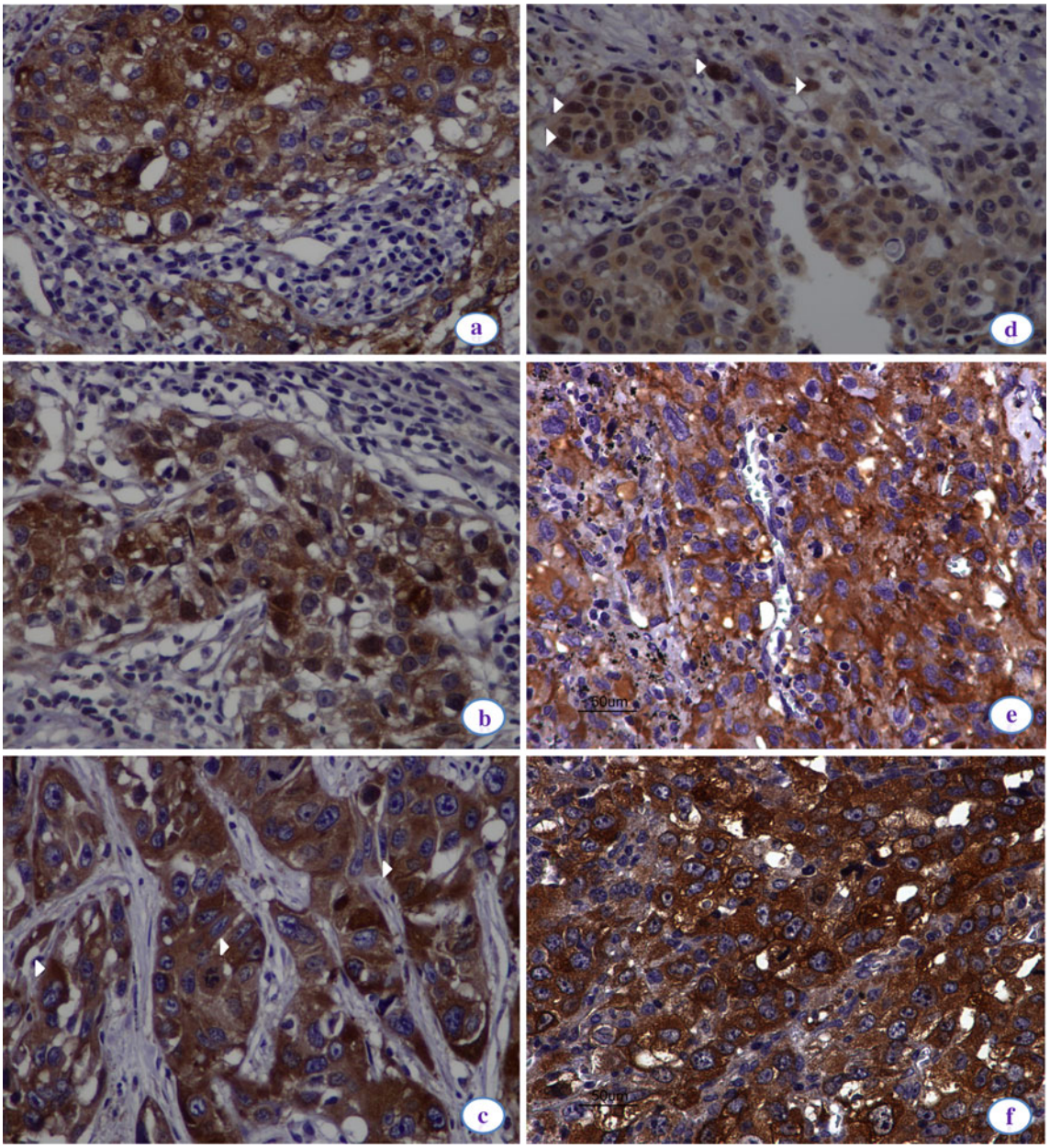

Fig. 1 **a** Representative histologic section of lung adenocarcinoma showing strong cytoplasmic immunopositivity for NF-κB2 (×40). **b** Strong nuclear and cytoplasmic staining for RelB in a representative histologic section of lung adenocarcinoma (×4O). **c** Strong diffuse cytoplasmic immunopositivity of NF-κB2 protein in invasive squamous cell carcinoma of the lung (×40). **d** Representative histologic of lung squamous cell carcinoma showing strong nuclear immunostaining and moderate cytoplasmic immunopositivity for RelB (×40)**. e** Strong cytoplasmic NF-κB2 expression in a representative section of human lung large cell carcinoma (×40). **f** Representative section of human lung large cell carcinoma with strong cytoplasmic RelB expression (×40)

NF-κB2 cytoplasmic expression is correlated with tumor grade

Using the two-tier grading system, we found that NF-κB2 levels in the cytoplasm were related to the grade of the tumor. Low-grade tumors had higher NF-κB2 levels compared to high-grade tumors ($p=0.046$). However, p52 in the nucleus was unrelated to grade. Moreover, RelB protein levels, independently of subcellular location, remained unchanged across grades.

RelB cytoplasmic expression is higher in squamous cell carcinoma

RelB cytoplasmic expression differed between NSCLC types. In particular, RelB expression in the cytoplasm of

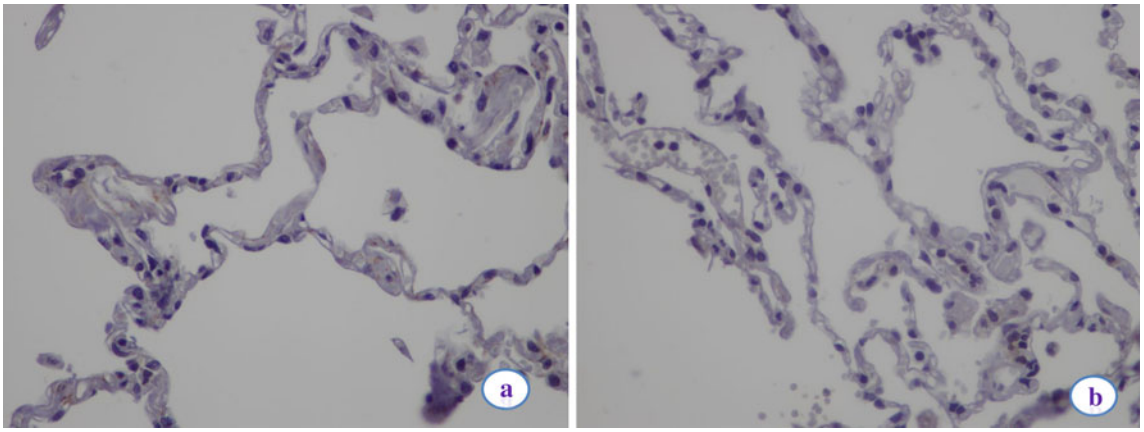

Fig. 2 **a** Negative immunostaining for NF-κB2 in alveolar epithelium and interstitium of adjacent nonneoplastic lung parenchyma (×40). **b** Negative immunostaining for RelB in alveolar epithelium and interstitium of adjacent nonneoplastic lung parenchyma (×40)

squamous cell carcinomas was higher than in the other NSCLC histological types ($p=0.008$). Moreover, expression levels were lower in adenocarcinomas than large cell carcinomas, although the difference was not significant. In addition, we observed a trend of higher nuclear RelB expression in the squamous cell subtype compared to other subtypes ($p=0.066$), although no differences were observed between adenocarcinomas and large cell carcinomas ($p=1.00$). Furthermore, NF-κB2 levels, independently of localization, did not differ between tumor types.

Correlation of protein levels between RelB and NF-κB2

NF-κB2 and RelB levels (cytoplasmic as well as nuclear) were positively correlated ($p=0.029$ and $p=0.004$, respectively). Additionally, RelB cytoplasmic and nuclear protein levels were correlated ($p<0.001$), although no such relation was noted for NF-κB2.

NF-κB2 in the cytoplasm is overexpressed in right lung tumors

In right lung tumors, cytoplasmic NF-κB2 levels were higher compared to left lung tumors. The difference was significant ($p=0.032$) when cytoplasmic expression was divided into three groups (low vs intermediate vs high). NF-κB2 nuclear expression and RelB nuclear or cytoplasmic expression were unrelated to primary site.

No correlation was found with age, sex, smoking, maximum tumor diameter, relapse rate, and overall survival

Patients' age was unrelated to the expression levels of NF-κB2 and RelB. Patients of both age groups, over and under the age of 65 (the median of our cohort), had the same NF-κB2 and RelB protein levels. Likewise, smoking, as estimated using the pack-years (median exposure of 80 pack-years), had no impact on the expression pattern of NF-κB2 and RelB. In addition, no significant correlation was found with maximum tumor diameter. Tumors with maximum diameter bigger or smaller than 4.5 cm, which was the median of our group, had similar levels of NF-κB2 and RelB. Furthermore, neither NF-κB2 nor RelB protein expression correlated with the regional disease recurrence and overall survival.

Discussion

NF-κB is a functionally pleiotropic factor implicated in the pathobiology of a variety of diseases [20]. In the last years, experimental evidence implicates the deregulation of the non-canonical NF-κB pathway in solid tumors, but its role in lung cancer pathogenesis and progression remains unknown [21].

In the present study, the immunohistochemical analysis of NF-κB2 and RelB proteins in NSCLC tissue samples revealed a statistically different expression pattern compared to adjacent nonneoplastic lung parenchyma. Cytoplasmic expression of both proteins was noted more frequently in neoplastic cells compared to adjacent nonneoplastic epithelium, while nuclear expression of both molecules was restricted to tumor tissue. These findings may reflect the activation of the alternative pathway of NF-κB in NSCLC patients. This is consistent with the observation of Lukashev et al. [22] that the TNF receptor family member, lymphotoxin-β receptor, whose activation results in the activation of the alternative pathway of NF-κB, is overexpressed in 87 to 96 % of a wide range of solid tumors, including lung cancer. Similarly, 51.9 and 58.9 % of NSCLC patients were positive for another activator of the alternative NF-κB pathway, CD40 and its ligand, CD154, respectively.

Moreover, CD40 expression in tumors is correlated with a poor prognosis since the activation of CD40 in cancer cells boosts the malignant potential of NCSLC [23, 24].

Furthermore, NF-κB2 and RelB seem to be expressed in the cytoplasm of cancer cells in a stage-dependent manner. NF-κB2 and RelB expression is lowest in patients with metastatic disease. However, previous studies in NK/T lymphomas, prostate, and esophageal tumors reported no relation of NF-κB2 and RelB expression with stage [25–27]. It is possible that the role of these molecules differs between different tumor types. Although our results should be treated with caution because of the small number of stage IV patients, they may reflect the different roles of NF-κB2 and RelB in the different stages of lung cancer progression. Additionally, it is documented that the final effect of NF-κB function may depend on the duration of NF-κB activation and the cellular context, and it can be either tumor suppressive or tumor promoting [28, 29]. This possible dual role of NF-κB during tumor progression needs to be clarified by further studies in NSCLC.

Moreover, supportive to the stage-dependent expression of NF-κB subunits is our finding that nuclear NF-κB (p52) levels are associated with lymph node metastasis. The reduced protein levels of NF-κB in the nucleus of cancer cells seem to be related to lymph node infiltration. In agreement with our findings, the nuclear localization of p65 (another member of the NF-κB family) in primary prostate tumors is a valuable marker for the prediction of lymph node metastasis [30]. It is possible that the activation of the alternative pathway of NF-κB and the subsequent nuclear translocation of NF-κB (p52) may hamper metastasis of the cancer cell. Perhaps the repeal of this brake, in a particular moment of the tumor's physical history, increases the lymph node metastatic potential. In addition, the higher levels of NF-κB2 in the cytoplasm were associated with low-grade tumors. This indicates that NF-κB2 in the cytoplasm may be correlated with an impediment of the dedifferentiation process. In prostate cancer, no relationship was noted between p52 nuclear expression and grade, although RelB was associated with tumor grade [25]. One intriguing point of our finding is that only the cytoplasmic NF-κB2 expression is correlated with tumor grade and not the nuclear.

In this study, for the first time, we found that RelB cytoplasmic expression is higher in squamous cell carcinomas compared to adenocarcinomas and large cell carcinomas. The difference between the histological groups may reflect the different microenvironments of these carcinomas that influence the activation of the NF-κB pathways in a cell type-specific manner. In agreement with our findings is the different molecular biology of the three NSCLC histological types [4].

NF-κB2 and RelB, the pivotal players of the alternative NF-κB pathway, are thought to have an active transcriptional activity when they are localized nuclearly. In our study, both were located mainly in the cytoplasm posing the question of whether cytoplasmic NF-κB2 and RelB maintain a biological function. Moreover, it would be of interest to investigate whether this cellular lodging reflects an escape mechanism of the malignant cell, which may trap p52 and RelB in the cytoplasm being benefitted more from their presence in the cytoplasm rather than of their absence from the nucleus.

Acknowledgments This research has been co-financed by the European Union (European Social Fund–ESF) and Greek national funds through the Operational Program "Education and Lifelong Learning" of the National Strategic Reference Framework (NSRF)–Research Funding Program: Heracleitus II. Investing in knowledge society through the European Social Fund.

Conflict of interest We declare that we have no conflict of interest.

References

1. Miller YE (2005) Pathogenesis of lung cancer: 100 year report. Am J Respir Cell Mol Biol 33(3):216–223
2. Aggarwal BB (2004) Nuclear factor-kappa-B: the enemy within. Cancer Cell 6(3):203–208
3. Jemal A, Siegel R, Ward E, Hao Y, Xu J, Thun MJ (2009) Cancer statistics, 2009. CA Cancer J Clin 59(4):225–249
4. Herbst RS, Heymach JV, Lippman SM (2008) Lung cancer. N Engl J Med 359(13):1367–1380
5. Sato M, Shames DS, Gazdar AF, Minna JD (2007) A translational view of the molecular pathogenesis of lung cancer. J Thorac Oncol 2(4):327–343
6. May MJ, Ghosh S (1997) Rel/NF-kappa B and I kappa B proteins: an overview. Semin Cancer Biol 8(2):63–73. doi:10.1006/scbi.1997.0057
7. Chen LF, Greene WC (2004) Shaping the nuclear action of NF-kappaB. Nat Rev Mol Cell Biol 5(5):392–401. doi:10.1038/nrm1368 nrm1368
8. Perkins ND (2007) Integrating cell-signalling pathways with NF-kappaB and IKK function. Nat Rev Mol Cell Biol 8(1):49–62. doi:10.1038/nrm2083
9. Hayden MS, Ghosh S (2008) Shared principles in NF-kappaB signaling. Cell 132(3):344–362. doi:10.1016/j.cell.2008.01.020
10. Karin M (2006) Nuclear factor-kappa B in cancer development and progression. Nature 441(7092):431–436. doi:10.1038/Nature04870
11. Grivennikov SI, Greten FR, Karin M (2010) Immunity, inflammation, and cancer. Cell 140(6):883–899. doi:10.1016/j.cell.2010.01.025
12. Okamoto T, Sanda T, Asamitsu K (2007) NF-kappa B signaling and carcinogenesis. Curr Pharm Des 13(5):447–462
13. Pacifico F, Leonardi A (2006) NF-kappa B in solid tumors. Biochem Pharmacol 72(9):1142–1152. doi:10.1016/j.bcp. 2006.07.032
14. Rayet B, Gelinas C (1999) Aberrant rel/nfkb genes and activity in human cancer. Oncogene 18(49):6938–6947
15. Tang X, Liu D, Shishodia S, Ozburn N, Behrens C, Lee JJ, Hong WK, Aggarwal BB, Wistuba II (2006) Nuclear factor-kappaB (NF-kappaB) is frequently expressed in lung cancer and preneoplastic lesions. Cancer 107(11):2637–2646. doi:10.1002/cncr.22315
16. Zhang Z, Ma J, Li N, Sun N, Wang C (2006) Expression of nuclear factor-kappaB and its clinical significance in nonsmall-cell lung cancer. Ann Thorac Surg 82(1):243–248. doi:10.1016/j.athoracsur.2006.01.049
17. Zhang D, Jin X, Wang F, Wang S, Deng C, Gao Z, Guo C (2007) Combined prognostic value of both RelA and IkappaB-alpha expression in human non-small cell lung cancer. Ann Surg Oncol 14(12):3581–3592. doi:10.1245/s10434-007-9560-z

18. Travis WD, World Health Organization, International Agency for Research on Cancer, International Association for the Study of Lung Cancer, International Academy of Pathology (2004) Pathology and genetics of tumours of the lung, pleura, thymus, and heart. IARC Press, Lyon
19. Taylor C (2006) Quantifiable internal reference standards for immunohistochemistry: the measurement of quantity by weight. Appl Immunohistochem Mol Morphol 14:253–259
20. Wong ET, Tergaonkar V (2009) Roles of NF-kappaB in health and disease: mechanisms and therapeutic potential. Clin Sci (Lond) 116(6):451–465. doi:10.1042/CS20080502
21. Dejardin E (2006) The alternative NF-kappa B pathway from biochemistry to biology: pitfalls and promises for future drug development. Biochem Pharmacol 72(9):1161–1179. doi:10.1016/j.bcp. 2006.08.007
22. Lukashev M, LePage D, Wilson C, Bailly V, Garber E, Lukashin A, Ngam-ek A, Zeng W, Allaire N, Perrin S, Xu X, Szeliga K, Wortham K, Kelly R, Bottiglio C, Ding J, Griffith L, Heaney G, Silverio E, Yang W, Jarpe M, Fawell S, Reff M, Carmillo A, Miatkowski K, Amatucci J, Crowell T, Prentice H, Meier W, Violette SM, Mackay F, Yang D, Hoffman R, Browning JL (2006) Targeting the lymphotoxin-beta receptor with agonist antibodies as a potential cancer therapy. Cancer Res 66(19):9617–9624. doi:10.1158/0008-5472.CAN-06-0217
23. Ishikawa K, Miyamoto M, Yoshioka T, Kato T, Kaji M, Ohbuchi T, Hirano S, Itoh T, Dosaka-Akita H, Kondo S (2008) Up-regulation of CD40 with juxtacrine activity in human nonsmall lung cancer cells correlates with poor prognosis. Cancer 113 (3):530–541. doi:10.1002/cncr.23618
24. Loskog AS, Eliopoulos AG (2009) The Janus faces of CD40 in cancer. Semin Immunol 21(5):301–307. doi:10.1016/j.smim.2009.07.001
25. Lessard L, Begin LR, Gleave ME, Mes-Masson AM, Saad F (2005) Nuclear localisation of nuclear factor-kappaB transcription factors in prostate cancer: an immunohistochemical study. Br J Cancer 93(9):1019–1023. doi:10.1038/sj.bjc.6602796
26. Kang MR, Kim MS, Kim SS, Ahn CH, Yoo NJ, Lee SH (2009) NF-kappaB signalling proteins p50/p105, p52/p100, RelA, and IKKepsilon are over-expressed in oesophageal squamous cell carcinomas. Pathology 41(7):622–625. doi:10.3109/00313020903257756
27. Liu X, Wang B, Ma X, Guo Y (2009) NF-kappaB activation through the alternative pathway correlates with chemoresistance and poor survival in extranodal NK/T-cell lymphoma, nasal type. Jpn J Clin Oncol 39(7):418–424. doi:10.1093/jjco/hyp037
28. Chen F, Castranova V (2007) Nuclear factor-kappaB, an unappreciated tumor suppressor. Cancer Res 67(23):11093–11098
29. Chen F, Beezhold K, Castranova V (2008) Tumor promoting or tumor suppressing of NF-kappa B, a matter of cell context dependency. Int Rev Immunol 27(4):183–204. doi:10.1080/08830180802130327
30. Lessard L, Karakiewicz PI, Bellon-Gagnon P, Alam-Fahmy M, Ismail HA, Mes-Masson AM, Saad F (2006) Nuclear localization of nuclear factor-kappaB p65 in primary prostate tumors is highly predictive of pelvic lymph node metastases. Clin Cancer Res 12 (19):5741–5745. doi:10.1158/1078-0432.CCR-06-0330

Virchows Arch (2012) 460:525–534
DOI 10.1007/s00428-012-1235-x

ORIGINAL ARTICLE

Smooth muscle actin expression in primary bone tumours

F. Hemingway · T. G. Kashima · G. Mahendra · A. Dhongre · P. C. W. Hogendoorn · F. Mertens · N. A. Athanasou

Received: 24 October 2011 / Revised: 29 February 2012 / Accepted: 30 March 2012 / Published online: 28 April 2012
© Springer-Verlag 2012

Abstract Alpha isoform of smooth muscle actin (SMA) expression has been reported in giant cell tumour of bone (GCTB) and other benign and malignant bone tumours, but the pattern of SMA expression and the precise nature of SMA-expressing cells in these lesions is uncertain. We determined by immunohistochemistry the expression of SMA and other muscle and vascular markers in normal bone, GCTB and a wide range of primary benign and malignant bone tumours. Cultured stromal cells of GCTB, chondroblastoma (CB), and aneurysmal bone cyst (ABC) were also analysed for SMA expression. SMA was only noted in blood vessels in normal bone. SMA was expressed by mononuclear stromal cells (MSC) cultured from GCTB, ABC and CB. SMA was strongly and diffusely expressed by MSC in non-ossifying fibroma, fibrous dysplasia, and "brown tumour" of hyperparathyroidism. SMA expression was also noted in GCTB, ABC, CB, chondromyxoid fibroma, malignant fibrous histiocytoma of bone and osteosarcoma. Little or no SMA was noted in Langerhans cell histiocytosis, simple bone cyst, Ewing's sarcoma, osteoblastoma, osteoid osteoma, enchondroma, osteochondroma, chondrosarcoma, myeloma, lymphoma, chordoma and adamantinoma. Our findings show that there is differential SMA expression in primary bone tumours and that identifying the presence or absence of SMA is useful in the differential diagnosis of these lesions. The nature of SMA-expressing cells in bone tumours is uncertain but they are negative for desmin and caldesmon and could represent either myofibroblasts or perivascular cells, such as pericytes.

Keywords Bone tumours · Alpha smooth muscle actin · Giant cells

Abbreviations

SMA	Alpha-smooth muscle actin
GCTB	Giant cell tumour of bone
CB	Chondroblastoma
ABC	Aneurysmal bone cyst
MSC	Mononuclear stromal cells
OS	Osteosarcoma
CMF	Chondromyxoid fibroma
GCRG	Giant cell reparative granuloma
SBC	Simple bone cyst
NOF	Non-ossifying fibroma
LCH	Langerhans cell histiocytosis
FD	Fibrous dysplasia

Introduction

Actin is a 42-kDa cytoskeletal microfilament protein that is ubiquitously expressed in all cell types. Actin interacts with a variety of membrane and cytoplasmic cytoskeletal proteins; it plays a role in cell contraction, adhesion and motility and is particularly abundant in muscle cells where

F. Hemingway · T. G. Kashima · G. Mahendra · A. Dhongre · N. A. Athanasou (✉)
Department of Pathology, Nuffield Department of Orthopaedics, Rheumatology and Musculoskeletal Sciences, University of Oxford, Oxford OX3 7LD, UK
e-mail: nick.athanasou@noc.anglox.nhs.uk

P. C. W. Hogendoorn
Department of Pathology, Leiden University Medical Centre, Leiden, The Netherlands

F. Mertens
Department of Clinical Genetics, University and Regional Laboratories, Skane University Hospital, Lund University, Lund, Sweden

it is bundled into myofilaments. There are several homologous actin isoforms and these have specificities for different cell types [1, 2]. Alpha actin is found in muscle cells and there are specific alpha actins for smooth, skeletal and cardiac muscle. Beta and gamma actin are found in muscle and non-muscle cells. The alpha isoform of smooth muscle actin (SMA) is known to be expressed in smooth muscle cells, myoepithelial cells, pericytes and myofibroblasts [3, 4]. Immunophenotypically, myofibroblasts are distinguished from smooth muscle cells by the absence of expression of desmin and caldesmon, and from pericytes by variable expression of SMA, desmin and other markers [5–7].

Specific monoclonal antibodies which recognise SMA are used to characterise soft tissue tumours of smooth muscle, myoepithelial and myofibroblast origin [3]. SMA has also been identified in a number of primary bone tumours, including leiomyosarcoma, malignant fibrous histiocytoma (MFH), osteosarcoma (OS), giant cell tumour of bone (GCTB) and chondromyxoid fibroma [8–13]. SMA expression has also been noted in leukaemia, myeloma and some secondary tumours of bone [14–16]; the nature of cells expressing SMA in these tumours has not been established. In normal bone, SMA expression has been reported in marrow stromal cells, osteoblasts and perivascular cells [14–16].

In this study, our aim has been to identify whether SMA expression is useful in the differential diagnosis of primary bone tumours and tumour-like lesions and to provide information on the nature of SMA-expressing cells in normal and

Table 1 Percentage of MSC in primary bone tumours showing SMA expression

Diagnosis	SMA staining			
	− (%)	+ (%)	++ (%)	+++ (%)
Osteogenic tumours				
Osteoblastoma (*N*=5)	100	0	0	0
Osteoid osteoma (*N*=5)	100	0	0	0
Osteosarcoma (*N*=17)	29	35	24	12
Telangiectatic osteosarcoma (*N*=11)	36	36	18	9
Giant cell-rich osteosarcoma (*N*=1)	0	100	0	0
Cartilage tumours				
Enchondroma (*N*=5)	100	0	0	0
Osteochondroma (*N*=5)	100	0	0	0
Chondroblastoma (*N*=20)	35	30	10	25
Chondromyxoid fibroma (*N*=11)	45	27	9	18
Chondrosarcoma (*N*=5)	100	0	0	0
Mesenchymal Chondrosarcoma (*N*=5)	80	20	0	0
Dedifferentiated Chondrosarcoma (*N*=5)	0	20	40	40
Giant cell-rich tumours/lesions				
Giant cell tumour (*N*=11)	0	0	36	64
Giant cell tumour recurrent/metastatic (*N*=8)	0	0	88	13
Giant cell granuloma of jaw (*N*=4)	0	25	75	0
Aneurysmal bone cyst (*N*=15)	0	40	60	0
Brown Tumour (*N*=3)	0	0	33	67
Non-ossifying fibroma (*N*=15)	0	0	27	73
Other benign tumours/lesions				
Fibrous dysplasia (*N*=16)	0	0	25	75
Simple bone cyst (*N*=5)	0	100	0	0
Langerhans cell histiocytosis (*N*=11)	91	9	0	18
Other malignant tumours				
Adamantinoma (*N*=5)	100	0	0	0
Chordoma (*N*=5)	100	0	0	0
Ewing sarcoma (*N*=5)	100	0	0	0
Malignant fibrous histiocytoma (*N*=12)	25	25	33	17
Myeloma (*N*=5)	100	0	0	0
Lymphoma (*N*=5)	100	0	0	0

SMA expression in (extravascular) mononuclear stromal cells (MSC) was scored semiquantitatively as follows: − no staining, + <10 % cells stained, ++ 10–50 % cells stained, +++ >50 % cells stained

N number of cases

pathological bone tissue. We have carried out a survey of the expression of SMA and other smooth muscle antigens in normal bone as well as in a wide range of tumour and tumour-like lesions of bone. To determine the identity of SMA-expressing cells we have also cultured mononuclear stromal cells (MSC) from several giant cell-rich lesions of bone, including GCTB, and examined whether these cells express SMA and other antigens.

Materials and methods

Specimen and tissue processing

Archival specimens of bone lesions were retrieved from the files of the Department of Pathology, Nuffield Orthopaedic Centre, Oxford, UK and the Department of Pathology Leiden University Medical Center, the Netherlands. The number and nature of lesions examined in this study are shown in Table 1. Bone specimens were decalcified in 5 % nitric or formic acid for 24 h prior to processing and embedding in paraffin wax. Sections (5 μm) of decalcified, formalin-fixed, paraffin-embedded bone specimens were cut onto silane-coated slides (Surgipath, Peterborough, UK) and incubated at 37°C for at least 24 h to improve tissue adhesion before immunohistochemistry was carried out using an indirect immunoperoxidase technique (ChemMate Envision, Dako UK). Tissue sections were dewaxed and rehydrated by successive immersion in xylene, graded ethanol and water. The monoclonal antibodies employed in this study are shown in Table 2. Antigen retrieval was not required for SMA and muscle-specific actin antibody staining but was required for other antibodies; this was carried out by microwave treatment (700 W, 2×4 min) in Target Retrieval Solution (Dako). Endogenous peroxidase was blocked in a 0.2 % (v/v) hydrogen peroxide solution in 80 % ethanol, and a protein serum block. Antigen expression was visualised by incubation with labelled polymer and diamenobenzidene. The sections were then counterstained with haematoxylin, dehydrated, cleared, and mounted.

SMA expression in (extravascular) MSC was scored semiquantitatively as follows: − no staining; + <10 % cells stained; ++ 10–50 % cells stained; +++ >50 % cells stained. Distinction of SMA staining of smooth muscle cells in the wall of blood vessels from MSC was carried out by staining serial sections with antibodies directed against endothelial cell markers (Factor VIII, CD31 and CD 34). All assays were scored by three independent observers (TGK, GM and NAA) who closely agreed on the findings. Cases with equivocal MSC staining or discordant scoring were reviewed by the pathologist together after immunohistochemical studies were repeated.

Analysis of SMA expression in cultured MSC from GCTB and other giant cell-rich lesions

MSC were isolated from 14 cases of GCTB, 13 cases of aneurysmal bone cyst (ABC) and two cases of chondroblastoma (CB) as previously described [17]. A small piece of tumour tissue was washed in sterile phosphate buffered saline, placed in a tissue culture flask and covered with α minimal essential medium (MEM; Lonza, Wokingham, UK) supplemented with 10 % heat-inactivated fetal bovine serum 50 IU/ml Penicillin, 50 μg/ml Streptomycin (Invitrogen, Paisley, UK) and 2 mM L-glutamine (Lonza, UK). Cultures were maintained at 37°C in 5 % CO_2, and the medium was replenished every 7 days. When the cells were 80 % confluent, the medium was removed and the cells were washed with α-MEM. The cells were incubated with trypsin for 5 min at 37°C and then α-MEM was added to inactivate the trypsin. The cells were pelleted and seeded onto 15 glass coverslips within a 6-cm Petri dish at 1×10^5 cells/dish. When the cells on the coverslips were 90 % confluent, they were fixed in acetone, allowed to dry and immunohistochemically stained for SMA

Table 2 Details of monoclonal antibodies employed in this study

Antigen	Antibody	Specificity	Dilution
Smooth muscle actin (SMA)	1A4	Smooth muscle cells Myofibroblasts Myoepithelial cells	1/50
Muscle specific actin	HHF 35	skeletal, cardiac and smooth muscle cells	1/50
Desmin	D33 and DE-R11	Smooth striated and muscle cells	1/100
Caldesmon	h-CD	H-caldesmon (smooth muscle cells)	1/100
Calponin	CALP	Calponin binding protein in smooth muscle cells and myofibroblasts	1/50
CD31	JC70	Endothelial cells	1/200
CD34	QBEnd 10	Endothelial cells	1/20
CD45	PD7/26	Leucocyte common antigen	1/50
CD68	KP-1	Pan-macrophage; osteoclast	1/50

and other smooth muscle and vascular markers as well as for CD45 and CD68 with the monoclonal antibodies PD7/26 and KP1, respectively (both obtained from Dako, UK).

In order to determine more precisely the nature of SMA-expressing MSC, the presence (and frequency) of telomere associations in short-term MSC cultures from six GCTBs was also performed as previously described [18].

Results

SMA expression in normal mature bone

In normal compact and cancellous bone, SMA was confined to the wall of blood vessels, some of which had an obvious smooth muscle wall which contained several layers of SMA+cells. Numerous small, thin-walled vascular channels were seen in fatty and haematopoietic marrow and immediately beneath bone-lining cells and osteoblasts covering the surface of bone trabeculae (Fig. 1). Although in some areas it appeared that there were small collections of SMA-positive cells in the stroma of fatty and haematopoietic marrow, serial sections revealed that these were related to thin-walled vascular channels. The fibrous periosteum did not contain cells expressing SMA or other muscle markers outside blood vessels; the cambium layer of periosteal cells covering bone also did not express SMA. Muscle-specific actin showed a similar pattern of expression to SMA. Desmin, calponin and caldesmon expression was also only noted in the smooth muscle wall of large- and medium-sized vessels and, unlike SMA, rarely stained small vessels. Articular cartilage was negative for SMA.

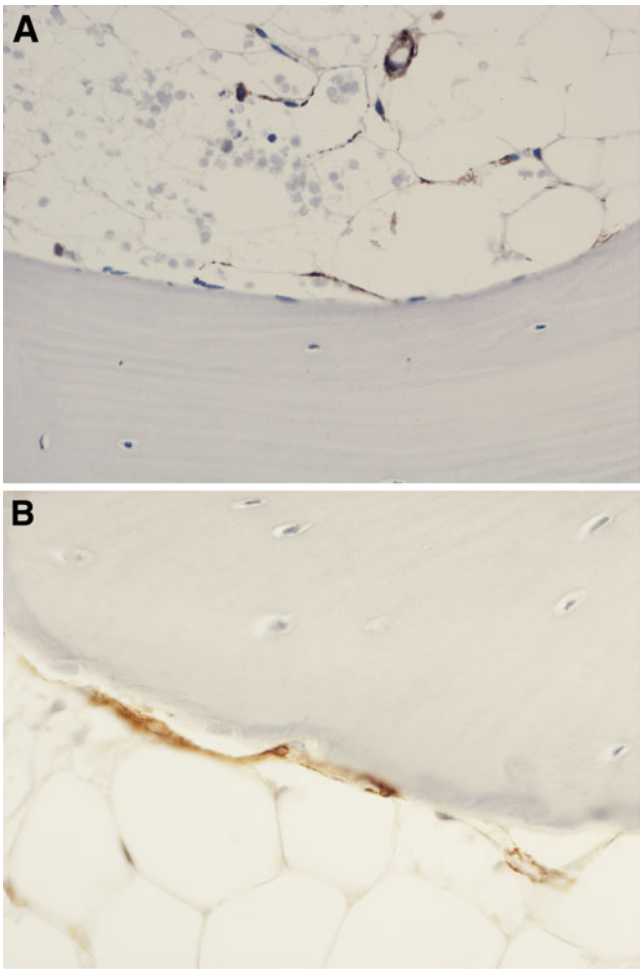

Fig. 1 **a** Low and **b** high-power view of normal bone showing SMA expression in the lining of vascular spaces, including those covering cancellous bone; bone lining cells are unstained

Analysis of SMA expression in tumours and tumour-like lesions of bone

SMA-expressing MSC (unrelated to the bone vasculature) were identified in a wide range of tumours and tumour-like lesions of bone (Table 1). These cells also expressed muscle-specific actin but were negative for desmin, calponin and caldesmon. We identified three patterns of SMA expression in the lesions analysed. A few tumours (non-ossifying fibroma [NOF], "brown tumour", fibrous dysplasia [FD]) consistently showed strong diffuse (++/+++) expression of SMA by MSC. The second group of tumours showed highly variable expression of SMA which was not uniformly distributed throughout the tumour. The third (and largest) group of tumours showed no obvious expression of SMA outside blood vessels. These three patterns were useful in distinguishing specific types and subtypes of bone tumours (Fig. 2).

Among giant cell-rich lesions of bone, diffuse strong (+++) expression of SMA was noted in NOF and the brown tumour of hyperparathyroid bone disease (Fig. 3). SMA was more variably expressed in GCTB (Fig. 4a), giant cell reparative granuloma (GCRG) and ABC (Fig. 4b); these tumours were well-vascularised as shown by staining for endothelial markers. SMA was expressed by MSC and not multinucleated osteoclast-like giant cells in all the giant cell-rich lesions of bone analysed. Most cases of chondromyxoid fibroma (CMF) and CB showed little (+) expression of SMA by MSC, but a few cases showed more pronounced staining (++) (Fig. 4c). SMA expression was not identified in Langerhans cell histiocytosis (LCH) or simple bone cyst (SBC) (Fig. 5), but was strongly and diffusely expressed in fibrous dysplasia (Fig. 3c).

No obvious difference in SMA expression was noted between primary and recurrent GCTBs. In some cases of GCTB, SMA expression was quite prominent at the advancing edge of the tumour, but in these areas the tumour was often highly vascular; SMA expression was also not particularly prominent in fibrotic areas of the lesion where

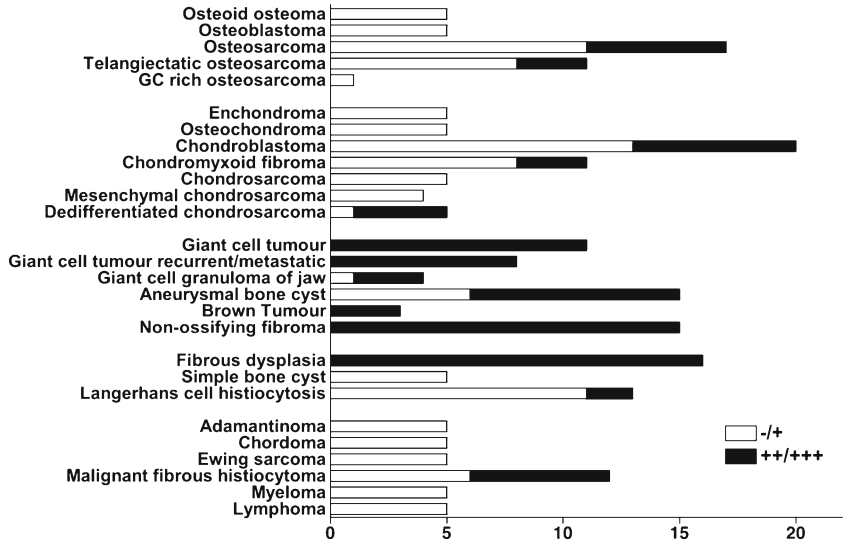

Fig. 2 Differential SMA expression in primary bone tumours. *empty rectangles* −/+, *filled rectangles* ++/+++ scored semiquantitatively

there were relatively few giant cells and there was proliferation of MSC.

MSC cultured from GCTB, ABC and CB expressed SMA and muscle-specific actin but not desmin (Fig. 6), calponin, caldesmon, the vascular marker CD31 and CD45 (leukocyte common antigen) or CD68, a macrophage marker. Cytogenetic analysis showed that cultured SMA + MSC from all the GCTBs contained telomere associations (mean: 25 % of cultured cells).

Fibroblast-like MSC and pleomorphic tumour cells expressed SMA in MFH and OS (Fig. 7a). OS showed a variable degree of SMA expression with most cases being +/++; a few cases, however, were entirely negative for SMA and some diffusely and strongly positive (+++). In contrast, SMA was not expressed outside blood vessels in the benign bone-forming tumours osteoid osteoma and osteoblastoma (Fig. 7b); plump osteoblasts and stromal MSC in these tumours did not express SMA. In Ewing's sarcoma, lymphoma, myeloma, adamantinoma and chordoma, SMA expression was also confined to the wall of blood vessels and neither tumour cells nor MSC expressed SMA. Chondromas, osteochondromas, conventional, mesenchymal and clear cell chondrosarcomas did not express SMA outside blood vessels. Dedifferentiated chondrosarcomas showing dedifferentiation towards OS or MFH variably (+/++) expressed SMA in the dedifferentiated but not the low-grade chondrosarcoma component (Fig. 7c).

Discussion

This study has shown that immunohistochemical expression of SMA is confined to blood vessels in normal adult cortical and cancellous bone and that it is not seen in marrow stromal cells, osteoblasts, osteocytes or bone lining cells. It has also found that SMA is differentially expressed by MSC in primary tumours and tumour-like lesions of bone. Diffuse strong expression of SMA was noted in several lesions including NOF, brown tumour of hyperparathyroidism and FD. In contrast to most giant cell-rich and cystic lesions of bone, little or no SMA expression was noted in LCH and SBC. Many primary benign and malignant bone tumours, including benign bone-forming tumours were negative for SMA, but MFH, OS and dedifferentiated chondrosarcoma variably expressed this marker.

Previous studies have shown that a variable number of actin-expressing cells are present in giant cell-rich containing lesions of bone [13, 19–22]. SMA expression has also been noted in giant cell tumours of soft tissue, skin and other extraskeletal sites [23–25]. In contrast to previous studies [13, 22], we did not identify actin expression by giant cells in GCTB or other giant cell-rich lesions of bone, although we did note that the giant cells in these lesions were often surrounded by thin-walled vessels or MSC expressing SMA and muscle-specific actin. SMA expression in GCTB was seen in both primary and recurrent GCTBs as well as in some tumours that produced lung nodules, a feature noted in previous studies [20, 26]; this suggests that SMA expression is not related to tumour invasion or an indicator of GCTB behaviour.

The differential diagnosis of giant cell-rich and cystic lesions of bone requires correlation of clinical, radiological and pathological findings. Interpretation of the histopathology of these lesions can be challenging and there are relatively few immunohistochemical markers which can usefully be employed to categorise these lesions. We found that SMA was strongly and diffusely expressed by MSC in NOF and brown tumour and that it was absent in LCH and SBC. Other giant cell-rich lesions of bone such

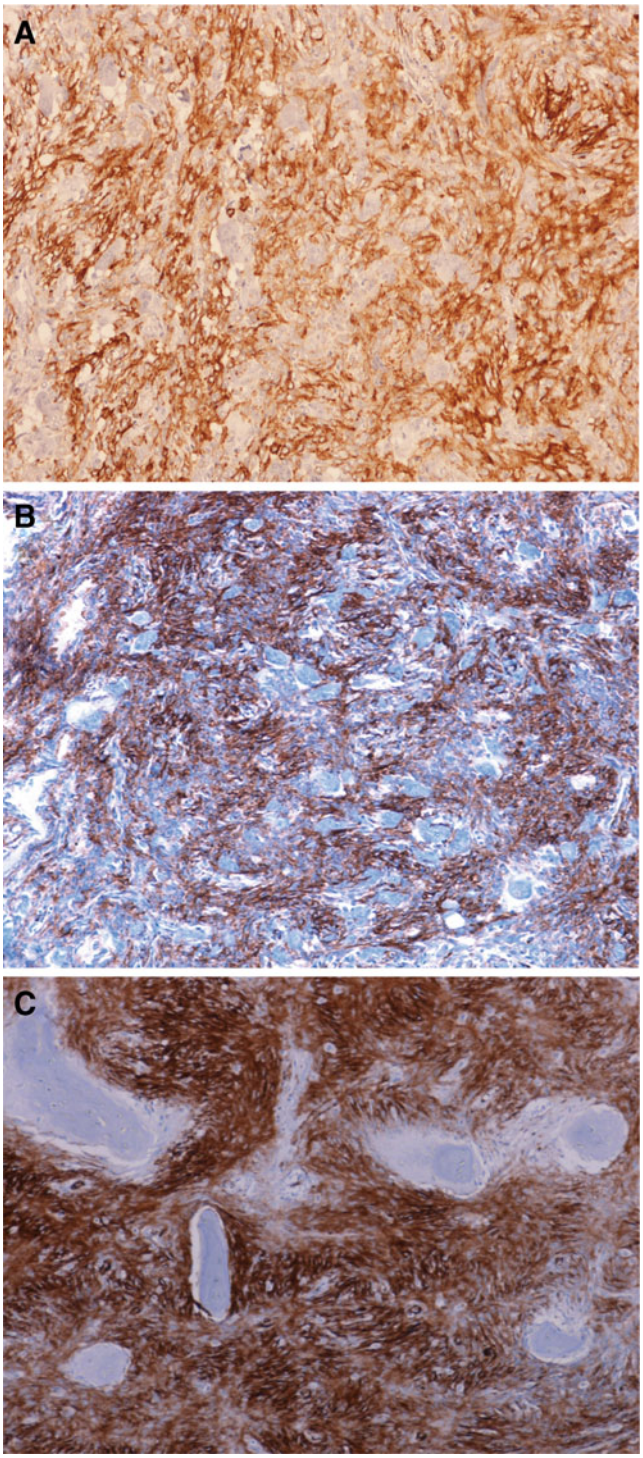

Fig. 3 Strong diffuse expression of SMA by MSC in: **a** non-ossifying fibroma, **b** "brown tumour" of hyperparathyroidism, **c** fibrous dysplasia

as GCTB, GCRG, ABC, CB, CMF and telangiectatic OS variably expressed SMA. Thus, with regard to cystic lesions of bone, expression of SMA may be useful in distinguishing ABC from SBC and, with regard to giant cell-rich lesions, absence of SMA may favour a diagnosis of LCH.

FD, a lesion which can occasionally contain focal giant cell-rich areas, was also distinguished by strong diffuse expression of SMA by intertrabecular MSC. FD enters

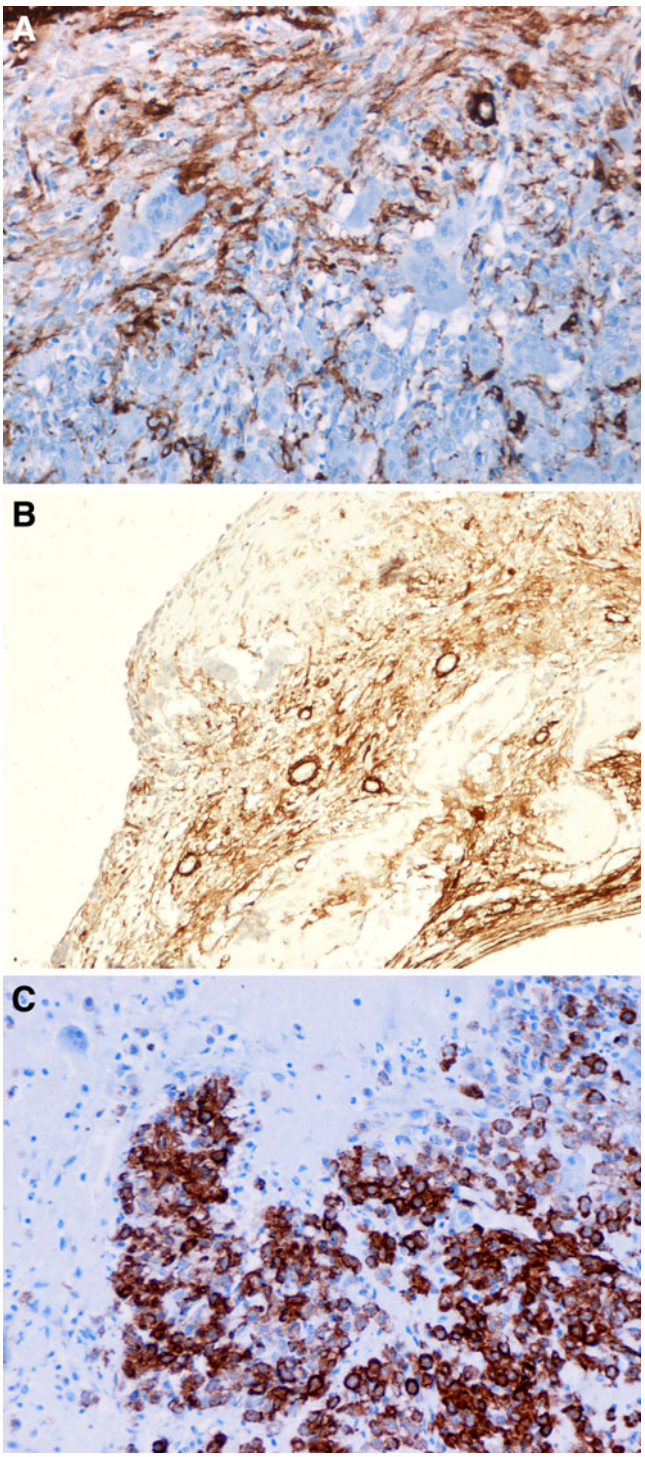

Fig. 4 SMA expression by MSC in: **a** giant cell tumour of bone, **b** aneurysmal bone cyst, **c** chondroblastoma

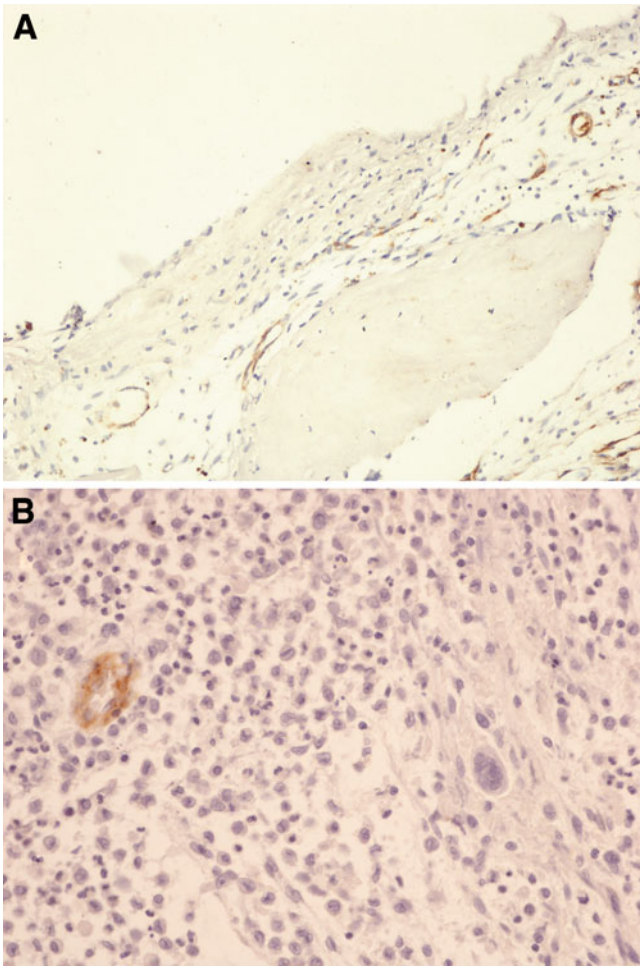

Fig. 5 Absence of (extravascular) SMA expression in **a** simple bone cyst, **b** Langerhans cell histiocytosis

into the differential diagnosis of many tumours, particularly fibro-osseous tumours of bone, such as MFH and OS. As noted in a previous study [12], we found that MFH showed relatively frequent but variable expression of SMA. We also noted SMA in most OS, including giant cell-rich and telangiectatic subtypes. In most cases of OS, SMA expression was restricted to a minority of MSC and tumour cells (+), but in some cases there was increased (++ or +++) expression. In contrast, osteoid osteoma and osteoblastoma did not show expression of SMA outside blood vessels. SMA expression may thus be useful in distinguishing benign bone-forming tumours from OS. Previous ultrastructural studies have shown that myofibroblast-like cells with a well-developed rough endoplasmic reticulum are present in FD and OS, particularly low-grade forms of OS [27]. The human SMA gene is a transcriptional target for the p53 tumour suppressor gene; expression of contractile proteins has been reported to be more common in low-grade OS and it has been suggested that SMA expression may have prognostic significance [10]. In the present study, we noted SMA expression in both high- and low-grade OS.

Many primary benign and malignant bone tumours showed no expression of SMA outside blood vessels. Osteochondroma, enchondroma as well as conventional, clear cell and mesenchymal chondrosarcoma did not express SMA; absence of SMA and calponin in conventional chondrosarcomas was similarly noted in a previous study [28]. Unsurprisingly, dedifferentiated chondrosarcomas showed SMA expression in the high-grade component exhibiting dedifferentiation towards MFH or OS. Other primary malignant bone tumours, including Ewing's sarcoma, myeloma, lymphoma, adamantinoma and chordoma, showed no expression of SMA outside blood vessels. Many of these tumours need to be considered in the differential diagnosis of round cell, spindle cell and pleomorphic sarcomas of bone. The status of SMA expression, taken with other immunohistochemical findings, may thus be useful in distinguishing these tumours.

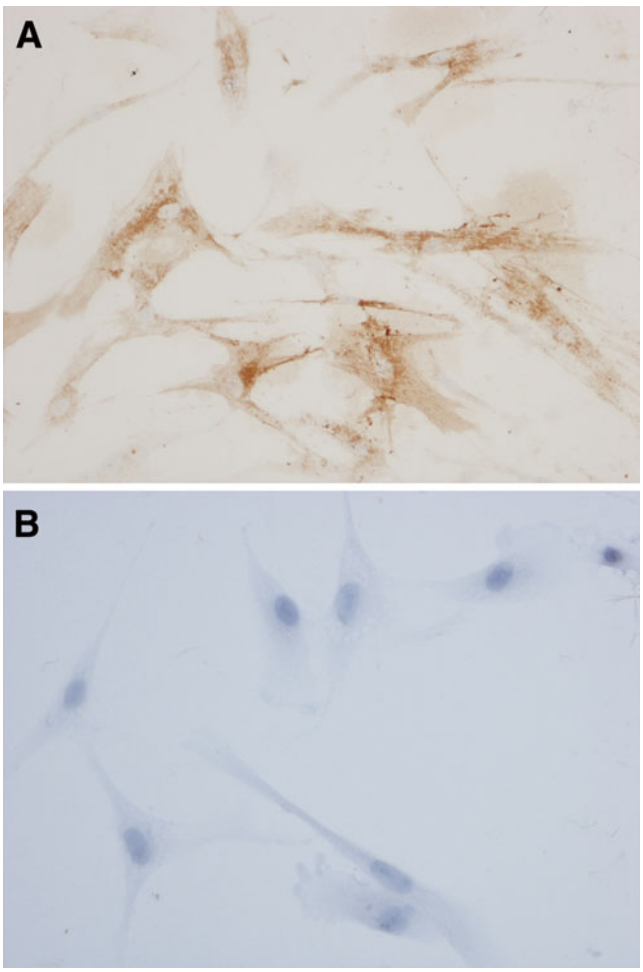

Fig. 6 MSC cultured from GCTB showing expression of **a** SMA but not **b** desmin

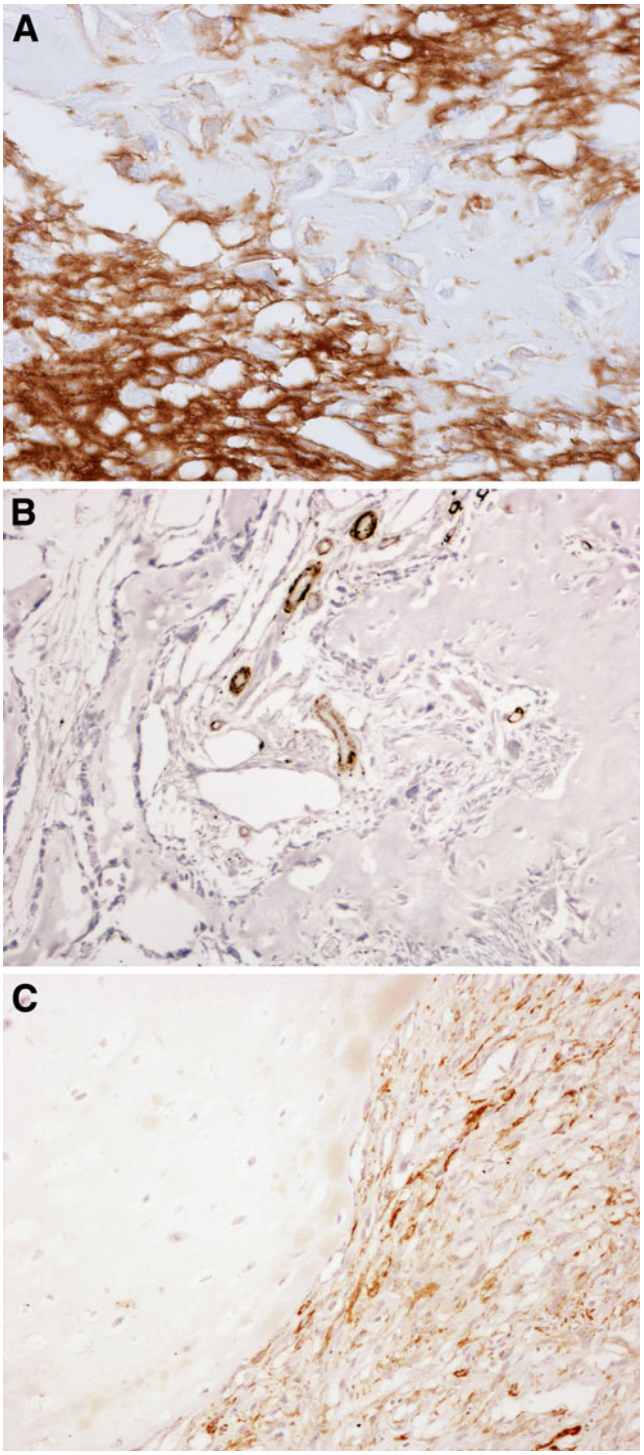

Fig. 7 SMA expression by tumour cells in **a** osteosarcoma but not **b** osteoblastoma or **c** low-grade chondrosarcoma component of a dedifferentiated chondrosarcoma; the dedifferentiated (MFH-like) component is positive for SMA

There are several reports of expression of SMA in normal adult bone marrow and in osteoblasts and bone lining cells [16, 29, 30]. One of the features which became apparent in the course of this study was the highly vascular nature of normal and pathological bone tissues; a dense meshwork of thin walled vessels is found in bone tumours and in normal bone marrow where a thin-walled vascular net is present over bone lining cells. This makes the assessment of extravascular SMA expression difficult to establish with certainty by immunohistochemistry and may account for the differences noted in SMA expression between the present and previous studies [14]. To verify that SMA was expressed by MSC in the extravascular component of the specimens analysed, we carried out staining with endothelial cell markers in serial sections. We also confirmed in cell culture studies of GCTB, ABC and CB that lesional SMA + mononuclear cells did not express endothelial, leucocyte or other smooth muscle cell markers. This was best seen in cell cultures of MSC derived from GCTB where cytogenetic analysis showed that these cells had telomere associations, a common feature of MSC in GCTB. SMA expression did not, however, obviously correlate with tumour vascularity, strong staining being noted, for example, in less-vascularised, fibrotic and well-vascularised cellular areas of GCTB.

We noted that SMA + MSC in many primary bone tumours also expressed muscle-specific actin but not desmin, calponin or H-caldesmon. This immunophenotypic profile has been noted in previous studies and believed to indicate that the SMA-expressing MSC in these lesions are reactive myofibroblasts [13, 22, 31]. Myofibroblast-like cells have been identified in several bone tumours in ultrastructural studies [27, 32–36]. We did not identify co-expression of calponin, which is typically expressed by myofibroblasts, on SMA-expressing cells. It remains possible, however, that the SMA-expressing cells in these lesions could represent this cell type as expression of smooth muscle markers by myofibroblast-like cells may depend on specific growth factor (e.g., transforming growth factor-β) stimulation [7, 21, 37]. Another cell type which expresses SMA (and more variably other smooth muscle-related antigens) is the pericyte [6]. Pericytes are perivascular cells which have been shown to be present in the bone marrow and other tissues; these cells are considered to represent a mesenchymal stromal cell precursor population which has the capacity for widely divergent differentiation into several mesenchymal cell types (including fibroblasts/myofibroblasts, chondroblasts and osteoblasts) [6, 38, 39]. Pericyte progenitor cells have been identified in the bone marrow, particularly in tumours [40]; these cells, like pericytes and myofibroblasts, can exhibit variable antigen expression. The precise nature and significance in terms of pathobiology of SMA-expressing MSC in bone tumours remains uncertain, but our findings suggest that identification of these cells may be useful in the differential diagnosis of primary bone tumours.

Acknowledgments This work was carried out by members of the EuroBoNet consortium, a Network of Excellence, supported by the European Union. The authors would like to thank Chris Lowe for typing the manuscript and NIHR BRU for help with this project.

Conflict of interest We declare that we have no conflict of interest.

References

1. Gunst SJ, Zhang W (2008) Actin cytoskeletal dynamics in smooth muscle: a new paradigm for the regulation of smooth muscle contraction. Am J Physiol Cell Physiol 295:C576–C587
2. Vandekerckhove J, Weber K (1978) At least six different actins are expressed in a higher mammal: an analysis based on the amino acid sequence of the amino-terminal tryptic peptide. J Mol Biol 126:783–802
3. Folpe A, Gown A (2008) Immunohistochemistry for analysis of soft tissue tumours. In: Weiss S, Goldblum J (eds) soft tissue tumours. Mosby Elsevier, Philadelphia, PA, pp 129–174
4. Perez-Montiel MD, Plaza JA, Dominguez-Malagon H, Suster S (2006) Differential expression of smooth muscle myosin, smooth muscle actin, h-caldesmon, and calponin in the diagnosis of myofibroblastic and smooth muscle lesions of skin and soft tissue. Am J Dermatopathol 28:105–111
5. Ceballos KM, Nielsen GP, Selig MK, O'Connell JX (2000) Is anti-h-caldesmon useful for distinguishing smooth muscle and myofibroblastic tumors? An immunohistochemical study. Am J Clin Pathol 114:746–753
6. Diaz-Flores L, Gutierrez R, Madrid JF, Varela H, Valladares F, Acosta E, Martin-Vasallo P, Diaz-Flores L Jr (2009) Pericytes. Morphofunction, interactions and pathology in a quiescent and activated mesenchymal cell niche. Histol Histopathol 24:909–969
7. Eyden B (2001) The myofibroblast: an assessment of controversial issues and a definition useful in diagnosis and research. Ultrastruct Pathol 25:39–50
8. Hasegawa T, Hirose T, Kudo E, Hizawa K, Usui M, Ishii S (1991) Immunophenotypic heterogeneity in osteosarcomas. Hum Pathol 22:583–590
9. Hasegawa T, Hirose T, Seki K, Hizawa K, Ishii S, Wakabayashi J (1997) Histological and immunohistochemical diversities, and proliferative activity and grading in osteosarcomas. Cancer Detect Prev 21:280–287
10. Salas S, Bartoli C, Deville JL, Gaudart J, Fina F, Calisti A, Bollini G, Curvale G, Gentet JC, Duffaud F, Figarella-Branger D, Bouvier C (2007) Ezrin and alpha-smooth muscle actin are immunohistochemical prognostic markers in conventional osteosarcomas. Virchows Arch 451:999–1007
11. Sugano I, Tajima Y, Ishida Y, Nagao T, Nagao K, Saga N, Ohno T, Miyakawa E (1997) Phalangeal intraosseous well-differentiated osteosarcoma of the hand. Virchows Arch 430:185–189
12. Ueda T, Araki N, Mano M, Myoui A, Joyama S, Ishiguro S, Yamamura H, Takahashi K, Kudawara I, Yoshikawa H (2002) Frequent expression of smooth muscle markers in malignant fibrous histiocytoma of bone. J Clin Pathol 55:853–858
13. Watanabe K, Tajino T, Kusakabe T, Saitoh A, Suzuki T (1997) Giant cell tumor of bone: frequent actin immunoreactivity in stromal tumor cells. Pathol Int 47:680–684
14. Gregoretti MG, Gottardi D, Ghia P, Bergui L, Merico F, Marchisio PC, Caligaris-Cappio F (1994) Characterization of bone marrow stromal cells from multiple myeloma. Leuk Res 18:675–682
15. Papadopoulos N, Simopoulos C, Kotini A, Lambropoulou M, Tolparidou I, Tamiolakis D (2001) Differential expression of alpha-smooth muscle actin molecule in a subset of bone marrow stromal cells, in b-cell chronic lymphocytic leukemia, autoimmune disorders and normal fetuses. Eur J Gynaecol Oncol 22:447–450
16. Schmitt-Graff A, Skalli O, Gabbiani G (1989) Alpha-smooth muscle actin is expressed in a subset of bone marrow stromal cells in normal and pathological conditions. Virchows Arch B Cell Pathol Incl Mol Pathol 57:291–302
17. Lau YS, Sabokbar A, Gibbons CL, Giele H, Athanasou N (2005) Phenotypic and molecular studies of giant-cell tumors of bone and soft tissue. Hum Pathol 36:945–954
18. Gorunova L, Vult von Steyern F, Storlazzi CT, Bjerkehagen B, Folleras G, Heim S, Mandahl N, Mertens F (2009) Cytogenetic analysis of 101 giant cell tumors of bone: nonrandom patterns of telomeric associations and other structural aberrations. Genes Chromosomes Cancer 48:583–602
19. O'Malley M, Pogrel MA, Stewart JC, Silva RG, Regezi JA (1997) Central giant cell granulomas of the jaws: phenotype and proliferation-associated markers. J Oral Pathol Med 26:159–163
20. Osaka S, Sugita H, Osaka E, Yoshida Y, Ryu J, Hemmi A, Suzuki K (2004) Clinical and immunohistochemical characteristics of benign giant cell tumour of bone with pulmonary metastases: case series. J Orthop Surg (Hong Kong) 12:55–62
21. Romeo S, Eyden B, Prins FA, Briaire-de Bruijn IH, Taminiau AH, Hogendoorn PC (2006) TGF-beta1 drives partial myofibroblastic differentiation in chondromyxoid fibroma of bone. J Pathol 208:26–34
22. Watanabe K, Tajino T, Sekiguchi M, Suzuki T (2000) h-Caldesmon as a specific marker for smooth muscle tumors. Comparison with other smooth muscle markers in bone tumors. Am J Clin Pathol 113:663–668
23. Hoang MP, Rogers BB, Albores-Saavedra J (2002) Giant cell tumor of the skin: a morphologic and immunohistochemical study of five cases. Ann Diagn Pathol 6:288–293
24. May SA, Deavers MT, Resetkova E, Johnson D, Albarracin CT (2007) Giant cell tumor of soft tissue arising in breast. Ann Diagn Pathol 11:345–349
25. O'Connell JX, Wehrli BM, Nielsen GP, Rosenberg AE (2000) Giant cell tumors of soft tissue: a clinicopathologic study of 18 benign and malignant tumors. Am J Surg Pathol 24:386–395
26. Alberghini M, Kliskey K, Krenacs T, Picci P, Kindblom L, Forsyth R, Athanasou NA (2010) Morphological and immunophenotypic features of primary and metastatic giant cell tumour of bone. Virchows Arch 456:97–103
27. Steiner GC, Forest M, Vacher-Lavenu MC (2006) Ultrastructure of low-grade intraosseous osteosarcoma of bone: a comparative study with fibrous dysplasia and parosteal osteosarcoma. Ultrastruct Pathol 30:293–299
28. Daugaard S, Christensen LH, Hogdall E (2009) Markers aiding the diagnosis of chondroid tumors: an immunohistochemical study including osteonectin, bcl-2, cox-2, actin, calponin, D2-40 (podoplanin), mdm-2, CD117 (c-kit), and YKL-40. APMIS 117:518–525
29. Kinner B, Spector M (2002) Expression of smooth muscle actin in osteoblasts in human bone. J Orthop Res 20:622–632
30. Peled A, Zipori D, Abramsky O, Ovadia H, Shezen E (1991) Expression of alpha-smooth muscle actin in murine bone marrow stromal cells. Blood 78:304–309
31. Vered M, Nasrallah W, Buchner A, Dayan D (2007) Stromal myofibroblasts in central giant cell granuloma of the jaws cannot distinguish between non-aggressive and aggressive lesions. J Oral Pathol Med 36:495–500
32. Emura I, Inoue Y, Ohnishi Y, Morita T, Saito H, Tajima T (1986) Histochemical, immunohistochemical and ultrastructural investigations of giant cell tumors of bone. Acta Pathol Jpn 36:691–702
33. Hanaoka H, Friedman B, Mack RP (1970) Ultrastructure and histogenesis of giant-cell tumor of bone. Cancer 25:1408–1423

34. Martinez-Tello FJ, Navas-Palacios JJ (1982) The ultrastructure of conventional, parosteal, and periosteal osteosarcomas. Cancer 50:949–961
35. Peuchmaur M, Forest M, Tomeno B, Abelanet R (1985) Multifocal nonosteogenic fibroma: report of a case with ultrastructural findings. Hum Pathol 16:751–753
36. Song S, Ewald AJ, Stallcup W, Werb Z, Bergers G (2005) PDGFRbeta + perivascular progenitor cells in tumours regulate pericyte differentiation and vascular survival. Nat Cell Biol 7:870–879
37. Aparisi T, Arborgh B, Ericsson JL (1979) Giant cell tumor of bone. Variations in patterns of appearance of different cell types. Virchows Arch A Pathol Anat Histol 381:159–178
38. Crisan M, Yap S, Casteilla L, Chen CW, Corselli M, Park TS, Andriolo G, Sun B, Zheng B, Zhang L, Norotte C, Teng PN, Traas J, Schugar R, Deasy BM, Badylak S, Buhring HJ, Giacobino JP, Lazzari L, Huard J, Peault B (2008) A perivascular origin for mesenchymal stem cells in multiple human organs. Cell Stem Cell 3:301–313
39. Crisan M, Corselli M, Chen CW, Peault B (2011) Multilineage stem cells in the adult: a perivascular legacy? Organogenesis 7:101–104
40. Eyden B (2004) Fibroblast phenotype plasticity: relevance for understanding heterogeneity in "fibroblastic" tumors. Ultrastruct Pathol 28:307–319

Virchows Arch (2012) 460:535–537
DOI 10.1007/s00428-012-1231-1

LETTER TO THE EDITOR

MDR3 immunostaining on frozen liver biopsy samples is not a sensitive diagnostic tool for the detection of heterozygous *MDR3/ABCB4* gene mutations

Aurélie Sannier · Nathalie Ganne · Maryline Tepper · Marianne Ziol

Received: 13 March 2012 / Accepted: 26 March 2012 / Published online: 13 April 2012
© Springer-Verlag 2012

Dear Editor,

We read with great interest the recent article of Wendum et al. [1] describing histological lesions observed in the liver of 13 adult patients with heterozygous *MDR3/ABCB4* gene mutations. They performed multidrug resistance P-glycoprotein 3 (MDR3) immunostaining on formalin-fixed paraffin-embedded sections of 11 patients and reported that the staining had a diffuse and strong canalicular pattern in patients and controls, except in one case who disclosed a faint staining. This finding suggested a lack of sensitivity of this technique for the diagnosis of *MDR3/ABCB4* heterozygous mutations.

Since we previously suggested that MDR3 immunostaining on frozen liver sections could be useful for the diagnosis of unexplained anicteric cholestasis in adult patients [2], we would like to contribute by providing our experience of MDR3 immunostaining realized on frozen liver biopsy sections of a new series of adult patients with *MDR3/ABCB4* mutations.

Between April 2007 and March 2011, 32 adult patients with unexplained anicteric cholestasis had *ABCB4* gene sequencing, using polymerase chain reaction amplification and DNA sequencing of exons 2 to 28 and all splice junctions. Among these 32 patients, ten carried six different *ABCB4* mutations. These ten patients (six females, 17–72 years of age) displayed various clinical characteristics: three fulfilled the criteria for low phospholipid-associated cholelithiasis syndrome [3]; one had an anteriority of intrahepatic cholestasis of pregnancy; and six had an unexplained anicteric cholestasis—two of them with associated elevated aminotransferase level. Histopathological analysis using Picrosirius red and hematoxylin–eosin-stained liver biopsy sections showed that nine patients had portal fibrosis (three F1, four F2, one F3, and one F4 according to Ishak fibrosis score); six of them displaying a jigsaw pattern of biliary-type fibrosis. Bile duct lesions corresponding to mild cholangitis could be observed in four patients. Ductopenia, defined as a loss of more than 50 % of bile ducts, was seen in two patients. Lastly, six cases showed a mild to moderate ductular reaction. The clinicopathological features are detailed in Table 1.

Frozen liver biopsies were available for 14 patients (five cases and nine controls). Immunohistochemistry was performed on 4-μm frozen sections by using MDR3 monoclonal antibody (clone $P3_{II\text{-}26}$) and MRP2 antibody (clone $M2_{III\text{-}6}$) as a control to check tissue immune reactivity. As shown in Fig. 1, we observed a diffuse and intense canalicular staining with MDR3 antibody, in the available frozen liver biopsies of the five patients with heterozygous *ABCB4* mutations and in the nine controls. Positive canalicular staining was also observed with MRP2 antibody, confirming the immunoreactivity of our samples.

These results are in contradiction with our previous report [2] in which no or faint MDR3 immunostaining was observed in frozen liver biopsies from four patients with

A. Sannier (✉) · M. Tepper · M. Ziol
Service d'Anatomie Pathologique, GHU Paris-Seine-Saint-Denis,
Hôpital Jean Verdier, AP-HP,
Avenue du 14 Juillet,
93143 Bondy Cedex, France
e-mail: aureliesannier@free.fr

N. Ganne · M. Ziol
Université Paris 13,
93000 Bobigny, France

N. Ganne
Service d'Hépato-gastroentérologie,
GHU Paris-Seine-Saint-Denis, Hôpital Jean Verdier, AP-HP,
Bondy, France

Table 1 Characteristics of patients with *ABCB4* mutations at the time of liver biopsy

Case	Sex	Age	Clinical data	Mutation category	Exon	Location and nucleotide change	Status of variant	Fibrosis score[a]	Bile duct lesions	MDR3 staining
1	F	40	LPAC	Missense	4	c.139C>T	Heterozygous	0	No	Diffuse
2	F	29	UC	Missense	19	c.2363G>A	Heterozygous	1	No	Diffuse
3	M	25	UC	Missense	13	c.1436C>T	Heterozygous	2	No	Diffuse
4	F	72	UC	Missense	19	c.2363G>A	Heterozygous	2	No	Diffuse
5	F	28	UC	Missense	19	c.2363G>A	Heterozygous	1	No	Diffuse
6	F	30	ICP	Missense	13	c.1436C>T	Heterozygous	1	No	ND
7	F	29	LPAC	Missense	23	c.2800G>A	Homozygous	2	Mild	ND
8	M	69	UC	Missense	15	c.1769G>A	Heterozygous	3	Mild	ND
9	M	23	LPAC	Insertion	12	c.1327dup	Heterozygous	2	Mild	ND
10	M	17	UC	Missense	15	c.1769G>A	Heterozygous	4	Mild	ND

LPAC low phospholipid-associated cholelithiasis, *UC* unexplained cholestasis, *ICP* intrahepatic cholestasis of pregnancy, *ND* not done

[a] According to Ishak scoring system

heterozygous *ABCB4* mutations. However, previous reports also described either a normal or a faint canalicular immunostaining on frozen liver biopsies in patients with heterozygous or homozygous *ABCB4* mutations [4–6]. In conclusion, MDR3 immunostaining on paraffin-embedded or frozen liver biopsy samples has a very limited value for the diagnosis of heterozygous *MDR3/ABCB4* mutations in adults.

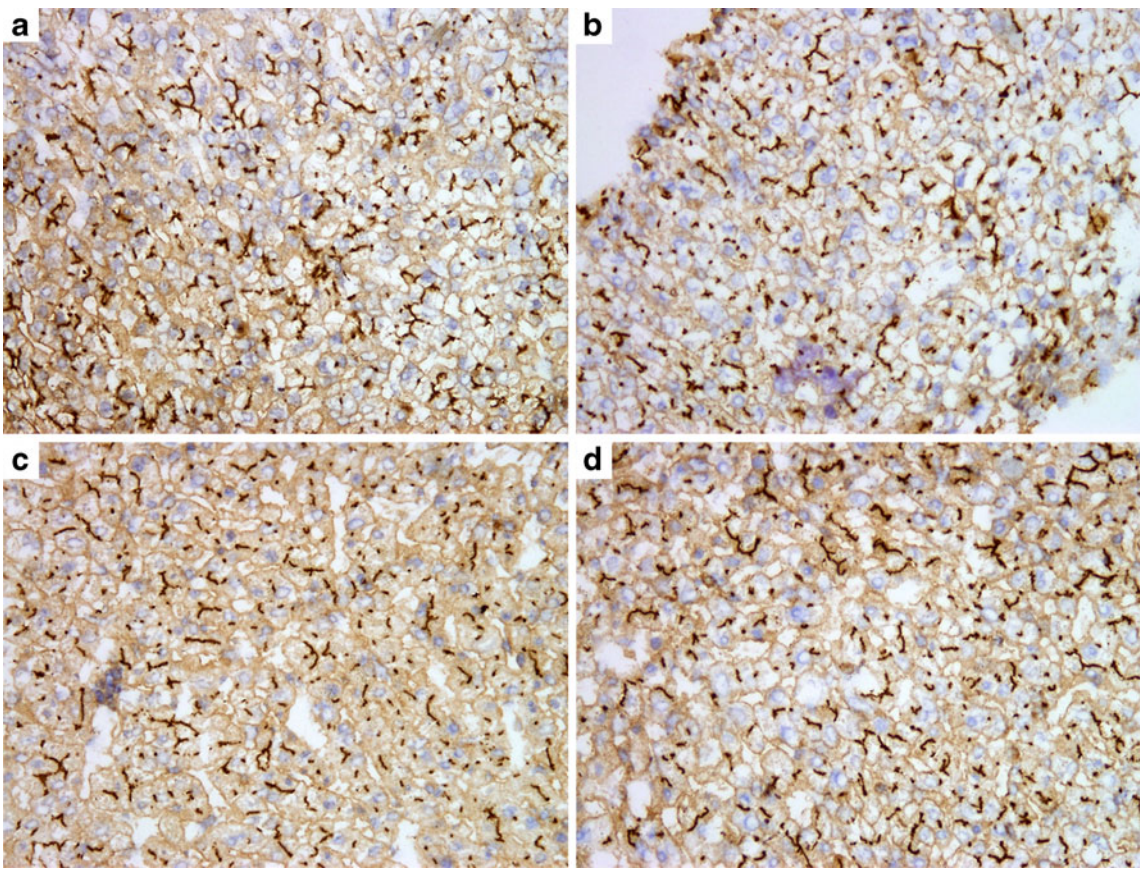

Fig. 1 MDR3 (**a**, **c**) and MRP2 (**b**, **d**) immunostainings on frozen liver biopsies. Strong and diffuse canalicular staining in a patient with *MDR3/ABCB4* heterozygous gene mutation (**a**, **b**) and a patient with unexplained anicteric cholestasis, without *MDR3/ABCB4* mutation (**c**, **d**)

References

1. Wendum D, Barbu V, Rosmorduc O, Arrivé L, Fléjou JF, Poupon R (2012) Aspects of liver pathology in adult patients with *MDR3/ABCB4* gene mutations. Virchows Arch 460:291–298
2. Ziol M, Barbu V, Rosmorduc O, Frassati-Biaggi A, Barget N, Hermelin B, Scheffer GL, Bennouna S, Trinchet JC, Beaugrand M, Ganne-Carrié N (2008) *ABCB4* heterozygous gene mutations associated with fibrosing cholestatic liver disease in adults. Gastroenterology 135:131–141
3. Rosmorduc O, Hermelin B, Boelle PY, Parc R, Taboury J, Poupon R (2003) *ABCB4* gene mutation-associated cholelithiasis in adults. Gastroenterology 125:452–459
4. Jacquemin E, De Vree JM, Cresteil D, Sokal EM, Sturm E, Dumont M, Scheffer GL, Paul M, Burdelski M, Bosma PJ, Bernard O, Hadchouel M, Elferink RP (2001) The wide spectrum of multidrug resistance 3 deficiency: from neonatal cholestasis to cirrhosis of adulthood. Gastroenterology 120:1448–1458
5. Lucena JF, Herrero JI, Quiroga J, Sangro B, Garcia-Foncillas J, Zabalegui N, Sola J, Herraiz M, Medina JF, Prieto J (2003) A multidrug resistance 3 gene mutation causing cholelithiasis, cholestasis of pregnancy, and adulthood biliary cirrhosis. Gastroenterology 124:1037–1042
6. Keitel V, Burdelski M, Warskulat U, Kuhlkamp T, Keppler D, Haussinger D, Kubitz R (2005) Expression and localization of hepatobiliary transport proteins in progressive familial intrahepatic cholestasis. Hepatology 41:1160–1172

Virchows Arch (2012) 460:539
DOI 10.1007/s00428-012-1238-7

INVITED COMMENTARY

Reply to the Sannier et al. letter entitled "MDR3 immunostaining on frozen liver biopsy is not a sensitive diagnosis tool for the detection of heterozygous *MDR3*/*ABCB4* gene mutation"

Dominique Wendum · Véronique Barbu · Olivier Rosmorduc · Lionel Arrivé · Jean-François Fléjou · Raoul Poupon

Received: 4 April 2012 / Accepted: 10 April 2012 / Published online: 1 May 2012
© Springer-Verlag 2012

Sir or Madam,

We read with great interest the letter by Sannier et al. The data presented are consistent with our publication [1].

The authors studied a new series of adult patients with unexplained cholestasis and heterozygous *MDR3*/*ABCB4* mutations. In five cases, a MDR3 immunostaining was performed on liver frozen sections and showed an intense canalicular staining similar to a normal staining. These results are in contradiction with their initial report that showed a faint MDR3 immunostaining in four patients with heterozygous *MDR3*/*ABCB4* mutations [2]. This discrepancy may be explained by technical hazards or by the type of *MDR3*/*ABCB4* mutations (indeed, the mutations were different in the two series).

It could be interesting to perform MDR3 immunostainings on the formalin-fixed paraffin-embedded liver tissues in these two series that would enable a comparison with our published data which were obtained with this technique. To conclude, it seems that *MDR3*/*ABCB4* heterozygous mutation diagnosis requires gene sequencing.

References

1. Wendum D, Barbu V, Rosmorduc O, Arrivé L, Fléjou JF, Poupon R (2012) Aspects of liver pathology in adult patients with MDR3/ABCB4 gene mutations. Virchows Arch 460 (3):291–298
2. Ziol M, Barbu V, Rosmorduc O, Frassati-Biaggi A, Barget N, Hermelin B, Scheffer GL, Bennouna S, Trinchet JC, Beaugrand M, Ganne-Carrie N (2008) ABCB4 heterozygous gene mutations associated with fibrosing cholestatic liver disease in adults. Gastroenterol 135:131–141

D. Wendum (✉) · J.-F. Fléjou
Service d'Anatomie et Cytologie Pathologiques,
APHP, Hôpital St Antoine,
184, rue du Faubourg St Antoine,
75012 Paris, France
e-mail: dominique.wendum@sat.aphp.fr

V. Barbu
Service de Biochimie, APHP, Hôpital St Antoine,
75012 Paris, France

O. Rosmorduc · R. Poupon
Service d'Hépatologie, APHP, Hôpital St Antoine,
75012 Paris, France

L. Arrivé
Service d'imagerie médicale, APHP, Hôpital St Antoine,
75012 Paris, France

D. Wendum · V. Barbu · O. Rosmorduc · L. Arrivé · J.-F. Fléjou · R. Poupon
Université Pierre et Marie Curie, UPMC, Univ Paris 06,
75005 Paris, France

D. Wendum · V. Barbu · O. Rosmorduc
INSERM, UMR_S938, CdR Saint-Antoine,
75012 Paris, France

Virchows Arch (2012) 460:541
DOI 10.1007/s00428-012-1221-3

ERRATUM

Erratum to: Immortalized bovine pancreatic duct cells become tumorigenic after transfection with mutant k-ras

Matthias Löhr · Petra Müller · Ira Zauner · Christian Schmidt · Birgit Trautmann · Frank Thévenod · Gabriel Capellá · Antonio Farré · Stefan Liebe · Ralf Jesenofsky

Published online: 23 March 2012
© Springer-Verlag 2012

Erratum to: Virchows Arch (2003) 438:581–590
DOI 10.1007/s004280100397

The author name listed as "Ralf Jesnowski," has been changed to "Ralf Jesenofsky"

The online version of the original article can be found at http://dx.doi.org/10.1007/s004280100397.

M. Löhr (✉)
Department of Medicine IV, Molecular Gastroenterology,
Medical Faculty of Mannheim, University of Heidelberg,
Theodor-Kutzer-Ufer 1–3,
68135 Mannheim, Germany
e-mail: matthias.loehr@med4.ma.uni-heidelberg.de

M. Löhr · P. Müller · C. Schmidt · S. Liebe · R. Jesenofsky
Department of Medicine, University of Rostock,
Rostock, Germany

I. Zauner · B. Trautmann
Department of Medicine I, University of Erlangen-Nuremberg,
Erlangen, Germany

F. Thévenod
Department of Physiology, University of Saarland,
Bad Homburg, Germany

G. Capellá · A. Farré
Laboratori d'Investigacio Gastrointestinal, Institut de Recerca,
Hospital de Sant Pau, Universita Autonoma,
Barcelona, Spain

Virchows Arch (2012) 460:543
DOI 10.1007/s00428-012-1222-2

ERRATUM

Erratum to: Gene expression profiles of microdissected pancreatic ductal adenocarcinoma

Robert Grützmann · Melanie Foerder · Ingo Alldinger · Eike Staub · Thomas Brümmendorf · Stefan Röpcke · Xinzhong Li · Glen Kristiansen · Ralf Jesenofsky · Bence Sipos · Matthias Löhr · Jutta Lüttges · Detlef Ockert · Günter Klöppel · Hans Detlev Saeger · Christian Pilarsky

Published online: 1 May 2012
© Springer-Verlag 2012

Erratum to: Virchows Arch (2003) 443:508–17
DOI 10.1007/s00428-003-0884-1

The author name listed as "Ralf Jesnowski," has been changed to "Ralf Jesenofsky"

The online version of the original article can be found at http://dx.doi.org10.1007/s00428-003-0884-1.

R. Grützmann · M. Foerder · I. Alldinger · D. Ockert · H. D. Saeger · C. Pilarsky (✉)
Department of Visceral, Thoracic and Vascular Surgery, University Hospital Carl Gustav Carus, Technical Universityof Dresden, Dresden, Germany
e-mail: Christian.Pilarsky@mailbox.tu-dresden.de

E. Staub · T. Brümmendorf · S. Röpcke · X. Li
metaGen Pharmaceuticals,
Berlin, Germany

G. Kristiansen
Department of Pathology, Charité,
Berlin, Germany

R. Jesenofsky · M. Löhr
Molecular Gastroenterology, II. Department of Medicine, Faculty of Clinical Medicine Mannheim, University of Heidelberg,
Heidelberg, Germany

B. Sipos · J. Lüttges · G. Klöppel
Department of Pathology, University of Kiel,
Kiel, Germany

Virchows Arch (2012) 460:545–553
DOI 10.1007/s00428-012-1237-8

REVIEW AND PERSPECTIVES

Cancer stem cell markers in breast neoplasias: their relevance and distribution in distinct molecular subtypes

Fernando Schmitt · Sara Ricardo · André Filipe Vieira · Maria Rita Dionísio · Joana Paredes

Received: 23 December 2011 / Revised: 29 March 2012 / Accepted: 10 April 2012 / Published online: 5 May 2012
© Springer-Verlag 2012

Abstract The identification and characterization of cancer stem cells might lead to more effective control of neoplastic disease, by directing therapies to the most aggressive cells. For that reason, the identification of cancer stem cells (CSCs) in breast tumours is one of the priorities in breast cancer research, which has resulted in many studies attempting to identify their presence based on the expression of specific molecular markers. In this review, we describe the main molecular markers that have been identified as being able to recognise CSCs in breast carcinomas, the major molecular pathways that regulate CSCs and their association with the different molecular subtypes.

Keywords Breast cancer · Cancer stem cells · Stem cell markers

Abbreviations

ALDH	Aldehyde dehydrogenase
ATM	Ataxia telangiectasia mutated gene
BCSC	Breast cancer stem cell
Bmi-1	Polycomb group repressor protein
BRCA1	Breast cancer 1, early onset
CD24	Heat-stable antigen
CD29	β1-integrin
CD44	Receptor for hyaluronic acid
CD49f	α6-integrin
CD61	β3-integrin
CD133	Prominin 1
CK5/6	Cytokeratin 5/6
CSC	Cancer stem cell
DCIS	Ductal carcinoma in situ
ECM	Extracellular matrix
EMT	Epithelial-to-mesenchymal transition
ER	Estrogen receptor
ESA	Epithelial-specific antigen
GPI	Glycosylphosphatidylinositol
HER2	Human epidermal growth factor receptor 2
HER2-OE	HER2 overexpressing molecular subtype
Ki67	Cellular proliferation marker
LOH	Loss of heterozygosity
mRNA	Messenger RNA
NOD/SCID	Non-obese diabetic/severe combined immunodeficient mice
SP	Side population
TIC	Tumour-initiating cell

F. Schmitt (✉) · S. Ricardo · A. F. Vieira · M. R. Dionísio · J. Paredes
IPATIMUP–Institute of Molecular Pathology and Immunology of Porto University,
Rua Dr. Roberto Frias s/n,
4200-465 Porto, Portugal
e-mail: fernando.schmitt@ipatimup.pt

F. Schmitt · J. Paredes
Medical Faculty of Porto University,
Porto, Portugal

S. Ricardo · A. F. Vieira
ICBAS–Abel Salazar Biomedical Science Institute,
Porto, Portugal

M. R. Dionísio
Gulbenkian Programme for Advanced Medical Education,
Lisbon, Portugal

Introduction

Breast cancer is a heterogeneous disease consisting of a growing number of biologically distinct subtypes. This

heterogeneity is reflected by differences in hormone receptor and human epidermal growth factor receptor 2 (HER2) expression status, diverse histological subtypes, as well as distinct biological behaviour, response to therapy and disease outcome [1]. This heterogeneity implies that in order to plan for the optimally effective therapy of each breast cancer subtype, it has become crucial to identify those cancer cells in a tumour that drive disease progression. The prevailing concept for many years was that the majority of the cells in a tumour have the potential to extensively proliferate and metastasize and should all be eliminated in order to effectively treat the disease. However, recent studies have suggested that the ability of tumours to proliferate, progress and propagate relies on a limited subpopulation of cells with stem cell-like properties, for which the term cancer stem cells (CSCs) has become mainstream [2]. These cancer stem cells share essential characteristics with normal adult stem cells, such as the capacity to self-renew through asymmetric cell division, producing one tumorigenic CSC and one non-tumorigenic cancer cell destined for terminal differentiation. This concept implies that cells in a cancer are hierarchically organised in a manner very similar to cells in a normal tissue: the progeny of a normal stem cell differentiates into phenotypically diverse cells with limited proliferative potential, and so, the progeny of CSCs also sustains genetic/epigenetic alterations analogous to the differentiation of normal cells, resulting in a population of phenotypically diverse non-tumorigenic cancer cells that compose the bulk of the tumour (Fig. 1a). These alterations are associated with loss of tumorigenic capacity, implying that the vast majority of cells in such carcinomas no longer contribute to disease progression [3].

Cancer stem cell model: rediscovery of an old story

Stem cells are present in many different somatic tissues and are important participants in their normal physiology. The progenitor cell and the mature cell populations that derive from it are organised in a hierarchical fashion, with the stem cell residing at the apex of the differentiation pathway [2]. Stem cells have three distinctive properties: (a) self-renewal (i.e. at cell division, one or both daughter cells retain the same biological properties as the parental cell); (b) the capacity to generate multiple cell lineages; and (c) the potential for sustained proliferation. Indeed, the attribute of self-renewal is especially notable because its subversion is highly relevant to oncogenesis and malignancy [4, 5]. Therefore, malignant cells harbouring the three features that define normal stem cells have been termed "cancer stem cells" (Fig. 1a).

Even though, recently, the awareness of this concept in cancer research has greatly expanded, it is not new. In 1855, Rudolf Virchow proposed the embryonal rest hypothesis, stating that cancer arises from the activation of "dominant" cells present in mature tissues that are remaining embryonic cells [6]. This theory, based on the morphological similarities between developing foetal cells and some cancer cells, was the first description of what we now call the CSC. Later, in 1875, this theory was expanded by other pathologists such as Julius Cohnheim, who proposed that misplacement of stem cells during embryonic development could lead later on in life to the development of tumours [7].

Back in 1937, Furth and Kahn established that engrafting of a single cell from a mouse tumour could initiate a new tumour in the recipient mouse [8]. The resulting tumours typically showed the same morphologic heterogeneity as the original tumour. Later, Kleinsmith and Pierce showed that malignant teratocarcinomas contain highly tumorigenic cells that, as single cells, have the capacity to differentiate into multiple mature, non-tumorigenic cell types [9]. The conclusion was drawn that teratocarcinomas tend to follow the pathways of development in embryonal tissues. To corroborate the previous findings, the same authors showed by radioactive pulse labelling of proliferating cells that these occurred almost exclusively in undifferentiated areas. At later time points, however, the DNA label appeared also in well-differentiated areas, which had to be derived from earlier labelled undifferentiated cells. These well-differentiated cells did not form tumours when transplanted into compatible recipients [10]. These results, among others, led Pierce to formulate the following early definition of the CSC concept [11]: "carcinomas are caricatures of tissue renewal, in that they are composed of a mixture of malignant stem cells".

Finally, in 1994, the first human CSC, the leukaemia stem cell, was identified in samples from patients with acute myeloid leukaemia [12] and it was proposed that blocked differentiation ("maturation arrest") was responsible for CSC proliferation and tumour growth [13]. Three years later, Blair and collaborators as well as Bonnet and Dick showed that only a small percentage of acute myeloid leukaemia cells (0.002–1 %), which phenotypically resembled hematopoietic stem cells, could transfer disease when transplanted into rodent recipients [14, 15]. These lines of evidence supported the notion that many, if not all cancers, depend on a small population of CSCs for their sustained growth and expansion. Since then, several investigators have documented the existence of CSCs in brain [16], breast [17], prostate [18] and lung cancers [19], among others.

Breast cancer stem cell markers

Finding breast CSCs (BCSCs) has been an important goal for many breast cancer researchers, who were trying to

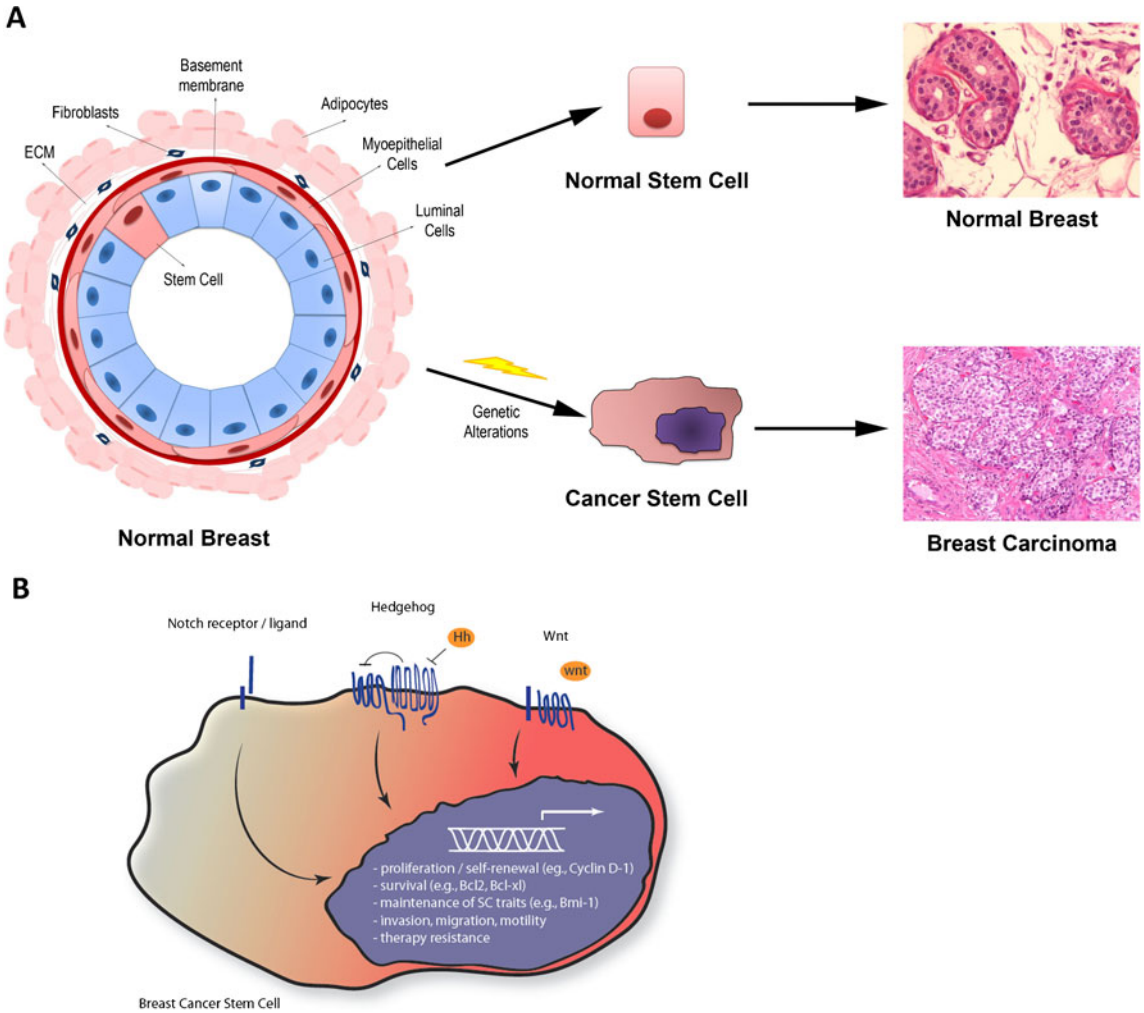

Fig. 1 **a** Schematic representation of the cellular components of a normal duct of the mammary gland. There is an outer layer of myoepithelial cells (*red*) surrounding an inner layer of luminal epithelial cells (*blue*). Stem cells of the normal mammary gland have two main distinctive properties: self-renewal and the capacity to develop into both lineages of fully breast-differentiated cells. Malignant cells harbouring the same features that define normal stem cells have been termed cancer stem cells, which originate due to the accumulation of genetic (or epigenetic) alterations that target the cellular components of the breast. **b** The three major signalling pathways involved in the maintenance of stem cell features in the breast cancer stem cell. The Notch, Wnt and Hedgehog molecules are well-known mediators of normal stem cell biology, which also mediate downstream effects in the transcription profile of cancer stem cells. These effects include the control of proliferation/self-renewal, survival, invasion and therapy resistance. Cancer stem cell therapy may encompass the modulation of these signalling pathways, which are over-activated in CSCs, without affecting normal breast physiology

define a universal marker or combination of markers able to specifically identify these cells in breast tumours and ultimately isolate them. Reviewing the literature, it appears that the most studied BCSC markers are the transmembrane proteins CD44 and CD24. A subpopulation of tumour cells that strongly express CD44 but not CD24 (the $CD44^{+}CD24^{-/low}$ phenotype) was identified as CSCs by Al-Hajj and collaborators [5], and this was subsequently confirmed by other authors. CD44 is a transmembrane glycoprotein, of which several isoforms exist, that normally regulates cell–cell adhesion and cell–matrix interactions, as well as cell migration. This glycoprotein binds mainly to hyaluronic acid, as well as to collagen, fibronectin, laminin and chondroitin sulphate—all important components of the ECM. It also binds the cytokine osteopontin [20]. Members of the CD44 family differ in their extracellular domain by the insertion of variable regions through alternative splicing [21]. The gene-encoding CD44 consists of 20 exons. In the standard form (CD44s), 10 of the 20 exons are transcribed. Multiple variant isoforms (CD44v1–v10) arise from alternative messenger RNA (mRNA) splicing of the other ten exons [22]. In contrast to the standard form of CD44, which is usually ubiquitously expressed on epithelial cells and lymphocytes, CD44 variants exhibit tissue-specific expression. Some of these variants, in particular splice variant CD44v6, are associated with aggressive tumour behaviour

in that their expression correlates with poor prognosis in a variety of human malignancies including breast cancer [23]. CD24 is a small, heavily glycosylated mucin-type protein, which is linked to the cell membrane via a GPI anchor. This molecule is involved in the regulation of cell proliferation and cell–cell interactions and it was shown to be expressed by normal pre-B lymphocytes (which lose its expression during the maturation into plasma cells), as well as in various haematological malignancies and solid tumours of some organs [24]. CD24 is the ligand of P-selectin and also an adhesion receptor expressed on activated endothelial cells and platelets, and this has led to the suggestion that it might play an important role in the metastatic process [25, 26]. Using a combination of these two cell surface markers, Al-Hajj and collaborators were the first to distinguish cancer cells that were tumorigenic in immunocompromised (non-obese diabetic/severe combined immunodeficient (NOD/SCID)] mice from non-tumorigenic cells, in a small number of breast tumours. In flow sorting experiments, they used the ESA as an epithelial cell marker with $CD44^{+}/CD24^{-/low}$ as CSC marker combination, after eliminating the non-epithelial cells that were stained for their lineage-specific markers (hematopoietic and endothelial) [5]. Since then, many more breast carcinomas have been reported to contain a subpopulation of $CD44^{+}/CD24^{-/low}$ cancer cells, which are capable of generating tumours in the NOD/SCID mice, even when implanted in very low numbers. In contrast, other cancer cell populations fail to generate tumours, even when implanted in high numbers. These reports therefore established tumourigenicity and self-renewal potential of these cells, in vitro and in vivo [27, 28].

Even though some clinical studies confirmed that $CD44^{+}/CD24^{-/low}$-expressing tumours have a poor prognosis [29–31], controversy remains concerning this issue [27, 32]. Shipitsin et al. demonstrated that genes specifically expressed in $CD44^{+}$ cells, among which many known stem cell markers, identified carcinomas with poor patient survival [33], suggesting that $CD44^{+}$ expression is prognostically relevant and justifying its consideration as a new therapeutic target for breast cancer. In contrast, Mylona et al. [32] observed that breast cancers with the opposite $CD44^{-}/CD24^{+}$ phenotype are associated with poor patient prognosis, in stark contrast with the CSC $CD44^{+}/CD24^{-/low}$ phenotype. Furthermore, Abraham et al. failed to confirm that the occurrence of $CD44^{+}/CD24^{-/low}$ tumour cells in breast cancer is associated with worse survival [27]. These contradictory data demanded additional efforts to find other markers that could complement the CSC markers CD44 and CD24, to arrive at an improved correlation with patient survival.

Along these lines, a new marker proposed for the identification of BCSCs is aldehyde dehydrogenase 1 (ALDH1). Ginestier et al. showed that normal human mammary epithelial cells and breast cancer cells with high ALDH1 activity have stem/progenitor cell properties [34]. This finding offered an important new potential molecular target for the study of breast CSCs. It was subsequently found that $ALDH1^{+}$ cells (putative CSCs) are significantly more resistant to platinum treatment and are biologically more aggressive, and that $ALDH1^{+}$ cancers are associated with poor patient prognosis [34–36]. Unlike the $CD44^{+}CD24^{-/low}$ phenotype, the $ALDH1^{+}$ phenotype consistently correlates with worse clinical outcome and with certain histological and clinical characteristics, such as high tumour grade, HER2 positivity and Ki67 proliferation status [37]. In addition, the ALDH1 marker can further divide the $CD44^{+}CD24^{-/low}$ cell population into fractions that are highly tumorigenic: while as few as 20 xenografted $ALDH1^{+}CD44^{+}CD24^{-/low}$ cells resulted in tumours, at this cell density, $ALDH1^{+}CD44^{+}CD24^{-/low}$ cells were not tumorigenic [34, 38]. Taken together, this evidence supports the notion that $ALDH1^{-}CD44^{+}CD24^{-/low}$ cells in a neoplastic population represent CSC-like cells. However, the fraction of $ALDH1^{+}$ cells in the $CD44^{+}CD24^{-/low}$ population in primary tumours is quite small (1.16 %) [34].

Another candidate marker for the BCSC phenotype is CD133, also known as Prominin-1 because of its location on cell membrane protrusions. Although initially considered a marker specific for haematopoietic stem cells, CD133 mRNA transcripts are also found in normal bone marrow and in a variety of other tissues [39]. Furthermore, CD133 is expressed in various solid tumours, including triple-negative invasive breast carcinomas, but more restricted in expression in comparison with other previously mentioned CSC markers, such as CD44 and ALDH1. In early-onset breast cancer 1 (BRCA1)-associated breast cancer cell lines, $CD133^{+}$-sorted cells have CSC properties, including greater colony-forming efficiency, higher proliferative activity and higher tumourigenicity in NOD/SCID mice [40]. Moreover, the expression of CD133 has been reported in the majority of inflammatory breast cancers, as well as in triple-negative tumours [41, 42].

Other markers, such as CD29 (β1-integrin), CD49f (α6-integrin) and CD61 (β3-integrin), have been used for the isolation of mammary CSCs. Vassilopoulos et al. [43] used CD24/CD29 or CD24/CD49f to identify a subpopulation of mammary tumour cells, while Vaillant et al. [44] found that CD61 identifies a cell subpopulation highly enriched for tumorigenic capacity in comparison with CD61-negative cells.

Complementary to the use of biomarkers to identify or isolate putative CSCs, by flow cytometry or immunolabeling using CD44 and CD24 antibodies or ALDH1 activity (using the ALDEFLUOR assay), functional assays have been extensively used for this purpose (Fig. 2). One of these methods is based on the capacity of purported stem cells to

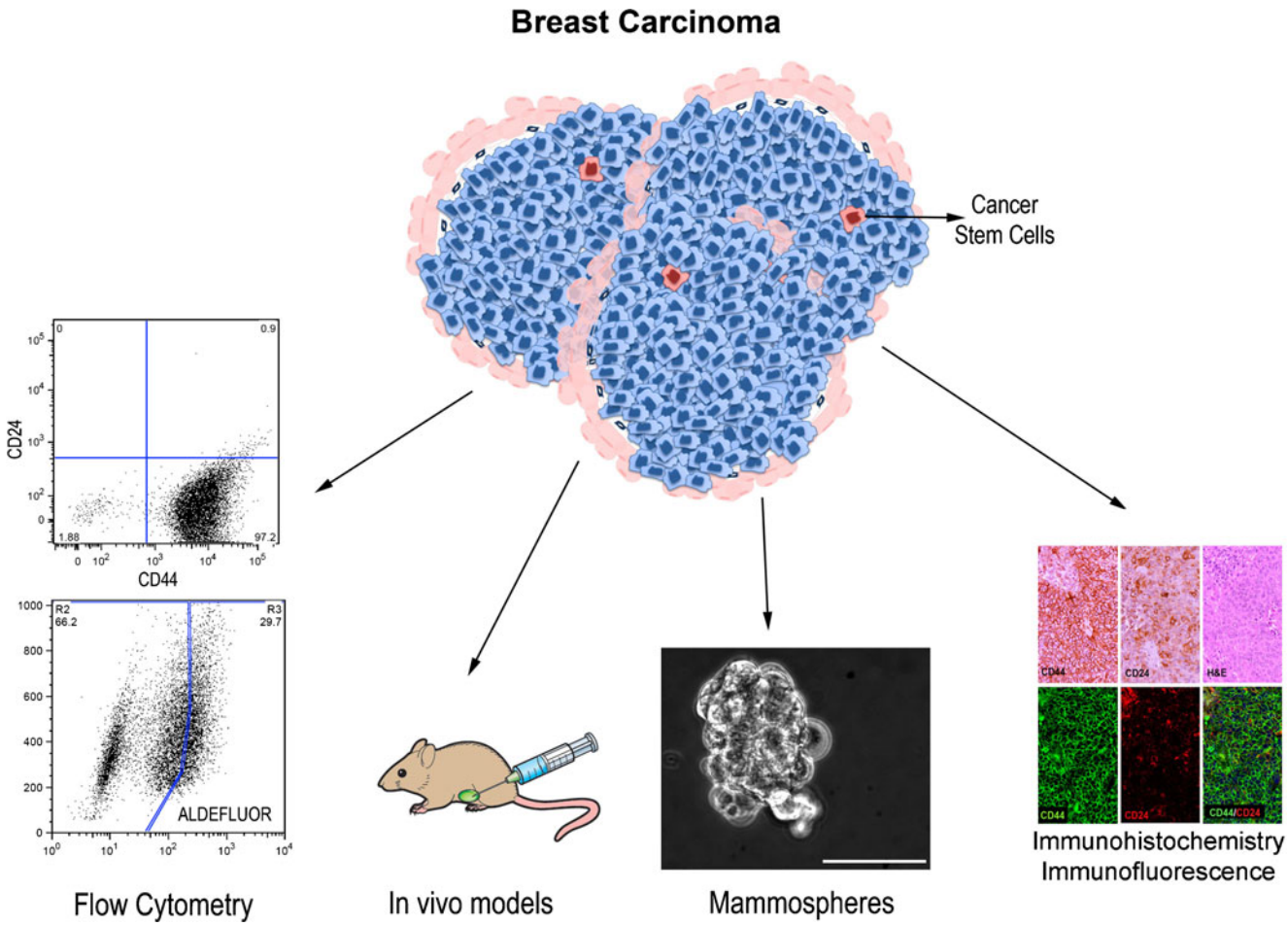

Fig. 2 Breast cancer stem cell identification and/or isolation rely in several breast CSC biomarkers and methodologies, including flow cytometry, in vivo tumorigenic models, mammospheres and histological immunostaining. Flow cytometry allows the identification and isolation of cancer cell subpopulations, using cell surface CSC markers, such as CD44/CD24, and ALDH1 activity (ALDEFLUOR assay). The mammosphere assay measures the survival of cancer cells in anchorage-independent conditions and constitutes an indicator of in vitro self-renewal capacity. Immunohistochemistry or immunofluorescence depend on the use of specific antibodies against breast CSC markers (such as CD44 and CD24), in order to detect the CSC phenotype in fixed paraffin-embedded tissue samples. The tumourigenic capability of CSCs subpopulations in immune-deficient mice allows proving the cancer stem cell properties in vivo (author's original images)

efflux a lipophilic fluorescent dye (Hoechst 33342), through the same mechanism they use to expulse drugs and which confers drug resistance. This dye excluding cell population has been called "side population" (SP). This method was initially described to isolate haematopoietic stem cells and was subsequently applied to breast cancer cell lines [45]. However, unsolved issues with potential toxicity of this dye for non-SP cells hinder the further application of this functional assay for the identification of BCSC subpopulations. Another important functional assay, used for breast epithelial stem cells, is the mammosphere-forming assay, in which mammary epithelial cells are cultured in a serum-free medium on a surface to which they do not adhere and are thus induced to form a three-dimensional cell cluster which is called mammosphere (Fig. 2). Pointi et al. employed a similar approach to derive mammospheres from human breast cancers and found CSCs within the cancer cell-derived mammospheres with the same phenotype as previously reported by Al-Hajj ($CD44^{+}CD24^{-/low}$) [46]. Since then, several other markers associated with a stem cell phenotype, such as components of the Notch and Wnt signalling pathways, have been found overexpressed in mammospheres from breast cancer cell lines [47].

Signalling pathways in breast cancer stem cells

Cancer stem cells share molecular markers with normal stem cells, but in addition, they show aberrant activation of self-renewal pathways, such as Wnt, Hedgehog and Notch, also operative in normal stem cells. Normal human mammary stem cells express high levels of the Notch-4

receptor, which are assumed to play an activating role in the stem cell compartment. Notch-4 and Notch-1 are involved in normal development of the mammary gland and mutated forms of these receptors are associated with the development of mouse mammary tumours [48]. Aberrant activation of Notch signalling is probably an early event in breast cancer, since this has been found in ductal carcinoma in situ (DCIS). High expression of Notch-1 in breast cancer is associated with worse prognosis, and a gamma-secretase inhibitor which blocks Notch signalling or a Notch-4-neutralising antibody reduced mammosphere formation from DCIS [48]. Notch-4 has been shown to be important for the self-renewal of cancer stem cells, and in xenotransplantation assays, it played an active role in tumour formation [49]. The Notch pathway activation and effects are heterogeneous and depend on the cellular context and on the in vivo model used. However, in both man and mice, the Notch pathway stimulates differentiation of mammary stem cells towards the luminal compartment. In man, this luminal cell fate determination is mediated by Notch-3, whereas in mice, Notch-1 seems to be more important [48, 50].

Stem cell self-renewal, maintenance and cell fate are also controlled by Hedgehog signalling in different tissues. In the mammary gland, strict regulation of the Hedgehog pathway is required for normal development and alterations in Hedgehog signalling cause defects during embryonic development resulting in an abnormal mammary gland [51]. Hedgehog signalling is activated in $CD44^{+}CD24^{-/low}$ human breast cancer stem cells [51], and stemness, measured by mammosphere-forming capacity, is increased upon the activation of this pathway [52]. Conversely, inhibition of Hedgehog signalling results in a reduction of the number of mammosphere-initiating cells and mammosphere size, effects that are mediated by Bmi-1 [51], which suggests that the Hedgehog pathway might provide new therapeutic targets.

Elucidation of Wnt signalling is complex, given the fact that there are 19 Wnt ligands, several Wnt receptors and involvement of this signalling pathway in embryogenesis, development, differentiation and proliferation. Inappropriate Wnt/β-catenin signalling can result in deregulated self-renewal. The activation of Wnt-1 causes expansion of the mammary stem cell compartment and an aberrant population of progenitor cells that have in vivo regenerative ability [44, 53]. Since in the presence of inappropriate Wnt signalling mammary glands express high levels of basal markers, Wnt is thought to induce dedifferentiation of mammary cells and confer a more stem-like phenotype. A role for Wnt signalling in the development of breast cancers of the basal-like subtype, and also the predictive capacity of Wnt signalling for brain metastasis, has been reported and the ligands Wnt5a/b have been identified as highly relevant for this subtype of breast cancer [54].

In addition to these main pathways, represented in Fig. 1b, many others have been implicated in the determination of breast stem cell fate. These pathways, when deregulated in cancer, might present new therapeutic targets. Molecules that interfere with these pathways should be tested in vitro with regard to their effect on the CSC compartment, and when found effective, subsequently in in vivo xenografted animal models of human cancer, before testing in patient tumours.

Cancer stem cells in molecular subtypes of breast cancer

In breast cancer, it is assumed that CSCs generate cells with aberrant and limited differentiation, which through mechanisms as yet unknown translate into the distinct breast cancer molecular subtypes. In this concept, each molecular subtype putatively is composed of cancer cells with a different level of differentiation; CSCs being most prevalent in the least differentiated molecular subtype (Fig. 3). Recently, our group demonstrated that of the molecular subtypes, the basal-like type harbours the highest percentage of tumour cells with a $CD44^{+}CD24^{-/low}$ and $ALDH1^{+}$ cancer stem cell phenotype [31]. This confirms earlier studies using breast cancer cell lines, which reported enrichment of $CD44^{+}/CD24^{-/low}$ and $CD44^{-}/CD24^{+}$ cell populations in basal-like and luminal molecular subtypes, respectively [55, 56];

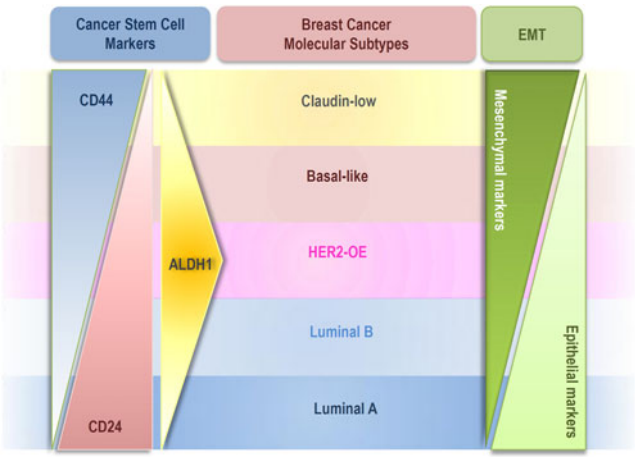

Fig. 3 Representation of the putative association between breast cancer molecular subtypes and the expression pattern of breast CSC biomarkers. In this hypothesis, each molecular subtype is enriched in cancer cells with distinct levels of differentiation, being CSCs more prevalent within the more undifferentiated molecular breast cancers, such as claudin-low tumours. Basal-like tumours have a phenotype close to the CSC phenotype but with an increase in the epithelial phenotype. This subtype of breast cancer and the Her-2 overexpressing molecular subtype have increased ALDH activity, a marker of the luminal progenitor of the breast. Luminal A and luminal B carcinomas present a mature differentiated cell profile, with the lowest expression of mesenchymal markers and an epithelial $CD24^{+}$ phenotype

the $CD44^+$ cells being more stem cell-like and $CD24^+$ cells more differentiated [37]. This is corroborated by data published by Honeth and collaborators, who showed that the $CD44^+/CD24^{-/low}$ CSC phenotype is significantly associated with basal-like breast cancers in human patients and in particular with BRCA1-inherited cancers [29]. However, ALDH1 is not associated with a particular molecular subtype of breast cancer [34, 35]. Even though $CD44^+CD24^{-/low}$ cells and $ALDH1^+$ cells are more frequently found in basal-like than in luminal tumours, $ALDH1^+$ cells are also commonly found in the HER2-overexpressing (HER2-OE) subtype [31]. This difference between basal-like and HER2-OE tumours may be due to a different cell-of-origin or to the induction of a stem-like transcriptional programme as a result of specific transforming genetic alterations (Fig. 3). In line with this notion, induced overexpression of HER2 expression in breast cancer cell lines increased the number of ALDEFLUOR-positive cells [57].

Moreover, basal-like tumours with a predominantly $CD44^+CD24^{-/low}$ CSC phenotype show a tendency towards worse prognosis, in agreement with earlier studies demonstrating an association between basal-like carcinomas and the $CD44^+CD24^{-/low}$ CSC phenotype [29, 37, 55, 56]. These results contribute to our understanding of the morphological and molecular heterogeneity of breast cancer. Furthermore, they suggest that the CSC phenotype may identify the cell-of-origin of the tumour, rather than the unique population of responsible for tumour progression, since the highly aggressive HER2-overexpressing tumours do not show increased expression of these markers.

Since basal type breast cancers have an increased stem cell-like population in comparison with other molecular subtypes, it has been hypothesised that in these tumours, a differentiation block exists, as the majority of the cells constituting the bulk of the tumour do not display a differentiated phenotype [51, 58]. The transformation of a basal-like mammary stem cell to a basal-like cancer cell may either be due to (a) LOH as a second hit in BRCA1 mutation carriers or (b) to the downregulation of BRCA1 expression in estrogen receptor (ER)-negative stem cells. This might result in the arrest of the luminal differentiation process, which fixes the cells in the undifferentiated phenotype of basal-like carcinomas with its unique expression of basal cytokeratins (CK5/6) [59]. Presumably, this goes along with an increment of telomerase activity, since BRCA1 suppresses telomerase expression, and in DNA repair defects, which generate inactivation or loss of the ataxia telangiectasia mutated (ATM) gene and as a result increased genomic instability, which may be the reason for the greater number of genomic gains and losses in sporadic and familial basal-like cancers [60].

Recently, a tumour-initiating cell (TIC) genomic signature, derived from $CD44^+/CD24^{-/low}$-sorted cells and mammospheres obtained from primary human breast tumours, was found to be exclusively enriched in a new molecular subtype referred to as claudin-low [61]. This new molecular subtype is characterised by the low expression of genes involved in tight junctions and cell–cell adhesion, including claudins 3, 4 and 7, Occludin and E-cadherin. It also displays epithelial-to-mesenchymal transition (EMT) features, such as high levels of expression of vimentin, Snail-1, Snail-2, TWIST1, TWIST2, ZEB1 and ZEB2. In addition, these tumours show low expression of luminal genes, inconsistent basal gene expression, high expression of lymphocyte and endothelial cell markers and lack of ER expression, and they were all diagnosed as grade II or III infiltrating ductal carcinomas. These tumour characteristics reflect a low level of tumour differentiation and fit with the CSC and EMT phenotypes [61].

Conclusion

The CSC model proposes that in tumours, like in normal tissues, a cellular hierarchy exists in which CSCs are the only cells endowed with an unlimited potential for proliferation and, as a consequence, capable of driving tumour growth and metastasis due to their stem cell-like characteristics [51]. The presently available markers that label cells with stem cell properties in tumours should be further tested for specificity, and additional markers, maybe in the form of specific gene signatures, are needed to further define and potentially target the CSC population of different breast cancer subtypes. However, in the design of novel effective anti-BCSC therapy strategies, the possibility that (a) marker expression is downregulated/silenced, (b) marker-negative BCSC cell clones evolve from marker-positive cell clones and (c) different BCSC subpopulations coexist in a single tumour or at different metastatic sites should be taken into consideration. Probably, in the future, it will be necessary to use a panel of BCSC markers, in order to effectively translate knowledge of CSCs into breast cancer benefit.

Acknowledgments This work was supported by a grant (project 96633–2010) from Fundação Gulbenkian, Portugal. The authors would also like to acknowledge Fundação Luso Britânica and Fundação para a Ciência e Tecnologia (FCT), Portugal, for fellowship support (A.F.V. was supported by SFRH/BD/41363/2007) and for the Programa Ciência 2007 (J.P.) [POPH-QREN-Tipology 4.2]. The Programme for Advanced Medical Education is sponsored by Fundação Gulbenkian, Fundação Champalimaud, Portuguese Ministry of Science, Technology and Higher Education and FCT, Portugal. IPATIMUP is an Associate Laboratory of the Portuguese Ministry of Science, Technology and Higher Education and is partially supported by FCT.

Conflict of interest We declare that we have no conflict of interest.

References

1. Weigelt B, Geyer FC, Reis-Filho JS (2010) Histological types of breast cancer: how special are they? Mol Oncol 4:192–208
2. Jordan CT, Guzman ML, Noble M (2006) Cancer stem cells. N Engl J Med 355:1253–1261
3. Shackleton M, Quintana E, Fearon ER, Morrison SJ (2009) Heterogeneity in cancer: cancer stem cells versus clonal evolution. Cell 138:822–829
4. Pardal R, Clarke MF, Morrison SJ (2003) Applying the principles of stem-cell biology to cancer. Nat Rev Cancer 3:895–902
5. Al-Hajj M, Wicha MS, Benito-Hernandez A, Morrison SJ, Clarke MF (2003) Prospective identification of tumorigenic breast cancer cells. Proc Natl Acad Sci USA 100:3983–3988
6. Virchow R (1855) Archiv fur Pathologische Anatomie und Physiologie fur Klinische Medizin, Volume 8.
7. Cohnheim V (1875) Congenitales, quergestreiftes Muskelsarkom der Nieren. Virchows Arch Pathol Anat Physiol Klin Med 65:64–69
8. Furth JK, Kahn MC (1937) The transmission of leukemia of mice with a single cell. Am J Cancer 31:276–282
9. Kleinsmith LJ, Pierce GB Jr (1964) Multipotentiality of single embryonal carcinoma cells. Cancer Res 24:1544–1551
10. Pierce GB, Wallace C (1971) Differentiation of malignant to benign cells. Cancer Res 31:127–134
11. Pierce GB, Speers WC (1988) Tumors as caricatures of the process of tissue renewal: prospects for therapy by directing differentiation. Cancer Res 48:1996–2004
12. Lapidot T, Sirard C, Vormoor J, Murdoch B, Hoang T, Caceres-Cortes J, Minden M, Paterson B, Caligiuri MA, Dick JE (1994) A cell initiating human acute myeloid leukaemia after transplantation into SCID mice. Nature 367:645–648
13. Sell S, Pierce GB (1994) Maturation arrest of stem cell differentiation is a common pathway for the cellular origin of teratocarcinomas and epithelial cancers. Lab Invest 70:6–22
14. Bonnet D, Dick JE (1997) Human acute myeloid leukemia is organized as a hierarchy that originates from a primitive hematopoietic cell. Nat Med 3:730–737
15. Blair A, Hogge DE, Ailles LE, Lansdorp PM, Sutherland HJ (1997) Lack of expression of Thy-1 (CD90) on acute myeloid leukemia cells with long-term proliferative ability in vitro and in vivo. Blood 89:3104–3112
16. Singh SK, Hawkins C, Clarke ID, Squire JA, Bayani J, Hide T, Henkelman RM, Cusimano MD, Dirks PB (2004) Identification of human brain tumour initiating cells. Nature 432:396–401
17. Dontu G, Al-Hajj M, Abdallah WM, Clarke MF, Wicha MS (2003) Stem cells in normal breast development and breast cancer. Cell Prolif 36(Suppl 1):59–72
18. Xin L, Lawson DA, Witte ON (2005) The Sca-1 cell surface marker enriches for a prostate-regenerating cell subpopulation that can initiate prostate tumorigenesis. Proc Natl Acad Sci USA 102:6942–6947
19. Kim CF, Jackson EL, Woolfenden AE, Lawrence S, Babar I, Vogel S, Crowley D, Bronson RT, Jacks T (2005) Identification of bronchioalveolar stem cells in normal lung and lung cancer. Cell 121:823–835
20. Orian-Rousseau V (2010) CD44, a therapeutic target for metastasising tumours. Eur J Cancer 46:1271–1277
21. Ponta H, Sherman L, Herrlich PA (2003) CD44: from adhesion molecules to signalling regulators. Nat Rev Mol Cell Biol 4:33–45
22. Tolg C, Hofmann M, Herrlich P, Ponta H (1993) Splicing choice from ten variant exons establishes CD44 variability. Nucleic Acids Res 21:1225–1229
23. Afify A, Purnell P, Nguyen L (2009) Role of CD44s and CD44v6 on human breast cancer cell adhesion, migration, and invasion. Exp Mol Pathol 86:95–100
24. Lim SC (2005) CD24 and human carcinoma: tumor biological aspects. Biomed Pharmacother 59(Suppl 2):S351–S354
25. Aigner S, Ramos CL, Hafezi-Moghadam A, Lawrence MB, Friederichs J, Altevogt P, Ley K (1998) CD24 mediates rolling of breast carcinoma cells on P-selectin. FASEB J 12:1241–1251
26. Kim HJ, Kim JB, Lee KM, Shin I, Han W, Ko E, Bae JY, Noh DY (2007) Isolation of CD24(high) and CD24(low/-) cells from MCF-7: CD24 expression is positively related with proliferation, adhesion and invasion in MCF-7. Cancer Lett 258:98–108
27. Abraham BK, Fritz P, McClellan M, Hauptvogel P, Athelogou M, Brauch H (2005) Prevalence of CD44+/CD24-/low cells in breast cancer may not be associated with clinical outcome but may favor distant metastasis. Clin Cancer Res 11:1154–1159
28. Snyder EL, Bailey D, Shipitsin M, Polyak K, Loda M (2009) Identification of CD44v6(+)/CD24− breast carcinoma cells in primary human tumors by quantum dot-conjugated antibodies. Lab Invest 89:857–866
29. Honeth G, Bendahl PO, Ringner M, Saal LH, Gruvberger-Saal SK, Lovgren K, Grabau D, Ferno M, Borg A, Hegardt C (2008) The CD44+/CD24− phenotype is enriched in basal-like breast tumors. Breast Cancer Res 10:R53
30. Buess M, Rajski M, Vogel-Durrer BM, Herrmann R, Rochlitz C (2009) Tumor-endothelial interaction links the CD44(+)/CD24(−) phenotype with poor prognosis in early-stage breast cancer. Neoplasia 11:987–1002
31. Ricardo S, Vieira AF, Gerhard R, Leitao D, Pinto R, Cameselle-Teijeiro JF, Milanezi F, Schmitt F, Paredes J (2011) Breast cancer stem cell markers CD44, CD24 and ALDH1: expression distribution within intrinsic molecular subtypes. J Clin Pathol 64:937–946
32. Mylona E, Giannopoulou I, Fasomytakis E, Nomikos A, Magkou C, Bakarakos P, Nakopoulou L (2008) The clinicopathologic and prognostic significance of CD44+/CD24(−/low) and CD44-/CD24 + tumor cells in invasive breast carcinomas. Hum Pathol 39:1096–1102
33. Shipitsin M, Campbell LL, Argani P, Weremowicz S, Bloushtain-Qimron N, Yao J, Nikolskaya T, Serebryiskaya T, Beroukhim R, Hu M, Halushka MK, Sukumar S, Parker LM, Anderson KS, Harris LN, Garber JE, Richardson AL, Schnitt SJ, Nikolsky Y, Gelman RS, Polyak K (2007) Molecular definition of breast tumor heterogeneity. Cancer Cell 11:259–273
34. Ginestier C, Hur MH, Charafe-Jauffret E, Monville F, Dutcher J, Brown M, Jacquemier J, Viens P, Kleer CG, Liu S, Schott A, Hayes D, Birnbaum D, Wicha MS, Dontu G (2007) ALDH1 is a marker of normal and malignant human mammary stem cells and a predictor of poor clinical outcome. Cell Stem Cell 1:555–567
35. Morimoto K, Kim SJ, Tanei T, Shimazu K, Tanji Y, Taguchi T, Tamaki Y, Terada N, Noguchi S (2009) Stem cell marker aldehyde dehydrogenase 1-positive breast cancers are characterized by negative estrogen receptor, positive human epidermal growth factor receptor type 2, and high Ki67 expression. Cancer Sci 100:1062–1068
36. Deng S, Yang X, Lassus H, Liang S, Kaur S, Ye Q, Li C, Wang LP, Roby KF, Orsulic S, Connolly DC, Zhang Y, Montone K, Butzow R, Coukos G, Zhang L (2010) Distinct expression levels and patterns of stem cell marker, aldehyde dehydrogenase isoform 1 (ALDH1), in human epithelial cancers. PLoS One 5:e10277
37. Park SY, Lee HE, Li H, Shipitsin M, Gelman R, Polyak K (2010) Heterogeneity for stem cell-related markers according to tumor subtype and histologic stage in breast cancer. Clin Cancer Res 16:876–887
38. Croker AK, Goodale D, Chu J, Postenka C, Hedley BD, Hess DA, Allan AL (2009) High aldehyde dehydrogenase and expression of cancer stem cell markers selects for breast cancer cells with enhanced malignant and metastatic ability. J Cell Mol Med 13:2236–2252
39. Miraglia S, Godfrey W, Yin AH, Atkins K, Warnke R, Holden JT, Bray RA, Waller EK, Buck DW (1997) A novel five-transmembrane

hematopoietic stem cell antigen: isolation, characterization, and molecular cloning. Blood 90:5013–5021
40. Wright MH, Calcagno AM, Salcido CD, Carlson MD, Ambudkar SV, Varticovski L (2008) Brca1 breast tumors contain distinct CD44+/CD24− and CD133+ cells with cancer stem cell characteristics. Breast Cancer Res 10:R10
41. Xiao Y, Ye Y, Yearsley K, Jones S, Barsky SH (2008) The lymphovascular embolus of inflammatory breast cancer expresses a stem cell-like phenotype. Am J Pathol 173:561–574
42. Zhao P, Lu Y, Jiang X, Li X (2011) Clinicopathological significance and prognostic value of CD133 expression in triple-negative breast carcinoma. Cancer Sci 102:1107–1111
43. Vassilopoulos A, Wang RH, Petrovas C, Ambrozak D, Koup R, Deng CX (2008) Identification and characterization of cancer initiating cells from BRCA1 related mammary tumors using markers for normal mammary stem cells. Int J Biol Sci 4:133–142
44. Vaillant F, Asselin-Labat ML, Shackleton M, Forrest NC, Lindeman GJ, Visvader JE (2008) The mammary progenitor marker CD61/beta3 integrin identifies cancer stem cells in mouse models of mammary tumorigenesis. Cancer Res 68:7711–7717
45. Hirschmann-Jax C, Foster AE, Wulf GG, Nuchtern JG, Jax TW, Gobel U, Goodell MA, Brenner MK (2004) A distinct "side population" of cells with high drug efflux capacity in human tumor cells. Proc Natl Acad Sci USA 101:14228–14233
46. Ponti D, Costa A, Zaffaroni N, Pratesi G, Petrangolini G, Coradini D, Pilotti S, Pierotti MA, Daidone MG (2005) Isolation and in vitro propagation of tumorigenic breast cancer cells with stem/progenitor cell properties. Cancer Res 65:5506–5511
47. Rappa G, Lorico A (2010) Phenotypic characterization of mammosphere-forming cells from the human MA-11 breast carcinoma cell line. Exp Cell Res 316:1576–1586
48. Raouf A, Zhao Y, To K, Stingl J, Delaney A, Barbara M, Iscove N, Jones S, McKinney S, Emerman J, Aparicio S, Marra M, Eaves C (2008) Transcriptome analysis of the normal human mammary cell commitment and differentiation process. Cell Stem Cell 3:109–118
49. Harrison H, Farnie G, Howell SJ, Rock RE, Stylianou S, Brennan KR, Bundred NJ, Clarke RB (2010) Regulation of breast cancer stem cell activity by signaling through the Notch4 receptor. Cancer Res 70:709–718
50. Bouras T, Pal B, Vaillant F, Harburg G, Asselin-Labat ML, Oakes SR, Lindeman GJ, Visvader JE (2008) Notch signaling regulates mammary stem cell function and luminal cell-fate commitment. Cell Stem Cell 3:429–441
51. Charafe-Jauffret E, Monville F, Ginestier C, Dontu G, Birnbaum D, Wicha MS (2008) Cancer stem cells in breast: current opinion and future challenges. Pathobiology 75:75–84
52. Moraes RC, Zhang X, Harrington N, Fung JY, Wu MF, Hilsenbeck SG, Allred DC, Lewis MT (2007) Constitutive activation of smoothened (SMO) in mammary glands of transgenic mice leads to increased proliferation, altered differentiation and ductal dysplasia. Development 134:1231–1242
53. Shackleton M, Vaillant F, Simpson KJ, Stingl J, Smyth GK, Asselin-Labat ML, Wu L, Lindeman GJ, Visvader JE (2006) Generation of a functional mammary gland from a single stem cell. Nature 439:84–88
54. Klemm F, Bleckmann A, Siam L, Chuang HN, Rietkotter E, Behme D, Schulz M, Schaffrinski M, Schindler S, Trumper L, Kramer F, Beissbarth T, Stadelmann C, Binder C, Pukrop T (2011) β-catenin-independent WNT signaling in basal-like breast cancer and brain metastasis. Carcinogenesis 32:434–442
55. Fillmore CM, Kuperwasser C (2008) Human breast cancer cell lines contain stem-like cells that self-renew, give rise to phenotypically diverse progeny and survive chemotherapy. Breast Cancer Res 10:R25
56. Sheridan C, Kishimoto H, Fuchs RK, Mehrotra S, Bhat-Nakshatri P, Turner CH, Goulet R Jr, Badve S, Nakshatri H (2006) CD44+/CD24− breast cancer cells exhibit enhanced invasive properties: an early step necessary for metastasis. Breast Cancer Res 8:R59
57. Korkaya H, Paulson A, Iovino F, Wicha MS (2008) HER2 regulates the mammary stem/progenitor cell population driving tumorigenesis and invasion. Oncogene 27:6120–6130
58. Charafe-Jauffret E, Ginestier C, Monville F, Finetti P, Adelaide J, Cervera N, Fekairi S, Xerri L, Jacquemier J, Birnbaum D, Bertucci F (2006) Gene expression profiling of breast cell lines identifies potential new basal markers. Oncogene 25:2273–2284
59. Liu S, Ginestier C, Charafe-Jauffret E, Foco H, Kleer CG, Merajver SD, Dontu G, Wicha MS (2008) BRCA1 regulates human mammary stem/progenitor cell fate. Proc Natl Acad Sci USA 105:1680–1685
60. Tommiska J, Bartkova J, Heinonen M, Hautala L, Kilpivaara O, Eerola H, Aittomaki K, Hofstetter B, Lukas J, von Smitten K, Blomqvist C, Ristimaki A, Heikkila P, Bartek J, Nevanlinna H (2008) The DNA damage signalling kinase ATM is aberrantly reduced or lost in BRCA1/BRCA2-deficient and ER/PR/ERBB2-triple-negative breast cancer. Oncogene 27:2501–2506
61. Hennessy BT, Gonzalez-Angulo AM, Stemke-Hale K, Gilcrease MZ, Krishnamurthy S, Lee JS, Fridlyand J, Sahin A, Agarwal R, Joy C, Liu W, Stivers D, Baggerly K, Carey M, Lluch A, Monteagudo C, He X, Weigman V, Fan C, Palazzo J, Hortobagyi GN, Nolden LK, Wang NJ, Valero V, Gray JW, Perou CM, Mills GB (2009) Characterization of a naturally occurring breast cancer subset enriched in epithelial-to-mesenchymal transition and stem cell characteristics. Cancer Res 69:4116–4124

Virchows Arch (2012) 460:555–567
DOI 10.1007/s00428-012-1244-9

REVIEW AND PERSPECTIVES

Macrophage-related diseases of the gut: a pathologist's perspective

Xavier Sagaert · Thomas Tousseyn · Gert De Hertogh · Karel Geboes

Received: 8 December 2011 / Revised: 15 March 2012 / Accepted: 26 April 2012 / Published online: 11 May 2012
© Springer-Verlag 2012

Abstract The resident macrophages of the gastrointestinal tract represent the largest population of macrophages in the human body and are usually located in the subepithelial lamina propria. This strategic location guarantees a first-line defense to the huge numbers of potentially harmful bacteria and antigenic stimuli that are present in the intestinal lumen. In non-inflamed mucosa, macrophages phagocytose and kill microbes in the absence of an inflammatory response. However, in the event of an epithelial breach and/or microbial invasion, new circulating monocytes and lymphocytes will be recruited to the damaged area of the gut, which will result in the secretion of proinflammatory mediators and engage a protective inflammatory response. Although macrophages are usually not conspicuous in normal mucosal samples of the gut, they can easily be detected when they accumulate exogenous particulate material or endogenous substances or when they become very numerous. These events will mostly occur in pathologic conditions, and this review presents an overview of the diseases which are either mediated by or affecting the resident macrophages of the gut.

Keywords Macrophages · Gut · Lysosomal disease · Infectious disease

X. Sagaert · T. Tousseyn · G. De Hertogh · K. Geboes
Department of Pathology UZ Leuven,
Leuven, Belgium

X. Sagaert (✉)
Department of Pathology, University Hospitals Leuven,
Minderbroederstraat 12,
3000 Leuven, Belgium
e-mail: xavier.sagaert@uzleuven.be

Introduction

Macrophages are ubiquitous in the mucosa of the digestive tract, but they are usually not conspicuous in normal mucosal samples of the colon. As all other tissue macrophages, they are derived from bone marrow stem cells through a very complex cascade of differentiation events, that amongst others, requires the presence of interleukin (IL)-1, IL-3, and IL-6 [1, 2]. Once they migrate into the gut, they are normally found in the upper part of the lamina propria, underneath the superficial small blood vessels just below the subepithelial collagen layer, where they are part of the first-line defense mechanism of the mucosa against harmful pathogens (referred to collectively as the innate immune system). Uniquely, resident macrophages of the gut are inflammation anergic as they will not induce an inflammatory response upon pathogen encounter [3]. In order to maintain their low-profile immune effector role, gut macrophages prominently display germline-encoded transmembrane Toll-like receptors as well as the cytosolic NOD-like receptors but do not express receptors for immunoglobulins or lipopolysaccharides [4, 5]. In the event of damage of the intestinal epithelium (e.g., infection, inflammatory bowel disease), circulating monocytes as well as B- and T-lymphocytes will join the resident macrophages of the gut and actively pursue the invading pathogens through phagocytosis and release of inflammatory mediators, resulting in neutralization and degradation of the harmful pathogen [5]. Importantly, in healthy mucosal conditions, the resident macrophages of the gut will continuously be replenished through the recruitment of new circulating monocytes into the gastrointestinal mucosa [6].

The cytoplasm of the macrophages commonly contains dense inclusions of varying sizes and shape, which explains a weak cytoplasmic positivity with Periodic Acid Schiff

(PAS) staining [7]. Immunohistochemical studies have shown that the macrophages of the gut express a variety of markers at their cell surface. They usually display the marker CD68, a heavily glycosylated, 110-kDa membrane protein, which can be highlighted with the monoclonal antibodies KP1 or PGM1 [8]. Although the biological function of CD68 has not been fully defined, it serves as a scavenger receptor for oxidized low density lipoproteins and may also be involved in cell–cell interactions [9–11]. Also, macrophages of the gut frequently show membranous positivity for HLA-DR (major histocompatibility class II), hereby reflecting their ability to present antigenic peptides to helper T-lymphocytes. In addition to CD68 and HLD-DR, macrophages can also show a positive staining pattern with antibodies directed against S100, the latter being a protein involved in regulation of numerous cell processes (protein phosphorylation, transcription factors, calcium homeostasis, the dynamics of cytoskeleton constituents, enzyme activities, cell growth and differentiation, and the inflammatory response) [12]. Some of the resident gut macrophages also have a strong membrane adenosine triphosphatase activity but weak acid phosphatase while others, especially in the colon, have a strong acid phosphatise activity [13].

Although mostly unnotified in routine histologic sections of normal gastrointestinal mucosa, macrophages of the gut are easily identified when exogenous particulate material (lipofuscin, hemosiderin, atmospheric dust) or endogenous material (mucin, glycogen, lipids) accumulate or when they become very numerous. These events will mostly occur in pathologic conditions, and this review presents an overview of the diseases which are either mediated by or affecting the resident macrophages of the gut.

Accumulation of exogenous material: pigmented macrophages

Melanosis coli, also called pseudomelanosis coli, is a pigmentation disorder of the colon wall, often identified at the time of endoscopy as a brownish discoloration in a moire pattern of the mucosa. The name *melanosis coli* is a misnomer, since the brown pigment is actually lipofuscin in macrophages, not melanin as the name implies (Fig. 1a, b). The most common cause of melanosis coli is the extended use of laxatives and commonly anthraquinone containing laxatives such as Senna and other plant glycosides [14]. However, other causes are identified, including an increase in colonic epithelial apoptosis. On biopsy, melanosis coli shows characteristic pigment-laden macrophages within the mucosa.

Hemosiderin-containing macrophages are highlighted by Perls iron staining and can be seen following hemorrhage and breakdown of red blood cells, after iron-ingestion, in gastric biopsies from alcoholics and in hemochromatosis (Fig. 1c, d). In a series of 500 patients with gastric biopsies, deposition of iron was found in 3.6 % of the cases with the Prussian blue stain [15]. Three patterns of siderosis were identified: (1) predominant deposition in stromal cells and in focal epithelial cells; (2) extracellular deposition, with focal deposition in stromal and epithelial cells; and (3) predominant deposition in antral and fundic glandular epithelium. The latter pattern is common in hemochromatosis. With iron ingestion, dark brown/green pigmentation can be seen on the surface of the epithelium in the oesophagus, the stomach and the small bowel in association with iron-containing macrophages in the lamina propria. Hemosiderin-laden macrophages are also occasionally seen in the lamina propria in the small intestine and colon following hemorrhage or ischemia. In the colon, they are further noticed in internal mucosal prolaps, in diverticular disease, endometriosis, and in hyperplastic, Peutz–Jeghers and adenomatous polyps with epithelial misplacement or pseudo-invasion [15–18].

Atmospheric dust can be found particularly in macrophages associated with Peyer's patches in the small intestine. It was observed as a dark brown granular pigment in all patients over the age of 6 years in two independent series (34 and 42 cases) [19, 20]. The macrophages are situated at the base of the human gut associated lymphoid tissue (GALT) [21]. They appear dark brown or black because of the pigment that is rich in aluminium, silicon, and titanium. Morphological and X-ray microanalysis and spectroscopy show three distinct types of microparticles: spheres of titanium dioxide, aluminosylicates, and mixed environmental silicates. Thus, the pigment seems partly derived from food additives and partly from the environment. It is most likely sampled by the microfold cells (so called M cells) overlying the Peyer's patches [21]. The pigment can also be found in the stroma around dilated submucosal lymphatics, in some transmural inflammatory aggregates, and in mesenteric lymph nodes. This occurs in both normal subjects and patients with a variety of diseases. The pathogenicity of this pigment is unclear. Titanium dioxide may possess proinflammtory and membranolytic activity but whether this is involved in the development of human disease needs further investigation.

Occasionally and without any clinical significance, accumulation of bile pigment can be observed in solitary macrophages in the lamina propria of the colon.

Accumulation of endogenous material: foamy macrophages

Accumulation of large clear cells in the intestinal lamina propria is mostly due to the storage of endogenous material

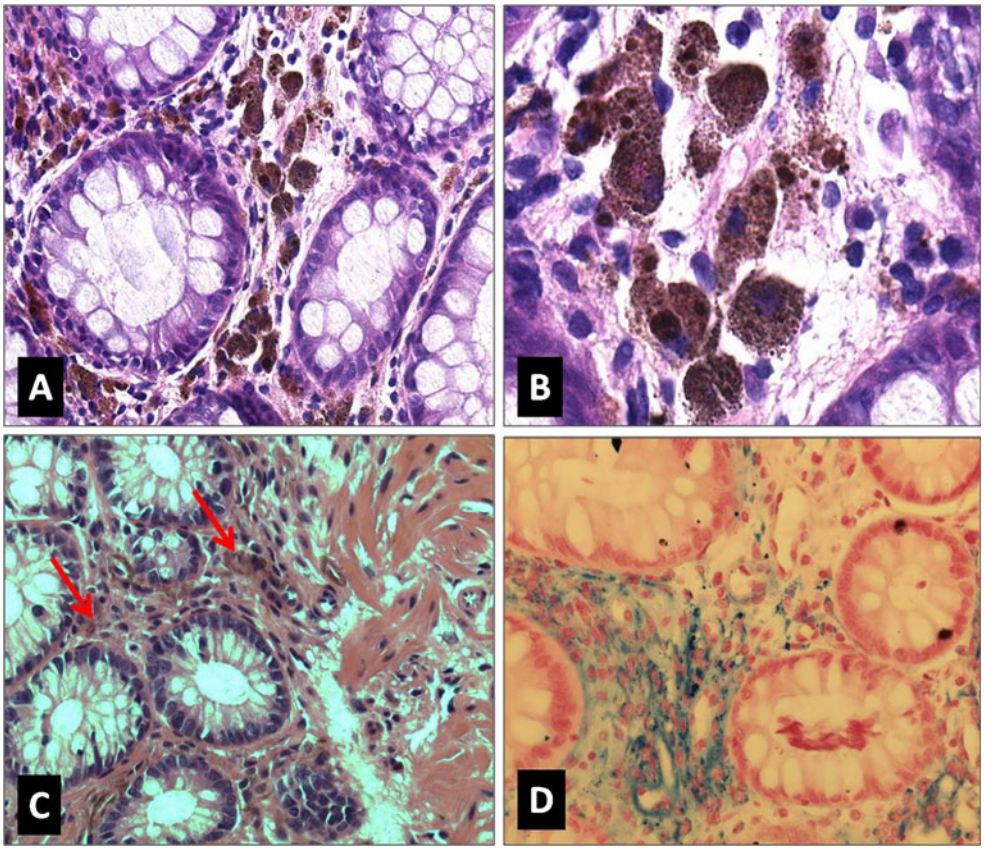

Fig. 1 Pigmented macrophages. **a** Hematoxylin eosin (HE) staining of a colonic biopsy with (pseudo)melanosis coli (magnification 400×); **b** HE staining of lipofuscin containing macrophages in (pseudo)melanosis coli (magnification 1,000×); **c** HE staining of a colonic biopsy with hemosiderin-containing macrophages, marked by the *arrows* (magnification 400×); **d** Perls iron staining highlights the hemosiderin-containing macrophages (*blue staining pattern*) in a patient with hemochromatosis (magnification 400×)

in the cytoplasm of macrophages. The nature of this intracellular material is very variable: the deposits may be microorganisms (e.g., Whipple's disease), normal mucins or lipids (as seen in low grade injury of the gut), or abnormal glycoproteins or glycolipids (as observed in "Metabolic disorders" section) (Table 1). In the presence of unusual aggregates of macrophages, sections should therefore be examined with a wide range of techniques, including stainings such as the PAS reaction and Oil-red O or Sudan black for lipids, in order to identify the nature of the stored material. Because the stored materials may be lipids of one type or another, frozen sections are often necessary as fat is usually dissolved out of the tissues during dehydration or paraffin embedding. Transmission electron microscopy (TEM) remains also an important tool for confirmation and morphological identification of the stored material. Occasionally, the presence of multiple foamy macrophages must be differentiated from mastocytosis by immunohistochemistry; although they may look histologically the same, foamy macrophages will be CD68 positive while mast cells will be tryptase positive.

Muciphages

Isolated foamy mucin containing histiocytes (muciphages) may be observed in the normal mucosa. They are diffusely distributed in the superficial lamina propria or in the basal mucosa and difficult to recognize without special stains. They may aggregate with other inflammatory cells. They usually contain neutral, weakly acidic, or strongly acidic mucin. The main type of acidic mucin is sialomucin [22, 23]. The majority of muciphages show a strong diffuse red to magenta pattern of PAS staining in the cytoplasm. The presence of these cells has been called "colon histiocytosis" but in our opinion, this term should be avoided, as muciphages are diagnostically non-specific. Small collections of these cells are seen in a large number of rectal biopsies (40–68 %) taken for a variety of reasons including diseases such as chronic idiopathic inflammatory bowel diseases and graft versus host disease [24]. They are more easily recognizable when they aggregate and become enlarged. In 25 out a series of 40 cases, variable-associated histologic changes were found such as epithelial regeneration, hyperplasia, and mild chronic inflammation, which may indicate that the presence of the muciphages is related to injury [25]. Overall, it seems thus that increase of macrophages is mainly seen in the terminal phase of repair after previous injury and/or in situations of low grade injury.

Xanthelasma

Aggregates of foamy histiocytes in biopsies can also occur in xanthomatous lesions. A xanthelasma is a 1–2-mm collection of foamy macrophages. Xanthomatosis

Table 1 Differential diagnosis of macrophages in the colon

Material in macrophages	Disorder	Staining pattern
Pigmented macrophages:accumulation of endogenous material		
Lipofuscin	Melanosis coli	PAS+
	Increased apoptosis	Melanin–
Hemosiderin	Mucosal hemorrhage	Iron+
	Metabolic storage disorder (hemochromatosis)	
Atmospheric dust		
Foamy macrophages: accumulation of exogenous material		
Microörganisms	Whipple's disease	PAS+, diastase PAS+
	Mycobacterium avium	Ziehl+
	Rhodococcus equi	
	Pneumocystis carinii	Grocott+
	Leishmaniasis	
	Histoplasmosis	
Mucins	Low grade injury (IBD, GVHD)	PAS+, mucicarmine+
	Terminal injury	alcian blue+
Abnormal glycoproteins/glycolipids	Lysosomal storage disease	PAS+
		Oil-red-O+
		Electron microscopy+
	Gangliosidoses	
Drugs		

is characterized by the presence of nodules or plaques which develop through the accumulation of foamy macrophages in the tissue, particularly in the mucosa. Occasionally, such a lesion can become pseudo-tumoral and induce symptoms. Accumulations of macrophages may have an impact on intestinal motility leading to ileus [26–28]. These conditions must not be confused with accumulation of lipid, pseudolipomatosis, or accumulation of histiocytes without a visible lesion. Another condition which has been reported is "multiple lipid islands" of the colonic mucosa. The condition is rare and appears as small, xanthomatous foci. Lipid is also accumulated in various other cell types including smooth muscle cells, histiocytes, pericytes, and enteroglia. Patients can have abdominal complaints which are probably not related to the accumulation of lipids. Therefore, the term "lipid proctitis" which has also been proposed for these condition may not be appropriate [29, 30]. Overall, it is however our impression that these so called "lipid islands" represent a variant of xanthomatosis.

Infectious diseases

Accumulation of foamy macrophages can also be seen in infections such as Whipple's disease, *Mycobacterium avium*, *Rhodococcus equi*, extrapulmonary pneumocystosis, leishmaniasis, and histoplasmosis.

Whipple's disease is a rare chronic disease initially presenting with weight loss, diarrhea, abdominal pain and arthralgia, but with the risk of malabsorption, neurological symptoms, and cardial complications when persisting [31, 32]. It predominantly affects middle-ages men, and is caused by the rod-shaped bacterium *Tropheryma whipplei.* Despite the ubiquitous natural occurrence of *T whipplei*, Whipple's disease is very rare and is generally not associated with other infections, hereby ruling out a major defective immune response. However, it was shown that intestinal macrophages in patients with Whipple's disease do have an impaired function. First, they are not able to degrade intracellular proteins and DNA from pathogens such as *Escherichia coli*, *Streptococcus pyogenes*, and *Candida tropicalis* (probably due to reduced CD11b expression) [33–35]. Second, they favor in vivo the development of a T-helper-2 response instead of a protective T-helper-1 response, as phytohemagglutinin-stimulated peripheral blood mononuclear cells from patients with Whipple's disease are characterized by a lower production of interferon-γ (IFN-γ) while interleukin (IL)-4 levels are increased, compared to controls [36]. Last, macrophages in Whipple's disease are characterized by a reduced production of IL-12 in response to *Staphylococcus aureus* or lipopolysaccharide in combination with IFN-γ, despite they retain their ability to produce normal levels of tumor necrosis factor [34, 37]. In Whipple's disease, the foamy macrophages (containing the intracellar pathogen) usually appear as a diffuse infiltration in the lamina propria of the

small intestine (Fig. 2a), although a more localized and even polypoid appearance has been noted. Whipple's disease of the colon is absolutely rare [38]. The presence of micro-organisms can be confirmed in endoscopic intestinal (duodenal) biopsies by both PAS staining (which will highlight PAS positive cytoplasmic inclusion in the foamy macrophages, representing the causative bacteria; Fig. 2b) and TEM. However, PAS staining remains nonspecific as PAS-positive macrophages are also seen in association with other infectious agents. As such, immunohistochemistry using *T. whipplei*-specific antibodies improves histological examination, and also polymerase chain reaction (PCR) may confirm the very nature of *T. whipplei* [39, 40]. Other diagnostic methods are limited to few reference laboratories and include cultivation and serology. All cases of Whipple's disease are treated with a prolonged antibiotic treatment, although the duration of treatment is not yet established [32, 41, 42].

T. whipplei is a distant relative of *M. avium-intracellulare*, and *Mycobacterium paratuberculosis* explaining in part why the clinicopathological presentation of Whipple's disease is similar to the diseases caused by these bacteria (Fig. 2c) [43, 44]. Ziehl staining may help in the differential diagnosis to confirm the presence of mycobacteria within the macrophages (Fig. 2d). Mycobacteria are environmental pathogens that predominantly enter the body through the gut via contaminated water or food. They can also enter the lungs by inhalation of liquid droplets. Mycobacteria cross the gut cell barrier either via active transport through M cells in the Peyer's patches of the small intestine or by receptor-mediated endocytosis into gut-lining epithelial cells. Macrophages are the preferred target cells of mycobacteria. Transport through M cells delivers mycobacteria directly to macrophages in the Peyer's patches of the small intestine, whereas receptor-mediated endocytosis of mycobacteria by gut epithelial cells leads to phagocytosis of bacteria by lamina propria macrophages. Phagocytosis by macrophages internalizes the Mycobacteria in a membrane-bound phagosome. Under normal conditions, the phagosome fuses with a lysosome containing degradative molecules to form a phagolysosome in which the bacteria are killed. However, pathogenic mycobacteria such as *Mycobacterium tuberculosis* and *M. avium-intracellulare* have developed mechanisms to prevent the fusion of lysosomes with phagosomes [45], resulting in survival and multiplication of the Mycobacteria in the phagosome, and in spread to other body parts when the macrophages migrate to other tissues. In immunocompetent hosts, prevention of this mycobacterial spread is achieved by the formation of a granuloma [46]. A granuloma sequesters infected macrophages in the center, surrounded by immune cells, predominantly CD4+ helper T lymphoctes. The fusion of infected macrophages to form

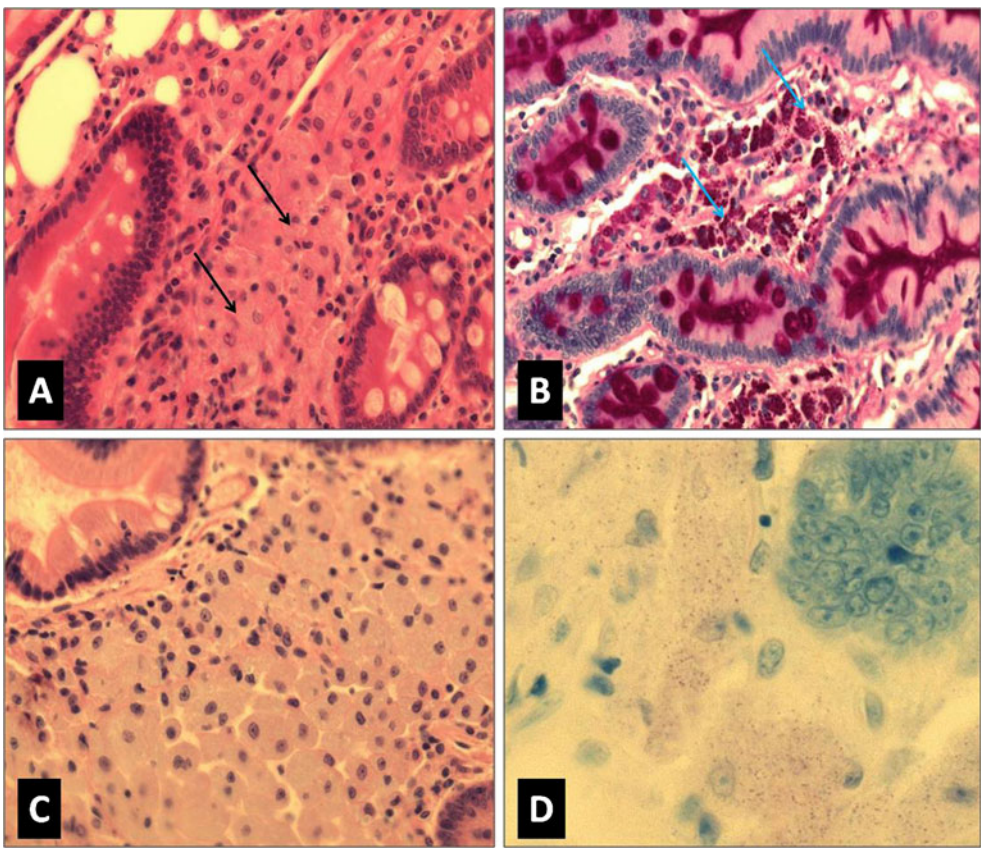

Fig. 2 Foamy macrophages in infectious diseases. **a** HE staining of a duodenal biopsy from a patient with Whipple's disease : multiple foamy macrophages, marked by *arrows*, are present (magnification 400×); **b** PAS staining confirms the presence of *Tropheryma whipplei* micro-organisms within the macrophages (marked by *arrows*) in the duodenal biopsy (magnification 1,000×); **c** HE staining of a colonic biopsy from a patient infected with *Mycobacterium avium-intracellulare* reveals accumulation of foamy macrophages (magnification 400×); **d** Ziehl staining highlights the presence of *Mycobacterium avium-intracellulare* micro-organisms within the foamy macrophages (magnification 1,000×)

foamy macrophage giant cells is thought to result from the release of mycolic acid products from infected cells. Later, the center of the granuloma may be filled with cell debris and live mycobacteria spilled from dead macrophages (caseation), and this poses a risk of spread if the granuloma ruptures. A sheath of collagen fibers produced by fibroblasts surrounds the cells inside. In immunodeficient patients, no granulomas are formed. The diagnosis of a gastrointestinal mycobacterial infection is often delayed and is usually made through a combination of radiologic, endoscopic, microbiologic, histologic, and molecular techniques. Antimicrobial treatment is the same as for pulmonary tuberculosis, although surgery is occasionally required [47, 48].

The soil actinomycete *R. equi* is a veterinary pathogen, originally isolated from horse lungs, that can cause substantial morbidity in patients that are both immunocompromised and occupationally or recreationally exposed to livestock and farming environments [49]. Only about 10–15 % of all *R equi* infections happens in the absence of any known immune compromise such as AIDS or organ transplants [50]. Although pulmonary involvement is a predominant feature in about 80 % of cases, the clinical spectrum of disease associated with *R. equi* (including gastrointestinal manifestations) is broad. As a facultative intracellular bacterium, *R. equi* survives and multiplies in macrophages and establishes its specific niche inside the host cell. Part of the virulence of *R. equi* is contributed to its ability to survive in macrophages, probably due to inadequate acidification of phagolysosomes [51, 52]. Little data are available on the immune response against *R. equi*, but in mice models. a T-helper-1 response is more protective against the pathogen than a T-helper-2 response, which may partly explain why patient with defective cell-mediated immune response are at risk [53–55]. Because *R. equi* is an unusual human pathogen, little systematic information is available on its treatment. Case studies suggest that infection can be managed by antibiotics alone, although surgical management might be beneficial for debulking of extensive disease [49]. Importantly, as immunosuppressive regimens used in settings of organ transplantation and treatment of chronic medical conditions become more widespread, knowledge of this organism becomes paramount to appropriate diagnosis and management of opportunistic infections in this population of patients. As such, endoscopic biopsies of the gut of an immunocompromised patient that reveal the presence of foamy macrophages with intracellular coccobacillary PAS-positive forms should make one suspicious of a possible *R. equi* infection.

Gastrointestinal pneumocystosis only occurs in an immunocompromised setting (AIDS, organ transplant) and is rarely encountered as compared to pulmonary pneumocystosis or other opportunistic infections. In recent years, however, the number of reported cases of extrapulmonary pneumocystosis has increased [56]. Several factors may be responsible for this increase. First, the increased longevity of AIDS patients may have increased the number of cases seen [57]. Second, it has been speculated but by no means proven, that strains of *Pneumocystis carinii* with different virulence factors may be responsible [57]. Third, some authors have argued that the use of aerosolized pentamidine for *P. carinii* pneumonia prophylaxis increases the likelihood of developing extrapulmonary pneumocystosis [58]. It is therefore important for physicians to recognize the various presentations, such as gastrointestinal symptoms of extrapulmonary *P. carinii* infection, which may be a clinical history of chronic diarrhea with accumulations of foamy macrophages in the endoscopic intestinal biopsies. PCR remains the gold standard to confirm the presence of *P. carinii* in the tissue.

Leishmaniasis, a vector-borne disease that is caused by obligate intra-macrophage protozoa and spread by female phlebotomine sandflies, is endemic in the (sub)tropics and around the Mediterranean. Its clinical modes of presentation can be divided into three main types: cutaneous leishmaniasis (which is mostly self-limiting), mucosal leishmaniasis (also known as espundia), and visceral leishmaniasis (also known as kala-azar, which is Hindi for black sickness or fever and which may affect the gut). In about 50 % of immunocompetent patients with visceral leishmaniasis, the protozoa will be present in the gut. Visceral leishmaniasis confined to the gut alone tends to occur in AIDS settings and is highly unusual in immunocompetent individuals with only few cases reported in literature [59, 60]. When microscopically encountering collections of foamy macrophages with PAS-positive cytoplasmatic inclusions in gut biopsies of a patient with an unidentified disease, one always has to think of visceral leishmaniasis. Diagnosis has to be confirmed either by visualization of the amastigote form of the parasite (in the gut biopsy and/or in aspirates from the bone marrow or lymph nodes) or by a serological antibody-detection test [61]. Importantly, the detection of parasites in blood or organs by culture or by using molecular techniques such as PCR is more sensitive than microscopic examination, but these techniques remain restricted to referral hospitals and research centres, despite efforts to simplify them [62]. The introduction of miltefosine and paromycin as well as the reduction in cost of liposomal amphotericin B have meant a breakthrough in the treatment of visceral leishmaniasis [63].

Involvement of the gut is very common in histoplasmosis: the causative organism, *Histoplasma capsulatum*, can be identified in the gastrointestinal tract of 70–90 % of patients with progressive disseminated histoplasmosis who undergo an autopsy [64–66]. However, gastrointestinal disease due to *H. capsulatum* is rarely recognized during life and is thought to cause clinical symptoms in only 3–12 % of

patients [67, 68]. This discrepancy raises the suspicion that histoplasmosis of the gut is an underdiagnosed entity, as symptoms may be nonspecific and histoplasmosis may not be considered in the differential diagnosis. This is an important issue to address, because the disease can have catastrophic consequences if diagnosis and treatment are delayed. Histoplasmosis of the gut can present in many ways, depending on whether the gut is involved as part of progressive dissemination of the infection, or as a result of local complications due to the infection and/or the healing process [69]. Both immunocompetent and immunocompromised patients can be affected, particularly individuals with AIDS, as was first reported in 1984 [68]. The small, 2–4 μm in diameter, uniform, ovoid-to-spherical organisms are often present in clusters within the cytoplasm of macrophages as seen on an hematoxylin eosin (HE) staining. The basophilic cytoplasm of *H. capsulatum* retracts from the relatively thin cell wall, hereby leaving a clear area or "halo-like" zone around the organism. The Gomori (Grocott) methenamine silver is usually the best special stain for demonstrating *H. capsulatum* in tissue. In addition, direct antigen detection in the blood or urine provides a rapid method for the diagnosis of disseminated histoplasmosis [67, 69]. The preferred treatment options vary with clinical scenario and severity of illness [70].

Non-typhoidal Salmonella serotypes are a leading cause of acute food borne disease worldwide. In immunocompetent individuals, they are associated with gastroenteritis, a localized infection of the terminal ileum and colon that manifests as fever, diarrhea, and intestinal cramping. However, a breach of mucosal barrier functions in immunocompromised individuals can result in the development of a life-threatening bacteremia. The most common human clinical isolates are *Salmonella enterica* serotypes *typhimurium* (*Salmonella typhimurium*) and *enteritidis* (*Salmonella enteritidis*) [71]. *Salmonella* serotypes are able to trigger intestinal inflammation and actively cross the intestinal epithelium, mainly but not exclusively through M cells in the follicle-associated epithelium of Peyer's patches. Once reaching the basal side of the epithelium, *Salmonella* serotypes are internalized by and survive in macrophages, dendritic cells, and neutrophils. The outcome of the interaction between *Salmonella* serotypes and dendritic cells or neutrophils is detrimental to the pathogen. In some hosts, Salmonella serotypes find a safe haven from humoral defenses and neutrophils within macrophages, and replication within this niche appears to be a prerequisite for the development of a systemic infection. In other hosts, macrophages can control bacterial growth and the infection remains localized to the intestine and mesenteric lymph nodes. Treatment with antibiotics will depend on severity of the disease and the clinical context (immunocompetent versus immunodeficient).

Although less frequently affected as compared to bacterial infections, macrophages may also be involved in viral infections such as CMV and HIV. CMV-gastritis, -enteritis, or -colitis may present with bleeding or ulceration and may cause necrotizing injury and perforation. It typically occurs in the clinical context of immunosuppression or AIDS and usually reflects disseminated infection. The inflammatory lesion in CMV gastro-entero-colitis shares features with CMV lung and retinal disease, including the presence of large viral inclusions (in macrophages, endothelial cells, fibroblasts, and smooth muscle cells), accumulation of mononuclear inflammatory cells, and tissue necrosis, suggesting a common pathogenesis involving the migration of blood mononuclear cells latently infected with CMV to tissue sites. Patients with HIV-gastritis, -enteritis, or -colitis mostly present with diarrhea and/or malabsorptive symptoms with or without other AIDS features such as Kaposi sarcoma. Histologically, the affected bowel will display atypical features, such as villus atrophy or colitis resembling ulcerative colitis. Importantly, one can only establish a diagnosis of HIV-gastritis, -enteritis, or -colitis when other possible infectious organisms have been ruled out.

Metabolic disorders

Metabolic disorders are the second clinically most important but rare cause for the accumulation of foamy macrophages. Functionally, the inborn metabolic disorders can be divided into three major groups: (a) disorders that give rise to intoxication such as errors of amino acid metabolism and metal intoxication such as hemochromatosis (see pigmented macrophages); (b) disorders involving energy metabolism such as disorders of glycolysis, glycogen metabolism, and gluconeogenesis, and (c) disorders involving complex molecules and cellular organelles. Group (a) diseases give rise to an acute or chronic intoxication. Lysosomal diseases and peroxisomal disorders belong to group (c) inborn errors of metabolism. In these conditions, symptoms are permanent, progressive, independent of intercurrent events, and unrelated to food intake. More than 40 lysosomal disorders are known. They are the main storage disorders. They are monogenic inborn errors of metabolism, caused by a defect of one or more enzymes involved in intracellular catabolism or in rare conditions such as cystinosis by a lysosomal membrane transport disorder. In the absence of the enzyme, the specific substrates accumulate in the cell which results in dysfunction. Accumulation of undegraded substrates in lysosomes due to the enzyme deficiency impairs the fusion between autophagosomes and lysosomes. This, in turn, leads to a progressive accumulation of poly-ubiquinated protein aggregates and of dysfunctional mitochondria. Accumulation of substrates may occur in different cell types including neurons,

endothelial cells, and macrophages. The stored substances are generally lipids and thus identification by morphology implies freshly frozen tissue. The precise diagnosis is based on biochemical tests. The individual storage diseases are rare, but the overall prevalence of these disorders is 1/6,000 births. In most of the disorders, the transmission is autosomal recessive. Exceptions to this are Fabry's and Hunter's disease which are X-linked recessive.

Lysosomal diseases can be classified according to the affected pathway and the specific substrate which is accumulated and new entities are still being identified. The major groups are sphingolipidoses (complex lipids), mucopolysaccharidoses (complex carbohydrates), glycoproteinoses or oligosaccharidoses and glycogenosis type II (the only glycogenosis which is of lysosomal origin). Lysosomal diseases are severe disorders with a heterogeneous clinical spectrum encompassing visceral, skeletal, and neurologic involvement and high morbidity and mortality. They can show differences in presentation according to the age of the patient which leads to a distinction between infantile, juvenile, and adult forms. On the other hand, different enzymatic defects may present with a similar clinical pattern. They can be classified clinically into three groups: leukodystrophies affecting mainly the brain; neurodegenerative or psychiatric-like diseases, and multisystemic diseases [72–74]. Examples of the multisystemic lysosomal diseases that affect the digestive tract are Gaucher's disease, Fabry's disease, Niemann–Pick's disease, Pompe's disease, Tangier disease, Wolmann's disease, and variant cholesterol ester storage disease and cystinosis (see Table 2). Several of these can involve the enteric nervous system and impair motility.

Table 2 Accumulation of endogeneous material in macrophages and/or endothelial cells in storage diseases

	Mucosal and submucosal macrophages	Endothelial cells
Tay Sach's disease	−	−
Krabbe disease	−	−
Gaucher's disease	−(+)	−
Fabry's disease	−	+
Batten's disease	−	+
Niemann Pick		
Type A	+	+
Type B	+	+
Type C	+	+
Pompe's disease	+	+
Tangier's dsease	+	−
Wolman's disease	+	+
Cholesteryl ester storage disease	+	+
Mucopolysaccharidoses	+	+
Cystinosis	+	−

Gaucher's disease is the most prevalent lysosomal disease [75, 76]. More than 1,600 patients from 13 countries are registered in a Gaucher registry [77]. It is caused by deficient glucocerebrosidase activity. The resulting accumulation leads to hepatosplenomegaly, anemia, thrombocytopenia, and various bone manifestations. Involvement of the digestive tract is uncommon. Hemorrhage associated with lymphoid hyperplasia of the ileum, bleeding esophageal varices secondary to liver disease, and the presence of a mesenteric mass inducing abdominal discomfort have been reported [78–80]. Accumulation of macrophages is unusual but has been described.

Fabry's disease is caused by a mutation affecting the alfa-galactosidase A gene [81]. Partial or complete deficiency of the enzyme results in pathologic metabolism of glycosphingolipids and accumulation of globotriaosylceramide (GB3). Renal involvement, cardiac disease, and neurological involvement are the most frequent features. In a review of 366 Fabry disease patients, gastrointestinal symptoms were present in 57 % of males and 47 % of females [82]. The most frequent symptoms were abdominal pain and diarrhea. Histological studies have demonstrated that GI involvement is very likely due to GB3 accumulation in neurons of Meissner's plexus, in endothelial cells of vessels and in smooth muscle cells [83]. Foamy macrophages are rarely reported. Coexistence of Fabry's disease with celiac disease and with Crohn's disease has been described [84].

Niemann–Pick's disease is a disorder which involves intracellular transport of cholesterol and glycolipids [85]. Two genes have been implicated, *NPC1* and *NPC2* [86]. Clinically, the disease is characterized by neurological and visceral symptoms. Different types have been recognized. In type B, a deficiency of sphingomyelinase results in accumulation of sphingomyeline in the macrophages [87, 88] (Fig. 3a, b, and d). Patients present with hepatosplenomegaly and hyperlipemia. Abnormalities of the myenteric plexus have been observed in infantile Niemann–Pick's disease [89]. Mucosal and submucosal accumulation of foamy histiocytes in the small and large intestine is rare. Nevertheless, a very rare condition, so called sea-blue histiocytosis, has been described in Niemann–Pick 's patients, which refers to the presence in the bone marrow, lung, and gut of scattered foci of aggregates of foamy macrophages that have a typical "sea-blue" appearance with May–Giemsa staining [90, 91] (Fig. 3d).

In Pompe's disease, a deficiency of lysosomal acid alpha-glucosidase, intralysosomal accumulation of glycogen is observed in multiple tissues, with skeletal and cardiac muscle most severely involved [91]. In the digestive tract, glycogen storage can be seen in endothelial cells and macrophages.

Tangier disease is characterized by almost complete absence of plasma-high density lipoprotein, deposition

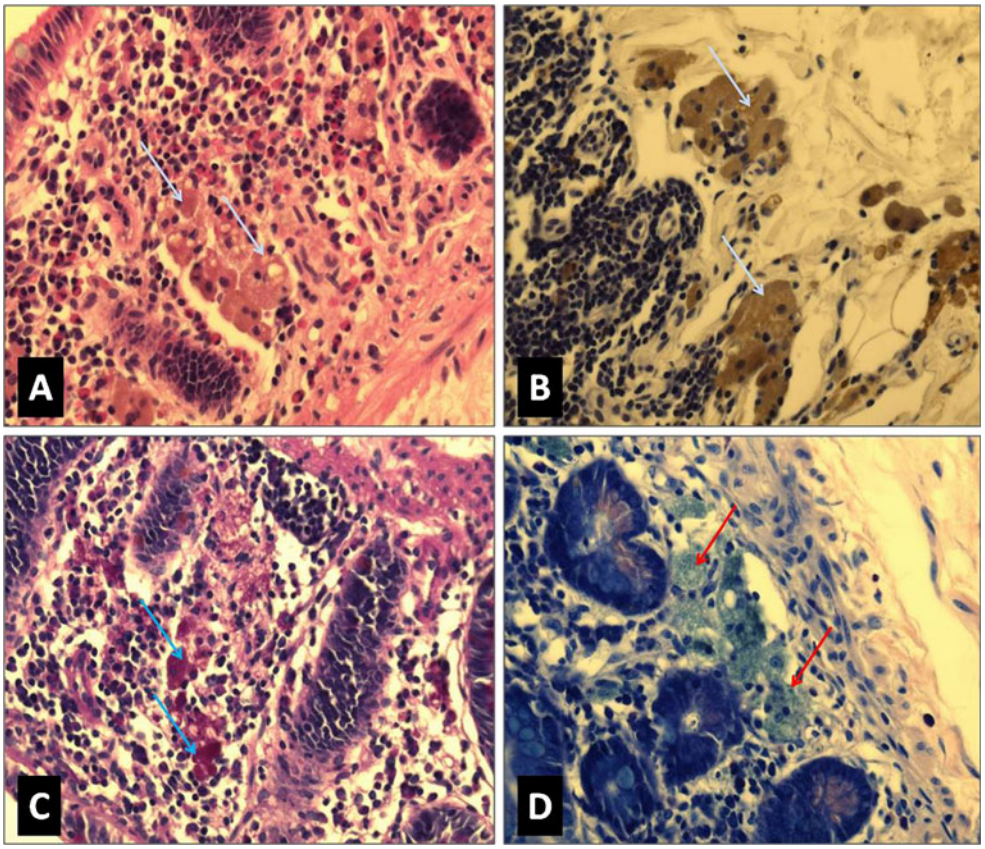

Fig. 3 Foamy macrophages in Niemann–Pick's disease. **a** HE staining of a colonic biopsy shows multiple foamy macrophages as marked by the *arrows* (magnification 400×); **b** CD68 staining marks multiple macrophages within the biopsy (magnification 400×); **c** PAS staining highlights the accumulation of endogenous material (sphingomyeline) within the macrophages (magnification 400×); **d** foamy macrophages in the gut display a typical sea-blue appearance with May–Giemsa staining

of cholesteryl esters in the reticulo-endothelial system and aberrant cellular lipid trafficking [92]. Large collections of cholesterol-laden macrophages can be seen in different tissues, including tonsils, thymus, lymph nodes, and colon [93].

In Wolman's disease, a disorder of infancy, nearly always fatal before the age of 1 year and in the variant cholesteryl ester storage disease (CESD) which can be more benign and may not be detected until adulthood, a similar accumulation of macrophages can be detected in the lamina propria of the colon and jejunum. Accumulation in the jejunum may lead to malabsorption [94–96].

In "cystinosis", abnormal accumulation of cystine is occurring in various tissues [97]. Some patients can have gastrointestinal symptoms related to intestinal dysmotility caused by intralysosomal cystine accumulation. In other patients, treatment with cysteamine may be responsible for the symptoms. Frozen sections and polarization may reveal the typical crystals, which tend to be rhomboidal. Counterstain with alcohol basic fucsin helps to demonstrate the crystals in macrophages and smooth muscle cells [98].

Inflammatory bowel disease

Although the etiology of inflammatory bowel diseases remains largely unknown, recent data demonstrated that inappropriate activation of the innate and adaptive mucosal immune response may contribute to its pathogenesis: several genomic loci, known to play a key role in the immune system and the maintenance of epithelial barrier integrity, have been implicated in the genomic susceptibility to ulcerative colitis and Crohn's disease [99, 100]. In line with these findings, other data suggested that a defective macrophage function may be responsible for the establishment of Crohn's disease [101, 102]. In addition, it was shown that macrophages isolated from Crohn's disease patients displayed decreased pro-inflammatory cytokine production following stimulation with heat-killed *E. coli*, as well as an altered cytokine secretion (e.g., increased IL-23 and decreased IL-12 secretion) in response to in vitro infection with *M. avium paratuberculosis* [103, 104]. While it seems evident that this macrophage dysfunction may contribute to the inflammatory exacerbation in inflammatory bowel diseases (especially Crohn's disease), further research is needed to investigate the precise role of macrophages in inflammatory bowel diseases.

Malakoplakia

Accumulation of histiocytes is further also observed in "Malakoplakia" section. Malakoplakia, ethymologically derived from the classic greek word "malacos" which means

soft, and "places", which means plaque is a granulomatous disorder that occurs mainly in the urinary tract. It was first described by Michaelis and Gutman in 1902. The condition is rare, with a total number of patients in the USA which is fewer than 500. The gastrointestinal tract is the second most common site of involvement (after the urinary tract), with mainly the descending colon, sigmoid, and rectum being most common sites affected. Other sites include the terminal ileum, stomach, appendix, and cecum. Grossly, the lesions may have three patterns: unifocal mucosal tan to yellow nodules or plaques, multinodular or polypoidal lesions, and large mass lesions. The clinical presentation may be diarrhea, abdominal pain, hemorrhage, or obstruction, but many cases are asymptomatic [105]. Histologically, malakoplakia is characterized by sheets of ovoid histiocytes (called von Hanseman cells) with accumulation of 5- to 15-mm granular basophilic PAS positive, diastase resistant inclusions and calcified Michaelis–Gutman bodies (Fig. 4a, b). By light microscopy, the Michaelis–Gutman bodies often exhibit a targetoid appearance with a dense central core. Michaelis–Gutman bodies can also occur extracellularly. They can be visualized by von Kossa stain for calcium or Prussian blue stain for iron. Gram-stain of the histiocytes may demonstrate Gram-negative bacteria.

The etiology of malakoplakia is not exactly known. Three possible mechanisms have been proposed for the pathogenesis: microorganisms, an abnormal immune response and an abnormal macrophage response because of defective lysosomal function. Several microorganisms have been implicated, particularly *E. coli* (found in more than 60 % of cases), *Klebsiella*, and *M. tuberculosis*. The partially digested bacteria accumulate in macrophages and lead to the deposition of calcium and iron on residual bacterial glycolipid. In the GI tract, malakoplakia has been reported in association with Whipple's disease, in renal (anal fistula) and liver transplant patients (sigmoid), in rectal prolapse, in ulcerative colitis, in the appendix (in association with eggs of Taenia and without apparent exogenous factor), and in severe combined immunodeficiency (SCID) [106–110]. The association between adenomatous polyp of the colon and cancer of the colon and malakoplakia is well documented in the literature. Local alteration of the gut flora has been postulated as the underlying mechanism (Table 3).

Table 3 Conditions associated with malakoplakia

1. Organ transplantation
2. Infections
—Tuberculosis
—Whipple's disease
1. Malignancy
2. Drugs
—Steroid use
—Cytotoxic chemotherapy
1. Ulcerative colitis

The diagnosis is rarely made clinically. Frequently, it is an unexpected histologic diagnosis made on biopsy or following resection by finding the combination of macrophages and neutrophils, but with a sprinkling of other inflammatory cells, together with the characteristic inclusions which may sometimes even be found on fine needle aspiration biopsy of the mass. The finding of a combination of neutrophils and macrophages is so uncommon that it should always prompt an immediate search for Michaelis–Gutmann bodies, and calcium or iron stains should be used to help demonstrate them. Because phagolysosomes are diastase-periodic acid-Schiff positive, macrophages will always be strongly positive, but this helps little in making the diagnosis. The differential diagnosis is with other sheets of inflammatory cells, such as what occurs in other xanthogranulomatous or inflammatory pseudotumors and which also may be bacterial. On biopsy, there is a theoretical distinction with Whipple's disease, in which the macrophages are also sudanophilic, but clinically these diseases have little in common.

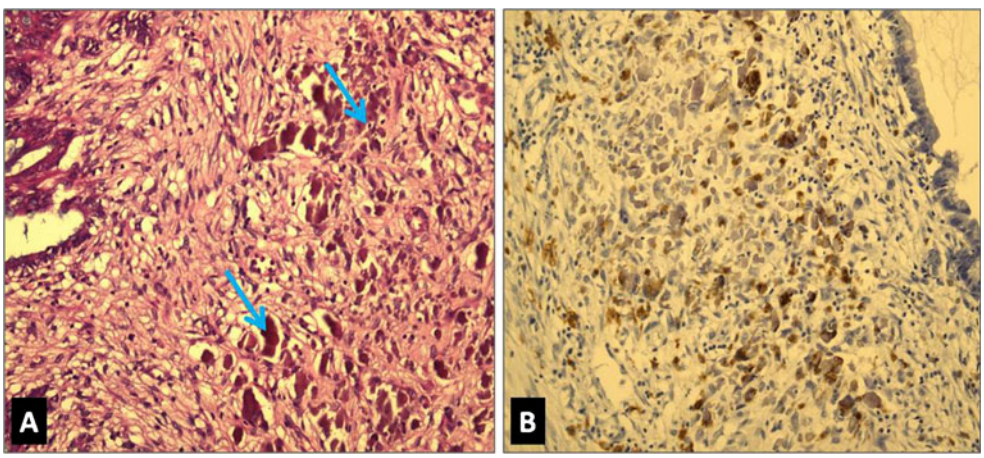

Fig. 4 Malakoplakia. **a** HE staining of a malakoplakia lesion in the colon, with the presence of multiple calcified Michaelis–Gutman bodies (marked by *arrows*) (magnification 200×); **b** CD68 staining highlights the sheets of ovoid histiocytes, also called von Hanseman cells, within the lesion (magnification 200×)

Conclusion

Although macrophages are usually not conspicuous in normal mucosal samples of the gut, they can easily be detected when they accumulate exogenous particulate material or endogenous substances, or when they become very numerous. However, the recognition of macrophage-related anomalies in the gut may challenge both clinicians and pathologists who are often unfamiliar with these problems. Moreover, the small size of the endoscopic sample may hamper an adequate diagnosis and classification. As a consequence, macrophage-related diseases of the gut are often overlooked and thus underdiagnosed. As such, when clinically suspected or when encountering easily detectable macrophages in endoscopic biopsies, clinicians and pathologists should communicate which each other to correlate their findings and to apply an array of special stainings in order to identify the underlying disease.

Conflict of interest statement We declare that we have no conflict of interest.

References

1. Valledor AF, Borras FE, Cullell-Young M, Celada A (1998) Transcription factors that regulate monocyte/macrophage differentiation. J Leukoc Biol 63:405–417
2. Gordon S, Clarke S, Greaves D, Doyle A (1995) Molecular immunobiology of macrophages—recent progress. Curr Opin Immunol 7:24–33
3. Smythies LE, Sellers M, Clements RH et al (2005) Human intestinal macrophages display profound inflammatory anergy despite avid phagocytic and bacteriocidal activity. J Clin Invest 115:66–75
4. Smythies LE, Shen RZ, Bimczok D et al (2010) Inflammation anergy in human intestinal macrophages is due to SMAD-induced I kappa B alpha expression and NF-kappa B inactivation. J Biol Chem 285:19593–19604
5. Smith PD, Smythies LE, Shen R, Greenwell-Wild T, Gliozzi M, Wahl SM (2011) Intestinal macrophages and response to microbial encroachment. Mucosal Immunol 4:31–42
6. Smythies LE, Maheshwari A, Clements R et al (2006) Mucosal IL-8 and TGF-beta recruit blood monocytes: evidence for cross-talk between the lamina propria stroma and myeloid cells. J Leukoc Biol 80:492–499
7. Eidelman S, Lagunoff D (1972) Morphology of normal human rectal biopsy. Hum Pathol 3:389–401
8. Kunisch E, Fuhrmann R, Roth A, Winter R, Lungershausen W, Kinne RW (2004) Macrophage specificity of three anti-CD68 monoclonal antibodies (KP1, EBM11, and PGM1) widely used for immunohistochemistry and flow cytometry. Ann Rheum Dis 63:774–784
9. Ramprasad MP, Terpstra V, Kondratenko N, Quehenberger O, Steinberg D (1996) Cell surface expression of mouse macrosialin and human CD68 and their role as macrophage receptors for oxidized low density lipoprotein. PNAS 93:14833–14838
10. Strobl H, Scheinecker C, Csmarits B, Majdic O, Knapp W (1995) Flow cytometric analysis of intracellular Cd68 molecule expression in normal and malignant hematopoiesis. Br J Haematol 90:774–782
11. Greaves DR, Gordon S (2002) Macrophage-specific gene expression: current paradigms and future challenges. Int J Hematol 76:6–15
12. Donato R (2003) Intracellular and extracellular roles of S100 proteins. Micros Res Technol 60:540–551
13. Selby WS, Poulter LW, Hobbs S, Jewell DP, Janossy G (1983) Heterogeneity of Hla-Dr-positive histiocytes in human intestinal lamina propria—a combined histochemical and immunohistological analysis. J Clin Pathol 36:379–384
14. Freeman HA (2008) "Melanosis" in the small and large intestine. World J Gastroenterol 14:4296–4299
15. Marginean EC, Bennick M, Cyczk J, Robert ME, Jain D (2006) Gastric siderosis—patterns and significance. Am J Surg Pathol 30:514–520
16. Yantiss RK, Goldman H, Odze RD (2001) Hyperplastic polyp with epithelial misplacement (inverted hyperplastic polyp): a clinicopathologic and immunohistochemical study of 19 cases. Mod Pathol 14:869–875
17. Parker RL, Dadmanesh F, Young RH, Clement PB (2004) Polypoid endometriosis—a clinicopathologic analysis of 24 cases and a review of the literature. Am J Surg Pathol 28:285–297
18. Kato S, Hashiguchi K, Yamamoto R et al (2006) Jumbo biopsy is useful for the diagnosis of colonic prolapsing mucosal polyps with diverticulosis. World J Gastroenterol 12:1634–1636
19. Shepherd NA, Crocker PR, Smith AP, Levison DA (1987) Exogenous pigment in Peyers-patches. Hum Pathol 18:50–54
20. Urbanski SJ, Arsenault AL, Green FHY, Haber G (1989) Pigment resembling atmospheric dust in Peyers patches. Mod Pathol 2:222–226
21. Powell JJ, Ainley CC, Harvey RSJ et al (1996) Characterisation of inorganic microparticles in pigment cells of human gut associated lymphoid tissue. Gut 38:390–395
22. Levine DS, Haggitt RC (1989) Normal histology of the colon. Am J Surg Pathol 13:966–984
23. Goldman H, Antonioli DA (1982) Mucosal biopsy of the rectum, colon, and distal ileum. Hum Pathol 13:981–1012
24. Lou TY, Teplitz C, Thayer WR (1971) Ultrastructural morphogenesis of colonic Pas-positive macrophages (colonic histiocytosis). Hum Pathol 2:421–439
25. Bejarano PA, Aranda-Michel J, Fenoglio-Preiser C (2000) Histochemical and immunohistochemical characterization of foamy histiocytes (muciphages and xanthelasma) of the rectum. Am J Surg Pathol 24:1009–1015
26. Coletta U, Sturgill BC (1985) Isolated xanthomatosis of the small bowel. Hum Pathol 16:422–424
27. Scheiman J, Elta G, Colturi T, Nostrant T (1988) Colonic xanthomatosis—relationship to disordered motility and review of the literature. Dig Dis Sci 33:1491–1494
28. Melling N, Bruder E, Dimmler A, Hohenberger W, Aigner T (2007) Localised massive tumourous xanthomatosis of the small intestine. Int J Colorectal Dis 22:1401–1404
29. Romeu J, Rybak B (1979) Lipid proctitis. N Engl J Med 301:1099–1100
30. Remmele W, Beck K, Kaiserling E (1988) Multiple lipid islands of the colonic mucosa—a light and electron-microscopic study. Pathol Res Pract 183:336–342
31. Schneider T, Moos V, Loddenkemper C, Marth T, Fenollar F, Raoult D (2008) Whipple's disease: new aspects of pathogenesis and treatment. Lancet Infect Dis 8:179–190
32. Desnues B, Al Moussawi K, Fenollar F (2010) New insights into Whipple's disease and *Tropheryma whipplei* infections. Microbes Infect 12:1102–1110

33. Marth T, Roux M, Vonherbay A, Meuer SC, Feurle GE (1994) Persistent reduction of complement receptor-3 alpha-chain expressing mononuclear blood-cells and transient inhibitory serum factors in Whipples-disease. Clin Immunol Immunopathol 72:217–226
34. Bai J, Sen L, Diez R et al (1996) Monocyte function in patients successfully treated for Whipple's disease. Acta Gastroenterologica Latinoam 26:85–89
35. Bjerknes R, Laerum OD, Odegaard S (1985) Impaired bacterial-degradation by monocytes and macrophages from a patient with treated Whipple's disease. Gastroenterology 89:1139–1146
36. Marth T, Kleen N, Stallmach A et al (2002) Dysregulated peripheral and mucosal Th1/Th2 response in Whipple's disease. Gastroenterology 123:1468–1477
37. Marth T, Neurath M, Cuccherini BA, Strober W (1997) Defects of monocyte interleukin 12 production and humoral immunity in Whipple's disease. Gastroenterology 113:442–448
38. Marcial MA, Villafana M (1997) Whipple's disease with esophageal and colonic involvement: endoscopic and histopathologic findings. Gastrointest Endosc 46:263–266
39. Fenollar F, Fournier PE, Robert C, Raoult D (2004) Use of genome selected repeated sequences increases the sensitivity of PCR detection of *Tropheryma whipplei*. J Clin Microbiol 42:401–403
40. Baisden BL, Lepidi H, Raoult D, Argani P, Yardley JH, Dumler JS (2002) Diagnosis of Whipple disease by immunohistochemical analysis—a sensitive and specific method for the detection of *Tropheryma whipplei* (the Whipple bacillus) in paraffin-embedded tissue. Am J Clin Pathol 118:742–748
41. Fenollar F, Raoult D (2010) How should classic Whipple disease be managed? Nat Rev Gastroenterol Hepatol 7:246–248
42. Feurle GE, Junga NS, Marth T (2010) Efficacy of ceftriaxone or meropenem as initial therapies in Whipple's disease. Gastroenterology 138:478–486
43. Mendoza JL, Lana R, Diaz-Rubio M (2009) Mycobacterium avium subspecies paratuberculosis and its relationship with Crohn's disease. World J Gastroenterol 15:417–422
44. Hamrock D, Azmi FH, O'Donnell E, Gunning WT, Philips ER, Zaher A (1999) Infection by *Rhodococcus equi* in a patient with AIDS: histological appearance mimicking Whipple's disease and *Mycobacterium avium-intracellulare* infection. J Clin Pathol 52:68–71
45. Ehrt S, Schnappinger D (2009) Mycobacterial survival strategies in the phagosome: defence against host stresses. Cell Microbiol 11:1170–1178
46. Almadi MA, Aljebreen AM, Sanai FM, Marcus V, AlMeghaiseeb ES, Ghosh S (2011) New insights into gastrointestinal and hepatic granulomatous disorders. Nat Rev Gastroenterol Hepatol 8:455–466
47. Radzi M, Rihan N, Vijayalakshmi N, Pani SP (2009) Diagnostic challenge of gastrointestinal tuberculosis: a report of 34 cases and an overview of the literature. Southeast Asian J Trop Med Public Health 40:505–510
48. Giouleme O, Paschos P, Katsaros M et al (2011) Intestinal tuberculosis: a diagnostic challenge—case report and review of the literature. Eur J Gastroenterol Hepatol 23:1074–1077
49. Yamshchikov AV, Schuetz A, Lyon GM (2010) *Rhodococcus equi* infection. Lancet Infect Dis 10:350–359
50. Kedlaya I, Ing MB, Wong SS (2001) *Rhodococcus equi* infections in immunocompetent hosts: case report and review. Clin Infect Dis 32:E39–E46
51. Toyooka K, Takai S, Kirikae T (2005) *Rhodococcus equi* can survive a phagolysosomal environment in macrophages by suppressing acidification of the phagolysosome. J Med Microbiol 54:1007–1015
52. Zink MC, Yager JA, Prescott JF, Wilkie BN (1985) In vitro phagocytosis and killing of *Corynebacterium equi* by alveolar macrophages of foals. Am J Vet Res 46:2171–2174
53. Nordmann P, Ronco E, Guenounou M (1993) Involvement of interferon-gamma and tumor-necrosis-factor-alpha in host defense against *Rhodococcus equi*. J Infect Dis 167:1456–1459
54. Nordmann P, Ronco E, Nauciel C (1992) Role of T-lymphocyte subsets in *Rhodococcus equi* infection. Infect Immun 60:2748–2752
55. Kanaly ST, Hines SA, Palmer GH (1993) Failure of pulmonary clearance of *Rhodococcus equi* infection in Cd4+ T-lymphocyte-deficient transgenic mice. Infect Immun 61:4929–4932
56. Kinchen K, Kinchen TH, Inglesby T (1998) *Pneumocystis carinii* infections of the small intestine. J Nat Med Assoc 90:625–627
57. Dieterich DT, Lew EA, Bacon DJ, Pearlman KI, Scholes JV (1992) Gastrointestinal pneumocystosis in HIV-infected patients on aerosolized pentamidine—report of 5 cases and literature-review. Am J Gastroenterol 87:1763–1770
58. Raviglione MC (1990) Extrapulmonary pneumocystosis—the 1st 50 cases. Rev Infect Dis 12:1127–1138
59. Alvarez-Nebreda ML, Alvarez-Fernandez E, Rada S et al (2005) Unusual duodenal presentation of leishmaniasis. J Clin Pathol 58:1321–1322
60. Salah MBH, Mekni A, Khanfir M et al (2006) Unusual presentation of visceral leishmaniasis in an immunocompetent patient. Med Mal Infect 36:167–169
61. Burns JM, Shreffler WG, Benson DR, Ghalib HW, Badaro R, Reed SG (1993) Molecular characterization of a kinesin-related antigen of *Leishmania chagasi* that detects specific antibody in African and American visceral leishmaniasis. PNAS 90:775–779
62. Reithinger R, Dujardin JC (2007) Molecular diagnosis of leishmaniasis: current status and future applications. J Clin Microbiol 45:21–25
63. Chappuis F, Sundar S, Hailu A et al (2007) Visceral leishmaniasis: what are the needs for diagnosis, treatment and control? Nat Rev Microbiol 5:873–882
64. Goodwin RA, Shapiro JL, Thurman GH, Thurman SS, Desprez RM (1980) Disseminated histoplasmosis—clinical and pathologic correlations. Medicine 59:1–33
65. Haggerty CM, Britton MC, Dorman JM, Marzoni FA (1985) Gastrointestinal histoplasmosis in suspected acquired immunodeficiency syndrome. West J Med 143:244–246
66. Goodwin RA, Desprez RM (1978) Histoplasmosis. Am Rev Respir Dis 117:929–956
67. Wheat LJ, Connollystringfield PA, Baker RL et al (1990) Disseminated histoplasmosis in the acquired-immune-deficiency-syndrome—clinical findings, diagnosis and treatment, and review of the literature. Medicine 69:361–374
68. Suh KN, Anekthananon T, Mariuz PR (2001) Gastrointestinal histoplasmosis in patients with AIDS: case report and review. Clin Infect Dis 32:483–491
69. Kahi CJ, Wheat LJ, Allen SD, Sarosi GA (2005) Gastrointestinal histoplasmosis. Am J Gastroenterol 100:220–231
70. Wheat J, Sarosi G, McKinsey D et al (2000) Practice guidelines for the management of patients with histoplasmosis. Clin Infect Dis 30:688–695
71. Rabsch W, Tschape H, Baumler AJ (2001) Non-typhoidal salmonellosis: emerging problems. Microbes Infect 3:237–247
72. Reuser AJJ, Drost MR (2006) Lysosomal dysfunction, cellular pathology and clinical symptoms: basic principles. Acta Paediatr 95:77–82
73. Parkinson-Lawrence EJ, Shandala T, Prodoehl M, Plew R, Borlace GN, Brooks DA (2010) Lysosomal storage disease: revealing lysosomal function and physiology. Physiology 25:102–115

74. Settembre C, Fraldi A, Rubinsztein DC, Ballabio A (2008) Lysosomal storage diseases as disorders of autophagy. Autophagy 4:113–114
75. Grabowski GA (2008) Lysosomal storage disease 1—phenotype, diagnosis, and treatment of Gaucher's disease. Lancet 372:1263–1271
76. Harmanci O, Bayraktar Y (2008) Gaucher disease: new developments in treatment and etiology. World J Gastroenterol 14:3968–3973
77. Charrow J, Andersson HC, Kaplan P et al (2000) The Gaucher registry—demographics and disease characteristics of 1698 patients with Gaucher disease. Arch Intern Med 160:2835–2843
78. Lim AKP, Vellodi A, McHugh K (2002) Mesenteric mass in a young girl—an unusual site for Gaucher's disease. Pediatr Radiol 32:674–676
79. Jones DR, Hoffman J, Downie R, Haqqani M (1991) Massive gastrointestinal hemorrhage associated with ileal lymphoid hyperplasia in Gauchers-disease. Postgrad Med J 67:479–481
80. Henderson JM, Gilinsky NH, Lee EY, Greenwood MF (1991) Gauchers-disease complicated by bleeding esophageal-varices and colonic infiltration by Gaucher cells. Am J Gastroenterol 86:346–348
81. Zarate YA, Hopkin RJ (2008) Lysosomal storage disease 3—Fabry's disease. Lancet 372:1427–1435
82. Mehta A, Ricci R, Widmer U et al (2004) Fabry disease defined: baseline clinical manifestations of 366 patients in the Fabry outcome survey. Eur J Clin Investig 34:236–242
83. O'Brien B, Shnitka T, McDougall R et al (1982) Pathophysiologic and ultrastructural basis for intestinal symptoms in Fabry's disease. Gastroenterology 82:957–962
84. Tumer L, Ezgu FS, Hasanoglu A et al (2004) The co-existence of Fabry and celiac diseases: a case report. Pediatr Nephrol 19:679–681
85. Kolodny EH (2000) Niemann–Pick disease. Curr Opin Hematol 7:48–52
86. Ory DS (2004) The Niemann–Pick disease genes—regulators of cellular cholesterol homeostasis. Trends Cardiovasc Med 14:66–72
87. Schuchman EH (2007) The pathogenesis and treatment of acid sphingomyelinase-deficient Niemann–Pick disease. J Inherit Metabol Dis 30:654–663
88. Horinouchi K, Erlich S, Perl DP et al (1995) Acid sphingomyelinase deficient mice—a model of type-A and type-B Niemann–Pick disease. Nat Genet 10:288–293
89. Galvis D, Nakazato Y, Wells T, Landing B (1987) Demonstration of myenteric plexus abnormalities in genetic diseases by a microdissection technique: preliminary studies. Am J Med Gen 3:329–342
90. Candoni A, Grimaz S, Doretto P, Fanin R, Falcomer F, Bembi B (2001) Sea-blue histiocytosis secondary to Niemann–Pick disease type B: a case report. Ann Hematol 80:620–622
91. van der Ploeg AT, Reuser AJJ (2008) Lysosomal storage disease 2—Pompe's disease. Lancet 372:1342–1353
92. Nofer JR, Remaley AT (2005) Tangier disease: still more questions than answers. Cell Mol Life Sci 62:2150–2160
93. Bale PM, Clifton-Bligh P, Benjamin BN, Whyte HM (1971) Pathology of Tangier disease. J Clin Pathol 24:609–616
94. Hoeg JM, Demosky SJ, Pescovitz OH, Brewer HB (1984) Cholesteryl ester storage disease and wolman disease—phenotypic variants of lysosomal acid cholesteryl ester hydrolase deficiency. Am J Hum Gen 36:1190–1203
95. Lambert I, Fransis S, Ectors N, Desreumaux P, Geboes K (2003) Macrophage collections in gastrointestinal biopsies and metabolic disorders: two unusual case reports. Histopathology 42:196–198
96. Boldrini R, Devito R, Biselli R, Filocamo M, Bosman C (2004) Wolman disease and cholesteryl ester storage disease diagnosed by histological and ultrastructural examination of intestinal and liver biopsy. Pathol Res Pract 200:231–240
97. Gahl WA, Thoene JG, Schneider JA (2002) Cystinosis. N Engl J Med 347:111–121
98. Dohil R, Newbury RO, Sellers ZM, Deutsch R, Schneider JA (2003) The evaluation and treatment of gastrointestinal disease in children with cystinosis receiving cysteamine. J Pediatr 143:224–230
99. Anderson CA, Massey DCO, Barrett JC et al (2009) Investigation of Crohn's disease risk loci in ulcerative colitis further defines their molecular relationship. Gastroenterology 136:523–529
100. Van Limbergen J, Wilson DC, Satsangi J (2009) The genetics of Crohn's disease. Annu Rev Genom Hum Genet 10:89–116
101. Xavier RJ, Podolsky DK (2007) Unravelling the pathogenesis of inflammatory bowel disease. Nature 448:427–434
102. Marks DJB, Harbord MWN, MacAllister R et al (2006) Defective acute inflammation in Crohn's disease: a clinical investigation. Lancet 367:668–678
103. Campos N, Magro F, Castro AR et al (2011) Macrophages from IBD patients exhibit defective tumour necrosis factor-alpha secretion but otherwise normal or augmented pro-inflammatory responses to infection. Immunobiology 216:961–970
104. Smith AM, Rahman FZ, Hayee B et al (2009) Disordered macrophage cytokine secretion underlies impaired acute inflammation and bacterial clearance in Crohn's disease. J Exp Med 206:1883–1897
105. Yousef GM, Naghibi B (2007) Malakoplakia outside the urinary tract—reply. Arch Pathol Lab Med 131:1512–1513
106. Boudny P, Kurrer MO, Stamm B, Laeng RH (2000) Malakoplakia of the colon in an infant with severe combined immunodeficiency (SCID) and CHARGE association. Pathol Res Pract 196:577–582
107. Jain M, Arora VK, Singh N, Bhatia A (2000) Malakoplakia of the appendix—an unusual association with eggs of *Taenia* species. Arch Pathol Lab Med 124:1828–1829
108. Guinaudeau E, Person B, Valo I, Tuech JJ, Rousselet MC (2002) Colonic malakoplakia and ulcerative colitis: report of a case. Gastroenterol Clin Biol 26:174–177
109. Kim PTW, Davis JE, Erb SR, Yoshida EM, Steinbrecher UP (2007) Colonic malakoplakia in a liver transplant recipient. Can J Gastroenterol 21:753–755
110. Cachia AR, Eshoo S, Kench J et al (2005) Synchronous malakoplakia and Whipple's disease. Pathology 37:315–317

Virchows Arch (2012) 460:569–575
DOI 10.1007/s00428-012-1241-z

ORIGINAL ARTICLE

Importance of assessing CK19 immunostaining in core biopsies in patients subjected to sentinel node study by OSNA

Felip Vilardell · Anna Novell · Javier Martin · Maria Santacana · Ana Velasco · M. J. Díez-Castro · Dolors Cuevas · M. Jose Panadés · Serafin González · Antonio Llombart · Edelmiro Iglesias · Xavier Matias-Guiu

Received: 22 December 2011 / Revised: 11 April 2012 / Accepted: 16 April 2012 / Published online: 4 May 2012
© The Author(s) 2012. This article is published with open access at Springerlink.com

Abstract Analysis of sentinel lymph node (SLN) by means of One-Step Nucleic Acid Amplification (OSNA) is being used increasingly as a very sensitive and quick method for intraoperative axillary staging in patients with breast cancer. This molecular diagnostic assay detects the expression level of cytokeratin 19 (CK19), a luminal epithelial cell marker broadly expressed in most breast carcinomas and not normally found in lymph nodes. Almost all breast cancers express this cytoskeleton protein, but some breast tumors have been found to lose the expression of CK19. CK19 immunostaining in core biopsies has been recommended in selecting patients eligible for OSNA analysis because SLNs with metastatic involvement by CK19-negative breast cancers may result in a false negative result by OSNA. However, the real frequency of CK19-negative breast cancer has to be elucidated. In this study, we have assessed the frequency and molecular profile of CK19-negative breast carcinomas in three series of cases. The first is a prospective series of 197 breast carcinomas, 111 of which were subjected to SLN evaluation by OSNA. The second is a retrospective series of 41 triple-negative (TN) breast carcinomas, and the third is a retrospective series of 68 breast cancer patients (matched core biopsies and metastatic lymph nodes) that had been evaluated by conventional procedures before the OSNA methodology was adopted in our institution. Our results not only demonstrate that lack of expression of CK19 is infrequent in breast cancers but also that performing CK19 immunohistochemical staining is important on diagnostic core biopsies in taking the decision of using OSNA methodology in the evaluation of sentinel nodes in breast cancer patients.

Keywords Breast carcinoma · OSNA · CK19 · Luminal · "Basal-like"

F. Vilardell · A. Novell · J. Martin · M. Santacana · A. Velasco · D. Cuevas · M. J. Panadés · X. Matias-Guiu
Department of Pathology and Molecular Genetics,
Hospital Universitari Arnau de Vilanova,
Lleida, Spain

M. J. Díez-Castro
Department of Nuclear Medicine,
Hospital Universitari Arnau de Vilanova,
Lleida, Spain

A. Llombart
Department of Medical Oncology,
Hospital Universitari Arnau de Vilanova,
Lleida, Spain

S. González · E. Iglesias
Unit of Breast Pathology, Department of Surgery,
Hospital Universitari Arnau de Vilanova,
Lleida, Spain

F. Vilardell (✉)
Servei d'Anatomia Patològica i Institut de Recerca Biomèdica de Lleida, Hospital Universitari Arnau de Vilanova,
Alcalde Rovira Roure 80,
25198, Lleida, Spain
e-mail: fvilardell@arnau.scs.es

Introduction

In the last 10 years, breast carcinoma has been categorized by means of cDNA microarray studies [1, 2] in five subtypes: luminal A and B, Her2, basal-like, and the more controversial normal breastlike. Luminal breast cancers show high expression levels of several luminal epithelial cell markers like CK7, CK8, CK18 and CK19, MUC1, bcl-2, estrogen receptors (ER), progesterone receptors (PR), GATA3, epithelial cell adhesion molecules, and lower expression levels of basal

CKs (CK5, CK14, and CK17). In contrast, breast cancers with a basal-like phenotype [3] are characterized by a protein expression pattern which is similar to that of myoepithelial cells, including a higher expression of high molecular weight cytokeratins, such as CK5, CK14 and CK17, smooth muscle markers, p63, CD10, EGFR/HER1, or beta-4 integrin, among others, and a lower expression of ER, PR, or HER2.

Currently, in clinical practice, the cytokeratin expression pattern of breast tumors usually is not assessed, and breast cancers are, as a rule, immunohistochemically classified into four immunophenotypes with very important implications [4, 5] in order to decide the more appropriate therapeutic approach: luminal A (ER+and/or PR+, HER2−), luminal B (ER+and/or PR+, and Ki67>14 % or HER2+), HER2 overexpressing (ER−, PR−, HER2+), and triple-negative (TN) phenotype (ER−, PR−, HER2−) [6]. Most TN breast cancers fit within the basal-like subgroup, although these two terms are not synonymous, and immunohistochemical assessment of EGFR and basal cytokeratins 5 and 6 is usually needed for better profiling of the basal-like phenotype among the TN tumors [7].

Sentinel lymph node (SLN) analysis by means of the One-Step Nucleic Acid Amplification (OSNA) assay is an increasingly used procedure for intraoperative staging of breast cancer patients [8]. The OSNA assay [9] (Sysmex, Kobe, Japan) is based on real-time amplification and quantitation of CK19 mRNA in homogenized samples of lymph nodes. In spite of the differences in cytokeratin expression pattern between luminal and basal-like breast cancers, luminal CK19 was chosen as the most suitable marker for identifying breast cancer metastases in lymph nodes by means of OSNA because virtually all (98.2 %) primary breast cancers were found to express this cytoskeletal protein [10]. CK19 mRNA has been described as having the highest sensitivity at nearly 90 % and was chosen as the best marker for OSNA assay among 45 potential mRNAs [8]. However, CK19 is not expressed in a small proportion of breast carcinomas including tumors with a luminal phenotype. Abd El-Rehim reported in 2004 [11] a consecutive series of 1944 breast carcinomas with 3.4 % (42/1230) of ER-positive tumors lacking CK19 expression. Similarly, Parikh et al. [12] reported in a cohort of 158 young women with stage I/II breast cancer, absence of CK19 expression in 6 % (4/66), and 30 % (21/62) of carcinomas with non-TN and TN phenotype, respectively.

In our institution, OSNA procedure is complemented with touch imprints as a quality control procedure. Between February 2009 and April 2011, nearly 450 breast carcinomas have been subjected simultaneously to OSNA and touch imprints. Concordant results were obtained in all but 13 of the cases, including three cases with isolated cells, eight cases with micrometastases, and one case with macrometastases, all of them regarded as negative by means of the touch imprints. One more discrepant case resulted in a SLN with malignant cells observed in the touch imprints but not detected by OSNA. This case turned out to be a grade I CK19-negative breast carcinoma with a luminal A immunophenotype and showed a high expression level of both ER and PR and a low Ki-67 proliferative index (4 %). The Her-2 expression was scored as negative (1+). A lymph node metastasis was seen in a touch imprint from the SLN but had not been detected by molecular procedures. The absence of expression of CK19 was confirmed by Sysmex Europe GmbH. The diagnostic core biopsy obtained several weeks before SLN analysis was also CK19-negative. Since this case was found, we routinely checked the status of CK19 in all newly diagnosed breast cancers on the diagnostic core biopsy. When CK19 expression is confirmed in the core biopsy, analysis of SLN is made by OSNA analysis in parallel with a touch imprint. If CK19 is negative, analysis of SLN is done by frozen section, touch imprints, and evaluation of formalin-fixed and paraffin-embedded samples, stained with hematoxylin and eosin (H&E), and immunostained with the pan-cytokeratin antibody AE1/AE3.

In order to assess the practical consequences of the absence of CK19 expression in breast cancer and to validate our strategy, we have conducted a prospective and retrospective study in order to determine the frequency of CK19-negative tumors within each of the four distinct immunophenotypes of breast carcinoma. Our results support the notion that the absence of expression of CK19 is rare in breast cancer but does occur in carcinomas with either a luminal or basal-like phenotype. Therefore, evaluation of CK19 in the diagnostic core biopsy may help in taking the decision as to the use of OSNA methodology in the evaluation of sentinel nodes in breast cancer patients.

Materials and methods

Patients and tumor specimens

Three different series of cases were studied. The first is a prospective consecutive series of 197 breast cancer core biopsies of patients who were diagnosed in Hospital Universitari Arnau de Vilanova, Lleida, Spain between April 2010 and April 2011. The mean age was 62.0 years (range 30 to 96 years). The histology of the cases included 182 (92.4 %) ductal breast carcinomas NOS, six (3.0 %) lobular breast carcinomas, and nine (4.6 %) belonging to other histologic subtypes. Tumor mean size was 18.2 mm. From them, 111 patients were subjected to sentinel node biopsy and OSNA evaluation.

Secondly, a retrospective series that included 41 TN breast carcinomas surgically resected from 2000 through 2010 was evaluated for CK5/6 and EGFR to identify breast cancers that have a basal-like phenotype. Subsequently, the CK19 status was checked in all the tumors from this series.

Thirdly, we included a retrospective series of 68 patients in which SLN was found to be positive for metastasis by

conventional pathological examination (touch imprints, frozen sections, and H&E and cytokeratin expression in formalin-fixed paraffin-embedded material) before the OSNA procedure was implemented in our institution on February 2009. Material available for these cases included sentinel node specimen and matched primary tumors.

OSNA

The OSNA assay for CK19 mRNA was introduced in our pathology department on February of 2009 as a routine method for analysis of SLN of breast cancer patients after a multicentric validation study performed under the auspices of Sociedad Española de Senología [12]. Between April 2010 and April 2011, 111 breast cancer patients from the first series were subjected to OSNA analysis of sentinel node. The OSNA protocol consisted of homogenization of tissue in a mRNA-stabilizing solution (Lynorhag, pH 3.5 Sysmex®) and subsequent isothermal (65 °C) amplification of cytokeratin 19 (CK19) using the Lynoamp amplification kit (Sysmex®) through a reverse transcriptase amplification assay (RT-LAMP) in a gene amplification detector RD-100i (Sysmex®) in compliance with the protocol previously described [8, 9]. The technique uses six primers, which increase the specificity and the speed of the reaction. In the OSNA assay, cases showing mRNA CK19 levels greater than 250 copies/μL were considered positive and were classified as micrometastases (number of copies >250 copies/μL <5,000 copies/μL) or macrometastases (number of copies >5,000 copies/μL) following system specifications based on prior calculations. Cases identified as "negative" (<250 copies/μL) by the system were further classified as isolated tumor cells (ITC) (no. of copies per microliter >100 but less than 250) or true negative if the number of copies per microliter was <100.

A positive OSNA reaction was found in 54 of the 111 cases of the first series (33 macrometastases, 19 micrometastases, and two ITC). In all cases, the OSNA analysis has been complemented with touch imprints, which are performed simultaneously with OSNA procedure. Concordance between OSNA results and touch imprints was observed in all but one of the patients, the latter corresponding to the first CK19-negative breast cancer mentioned above.

Immunohistochemistry

ER, PR, Ki-67, and Her-2

The immunophenotype of the three series of tumors was assessed in real time by means of immunolabeling for ER, PR, Ki-67, and Her-2 on the diagnostic core biopsies. For immunohistochemical analysis of ER, PR, and Ki-67 in the prospective consecutive series, the tissue sections were deparaffinized and endogenous peroxidase activity was blocked with Peroxidase-Blocking Reagent for 10 min. For ER and PR immunostaining, epitope retrieval was performed by heating at 95 °C in Target Retrieval Solution, High pH (50× Tris/EDTA buffer, pH 9) of Dako® for 20 min. The slides were subsequently incubated for 25 min with monoclonal mouse antihuman ERα antibody (clone 1D5, isotype IgG1, kappa) for ER staining and with monoclonal mouse antihuman PR antibody (clone PgR 636, isotype IgG1, kappa) for assessment of PR expression. The expression of ER and PR was graded semiquantitatively by considering the percentage and intensity of the staining applying the following formula: Histoscore=1×(% light staining)+2×(% moderate staining)+3×(% strong staining). The Allred score 7 is used as well. In order to assess the proliferative index, antigen retrieval was performed by heating at 95 °C in Target Retrieval Solution, High pH (50× Tris/EDTA buffer, pH 6.1) of Dako® for 20 min and incubation with monoclonal mouse antihuman Ki-67 antigen (clone MIB-1) for 20 min. Ki-67-positive nuclei were scored in the tumor areas showing the highest number of stained nuclei. In all cases, the slides were incubated with EnVision™ FLEX of Dako® as secondary antibody for 20 min, with chromogen diaminobenzidine tetrahydrochloride for 10 min and finally, counterstained with hematoxylin, dehydrated with ethanol, and mounted. Her-2 immunolabeling was performed following the HercepTest™ of Dako®. The antigen retrieval was by heating at 97 °C for 40 min with HercepTest™ Epitope Retrieval Solution (containing detergent 10×) (0.1 mol/L citrate buffer with a detergent). The slides were incubated with the primary antibody HercepTest™ Rabbit Anti-Human HER2 Protein for 30 min and with HercepTest™ Visualization Reagent for 30 min as secondary antibody.

Basal-like immunophenotype

All tumors which showed a TN phenotype were subsequently immunostained for EGFR and CK5/6 in order to characterize them as "basal-like" or "non basal-like." EGFR immunostaining was performed using the kit EGFR pharmDx of Dako®. The samples were digested for 5 min with proteinase K for antigen retrieval and incubated for 30 min with the primary antibody Mouse Antihuman EGFR protein. Subsequently, they were incubated for 30 min with the secondary antibody Labelled Polymer-HRP. CK5/6 was assessed by means of the PT Link Pre-treatment Module of Dako®, using Target Retrieval Solution, High pH, for 20 min for antigen retrieval and a 20-min incubation with the primary antibody Monoclonal Mouse Anti-Human clone D5/16 B4. The slides were incubated with EnVision™ FLEX of Dako® as secondary antibody for 20 min. CK 5/6 and EGFR were scored following qualitative criteria. TN tumors showing either CK5/6 or EGFR expression, even

if focal, were regarded as tumors with a "basal-like" phenotype [7].

CK19 immunostaining

Finally, CK19 was assessed by incubation with the RCK108 primary antibody for 20 min. Methodology was similar to that performed for ER and PR, and the samples were incubated with EnVision™ FLEX of Dako® as secondary antibody for 20 min.

Statistics

For statistical evaluation of the data reported in Table 2, the Statistical Package for Social Science (SPSS) software was used. The contingency tables for clinicopathological correlations were analyzed by means the χ^2 test.

Results

Results are summarized in Tables 1 and 2.

Prospective series of 197 breast carcinomas

First, we evaluated a prospective series of 202 consecutive, unselected breast cancers, 111 of which were subjected to SLN evaluation by OSNA. In that series, the expression of CK19 had been assessed in 197 cases. This series comprised 57 (28.9 %) luminal A cases (ER+and/or PR+, Ki67<14 %, Her2−), 103 (52.3 %) luminal B cases (ER+and/or PR+, Ki67>14 % or Her2+), 14 (7.1 %) Her2 cases (ER−, PR−, Her-2+), and 23 (11.7 %) TN cases, with 16 (7.9 %) basal-like tumors by means of immunolabeling with CK5/6 and EGFR.

In this series, a total of six (3.04 %) CK19-negative breast carcinomas were found. Five of the six carcinomas lacking CK19 expression were positive for ER and regarded as carcinomas with a luminal phenotype (5/160, 3.1 %), two of them with a luminal A phenotype and the remaining three with a luminal B phenotype. The sixth CK19-negative case was a TN carcinoma, with a basal-like phenotype (1/24, 4.2 %). The first luminal-type carcinoma was the case described in the "Introduction," a grade I breast carcinoma with high expression of ER and PR, low Ki67 index (luminal A), and a metastatic sentinel node that was misinterpreted by OSNA. The second CK19-negative case, with a luminal A phenotype, was not treated in our center. In the third luminal-type tumor (luminal B), lymph node metastases were demonstrated by means an axillary fine-needle aspiration as well as in the basal-like one. In the fourth and fifth luminal carcinomas (luminal B) lacking expression of CK19, the SLNs were examined by means of frozen and paraffin-embedded sections. Such a decision was taken after CK19 staining turned out negative in the diagnostic core biopsy. A micrometastasis was detected in one case by means of immunolabeling for cytokeratins using the AE1/AE3 antibody and a macrometastasis (9 mm) in the other case, which was seen in the frozen section. Then, we checked the expression of CK19 in these two metastases.

Table 1 Characteristics of the prospective series of 197 breast cancer cases in which CK19 expression has been assessed

Age (years)	
Mean	62.05
Median±SD	63±15.25
Range	30–96
Histology	
Ductal	182 (92.4 %)
Lobular	6 (3.0 %)
Other	9 (4.6 %)
Tumor size (mm)	
Mean	18.2
T1 (<2.0)	110
≥T2 (≥2.0)	54
Tumor grade	
Grade I	56 (28.4 %)
Grade II	104 (52.7 %)
Grade III	15 (7.6 %)
NA	22
Nodal status	
Total assessed	174 (87.9 %)
Negative	77 (38.9 %)
Positive	97 (49.0 %)
ER status	
Negative	37 (18.8 %)
Positive	160 (81.2 %)
Her2 status	
Negative	170 (86.3 %)
Positive	27 (13.7 %)
Ki67	
Low (<14 %)	61 (31.0 %)
High (>14 %)	136 (69.0 %)
Immunophenotype	
Luminal	
—Luminal A	57 (28.9 %)
—Luminal B (ER+and Her2+ or Ki67>14 %)	103 (52.3 %)
—Total luminal	160 (81.2 %)
Her-2	14 (7.1 %)
Triple-negative	23 (11.7 %)
Cytokeratin 19 status	
Positive	191 (96.5 %)
Negative	6 (3.0 %)
Undone	5 (0.5 %)

Table 2 Association between CK19 status and patient features

	CK19 status		
	Positive	Negative	*p* value
Age (years)			
<Mean	89	2	0.048
>Mean	102	4	
Histology			
Ductal (NOS)	176	6	0.920
Lobular	6	0	
Other	9	0	
Tumor size (cm)			
T1 (<2.0)	105	5	0.249
T2 (≥2.0)	54	0	
Tumor grade			
Grade I	54	2	0.123
Grade II	101	3	
Grade III	15	1	
Nodal status			
Negative	77	0	0.096
Positive	92	5	
ER status			
Negative	36	1	0.000
Positive	155	5	
Her2 status			
Negative	161	6	0.036
Positive	27	0	
Triple-negative status			
Positive	22	1	0.791
Negative	169	5	
Immunophenotype			
Luminal A (ER+, Ki67<14 %, Her-2−)	55	2	0.754
Luminal B (ER+, Ki67>14 % or Her-2+)	100	3	
Her-2	14	0	
Triple-Negative	22	1	
Immunophenotype			
Luminal A and B	155	5	0.000
Her-2	14	0	
Triple-negative	22	1	

The micrometastasis from the fourth CK19-negative luminal tumor was CK19-negative as well. The macrometastasis from the fifth CK19-negative luminal carcinoma, however, showed some isolated CK19-positive cells (Fig. 1). When the immunohistochemical profile of the tumors had been initially assessed in core biopsies samples, we compared this with the CK19 status of this primary tumor on the surgical specimen to rule out the possibility that the core biopsy was not representative for the whole tumor in terms of CK19 expression. This primary carcinoma was mostly CK19-negative, but there were some small areas with immunolabeling for CK19, and these areas were not present in the core biopsy.

Retrospective series of 41 triple-negative (TN) breast carcinomas

The series of 41 TN breast carcinomas consisted of 30 tumors with a basal-like phenotype and nine carcinomas with a nonbasal-like TN phenotype. In two cases, we could not test retrospectively the expression of CK5/6 and EGFR in order to further characterize these as basal-like or "non-basal-like. No tumor from this series was CK19-negative.

Retrospective series of 68 cases with metastases in SLN before OSNA implementation

SLN was evaluated in 211 breast cancer cases before the OSNA methodology was adopted in our institution. All the SLNs had been studied by means conventional pathological and immunohistochemical examination, and the cases were retrospectively reviewed in order to find CK19-negative metastases which could have originated false negative results by OSNA. Eighty-six SLNs had been positive for metastasis, 23 with micrometastases, and 63 with macrometastases, but in 18 cases, the metastatic focus was exhausted in the remaining material. Of the other 68 cases with metastatic foci still present, all but one case was CK19-positive. In this case, the expression of CK19 was checked in the surgical specimen of the matched primary tumor, and the tumor was homogeneously CK19-negative.

Discussion

The OSNA methodology for detection of axillary metastasis in breast cancer is becoming a standard procedure and is based on measuring the expression level of CK19 in the SLN. CK19 was chosen as the optimal molecule because of its broad expression in most breast carcinomas, without notable expression in hematopoietic cells [10]. Validation studies published to date [13–17] show that OSNA is a reliable quantitative test of intraoperative metastasis detection in SLNs of breast cancer patients.

In general, breast cancer is regarded to arise from luminal epithelial cells of the terminal duct lobular unit (TDLU) which express several cytokeratins such as CK7, CK8, CK18, and CK19 [1]. This suggests that virtually all breast carcinomas express CK19, but still there is the possibility that some breast cancers loose CK19 expression during tumor development and progression. This may be a challenge for the accuracy of OSNA in evaluating SLN. Moreover, a smaller group of breast carcinomas express some

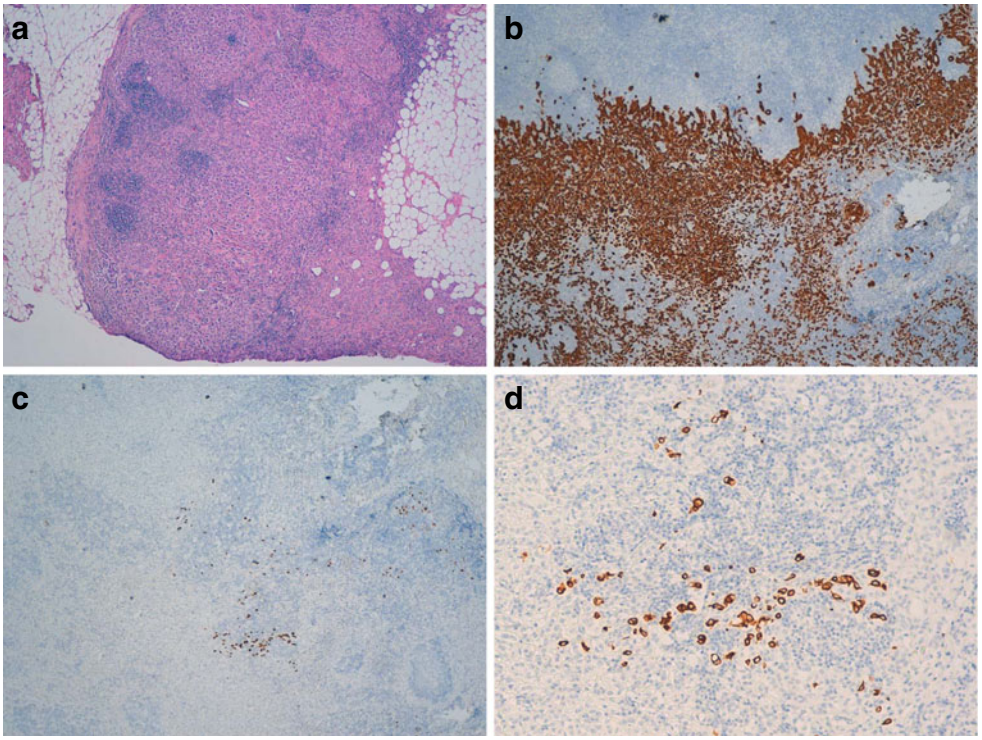

Fig. 1 Sentinel lymph node from the fourth luminal A CK19-negative breast carcinoma. **a** Lymph node section showing a macrometastasis of 9 mm in maxim diameter. **b** View of the metastatic population of cells by means of CKAE1/AE3 pan-cytokeratin immunostaining of the same section. CK19 immunostaining of the same lymph node section (**c** and **d**). Only a small proportion of metastatic cells express CK19. **a** H&E staining, original magnification×40. **b** Original magnification×200. **c** Original magnification×40. **d** Original magnification×200

cytokeratins normally found in the outer basal layer of myoepithelial cells of the mammary ductules, such as CK5, CK14, and CK17, and, for this reason, are designated basal-like [3, 6]. Consequently, breast cancers lacking CK19 expression might occur only in the basal-like subtype of breast cancer or might also contain luminal breast carcinomas with loss of CK19 expression.

A few studies have addressed the frequency of CK19-negative breast cancers. Parikh et al. (2008) [12] reported lack of CK19 expression in 20.5 % of 158 breast carcinomas in a tissue microarray. Moreover, they found a statistically significant association between lack of CK19 expression and the TN phenotype (30 % of TN breast cancers were CK19-negative). However, four of their 27 CK19-negative tumors were not triple-negative, which in their series amounted to 6 %. Similarly, Abd El-Rehim et al. (2004) [11] reported lack of CK19 expression in 3.4 % of luminal (ER+) breast cancers. Very recent works [18] have assessed the expression of CK19 in different histological types of breast cancer but without consideration of their molecular profile.

A case of discordance between metastatic cells seen in a touch imprint of a SNL but not detected by means of the OSNA assay, allowed us to find a grade I ductal carcinoma with a luminal A phenotype which did not express CK19. The lack of CK19 expression was confirmed by Sysmex Europe GmbH. From then on, we assessed the CK19 status of all newly diagnosed breast carcinomas. To date, from a consecutive series of 197 breast cancers in which CK19 expression was assessed, we found lack of CK19 expression in 3.5 % (2/57) of breast cancers with a luminal A phenotype (ER/PR+, Her2−, Ki67<14 %), 2.9 % (3/103) of breast cancers with a luminal B phenotype (ER/PR+and Ki67>14 % or Her2+), and 4.2 % (1/24) in triple-negative carcinomas. We did not find any CK19-negative tumor with a pure Her2-positive phenotype. We conclude from these results and literature review that absence of CK19 expression can be expected in around 4 % to 7 % of breast carcinomas with either a luminal or nontriple-negative phenotype (which can include the Her2 phenotype). It is conceivable that in some breast cancers, the lack of CK19 expression might be due to an absence of translation of the transcript CK19 mRNA. In these cases, the OSNA assay would be able to detect and amplify CK19 mRNA in the absence of protein. Nonetheless, it seems rational to check, as a rule, the expression of CK19 by immunohistochemistry in all newly diagnosed breast carcinomas in order to decide whether the analysis of SLN should preferably be done using the OSNA assay or conventional procedures. In one of the five luminal carcinomas lacking CK19 expression on the core biopsy, a macrometastasis was found in the SLN by means of cytology and frozen section examination. Just a few isolated cells of this macrometastasis expressed CK19. OSNA assay might have interpreted as isolated cells this macrometastasis. Interestingly, in this case, evaluation of CK19 in the surgical specimen also demonstrated the occasional presence of CK19-positive cells, which had not been seen in the diagnostic core biopsy, thus demonstrating that CK19 expression heterogeneity can also be an additional problem in the strategy of using CK19 evaluation in the core biopsy as an indicator of eligibility for OSNA evaluation in SLNs.

Furthermore, we decided to study retrospectively a series of 68 breast cancer patients that underwent SLN evaluation by conventional pathological assessment before OSNA assay was implemented in order to assess the number of cases that might have been misinterpreted as negative had they been assessed by OSNA because of lack of CK19 immunostaining. We found one case of SLN metastasis which was CK19-negative, which translates into a 1.4 % of false negative rate of SLN assessment using the OSNA assay. Interestingly, in this case, CK19 was not expressed in the core biopsy, suggesting that the absence of CK19 expression in the SLN might have been predicted by the evaluation of the core biopsy.

Based on our results, we conclude that even though the overall prevalence of CK19-negative breast carcinomas is very low, they do occur not only in tumors with a triple-negative or basal-like phenotype but also in breast cancers with a luminal phenotype, in which expression of luminal cytokeratins including CK19 is expected to be the rule. Therefore, expression of CK19 should be routinely assessed in all newly diagnosed primary breast carcinomas in order to decide whether the intraoperative axillary staging should be performed by means of cytology and pan-cytokeratins immunostaining on SLN sections or by means of real-time amplification and quantitation of CK19.

Conflict of interest The authors declare that they have no conflict of interest.

Open Access This article is distributed under the terms of the Creative Commons Attribution License which permits any use, distribution, and reproduction in any medium, provided the original author(s) and the source are credited.

References

1. Moll R, Franke WW, Schiller DL, Geiger B, Krepler R (1982) The catalog of human cytokeratins: patterns of expression in normal epithelia, tumors and cultured cells. Cell 31:11–24, Review
2. Perou CM, Sørlie T, Eisen MB, van de Rijn M, Jeffrey SS, Rees CA, Pollack JR, Ross DT, Johnsen H, Akslen LA, Fluge O, Pergamenschikov A, Williams C, Zhu SX, Lønning PE, Børresen-Dale AL, Brown PO, Botstein D (2000) Molecular portraits of human breast tumours. Nature 406:747–52
3. Rakha EA, Reis-Filho JS, Ellis IO (2008) Basal-like breast cancer: a critical review. J Clin Oncol 26:2568–81
4. Harvey JM, Clark GM, Osborne CK, Allred DC (1999) Estrogen receptor status by immunohistochemistry is superior to the ligand-binding assay for predicting response to adjuvant endocrine therapy in breast cancer. J Clin Oncol 17:1474–81
5. Goldhirsh A, Wood WC, Coates AS, Gelber RD, Thürlimann B, Senn HJ, Panel members (2011) Strategies for subtypes—dealing with the diversity of breast cancer: highlights of the St. Gallen International Expert Consensus on the Primary Therapy of Early Breast Cancer. Ann Oncol 22:1736–47
6. Nielsen TO, Hsu FD, Jensen K, Cheang M, Karaca G, Hu Z, Hernandez-Boussard T, Livasy C, Cowan D, Dressler L, Akslen LA, Ragaz J, Gown AM, Gilks CB, van der Rijn M, Perou CM (2004) Immunohistochemical and clinical characterization of the basal-like subtype of invasive breast carcinoma. Clin Cancer Res 10:5367–74
7. Collins LC, Martyniak A, Kandel MJ, Stadler ZK, Masciari S, Miron A, Richardson AL, Schnitt SJ, Garber JE (2009) Basal cytokeratin and epidermal growth factor receptor expression are not predictive of BRCA1 mutation status in women with triple-negative breast cancers. Am J Surg Pathol 33:1093–7
8. Tsujimoto M, Nakabayashi K, Yoshidome K, Kaneko T, Iwase T, Akiyama F, Kato Y, Tsuda H, Ueda S, Sato K, Tamaki Y, Noguchi S, Kataoka TR, Nakajima H, Komoike Y, Inaji H, Tsugawa K, Suzuki K, Nakamura S, Daitoh M, Otomo Y, Matsuura N (2007) One-step nucleic acid amplification for intraoperative detection of lymph node metastasis in breast cancer patients. Clin Cancer Res 13:4807–4816
9. Visser M, Jiwa M, Horstman A, Brink AA, Pol RP, van Diest P, Snijders PJ, Meijer CJ (2008) Intra-operative rapid diagnostic method based on CK19 mRNA expression for the detection of lymph node metastases in breast cancer. Int J Cancer 122:2562–7
10. Chu PG, Weiss LM (2002) Keratin expression in human tissues and neoplasms. Histopathology 40:403–39
11. Abd El-Rehim DM, Pinder SE, Paish CE, Bell J, Blamey RW, Robertson JF, Nicholson RI, Ellis IO (2004) Expression of luminal and basal cytokeratins in human breast carcinoma. J Pathol 203:661–71
12. Parikh RR, Yang Q, Higgins SA, Haffty BG (2008) Outcomes in young women with breast cancer of triple-negative phenotype: the prognostic significance of CK19 expression. Int J Radiat Oncol Biol Phys 70:35–42
13. Bernet L, Cano R, Martinez M, Dueñas B, Matias-Guiu X, Morell L, Palacios J, Rezola R, Robles-Frias M, Ruiz I, Velasco A, Vieites B, Sevilla F, Torro J, Medrano J, Ballester B (2011) Diagnosis of the sentinel lymph node in breast cancer: a reproducible molecular method: a multicentric Spanish study. Histopathology 58:863–9
14. Feldman S, Krishnamurthy S, Gillanders W, Gittleman M, Beitsch PD, Young PR, Streck CJ, Whitworth PW, Levine EA, Boolbol S, Han LK, Hermann R, Hoon DS, Giuliano AE, Meric-Bernstam F (2011) A novel automated assay for the rapid identification of metastatic breast carcinoma in sentinel lymph nodes. Cancer 117:2599–607
15. Schem C, Maass N, Bauerschlag DO, Carstensen MH, Löning T, Roder C, Batic O, Jonat W, Tiemann K (2009) One-step nucleic acid amplification-a molecular method for the detection of lymph node metastases in breast cancer patients; results of the German study group. Virchows Arch 454:203–10
16. Snook KL, Layer GT, Jackson PA, de Vries CS, Shousha S, Sinnett HD, Nigar E, Singhal H, Chia Y, Cunnick G, Kissin MW (2011) Multicenter evaluation of intraoperative molecular analysis of sentinel lymph nodes in breast carcinoma. Br J Surg 98:527–35
17. Castellano I, Macrì L, Deambrogio C, Balmativola D, Bussone R, Ala A, Coluccia C, Sapino A (2012) Reliability of whole sentinel lymph node analysis by one-step nucleic acid amplification for intraoperative diagnosis of breast cancer metastases. Ann Surg 255:334–42
18. Alvarenga CA, Paravidino PI, Alvarenga M, Dufloth R, Gomes M, Zeferino LC, Schmitt F (2011) Expression of CK19 in invasive breast carcinomas of special histological types: implications for the use of one-step nucleic acid amplification. J Clin Pathol 64:493–7

Virchows Arch (2012) 460:577–585
DOI 10.1007/s00428-012-1242-y

ORIGINAL ARTICLE

Performance characteristics of Pap test, VIA, VILI, HR-HPV testing, cervicography, and colposcopy in diagnosis of significant cervical pathology

Adhemar Longatto-Filho · Paulo Naud · Sophie FM Derchain · Cecília Roteli-Martins · Sílvio Tatti · Luciano Serpa Hammes · Luis Otavio Sarian · Mojca Eržen · Margherita Branca · Jean Carlos de Matos · Renata Gontijo · Marina Y. S. Maeda · Temístocles Lima · Silvano Costa · Stina Syrjänen · Kari Syrjänen

Received: 17 October 2011 / Revised: 13 March 2012 / Accepted: 23 April 2012 / Published online: 5 May 2012
© Springer-Verlag 2012

Abstract We sought to evaluate the performance of diagnostic tools to establish an affordable setting for early detection of cervical cancer in developing countries. We compared the performance of different screening tests and their feasibility in a cohort of over 12,000 women: conventional Pap smear, liquid-based cytology, visual inspection with acetic acid (VIA), visual inspection with Iodine solution (VILI), cervicography, screening colposcopy, and high-risk human papillomavirus (HPV) testing (HR-HPV) collected by physician and by self-sampling. HR-HPV assay collected by the physician has the highest sensitivity (80 %), but high unnecessary referrals to colposcopy (15.1 %). HR-HPV test in self-sampling had a markedly lower (57.1 %) sensitivity. VIA, VILI, and cervicography had a poor sensitivity (47.4, 55, and 28.6 %, respectively). Colposcopy presented with sensitivity of 100 % in detecting CIN2+, but the lowest specificity (66.9 %). Co-testing with VIA and VILI Pap test increased the sensitivity of stand-alone Pap test from 71.6 to 87.1 % and 71.6 to 95 %, respectively, but with high number of unnecessary colposcopies. Co-testing

A. Longatto-Filho
Life and Health Sciences Research Institute (ICVS),
School of Health Sciences, University of Minho,
Braga, Portugal

A. Longatto-Filho
ICVS/3B's—PT Government Associate Laboratory,
Braga, Guimarães, Portugal

A. Longatto-Filho (✉)
Laboratory of Medical Investigation (LIM) 14,
Faculty of Medicine, University of São Paulo,
1246-903 São Paulo, Brazil
e-mail: longatto@ecsaude.uminho.pt

P. Naud · L. S. Hammes · J. C. de Matos
Hospital de Clinicas de Porto Alegre,
Porto Alegre, Brazil

S. F. Derchain · L. O. Sarian · R. Gontijo
Universidade Estadual de Campinas,
Campinas, Brazil

C. Roteli-Martins · T. Lima
Hospital Leonor Mendes de Barros (HLMB),
São Paulo, Brazil

S. Tatti
First Chair Gynecology Hospital de Clinicas,
Buenos Aires, Argentina

L. S. Hammes
Institute of Education and Research,
Hospital Moinhos de Vento,
Porto Alegre, Brazil

M. Eržen
SIZE Diagnostic Center,
Ljubljana, Slovenia

M. Branca
Unit of Cytopathology, National Centre of Epidemiology,
Surveillance and Promotion of Health,
National Institute of Health (ISS),
Rome, Italy

with HR-HPV importantly increased the sensitivity of Pap test (to 86 %), but with high number of unnecessary colposcopies (17.5 %). Molecular tests adjunct to Pap test seems a realistic option to improve the detection of high-grade lesions in population-based screening programs.

Keywords Cancer prevention · Pap test · Hybrid capture · Colposcopy · Screening program

Introduction

Cervical cancer (CC) is a preventable disease that still causes 250,000 deaths per year, with most of them (80 %) occurring in developing countries. Many of these women have never or rarely been screened because of the lack of organized screening programs. Paradoxical enough, in many developing countries with organized screening programs implemented, as in Brazil, CC incidence and mortality rates have not changed significantly during the past decades [1].

Pap smear is the time-honored means to drastically reduce CC incidence and mortality, as proven, e.g., in the Nordic countries with organized screening programs based on conventional Pap smear. However, many developing countries, e.g., in Latin America, has not been able to implement such highly effective programs because of the complex setting required (i.e., collection, processing, and interpretation). During the past several years, it has also become increasingly clear that Pap smear suffers from inherent limited sensitivity in detecting CC and its precursor lesions [2, 3].

Given these limitations of Pap smear screening, the need for optional screening tools has been widely recognized, and several multicenter trials have been completed or are ongoing mostly in the developing world with a high incidence and mortality of CC. These alternative screening methods subjected to extensive testing recently include: (a) human papillomavirus (HPV) detection; (b) visual methods: visual inspection with acetic acid (VIA), visual inspection with Lugol iodine (VILI), cervicography, screening colposcopy, spectroscopy, speculoscopy; and (c) cytological methods: liquid-based cytology (LBC) or cytology automation.[2]

Latin America is among the regions with the highest incidence and mortality rates of CC and, for this reason, also the site of recent studies evaluating these alternative screening methods. Despite the fact that Brazil and Argentina are emerging countries in this region, CC incidence rates have not decreased over time in these countries, and this disease remains to be an important public health problem. Some years ago, we designed a multicenter study in these two countries, known as the Latin American Screening (LAMS) study, aiming to evaluate the performance of optional diagnostic tools to establish an effective, feasible, and affordable setting for early detection of CC, which is a public health priority in these countries. In this communication, we present the data comparing the performance of these screening tests in the LAMS study cohort of over 12,000 women.

Materials and methods

General study design

The LAMS study is a European Commission-funded, multicenter screening trial, targeting the female populations in two Latin American countries: Brazil and Argentina. LAMS study compared the performance of different screening tests and their feasibility in a cohort of over 12,000 women: conventional Pap smear, LBC, VIA, VILI, cervicography, screening colposcopy, high-risk HPV testing (HR-HPV) collected by physician and by self-sampling. The study design and baseline data have been described in detail in previous publications [2–4]. Briefly, LAMs study is a combination of cross-sectional and prospective cohort in regions with different incidence rates of cervical cancer with two principal goals: to evaluate the feasibility of eight different tests for screening proposals, hypothesizing that different incidences of cervical cancer depend on different exposures for different risk factors [2]. Consecutive women from the cities of Campinas (Brazil), São Paulo (Brazil), Porto Alegre (Brazil), and Buenos Aires (Argentina) were invited to gynecological consultations and tests examination. All centers performed conventional Pap smear, Hybrid Capture 2 (HCII), and VIA, but only Porto Alegre performed VILI. In order to guarantee standardized exams with high quality, all centers provided specialists in gynecology and well-trained nurses to collect the samples for HCII and Pap smear, as well as to perform VIA and VILI [2–4].

M. Y. S. Maeda
Adolfo Ltz Instiute,
São Paulo, Brazil

S. Costa
Department of Obstetrics and Gynecology,
S.Orsola-Malpighi Hospital,
Bologna, Italy

S. Syrjänen
Department of Oral Pathology, University of Turku,
Turku, Finland

K. Syrjänen
Department of Oncology and Radiotherapy,
Turku University Hospital,
Turku, Finland

Women who tested positive in at least one of these assays were referred for colposcopic examination. Whenever colposcopy revealed any abnormal pattern, a directed biopsy was taken. Patients with cervical intraepithelial neoplasia (CIN)2+ were submitted for prompt treatment. Patients with low-grade lesions (CIN1 or evidence of HPV infection without CIN) and/or abnormal Pap smear and/or positive HR-HPV assay were prospectively followed-up for 3 years.

At the first visit, when consented to participate in the trial, all patients were asked to fill in a detailed questionnaire recording their demographic characteristics and risk factors of CC/CIN. In addition to evaluation of the different screening tests, LAMS study is also a combination of a population-based cross-sectional (prevalence) study and a prospective cohort study of women enrolled in these two countries. In this communication, we will focus only on the screening test performance in detecting high-grade cervical lesions (CIN2+) and CC.

PAP test evaluation

Cervical cytology was tested in three arms: conventional and two different LBC techniques. LBC comprising Sure-Path® (named Autocyte at the time of study, BD, Burlington, USA) and DNA-Citoliq® (Digene, São Paulo, Brazil). Interpretation of the smears follows the Bethesda 2001 system. For analysis, when not otherwise indicated, Pap smear results equal or worse than atypical squamous cells of undetermined significance (ASC-US) were considered positive.

HPV testing

HR-HPV testing was done by HCII assay, using cervical swabs (collected by a physician) and self-sampling devices (tampons), as described previously [2–4]. HCII assay was performed using the automated system according to the manufacturer's protocol. The samples were analyzed only for the presence of high-risk HPV types 16, 18, 31, 33, 35, 39, 45, 51, 52, 56, 58, 59, and 68. The usual limit of 1 pg/ml of HPV16 DNA was used as the positive control. Samples were classified as HR-HPV positive, if the relative light unit reading of the luminometer was equal to or greater than 1.0 pg/ml.

Visual inspection with acetic acid

After sample collection for Pap test and HCII, 5 % acetic acid was applied on the cervix through embedded cotton at the edge of a Cherron forceps. One minute thereafter, the cervix was illuminated with a 100-W bright lamp and examined by naked eyes. The examiner's visual impression, classified according to the Atlas of Visual Inspection, was then recorded as the result of the examination. Results of VIA were classified as: (1) normal; (2) abnormal; and (3) suggesting cancer. The category of normal includes cases with the presence of cervical mucus, squamous metaplasia, ectopy, cervicitis, Naboth cysts, and polyps. Lesions suggestive of condyloma, CIN1, CIN2, and CIN3 were included in the abnormal category, and lesions suggesting cancer were recorded separately.

Visual inspection with Lugol iodine

After use of acetic acid, Lugol iodine was also applied on the cervix through an embedded cotton at the edge of a Cherron. Immediately after, the cervix was again illuminated with a 100-W bright lamp and examined by naked eyes. The examiner's visual impression, classified according to the Atlas of Visual Inspection, was then recorded as the result of the examination. Results of VILI were classified as normal, abnormal, and suggesting cancer, similar to VIA.

Cervicography

The cervix was visualized in a self-retaining speculum, and a specifically designed handheld camera (Cerviscope®, National Testing Laboratories, NTL, MO, USA) was used to take the photographs (cervigrams), using a special film. All cervigrams were interpreted by one of the authors, who are an NTL-authorized reader of cervigrams (S. Costa, Bologna, Italy). The examination of each patient was classified as technically defective (no definite diagnosis), negative, atypical, and positive.

Screening colposcopy and referral colposcopy

In one clinic (Buenos Aires), all patients were systematically examined by colposcopy. In all other clinics, patients were referred to colposcopy only if they had at least one of the screening tests abnormal. Colposcopy was performed according to the International Federation of Cervical Pathology and Colposcopy 1990 nomenclature. Any lesions suggestive of CIN or worst were defined as an abnormal colposcopy: aceto-white epithelium, punctuation, mosaic, leukoplakia, iodine negative area, abnormal blood vessels, and colposcopic findings suggestive of invasive carcinoma. All colposcopic abnormalities were subjected to punch biopsy for histological confirmation.

Cervical biopsies

Directed punch biopsies and conization samples were fixed in 10 % formalin and embedded in paraffin. The 5-μm-thick paraffin sections were routinely stained with hematoxylin–eosin and examined among the daily routine at the pathology departments of the four clinics. The commonly agreed CIN nomenclature was used for diagnosis of cervical pathology; CIN1 and/or HPV infection were considered as

low-grade CIN, whereas CIN2 and/or CIN3 were classified as high-grade CIN.

Final screening diagnosis

At the end of the screening phase, gold standard diagnosis was defined and used as an endpoint to calculate the performance indicators for the screening tests. Patients were stratified into two main categories:

1. Patients with normal cervix or cervical lesion equal to or less than CIN 1—the patient was considered to have a normal cervix if: (1) all screening tests were negative; (2) any screening test was abnormal but colposcopy revealed no lesion; or (3) any screening test and colposcopy was abnormal, but biopsy did not reveal any lesion.
2. Patients with biopsy-proven cervical lesions equal to or greater than CIN2 (CIN2+)—the patient was classified as CIN2+ based on the worst diagnosis in the biopsy or cervical conization.

Women with high-grade intraepithelial lesion (HSIL) cytology but normal colposcopy and/or normal biopsy were re-evaluated either by endocervical curettage or cold knife conization, based on the case characteristics and local management practices.

Unnecessary colposcopy referrals

We also calculated the percentage of unnecessary referrals to colposcopy. This number was defined as the proportion of the total number of patients who were referred to colposcopy and did not have CIN2 + .

Statistical analysis

Statistical analyses were performed using the SPSS program package (SPSS for Windows, version 12, USA). Performance indicators: sensitivity, specificity, positive predictive value, negative predictive value, and their 95 % confidence interval (95 % CI), of the diagnostic tests in predicting biopsy-confirmed CIN2+ were calculated using Epi Info (Centers for Disease Control and Prevention, version 3.5.1, USA). In all calculations, $p<0.05$ was considered statistically significant. When sensitivity, specificity, positive predictive value, and negative predictive value are presented, we also give the disease (CIN2+) prevalence, because of its major impact on these performance indicators.

Results

The four clinics examined a total of 12,114 women between February 2002 and June 2003, comprising the original LAMS study cohort. The mean (±SD) age of these women at enrolment was 37.9±11.2 years.

The majority of the women were White (74.7 %) in origin, followed by mixed (15.9 %), Black (8.6 %), and other race (0.8 %). A total of 31.6 % reported to be single. Only 0.1 % had not yet started their sexual activity. The mean age of first sexual intercourse was 18.5±3.9 years, and 86.9 % reported four or less sexual partners in a lifetime. Regarding participation in CC screening, 89.6 % reported at least one previous Pap smear, with a mean of 7.1±6.3 Pap smears in a lifetime.

Table 1 gives the numbers of all screening tests performed by each clinic. Conventional Pap smear, VIA, and HR-HPV testing were performed in all clinics, while the other screening tests were performed as specified.

Table 2 summarizes the final screening diagnosis at each clinic. The overall prevalence of CIN2+ (1.4 %) was not markedly less than the prevalence of CIN1/HPV (2.5 %), and that women in Buenos Aires presented with a higher prevalence of CIN lesions than the women at other clinics. Importantly, the percentage of patients who did not complete the screening phase of the study was very low (1.3 %).

Performance of conventional Pap smear and the two LBC assays in detecting CIN2+ lesions is summarized in Table 3. Specificity is very high in all settings. However, the sensitivity of all three cytological tests decreases substantially in parallel with the increasing cutoff (ASC-US, LSIL, and HSIL) used for colposcopic referral. Using the LSIL or HSIL cutoff, conventional Pap smear and LBC did not differ in the number of unnecessarily referrals to colposcopies, in contrast to ASC-US cutoff, where more variation was obvious.

Because (a) sensitivity of the screening tests varies according to the disease prevalence and (b) the same patients were not subjected to all three modalities of cytology, the prevalence of CIN2+ was slightly different for the three tests: 1.5, 1.3, and 1.2 % for conventional Pap smear, SurePath, and DNA-Citoliq groups, respectively (chi-square test, $p<0.001$).

Table 4 presents the performance of the other screening tests in detecting CIN2+. HCII assay collected by the physician has a high sensitivity (80 %), but at the expense of a high number of unnecessary referrals to colposcopy (15.1 %). HCII test in self-sampling had a markedly lower (57.1 %) sensitivity. VIA, VILI, and cervicography (any lesion cutoff) had a poor sensitivity (47.4, 55. and 28.6 %, respectively), with variable rates of unnecessary referrals to colposcopy (10.7, 21.8, and 3.4 %, respectively). Screening colposcopy presented with sensitivity of 100 % in detecting CIN2+, but the lowest specificity (66.9 %) of all tests analyzed in this setting.

Table 5 gives the performance indicators for different combinations used in co-testing for CIN2+ detection. Because co-testing with HCII and VIA/VILI resulted in very high number of unnecessary colposcopies, this combination was excluded from this analysis.

Table 1 Number of screening tests performed by each clinic

Screening test	Number of screening tests performed[a]			
	Porto Alegre, Brazil	São Paulo, Brazil	Campinas, Brazil	Buenos Aires, Argentina
Conventional cytology	3,039	1,372	2,615	3,437
LBC Sure-Path	–	320	–	–
LBC DNA-Citoliq	–	1,307	–	–
VIA	3,039	2,999	2,618	3,437
VILI	3,039	–	–	–
Cervicography	–	–	345	–
Screening colposcopy	–	–	–	3,437
HR-HPV testing (collected by physician)	1,104	808	1,562	940
HR-HPV testing (self-sampling)	–	311	–	–

[a]Blank cells indicate that the tests were not performed at that site

Co-testing with VIA (cutoff any lesion) and conventional Pap smear (ASC-US cutoff) increased the sensitivity of stand-alone Pap test from 71.6 % (Table 3) to 87.1 %, resulting in 13.3 % of unnecessary colposcopies. Similarly, adding VILI (any lesion cutoff) also increased sensitivity of conventional Pap smear (from 71.6 to 95 %), but at the expense of a high number of unnecessary colposcopies (23.7 %). Co-testing with HCII also increased the sensitivity of conventional Pap (to 86 %), but the number of unnecessary colposcopies (17.5 %) was higher than that of stand-alone VIA.

When the Pap test cutoff was raised to LSIL, the number of unnecessary colposcopies slightly decreases, but sensitivity is slightly compromised. The best combination was VIA (cutoff of any lesion) with Pap smear (LSIL) showing the lowest percentage of unnecessary referrals to colposcopy (11.7 %) and still having a high sensitivity (81.9 %).

Co-testing with combined VILI and VIA presented with sensitivity of 62.5 %, which is higher than that of either test alone; 47.4 % (VIA) and 55.0 % (VILI). However, this combination resulted in unacceptably high (22.5 %) percentage of unnecessary referrals to colposcopy.

Discussion

Conducted in the first years of 2000s, the LAMS study is among the first large cohorts in Latin America designed to compare multiple screening tests for early detection of CC. A part of reporting of the results is somewhat delayed from the study onset because the prospective arm took several more years to complete, i.e., to ensure a reasonable follow-up time. The main goal of the LAMS study was to furnish supportive elements to the Public Health Authorities (PHA), assisting their decisions about the best algorithms to be incorporated in the future screening programs. Indeed, when a new screening program is implemented, the PHA should be able to appropriately handled by all patients who have a positive screening test and would need further evaluation. It is a common knowledge that this can be a major problem in many screening settings. Because of this, in the present study, the numbers of unnecessary referrals to colposcopy are included as a key element in all performance calculations of stand-alone tests and their combinations.

In the LAMS setting, the conventional Pap smear showed the same sensitivity as previously reported in other large

Table 2 Final screening diagnosis at each clinic

Final diagnosis	Porto Alegre, Brazil *N* (%)	São Paulo, Brazil *N* (%)	Campinas, Brazil *N* (%)	Buenos Aires, Argentina *N* (%)	Total *N* (%)
Normal cervix	2,934 (96.4)	2,827 (94.2)	2,496 (94.8)	3,219 (93.7)	11,476 (94.7)
CIN1 and/or HPV infection	54 (1.8)	59 (2.0)	51 (1.9)	140 (4.1)	304 (2.5)
CIN2+	40 (1.3)	28 (0.9)	31 (1.2)	76 (2.2)	175 (1.4)
Screening not completed	15 (0.5)	86 (2.9)	56 (2.1)	0 (0)	157 (1.3)
Other diagnosis	0 (0)	0 (0)	0 (0)	2 (1.1)	2 (0.0)
Total	3,043 (100)	3,000 (100)	2,634 (100)	3,437 (100)	12,114 (100)

Chi-square test, $p<0.001$

CIN cervical intraepithelial neoplasia, *CIN2+* cervical intraepithelial neoplasia equal to or higher than CIN2

Table 3 Accuracy of the three cytological techniques in detecting CIN2+ in a scenario of 1.2 to 1.5 % disease prevalence

Cytological methods	Sensitivity	Specificity	PPV	NPV	Unnecessary referral to colposcopy
(For ASC-US + diagnoses)					
Conventional Pap smear	71.6 % (63.7–78.4)	96.5 % (96.1–96.8)	23.5 % (19.8–27.7)	99.6 % (99.4–99.7)	3.5 %
Liquid-based cytology (Sure-Path)	100.0 % (39.6–100)	97.1 % (94.5–98.6)	30.8 % (10.4–61.1)	100.0 % (98.5–100)	2.8 %
Liquid-based cytology (DNA-Citoliq)	73.3 % (44.8–91.1)	91.8 % (90.1–93.2)	9.7 % (5.2–17.1)	99.7 % (99.0–99.9)	8.1 %
(For LSIL + diagnoses)					
Conventional Pap smear	60.6 % (52.5–68.3)	98.5 % (98.2–98.7)	37.9 % (31.9–44.3)	99.4 % (99.2–99.5)	1.5 %
Liquid-based cytology (Sure-Path)	75.0 % (21.9–98.7)	98.4 % (96.1–99.4)	37.5 % (10.2–74.1)	99.7 % (97.9–100)	1.6 %
Liquid-based cytology (DNA-Citoliq)	46.7 % (22.3–72.6)	97.3 % (71.1–84.6)	17.5 % (7.9–33.4)	99.3 % (87.8–97.1)	2.6 %
(For HSIL + diagnoses)					
Conventional Pap smear	53.5 % (45.4–61.5)	99.6 % (99.4–99.7)	65.9 % (56.8–73.9)	99.3 % (99.1–99.4)	0.4 %
Liquid-based cytology (Sure-Path)	25.0 % (1.3–78.1)	99.7 % (98.0–100)	50.0 % (2.7–97.3)	99.1 % (97.0–99.8)	0.3 %
Liquid-based cytology (DNA-Citoliq)	46.7 % (22.3–72.6)	99.2 % (98.5–99.6)	41.2 % (19.4–66.5)	99.4 % (98.7–99.7)	0.8 %

95 % confidence interval (95 % CI) was proposed for all performance indicators (in parentheses)

95 % CI 95 % confidence interval, *PPV* positive predictive value, *NPV* negative predictive value, *CIN2+* cervical intraepithelial neoplasia equal to or higher than CIN2, *ASC-US* atypical squamous cells of undetermined significance, *LSIL* low-grade squamous intraepithelial lesion, *HSIL* high-grade squamous intraepithelial lesion

cohort studies [5–8]. This limited sensitivity (declining in parallel with the increasing cutoff (ASC-US to HSIL); Table 3) corroborates the inherent limitation of this test and the need of being repeated regularly. When using LSIL + cutoff, Sure-Path LBC had a higher sensitivity than conventional Pap smear or DNA-Citoliq. However, when using HSIL + cutoff, conventional Pap smear performed better than the two LBC methods. Some caution should be practiced, however, while interpreting these differences because of the sampling bias, i.e., a marked disparity in the number of cases examined by the three cytological methods. Of the LBC methods, Sure-Path was tested in only 320 women, while DNA-Citoliq was used for 1,307 women, all being collected at one center only (Leonor Mendes de Barros Hospital), which is a hospital that examines women at low-medium risk for CC [9–12]. The remaining 10,463 cytology samples were collected in all four

Table 4 Accuracy of the other screening methods in detecting CIN2+

Method (cutoff)	Sensitivity (95 % CI)	Specificity (95 % CI)	PPV (95 % CI)	NPV (95 % CI)	Unnecessary referral to colposcopy	Disease prevalence
HR-HPV Testing – physician (positive)	80.0 % (68.4–88.3)	84.6 % (83.5–85.7)	7.9 % (6.0–10.1)	99.6 % (99.3–99.8)	15.1 %	1.6 %
HR-HPV Testing - self-sampling (positive)	57.1 % (20.2–88.2)	85.7 % (97.7–98.8)	9.09 % (3.0–22.6)	98.8 % (99.6–100)	14 %	2.5 %
VIA (any lesion)	47.4 % (39.9–55.1)	89.3 % (88.6–89.7)	6.1 % (4.9–7.6)	99.1 % (98.9–99.3)	10.7 %	1.5 %
VIA (suggesting cancer)	10.3 % (6.4–16.0)	99.9 % (99.9–100.0)	81.8 % (59.0–94.0)	98.7 % (98.5–98.9)	0.03 %	1.5 %
VILI (any lesion)	55.0 % (38.7–70.4)	77.9 % (76.3–79.3)	3.2 % (2.1–4.9)	99.2 % (98.8–99.5)	21.8 %	1.3 %
VILI (suggesting cancer)	7.5 % (2.0–21.5)	99.9 % (99.7–100.0)	60.0 % (17.0–92.7)	98.8 % (98.3–99.1)	0.07 %	1.3 %
Cervicography (any lesion)	28.6 % (5.1–69.7)	96.6 % (93.8–98.2)	15.4 % (2.7–46.3)	98.4 % (96.1–99.4)	3.4 %	2.1 %
Screening Colposcopy (any lesion)	100.0 % (94.0–100)	66.9 % (65.3–68.5)	6.4 % (5.1–8.0)	100.0 % (99.8–100)	32.5 %	2.2 %

95 % CI 95 % confidence interval, *PPV* positive predictive value, *NPV* negative predictive value, *CIN* cervical intraepithelial neoplasia, *VIA* visual inspection with acetic acid, *VILI* visual inspection with Lugol iodine, *HR-HPV* high-risk human papillomavirus

Table 5 Accuracy of co-testing with different combinations in detecting CIN2+

Method (cutoff)	Sensitivity (95 % CI)	Specificity (95 % CI)	PPV (95 % CI)	NPV (95 % CI)	Unnecessary referral to colposcopy	Disease prevalence
Co-testing with conventional Pap smear (ASC-US+) and other screening test						
Conventional Pap (ASC-US+) and/or VIA (any lesion)	87.1 % (80.5–91.8)	86.5 % (85.8–87.2)	8.9 % (7.6–10.5)	99.8 % (99.6–99.9)	13.3 %	1.5 %
Conventional Pap (ASC-US+) and/or VILI (any lesion)	95.0 % (81.8–99.1)	76.0 % (74.4–77.5)	5.0 % (3.6–6.9)	99.9 % (99.6–100)	23.7 %	1.3 %
Conventional Pap (AS-CUS+) and/or HR-HPV testing—physician (positive)	86.0 % (73.7–93.3)	82.3 % (80.9–83.5)	7.3 % (5.5–9.6)	99.7 % (99.4–99.9)	17.5 %	1.6 %
Co-testing with conventional Pap smear (LSIL+) and other screening test						
Conventional Pap (LSIL+) and/or VIA (any lesion)	81.9 % (74.8–87.5)	88.1 % (87.5–88.7)	9.5 % (8.0–11.2)	99.7 % (99.5–99.8)	11.7 %	1.5 %
Conventional Pap (LSIL+) and/or VILI (any lesion)	92.5 % (78.5–98.0)	77.1 % (75.6–78.6)	5.1 % (3.7–7.0)	99.9 % (99.6–100)	22.6 %	1.3 %
Conventional Pap (LSIL+) and/or HR-HPV Testing—physician (positive)	82.5 % (69.6–90.8)	83.5 % (82.2–84.7)	7.5 % (5.6–9.9)	99.7 % (99.4–99.8)	16.3 %	1.6 %
Co-testing with visual screening tests						
VIA (any lesion) and/or VILI (any lesion)	62.5 % (45.8–76.8)	77.2 % (75.6–78.6)	3.5 % (2.3–5.3)	99.4 % (98.9–99.6)	22.5 %	1.3 %

95 % CI 95 % confidence interval, *PPV* positive predictive value, *NPV* negative predictive value, *CIN* cervical intraepithelial neoplasia, *VIA* visual inspection with acetic acid, *VILI* visual inspection with Lugol iodine, *HR-HPV* high-risk human papillomavirus, *ASC-US* + atypical squamous cells of undetermined significance or worst cytological finding, *LSIL* + low-grade intraepithelial lesions or worst cytological finding

centers, covering high prevalence areas of high-grade cervical lesions. Because the disease prevalence critically affects the test performance (sensitivity, PPV), the differences observed between the three cytological methods must be interpreted with this preservation. Interestingly, however, when correlated to the biopsy results, Sure-Path high-grade cases had 100 % concordance with the histological diagnosis, while DNA-Citoliq did only 40 % and Pap smear in 68.1 % (data previously reported; see reference [3]).

As previously reported [4], VIA and VILI as stand-alone tests in the LAMS setting did not show the same good performance indicators as previously reported in other settings [13–18]. In our cohort, both sensitivity and specificity of VIA and VILI were lower than those of conventional Pap smear, except when the "suggesting cancer" cutoff was used, when both VIA and VILI were almost 100 % specific (Table 4). Most of the published reports on VIA/ILI are from the same authors and based on data from India or Africa, i.e., in geographic areas with very high prevalence of CC and high-grade CIN, which certainly influences the performance of VIA and VILI [13–19].

Of all optional screening tools, HPV testing by HCII assay is among the most intensely studied diagnostic methods, assessed in several randomized controlled trials, and subjected to repeated meta-analyses [5, 6, 14, 20, 21]. In the LAMS setting, HCII testing in samples collected by physicians was not capable of detecting all CIN2+ cases but still presented a high (80 %) sensitivity. Of note, however, is the fact that 15 % of all patients examined by HCII assay in our trial were referred unnecessarily to colposcopy and needed further evaluation by colposcopy (Table 4). This is consistent with our recently published data implicating that the sensitivity of HPV testing (and Pap) will increase in older women, i.e., those beyond 35 years [19]. The local prevalence to HPV infections must be considered while planning to use this (and any) HPV assay as stand-alone test or combined with Pap (or other) test, in order to avoid unnecessary costs due to triage with supplementary examination [6, 13, 20–23].

In low-resource settings, self-sampling for HPV testing (by HCII) may help in detecting women with high-grade lesions [24]. In the LAMS setting, like in other studies, the

high rate of unnecessary referrals to colposcopy is a major problem, and the sensitivity of HCII self-sampling is lower than in cases when the samples are collected by physicians (Table 4). The findings of this study are in alignment with a previous analysis in one clinic (São Paulo), when we reported that self-sampling had a worse performance as compared with HCII testing from physician-collected samples [24]. The characteristics of the local facilities for collection of these samples must be carefully weighted prior to considering the introduction of self-sampling for HCII assay. Importantly, positive HPV test could be due to vaginal or vulvar infection and/or not necessarily linked with cervical lesion but just an indication of a transient infection. It is important to realize that in the present study, the number of samples included in this arm (n=311) is far too small when compared to other studies reporting a better performance for self-sampling, and this could contribute to our inferior results.

Of all tests evaluated in our study, cervicography had the lowest sensitivity in detecting CIN2+ (Table 4). This was not completely unexpected because, as determined from the published data, the sensitivity of cervicography varies significantly. Several potential biases have been listed to explain the wide variation of cervicography performance and its inherent limitations, including the quality of the equipment as well as the expertise of cervigram readers [23, 25–28]. All these limitations have contributed to the fact that cervicography is no longer considered as a viable option to replace Pap test or HPV assay in CC screening.

The last of the optional screening tests evaluated in the LAMS study is screening colposcopy, performed in one of the four clinics (Table 1) [2]. To make the data analysis comparable with the other screening tests, we considered that a patient with an abnormal screening colposcopy would necessitate a second colposcopy to evaluate the need for (and perform) the biopsy. With this approach, we identified that from the 3,437 screening colposcopies performed, 1,188 needed further evaluation by a second colposcopy, and only 76 patients had a significant biopsy-proven cervical lesion. These figures clearly indicate that colposcopy is not optimally tailored for screening purposes, despite its very high (100 %) sensitivity [2].

In addition to using the diagnostic assays as stand-alone tests, combining a test with high sensitivity with one demonstrating high specificity seems an attractive option [16]. When this was done in the present setting (Table 5), VIA and conventional Pap test disclosed the best balance of sensitivity, specificity, and unnecessary referrals to colposcopy. Thus, combining VIA and Pap test (ASC-US cutoff) increased the sensitivity of stand-alone Pap from 71.6 to 87.1 %. The combination of VILI and Pap test provided even higher sensitivity (95 %) but increased the unnecessary referrals to colposcopy almost twofold. These data might be of major practical importance because both VIA and VILI play a pivotal role in developing countries, and co-testing with Pap could importantly improve the efficacy of CC screening in these settings.

In the prevention of any disease, the primary prevention should always be the first choice whenever available, exceeding the capabilities of secondary prevention measures, e.g., screening. There is no doubt that in this respect, HPV vaccines are an important tool to improve the prevention of CC. Effective as this primary prevention of CC by HPV vaccination might prove to be, it should be taken into account that even if all HPV genotypes (currently two and four only) could be covered by the future vaccines, and even if all women were able to obtain the vaccination, there are hundreds of millions of women who have already been exposed to HPV and will need to be continuously monitored for CC and CIN. In this respect, the data elaborated in the LAMS study could substantially contribute to the public policies regarding CC screening in these two countries. At the same time, however, there is no doubt that introduction of molecular tests adjunct to Pap test seems urgent to improve the detection of high-grade lesions in population-based screening programs [28]. Specifically, the new generation of RNA tests such as Aptima that detects E6/E7 mRNA from 14 high-risk types was tailored to have similar sensitivity than DNA tests but significantly more specific [29]. Aptima was demonstrated to have the highest absolute risk for biopsy-proven CIN3+ and CIN2+ when compared with cytology and HCII testing, respectively [30]. This is a remarkable new data that could represent an important improvement to screening proposes and avoid unnecessary colposcopies

Acknowledgments This study has been supported by the European Commission, INCO-DEV Programme (contract# ICA4-CT-2001-10013). The generous contribution of DIGENE Corporation (USA) donating the HCII tests at our disposal is gratefully acknowledged.

Conflict of interest The authors declare that any conflict of interest, mainly financial agreement with companies whose products, are alluded to in the paper.

References

1. Estimate 2010: Incidence of cancer in Brazil. [eletronic] Rio de Janeiro: Brazilian National Cancer Institute; 2009 [cited 2010 04/01/2010]; Available from: http://www.inca.gov.br/estimativa/2010/conteudo_view.asp?ID=5
2. Syrjänen K, Naud P, Derchain S, Roteli-Martins C, Longatto-Filho A, Tatti S, Branca M, Erzen M, Hammes LS, Matos J, Gontijo R, Sarian L, Braganca J, Arlindo FC, Maeda MY, Lörincz A, Dores GB, Costa S, Syrjänen S (2005) Comparing PAP smear cytology, aided visual inspection, screening colposcopy, cervicography and HPV testing as optional screening tools in Latin America. Study design and baseline data of the LAMS study. Anticancer Res 25 (5):3469–80

3. Longatto-Filho A, Maeda MY, Erzen M, Branca M, Roteli-Martins C, Naud P, Derchain SF, Hammes L, Matos J, Gontijo R, Sarian LO, Lima TP, Tatti S, SyrjäneS SK (2005) Conventional Pap smear and liquid-based cytology as screening tools in low-resource settings in Latin America: experience of the Latin American screening study. Acta Cytol 49(5):500–6
4. Sarian LO, Derchain SF, Naud P, Roteli-Martins C, Longatto-Filho A, Tatti S, Branca M, Erzen M, Serpa-Hammes L, Matos J, Gontijo R, Bragança JF, Lima TP, Maeda MY, Lörincz A, Dores GB, Costa S, Syrjänen S, Syrjänen K (2005) Evaluation of visual inspection with acetic acid (VIA), Lugol's iodine (VILI), cervical cytology and HPV testing as cervical screening tools in Latin America. This report refers to partial results from the LAMS (Latin AMerican Screening) study. J Med Screen 12(3): 142-9
5. Arbyn M, Sankaranarayanan R, Muwonge R, Keita N, Dolo A, Mbalawa CG, Nouhou SB, Wesley R, Somanathan T, Sharma A, Shastri S, Basu P (2008) Pooled analysis of the accuracy of five cervical cancer screening tests assessed in eleven studies in Africa and India. Int J Cancer 123(1):153–60
6. Koliopoulos G, Arbyn M, Martin-Hirsch P, Kyrgiou M, Prendiville W, Paraskevaidis E (2007) Diagnostic accuracy of human papillomavirus testing in primary cervical screening: a systematic review and meta-analysis of non-randomized studies. Gynecol Oncol 104 (1):232–46
7. Nanda K, McCrory DC, Myers ER, Bastian LA, Hasselblad V, Hickey JD (2000) Matchar DB (2000) Accuracy of the Papanicolaou test in screening for and follow-up of cervical cytologic abnormalities: a systematic review. Ann Intern Med 132(10):810–9
8. Fahey, M.T., Irwin L, P. Macaskill P Meta-analysis of Pap test accuracy. Am J Epidemiol 141(7): 680-9.
9. Arbyn M, Bergeron C, Klinkhamer P, Martin-Hirsch P, Siebers AG (2008) Bulten J Liquid compared with conventional cervical cytology: a systematic review and meta-analysis. Obstet Gynecol 111 (1):167–77
10. Ronco G, Cuzick J, Pierotti P, Cariaggi MP, Dalla Palma P, Naldoni C, Ghiringhello B, Giorgi-Rossi P, Minucci D, Parisio F, Pojer A, Schiboni ML, Sintoni C, Zorzi M, Segnan N, Confortini M (2007) Accuracy of liquid based versus conventional cytology: overall results of new technologies for cervical cancer screening: randomised controlled trial. BMJ doi: 10.1136/bmj.39196.740995.BE
11. Davey E, Barratt A, Irwig L, Chan SF, Macaskill P, Mannes P, Saville AM (2006) Effect of study design and quality on unsatisfactory rates, cytology classifications, and accuracy in liquid-based versus conventional cervical cytology: a systematic review. Lancet 367(9505):122–32
12. Austin R, Ramzy I (1998) Increased detection of epithelial cell abnormalities by liquid-based gynecologic cytology preparations. A review of accumulated data. Acta Cytol 42(1):178–84
13. Sangwa-Lugoma G, Mahmud S, Nasr SH, Liaras J, Kayembe PK, Tozin RR, Drouin P, Lorincz A, Ferenczy A, Franco EL (2006) Visual inspection as a cervical cancer screening method in a primary health care setting in Africa. Int J Cancer 119(6):1389–95
14. Sankaranarayanan R, Nene BM, Dinshaw KA, Mahe C, Jayant K, Shastri SS, Malvi SG, Chinoy R, Kelkar R, Budukh AM, Keskar V, Rajeshwarker R, Muwonge R, Kane S, Parkin DM, Chauhan MK, Desai S, Fontaniere B, Frappart L, Kothari A, Lucas E, Panse N (2005) A cluster randomized controlled trial of visual, cytology and human papillomavirus screening for cancer of the cervix in rural India. Int J Cancer 116(4):617–23
15. Muwonge R, Walter SD, Wesley RS, Basu P, Shastri SS, Thara S, Mbalawa CG, Sankaranarayanan R (2007) Assessing the gain in diagnostic performance when two visual inspection methods are combined for cervical cancer prevention. J Med Screen 14(3):144–50
16. Mahe C, Gaffikin L (2005) Screening test accuracy studies: how valid are our conclusions? Application to visual inspection methods for cervical screening. Cancer Causes Control 16(6):657–66
17. Gaffikin L, Lauterbach M, Blumenthal PD (2003) Performance of visual inspection with acetic acid for cervical cancer screening: a qualitative summary of evidence to date. Obstet Gynecol Surv 58 (8):543–50
18. Sankaranarayanan R, Wesley R, Thara S, Dhakad N, Chandralekha B, Sebastian P, Chithrathara K, Parkin DM, Nair MK (2003) Test characteristics of visual inspection with 4 % acetic acid (VIA) and Lugol's iodine (VILI) in cervical cancer screening in Kerala, India. Int J Cancer 106(3):404–8
19. Syrjänen K, Derchain S, Roteli-Martins C, Longatto-Filho A, Hammes LS, Sarian L (2008) Value of conventional pap smear, liquid-based cytology, visual inspection and human papillomavirus testing as optional screening tools among Latin American women <35 and > or =35 years of age: experience from the Latin American Screening Study. Acta Cytol 52(6):641–53
20. Sankaranarayanan R, Nene BM, Shastri SS, Jayant K, Muwonge R, Budukh AM, Hingmire S, Malvi SG, Thorat R, Kothari A, Chinoy R, Kelkar R, Kane S, Desai S, Keskar VR, Rajeshwarkar R, Panse N, Dinshaw KA (2009) HPV screening for cervical cancer in rural India. N Engl J Med 360(14):1385–94
21. Cuzick J, Clavel C, Petry KU, Meijer CJ, Hoyer H, Ratnam S, Szarewski A, Birembaut P, Kulasingam S, Sasieni P, Iftner T (2006) Overview of the European and North American studies on HPV testing in primary cervical cancer screening. Int J Cancer 119(5):1095–101
22. De Vuyst H, Claeys P, Njiru S, Muchiri L, Steyaert S, De Sutter P, Van Marck E, Bwayo J, Temmerman M (2005) Comparison of Pap smear, visual inspection with acetic acid, human papillomavirus DNA-PCR testing and cervicography. Int J Gynaecol Obstet 89 (2):120–6
23. Longatto-Filho A, Roteli-Martins C, Hammes L, Etlinger D, Pereira SM, Erzen M, Branca M, Naud P, Derchain SF, Sarian LO, Matos J, Gontijo R, Lima T, Maeda MY, Tatti S, Syrjänen S, Syrjänen K (2008) Self-sampling for human papillomavirus (HPV) testing as cervical cancer screening option. Experience from the LAMS study. Eur J Gynaecol Oncol 29(4):327–32
24. Cronjé HS, Parham GP, Cooreman BF, de Beer A, Divall P, Bam RH (2003) A comparison of four screening methods for cervical neoplasia in a developing country. Am J Obstet Gynecol 188 (2):395–400
25. Costa S, Sideri M, Syrjänen K, Terzano P, De Nuzzo M, De Simone P, Cristiani P, Finarelli AC, Bovicelli A, Zamparelli A, Bovicelli L (2000) Combined Pap smear, cervicography and HPV DNA testing in the detection of cervical intraepithelial neoplasia and cancer. Acta Cytol 44(3):310–8
26. Schneider DL, Herrero R, Bratti C, Greenberg MD, Hildesheim A, Sherman ME, Morales J, Hutchinson ML, Sedlacek TV, Lorincz A, Mango L, Wacholder S, Alfaro M, Schiffman M (1999) Cervicography screening for cervical cancer among 8460 women in a high-risk population. Am J Obstet Gynecol 180:290–8
27. De Sutter P, Coibion M, Vosse M, Hertens D, Huet F, Wesling F, Wayembergh M, Bourdon C, Autier P (1998) A multicentre study comparing cervicography and cytology in the detection of cervical intraepithelial neoplasia. Br J Obstet Gynaecol 105(6):613–20
28. Schiffman M, Wentzensen N, Wacholder S, Kinney W, Gage JC, Castle PE (2011) Human papillomavirus testing in the prevention of cervical cancer. J Natl Cancer Inst 103(5):368–83
29. Clad A, Reuschenbach M, Weinschenk J, Grote R, Rahmsdorf J, Freudenberg N (2011) Performance of the Aptima high-risk human papillomavirus mRNA assay in a referral population in comparison with Hybrid Capture 2 and cytology. J Clin Microbiol 49(3):1071–6
30. Monsonego J, Hudgens MG, Zerat L, Zerat JC, Syrjänen K, Smith JS (2012) Risk assessment and clinical impact of liquid-based cytology, oncogenic human papillomavirus (HPV) DNA and mRNA testing in primary cervical cancer screening (The FASE Study). Gynecol Oncol 125(1):175–180

Virchows Arch (2012) 460:587–600
DOI 10.1007/s00428-012-1234-y

ORIGINAL ARTICLE

TGF-beta/Smad pathway and *BRAF* mutation play different roles in circumscribed and infiltrative papillary thyroid carcinoma

C. Eloy · J. Santos · J. Cameselle-Teijeiro · P. Soares · M. Sobrinho-Simões

Received: 4 February 2012 / Revised: 13 March 2012 / Accepted: 26 March 2012 / Published online: 20 April 2012
© Springer-Verlag 2012

Abstract Poorly circumscribed growth pattern, extrathyroid extension and high intratumoural lymph vessel density are significantly associated to nodal metastatization in papillary thyroid carcinoma (PTC). It was also shown that transforming growth factor beta (TGF-beta)/Smad-dependent pathway activity is associated with local invasion, nodal metastatization and *BRAF*-mutated PTCs. We analysed the immunoexpression of TGF-beta, Smad2/Smad3, Smad4 and Smad7 in a series of 42 cases of classic PTC and 33 cases of follicular variant of PTC with known clinico-pathological and follow-up data, as well as *BRAF* and *RAS status*. The 75 PTCs were divided into poorly circumscribed (PCPTC) (n=53) and well circumscribed (WCPTC) (n=22) according to their borders. Nodal metastases were not detected in any WCPTC regardless of the presence of immunoexpression for TGF-beta, Smad2/Smad3, Smad4 and Smad7 and occurrence of *BRAF* mutation (in 20 % of WCPTCs). Increased cytoplasmatic expression of TGF-beta at the periphery of PCPTC was associated to morphological features of invasiveness, featuring the so-called epithelial-to-mesenchymal transition (EMT), and presence of nodal metastases, as well as to the occurrence of *BRAF* mutation which did not significantly alter, per se, the frequency of nodal metastases. The nuclear expression of Smad7 was more frequent in WCPTCs than in PCPTCs and was associated with unicentricity and absence of extrathyroid extension, vascular invasion and nodal metastases. We conclude that nodal metastases are associated to poorly circumscribed, locally invasive PTCs that exhibit low levels of nuclear Smad7 and a peripheral EMT phenotype displaying TGF-beta overexpression, regardless of the occurrence of *BRAF* mutation.

Keywords Papillary thyroid carcinoma · BRAF · TGF-beta · Smad7 · Prognosis

Electronic supplementary material The online version of this article (doi:10.1007/s00428-012-1234-y) contains supplementary material, which is available to authorized users.

C. Eloy · M. Sobrinho-Simões
Pathology Department, Hospital de São João,
Porto, Portugal

C. Eloy · P. Soares · M. Sobrinho-Simões
Pathology Department, Medical Faculty of the University of Porto,
Porto, Portugal

C. Eloy · J. Santos · P. Soares · M. Sobrinho-Simões
IPATIMUP (Institute of Molecular Pathology and Immunology of the University of Porto),
Porto, Portugal

C. Eloy
Dentistry Faculty of the University of Porto,
Porto, Portugal

J. Cameselle-Teijeiro
Department of Pathology, Clinical University Hospital,
Health Research Institute of Santiago de Compostela (IDIS),
University of Santiago de Compostela,
Santiago de Compostela, Spain

C. Eloy (✉)
Anatomic Pathology Department, Hospital de São João,
Alameda Professor Hernani Monteiro,
4200-451 Porto, Portugal
e-mail: catarinaeloy@hotmail.com

Introduction

The large majority of papillary thyroid carcinomas (PTCs) evolve favourably [1] although a subset of cases may progress adversely leading to the development of recurrences and/or metastases [1–3]. Most cases of classic PTC (CPTC)

are poorly circumscribed, display a peripheral invasive front and give frequently rise to lymph node metastases [1], whereas many cases of the follicular variant of PTCs (FVPTCs) are encapsulated, sharing some of the clinico-pathological features of follicular carcinoma such as vascular invasion and distant metastases, as well as its most frequent molecular alterations, *RAS* mutations and *PAX8/PPARgamma* rearrangements [4–7]. There is also a poorly circumscribed/infiltrative subtype of FVPTC that, like CPTC, discloses a high intratumoural lymph vessel density and is prone to give rise to lymph node metastases [5, 6, 8]. It has been shown that *BRAF* V600E mutation is particularly prevalent in CPTC, as well as in PTC with a prominent papillary growth pattern such as Warthin-type and tall cell variant of PTC [9], in contrast to its low prevalence in FVPTC [9–11].

In a recent clinico-pathological study of 75 cases of PTC (42 CPTCs and 33 FVPTCs), we observed that poorly circumscribed/infiltrative growth pattern and extra-thyroid extension, rather than the presence of *BRAF* V600E, were significantly associated with the occurrence of lymph node metastases [11]. The infiltrative growth pattern of most non-encapsulated forms of PTC is mainly the result of increased motility and of tumour cell's invasiveness [12–14] which are features related to the so-called epithelial-to-mesenchymal transition (EMT). At PTC's infiltrative periphery, the neoplastic cells displayed loss of polarity/cohesiveness [14], decreased expression of beta-catenin and E-cadherin at the cell membrane [15], increased nuclear expression of STAT3 [Couto et al., unpublished results], increased cytoplasmatic expression of vimentin [15], fibronectin 1[12], met [16], ret [17], cytokeratin 5/6 [18] and galectin-3 [19], and increased nuclear expression of cyclin D1 [20].

The above-mentioned alterations at the infiltrative edge of the tumours reflect probably the crosstalk between tumour cells and cellular and non-cellular elements of the stroma, in part mediated by integrin-related epithelial-to-stromal connections which are enhanced at PTC's periphery [21]. Dendritic cells were found to be located at the tumour's invasion edge in a small series of PTC [22] and, together with lymphocytes, appear to be decreased in PTCs with distant metastases [23], while increased density of tumour-associated macrophages in poorly differentiated carcinomas correlate with invasion and decreased survival [24].

EMT is partially regulated by transforming growth factor beta (TGF-beta) in PTC cell lines [25–28] and in animal models [29]. TGF-beta is one of the members of the TGF-beta superfamily and occurs in three isoforms—TGF-beta1, TGF-beta2 and TGF-beta3—that function via the same membrane receptor signalling system [30]. In TGF-beta/Smad-dependent pathway, the activated TGF-beta receptor complex propagates the signal inside the cell through the phosphorylation of receptor-regulated Smad2 and Smad3 downstream proteins localised in the cytoplasm [30–32]. Phosphorylated Smad2 and Smad3 form heteromeric complexes with Smad4 and re-localise to the nucleus where they regulate gene transcription [30–32]. Inhibitory Smad7 acts in an opposite manner and antagonises TGF-beta/Smad-dependent signalling, inducing TGF-beta receptor degradation and thus preventing Smad2 and Smad3 phosphorylation [31, 32]. TGF-beta/Smad-dependent pathway activation induces major growth-suppressive effects on epithelial cells in general [32], and on animal [33–35] and human [36, 37] thyroid cell lines, as well as on some PTC cell lines [25, 28], in particular. TGF-beta is also related to inhibition of migration and invasiveness in some PTC cell lines [25]. The expression of TGF-beta, Smad2, Smad3 and Smad7 has been detected in multinodular goitres [38–40] and in follicular adenomas of some series [40, 41], but not in other series of thyroid lesions where TGF-beta was the only element searched [42].

In tumours, TGF-beta expression has been detected in 52–100 % of PTC cases [38, 40–43] and, whenever specifically studied at the tumour's periphery, was associated to the occurrence of extra-thyroid extension and lymph node metastases [26]. Similarly, phosphorylated Smad2/Smad3 (P-Smad2/3) has been detected in every case of PTC [40], while Smad4 is expressed in 75 % of PTC cases [40] and in every PTC cell line [44, 45]. Smad7 expression has been detected in 80 % of PTCs and PTC cell lines [40, 44].

In tumour cells, particularly when exhibiting an EMT phenotype characterised by mesenchymal-type features [12], the response to TGF-beta growth-suppressive effect can be partially or totally abrogated via interferences in the signalling pathways that mediate its action [26, 29, 37, 46–48]. TGF-beta anti-proliferative effects were reported as attenuated in cases of multinodular goitre [49], in anaplastic carcinoma cell lines [50], as well as in rat thyroid cell lines [51]. At the EMT, the TGF-beta-altered cell response has been associated to the development of pro-oncogenic effects, namely through the inhibition of cell adhesion and enhancement of motility [32, 52].

Besides playing a functional role in tumour cell migration, invasion and EMT in vitro, TGF-beta and high TGF-beta/Smad-dependent pathway activity are associated with invasion, nodal metastasising and *BRAF*-mutated PTCs [26]. It has been reported that oncogenic *BRAF* stimulates TGF-beta secretion in vitro [26]. *BRAF* is thought to play a major role in extracellular matrix remodelling [52] and is required for TGF-beta-induced EMT during progression from PTC to poorly differentiated carcinoma in an animal model [29]. Finally, it has been shown that *BRAF* suppresses the expression of E-cadherin, which is a typical finding at the infiltrative edge of poorly circumscribed PTCs, and that this effect can be abrogated with both TGF-beta and mitogen-activated protein kinase (MAPK) inhibitors [26].

We decided to analyse the immunohistochemical expression of TGF-beta1 and TGF-beta2 and their downstream phosphorylated Smad2/Smad3 and Smad4 elements, and of the inhibitory Smad7, in well-circumscribed and poorly circumscribed PTCs (WCPTC and PCPTC, respectively). The study was made using the previously analysed series of 75 carcinomas in which *BRAF* and *N-RAS status* had been characterised [11], in order to clarify the putative relationship between functioning TGF-beta/Smad-dependent pathway and *BRAF* mutation in the two PTC subtypes: WCPTC and PCPTC.

Material and methods

Part of the clinico-pathological data of the 75 cases has been previously reported [8, 11].

Tumour samples

A series of 75 PTC cases was retrieved from the Cancer Registry of the Pathology Department of Hospital de São João: 42 CPTCs and 33 FVPTCs. Both groups (CPTC and FVPTC) included cases with lymph node metastases (+M) (mean follow-up of 5.9 years; range 1 to 14 years) and cases without metastases and long-term follow-up (−M) (mean follow-up of 18.8 years; range 10 to 24 years). Three cases (two CPTCs and one FVPTC) disclosed, together with lymph node metastases, lung metastases (Tables 1 and 2). Both groups included tumours larger than 1 cm and small tumours, 1 cm or less in diameter, that were classified according to their pattern of growth as CPTC or FVPTC. None of the patients died from the disease.

All samples had been fixed in formalin and included in paraffin. Clinical data were collected from the pathology reports and clinical files. H&E slides were retrieved from the archives and reviewed independently by two pathologists (CE and MSS) and the tumours were classified using the WHO criteria [1]. Cases with doubtful PTC features were excluded. Due to their scarcity, variants of PTC such as tall cell, columnar cell and sclerosing diffuse variant were not included. WCPTCs were those with expansive growth pattern along the whole periphery and those limited by a capsule with none or only minimal focal invasion. PCPTCs were those with infiltrative growth pattern or with an extensively invaded capsule. Vascular invasion was considered to be present whenever one image of unequivocal venous vessel invasion was observed.

Mutation screening

The detection of *BRAF* (exon 15) and *N-RAS* (exon 2) mutations was performed as previously described [11] in 10-μm sections of 65 tumours: 34 CPTCs and 31 FVPTCs. The remaining ten cases had insufficient available material for performing the molecular study.

Immunohistochemistry

Immunohistochemical staining was performed using streptavidin–biotin technique as previously described [8]. Briefly, endogenous peroxidase was blocked with 3 % hydrogen peroxidase in methanol (Panreac) for 10 min in a humid chamber and then avidin blocking and biotin blocking were performed (Lab Vision, Thermo Scientific). In order to block unspecific bounding to hydrophobic epitopes, the sections were immersed in Ultra V Block (Lab Vision, Thermo Scientific) for 10 min at room temperature. Slides were incubated overnight at 4°C with TGF-beta1/2 rabbit polyclonal antibody (from here on designated as TGF-beta) in a 1:50 dilution (TGF-beta1(V), Santa Cruz Biotechnology, CA) against a peptide in the C-terminus of precursor and mature human TGF-beta1 and TGF-beta2 ligands; P-Smad2/3 rabbit polyclonal antibody in a 1:100 dilution (P-Smad2/3 (Ser 423/425), Santa Cruz Biotechnology, CA) against C-terminus of both phosphorylated Smad2 and Smad3; Smad4 monoclonal mouse antibody in a 1:100 dilution (Smad4 (B-8), Santa Cruz Biotechnology, CA) and Smad7 mouse monoclonal antibody in a 1:100 dilution (Smad7 (Z8-B), Santa Cruz Biotechnology, CA). Then, the slides were incubated with biotinylated secondary goat antibody and streptavidin–peroxidase complex (Lab Vision, Thermo Scientific) for 10 min at room temperature. Tissue microarrays with adequate positive and negative controls were used in every set of staining.

Semiquantitative assessment of TGF-beta and Smads expression

The TGF-beta expression in the tumour cells was evaluated in the centre and in the periphery of all carcinomas (CPTC and FVPTC) and in the respective remaining thyroid tissue, which was used as an internal control tissue, in order to reduce the influence of fluctuations of the physiological expression in each case. TGF-beta expression detected in cells of the control tissue was considered as the basal expression.

TGF-beta expression in the tumour cells located in the centre of each tumour was compared with the expression in the respective control tissue, and the TGF-beta expression in the tumour cells located in the periphery of each tumour was compared with the expression in the respective centre of the tumour. The mean expressions observed in each location were also compared. The centre of the tumour comprised the bulk of the tumour, i.e. the whole neoplastic tissue except the subcapsular areas and/or the invasive front. The periphery of the tumour comprised the rim of tumour cells

Table 1 Clinico-pathological, molecular and immunohistochemical features of the CPTC cases

Case number	Gender	Age (years)	Follow-up (years)	Tumour size (cm)	GP	MC	EE	VI	*BRAF*	*N-RAS*	Intensity of expression			P-Smad2/3 C (n/c)	P-Smad2/3 CT (n/c)	Smad4 C (n/c)	Smad4 CT (n/c)	Smad7 C (n/c)	Smad7 CT (n/c)	LNM
											TGF-beta C	TGF-beta P	TGF-beta CT							
1	M	58	17	0.8	PC	−	−	−	ND	ND	3	2	1	+/−	−/+	−/+	−/+	+/+	−/+	−
2	F	66	19	1.5	WC	−	−	−	ND	ND	2	2	1	+/+	+/−	−/+	+/+	+/+	+/−	−
3	F	31	21	3.5	PC	+	−	−	−	−	3	3	2	+/+	+/−	−/+	+/+	+/+	+/−	−
4	F	59	21	0.6	PC	+	−	−	−	−	2	2	1	+/+	+/−	−/+	+/+	+/+	+/−	−
5	F	37	21	1.0	WC	+	−	−	ND	ND	3	3	2	+/−	+/+	−/+	−/+	+/+	+/+	−
6	F	35	18	0.3	PC	−	−	−	ND	ND	2	3	0	+/−	+/−	+/+	+/+	+/−	+/−	−
7	F	40	18	1.5	PC	−	−	−	V600E	−	3	3	1	+/+	+/−	−/+	−/+	+/−	+/−	−
8	F	38	18	0.5	PC	−	−	−	ND	ND	2	2	0	+/+	+/+	−/+	−/+	+/+	+/−	−
9	M	25	20	1.2	PC	−	−	+	−	−	2	1	1	+/+	+/−	−/+	−/+	+/+	+/−	−
10	F	30	21	0.6	PC	+	−	−	V600E	−	2	3	2	+/+	+/−	−/+	+/+	−/+	−/+	−
11	F	40	20	2.2	WC	−	−	−	−	−	1	2	2	+/+	+/−	−/+	−/+	+/+	+/+	−
12	F	50	20	3.0	WC	−	−	−	V600E	−	1	1	0	+/−	+/−	−/+	−/+	+/−	+/−	−
13	F	25	17	2.1	WC	−	−	−	V600E	−	1	1	1	+/+	+/−	−/+	+/+	+/+	+/−	−
14	F	45	22	4.5	WC	+	−	−	V600E	Q61R	2	3	2	+/−	+/+	+/+	−/+	+/+	+/−	−
15	F	23	24	2.5	PC	−	−	−	−	−	3	3	2	+/+	+/+	−/+	+/+	+/+	+/+	−
16	M	65	24	2.3	PC	−	−	−	−	−	3	3	2	+/+	+/+	−/+	+/+	+/+	+/+	−
17	F	21	19	2.0	PC	−	−	+	V600E	−	1	2	0	+/+	+/−	−/+	+/+	+/+	+/−	−
18	F	79	23	2.8	PC	−	+	−	−	−	3	3	1	+/+	−/−	−/+	−/+	+/+	+/−	−
19	F	65	16	3.5	PC	−	+	−	V600E	−	1	2	0	+/+	+/−	−/+	+/−	+/−	+/−	−
20	F	28	24	2.5	PC	−	−	+	−	−	3	3	0	+/+	+/+	−/+	+/+	+/+	+/−	−
21	F	28	20	2.0	PC	−	−	+	V600E	−	3	3	0	+/+	+/−	−/+	+/+	+/+	+/+	−
22	F	43	18	1.5	WC	+	−	+	−	−	1	1	0	+/+	+/−	−/+	+/+	+/+	+/+	−
23	F	47	16	4.5	PC	−	+	+	V600E	−	1	3	1	+/+	+/−	−/+	+/+	+/+	+/−	−
24	F	28	5	0.9	PC	−	−	−	V600E	−	1	2	1	+/+	+/−	+/+	+/+	+/+	+/−	+
25	F	21	6	1.2	PC	−	−	−	−	−	1	2	2	+/+	+/+	+/+	+/+	−/+	+/−	+
26	F	22	14	1.9	PC	+	−	−	−	−	1	1	1	+/+	+/−	−/+	+/+	+/+	+/−	+
27	F	30	3	1.3	PC	−	+	+	−	−	2	3	2	+/+	+/−	−/+	+/+	−/+	+/−	+
28	F	56	3	0.7	PC	+	−	−	−	−	3	3	2	+/+	+/−	−/+	+/+	−/+	+/−	+
29	F	18	3	1.5	PC	+	+	+	−	−	3	3	2	+/+	+/−	+/+	+/+	−/+	+/−	+
30	M	22	4	1.1	PC	+	−	−	−	−	2	3	2	+/−	+/−	+/+	+/+	−/−	+/−	+
31	F	22	6	0.8	PC	−	−	−	ND	ND	1	2	2	+/+	+/−	−/+	+/+	−/+	+/−	+
32	F	56	3	0.8	PC	+	−	−	ND	ND	1	2	1	+/+	+/−	−/+	+/+	−/+	+/+	+
33	M	42	5	1.6	PC	+	+	−	−	−	2	3	3	+/+	+/−	−/+	+/+	−/+	+/−	+
34	F	38	7	3.0	PC	+	−	+	V600E	−	1	1	2	+/+	+/−	−/+	+/+	−/+	+/−	+
35	F	35	5	1.7	PC	−	−	+	V600E	−	0	2	2	+/+	+/−	−/+	+/+	−/+	+/−	+
36	M	11	9	6.0	PC	+	+	+	−	−	1	2	0	+/+	+/−	−/+	+/+	+/−	+/−	+[a]
37	F	56	4	2.4	PC	−	+	−	−	−	1	2	2	+/+	+/−	−/+	+/+	−/+	+/−	+[a]

Table 1 (continued)

Case number	Gender	Age (years)	Follow-up (years)	Tumour size (cm)	GP	MC	EE	VI	*BRAF*	*N-RAS*	Intensity of expression			P-Smad2/3 C (n/c)	P-Smad2/3 CT (n/c)	Smad4 C (n/c)	Smad4 CT (n/c)	Smad7 C (n/c)	Smad7 CT (n/c)	LNM
											TGF-beta C	TGF-beta P	TGF-beta CT							
38	F	83	1	7.5	PC	–	+	–	V600E	–	0	3	ND	+/+	ND	–/+	ND	–/+	ND	+
39	F	18	4	3.6	PC	+	–	+	–	–	2	2	1	+/+	+/–	+/+	+/+	–/+	+/–	+
40	M	14	4	2.5	PC	+	+	–	–	–	1	2	1	+/+	+/–	+/+	+/+	–/–	+/–	+
41	F	32	9	1.1	PC	–	+	–	V600E	–	0	2	1	+/–	+/–	–/+	+/+	+/–	+/–	+
42	F	56	10	7.5	PC	+	+	–	ND	ND	1	2	1	+/+	+/–	–/+	+/+	–/+	+/–	+

M male, *F* female, + presence, – absence, *GP* growth pattern, *MC* multicentricity, *EE* extra-thyroid extension, *VI* vascular invasion, *WC* well circumscribed, *PC* poorly circumscribed, *ND* not determined, *C* expression in the centre of the tumour, *P* expression in the tumour periphery, *CT* expression in the control tissue, *n* nuclear, *c* cytoplasmatic, *LNM* lymph node metastases

[a] Cases with concurrent distant metastases

underneath the capsule or at the expansive periphery in WCPTC and in the invasive front in PCPTC. TGF-beta expression was cytoplasmatic and was graduated in four categories that were considered to represent continuous and crescent immunostaining intensity: negative 0 (weak staining in less than 25 % of cells), positive 1 (weak staining in at least 25 % of cells or moderate intensity in less than 25 % of cells), positive 2 (moderate intensity in at least 25 % of cells or intense staining in less than 25 % of cells) and positive 3 (intense staining in at least 25 % of cells).

The expression of P-Smad2/3, Smad4 and Smad7 was nuclear and cytoplasmatic and was evaluated in all CPTC and FVPTC tumours and in the respective remaining thyroid tissue, which was used as an internal control tissue and considered the basal expression. The expression of P-Smad2/3, Smad4 and Smad7 in the centre of the tumour and at the periphery was considered too difficult to distinguish and, therefore, assumed as similar. The expression was graduated in two categories: negative (weak staining in less than 25 % of cells) and positive (weak, moderate or intense staining in at least 25 % of cells), regarding each subcellular location (nuclear or cytoplasmatic) separately.

Statistical analysis

The results are expressed as absolute values, percentages and/or mean ± standard deviation. The χ^2 test with Yates's correction and the Student's *t* test (unpaired) were used in the statistical analysis. Two values were considered significantly different whenever $p<0.05$ and suggestively different whenever $p<0.1$.

Results

1. Clinico-pathological and molecular features

   CPTC and FVPTC groups displayed similar features except the prevalence of poorly circumscribed tumours (83.3 % of CPTC and 54.4 % of FVPTC, $p=0.010$), vascular invasion (26.6 % of CPTC and 57.6 % of FVPTC, $p=0.018$) and *BRAF* V600E mutation (41.2 % of CPTC and 16.1 % of FVPTC, $p=0.032$). A detailed description of the clinico-pathological and molecular features of the 75 cases has been previously reported [8, 11].

2. CPTC versus FVPTC

   (a) TGF-beta expression

   TGF-beta expression was observed in all but two FVPTC−M cases and was detected in the centre of 88.0 % of tumours (95.2 % of CPTC and 81.8 % of FVPTC), at the periphery of 94.7 % of tumours (100 % of CPTC and 87.9 %

Table 2 Clinico-pathological, molecular and immunohistochemical features of the FVPTC cases

Case number	Gender	Age (years)	Follow-up (years)	Tumour size (cm)	GP	MC	EE	VI	*BRAF*	*N-RAS*	Intensity of expression			P-Smad2/3 C (n/c)	P-Smad2/3 CT (n/c)	Smad4 C (n/c)	Smad4 CT (n/c)	Smad7 C (n/c)	Smad7 CT (n/c)	LNM
											TGF-beta C	TGF-beta P	TGF-beta CT							
1	F	32	22	2.0	WC	−	−	+	−	−	2	0	2	+/+	+/−	−/+	+/+	+/+	+/−	−
2	F	26	21	1.8	PC	+	−	+	V600E	−	2	3	1	+/+	+/−	−/+	+/+	+/+	+/+	−
3	F	59	19	0.5	WC	−	−	−	−	−	0	0	0	+/−	+/−	−/+	+/−	+/−	+/−	−
4	F	51	18	1.4	WC	−	−	−	−	−	2	3	1	+/+	+/−	+/+	+/+	+/+	+/−	−
5	F	36	18	0.5	PC	−	−	−	V600E	−	1	1	1	+/+	+/−	+/+	+/+	+/−	+/−	−
6	F	39	15	1.0	WC	+	−	−	−	Q61R	1	1	0	+/−	+/−	+/+	+/+	+/+	+/−	−
7	F	48	13	0.6	WC	−	−	−	−	−	1	0	0	+/+	+/+	+/+	+/+	+/−	+/−	−
8	F	33	20	0.2	PC	−	−	−	−	−	3	3	0	+/+	+/+	+/+	+/+	+/+	+/−	−
9	F	30	15	0.5	WC	−	−	−	−	−	1	1	0	+/+	+/+	−/+	+/+	+/−	+/−	−
10	F	21	21	0.6	PC	−	−	−	−	−	1	3	1	+/−	+/−	−/+	+/+	+/−	+/−	−
11	F	37	18	0.3	PC	−	−	+	−	−	1	1	1	+/−	+/−	−/+	+/+	+/−	+/−	−
12	F	28	21	2.8	WC	+	−	+	−	−	2	3	0	+/+	+/−	−/+	+/+	+/+	+/+	−
13	F	34	20	3.5	WC	−	−	−	−	−	0	0	0	+/−	+/−	+/+	−/+	+/−	+/−	−
14	M	61	22	4.0	WC	−	−	+	V600E	−	2	2	2	+/+	+/−	−/+	+/+	+/+	+/−	−
15	M	35	20	3.5	WC	−	−	+	−	Q61R	1	1	1	+/+	+/−	−/+	+/+	+/−	+/−	−
16	F	50	20	2.5	WC	−	−	−	−	−	1	1	1	+/−	+/−	−/+	−/+	+/−	+/−	−
17	F	47	23	3.0	PC	−	−	−	−	Q61R	2	3	0	+/−	+/−	+/+	+/+	+/+	+/−	−
18	F	49	14	3.0	WC	+	−	+	−	−	2	1	1	+/+	+/+	−/+	+/+	+/+	+/−	−
19	F	35	21	1.7	PC	+	−	+	ND	ND	3	3	1	+/+	+/−	−/+	+/+	+/+	+/−	−
20	F	32	13	4.7	PC	+	−	+	−	−	2	3	2	+/+	+/−	+/+	+/+	+/+	+/−	−
21	F	52	13	2.5	WC	+	−	−	−	−	1	1	2	+/−	+/−	+/+	+/+	+/−	+/−	−
22	F	66	13	2.5	WC	+	−	−	−	−	1	1	0	+/+	+/−	+/+	+/+	+/−	+/−	−
23	F	58	13	1.5	PC	+	−	+	V600E	−	0	1	1	+/+	+/−	−/+	+/+	+/+	+/−	−
24	F	54	10	1.8	PC	+	−	+	−	−	1	2	1	+/+	+/+	−/+	+/+	+/+	+/−	−
25	M	45	20	4.0	WC	−	−	−	−	−	1	1	1	+/−	+/−	−/+	+/+	+/−	+/−	−
26	M	57	3	9.5	PC	−	+	+	−	−	2	2	1	+/+	+/+	+/+	+/+	−/+	+/−	+
27	F	56	3	0.8	PC	+	−	+	−	−	1	2	2	+/+	+/−	+/+	+/+	−/−	+/−	+
28	M	21	4	2.5	PC	−	+	+	−	−	1	2	0	+/+	+/−	−/+	+/+	−/+	+/−	+
29	F	20	14	1.0	PC	+	−	+	ND	ND	0	1	2	+/−	+/−	−/+	+/+	−/−	+/−	+
30	F	49	4	2.2	PC	−	−	+	−	−	0	1	0	+/−	+/−	−/+	+/+	−/−	+/−	+
31	F	43	10	4.0	PC	+	+	+	−	−	0	1	0	+/−	+/−	−/+	+/+	−/−	+/−	+

Table 2 (continued)

Case number	Gender	Age (years)	Follow-up (years)	Tumour size (cm)	GP	MC	EE	VI	*BRAF*	*N-RAS*	Intensity of expression			P-Smad2/3 C (n/c)	P-Smad2/3 CT (n/c)	Smad4 C (n/c)	Smad4 CT (n/c)	Smad7 C (n/c)	Smad7 CT (n/c)	LNM
											TGF-beta C	TGF-beta P	TGF-beta CT							
32	F	43	10	1.5	PC	+	+	+	V600E	–	1	3	1	+/–	+/–	–/+	+/+	+/–	+/–	+
33	M	63	7	1.8	PC	–	–	+	–	–	1	3	1	+/–	+/–	–/+	+/+	–/+	+/–	+[a]

M male, *F* female, + presence, – absence, *GP* growth pattern, *MC* multicentricity, *EE* extra-thyroid extension, *VI* vascular invasion, *WC* well circumscribed, *PC* poorly circumscribed, *ND* not determined, *C* expression in the centre of the tumour, *P* expression in the tumour periphery, *CT* expression in the control tissue, *n* nuclear, *c* cytoplasmatic, *LNM* lymph node metastases

[a] Case with concurrent distant metastases

of FVPTC) and in the control tissues in 73.0 % of cases (78.6 % of CPTC and 63.3 % of FVPTC).

In comparison with the respective control tissue, the centre of the carcinomas disclosed basal or overexpression of TGF-beta in 83.8 % of cases. The TGF-beta expression at the periphery of each tumour was similar or higher than the TGF-beta expression in the centre in all but one CPTC−M and three FVPTC−M cases (94.7 %) (Tables 1 and 2 and Fig. 1).

The mean intensity of TGF-beta expression in the centre of the tumours, in comparison with the respective control tissue, was much higher in PTC −M than in PTC+M ($p<0.0001$). The mean intensity of TGF-beta expression at the periphery, compared with the respective centre of the tumours, was significantly higher in PTC+M than in PTC−M ($p=0.0001$) and was also significantly higher in tumours with poorly circumscribed growth pattern ($p<0.0007$), extra-thyroid extension ($p=0.002$) and *BRAF* V600E mutation ($p=0.029$).The Supplemental table summarises the result of the comparison between CPTC and FVPTC.

(b) P-Smad2/3 expression

P-Smad2/3 nuclear expression was observed in all tumours (Fig. 2a, b) and in all but two control tissues of the CPTC−M group (97.3 %) (Fig. 2c).

P-Smad2/3 cytoplasmatic expression was observed in 72.0 % of tumours and in 18.9 % of control tissues. In comparison to the respective control tissue, P-Smad2/3 had a basal level or was underexpressed in the cytoplasm of tumour cells in 43.2 % of the cases. Tumours with basal or underexpression of cytoplasmatic P-Smad2/3 belonged more frequently to the group of FVPTC than to the CPTC group (60.6 and 29.3 %, respectively; $p=0.010$) and tended to have more often wild-type *BRAF* than mutated *BRAF* ($p=0.053$) (Tables 1 and 2). P-Smad2/3 expression was not significantly associated to any other clinical, pathological or molecular features.

(c) Smad4 expression

Smad4 nuclear expression was observed in 26.7 % of tumours and 85.1 % of control tissues (Fig. 2d–f). Smad4 had a basal level or was overexpressed in the nuclei of tumour cells in 39.2 % of the cases in comparison with the respective control tissue. Vascular invasion was significantly less frequent in tumours with basal or overexpressed nuclear Smad4 ($p=0.004$), particularly in the FVPTC group ($p=0.003$). Smad4 cytoplasmatic expression was observed in all tumours and in all but two control tissues of the PTC−M group (97.3 %).

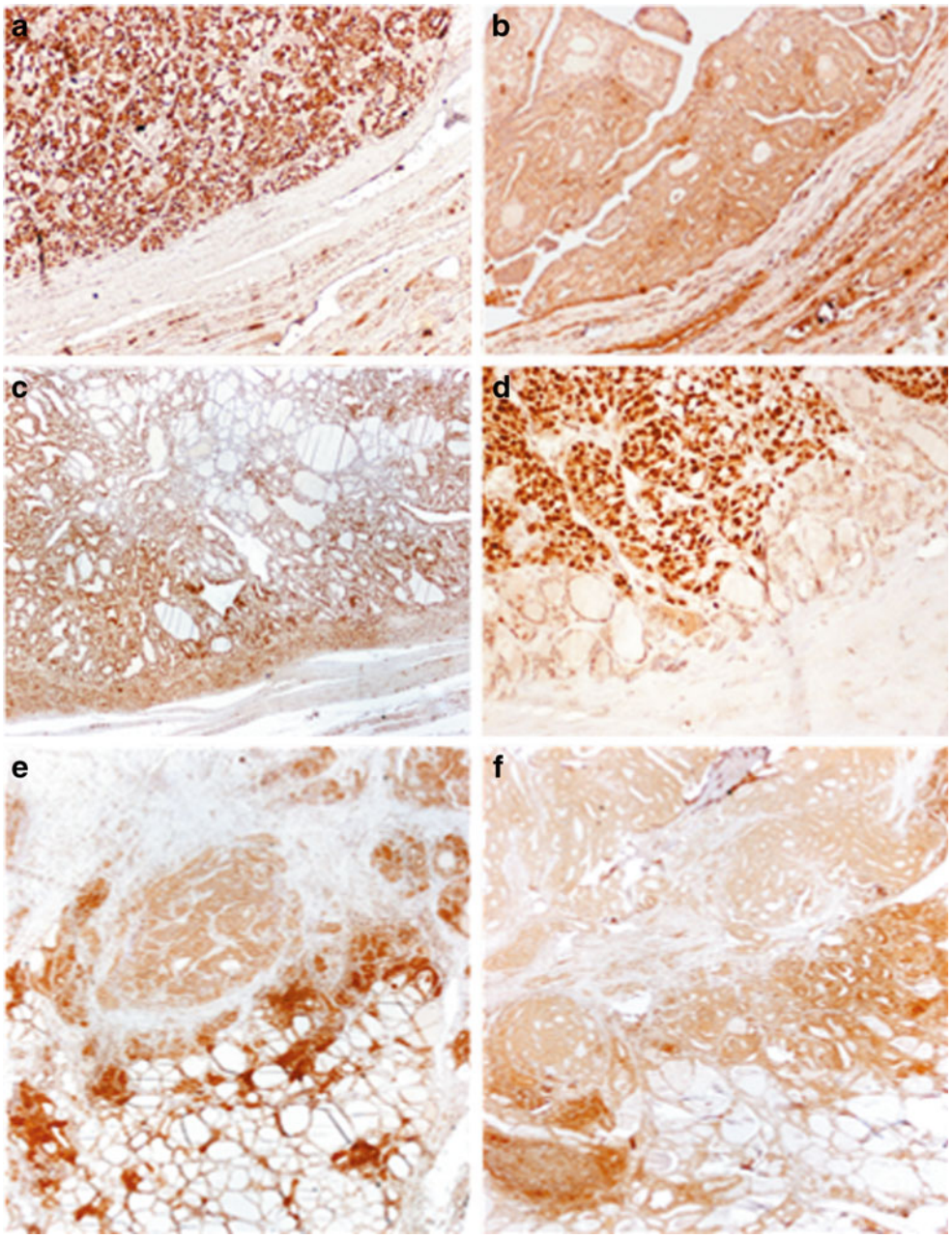

Fig. 1 TGF-beta expression at the centre and at the periphery of the tumours. **a** Well-circumscribed *BRAF*-mutated FVPTC−M with similar expression at the centre and at the periphery (case 14, ×200). **b** Well-circumscribed wild-type *BRAF* FVPTC−M with increased expression at the periphery (case 12, ×200). **c** Poorly circumscribed wild-type *BRAF* FVPTC+M with lung metastases and increased expression at the periphery (case 33, ×200). **d** Well-circumscribed wild-type *BRAF* FVPTC−M with decreased expression at the periphery (case 18, ×200). **e** Poorly circumscribed wild-type *BRAF* CPTC+M with increased expression at the periphery (case 33, ×40). **f** Poorly circumscribed *BRAF*-mutated CPTC−M with increased expression at the periphery (case 17, ×40)

(d) Smad7 expression

Smad7 nuclear expression was observed in 69.3 % of tumours and in all but two control tissues of the CPTC−M group (97.3 %) (Fig. 2g–i).

Smad7 had a basal level or was overexpressed in the nuclei of the tumour cells in 71.6 % of tumours in comparison with the respective control tissue. There was a significant association between basal to overexpressed Smad7 in the nuclei of the tumour cells and well-circumscribed growth pattern (p=0.0001), unicentric CPTC (p=0.048), absence of vascular invasion in FVPTC (p=0.013), absence of extra-thyroid extension in FVPTC (p=0.023) and absence of lymph node metastases in both CPTC and FVPTC (p<0.0001).

Smad7 cytoplasmatic expression was observed in 66.7 % of tumours and in 14.9 % of the control tissues. Smad7 had a basal level or was underexpressed in the cytoplasm of the tumour cells in 48.6 % of cases in comparison with the respective control tissue, both in CPTC and FVPTC. Smad7 cytoplasmatic expression was not significantly associated to any clinical, pathological or molecular feature.

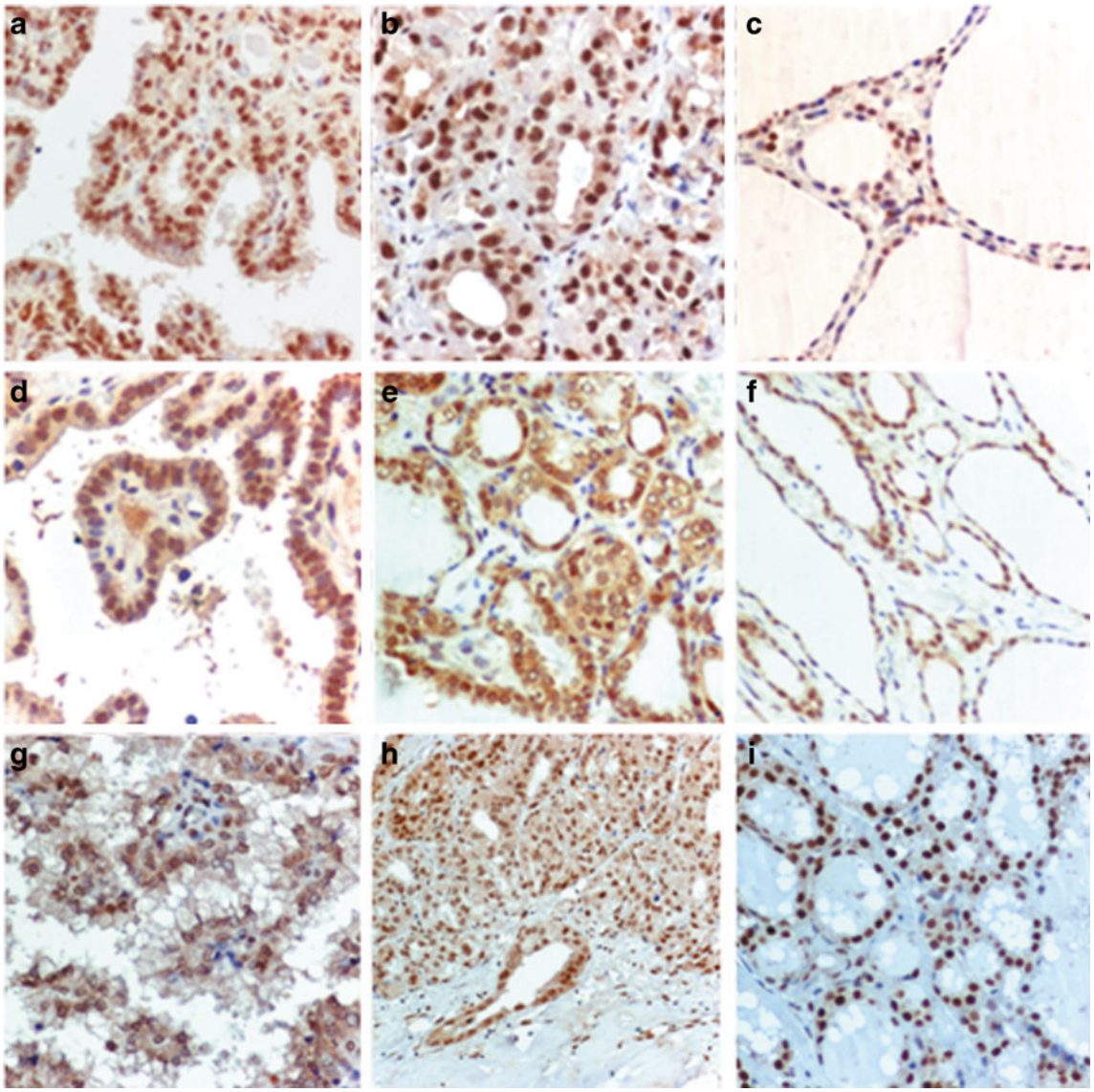

Fig. 2 Expression of P-Smad2/3: **a** Papillary areas of the centre of the tumour (case 26 of CPTC group, ×200). **b** Follicular areas of the centre of the tumour (case 28 of FVPTC group, ×400). **c** Control tissue (case 2 of CPTC group, ×400). Expression of Smad4: **d** Papillary areas of the centre of the tumour (case 39 of CPTC group, ×200). **e** Follicular areas of the centre of the tumour (case 27 of FVPTC group, ×200). **f** Control tissue (case 27 of FVPTC group, ×200). Expression of Smad7: **g** Papillary areas of the centre of the tumour (case 9 of CPTC group, ×400). **h** Follicular areas of the periphery of the tumour (case 1 of FVPTC group, ×100). **i** Control tissue (case 1 of FVPTC group, ×200)

3. WCPTC versus PCPTC

None of the 22 WCPTCs had lymph node metastases, while 50.9 % of the 53 PCPTCs had given rise to lymph node metastases. Globally, the difference between the mean TGF-beta expression in the centre of the tumours and in the control tissue was similar in WCPTC and in PCPTC (p=0.839), whereas the difference between the mean TGF-beta expression in the periphery of the tumours and in the centre of the tumours was much higher in PCPTC than in WCPTC (p=0.0007).

In 63.6 % of WCPTC cases (14 out of 22), the TGF-beta expression was nearly homogeneous, absent or low/moderate, throughout the tumour. In PCPTC, the PTC−M cases disclosed a significantly more intense expression of TGF-beta in the centre of the tumours than in the control tissue (p<0.0001), whereas in PTC +M cases, the cells in the periphery of the tumours presented a significantly more intense expression of TGF-beta than those in the centre of the tumours (p=0.017) (Table 3).

The *BRAF* V600E mutation was detected in 20.0 % of WCPTC including four WCPTC cases disclosing similar or higher TGF-beta expression in the periphery than in the centre, while none of the three WCPTCs with a lower TGF-beta expression in the periphery than

Table 3 Comparison between the immunohistochemical patterns of expression at the centre and at the periphery of the tumours in well and poorly circumscribed PTCs (WCPTC and PCPTC)

Features		TGF-beta intensity of expression (mean ± SD)				Smad4 nuclear expression (%)		Smad7 nuclear expression (%)	
		C-CT	*p*	P-C	*p*	C-CT	*p*	C-CT	*p*
WCPTC	VI		0.376		0.641		0.005		>0.999
	Present	0.7±0.8		0.0±0.6		0.0		100.0	
	Absent	0.4±0.7		0.1±0.5		70.6		100.0	
PCPTC	Multicentricity		0.053		0.935		0.381		0.167
	Present	0.1±0.9		0.7±0.6		26.1		47.8	
	Absent	0.8±1.3		0.7±0.9		39.3		67.9	
	EE		0.398		0.048		0.746		0.119
	Present	0.3±0.9		1.0±0.7		26.7		40.0	
	Absent	0.6±1.3		0.6±0.7		50.0		66.7	
	LNM		<0.0001		0.017		0.771		<0.0001
	Present	−0.2±0.9		0.9±0.6		30.8		19.2	
	Absent	1.2±1.1		0.4±0.8		36.0		100.0	

EE extra-thyroid extension, *VI* vascular invasion, *C* expression in the centre of the tumour, *P* expression in the tumour periphery, *CT* expression in the control tissue, *LNM* lymph node metastases

in the centre were *BRAF*-mutated tumours. The group of WCPTC cases with similar or higher TGF-beta expression at the periphery than in the centre had similar clinico-pathological features and no lymph node metastases, independently of the *BRAF* mutational *status* (Tables 1 and 2).

The *BRAF* mutation was detected in 15 PCPTCs (33.3 %) disclosing similar or higher TGF-beta expression in the periphery than in the centre. PCPTC cases with similar or higher TGF-beta expression at the periphery than in the centre disclosed lymph node metastases in 40.0 % of *BRAF*-mutated tumours and in 56.7 % of tumours with wild-type *BRAF*. Smad4 nuclear expression in WCPTC subgroup was detected only in tumours without vascular invasion (p=0.005) (Table 3), whereas in PCPTC, Smad4 nuclear expression was not significantly associated to any clinical, pathological or molecular features.

Discussion and conclusions

The results we have obtained confirm the prognostic prominence of staging over cytological and molecular features and the major importance of architecture (expansive versus infiltrative growth pattern) and topography (different immunohistochemical characteristics of tumour cells according to their peripheral or central location) in the understanding of PTC development. It is known that the neoplastic cells at the tumour periphery differ substantially from those in the bulk of the tumours regarding the expression of several structural and functional proteins (e.g. cytokeratins, vimentin, beta-catenin, E-cadherin, fibronectin 1 and TGF-beta) [12, 15, 18, 26].

The role of TGF-beta in thyroid cell signalling and in thyroid carcinogenesis, like in many other models, is very complex and profoundly influenced by the cellular and tissue context [26], thus being better evaluated in tissue samples than in cell lines. In the present study, we observed signs of the dual role of TGF-beta regarding the co-existence in the same tumour of signs of activation and of inhibition of TGF-beta/Smad-dependent pathway according to the location of the neoplastic cells.

The tumour-suppressive effect of TGF-beta/Smad-dependent pathway that had been firmly established in thyroid cell lines [33–37] and in some PTC cell lines [25, 28] was found to be abrogated at the periphery of PTC [12, 26], where increased vimentin expression and loss of E-cadherin with increased motility and invasiveness configure an EMT-invasive phenotype [12]. We observed, particularly in the poorly circumscribed tumours, that TGF-beta expression was stronger in the invasive front than in the central regions of the tumours, and that an increased TGF-beta expression at the periphery of the tumours was associated to the occurrence of extra-thyroid extension and lymph node metastases, as previously reported by Riesco-Eizaguirre et al. [26].

Our subdivision of PTCs into well and poorly circumscribed carcinomas (WCPTC and PCPTC, respectively) goes further than the usual division into CPTC and FVPTC and provides interesting results: in WCPTC (no infiltrative features and no lymph node metastases), the mean

increment of TGF-beta immunoexpression from the centre to the periphery was very low in comparison with PCPTC, in line with the above-mentioned association between TGF-beta expression at the periphery and invasiveness, also reported by other authors [26]. We detected TGF-beta and P-Smad2/3 expressions in the centre of all cases of WCPTC and PCPTC and control tissues (except in nine TGF-beta-negative cases), as it had been reported previously [38, 40, 42–44], thus highlighting the existence of signs of functioning TGF-beta/Smad-dependent pathway in PTC.

Smad4 nuclear expression is considered as indicative of a functioning TGF-beta/Smad-dependent pathway [40, 44, 45], but the nuclear translocation of phosphorylated Smad2 in response to TGF-beta does not require the presence of Smad4 [30], as our results also indicate. In the present study, all tumours expressed Smad4 in the cytoplasm of the neoplastic cells, like it had been observed by Matsuo et al. [40] and Cerutti et al. [44], whereas Smad4 nuclear expression was detected in 27 % of tumours. In WCPTC, Smad4 nuclear expression was detected only in cases without vascular invasion. The nuclear expression of Smad4 in PTC cells had not been detected previously to the best of our knowledge. The percentage of cases with Smad4 nuclear expression may be related with an impaired nuclear translocation of Smad2/3–Smad4 complexes as a sort of end result of Smad4 mutations that were detected in another series in 21 % of PTCs [53]. Unfortunately, the absence of available material for the molecular search of Smad4 mutations in the present series did not allow the confirmation or the rejection of this hypothesis. Whatever the mechanisms involved in the process, we found that signs of functioning TGF-beta/Smad-dependent pathway in the centre of the tumours, namely basal or overexpression of TGF-beta and nuclear Smad4, were associated to low vascular invasiveness and absence of lymph node metastases, respectively.

Smad7 nuclear expression has been associated to loss of TGF-beta/Smad-dependent pathway inhibition [54] and was found to be at basal or overexpressed levels in 72 % of the cases of the present series—a percentage similar to that reported in another series of PTC [40]. We found that Smad7 nuclear expression was associated to low neoplastic invasiveness, namely to well-circumscribed growth pattern, and to unicentricity in CPTC and to the absence of extra-thyroid extension and vascular invasion, in FVPTC. More importantly, the Smad7 nuclear expression was associated to the absence of lymph node metastases both in CPTC and FVPTC.

The encapsulated, non-angioinvasive FVPTC is the prototype of a carcinoma with an extremely benign course [55] and discloses a very low intratumoural lymph vessel density [8]. In the present series, and in almost every series on record, most WCPTCs display a capsule and are apparently protected from the cascade of TGF-beta oncogenic effects occurring at the periphery of PCPTC. The WCPTCs that do not disclose invasive front and EMT features (independently of the occurrence of *BRAF* mutation), nor lymph node metastases, present often a nearly homogeneous TGF-beta expression throughout the tumour.

At variance with TGF-beta, *BRAF* mutation has been found to promote growth and cell invasiveness [56]. The putative relationship between alterations of the TGF-beta/Smad-dependent pathway and *BRAF* mutation is difficult to evaluate in an observational study like the present one. Despite acknowledging this limitation, we think our findings suggest the existence of a synergic influence of TGF-beta over *BRAF*-mutated neoplastic cells in the periphery of the tumours.

BRAF V600E mutation was more frequently detected in the subset of tumours with higher increment of TGF-beta expression at the periphery. This finding concurs with the results of Riesco-Eizaguirre et al. [26] and suggests that, at the periphery of the tumours, the association of high levels of TGF-beta expression with *BRAF* mutation and invasiveness, as previously described in animal models [29], PTC cell lines and PTCs [26], reflects a synergic interaction that may potentiate the oncogenic effect of *BRAF* mutation [11]. In the present series, the occurrence of *BRAF* mutation did not significantly alter, per se, the frequency of lymph node metastases, thus highlighting the complexity of the process and reinforcing the importance of growth pattern and invasion.

Considering that the increased expression of TGF-beta at the periphery of the tumours may functionally articulate with *BRAF* V600E mutation [29], the reason underlying this particular topographic immunoexpression of TGF-beta remains unclear. Since the *BRAF* mutation occurs, at least in most *BRAF*-positive cases, in every tumour cell, the TGF-beta expression increment should be detected, in case it was a direct result of the *BRAF* mutation, throughout the whole neoplastic tissue. It is likely that this increment of TGF-beta at the periphery of the tumours is influenced by the crosstalk between the neoplastic cells and cellular and non-cellular stromal elements, such as tumour-associated macrophages [24, 29], dendritic cells [22], lymphocytes [23] and basement membrane components [29]. A similar interaction with *BRAF* has been recently described with STAT3 which is highly expressed in the periphery of *BRAF*-mutated PTCs and has been found to result from the crosstalk between neoplastic cells and stromal elements [Couto et al., unpublished results]. The aforementioned need of co-existing factors in the setting of *BRAF* oncogenic mutation provides an explanation for the low prevalence of *BRAF*-positive PTCs in young patients [11].

Other interactions between TGF-beta signalling pathways and MAPK pathway have been advanced, namely through oncogenic *RAS* that is thought to be required for

the disruption of TGF-beta growth-suppressive effects in cell lines [51]. In our series, *N-RAS* Q61R mutation occurred in 6 % of cases without any significant association with pathological signs of invasiveness, but the number of positive cases is too small to allow any definite conclusion on this issue.

Summing up, the signs of functioning TGF-beta/Smad-dependent signalling pathway in the central areas of the tumours are associated to low invasiveness and absence of lymph node metastases while, at the periphery, TGF-beta expression is associated to invasiveness and occurrence of lymph node metastases, both in CPTC and in cases of the poorly circumscribed form of FVPTC. Our findings support the assumption that TGF-beta acts synergically with *BRAF* and probably with other cellular and molecular stromal factors at the periphery of the tumours, leading to neoplastic progression and acquisition of invasive properties by cancer cells.

Our results indicate that Smad7 nuclear expression in the centre of the tumours appears to be a marker of favourable evolution, unrelated to the occurrence of *BRAF* mutation. We suggest that preoperative detection of Smad7 nuclear expression should be evaluated by fine-needle aspiration in a large series of PTCs with thorough clinical, imaging and follow-up data, as it may constitute a valuable tool for risk stratification of patients. We conclude that nodal metastases are associated to poorly circumscribed, locally invasive PTCs that exhibit low levels of nuclear Smad7 and a peripheral EMT phenotype displaying TGF-beta overexpression, regardless of the occurrence of *BRAF* mutation.

Acknowledgments This work was partially supported by the grant Prof. Edward Limbert SPEND/GENZYME—Year 2007. Part of the data reported in this study was obtained in the project 'Identificação de factores prognósticos e de selecção terapêutica em carcinomas diferenciados da tireoide', which is supported by Fuandação Calouste Gulbenkian. IPATIMUP is an Associate Laboratory of the Portuguese Ministry of Science, Technology and Higher Education and is partly supported by the Fundação para a Ciência e Tecnologia. J. C-T was supported by grant PS09/02050-FEDER from Instituto de Salud Carlos III, Ministry of Science and Innovation, Spain.

Conflict of interest The authors declare no conflict of interest.

References

1. DeLellis RA, Lloyd RV, Heitz PU, Eng C (2004) World Health Organization classification of tumours. Pathology and genetics of tumours of endocrine organs. IARC, Lyon
2. Tubiana M, Schlumberger M, Rougier P, Laplanche A, Benhamou E, Gardet P, Caillou B, Travagli JP, Parmentier C (1985) Long-term results and prognostic factors in patients with differentiated thyroid carcinoma. Cancer 55:794–804
3. Gilliland FD, Hunt WC, Morris DM, Key CR (1997) Prognostic factors for thyroid carcinoma. A population-based study of 15,698 cases from Surveillance, Epidemiology and End Results (SEER) program 1973–1991. Cancer 79:564–573
4. Castro P, Rebocho AP, Soares RJ, Magalhães J, Roque L, Trovisco V, Vieira de Castro I, Cardoso de Oliveira M, Fonseca E, Soares P, Sobrinho-Simões M (2006) PAX8-PPARgamma rearrangement is frequently detected in the follicular variant of papillary thyroid carcinoma. J Clin Endocrinol Metab 91:213–220
5. Sobrinho-Simões M, Preto A, Rocha AS, Castro P, Máximo V, Fonseca E, Soares P (2005) Molecular pathology of well-differentiated thyroid carcinomas. Virchows Arch 447:787–793
6. Castro P, Fonseca E, Magalhães J, Sobrinho-Simões M (2022) Follicular, papillary, and "hybrid" carcinomas of the thyroid. Endocr Pathol 13:313–320
7. Rivera M, Ricarte-Filho J, Knauf J, Shaha A, Tuttle RM, Fagin JA, Ghossein RA (2010) Molecular genotyping of papillary thyroid carcinoma follicular variant according to its histologic subtypes (encapsulated vs infiltrative) reveals distinct BRAF and RAS mutation patterns. Mod Pathol 23:1191–1200
8. Eloy C, Santos J, Soares P, Sobrinho-Simões M (2011) Intratumoural lymph vessel density is related to presence of lymph node metastases and separates encapsulated from infiltrative papillary thyroid carcinoma. Virchows Archiv 459:595–605
9. Trovisco V, Soares P, Preto A, de Castro IV, Lima J, Castro P, Máximo V, Botelho T, Moreira S, Meireles AM, Magalhães J, Abrosimov A, Cameselle-Teijeiro J, Sobrinho-Simões M (2005) Type and prevalence of BRAF mutations are closely associated with papillary thyroid carcinoma histotype and patients' age but not with tumour aggressiveness. Virchows Arch 446:589–595
10. Adeniran AJ, Zhu Z, Gandhi M, Steward DL, Fiddler JP, Giordano TJ, Biddinger PW, Nikiforov YE (2006) Correlation between genetic alterations and microscopic features, clinical manifestations, and prognostic characteristics of thyroid papillary carcinomas. Am J Surg Pathol 30:216–222
11. Eloy C, Santos J, Soares P, Sobrinho-Simões M (2011) The preeminence of growth pattern and invasiveness and the limited influence of *BRAF* and *RAS* mutations in the occurrence of papillary thyroid carcinoma lymph node metastases. Virchows Arch 459:265–276
12. Vasko V, Espinosa AV, Scouten W, He H, Auer H, Liyanarachchi S, Larin A, Savchenko V, Francis GL, de la Chapelle A, Saji M, Ringel MD (2007) Gene expression and functional evidence of epithelial-to-mesenchymal transition in papillary thyroid carcinoma invasion. Proc Natl Acad Sci U S A 104:2803–2808
13. Vasko VV, Saji M (2007) Molecular mechanisms involved in differentiated thyroid cancer invasion and metastasis. Curr Opin Oncol 19:11–17
14. Liu Z, Kakudo K, Bai Y, Li Y, Ozaki T, Miyauchi A, Taniguchi E, Mori I (2011) Loss of cellular polarity/cohesiveness in the invasive front of papillary thyroid carcinoma, a novel predictor for lymph node metastasis; possible morphological indicator of epithelial mesenchymal transition. J Clin Pathol 64:325–329
15. Jensen K, Patel A, Hoperia V, Larin A, Bauer A, Vasko V (2010) Dynamic changes in e-cadherin gene promoter methylation during metastatic progression in papillary thyroid cancer. Exp Ther Med 1:457–462
16. Scarpino S, Cancellario d'Alena F, Di Napoli A, Pasquini A, Marzullo A, Ruco LP (2004) Increased expression of Met protein is associated with up-regulation of hypoxia inducible factor-1 (HIF-1) in tumour cells in papillary carcinoma of the thyroid. J Pathol 202:352–358
17. Miki H, Kitaichi M, Masuda E, Komaki K, Yamamoto Y, Monden Y (1999) ret/PTC expression may be associated with local invasion of thyroid papillary carcinoma. J Surg Oncol 71:76–82
18. Fonseca E, Nesland JM, Höie J, Sobrinho-Simões M (1997) Pattern of expression of intermediate cytokeratin filaments in the

thyroid gland: an immunohistochemical study of simple and stratified epithelial-type cytokeratins. Virchows Arch 430:239–245
19. Herrmann ME, LiVolsi VA, Pasha TL, Roberts SA, Wojcik EM, Baloch ZW (2002) Immunohistochemical expression of galectin-3 in benign and malignant thyroid lesions. Arch Pathol Lab Med 126:710–713
20. Jung CK, Kang YG, Bae JS, Lim DJ, Choi YJ, Lee K-Y (2010) Unique patterns of tumour growth related with the risk of lymph node metastasis in papillary thyroid carcinoma. Mod Pathol 23:1201–1208
21. Hood JD, Cheresh DA (2002) Role of integrins in cell invasion and migration. Nat Rev Cancer 2:91–100
22. Scarpino S, Stoppacciaro A, Ballerini F, Marchesi M, Prat M, Stella C, Sozzani S, Allavena P, Mantovani A, Ruco LP (2000) Papillary carcinoma of the thyroid: hepatocyte growth factor (HGF) stimulates tumor cells to release chemokines active in recruiting dendritic cells. Am J Pathol 156:831–837
23. Fiumara A, Belfiore A, Russo G, Salomone E, Santonocito GM, Ippolito O, Vigneri R, Gangemi P (1997) In situ evidence of neoplastic cell phagocytosis by macrophages in papillary thyroid cancer. J Clin Endocrinol Metab 82:1615–1620
24. Ryder M, Ghossein RA, Ricarte-Filho JC, Knauf JA, Fagin JA (2008) Increased density of tumor-associated macrophages is associated with decreased survival in advanced thyroid cancer. Endocr Relat Cancer 15:1069–1074
25. Hölting T, Zielke A, Siperstein AE, Clark O, Duh QY (1994) Transforming growth factor-beta1 is a negative regulator for differentiated thyroid cancer: studies of growth, migration, invasion, and adhesion of cultured follicular and papillary thyroid cancer cell lines. J Clin Endocrinol Metab 79:806–813
26. Riesco-Eizaguirre G, Rodríguez I, De la Vieja A, Costamagna E, Carrasco N, Nistal M, Santisteban P (2009) The BRAFV600E oncogene induces transforming growth factor beta secretion leading to sodium iodide symporter repression and increased malignancy in thyroid cancer. Cancer Res 69:8317–8325
27. Kimura ET, Matsuo SE, Ricarte-Filho JC (2007) TGFbeta, activin and SMAD signaling in thyroid cancer. Arq Bras Endocrinol Metab 51:683–689
28. Matsuo SE, Leoni SG, Colquhoun A, Kimura ET (2006) Transforming growth factor-β1 and activin A generate antiproliferative signaling in thyroid cancer cells. J Endocrinol 190:141–150
29. Knauf JA, Sartor MA, Medvedovic M, Lundsmith E, Ryder M, SalzanoM NYE, Giordano TJ, Ghossein RA, Fagin JA (2011) Progression of BRAF-induced thyroid cancer is associated with epithelial-mesenchymal transition requiring concomitant MAP kinase and TGFβ signaling. Oncogene 30:3153–3162
30. Massagué J (1998) TGFb-signal transduction. Annu Rev Biochem 67:753–791
31. ten Dijke P, Hill CS (2004) New insights into TGF-β-Smad signaling. Trends Biochem Sci 29:265–273
32. Elliott RL, Blobe GC (2005) Role of transforming growth factor beta in human cancer. J Clin Oncol 23:2078–2093
33. Nicolussi A, D'Inzeo S, Santulli M, Colletta G, Coppa A (2003) TGF-beta control of rat thyroid follicular cells differentiation. Mol Cell Endocrinol 207:1–11
34. Morris JC 3rd, Ragnanathan G, Hay ID, Nelson RE, Jiang NS (1988) The effects of transforming growth factor-beta on growth and differentiation of the continuous rat thyroid follicular cell line, FRTL-5. Endocrinology 123:1385–1394
35. Franzén A, Piek E, Westermark B, ten Dijke P, Heldin N-E (1999) Expression of transforming growth factor-beta1, activin A, and their receptors in thyroid follicle cells: negative regulation of thyrocytes growth and function. Endocrinology 140:4300–4310
36. Bravo SB, Pampín S, Cameselle-Teijeiro J, Carneiro C, Domínguez F, Barreiro F, Alvarez CV (2003) TGF-β-induced apoptosis in human thyrocytes is mediated by p27kip1 reduction and is overridden in neoplastic thyrocytes by NF-κB activation. Oncogene 22:7819–7830
37. Pisarev MA, Thomasz L, Juvenal GJ (2009) Role of transforming growth factor beta in the regulation of thyroid function and growth. Thyroid 19:881–892
38. Kimura ET, Kopp P, Zbaeren J, Asmis LM, Ruchti C, Maciel RM, Studer H (1999) Expression of transforming growth factor beta1, beta2, and beta3 in multinodular goiters and differentiated thyroid carcinomas: a comparative study. Thyroid 9:119–125
39. Morosini PP, Taccaliti A, Montironi R, Scarpelli M, Diamanti L, Simonella G, Mancini V, Petrelli MD, Mantero F (1996) TGF-beta1 immunohistochemistry in goiter: comparison of patients with recurrence or no recurrence. Thyroid 6:417–422
40. Matsuo SE, Fiore AP, Siguematu SM, Ebina KN, Fruglietti CU, Ferro MC, Kulcsar MA, Kimura ET (2010) Expression of SMAD proteins, TGF-beta/activin signaling mediators, in human thyroid tissues. Arq Bras Endocrinol Metab 54:406–412
41. Imamura Y, Jin L, Grande JP, Li C-Y, Zheng TR, Erickson LA, Lloyd RV (1998) Analysis of TGF-B and TGF-B-RII in thyroid neoplasms from the United States, Japan, and China. Endocr Pathol 9:209–216
42. Jasani B, Wyllie FS, Wright PA, Lemoine NR, Williams ED, Wynford-Thomas D (1990) Immunocytochemically detectable TGF-β associated with malignancy in thyroid epithelial neoplasia. Growth Factors 2:149–155
43. Lloyd RV, Ferreiro JA, Jin L, Sebo TJ (1997) TGFB, TGFB receptors, Ki-67, and p27(Kip)l expression in papillary thyroid carcinomas. Endocr Pathol 8:293–300
44. Cerutti JM, Ebina KN, Matsuo SE, Martins L, Maciel RM, Kimura ET (2003) Expression of Smad4 and Smad7 in human thyroid follicular carcinoma cell lines. J Endocrinol Invest 26:516–521
45. D'Inzeo S, Nicollussi A, Ricci A, Mancini P, Porcellini A, Nardi F, Coppa A (2010) Role of reduced expression of SMAD4 in papillary thyroid carcinoma. J Mol Endocrinol 45:229–244
46. Massagué J (2008) TGFbeta in cancer. Cell 134:215–230
47. Nicolussi A, D'Inzeo S, Gismondi A, Coppa A (2006) Reduction of invasive potential in K-ras-transformed thyroid cells by restoring of TGF-beta pathway. Clin Exp Metastasis 23:237–248
48. Mulder KM (2000) Role of Ras and Mapks in TGFbeta signaling. Cytokine Growth Factor Rev 11:23–35
49. Asmis LM, Kaempf J, Von Gruenigen C, Kimura ET, Wagner HE, Studer H (1996) Acquired and naturally occurring resistance of thyroid follicular cells to the growth inhibitory action of transforming growth factor-b1 (TGF-β1). J Endocrinol 149:485–496
50. Heldin NE, Bergström D, Hermansson A, Bergenstrahle A, Nakao A, Westermark B, ten Dijke P (1999) Lack of responsiveness to TGF-beta1 in a thyroid carcinoma cell line with functional type I and type II TGF-beta receptors and Smad proteins, suggests a novel mechanism for TGF-beta insensivity in carcinoma cells. Mol Cell Endocrinol 153:79–90
51. Coppa A, Mincione G, Mammarella S, Ranieri A, Colletta G (1995) Epithelial rat thyroid cell clones, escaping from transforming growth factor b negative growth control, are still inhibited by this factor in the ability to trap iodine. Cell Growth Differ 6:281–290
52. Mesa C Jr, Mirza M, Mitsutake N, Sartor M, Medvedovic M, Tomlinson C, Knauf JA, Weber GF, Fagin JA (2006) Conditional activation of RET/PTC3 and BRAFV600E in thyroid cells is associated with gene expression profiles that predict a preferential role of BRAF in extracellular matrix remodeling. Cancer Res 66:6521–6529
53. Lazzareschi D, Nardi F, Turco A, Ottini L, DÁmico C, Mariani-Constantini R, Gulino A, Coppa A (2005) A complex pattern of mutations and abnormal splicing of Smad4 is present in thyroid tumours. Oncogene 24:5344–5354

54. Itóh S, Landström M, Hermansson A, Itoh F, Heldin CH, Heldin NE, ten Dijke P (1998) Transforming growth factor beta1 induces nuclear export of inhibitory Smad7. J Biol Chem 273:29195–29201
55. Piana S, Frasoldati A, Di Felice E, Gardini G, Tallini G, Rosai J (2010) Encapsulated well-differentiated follicular-patterned thyroid carcinomas do not play a significant role in the fatality rates from thyroid carcinoma. Am J Surg Pathol 34:868–872
56. Nikiforova MN, Kimura ET, Gandhi M, Biddinger PW, Knauf JA, Basolo F, Zhu Z, Giannini R, Salvatore G, Fusco A, Santoro M, Fagin JA, Nikiforov YE (2003) BRAF mutations in thyroid tumors are restricted to papillary carcinomas and anaplastic or poorly differentiated carcinomas arising from papillary carcinomas. J Clin Endocrinol Metab 88:5399–5404

Virchows Arch (2012) 460:601–609
DOI 10.1007/s00428-012-1239-6

ORIGINAL ARTICLE

Clinicopathological correlations of mTOR and pAkt expression in non-small cell lung cancer

Mee-Hye Oh · Hyun Ju Lee · Seol Bong Yoo · Xianhua Xu · Jae Sung Choi · Yong Hoon Kim · Seok Yeol Lee · Choon-Taek Lee · Sanghoon Jheon · Jin-Haeng Chung

Received: 11 March 2012 / Accepted: 16 April 2012 / Published online: 5 May 2012
© Springer-Verlag 2012

Abstract The Akt/mammalian target of rapamycin (mTOR) pathway is up-regulated in many human cancers, and agents targeting the mTOR pathway are in various stages of clinical development and application. Expression of pAkt and mTOR was studied by immunohistochemical analysis of 574 surgically resected non-small cell lung cancer (NSCLC) specimens on a tissue microarray. The results were correlated with clinicopathological features. Expression of mTOR showed a strong correlation with the expression of pAkt ($p<0.001$) and was significantly associated with female gender, tumor size of ≤3 cm, adenocarcinoma (ADC), non-smoker status, and lower pathological stage. Expression of pAkt was correlated with older age (≥65), ADC, non-smoker status, and lower T stage. Univariate survival analysis revealed that the mTOR- and pAkt-positive group had a significantly longer cancer-specific survival than the mTOR- and pAkt-negative group ($p=0.038$ and 0.024, respectively). Coexpression of pAkt and mTOR correlated with better prognosis than either single- or double-negative pAkt and mTOR groups ($p=0.016$). However, multivariate analysis proved that mTOR and pAkt expression are not independent prognostic factors for cancer-specific survival. Expression of pAkt and mTOR expression is more significantly associated with ADC than squamous cell carcinoma. Although pAkt/mTOR expression is not an independent prognostic marker, expression of these proteins is associated with better prognosis.

Keywords Non-small cell lung cancer · mTOR · pAkt · Prognosis

Lung cancer is the leading cause of cancer-related deaths worldwide in both men and women with over one million cases diagnosed yearly [1]. Non-small cell lung cancer (NSCLC) accounts for >80% of all lung cancers. Only a

M.-H. Oh · H. J. Lee
Department of Pathology, Soonchunhyang University Cheonan Hospital, Soonchunhyang University College of Medicine, Cheonan, Republic of Korea

J. S. Choi · Y. H. Kim
Department of Internal Medicine, Soonchunhyang University Cheonan Hospital, Soonchunhyang University College of Medicine, Cheonan, Republic of Korea

S. Y. Lee
Department of Thoracic and Cardiovascular Surgery, Soonchunhyang University Cheonan Hospital, Soonchunhyang University College of Medicine, Cheonan, Republic of Korea

S. B. Yoo · X. Xu · J.-H. Chung (✉)
Department of Pathology, Seoul National University Bundang Hospital, Seoul National University College of Medicine, 300 Gumidong, Bundang-gu, Seongnam, Gyeonggi-do 463-707, Republic of Korea
e-mail: chungjh@snu.ac.kr

C.-T. Lee
Department of Internal Medicine, Seoul National University Bundang Hospital, Seoul National University College of Medicine, Seongnam, Republic of Korea

S. Jheon
Department of Thoracic and Cardiovascular Surgery, Seoul National University Bundang Hospital, Seoul National University College of Medicine, Seongnam, Republic of Korea

minority of NSCLC patients is eligible for curative treatment. Despite progress in the multimodality treatment of lung cancer, prognosis is still poor with 5-year survival rates of 10 to 15 %. Even in patients with resected stage IA tumors, the survival rate only ranges from 66 to 85 % [2]. Several studies have investigated the benefit of postoperative adjuvant chemotherapy and/or radiotherapy. Stage Ia and Ib patients without lymph node involvement fail to demonstrate consistent survival advantages after these treatments [3, 4]. Further elucidation of the molecular mechanisms underlying lung cancer progression is essential for the development of new effective therapeutic agents. Recent studies have been performed in which treatment has been personalized by selecting those patients likely to respond to a particular chemotherapeutic regimen. This approach may contribute to improved treatment efficacy while avoiding unnecessary side effects [5].

The PI3K/Akt/mTOR pathway is a prototypical survival pathway that is activated in many types of cancer [6–8]. Mechanisms leading to pathway activation include loss of function of the tumor suppressor PTEN, amplification or mutation of PI3K, amplification or mutation of Akt, activation of growth factor receptors, and exposure to carcinogens. Once activated, signaling through Akt can be propagated to a diverse array of substrates, including mTOR, a key regulator of protein translation [9]. Moreover, activation of the Akt/mTOR pathway confers resistance to many types of cancer therapy [10–14] and is a poor prognostic factor for many cancers [15–20]. However, the prognostic significance and predictive value for response to therapy targeting activated Akt (phosphorylated Akt) or mTOR is not clearly established in the lung cancer patients. Because mTOR inhibitors are currently undergoing clinical trials in advanced NSCLC, it is important to detect specific target molecules of the mTOR pathway as well as to identify and select the patients who would benefit from mTOR pathway inhibition. Whether the inhibitors of specific pathways can be put into clinical practice remains to be seen and these trials should be preceded by detailed appraisals of biomarker expression in the tumor cells. In order to evaluate the clinical significance of the pAkt/mTOR pathway, we investigated the intratumoral expression of pAkt and mTOR in NSCLC.

Patients and methods

Patients and tissues

We retrospectively obtained formalin-fixed and paraffin-embedded tissues from 574 resected primary NSCLC cases; 456 tumors were obtained from the Seoul National University Bundang Hospital between May 2003 and December 2008 and, 118 tumors were obtained from the Soonchunhyang University Cheonan Hospital between January 1996 and October 2009. Tumors from patients who died from causes other than lung carcinoma and recurrent or metastatic tumors were excluded from this study. The patients with NSCLC consisted of 398 men and 176 women. The mean patient age was 63.4 years (standard deviation, 9.8; range, 21–84 years), and the mean tumor size was 3.6 cm (standard deviation, 1.9; range, 0.4–16 cm).

Hematoxylin and eosin (H & E) stained slides were reviewed in each case to confirm the original diagnosis. Two pathologists (M.H.O. and J.H.C) independently reviewed these slides to select the most representative areas based on the World Health Organization criteria [21]. Tumor specimens were histopathologically diagnosed as adenocarcinoma (ADC; n=297), squamous cell carcinoma (SCC; n=227), large cell carcinoma (n=4), adenosquamous cell carcinoma (n=11), large cell neuroendocrine carcinoma (n=14), typical carcinoid (n=2), atypical carcinoid (n=2), sarcomatoid carcinoma (n=16), mixed large cell neuroendocrine carcinoma (n=1), and SCC (n=1).

The pathological stage of each tumor was assigned following the guidelines from the 7th edition of TNM classification [22]. The total sample set was composed of 140 stage Ia, 117 stage Ib, 101 stage IIa, 59 stage IIb, 126 stage IIIa, 11 stage IIIb, and 20 stage IV tumors. The patient medical records were collected to obtain information regarding patient age, gender, performance status using the Zubrod scale [23], and smoking status. Further data regarding patient survival status and cause of death were obtained from the medical records and/or interview with the family. The median follow-up period for all patients was 35.0 months, with a range of 1 to 153 months. This study was approved by the local institution review board.

Construction of tissue microarray

The most representative tumor area was carefully marked on H & E stained slides of sample tissue cores (2 mm in diameter) from formalin fixed, paraffin embedded tissue blocks. Representative cores were arranged in a trephine apparatus (Superbiochips, Laboratories, Seoul, Korea). A core was sampled from each tumor and included in the tissue microarray (TMA) block. One section from the block was stained with H & E for tissue confirmation.

Immunohistochemistry for mTOR and pAkt

Expression of mTOR and pAkt was analyzed by immunohistochemistry (IHC). Details of the materials and methods used in this study have been reported previously [24] and will be briefly described here. From the TMA blocks, 4-μm thick sections were transferred to poly-L-lysine-coated glass slides and incubated in a dry oven at 60°C for 1 h. They

were then dewaxed in xylene (three changes), rehydrated in a graded series of decreasing ethanol concentrations, and rinsed in Tris-buffered saline (pH 7.4). Endogenous peroxidase activity was inactivated with 5 % hydrogen peroxide in methanol for 15 min at 37°C. For mTOR staining, antigen retrieval was performed using microwave treatment in pH 6.0 epitope retrieval solution for 20 min. The tissue was then incubated with a rabbit monoclonal antibody against mTOR (1:100, clone 49F9, Cell Signaling Technology, Danvers, MA, USA) in a humidified chamber at 4°C for 16 h. Secondary antibody was applied using a Bond Polymer Refine Detection kit (Leica, Mt Waverley, Australia). Diaminobenzidine was used as the chromogen, and the sections were counterstained with Mayer's hematoxylin. For pAkt staining, antigen retrieval was achieved by incubation in a pressure cooking chamber in pH 9.0 Tris-EDTA buffer for 2 min. The tissue was then incubated with a rabbit monoclonal antibody against pAkt (1:50, clone 736E11, Cell Signaling Technology, Danvers, MA, USA) in a humidified chamber at 4°C for 16 h. The immunohistochemical reaction was visualized using the Ultravision LP kit (Lab Vision, Fremont, CA, USA) according to the manufacturer's protocol. Diaminobenzidine was used as the chromogen, and the sections were counterstained with Mayer's hematoxylin. Positive controls, consisting of cases with known reactivity for the antibody, and negative controls, obtained by omitting the primary antibody, were included.

Immunohistochemical assessment

Expression of mTOR was detected at the apical membrane of normal bronchial epithelial cells, but not in pneumocytes in the normal alveolar wall. Tumor cells were judged as positive if cytoplasmic and circumferential membranous staining was present. Expression of pAkt expression was not detected in normal bronchial epithelial cells or alveolar pneumocytes. Tumor cells were judged as positive for pAkt if membranous, cytoplasmic and/or nuclear staining was present. Immunohistochemical staining was separately evaluated by two investigators (M.H.O. and J.H.C.). In the rare instance of a discrepancy in judgment, agreement was obtained by discussion at a multihead microscope. A semiquantitative immunohistochemical score was assigned that included assessment of both the intensity of staining and the extent of staining. To measure the intensity, a score of 0 to 3 (corresponding to negative, weak, moderate, and strong positivity) was recorded. The extent of staining was scored as 0 (0 %), 1 (1–10 %), 2 (11–50 %), and 3 (51–100 %), according to the percentage of cells stained positive for each protein. The sum of the intensity and extent score was used as the final score (0–6). Tissues having a final score ≥3 were considered positive. Similar semiquantitative scoring systems have been successfully used for other TMA evaluations [17].

Statistical analysis

Statistical significance of the data was assessed using Statistical Package, SPSS version 14.0 for Windows (SPSS Inc, Chicago, IL, USA). Associations between the mTOR/pAkt expression and the clinicopathological characteristics were analyzed using the Pearson χ^2 or Fisher's exact test according to the test conditions. Kaplan–Meier analysis was performed for analysis of survival curves, and statistical significance was assessed using the log-rank test. Cancer-specific survival was defined as the time from the date of surgery to the last follow-up visit or cancer-related death. Univariate analysis of cancer-specific survival was performed using the Kaplan–Meier method. Multivariate Cox proportional hazard regression analysis was used to assess the prognostic significance between mTOR/pAkt expression, the other clinicopathological characteristics, and survival. Overall, 95 % confidence intervals were used throughout the analyses. Statistical significance was defined as $p<0.05$.

Results

mTOR and pAkt immunoreactivity

In the non-neoplastic pulmonary parenchyma, mTOR was expressed on the apical membrane of the bronchial epithelium, but not in pneumocytes on the alveolar wall. Expression of pAkt was not detected in normal bronchial epithelial cells or alveolar pneumocytes. Expression of mTOR in NSCLC appeared mainly in the cytoplasm and circumferential membrane (Fig. 1a–d). After evaluation and scoring of the 574 immunostained NSCLC specimens, 126 (22 %) scored 0, 73 (13 %) scored 2, 64 (11 %) scored 3, 86 (15 %) scored 4, 100 (17 %) scored 5, and 125 (22 %) scored 6. The cases were subdivided into an mTOR-negative group (scores of 0 or 2, $n=198$ (35 %)) and an mTOR-positive group (scores of 3, 4, 5, or 6; $n=376$ (65 %)) for statistical analysis. Expression of pAkt in NSCLC was detected in the membrane, cytoplasm and/or nucleus (Fig. 2a–d). Among the 574 NSCLC specimens, 291 (51 %) revealed a score of 0, 13 (2 %) scored 2, 14 (2 %) scored 3, 230 (40 %) scored 4, 22 (4 %) scored 5, and 4 (1 %) scored 6. The cases were subdivided into a pAkt-negative group (scores of 0 or 2, $n=304$ (53 %)) and a pAkt-positive group (scores of 3, 4, 5, or 6, $n=270$ (47 %)) for statistical analysis.

Correlations between mTOR/pAkt expression and clinicopathologic parameters

Expression of mTOR showed strong correlation with expression of pAkt ($p<0.001$). The expression of mTOR was

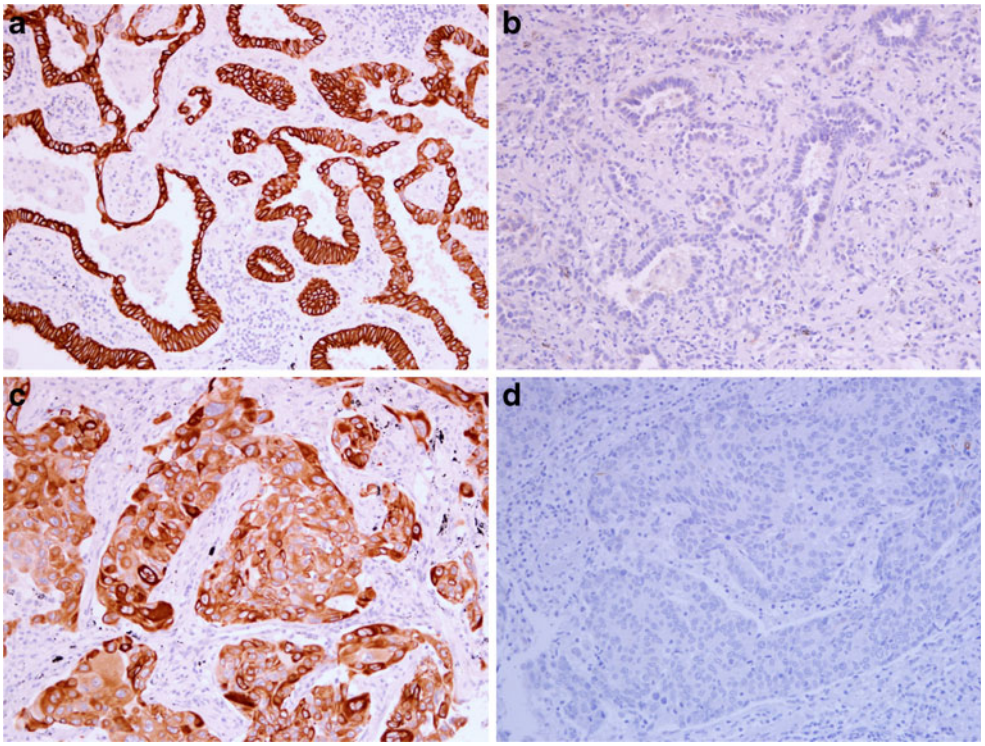

Fig. 1 Immunohistochemical staining of mTOR expression in NSCLC: **a** ADC; mTOR-positive expression, **b** ADC; mTOR-negative expression, **c** SCC; mTOR-positive expression, **d** SCC; mTOR-negative expression. *NSCLC* non-small cell lung cancer, *ADC* adenocarcinoma, *SCC* squamous cell carcinoma

significantly higher in the tumors with the following clinicopathological characteristics: female gender, smaller tumor size (≤3 cm), ADC histology rather than SCC histology, non-smoker staus, and early pathological stage. A weak correlation between mTOR expression and T status was also found without reaching statistical significance. Other clinicopathologic variables, including age, performance status, pleural invasion, venous invasion, lymphatic invasion, perineural invasion, nodal status, *EGFR* mutation status in ADC, and metastasis showed no correlation with mTOR expression.

The expression of pAkt was significantly higher in the tumors with the following characteristics; older age patient,

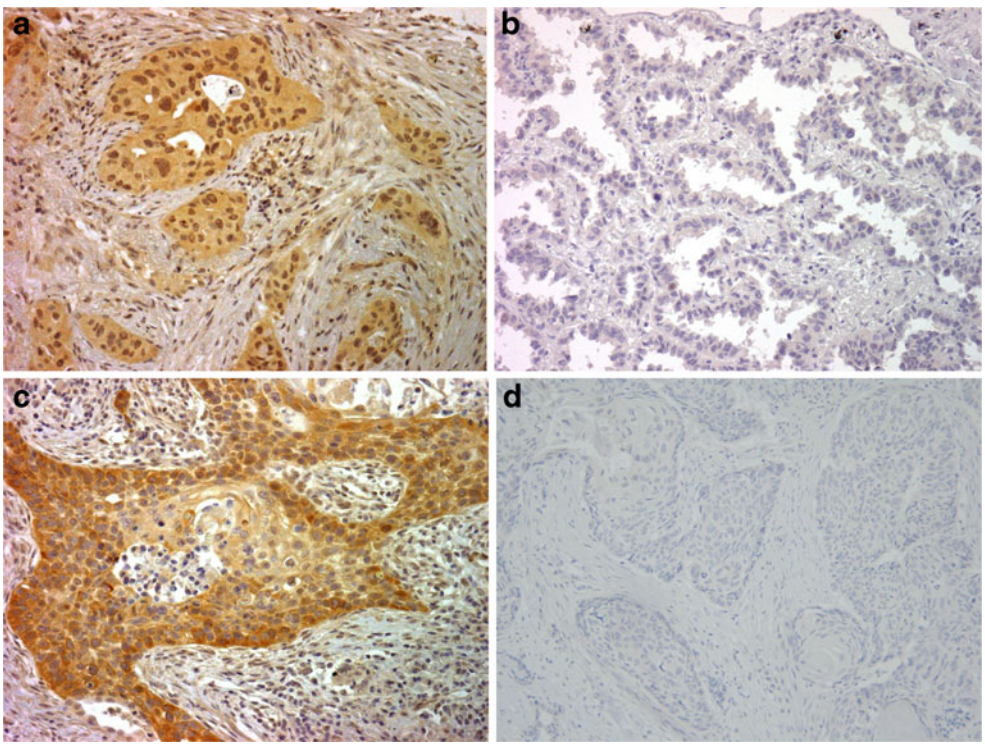

Fig. 2 Immunohistochemical staining of pAkt expression in NSCLC: **a** ADC; pAkt-positive expression, **b** ADC; pAkt-negative expression, **c** SCC; pAkt-positive expression, **d** SCC; pAkt-negative expression. *NSCLC* non-small cell lung cancer, *ADC* adenocarcinoma, *SCC* squamous cell carcinoma

Table 1 Distribution of mTOR and pAkt status in 574 patients with NSCLC

Variable	*N* (%)	mTOR			pAkt		
		Negative	Positive	*p*	Negative	Positive	*p*
Total	574 (100)	198 (35)	376 (65)		304 (53)	270 (47)	
pAkt							
Negative		139 (46)	165 (54)	<0.001			
Positive		59 (22)	211 (78)				
Sex							
Male	398 (69)	168 (42)	230 (58)	<0.001	221 (56)	177 (44)	0.064
Female	176 (31)	30 (17)	146 (83)		83 (47)	93 (53)	
Age (year)							
<65	282 (49)	90 (32)	192 (68)	0.219	162 (57)	120 (43)	0.034
≥65	292 (51)	108 (37)	184 (63)		142 (49)	150 (51)	
Tumor size (cm)							
≤3	288 (50)	80 (28)	208 (72)	0.001	141 (49)	147 (51)	0.054
>3	286 (50)	118 (41)	168 (59)		163 (57)	123 (43)	
Histology							
ADC	297 (52)	42 (14)	255 (86)	<0.001	135 (46)	162 (54)	0.001
SCC	227 (40)	136 (60)	92 (40)		141 (62)	87 (38)	
Others	49 (8)	20 (41)	29 (59)		28 (57)	21 (43)	
PS							
0 and 1	427 (94)	118 (28)	309 (72)	0.403	181 (42)	246 (58)	0.565
2 and 3	29 (6)	10 (35)	19 (65)		14 (48)	15 (52)	
No data	118						
Smoking							
Non-smoker	216 (38)	37 (17)	179 (83)	<0.001	97 (45)	119 (55)	0.003
Smoker	358 (62)	161 (45)	197 (55)		207 (58)	151 (42)	
Pleural invasion							
Absent	333 (58)	119 (36)	214 (64)	0.462	180 (54)	153 (46)	0.538
Present[a]	241 (42)	79 (33)	162 (67)		124 (52)	117 (48)	
Venous invasion							
Absent	494 (86)	166 (34)	328 (66)	0.264	262 (53)	232 (47)	0.929
Present	80 (14)	32 (40)	48 (60)		42 (53)	38 (47)	
Lymphatic invasion							
Absent	349 (61)	119 (34)	230 (66)	0.803	189 (54)	160 (46)	0.476
Present	225 (39)	79 (35)	146 (65)		115 (51)	110 (49)	
Perineural invasion							
Absent	536 (93)	181 (34)	355 (66)	0.169	280 (52)	256 (48)	0.193
Present	38 (7)	17 (45)	21 (55)		24 (63)	14 (37)	
Tumor status							
T1	197 (34)	54 (27)	143 (73)	0.066	88 (45)	109 (55)	0.032
T2	267 (47)	99 (37)	168 (63)		156 (58)	111 (42)	
T3	85 (15)	35 (41)	50 (59)		47 (55)	38 (45)	
T4	25 (4)	10 (40)	15 (60)		13 (52)	12 (48)	
Nodal status							
N0	334 (58)	110 (33)	224 (67)	0.116	175 (52)	159 (48)	0.324
N1	125 (22)	53 (42)	72 (58)		74 (59)	51 (41)	
N2	112 (19)	35 (31)	77 (69)		54 (48)	58 (52)	
N3	3 (1)	0 (0)	3 (100)		1 (33)	2 (67)	
Metastasis							
M0	555 (97)	193 (35)	362 (65)	0.446	295 (53)	260 (47)	0.619
M1	19 (3)	5 (26)	14 (74)		9 (47)	10 (53)	
Pathologic Stage							
I	257 (45)	74 (29)	183 (71)	0.001	134 (52)	123 (48)	0.684
II	160 (28)	76 (48)	84 (52)		91 (57)	69 (43)	
III	137 (24)	43 (31)	94 (69)		69 (50)	68 (50)	
IV	20 (3)	5 (25)	15 (75)		10 (50)	10 (50)	

NSCLC non-small cell lung cancer, *ADC* adenocarcinoma, *SCC* squamous cell carcinoma, *PS* performance status

[a] Visceral and/or parietal invasion

ADC histology rather than SCC histology, non-smoker status, and lower T stage. Smaller tumor size and female gender showed a non-significant trend to correlate with pAkt expression. Other clinicopathological variables, including performance status (PS), pleural invasion, venous invasion, lymphatic invasion, perineural invasion, nodal status, metastasis, *EGFR* mutation status in ADC, and pathological stage showed no correlation with pAkt expression (Table 1).

Survival analysis

At the time of analysis, the number of cancer-specific deaths was 171 (30 %). Univariate survival analysis included expression of mTOR and pAkt, sex, age, histology, smoker status, tumor size, PS, pleural invasion, venous invasion, lymphatic invasion, perineural invasion, TNM, and pathological stage to evaluate significance of each variable upon cancer-specific survival (Table 2). The groups positive for mTOR and pAkt displayed a significantly longer cancer-specific survival than the groups negative for mTOR and pAkt, respectively (p=0.038 and 0.024, respectively; Fig. 3a, b). Patients with tumors coexpressing mTOR and pAkt showed better prognosis than either single-negative group or the group lacking expression of both mTOR and pAkt (p=0.016; Fig. 3c). Among the above-mentioned variables, female gender (p=0.017), younger age (p=0.010), ADC (p=0.030), smaller tumor size (p<0.001), pleural invasion (p<0.001), venous invasion (p=0.001), lymphatic invasion (p=0.002), TNM (p<0.001), and pathological stage (p<0.001) correlated with significantly longer survival. To evaluate whether mTOR/pAkt positivity in NSCLC is an independent predictor of cancer-specific survival, a multivariate analysis using the Cox proportional hazard model was performed. The four variables of age (p=0.013), nodal status (p=0.049), metastasis (p=0.027), and pathologic stage (p=0.014) were significant prognostic factors for NSCLC patients. Multivariate analysis demonstrated that mTOR/pAkt expression was not an independent prognostic factor for cancer-specific survival. Analysis of ADCs only indicated that the following are independent prognostic factors; age (p=0.003), smoking status (p=0.006), tumor size (p=0.014), PS (p<0.001), nodal status (p=0.040), and metastasis (p=0.010). A similar analysis of SCCs only indicated that smoking (p=0.002) and pathological stage (p=0.015) are independent prognostic factors. Only smoking status, regardless of tumor histology, was identified as a consistent independent prognostic factor for cancer-specific survival (Table 3). Among early stage tumors (stages I and II only), univariate survival analysis showed results similar to those from all NSCLC cases. Expression of mTOR and pAkt was correlated with longer survival (p=0.001 and 0.001, respectively) and patients coexpressing mTOR and pAkt showed better prognosis (p<0.001). Female gender (p=0.014), ADC (p=0.001), smaller tumor size (p<0.001), PS (p<0.001), absence of pleural invasion (p=0.041), lower tumor status (p=0.023), and nodal status (p=0.048) also correlated with longer survival. Using multivariate survival analysis, PS (p<0.001), and nodal status (p=0.016) were demonstrated to be independent prognostic factors for early stage tumors (Table 3).

Table 2 Univariate analysis results of cancer-specific survival in 574 patients with NSCLC

Univariate	Cancer-specific survival (p value)
mTOR expression (negative vs. positive)	0.038
pAkt expression (negative vs. positive)	0.024
mTOR/pAkt expression (+/+ vs. +/− or −/+ vs. −/−)	0.016
Sex (male vs. female)	0.017
Age (≥65 vs. <65)	0.010
Histology (ADC vs. SCC)	0.030
Smoking (non-smoker vs. smoker)	0.117
Size (>3 vs. ≤3)	<0.001
Performance status (0.1 vs. 2.3)	0.140
Pleural invasion[a]	<0.001
Venous invasion[a]	0.001
Lymphatic invasion[a]	0.002
Perineural invasion[a]	0.125
Tumor status (1, 2, 3, and 4)	<0.001
Nodal status (0, 1, 2, and 3)	<0.001
Metastasis status (0 and 1)	<0.001
Pathologic stage (I, II, III, and IV)	<0.001

NSCLC non-small cell lung cancer, *ADC* adenocarcinoma, *SCC* squamous cell carcinoma

[a] Absent vs. present

Discussion

The results of the current study demonstrate that mTOR expression correlates with pAkt expression, which suggests that pAkt is an important activator of the mTOR signaling pathway. Among clinicopathological parameters, female gender, ADC histology, tumor size ≤3cm, non-smoker, and earlier pathological stage were associated with mTOR expression. Expression of pAkt was correlated with age ≥65 years, ADC histology, non-smoker status, and lower T stage. Both mTOR and pAkt expression were significantly associated with ADC histology and non-smoker status. In previous reports, there have been no indications of a specific correlation between histologic type and mTOR or pAkt expression.

Expression of mTOR was higher in pAkt-positive NSCLCs than in pAkt-negative NSCLCs. This result

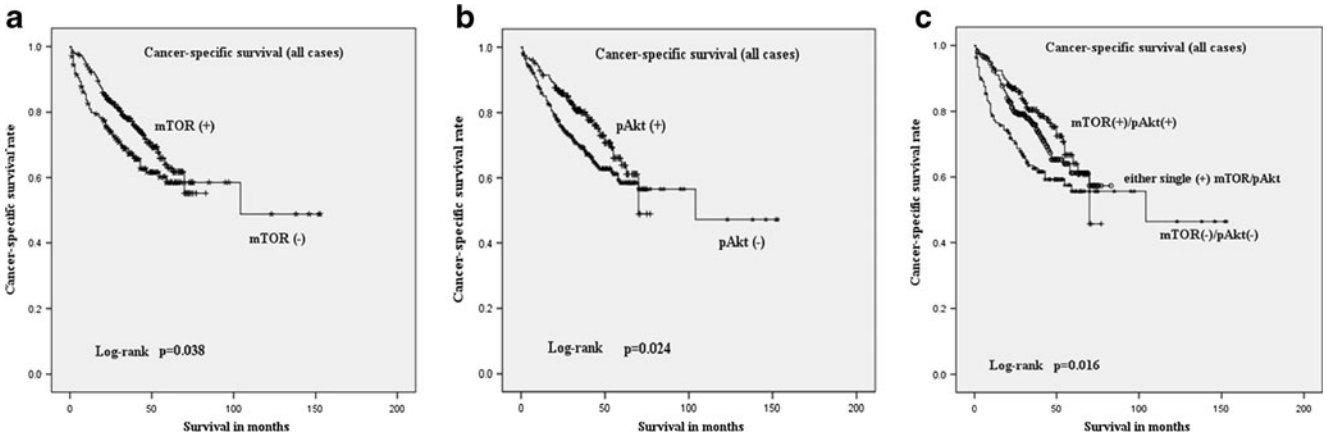

Fig. 3 Kaplan-Meier cancer-specific survival curve for mTOR and pAkt in NSCLC cases (n=574): **a** mTOR (p=0.038), **b** pAkt (p=0.024), **c** mTOR/pAkt (p=0.016). *NSCLC* non-small cell lung cancer

demonstrates that mTOR expression is closely related to pAkt expression. Therefore, pAkt activity is one of the important mechanisms for the activation of the mTOR signaling pathway in lung cancer. The patients with mTOR expression showed longer survival in this study. A novel finding of our study is that the NSCLC patients with tumors that are positive for pAkt as well as for mTOR showed the longest survival, and the patients with tumors are negative for pAkt and mTOR displayed shorter survival than either single-negative group. Although Kaplan-Meier analysis revealed that the expression of both mTOR (p=0.038) and pAkt (p=0.024) is significantly correlated with better prognosis (Table 2), we found that neither expression of mTOR nor of pAkt is an independent prognostic factor in multivariate analysis. These results are identical to the survival analysis of early stage (stages I and II) resected NSCLC in this study (Table 3).

Controversial results regarding pAkt/mTOR pathway expression and clinical outcomes have been reported. Recently, Dhillon et al. [19] described a significant correlation between mTOR overexpression and poor survival in resected early stage (stages I and II) NSCLC. In contrast, Anagnostou et al. [25] have insisted that high expression of mTOR is associated with better outcome for patients harboring early stage lung adenocarcinoma. Recently, Lee et al. reported that mTOR activation induces tumor suppressors

Table 3 Univariate analysis results of cancer-specific survival in patients with ADC (n=297), SCC (n=228), and early stage (stages I and II, n=417) NSCLC, respectively

Univariate	Cancer-specific survival (p value)		
	ADC	SCC	Stages I and II
mTOR expression (negative vs. positive)	0.728	0.265	0.001
pAkt expression (negative vs. positive)	0.013	0.615	0.001
mTOR/pAkt expression (+/+ vs. +/− or −/+ vs. −/−)	0.182	0.39	<0.001
Sex (male vs. female)	0.122	0.787	0.014
Age (≥65 vs. <65)	0.001	0.838	0.075
Histology (ADC vs. SCC)			0.001
Smoking (non-smoker vs. smoker)	0.006	0.01	0.287
Size (>3 vs. ≤3)	<0.001	0.137	<0.001
Performance status (0.1 vs. 2.3)	<0.001	0.757	<0.001
Pleural invasion[a]	0.001	0.019	0.041
Venous invasion[a]	0.002	0.016	0.795
Lymphatic invasion[a]	0.004	0.032	0.912
Perineural invasion[a]	0.042	0.933	0.467
Tumor status (1, 2, 3, and 4)	<0.001	<0.001	0.023
Nodal status (0, 1, 2, and 3)	<0.001	0.001	0.048
Metastasis status (0 and 1)	0.001	0.06	
Pathologic stage (I, II, III, and IV)	<0.001	<0.001	

NSCLC non-small cell lung cancer, *ADC* adenocarcinoma, *SCC* squamous cell carcinoma, *PS* performance status

[a]Absent vs. present

that inhibit leukemogenesis after PTEN deletion, which suggests that mTOR activation is involved not only in the oncogenic pathway, but also in tumor suppressor gene induction under specific circumstances [26]. Therefore, the clinical implications of mTOR activation and its potential role as a target for therapy in NSCLC should be interpreted more cautiously, and further study regarding PTEN status is required. Diverse opinions also exist regarding prognosis in relation to pAkt expressions. A large majority of studies have asserted that pAkt expression is correlated with poor prognosis in NSCLC [11, 17, 26], breast cancer [27], gastric cancer [20], and renal cell carcinoma [15]. However, Chan et al. [28] have reported that pAkt expression is not significantly related to patient survival, but is inversely related to tumor grade and size in breast cancer. Masson et al. [29] also have asserted that pAkt protein expression has no prognostic significance in lung cancer, but pAkt expression is associated with severe dysplasia of the bronchial wall. These observations suggest early involvement of PI3K/Akt pathway in lung cancer. To our knowledge, there has been no report to date suggesting that pAkt expression is associated with better outcome in NSCLC. Our contradictory results could be explained as follows; (1) the absence of standard or universally accepted criteria to evaluate pAkt/mTOR pathway expression by immunohistochemistry might lead to different results and (2) each organ might employ different mechanisms for activating mTOR signaling. Therefore, detailed and standardized immunohistochemical assessment of pAkt/mTOR pathway expression is recommended.

Our study provides new insight into the relationship between the pAkt/mTOR pathway and clinical outcome in NSCLC. However, we cannot exclude selection bias because all the enrolled patients were surgically resectable. Furthermore, our study is retrospective and sampling might be a limitation as only one TMA core was included per case. These limitations of our study might restrict the generalizability of our results.

In summary, this study demonstrates that: (1) pAkt/mTOR pathway expression is associated with better prognosis in NSCLC, (2) pAkt and mTOR expression is higher in tumors with ADC histology than SCC in Korean NSCLC patients, and (3) pAkt is one of the possible mechanisms for activation of the mTOR signaling pathway in lung cancer.

Conflict of interest statement None declared.

References

1. Jemal A, Siegel R, Ward E et al (2007) Cancer statistics, 2007. CA Cancer J Clin 57:43–66
2. Tsuchiya T, Akamine S, Muraoka M et al (2007) Stage IA non-small cell lung cancer: vessel invasion is a poor prognostic factor and a new target of adjuvant chemotherapy. Lung Cancer 56:341–348
3. Douillard JY, Rosell R, De Lena M et al (2006) Adjuvant vinorelbine plus cisplatin versus observation in patients with completely resected stage IB-IIIA non-small-cell lung cancer (Adjuvant Navelbine International Trialist Association [ANITA]): a randomised controlled trial. Lancet Oncol 7:719–727
4. Wakelee H, Dubey S, Gandara D (2007) Optimal adjuvant therapy for non-small cell lung cancer—how to handle stage I disease. Oncologist 12:331–337
5. Wang X, Zhao J, Yang L et al (2010) Positive expression of ERCC1 predicts a poorer platinum-based treatment outcome in Chinese patients with advanced non-small-cell lung cancer. Med Oncol 27:484–490
6. Yuan ZQ, Sun M, Feldman RI et al (2000) Frequent activation of AKT2 and induction of apoptosis by inhibition of phosphoinositide-3-OH kinase/Akt pathway in human ovarian cancer. Oncogene 19:2324–2330
7. Sun M, Wang G, Paciga JE et al (2001) AKT1/PKBalpha kinase is frequently elevated in human cancers and its constitutive activation is required for oncogenic transformation in NIH3T3 cells. Am J Pathol 159:431–437
8. Altomare DA, Tanno S, De Rienzo A et al (2002) Frequent activation of AKT2 kinase in human pancreatic carcinomas. J Cell Biochem 87:470–476
9. LoPiccolo J, Blumenthal GM, Bernstein WB et al (2008) Targeting the PI3K/Akt/mTOR pathway: effective combinations and clinical considerations. Drug Resist Updat 11:32–50
10. Schuurbiers OC, Kaanders JH, van der Heijden HF et al (2009) The PI3-K/AKT-pathway and radiation resistance mechanisms in non-small cell lung cancer. J Thorac Oncol 4:761–767
11. Murakami D, Tsujitani S, Osaki T et al (2007) Expression of phosphorylated Akt (pAkt) in gastric carcinoma predicts prognosis and efficacy of chemotherapy. Gastric Cancer 10:45–51
12. Brognard J, Clark AS, Ni Y et al (2001) Akt/protein kinase B is constitutively active in non-small cell lung cancer cells and promotes cellular survival and resistance to chemotherapy and radiation. Cancer Res 61:3986–3997
13. Clark AS, West K, Streicher S et al (2002) Constitutive and inducible Akt activity promotes resistance to chemotherapy, trastuzumab, or tamoxifen in breast cancer cells. Mol Cancer Ther 1:707–717
14. West KA, Castillo SS, Dennis PA (2002) Activation of the PI3K/Akt pathway and chemotherapeutic resistance. Drug Resist Updat 5:234–248
15. Pantuck AJ, Seligson DB, Klatte T et al (2007) Prognostic relevance of the mTOR pathway in renal cell carcinoma: implications for molecular patient selection for targeted therapy. Cancer 109:2257–2267
16. Akcakanat A, Sahin A, Shaye AN et al (2008) Comparison of Akt/mTOR signaling in primary breast tumors and matched distant metastases. Cancer 112:2352–2358
17. Lim WT, Zhang WH, Miller CR et al (2007) PTEN and phosphorylated AKT expression and prognosis in early- and late-stage non-small cell lung cancer. Oncol Rep 17:853–857
18. Balsara BR, Pei J, Mitsuuchi Y et al (2004) Frequent activation of AKT in non-small cell lung carcinomas and preneoplastic bronchial lesions. Carcinogenesis 25:2053–2059
19. Dhillon T, Mauri FA, Bellezza G et al (2010) Overexpression of the mammalian target of rapamycin: a novel biomarker for poor survival in resected early stage non-small cell lung cancer. J Thorac Oncol 5:314–319
20. Lee S, Kim YC, Lee HM et al (2010) Prognostic value of phosphorylated Akt and survivin expression in gastric adenocarcinoma. Korean J Pathol 44:252–258

21. Travis WD BE, Muller-Hermelink HK et al (2004) World Health Organization International Histological Classification of Tumours, Pathology and genetics of tumours of the lung, pleura, thymus and heart. IARC Press, Lyon
22. Travis WD (2009) Reporting lung cancer pathology specimens. Impact of the anticipated 7th Edition TNM classification based on recommendations of the IASLC Staging Committee. Histopathology 54:3–11
23. Zubrod C, Scheiderman M, Frei E III et al (1960) Cancer appraisal of methods for the study of chemotherapy of cancer in men: thiophosphoramide. J Chronic Dis 11:7–33
24. Lin F, Zhang PL, Yang XJ et al (2006) Morphoproteomic and molecular concomitants of an overexpressed and activated mTOR pathway in renal cell carcinomas. Ann Clin Lab Sci 36:283–293
25. Anagnostou VK, Bepler G, Syrigos KN et al (2009) High expression of mammalian target of rapamycin is associated with better outcome for patients with early stage lung adenocarcinoma. Clin Cancer Res 15:4157–4164
26. David O, Jett J, LeBeau H et al (2004) Phospho-Akt overexpression in non-small cell lung cancer confers significant stage-independent survival disadvantage. Clin Cancer Res 10:6865–6871
27. Yu P, Zhou L, Ke W et al (2010) Clinical significance of pAKT and CD44v6 overexpression with breast cancer. J Cancer Res Clin Oncol 136:1283–1292
28. Chan S (2004) Targeting the mammalian target of rapamycin (mTOR): a new approach to treating cancer. Br J Cancer 91:1420–1424
29. Massion PP, Taflan PM, Shyr Y et al (2004) Early involvement of the phosphatidylinositol 3-kinase/Akt pathway in lung cancer progression. Am J Respir Crit Care Med 170:1088–1094

Virchows Arch (2012) 460:611–619
DOI 10.1007/s00428-012-1243-x

ORIGINAL ARTICLE

Microvessel density is high in clear-cell renal cell carcinomas of Ukrainian patients exposed to chronic persistent low-dose ionizing radiation after the Chernobyl accident

A. M. Romanenko · A. Ruiz-Saurí · L. Morell-Quadreny · G. Valencia · A. F. Vozianov · A. Llombart-Bosch

Received: 23 December 2011 / Revised: 26 March 2012 / Accepted: 26 April 2012 / Published online: 13 May 2012
© Springer-Verlag 2012

Abstract During the 25-year period subsequent to the Chernobyl accident, the morbidity of malignant renal tumors in Ukraine has increased from 4.7 to 10.7 per 100,000 of the total population. Recent studies of our group have shown that increases in morbidity, aggressiveness, and proliferative activity of renal cell carcinomas (RCCs), especially clear-cell renal cell carcinoma (CCRCC), in Ukrainian patients continuously inhabiting the radio-contaminated areas could be explained by specific molecular changes influenced by the so-called "chronic persistent low-dose ionizing radiation" (CPLDIR) exposure. This study aimed to examine the role of angiogenesis in CCRCC carcinogenesis associated with CPLDIR in patients living more than 20 years in cesium 137 (^{137}Cs) contaminated areas after the Chernobyl accident in Ukraine. Paraffin-embedded specimens of 106 CCRCs were studied: Control cases were 18 tumors from Spanish patients (group 1), 25 tumors from Ukrainian patients from so-called clean areas without known radio-contamination (group 2), and 63 tumors from Ukrainian patients from radio-contaminated areas (group 3). For intratumoral microvessel density (MVD) determination, anti-CD31 antibody was used. A computerized image analysis program was used to quantitatively calculate the vascular density. Seventy-three percent of group 3 and 72 % of group 2 CCRCCs displayed the highest MVD. A striking increase in MVD was seen in group 3 CCRCCs, in comparison with groups 1 and 2 ($p<0.001$). The majority of the hot spot vessels in group 3 was poorly differentiated. Moreover, MVD values for total vessels as well as for capillaries and tumor grade were strongly correlated. When we compared only tumor–node–metastasis tumor stages I and II, the differences remained statistically significant ($p<0.1$). The ratio of the average total vessels and capillaries in the Ukrainian groups combined was 1.65:1 in comparison to the Spanish group. Our results provide evidence that CPLDIR exposure increases MVD (particularly capillary) in CCRCCs and is associated with a higher histological grade.

Grant for temporary stay for invited professors, number UV-ESTPC-07-393, Valencia University, Spain.

A. M. Romanenko
Department of Pathology, Institute of Urology,
Academy of Medical Sciences of Ukraine,
Kiev, Ukraine
e-mail: romanenkoa5@hotmail.com

A. M. Romanenko · A. Ruiz-Saurí · G. Valencia · A. Llombart-Bosch (✉)
Department of Pathology, Valencia University Medical School,
Valencia, Spain
e-mail: Antonio.llombart@uv.es

A. Ruiz-Saurí
e-mail: Amparo.Ruiz-Sauri@uv.es

G. Valencia
e-mail: gvalenci@uninorte.edu.co

L. Morell-Quadreny
Department of Pathology, University Hospital Ribera,
Alzira, Spain
e-mail: LMorell@Hospital-Ribera.com

G. Valencia
Universidad del Norte,
Barranquilla, Colombia

A. F. Vozianov
Institute of Urology, Academy of Medical Sciences of Ukraine,
Kiev, Ukraine
e-mail: romanenkoa5@hotmail.com

Keywords Conventional renal cell carcinoma · Ionizing radiation · Angiogenesis · Microvessel density · CD31antibody

Introduction

Clear-cell renal cell carcinoma (CCRCC) is the most common subtype of malignant renal tumors, representing 80 % of renal cell carcinomas (RCCs). CCRCC is known as a highly vascularized cancer, resistant to conventional chemotherapy and radiotherapy. At time of diagnosis, 20–30 % of patients with renal cell carcinoma (RCC) have metastases. Metastatic RCC has an overall poor response to cytotoxic chemotherapy and cytokine therapies [1, 2], but it is a highly vascular tumor and hence an ideal candidate for antiangiogenic therapy [3].

During the 25-year period subsequent to the Chernobyl accident, the incidence of malignant renal tumors in Ukraine has increased from 4.7 to 10.7 per 100, 000 [4]. Recent studies of our group have shown that increases in morbidity, aggressiveness, and proliferative activity of RCCs, especially CCRCCs, in Ukrainian patients that have continuously inhabited the radio-contaminated areas, might be explained by specific molecular events, influenced by chronic persistent low-dose ionizing radiation (CPLDIR) exposure [5–9].

The biological effects of long-term exposure to low-dose IR and its relationship with carcinogenesis have received a great deal of attention in the last decade [10–13]. Angiogenesis is intimately involved in the major biological processes associated with tumor growth, such as increased aggressive clinical behavior as well as increased resistance to chemotherapy, which justifies studies on the effect of long-term exposure to low-dose IR on tumor vascularization and angiogenesis in RCCs in Ukrainian patients.

Angiogenesis is a process of development and growth of new capillaries from pre-existing vessels. Neoplasms need to form new blood vessels in order to continue to grow, which explains the current concept of angiogenesis dependence of cancer [14, 15]. As a result, antiangiogenesis has become an important component in the treatment of several types of cancers, particularly of RCC [16–18].

To further increase in size, tumor cells express molecules that initiate tumor vascularization. Cellular stress factors, including hypoxia, nutrient deprivation, and especially reactive oxygen species (ROS), which are known to be produced directly or indirectly by IR, are important stimuli of angiogenic signaling [19–21].

Microvessel density (MVD), a surrogate marker for tumor angiogenesis, is accepted as an important prognostic indicator in several malignant neoplasms, such as breast, prostate, and squamous cell carcinoma of head and neck [22, 23]. The value of MVD as a predictor of patient prognosis in RCC is controversial. Several studies have shown a positive correlation between MVD and survival [24–26], while others revealed a negative correlation [27–29], and some reports no correlation at all [30, 31].

Markers used to identify blood vessels heterogeneously stain tumor vessels and reveal different characteristics of tumor vasculature [32]. CD 31 is a panvascular marker often used for immunohistochemical evaluation of MVD.

The goal of the present investigation was to examine MVD determined by CD-31 expression in CCRCCs influenced by long-term low-dose IR exposure in Ukrainian patients who lived for more than 20 years in radio-contaminated areas. To this end, we selected two groups of patients with CCRCCs from Ukraine, representing varying degrees of exposure to IR. As controls, patients from a nonirradiated homologous geographical area, as well as an analogous series of tumors from the University Clinical Hospital of Valencia (Spain) were selected.

Materials and methods

Case selection

Paraffin-embedded tissue blocks of clear-cell renal cell carcinoma (CCRCC) from 106 patients (61 men and 45 women; male/female ratio, 1.4:1) were selected for the present study. The control group 1 consisted of 18 patients with primary CCRCCs who underwent surgery between 2005 and 2007 in the University Clinical Hospital of Valencia (Spain). Ukrainian patients [25] who underwent surgery between 2005 and 2007 in the Institute of Urology, Academy of Medical Sciences of Ukraine in Kiev (Ukraine) from areas without known radio-contamination constituted group 2. Patients (63) from radio-contaminated areas, including the city of Kiev, constituted group 3. These patients resided in the same areas during the pre- and post-Chernobyl accident periods.

All tumors were evaluated with regard to pT stage, grade, and histological subtype. RCC staging was according to the AJCC 2002 tumor–node–metastasis (TNM) classification system [33, 34]. Tumor grade was determined using the Fuhrman grading system [35]. Tumor histology was classified according to the 2004 WHO criteria. We also assessed the presence of sarcomatoid changes, inflammatory response, and tumor necrosis. Pathological findings were reviewed by two pathologists specializing in genitourinary pathology. Cases in which the pathologists could not reach an agreement were excluded from the study.

Immunohistochemistry

Immunostaining with the endothelial cell marker CD 31 was performed on paraffin-embedded archival tissue following the avidin–biotin immunoperoxidase technique, as previously described [36]. Antigen retrieval was obtained incubating the samples with citrate buffer and heating in an autoclave (5 min, 1.5 atm). The primary antibody used was a prediluted monoclonal antibody anti-CD31 (clone-TUK3) from Dako. 3,3′-Diaminobenzidine and imidazole (0.01 M) were used as chromogen, and the sections were counterstained with methyl green. Microvessels of the normal adjacent kidney tissue served as positive control, and omission of the primary antibody was used as negative control. The IHC sections were read independently by at least two pathologists, without knowledge of the patient group.

Assessment of microvessel density

Representative areas of the invasive component of the CCRCCs tissue were selected for evaluation in each case. Any single brown-stained cell or cluster of cells clearly distinguishable from the background was counted as a vessel. The presence of either lumen alone or lumen with erythrocytes, although often visible, was not required to classify a structure as a vessel. We classified CD31-positive cell groups without a lumen as undifferentiated vessels. The lumen diameter had to be smaller than approximately eight red blood cells. Areas of fibrosis, necrosis, and inflammation and vessels with a muscle wall were excluded from counting.

MVD was assessed in vascular hot spots identified by light microscopy using a ×4 objective. Five equal areas were then photographed with a ×20 objective (magnification ×200) (each field representing an area of 0.596 mm^2). For each slide, the mean number of microvessels from these five areas per 0.596 mm^2 was calculated according to the criteria reported by Weidner [38]. MVD was determined without knowledge of the patients' outcome, the presence or absence of metastasis, or any other pertinent variable. Measurements were taken using the Image Pro-Plus 5.1 Image Analysis System (Media-Cybernetics).

Statistical analysis

Statistical analysis was performed in order to determine whether pathological and IHC data were correlated, within and between the different patient groups. We applied a χ^2 test for statistical analysis between qualitative variables. ANOVA and mean difference tests were used to assess the relationships between qualitative and quantitative variables. All analyses were made using the SPSS v17.0 software package.

Results

TNM stage, grade, and pathological features of CCRCCs of the patients in the different groups are summarized in Table 1.

Table 1 Patient characteristics: epidemiological and pathological features

	Group 1	Group 2	Group 3	Significance
Males	12	12	37	NS
Females	6	13	26	
Mean age (range)	63 (29–81)	56 (40–73)	57 (30–80)	NS
Year surgery	2005–2007	2005–2007	2005–2007	
Contamination level in soil[a] (Ci/km^2)	NC	NC	0.5–30	
Mean size (range)	5.27 cm (3–12)	4.84 cm (3–9)	6.58 cm (2–15)	$F=5.146$, $p=<0.01$
Tumor stage				
pT1a	6	6	9	NS
pT1b	9	16	28	
pT2	3	–	17	
pT3	–	3	9	
Grade				
1	4	9	7	$\chi^2=13.44$, $p<0.05$
2	7	2	18	
3	5	6	23	
4	2	8	15	
Sarcomatoid changes	3 (16 %)	10 (40 %)	24 (38 %)	NS
Inflammatory changes	17 (94 %)	10 (40 %)	21 (33 %)	$\chi^2=29.61$, $p<0.001$
Necrosis	3 (16 %)	10 (40 %)	14 (76 %)	$\chi^2=34.11$, $p<0.001$

NC noncontaminated areas

[a]Contamination data from Raes et al. [37]

The tumors were significantly larger in group 3 compared with groups 1 and 2. In addition, higher TNM stage and Fuhrman grade were found in tumors from group 3 ($p<0.05$). CCRCCs from groups 2 and 3 presented sarcomatoid patterns more frequently than tumors from group 1.

An intratumoral inflammatory reaction containing lymphocytes, histiocytes, and macrophages was found more frequently in group 1, but this difference was not statistically significant. Tumor necrosis was more frequent in groups 2 and 3 ($p<0.001$). Gender and age of the patients were not significantly different between groups.

Sclerosing proliferative irradiation nephropathy , characterized by medullary and less cortical peritumoral fibrous tissue, with degenerative epithelial cell pyknosis and frank necrosis in proximal and distal tubules and collecting ducts, and glomerular changes simulating membranous nephropathy, were detected in group 3 kidneys. In addition, in the medullary region of the kidney, extensive areas of epithelial detachment and degeneration with development of widened enlarged loops resembling cheese holes were seen. These were more frequent in group 3 than in group 2, but absent in group 1.

Additionally, a positive correlation was found between tumor grade and sarcomatoid transformation as well as the amount of necrosis within the histological slide, both processes being associated with high-grade CCRCCs. There were no significant relationships among tumor grade and sex, age, TNM, and intratumoral inflammatory response.

Microvessel density

Vascular density was evaluated using CD31 staining to define vascular structures. The mean count (±SD) of all CD31-stained vessels was 277.77 (±62.36), 470.24 (±111.36) and 457.84 (±104.10) for groups 1, 2, and 3, respectively. MVD counts were classified into four levels for each group as summarized in Table 2 and shown in Fig. 1.

The value of the MVD for capillary vessels only classified into four levels for different CCRCCs groups is summarized in Table 2 and shown in Fig. 2. A striking increase in capillaries with the highest capillary density levels (201–250 and >251) was seen in three CCRCCs, in comparison with groups 1 and 2 CCRCCs ($\chi^2=25.82$; $p<0.001$). This is illustrated in Fig. 3. It is significant to note that the majority of hot spot vessels in group 3 were undifferentiated. They had no lumen, had a thicker vessel wall, and had smaller size than differentiated vessels. The highest capillary MVD levels (>251) were not detected in group 1, in which the more differentiated vessels were predominant.

Regarding Ukrainian groups, the MVD of large caliber vessels was 15.64 (±5.64) and 14.98 (±9.07); the MVD for mid-caliber vessels was 230.64 (±69.41) and 215.63

Table 2 Results of microvascular density in relation to groups and tumor grade

Groups					Tumor grade			
	1	2	3	Significance	1	2	3+4	Significance
Total vessels								
Mean	277.77	470.24	457.84	$F=25.17$,	442.35	383.85	448.83	NS
SD	62.36	111.36	104.10	$p<0.001$	92.70	131.00	116.02	
Total vessels								
<300	10	1	5	$\chi^2=40.48$,	2	7	7	NS
301–400	8	6	12	$p<0.001$	4	7	15	
401–500	–	10	25		10	7	18	
>500	–	8	21		4	6	19	
Total vessels large caliber								
Mean	9.72	15.64	14.98	$F=3.217$,	15.45	14.85	13.44	NS
SD	8.93	5.64	9.07	$p<0.05$	8.98	10.91	7.26	
Total vessels mid caliber								
Mean	116.61	230.64	230.64	$F=21.78$,	201.25	187.07	212.05	NS
SD	41.19	69.41	69.41	$p<0.001$	61.08	77.78	71.92	
Total capillary								
Mean	151.44	223.96	227.22	$F=13.90$,	225.65	187.92	222.50	$F=2.607$,
SD	55.49	53.84	55.19	$p<0.001$	43.47	67.01	61.21	$p=0.056$, NS
Total capillary								
<150	8	1	4	$\chi^2=25.82$,	–	6	7	$\chi^2=20.27$,
151–200	6	10	20	$p<0.001$	5	12	19	$p<0.05$
201–250	4	5	14		10	3	10	
>250	–	9	25		5	6	23	

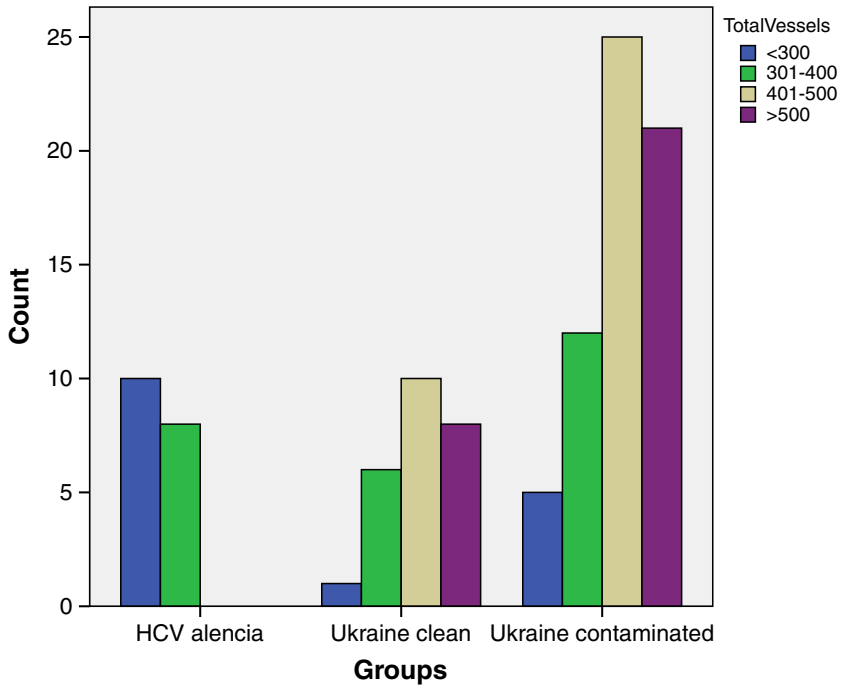

Fig. 1 Number of cases grouped according to the MVD of total vessels in the three populations analyzed

(±62.46) for CCRCCs groups 2 and 3, respectively; capillary MVD in the same groups was 223.96 (±53.84) and 227.22 (±55.19), respectively, without significant differences. The same correlation was observed for total MVD, which was 470.24 (±111.36) and 457.84 (±104.10) in CCRCCs of groups 2 and 3, respectively.

However, the MVD of large caliber vessels (9.72±8.93), the MVD of mid-caliber vessels (116.61, ±41.19), the capillary MVD (151.44, ±55.49), as well as the MVD for all vessels (277.34, ±62.36) in CCRCCs from group 1 was significantly lower than in both Ukrainian groups 2 and 3 ($p<0.001$).

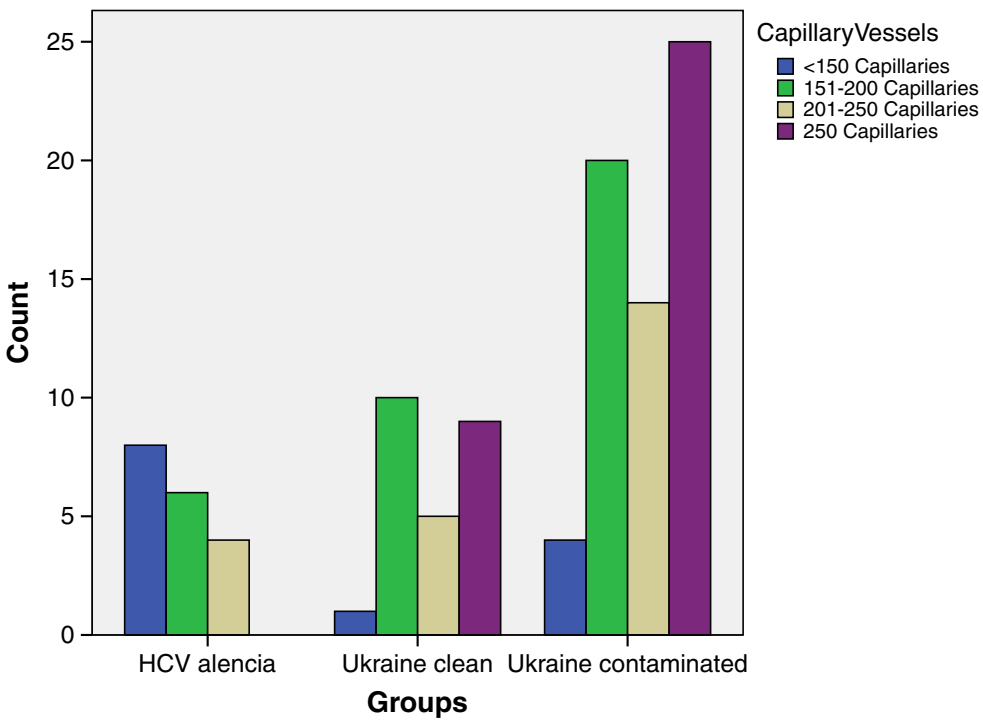

Fig. 2 Number of cases grouped according to the MVD of capillary vessels in the three populations analyzed

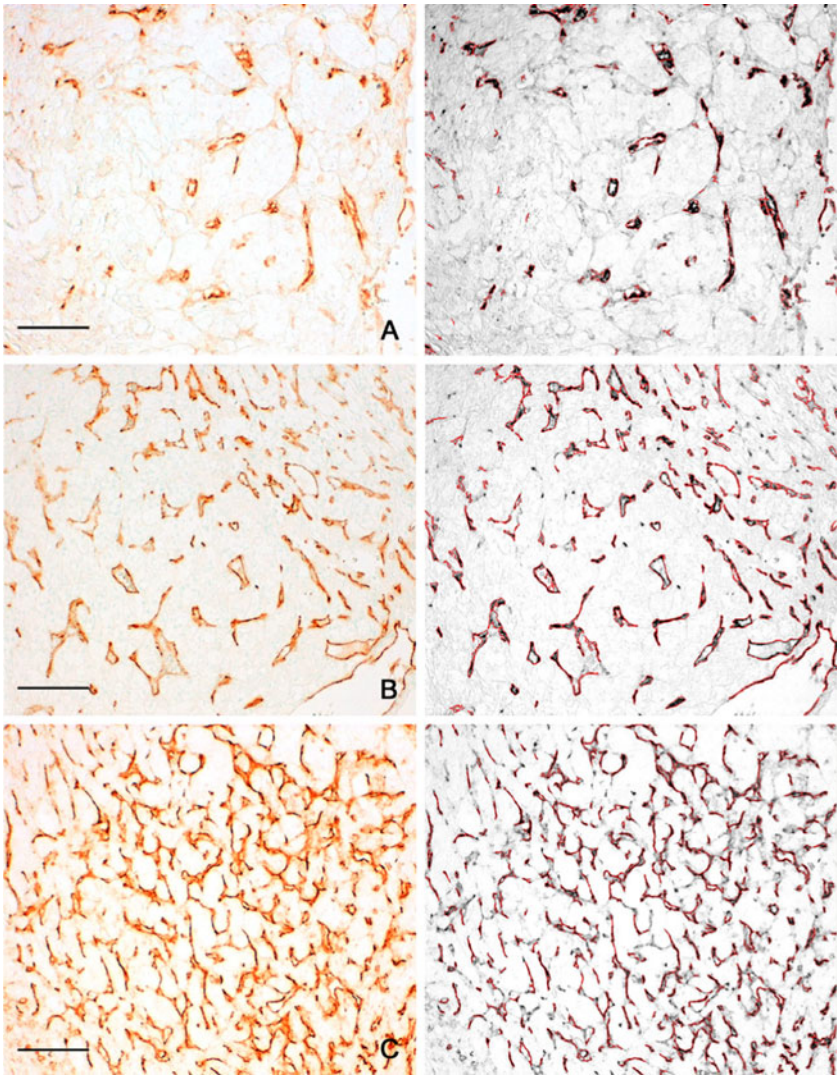

Fig. 3 **a**–**c** Serial sections of CCRCCs tissue stained with CD31, which clearly revealed the differentiated and undifferentiated blood vessels. *Adjacent* The corresponding marking for morphometric study. **a** Case from Valencia. **b** Vase from Kiev noncontaminated. **c** from Kiev contaminated. Magnification ×20

Moreover, strong statistical correlations were found between tumor grade and MVD for total vessels as well as capillary MVD. The highest total MVD (from 301 to 500 and >500) and the highest capillary MVD (from 150 to 250 and >250) was detected in grade 3+4 CCRCCs ($p<0.05$).

Table 3 Comparison of MVD between low TNM stages (I and II)

Group	*N*	Mean of total vessels	Mean capillaries
1 (CCRCC-Valencia)	18	277.77	151.44
2 (CCRCC-Ukraine clean area)	22	466.31	223.77
3 (CCRCC-Ukraine contaminated area)	54	454.77	225.07
Total	94		

N patients with TNM stages I and II, *X TV* mean of total vessels, *X CAP* mean of capillaries

A significant decrease in MVD was seen in group 1 CCRCCs, compared with groups 2 and 3 ($F=25.17$; $p<0.001$). Moreover, 72 % of group 2 and 73 % of group 3 CCRCCs showed the highest MVD (between 401 and 500 and >501) with significant differences with group 1. When we compared only TNM tumor stages I and II, the differences remained statistically significant ($p<0.01$). The ratio of average total vessel MVD and capillary MVD in the groups 2 and 3 combined was (1.65:1) with respect to the Spanish group. These data are summarized in Table 3 and shown in Fig. 4.

Discussion

Our study demonstrates a striking increase in vascular density in Ukrainian CCRCCs, in comparison with equivalent Spanish cases. Particularly significant is the increase in capillary density, which was highest in the Ukrainian group 3 patients living continuously in the radio-contaminated

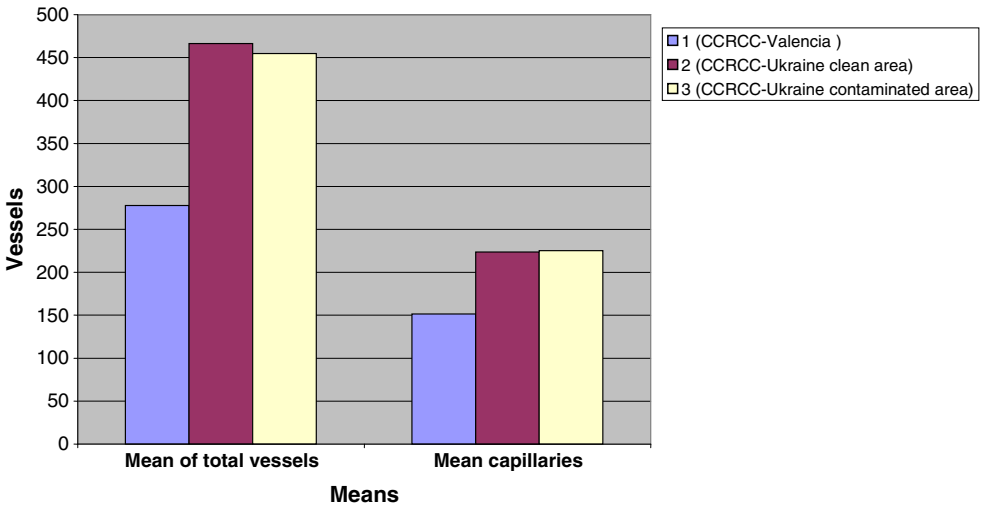

Fig. 4 Comparison of MVD between low TNM stages (I and II)

areas. We speculate that these very high MVD levels might result not only from the newly formed capillaries but also from the development of undifferentiated microvessels stained by CD31 antibody [39, 40].

We found no significant differences in mean or median MVD values between the Ukrainian groups 2 and 3 for capillaries or the large and mid-caliber vessels or for the total vessel counts. This might be explained on the assumption that the Ukrainian control group 2, which included tumors from so-called clean areas (without officially indicated radio-contamination), may have had chemical or radioactive contamination from food and vegetables coming from radio-contaminated areas, since all of Ukraine is considered to be an ecological disaster area.

It is well known that angiogenesis is one of the most important factors in vascularization, growth, and metastasis of tumor tissue [14, 41, 42]. The transition from the latent phase to the invasive and metastatic phase of a cancer is linked to what is called "the angiogenic switch," which also allows the transcription from low invasive and poorly vascularized tumors to highly invasive and angiogenic tumors [43, 44].

The highest levels of undifferentiated vessels and capillaries in group 3 CCRCCs of the Ukrainian patients who lived for longer than 20 years in ^{137}Cs-contaminated areas might be, in our opinion, a result of *CPLDIR* effects. Recent studies have revealed that a number of cellular stress factors, including hypoxia and ROS that are generated by chronic persistent low-dose IR exposure, can specifically activate certain signaling pathways and thus contribute to tumor development through the regulation of cellular proliferation and angiogenesis [19, 45].

In addition, overexpression of rat sarcoma viral oncogene (*Ras*) has been linked to vascularization of tumors [14]. This suggestion is supported by a recent study by our group in which some Ukrainian CCRCCs demonstrate a striking increase in aggressiveness and proliferative activity associated with strong K-ras and Raf-1 (murine sarcoma 3611 oncogene) protein expression [5].

In contrast with the existing opinion that activating *Ras* or *Raf* mutations are rare in RCCs [46], our recent data on Ukrainian CCRCCs influenced by long-term exposure to low-dose IR [47] indicate that K-Ras and Raf-1protein overexpression is associated with MAPK pathway activation, which is known to be a critical component of ROS mediated signaling [48].

Indeed, the *Ras/Raf/MEK/MAPK* signal transduction cascade stabilizes hypoxia inducible factor-1α (HIF-1α) and upregulates the transcription of vascular endothelial growth factor-A. Moreover, ROS stabilize HIF-1a protein, which, in turn, responds to these changes by specifically decreasing the oxygen (or hypoxia) levels and upregulates several genes to promote survival in low-oxygen conditions, thus promoting angiogenesis, which might be related to the metastatic process and to poorly differentiated variants of CCRCCs [49].

In contrast with earlier studies [26, 50], which showed that MVD does not correlate with stage and histological grade of CCRCCs, our results confirm the positive correlation between tumor grade and total intratumoral MVD, as well as capillary MVD, especially in the Ukrainian CCRCCs groups. These differences may be due to the fact that microvascularization of CCRCC differs from that of other types of renal carcinoma.

Thus, we conclude that microvessel density determined with CD31 may represent a prognostic parameter for clear-cell renal cell carcinoma in patients exposed to CPLDIR. The results of our study are in agreement with other recent studies that demonstrate the relationship between MVD and angiogenesis and prognosis in CCRCCs, in addition to histologic grade, presence of tumor necrosis and sarcomatoid areas,

presence of metastasis, and tumor proliferative activity [51, 52].

The controversial significance of MVD determined by CD31 as a prognostic indicator in RCCs could result from many non-mechanistic factors, including sample size, the different blood vessel markers chosen for IHC characterization, the quality of IHC staining, the method of vasculature quantification, as well as the methods of interpretation.

In conclusion, the present study shows that CCRCC patients exposed to long-term low-dose IR effects [living for more than 20 years in radio-contaminated (^{137}Cs) areas of Ukraine], have a striking increase in CCRCC MVD (particularly, capillary) which is strongly associated with high histological grade, sarcomatoid transformation, intratumoral necrosis, and decreased inflammatory response.

Acknowledgments This study is supported by grants: Conselleria Sanitat Comunitat Valenciana, ref. no. 909/2007 and Fundación Instituto Valenciano de Oncología (IVO) Valencia. Spain.

Conflict of interest statement We declare that we have no conflict of interest.

References

1. Yagoda A, Petrylak D, Thompson S (1993) Cytotoxic chemotherapy for advanced renal cell carcinoma. Urol Clin Nort Am 20:303–321
2. Fossa SD (2000) Interferon in metastatic renal cell carcinoma. Semin Oncol 27:187–193
3. Dennis Smith A, Lieber ML, Shah SN (2010) Assessing tumor response and detecting recurrence in metastatic renal cell carcinoma on targeted therapy: importance of size and attenuation on contrast enhanced CT. Am J Roentgenol 194:157–165
4. Saydackova NA, Starceva LM, Kravchuk NC (2007) The state of urological assistance for the population in Ukraine. Annual report. Ministry of Health in Ukraine, Kiev, pp 146–153
5. Romanenko A, Morrell-Quadreny L, Nepomnyaschy V, Vozianov A, Llombart-Bosch A (2000) Pathology and proliferative activity of renal-cell carcinomas and renal oncocytomas in patients with different radiation exposure after the Chernobyl accident in Ukraine. Int J Cancer 87:880–883
6. Romanenko A, Morrell-Quadreny L, Nepomnyaschy V, Vozianov A, Llombart-Bosch A (2001) Radiation sclerosing proliferative atypical nephropathy of peritumoral tissue of renal-cell carcinomas after the Chernobyl accident in Ukraine. Virchows Arch 438:146–153
7. Romanenko A, Morrell-Quadreny L, Lopez-Guerrero JA, Pellin A, Nepomnyaschy V, Vozianov A, Llombart-Bosch A (2004) The INK4a/ARF locus: role in cell cycle control for renal cell epithelial tumor growth after the Chernobyl accident. Virchows Arch 445:298–304
8. Romanenko A, Morrell-Quadreny L, Ramos D, Vozianov A, Llombart-Bosch A (2006) Alteration of apoptotic regulatory molecules in conventional renal cell carcinoma influenced by chronic long-term low-dose radiation exposure in humans revealed by tissue microarray. Cancer Genomics Proteomics 3:107–112
9. Romanenko A, Morrell-Quadreny L, Ramos D, Nepomnyaschy V, Vozianov A, Llombart-Bosch A (2006) Extracellular matrix alterations in conventional renal cell carcinomas by tissue microarray profiling influenced by persistent, long-term, low-dose ionizing radiation exposure in humans. Virchows Arch 448:584–590
10. Clarke RH (2001) Control of low-level radiation exposure: what is the problem and how can it be solved? Health Phys 80:391–396
11. Christensen R, Alsner J, Brandt Sorensen F, Dagnaes-Hansen F, Kolvraa S, Serakinci N (2008) Transformation of human mesenchymal stem cells in radiation carcinogenesis: long-term effect of ionizing tadiation. Regen Med 3(6):849–861
12. Mullenders L, Atkinson M, Peretzke H, Sabatier L, Bouffler S (2009) Assessing cancer risks of low-dose radiation. Nat Rev Cancer 9(8):596–604
13. Wilson PF, Nham PB, Urbin SS, Hinz JM, Jones IM, Thompson LH (2010) Inter-individual variation in DNA double-strand break repair in human fibroblasts before and after exposure to low doses of ionizing radiation. Mutat Res 683:91–97
14. Bergers G, Benjamin LE (2003) Tumorigenesis and the angiogenic switch. Nat Rev Cancer 3:401–410
15. Kerbel RS (2008) Tumor angiogenesis. N Engl J Med 358:2039–2049
16. Zhang Y, Jiang X, Qin X, Ye D, Yi Z, Liu M, Bai O, Fang J, Chen Y (2010) RKTG inhibits angiogenesis by suppressing MAPK-mediated autocrine VEGF signaling and is downregulated in clear-cell renal cell carcinoma. Oncogene 29:5404–5415
17. Hanahan D, Weinberg RA (2011) Hallmarks of cancer: the next generation. Cell 144:646–674
18. Ravasio R, Ortega C, Sabbatini R, Porta C (2011) Bevacizumab plus interferon-a versus sunititab for first-line treatment of renal cell carcinoma in Italy: a cost-minimization analysis. Clin Drug Investig 31:507–517
19. North S, Moenner M, Bikfalvi A (2005) Recent developments in the regulation of the "angiogenic switch" by cellular stress factors in tumors. Cancer Lett 218:1–14
20. Ushio-Fukai M, Nakamura Y (2008) Reactive oxygen species and angiogenesis: NADPH oxidase as target for cancer therapy. Cancer Lett 266:37–52
21. Kim J, Koyanagi T, Mochly-Rosen D (2011) PKCo activation mediates angiogenesis via NADPH oxidase activity in PC-3 prostate cancer cells. Prostate 71:946–954
22. Weidner N (1995) Current pathologic methods for measuring intratumoral microvessel density within breast carcinoma and other solid tumors. Breast Cancer Res Treat 36:169–180
23. Uzzan B, Nicolas P, Cucherat M, Perret GY (2004) Microvessel density as a prognostic factor in women with breast cancer: a systematic review of the literature and meta-analysis. Cancer Res 64:2941–2955
24. Delahunt B, Bethwaite PB, Thornton A (1997) Prognostic significance of microscopic vascularity for clear cell renal cell carcinoma. Br J Urol 80:401–404
25. Herbst C, Kosmehl H, Stiller KJ (1998) Evaluation of microvessel density by computerized image analysis in human renal cell carcinoma. Correlation to pT category, nuclear grade, proliferative activity and occurrence of metastasis. J Cancer Res Clin Oncol 124:141–147
26. Gontero P, Ceratti G, Guglielmetti S, Andorno A, Terrone C, Bonvini D, Faggiano F, Tizzani A, Frea B, Valente G (2008) Prognostic factors in a prospective series of papillary renal cell carcinoma. BJU Int 102:697–702
27. Nativ O, Sabo E, Reiss A (1998) Clinical significance of tumor angiogenesis in patients with localized renal cell carcinoma. Urol 51:693–696
28. Yildiz E, Ayan S, Goze F, Gultekin EY (2008) Relation of microvessel density with microvascular invasion, metastasis and prognosis in renal cell carcinoma. BJU Int 101:758–754
29. Sharma SG, Aggarwal N, Gupta SD, Singh MK, Gupta R, Dinda AK (2010) Angiogenesis in renal cell carcinoma: correlation of microvessel density and microvessel area with other prognostic factors. Int Urol Nephrol 10:9779–9787
30. Yilmazer D, Han U, Onal B (2007) A comparison of the vascular density of VEGF expression with microvascular density

determined with CD34 and CD31 staining and conventional prognostic markers in renal cell carcinoma. Int Urol Nephrol 39:691–698
31. Bhattacharyya NK, Chatterjee U, Sarkar S, Kundu AK (2008) A study of proliferative activity, angiogenesis and nuclear grading in renal cell carcinoma. Indian J Pathol Microbiol 51:17–21
32. Llombart-Bosch A, Lopez-Guerrero JA, Carda Batalla C, Ruiz-Sauri A, Peydro-Olaya A (2003) Structural basis of tumoral angiogenesis. Adv Exp Med Biol 532:69–89
33. Sobin LH and Wittekind C (eds) (2002) TNM classification of malignant tumors, 6th edn. Wiley-Liss, New York
34. Eble JN, Sauter G, Epstein JI, Sesterhenn IA (eds) (2004) Pathology and genetic of tumors of the urinary system and male genetic organs. World Health Organization Classification of Tumors. IARC, Lyon
35. Fuhrman SA, Lesky LC, Limas C (1982) Prognosis significance of morphologic parameters in renal cell carcinoma. Am J Surg Pathol 6:655–663
36. Sales A, Ruiz A, Llombart-Bosch A (1999) Comparative morphometric evaluation of microvessel density and nuclear area in ductal carcinoma in situ and hyperplasticductal breast lesions. Breast 8:21–25
37. Raes F, De Cort M, Graziani G (1991) Multi-fractal nature of radioactivity deposition on soil after the Chernobyl accident. Health Phys 61:271–28
38. Weidner N, Folkman J, Pozza F, Bevilacqua P, Allred EN, Moore DH, Meli S, Gasparini G (1992) Tumor angiogenesis: a new significant and independent prognostic indicator in early-stage breast carcinoma. J Natl Cancer Inst 84:1875–1887
39. Lao X, Qian CN, Zhand ZF, Tan MH, Kort XJ, Resau JH, The BT (2007) Two distinct types of blood vessels in clear cell renal cell carcinoma have contrasting prognostic implications. Clin Cancer Res 13:161–169
40. Qian CN, Huang D, Wondergem B, The BT (2009) Complexity of tumor vasculature in clear cell renal cell carcinoma. Cancer 115:2282–2289
41. Fox SB (1997) Tumor angiogenesis and prognosis. Histopathol 30:294–301
42. Jain L, Vargo CA, Danesi R, Sissung TM, Price DK, Venzon D, Venitz J, Figg WG (2009) The role of vascular endothelial growth factor SNPs as predictive and prognostic markers for major solid tumors. Mol Cancer Ther 8:2496–2508
43. Shinkaruk S, Bayle M, Lain G, Deleris G (2003) Vascular endothelial cell growth factor (VEGF), an emerging target for cancer chemotherapy. Curr Med Chem Anticancer Agents 3:95–117
44. Reuter S, Gupta SC, Chaturvedi MM, Aggarwal BB (2010) Oxidative stress, inflammation, and cancer: how they linked? Free Radic Biol Med 49:1603–1616
45. Storz P (2005) Reactive oxygen species in tumor progression. Front Biosci 10:1881–1896
46. Rochlitz CF, Peter S, Willroth G, de Kant E, Lobeck H, Huhn D (1992) Mutations in the *ras* protooncogenes are rare events in renal cell cancer. Eur J Cancer 28:333–336
47. Romanenko AM, Morimura K, Kinoshita A, Wanibuchi H, Takahashi S, Zaparin WK, Vinnichenko VI, Vozianov AF, Fukushima Sh (2006) Upregulation of fibroblast growth factor3 and epidermal growth factor receptors, in association with Raf-1, in urothelial dysplasia and carcinoma in situ after the Chernobyl accident. Cancer Sci 97:1168–1174
48. Suzuki K, Kodama S, Watenabe M (2001) Extremely low-dose ionizing radiation causes activation of mitogen-activated protein kinase pathway and enhances proliferation of normal human diploid cells. Cancer Res 61:5396–5401
49. Chandel NS, Maltere E, Goldwasser E, Mathieu CE, Simon MC, Schumacker PT (1998) Mitochondrial reactive oxygen species trigger hypoxia-induced transcription. Proc Natl Acad Sci USA 95:11715–11720
50. MacLennan GT, Bostwick DG (1995) Microvessel density in renal cell carcinoma: lack of prognostic significance. Urol 46:27–30
51. Kavantzas N, Paraskevakou H, Tseleni-Balafouta S, Aroni K, Athanassiades P, Agrogiannis G, Patsouris E (2007) Association between microvessel density and histologic grade in renal cell carcinomas. Pathol Oncoly Res 13:145–148
52. Puscasiu D, Tatu C, Tatu RF, Potencz E, Popescu R, Muntean I, Verdes D (2011) The significance of angiogenesis and tumoral proliferation in renal cell carcinoma. Rom J Morphol Embryol 52:369–372

Virchows Arch (2012) 460:621–628
DOI 10.1007/s00428-012-1240-0

ORIGINAL ARTICLE

NR4A3 rearrangement reliably distinguishes between the clinicopathologically overlapping entities myoepithelial carcinoma of soft tissue and cellular extraskeletal myxoid chondrosarcoma

Uta Flucke · Bastiaan B. J. Tops · Marian A. J. Verdijk · Patricia J. H. van Cleef · Peter H. van Zwam · Pieter J. Slootweg · Judith V. M. G. Bovée · Robert G. Riedl · David H. Creytens · Albert J. H. Suurmeijer · Thomas Mentzel

Received: 18 November 2011 / Revised: 30 March 2012 / Accepted: 16 April 2012 / Published online: 9 May 2012
© The Author(s) 2012. This article is published with open access at Springerlink.com

Abstract Myoepithelial carcinoma of soft tissue (MEC) and cellular extraskeletal myxoid chondrosarcoma (cEMC) share striking similarities. In this paper, we compare ten MECs with five cEMCs. MEC patients had an equal gender distribution. The age range was 15–76 years (mean, 42 years). Tumours were located on extremities, pelvic girdle, vulva and neck. Follow-up, available for nine patients, ranged from 4 to 85 months (mean, 35 months). Five patients were alive without evidence of disease, two were alive with disease and two died 8 months after the initial diagnosis. cEMCs were from three males and two females with an age range of 37–82 years (mean, 57 years); they presented in extremities, shoulder and paravertebral/cervical. Follow-up, available for four patients, ranged from 6 to 220 months (mean, 61 months). All patients were alive, two with recurrences and/or metastases and two without evidence of disease. Morphologically, the distinction between these two entities was difficult since all cases exhibited features typically seen in myoepithelial tumours. Immunohistochemically, MECs expressed pan-keratin (80 %), epithelial membrane antigen (EMA; 57 %), S100 (50 %), alpha-smooth muscle actin (ASMA; 75 %), calponin (67 %) and p63 (25 %). S100 and EMA were expressed in 40 % of cEMC cases respectively with additional immunoreactivity for p63, ASMA and glial fibrillary acidic protein in one case. Pan-keratin was negative in all neoplasms. *NR4A3* rearrangement was present in four of four cEMCs and in none of the MECs. In contrast, three of nine (33 %) MECs and four of five (80 %) cEMCs showed an *EWSR1* rearrangement. In summary, MECs and cEMCs share clinical, morphological, immunohistochemical and genetic characteristics. The pathognomic rearrangement of *NR4A3* is a useful diagnostic feature in identifying cEMCs.

U. Flucke (✉) · B. B. J. Tops · M. A. J. Verdijk · P. J. H. van Cleef · P. H. van Zwam · P. J. Slootweg
Department of Pathology,
Radboud University Nijmegen Medical Center,
P.O. Box 9101, 6500 Nijmegen, The Netherlands
e-mail: u.flucke@pathol.umcn.nl

J. V. M. G. Bovée
Department of Pathology, Leiden University Medical Center,
Leiden, The Netherlands

R. G. Riedl
Department of Pathology, Maastricht University Medical Center,
Maastricht, The Netherlands

D. H. Creytens
Department of Pathology, University Hospital Antwerp,
Antwerp, Belgium

A. J. H. Suurmeijer
Department of Pathology, University Medical Center Groningen,
Groningen, The Netherlands

T. Mentzel
Dermatopathologie Bodensee,
Friedrichshafen, Germany

Keywords Myoepithelial carcinoma of soft tissue · Extraskeletal myxoid chondrosarcoma · Soft tissue tumours · *EWSR1* rearrangement · *NR4A3* rearrangement

Introduction

Myoepithelial tumours of the soft tissue were initially characterised in a series by Kilpatrick et al. [1]. Later on, criteria for malignancy were established and the clinicopathological features expanded [2, 3]. Histologically, these tumours show the same broad variation in morphology as seen in their salivary gland counterparts [1–4].

Extraskeletal myxoid chondrosarcomas (EMCs) reveal a cord- or lace-like arrangement of small round to spindle-shaped cells with distinct eosinophilic cytoplasm distributed in a prominent myxoid stroma. In cellular lesions (cEMCs), amounting to one third of the cases, there is a greater morphological diversity [5–11]. Although the age range is broad for both entities, the peak incidence for EMC is the sixth and for MEC the fourth decade [2, 4, 12]. Furthermore, a significant subset of malignant myoepithelial tumours or myoepithelial carcinomas (MECs) occurs in children in contrast to EMCs which show a very low incidence in this cohort [3, 5, 8, 12, 13]. Both, myoepithelial tumours and EMCs arise predominantly in the proximal lower extremity but EMCs are more often located in the deep soft tissue [2, 4, 12]. Whereas EMCs have a protracted clinical course with a 10-year survival rate up to 88 % [5, 8, 14–16], MECs typically demonstrate aggressive behaviour, particularly in the pediatric population [2, 3]. Whether or not also cEMCs have a worse prognosis remains controversial [5–10].

Histologically, cEMC can be morphologically similar to myoepithelial tumours but the latter have a broader immunohistochemical profile [2–4, 12]. Gene fusions involving *NR4A3* (*nuclear receptor subfamily 4, group A, member 3*) located at 9q22 are characteristic for EMC and have never been described in myoepithelial tumours. In contrast, both tumour types harbour *EWSR1* (*Ewing sarcoma breakpoint region 1;* 22q12.2) rearrangement [3, 12, 17–25].

In this paper, we report on the morphological, immunohistochemical and molecular overlap of MEC and cEMC.

Material and methods

We searched the surgical pathology and referral files of the authors for the diagnoses myoepithelial tumours of soft tissue and EMC. Slides were reviewed and the diagnoses were based on criteria according to the recent WHO classification [26]. Myoepithelial tumours with moderate to severe nuclear atypia (vesicular or coarse chromatin, prominent, often large nucleoli, or nuclear pleomorphism) and EMCs with cellular features were included in our study. Clinical details and follow-up were obtained from the referring pathologists (see "Acknowledgement"). Cases 8 and 10 were published earlier [3, 27, 28].

In all cases, the tissue was fixed in 4 % buffered formalin, routinely processed and embedded in paraffin; 2–4-μm-thick sections were stained with hematoxylin and eosin. Immunohistochemical methods consisted of the labelled Streptavidin Biotin technique using commercially available antibodies as listed in Table 1. Appropriate positive and negative controls were used throughout.

Fluorescence in situ hybridisation analysis

Fluorescence in situ hybridisation (FISH) was performed as described earlier. For *EWSR1,* a directly FITC/Rhodamine-labelled break apart-probe (Abbott, Bergisch Gladbach, Germany) was used [29]. FISH probes to detect a *NR4A3* rearrangement (break apart probe) were generated in-house. BAC clones RP11-624K13 (centromeric), RP11-412F16 (centromeric), RP11-121L12 (telomeric) and RP11-467B11 (telomeric) were obtained from the BACPAC Resources Center (Oakland, CA). Clones were either labelled with biotin or digoxigenin using a nick translation kit, according to manufacturer's instructions (Roche, Basel, Switzerland). Copy numbers of chromosome 9 were assessed using a centromere probe (CEP9). A negative control was used for each tumour. A case was considered having a break when at least 10 of 50 counted tumour cells (20 %) showed separation of a red and green signal.

Reverse transcription polymerase chain reaction

RNA was isolated from formalin-fixed, paraffin-embedded material by proteinase K digestion, followed by phenol/chloroform extraction and *n*-propanol precipitation. cDNA synthesis was performed in a 24-μl reaction containing 1 μg

Table 1 Details of used immunohistochemical antibodies

Antibody	Clone	Dilution	Source
ASMA	1A4	1:500	DAKO, Glostrup, Denmark
EMA	Mc5	1:400	BioGenex, San Ramon, USA
CD34	HPCA-1	1:100	BD Biosciences, San Jose, USA
Pan-cytokeratin	MNF116	1:500	DAKO, Glostrup, Denmark
Pan-cytokeratin	AE1/3	1:50	DAKO, Glostrup, Denmark
S-100 protein	polyclonal	1:2000	DAKO, Glostrup, Denmark
P63	4A4	1:5000	Thermo Fisher Scientific, USA
GFAP	GA-5	1:200	DCS, Hamburg, Germany
Calponin	CALP	1:400	DAKO, Glostrup, Denmark

of RNA, 1 μg of random hexamers (Promega) and 20 nmol dNTPs (Invitrogen) and heated at 65°C for 5 min. Next, 2 μl of RNasin (Promega), 8 μl of ×5 first-strand buffer (Invitrogen), 4 μl of 0.1 M DTT (Invitrogen) and 2 μl of Superscript II (Invitrogen) were added and the sample was heated accordingly: 20°C for 10 min, 42°C for 60 min and 95°C for 3 min.

For EMC, most potential translocation-specific *EWSR1-NR4A3* and *TAF15-NR4A3* fusion products were detected using primers targeting *EWSR1* (exon 7: TCCTACAGCCAAGCTC CAAGTC and exon 11: GACTCTAGATGATCTGGCAGAC, RefSeq: NM_005243.3), *TAF15 (TAF15 RNA polymerase II)* (exon 6: AGCAGTCAAATTATGATCAGCAGC, RefSeq: NM_003487.2) and *NR4A3* (exon 3: CCTGGAGGG GAAGGGCTATATTGGG, RefSeq: NM_006981.3).

Results

Clinical findings

Clinical details are summarised in Table 2. The MEC cohort consisted of five males and five females with an age range of 15–76 years (mean, 42 years). The tumours were located on the extremities (n=4) with one case each on the thigh, calf, forearm and hand. Other sites were vulva (n=2), gluteal (n=1), sacral (n=1) and the neck region (n=1). In one case, the exact anatomic site was not known. Seven MECs were situated in the deep soft tissue and two subcutaneous. One superficially located tumour of the vulva showed exophytic growth. All patients underwent surgical treatment. Complete resection was reached in seven cases and marginal excision in one case. Tumour-positive margins were reported in two cases. Follow-up, available for nine patients, ranged from 4 to 85 months (mean, 35 months). Five patients were alive without evidence of disease at 12, 34, 39, 60 and 70 months, respectively. Two patients were alive with disease 4 and 85 months after the initial diagnosis, the latter with a second local recurrence. Two patients died of disease 8 months after the initial diagnosis. Case 10 was the first local recurrence on the hand with secondary bone involvement. Three patients presented with lung metastases. Involvement of regional lymph nodes was additionally observed in two of them, and one patient had bone metastases.

The five cases of EMC were from three males and two females with an age range of 37–82 years (mean, 57 years). Two lesions were located in the deep soft tissue of the thigh and one in the subcutis and soft tissue of the shoulder. One tumour each arose at the ankle and the paravertebral/cervical region. All patients but one (n=4) underwent resection. Tumour free resection margins were reported in three cases (wide margins in two cases and marginal resection in one case). In Case 14, the resection status was not known. Follow-up, available for four patients, ranged from 6 to 220 months

Table 2 Clinical data

Case No	Sex/Age	Primary Site	Size (cm)	Therapy	Follow-up (months)	Rec (Met)
MEC						
1	F/36 years	na/sc	4.5	R0	NA	
2	F/21 years	Thigh/deep	5.0	R0	70, NER	
3	F/53 years	Vulva/exophytic	3.5	R0	60, NER	
4	F/75 years	Vulva	3.5	R0	34, NER	
5	M/36 years	Forearm/deep	10	R0	8, DOD	Lung
6	F/15 years	Neck/deep	4	R2	85, AWD	2 rec
7	M/15 years	Sacral/deep	5	R0	39, NER	
8	M/17 years	Calf/deep	12	R0, perf,amp	8, DOD	Bone, lung, LN
9	M/71 years	Buttock/sc	15	R1	4, AWD	Lung, LN
10	M/76 years	Hand/deep, bone invasion	4.5	RM	12, NER	1 rec
EMC						
11	M/61 years	Thigh/deep	8.1	R0	12, NER	
12	M/58 years	Thigh/deep	10	R0	6, NER	
13	F/37 years	Shoulder/sc, deep	15	NT	6, AWD	LN
14	M/82 years	Paravertebral/cervical	NA	RX	NA	
15	F/46 years	Ankle	1	RM	220, AWD	4 rec, lung

Mos months, *Rec* recurrence, *Met* metastases, *Sc* subcutis, *LN* lymph node, *NER* no evidence of recurrence, *AWD* alive with disease, *DOD* death of disease, *NA* not available, *NT* no treatment, *Perf* limb perfusion, *Amp* amputation, *R0* complete resection, *RM* marginal resection, *R1* resection with histological positive margins, *R2* resection with macroscopically positive margins, *RX* resection with unknown margins

(mean, 61 months). No patient died of the disease so far. Case 15 was the 4th recurrence of a tumour with primarily classical morphological features. This patient had also pulmonary spread. Another patient was known with regional lymph node involvement (Case 13).

Pathological findings

Grossly, the neoplasms were described as white or yellowish nodules, solid, gelatinous and also cystic in appearance. Haemorrhage and necrosis was seen in some of the lesions. The size range for MECs was 3.5 to 15 cm (mean, 6.7 cm) and for EMCs 1 to 15 cm (mean, 8.5 cm). In one EMC, the size was unknown.

Histologically, most cases demonstrated a (multi)nodular configuration with expansive margins and an incomplete pseudo-capsule. Infiltrative margins were focally seen. MECs showed in most of the cases varying growth patterns such as trabecular, reticular, nested and solid. A pure trabecular pattern was seen in two cases. Six tumours were composed of different cell types, including spindle, epithelioid, plasmacytoid and/or clear cells. Round cell morphology associated with clear cell features was observed in two cases and a pure epithelioid phenotype in two other cases (Fig. 1). Osteoclast-like giant cells were scattered in Cases 1 and 4. All cases exhibited moderate to severe nuclear atypia with vesicular or coarse chromatin (Fig. 2). Prominent nucleoli were conspicuous in seven cases. Mitoses ranged from one to six per ten HPF. The matrix was (chondro)myxoid in eight cases with pseudocystic changes in two cases. Five tumours showed stromal hyalinisation. Areas of haemorrhage and tumour necrosis were observed in one and two cases, respectively.

All EMC cases had focally classical features with strands and cords of small, uniform round to spindle-shaped cells set in a prominent myxoid matrix. There were round to oval nuclei and limited deeply eosinophilic cytoplasm. The tumour nodules, separated by fibrous septa, often showed peripheral cell condensation. In the cellular areas, sheets and nests of tumour cells were present. A trabecular and reticular-cystic pattern as well as loosely arranged cells occurred variably. The lesional cells were epithelioid and/or spindle shaped and slightly pleomorphic (Figs. 3 and 4). Case 13 showed increased pleomorphism, cytoplasmic vacuoles, multinucleated giant cells and prominent necrosis. In two cases, larger nuclei and prominent nucleoli were seen (Cases 11 and 12). Rhabdoid cytology was observed in Case 12. For all cases, the mitotic activity was very low and did not exceed one mitosis/ten HPF. In the cellular areas, the myxoid matrix was scant or even absent.

Immunohistochemically, eight of ten (80 %) myoepithelial carcinomas were, at least focally, positive for pan-cytokeratin and four of seven (57 %) for epithelial membrane antigen (EMA). The two cases negative for pan-cytokeratin expressed

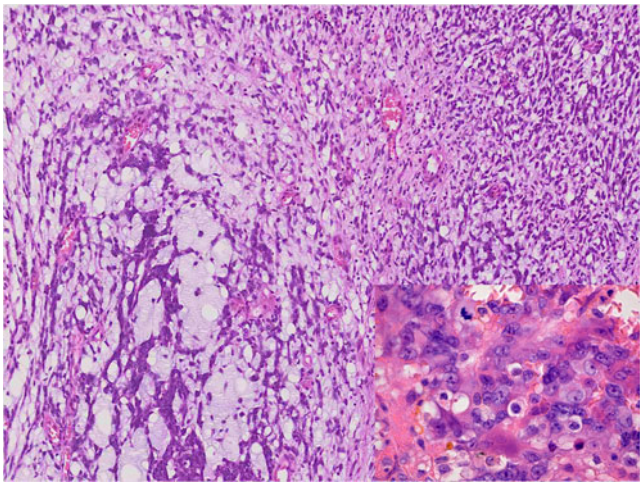

Fig. 2 Note the nuclear pleomorphism, more often seen in MEC (Case 3)

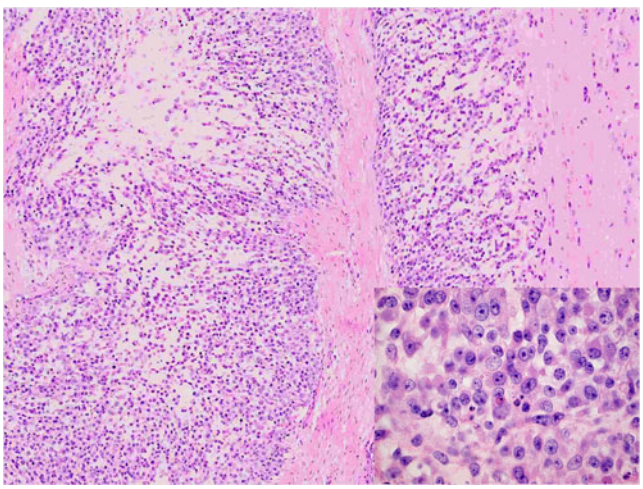

Fig. 1 This case of MEC showed a reticular and cord-like pattern of epithelioid cells set in a prominent myxoid matrix (Case 5)

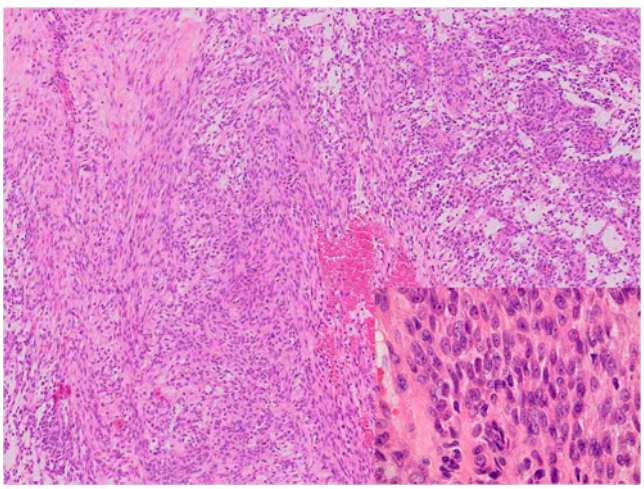

Fig. 3 Monomorphic epithelioid and spindle-shaped cells in a cellular EMC (Case 11)

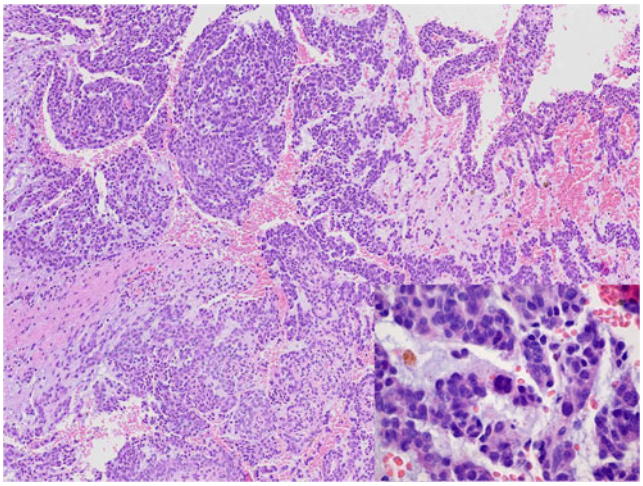

Fig. 4 Solid and reticular arrangement of slightly polymorphic epithelioid cells in a cellular EMC

EMA. Two of eight cases showed nuclear immunoreactivity for p63 (25 %). Alpha-smooth muscle actin (ASMA) was detected in six of eight (75 %) and calponin in four of six cases (67 %). A focal expression of S100 was seen in five of ten cases (50 %). Glial fibrillary acidic protein (GFAP), in four cases performed, was negative in all four. In cEMCs, S100 and EMA were each expressed in two of five cases (40 %). One of the mentioned S100-positive cases (Case 11) showed a broader pattern of marker expression with additional immunoreactivity for (Fig. 5) p63 and focally for ASMA and GFAP. Pan-cytokeratin was negative in all neoplasms (Table 3).

FISH and RT-PCR analysis

In three of nine (33 %) MECs, a *EWSR1* rearrangement was observed by FISH. One case failed for analysis due to poor hybridisation. No tumour showed a *NR4A3* rearrangement. Aberrations of chromosome 9 were seen in two instances. One of them harboured a polysomy and one a heterozygous deletion. All EMCs successfully tested (four of five) exhibited a *NR4A3* rearrangement (Fig. 6). One case failed for reverse transcription polymerase chain reaction (RT-PCR) and *NR4A3*-FISH. Three cases showed a *EWSR1* rearrangement by FISH. In one of them, a fusion of *TAF15-NR4A3* was additionally detected by RT-PCR. In Case 15, *NR4A3* was rearranged (by FISH) but a fusion with *EWSR1* or *TAF15* was not found (RT-PCR). *EWSR1-NR4A3* was evident in one neoplasm (Table 4).

Discussion

The first myoepithelial tumour of the soft tissue was published by Stout and Gorman in 1959 in a series of cutaneous lesions [30]. In the largest series to date, moderate to severe atypia

Table 3 Immunohistochemistry

Case	Pan-CK	EMA	p63	ASMA	S100	GFAP	Calponin
MEC							
1	–	+	–	f +	–	nd	+
2	+	nd	–	f +	f +	–	f +
3	f +	nd	–	f +	–	nd	f +
4	–	+	–	f +	–	–	nd
5	f +	–	nd	f+	–	nd	nd
6	+	nd	+	+	–	nd	nd
7	+	+	–	–	f +	–	–
8	+	–	nd	nd	+	–	+
9	+	–	–	–	f+	nd	–
10	+	+	+	nd	f+	nd	nd
	8/10	4/7	2/8	6/8	5/10	0/4	4/6
	80 %	57 %	25 %	75 %	50 %	0 %	67 %
EMC							
11	–	–	+	f +	f +	f+	nd
12	–	–	–	–	f +	–	nd
13	–	f+	nd	–	–	–	nd
14	–	–	–	–	–	–	nd
15	–	f +	–	–	–	–	nd
	0/5	2/5	1/4	1/5	2/5	1/5	
	0 %	40 %	25 %	20 %	40 %	20 %	

f focally, *nd* not done

(vesicular or coarse chromatin, prominent, often large nucleoli or nuclear pleomorphism) was determined as indicating malignancy [2]. The wide morphological and immunohistochemical diversity, presumably a result of the plasticity of myoepithelial cells, is the cause of the many differential diagnoses, which include most importantly the cellular variant of extraskeletal myxoid chondrosarcoma, furthermore atypical/malignant ossifying fibromyxoid tumour, undifferentiated carcinoma,

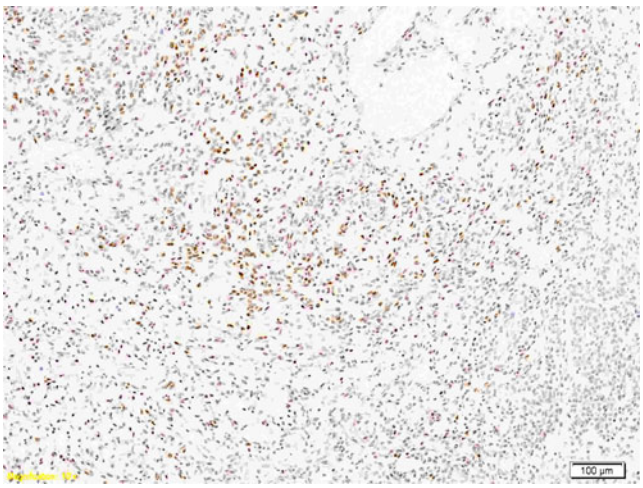

Fig. 5 p63 was positive in one of the cellular EMC cases (Case 11)

Table 4 Molecular analyses (FISH*, RT-PCR)

Case	*EWSR1**	*NR4A3*/cep 9*	TAF15-NR4A3	EWSR1-NR4A3
MEC				
1	+	−		
2	+	Heterozygote deletion chr. 9		
3	−	−		
4	−	−		
5	−	nd	−	−
6	+	−		
7	−	−		
8	−	Polysomy chr. 9		
9	−	−		
10	×	×		
EMC				
11	+	nd	+	−
12	nd	nd	−	+
13	+	+	×	×
14	+	×	×	×
15	nd	+	−	−

"+" rearrangement, "−" no rearrangement, "×" analysis failed, *nd* not done

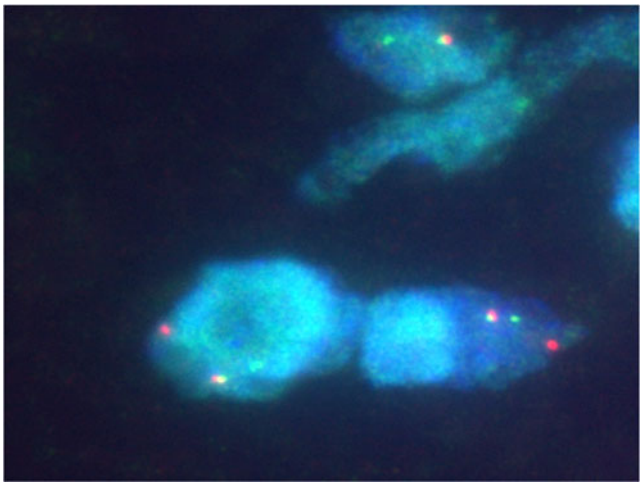

Fig. 6 *NR4A3* rearrangement by FISH showing break-apart signal. This was observed in all EMC cases successfully tested

epithelioid MPNST and proximal type epithelioid sarcoma. In cases with round cell morphology, Ewing sarcoma, myxoid/round cell liposarcoma and poorly differentiated synovial sarcoma are to be considered, at least in small samples [2–4].

The occurrence of myoepithelial tumors at different sites possibly reflects an aberrant gene expression pattern during oncogenesis rather than an origin from a specific cell lineage [3]. This is supported by the evidence of *EWSR1* rearrangement in a subset of benign and malignant myoepithelial tumours of skin, soft tissue, bone and visceral locations (lung) [25, 31]. The hitherto identified fusion genes are *POU5F1*, *PBX1* and *ZNF444* [23–25]. Other more heterogenous genetic changes are also identified including recurrent aberrations of chromosome 9 [27, 32–34]. Recently, a *pleomorphic adenoma gene 1* (*PLAG1*) rearrangement was discovered in a subset of benign mixed tumours of skin and soft tissues (with well-formed ducts). It seems that this genetic abnormality excludes *EWSR1* rearrangement [35]. Whether malignant myoepithelial/mixed tumours possess similar features remains unresolved as yet.

When Enzinger designated extraskeletal myxoid chondrosarcoma as a distinct entity he already mentioned a resemblance with salivary gland type, mixed tumours of deep fascial region of thigh with reference to the report by Dutra in 1960 [5, 36]. Classical cases of EMC have a typical histomorphology with uniform small round to spindle-shaped cells with deeply eosinophilic cytoplasm. The cells are arranged in a delicate network set in a copious myxoid stroma. Cellular variants, representing approximately one third of the cases, show greater morphologic heterogeneity, often resembling myoepithelial tumours [2, 4, 5, 8, 10, 11, 25, 33, 37, 38].

Both tumour types share features such as lobular/multinodular architecture, variable amounts of myxoid stroma and a reticular growth pattern. The stromal component in cellular areas can be poor or even absent. The cells are variably epithelioid, round and spindle shaped. Rhabdoid cytology may also be present in both. Unlike myoepithelial carcinomas, moderate to severe nuclear atypia is much less common in cEMC and can therefore be a helpful discriminating sign. This was also a finding in our series. Ductular structures and metaplastic cartilage or bone, present in not more than 20 % of soft tissue myoepithelial tumours, are not a feature of EMC [2–8, 10, 38–41]. None of our MECs demonstrated one of these characteristics.

Immunohistochemically, soft tissue myoepithelial tumours usually show expression of keratins (90–95 %), EMA (60 %), S100 (85 %), GFAP (50 %), calponin (90 %), SMA (40 %) and p63 (40 %) [4, 42]. In contrast, EMCs are often focally, positive for S100. GFAP, EMA, ASMA and keratins are expressed in a minority of cases, mostly with a focal staining pattern [2, 4, 6–8, 10, 12, 33, 38–41]. In our series, pankeratin was the most distinctive marker expressed in 80 % of MECs but in none of the EMCs. Although our series is small, this result mirrors those by others [8]. p63, labelling myoepithelial cells at different sites, is positive in circa 40 % of MECs and can be exceptionally positive in EMCs as we found in one of our cases [42].

Loss of *SMARCB1/INI1* is also an overlapping feature of the described entities and has been demonstrated in a subset of cases. Whereas underlying genetic alterations (homozygous deletion and frameshift mutation) have been detected in some EMCs, genetic aberrations have not been investigated in

myoepithelial carcinomas as yet [3, 39]. Interestingly, the SMARCB1/INI1-negative EMC cases lack a typical major fusion gene transcript [39]. This raises the question whether these cases are more related to myoepithelial tumours. EMCs are defined by specific reciprocal translocations, involving the pathognomonic *NR4A3.* The described fusion partners are, in decreasing frequency, *EWSR1, TAF15, TCF12* and *TGF* [17–22].

By RT-PCR or FISH analysis, *NR4A3* rearrangement was found in all of our successfully tested EMCs. In one case, we detected besides a *TAF15-NR4A3* fusion an additional *EWSR1* rearrangement which is in line with another reported more complex rearranged case [43]. Furthermore, 33 % of our myoepithelial carcinomas showed *EWSR1* rearrangement, consistent with the results by Antonescu et al. [25]. We did not find *NR4A3* rearrangement in any of the myoepithelial carcinomas, but as previously reported, changes of chromosome 9 as a recurrent aberration were seen in two of our cases [27, 34].

In summary, myoepithelial carcinoma of soft tissue and cellular extraskeletal myxoid chondrosarcoma share clinical, morphological, immunohistochemical and genetic similarities. The pathognomic rearrangement of *NR4A3* and the general lack of keratin expression identify most cases of cEMC. The seemingly poorer outcome especially in young patients with myoepithelial carcinomas and possible different treatment options make discrimination between these different entities necessary.

Acknowledgements The authors thank the following pathologists for kindly providing case material and clinical follow-up when available: Dr. van der Linden, Dr. Nooijen, ‘s Hertogenbosch (Cases 5 and 11), Dr. Theunissen, Heerlen (Case 13); Dr. Blomjous, Tilburg, The Netherlands (Case 12); Dr. Karhoff, Limburg (Case 1), Dr. Neumann, Marburg (Case 2), Dr. Wellens, Spaichingen (Case 3), Dr. Knolle, Dr. Grafik, Dessau (Case 4) and Prof. Dr. Holzhausen, Halle, Germany (Case 14). We are also grateful to Dr. Fletcher, Boston, MA for confirming the diagnoses in six of our cases.

Conflict of interest statement We declare that we have no conflict of interest.

Open Access This article is distributed under the terms of the Creative Commons Attribution License which permits any use, distribution, and reproduction in any medium, provided the original author(s) and the source are credited.

References

1. Kilpatrick SE, Hitchcock MG, Kraus MD, Calonje E, Fletcher CDM (1997) Mixed tumors and myoepitheliomas of soft tissue: a clinicopathologic study of 19 cases with a unifying concept. Am J Surg Pathol 21:13–22
2. Hornick JL, Fletcher CDM (2003) Myoepithelial tumors of soft tissue. A clinicopathologic and immunohistochemical study of 101 cases with evaluation of prognostic parameters. Am J Surg Pathol 27:1183–1196
3. Gleason BC, Fletcher CDM (2007) Myoepithelial carcinoma of soft tissue in children: an aggressive neoplasm analysed in a series of 29 cases. Am J Surg Pathol 31:1813–1824
4. Gleason BC, Hornick JL (2008) Myoepithelial tumours of skin and soft tissue: an update. Diagn Histopathol 14:552–562
5. Enzinger FM, Shiraki M (1972) Extraskeletal myxoid chondrosarcoma. An analysis of 34 cases. Hum Pathol 3:421–435
6. Antonescu CR, Argani P, Erlandson RA, Healey JH, Ladanyi M, Huvos AG (1998) Skeletal and extraskeletal myxoid chondrosarcoma: a comparative clinicopathologic, ultrastructural, and molecular study. Cancer 83:1504–1521
7. Lucas DR, Fletcher CDM, Adsay NV, Zalupski MM (1999) High grade extraskeletal myxoid chondrosarcoma: a high-grade epithelioid malignancy. Histopathology 35:201–208
8. Meis-Kindblom JM, Bergh P, Gunterberg B, Kindblom LG (1999) Extraskeletal myxoid chondrosarcoma: a reappraisal of its morphologic spectrum and prognostic factors based on 117 cases. Am J Surg Pathol 23:636–650
9. Oliveira AM, Sebo TJ, McGrory JE, Gaffey TA, Rock MG, Nascimento AG (2000) Extraskeletal myxoid chondrosarcoma: a clinicopathologic, immunohistocheicl, and ploidy analysis of 23 cases. Mod Pathol 13:900–908
10. Okamoto S, Hisaoka M, Ishida T, Imamura T, Kanda H, Shimajiri S, Hashimoto H (2001) Extraskeletal myxoid chondrosarcoma: a clinicopathologic, immunohistochemical, and molecular analysis of 18 cases. Hum Pathol 32:1116–1124
11. Noguchi H, Mitsuhashi T, Seki K, Tochigi N, Tsuji M, Shimoda T, Hasegawa T (2010) Fluorescence in situ hybridization analysis of extraskeletal myxoid chondrosarcomas using EWSR1 and NR4A3 probes. Hum Pathol 41:336–342
12. Hisaoka M, Hashimoto H (2005) Extraskeletal myxoid chondrosarcoma: updated clinicopathological and molecular genetic characteristics. Pathol Int 55:453–463
13. Hachitanda Y, Tsuneyoshi M, Daimaru Y, Enjoji M, Nakagawara A, Ikeda K, Sueishi K (1988) Extraskeletal myxoid chondrosarcoma in young children. Cancer 61:2521–2526
14. Saleh G, Evans HL, Ro JY, Ayala AG (1992) Extraskeletal myxoid chondrosarcoma. A clinicopathologic study of ten patients with long-term follow-up. Cancer 70:2827–2830
15. Kawaguchi S, Wada T, Nagoya S, Ikeda T, Isu K, Yamashiro K, Kawai A, Ishii T, Araki N, Myoui A, Matsumoto S, Umeda T, Yoshikawa H, Hasegawa T (2003) Extraskeletal myxoid chondrosarcoma: a multi-institutional study of 42 cases in Japan. Cancer 97:1285–1292
16. Drilon AD, Popat S, Bhuchar G, D’Adamo DR, Keohan ML, Fisher C, Antonescu CR, Singer S, Brennan MF, Judson I, Maki RG (2008) Extraskeletal myxoid chondrosarcoma. A retrospective review from 2 referral centers emphasizing long-term outcomes with surgery and chemotherapy. Cancer 113:3364–3371
17. Sciot R, Dal Cin P, Fletcher C, Samson I, Smith M, de Vos R, Van Damme B, Van den Berghe H (1995) t(9;22) (q22-31;q11-12) is a consistent marker of extraskeletal myxoid chondrosarcoma: evaluation of three cases. Mod Pathol 8:765–768
18. Bjerkehagen B, Dietrich C, Reed W, Micci F, Saeter G, Berner A, Nesland JM, Heim S (1999) Extraskeletal myxoid chondrosarcoma: multimodal diagnosis and identification of a new cytogenetic subgroup characterized by t(9;17)(q22;q11). Virchows Arch 435:524–530
19. Sjögren H, Meis-Kindblom J, Kindblom LG, Aman P, Stenman G (1999) Fusion of the *EWS*-related gene *TAF2N* to *TEC* in extraskeletal myxoid chondrosarcoma. Cancer Res 59:5064–5067
20. Sjögren H, Wedell B, Meis-Kindblom JM, Kindblom LG, Stenman G (2000) Fusion of the NH2-terminal domain of the basic helix-loop-helix protein TCF12 to TEC in extraskeletal myxoid chondrosarcoma with translocation t(9;15)(q22;q21). Cancer Res 60:6832–6835

21. Panagopoulos I, Mertens F, Isaksson M, Domanski HA, Brosjö O, Heim S, Bjerkehagen B, Sciot R, Dal Cin P, Fletcher JA, Fletcher CD, Mandahl N (2002) Molecular genetic characterization of the *EWS/CHN* and *RBP56/CHN* fusion genes in extraskeletal myxoid chondrosarcoma. Genes Chromosom Cancer 35:340–352
22. Hisaoka M, Ishida T, Imamura T, Hashimoto H (2004) TFG is a novel fusion partner of NOR1 in extraskeletal myxoid chondrosarcoma. Genes Chromosom Cancer 40:325–328
23. Brandal P, Panagopoulos I, Bjerkehagen B, Gorunova L, Skjeldal S, Micci F, Heim S (2008) Detection of a t(1;22)(q23;q12) translocation leading to an EWSR1-PBX1 fusion gene in a myoepithelioma. Genes Chromosom Cancer 47:558–564
24. Brandal P, Panagopoulos I, Bjerkehagen B, Heim S (2009) t(19;22)(q13;12) Translocation leading to the novel fusion gene EWSR1-ZNF444 in soft tissue myoepithelial carcinoma. Genes Chromosom Cancer 48:1051–1056
25. Antonescu CR, Zhang L, Chang NE, Pawel BR, Travis W, Katabi N, Edelman M, Rosenberg AE, Nielsen GP, Dal Cin P, Fletcher CDM (2010) *EWSR1-POU5F1* fusion in soft tissue myoepithelial tumors. A molecular analysis of sixty-six cases, including soft tissue, bone and visceral lesions showing common involvement of EWSR1 gene rearrangement. Genes Chromosom Cancer 49:1114–1124
26. Fletcher CDM, Unni K, Mertens F (eds) World Health Organization Classification of Tumours. Pathology and genetics of tumours of soft tissue and bone. IARC Press, Lyon, pp 198–199, 213–215
27. van den Berg E, Zorgdrager H, Hoekstra HJ, Suurmeijer AJH (2004) Cytogenetics of a soft tissue malignant myoepithelioma. Cancer Genet Cytogenet 151:87–89
28. Bell E, Van der Biezen JJ, Werker PM (2009) Parachordoma: a very rare tumor of the hand. J Hand Surg Eur 34:814–816
29. Hantschke M, Mentzel T, Rütten A, Palmedo G, Calonje E, Lazar AJ, Kutzner H (2010) Cutaneous clear cell sarcoma: a clinicopathologic, immunohistochemical, and molecular analysis of 12 cases emphasizing its distinction from dermal melanoma. Am J Surg Pathol 34:216–220
30. Stout AP, Gorman JG (1959) Mixed tumors of the skin of the salivary gland type. Cancer 12:537–543
31. Flucke U, Palmedo G, Blankenhorn N, Slootweg PJ, Kutzner H, Mentzel T (2011) *EWSR1* gene rearrangement occurs in a subset of cutaneous myoepithelial tumors: a study of 18 cases. Mod Pathol 11:1444–1450. doi:10.1038/modpathol.2011.108
32. Pauwels P, Dal Cin P, Roumen R, van den Berghe H, Sciot R (1999) Intramuscular mixed tumour with clonal chromosomal changes. Virchows Arch 434:167–171
33. Folpe AL, Agoff SN, Willis J, Weiss SW (1999) Parachordoma is immunohistochemically and cytogenetically distinct from axial chordoma and extraskeletal myxoid chondrosarcoma. Am J Surg Pathol 23:1059–1067
34. Hallor KH, Teixeira MR, Fletcher CDM, Bizarro S, Staaf J, Domanski HA, Vult von Steyern F, Panagopoulos I, Mandahl N, Mertens F (2008) Heterogeneous genetic profiles in soft tissue myoepitheliomas. Mod Pathol 21:1311–1319
35. Bahrami A, Dalton JD, Krane JF, Fletcher CDM (2011) A subset of cutaneous and soft tissue mixed tumors are genetically linked to their salivary gland counterpart. Genes Chromosom Cancer. doi:10.1002/gcc.20938
36. Dutra FR (1960) Mixed tumor, salivary gland type, of deep fascial region of thigh. Arch Path 70:562–564
37. Fletcher CDM (2007) Soft tissue tumors. In: Fletcher CDM (ed) Diagnostic histopathology of tumors, 3rd edn. Churchill Livingstone, Philadelphia, pp 1573–1574
38. Dei Tos AP, Wadden C, Fletcher CDM (1997) Extraskeletal myxoid chondrosarcoma: an immunohistochemical reappraisal of 39 cases. Appl Immunohistochem 5:73–77
39. Kohashi K, Oda Y, Yamamoto H, Tamiya S, Oshiro Y, Izumi T, Taguchi T, Tsuneyoshi M (2008) SMARCB1/INI1 protein expression in round cell soft tissue sarcomas associated with chromosomal translocation involving EWS: a special reference to SMARCB1/INI1 negative variant extraskeletal myxoid chondrosarcoma. Am J Surg Pathol 32:1168–1174
40. Oshiro Y, Shiratsuchi H, Tamiya S, Oda Y, Toyoshima S, Tsuneyoshi M (2000) Extraskeletal myxoid chondrosarcoma with rhabdoid features, with special reference to its aggressive behavior. Int J Surg Pathol 8:145–152
41. Abramovici LC, Steiner GC, Bonar F (1995) Myxoid chondrosarcoma of soft tissue and bone: a retrospective study of 11 cases. Hum Pathol 26:1215–1220
42. Jo VY, Fletcher CDM (2011) p63 immunohistochemical staining is limited in soft tissue tumors. Am J Clin Pathol 236:762–766
43. Turc-Carel C, Dal Cin P, Rao U, Karakousis C, Sandberg AA (1988) Recurrent breakpoints at 9q31 and 22q12.2 in extraskeletal myxoid chondrsarcoma. Cancer Genet Cytogenet 30:145–150

Virchows Arch (2012) 460:629–636
DOI 10.1007/s00428-012-1236-9

ORIGINAL ARTICLE

Intratumoral hemorrhage, vessel density, and the inflammatory reaction contribute to volume increase of sporadic vestibular schwannomas

Maurits de Vries · Pancras C. W. Hogendoorn · Inge Briaire-de Bruyn · Martijn J. A. Malessy · Andel G. L. van der Mey

Received: 27 January 2012 / Revised: 6 March 2012 / Accepted: 2 April 2012 / Published online: 4 May 2012
© The Author(s) 2012. This article is published with open access at Springerlink.com

Abstract Vestibular schwannomas show a large variation in growth rate, making prediction and anticipation of tumor growth difficult. More accurate prediction of clinical behavior requires better understanding of tumor biological factors influencing tumor progression. Biological processes like intratumoral hemorrhage, cell proliferation, microvessel density, and inflammation were analyzed in order to determine their role in vestibular schwannoma development. Tumor specimens of 67 patients surgically treated for a histologically proven unilateral vestibular schwannoma were studied. Preoperative magnetic resonance imaging (MRI) scans were used to determine tumor size and to classify tumors as homogeneous, inhomogeneous, and cystic. Immunohistochemical studies evaluated cell proliferation (histone H3 and Ki-67), microvessel density (CD31), and inflammation (CD45 and CD68). Intratumoral hemorrhage was assessed by hemosiderin deposition. The expression patterns of these markers were compared with tumor size, tumor growth index, MRI appearance, patients' age, and duration of symptoms. No relation between cell proliferation and clinical signs of tumor volume increase or MRI appearance was found. Intratumoral hemosiderin, microvessel density, and inflammation were significantly positively correlated with tumor size and the tumor growth index. Cystic and inhomogeneous tumors showed significantly more hemosiderin deposition than homogeneous tumors. The microvessel density was significantly higher in tumors with a high number of CD68-positive cells. The volume increase of vestibular schwannomas is not based on cell proliferation alone. Factors like intratumoral bleeding, (neo)vascularization, and intensity of the inflammatory reaction also influence tumor volume.

Keywords Vestibular schwannoma · Neuropathology · Tumor biology

Introduction

Vestibular schwannomas (acoustic neuromas) are benign tumors originating from the myelin-forming Schwann cells of the vestibular branch of the eighth cranial nerve in the internal auditory canal or cerebellopontine angle. Clinically, these tumors grow slowly and progressively, eventually causing brainstem compression.

One of the problems in the treatment of these tumors is the large variation in the evolution of increase in volume in time. Why this is so variable remains largely unknown, but clinically, this makes prediction and anticipation of the evolution of symptoms difficult. Current therapeutic management is mainly based on symptoms and radiological assessment. Unfortunately, these indicators do not always correlate with actual tumor volume increase. More accurate prediction of tumor expansion rate could lead to more

Electronic supplementary material The online version of this article (doi:10.1007/s00428-012-1236-9) contains supplementary material, which is available to authorized users.

P. C. W. Hogendoorn (✉) · I. Briaire-de Bruyn
Department of Pathology, Leiden University Medical Center, P.O. Box 9600, 2300 RC Leiden, The Netherlands
e-mail: p.c.w.hogendoorn@lumc.nl

M. J. A. Malessy
Department of Neurosurgery, Leiden University Medical Center, P.O. Box 9600, 2300 RC Leiden, The Netherlands

M. de Vries · A. G. L. van der Mey
Department of Otolaryngology, Leiden University Medical Center, P.O. Box 9600, 2300 RC Leiden, The Netherlands

balanced decision-making regarding therapeutic actions when a vestibular schwannoma is diagnosed.

Accurate assessment of potential tumor volume increase requires better understanding of tumor biological (growth) factors and concurrent pathological events like cyst formation. To gain more insight in the role of these factors, we assessed the relationships between (immuno)histopathological markers, radiological observations on tumor appearance, and clinical growth of vestibular schwannomas.

One way for tumors to expand is by cell proliferation. A well-known proliferation marker is the Ki-67 antigen [1, 2], which is present during all phases of the cell cycle but is absent in noncycling cells. A less known indicator for proliferation is the phosphorylated histone H3 protein, which is expressed during mitosis [3–5]. Both these markers were included in this study.

In addition to proliferation, we investigated to what extent intratumoral hemorrhage, microvessel density, and the degree of inflammation are involved in tumor expansion. To quantify intratumoral hemorrhage, hemosiderin (i.e., iron) deposition was evaluated. The endothelial marker CD31 was used to measure microvessel density, and the degree of inflammation was determined by quantifying the number of leukocytes and macrophages through the expression of the markers CD45 and CD68, respectively.

Material and methods

Patients

From the vestibular schwannoma database at the Leiden University Medical Center, a total of 67 patients (26 males and 41 females) were identified. They involved a group of patients surgically treated for a histologically proven vestibular schwannoma from January 2000 to November 2005. The main criteria for surgical treatment were clinical symptoms (e.g., progressive or debilitating vertigo and hearing loss) and tumor size, both initial as well as in terms of progression over time. Patients' personal preference was also of great importance in deciding if and when to apply treatment. Only cases of unilateral sporadic schwannomas were selected, patients diagnosed with NF2 were excluded.

Tumor measurement

Information on radiological data was obtained from radiology records which are all composed according to specific clinical and scientific incentives. These standardized reports include measurement of the greatest tumor diameter according to the guidelines of the American Academy of Otolaryngology Head and Neck Surgery [6]. Additionally, the reports comprise evaluation of tumor density based on gadolinium-enhanced T1-weighted as well as T2-weighted scans. Depending on the presence of microcystic and or macrocystic components, tumors were classified as homogeneous, inhomogeneous, or cystic. All patient data were prospectively discussed at a multidisciplinary conference attended by representatives of the neurosurgery, radiology, radiotherapy, pathology, and otolaryngology department. Clinical and radiological data were cross checked before being entered in the vestibular schwannoma database (for the exact patient characteristics, including figures illustrating cystic, inhomogeneous, and homogeneous tumors, see Electronic supplementary material Figs. 1, 2, and 3).

Immunohistochemistry

The immunohistochemical tests were conducted at the Department of Pathology of the Leiden University Medical Center. The tests were conducted on specimens preserved in formalin and stored in paraffin. All assessments were performed on tissue sections obtained from one single tumor block per tumor sample. Immunohistochemical reactions were performed according to standard laboratory methods [7]. In brief, heat-induced antigen retrieval was performed using microwave treatment of all sections after dewaxing and rehydration, followed by blocking of endogenous peroxidase with 3 % H_2O_2 in methanol. Incubation with primary antibodies was overnight (for sources, working dilutions, and positive controls used, see Table 1). Subsequently, sections were incubated with poly-HRP-antimouse/rabbit/rat conjugate. Visualization was carried out with a H_2O_2–diaminobenzidine solution. All washing procedures were performed in phosphate-buffered saline. Slides were counterstained with hematoxylin. In addition to the immunohistochemical stains, hemosiderin staining was performed.

Microscopic analysis

In order to obtain an overall impression of the staining pattern of each marker, all sections were first evaluated using a × 10 objective lens. Hemosiderin, CD45, and CD68 displayed an irregular/patchy staining pattern, making

Table 1 Antibody concentrations and positive control tissues used

Antibody	Supplier	Concentration	Positive control
Ki-67	DAKO	1:800	Tonsil
Histone H3	Comproscientific	1:3,200	Tonsil
CD31	DAKO	1:150	Tonsil
CD45	DAKO	1:4,000	Tonsil
CD68	DAKO	1:20,000	Tonsil

computer-assisted analysis less reliable. For this reason, further analysis of these markers was performed manually in a semiquantitative score. Per specimen, 10 randomly chosen fields of view (FOV) were evaluated at a × 40 objective lens. Scoring was independently assessed by two authors. The degree of staining was scored as follows: 0, absent; 1, mild; and 2, strong.

Staining for Ki67 and histone H3 showed a more homogeneous distribution, permitting the application of a computer-based image analysis method in order to determine the index of proliferation. In brief, of each specimen, five randomly chosen digital snapshots were taken. Positively stained nuclei were identified through spectrometry using a Leica DM4000B microscope fitted with a CRI Nuance spectral analyzer (Cambridge Research and Instrumentation, Inc., Woburn, MA, USA). Using Mirax software (Zeiss, Germany) and ImageJ (National Institutes of Health, Bethesda, MD, USA), the number of pixels representing positively stained nuclei was determined, as well as the number of pixels representing the total nuclear area in one FOV. The index of proliferation was calculated by dividing the number of immunopositive pixels by the number of pixels representing the total nuclear area. The mean value of the five snapshots was used for statistical analysis.

Microvessel density was determined with the Chalkley point overlap morphometric technique, which allows for rapid analysis with a relatively low interobserver variability [8]. This method has been described in detail [9, 10]. In brief, CD31 stained sections were scanned for hot spots of high vascular density. Using an ocular grid with 25 random points, microvessel density was scored in these hot spots with a × 20 objective lens. The grid was oriented to permit the maximum number of points to hit the stained microvessels (Fig. 1). The Chalkley count was the mean of the maximum number of points hitting a microvessel in three hot spots per tumor specimen.

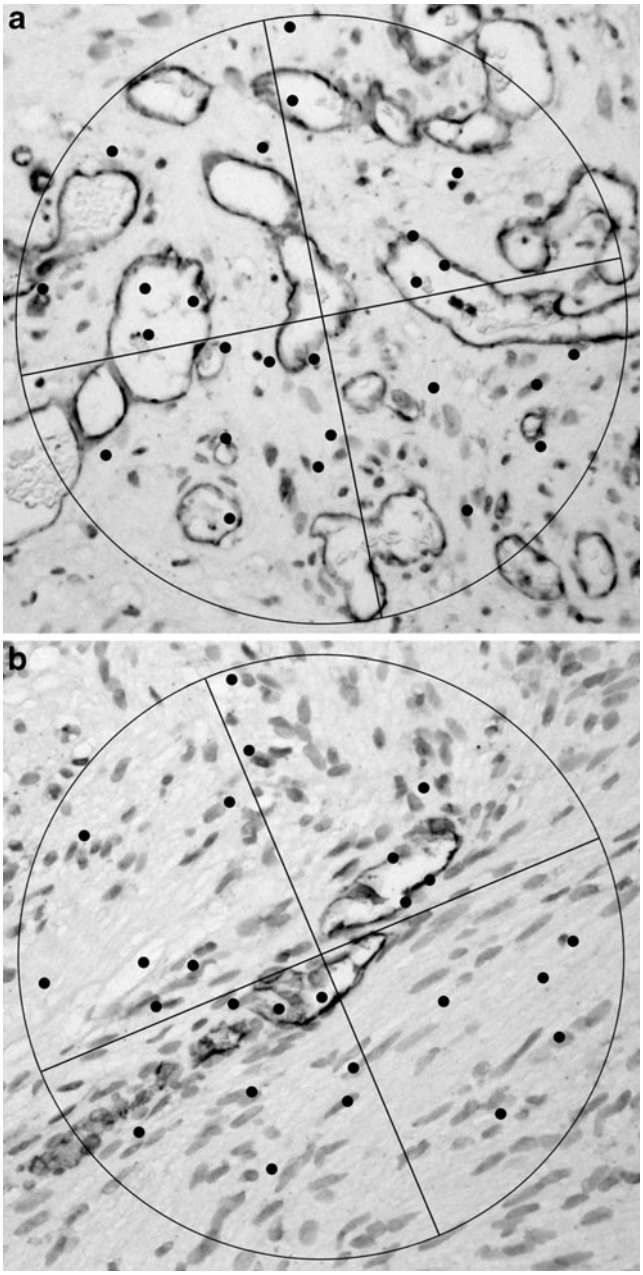

Fig. 1 Examples of Chalkley counts in vascular hotspots, specimen **a** and **b** score 10 and 6, respectively (original magnification×200)

Tumor growth index

Accurate measurement of tumor growth depends on serial magnetic resonance imaging (MRI) scanning over a longer period of time. Because only six patients in our selection underwent serial MRI scanning prior to surgery, this method of growth assessment could not be used in our study. We used the tumor growth index as a surrogate parameter. This index has been described earlier regarding vestibular schwannoma growth [11, 12]. Its basic assumption is that the age of onset of the tumor varies randomly. The tumor growth index is calculated by dividing the maximal tumor diameter by the age of the patient.

Statistical analysis

For evaluation of the relationships between the tumor biological markers and parameters of clinical growth, the Spearman rank correlation test was used. The difference in hemosiderin deposition between cystic and inhomogeneous tumors versus homogeneous tumors was determined by the chi-square test. Tumor size of cystic and inhomogeneous tumors versus homogeneous tumors was compared with the unpaired t test. The relation between microvessel density and CD68 expression was evaluated using the one-way

analysis of variance (ANOVA) and Scheffe test. For all statistical tests, $p<0.05$ was considered as significant. All calculations were performed using SPSS Inc. software, version 17.0.

Results

A total of 67 patients (age: range, 15–72 years; mean, 49.04± 14.06 years) was studied. Maximum tumor diameter varied between 5 and 50 mm (mean, 24.03±11.52 mm) and the tumor growth index (which does not represent actual increase in size but a parameter for tumor growth rate) varied between 0.07 and 2.11 mm/year (mean, 0.56±0.40 mm/year).

The mean value of the Ki-67 index in this studied group was 0.6 % (range, 0.1–1.8 %). For the histone H3 index, the mean value was 3.9 % (range, 0.4–15.5 %). No significant correlation was found between the Ki-67 or histone H3 index and maximal tumor diameter, tumor growth index, and radiologically measured tumor growth.

The number and distribution of hemosiderin-, CD45-, and CD68-positive cells in the tissue sections were very heterogeneous. Some specimens showed no staining at all, yet other specimens showed a substantial number of positive cells (Fig. 2). The mean Chalkley count was 9.59 (range, 3.3–23.0; SD, 3.70). The Spearman rank correlation test demonstrated several significant positive correlations between these markers (Table 2, for the corresponding scattergrams, see Electronic supplementary material Figs. 4, 5, and 6).

The number of hemosiderin-positive cells correlated with tumor size ($p<0.001$; $r=0.39$) and tumor growth index ($p<0.006$; $r=0.33$). CD45 expression correlated with tumor size ($p<0.006$; $r=0.33$) and tumor growth index ($p<0.002$; $r=0.38$), and CD68 expression also correlated with tumor size ($p<0.0001$; $r=0.46$) and tumor growth index ($p<0.0001$, $r=0.48$).

The Chalkley count demonstrated a positive correlation with tumor size ($p<0.001$; $r=0.40$) and tumor growth index ($p<0{,}002$; $r=0.37$). Furthermore, the Chalkley count showed a significant correlation with the number of hemosiderin-positive cells ($p<0.003$; $r=0.36$), CD45-positive cells ($p<0.021$ $r=0.28$), and CD68-positive cells ($p<0.0001$; $r=0.47$). A one-way ANOVA and a Scheffe test confirmed the positive relation between the number of CD68-positive cells and microvessel density. Tumors with a high number of CD68-positive cells displayed a significantly higher microvascular density than tumors with low or no CD68-positive cells (Fig. 3).

In 61 patients, the tumors were morphologically classified based on their MRI appearance. Twenty-four tumors were classified as homogeneous, 8 as inhomogeneous, and 29 as cystic. Cystic and inhomogeneous tumors were significantly larger than homogeneous tumors (Table 3). Cystic and inhomogeneous tumors also displayed a significantly higher number of hemosiderin-positive cells than homogeneous tumors (Table 3).

No statistically significant correlations or differences were observed when patient age or duration of symptoms was taken into account.

Discussion

To gain more insight into the mechanisms responsible for volume increase of vestibular schwannomas, possible correlations between histopathological markers and radiological and clinical characteristics of vestibular schwannomas were investigated. For studying the growth rate of a tumor, serial radiological observation is the preferred method. As most patients in this study were operated on shortly after diagnosis, in the majority of cases, only one preoperative MRI scan was obtained, which excluded this approach. As a surrogate, we used the growth index, which is only a rough estimate of the rate of tumor volume increase but allowed us to include a larger number of patients in the study.

To evaluate the role of proliferative activity in the volume increase of vestibular schwannomas, the cell cycle markers Ki-67 and histone H3 were used. Ki-67 as a parameter of growth of vestibular schwannomas has been studied by Niemczyk et al. [2], who compared clinically stable vestibular schwannomas with clinically growing cases. They found a significant difference in Ki-67 labeling index between the two groups. The mean labeling index in the growing tumors was 3.17 % compared to 1.11 % in the stable tumors. Overall, the Ki-67 index ranged from 0.22 to 5 %, with an average of 1.86 %. Gomez et al. [13] also investigated cell proliferation in vestibular schwannomas, but did not find a significant correlation between tumor growth and Ki-67 labeling index, which ranged from 0.2 to 2.2 %. We conclude that the labeling index of Ki-67 in our study (ranging from 0.1 to 1.8 %, with a mean of 0.6 %) is comparable with earlier published data.

Histone H3 as a proliferation marker has not been studied in vestibular schwannomas before. We did not find a correlation between the histone H3 labeling index and the tumor growth index. Taken together, our data and those from the literature indicate that cell proliferation is not a decisive factor in the expansion of vestibular schwannomas.

Degenerative changes such as cysts may contribute to tumor volume increase. Reports on the incidence of cyst formation in vestibular schwannomas vary between 5.7 and 48 %, with more recent studies indicating incidences of approximately 10 % [14–17]. Cystic tumors can display a relatively rapid increase in volume and generally become larger than noncystic tumors [18]. This also applies to our case series, the cystic and inhomogeneous tumors being

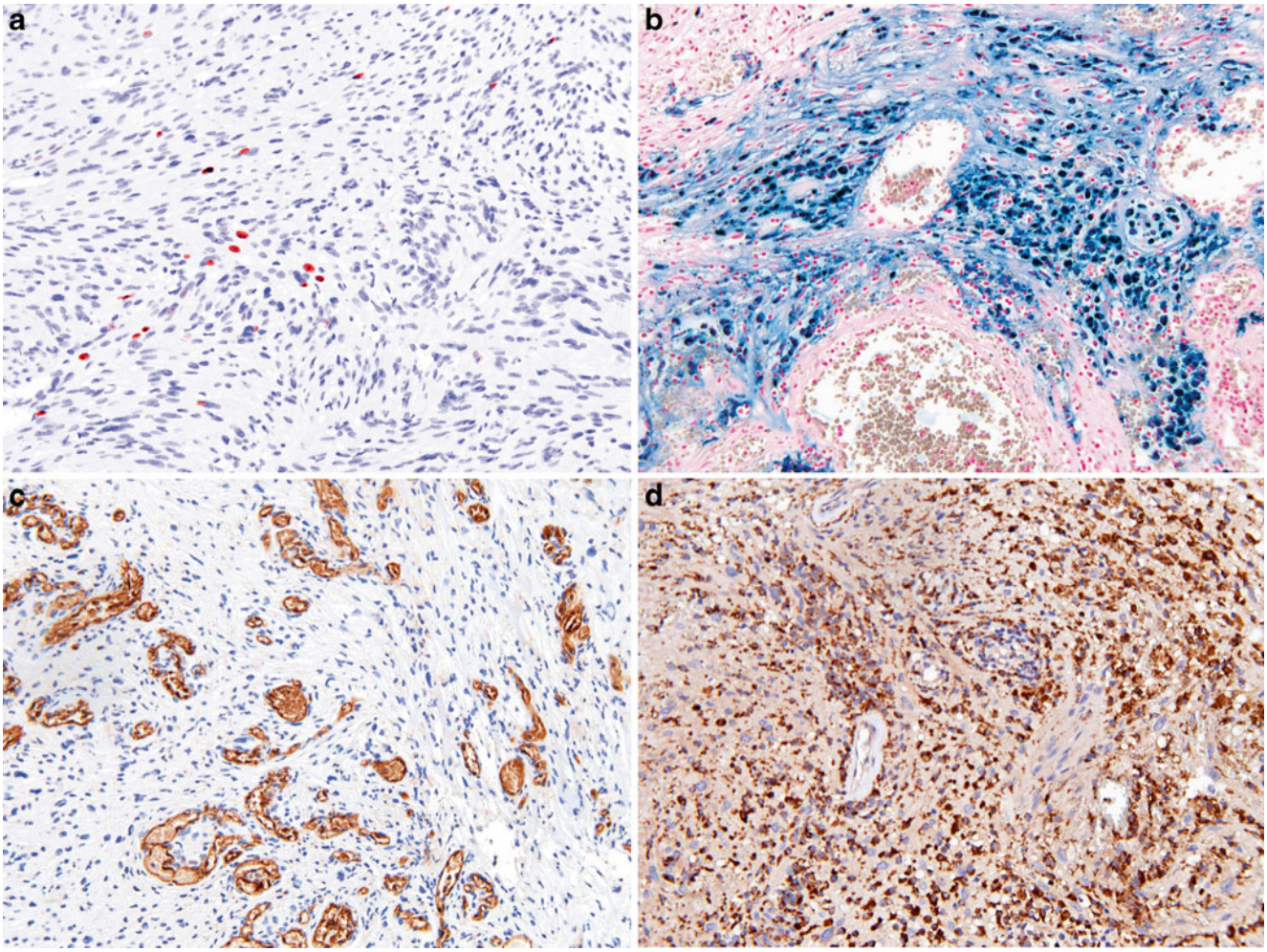

Fig. 2 **a** Proliferating cells (Ki-67/histone H3), **b** intratumoral bleeding (hemosiderin), **c** high microvessel density (CD31), and **d** intratumoral inflammation (CD45/CD68) (original magnification×400)

significantly larger than the homogeneous tumors. The mechanisms responsible for cyst formation in vestibular schwannomas remain unclear. Gomez et al. [13] demonstrated a significant correlation between hemosiderin deposition, tumor size, and tumor heterogeneity and suggested that hemosiderin resorption might induce cyst formation. The same suggestion is made by Park et al. [19]. Our results are in line with these studies. We found significantly more hemosiderin deposition in cystic and inhomogeneous tumors compared to homogeneous tumors. The significant correlations between hemosiderin deposition and tumor size and tumor growth index also support this notion.

These results may offer a clue in the search for markers of tumor volume increase. Both cysts and iron deposition are radiologically demonstrable and might, therefore, constitute clinically applicable markers. A radiological study on pituitary macroadenomas by Stadlbauer et al. [20] described a significant difference in spectral signals measured in hemorrhagic versus nonhemorrhagic tumors. The authors suggested that the paramagnetic effect of hemosiderin deposition in hemorrhagic

Table 2 Spearman's correlation test for pathological markers and clinical characteristics

		Ki-67	Histone H3	CD45	CD68	Siderin[a]	MVD
Size	Correlation coefficient	0.129	0.326	0.333**	0.457**	0.392**	0.397**
	Significance (two-tailed)	0.301	0.120	0.006	0.000	0.001	0.001
TGI	Correlation coefficient	0.091	0.275	0.375**	0.482**	0.330**	0.373**
	Significance (two-tailed)	0.466	0.243	0.002	0.000	0.006	0.002
MVD	Correlation coefficient	0.140	0.240	0.281*	0.472**	0.363**	–
	Significance (two-tailed)	0.261	0.102	0.021	0.000	0.003	–

TGI tumor growth index, *MVD* microvessel density

[a]Hemosiderin

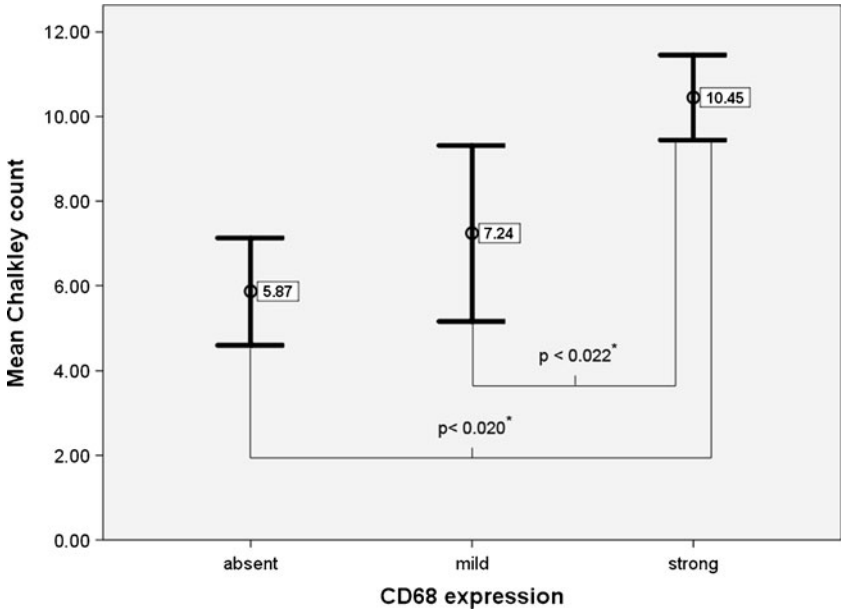

Fig. 3 Relation between CD68 expression and microvessel density. The mean Chalkley count is significantly higher in tumors with strong CD68 expression. *Asterisk* denotes statistical differences calculated with the Scheffe test

tumors on the MR images might provide an explanation. Using this approach to study iron deposition and cyst formation in vestibular schwannomas might establish a causal relationship between intratumoral hemorrhage and cyst formation.

Although vestibular schwannomas are relatively slow-growing neoplasms, they depend for further growth on a functional vascular system, as any other tumor [21]. The positive correlation between microvessel density and tumor size and tumor growth index we found is consistent with other published data [22, 23]. These findings suggest that angiogenesis may be important for the volume increase of vestibular schwannomas. Determining the degree of vascularization of vestibular schwannomas might also be possible using MRI diffusion or perfusion techniques [24–26]. Further research into this hypothesis could lead to another clinically applicable marker of tumor volume increase. These results also suggest that antiangiogenesis therapy might contribute to controlling tumor growth.

The degree of inflammation measured by the expression of CD68 and CD45 showed a positive significant correlation with tumor size and tumor growth index. Similar correlations have not been reported in the literature yet. In a study performed by Brieger el al. [27] on angiogenic growth factors in vestibular schwannomas, tumor-infiltrating CD68-positive lymphocytes were not detected. Labit et al. [28] only found a correlation between the number of CD45-positive cells and the duration of symptoms. The mechanism responsible for or the significance of an inflammatory reaction in vestibular schwannomas has not been elucidated as yet. Studies on breast cancer have addressed the role of the inflammatory microenvironment in tumor progression [29–35]. It has been proposed that inflammation which triggers angiogenesis might contribute to tumor progression. Macrophage activity is a major determinant of the intratumoral inflammatory milieu but other components of the inflammatory infiltrate also seem to modulate tumor behavior [36]. The significant associations between the degree of inflammation (i.e., CD45 and CD68) and tumor size and tumor growth index and, in addition, the significant increase of microvessel density in tumors with a higher number of CD68-positive cells (Fig. 3) suggest that similar processes take place in vestibular schwannomas. Several approaches targeting macrophage activity are currently under investigation [37, 38], making additional research of the inflammatory

Table 3 MRI appearance compared by hemosiderin deposition and size

MRI	Hemosiderin deposition[a]						Size[b]	
	Absent	Mild	Strong	χ^2	*df*	*p* value	Mean ± SD	*p* value
Homogeneous	15	7	2	8.67	2	<0.013	13.46±8.44	<0.0001
Inhomogeneous/cystic	10	15	12				30.46±8.43	

MRI magnetic resonance imaging

[a] Chi-square test

[b] Independent *t* test

process in vestibular schwannomas even more interesting. The first step would be further typing of inflammatory cells present in vestibular schwannomas. Furthermore, their activation state and relationship with angiogenic growth factors should be examined.

The results of this study indicate that tumor volume increase of vestibular schwannomas is not based on cell proliferation alone. Contributing factors are intratumoral hemorrhage, vascularization, and degree of inflammation.

Acknowledgements The authors want to thank Frans Prins and Carlos de Andrea for their assistance on the analysis of our histological data.

Disclosure The authors report no conflict of interest concerning the materials or methods used in this study or the findings specified in this paper.

Open Access This article is distributed under the terms of the Creative Commons Attribution License which permits any use, distribution, and reproduction in any medium, provided the original author(s) and the source are credited.

References

1. Szeremeta W, Monsell EM, Rock JP, Caccamo DV (1995) Proliferation indices of vestibular schwannomas by Ki-67 and proliferating cell nuclear antigen. Am J Otol 16(5):616–619
2. Niemczyk K, Vaneecloo FM, Lecomte MH, Lejeune JP, Lemaitre L, Skarzynski H et al (2000) Correlation between Ki-67 index and some clinical aspects of acoustic neuromas (vestibular schwannomas). Otolaryngol Head Neck Surg 123(6):779–783
3. Davidson EJ, Morris LS, Scott IS, Rushbrook SM, Bird K, Laskey RA et al (2003) Minichromosome maintenance (Mcm) proteins, cyclin B1 and D1, phosphohistone H3 and in situ DNA replication for functional analysis of vulval intraepithelial neoplasia. Br J Cancer 88(2):257–262
4. Brenner RM, Slayden OD, Rodgers WH, Critchley HO, Carroll R, Nie XJ et al (2003) Immunocytochemical assessment of mitotic activity with an antibody to phosphorylated histone H3 in the macaque and human endometrium. Hum Reprod 18(6):1185–1193
5. Takahashi H, Murai Y, Tsuneyama K, Nomoto K, Okada E, Fujita H et al (2006) Overexpression of phosphorylated histone H3 is an indicator of poor prognosis in gastric adenocarcinoma patients. Appl Immunohistochem Mol Morphol 14(3):296–302
6. (1995) Committee on Hearing and Equilibrium guidelines for the evaluation of hearing preservation in acoustic neuroma (vestibular schwannoma). American Academy of Otolaryngology-Head and Neck Surgery Foundation, INC. Otolaryngol Head Neck Surg 113 (3):179–180.
7. Bovee JV, van den Broek LJ, de Boer WI, Hogendoorn PC (1998) Expression of growth factors and their receptors in adamantinoma of long bones and the implication for its histogenesis. J Pathol 184 (1):24–30
8. Vermeulen PB, Gasparini G, Fox SB, Colpaert C, Marson LP, Gion M et al (2002) Second international consensus on the methodology and criteria of evaluation of angiogenesis quantification in solid human tumours. Eur J Cancer 38(12):1564–1579
9. Fox SB, Leek RD, Weekes MP, Whitehouse RM, Gatter KC, Harris AL (1995) Quantitation and prognostic value of breast cancer angiogenesis: comparison of microvessel density, Chalkley count, and computer image analysis. J Pathol 177(3):275–283
10. de Andrea CE, Wiweger MI, Bovee JV, Romeo S, Hogendoorn PC (2011) Peripheral chondrosarcoma progression is associated with increased type X collagen and vascularisation. Virchows Arch 460 (1):95–102
11. Koutsimpelas D, Stripf T, Heinrich UR, Mann WJ, Brieger J (2007) Expression of vascular endothelial growth factor and basic fibroblast growth factor in sporadic vestibular schwannomas correlates to growth characteristics. Otol Neurotol 28(8):1094–1099
12. Bedavanija A, Brieger J, Lehr HA, Maurer J, Mann WJ (2003) Association of proliferative activity and size in acoustic neuroma: implications for timing of surgery. J Neurosurg 98(4):807–811
13. Gomez-Brouchet A, Delisle MB, Cognard C, Bonafe A, Charlet JP, Deguine O et al (2001) Vestibular schwannomas: correlations between magnetic resonance imaging and histopathologic appearance. Otol Neurotol 22(1):79–86
14. Jeng CM, Huang JS, Lee WY, Wang YC, Kung CH, Lau MK (1995) Magnetic resonance imaging of acoustic schwannomas. J Formos Med Assoc 194(8):487–493
15. Fundova P, Charabi S, Tos M, Thomsen J (2000) Cystic vestibular schwannoma: surgical outcome. J Laryngol Otol 114(12):935–939
16. Jones SE, Baguley DM, Moffat DA (2007) Are facial nerve outcomes worse following surgery for cystic vestibular schwannoma? Skull Base 17(5):281–284
17. Sinha S, Sharma BS (2008) Cystic acoustic neuromas: surgical outcome in a series of 58 patients. J Clin Neurosci 15(5):511–515
18. Charabi S, Mantoni M, Tos M, Thomsen J (1994) Cystic vestibular schwannomas: neuroimaging and growth rate. J Laryngol Otol 108 (5):375–379
19. Park CK, Kim DC, Park SH, Kim JE, Paek SH, Kim DG et al (2006) Microhemorrhage, a possible mechanism for cyst formation in vestibular schwannomas. J Neurosurg 105(4):576–580
20. Stadlbauer A, Buchfelder M, Nimsky C, Saeger W, Salomonowitz E, Pinker K et al (2008) Proton magnetic resonance spectroscopy in pituitary macroadenomas: preliminary results. J Neurosurg 109 (2):306–312
21. Folkman J (1971) Tumor angiogenesis: therapeutic implications. N Engl J Med 285(21):1182–1186
22. Charabi S, Simonsen K, Charabi B, Jacobsen GK, Moos T, Rygaard J et al (1996) Nerve growth factor receptor expression in heterotransplanted vestibular schwannoma in athymic nude mice. Acta Otolaryngol 116(1):59–63
23. Charabi S (1997) Acoustic neuroma/vestibular schwannoma in vivo and in vitro growth models. A clinical and experimental study. Acta Otolaryngol Suppl 530:1–27
24. van Rijswijk CS, Kunz P, Hogendoorn PC, Taminiau AH, Doornbos J, Bloem JL (2002) Diffusion-weighted MRI in the characterization of soft-tissue tumors. J Magn Reson Imaging 15(3):302–307
25. Bonneville F, Savatovsky J, Chiras J (2007) Imaging of cerebellopontine angle lesions: an update. Part 2: intra-axial lesions, skull base lesions that may invade the CPA region, and non-enhancing extra-axial lesions. Eur Radiol 17(11):2908–2920
26. Pedrosa I, Alsop DC, Rofsky NM (2009) Magnetic resonance imaging as a biomarker in renal cell carcinoma. Cancer 115(10 Suppl):2334–2345
27. Brieger J, Bedavanija A, Lehr HA, Maurer J, Mann WJ (2003) Expression of angiogenic growth factors in acoustic neurinoma. Acta Otolaryngol 123(9):1040–1045
28. Labit-Bouvier C, Crebassa B, Bouvier C, Andrac-Meyer L, Magnan J, Charpin C (2000) Clinicopathologic growth factors in vestibular schwannomas: a morphological and immunohistochemical study of 69 tumours. Acta Otolaryngol 120(8):950–954
29. Buddingh EP, Kuijjer ML, Duim RA, Burger H, Agelopoulos K, Myklebost O et al (2011) Tumor-infiltrating macrophages are

associated with metastasis suppression in high-grade osteosarcoma: a rationale for treatment with macrophage activating agents. Clin Cancer Res 17(8):2110–2119
30. Colotta F, Allavena P, Sica A, Garlanda C, Mantovani A (2009) Cancer-related inflammation, the seventh hallmark of cancer: links to genetic instability. Carcinogenesis 30(7):1073–1081
31. Hsu HP, Shan YS, Lai MD, Lin PW (2010) Osteopontin-positive infiltrating tumor-associated macrophages in bulky ampullary cancer predict survival. Cancer Biol Ther 10(2):144–154
32. Lin EY, Nguyen AV, Russell RG, Pollard JW (2001) Colony-stimulating factor 1 promotes progression of mammary tumors to malignancy. J Exp Med 193(6):727–740
33. Mantovani A, Romero P, Palucka AK, Marincola FM (2008) Tumour immunity: effector response to tumour and role of the microenvironment. Lancet 371(9614):771–783
34. Ojalvo LS, Whittaker CA, Condeelis JS, Pollard JW (2010) Gene expression analysis of macrophages that facilitate tumor invasion supports a role for Wnt-signaling in mediating their activity in primary mammary tumors. J Immunol 184(2):702–712
35. Qian B, Deng Y, Im JH, Muschel RJ, Zou Y, Li J et al (2009) A distinct macrophage population mediates metastatic breast cancer cell extravasation, establishment and growth. PLoS One 4(8): e6562
36. Solinas G, Germano G, Mantovani A, Allavena P (2009) Tumor-associated macrophages (TAM) as major players of the cancer-related inflammation. J Leukoc Biol 86(5):1065–1073
37. Allavena P, Signorelli M, Chieppa M, Erba E, Bianchi G, Marchesi F et al (2005) Anti-inflammatory properties of the novel antitumor agent yondelis (trabectedin): inhibition of macrophage differentiation and cytokine production. Cancer Res 65(7):2964–2971
38. Mukhtar RA, Nseyo O, Campbell MJ, Esserman LJ (2011) Tumor-associated macrophages in breast cancer as potential biomarkers for new treatments and diagnostics. Expert Rev Mol Diagn 11 (1):91–100

Virchows Arch (2012) 460:637–649
DOI 10.1007/s00428-012-1233-z

ORIGINAL ARTICLE

Ultrastructural scoring of skin biopsies for diagnosis of vascular Ehlers–Danlos syndrome

Kim-Thanh Ong · Henri Plauchu · Simone Peyrol · Elisabeth Roux · Elisabeth Errazuriz · Philippe Khau Van Kien · Brigitte Arbeille · Alain Gaulier · Gabriela Georgescou · Patrick Collignon · Dominique P. Germain · Marie-Noëlle Gaveau · Jérôme Perdu · Stéphane Laurent · Patrick Bruneval · Pierre Boutouyrie

Received: 29 December 2011 / Revised: 7 March 2012 / Accepted: 26 March 2012 / Published online: 2 May 2012
© Springer-Verlag 2012

Abstract Vascular Ehlers–Danlos syndrome (vEDS) results from a mutation in the gene encoding alpha-1, type III procollagen (*COL3A1*) and confers fragility to skin, ligament and vascular tissue. We tested the value of skin biopsy for diagnosis of vEDS through an ultrastructure scoring procedure. Study design was a multicentric, case–control, blinded trial consisting of two phases: phase 1 was to identify an ultra-structure score providing the best discriminative value for vEDS and phase 2 was to replicate this result in a different population. We enrolled 103 patients, 66 cases defined through the revised nosology for Ehlers–Danlos syndromes and 37 control subjects selected from patients referred for other pathologies. Ultrastructure of extracellular matrix was read by three to five experienced pathologists

K.-T. Ong · J. Perdu · S. Laurent · P. Bruneval · P. Boutouyrie
Assistance Publique–Hôpitaux de Paris, Hôpital Européen Georges Pompidou, Inserm U970, Université Paris Descartes, Paris, France

H. Plauchu
Hospices Civils de Lyon, Hôpital Louis Pradel, Service de génétique clinique, Université de Lyon, Lyon, France

S. Peyrol · E. Roux · E. Errazuriz
Centre Commun d'Imagerie Laennec, Université de Lyon, Lyon, France

P. K. Van Kien
CHU Montpellier, Laboratoire de Génétique Moléculaire, Centre de Compétences Maladies Vasculaires Rares, Montpellier, France

B. Arbeille · G. Georgescou
CHU Tour, Centre commun de Microscopie Electronique, Université François Rabelais, Tours, France

A. Gaulier
CH d'Argenteuil Victor Dupouy, Laboratoire d'Anatomie et Cytologie Pathologiques, Argenteuil, France

P. Collignon
Assistance Publique–Hôpitaux de Marseille, Service de génétique, Hôpital de la Timone, Marseille, France

D. P. Germain
Assistance Publique–Hôpitaux de Paris, Hôpital Raymond Poincaré, Garches, Université de Versailles Saint-Quentin-en-Yvelines, Versailles, France

M.-N. Gaveau
Association Française des Syndromes d'Ehlers–Danlos, Tours, France

P. Bruneval (✉)
Service d'anatomo-pathologie and INSERM U970, Hôpital Européen Georges Pompidou, Assistance Publique–Hôpitaux de Paris, Université Paris Descartes, Paris, France
e-mail: patrick.bruneval@egp.aphp.fr

blinded for diagnosis. We used the receiver operating curves and logistic regression analysis for ranking ultrastructure scores. We created a detailed description of lesions observed in vEDS patients with 27 items (coded 0 or 1). In the phase 1 (17 cases and 20 controls), abnormal fibroblast shape, presence of lysosomes in the fibroblast and abnormal basal lamina were found to be independent discriminative items. Addition of these three items (defining an ultrastructure score) had the best diagnosis value (area under the curve (AUC)=0.96). In the phase 2 (49 cases, 17 controls), ultrastructure score provided odds ratio of 9.76 (95 % CI 2.91–32.78), and AUC of 0.90. The ultrastructure score of skin biopsy has predictive value for the diagnosis of vEDS. Presence of two or more signs (either abnormal fibroblast, presence of lysosomes in the fibroblast or abnormal basal lamina) is very evocative of vEDS.

Keywords Skin biopsy · Diagnosis · Vascular Ehlers–Danlos syndrome · Ultrastructure · Score · Fibroblast · Case–control · Blinded study

Introduction

The diagnosis of vascular Ehlers–Danlos syndrome (vEDS) is still challenging, despite the fact that this extracellular matrix (ECM) disease is due to alteration in *COL3A1*, the unique gene which encodes for alpha 1, type III (pro) collagen [1], because of the rate of negative genetic testing among patients with typical clinical presentation[2]. Type III collagen is strongly expressed in vascular tissue, ligament and skin, so that ECM structure and organization can be explored in skin biopsy, more accessible than vascular samples. The nanometric resolution of transmission electron microscopy allows to clearly visualise the polymeric forms of the collagens, their structural characteristics and the changes in their co-distribution. Ultrastructure of ECM from skin biopsy could contribute to diagnosis of vEDS [3, 4], together with other techniques such as dermal fibroblast culture for type III collagen properties [5] and the screening for *COL3A1* mutation [6].

The major issue when using complex data such as tissue sections is to propose a reading framework for exemplifying specific patterns for a given disease. Synthesis, maturation and physiological organization of major ECM proteins, particularly collagen because of its crystalline structure [7], can be observed by transmission electron microscopy on ultra-thin skin section (≈60 nm). We hypothesized that positive diagnosis of vEDS could be done by using ultrastructure of skin biopsies after adapting a previously published scoring of dermal ultrastructural lesions [8]. The objectives were triple: first, to make a detailed description of lesions observed in vEDS patients and create a reference atlas for normal skin biopsy; second, to identify the combination of items providing the best discriminative value for vEDS in a sample of 37 subjects; and third, to replicate this result in a different sample of 66 subjects.

Materials and methods

Sample

Patients were included at five multidisciplinary clinic centres concerning ECM diseases in France (Lyon, Marseille, Montpellier, Tours and Paris). Cases (n=66) were defined through a multistage workup. First, they were classified according to the revised nosology for Ehlers–Danlos syndrome (Villefranche 1997) [1]. The major clinical signs were numbered from M1 to M4. The minor criteria were numbered from m1 to m11 (Table 1). We added to the Beighton's list the "premature membrane rupture" as minor sign m10 and "absent lip frenula" as minor sign m11. We kept the heredity criteria as a minor one (m 9) if the diagnosis was probable in first-degree relative. In a majority of cases, COL3A1 mutation confirmed the diagnosis [9, 10]. In case of negative genetic testing, inclusion of cases was to be confirmed by a panel decision of members of the steering committee and with the mandatory opinion of a specialised geneticist [10]. Control subjects (n=37) were chosen among patients referred for other pathologies (type I or III Ehlers–

Table 1 Conventional designation of the clinical diagnostic criteria (according to Beighton P et al. [1]) and update

Major criteria (M)	
Thin, translucent skin	M1
Arterial/intestinal/uterine fragility or rupture	M2A, M2I, M2U
Extensive bruising	M3
Characteristic facial appearance	M4
Minor criteria (m)	
Acrogeria	m1
Hypermobility of small joints	m2
Tendon and muscle rupture	m3
Talipes equinovarus (clubfoot)	m4
Early-onset varicose veins	m5
Arterio-venous, carotid-cavernous sinus fistula	m6
Pneumo-thorax/pneumo-hemothorax	m7
Gingival recession	m8
Positive family history, sudden death in close relative	m9
Premature membrane rupture	m10
Absent inferior lip frenula	m11

Danlos, $n=12$; unaffected siblings of smooth muscle myosin heavy chain mutation [11], $n=11$; tissular fragility syndromes not fulfilling vEDS criteria, $n=10$; and Fabry disease, $n=4$).

All biopsies were done for clinical care and diagnostic purpose. All patients gave their written informed consent.

Skin biopsy

The skin biopsy was taken on the internal face of one arm in order to avoid additional UV radiation alterations due to sun exposure. After percutaneous local anaesthesia for 20 min, a 5×1-mm crescent-like skin sample was cut using a clamped curved forceps as a guide. The skin biopsy was divided in two parts with respect of the dermal–epidermal polarization: one part was immediately immersed in sterile physiological serum for cell culture, and the other, immersed in aldehyde fixative for ultrastructural preservation.

Electron microscopy, guide for observation and scoring, reference atlas

Preparative methods

The polarity of the skin biopsy was respected during the whole treatment: double fixation in Na-cacodylate/HCl buffered with 2 % glutaraldehyde and 1 % osmium tetroxide; dehydration in graded ethanol; impregnation and flat-embedding in epon polymerized at 60 °C for 3 days; semi-thin and ultra-thin sectioning on Reichert Ultracut E; collection of sections on 200 mesh copper grids; contrast with uranyl acetate in methanol and lead citrate (Richardson); observation on 1200CX Jeol Transmission electron microscope equipped with Megaview II SIS digital camera and AnalySIS software for image treatment; and morphometric analysis and diffusion as patient specific repertoires.

Method of observation

The skin biopsy section was systematically examined from the epidermis to the deep reticular dermis: (a) the dermal–epidermal junction, which includes the basal lamina, the structures involved in epidermal anchorage and the structures involved in dermal anchorage to the basal lamina (type VII collagen for the collagenic fibrils, oxytalanic fibres for the elastic fibres); (b) the cytological characters of the fibroblastic population distributed among all the dermal layers; (c) the ultrastructural characters of the collagen fibrils and of the elastic fibres and the organization pattern of the collagenic framework and of the elastic network; and (d) the capillary vessel walls and the peri-vascular connective matrix, with eventual sites of red blood cell exfiltration and peculiar fibrosing process.

All these signs were documented in the "scoring list" where pathological forms were quoted "1" and normal aspect "0" (Table 2).

Morphometric analysis of the dermal collagen fibres

During the observation of the deep reticular dermis, pictures of five largest orthogonally sectioned collagen fibre bundles were done at magnification×50,000. The bundles were chosen at distance from vessels, neural endings or glands. The magnification was convenient for precise measurement of the collagen fibre diameter. The diameter of 98 contiguous collagen fibres (excluding flower-like sections) was measured in each picture, and five histograms of size distribution were drawn and compiled (for a total of 490 measurements), allowing to document items 9–15.

Methodological and statistical aspects

Because reading of images is highly subjective, we built an atlas of reference iconography and of the morphometric data. All images were compared to the reference images for each item for identifying abnormal aspects. Selection of typical images was performed by the group of pathologists after several working sessions. Because induction bias (different reading if the investigator is oriented for diagnosis) is unavoidable, all images were anonym, and the reader was blinded as to the status of the patient. Unblinding was done after all readings were done and the database, frozen. Reading was performed by three experienced pathologists for phase 1, and five for phase 2. The item was considered present if 2/3 for phase 1 (3/5 for phase 2) of readers agreed. Agreement between readers was tested in phase 1. R values for scores ranged from 0.79 to 0.89, while coefficient of variation between readers ranged from 13 to 14 %.

Data were expressed as mean±SD. First, comparisons of categorical and quantitative variables were performed using Chi² tests and Wilcoxon rank test, respectively. Second, the independent discriminative items for the diagnosis of vEDS were assessed by logistic regression analysis. The third step was to construct a score that combined the independent items. Diagnostic values of score and isolated items were assessed by receiver operating characteristic (ROC) curve analysis. ROC curves were compared two by two by using area under the curves (AUCs) and SEs, and hypothesis tests above use the empirical approach for correlated (paired) samples (REF). Comparison of

Table 2

Panel 1 Patient :

(27 criteria: presence:1, absence:0; maximal score: 35, minimal score 0)

Fibroblasts

1. Shape 0 = fusiform, Normal
1 = tortuous, shrinked, osmiophilic =Degenerescent ……
2. Swelling of the rough endoplasmic reticulum ……
Size of mitochondria +1
Size like nucleus +2
Size larger than nucleus +3
3. Presence of lysosomes (absence =0 = normal; presence =1) ……..

Collagen fibres: isolated specimens in the reticular dermis

4. Curly or angled shape……

Bundles of collagen fibres

- ***Longitudinal section*:**

5. Sinusoidal shape……..
6. Irregular width of the fibres ……..……
7. Presence of ruptures or gaps…… …..
8. Variable stain along the fibres……..……..……

- ***Cross section*:**

9. Irregular diameter of the constitutive fibres ……
10. At least one pick below 80-90 nm (yes: +1, no: 0) ……
11. Fibres with diameter >120nm (more than 5 per image)……..…….
12. Number of bimodal diagrams (none 0, +1, +2, +3, +4, or +5)……..
13. Flower-like or non discoidal contour ……
14. Variable stain density……..……..……
15. Presence of finely granular material adjoining the fibres...……

Elastic fibres

- ***Longitudinal sections* :**

16. Atonic ribbon-like shape…..…….....
17. Hirsute, branchy, fragmented, dotted with holes……
18. Presence of fibrillo-granular material (different from elastin-associated microfibrils) in close contact with the elastic fibre……..
19. Broken fibres...…….

- ***Cross sections* :**

20. Default of elastin (heterogeneous contrast, speckled aspect)…….

Dermo-epidermal junction

21. Foliated, cumulative basal lamina……
22. Finely granular material ……..
23. Aggregate of elastin-associated micro-fibrils.……

Dermis, general aspect

24. Density:
Dermal-epidermal junction and superficial dermis …….
Loose organization =0 =normal;
Dense organization =1 =Abnormal;
Topographically heterogeneous along the section =0.5
Reticular Dermis (medium part): …….
Dense organization =0 = normal
Loose organization – scarce collagen fibre bundles =1 = Abnormal
Topographically heterogeneous =0.5
Reticular Dermis (deep part) : ……..……
Dense organization =0 =normal
Loose organization =1 =Abnormal)
Topographically heterogeneous =0.5
25. Presence of type VI collagen polymers ……..
26. Presence of wide pools of finely granular material ……

Blood vessels

27. Presence of red blood cell inserted in the vessel wall or outside capillaries....

TOTAL ……..……..

diagnostic value of scores was by area under the ROC curves. All tests were two-side and p values <0.05 were considered as significant. All analyses were performed using NCSS 2007 (G. Hintze, Kaysville, USA).

Results

From 1993 to 2007, 103 patients diagnosed clinically with Ehlers–Danlos syndrome were enrolled for skin biopsies (66 cases and 37 controls). Cases were younger than controls (32 years for cases and 37 years for controls, p=0.02), and sex ratio was similar (30 % of male for cases and 40 % of male for controls). Table 3 will show the median score of each item in the control and vEDS group in phase 1; Table 4, the Z value, odds ratio, and AUC of items 1, 2, 3, 6, 9, 11 and 21 in phase 1; and Table 5, the predictive value between simple (1, 3, 21) and combined items (1+3+21) in phase 1.

Electron microscopy findings

In vEDS, *fibroblasts* were primarily targeted by the lesional process. The spreading attachment upon ECM was restricted because of matrix components scarcity; the cell processes were unextended and showed multiple folds deprived of any support (Table 2, item 1) (Fig 1a–c). Fibroblast necrosis was frequently observed (Fig 1d) and might affect several cells around capillary vessels. The rough endoplasmic reticulum

Table 3 Median score of each item in the control and vEDS group in the phase 1

	Control (95 % CI)	vEDS (95 % CI)	p
Number of patients	20	17	
Fibroblasts			
Shape (item 1)	1 (0–1.5)	2 (2–2)	**0.001**
Swelling of the rough endoplasmic reticulum (item 2)	2.5 (1–3)	3 (3–4.5)	**0.04**
Presence of lysosomes (item 3)	0 (0–1)	1 (1–1)	**0.02**
Collagen fibres			
Curly or angled shape (item 4)	3 (2–3)	3 (2–3)	0.94
Bundles of collagen fibres			
Sinusoidal shape (item 5)	2 (1.5–2.5)	2 (2–3)	0.41
Irregular width of the fibres (item 6)	1 (0–2)	2 (2–3)	**0.001**
Presence of ruptures or gaps (item 7)	2.2 (2–3)	3 (2–3)	0.58
Variable stain along the fibres (item 8)	0 (0–1)	1 (1–2)	0.09
Irregular diameter (item 9)	1 (0–3)	3 (2–3)	**0.01**
At least one pick <80–90 nm (item 10)	1.5 (0–3)	0 (0–3)	0.61
Fibres with diameter >120 nm (item 11)	0 (0–0)	3 (0–3)	**0.04**
Number of bimodal diagrams (item 12)	1.5 (0–3)	0 (0–6)	0.83
Flower-like or non-discoidal contour (item 13)	0 (0–1)	1 (0–2)	0.32
Variable stain density (item 14)	0 (0–0.5)	0 (0–1)	0.65
Presence of finely granular material adjoining the fibres (item 15)	2 (1–3)	2.5 (2–3)	0.50
Elastic fibres			
Atonic ribbon-like shape (item 16)	1 (1–2)	1 (1–2)	0.59
Hirsute, branchy, fragmented, dotted with holes (item 17)	3 (1.5–3)	3 (3–3)	0.12
Presence of fibrillo-granular material (item 18)	2.5 (1–3)	2 (0.5–3)	0.44
Broken fibres (item 19)	1 (0–1)	1 (0–2)	0.94
Default of elastin (item 20)	2 (1–3)	2 (2–3)	0.22
Dermo-epidermal junction			
Foliated, cumulative basal lamina (item 21)	1 (1–2)	3 (2–3)	**0.002**
Finely granular material (item 22)	2 (1–3)	3 (2–3)	0.20
Aggregate of elastin-associated micro-fibrils (item 23)	1 (0–1)	0 (0–1)	0.47
Dermis, general aspect			
Density (item 24)	1.7 (1.5–3)	1.5 (1–2)	0.37
Presence of type VI collagen polymers (item 25)	0 (0–1)	1 (0–3)	0.16
Presence of wide pools of finely granular material (item 26)	2 (1–2)	1 (0–3)	0.87
Blood vessels			

Bold items are items which differ significantly between EDS and controls and were further tested in multivariate models.

Table 4 Z value, odds ratio, and AUC of items 1, 2, 3, 6, 9, 11 and 21 in phase 1

	Z value	Odds ratio (95 % CI)	AUC	*p*
Item 1	2.66	4.42 (1.48–13.25)	0.78	0.008
Item 2	2.01	1.60 (1.01–2.53)	0.69	0.044
Item 3	2.14	4.20 (1.13–15.62)	0.70	0.032
Item 6	2.91	3.88 (1.55–9.70)	0.80	0.004
Item 9	2.53	2.51 (1.23–5.11)	0.73	0.011
Item 11	2.40	1.62 (1.02–2.59)	0.67	0.040
Item 21	2.88	3.99 (1.55–10.26)	0.79	0.004

exhibited various degrees of dilatation due to the intracisternal stasis of abnormal protein (Table 2, item 2). Mast cells were frequently present in close contact with injured fibroblasts. Lysosomes, very uncommon in normal in vivo fibroblasts, were often observed and confined in the cytoplasm of vEDS syndrome fibroblasts (Table 2, item 3), (Fig 2). They displayed some diversity (Fig 2a), presenting as membrane-bound dense bodies (Fig 2b) or vacuolated vesicles (Fig 2c, d).

The *collagen fibrous framework* was affected: the constitutive periodically cross-striated fibrils were folded, flexible in appearance, expanded and showed unusual shapes and contrast affinity (Table 2, items 4, 8, 13 and 14), (Fig 3a). The largest collagen fibre bundles in the deep reticular dermis were not rigid but bended as sinusoids (Fig 3b); patches of missing collagen fibres introduced gaps in the axis of the bundles (Table 2, items 5 and 7). Sections in the long axis of the collagen fibrils appeared unequal (Fig 3c, d). The diameter measurements of cross-sectioned collagen fibrils made obvious the evidence of a wide disparity (Table 2, items 6 and 9). The bi-modality of Gaussian curves in patients with vEDS cases allowed to distinguish one major population of fibres with small diameter (<80 nm) and a minor one with large diameter (>100 nm) (Table 2, items 10 and 12) (Fig 3a).

The *elastic network* was affected in the reticular dermis. The elastic fibres showed a ribbon-like shape (Table 2, item 16) among the rarefied fibrous collagen matrix. In the absence of strong collagen fibre support, they appeared weakened in their deployment (Table 2, item 17), in their structure (Table 2, item 20) and sometimes gave evidence of breaking (Table 2, item 19).

The lesion of the *dermal–epidermal junction* was focused on the basal lamina which objectified the complex bipolar plane of attachment between epidermis and dermis: the thickness was irregular, either thickened or thinned, and additional sheaths of basal lamina formed loops running down in the dermis (Table 2, item 21) (Fig 4b). Type VII collagen and oxytalan fibres were regularly anchored to this modified basal lamina.

The background deposition of unidentified finely granular material (Table 2, item 22) gave an unusual electron density to the superficial dermis which contrasted with an aspect of *matrix vacuity* of the adjacent reticular dermis (Table 2, item 24) (Fig 4a). Wide pools of unidentified fine granular material often spread into the matrix collagen-free spaces (Fig 1a) and stuck to collagen fibre bundles or elastic fibres (Table 2, item 15, 18 and 26) (Fig 4c). In such dermal matrix configuration, the lymphatic microvasculature appeared widened and belt by a continuous vessel wall composed of joined endothelial cells and a thin regular elastic and collagen tie (Fig 1c). As a consequence of the matrix default, capillary vessel walls also appeared widened with frequent unmasking of *type VI collagen* polymers (Fig 4c) among or in the vicinity of the supernumerary basal laminas (Table 2, item 25). Evidence of vessel wall dissection was incidentally observed as well as the presence of red blood cells outside vessels (Table 2, item 27) (Fig 4d).

Predictive value of scoring

The first phase was performed in 37 subjects (17 cases and 20 controls). Each of the 27 items of the score was quoted by comparison to the reference atlas, blinded as to the name and diagnosis of the patient. The score of each item is listed in Table 3. For items 1, 2, 3, 6, 9, 11 and 21, the score was significantly greater in the cases than in the control group. By using logistic regression analysis, we could obtain the Z value, AUC of items 1, 2, 3, 6, 9, 11 and 21 (Table 4). We

Table 5 Predictive value between simple (1, 3, 21) and combined items (1+3+21) in phase 1

	Z value	Odds ratio (95 % CI)	AUC	*p*
Item 1	3.22	14 (2.81–69.76)	0.79 [0.58–0.89]	0.001
Item 3	2.49	7 (1.51–32.48)	0.71 [0.51–0.83]	0.123
Item 21	2.86	12.86 (2.23–74.08)	0.79 [0.60–0.89]	0.004
Item 1+3+21	3.42	#NA	0.96 [0.85–0.99]	0.001

Odds ratio impossible to calculate (*#NA*) because of quasi complete separation of data (only 1 control misclassified as vEDS and 1 vEDS misclassified as control). AUC comparison: #1 vs. #3, $p=0.50$; #1 vs. #21, $p=0.48$; #(1+3+21) vs. (#1, #3, #21), $p<0.05$

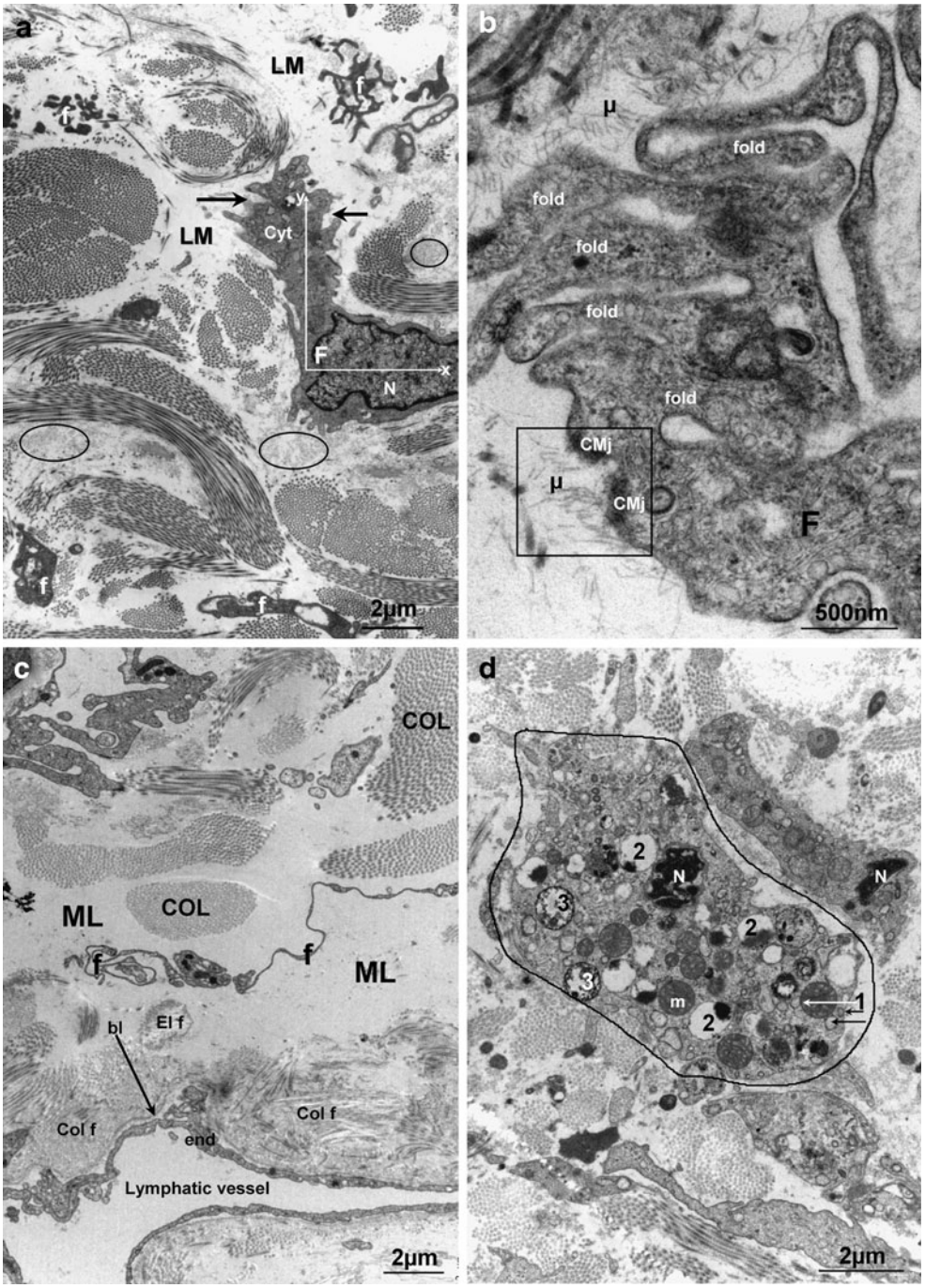

Fig. 1 Fibroblasts in vEDS syndrome (item 1). **a** The major fibroblast (*F*) incidence shows the right angle between the axes of the pericaryon (*white axis x*, *N* nucleus) and the main cytoplasmic process (*white axis y*, *Cyt* cytoplasm); the cytoplasmic membrane is creased (*black arrows*) in front of the lacunary matrix (*LM*) and the patches of fibrillo-granular material (*ellipse*). Distinct fibroblastic processes (*white f*) are disposed in the four corners: they are slender, osmiophilic, dot-like- or star-like-shaped. **b** Higher magnification: folding of an unexpended fibroblast (*F*) cytoplasmic process (*fold*: thin multiple folds of cytoplasm). Frame: cell-matrix junctions (*CMj*) link the fibroblast to elastin-associated micro-fibrils (*µ*). **c** In the centre, very slender fibroblastic processes (*f*), devoid of matrix anchorage in the plane of section, float in a wide matrix lacuna (*ML*) where collagen fibre bundles (*COL*) are disjoined. At the *bottom*, a lymphatic vessel is gaping; the lymphatic wall is composed of a continuous endothelium (*end*), a distinct basal lamina (*bl*) and a rather dense collagenous/elastic fibrillar sheath (*Col f* collagen fibres, *El f* elastic fibre). **d** Necrotic fibroblast in the center (*encircled*): nucleus (*N*) is pycnotic, mitochondrias (*m*) are enlarged and rounded, endoplasmic reticulum is vesiculated (*1*) and some enlarged rounded cisternae contain dark residues (*2*), and autophagocytosis vesicles are characterised by a dense membranous envelope and a heterogeneous content (*3*)

then assessed the independency of each item by combining two or more items introduced together in the logistic model. Items 1, 3 and 21 were identified as independent discriminative items for the diagnosis of vEDS. The addition of values for item 1, 3 and 21 was named ultrastructure score, ranging between 0 and 3. By using ROC curves analysis, we compared the predictive value between simple and combined parameters (Table 5). Ultrastructure score had the best behaviour, with quasi-complete separation of patients and controls (only one control misclassified as vEDS and one vEDS misclassified as control; AUC (0.96) compared to individual items). Figure 5 shows the ROC for items 1, 3 and 21 and the combined ultrastructural score

We replicated the findings of the first phase (37 patients) in a new sample of 66 patients (phase 2). In this phase, we had 49 cases and 17 controls. New expert readers examined TEM preparations of skin biopsies and gave score for three items: 1, 3 and 21. Then, each score was codified like in the first phase, and the ultrastructure score was obtained for each

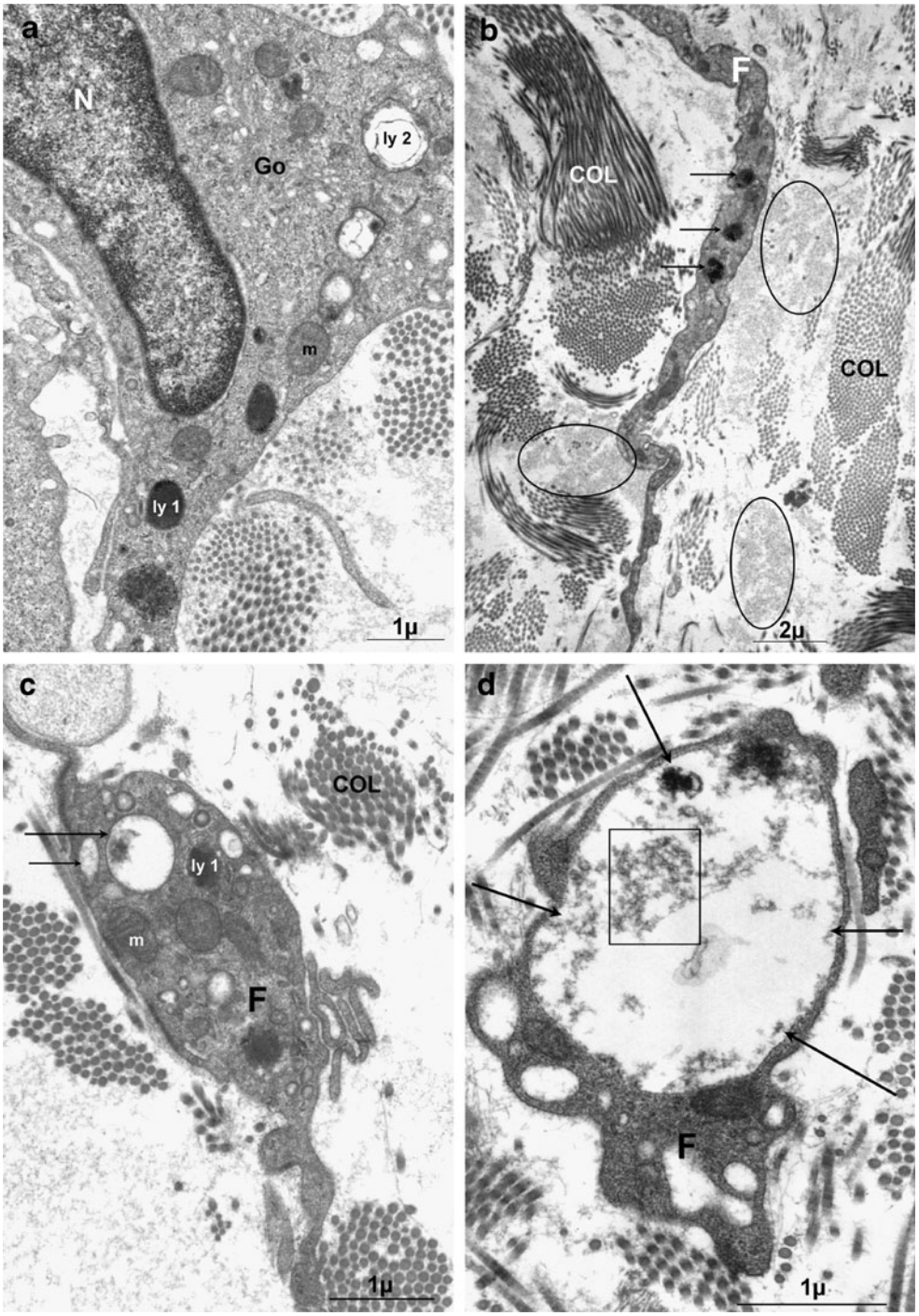

Fig. 2 Lysosomes in fibroblasts (item 3). **a** Lysosomes (ly) are distributed around the Golgi area (*Go*): primary lysosomes (*ly 1*) are homogeneously electron-dense; secondary lysosomes (*ly 2*) are vacuolated and contain heterogeneous material. **b** Electron-dense lysosomes (*arrows*) in a fibroblastic process (*F*). Patches of fibrillo-granular deposit (*ellipse*) are disposed in contact with the fibroblast and with collagen fibre bundles (*COL*). **c** Cytoplasmic process of a fibroblast (*F*): *arrows* point two different vesicles: the smaller one is an endoplasmic reticulum *cisterna* containing proteic deposits; the larger one is bounded by a dense membrane and contains heterogeneous material, such as an autophagocytotic vesicle. (*ly1* primary lysosome, *m* mitochondria, *COL* collagen fibre bundle). **d** Large vacuolated vesicle (*arrows*) in a fibroblastic process (*F*): the heterogneous content evokes accumulation of degraded immature proteic material (*frame*)

patient. By using logistic regression analysis, ultrastructure score had odds ratio of 9.76 (95 % CI 2.91–32.78), corresponding to an AUC of 0.90 [0.76–0.96].

At the last step of our study, we grouped the patients in phases 1 and 2 and did an analysis in 103 patients. We found that odds ratio of ultrastructure-score was 11.44 (95 % CI 4.72–27.75) with an AUC of 0.92 [0.85–0.96]. Cut-off values of 1 lead to a sensitivity of 0.98 and specificity of 0.30. Cut-off values of 2 lead to a sensitivity of 0.96 and specificity of 0.73. Cut-off values of 3 lead to a sensitivity of 0.74 and specificity of 0.94. The ultrastrucure score provided similar AUC, whether samples were issued from patients with proved mutation (0.93 [0.83–0.97]) or not (0.92 [0.83–0.96]).

Discussion

The main finding of the present study is that three independent items of the ultrastructure of skin biopsy were

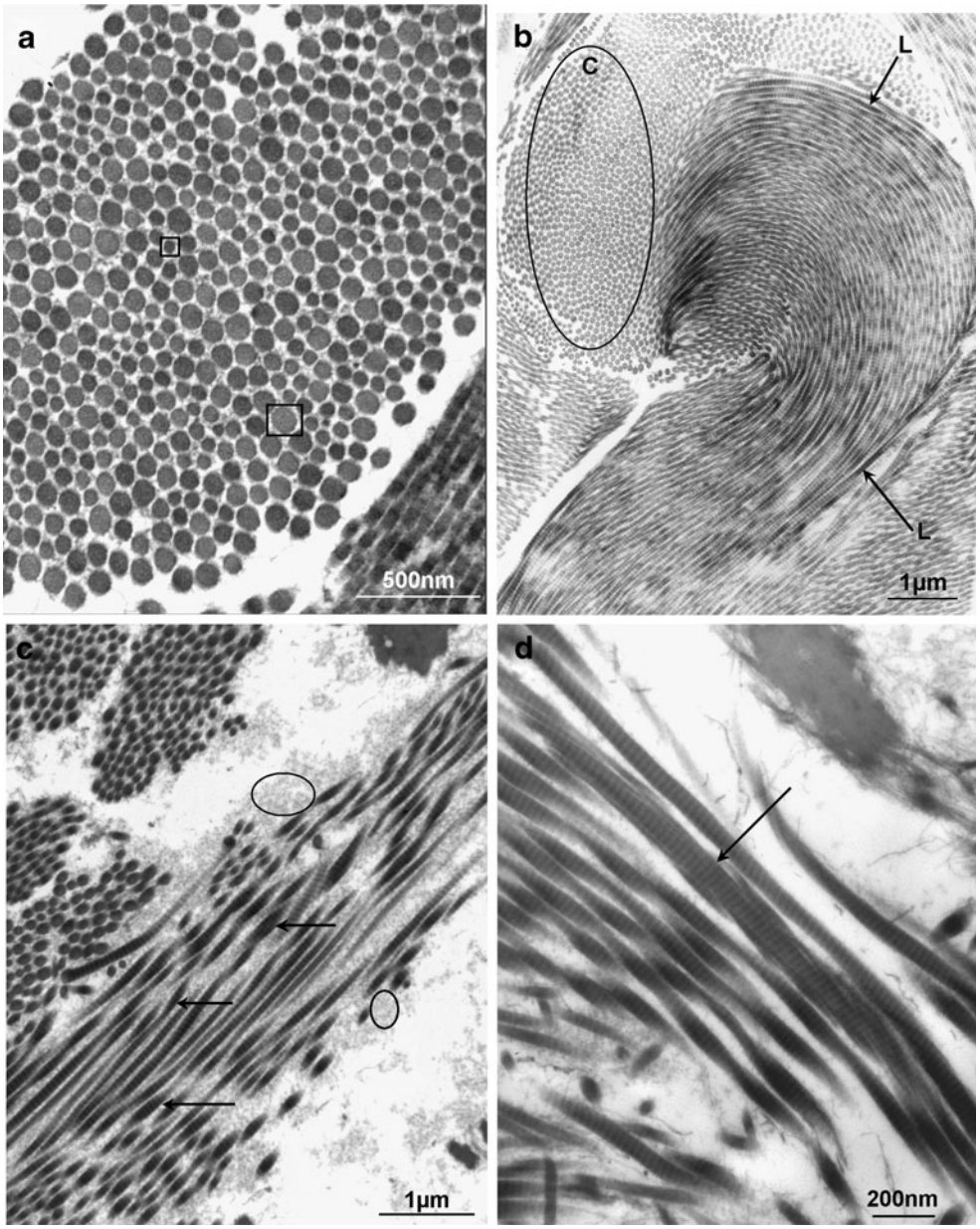

Fig. 3 Extracellular matrix in vEDS. **a** Cross section of a collagen fibre bundle in the reticular dermis: the collagen fibrils show various sizes and electron densities. Two sections of collagen fibrils are framed in order to be compared:. one shows a smaller diameter and a higher electron density, the other shows a larger diameter and a lower electron density (item 14). **b** Medium part of the reticular dermis: the collagen fibre bundle has a sinusoidal shape as suggested by the consecutive cross (*C*) and longitudinal (*L*) section incidences along the bundle (inside the ellipse, all the collagen fibres are cross-sectioned) (item 5) **c** Sections along the axis of collagen fibrils show a "fish-like" aspect (*arrow*) and emphasize the varying width (item 6). Finely granular material is adjoining the fibrils (*ellipse*) (item 15). **d** Higher magnification of the "fish-like" sections of collagen fibrils: one diagonally disposed fibril (*arrow*) has a large diameter (>120 nm)

identified as having a good diagnosis value for vEDS, and that this result could be replicated on a different set of patients and by different readers. The diagnosis value of this ultrastructure score is excellent, leading to AUC above 0.90 on ROC curves.

Pathophysiological considerations

Most dermal items characterised in this study were previously proposed for their potential specific relevance with regards to Ehlers–Danlos syndrome diagnosis and classification [8]; however, this study had no control group.

The first surprise of the present paper was to have observed that collagen fibre size and bundle characteristics did not discriminate between vEDS and controls. Although some items (6, 9 and 11) were associated with diagnosis in univariate analysis, these differences disappeared in multivariate analysis. Discovery of type III collagen as the target protein [12] and of *COL3A1* alteration as the primary target in vEDS [13] naturally focused attention on cross-striated collagen fibrils known to result from the interactive co-polymerization of the major collagen types I [14], III and V [7, 15, 16]. Small fibril diameter (about 60 nm) was reported as a constant finding [17]. Here, we observed the presence of a bi-modal distribution curve of the fibril diameter in several patients with confirmed vEDS, but not in all. When tested for specificity of this sign for vEDS, none of the collagen fibre characteristic was significantly and

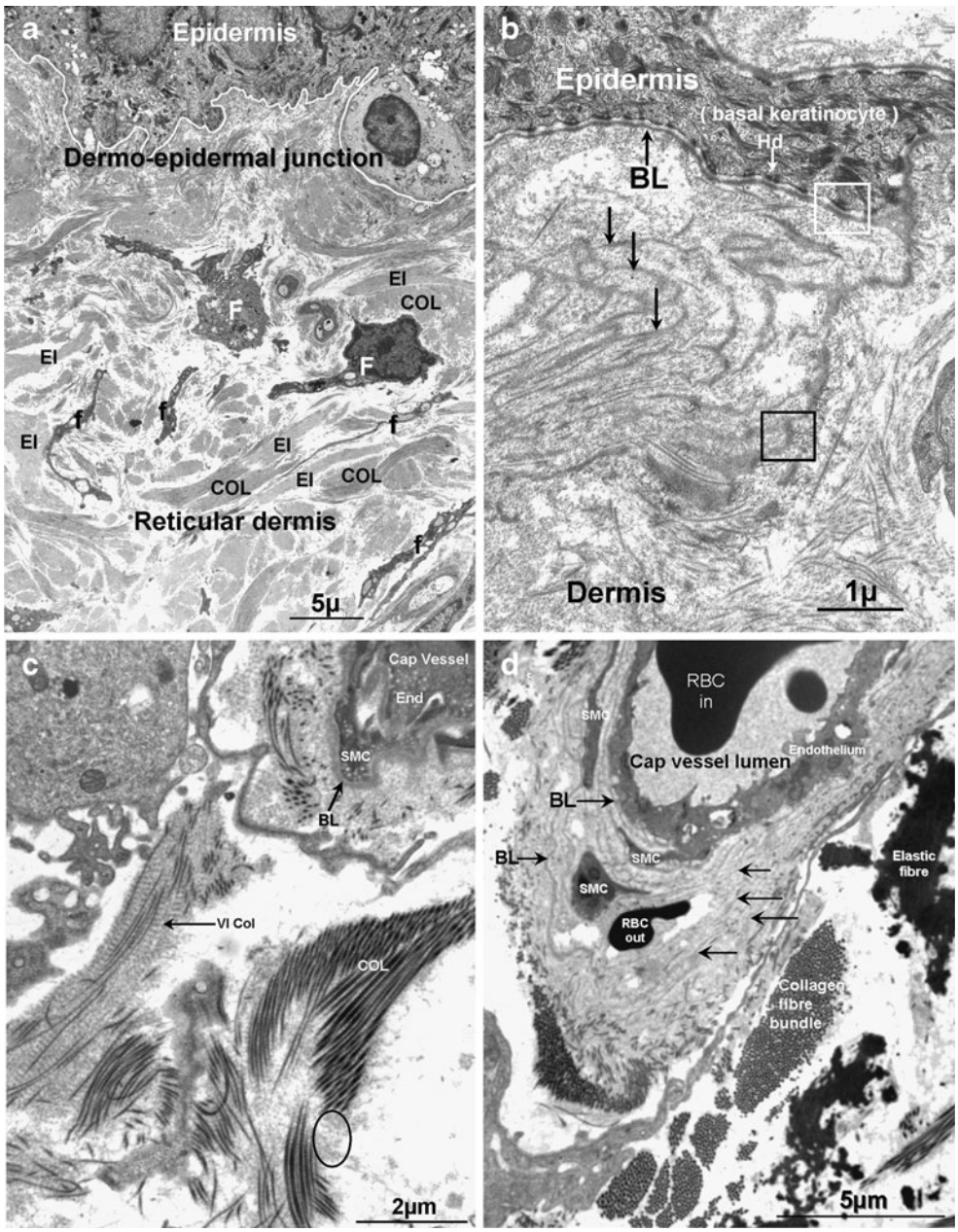

Fig 4 Dermal–epidermal junction and reticular dermis. **a** Extracellular matrix organization of the superficial reticular dermis. In contact with the epidermis, the dermal–epidermal junction shows a dense organization (the sub-epidermal basal lamina is underlined by a *white line*). In contrast, the lower part shows a loose organization: fibroblasts (*F*) and their fine processes (*f*) float in a lacunar matrix where collagen fibre bundles (*COL*) and elastic fibres (*El*) form a slender framework (item 24). **b** Detail of segment of dermal–epidermal junction with foliated basal lamina. In contact with the epidermis, the basal lamina (*BL*) is continuous and shows regular proteic condensations in front of the keratinocytic hemidesmosomes (*Hd* and *white frame*). Multiple sheets of basement membrane material are accumulated beneath (*black arrows*); structures of hemidesmosome attachment are yet present along (*black frame*) (item 21). **c** Type VI collagen polymers (*VI Col*) near to a capillary vessel wall (*Cap Vessel* lumen of the capillary vessel, *End* endothelial cell, *SMC* smooth muscle cell, *BL* basal lamina) (item 25). Granular material (*ellipse*) is stuck to collagen fibre bundles (*COL*) (item 26). **d** Capillary vessel dissection. A large section of red blood cell (*RBC in*) is present in the lumen of the capillary vessel (*Cap vessel lumen*). The vessel wall is composed of endothelial cells (*Endothelium*) and smooth muscle cells (*SMC*) with encircling basal laminas (*BL*) which cumulate several sheets (*arrows*). One red blood cell (*RBC out*) is inserted between supernumerary basal laminas, thus indicating capillary leakage (item 27)

independently associated. Thin collagen fibrils might be formed when normal type III collagen availability is depleted as a consequence either of senescence process or of protein synthesis and maturation disturbance of genetic origin. Nevertheless, these items (9, 10 and 12), either collagen framework depletion or loose matrix organization of the

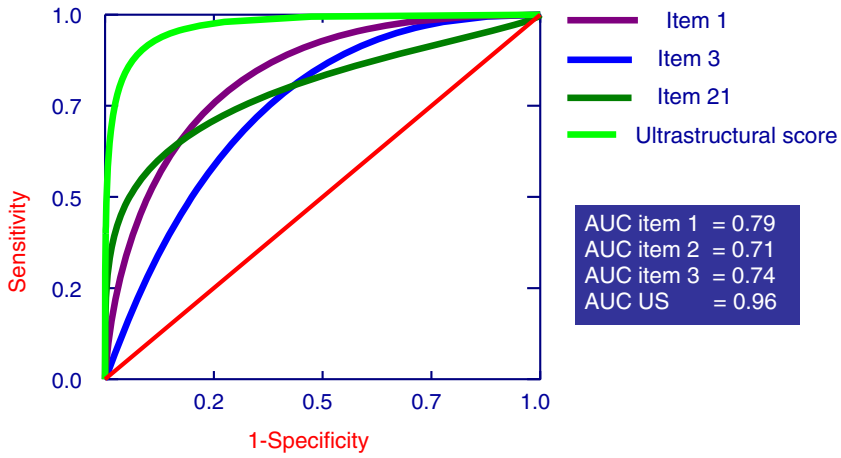

Fig. 5 Receiver operating curves for items 1, 3 and 21, and combined ultrastructural Score. *AUC* stands for area under the curve and *US* stands for ultrastructural score

reticular dermis (item 24) did not come out as specific for vEDS. This is surprising since these items were quantitative measures. Yet these features are supposed to contribute to the loss of dermal density and strength, participating to the three major clinical signs of vEDS (thin, translucent skin, extensive bruising and characteristic facial appearance).

Fibroblasts, (here dermal fibroblasts) were ideal candidates for finding specific signs for vEDS since they synthesise abnormal *COL3A1*. Rough endoplasmic reticulum (RER) cisternae are described as dilated, up to complete cytoplasm stuffing [17–20] by sequestered alpha 1, type III pro-collagen chains, which cannot be further processed because of its abnormal structure [21]. Fibroblastic RER dilatation (item 2) did not come out as specific for vEDS. This lack of specificity might be caused by the fact that it has been also observed in other disorders in which protein secretion was inefficient [22]. Intracytoplasmic secondary lysosomes were not previously described in vEDS studies. However, their presence came out of the present analysis as highly specific ultrastructural stigmata of vEDS. In parallel to vEDS heterogeneity due to the wide panel of mutations which may alter *COL3A1*, different steps of type III collagen intracellular processing and extracellular maturation might be stopped or not properly achieved. Without type III collagen identification in these lysosomes, we are reduced to alternative hypotheses. Either abnormal type III collagen products, which cannot be further processed, are segregated in the fibroblast in order to be degraded by autophagy process. Alternatively, depleted connective matrix reciprocally disturbs cell–matrix interactions and fibroblastic deployment, thus leading to exacerbated cell susceptibility to all the types of matrix-mediated aggressions (mechanical or humoral). The fact that fibroblast aspect (item 1) discriminates between vEDS and controls could be interpreted in terms of stress on cells, leading to degeneration and early cell death.

Foliated, cumulative basal lamina of the dermal–epidermal junction definitely discriminated vEDS and controls. This earlier described [17] feature suggests overexpression of basal lamina components (basically type IV collagen, laminin, but also basement membrane glycoproteins and proteoglycans) which is difficult to correlate with Type III collagen depletion. The presence of type III collagen at the dermal–epidermal junction is known since a long time [23] as a component of the thin fibrillar stuffing disposed beneath the basal lamina and around dermal blood capillary vessels, but its function was not yet defined. At the light of the vEDS clinical signs M1, m5 and m6, skin and vascular fragility was emphasized, indicating the role of the type III collagen fibrillar component in consolidation both of the skin interface and of the vascular walls. The patchy distribution of sub-epidermal basal lamina accumulation might reflect the long-term history of slight mechanical aggressions over the skin of the patient against a defective dermal support; keratinocytes and vEDS dermal fibroblasts should supply to this defect by an over-production of their common interface: the basal lamina with all its glycoproteic and proteoglycanic annexes which ensure stability and strength to the skin as a protective tissue. A similar proposition could be done for the vessel walls, the basal lamina of which is often foliated, sometimes with red blood cells interposed between their multiple layers. Because skin and blood vessels are subject to mechanical stress, the abnormalities of basement membrane (mainly type VI collagen) could represent an adaptive response of fragile structure (lack of type III collagen) to mechanical stress. Such large type VI collagen polymers were already observed in vEDS dermis, close to perineurial basement membrane, and also in the ECM associated to remodelled vessel walls, in diabetic patients [23], in burn-scar recovery and among the neoangiogenesis of stromal reaction [24].

This study has several strengths. First, the reading procedure was made in a large subset of patients and controls using blinding procedure, thus limiting the induction bias. Second, the reading framework was based on literature and further refined by highly experienced pathologists. This grid was preestablished and prospectively applied to the first cohort for

selection of items, then in a distinct sample for replication. This study has also weaknesses. First, the genetic diagnosis was not available for all patients. If the analysis was limited to the cases confirmed by genetic testing, results were similar. Second, control subjects are not, strictly speaking, normal because we had to have biopsies for a clinical indication (except healthy relatives of patients with mutations in *MYH11*). We chose to include patients with other type of connective tissue disorder as controls. They were, however, undistinguishable from normal subjects [9]. This choice was deliberate since the differential diagnosis has to be usually done between patients with other forms of connective tissue disorders.

Application of the present findings and clinical perspective

The score for ultrastructure abnormalities of skin is easy to use. Presence of two or more signs (either abnormal fibroblast, presence of lysosomes in the fibroblast or abnormal basal lamina) is very evocative of the diagnosis. Templates are provided for guiding the pathologist (internet site: http://www.afsed.com/accueil.htm).

As emphasized in the ("Introduction") section, positive diagnosis of vEDS is still problematic. Many patients present with incomplete phenotype, and in such population, the yielding of genetic testing is low [2, 10]. Given the very high diagnostic performance of the ultrastructure score, its simplicity (only three independent items) and the availability of reference images, experienced pathologists could apply the scoring to patients negative for *COL3A1* mutation. Evocative signs for vEDS could then confirm the diagnosis and allow the introduction of preventive treatment, among them, Celiprolol [10].

Acknowledgments We thank the electron microscopy team of Tours for the dispositions of the skin biopsies of the vEDS patients in the CHU Tours: Mrs. Monique Lemesle for excellent electron microscopy technique until contrasted ultra-thin sections were ready to observe and Mr. Pierre-Yves Sizaret and Mr Pierre Ivan RaynaL for argentic and numeric photograph communication. We thank Marie-Thérèse Zabot of the centre of Biology of Hôpital Louis Pradel in Lyon, who practised the initial series of skin biopsies and founded the bank of fibroblasts in1986. This study was done with the support from the Association Française des Syndromes d'Ehlers–Danlos.

Conflict of interest Association Française des Syndromes d'Ehlers–Danlos was the sponsor of the study and was involved in study design. The authors state no conflict of interest.

References

1. Beighton P, De PA, Steinmann B et al (1998) Ehlers–Danlos syndromes: revised nosology, Villefranche, 1997. Ehlers–Danlos National Foundation (USA) and Ehlers–Danlos Support Group (UK). Am J Med Genet 77:31–37
2. Pepin M, Schwarze U, Superti-Furga A et al (2000) Clinical and genetic features of Ehlers–Danlos syndrome type IV, the vascular type. N Engl J Med 342:673–680
3. Holbrook KA, Byers PH (1989) Skin is a window on heritable disorders of connective tissue. Am J Med Genet 34:105–121
4. Smith LT, Schwarze U, Goldstein J et al (1997) Mutations in the COL3A1 gene result in the Ehlers–Danlos syndrome type IV and alterations in the size and distribution of the major collagen fibrils of the dermis. J Invest Dermatol 108:241–247
5. Zoppi N, Gardella R, De PA et al (2004) Human fibroblasts with mutations in COL5A1 and COL3A1 genes do not organize collagens and fibronectin in the extracellular matrix, down-regulate alpha2beta1 integrin, and recruit alphavbeta3 Instead of alpha5beta1 integrin. J Biol Chem 279:18157–18168
6. Malfait F, Symoens S, De BJ et al (2007) Three arginine to cysteine substitutions in the pro-alpha (I)-collagen chain cause Ehlers–Danlos syndrome with a propensity to arterial rupture in early adulthood. Hum Mutat 28:387–395
7. van der Rest M, Garrone R (1990) Collagens as multidomain proteins. Biochimie 72:473–484
8. Hausser I, Anton-Lamprecht I (1994) Differential ultrastructural aberrations of collagen fibrils in Ehlers–Danlos syndrome types I-IV as a means of diagnostics and classification. Hum Genet 93:394–407
9. Plancke A, Holder-Espinasse M, Rigau V et al (2009) Homozygosity for a null allele of COL3A1 results in recessive Ehlers–Danlos syndrome. Eur J Hum Genet 17:1411–1416
10. Ong KT, Perdu J, De BJ et al (2010) Effect of celiprolol on prevention of cardiovascular events in vascular Ehlers–Danlos syndrome: a prospective randomised, open, blinded-endpoints trial. Lancet 376:1476–1484
11. Zhu L, Vranckx R, Van Khau KP et al (2006) Mutations in myosin heavy chain 11 cause a syndrome associating thoracic aortic aneurysm/aortic dissection and patent ductus arteriosus. Nat Genet 38:343–349
12. Pope FM, Martin GR, Lichtenstein JR et al (1975) Patients with Ehlers–Danlos syndrome type IV lack type III collagen. Proc Natl Acad Sci U S A 72:1314–1316
13. Superti-Furga A, Gugler E, Gitzelmann R et al (1988) Ehlers–Danlos syndrome type IV: a multi-exon deletion in one of the two COL3A1 alleles affecting structure, stability, and processing of type III procollagen. J Biol Chem 263:6226–6232
14. Liu X, Wu H, Byrne M et al (1997) Type III collagen is crucial for collagen I fibrillogenesis and for normal cardiovascular development. Proc Natl Acad Sci U S A 94:1852–1856
15. Canty EG, Kadler KE (2005) Procollagen trafficking, processing and fibrillogenesis. J Cell Sci 118:1341–1353
16. Myllyharju J, Kivirikko KI (2004) Collagens, modifying enzymes and their mutations in humans, flies and worms. Trends Genet 20:33–43
17. Byers PH, Holbrook KA, McGillivray B et al (1979) Clinical and ultrastructural heterogeneity of type IV Ehlers–Danlos syndrome. Hum Genet 47:141–150
18. Byers PH, Barsh GS, Holbrook KA (1981) Molecular mechanisms of connective tissue abnormalities in the Ehlers–Danlos syndrome. Coll Relat Res 1:475–489
19. Holbrook KA, Byers PH (1982) Structural abnormalities in the dermal collagen and elastic matrix from the skin of patients with inherited connective tissue disorders. J Invest Dermatol 79(Suppl 1):7 s–16 s
20. Vitellaro-Zuccarello L, Cheli F, Esposito R et al (1985) Ultrastructural study of the dermis in a case of type IV Ehlers–Danlos syndrome. J Submicrosc Cytol 17:695–701
21. Bateman JF, Boot-Handford RP, Lamande SR (2009) Genetic diseases of connective tissues: cellular and extracellular effects of ECM mutations. Nat Rev Genet 10:173–183

22. Willing MC, Cohn DH, Starman B et al (1988) Heterozygosity for a large deletion in the alpha 2(I) collagen gene has a dramatic effect on type I collagen secretion and produces perinatal lethal osteogenesis imperfecta. J Biol Chem 263:8398–8404
23. Peyrol S, Hugues B, Grimaud JA et al (1984) Collagen heterogeneity of thickened basement membranes of human diabetic dermis: tissular immunolabelling of collagen types I, III and IV by light and electron microscopy. Cell Mol Biol 30:43–57
24. Peyrol S, Galateau-Salle F, Raccurt M et al (2000) Selective expression of lysyl oxidase (LOX) in the stromal reactions of broncho-pulmonary carcinomas. Histol Histopathol 15:1127–1135

Virchows Arch (2012) 460:651–658
DOI 10.1007/s00428-012-1246-7

ORIGINAL ARTICLE

Temporal differences of onset between primary skin lesions and regional lymph node lesions for tularemia in Japan: a clinicopathologic and immunohistochemical study of 19 skin cases and 54 lymph node cases

Shigeyuki Asano · Kikuo Mori · Kazuki Yamazaki · Tetsutaro Sata · Takayuki Kanno · Yuko Sato · Masaru Kojima · Hiromi Fujita · Yasushi Akaike · Haruki Wakasa

Received: 1 March 2012 / Revised: 17 April 2012 / Accepted: 2 May 2012 / Published online: 17 May 2012
© The Author(s) 2012. This article is published with open access at Springerlink.com

Abstract For tularemia, a zoonosis caused by the gram-negative coccobacillus *Francisella tularensis*, research of the relation between skin lesions and lymph node lesions has not been reported in the literature. This report describes skin lesions and lymph node lesions and their mutual relation over time for tularemia in Japan. Around the second day after infection (DAI), a subcutaneous abscess was observed (abscess form). Hand and finger skin ulcers formed during the second to the fourth week. Subcutaneous and dermal granulomas were observed with adjacent monocytoid B lymphocytes (MBLs) (abscess–granulomatous form). From the sixth week, large granulomas with central homogeneous lesions emerged diffusely (granulomatous form). On 2–14 DAI, *F. tularensis* antigen in skin lesions was detected in abscesses. During 7–12 DAI, abscesses with adjacent MBLs appeared without epithelioid granuloma (abscess form) in regional lymph nodes. During the second to fifth week, granulomas appeared with necrosis (abscess–granulomatous form). After the sixth week, large granulomas with a central homogeneous lesion (granulomatous form) appeared. *F. tularensis* antigen in lymph node lesions was observed in the abscess on 7–92 DAI. Apparently, *F. tularensis* penetrates the finger skin immediately after contact with infected hares. Subsequently, the primary lesion gradually transfers from skin to regional lymph nodes. The regional lymph node lesions induced by skin lesion are designated as dermatopathic lymphadenopathy. This study revealed temporal differences of onset among the skin and lymph node lesions.

Keywords Tularemia · Primary skin lesions · Regional lymph node lesions · Temporal differences of onset

S. Asano (✉) · K. Mori · K. Yamazaki
Department of Pathology, Iwaki Kyoritsu General Hospital,
16 Kusehara, Mimaya-machi, Uchigo,
Iwaki 973-8555, Japan
e-mail: patho.asano@gmail.com

T. Sata · T. Kanno · Y. Sato
Department of Pathology, National Institute of Infectious Diseases,
Tokyo, Japan

M. Kojima
Department of Pathology, Dokkyo University School of Medicine,
Tochigi, Japan

H. Fujita
Ohara Laboratory Institute,
Fukushima, Japan

Y. Akaike
Department of Pathology, Shimotsuga General Hospital,
Tochigi, Japan

H. Wakasa
Tohoku Bunka Gakuen University,
Sendai, Japan

Introduction

Tularemia is a zoonosis caused by the gram-negative coccobacillus *Francisella tularensis*, the etiologic agent of the disease [1–5]. Soken Honma, a physician in Mito, Ibaraki Prefecture, Japan, described tularemia as "hare meat poisoning" (1837) [3] in the oldest report of the disease. In California, USA, McCoy (1911) [6] reported a plague-like disease affecting squirrels.

Ohara and Kitamura [3, 7] confirmed its transmissibility to humans. *F. tularensis* was named after Francis and the town in which the bacterium was isolated: Tulare, California, USA (1921) [6]. In Japan, Hachiro Ohara established the Ohara Institute in Fukushima for the active study of tularemia (1925) [3]. Japanese armed forces (1932–1945) and the U.S. Army (1950–1960) undertook studies to develop tularemia bacteria for use as a biological weapon [1, 8, 9].

After bioterrorism with anthrax in 2001, the Centers for Disease Control (CDC) classified tularemia into the most dangerous pathogen group, category A, along with smallpox and anthrax [10]. Thereafter, cases of tularemia have been reported worldwide [2, 11, 12], but it has become an exceedingly rare disease in Japan. Although the incidence of this disease has decreased, its details must be reviewed because of its potential for use in acts of bioterrorism [1, 8, 10, 13] and because of the danger it presents as an infectious disease transmitted by animals [1, 3, 7].

Research of lymph node lesions [7] has been more common for this disease, but skin lesions and the relation between primary skin lesions and lymph node lesions has not described in the literature. This report of cases in Japan describes primary skin lesions and lymph node lesions and their mutual relation over time for tularemia in terms of clinicopathology and immunohistochemistry.

Materials and methods

Between 1950 and 1965, data of 19 skin cases and 54 lymph node cases were collected at the Ohara Laboratory Institute, Fukushima Japan. All patients files reserved at the Institute were used for this research. These files contained clinical data including symptoms, intimate contact day from infected hares, onset day and biopsy day for each patient. In addition, laboratory examinations such as serum agglutinin and skin test against *F. tularensis* showed positive.

Sections cut from 10 % formalin-fixed paraffin-embedded skin and lymph node samples were stained with hematoxylin–eosin (HE), Giemsa, periodic acid-Schiff (PAS), and Watanabe's silver impregnation.

For immunohistochemical examination, formalin-fixed tissue sections (4-μm thick) were deparaffinized in xylene and redehydrated in graded alcohols and distilled water. All tissue sections were incubated in 0.01 M citrate buffer (pH 6.0) (Koso Chemical Co., Ltd., Tokyo, Japan) using standard microwave or autoclave heating technique for 15, 20 min, respectively. Furthermore, immunohistochemical examination of deparaffinized sections was performed using an automated stainer (Ventana Medical Systems Inc., Arizona, USA) according to the manufacturer's instructions. Then, they were mounted with Malinol mounting (Muto Pure Chemicals Co. Ltd., Tokyo, Japan).

The panel of antibodies against CD 3 (Roche Diagnostics Corp., Ventana Medical Systems Inc.), CD 4, CD10 (Nichirei Corp., Tokyo Japan), CD 5, CD 8, CD 20, CD 30, CD 68 (all Dako, Carpinteria, Ca, USA), CD 83 (Novocastra Laboratories Ltd., U.K.), CD 163 (Lab Vision Corp., USA), CD 204 (Dr. Takeya, Kumamoto, Japan), Langerin (Novocastra Laboratories Ltd.), S-100 (Dako), D2-40 (Nichirei Corp.), Fascin, HLA-DR, IgG, IgA, IgM, κ, λ (all Dako), and anti-*F. tularensis* antibody (Dr. Hotta, NIID, Japan) were used. Sections with known reactivity to the assayed antibodies served as positive controls. Negative controls consisted of each case tissue incubated with normal mouse serum instead of the antibody against *F. tularensis* (Table 1).

Results

Clinical findings

Clinical features of the skin lesions (19 cases) and lymph node lesions (54 cases) are presented in Tables 2 and 3 and almost all patients had visited the doctor for common cold-like symptoms such as a sudden high fever (38–40°C) with chill, headache, back pain, cough, and sore throat. Most patients were male agricultural workers. Almost all patients had been infected during skinning of hares and during cooking of infected hare meat. Skin lesions and lymphadenopathy mainly included finger skin and subcutaneous lesions and regional axillary and elbow lymph nodes, respectively. There were no fatal cases.

Pathological findings

Skin lesion

In the early phase (1–8 days after infection, DAI), no ulceration was found. Many inflammation-related cells such as lymphocytes and plasma cells were observed, along with cell debris and necrosis without neutrophils in deeper dermis and subcutaneous regions under the superficial dermis (abscess form) (Fig. 1a). *F. tularensis* antigens were detected mainly in abscess and necrotic areas (Fig. 1b). Many S-100+, CD68+, CD83+, Fascin+, and CD163+ cells were found in dilated lymph vessels of dermal papillae. Furthermore, irregularly shaped abscesses and many S-100+ and Langerin+ dendritic cells were apparent in dilated lymph vessels around abscess and necrotic subcutaneous sites. Mainly CD20+ B cells are scattered near the abscess.

In the later phase, 14–20 DAI, ulcers appear (Figs. 1c, d). Marked dilated lymph vessels are apparent at the bottom of ulcers and dermal papillae where lymphocytes, dendritic cells, and apoptotic cells were phagocytized by macrophages

Table 1 Antibodies used in this immunohistochemical study

Antibody	Clone	Specificity	Source	Clonality	Retrieval	Dilution
CD3	2GV6	T cells	Roche	M	Mic	1:1
CD4	1 F6	Helper/inducer T cells	Nichirei	M	Mic	1:1
CD5	CD5/5456	T cells	Dako	M	Mic	1:100
CD8	C8/144B	Cytotoxic/suppressor T cells	Dako	M	Mic	1:1
CD10	56 C6	CALLA, Immature B cells, germinal center B cells	Nichirei	M	Mic	1:1
CD20	L26	B cells	Dako	M	Mic	1:1
CD30	Ber-H2	Activated B cells	Dako	M	Mic	1:100
CD68	KP1	Macrophage, plasmacytoid T cells	Dako	M	Mic	1:50
CD83	1H4b	Dendritic cells, Langerhans cells	Novo	M	Mic	1:20
CD163	10D6	Macrophage scavenger receptor	Lab	M	Mic	1:50
CD204		Macrophage scavenger receptor	[a]	M	Mic	1:1
Langerin	12D6	Langerhans cells	Novo	M	Mic	1:100
S-100		Langerhans cells, melanocyte, Schwan cells	Dako	P	Non	1:1
D2-40	D2-40	Lymph vessel	Nichirei	M	Mic	1:1
Fascin	55 K-2	Dendritic cells, interdigitating reticulum cells	Dako	M	Mic	1:50
HLA-DR	TAL.1B5	Langerhans cells, Macrophages, B cells, activated T cells	Dako	M	Mic	1:25
IgG		IgG	Dako	P	Non	1:1
IgA		IgA	Dako	P	Mic	1:1
IgM		IgM	Dako	P	Mic	1:1
κ	R10-21-f3	κ	Dako	M	Non	1:1
λ	N10/2	λ	Dako	M	Non	1:1
F.tularensis		*F.tularensis*	[b]	P	Auto	1:1

Roche Roche Diagnostics, Arizona, USA, *Nichirei* Nichirei, Tokyo, Japan, *Dako* Dako, Ca, USA, *Novo* Novocastra, UK, *Lab* Lab Vision, USA
M monoclonal, *P* polyclonal, *Mic* microwave, *Auto* autoclave, *Non* non treated
[a] Anti-CD204 antibody and [b] anti-*F. tularensis* antibody were supplied from Dr. Takeya and Dr. Hotta, respectively

(Fig. 1e). Subcutaneous areas show several immature granulomas with radiative patterns of epithelioid cells (abscess–granulomatous form) (Fig. 1f). Giant cells and inflammation were observed. Many S-100+, CD68+, CD163+, CD204+, Fascin+, and T cells were found in and around granulomas.

Table 2 Summary of clinical findings of skin lesions, 19 cases

Age distribution	19–69	Mean 43 years, median 44 years
Male:female ratio	4:1	
Occupation	Farmer	13 cases (68 %)
	Charcoal maker	2
	Other	4
Day after infection	1–96 days	Mean 30 days, median 19 days
Site	Skin (hand finger)	4 cases
	Subcutaneous (axillary, elbow)	14
	Unknown	1

Aggregations of monocytoid B lymphocytes (MBLs) were adjacent to the granulomas (Fig. 1g).

Dilated lymph vessels become more numerous during 28–42 DAI and similar cells to those in the previous phase appear at the bottom of the ulcer of dermis. Numerous granulomas are also observed not only in subcutaneous areas but also in superficial dermis. In addition, numerous multinucleated giant cells appear near the granulomas.

In the last phase, skin ulcers are scarred after around the sixth week. During 51–96 DAI, many irregularly shaped fused epithelioid granulomas with central homogeneous lesions are observed in subcutaneous and dermis areas (granulomatous form) (Fig. 1h). Similar cells to those in the previous phase appear in and around granulomas. Giant cells are observed occasionally at epithelioid granulomas. Aggregations of MBLs, adjacent to the granulomas, were also observed in this phase. Many S-100+, CD68+, and CD163+ cells were also observed in marked distended lymph vessels of dermal papillae.

The *F. tularensis* antigen of the skin lesion was detected only in the abscess, except with granuloma at 2–14 DAI (Fig. 2).

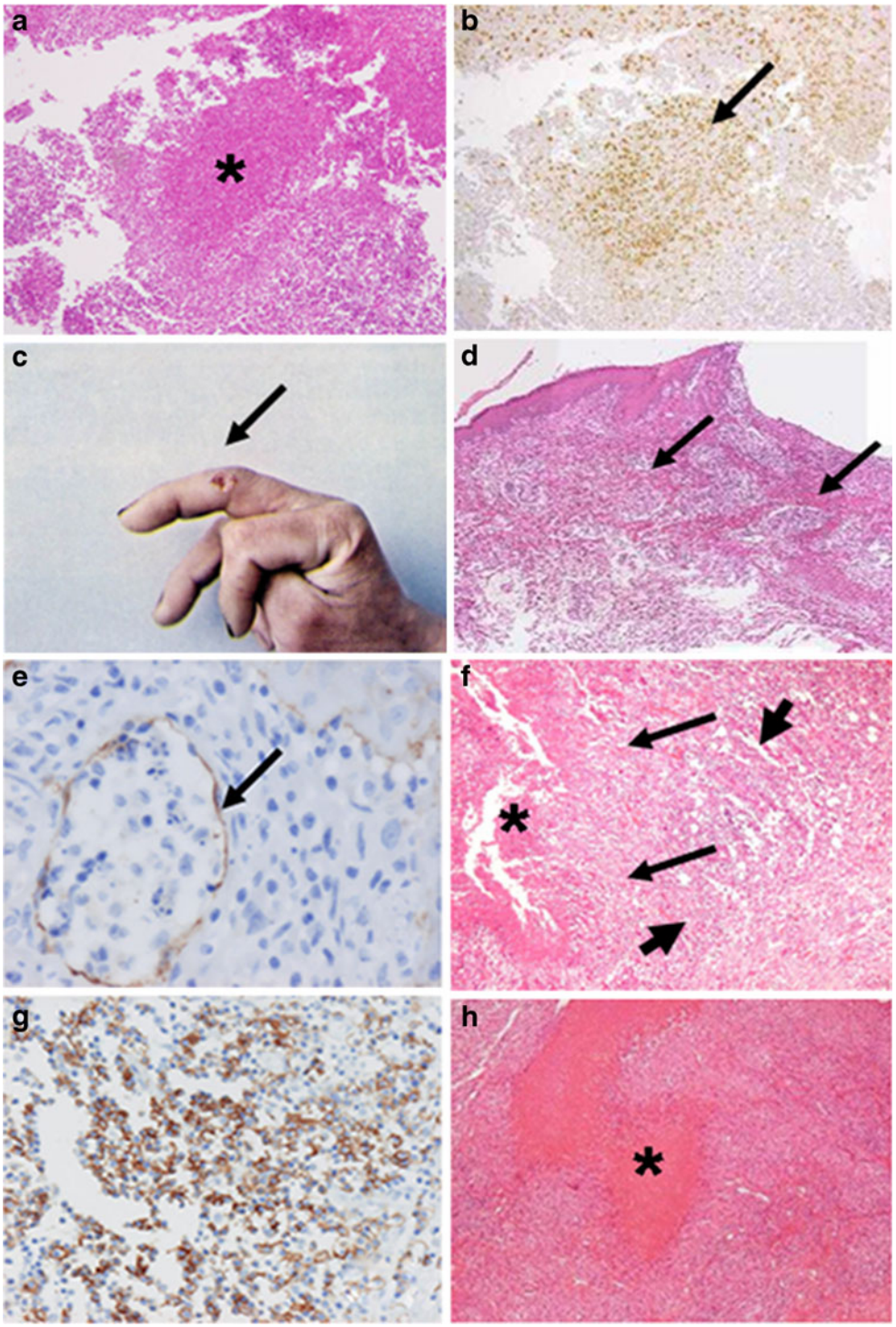

Fig. 1 Skin and subcutaneous. **a** Central necrosis and abscess (*asterisk*) of subcutaneous area with marginal lymphocytes (4 DAI). **b** Immunostaining. *F. tularensis* antigens (*arrow*) were detected mainly in abscesses and necrotic areas (4 DAI) (anti-*F. tularensis* antibody). **c** Skin ulcer (*arrow*) of the right middle finger (14 DAI). **d** Various sizes of granulomas (*arrow*) at ulcer base of dermis. **e** Lymphocytes, apoptotic cells, and macrophages were observed within marked distended lymph vessels (*arrow*) (30 DAI). (Anti-D2-40 antibody). **f** Epithelioid granuloma (*arrow*) in dermis with central necrosis (*asterisk*) was adjacent to CD 20+ lymphocyte aggregation (*bold arrow* = *italic*). **g** Enlargement of **f**. Many CD 20 + lymphocytes (monocytoid B lymphocytes; MBLs) aggregated near the granuloma (19 DAI). **h** Large irregularly shaped epithelioid granuloma with central homogeneous lesion (*asterisk*) in dermis. No antigen was detected in the lesion (75 DAI)

Lymph node lesion

During 7–12 DAI, sinus histiocytosis and follicular hyperplasia appeared. Small abscesses and mononuclear cells appeared (abscess form) (Fig. 3a). *F. tularensis* antigens were detected mainly in abscess and necrotic areas (Fig. 3b). Adjacent to abscesses, MBLs aggregation was observed. Some cases show marked periadenitis because of acute inflammation.

During the second to fifth week after infection, small epithelioid granulomas with central necrosis were apparent beneath the capsular area and medulla of lymph nodes (abscess–granulomatous form) (Figs. 3c, d). The epithelioid cells of the granulomas occasionally showed a radiative

Table 3 Summary of clinical findings of lymphadenopathy, 54 cases

Age distribution	8–69		Mean 39 years, median 37 years
Male:female ratio	4:1		
Occupation	Farmer		40 cases (74 %)
	Charcoal maker		3
	Carpenter		2
	Other (teacher, woodcutter, charcoal maker, hotel worker) furrier, child)		9
Day after infection	6–133 days		Mean 33 days, median 24 days
Site	Axillary (76 %)	Left	21
		Right	21
		Bilateral	4
	Elbow (7 %)	Left	1
		Right	3
	Mandible		1
	Unknown		3

pattern. Many S-100+, CD68+, CD163+, CD204+, Fascin+, HLA-DR+, and T cells were found in and around granulomas.

The MBLs were adjacent to the granuloma, as in an earlier phase (Fig. 3e). Regarding lymphocyte distribution in and around granulomas, CD4/CD8 T cell ratios were 2.3, 1.1, and 2.0, respectively, at abscesses, granulomas, and outer layers of granulomas (Fig. 3f). Furthermore, numerous multinucleated giant cells are scattered in granulomatous lesions.

After the sixth week, many large granulomas with central homogeneous lesions resembling tuberculous nodes (granulomatous form) were present. They were mutually fused, forming irregularly shaped granulomas (Fig. 3g). Similar cells to those in the previous phase appear in and around granulomas. Many MBLs were observed as adjacent to granulomas, as noted for the prior phase (Fig. 3h). In addition, many multinucleated giant cells were observed in granulomatous lesions.

F. tularensis antigen was observed from 7–92 DAI in the abscess, except that with granuloma (Fig. 2).

Discussion

From their pathological study of the tularemia, Kitamura et al. [7] described lymph node and skin phenomena. According to their report, lymph node lesions are classifiable with time into three forms: abscess form, abscess–granulomatous form, and granulomatous form. Skin ulcers form in the first week and scar tissue formation is observed in the second to fifth week after onset. Healing of skin lesions might be more rapid than that of lymph nodes [7].

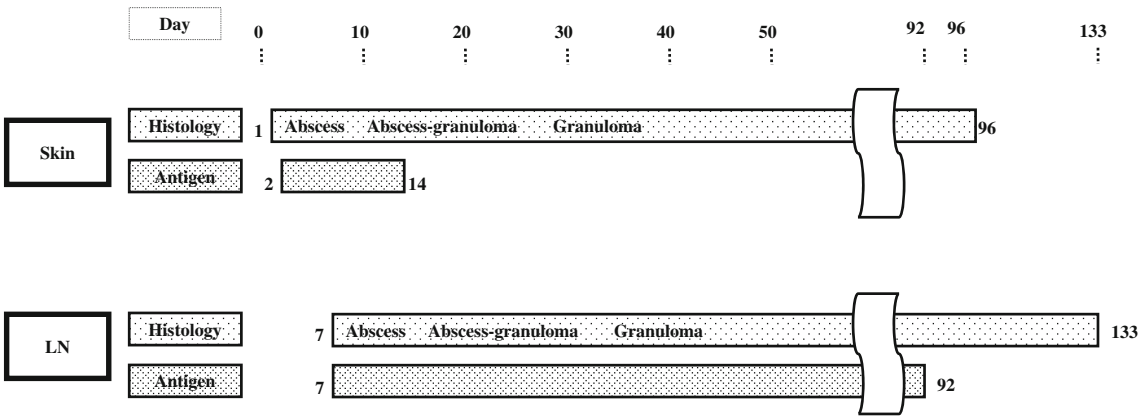

Fig. 2 Histology and *F. tularensis* antigen of skin and lymph node. *F. tularensis* antigen was detected during 2–14 DAI, and 7–92 DAI, in abscess and necrotic area of skin and lymph node, respectively. *Day*, days after infection (numbers of columns denote days); *LN*, lymph node; *Antigen*, antigen for *F. tularensis*; Histology was classified into three forms: abscess, abscess–granulomatous, and granulomatous [7]

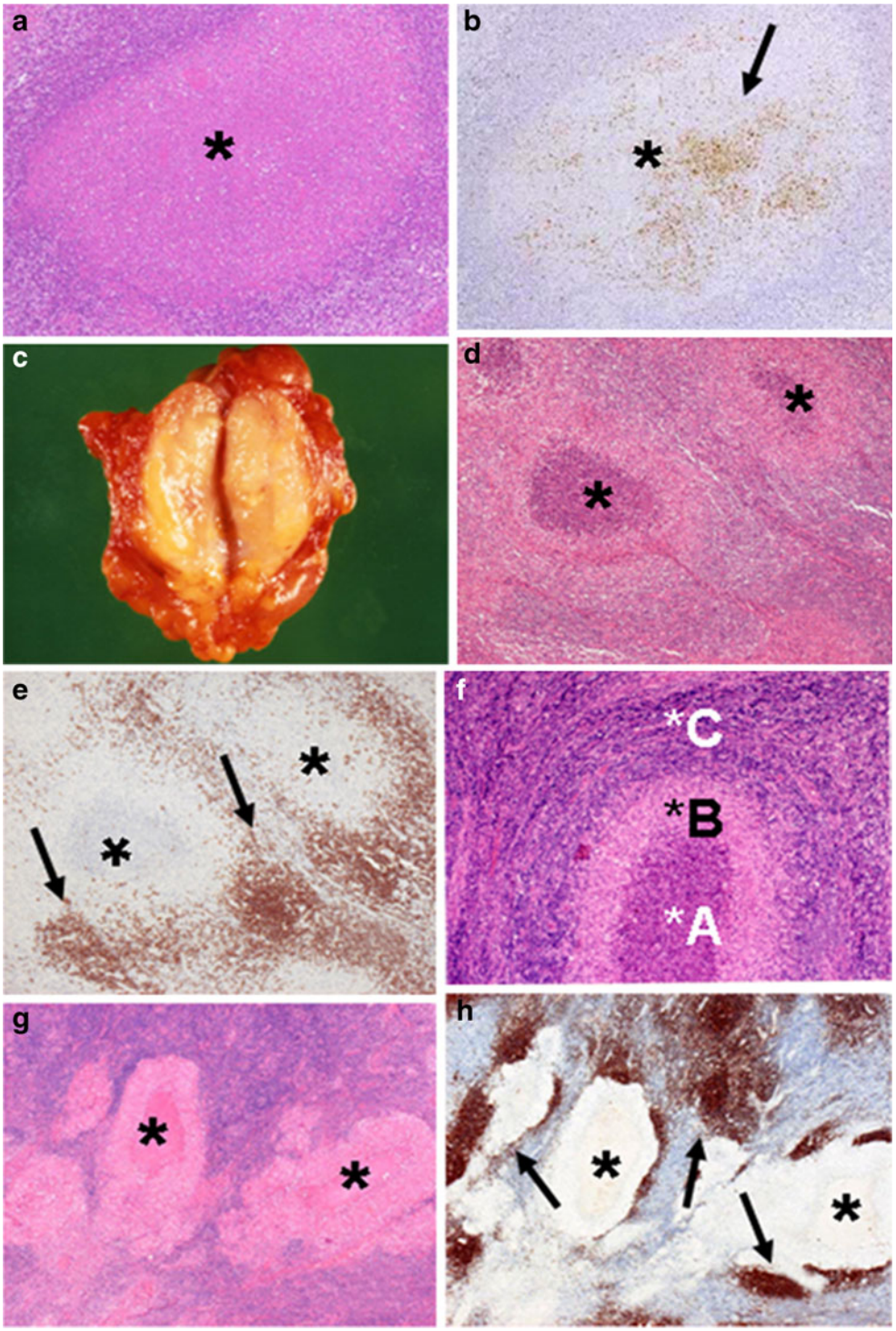

Fig. 3 Abscess form lymph node lesion (10 DAI). **a** Abscess and necrosis lesion (*asterisk*) without epithelioid granuloma located in the paracortex of a lymph node (10 DAI). **b** *F. tularensis* antigens (*arrow*) were mainly present in abscesses and necrosis lesions (*asterisk*) (10 DAI). (Anti-*F. tularensis antibody).* **c** Abscess–granulomatous form lymph node lesion (14 DAI). Marked swelled axillary lymph node on the cut section. **d** Central abscess and necrosis lesion (*asterisk*) was surrounded by thick epithelioid cell granuloma (14 DAI). **e** CD20+ monocytoid B lymphocytes (MBLs) aggregations (*arrow*) were adjacent to granuloma. *Asterisk*, abscess and necrosis lesion (14 DAI). **f** CD4/CD8 ratio was 2.3 (**A*), 1.1 (**B*), and 2.0 (**C*) in abscess–granulomatous form of lymph node. **g** Granulomatous form lymph node lesion (92 DAI). Large irregular granuloma with central homogeneous lesion (*asterisk*). Very few antigens were detected in abscesses. **h** CD20+ cells (MBLs) aggregations (*arrow*) were adjacent to the outer layer of epithelioid cell granuloma. *Asterisk*, central homogeneous lesion

Our study revealed that the primary skin lesions, especially in subcutaneous lesions, induced by *F. tularensis* occurred from 2 DAI and that lymph node lesions developed during 7–14 DAI. The time difference of onset was apparent among these skin and lymph node cases.

Molecular biological analysis showed that DNA sequences of *F. tularensis* from the infected hare coincided with that of regional lymph node of the patient [in prepare]. It may be concluded that *F. tularensis* penetrates intact human skin after direct contact with an infected hare. Subsequently, it is transported via the skin lymphatic stream to subcutaneous regions and then to regional lymph nodes [14, 15]. The most common skin ulcers occurred on the finger skin up to the second week after infection, and scars formed up to the sixth week in this study. Many antigen presenting cells (APCs) such as histiocytes, leukocytes, lymphocytes, and

Langerhans cells were observed within dilated lymph vessels in the primary skin lesion. Many recruited APCs at the subcutaneous region or lymph node, contributing to production of abscesses and granuloma formation. During this period, granulomas with marked inflammation were formed at the base of the ulcer, and *F. tularensis* was detected only at abscesses. As described above, regional lymph node lesions induced by skin disease are designated as dermatopathic lymphadenopathy (DPL) [16]. The primary skin lesion gradually transfers from the skin to regional lymph nodes [14, 17].

Dermatopathic lymphadenopathy (DPL) is a commonly paracortical hyperplasia of a regional lymph node induced by chronic skin diseases such as erythroderma and mycosis fungoides. It persists even after distinct skin lesions have disappeared by the time of lymph node biopsy [16]. In general, the pathological finding of DPL is characterized by the presence of eosinophils, histiocytes, lymphoblasts, and Langerhans cells appearing as a pale area in the paracortex in the lymph node. In contrast, in tularemic lymph nodes, cells of such kinds do not appear because the primary skin lesions are acute dermatitis induced by *F. tularensis* [7]. Based on the discussion presented above, tularemic lymphadenopathy can be regarded as DPL of an acute type.

Secondary skin lesions on the hand, leg, and neck caused by an allergic reaction to bacteria are papular or papulovesicular eruptions that occur around 10 DAI. They might occur bilaterally, symmetrically, or as widely distributed, and can take 2 weeks to subside. Erythema nodosum and erythema multiforme are also secondary skin lesions. *F. tularensis* was also detected from erythema multiforme vesicle fluid [18, 19]. However, secondary skin lesions do not produce ulcers as primary skin lesions do [20, 21].

Earlier reports have described that *F. tularensis* antigen was detected only in the abscesses of skin and lymph node lesions [14]. The long-lasting antigen against *F. tularensis* in the lymph nodes might contribute to the sustained presence of serum antibodies. Furthermore, CD4+ T cells, which affect B cells to stimulate antibody production, were present in greater numbers in granuloma than CD8+ T cells were. The factors described above contributed to antibody production. However, the antigen was apt to diminish after mature granuloma formation.

In the early phase of tularemia, numerous neutrophils, monocytoid B cells (MBLs), histiocytic cells, T cells, S-100+, Langerin+, CD83+, CD163+ dendritic cells are found in lesions. An MBL cluster was occasionally observed adjacent to a microabscess from the abscess forming phase. During abscess and granuloma formation, macrophages might recruit MBLs with subsequent infiltration of neutrophils, followed by necrosis and eventual granuloma formation [22]. Furthermore, inflammatory cells such MBLs, CD68+, CD163+, CD204+ macrophages, S-100+, Langerin+, CD83+, CD163+ dendritic cells and T lymphocytes can be regarded as playing an important role for granuloma formation in tularemia, as in cat scratch disease [23].

It is occasionally difficult to distinguish tularemia from tuberculosis because they have similar granulomas. Tularemia, which has clinically acute inflammation, begins with much more rapid progress than that of tuberculosis. Regarding histologic characteristics of tularemia, the epithelioid cell layer is generally thicker than that of tuberculosis, with disappearance of argyrophilic fibers in the center of the granulomas of tularemia. Moreover, the nuclei of giant cells in tularemia are fewer than in tuberculosis [7].

Recently, rapid assay for detection of *F. tularensis* in formalin-fixed paraffin-embedded lymph nodes has become available for differential diagnosis by polymerase chain reaction (PCR) [19, 24]. As a biosecurity issue, it is necessary to design a molecular diagnosis system for *F. tularensis* to distinguish strains of subsp. *holarctica*, a common strain in Japan [25], from strains of other subspecies including strains of the highly virulent subsp. *tularensis* [2, 26].

Acknowledgement This study was supported in part by a grant for research on Emerging and Re-emerging Infectious Disease (H22 Shinko-Ippan-6) from the Ministry of Health, Labour, and Welfare, Japan.

The authors appreciate support of anti-CD 204 antibody from Dr. M. Takeya, Dept. of Pathology, Kumamoto University, Kumamoto, Japan, and of anti-*F. tularensis* antibody, from Dr. T. Hotta, Dept. of Veterinary Science, National Institute of Infectious Diseases, Tokyo, Japan.

Conflict of interest We declare that we have no conflict of interest.

Open Access This article is distributed under the terms of the Creative Commons Attribution License which permits any use, distribution, and reproduction in any medium, provided the original author(s) and the source are credited.

References

1. Denis DT, Inglesby TV, Henderson DA et al (2001) Tularemia as a biological weapon. Medical and public health management. JAMA 285:2763–2773
2. Johansson A, Ibrahim A, Goeransson I et al (2000) Evaluation of PCR-based methods for discrimination of *Francisella* species and development of a specific PCR that distinguished two major subspecies of *Francisella tularensis*. J Clin Microbiol 38:4180–4185
3. Ohara S, Ichikawa K (1962) The distribution of Yato-byo and its clinical observations. Ohara nenpou (in Japanese) 11:1–22
4. Olsufjev NG, Meschcheryakova IS (1983) Subspecific taxonomy of *Francisella tularensis*. Int J Syst Bacteriol 33:872–874
5. Vogler AJ, Birdsell D, Price LB et al (2009) Phylogeography of *F. tularensis*: global expansion of a highly fit clone. J Bacterio 191:2472–2484
6. Francis E (1925) Tularemia. JAMA 84:1243–1250

7. Kitamura S, Fukuda M, Takeda H et al (1956) Pathology of tularemia. Acta Pathol Jap 6:719–764
8. Christopher GW, Cieslak TJ, Pavlin JA et al (1997) Biological warfare: a histological perspective. JAMA 278:412–418
9. Harris S (1992) Japanese biological warfare research on humans: a case study of microbiology and ethics. Ann N Y Acad Sci 666:21–52
10. Inglesby TV, O'Toole T, Henderson DA et al (2002) Anthrax as a biological weapon: updated recommendations for management. JAMA 287:2236–2252
11. Dahlstrand S, Ringetz O, Zetterberg B (1971) Airborne tularemia in Sweden. Scand J Infect Dis 3:7–16
12. Syrjälä H, Kujara P, Salminen A (1985) Airborne transmission of tularemia in farmers. Scand J Infect Dis 17:371–375
13. Kuroda M, Serizawa M, Okutani A et al (2010) Genome-wide single nucleotide polymorphism typing method for identification of *Bacillus anthracis* species and strains among *B. cereus* group species. J Clin Microbiol 48:2821–2829
14. Guarner J, Gree PW, Bartlett J et al (1999) Immunohistochemical detection of *Francisella tularensis* in formalin-fixed paraffin- embedded tissue. Appl Immunohistochem Mol Morphol 7:122–126
15. Ryan TJ, Mortimer PS, Jones RL (1986) Lymphatics of the skin (neglected but important). Inter J Dermatol 25:411–419
16. Asano S, Muramatsu T, Kanno H et al (1987) Dermatopathic lymphadenopathy-electronmicroscopic, enzyme-histochemical and immunohistochemical study. Acta Pathol Jap 37:887–900
17. Tärnvik A, Berglund L (2003) Tularaemia. Eur Respir J 21:361–373
18. Foshay L (1940) Tularemia: a summary of certain aspects of the disease including methods for early diagnosis and the results of serum treatment in 600 patients. Medicine 19:1–83
19. Golovliov I, Ericsson M, Sandström G et al (1997) Identification of proteins of *Francisella tularensis* induced during growth in macrophages and cloning of the gene encoding a prominently induced 23-kilodalton protein. Infect Immun 65:2183–2189
20. Ohara S, Hoshishima K (1957) Diagnosis of Yato-byo (Ohara disease, tularemia in Japan). Fukushima J Med Sci 4:51–61
21. Syrjälä H, Karvonen J, Salminen A (1984) Skin manifestations of tularemia: a study of 88 cases in northern Finland during 16 years (1967–1983). Acta Derm Venereol 64:513–516
22. Chang KL, Arber DA, Gaal KK et al (2006) Lymph nodes and spleen. In: Silverberg SG, DeLellis RA, Frable WJ et al (eds) Principles and practice of surgical pathology and cytopathology, 4th edn. Churchill Livingstone, Philadelphia, pp 507–608
23. Kojima M, Nakamura S, Kurabayashi Y et al (1995) Suppurative lesions without prominent epithelioid cell response in abscess-forming granulomatous lymphadenitis. Path Res Pract 191:1072–1077
24. Versage JL, Severin DDM, Chu MC et al (2003) Development of a multitarget real-time TaqMan PCR assay for enhanced detection of *Francisella tularensis* in complex specimens. J Clin Microbiol 41:5492–5499
25. Kuroda M, Sekizawa T, Shinya F et al (2012) Detection of a possible bioterrorism agent, *Francisella* sp., in a clinical specimen by use of next-generation direct DNA sequencing. J Clin Microbiol 50:1810–1812
26. Byström M, Böchen S, Magnusson A et al (2005) Tularemia in Denmark: identification of a *Francisella tularensis* subsp. *holarctica* strain by real-time PCR and high-resolution typing by multiple-locus variable-number tandem repeat analysis. J Clin Microbiol 43:5355–5358